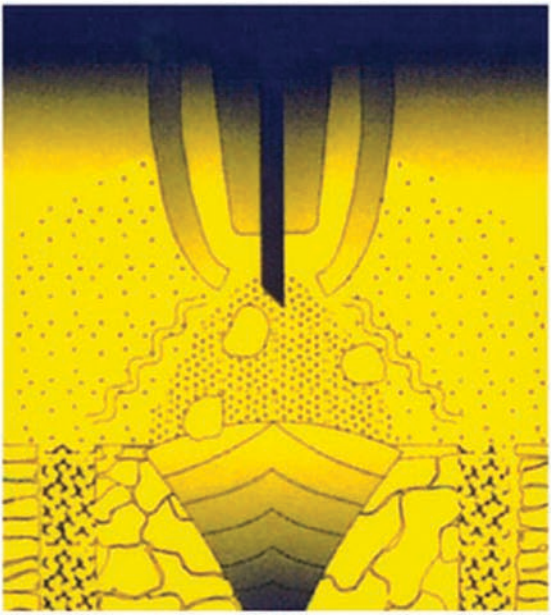
PHYSIKS TEXTBOOK

WILEY-VCH

Robert W. Messler, Jr.

Principles of Welding

Processes, Physics, Chemistry, and Metallurgy



PRINCIPLES OF WELDING

Processes, Physics, Chemistry, and Metallurgy

ROBERT W. MESSLER, Jr.
Materials Science and Engineering Department
Rensselaer Polytechnic Institute
Troy, NY



WILEY-VCH Verlag GmbH & Co. KGaA

This Page Intentionally Left Blank

PRINCIPLES OF WELDING

This Page Intentionally Left Blank

PRINCIPLES OF WELDING

Processes, Physics, Chemistry, and Metallurgy

ROBERT W. MESSLER, Jr.
Materials Science and Engineering Department
Rensselaer Polytechnic Institute
Troy, NY



WILEY-VCH Verlag GmbH & Co. KGaA

All books published by Wiley-VCH are carefully produced.
Nevertheless, authors, editors, and publisher do not warrant the information contained in these books, including this book, to be free of errors.
Readers are advised to keep in mind that statements, data, illustrations, procedural details or other items may inadvertently be inaccurate.

Library of Congress Card No.:
Applied for

British Library Cataloging-in-Publication Data:
A catalogue record for this book is available from the British Library

Bibliographic information published by
Die Deutsche Bibliothek
Die Deutsche Bibliothek lists this publication in the Deutsche Nationalbibliografie; detailed bibliographic data is available in the Internet at <http://dnb.ddb.de>.

© 1999 by John Wiley & Sons, Inc.
© 2004 WILEY-VCH Verlag GmbH & Co. KGaA, Weinheim

All rights reserved (including those of translation into other languages).
No part of this book may be reproduced in any form – nor transmitted or translated into machine language without written permission from the publishers.
Registered names, trademarks, etc. used in this book, even when not specifically marked as such, are not to be considered unprotected by law.

Printed in Singapore
Printed on acid-free paper

Cover Illustration Avram Kaufman
Printing and Bookbinding Markono Print Media Pte Ltd, Singapore

ISBN-13: 978-0-471-25376-1
ISBN-10: 0-471-25376-6

CONTENTS

PREFACE xix

I THE PROCESS AND PROCESSES OF WELDING

1 INTRODUCTION TO THE PROCESS OF WELDING 3

1.1 What Is Welding? / 3
1.2 The Evolution of Welding as a Process / 6
1.3 The Nature of an Ideal Weld: Achieving Continuity / 7
1.4 Impediments to Making Ideal Welds in the Real World / 10
1.5 What It Takes to Make a Real Weld / 12
1.6 Advantages and Disadvantages of Welding / 14
1.7 Summary / 15
References and Suggested Reading / 15

2 CLASSIFYING WELDING PROCESSES 17

2.1 Why Classify Processes? / 17
2.2 Mechanisms for Obtaining Material Continuity / 18
2.3 The Roles of Temperature and Pressure / 21
2.4 Alternative Bases for Classification / 23
2.4.1 Fusion Versus Nonfusion / 23
2.4.2 Pressure Versus Nonpressure / 25
2.4.3 Energy Source for Welding / 25

2.4.4 Interface Relationships and Classification by Energy Transfer Processes / 27
2.4.5 Other Bases for Classification and Subclassification / 28
2.5 Allied Processes / 35
2.6 The AWS Classification Scheme / 37
2.7 Summary / 39
References and Suggested Reading / 39

3 FUSION WELDING PROCESSES **40**

3.1 General Description of Fusion Welding Processes / 40
3.2 Chemical Fusion Welding Processes / 41
3.2.1 Oxyfuel Gas Welding / 41
3.2.2 Aluminothermic Welding / 46
3.3 Electric Arc Welding Processes / 49
3.3.1 Nonconsumable Electrode Arc Welding Processes / 50
3.3.1.1 Gas–Tungsten Arc Welding / 51
3.3.1.2 Plasma Arc Welding / 55
3.3.1.3 Magnetically Impelled Arc Butt Welding / 57
3.3.2 Consumable Electrode Arc Welding Processes / 60
3.3.2.1 Gas–Metal Arc Welding / 60
3.3.2.2 Shielded-Metal Arc Welding / 64
3.3.2.3 Flux-Cored Arc Welding / 66
3.3.2.4 Submerged Arc Welding / 68
3.3.2.5 Electrogas Welding / 69
3.3.2.6 Electroslag Welding / 70
3.4 Resistance Welding Processes / 71
3.4.1 Resistance Spot, Resistance Seam, and Projection Welding / 71
3.4.2 Flash, Upset, and Percussion Welding / 74
3.5 High-Intensity Radiant Energy or High-Density Beam Welding Processes / 77
3.5.1 High-Energy-Density (Laser and Electron) Beam Welding Processes / 80
3.5.2 Focused IR and Imaged Arc Welding / 86
3.5.3 Microwave Welding / 88
3.6 Summary / 92
References and Suggested Reading / 93

4 NONFUSION WELDING PROCESSES 94

4.1 General Description of Nonfusion Welding Processes / 94
4.2 Pressure (Nonfusion) Welding Processes / 97
4.2.1 Cold Welding Processes / 98
4.2.2 Hot Pressure Welding / 99
4.2.2.1 Pressure Gas Welding / 100
4.2.2.2 Forge Welding / 101
4.2.3 Roll Welding / 102
4.2.4 Explosion Welding / 103
4.3 Friction Welding Processes / 105
4.3.1 Radial and Orbital Welding / 107
4.3.2 Direct-Drive Versus Inertia-Drive (Friction) Welding / 107
4.3.3 Angular and Linear Reciprocating (Friction) Welding / 108
4.3.4 Ultrasonic (Friction) Welding / 109
4.3.5 Friction Stir Welding / 112
4.3.6 Friction Surfacing / 113
4.4 Diffusion Joining Processes / 113
4.4.1 Diffusion Welding / 114
4.4.1.1 Conventional Diffusion Welding / 118
4.4.1.2 Deformation Diffusion Welding / 118
4.4.1.3 Resistance Diffusion Welding / 118
4.4.1.4 Continuous Seam Diffusion Welding / 118
4.4.2 Diffusion Brazing / 119
4.4.3 Combined Forming and Diffusion Welding / 119
4.5 Solid-State Deposition Welding Processes / 120
4.6 Inspection and Repair of Nonfusion Welds / 120
4.7 Summary / 123
References and Suggested Reading / 123

II THE PHYSICS OF WELDING

5 ENERGY FOR WELDING 127

5.1 Introduction to the Physics of Welding / 127
5.2 Sources of Energy for Welding / 127

5.3 Source Energy, Transferred Power, Energy Density, and Energy Distribution / 128
5.3.1 Energy Available at a Source (Energy Level or Capacity / 128
5.3.2 Transferred Power / 130
5.3.3 Source Intensity or Energy Density / 130
5.3.4 Energy Distribution / 131
5.4 Energy Input to a Weld / 132
5.5 Causes of Loss During Energy Transfer From Source to Work / 134
5.6 Transfer Efficiency of Processes / 134
5.7 Effects of Deposited Energy: Good and Bad / 138
5.7.1 Desirable Melting, Fluxing, or Softening / 139
5.7.2 Adverse Effects of Heat in and Around the Weld / 141
5.8 Effects of Energy Density and Distribution / 142
5.9 Summary / 144
References and Suggested Reading / 146

6 THE FLOW OF HEAT IN WELDS 147

6.1 General Description of the Flow of Heat in Welds / 147
6.2 Weld Joint Configurations / 148
6.2.1 Types of Weld Joints / 148
6.2.2 General Weld Design Guidelines / 152
6.2.3 Size of a Weld and Amount of Welding / 154
6.3 The Welding Thermal Cycle / 154
6.4 The Generalized Equation of Heat Flow / 158
6.5 Analysis of Heat Flow During Welding / 161
6.5.1 Rosenthal's Simplified Approach / 162
6.5.2 Modifications to Rosenthal's Solutions / 165
6.5.3 Dimensionless Weld Depth Versus Dimensionless Operating Parameter / 167
6.6 Effect of Welding Parameters on Heat Distribution / 168
6.7 Prediction of Weld Zones and Weld Cooling Rates / 172
6.7.1 Zones in Fusion-Welded Materials / 172
6.7.2 Simplified Equations for Approximating Welding Conditions / 173
6.7.2.1 Peak Temperatures / 174
6.7.2.2 Width of the Heat-Affected Zone / 174
6.7.2.3 Solidification Rate / 174
6.7.2.4 Cooling Rates / 175

6.8 Weld Simulation and Simulators / 176
6.9 Summary / 178
References and Suggested Reading / 178

7 THERMALLY INDUCED DISTORTION AND RESIDUAL STRESSES DURING WELDING 181

7.1 Origin of Thermal Stresses / 181
7.2 Distortion Versus Residual Stresses / 183
7.2.1 Causes of Residual Stresses in Weldments / 185
7.2.1.1 Residual Stresses From Mismatch / 186
7.2.1.2 Residual Stresses From Nonuniform, Nonelastic Strains / 189
7.2.2 Causes of Distortion in Weldments / 190
7.3 Typical Residual Stresses in Weldments / 191
7.4 Effects of Distortion / 194
7.5 Effects of Residual Stresses / 196
7.6 Measurement of Residual Stresses in Weldments / 197
7.6.1 Stress–Relaxation Techniques / 199
7.6.1.1 A Sectioning Technique Using Electric-Resistance Strain Gauges / 199
7.6.1.2 The Rosenthal–Norton Section Technique / 201
7.6.1.3 The Mathar–Soete Hole Drilling Technique / 202
7.6.1.4 The Gunnert Drilling Technique / 202
7.6.2 The X-ray Diffraction Technique / 204
7.7 Residual Stress Reduction and Distortion Control / 206
7.7.1 The Interplay Between Residual Stresses and Distortion / 206
7.7.2 Prevention Versus Remediation / 206
7.7.3 Controlling or Removing Residual Stresses / 207
7.7.4 Controlling or Removing Distortion / 208
7.8 Numerical Methods for Estimating Residual Stresses / 210
7.9 Summary / 211
References and Suggested Reading / 214

8 THE PHYSICS OF WELDING ENERGY OR POWER SOURCES 216

8.1 Electricity for Welding / 216
8.2 The Physics of an Electric Arc and Arc Welding / 223
8.2.1 The Physics of an Electric Arc / 223

8.2.1.1 The Welding Arc / 224
8.2.1.2 The Arc Plasma / 224
8.2.1.3 Arc Temperature / 224
8.2.1.4 Arc Radiation / 226
8.2.1.5 Arc Electrical Features / 226
8.2.1.6 Effect of Magnetic Fields on Arcs / 228
8.2.2 Volt–Ampere Characteristics for Welding / 231
8.2.2.1 Constant-Current Power Sources / 232
8.2.2.2 Constant-Voltage Power Sources / 232
8.2.2.3 Combined Characteristic Sources / 234
8.3 The Physics of a Plasma / 234
8.4 The Physics of Resistance (or Joule) Heating and Resistance Welding / 237
8.4.1 Joule Heating / 237
8.4.2 The Resistance Welding Cycle / 239
8.4.3 Resistance Welding Power Supplies / 239
8.5 The Physics of Electron Beams / 243
8.5.1 Electron-Beam Generation / 245
8.5.2 Electron-Beam Control / 248
8.5.3 Role of Vacuum in EB Welding / 252
8.5.4 Electron-Beam–Material Interactions / 253
8.6 The Physics of Laser Beams / 256
8.6.1 Laser Light / 256
8.6.2 Laser Generation / 256
8.6.2.1 Nd:YAG Lasers / 258
8.6.2.2 CO_2 Lasers / 259
8.6.3 Laser-Beam Control / 259
8.6.4 Laser-Beam–Material Interactions / 260
8.6.5 Benefits of Laser-Beam and Electron-Beam Welding / 263
8.7 The Physics of a Combustion Flame / 265
8.7.1 Fuel Gas Combustion or Heat of Combustion / 265
8.7.2 Flame Temperature / 265
8.7.3 Flame Propagation Rate or Combustion Velocity / 266
8.7.4 Combustion Intensity / 266
8.8 The Physics of Converting Mechanical Work to Heat / 266
8.9 Summary / 268

References and Suggested Reading / 269

9 MOLTEN METAL TRANSFER IN CONSUMABLE ELECTRODE ARC WELDING 270

9.1 Forces Contributing to Molten Metal Transfer in Welding / 270
- 9.1.1 Gas Pressure Generation at Flux-Coated or Flux-Cored Electrode Tips / 271
- 9.1.2 Electrostatic Attraction / 272
- 9.1.3 Gravity / 272
- 9.1.4 Electromagnetic Pinch Effect / 272
- 9.1.5 Explosive Evaporation / 272
- 9.1.6 Electromagnetic Pressure / 273
- 9.1.7 Plasma Friction / 273
- 9.1.8 Surface Tension / 273

9.2 Free-Flight Transfer Modes / 274
- 9.2.1 Globular Transfer / 275
- 9.2.2 Spray Transfer / 276

9.3 Bridging of Short-Circuiting Transfer Modes / 278

9.4 Pulsed-Arc or Pulsed-Current Transfer / 279

9.5 Slag-Protected Transfer / 280

9.6 Variations of Major Transfer Modes / 281

9.7 Effect of Welding Process Parameters and Shielding Gas on Transfer Mode / 282
- 9.7.1 Effects on Transition Current / 282
- 9.7.2 Shielding Gas Effects / 285
- 9.7.3 Process Effects / 287
- 9.7.4 Operating Mode or Polarity Effects / 288

9.8 Summary / 289

References and Suggested Reading / 289

10 WELD POOL CONVECTION, OSCILLATION, AND EVAPORATION 291

10.1 Origin of Convection / 291
- 10.1.1 Generalities on Convection in Weld Pools / 292
- 10.1.2 Buoyancy or Gravity Force / 294
- 10.1.3 Surface Gradient Force or Marangoni Convection / 295
- 10.1.4 Electromotive Force or Lorentz Force / 296
- 10.1.5 Impinging or Friction Force / 297
- 10.1.6 Modeling Convection and Combined Force Effects / 298

10.2 Effects of Convection / 298
10.2.1 Effect of Convection on Penetration / 300
10.2.2 Effect of Convection on Macrosegregation / 301
10.2.3 Effect of Convection of Porosity / 304
10.3 Enhancing Convection / 305
10.4 Weld Pool Oscillation / 306
10.5 Weld Pool Evaporation and Its Effects / 307
10.6 Summary / 310
References and Suggested Reading / 310

III THE CHEMISTRY OF WELDING

11 MOLTEN METAL AND WELD POOL REACTIONS 315

11.1 Gas–Metal Reactions / 316
11.1.1 Gas Dissolution and Solubility in Molten Metal / 317
11.1.2 Solid Solution Hardening and Phase Stabilization / 323
11.1.3 Porosity Formation / 326
11.1.4 Embrittlement Reactions / 327
11.1.5 Hydrogen Effects / 328
11.1.5.1 Hydrogen Embrittlement / 329
11.1.5.2 Hydrogen Porosity / 331
11.1.5.3 Hydrogen Cracking / 332
11.2 Molten Metal Shielding / 333
11.2.1 Shielding Gases / 333
11.2.2 Slags / 335
11.2.3 Vacuum / 335
11.2.4 Self-Protection and Self-Fluxing Action / 336
11.3 Slag–Metal Reactions / 337
11.3.1 Deoxidizing/Denitriding (or Killing) Versus Protection / 337
11.3.2 Flux-Protected Welding Processes / 339
11.3.3 Shielding Capacities of Different Processes / 340
11.3.4 Slag Formation / 341
11.3.5 Slag–Metal Chemical Reactions / 342
11.3.6 Flux Types / 342

11.3.7 Common Covered- and Cored-Electrode Flux Systems / 344
11.3.7.1 Shielded Metal Arc Welding Electrode Coatings / 344
11.3.7.2 Flux-Cored Arc Welding Fluxes / 344
11.3.7.3 Submerged Arc Welding Fluxes / 344
11.3.8 Basicity Index / 344
11.3.9 Thermodynamic Model for Welding Slag–Metal Reactions / 348
11.4 Summary / 354
References and Suggested Reading / 356

12 WELD CHEMICAL HETEROGENEITY 359

12.1 Weld (Pool) Dilution / 360
12.2 Microsegregation and Banding in the Weld Metal / 363
12.3 Unmixed and Partially Mixed Zones / 365
12.4 Impurities in the Weld Metal / 366
12.5 Macrosegregation in Dissimilar Welds / 368
12.6 Summary / 370
References and Suggested Reading / 370

IV THE METALLURGY OF WELDING

13 WELD FUSION ZONE SOLIDIFICATION 375

13.1 Equilibrium Versus Nonequilibrium / 378
13.2 Solidification of a Pure Crystalline Material / 381
13.2.1 Criteria for Equilibrium at T_E and Constant Pressure / 381
13.2.2 Pure Material Growth Modes / 382
13.2.3 Homogeneous Versus Heterogeneous Nucleation / 384
13.2.3.1 Homogeneous Nucleation / 384
13.2.3.2 Super- or Undercooling / 388
13.2.3.3 Effect of Radius of Curvature on Supercooling / 388
13.2.3.4 Heterogeneous Nucleation / 389
13.2.4 Epitaxial and Competitive Growth / 392
13.2.5 Effect of Weld Pool Shape on Structure / 395

13.2.6 Competing Rates of Melting and Solidification / 399
13.2.7 Effect of Nonequilibrium on Pure Material Solidification / 402
13.3 Equilibrium Solidification of an Alloy / 402
13.3.1 Prerequisites for the Solidification of Alloys / 403
13.3.2 Equilibrium Solidification of a Hypothetical Binary Alloy (Case 1) / 403
13.4 Nonequilibrium Solidification of Alloys / 406
13.4.1 Boundary Conditions for Solidification of Alloys / 406
13.4.2 Equilibrium Maintained Throughout the System at all Times: Microscopic Equilibrium (Case 1) / 407
13.4.3 Complete Liquid Mixing/No Diffusion in the Solid (Case 2) / 408
13.4.3.1 Expression for the Composition of Solid at the Advancing Solid–Liquid Interface / 410
13.4.3.2 Calculation of the Average Composition of the Solid for Case 2 / 411
13.4.4 No Liquid Mixing/No Diffusion in the Solid (Case 3) / 413
13.4.4.1 Trace of Average Composition in the Solid for Case 3 / 420
13.4.4.2 Expression for the Initial Transient in the Composition of the Solid Formed / 420
13.4.4.3 Some Limitations of the Classic Models / 421
13.4.5 Other Effects of Rapid Solidification / 422
13.4.5.1 Nonequilibrium Solute Partitioning / 422
13.4.5.2 Nonequilibrium Phases / 422
13.5 Consequences of Nonequilibrium Solidification / 423
13.5.1 Interdendritic Microsegregation / 423
13.5.2 Solidus Suppression / 425
13.5.3 Substructure Formation / 426
13.5.3.1 Constitutional Supercooling / 426
13.5.3.2 Effect of Cooling Rate on Substructure / 430
13.5.3.3 Interface Stability / 432
13.5.3.4 Nucleation of New Grains Within the Fusion Zone / 438
13.5.3.5 Controlling Substructure / 438
13.5.4 Centerline Segregation / 443
13.6 Fusion Zone Hot Cracking / 443
13.6.1 Mechanism of Hot Cracking / 444

13.6.2 Remediation of Hot Cracking / 447
13.6.2.1 Control of Weld Metal Composition / 447
13.6.2.2 Control of Solidification Structure / 448
13.6.2.3 Use of Favorable Welding Conditions / 448
13.7 Summary / 449
References and Suggested Reading / 450

14 EUTECTIC, PERITECTIC, AND POSTSOLIDIFICATION FUSION ZONE TRANSFORMATIONS 454

14.1 Eutectic Reactions or Solidification of Two-Phase Alloys / 455
14.1.1 Solidification at the Eutectic Composition / 455
14.1.2 Solidification of Two-Phase Alloys at Noneutectic Compositions / 460
14.1.3 Morphology of Eutectic Phases / 462
14.2 Peritectic Reactions / 462
14.2.1 Equilibrium Conditions (Case 1) / 463
14.2.1.1 Alloys Below the Solubility Limit of the Solid Phase in the Peritectic / 463
14.2.1.2 Alloys Between the Solubility Limit and the Peritectic Composition / 466
14.2.1.3 Alloys With the Peritectic Composition / 467
14.2.1.4 Alloys Beyond the Peritectic Composition, but Within the L + S Range / 468
14.2.1.5 Alloys Past the L + S Range of a Peritectic in the Liquid Field / 469
14.2.2 Nonequilibrium Conditions / 469
14.2.2.1 No Diffusion in the Solid/Complete Mixing in the Liquid (Case 2) / 470
14.2.2.2 No Diffusion in the Solid/No Mixing, Only Diffusion in the Liquid (Case 3) / 472
14.3 Transformations in Ferrite + Austenite or Duplex Stainless Steels / 472
14.4 Kinetics of Solid-State Phase Transformations: Nonequilibrium Versus Equilibrium / 480
14.5 Austenite Decomposition Transformations / 489
14.5.1 Equilibrium Decomposition to Ferrite + Pearlite (The Eutectiod Reaction) / 491

14.5.2 Nonequilibrium Decomposition to Other Ferrite Morphologies (Very Slow to Moderately Slow Cooling Rates) / 493
14.5.3 Nonequilibrium Transformation to Bainite (Faster Cooler Rates) / 494
14.5.4 Nonequilibrium Transformation to Martensite (Very Fast Cooling Rates) / 495
14.6 Sigma and Chi Phase Formation / 498
14.7 Grain Boundary Migration / 499
14.8 Summary / 499
References and Suggested Reading / 499

15 THE PARTIALLY MELTED ZONE **501**

15.1 Origin and Location of the Partially Melted Zone / 501
15.2 Constitutional Liquation / 505
15.3 Defects Arising in the PMZ / 508
15.3.1 Conventional Hot Cracking and Liquation Cracking in the PMZ / 508
15.3.2 Loss of Ductility in the PMZ / 509
15.3.3 Hydrogen-Induced Cracking in the PMZ / 510
15.4 Remediation of Defects in the PMZ / 511
15.5 Summary / 512
References and Suggested Reading / 513

16 THE WELD HEAT-AFFECTED ZONE **514**

16.1 Heat-Affected Zones in Welds / 514
16.2 The HAZ in Work-Hardened or Cold-Worked Metals and Alloys / 515
16.2.1 The Physical Metallurgy of Cold Work/Recovery/Recrystallization/Grain Growth / 515
16.2.2 Cold Worked Metals and Alloys in Engineering / 520
16.2.3 Avoiding or Recovering Property Losses in Work-Hardened Metals or Alloys / 523
16.2.4 Development of a Worked Zone in Pressure-Welded Materials / 525
16.3 The HAZ in a Solid-Solution-Strengthened Metal or of an Alloy / 526
16.3.1 The Physical Metallurgy of Solid-Solution Strengthening or Alloying / 526

16.3.2 Major Engineering Alloys Consisting of Single-Phase Solid Solutions / 529
16.3.3 Maintaining Properties in Single-Phase Solid-Solution-Strengthened Alloys / 529
16.4 The HAZ in Precipitation-Hardened or Age-Hardenable Alloys / 529
16.4.1 The Physical Metallurgy of Precipitation- or Age-Hardenable Alloys / 529
16.4.2 Important Precipitation-Hardenable Alloys in Engineering / 536
16.4.3 Avoiding or Recovering Property Losses in Age-Hardenable Alloys / 536
16.5 The HAZ in Transformation-Hardenable Alloys / 543
16.5.1 The Physical Metallurgy of Transformation-Hardenable Alloys / 543
16.5.2 Some Important Engineering Alloys Exhibiting Transformation Hardening / 545
16.5.3 Welding Behavior of Carbon and Alloy Steels / 545
16.5.3.1 Behavior of Carbon Steels / 545
16.5.3.2 Behavior of Alloy Steels / 547
16.6 The HAZ in Corrosion-Resistant Stainless Steels / 550
16.6.1 The Physical Metallurgy of Stainless Steels / 550
16.6.2 Major Stainless Steels Used in Engineering / 553
16.6.3 Sensitization of Austenitic Stainless Steels by Welding / 553
16.6.4 Welding of Ferritic and Martensitic Stainless Steels / 561
16.7 The HAZ in Dispersion-Strengthened or Reinforced Alloys / 564
16.8 HAZ Defects and Their Remediation / 566
16.8.1 Liquation Cracking / 567
16.8.2 Reheat or Strain-Age Cracking / 570
16.8.3 Quench Cracking and Hydrogen Cold Cracking / 571
16.8.4 Weld Decay, Knife-Line Attack, and Stress Corrosion Cracking / 571
16.8.5 Lamellar Tearing / 573
16.9 Summary / 574
References and Suggested Reading / 574

17 WELDABILITY AND WELD TESTING 577

17.1 Weldability Testing / 578
17.2 Direct Weldability or Actual Welding Tests / 578

17.2.1 Fusion and Partially Melted Zone Hot-Cracking Tests / 580
17.2.1.1 Finger Test / 582
17.2.1.2 Houldcroft and Battelle Hot-Crack Susceptibility Tests / 582
17.2.1.3 Lehigh Restraint Test / 583
17.2.1.4 Variable-Restraint (or Varestraint) Test / 583
17.2.1.5 Murex Hot-Cracking Test / 584
17.2.1.6 Root-Pass Crack Test / 584
17.2.1.7 Keyhole-Slotted-Plate Test / 585
17.2.1.8 Navy Circular-Fillet-Weldability (NCFW) Test / 586
17.2.1.9 Circular-Groove Cracking and Segmented-Groove Tests / 586
17.2.1.10 Circular-Patch Test / 588
17.2.1.11 Restrained-Patch Test / 588
17.1.1.12 Sigmajig Test / 588
17.2.2 Heat-Affected Zone General Cold-Cracking Weldability Tests / 589
17.2.3 Hydrogen Cracking Testing / 592
17.2.3.1 Implant Test / 595
17.2.3.2 RPI Augmented Strain Cracking Test / 596
17.2.3.3 Controlled-Thermal-Severity (CTS) Test / 596
17.2.3.4 Lehigh Slot Weldability Test / 598
17.2.3.5 Wedge Test / 598
17.2.3.6 Tekken Test / 598
17.2.3.7 Gapped-Bead-on-Plate or G-BOP Test / 598
17.2.4 Reheat or Strain-Age Cracking Test / 601
17.2.4.1 Compact Tension Test / 601
17.2.4.2 Vinckier Test / 601
17.2.4.3 Spiral Notch Test / 603
17.2.5 Lamellar Tearing Tests / 603
17.2.5.1 Lehigh Cantilever Lamellar Tearing Test / 603
17.2.5.2 Tensile Lamellar Tearing Test / 604
17.3 Indirect Weldability Tests or Tests of Simulated Welds / 606
17.4 Weld Pool Shape Tests / 606
17.5 Weld Testing / 607
17.5.1 Transverse- and Longitudinal-Weld Tensile Tests / 608
17.5.2 All-Weld-Metal Tensile Tests / 609

17.5.3 Bend Ductility Tests / 609
17.5.4 Impact Tests / 610
17.5.5 Other Mechanical Tests / 610
17.5.6 Corrosion Tests / 615
17.5.6.1 General Corrosion and Its Testing / 615
17.5.6.2 Crevice Corrosion and Its Testing / 617
17.5.6.3 Pitting Corrosion and Its Testing / 617
17.5.6.4 Intergranular Corrosion and Its Testing / 617
17.5.6.5 Stress Corrosion and Its Testing / 621
17.6 Summary / 621
References and Suggested Reading / 622

CLOSING THOUGHTS **625**

APPENDICES **627**

INDEX **639**

This Page Intentionally Left Blank

PREFACE

Perhaps no secondary process has been and continues to be more important to the survival, comfort, and advancement of humankind than welding. It has let us build our world. It enables the planting and harvesting of our crops through the manufacture of tillers, tractors, and combines. It enables processing of our food through the manufacture of crushers, cookers, and conveyors. It enables the mining of minerals and metals, the building blocks of all structures, through the manufacture of drills, excavators, and trams. It enables the transport of grown, mined, and manufactured goods across town, across states, across nations, and across oceans through the manufacture of trucks, trains, and ships. It enables transportation through the manufacture of cars, buses, and planes. It enables the maintenance of our security, and the general security of the world, through the manufacture of tanks, missiles, and submarines. It enables the generation and transmission of power, the communication of information, and on and on and on! Yet, learning about this essential but complex process has never been easy, and this has led to less-than-optimal understanding and implementation and advancement.

Despite the essential nature of the process, there has never been a comprehensive treatise on welding that could be used as a primer for students of welding as well as a refresher and lifelong reference for both neophytes and seasoned practitioners. There have been good, comprehensive basic and advanced treatments dealing with the specific processes of welding, but these unanimously fail to deal with the physics and chemistry no less the metallurgy of weld formation. Contrarily, there have been good, comprehensive treatments of the physics, chemistry, and metallurgy of weld formation, but these either fail to deal with the general and specific processes for making welds or gloss over the subject in a chapter or less.

The time has come for the critically important process of welding to be treated comprehensively, in one source, in precise, unambiguous language, in readable format, and in sufficient depth to satisfy the experienced engineer but sufficiently clear and concise so as not to overwhelm the new student of welding or the interested layperson.

The book is divided into four parts and seventeen chapters. Part One addresses the process and processes of welding. Chapter 1 introduces the reader to what welding is, how it evolved as a process, what it means to make a weld, ideally and in the real world, and the advantages and shortcomings of welding. Chapter 2 considers why welding processes should be classified, and presents alternative ways of accomplishing that classification. Based on whether the process requires melting and solidification to produce a weld, or whether a weld is made in the solid state without melting, Chapters 3 and 4 describe fusion and nonfusion welding processes, respectively, by principal source of energy. These two chapters are about as comprehensive in scope, yet of reasonable depth, as presented in any single reference of this sort.

Part Two addresses the physics of welding. Chapter 5 looks at the sources, characterization, roles, and favorable and unfavorable effects of energy for making welds. Chapter 6 describes how heat flows in a weld and in weldments and what the effects of that heat are. Chapter 7 discusses thermally induced distortion and residual stresses during welding. Chapter 8 explains the physics underlying each major category of welding by energy source in the only treatment of its kind. Chapters 9 and 10 deal with the physics of molten metal transfer from consumable electrodes to the weld pool and of molten metal movement within the weld pool, respectively.

Part Three addresses the chemistry of welding in two chapters. Chapter 11 describes molten metal and weld pool reactions with the environment, the means of providing protection from such adverse reactions, and the means of providing additional metallurgical refinement. Chapter 12 looks at the origins and consequences of chemical heterogeneity in the weld pool and final weld.

Part Four considers the all-important metallurgy of welding. Chapter 13 addresses the phenomena of melting and solidification in pure metals and alloys, under nonequilibrium as well as equilibrium conditions, looking at the development of structure, substructure, and defects, and does so to a level and with clarity unparalleled in welding texts. Chapter 14 presents an almost unique treatment of eutectic and peritectic reactions in two-phase alloys, as well as major postsolidification transformations that can occur in the fusion zone. Chapter 15 addresses the unheralded and poorly understood partially melted zone and looks at some particular problems that can arise there. Chapter 16 addresses the heat-affected zone, considering what can happen as a consequence of the heat of welding based on how the base material obtains its strength and other properties in the first place. Finally, Chapter 17 addresses the testing of a material's weldability and a weld's properties.

I have attempted to create a unique welding reference. It's not encyclopedic in scope, depth, or drudgery; but neither is it an overly simplistic pseudo-text

that fails to present and expound upon the principles underlying this critical group of production processes. It clearly explains theory, but never fails to mention where and how reality deviates from theory. It's what I looked for more than twelve years of teaching welding to engineering undergraduates and graduates, practicing engineers involved with welding directly or peripherally, and welders desirous of knowing more about their chosen trade. I hope it succeeds by being informative, interesting, and, perhaps, enlightening and entertaining. If so, I've created the book I wished I had 35 years ago.

To accompany this book, or simply to aid study of the principles of welding, *Work, Practice, and Thinking Problems* is available on floppy disk directly from the author at email address messlr@rpi.edu or at Rensselaer Polytechnic Institute, Materials Science and Engineering Department, Troy, NY 12180-3590.

A book like this cannot be written without help. The information that found its way into this book is the sum of the knowledge obtained from others by whom the author has been touched. Sometimes that touch was through another's writings, as is the case from unseen "friends" and colleagues like George Linnert, James Lancaster, Kenneth Easterling, Sindo Kou, and Henri Granjon. Other times that touch was quite personal, as was the case of mentors at RPI like Carl D. Lundin, John J. McCarthy, Ernest F. Nippes, and, most of all, Warren F. "Doc" Savage.

Making a book read well and look good is also a tedious task. In this case, the selfless assistance of some reviewers unknown to me and the professionalism of the editorial staff at John Wiley & Sons, Inc. is gratefully acknowledged. Artwork for the new figures was made possible by a talented former student, Suat Genc, to whom I am very grateful. Countless hours of research in libraries were shared with my student Leijun Li, a truly scholar and wonderful protegé, of whom I am extremely proud. The cover design was the brainchild of my daughter Victoria and the illustration was by her (and my) dear friend Avrau Kaufman.

To my wife, Joan, and daughters, Kerri and Vicki, I thank you for your endless patience with a compulsive personality, and for your understanding and love.

Writing a book like this can be a lonely process—hours and hours at the library and at the word-processor. But it really wasn't lonely for me. Just as I, and many others, sometimes feel Doc Savage's presence while I'm lecturing in a classroom, I frequently felt Doc's presence while writing this book. Sometimes that presence was felt when I tried to take a short cut or gloss over a point. Sometimes it was when I was tackling a particularly tough topic, like peritectic reactions. But, it was always a great support to feel the presence of a truly gifted mentor. I'm grateful for the chance to have known Doc, and for his eternal presence. Thanks, Doc!

ROBERT W. MESSLER, JR.

January 5, 1999

This Page Intentionally Left Blank

PART 1

THE PROCESS AND PROCESSES OF WELDING

This Page Intentionally Left Blank

CHAPTER 1

INTRODUCTION TO THE PROCESS OF WELDING

1.1. WHAT IS WELDING?

In its broadest context, welding is *a process in which materials of the same fundamental type or class are brought together and caused to join (and become one) through the formation of primary (and, occasionally, secondary) chemical bonds under the combined action of heat and pressure* (Messler, 1993). Common dictionaries tend to narrow the definition somewhat, as typified by the definition given in *The American Heritage Dictionary*[1]: "To join (metals) by applying heat, sometimes with pressure and sometimes with an intermediate or filler metal having a high melting point." The definition found in ISO standard R 857 (1958) states, "Welding is an operation in which continuity is obtained between parts for assembly, by various means," while the motto on the coat of arms of The Welding Institute (commonly known as TWI) simply states "e duobus unum," which means "from two they become one." All slightly different, but all similar in essential ways. Let's pause for a moment to consider those essential ways.

First and foremost is the central point that *multiple entities are made one by establishing continuity*. Here, continuity implies the absence of any physical disruption on an atomic scale, that is, no gaps, unlike the situation with mechanical attachment or mechanical fastening where a physical gap, no

[1]Second College Edition by Houghton Mifflin, Boston, MA, 1985.

matter how tight the joint, always remains.[2] Continuity as used here does not imply homogeneity of chemical composition through or across the joint, but it does imply the continuation of like atomic structure. A weld can be made homogeneous, as when two parts made from the same austenitic stainless steel are joined with a filler of the same alloy, or they can be made to be intentionally dissimilar (heterogeneous), as when two parts made from gray cast iron are joined with a bronze filler metal. Similarly, two polymers or plastics[3] can be joined and made to be homogeneous if they are of identical (or essentially identical) type or composition, as when two pieces of thermoplastic polyvinyl chloride are thermally bonded or welded, or heterogeneous when two unlike but compatible thermoplastics are joined by thermal bonding. Alternatively, a compatible thermoplastic filler could be used as what is called an adhesive, and, when this is the situation, the result can also correctly be called a weld.

The key in each case is that even when the material across the joint is not identical in composition (i.e., homogeneous), it is essentially the same in atomic structure, thereby allowing the formation of chemical bonds: primary metallic bonds between similar or dissimilar metals, primary ionic or covalent or mixed ionic–covalent bonds between similar or dissimilar ceramics, and secondary hydrogen, van der Waals, or other dipolar bonds between similar or dissimilar polymers. The problem comes about when the materials to be joined are fundamentally different in structure at the atomic or (for polymers) molecular level. When this is the case, welding by the strictest definition (e.g., that of Messler, 1993, above) cannot be made to occur. An example is the joining of metals to ceramics or even thermoplastic to thermosetting polymers. In both cases, the fundamental nature of the bonding that must take place differs from that in at least one of the joint elements. For metals to ceramics, the metallic joint element is held together by metallic bonds, while the ceramic joint element is held together by either ionic or covalent or mixed ionic–covalent bonds. Clearly, there must be a disruption of bonding type across the interface of these fundamentally different materials. And for the case of a thermoplastic being joined to a thermoset, a degree of ionic bonding can occur in the thermoset to cause cross-linking, but not so in the thermoplastic. Thus, a dissimilar adhesive alloy is required to bridge this fundamental incompatibility (Messler, 1993). In short, the key is achieving continuity of structure by forming chemical bonds, and this limits possibilities to like types or classes even if not identical compositions of materials. More is said about how to achieve this essential continuity in Section 1.3.

[2]Not incidentally, the persistence of a physical gap, no matter how tight it might be made, is what gives mechanical attachment or fastening its essentially unique and often desirable capability for allowing intentional disassembly without damaging the elements comprising the joint, or, under the right circumstances, for relative motion to take place between parts held in proximity and alignment, and, under the wrong circumstances, for fluids to leak through the joint.

[3]The preferred term in materials science for plastics is polymers, and so that term will be used throughout this work.

The second common and essential point among definitions is that *welding applies not just to metals.* It can and often does apply equally well to certain polymers (e.g., thermoplastics), crystalline oxide or nonoxide ceramics, intermetallic compounds, and glasses. The process being performed may not always be called welding—it may be called thermal bonding for thermoplastics, or fusion bonding or fusing for glasses—but it is welding! With the emergence and increasing application of so many different materials of different fundamental types, welding will remain a viable process for joining.

The third essential point is that *welding is the result of the combined action of heat and pressure.* There is a widely held perception that welding is performed by heating and melting materials, and thats it! In fact, as we will learn in Section 1.3, welds (as defined above) can be produced over a wide spectrum of combinations of heat and pressure: from essentially no pressure when heat is sufficient to cause melting, to where pressure is great enough to cause gross plastic deformation when no heat is added and welds are made cold. Welding is a highly versatile and flexible joining process, enabling the joining of many different materials into many different structures to obtain many different properties for many different purposes.

The fourth essential point is that *an intermediate or filler material*[4] *of the same type, even if not same composition, as the base material(s) may or may not be required.* There are a host of reasons why such a filler might be required or desired, and these are presented in Chapter 2. Once again, the option of employing an intermediate or filler or not adds to process flexibility and versatility.

The fifth and final essential point is that *welding is used to join parts, although it does so by joining materials.* It is this goal that often places additional constraints and demands on the welding process as it is selected and applied. Creating a weld between two materials requires producing chemical bonds by using some combination of heat and pressure. How much heat and how much pressure is partially dictated by the inherent nature of the material(s) being joined. But, how much heat and how much pressure also depends on the nature of the actual parts or physical entities being joined. Among other things, part shape, critical part dimensions, and part and assembly (i.e., joint) properties must also be dealt with by preventing intolerable levels of distortion, residual stresses, or disruption of chemical composition and microstructure. The key point here is that welding is a secondary manufacturing process used to produce an assembly or structure from parts or structural elements.

So, now that we understand what is meant by welding, lets take a brief look at how it evolved as a process over time.

[4]In fact, there is a subtle but important difference between the use of an intermediate and a filler. A filler is used to provide a supply of atoms to help fill gaps on a microscopic or macroscopic scale to allow a weld to be created (see Section 1.4), while an intermediate or intermediary is (or ought to be) used to bridge incompatibilities in chemical, physical, or mechanical properties (Messler, 1993). Intermediate material is never melted, while filler material usua'ly, but not necessarily, is.

1.2. THE EVOLUTION OF WELDING AS A PROCESS

Next to mechanical attachment and fastening, which began when humans or, perhaps, humanoids wedged and later lashed stones into sticks to produce clubs and spears for hunting, welding is unquestionably the oldest method for joining materials. Welding is, in fact, an ancient art. The bonding of metals was a much more acute and challenging problem for our ancient ancestors than it is today. Primitive equipment for extracting and refining metals won from ores was on a very small scale, largely as the result of severely limited sources for heating. The forming of small pieces of metal into useful parts was the earliest example of what has been called *adaptive metallurgy*. Within a few centuries, the acute problem arose of joining these small parts into larger assemblies. While mechanical fastening in one form or another (e.g., coforging or riveting) was often the answer, crude welds were also used. Examples of bracelets from prehistoric times have been discovered that were made by hammering nuggets of gold or silver into rods, forming the rods into circles or segments of a circle, and then forging the ends together to form a continuous ring. This earliest welding process is called forge welding. The challenging problem was that to make bigger and better welds required larger and more intense sources of heat.

Founding (or foundry) processes in early metallurgy (or alchemy) came along much later. It was late in the Bronze Age before the casting of metals like gold, silver, lead, tin, and copper, and thus pewter and bronzes, into final shapes became popular. However, foundry equipment grew in scale much more quickly than did forging equipment. Not surprisingly, castings were used in preference to weldments for the production of large or complex-shaped metal parts, even though wrought metal properties of strength and toughness were recognized to be superior. Unfortunately, wrought welds were more expensive and of variable quality. Welding suffered still more with the emergence of the Machine Age, where dimensional tolerances became important for interchangeability and mass manufacturing.

The key discoveries that led to the emergence of welding as a viable manufacturing process were made in the latter half of the nineteenth century. Miossan of France, in 1881, originated the use of the carbon arc for melting metals. In Russia, Bernandos applied this arc to the welding of metals in 1887, and shortly thereafter, Slavianoff experimented with consumable metal electrodes for arc welding. The first patents for metal-arc welding in the United States were granted in 1889 to Coffin.

Paralleling the emergence and evolution of welding with an electric arc was the evolution of welding with mixtures of air and organic fuels. Although known and practiced even in prehistoric times primarily using fanned charcoal fires, it wasn't until the invention of the oxyacetylene blowpipe by Le Chatelier in 1895 that modern torch welding systems emerged. Oxyacetylene welds in steel were vastly superior to welds made with carbon or bare-wire electric arcs, so much so that arc processes were nearly superseded (at least for stressed structural welds) until 1914. In that year,

the Swedish engineer Kjellberg introduced shielding for both carbon and metal arcs.

The history of resistance welding followed a different and much less complicated path. In 1865, Joule, the famous British physicist, made a weld between two resistance-heated wires by forging them together while hot. The American engineer and inventor Elihu Thomson was the first to successfully use contact resistance as a heat source for welding in 1877. The process of resistance spot welding sprang virtually full-blown from Thomson's work, and essentially all developments in resistance welding since have been basically engineering refinements.

The beginning of what might be called modern industrial welding hinged on two key factors. First, advances in energy sources (e.g., capacitor-discharge, constricted arcs, plasma arcs, and laser or electron beams) produced ever more intense heat to enable welds to be made in higher-melting metals and alloys, larger structures, thicker sections, and with greater speed. Second, and not at all incidentally, advances occurred in response to a critical change in the psychology of product designers that took place over time but occurred fastest in the 1930s. That change was a shift from Do we dare use welding in fabrication? to How do we use welding in fabrication? By no means is this important evolution in design psychology over. In fact, for many industries, aerospace being a prime example, the battle is still being fought.

It is not the intent of this book to present the entire long and fascinating history of welding. That is left to the interested reader to find elsewhere, although the task of finding good historical information is not simple. There are few comprehensive histories, but many brief histories of specific processes in many sources. One of the better sources, albeit a difficult one to search, is patents. To help a little, Figure 1.1 shows a reasonable time line of some of the major developments in welding as a joining process. This time line was derived from *Jefferson's New Welding Encyclopedia*, 18th edition (American Welding Society, 1997), which is itself a superb source of history in many of the topics covered.

1.3. THE NATURE OF AN IDEAL WELD: ACHIEVING CONTINUITY

Understanding exactly what happens when two pieces of metal (or other like-species of material) are brought into contact is crucial to understanding how welds are formed and how welding might be performed. It all goes back to how two atoms (or ions, or molecules) behave when they are brought together.

When two or more atoms are separated by what for all intents and purposes is an infinite distance, they do not sense one another's presence, that is, there is no force of attraction or repulsion between them. As they are brought together from this infinite separation, however, a force of electrostatic or Coulombic attraction arises between the positively charged nuclei and negatively charged electron shells or clouds. (For neutral atoms, this force is

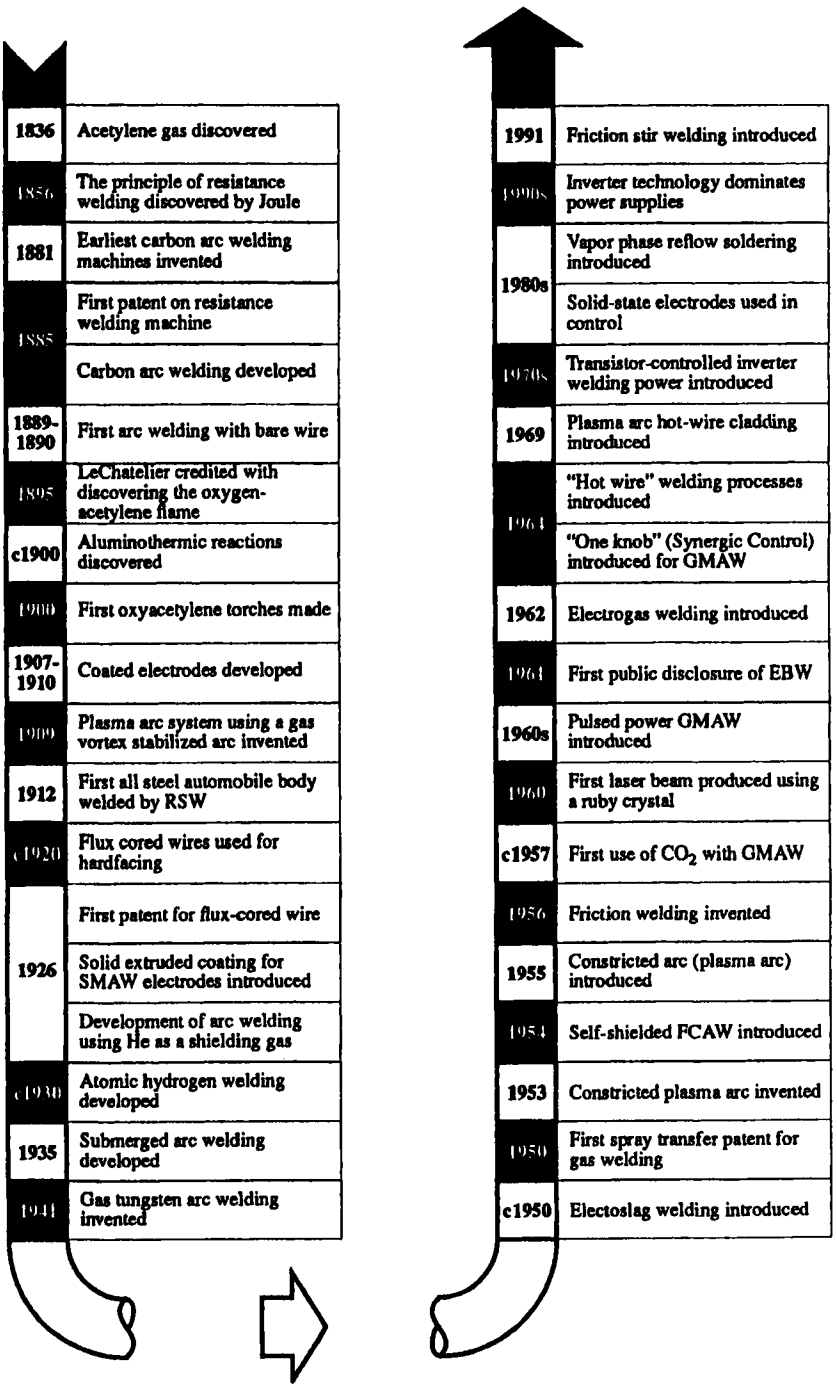


Figure 1.1 Time line of highlights in the development of welding as a joining process (Based on information from Appendix 1, *Jefferson's New Welding Encyclopedia*, 18th ed., pp. 615–617, American Welding Society, Miami, FL, 1997).

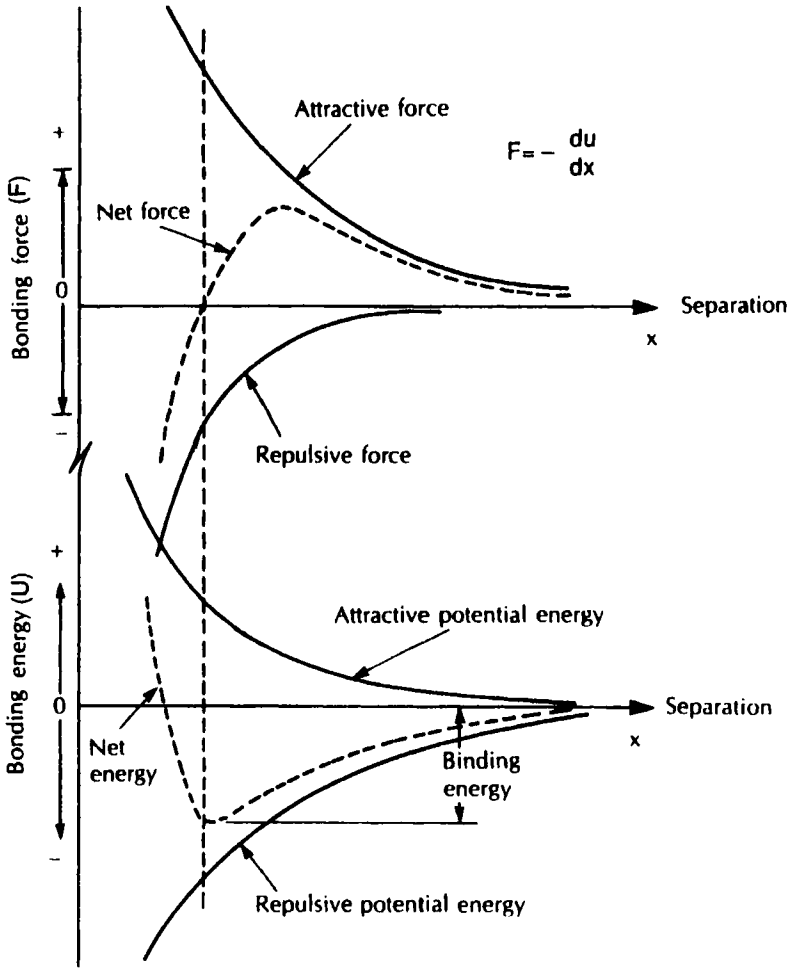


Figure 1.2 The forces and potential energies involved in bond formation leading to welding. (From *Joining of Advanced Materials* by R. W. Messler, Jr., published in 1993 by and used with permission of Butterworth-Heinemann, Woburn, MA).

actually the result of a slight shift in positive and negative charge centers to induce a dipole. For oppositely charged ions, that is, negative anions and positive cations, no such shift is necessary. For molecules, permanent dipoles may exist for some polar types, while induced dipoles are created for other types.) This force of attraction increases with decreasing separation. The potential energy of the separated atoms also decreases as the atoms come together. This is shown in plots of force and potential energy in Figure 1.2.

As the distance of separation decreases to the order of a few atom diameters, the outermost electron shells of the approaching atoms begin to feel one another's presence, and a repulsion force between the negatively charged

electron shells increases more rapidly than the attractive force.[5] The attractive and repulsive forces combine to create a net force, which at some separation distance becomes zero as the two forces exactly offset one another. This separation is known as the *equilibrium interatomic distance* or *equilibrium interatomic spacing*. At this equilibrium spacing, the net potential energy[6] is a minimum, the aggregate of atoms is stable, and the atoms are said to be bonded. When all of the atoms in an aggregate are at their equilibrium spacing, each and every one achieves a stable outer electron configuration by sharing or transferring electrons.[7] What has just been described for neutral atoms can also occur for molecules having permanent or induced dipoles or for oppositely charged ions, leading to the formation of aggregates of molecules in polymers or ions in ionically bonded compounds called ceramics, respectively.

The tendency for atoms to bond is the fundamental basis for welding. All that is required to produce a weld is to bring atoms together to their equilibrium spacing in large numbers to produce aggregates, and to bring separate aggregates together to do the same for atoms comprising their surfaces at mating interfaces. For metals, intermetallics, and most ceramics, this aggregate is crystalline. That is, all of the atoms comprising the aggregate take up regular positions on a three-dimensional arrangement of points in space called a crystal lattice. The result of bonding is the creation of continuity (referred to earlier) between aggregates or crystals, and the formation of an ideal weld. What makes the weld ideal is that there is no remnant of any gap, and the strength of the joint would be the same as the cohesive strength of the weakest material comprising the joint. However, there is a challenge, which is how to obtain continuity.

Figure 1.3 shows a simple schematic of the nature of continuity in a crystalline metal.

1.4. IMPEDIMENTS TO MAKING IDEAL WELDS IN THE REAL WORLD

Making an ideal weld doesn't sound too difficult. All that is required is to bring large numbers of atoms comprising two separate aggregates together to the equilibrium spacing for the atom species at the mating surfaces of these aggregates. Once this is done, bonds will form and an ideal weld will result. Unfortunately, in the real world, there are several impediments to making ideal welds.

[5]The attractive force increases inversely to the appropriate n power of the atomic separation, while the repulsive force increases as the approximate m power of the atomic separation, where $n < m$, m is usually 12, and n is usually 2–6, depending on ultimate bond type.

[6]The potential energy and the forces of attraction and repulsion are related by the relationship $F = -dU/dx$, where F is the force of attraction or repulsion, U is the potential energy of attraction or repulsion, and x is the distance of separation. By convention, attraction is negative and repulsion is positive, based on how work must be done to change the separation.

[7]Electrons are shared in covalent and metallic (also known as extended covalent) bonds, while there is a transfer of electrons from one atom to the other in a bonded pair in ionic bonds.

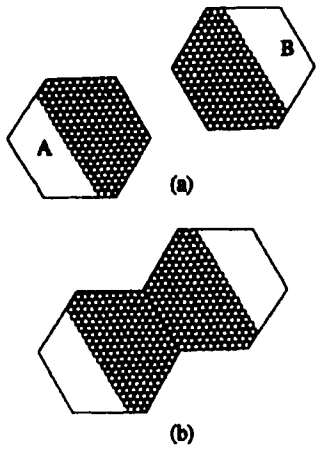


Figure 1.3 The nature of continuity in a metal, with constituent atoms of parts A and B, (a) initially belonging to two separate aggregates (e.g., crystals, grains, or parts), and (b) forming a single assembly or aggregate after welding.

If two perfectly flat surfaces of aggregates of atoms are brought together to the equilibrium spacing for the atomic species involved, bond pairs form and the two pieces are welded together perfectly. In this case, there is no remnant of a physical interface and there is no disruption of the structure of either material involved in the joint.[8] This ideal situation is shown in Figure 1.4a, b. The resulting weld has the strength expected from the atom-to-atom binding energy determined from the depth of the well in the net potential energy curve in Figure 1.2, so the joint efficiency is 100%.[9]

In reality, two materials never have perfectly smooth, planar surfaces, so perfect matching up of all atoms across an interface at equilibrium spacing never occurs. Thus, a perfect joint or ideal weld can never be formed simply by bringing the two material aggregates together. Real materials have surfaces that are highly irregular on a microscopic, even if not macroscopic, scale. Peaks and valleys (known generically as asperities) of several to hundreds or even thousands of atoms high or deep lead to very few points of intimate contact at which the equilibrium spacing can be achieved. This is shown in Figure 1.4c. Typically, only one out of approximately every billion (10^9) atoms on a well-machined (e.g., 4 rms finish) surface come into contact to be able to create a bond, so the strength of the joint is only about one-billionth (10^{-9}) of the theoretical cohesive strength that can be achieved. This situation is made even worse by the presence of oxide or other tarnish layers and associated adsorbed moisture layers usually found on real materials. As shown in Figure 1.4d–g,

[8]This case applies to a crystalline or a noncrystalline (i.e., amorphous) material, with either the crystalline or the amorphous structure being preserved across the interface.

[9]"Joint efficiency" is defined as the ratio of the stress that can be sustained in the joint itself to the stress that can be sustained in the base material elements comprising the joint (Messler 1993).

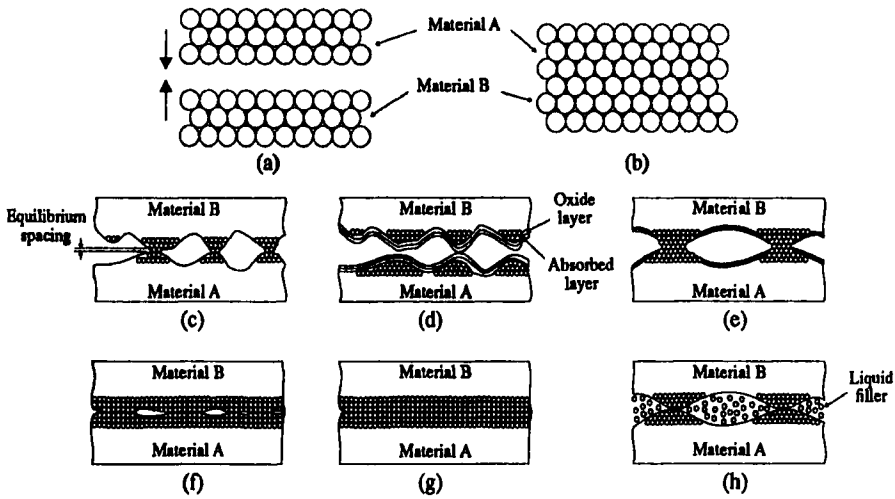


Figure 1.4 Two perfectly smooth and clean versus two real materials being brought together to attempt to form a weld. An ideal surface (a) to produce an ideal or perfect weld (b). Various real surfaces (c and d) being progressively forced together by pressure (e and f) to form a near-perfect weld (g). Melting to provide a supply of atoms (h) to form a near-perfect weld (g). (Modified but from *Joining of Advanced Materials* by R. W. Messler, Jr., published in 1993 by and used with permission of Butterworth-Heinemann, Woburn, MA.)

bonding, and thus welding, can be achieved only by removing or disrupting these layers and bringing the clean base material atoms to the equilibrium spacing for the materials involved. Obviously, any other form of surface contamination, such as paint or grease or oil, only further exacerbates this situation.

1.5. WHAT IT TAKES TO MAKE A REAL WELD

To make a real weld, that is, to obtain continuity, requires overcoming the impediments of surface roughness and few points of intimate contact and intervening contaminant layers. There are two ways of improving the situation: (1) cleaning the surface of real materials, and (2) bringing most, if not all, of the atoms of those material surfaces into intimate contact over large areas. There are, in turn, two ways of cleaning the surface: (1) chemically, using solvents to dissolve away contaminants or reducing agents to convert oxide or tarnish compounds to the base metals, and (2) mechanically, using abrasion or other means to physically disrupt the integrity of oxides or tarnish layers. Obviously, once the surfaces to be joined by welding are cleaned, they must be

kept clean until the weld is actually produced. This requires shielding. So important is cleanliness to the production of sound welds that every viable process for making welds must somehow provide and/or maintain cleanliness in the joint area.

There are also, it turns out, two ways of bringing atoms together in large numbers to overcome asperities. The first is to apply heat; the second is to apply pressure. Heating helps promote weld formation in several ways. In the solid state, heating helps by (1) driving off volatile adsorbed layers of gases or moisture (usually hydrogen-bonded waters of hydration) or organic contaminants; (2) either breaking down the brittle oxide or tarnish layers through differential thermal expansion or, occasionally, by thermal decomposition (e.g., copper oxide and titanium oxide), or, at least, disrupting the continuity of these layers; and (3) lowering the yield strength of the base materials and allowing plastic deformation under pressure to bring more atoms into intimate contact across the interface. This latter process is shown in Figure 1.4d–g. Alternatively, heating could help by causing melting of the substrate materials to take place, thereby allowing atoms to rearrange by fluid flow and come together to equilibrium spacing, or by melting a filler material to provide an extra supply of atoms of the same or different but compatible types as the base material. Melting is shown in Figure 1.4h.

As opposed to heat, pressure helps welding to take place by (1) disrupting the adsorbed layers of gases or moisture by macro- or microscopic deformation, (2) fracturing brittle oxide or tarnish layers to expose clean base material atoms, and (3) plastically deforming asperities to increase the number of atoms, and thus the area, in intimate contact (see Figure 1.4e). Figure 1.4g shows a perfect or near-perfect weld achieved by either route.

The relative amounts of heat and pressure necessary to create welds vary from one extreme to the other. Very high heat and little or no pressure can produce welds by relying on the high rate of diffusion in the solid state at elevated temperatures or in the liquid state produced by melting or fusion.[10] Little or no heat with very high pressures can produce welds by forcing atoms together by plastic deformation on either a gross or macroscopic scale (as in forge welding) or on a microscopic scale (as in friction welding), and/or by relying on atom transport by solid-phase diffusion to cause intermixing and bonding. Most real welding processes (as will be seen in Section 2.4.1 and Chapter 3) involve a fair amount of heat and only enough pressure to hold the joint elements together during welding, but there are processes that predominantly employ pressure (as will be seen in Section 2.4.2 and Chapter 4).

In Chapter 2, welding processes are classified based on their characteristics. As part of the discussion there, the actual mechanisms for obtaining material continuity are presented.

[10]As used throughout this book, fusion is synonymous with melting. In some other books, fusion may refer more broadly to having achieved the atomic continuity discussed earlier.

1.6. ADVANTAGES AND DISADVANTAGES OF WELDING

Like all joining processes (in fact, like all processes!), welding offers several advantages but has some disadvantages as well. The most significant advantage of welding is undoubtedly that it provides exceptional structural integrity, producing joints with very high efficiencies. The strength of joints that are welded continuously (i.e., full length, without intentional skipped areas) can easily approach or exceed the strength of the base material(s). The latter situation is made possible by selecting a joint design that provides greater cross-sectional area than the adjoining joint elements and/or filler that is of higher strength than the base material(s). Another advantage of welding is the wide range of processes and approaches that can be selected and the correspondingly wide variety of materials that can thus be welded. Almost all metals and alloys, many (thermoplastic) polymers, most if not all glasses, and some ceramics can be welded, with or without auxiliary filler.

Still other advantages of welding are that (1) there are processes that can be performed manually, semiautomatically, or completely automatically; (2) some processes can be made portable for implementation in the field for erection of large structures on site or for maintenance and repair of such structures and equipment; (3) continuous welds provide fluid tightness (so welding is the process of choice for fabricating pressure vessels); (4) welding (better than most other joining processes) can be performed remotely in hazardous environments (e.g., underwater, in areas of radiation, in outer space) using robots; and (5) for most applications, costs can be reasonable. The exceptions to the last statement are where welds are highly critical, with stringent quality requirements or involving specialized applications (e.g., very thick section welding).

The single greatest disadvantage of welding is that it precludes disassembly. While often chosen just because it produces permanent joints, consideration of ultimate disposal of a product (or structure) at the end of its useful life is causing modern designers to rethink how they will accomplish joining. A prime example is the need for the regulatory authorities in former West Germany to dismantle the nuclear reactors in former East Germany that have designs similar to the reactor that failed in Chernobyl in the former USSR.

A second major disadvantage of many welding processes is that the requirement for heat in producing many welds can disrupt the base material microstructure and degrade properties. Unbalanced heat input can also lead to distortion or the introduction of residual stresses that can be problematic from several standpoints. A third serious consideration, but not necessarily a disadvantage, is that welding requires considerable operator skill, or, in lieu of skilled operators, sophisticated automated welding systems. Both of these, along with the aforementioned specialized applications, can lead to high cost.

Table 1.1 summarizes the major advantages and disadvantages or limitations of welding as a means of joining materials or parts into parts or assemblies or structures.

TABLE 1.1 Advantages and Disadvantages of Welding as a Joining Process

Advantages	Disdvantages
1. Joints of exceptional structural integrity and efficiency, will not accidently loosen or disassemble	1. Impossible to disassemble joints without destroying detail parts
2. Wide variety of process embodiments	2. Heat of welding degrades base properties
3. Applicable to many materials within a class	3. Unbalanced heat input leads to distortion or residual stresses
4. Manual or automated operation	4. Requires considerable operator skill
5. Can be portable for indoor or outdoor use	5. Can be expensive (e.g., thick sections)
6. Leak-tight joints with continuous welds	6. Capital equipment can be expensive (e.g., electron-beam guns and vacuum chambers)
7. Cost is usually reasonable	

Source: After R. W. Messler's *Joining of Advanced Materials*, Table 6.1, published in 1993 by Butterworth-Heinemann, Stoneham, MA, with permission.

1.7. SUMMARY

Producing welds is fundamentally a simple process: Just cause large numbers of atoms of the base materials comprising joint elements to come together to equilibrium spacing. The result will be one piece from many, with continuity of structure and properties at both a microscopic and macroscopic level. In reality, the situation is complicated by the presence of asperities on the surfaces of real parts that limit the points of intimate contact, as well as by the presence of intervening layers of contaminants in the form of oxide or tarnish layers, adsorbed gases or moisture, or paint, grease, oil, or dirt. The two principal means to overcome these impediments are to employ heat and pressure in some combination, from one extreme to the other. When done well, welding offers several advantages over other methods of joining, but, as for all things in life, not without some limitations and sacrifices.

REFERENCES AND SUGGESTED READINGS

Messler, R. W., Jr., 1993, *Joining of Advanced Materials*, Butterworth-Heinemann, Woburn, MA.

Suggested readings on the history of welding:

Cary, H. B., 1998, *Modern Welding Technology*, 4th ed., Prentice Hall, Engelwood Cliffs, NJ.

O'Brien, R. L. (editor), 1997, *Jefferson's New Welding Encyclopedia*, 18th ed., American Welding Society, Miami, FL.

For a more complete discussion of the bonding of atoms to form aggregates:

Callister, W. D., 1997, *Materials Science and Engineering*, 4th ed., Wiley, New York.

CHAPTER 2

CLASSIFYING WELDING PROCESSES

2.1. WHY CLASSIFY PROCESSES?

When one recalls that welding is *a process in which materials of the same fundamental type or class are joined together through the formation of primary (or, occasionally, secondary) bonds under the combined action of heat and pressure*, it should come as no surprise that an extremely wide variety of specific process embodiments (called processes) exist. As is the case for any large group of somehow related items or entities, there is a need or, at least, a desirability for classifying them. Proper classification helps clarify fundamental differences in these processes, showing complementarity as well as diversity. Taken together, shared characteristics and differences can aid in selection of suitable or necessary alternatives. In the case of processes or materials, proper classification also helps identify technology gaps, analogous to "missing links" in animal classifications. Once such gaps have been identified, a new process (or material) can be invented or developed to fill that gap.

For complex entities, there can be many bases for classification or for creating a taxonomy. This is certainly the case for welding processes. To make the point about "many bases for classification" clear, let's look at a familiar example, namely, the classification of animals. To keep the example simple, let's restrict ourselves to only vertebrate animals, i.e., those having a spine.

On first looking at all of the vertebrate animals, it is easy to be overwhelmed by the tremendous diversity; snakes to mice to dogs to cows to giraffes to elephants to whales to porpoises to minnows to sparrows to eagles to ostriches to humans. What is it that differentiates, yet relates, all of these diverse animals? It is certainly not obvious. Or is it? The easy thing to do is look at

the obvious. But what is that? Size? (Which would group mice with minnows and sparrows, and giraffes with elephants and whales.) The presence or absence of fur or feathers or scales? (Which would group mice with dogs and cows and giraffes, sparrows with eagles and ostriches, and snakes with minnows.) Number of legs? (Which would group snakes with whales and porpoises and minnows, sparrows with eagles and ostriches and humans, and mice with dogs, cows, giraffes and elephants.) But, such groupings are not satisfactory because they fail to capture *essential* characteristics or traits. The ultimate result is groupings as mammals, reptiles, fish, and birds. And, within mammals, at some lower level, as lions, tigers, and bears.... The challenge in classifying welding processes is to decide on a proper basis — What it is that fundamentally relates or differentiates one and another?

Before we look at alternative bases for classifying welding processes, let's review how material continuity is obtained to produce a weld, and what the roles of temperature (or heat) and pressure are.

2.2. MECHANISMS FOR OBTAINING MATERIAL CONTINUITY

What is fundamentally desired and required to produce a weld between two pieces of material is to obtain material continuity. Let's look at the fundamental mechanisms by which this can be accomplished. Our discussion will focus on obtaining continuity between crystalline (versus amorphous or semicrystalline) materials in particular, and, metals (as opposed to ceramics). The discussion, however, pertains generally to all materials, but with some subtleties for noncrystalline types such as polymers and glasses.

There are three distinctive mechanisms for obtaining metallic continuity, as articulated well by Granjon (1991) in his fine book: (1) solid-phase plastic deformation, without or with recrystallization, (2) diffusion, and (3) melting and solidification. These are shown schematically in Figures 2.1.

Atoms comprising two pieces of crystalline metal, whether pure or alloyed, can be brought together sufficiently close to ensure that bonds are established at their equilibrium spacing as the result of mutual attraction, while simultaneously excluding extraneous atoms from contaminants (oxide, tarnish, adsorbed gases or moisture, etc.), by employing plastic deformation in the solid phase. The bringing together, called "rapprochement," is permanent because of the formation of these bonds. This plastic deformation, while made to occur entirely in the solid phase, can be caused to occur with or without heat, that is, in the hot or cold state. When caused to occur in the cold state, the metallic crystal lattices of each piece involved in the joining process are deformed or strained to achieve continuity, and left in the strained state (see Figure 2.1a). As a result, strain or work hardening occurs, with attendant changes in properties at the newly created interface. When caused to occur in the hot state (above approximately 0.4–0.5 of the absolute melting temperature of the metal or alloy), metallic continuity is further enhanced by the process of dynamic

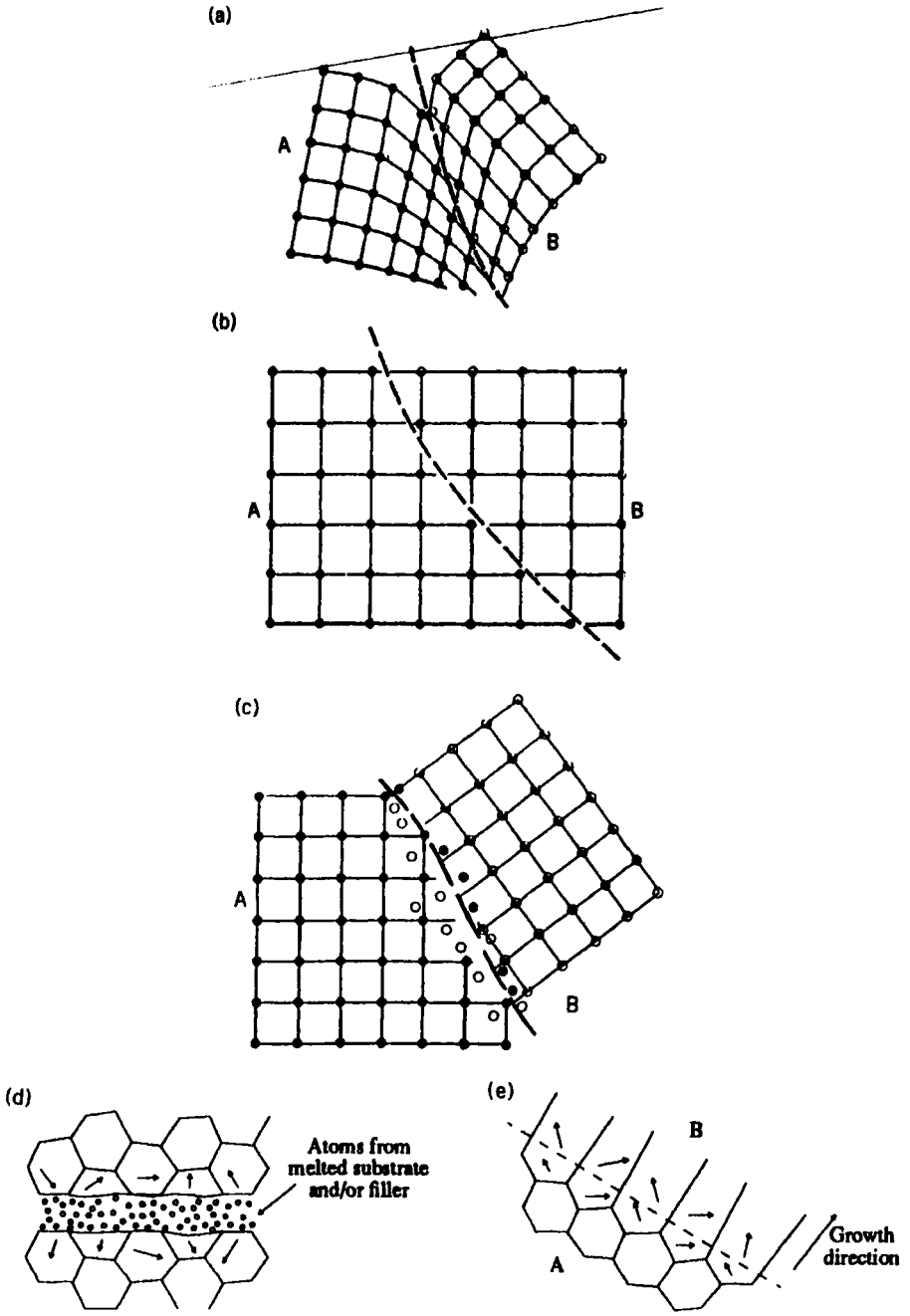


Figure 2.1 Achieving metallic continuity by bringing atoms together using (a) cold deformation and lattice strain or (b) hot deformation and dynamic recrystallization; (c) solid-phase diffusion across the original interface (shown by a dotted line); and (d) liquid provided by melting the parent materials (or substrates), without or with additional filler, and (e) establishing a bond upon epitaxial solidification of this liquid.

recrystallization.[1] Recrystallization involves atomic rearrangement under the driving force of the strain energy, and establishes a common orientation of atoms across the original interface (see Figure 2.1b). Recrystallization also removes the effects of cold work on microstructure (e.g., increased dislocation density and lattice distortion), and restores base metal properties. Not surprisingly, cold deformation leads to what are called *cold welding processes*, while hot deformation leads to a host of *hot deformation welding processes.*

The degree of plastic deformation, whether caused to occur cold or hot, can also vary from gross, macroscopic movement of metal to microscopic movement. Not surprisingly, greater degrees of plastic deformation tend to be more disruptive to intervening contaminating layers of oxide and tarnish, thereby facilitating bonding and weld formation.

For all of the preceding discussion, deformation results in the formation of a common grain texture in the joined pieces. Continuity actually is established grain to grain across the original interface, with all recrystallization events that occur emanating from individual nuclei which are the product of both joint elements. It is this growth of grains across the original interface that produces the actual weld and eliminates the original physical interface.

The second mechanism for obtaining metallic continuity is diffusion, which is *the transport of mass from one place or piece to another across an interface through atom movement.* This is shown schematically in Figure 2.1c. Diffusion can take place entirely in the solid phase or in the presence of a liquid. When it takes place entirely in the solid phase on both sides of a joint interface, atoms move in both directions across the interface under the influence of temperature (heat) *and* pressure. Welding processes relying on solid-phase diffusion are said to be occurring by diffusion and are called *diffusion welding processes*, but they really also rely on simultaneous recrystallization. Hence the need for simultaneous heat and pressure.

If material comprising one of the elements of a joint becomes completely or partially liquid, even for only a moment (i.e., if it is transient), while material in the other element of the joint remains solid (because it is less easily melted), diffusion allows the atoms of the liquid to pass through this interface into the crystalline lattice of the solid, creating a very thin layer of alloy along the interface. In the other direction, atoms from the solid joint element can and may pass into the liquid, but they become highly diluted in the liquid mass, causing only a minute change in its chemical composition. This latter situation (involving liquid in diffusion) is what prevails in both *brazing* and *soldering*, which are subcategories of welding, and *braze welding*, which is a variant of welding and brazing (Messler, 1993). (Incidentally, diffusion is involved in most

[1]Dynamic recrystallization is recrystallization that takes places simultaneously with plastic deformation, as the result of an immediate driving force (from increased energy from stored strain) and sufficient atomic mobility (from temperature). If the temperature (and atomic mobility) is not sufficiently high, recrystallization cannot occur until the temperature is raised during subsequent heat treatment (recrystallization annealing).

welding, especially when melting and solidification are involved, but also when deformation is caused to occur hot. The effects are most pronounced, however, when there is a difference in the chemical composition of the two joint elements, thus providing a chemical driving force as found in Fick's first law (flux $J = -D(dc/dx)$, where D is the diffusion coefficient and dc/dx is the prevailing composition gradient).

The third mechanism for obtaining metallic continuity involves gross mass and atom transport via melting and flow and microscopic transport via diffusion during solidification of the base metals. Here, metallurgical continuity is the result of *epitaxial growth.* In growth by epitaxy, solidifying crystals at the interface build upon the crystals or grains of the unmelted, solid parent base metal. In so doing, they take up the substrate's crystal or grain structure and orientation and grow competitively (see Section 13.2.2). (Similar epitaxial growth can occur when metal in the vapor phase condenses onto a solid substrate.) Grain boundaries of at least some of the more favorably oriented parent metal cross the interface without discontinuity. This is illustrated in Figure 2.1d and e. This final mechanism is seen in all welding processes in which melting or fusion occurs, with total or partial participation of the parent metal(s) in the development of the weld metal zone.

The preceding three mechanisms contribute separately or in combinations to the establishment of metallurgical continuity in every welding process. Sometimes they rely on deformation, sometimes they rely on melting and solidification, and almost always they involve diffusion, alone or together with other mechanisms, to create common grain structure across an original interface by strain, recrystallization, or epitaxial growth.

2.3. THE ROLES OF TEMPERATURE AND PRESSURE

Obtaining continuity between two pieces made from metals or other, like-class materials, whether enabled by plastic deformation entirely in the solid state (without or with recrystallization), by diffusion (entirely in the solid state or with assistance from the presence of some liquid, even if transient), or by melting and then solidification (relying on the presence of liquid and subsequent epitaxial growth), always requires some combination of heat (or temperature) and pressure. This dependence was apparent from most definitions presented in Section 1.1. Let's briefly look once again at the roles that temperature and pressure play in this process of obtaining material continuity, and then we can move on to considering alternate bases for classifying processes.

Heating and elevated temperature help obtain material continuity and, thereby, promote weld formation in several ways. In the solid state, heating helps by driving off volatile adsorbed layers of gases, moisture, or organic contaminants, thereby exposing clean base material to enable formation of

bonds once atoms are brought sufficiently close together. Heating also tends to either break down the brittle oxide or tarnish layers through differential thermal expansion, causing it to spall off, or, occasionally, causing these oxides or other tarnish compounds to thermally decompose, dissociate or dissolve. Examples of layers that decompose or dissolve are copper oxide and titanium oxide, respectively. In both cases, the integrity of the intervening layer of contaminant is disrupted and clean underlying base metal is exposed, enabling the formation of metal-to-metal bonds. Another way heating helps in the solid state is by lowering the yield or flow strength of the base materials and allowing plastic deformation under pressure to bring more atoms into intimate contact across the interface, or requiring less pressure to do so. (This particular sequence of events is shown in Figure 1.4d–g). And heating promotes dynamic recrystallization during plastic deformation welding processes, causing new grains to nucleate at and grow across the original interface.

Heating or elevated temperature can help in two other ways. First, heating accelerates the rates of diffusion of atoms. Faster diffusion rates facilitate achievement of continuity in either the solid state or in the presence of a liquid layer at the interface. Second, heating melts the substrate materials, so that atoms can rearrange by fluid flow and come together to equilibrium spacing, or melts a filler material to provide an extra supply of atoms of the same or different but compatible species as the base material. (This latter scenario is shown in Figure 1.4h and Figure 2.1d.)

Pressure helps welding to take place by (1) disrupting the adsorbed layers of gases or moisture by macro- or microscopic deformation, (2) fracturing brittle oxide or tarnish layers to expose clean base material atoms, and (3) plastically deforming asperities to increase the number of atoms (and the area) that come into intimate contact (see Figure 1.4e). Figure 1.4g shows a perfect (or near-perfect) weld achieved by either route.

The relative amounts of heat (or temperature) and pressure necessary to create welds vary from one extreme to the other. Very high heat and little or no pressure can produce welds by relying on the high rate of diffusion in the solid state at elevated temperatures or in the liquid state produced by melting or fusion. Little or no heat with very high pressures can produce welds by forcing atoms together by plastic deformation on either a gross or macroscopic scale (as in forge welding) or a microscopic scale (as in friction welding), and/or by relying on atom transport by solid-state diffusion to cause intermixing and bonding (as in diffusion welding).

As will be seen in Chapter 3, most real welding processes involve a fair amount of heat and only enough pressure to hold the joint elements together during welding. But, there are processes that predominantly employ pressure and may or may not employ heat (Chapter 4).

Now let's look at some alternative bases for classifying welding processes.

2.4. ALTERNATIVE BASES FOR CLASSIFICATION

2.4.1. Fusion Versus Nonfusion

Most welding processes rely on heat more than on pressure to accomplish joining by creating atomic bonding across the joint interface. This is true whether that heat is sufficient to cause melting or fusion, or is only enough to soften the material in the solid state to facilitate plastic deformation and/or speed up solid-phase diffusion. When significant melting is involved and necessary for welding to take place, the processes are called *fusion welding processes.* For fusion welding processes, bond formation is aided by melting providing a supply of highly mobile atoms throughout the interface, filling gaps caused by microscopic surface asperities or fit-up (for square-butt joints), whether or not auxiliary filler material is employed (see Figure 2.1d).

In fact, in fusion welding, the liquid produced can actually participate in two ways: (1) to aid principally in fluxing (i.e., cleaning by chemical reaction or dissolution) the abutting or faying joint surfaces, or (2) to aid principally in bonding. In the first case, liquid is present early in the process, acts to clean or flux the surfaces to be joined, and then is largely expelled during a later (often final) stage of the process where pressure tends to prevail as the means for obtaining final metallic continuity. In the second case, liquid participates throughout the process, initially cleaning and later providing metallurgical continuity. This fine distinction is important when fusion welding processes also employ a significant level of pressure to produce a weld. For fusion welding processes, the source of heat can be chemical (reaction exothermy), electrical (arc or resistance), high-energy beams, or others (microwave, induction, etc.).[2]

If melting does not occur or is not principally responsible for causing welding (i.e., bond formation), the processes are called *nonfusion welding processes.* Heat may still be involved, however, either to reduce the power needed to cause plastic deformation or to speed diffusion, or both.

Irrespective of the particular source of heating in fusion welding, fusion welds exhibit distinct microstructural regions as a direct result of the various effects of the heat. Figure 2.2a shows a schematic of a typical fusion weld in a pure and in an alloyed crystalline metallic (or ceramic) material. Where heating caused the temperature of the pure material to rise above its melting point or the alloy to rise above its liquidus temperature, complete melting or fusion occurred, producing a *fusion zone* (*FZ*). Outside this region or zone, where the temperature of the alloy was below the liquidus but above the solidus, a *partially-melted zone* (*PMZ*) was produced. Since the pure material melts at

[2]Some fusion processes are thought to employ mechanical means for generating heat, often from friction, but, usually, the little bit of melting that occurs is not necessary for bonding. The predominant mechanism for obtaining metallic continuity is deformation.

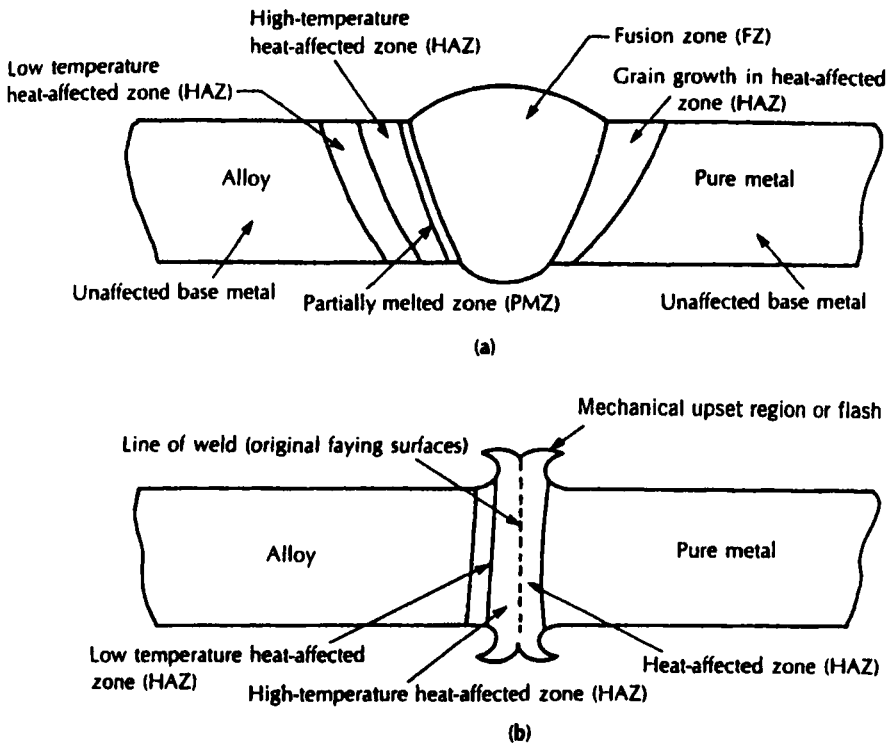


Figure 2.2 The various microstructural zones formed in (a) fusion and (b) nonfusion welds between a pure metal (left) and an alloy (right). (From *Joining of Advanced Materials* by R. W. Messler, Jr., published in 1993 by and reprinted with permission of Butterworth-Heinemann, Woburn, MA.)

one distinct and unique temperature, as opposed to over a range of temperatures, no PMZ is found in pure metals or ceramics (ionic or covalent or mixed ionic–covalent compounds). Still farther from the centerline of the heat source and the resulting weld, the temperature was lower, but may have been high enough to have caused some observable microstructural changes due to solid-phase transformations. These transformations may be due to allotropic phase changes, recrystallization and/or grain growth (in cold-worked materials), or aging, overaging, or resolutioning (or reversion) in precipitation-hardenable systems. When such observable microstructural changes occur, the region is referred to as the *heat-affected zone* (*HAZ*).[3] At some point far from

[3]It is possible for there to be more than one distinct heat-affected zone, if several different processes or reactions can and do occur in the material system at different temperatures. One example is a cold-worked alloy that exhibits a phase transformation. Here, there is a region in which recrystallization and grain growth occur at a relatively low temperature, and a region of phase change at a higher temperature. These different regions are often referred to as high-temperature and low-temperature heat-affected zones.

the weld (and heat source) centerline, the temperature did not rise high enough to cause any noticeable change in the microstructure.[4] In fact, temperature may not have risen at all if far enough away from the heat source (or weld centerline). This region is called the *unaffected base material.*

The precise number of distinct zones, and the width of these zones, occurring in a material subjected to heat during welding depends on the specific reactions or transformations that can occur in that particular material. In a nonfusion, solid-phase or solid-state weld, there is no fusion zone,[5] and little or no heat-affected zone, depending on how much of a role heat played in allowing plastic deformation (whether by pressure or friction) to occur. Figure 2.4b schematically shows a nonfusion weld in a pure and an alloyed material. Note that there is often an indication of plastic deformation or "upsetting" at the original faying surfaces of the joint. This is commonly called an upset region or flash, depending on the particular process (see Section 3.4.2).

2.4.2. Pressure Versus Nonpressure

A growing number of welding processes depend on or are facilitated by the application of pressure to bring the atoms of the material substrates to be joined close enough together to obtain continuity and achieve bond formation across the interface. These processes are called *pressure welding* or *pressure bonding processes.* The pressure required in pressure welding processes is considerably greater than the pressure required with essentially all fusion welding processes in which pieces to be joined are simply held together during the process of joining. The exception may be for many of the resistance welding processes in which a forging cycle is typically included in the overall welding schedule. (More is said about this in Section 3.4.)

As described earlier, the effect of pressure in accomplishing welding is multifold. First, it increases the number and area of contacts between mating substrates through plastic deformation of the highest asperities, bringing lower-height asperities into contact. Second, it enhances diffusion of atoms across the interface by increasing the temperature locally as the result of the mechanical work done by the macroscopic deformation process or microscopic friction (really, deformation) process and, to a lesser extent, through stress-enhanced diffusion. Obviously, both of these effects require that the materials being welded exhibit reasonable plastic behavior. Metals and their alloys typically do; ceramics typically do not. Finally, pressure holds the joint elements together while bonding takes place. Fixturing or holding pressures are

[4]In fact, unnoticeable changes may occur, such as recovery in a cold-worked material, but this is not usually considered as part of the heat-affected zone.

[5]The fact that heating from gross plastic deformation or friction may be intense enough to cause localized melting during nonfusion welding may result in a vestigial region of melting. But such a vestige is usually undesirable, because it indicates that scrubbing action to remove any intervening oxide or tarnish layers was probably inadequate, and should not be considered as a fusion zone in the true sense.

normally only of the order of a few pounds per square inch (or a fraction of a MPa), while the pressures used to cause plastic deformation are normally thousands or tens of thousands of pounds per square inch (or tens to hundreds of MPa).

Very few pressure welding processes are done cold. Most pressure welding is facilitated by heating, from various sources, to reduce the yield or flow strength of the materials to ease plastic deformation, and thereby reduce the power required to make the weld. Heating also speeds diffusion, which also helps make the weld. However, in true pressure welding processes, pressure is far more important than heat, and certainly melting or fusion is not necessary to produce the weld, although some melting may occur. When welding is accomplished without any heating, the process is called *cold welding*, (for some practical examples, see Section 4.1.1).

Non-pressure welding processes rely on heat only, with little or no pressure except to hold the joint elements together. In fact, welding processes that do not require pressure are not generally referred to as nonpressure welding, they are just called welding.

Various pressure welding processes are listed in Table 2.1, while pressure versus nonpressure processes in an overall taxonomy of welding processes are shown in Figure 2.3. Individual pressure welding processes are described later: pressure fusion welding processes in Section 3.4, and pressure nonfusion welding processes in Section 4.1.

2.4.3. Energy Sources for Welding

Besides classifying welding processes by whether temperature or pressure is more important in establishing metallic continuity, it is fairly common to classify welding processes by the specific type of source employed to provide the energy needed to produce welds. In theory, there are only three fundamental sources of energy: (1) chemical, (2) electrical, and (3) mechanical. In practice, there are many important subtypes within these fundamental energy sources: (1) Chemical sources may generate heat from either (a) exothermic combustion of a fuel-gas using air or oxygen or (b) an exothermic chemical reaction between some combination of a metal and an oxide or another metal or oxygen. (2) Electrical sources generate heat from (a) an electric arc or plasma between an electrode and the weldment, (b) resistance (I^2R) heating of the work as part of an electrical circuit or by (c) induction, (d) excitation through irradiation by a high-energy beam by converting the kinetic energy of particles in the beam upon collision with the work, or (e) excitation by an electromagnetic source of infrared or microwave radiation (related to induction). (3) Mechanical sources generate heat by the conversion of work through (a) plastic deformation under pressure or (b) friction. Diffusion as a means of obtaining metallic continuity really requires only heat, which is provided by one of these aforementioned sources, but usually by gas combustion (in a gas-fired furnace), radiant heating (in an electric furnace or autoclave), or conduction heating (in a resistance-heated press).

TABLE 2.1 Pressure Welding Processes by Energy Source

Energy Source		
Mechanical	Chemical	Electrical
Cold welding (CW)	Pressure gas welding (PGW)	Stud arc welding (SW)[a]
Hot pressure welding (HPW)	Exothermic pressure welding	Magnetically impelled arc butt (MIAB) welding[a]
Forge welding (FOW)	Pressure Thermit	Resistance spot welding (RSW)[a]
Roll welding (ROW)	Forge welding (FOW)	Resistance seam welding (RSEW)[a]
Friction welding (FRW)		Projection welding (PW)[a]
Ultrasonic welding (USW)		Flash welding (FW)[a]
Friction stir welding		Upset welding (UW)[a]
Explosion welding (EXW)		Percussion welding (PEW)[a]
Deformation diffusion welding (DFW)		Resistance diffusion welding
Continuous seam DFW (CSDW)		
Creep isostatic pressure welding (CRISP)		
Superplastic forming/ diffusion bonding (SPF/DB)		

[a]All involve some fusion, which may or may not be essential to the formation of the weld, depending on the degree of deformation from pressure.

Source: From *Joining of Advanced Materials* by R. W. Messler, Jr., published in 1993 by and used with permission of Butterworth-Heinemann, Woburn, MA.

Table 2.2 lists fusion processes by energy source, while Table 2.1 lists nonfusion processes by energy source.

2.4.4. Interface Relationships and Classification by Energy Transfer Processes

In Chapter 1, the critical importance of obtaining metallic (or, more broadly, material) continuity between atoms across an interface was described in great detail. When we examine the circumstances by which metallurgical continuity is achieved, a simple, yet elegant, classification scheme for welding processes emerges. The scheme is based on the fact that all processes involve at least one of the three operations occurring at an interface, as articulated by Granjon (1991), and as paraphrased next:

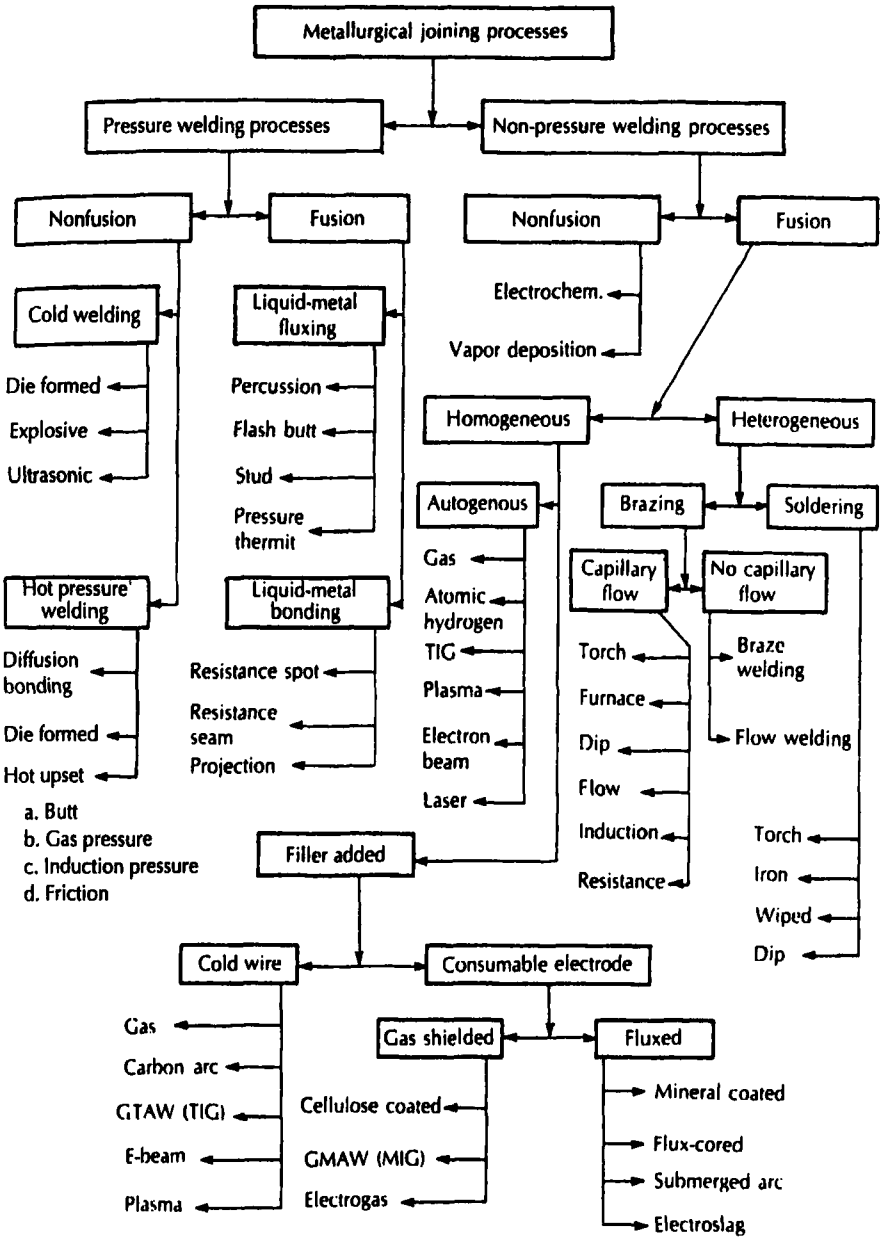


Figure 2.3 Taxonomy of welding processes. (From *Joining of Advanced Materials* by R. W. Messler, Jr., published in 1993 by and used with permission of Butterworth-Heinemann, Woburn, MA.)

TABLE 2.2 Fusion Welding Processes by Energy Source

Energy Source		
Chemical		Radiant Energy
Oxy-fuel gas welding (OFW)		Laser beam welding (LBW)
Torch brazing (TB)		Electron-beam welding (EBW)
Exothermic welding/ aluminothermic or Thermic welding (TW)		Infrared welding/brazing (IB)
Reaction brazing/ transient liquid phase bonding (TLPB)		Imaging arc welding
		Microwave welding
		Furnace brazing (FB)
		Dip brazing (DB)
Electric Arc or Resistance		
Permanent Electrode Arc	Consumable Electrode Arc	Resistance
Gas tungsten arc welding (GTAW)	Gas metal arc welding (GMAW)	Resistance spot welding (RSW)
Plasma arc welding (PAW)	Shielded metal arc welding (SMAW)	Resistance seam welding (RSEW)
Carbon arc welding (CAW)	Flux-cored arc welding (FCAW)	Projection welding (RPW)
Stud arc welding (SW)	Submerged arc welding (SAW)	Flash welding (FW)
Atomic hydrogen welding (AHW)	Electrogas welding (EGW)	Upset welding (UW)
Magnetically-impelled arc butt (MIAB) welding	Electroslag welding (ESW)[a]	Percussion welding (PEW)
		Induction welding/ induction brazing (IB)

[a]Electroslag welding (ESW) begins with an arc to heat flux until its molten and electrically conductive, at which time subsequent heating arises from the resistance of the flux to current passage (Joule heating).

Source: From *Joining of Advanced Materials* by R. W. Messler, Jr., published in 1993 by and used with permission of Butterworth-Heinemann, Woburn, MA.

a. Liquid/solid interface reactions or processes, in which bonds are obtained by epitaxial solidification of a liquid phase in contact with a solid parent metal.

b. Solid/solid interface reactions or processes, in which bonds are obtained from solid-state contact between the parts of the assembly by some means involving pressure.

c. Vapor/solid interface reactions or processes, in which filler condensed from the vapor state onto a parent metal remains in the solid state to directly produce a bond (as in surface coating) or assist in the production of bonds (as in some cases of brazing). (This last approach has only recently appeared as actual process embodiments.)

Granjon (1991) goes on to describe how the first two classes above break down further as follows:

a.1. "Liquid/solid interface reactions or processes with melting and intermixing of the parent metal, without or with the participation of a filler metal, to produce a weld upon solidification." Without filler, the process is said to be *autogenous*. This heading encompasses all fusion welding processes.

a.2. "Liquid/solid interface reactions or processes without melting or fusion of the parent metal participating in the formation of a bond made possible by a heterogeneous filler that melts to cause both fluxing and establishment of continuity." This heading encompasses brazing and braze welding and soldering.

b.1. "Solid/solid interface reactions or processes enabled by the prior formation of a transient liquid or viscous phase, itself arising from the parent metal, which is eliminated during later stages of the welding operation." This elimination can occur all at once (as in flash or some friction welding) or step by step (as in explosive welding). The heading encompasses both fusion welding processes involving a high degree of pressure (pressure fusion welding processes) and some nonfusion processes.[6]

b.2. "Solid/solid interface reactions or processes in which there is direct bond formation in the solid state" as the result of cold or hot macroscopic deformation (pressure) or microscopic deformation (friction). This heading encompasses virtually all nonfusion welding processes.

These interface situations and the mechanism for obtaining continuity and bonding resulting from them are achieved through three actions, singly or in combinations: (1) use of a filler metal (designated by Granjon by "m"); (2) application of pressure to the parts being assembled, with consequent overall macroscopic or localized microscopic deformation (designated by "p"); and (3) intervention caused by temperature variation at the interface (designated by "t").

[6]Recall that in nonfusion welding processes melting and the presence of liquid is fairly incidental to production of the final welding, except as that liquid provides a fluxing action (see Section 11.2.4).

It still remains to distinguish individual welding processes by the nature of the energy used to actually establish metallic continuity across the interface boundary. This task was performed by two working groups from the International Institute of Welding (IIW) with a view to classifying literature on welding. A list of nine processes of energy transfer at the interface was developed (Doc IIS VI-582-86: "List of Welding and Allied Processes, With Their Definitions, Classified According to Energy Source"). That list has permitted a much finer distinction among welding and allied[7] processes than was possible with previous classification schemes. Six of the nine transfer processes were presented by Granjon (1991) and are paraphrased briefly here.

Gas Transfer. This group includes processes in which the energy necessary to form bonds is obtained at the interface by heat (or califoric) exchange between the parent metal, and possibly filler, and a hot gas or gas mixture. Included here are all processes using a flame as well as a plasma, because this latter source transfers energy provided by the ionized gas jet constituting the plasma.

Electric Arc Transfer. This is by far the most important mode of energy transfer from the standpoint of number of process variations and tonnage of products welded thereby. In most cases, the electric arc heats the base metal, and any filler that might be employed, to the point of melting to allow bonding upon solidification. These are collectively called *arc welding processes.* There is also a variant in which an electric arc melts just the filler (leaving a much-higher melting parent metal unmelted), the prominent example being braze welding. Finally, there is the case in which the electric arc is maintained between the actual pieces being welded (as both electrodes in the circuit). Here, the arc melts the base metals, the liquid fluxes the faying surfaces, and the pieces are forced together to expel most of the liquid. The best known example is magnetically impelled arc butt welding to achieve welds between circular parts.

Radiation Transfer. In this group of processes, an intense beam of electromagnetic energy is focused on the work to cause melting of the substrates (and any filler) to produce bonding upon solidification. This heading encompasses the electron- and laser-beam processes, and the less-well-known, and more anecdotal, high-energy-source images, including solar energy or electric arcs (i.e., focused infrared or imaging arc processes, respectively).

Transfer by Mechanical Effect. In this group, energy resulting from a mechanical effect (deformation or friction) is the sole source of activation energy at the interface being welded. In all cases, energy is obtained by the displacement of mass. Welds are usually made in the solid state, but can involve an intermediary transient liquid or viscous phase, as with some friction

processes and with explosion welding. In most cases, this heading encompasses the more traditional solid-phase or nonfusion welding processes.

Transfer by Passage of an Electric Current. In this group of processes, an electric current is passed through the parts being welded, as a direct path in the electric circuit. Heat is generated by the I^2R (Joule) effect. Parts are usually in direct contact throughout the welding process, but need not be if first heated by the internal resistance and then forced (forged) together. Heating is almost always to the point that melting of the base metals occurs, at least locally. This group encompasses all of the traditional resistance welding processes, including those that use the liquid phase formed strictly for fluxing (as in flash welding) and those that use the liquid formed for actual bond formation (as in resistance spot welding).

Miscellaneous Processes. A small number of processes escape classification into any of the other eight categories of which five have been described on the basis of the energy transfer process. Most examples rely on diffusion and include many brazing processes, as well as diffusion brazing and diffusion welding. Other examples involve chemical reactions that occur in the solid state and either never produce any liquid (as in reaction bonding) or produce a transient liquid (as in aluminothermic or exothermic welding).

Based on these energy transfer processes at interfaces, welding processes can be classified as shown in Table 2.3 and as grouped in Table 2.4 (after Granjon, 1991). This scheme for classifying welding and allied processes is elegant in its simplicity and precision, but is generally more than is needed. In this book, the more traditional classification based on fusion versus nonfusion is used (see Chapters 3 and 4). The interested reader is encouraged to read Granjon's fuller treatment.

2.4.5. Other Bases for Classification and Subclassification

Autogenous Versus Homogeneous Versus Heterogeneous Fusion Welding. Within fusion welding, the specific processes can be further subclassified by whether an auxiliary filler material is needed and, if so, whether that filler has the same composition as the base material or a different one. When no filler is required or employed, the process is said to be *autogenous*. The source of atoms (or molecules or ions) required to help fill gaps at the interface due to microscopic asperities or imperfect macroscopic fit-up come from the melted base materials themselves. For autogenous welding to produce structurally sound and attractive welds, the base materials comprising the joint must be the same or highly compatible to allow mixing without problems, and the fit-up of the joint elements must be good (i.e., with little gap) to preclude underfill of the finished joint.

TABLE 2.3 Classification of Welding Processes by Type of Interface for obtaining Continuity, and Energy Transfer Process

Type of interface and conditions for obtaining continuity						Energy transfer process						
Interface	Mode of substrate participation		Filler m	Pressure p	Temperature t	Gas A	Electric arc B	Radiation C	Mechanical D	Passage of current E	Miscellaneous F
a : Liquid/Solid	a.1 With fusion of parent metal	a.1.1	O	O	X	●	●	●			
		a.1.2	O	X	X	●				●	
		a.1.3	X	O	X	●	●	●			●
		a.1.4	X	X	X						
	a.2 Without fusion of parent metal	a.2.1	X	O	X	●	●			●	●
		a.2.2	O	X	X	●					
b : Solid/Solid	b.1 Formation of a transient liquid of viscous phase from parent metal	b.1.1	O	X	X		●		●	●	
		b.1.2	O	X	O				●		
		b.1.3	X	O	X						●
	b.2 Direct bond in solid state	b.2.1	O	X	O				●		
		b.2.2	O	X	X	●				●	●

Source: From *Fundamentals of Welding Metallurgy* by H. Granjon, published in 1991 by and used with permission of Abington Publishing of Woodhead Publishing Ltd., Cambridge, U.K.

TABLE 2.4 Listing of Welding and Brazing Processes by Category from Table 2.3

a.1.1A	Welding without filler metal (flame or plasma)
a.1.3A	Welding with filler metal (flame or plasma)
a.2.1A	Gas brazing and braze welding
a.2.2A	Gas pressure welding
a.1.1B	Arc welding without filler metal with nonfusible electrode (TIG)
a.1.3B	Arc welding with nonfusible electrode (TIG) with filler metal
	Arc welding with electrode or submerged-arc welding and vertical electroslag welding
a.2.1B	Arc braze welding
a.1.1B	Rotating arc welding
a.1.1C	Electron-beam welding
or	Laser-beam welding
a.1.3C	Solar energy or arc image welding
b.1.1D	Friction welding
b.1.2D	Explosion welding
b.2.1D	Cold pressure welding
	Ultrasonic welding
a.1.2E	Resistance spot welding
	Resistance brazing
b.1.1E	Flash welding–high-frequency induction welding
b.2.2E	Resistance butt welding
a.2.1F	Brazing
b.1.3F	Brazing–diffusion
b.2.2F	Diffusion welding
a.1.3F	Aluminothermic processes
a.2.0F	Hand soldering
b.2.2F	Forge welding

Source: From *Fundamentals of Welding Metallurgy* by H. Granjon, published in 1991 by and used with permission of Abington Publishing of Woodhead Publishing Ltd., Cambridge, UK.

When filler is required or employed, the process is called *homogeneous* if the filler's composition is the same as the base material, and *heterogeneous* if it is different. For a process to be homogeneous, all parts comprising the joint must have the same composition (e.g., AISI 304 austenitic stainless steel welded to AISI 304 austenitic stainless steel using an AWS 304 filler metal). If the elements comprising the joint are of different compositions, the filler must be compatible with all of the materials (e.g., nickel filler between gray cast iron and mild structural steel, if there were such a need) and the process is heterogeneous.

Filler is often needed in fusion welding to make up volume in a joint. First, it compensates for the shrinkage that nearly always accompanies the solidification of a molten metal (one exception being Bi), and, second, it adds material where there is none due to poor fit. As mentioned earlier, filler also facilitates joining by bridging gaps at the joint faying surfaces by adding atoms, and, since

it is in the molten state, also facilitates diffusion. For joints that comprise two materials of the same type but of different compositions (e.g., mild- to high-strength low-alloy steels), the filler often is selected to make the two material compositions compatible (e.g., an austenitic stainless steel such as 308 or 309). Fillers are available in several different forms: stick electrodes, which are consumed by the heat of the arc to provide metal; wires which are either preplaced in the joint or fed into the joint during welding; shims which are preplaced in the joint; or powders, which are usually added to the joint during welding through an arc or gas flame.

Autogenous, homogeneous, and heterogeneous processes are shown in the taxonomy in Figure 2.3.

Nonconsumable (or Permanent) Versus Consumable Electrode Arc Welding Processes. In arc welding processes, the electrode used to strike an arc with the workpiece may serve only as the means for carrying current to the arc, or it can be consumed in the arc, contributing filler as well as heat to the weld. The first case is referred to as a *nonconsumable* or *permanent electrode process*, and the second case is referred to as a *consumable electrode process.* Figure 2.3 shows the position of nonconsumable and consumable electrode arc welding processes in the taxonomy of welding processes, while Table 2.2 distinguishes between these two important groups.

Continuous Versus Discontinuous Consumable Electrode Arc Welding Processes. Consumable electrodes used in fusion arc welding processes can be *continuous* in form, consisting of long wires fed into the arc by a mechanized device, or *discontinuous*, consisting of discrete lengths of rods or wire fed manually or by a mechanized device. This distinction is of significance primarily in the difference in productivity between the two broad types. Continuous consumable electrode processes are far easier to automate and, whether operated manually or automatically, result in less down-time to change electrodes and, thus, in overall higher deposition rates (over long times, as opposed to short runs). Figure 2.3 and Table 2.2 indicate whether a particular arc welding process employs a continuous or discontinuous consumable electrode.

2.5. ALLIED PROCESSES

As stated earlier, the general processes of brazing and soldering are really just sub-categories of welding. This is particularly obvious when one looks at similarities and differences from the standpoint of the interfaces involved and the energy transfer processes employed (Section 2.4.4). There are, however, processes that use the same energy sources (and, therefore, perhaps involve the same energy transfer processes at similar interfaces) as welding processes, but with an objective distinctly different than welding. These include the

following major groups: (1) thermal cutting, (2) thermal spraying, (3) surface heat treatment (or other modification), and (4) heat straightening or heat shaping.

Thermal cutting processes have as their goal the removal of material (as opposed to addition, as in welding) to produce planar shapes used more as the starting point for further fabrication than as finished parts. Heat is applied along a path to cause localized melting, and the molten material is forced out of the path by some force, such as gravity or pressurized gas or the frictional force of the energy stream itself. Possible heat sources include oxyfuel flames; intense arcs from special, nonconsumable (gas–tungsten arc) or highly exothermic consumable (shielded metal arc) electrodes; plasmas; and intense beams (of electrons or laser). Processes are called *flame cutting*, *arc cutting*, *plasma cutting*, and *laser-beam* or *electron-beam cutting* respectively. Thermal cutting processes should be distinguished from the perhaps better-known mechanical cutting processes, which include sawing, shearing, abrasive wheel cutting, and less well known abrasive jet and water-jet cutting. The latter processes, if done properly, can offer the advantage of not heating material in the vicinity of the cut with potential degradation from some mechanism (e.g., oxidation, transformation), and impose minimal mechanical forces on the work. Except for abrasive jet or water jet mechanical cutting, thermal cutting offers the advantage of low force, and, thus, no requirement for holding or fixturing.

Thermal spraying processes have as their common goal the application of a protective or decorative coating to a part using an intense stream of material in a particulate form. Four major variations exist, named for the energy source employed: (1) (oxygas) combustion spraying, (2) (metal) arc spraying (originally called metallizing), (3) plasma spraying, and (4) detonation spraying. The starting form of the material to be deposited varies (from wire to powder), but eventually every process heats the material to be deposited to near or above melting and propels it so that when it strikes the workpiece, it adheres to the unmelted substrate. Recently, thermal spraying (as well as some welding processes) have been used to produce actual three-dimensional shapes in what is called *spray forming* or *shape welding*, and also to consolidate reinforcing filaments wound onto removable mandrels.

The localized nature of some heat sources used in welding means that they can be used to heat the surface of a part to below the point of melting to cause modification of the microstructure near the surface. Such processes include the well-known surface heat treatment processes of *flame hardening* and *induction hardening*, and the less-well-known *laser* or *electron-beam surface modification processes*. In the case of the latter two processes, the beam heat source is so intense that heating and subsequent cooling is very rapid, so that unique microstructure can be produced, beyond simple transformation hardening by the formation of martensite in suitable steels. For example, an amorphous or glassy layer can actually be produced in some instances. This glassy layer can have unusual and desirable properties, such as high wear or corrosion resistance.

Finally, flames can be used to straighten warped metal parts and structures or shape them by localized heating and cooling to cause localized thermal expansion and contraction. The resulting thermally induced stresses cause distortion that, when properly controlled, can remove (or offset) unwanted warpage or other distortion, or create a desired bow (e.g., the hump-back on a flat-bed trawler). The process, more an art than a science, is known as *flame straightening* or *heat forming.*

Despite their importance in manufacturing and their obvious relationship to welding, no further mention is made of these allied processes.

2.6. THE AWS CLASSIFICATION SCHEME

The American Welding Society (AWS) has developed its own classification of welding processes, including allied processes like brazing and soldering and others. This classification embodies many of the classification schemes described in the preceding subsections, but in a much less rigorous and overtly expressed fashion. The AWS scheme is directed more at the practicing welder than at the engineer or researcher, and so tends to be simpler.

In coming up with a classification scheme, the AWS made each welding process definition as complete as possible so that it suffices without reference to any other definition. Key to their definitions, the AWS defines a process as "a distinctive progressive action or series of actions involved in the course of producing a basic type of result." Furthermore, the Society formulated process definitions from the operational as opposed to metallurgical point of view. Thus, definitions prescribe the significant elements of operation instead of the significant metallurgical characteristics.

The starting point for classification is the definition of welding as "a joining process that produces coalescence of materials by heating them to the melting temperature with or without the application of pressure or by the application of pressure alone and with or without the use of filler material." What resulted is an official grouping and listing of more than 40 welding processes along with nearly a dozen each of brazing and soldering processes. Processes are grouped according to the "mode of energy transfer" as the primary consideration. A secondary factor is the "influence of capillary attraction in effecting distribution of filler metal" in the joint. Capillary attraction distinguishes the welding processes grouped under "brazing" and "soldering" from "arc welding," "gas welding," "resistance welding," "solid-state welding," and "other processes." The distinguishing feature of the latter groups of welding processes is the mode of energy transfer. "Adhesive bonding" is also included since it is being increasingly used to join metals.

The AWS deliberately omitted the designation of *pressure* or *nonpressure* since the factor of pressure is an element of operation of the applicable process. The designation of fusion welding is not recognized as a grouping, since fusion is involved with many processes. There are many other terms or factors that are or are not included.

The AWS Classification of Welding Processes is shown in Figure 2.4. Appendix A contains two tables, A1 and A2, that list the designation of all welding and allied processes by letter and an alphabetical cross reference.

Other prominent welding societies (such as the British Welding Institute and the Canadian Welding Research Institute) employ similar classifications, but may refer to the type of energy involved as "thermochemical," "electrothermic," "mechanical energy," or "focalized energy."

The point of this entire chapter has been that there is not one way for classifying welding processes that is necessarily right to the exclusion of all other schemes. Its largely a matter of what works for you for what you are looking to emphasize.

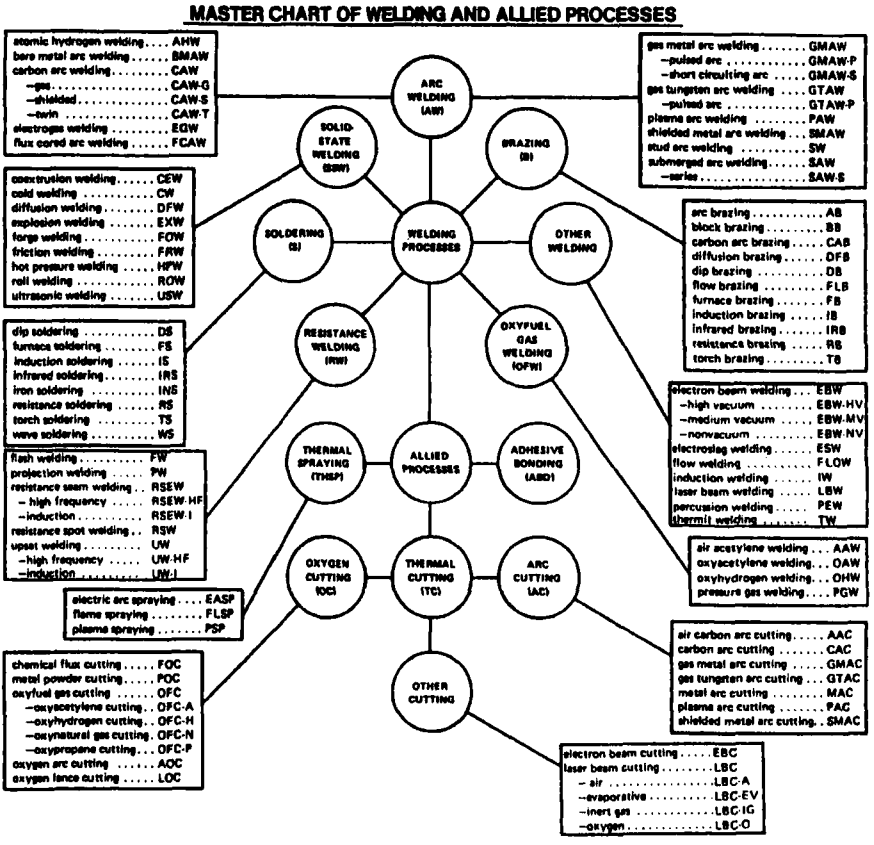


Figure 2.4 The classification scheme of the American Welding Society (AWS) in the form of a "Master Chart of Welding and Allied Processes." (From the Appendix of *Jefferson's New Welding Encyclopedia*, 18th ed., edited by R. L. O'Brien, published in 1997 by and used with permission of the American Welding Society, Miami, FL.)

2.7. SUMMARY

As for any collection of somehow related but different items or entities, it is highly desirable to classify welding processes. Doing so brings order where there may have appeared to have been chaos, and serves to point out similarities, differences, and kinships. Classification also points out gaps to be filled by future invention or development. Deciding on a proper basis for classifying welding processes, on the other hand, is nontrivial. Welding processes are, by their nature complex, involving different sources of energy, different mechanisms for obtaining material continuity on an atomic scale, different interfacial reactions by which continuity is achieved, and different means of transferring energy at the operative interface. Several traditional bases for classification, as well as a rather recent and elegant scheme developed by the IIW, were presented.

The next task is to describe the key processes in two widely used categories of classification: fusion and nonfusion welding processes.

REFERENCES AND SUGGESTED READINGS

Granjon, H., 1991, *Fundamentals of Welding Metallurgy*, Abington Publishing, Woodhead Publishing, Cambridge, UK.

Messler, R. W., Jr., 1993, *Joining of Advanced Materials*, Butterworth-Heinemann, Woburn, MA.

Suggested reading on allied processes

ASM International, 1984, *Thermal Spraying: Practice, Theory, and Application*, ASM International, Metals Park, OH. [Thermal spraying].

Boyer, H. E. (Editor), 1984, *Practical Heat Treating*, ASM International, Metals Park, OH. [Flame and induction surface hardening].

Houck, D. L., 1989, *Thermal Spray Technology: New Ideas and Processes*, Proceedings of ASM Conference, ASM International, Materials Park, OH. [Thermal spraying].

O'Brien, R. L. (editor), 1990, *Welding Handbook*, Vol. 2: *Welding Processes*, 8th ed., American Welding Society, Miami, FL. [Thermal cutting processes, Chapters 14–16; thermal spraying, Chapter 28].

Stewart, J. P., 1981, *Flame Straightening Technology for Welders*, AWS, Miami, FL. [Flame straightening].

CHAPTER 3

FUSION WELDING PROCESSES

3.1. GENERAL DESCRIPTION OF FUSION WELDING PROCESSES

In fusion welding processes, part edges or joint faying surfaces (or, for surface overlay, cladding, or hardfacing, the surfaces to be overlaid) are heated to above the melting point for a pure material or above the liquidus for alloys. In this way, atoms from the substrate(s) are brought together in the liquid state to establish material continuity and create large numbers of primary bonds across the interface after solidification has taken place. Sometimes, filler material must also be melted and added to completely fill the joint gap (or for overlaying, etc., to cover the surface). *Fusion welding processes* include all of those processes in which the melting or fusion of portions of the substrate(s), with or without added filler, plays a principal role in the formation of bonds to produce a weld.[1] As shown in Figure 2.2, all fusion welds contain a distinct fusion zone (FZ), as well as heat-affected zones (HAZ) and unaffected base material. In alloys, there is also a partially melted zone (PMZ) between the FZ and HAZ.

The following sections highlight the principal characteristics of the major fusion welding processes (more complete coverage is available in numerous references, including those given at the end of this chapter). These processes include, in order, (1) processes employing a chemical energy source, including (a) gas welding employing a combustible fuel as the source of heat, or (b) an

[1] There are some processes in which some melting or fusion occurs, but the principal mechanism by which material continuity is obtained is plastic deformation under pressure. Any liquid phase formed is largely superfluous, other than for the fact that it serves to clean the surface(s) being welded through a fluxing action.

exothermic reaction between solid (or solid and gaseous) reactants (i.e., an aluminothermic reaction) as the source of heat; (2) processes employing an electric arc as the energy source, including arcs between (a) a nonconsumable electrode as a source of heat, or (b) a consumable electrode, as a source of both heat and filler metal; (3) processes that develop heat by internal resistance or Joule heating of the workpiece, whether as the result of direct current flow through workpieces that are part of a circuit or currents induced in a workpiece by fluctuating electromagnetic fields; and (4) processes that develop heat from a high-intensity radiant energy, often beam, source through the conversion of the kinetic energy of fast-moving particles in that irradiating flux or beam.

Lets begin.

3.2. CHEMICAL FUSION WELDING PROCESSES

Chemical energy stored in a variety of forms can be converted to useful heat. There is a subset of fusion welding processes that develops the heat needed to cause melting by the transfer of energy from an exothermic chemical reaction to the work. These are *chemical fusion welding processes*, and include two major types: (1) those that employ an exothermic chemical reaction involving the combustion of a fuel gas in oxygen, called *oxyfuel gas welding* (or gas welding); (2) those that employ a highly exothermic chemical reaction between solid-phase particulate materials (or solid particles and a gas), generally referred to as *aluminothermic reactions* (or, more narrowly, Thermit welding).

3.2.1. Oxyfuel Gas Welding

In general, *oxyfuel gas welding* (OFW[2]) includes any welding process in which the source of heat for welding is the exothermic chemical combustion of a fuel gas with oxygen. While natural gas/methane, propane, propylene, butane, or other hydrocarbon gases, or even hydrogen, can be used, oxyacetylene welding, which uses acetylene gas as the fuel, is the most commonly used oxyfuel gas welding process due to its high flame temperature (i.e., intense source energy). *Oxyacetylene welding* (OAW) derives the heat needed to cause melting of the substrates and, almost always, filler from two stages of combustion. In the first stage, known as primary combustion, the acetylene fuel gas partially reacts with oxygen provided from a pressurized gas cylinder to form carbon monoxide and hydrogen:

$$C_2H_2 + O_2 \text{ (cylinder)} = 2CO + H_2 \tag{3.1}$$

[2] Throughout this book, wherever possible, the AWS designation and shorthand code for a welding process are used.

This reaction is exothermic and is responsible for about one-third of the total heat generated by the complete combustion of acetylene. The dissociation of acetylene to carbon and hydrogen releases 227 kJ/mol of acetylene at 15°C (50°F), while the partial combustion of the carbon to form carbon monoxide releases 221 kJ/mol of carbon. No combustion of the hydrogen takes place at this stage. The total heat released by the primary reaction is 448 kJ/mole (501 Btu/ft^3) of acetylene.

In the second stage of oxyacetylene or other fuel gas welding, known as secondary combustion, which occurs immediately after the primary combustion, the carbon monoxide resulting from partial combustion of the carbon dissociated from the acetylene (or other fuel gas) reacts further with oxygen, this time from the surrounding air, to form carbon dioxide, while the hydrogen from the primary combustion dissociation of acetylene (or other fuel gas) reacts with oxygen in the air to form water:

$$2CO + O_2(\text{air}) = 2CO_2 \tag{3.2}$$

$$H_2 + 0.5O_2(\text{air}) = H_2O \tag{3.3}$$

These reactions are also exothermic and are responsible for two-thirds of the total heat generated by burning the dissociation products of the acetylene completely. Burning of hydrogen to produce water vapor releases 242 kJ/mol of hydrogen, while further oxidation of carbon monoxide releases an additional 285 kJ/mol of carbon monoxide, or 570 kJ/mol for the reaction. The total heat released by the second reaction is thus 812 kJ/mol (907 Btu/ft^3) of acetylene.

The actual primary and secondary combustion reactions occur in the gas flame of an oxygen–acetylene torch in two distinct regions, as shown in Figure 3.1a. Primary combustion occurs in an inner cone, while secondary combustion occurs in an outer flame. Although only accounting for one-third of the total heat of the overall combustion reaction (448 kJ/mol out of 1260 kJ/mole), the inner cone tends to be more concentrated in volume, and so is hotter (i.e., the energy is more dense). Thus, the welder tends to work with the tip of the inner cone near the workpiece to cause melting, using the outer flame to provide a degree of shielding of the molten weld metal and hot, newly formed weld by the carbon dioxide, to provide preheating to aid in initial melting and to slow down cooling once the weld has been made (thereby sometimes avoiding adverse postsolidification or heat-affected zone transformations; see Chapters 14 and 16, respectively.

Similar combustion reactions can be written and energy balances performed for other fuel gas mixtures with oxygen, with different amounts of energy being liberated and different flame temperatures being produced for each. Table 3.1 shows the flame temperatures for several common fuel gas–oxygen mixtures. (Determination of flame temperature is nontrivial, and is discussed in Section 8.7.2).

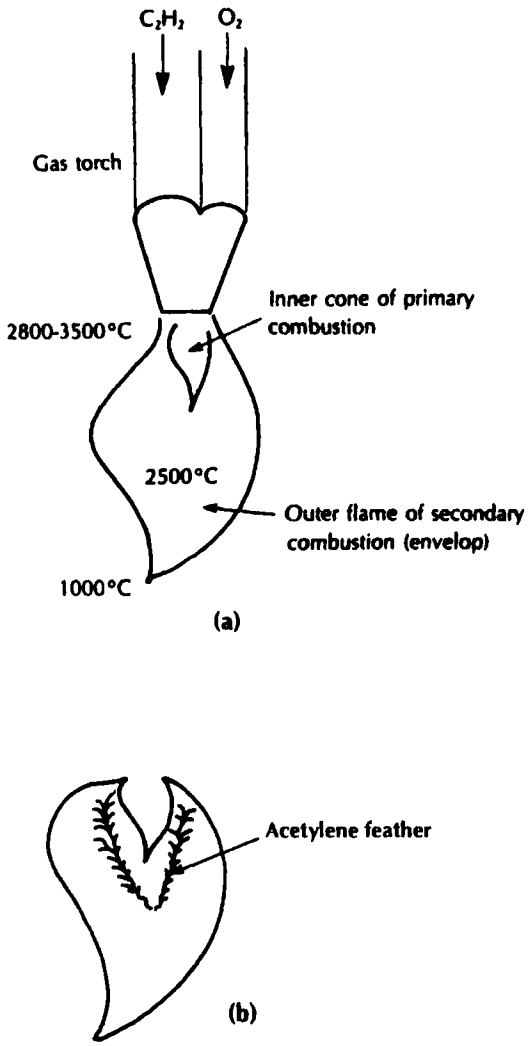


Figure 3.1 Primary and secondary combustion regions in an oxyfuel gas welding flame (a) and the presence of an acetylene feather indicating a reducing flame (b). (From *Joining of Advanced Materials* by R. W. Messler, Jr., published in 1993 by and used with permission from Butterworth-Heinemann, Woburn, MA.)

The exact chemical nature, or reactivity, of the flame in oxyfuel gas welding processes, such as oxyacetylene welding, can be adjusted to be chemically neutral, chemically reducing, or chemically oxidizing. The neutral flame occurs when the molar ratio of acetylene (C_2H_2) to oxygen (O_2) is as it should be in the balanced chemical reaction (e.g., 1:1 in Eq. 2.1). By supplying excess acetylene to the flame, primary combustion becomes incomplete, leaving some

TABLE 3.1 Flame Temperatures and Other Key Features for Various Oxyfuel Gas Welding Processes

Fuel Gas	Formula	Specific Gravity[a]	Volume to Weight Ratio[a]		Oxygen-to-Fuel Gas Combustion Ratio[b]
		Air = 1	ft^3/lb	m^3/kg	
Acetylene	C_2H_2	0.906	14.6	0.91	2.5
Propane	C_2H_3	1.52	8.7	0.54	5.0
Methylacetylene-propadiene (MPS)[d]	C_3H_4	1.48	8.9	0.55	4.0
Propylene	C_3H_6	1.48	8.9	0.55	4.5
Natural gas (methanol)	CH_4	0.62	23.6	1.44	2.0
Hydrogen	H_2	0.07	188.7	11.77	0.5

[a]At 60°F (15.6°C).
[b]The volume units of oxygen required to completely burn a unit volume of fuel gas. A portion of the oxygen is obtained from the atmosphere.
[c]The temperature of the neutral flame.

unburned acetylene. The remaining acetylene burns during secondary combustion in the outer flame, producing a tell-tale blue "acetylene feather," as illustrated in Figure 3.1b, and rendering the flame reducing. The neutral flame is attained when the flow of oxygen from the pressurized gas cylinder is increased to the point where the feather just disappears. Increasing the flow of oxygen still further results in an oxidizing flame, where there is actually some oxygen left unreacted in the products.

The reducing flame is good for removing oxides from metals, such as aluminum or magnesium, that are being welded, and for preventing oxidation reactions during welding, such as decarburization (i.e., C to CO_2) in steels. The oxidizing flame causes the metal being welded to form an oxide. This can be useful for preventing the loss of high vapor-pressure components, such as zinc out of brass, through the formation of an impermeable "oxide skin" (here, copper oxide).

All oxyfuel gas flames can be similarly adjusted, and for all, the procedure for lighting and extinguishing the flame is the same. First, the valve on the fuel gas line is opened and the fuel gas is lit with a spark, usually from a flint/steel ignitor. The resulting flame is yellow, "soft," and very sooty. Next, the valve on the oxygen line is opened, at which point the flame becomes very intense and usually white. To achieve final adjustment, the oxygen flow should be reduced until the acetylene feather just appears, at which point the flame is just becoming reducing. Bringing the oxygen flow rate up to just eliminate the feather renders the flame neutral. Further increase or decrease in oxygen flow

TABLE 3.1 (*Continued*)

Flame Temperature for Oxygen[c]		Heat of Combustion					
		Primary		Secondary		Total	
°F	°C	Btu/ft^3	MJ/m^3	Btu/ft^3	MJ/m^3	Btu/ft^3	MJ/m^3
5589	3087	507	19	963	36	1470	55
4579	2526	255	10	2243	94	2498	104
5301	2927	571	21	1889	70	2460	91
5250	2900	438	16	1962	73	2400	89
4600	2538	11	0.4	989	37	1000	37
4820	2660					325	12

[d]May contain significant amounts of saturated hydrocarbons.

Source: Welding Handbook, Vol. 2: *Welding Processes,* 8th ed., edited by R. L. O'Brien, published in 1991 by and used with permission of American Welding Society, Miami, FL.

rate from this point renders the flame increasingly more oxidizing or reducing, respectively. To shut the torch off, first the fuel supply and then the oxygen supply is shut off. This is done to prevent the fuel gas from seeking oxygen for combustion when the oxygen valve is closed by tracking up along the oxygen fuel line, to the valve or beyond, and possibly causing an explosion. As an additional safety measure, special check valves or flash-suppressing valves are often used.

The oxyacetylene gas welding process is simple and highly portable. It requires inexpensive equipment, consisting of pressurized cylinders of oxygen and acetylene, gas regulators for controlling pressure and flow rate, a torch for mixing the gases for combustion, and hoses for delivering the gases from the cylinders to the torch. A schematic of a typical torch is shown in Figure 3.2. The process suffers from limited source energy, so welding is slow and total heat input per linear length (see Section 5.4) of weld can be high.[3] Also, the nature of the process limits the amount of protective shielding provided to the weld, so welding of the more reactive metals (e.g., titanium) is generally impossible. To offset this shortcoming, oxyacetylene welding may employ a flux

[3] The heat input per linear length of weld is an important measure of how much thermal distortion or metallurgical transformation (i.e., heat-affected zone) can be expected. The analogy is of running one's finger through a candle flame. Moving quickly causes no burning sensation, but going slowly does—even though the temperature of the candle flame is the same in both instances. Moving faster reduces the heat input. Likewise, welding at high speeds results in a lower heat input per unit length of weld than welding slowly. More is said about heat input in Chapter 5.

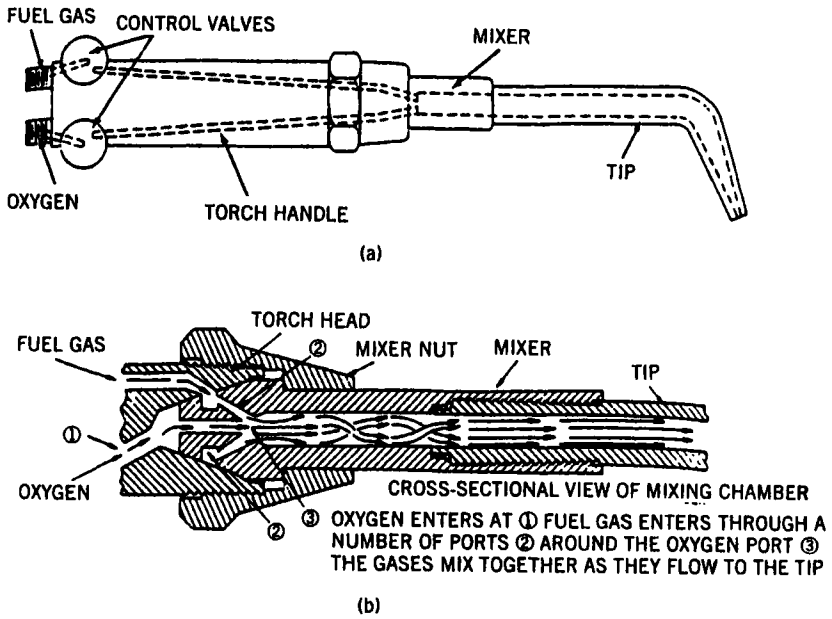


Figure 3.2 Schematic of the basic elements of an oxyfuel gas welding torch (a) and the detail design of a typical gas mixer for a positive-pressure type torch (b). (From *Joining of Advanced Materials* by R. W. Messler, Jr., published in 1993 by and used with permission from Butterworth-Heinemann, Woburn, MA).

or fluxing agent to provide additional protection to the weld, to prevent oxidation during welding, and/or to clean the workpiece of oxide to promote flow and wetting[4] by any filler metal.

Oxyfuel gas welding processes can be used for cutting, gouging (grooving), or piercing (producing holes), as well as for welding. For cutting, gouging, or piercing, the process involves melting the base material and blowing the molten material away with a jet of air or oxygen from a compressed source. Oxyfuel gas processes can also be used for flame straightening or shaping. Torch designs, for the most part, are the same.

3.2.2. Aluminothermic Welding

Aluminothermic welding is commonly known as *Thermit welding (TW)*.[5] As a subset, these processes use the heat from highly exothermic chemical reactions of solid, particulate materials (or, occasionally, solid particles and a gas) to

[4] Wetting is the phenomenon of a liquid attaching to a solid at a low angle of contact, tending to form a film rather than beads. The more complete the wetting, the smaller the angle of contact, and the more the liquid spreads as a film. The basis for wetting is surface energy reduction.

[5] Thermit is the term commonly used to identify this generic subset of processes, although it is, in reality, a registered trademark referring to a more narrow set of reactions.

produce melting and joining, also called coalescence, between metals. Most often, the reactants employed are oxides with low heats of formation and metallic reducing agents, which when oxidized have high heats of formation, but combinations of two metals or a metal and a nonmetal (e.g., H, C, O, N, B, Si, S, or Se) that will react exothermically to produce a compound with a high heat of formation can also be used. The excess heat of formation of the reaction products, in either case, provides the energy to produce the weld.

As an example, if finely divided aluminum and metal oxides of, say, iron or copper are blended and ignited by means of an external heat source, the aluminothermic reaction (after which the entire group is named) will proceed according to the following general reaction:

$$\text{Metal oxide} + \text{aluminum} \rightarrow \text{aluminum oxide} + \text{metal} + \text{heat}$$

The reaction is so exothermic that the heat liberated results in the metal formed as a reaction product being liquid. The most common Thermit reactions used to produce welds are

$$\tfrac{3}{4}Fe_3O_4 + 2Al \rightarrow \tfrac{9}{4}Fe + Al_2O_3 \qquad (\Delta H = 838\,\text{kJ/mol of oxide}) \quad (3.4)$$

$$3FeO + 2Al \rightarrow 3Fe + Al_2O_3 \qquad (\Delta H = 880\,\text{kJ/mol of oxide}) \quad (3.5)$$

$$Fe_2O_3 + 2Al \rightarrow 2Fe + Al_2O_3 \qquad (\Delta H = 860\,\text{kJ/mol of oxide}) \quad (3.6)$$

$$3CuO + 2Al \rightarrow 3Cu + Al_2O_3 \qquad (\Delta H = 1210\,\text{kJ/mol of oxide}) \quad (3.7)$$

$$3Cu_2O + 2Al \rightarrow 6Cu + Al_2O_3 \qquad (\Delta H = 1060\,\text{kJ/mol of oxide}) \quad (3.8)$$

By causing the reaction to take place such that this molten metal product can reach and fill a joint, a weld can be made. In Thermit welding as it is usually practiced, the reaction is made to take place in a vessel located above a mold around the aligned and abutted joint elements. Once the reaction takes place, the molten metal product, being denser than the solid Al_2O_3 product, pours down into the mold under the influence of gravity and casts into the joint to create a weld. To help the reaction proceed, especially for large volumes of reactant and large welds to be made, the mold is often preheated. A typical arrangement for Thermit welding is shown schematically in Figure 3.3, where concrete reinforcing steel bar is being welded in either a horizontal or vertical orientation. This and the joining of steel railroad rails and heavy copper electric cables or buss bars to terminal connectors are common applications of this process.

While the theoretical maximum temperature that results from such reactions can be calculated from the reaction thermodynamics, the actual maximum temperature achieved is less precise because the reaction does not take place adiabatically. In the case of the most common reaction (given by Eq. 3.4), the

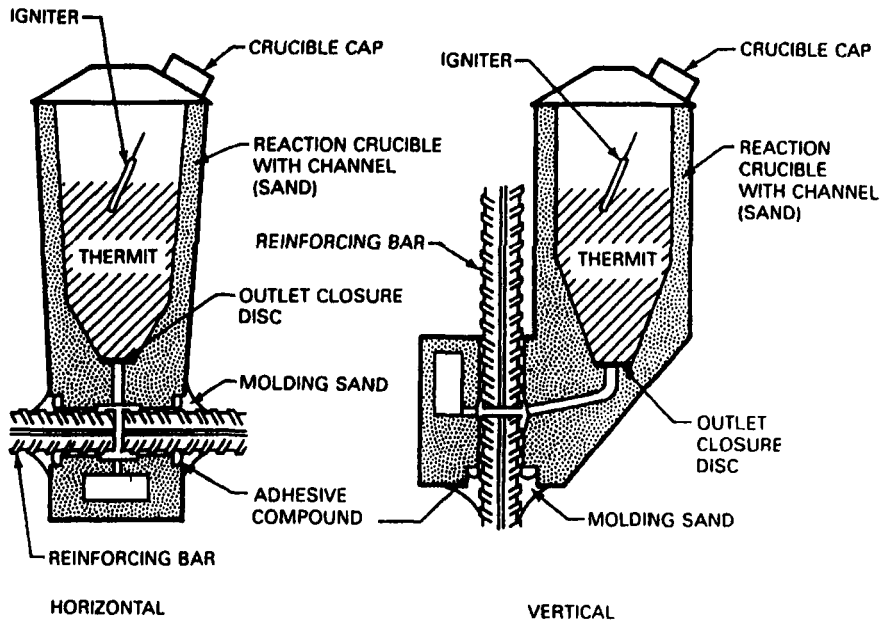


Figure 3.3 Typical arrangement of the Thermit process for welding concrete reinforcing steel bars, horizontally or vertically. (From *Welding Handbook,* Vol. 2: *Welding Processes,* 8th ed., edited by R. L. O'Brien, published in 1991 by and used with permission of the American Welding Society, Miami, FL.)

maximum theoretical temperature is approximately 3200°C (5800°F). Even though the actual maximum temperature probably ranges between 2200°C (4000°F) and 2400°C (4350°F) due to various losses, there is more than enough superheat in the molten metal product to cause melting of the surfaces of the abutting joint elements, thereby producing a real weld.

More recently, as the result of work by Merzhanov et al. (1972) in Russia, a host of exothermic reactions have been studied and used to accomplish surface welding or overlaying by causing the reaction to take place in reactant packed on the surface, and cladding by causing the reaction to take place in reactant sandwiched between layers. Reactions to produce refractory oxides, carbides, nitrides, carbonitrides, borides, silicides, and other nonoxide ceramics as well as intermetallics (e.g., aluminides) have been studied (Hlavacek, 1991) and offer potential to join ceramics to one another and to metals. The former processes are generically classified by the AWS as *exothermic welding* processes, while the latter are classified as *exothermic brazing* processes, the difference being whether any melting of the substrate(s) occurs, as it must to be considered welding. Alternative names for these processes, because of the propagating and simultaneous modes in which the process can take place are: *self-propagating high-temperature synthesis* (SHS) and *combustion synthesis* (CS).

3.3. ELECTRIC ARC WELDING PROCESSES

Energy can be obtained from an electrical or electromagnetic source in three distinct ways: (1) an electric arc; (2) resistance (I^2R or Joule losses) to either the direct flow of current in a circuit or currents induced in the workpiece; and (3) high-intensity radiant energy or beams in which the kinetic energy of particles in the irradiating field or beam is converted to heat by collisions with atoms in the workpiece. Processes relying on each source are discussed in Sections 3.3–3.5.

Fusion welding processes that employ an electric arc as a heat source are called *arc welding processes.* More processes use this source than any other source, primarily because heat for fusion can be effectively generated, concentrated, and controlled. Examples are listed in Table 3.2. The arc in arc welding is created between an electrode and a workpiece or a weldment, each at different polarities. The arc itself consists of thermally emitted electrons and positive ions from this electrode and the workpiece. These electrons and positive ions are accelerated by the potential field (voltage) between the source (one electrode) and the work (the opposite charged electrode), and produce heat when they convert their kinetic energy by collision with the opposite charged element. Although electrons are far less massive than all positive ions (approximately 1/1850th the mass of a proton or positive hydrogen ion), they have much greater kinetic energy because they can be accelerated to much higher velocities under the influence of a given electric field. Since kinetic

TABLE 3.2 Examples of Fusion Arc Welding Processes

Atomic hydrogen (arc) welding	AHW
Carbon arc welding	CAW
Electrogas welding	EGW
Electroslag welding[a]	ESW[a]
Flux-cored arc welding	FCAW
Gas metal arc welding	GMAW
Gas tungsten arc welding	GTAW
Magnetically impelled arc butt welding	MIAB
Plasma arc welding	PAW
Shielded metal arc welding	SMAW
Stud arc welding	SW
Submerged arc welding	SAW

Note: Flash welding and upset welding also involve the establishment of an electric arc, but are classified as resistance, not arc, welding processes.

[a]ESW begins with an arc to heat the flux until it is molten and electrically conductive, at which time subsequent heating arises from the resistance to the passage of current (i.e., Joule heating).

energy is one-half the product of mass and the square of velocity, this is fairly apparent.

The electrode in the above circuit can be intended to be permanent, serving solely as a source of electrons or positive ions, or consumed, in which case it serves both as a source of energy for welding from these particles and as a filler to the weld joint. If the electrode is intended to be permanent, the processes are called permanent electrode arc welding processes or, more commonly, nonconsumable electrode arc welding processes. If the electrode is intended to be consumed, the processes are called consumable electrode arc welding processes.

For nonconsumable electrode arc welding processes, if filler metal is required, it must be added from a supplemental source (e.g., filler wire). Nonconsumable electrodes are usually composed of tungsten or carbon (graphite), because of their very high melting temperatures, but must be protected from oxidation by an inert shielding gas. Consumable electrodes are often composed of the metal or alloy needed in the filler, and come in the form of rods or "sticks" (discontinuous electrodes) or wires (continuous electrodes). They too need to be protected so that the molten metal they produce is not oxidized and contaminated during transfer to the workpiece to produce a weld.

Whether the arc welding process employs a nonconsumable or consumable electrode, shielding must be provided to the weld by a chemically inert or nonoxidizing gas generated by decomposing or dissociating the coating on or flux core in a consumable electrode, or from an external inert gas source (e.g., pressurized gas cylinder) for all nonconsumable and many consumable electrode processes. This shielding is to prevent oxidation of the highly reactive molten weld metal during its transfer to the workpiece to produce the weld, of the newly produced molten weld pool, and of the very hot metal in the just-solidified weld. Shielding gases (from whatever source) also help to stabilize the arc by providing an additional supply of electrons and positive ions.

Several of the more common arc welding processes are described below, nonconsumable electrode processes first, then consumable electrode processes.

3.3.1. Nonconsumable Electrode Arc Welding Processes

There are six predominant arc welding processes that employ nonconsumable electrodes: (1) gas–tungsten arc welding (GTAW), (2) plasma arc welding (PAW), (3) carbon arc welding (CAW), (4) stud arc welding (SW) or arc stud welding, (5) atomic hydrogen welding (AHW), and (6) magnetically impelled arc butt (MIAB) welding. The carbon arc and atomic hydrogen processes are rarely used anymore and the magnetically impelled arc butt process (a rotating arc process as referred to in Section 2.4.4) is practiced rarely outside of Eastern Europe, Ukraine, and Russia, although it has potential. The arc stud process has a highly specialized role for attaching threaded or unthreaded studs to structures using the heat generated by an arc between the stud and the

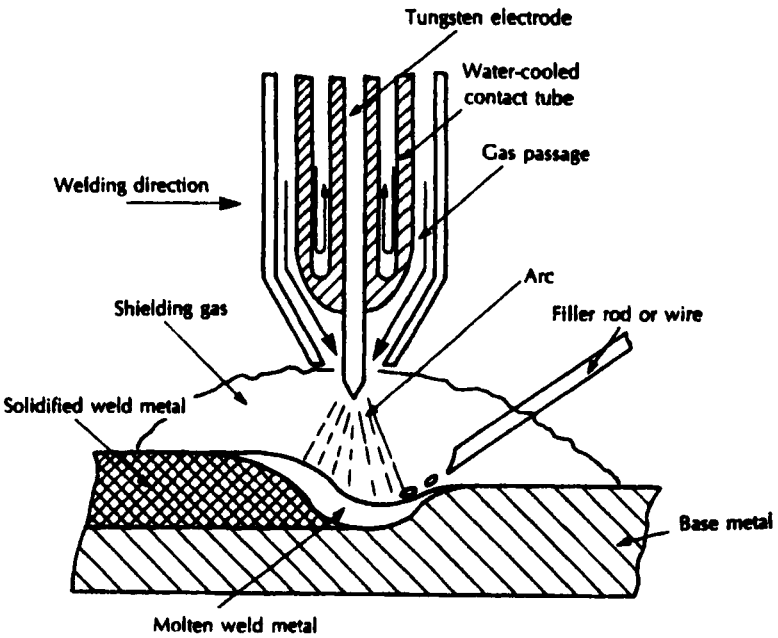


Figure 3.4 Schematic of a gas–tungsten arc welding (GTAW) process, including torch, weld, and electrical hookup. (From *Joining of Advanced Materials* by R. W. Messler, Jr., published in 1993 by and used with permission from Butterworth-Heinemann, Woburn, MA).

workpiece and applying a light pressure. These studs are then subsequently used to enable mechanical attachment or fastening (Messler, 1993).

Gas–tungsten arc and plasma arc welding are described in some detail, and the somewhat unusual magnetically impelled arc butt (MIAB) process is described briefly. The other processes are not described at all.

3.3.1.1. Gas–Tungsten Arc Welding. *Gas-tungsten arc welding (GTAW)* uses a permanent, nonconsumable tungsten electrode to create an arc to a workpiece. This electrode is shielded by an inert gas, such as argon or helium (or a mixture of the two), to prevent electrode degradation; hence the older, common names tungsten–inert gas (TIG[6]) and heli-arc welding. As shown in Figure 3.4, current from the power supply is passed to the tungsten electrode of a torch through a contact tube. This tube is usually (but may not be) water-cooled to prevent overheating. The gas–tungsten arc welding process can be performed with or without filler (autogenously). When no filler is employed, joints must be thin and have a close-fitting square-butt configuration.

[6] TIG is a trade name of the Linde Company.

The GTAW process, as well as several other arc welding processes to be described later (e.g., SMAW, GMAW, and FCAW), can be operated in several different current modes, including direct current (DC), with the electrode negative (EN) or positive (EP), or alternating current (AC). These different current or power modes result in distinctly different arc and weld characteristics.

When the workpiece or weldment is connected to the positive (+) terminal of a direct current power supply, the operating mode is referred to as direct current straight polarity (DCSP) or direct current electrode negative DC− or DCEN). When the workpiece is connected to the negative terminal of a direct current power supply, the operating mode is referred to as direct current reverse polarity (DCRP) or direct current electrode positive (DC+ or DCEP). In DCSP, electrons are emitted from the tungsten electrode and accelerated to very high speeds and kinetic energies while traveling through the arc. These high-energy electrons collide with the workpiece, give up their kinetic energy, and generate considerable heat in the workpiece. Consequently, DCSP results in deep penetrating, narrow welds, but with higher workpiece heat input. About two-thirds of the net heat available from the arc (after losses from various sources) enters the workpiece. High heat input to the workpiece may or may not be desirable, depending on factors such as required weld penetration, required weld width, workpiece mass, susceptibility to heat-induced defects or degradation, and concern for distortion or residual stress.

In DCRP, on the other hand, the heating effect of the electrons is on the tungsten electrode rather than on the workpiece. Consequently, larger water-cooled electrode holders are required, shallow welds are produced, and workpiece heat input can be kept low. This operating mode is good for welding thin sections or heat-sensitive metals and alloys. This mode also results in a scrubbing action on the workpiece by the large positive ions that strike its surface, removing oxide and cleaning the surface. This mode is thus preferred for welding metals and alloys that oxidize easily, such as aluminum or magnesium.

The DCSP mode is much more common with nonconsumable electrode arc processes than the DCRP mode. There is, however, a third mode, employing alternating current or AC. The AC mode tends to result in some of the characteristics of both of the DC modes, during the corresponding half cycles, but with some bias toward the straight polarity half-cycle due to the greater inertia (i.e., lower mobility) and, thus, greater resistance of large positive ions. During this half-cycle, the current tends to be higher due to the extra emission of electrons from the smaller, hotter electrode versus larger, cooler workpiece. In the AC mode, reasonably good penetration is obtained, along with some oxide cleaning action.

Figure 3.5 summarizes the characteristics of the various current or operating modes of the GTAW process described above. (Incidentally, many of these effects are far less pronounced with other electric arc welding processes employing consumable electrodes. Most particularly, there is little difference in

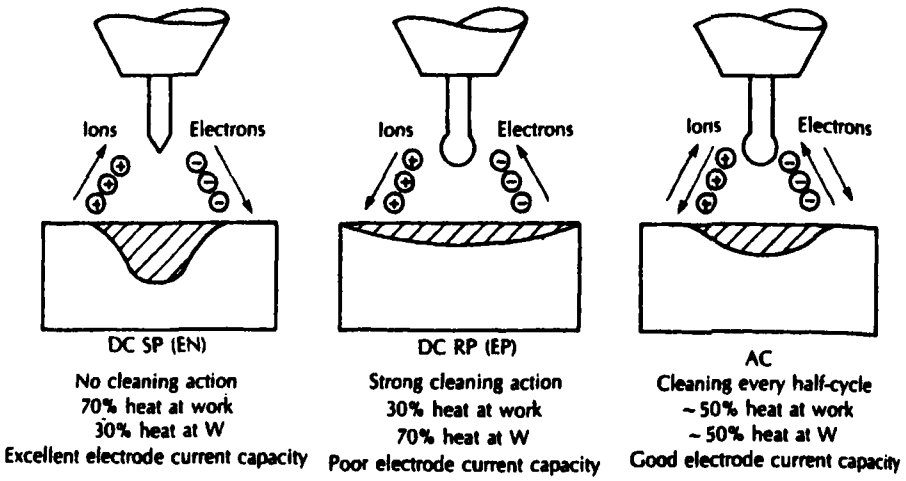


Figure 3.5 Schematic summary of the characteristics of the various operation modes possible for the gas–tungsten arc welding (GTAW) process. (From *Joining of Advanced Materials* by R. W. Messler, Jr., published in 1993 by and used with permission from Butterworth-Heinemann, Woburn, MA).

penetration between DCSP and DCRP. This is so since the concentration of heat at the electrode with RP aids in melting the consumable electrode, as is desired, but this heat is returned to the weld when the molten metal droplets transfer to the pool. On the other hand, the cleaning action of the RP mode at the workpiece still takes place.)

In modern welding power supplies designed specifically for GTA welding, there is the added capability for *square-wave* AC and for *wave balancing*. In square-wave AC, solid-state electronic devices reshape the sinusoidal wave provided as input to the power supply from line voltage to give it a square shape; positive for half a cycle and negative for half a cycle. This shape turns out to be advantageous during the transition from one half-cycle to the other, where the voltage and resulting current pass through zero. For normal sinusoidal waveforms, as this transition is taking place, the voltage just before and just after the reversal approaches zero relatively slowly compared to the rate of change for a square wave. The effect of the much more rapid (essentially instantaneous) reversal with a square wave is to avoid possible momentary loss and subsequent difficulty of reestablishing the arc.

In wave balancing, there is the capability of shifting the relative magnitude of the straight and reverse half-cycles, thereby shifting the characteristics of the altered waveform. This is done by applying a DC bias voltage to the AC, whether of sinusoidal or square waveform. The advantage is the ability to fine-tune the waveform for the particular material being welded, obtaining just the degree of straight (penetrating) or reverse (cleaning) half-wave behavior desired. Regardless of mode or waveform, power supplies for GTAW are

generally of a constant current (CC) type. These, as well as constant voltage (CV) and combined characteristic (CC/CV) type supplies, are described in Section 8.2.2.

Square versus normal sinusoidal wave form and wave balancing are shown schematically in Figure 3.6.

The electron emission of tungsten electrodes is occasionally enhanced by adding 1–2% thorium oxide or cerium oxide (or other rare-earth oxides) to the tungsten. This addition improves the current-carrying capacity of the electrode, results in less chance for contamination of the weld by expulsion of tungsten due to localized electrode overheating and melting, and allows for greater arc stability and easier initiation.

As mentioned earlier, both argon and helium are used for shielding with the GTAW process. Argon offers better shielding since it is heavier and tends to stay on the work. Arc initiation is also easier, since the binding energy (i.e., work potential) for electrons in the completely filled outermost electron shell (some of which must be stripped from this shell to provide a conducting

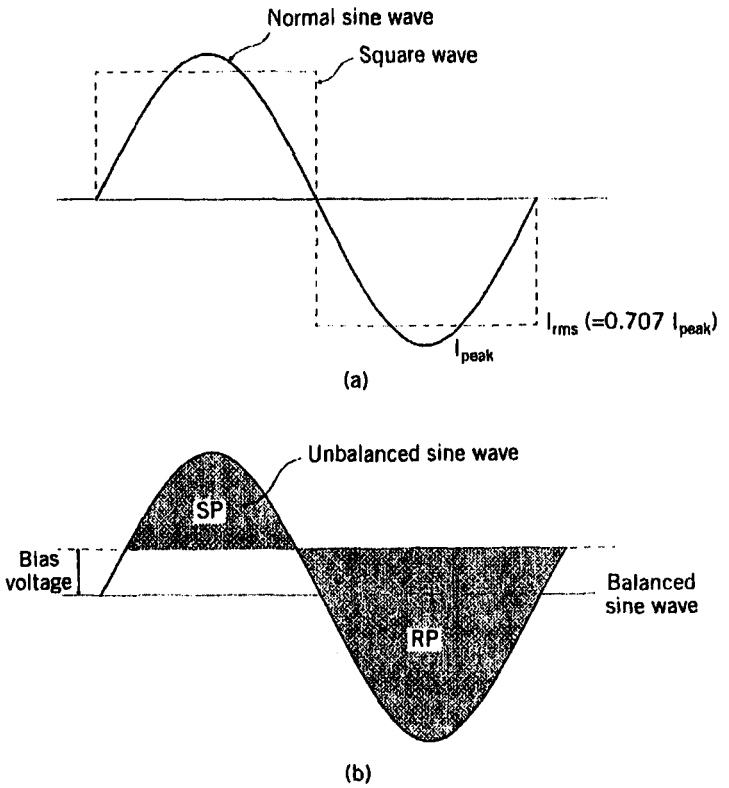


Figure 3.6 Schematic of (a) square versus normal sinusoidal wave AC forms, and (b) wave balancing in the AC operating mode.

plasma) is lower than for helium. The advantage of helium is a hotter arc, which is the result of the higher work potential compared to argon. By using mixtures of these two inert gases, mixed characteristics can be obtained.

In summary, the GTAW process is good for welding thin sections due to its inherently low heat input (especially in the DCRP mode), offers better control of weld filler dilution (see Section 12.1) by the substrate than many other processes (again due to low heat input), and is a very clean process (as a result of the excellent protection afforded by inert argon or helium or argon–helium mixtures). Its greatest limitation is its slow deposition rate (only about 1–2 lbs. or 0.5–1 kg. per hour), although this can be overcome by employing a "hot wire" variation in which the filler wire is resistance heated by being included in the circuit at a lower potential than the electrode. Deposition rate can also be increased to compete with GMAW, SMAW, and FCAW by using much larger, water-cooled electrodes with much higher currents (e.g., upward of a thousand amperes versus around a hundred amperes), or by using a fairly recent variation of the process that employs supplemental flux (*fluxed gas–tungsten arc welding*). In both of these variations, the process must be mechanized, however, to deal with the greater volumes of molten weld metal.

3.3.1.2. Plasma Arc Welding. *Plasma arc welding (PAW)* is similar to gas–tungsten arc welding in that it too employs a nonconsumable tungsten electrode to produce an arc to a workpiece. The difference is that in plasma arc welding the converging action of inert gas at an orifice in the nozzle of the welding torch (Figure 3.7) constricts the arc, resulting in several advantages over the GTAW process. These advantages include greater energy concentration (i.e., higher energy density), higher heat content (or source intensity), improved arc stability, deeper penetration capability, higher welding speeds, and, usually, cleaner welds, since the tip of the tungsten electrode cannot accidentally be touched to the workpiece causing contamination. Figure 3.8 schematically shows a comparison of the GTAW and PAW processes.

The plasma in PAW is created by the low-volume flow of argon through the inner orifice of the PAW torch (see Figure 3.7). A high-frequency pilot arc established between the permanent tungsten electrode and the inner nozzle ionizes the orifice gas and ignites the primary arc to the workpiece. When the workpiece is connected electrically to the welding torch such that it is of opposite polarity to the permanent electrode, the plasma is drawn to the workpiece electrically, and the plasma generation is referred to as operating in the transferred arc mode. When the workpiece is not connected electrically to the torch, and the plasma is simply forced to the workpiece by the force of the inert gas, the plasma generation is referred to as operating in the nontransferred mode (see Figure 3.9). The transferred arc mode is usually employed for welding or cutting, while the nontransferred arc mode is usually employed for thermal spraying. Concentric flow of inert gas from an outer gas nozzle provides shielding to the arc and the weld in PAW. This shielding gas can be argon, helium, or argon mixed with helium or hydrogen to obtain subtle differences in arc characteristics.

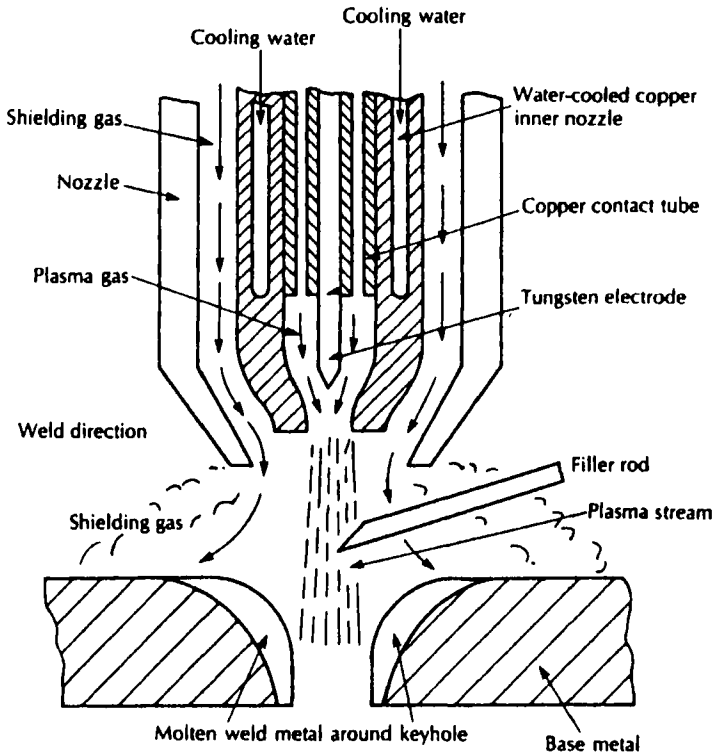


Figure 3.7 Schematic of a plasma arc welding (PAW) torch. (From *Joining of Advanced Materials* by R. W. Messler, Jr., published in 1993 by and used with permission from Butterworth-Heinemann, Woburn, MA.)

Two distinctly different welding modes are possible with the plasma arc welding process: the *melt-in* or *conduction mode* and the *keyhole mode*. In the melt-in or conduction mode, heating of the workpiece occurs by conduction of heat from the plasma's contact with the workpiece surface inward. This mode is good for joining thin sections (e.g., 0.025–1.5 mm or 0.001–0.060 in.) and making fine welds at low currents, and for joining thicker sections (e.g., up to 3 mm or 0.125 in.) at high currents. In the keyhole mode, the high energy density of a very high-current plasma vaporizes a cavity through the workpiece and creates a weld by moving the keyhole, analogous to a hot wire through wax. Penetration is great, since the vapor cavity tends to "trap" energy by internal reflection. Molten metal surrounding the vapor cavity is drawn by surface tension or capillary forces to fill the cavity at the trailing edge of the weld. This mode is excellent for welding applications requiring deep penetration, to approximately 20 mm (0.8 in.). These two modes are shown schematically in Figure 3.10. The keyhole mode arises whenever the energy density in the source exceeds a certain level, around 10^9 to 10^{10} W/m^2. It is particularly

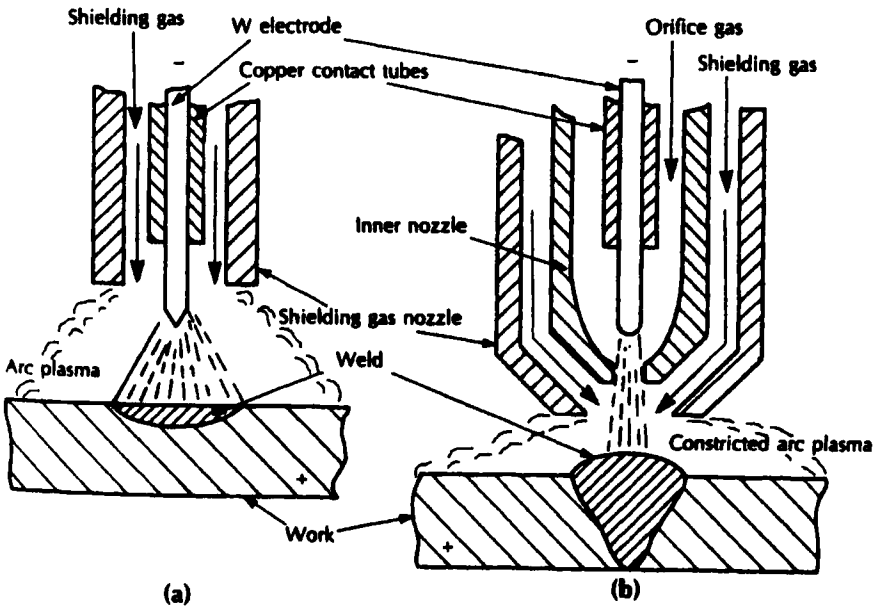


Figure 3.8 Schematic comparison of the (a) the gas–tungsten arc welding (GTAW) and (b) plasma arc welding (PAW) processes. (From *Joining of Advanced Materials* by R. W. Messler, Jr., published in 1993 by and used with permission from Butterworth-Heinemann, Woburn, MA.)

important in the high-intensity beam processes discussed in Section 3.5. More traditional, lower-energy-density arc welding processes all operate in the melt-in or conduction mode.

The single greatest disadvantage of plasma arc welding is the required equipment. Power sources, gas controllers, and torches are all more complicated and expensive than for GTAW, and the torches tend to be large, making handling difficult during manual operation.

As for gas–tungsten arc, plasma arc torches can be used with some modification for cutting, gouging, or piercing.

3.3.1.3. Magnetically Impelled Arc Butt Welding. *Magnetically impelled arc butt (MIAB) welding* (sometimes referred to as rotating arc welding) is a rapid, clean, and reliable arc welding process that employs forging to produce the finished weld. As such, it is classified as an electric arc welding process since that is the energy source for producing melting or fusion, even though pressure from forging is needed to complete the weld. It is thus a fusion arc pressure welding process, and, in that way, is related to arc stud welding, which is not described herein.

The MIAB welding process is well established in Europe (especially Eastern Europe) and the independent states of the former Soviet Union, finding

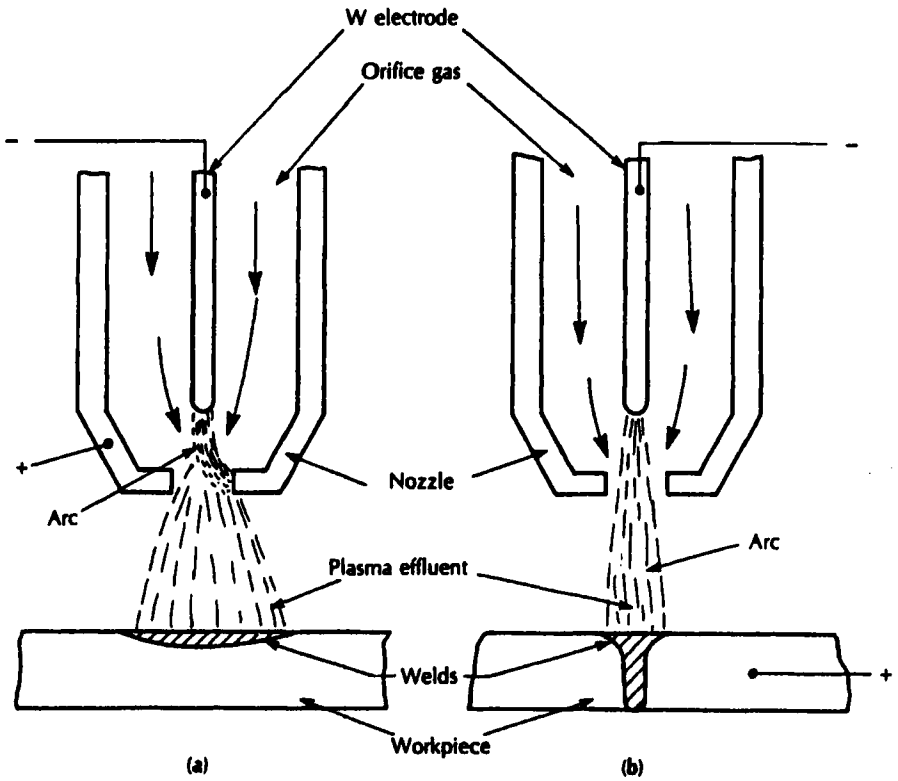


Figure 3.9 Schematic comparison of the (a) nontransferred and (b) transferred arc modes of plasma generation. (From *Joining of Advanced Materials* by R. W. Messler, Jr., published in 1993 by and used with permission from Butterworth-Heinemann, Woburn, MA.)

application in the automotive industry for the fabrication of tubular-section butt welds and, to a lesser extent, tube-to-plate welds. Tubes can have circular or noncircular cross sections, with walls ranging from 0.5 to 5 mm or more (0.020 to 0.200 in.) thick. Steel as well as aluminum alloy has been welded successfully in mass production, producing welds with exceptional quality even for safety-critical applications.

In practice, MIAB welding is fully automated. An arc drawn between aligned but properly gapped tube ends is impelled to move (rotate) around the joint line by an interaction of the arc current and an externally applied magnetic field (explained in Section 8.2.1.6), hence the name. Once the arc has heated the ends of the tubes to cause localized melting and adjacent softening in the heat-affected zone, the parts are forged together. This expels most of the molten metal present and a solid-phase bond is formed. The principle of operation is shown schematically in Figure 3.11; typical placement of the magnets used to apply the propelling force to the arc is shown in Figure 3.12.

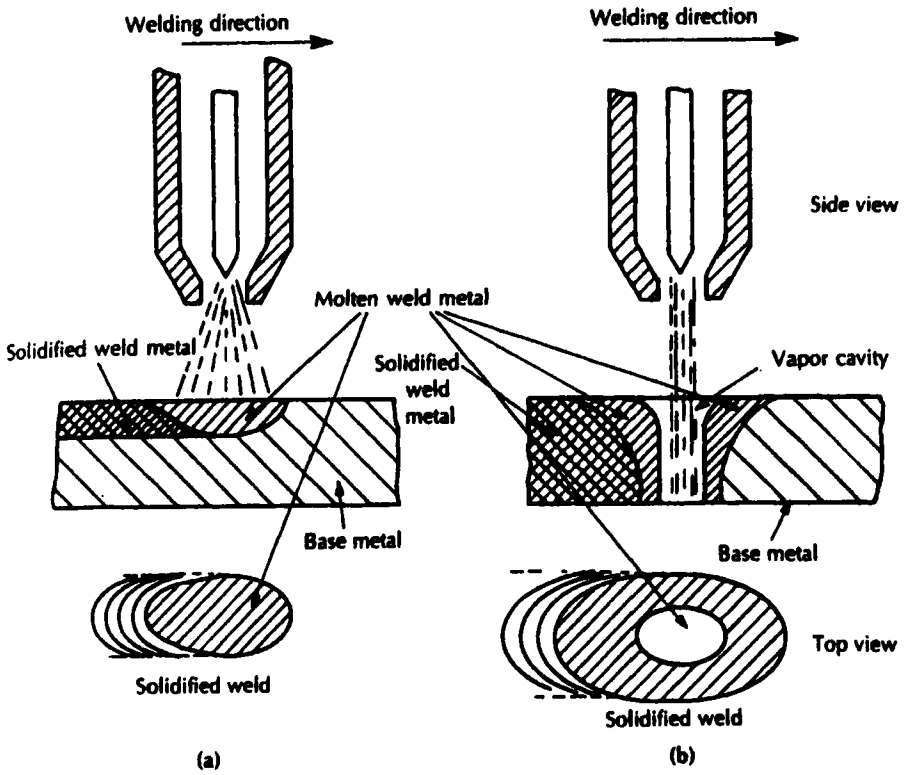


Figure 3.10 Schematic comparison of the (a) melt-in and (b) keyhole modes, exemplified by plasma arc welding (PAW), but found in other high-energy-density processes like electron- and laser-beam welding (EBW and LBW). (From *Joining of Advanced Materials* by R. W. Messler, Jr., published in 1993 by and used with permission from Butterworth-Heinemann, Woburn, MA.)

The major benefits of MIAB welding are (1) no rotation of either component (thereby overcoming problems with asymmetrical parts encountered with many friction welding processes), (2) short welding times (e.g., 2–4 s for 2 to 4-mm [0.040- to 0.080-in.]-thick low-carbon steel tube), (3) low material loss, (4) low fumes and spatter, and (5) relatively low required arc current.

As opposed to flash and upset welding (Section 3.4.2), MIAB welding does not use resistance to accomplish heating at the joint, but, rather, an electric arc. This makes it an arc rather than a resistance welding process. The fact that forging removes most molten metal suggests that the process could be considered nonfusion; after all, the role of the liquid is largely fluxing (as described in Section 11.2.4). The process is considered a nonconsumable electrode arc process because the intent is not to consume the parts being welded and used as electrodes, but to preserve those parts.

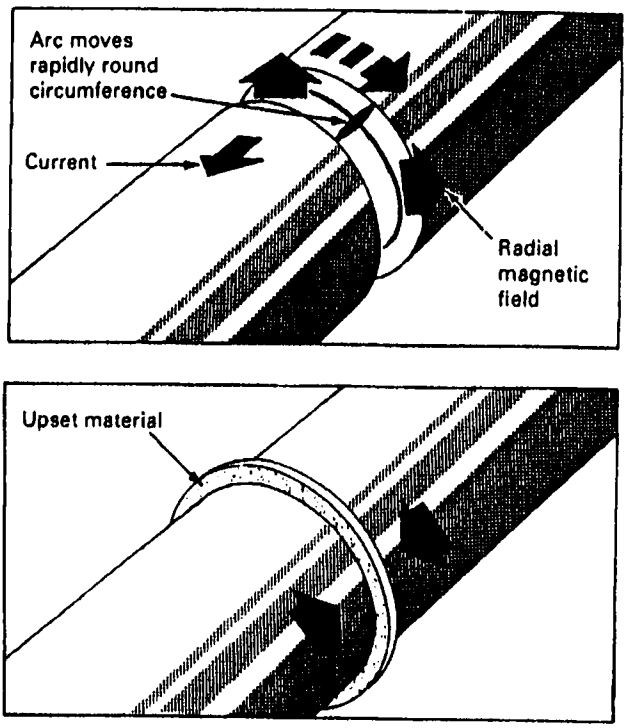


Figure 3.11 Schematic of the operation of the magnetically impelled arc butt (MIAB) welding process. (From "Magnetically Impelled Arc Butt Welding: Development and Applications" by P. Hone, in *Proceedings of Sheet Metal Welding Conference III*, organized and sponsored by the Detroit Section of the American Welding Society, 25–27 October 1988, and used with permission.)

3.3.2. Consumable Electrode Arc Welding Processes

There are six predominant *consumable electrode arc welding processes*: (1) gas–metal arc welding (GMAW), (2) shielded-metal arc welding (SMAW), (3) flux-cored arc welding (FCAW), (4) submerged arc welding (SAW), (5) electrogas welding (EGW), and (6) electroslag welding (ESW). The gas–metal arc and electrogas welding processes employ an inert gas shield provided from an external source, while the shielded-metal and flux-cored arc welding processes achieve shielding from gases generated from within the consumable electrode during melting. The submerged arc and electroslag welding processes achieve shielding of the molten weld metal with a molten slag cover. Each of these processes is described below.

3.3.2.1. Gas-Metal Arc Welding. The *gas–metal arc welding* (*GMAW*) (or metal–inert gas, MIG) process employs a continuous consumable (usually)

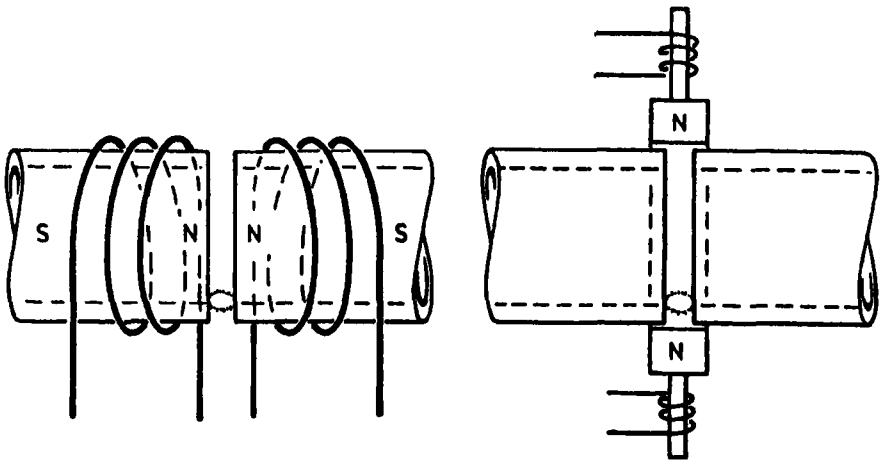


Figure 3.12 Schematic of the typical placement of magnets for propelling the arc in MIAB welding. (From "Magnetically Impelled Arc Butt Welding: Development and Applications" by P. Hone, in *Proceedings of Sheet Metal Welding Conference III*, organized and sponsored by the Detroit Section of the American Welding Society, 25–27 October 1988, and used with permission.)

solid wire electrode and an externally supplied inert shielding gas. A schematic of the process is shown in Figure 3.13. The consumable wire electrode produces an arc with a workpiece made part of the electric circuit and provides filler to the weld joint. The wire is fed to the arc by an automatic wire feeder, of which both push and pull types are employed, depending on the wire composition, diameter, and welding application.

The externally supplied shielding gas plays dual roles in GMAW, as it does in the gas-shielded form of the FCAW and in the EGW processes: First, it protects the arc and the molten or hot, cooling weld metal from air. Second, it provides desired arc characteristics through its effect on ionization. A variety of gases can be used, depending on the reactivity of the metal being welded, the design of the joint, and the specific arc characteristics that are desired.

Constant voltage (CV) DC welding power supplies can be used, hooked up as shown in Figure 3.13. Either DCSP (DCEN) or DCRP (DCEP) may be used, depending on the particular wire and desired mode of molten metal transfer, but the DCRP (DCEP) mode is far more common. The reason is that in the RP mode, electrons from the negative workpiece strike the positive wire to give up their kinetic energy in the form of heat to melt and consume the wire. As opposed to GTAW, in GMAW the heat given up to the wire to melt it is recovered to help make the weld when the molten metal from the wire is transferred to the workpiece.

A distinct advantage of GMAW is that the mode of molten metal transfer from the consumable wire electrode can be intentionally changed and control-

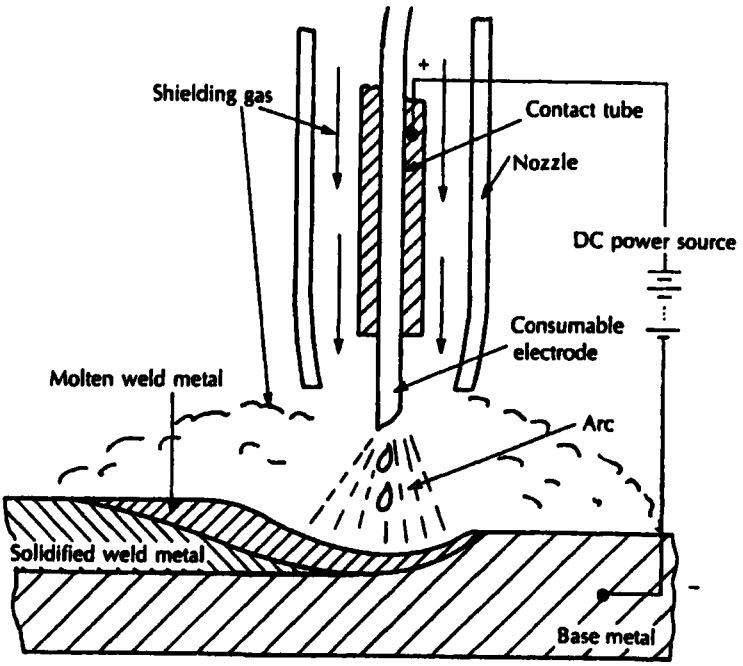


Figure 3.13 Schematic of the gas–metal arc welding (GMAW) process showing torch, weld and electrical hookup (From *Joining of Advanced Materials* by R. W. Messler, Jr., published in 1993 by and used with permission from Butterworth-Heinemann, Woburn, MA.)

led through a combination of shielding gas composition, power source type, electrode type and form, arc current and voltage, and wire feed rate. There are three predominant metal transfer modes: spray, globular, and short-circuiting. There is also a pulsed current or pulsed arc mode, which is not specifically related to the molten metal transfer mode. (More is said about these various modes in Chapter 10.)

The spray transfer mode is characterized by an axial transfer of fine, discrete molten particles or droplets from the consumable electrode to the work at rates of several hundred per second. The metal transfer is very stable, directional, and essentially free of spatter.[7] Spray transfer is produced by welding in the direct current electrode positive (i.e., DC+) mode at high voltages and amperages above some critical value related to the electrode diameter. Argon or argon–helium mixtures are usually employed when welding reactive metals

[7] Spatter refers to molten metal from the consumable (filler wire) electrode that fails to be captured by the weld pool, and runs away to stick on the workpiece surface or drop to the ground. Since spatter represents lost energy and mass, it is undesirable. Furthermore, it is often necessary to remove spatter that has adhered to the workpiece surface (by chipping or machining) for cosmetic reasons, for fit, or so as not to degrade fatigue resistance.

like aluminum, titanium, and magnesium, while small amounts of carbon dioxide (20%) or oxygen (2%) are usually added when welding ferrous alloys to stabilize the arc and give the weld a better and more regular contour.[8] The high arc energy and heat associated with the spray transfer mode limits the effectiveness for joining sheet-gage metals, but the strong directional spray can be useful for welding out of position (i.e., in a vertical plane horizontally or vertically up or down, or in a horizontal plane overhead).

Globular transfer is characterized by large globules of molten metal formed at the tip of the consumable electrode and then released and carried to the workpiece predominantly by gravity and, to a lesser extent, by arc forces including Lorentz pinching and friction. The rate of droplet transfer is slow, typically around 1 to 10 droplets per second. Spatter is usually considerable compared to spray transfer. When argon or argon–helium is used as for shielding, welding currents must be kept low to achieve this mode. Carbon dioxide-rich gases are usually employed when this mode is desired.

Unlike the spray and globular modes, which are known as free-flight modes, in the short-circuiting mode, welding currents and voltages are kept low and the slow-forming molten globules at the end of the consumable electrode are periodically touched to the weld puddle, bridging the electrode–workpiece gap, to cause their release through surface tension forces. This short-circuiting occurs at rates in excess of 50 per second, but requires special power sources. The low currents required for this mode enable the welding of thin sections without melt-through or overwelding. Out-of-position welding is facilitated by the direct transfer of the molten metal through contact. If done properly (i.e., at proper settings of voltage and wire feed speed) spatter is minimized with this transfer mode. The bridging described leads to the alternate classification of the short-circuiting mode as bridging mode transfer.

Rather than employing constant currents during welding, as is usually the case, it is possible to superimpose intermittent, high-amplitude pulses on a low-level steady current that maintains the arc. This is known as the pulsed current or pulsed arc mode. Here, "mode" refers to the mode of current and not the mode of molten metal transfer. This technique allows spray transfer to be obtained at appreciably reduced current levels, during the high-amplitude pulses. Argon-rich gases are essential, and programmable power sources are required, but several advantages are obtained. Relatively large-diameter wires can be used to weld either thin or thick sections, in or out of position.[9]

The globular, short-circuit, and pulsed-arc transfer modes usually employ the direct current electrode negative (DC−) operating mode, while the spray transfer mode usually employs the electrode positive (DC+) operating mode. A schematic of the various major metal transfer modes is shown in Figure 3.14. More will be said about molten metal transfer in Chapter 10.

[8] The contour of a weld refers to the shape of its top bead or crown bead.

[9] Out-of-position welding refers to welding in a position other than with the workpiece in a horizontal plane and the weld deposit being made from above and using the force of gravity to assist in molten metal transfer, which is referred to as in-position.

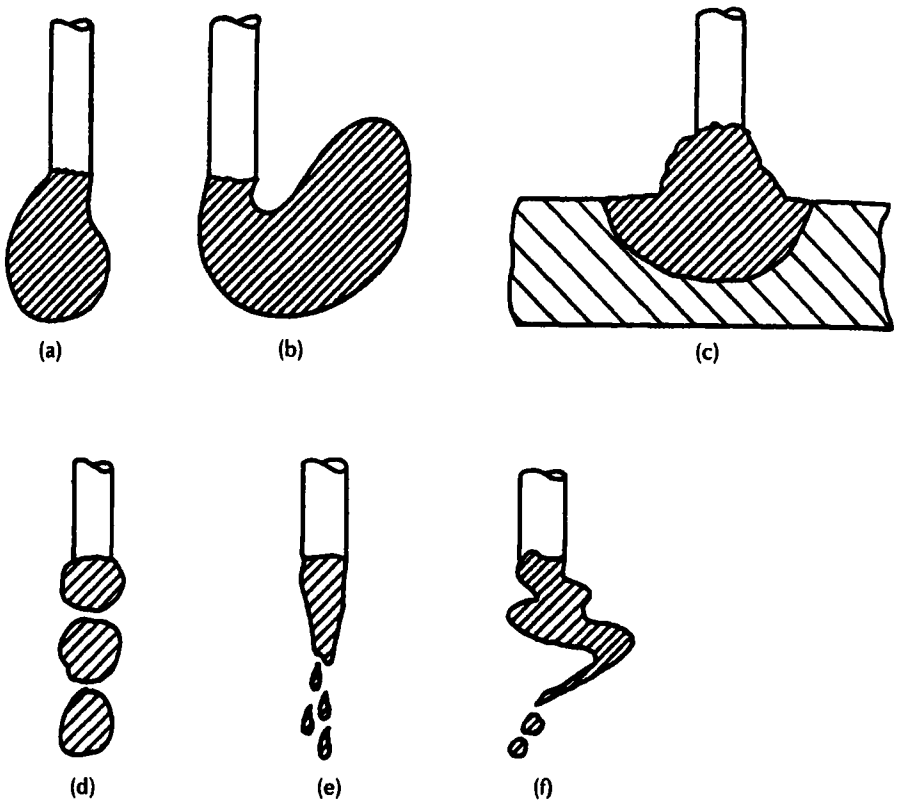


Figure 3.14 Schematic of the predominant modes of molten metal transfer in the gas–metal arc welding (GMAW) process: (a) drop globular, (b) repelled globular, (c) short-circuiting, (d) projected spray, (e) streaming spray, and (f) rotating spray. (From *Joining of Advanced Materials* by R. W. Messler, Jr., published in 1993 by and used with permission from Butterworth-Heinemann, Woburn, MA.)

In summary, the GMAW process offers flexibility and versatility, is readily automated, requires less manipulative skill than SMAW, and enables high deposition rates (5–20 kg or 10–40 lb per hour) and efficiencies[10] (80–90%). The greatest shortcoming of the process is that the power supplies[11] typically required are expensive.

3.3.2.2. Shielded-Metal Arc Welding. The *shielded metal arc welding* (*SMAW*) process is also known as the stick welding process. As shown in Figure 3.15, metal coalescence is produced by the heat from an electric arc that

[10] Efficiency, in this case, refers to the efficiency with which energy is transferred from the heat source (here, a torch) to the workpiece for use in making the weld (see Section 5.6).

[11] Constant-voltage (CV) power supplies are employed. These and constant-current (CC) types are described in various references (given at the end of this chapter), and in Section 8.2.2, but not here.

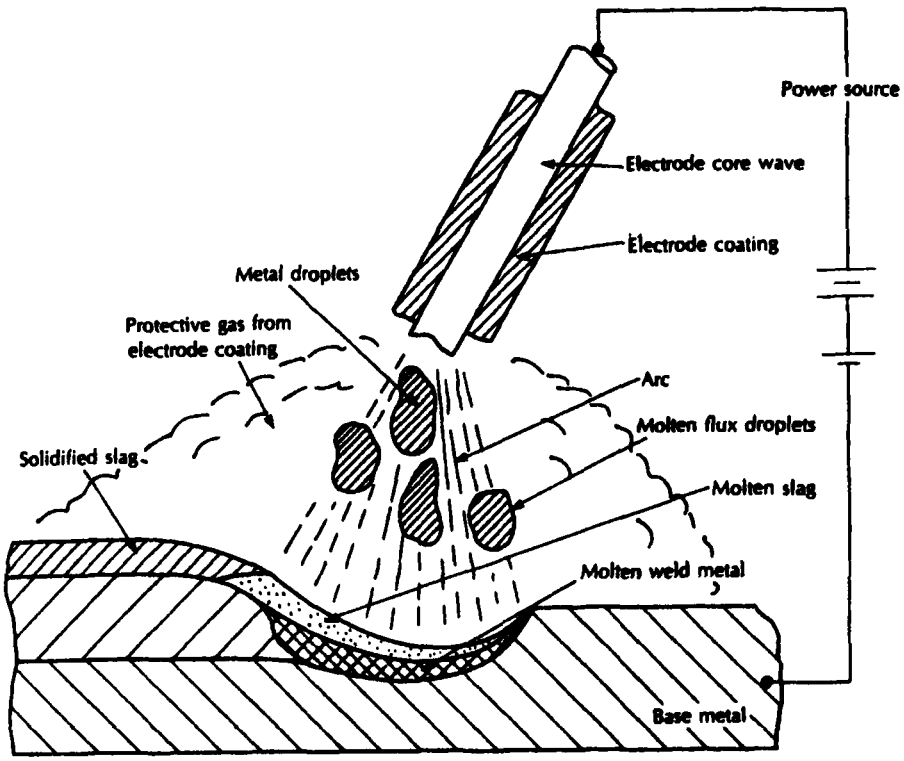


Figure 3.15 Schematic of the shielded-metal arc welding (SMAW) process, including electrode holder and electrode, weld, and electrical hookup (From *Joining of Advanced Materials* by R. W. Messler, Jr., published in 1993 by and used with permission from Butterworth-Heinemann, Woburn, MA.)

is maintained between the tip of flux-coated (or "coated" or "covered"), discontinuous consumable (or "stick") electrode and the surface of the base metal being welded. A core wire conducts the electric current from a constant-current power supply to the arc and provides most of the filler metal to the joint. Some portion of the arc heat is lost to the electrode by conduction, and some source power is lost as I^2R heat.

The covering, coating, or flux on an SMAW electrode, or, later, in the core of an FCAW wire, performs many functions. First, it provides a gaseous shield to protect the molten metal of the weld from the air. This shielding gas is generated by either the decomposition or dissociation of the coating, which may be of several types: cellulosic, which generates H_2, CO, H_2O and CO_2; rutile (TiO_2), which generates up to 40% H_2; or limestone ($CaCO_3$), which generates CO_2 and CaO slag and little or no H_2. The latter type is thus known as a low-hydrogen coating. For cellulosic coatings, gas generation is by thermal decomposition; for rutile and limestone, gas generation is by dissociation. The

different types are selected for different applications, where hydrogen can or cannot be tolerated.[12]

The second thing a coating does is provide deoxidizers and fluxing or reducing agents as molten metal compounds to deoxidize or denitrify and cleanse the molten weld metal, as in metallurgical refining. Once solidified, the slag that is formed from the flux protects the already solidified, but still hot and reactive, weld metal from oxidation. It also aids out-of-position welding by providing a shell or mold in which molten weld metal can solidify.

The third thing a coating does is provide arc stabilizers in the form of readily ionized compounds (e.g., potassium oxalate or lithium carbonate) to help initiate the arc and keep the arc steady and stable by helping to conduct current by providing a source of ions and electrons.

Finally, the coating can provide alloying elements or grain refiners and/or metal fillers to the weld. The former help achieve and control the composition and/or microstructure of the weld (adding to the composition of the core wire), while the latter increase the rate of deposition of filler metal (adding to the metal from the core wire). Both of these offer advantages in electrode manufacturing.

SMAW can operate with both direct current (DC) power supplies, with the electrode positive or negative, or alternating current (AC) power supplies, depending on coating design. Typically, currents range from 50 to 300 A, largely based on electrode diameter, at 10–30 V, resulting in 1- to 10-kg (2- to 20-lb) per hour deposition rates.

Advantages of SMAW are that it is simple, portable, and requires inexpensive equipment (power supply, electrode holder, and cables). The process is versatile, enabling joining and coating or overlaying for restoring dimensions or enhancing wear resistance (hardfacing or wear facing) for fabrication, assembly, maintenance, or repair, in-plant or in the field. Shortcomings of the process are that it offers only limited shielding protection compared to inert gas shielded processes, provides limited deposition rates compared to many other arc welding processes, and is usually performed manually, rather than automatically. Like all manual processes, but even more than most, SMAW requires fair operator skill for best results.

3.3.2.3. Flux-Cored Arc Welding. *Flux-cored arc welding* (*FCAW*) or *open-arc welding* is similar to SMAW in that it is self-shielding; however, the gas- and flux-generating flux is contained in the core of a roll-formed and/or drawn tubular wire, rather than on the outside of a core wire as a coating. The cored wire serves as a continuous consumable electrode, with the filler in the core fulfilling the same functions as the coating in SMAW—providing self-shielding gases, slagging ingredients, arc stabilizers, and alloy additions and deposition rate enhancers. The self-shielding provided by the generation of gases from the core through the arc is more effective than when gas is generated from an external coating. By the time gas that is generated (usually by dissociation of

[12] Hydrogen-generating types of coatings should be avoided when hardenable (i.e., martensite-forming) steels are being welded to avoid hydrogen embrittlement. Martensite formation and hydrogen embrittlement are discussed in Chapter 16.

some core ingredient) reaches the air to be swept away, it has fulfilled its shielding function. For this reason FCAW is an excellent choice for welding in the field, and it is here that it got the name open arc welding.

The FCAW process can also be operated in a gas-shielded mode, in which case it is closely related to the gas–metal arc welding (GMAW) process. Both employ a continuous consumable electrode, both provide filler, and both use an externally provided gas to shield the arc and the weld metal. In either mode (with or without gas shielding), FCAW can be operated with DC power supplies, with the electrode positive or negative, depending on the particular wire type and formulation.

Figure 3.16 shows the self-shielded and gas-shielded forms of FCAW. Process advantages include high deposition rates (e.g., 2–15 kg or 10–30 lb per hour), with actual rates being high due to the continuous operation at higher currents than SMAW; larger, better contoured welds than SMAW; portability; and excellent suitability for use in the field.

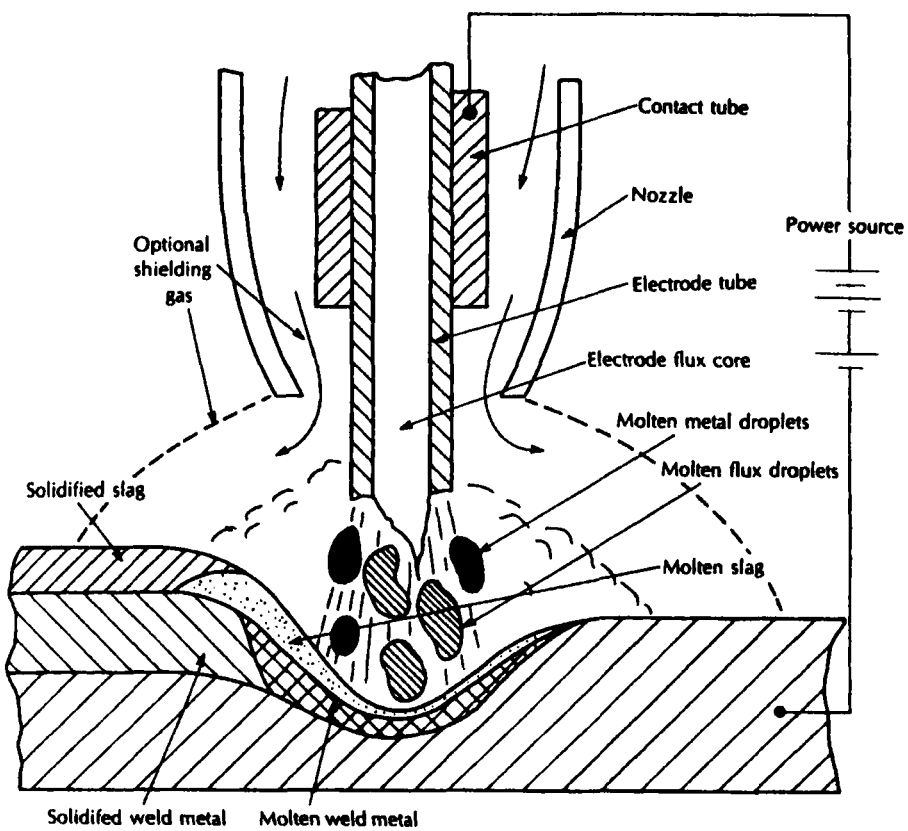


Figure 3.16 Schematic of the self-shielded and gas-shielded forms of the flux-cored arc welding (FCAW) process, including torch and wire, weld, and electrical hookup (From *Joining of Advanced Materials* by R. W. Messler, Jr., published in 1993 by and used with permission from Butterworth-Heinemann, Woburn, MA.)

3.3.2.4. Submerged Arc Welding. In the *submerged arc welding* (*SAW*) process, shown in Figure 3.17, the arc and the molten weld metal are shielded by a covering envelope of molten flux and a layer of unfused granular flux particles. Since the arc is literally buried (or submerged) in the flux, it is not visible. As a result, the process is relatively free of the intense radiation of heat and light typical of most open arc welding processes (e.g., GMAW, SMAW, and FCAW), and resulting welds are very clean. The SAW process employs a continuous solid wire electrode that is consumed to produce filler. The efficiency of transfer of energy from the electrode source to the workpiece is very high (usually over 90%), since losses from radiation, convection, and spatter are minimal (see Sections 5.5 and 5.6).

The sub-arc process is always mechanized, because currents are very high (500 to over 2000 A), deposition rate is very high (27–45 kg or 60–100 lb per hour), and reliability is high. Also, the process must be controlled without relying on feedback of visible signs from the arc, which is so important to the other open arc processes. Thin sections can be welded at very high velocities (up to 500 cm or 200 in. per minute), while very thick sections can be welded at lower velocities, even in the direct current electrode positive (or DCRP) operating mode. At very high currents (over 1000 A), AC is often used to avoid problems with arc blow.[13] The process can be operated with multiple wires or with strip electrodes to further increase deposition rate (the latter occasionally is called strip welding, but this name is applied elsewhere, especially hard surfacing). Welding is restricted to flat and horizontal positions, because of the effects of gravity on the large molten puddles that typify the process, however,

[13] Arc blow refers to the deflection of an arc by the induced electromagnetic fields in conductive materials. It can occur for any arc welding process, and is discussed in more detail in Chapter 8.

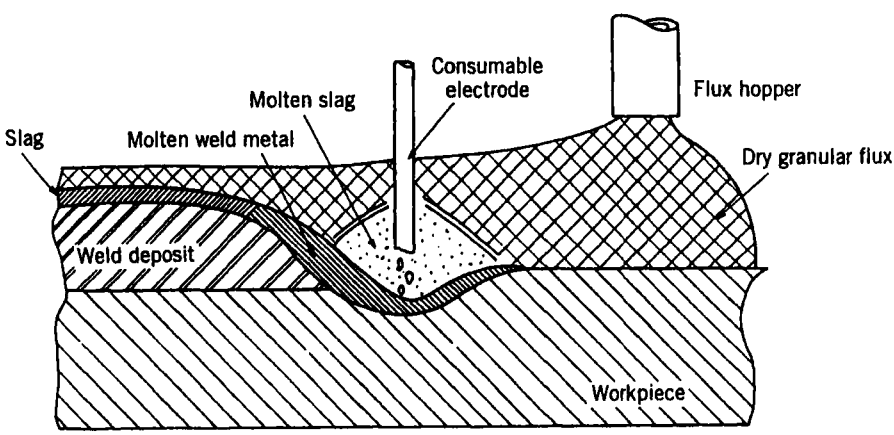


Figure 3.17 Schematic of the submerged arc welding (SAW) process, including torch, weld, and flux hopper. (From *Joining of Advanced Materials* by R. W. Messler, Jr., published in 1993 by and used with permission from Butterworth-Heinemann, Woburn, MA.)

a variant of the process at the world-renowned E.O. Paton Electric Welding Institute in Kiev, Ukraine, allows overhead welding. As already mentioned, the inability to observe the puddle directly can hinder control.

The granular flux employed in the SAW process is specially formulated, often containing additives to compensate for the loss of volatile alloying elements (such as chromium) from the filler. Approximately one kilogram of flux is consumed for every kilogram of filler deposited.

3.3.2.5. Electrogas Welding. The *electrogas welding* (*EGW*) process is a heavy-deposition-rate arc welding process, even more so than SAW. The process operates under an inert gas shield provided to a joint enclosed with water-cooled dams, shoes or backing plates, as shown in Figure 3.18. Deposition rate can be as high or higher than SAW, and the quality of weld deposit is excellent, due to the extremely effective shielding provided by the inert gas

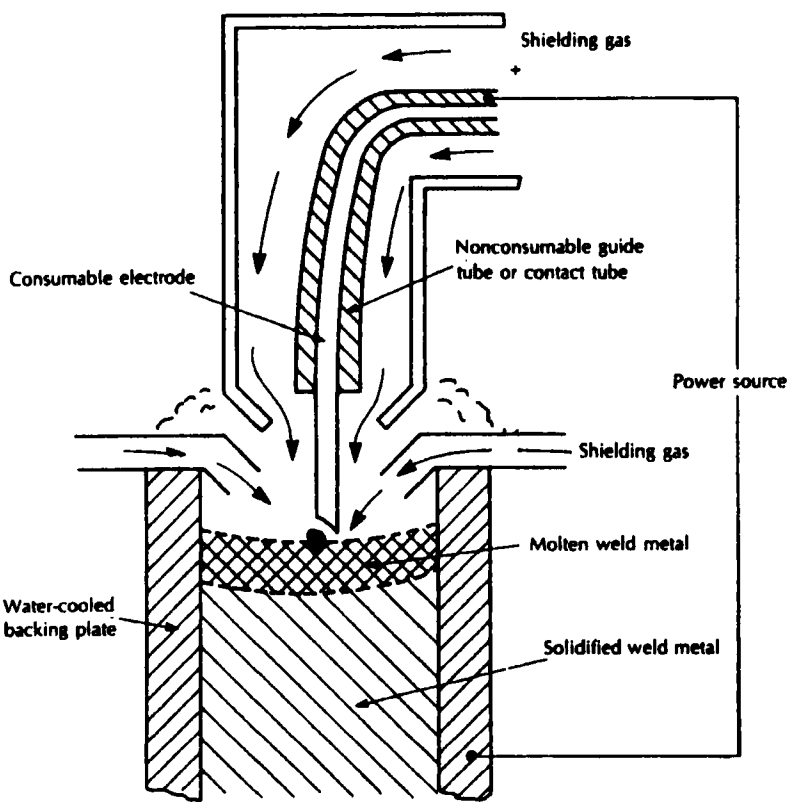


Figure 3.18 Schematic of the electrogas welding (EGW) process, including torch, weld, mold, and electrical hookup. (From *Joining of Advanced Materials* by R. W. Messler, Jr., published in 1993 by and used with permission from Butterworth-Heinemann, Woburn, MA.)

coverage. A drawback is that the process can be employed only for welding vertically up, but, in this mode, requires little joint preparation for fit-up.

3.3.2.6. Electroslag Welding. The *electroslag welding* (*ESW*) process is not a true arc welding process. The energy for melting the base metal and filler is provided by a molten bath of slag that is resistance heated by the welding current. An arc is employed only to melt the flux initially, after being struck at the bottom of the joint. Welds are produced in the vertical up direction (and, occasionally, in horizontal fillets), with the joint edges being melted and fused by molten weld filler metal contained in the joint by water-cooled dams or shoes, as shown in Figure 3.19. The molten flux or slag provides excellent

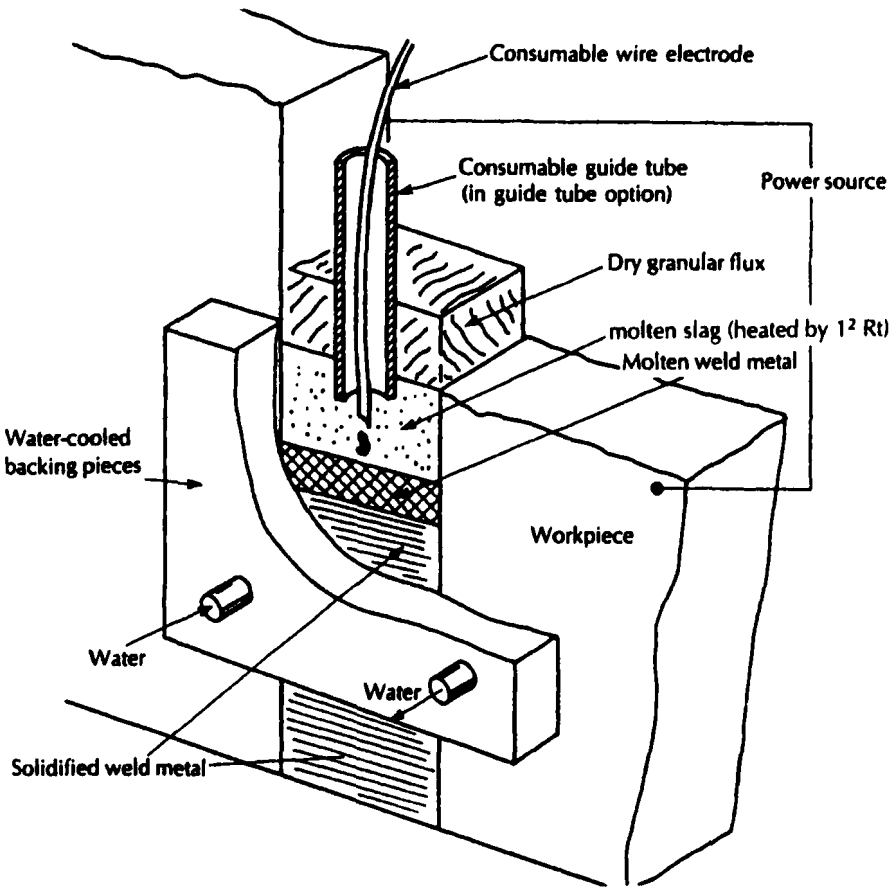


Figure 3.19 Schematic of the electroslag welding (ESW) process, including torch, weld, weld mold, and electrical hookup (From *Joining of Advanced Materials* by R. W. Messler, Jr., Figure 6.22, page 215, published in 1993 by and used with permission from Butterworth-Heinemann, Woburn, MA.)

protection to the weld. Deposition rates are typically 7–13 kg (or 15–30 lb) per hour per electrode, and multiple electrodes can be employed. In the guide tube mode of this process, a consumable, thick-walled tube is employed to provide additional filler and guide the continuous wire to the bottom of the joint. Here, deposition rate can easily reach 15–25 kg (35–55 lbs) per hour per electrode/guide tube.

Neither electrogas nor electroslag welding is very widely practiced in the United States, although both are practiced elsewhere, especially in the former Soviet states.

3.4. RESISTANCE WELDING PROCESSES

As a group, *resistance welding* (*RW*) processes generate heat through the resistance to the flow of electric current in parts being welded. The parts are usually an integral part of the electrical circuit, with heat generation and welding taking place at the points of contact. Some processes also rely on resistance heating, but in this case internally as the result of field-induced currents. All are called resistance welding processes, however.

As shown in Figure 3.20, contact resistance, especially at faying surfaces, heats the area locally by I^2R or Joule heating, resulting in melting and the formation of a nugget. For the process to work properly, the contact resistance must be higher at the point to be welded than anywhere else. Pairs of water-cooled electrodes, made of copper or copper alloyed with refractory metals to improve erosion resistance, conduct current to the joint, apply pressure by clamping to improve contact (i.e., reduce the contact resistance) at the electrode-to-workpiece interface, and help contain the molten metal in the nugget. The electrical hookup is shown in Figure 3.21. The principal process variables are welding current (usually several thousands to tens of thousands of amperes), welding time (of the order of $\frac{1}{4}$ s), electrode force, and electrode shape. Such DC power to the weld is provided from either single-phase or three-phase AC line voltages of 440–480 V using step-down transformer/rectifiers, for example (see Section 8.4.3). Usually, the process is used to join overlapping sheets or plates as lap joints, which may have different thicknesses.

At least six major types of processes rely on direct resistance heating to produce welds, with several variations within certain types: (1) resistance spot welding (RSW); (2) resistance seam welding (RSEW), employing high frequency (RSEW-HF) or induction (RSEW-I); (3) projection welding (PW); (4) flash welding (FW); (5) upset welding (UW), employing high frequency (UW-HF) or induction (UW-I); and (6) percussion welding (PEW).

3.4.1. Resistance Spot, Resistance Seam, and Projection Welding

Resistance spot welding (RSW) consists of a series of discrete nuggets produced by resistance heating. Nuggets or welds are usually produced directly under the

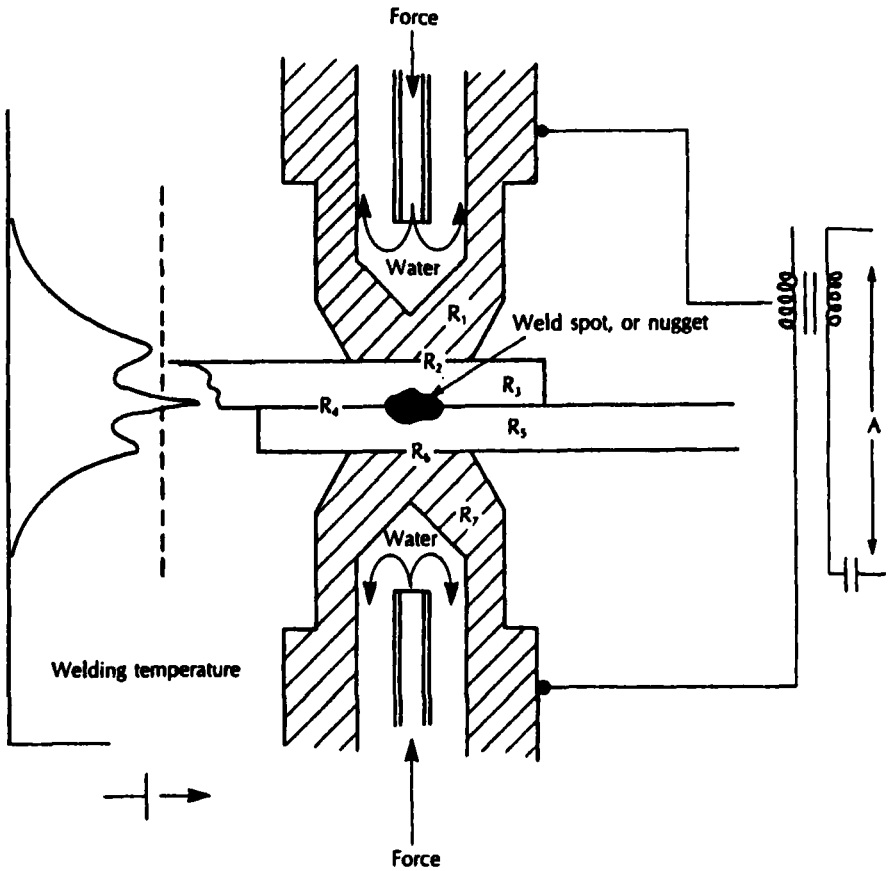


Figure 3.20 Schematic of the resistance (spot) welding (RSW) process showing it to be a circuit consisting of a series of resistors (R_1 through R_7), with heating intended to be greatest at the point(s) of contact of faying surface(s) between workpieces to create a weld nugget. (From *Joining of Advanced Materials* by R. W. Messler, Jr., published in 1993 by and used with permission from Butterworth-Heinemann, Woburn, MA.)

electrodes, but not necessarily if there is another more favorable path, called a shunt, for the current. Spot welding usually requires access to both sides of the work, but can be accomplished from one side using a series-welding technique where current passes from one electrode on the face of the work, through the work to produce a weld at the interface of the workpieces, through the workpiece farthest from the electrode, back through the workpieces to produce a second weld, and into a second electrode contacting the front face of the work. Figure 3.22 schematically shows normal resistance spot and series resistance spot welds being made.

The purpose of the forging pressure cycle within the overall weld schedule of current and pressure versus time is multifold. First, pressure holds workpie-

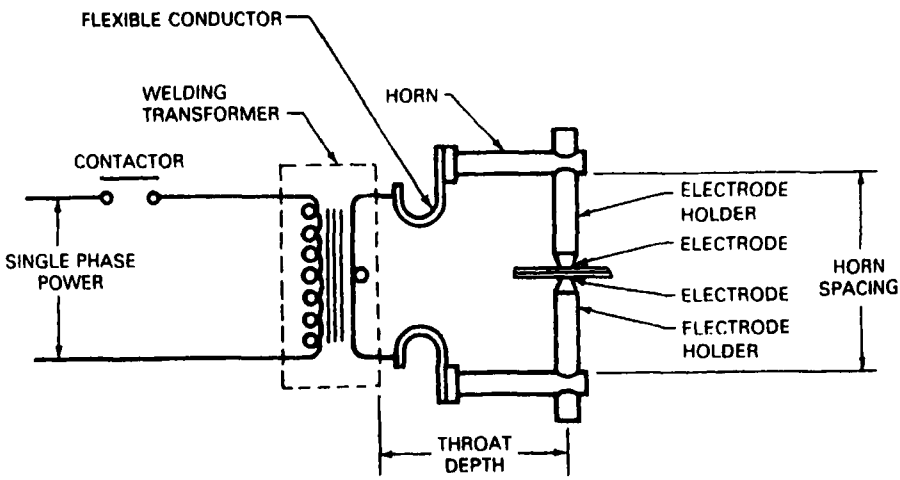
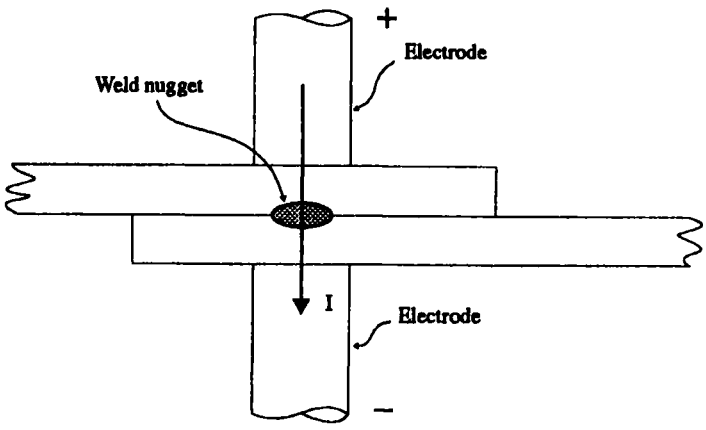


Figure 3.21 Schematic of a typical single-phase spot welding circuit. (From *Welding Handbook, Volume Two: Welding Processes*, 8th ed., R. L. O'Brien (Editor), published in 1991 by and used with permission of the American Welding Society, Miami, FL.)

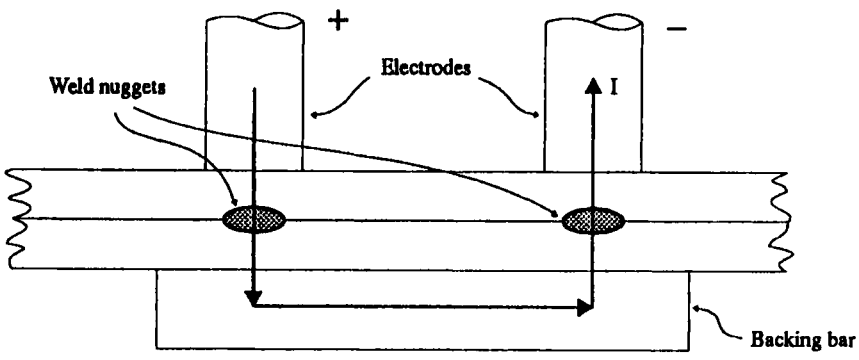
ces together to contain the molten nugget as it forms and expands as solid transforms to liquid. It is important to hold this liquid in the nugget under pressure, or it is expelled from the nugget at the faying surfaces. Expelled liquid (called expulsion or spitting) leaves insufficient liquid in the nugget to form a continuous solid weld. Large voids can result, seriously weakening the weld. Second, pressure is used to help control the contact resistance and, thus, rate of melting at the interface. Higher pressure lowers contact resistance by pressing more high points into intimate contact. Third, for some welding applications, pressure is needed to literally forge the work surfaces together in the vicinity of the weld. Use of pressure in this way is restricted to situations where surface indentations are tolerable. Incidentally, the ideal nugget in a two-ply joint from pieces with equal thickness is 0.6–0.7 of the combined thickness of the joint.

Resistance seam welding (RSEW) consists of a series of overlapping spots to produce an apparently continuous seam or resistance heating along the edges of two pieces being forced into contact along a seam in what is known as *mash welding*. Use of high-frequency AC or induction allows the edges of parts to be welded as they are brought together, perhaps by a continuous forming process. Figure 3.23 schematically shows a seam produced from overlapping spots made at the point of contact created by two opposing wheels (Figure 3.23a), with timed current pulses or groups of pulses producing each spot, as well as a seam along abutting edges of two workpieces as they are brought together (Figure 3.23b).

In projection welding (PW), projections or dimples in overlapping joint elements are employed to concentrate the current during welding, focusing the



(a)



(b)

Figure 3.22 Schematic of (a) normal resistance spot welding (RSW) and (b) series spot welding.

weld energy and helping to locate the weld more precisely. Figure 3.24 shows projection welding schematically.

Figure 3.25 shows simple schematics comparing the three major resistance welding processes: spot, seam, and projection.

3.4.2. Flash, Upset, and Percussion Welding

Flash welding (FW) is classified as a resistance welding process, but it is unique. Heating at the faying surface is by combined resistance and arcing. Two parts

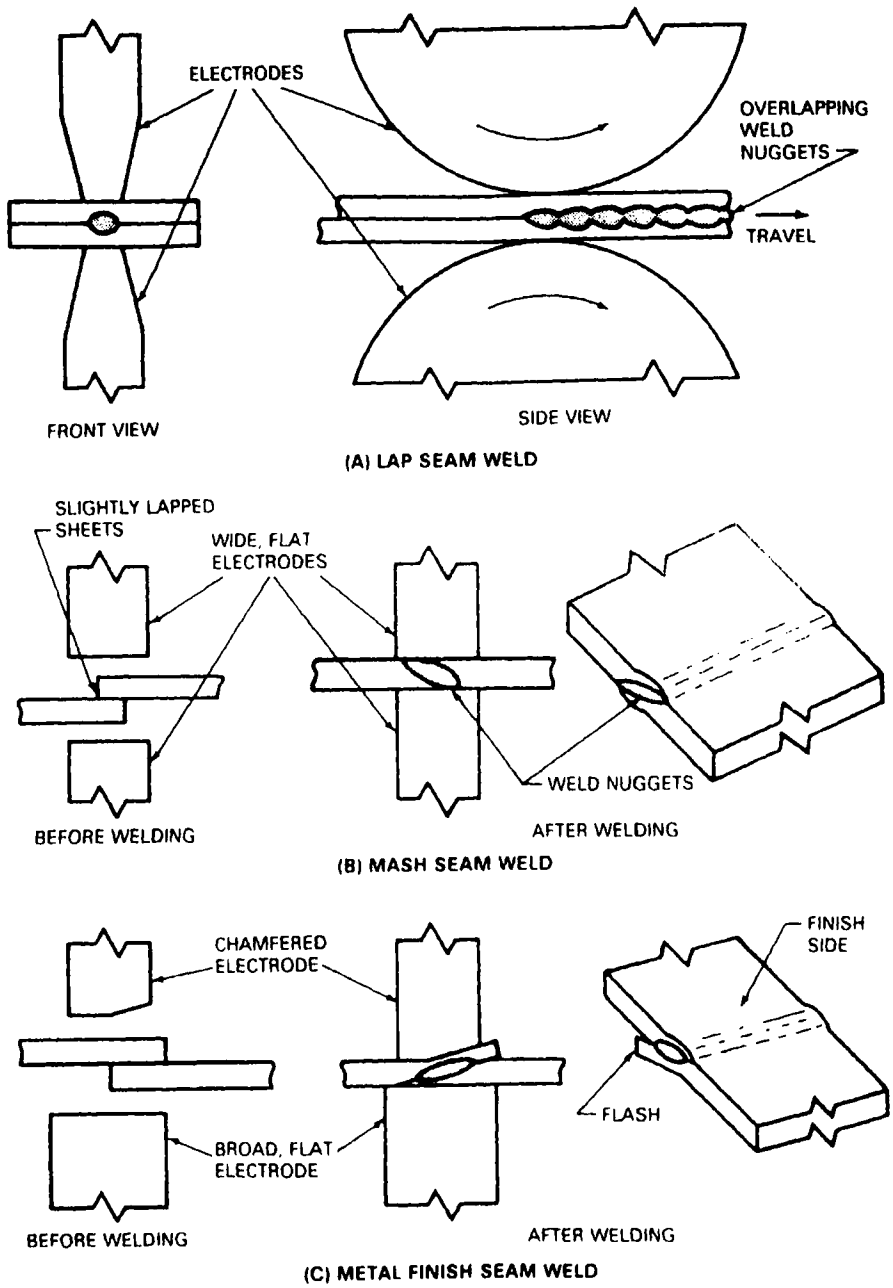


Figure 3.23 Schematic of (a) normal resistance seam welding (RSEW) using overlapping spot welds, and (b) continuous seam welding as edges of two workpieces are forced together under the influence of a high-frequency or induced current (From *Welding Handbook*, Vol. 2: *Welding Processes*, 8th ed., edited by R. L. O'Brien, published in 1991 by and used with permission of the American Welding Society, Miami, FL.)

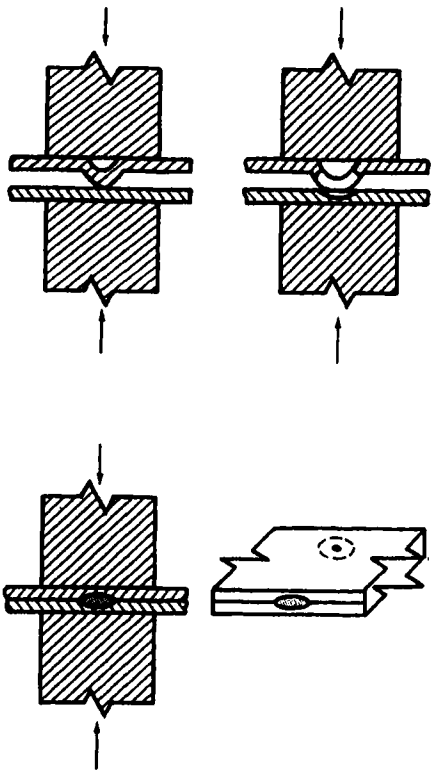


Figure 3.24 Schematic of projection welding (PW). (From *Welding Handbook,* Vol. 2: *Welding Processes,* 8th ed., edited by R. L. O'Brien, published in 1991 by and used with permission of the American Welding Society, Miami, FL.)

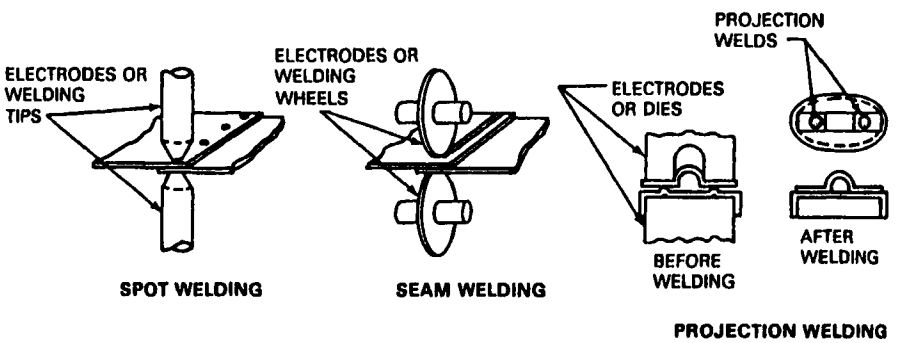


Figure 3.25 Simple schematics depicting the basic processes of spot, seam, and projection resistance welding. (From *Welding Handbook,* Vol. 2: *Welding Processes,* 8th ed., edited by R. L. O'Brien, published in 1991 by and used with permission of the American Welding Society, Miami, FL.)

to be welded are each made an electrode of opposite polarity by hooking them up into an electric circuit. As an initial gap between the two is reduced, high points on the faying surface of each begin to cause arcing, heat, soften and melt, and explode. Shortly after this point, the next highest points come into proximity and arc, heat, melt, and explode—and so on. This continues until the overall faying surfaces of parts to be joined are heated to a temperature sufficient to allow welding when a force is applied to consummate a weld. Molten metal is expelled, the hot metal is plastically upset, a weld is produced, and a "flash" of frozen expelled metal is formed.

Closely related to flash welding is *upset welding* (UW). The major differences are that the two parts to be welded are in contact from the outset of the process and the amount of gross plastic deformation or upsetting that is employed to produce the weld after suitable resistance heating of the entire joint area is much greater. Figure 3.26 shows flash welding schematically, along with a schematic of a typical flash weld, while Figure 3.27 shows upset welding and an upset weld schematically.

Percussion welding (also known as capacitor-discharge welding) produces welds through resistance heating by the rapid release of electrical energy from a storage device (e.g., capacitor). Figure 3.28 shows percussion welding schematically.

In all resistance welding processes, the rate of heating is extremely rapid, the time for which the weld is molten is extremely short, and the rate of cooling is usually rapid. This allows these processes to be used where heat input must be limited. On the other hand, resistance welding processes are capable of welding even the most refractory metals and alloys, due to the intense heating that can be made to occur (limited only by the current that can be applied, and the time for which it can be applied). High speed also allows the processes to be operated without shielding because of the combined effects of short time at temperature, limited access for air, and favorable effects of forging pressure to breakdown any oxide.

In RSW, RSEW, PW, and PEW, the presence of liquid is essential for the creation of a weld; thus, these are fusion welding processes, albeit ones that require substantial pressure. In FW and UW, on the other hand, liquid only serves to flux the faying surfaces, while forging (deformation) produces the weld, expelling virtually all of the liquid. In this sense, these two processes could be considered nonfusion pressure welding processes.

3.5. HIGH-INTENSITY RADIANT ENERGY OR HIGH-DENSITY BEAM WELDING PROCESSES

There is a group of processes that employs a source of high-intensity electromagnetic radiation to cause fusion and produce welds. The better known of these are the high-energy-density beam processes, including electron-beam and laser-beam welding. Less well known are those processes that employ a focused

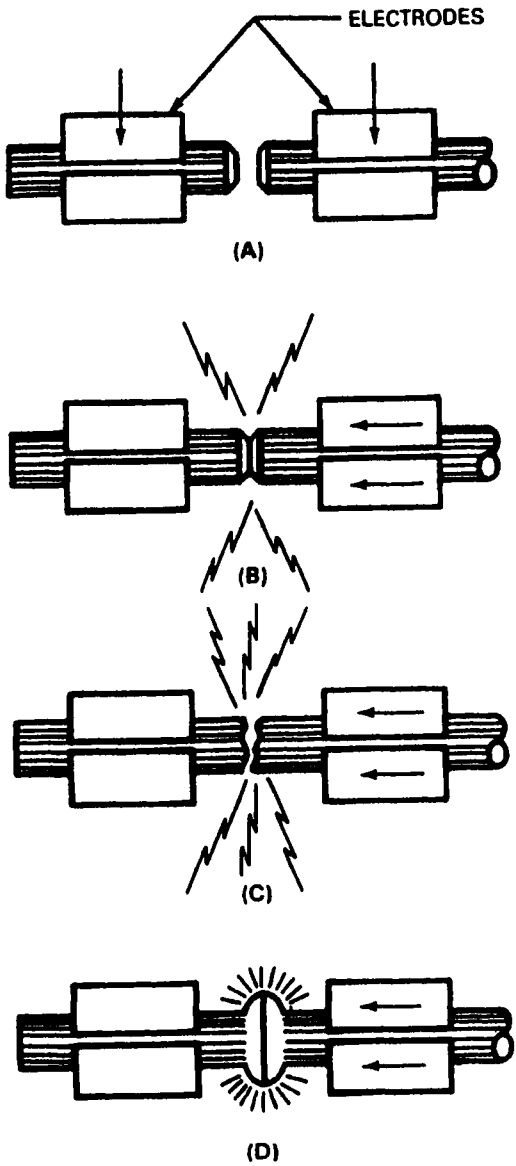


Figure 3.26 Schematic of (A through C) flash welding (FW) and a typical flash weld (D). (From *Welding Handbook,* Vol. 2: *Welding Processes,* 8th ed., edited by R. L. O'Brien, published in 1991 by and used with permission of the American Welding Society, Miami, FL.)

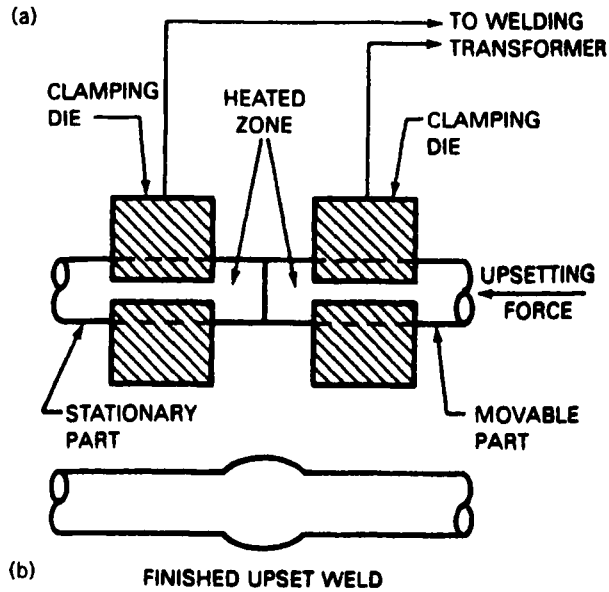


Figure 3.27 Schematic of (a) upset welding (UW) and (b) a typical upset weld. (From *Welding Handbook*, Vol. 2: *Welding Processes*, 8th ed., edited by R. L. O'Brien, published in 1991 by and used with permission of the American Welding Society, Miami, FL.).

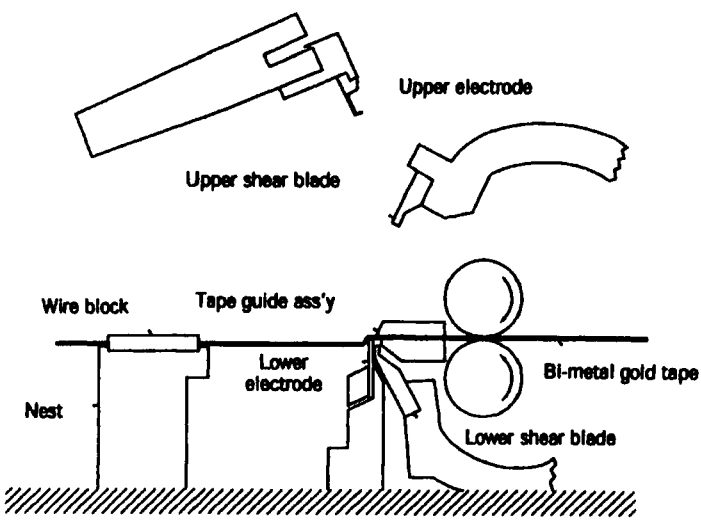


Figure 3.28 Schematic of percussion welding (PEW). (After "Principles and Practices in Contact Welding," by K. N. Petry, J. J. Buckenberger, J. E. Voytko, and D. R. Lipphart, *Welding Journal*, **49**(2), 1970, published by and used with permission of the American Welding Society, Miami, FL.)

beam of electromagnetic energy to either heat a workpiece by concentration of the irradiating energy at the point at which it is absorbed or to excite the atoms comprising the workpiece to cause heating sufficient to lead to melting and weld production. These latter processes include focused IR and imaged arc welding and microwave welding, respectively.

3.5.1. High-Energy-Density (Laser and Electron) Beam Welding Processes

Often, the density of the energy available from a heat source for welding or for cutting is more important than the total source energy (as explained in Chapter 5). The two major types of high-energy-density welding processes are (1) *electron-beam welding* (EBW) and (2) *laser-beam welding* (LBW), although a third, yet to be developed possibility is ion-beam welding. Both processes use a very high-intensity beam of electromagnetic energy as the heating source for welding; the first in the form of electrons, the second in the form of photons. The energy density in both of these processes is approximately 10^{10} to 10^{13} W/m^2 versus 5×10^6 to 5×10^8 W/m^2 for typical arc welding processes. Conversion of the kinetic energy of the electrons (in EBW) or photons (in LBW) into heat occurs as these particles strike the workpiece, leading to melting and vaporization. Both processes usually operate in this keyhole mode, so penetration can be high, producing deep, narrow, parallel-sided (high aspect) fusion zones with narrow heat-affected zones and minimal angular distortion due to nonuniform weld metal shrinkage or thermal expansion and contraction.

The *electron-beam welding* (EBW) process is almost always performed autogenously,[14] so joint fit-up, usually as straight or square butts, must be excellent. Filler metal can be added as wire for shallow EB welds or to correct underfill in deep-penetration welds to improve cosmetics. It can also be added as preplaced shim stock. Laser-beam welding is usually done autogenously also, but can employ fillers unless penetration becomes excessive. Shielding for the EBW process is provided by the vacuum (typically, 10^{-3} to 10^{-5} atm) required to allow the beam of electrons to flow to the workpiece unimpeded by collisions with molecules in air or another gaseous atmosphere. Shielding for the LBW process is accomplished with inert gases, either in dry boxes or from special shrouds over the vicinity of the weld puddle, although the process could also be performed in vacuum.

While the high-energy beam of electrons in electron-beam welding is readily absorbed and the kinetic energy is converted to heat by all materials, this is not so for an intense beam of photons in laser welding. Some materials reflect photons, or light, depending on the specularity of the particular material and the wavelength of the photons or laser light. As a result, since the efficiency of

[14] It is possible to provide filler by preplacing shim material in the point, or by laying lengths of wire or shims in an underfilled weld and rewelding with reduced energy, partial penetration to improve the cosmetics of the weld crown.

electron absorption is high, the transfer efficiency of electron-beam welding is also high, approaching 90% and greater. Since the efficiency of absorption of photons can vary, process transfer efficiency can also vary, from a low of around 10% or less for highly reflective materials (like aluminum) to upward of 90% for nonreflective and absorptive materials (like graphite). Thus, penetration capability with laser-beam welding varies greatly, depending on material, and the process can be made to operate in either a melt-in or keyhole mode as a result.

Schematics of these two processes are shown in Figure 3.29.

Electron beams are produced in what is called a gun by thermionically extracting them from a heated filament or cathode and accelerating them across a high potential achieved using one or more annular anodes along a high-vacuum column. The stream of accelerated electrons is focused into a beam of very high energy density using a series of electromagnetic coils or lenses. The electrons then pass from the column to a work chamber to the workpieces to produce a weld. A typical gun, column, and work chamber are shown schematically in Figure 3.30. More details on the physics of EB welding can be found in Section 8.5.

While virtually all electron-beam welding is performed in a vacuum to prevent disruption of the high-speed/high-energy electrons by collisions with molecules in air or another gaseous atmosphere, there are exceptions. In fact, it has long been a goal to free electron-beam welding from the confines of a vacuum to make it more practical and less expensive due to the high capital cost of vacuum chambers. There are several possibilities, each with its drawbacks and each in a fairly to completely embryonic state of development.

First, there have been attempts to weld with beams of high-energy electrons in atmosphere. This can and has been done, although the distance between the beam source or exit from the source (called an electron-beam gun) and the work must be quite short (of the order of a few centimeters) to minimize interaction between electrons and gas molecules before interaction between electrons and the workpiece. A schematic of such a nonvacuum system is shown in Figure 3.31.

Very recently, there has been discussion of the potential of electron beams operating in the relativistic range. This means, the electrons have been accelerated by tremendously high-potential fields of millions of volts to near the speed of light. In this regime, it has been reported that the beam of electrons tends to remain focused and has minimal interaction with gas molecules, allegedly as the result of some electromagnetic pinching effect resulting from ionized atoms and molecules in the air.

More practically, there have been successes in welding in what is called a "soft" (as opposed to "hard") vacuum. Soft vacuums are generally only a tenth or a hundredth of an atmosphere of pressure, and can be obtained with differential pumping systems and a series of pressure locks. Examples of such systems have been used in the automotive industry to produce hermetically tight seals in components like catalytic converters.

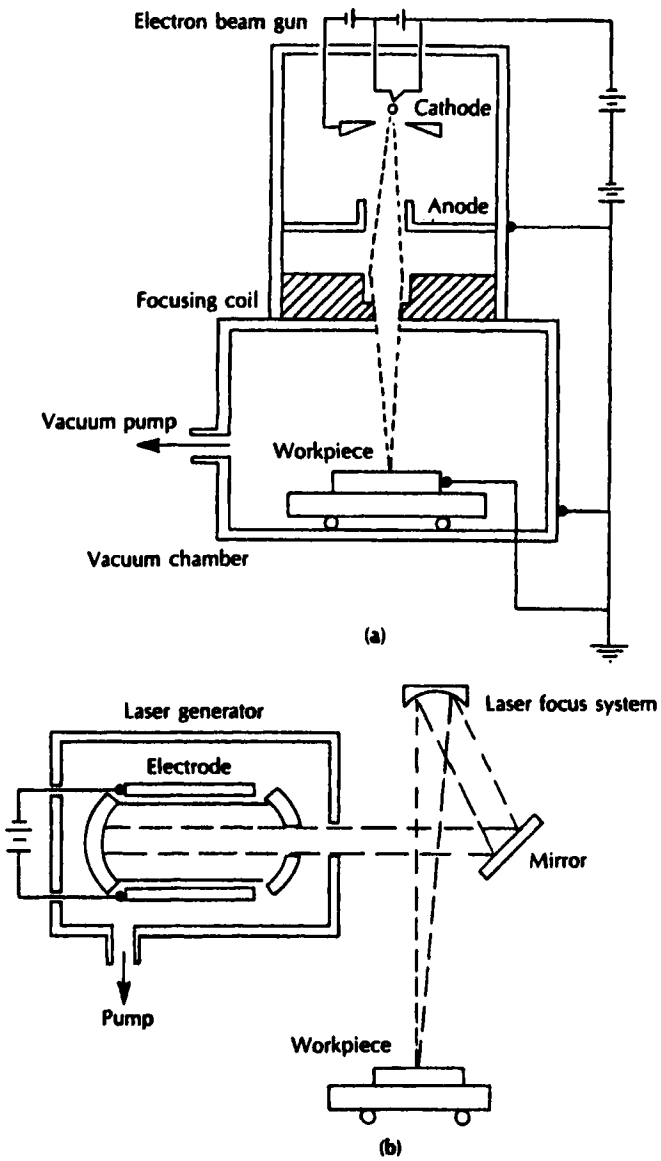


Figure 3.29 Schematic of (a) electron-beam welding (EBW) and (b) laser-beam welding (LBW) system. (From *Joining of Advanced Materials* by R. W. Messler, Jr., published in 1993 by and used with permission from Butterworth-Heinemann, Woburn, MA.)

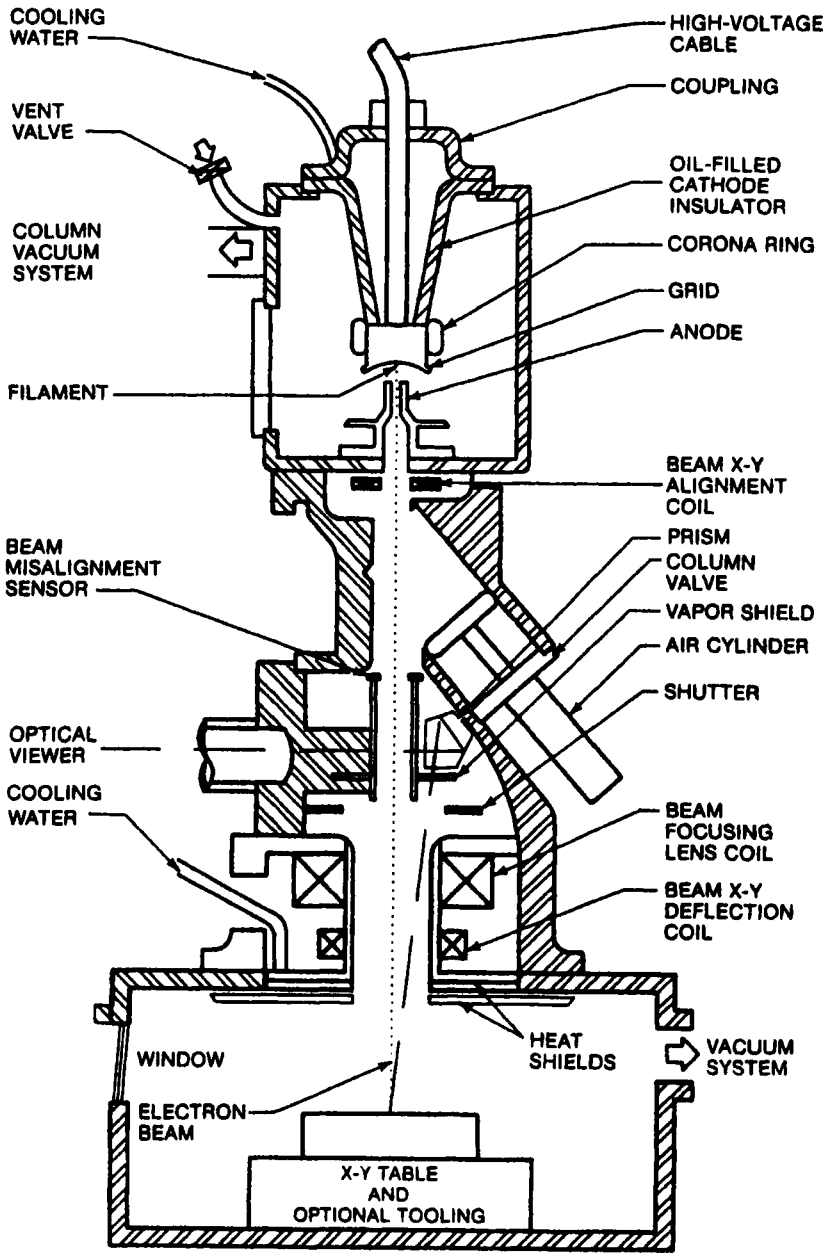


Figure 3.30 Schematic cross section of a hard-vacuum EBW gun, column, and work chamber. (From *Welding Handbook*, Vol. 2: *Welding Processes*, 8th Edition, ed., edited by R. L. O'Brien, published in 1991 by and used with permission of the American Welding Society, Miami, FL.)

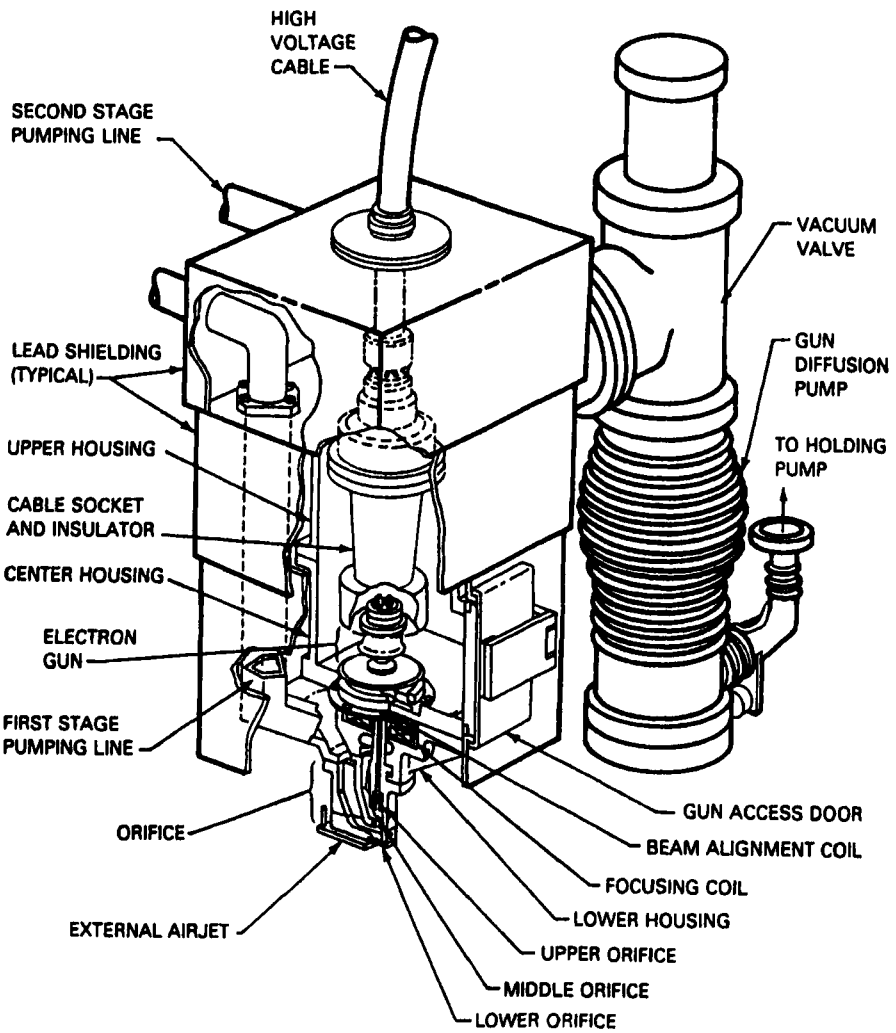


Figure 3.31 Schematic of a nonvacuum electron-beam gun column assembly. (From *Welding Handbook,* Vol. 2: *Welding Processes,* 8th ed., edited by R. L. O'Brien, published in 1991 by and used with permission of the American Welding Society, Miami, FL.)

Finally, there has been success with what are called sliding-seal electron-beam or moving-chamber systems. In SSEB, rather than bringing the work to the vacuum environment to allow electron-beam welding to be performed, the vacuum is brought to the work. This is accomplished through the use of a small vacuum chamber, shaped to fit tight up against the workpiece, with the electron-beam weld executed through a system of holes and slots often moving the chamber. An example is shown in Figure 3.32.

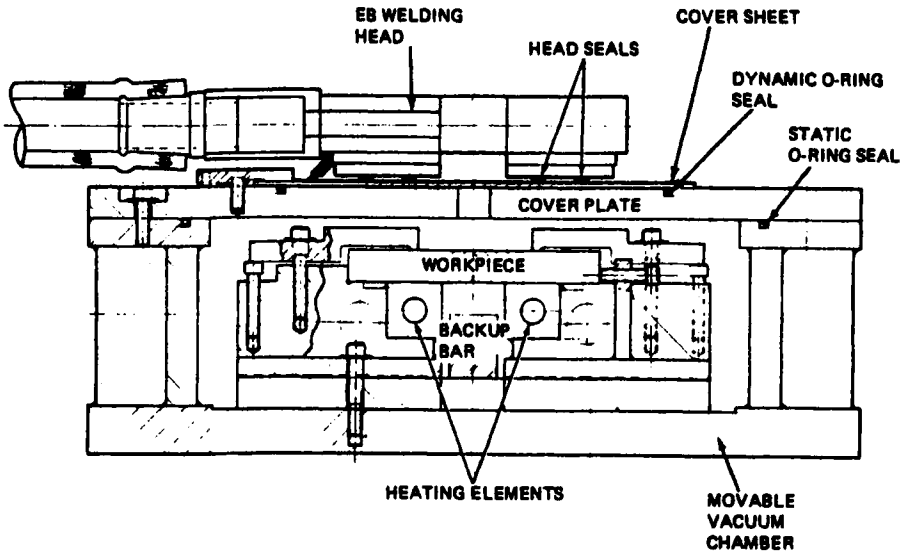


Figure 3.32 Schematic of a sliding-seal electron-beam (SSEB) welding system. (From "Sliding-Seal Electron-Beam Slot Welding of an Aircraft Wing Closure Beam," by R. W. Messler, Jr., *Welding Journal,* 60(9), published in 1981 by and used with permission of the American Welding Society, Miami, FL.)

The three basic modes of electron-beam welding, corresponding to three levels of vacuum referred to earlier, are shown schematically in Figure 3.33.

The sources for high-energy laser beams are of two types: (1) solid-state lasers and (2) gas lasers. The principal example of the former is Nd:YAG, while the principal example of the latter is CO^2. Schematics of a solid-state and a gas laser are shown in Figures 3.34 and 3.35. Without going into details here, there are three types of gas laser sources: (1) slow axial flow, (2) fast axial flow, and (3) transverse flow. Each type has its relative advantages and disadvantages, and the interested reader is referred to some excellent sources given at the end of this chapter. Schematic illustrations of each type are shown in Figure 3.35. Details of the physics of LB welding (as well as EB welding) can be found in Section 8.6 (and 8.5).

Comparative advantages and disadvantages of the two processes are given in Table 3.3. For both processes, three of the most significant advantages are (1) virtually unlimited melting power (due to the energy and energy density available in the beams); (2) precise placement of energy (due both to the fineness of the beam and the accuracy of beam focusing and delivery systems using optics or electrooptics); and (3) precise control of energy dosage (through source electronics). Both processes have also demonstrated the potential for use in outer space, to help fabricate structures there. The high depth-to-width ratio of LBW operating in the keyhole mode and, especially, EBW welds versus

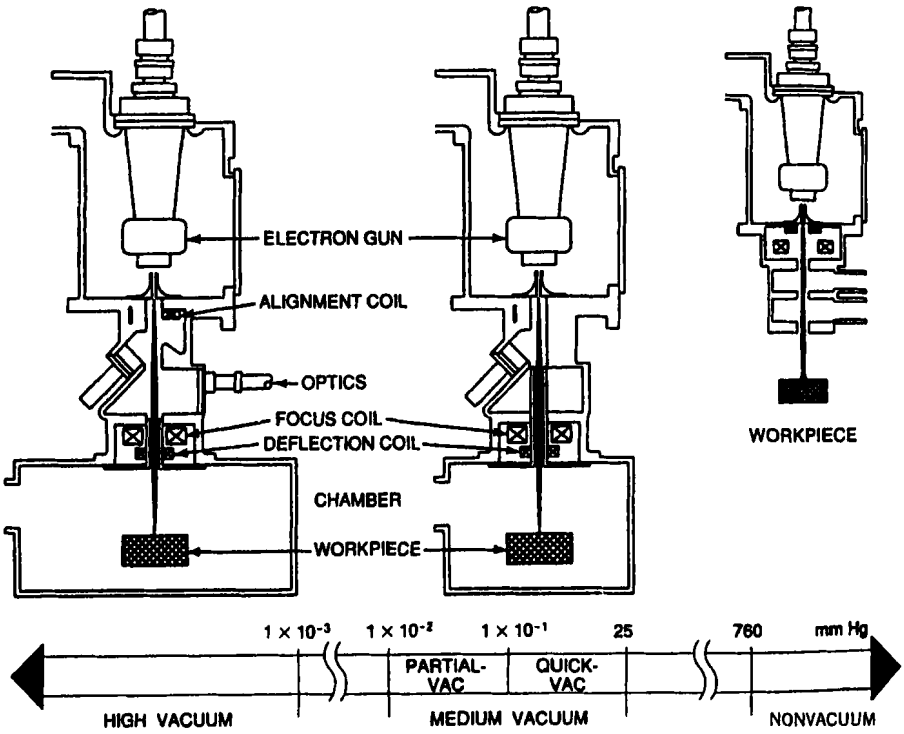


Figure 3.33 Schematic of the three basic modes of electron-beam welding, corresponding to three levels of vacuum. (From *Welding Handbook,* Vol. 2: *Welding Processes,* 8th ed., edited by R. L. O'Brien, published in 1991 by and used with permission of the American Welding Society, Miami, FL.)

welds made by conventional arc welding processes is shown schematically in Figure 3.36.

3.5.2. Focused IR and Imaged Arc Welding

Rather than using the radiation of an extremely intense beam of electromagnetic energy in the form of electrons (in EBW) or monochromatic and coherent photons (in LBW), it is possible, although much less common, to simply use focused light. The two possibilities are *focused IR* and *imaged arc welding* processes.

Infrared radiation from the sun or an artificial light source can be used to make welds provided the radiation is focused into an intense, high-density spot directed onto the work. When the sun is used, the process (although rare) is called solar welding. Artificial IR sources are often high-intensity, quartz heat lamps that produce light with a wavelength of about 1 μm. Figure 3.37 shows a focused IR system schematically.

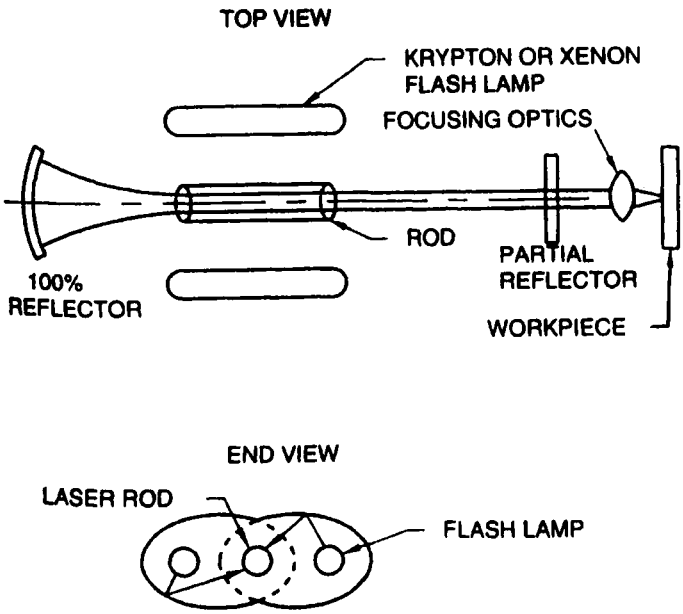


Figure 3.34 Schematic of a solid-state laser source (From *Welding Handbook,* Vol. 2: *Welding Processes,* 8th ed., edited by R. L. O'Brien, published in 1991 by and used with permission of the American Welding Society, Miami, FL.)

Because the heating power of focused IR sources is limited, the process (especially using artificial sources) is most often used to weld thermoplastic polymers, but could be used to weld low-melting point metals (e.g., Pb, Sn, and Zn or their alloys, pewter, babbitt metal, etc.). For some polymers, a through-transmission variation has been developed. Here, the IR radiation is passed through a transparent polymer to an absorbing interface. At this interface, the IR is absorbed, the interface heats and melts, and a weld is made. Xenon lamp sources have also been used for flash soldering by reflow. The principal advantage of focused IR welding is relative low cost, especially if the source is the sun. However, there are, without question, practical problems in capturing, focusing, directing, and moving the energy.

In a process known as *imaged arc* or *arc image welding*, little or no information seems to be available, and most of what is known by the author (and many others) is anecdotal. In principle, what is done is to focus a high-intensity electric arc or plasma arc using suitable optics largely relying on reflection using parabolic mirrors. The imaged arc is then directed onto the workpieces, intense heating and melting takes place, and a weld is made. An obvious and possibly useful advantage is freedom from the electromotive Lorentz forces associated with conventional arc welding, which can lead to unwanted induced currents and arc deflection (see Section 8.1) or weld pool convection (see Section 9.1.3).

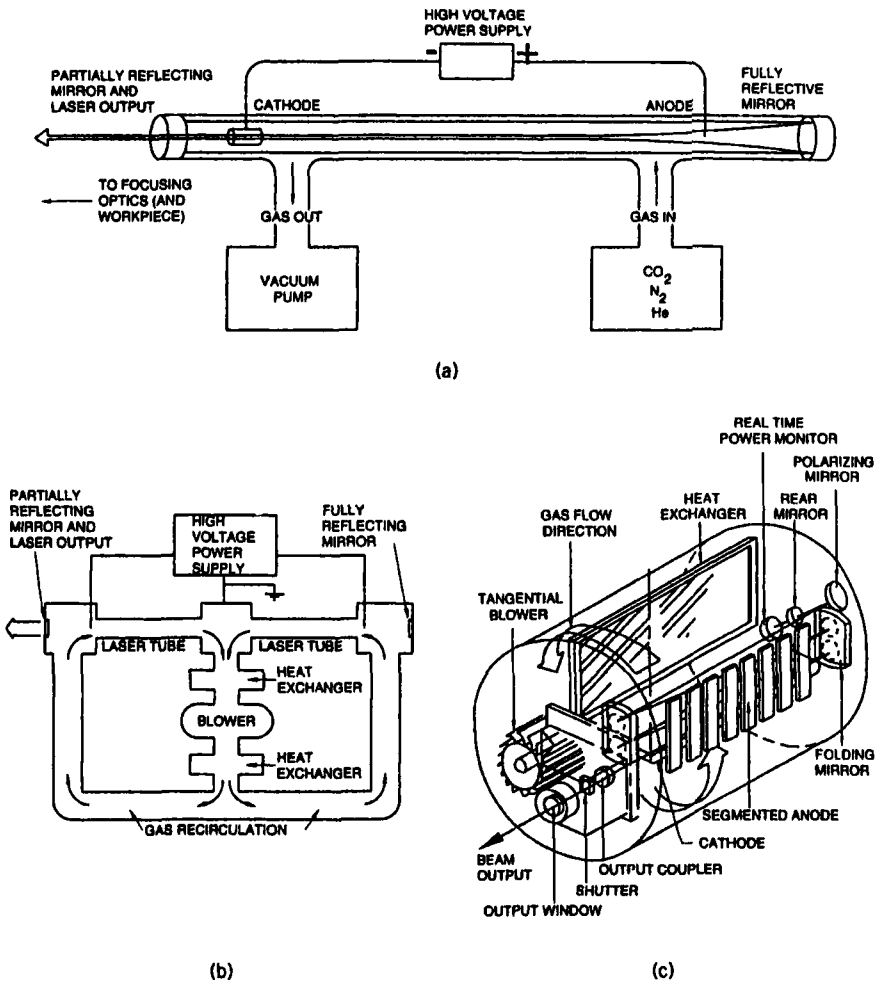


Figure 3.35 Schematic of (a) slow axial flow, (b) high axial flow, and (c) transverse flow lasers (From *Welding Handbook,* Vol. 2: *Welding Processes,* 8th ed., edited by R. L. O'Brien, published in 1991 by and used with permission of the American Welding Society, Miami, FL.)

3.5.3. Microwave Welding

The use of induction heating, as employed in some variations of resistance welding, is reserved for conductive materials (chiefly metals and alloys) in which eddy currents can be produced to generate thermal energy by Joule I^2R heating. In the case of nonconductive materials, in which direct Joule heating by induction methods is not possible, a related process called *high-frequency dielectric heating* can be used. The process is called microwave heating and can

TABLE 3.3 Comparative Advantages and Disadvantages of Electron-Beam and Laser-Beam Welding Processes

EBW	LBW
1. Deep penetration in all materials	1. Deep penetration in many materials, but *not* in metals that reflect laser light of specific wavelengths because they are specular or because their vapors are reflective
2. Very narrow welds	2. Can be narrow (in keyhole mode)
3. High energy density/low linear input heat	3. Same
4. Best in vacuum, to permit electrons to move unimpeded	4. Can operate in air, inert gas, or vacuum
5. Usually requires tight-fitting joints	5. Same
6. Difficult to add filler for deep welds, except as preplaced shim	6. Same
7. Equipment is expensive	7. Same
8. Very efficient electrically (99%)	8. Very inefficient electrically ($\sim$12%)
9. Generates x-ray radiation	9. No x-rays generated

Source: Joining of Advanced Materials by R. W. Messler, Jr., published in 1993 by and used with permission from Butterworth-Heinemann, Woburn, MA.

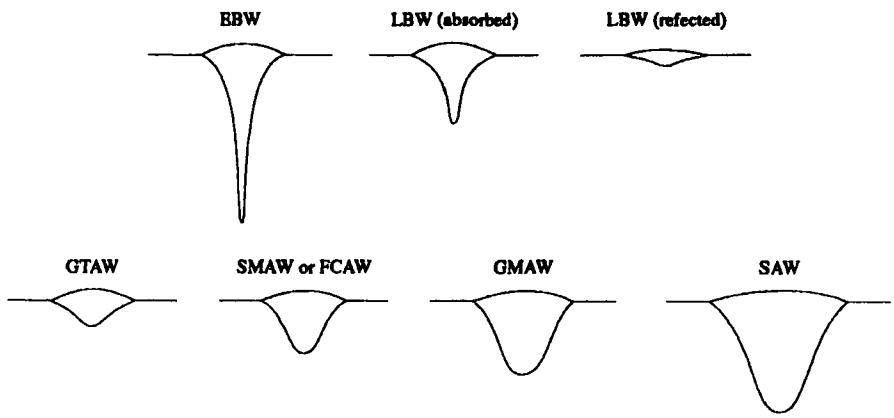
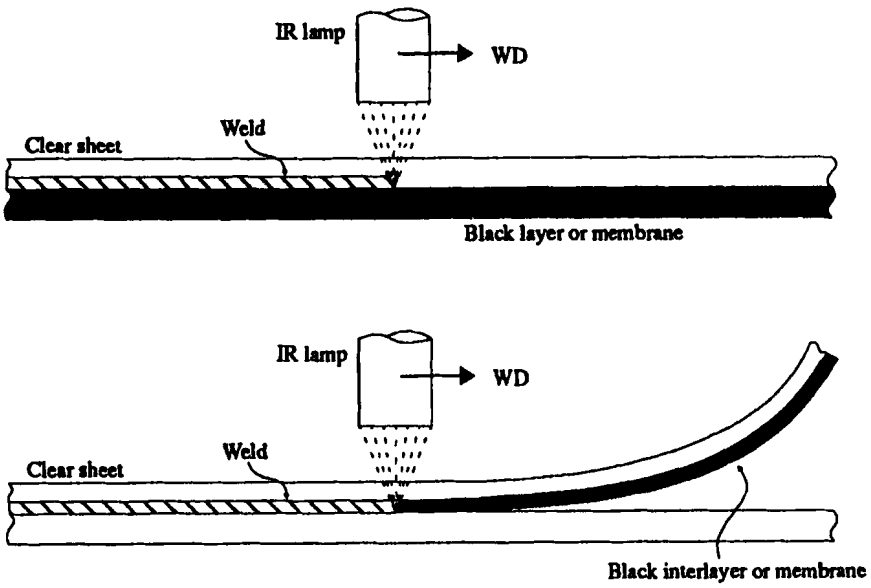
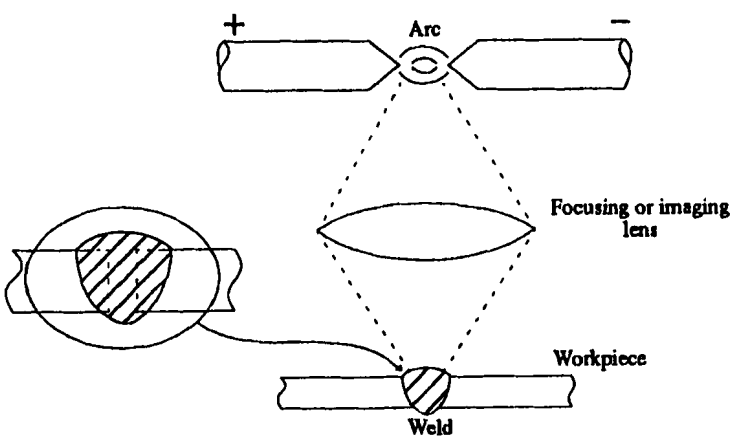


Figure 3.36 Schematic comparison of typical EB, LB, and conventional arc (e.g., GTA, GMA, SMA, FCA, or SA) welds.



(a)



(b)

Figure 3.37 Schematic of (a) the focused IR and (b) imaging-arc welding processes.

be the basis for welding, as well as brazing and soldering. Microwave heating dates back to the 1930s when it was used to vulcanize rubber (Puschner, 1966). More recently, it has been used to dry wood and textile products as well as grain and sugar.

The use of microwave electromagnetic radiation (in the frequency range of approximately 0.05–50 GHz, with some limitations, since this frequency range is shared in use for radio transmission/reception) as a means of heating materials is well known from that time-saving appliance, the microwave oven. Similar in principle, *microwave welding* uses the energy of microwaves to cause ions or polar molecules to oscillate rapidly, producing heat from inside the material. Unlike the kitchen appliance, which operates with a microwave source of several hundred watts at a frequency of 2.54 GHz, sources used for welding are capable of delivering thousands or tens of thousands of watts at frequencies from 5 to 50 GHz or more.

For there to be an interaction between the electromagnetic microwave energy and the material, the material must be composed of or at least contain either ions or polar molecules, that is, it must be a nonconducting dielectric, rather than a conductor. Thus, ceramics and polymers are normally heated and welded using microwave sources. Metals can be heated indirectly by being placed in a ceramic vessel, which is heated by the microwaves and, in turn, heats the metal by conduction.

Two types of microwave generators are employed: (1) magnetron sources and (2) klystron tube sources. Both sources employ a waveguide to direct the field energy. The magnetron source is capable of frequencies up to 1 GHz and power levels up to hundreds of kilowatts, with power capability decreasing with increasing frequency. Magnetrons are the preferred source for industrial applications of microwave energy. Klystrons are used to generate microwaves at higher frequencies. Waveguides are used as "horns" to direct the microwave energy from the source to the target workpiece(s). While simple in geometry (usually just rectangular tubes), the dimensions are precisely controlled to prevent unwanted attenuation of the microwaves from the source on their way to the target.

Research has shown that several different ceramics can be welded by heating to above or near the point of melting. A key to the microwave welding process is achieving coupling between the microwave energy and the material. What is meant here is that different materials absorb microwave (MW) energy to a greater or lesser extent, depending on (1) the materials character (whether it is composed of ions or polar molecules, and what ones); (2) the frequency of the MW energy (due to loss factor effects); and (3) the temperature of the material being irradiated (with absorption increasing with increasing temperature). To produce a weld between two pieces of ceramic of similar or different type and/or composition, the interface is often packed with a mixture of the ceramics in powdered form along with powdered glass or frit. This mixture tends to preferentially absorb the MW energy, and thus preferentially heat, and soften or melt.

Microwave welding is, for the most part, in an embryonic state, except as it is being used for welding plastics. The process has tremendous potential, however, for hard-to-weld ceramics.

Figure 3.38 shows schematically how microwave welding occurs.

3.6. SUMMARY

A large number of very diverse processes are dependent on melting a portion of the substrate(s) followed by solidification to cause metallic continuity to produce a weld. These are collectively called fusion welding processes. Major groups include (1) processes employing a chemical energy source, including (a) gas welding employing a combustible fuel as the source of heat, or (b) an exothermic solid-phase (aluminothermic) reaction as the source of heat; (2) processes employing an electric arc as the energy source, including arcs between (a) a nonconsumable electrode as a source of heat, or (b) a consumable electrode, as a source of both heat and filler metal; (3) processes that develop heat by internal resistance or Joule heating of the workpiece, whether

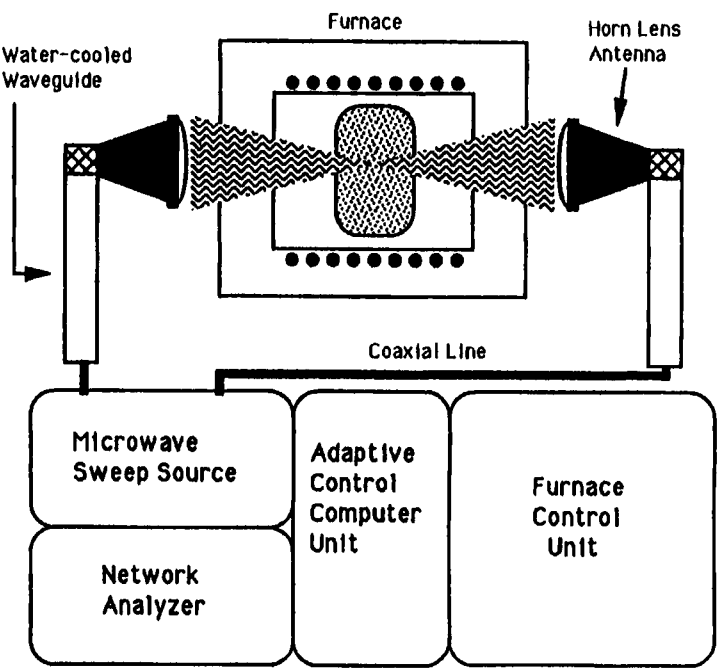


Figure 3.38 Schematic of a microwave welding system. (From *In Situ Monitoring of Porosity in Alumina During Sintering Using Ultrasonic and Microwave Energy,* Thesis, P. Komarenko, May 1992, Rensselaer Polytechnic Institute, Troy, NY, with permission.)

as the result of direct current flow in a circuit or currents induced in a part; and (4) processes that develop heat from a high-intensity radiant energy or beam source through the conversion of the kinetic energy of fast-moving particles in that irradiating beam.

The diversity of types is the reason fusion welding processes predominate in the fabrication of weldments as well as the overlaying, cladding, or hardfacing of parts, in both number of applications and tonnage of product produced.

REFERENCES AND SUGGESTED READINGS

Hlavacek, V., 1991, "Combustion synthesis: a historical perspective," *Ceramic Bulletin*, **70**, 240–246.

Merzhanov, A. G., Skhiro, V. M., and Borovinskaja, P., 1972, "Self-propagating high-temperature synthesis of refractory inorganic compounds," USSR Pat. No. 255,221, *Dokl. Akad. Nauk. SSSR*, **204**, 366–371.

Messler, R. W., Jr., 1981, "Sliding-seal electron-beam slot welding of an aircraft wing closure beam," *Welding Journal*, **60**(9), 31–39.

Messler, R. W., Jr., 1993, *Joining of Advanced Materials*, Butterworth-Heinemann, Woburn, MA.

Puschner, H., 1966, *Heating With Microwaves*, Springer, New York.

Suggested readings [by process]

Arata, Y., 1986, *Plasma, Electron and Laser Beam Technology*, ASM, Metals Park, OH. [PAW, EBW, and LBW].

Cary, H. B., 1994, *Modern Welding Technology*, 3d ed., Prentice Hall, Englewood Cliffs, NJ. [Variety of processes].

Dawes, C., 1992, *Laser Welding*, McGraw-Hill, Cambridge, UK. [LBW].

Grimm, R. A., 1996, "Welding processes for plastics," Edison Joining Technology Center, Edison Welding Institute, Columbus, OH. [Processes for plastics].

Hone, P., 1988, "Magnetically impelled arc butt (MIAB) welding: developments and applications," AWS Detroit Section *Proceedings of the Sheet Metal Welding Conference III*, Detroit, MI, 25–27 October, 1988. [MIAB welding].

OBrien, R. L. (Editor), 1991, *AWS Welding Handbook, Vol. 2: Welding Processes*, 8th ed., American Welding Society, Miami, FL. [Variety of processes].

Resistance Welding Manual, 1990, 4th ed., American Welding Society, Miami, FL. [Resistance welding processes].

Schultz, H., 1993, *Electron Beam Welding*, Abington, Cambridge, UK. [EBW].

Submerged-Arc Welding, 1989, Abington, Cambridge, UK. [SAW].

TIG and Plasma Arc, 1990, Abington, Cambridge, UK. [GTAW and PAW].

CHAPTER 4

NONFUSION WELDING PROCESSES

4.1. GENERAL DESCRIPTION OF NONFUSION PROCESSES

Nonfusion welding processes accomplish welding by bringing the atoms (or ions or molecules) of the materials to be joined to equilibrium spacing principally, but not exclusively, through plastic deformation due to the application of pressure at temperatures below the melting point of the base material(s) and without the addition of any filler that melts. Chemical bonds are then formed and a weld is produced as a direct result of the continuity obtained, always with the added assistance of solid-state diffusion. Often some heat is generated by or supplied to the process to allow plastic deformation to occur at lower stresses and to accelerate interdiffusion without causing or, at least, depending on melting (which, in the context of welding, constitutes fusion); hence the name nonfusion processes. The key feature of all nonfusion welding processes is that *welds can be produced without the need for melting or fusion.*

The three principal ways in which nonfusion welding is made to occur are (1) by pressure and gross deformation, in what is called *pressure welding*; (2) by friction and microscopic deformation, called *friction welding*; and (3) by diffusion, without or with some deformation, called *diffusion welding.* A fourth way is beginning to receive attention, namely processes that rely on solid-phase deposition, whether from an electrochemical reaction or vapor condensation, in what is called *solid-state deposition welding.* It is important to note that solid-phase diffusion (actually interdiffusion) between base materials or base materials and occasionally an intermediate is always involved in nonfusion welding, as it is to some degree in all welding processes, depending on temperature. Subclassification by the four methods just given simply refers to the predominant means of obtaining material continuity, with the fourth,

electro- or vapor deposition, just beginning to emerge as welding process embodiments.

While other sources of energy are possible (such as chemical reactions), mechanical energy is the most common and includes pressure sources and friction sources.[1] Both produce heat along with gross material transport as the result of the work done in causing deformation, but on a macroscopic scale for the pressure processes and on a microscopic scale for the friction processes. With chemical sources, bonds are formed in the solid state as the result of a chemical reaction. No deformation, either macroscopic or microscopic, is necessary. Examples are the aforementioned vapor deposition process and an electrochemical deposition process. While electrical sources could be used as a source for energy during nonfusion welding, most of the time the heat generated would (or could) cause melting, so the process would (or could) be occurring by fusion. An exception is when resistance is used to heat workpieces to the point at which they plastically soften, are squeezed together to obtain continuity, and diffusion weld together under the influence of the resistance heating (see Section 4.4.1.3).

There are eight major nonfusion welding processes: (1) cold welding, (2) hot pressure welding (using either pressure gas or forging); (3) roll (pressure) welding (hot, warm, or even cold); (4) explosion welding (which appears cold, but locally is occurring hot), (5) friction welding (using any of several types of motion), (6) ultrasonic welding (which is really friction welding with motion on a very small scale), (7) diffusion welding and diffusion brazing, and (8) deposition processes (using electrochemical reactions or vapor condensation). These are listed in Table 4.1.

Cold welding, hot pressure gas welding, forge welding, roll welding, and explosion welding all rely on substantial pressure to cause gross or macroscopic plastic deformation to produce a weld. Friction and, especially, ultrasonic welding rely on friction to cause heating and bring atoms or molecules together by microscopic plastic deformation to produce a weld. Diffusion welding relies on heating to accelerate diffusion to produce welds through mass transport in the solid state, with pressure sometimes playing a relatively minor role. Deposition processes rely on solid-phase diffusion once one material has been deposited onto another. No pressure is involved or required.

Nonfusion welding processes, as a group, offer several advantages over fusion processes. The general absence of melting and, typically, the low heat involved, minimally disrupt the microstructure of the materials being joined. As shown in Figure 2.2, there is no fusion zone and, usually, a minimal heat-affected zone in nonfusion welds. By precluding the need for melting, intermixing of the materials involved in the joint is minimal on a macroscopic

[1] Naturally, friction processes also involve pressure, since the force of friction arises from the product of the applied normal force and the coefficient of friction, $F = \mu N$. The coefficient of friction, μ, in turn, is determined by the state of the surface, which includes roughness and atomic cleanliness (i.e., freedom from oxide or tarnish or other contamination), as well as the presence of any lubricant.

TABLE 4.1 List of the Eight Major Nonfusion Welding Processes With Variations Within Each

1. Cold welding (CW)
    - Press welding
    - Forge welding
    - Roll welding
    - Toggle welding
    - Hydrostatic impulse welding
    - Shock-wave impulse welding
2. Hot pressure welding (HPW)
    - Pressure gas welding (PGW)
    - Forge welding (FOW)
3. Roll pressure welding (ROW)
    - Hot, warm, or cold roll welding
4. Explosion welding (EXW)
5. Friction welding (FRW)
    - Radial friction welding
    - Orbital friction welding
    - Rotational friction welding
        - Direct-drive welding
        - Inertia welding
    - Angular (reciprocating) friction welding
    - Linear (reciprocating) friction (or vibration) welding
    - Friction stir welding
    - Friction surfacing
6. Ultrasonic welding (USW)
    - Spot, ring, line, and seam USW
    - Microminiature welding
    - Microminiature thermosonic welding
7. Diffusion welding (DFW)
    - Conventional diffusion welding
    - Deformation diffusion welding
    - Resistance diffusion welding
    - Continuous seam diffusion welding (CSDW)
    - Diffusion brazing (DFB)
    - Combined forming/welding
        - Creep isostatic pressing (CRISP)
        - Superplastic forming/diffusion bonding (SPF/DB)
8. Solid-state deposition welding
    - Electrochemical deposition
    - Vapor deposition
    - Chemical vapor deposition
    - Chemical reaction bounding

TABLE 4.2 Relative Advantages and Shortcomings of Nonfusion Welding Processes

Advantages	Shortcomings
1. General absence of melting and, thus, solidification (so, structure is retained)	1. Stringent requirements for cleaning joint faying surfaces for some processes (e.g., CW, ROW, HPW, DFW, and solid-state deposition welding)
2. Low heat input (minimally disrupts microstructure)	2. Elaborate tooling is required for some processes (e.g., DFW)
3. Wide variety of process embodiments	3. Challenging inspection of joint quality
4. Applicable to many materials within a class as well as between classes (since there is little or no intermixing)	4. Repairing process-induced defects is difficult to impossible
5. High joint efficiency is possible for many situations where the same cannot be said for fusion welding processes	5. Processes require specialized equipment are rarely portable, and almost always must be automated

scale, so materials of dissimilar compositions can often be joined. Nonfusion processes are thus ideal for joining dissimilar materials, even from different basic classes or of totally different basic types, that would otherwise be chemically incompatible. A principal example is ceramic-to-metal joining, or, as some authors incorrectly call it, "welding." The joint resulting from nonfusion welding typically is of very high efficiency. In fact, only a nonfusion process could ever produce a "perfect" weld; indistinguishable from the base material(s) in structure and properties. Process disadvantages relate to the surface preparation and tooling required to produce acceptable joints and difficulties associated with inspecting and repairing defective joints. Relative advantages and shortcomings of nonfusion welding processes, as a group, are listed in Table 4.2.

Let's now look at the major subcategories and specific processes.

4.2. PRESSURE (NONFUSION) WELDING PROCESSES

As the name implies, nonfusion *pressure welding processes* primarily depend on the application of significant pressure to obtain metallic continuity and produce welds. Pressure processes can be performed cold or hot, so the first major subdivisions are *cold welding* and *hot pressure welding* processes. However, there are also processes that depend on rolling (from pressure rolls) or explosions (from explosives) for the pressure needed to obtain metallic continuity. The former can be performed hot or cold, while the latter are said

to occur cold, but really rely on heat that is highly localized at the joint interface arising from highly localized high-strain-rate plastic deformation and friction heating by violently expelled air.

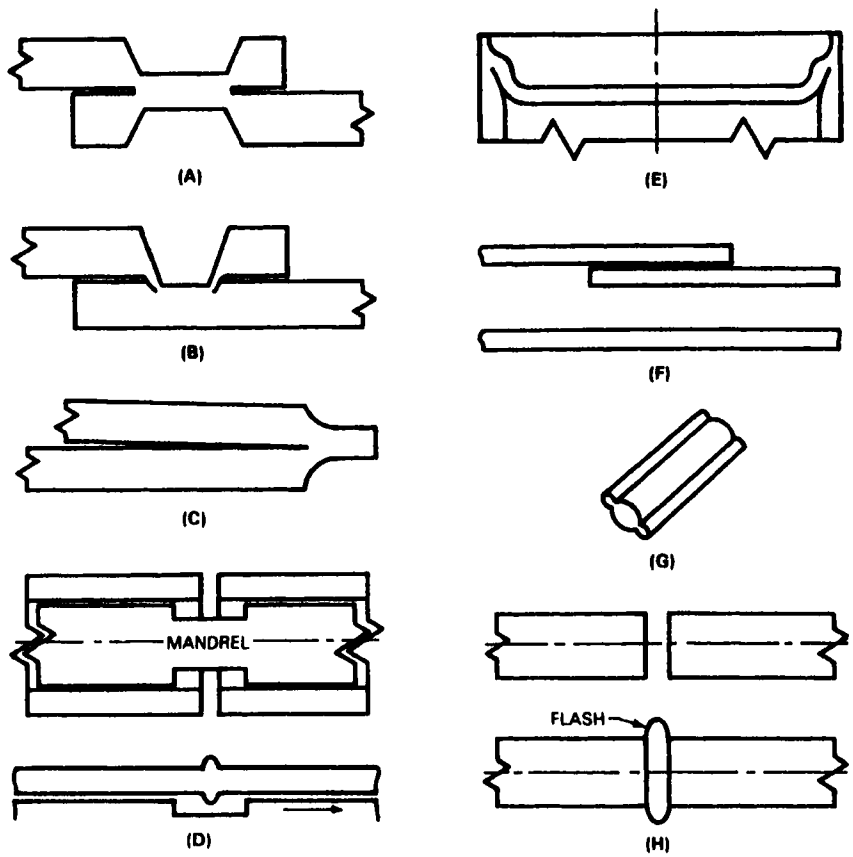
4.2.1. Cold Welding Processes

According to the American Welding Society (AWS), "Cold welding (CW) is a solid-state process in which pressure is used at room temperature to produce coalescence of metals with substantial plastic deformation at the weld." As a subgroup, cold welding processes are characterized by a notable absence of heat, whether applied from an external source or generated internal to the process itself. To achieve the required plastic deformation, at least one of the metals to be joined must be highly ductile and not exhibit extreme work hardening. Given this requirement, face-centered cubic (fcc) metals and alloys are best suited to cold welding. Prime examples of materials that are easily cold-welded are Al, Cu, and Pb, and, to a lesser degree, Ni and soft alloys of these metals such as brasses, bronzes, babbitt metals, and pewter. The precious metals, Au, Ag, Pd, and Pt, are also ideally suited to cold welding, as they are face-centered cubic (soft) and are almost free of oxides that can interfere with obtaining needed metallic continuity. (Recall, cold welding of precious metals is the oldest known welding process, as mentioned in Chapter 2.)

Cold welding is ideally suited to the joining of dissimilar metals since no intermixing of the base metals is required or obtained. This allows inherent chemical incompatibilities that would prevent or make fusion welding difficult to be overcome. The best example is the cold welding of relatively pure aluminum to relatively pure copper to produce electrical connections. Of course, there is the possibility that brittle intermetallics (e.g., Al_2Cu) will form later, either during postweld heat treatment or in service, say by resistance heating in the electrical connector.

Typical joint configurations for producing cold welds are shown in Figure 4.1. Note that every configuration is designed to allow or facilitate significant plastic deformation either in butts or laps. Typical lap weld indentor configurations used in cold welding are shown in Figure 4.2. The power for producing deformation may be applied by mechanical or hydraulic presses, rolls (as in roll welding, Section 4.2.3), or special tools (e.g., hand-operated toggle cutters). An impulse from a hydraulic or electrical source (e.g., capacitor discharge) can also be employed to force material together to effect a weld. Regardless of the method by which pressure is applied and metal is deformed, successful cold welding requires clean metal faces in contact to allow metallic continuity to be obtained. Cleaning can be accomplished mechanically using brushes or abrasives or chemically using acidic or alkaline etchants or pickling solutions, or using both methods.

Applications for cold welding are quite limited, largely by the requirement of stringent cleanliness, which is not easy to obtain in production environments. Nonetheless, when freedom from heat effects is critical, cold welding is obviously the best choice.



(A) LAP WELD, BOTH SIDES INDENTED; (B) LAP WELD, ONE SIDE INDENTED; (C) EDGE WELD, BOTH SIDES INDENTED; (D) BUTT JOINT IN TUBING, BEFORE AND AFTER WELDING; (E) DRAW WELD; (F) LAPPED WIRE, BEFORE AND AFTER WELDING; (G) MASH CAP JOINT; (H) BUTT JOINT IN SOLID STOCK, BEFORE AND AFTER WELDING.

Figure 4.1 Schematic of typical joints for producing cold welds. (From *Welding Handbook*, Vol. 2: *Welding Processes*, 8th ed., edited by R. L. O'Brien, published in 1991 by and used with permission of the American Welding Society, Miami, FL.)

4.2.2. Hot Pressure Welding

According to the AWS, "Hot pressure welding (HPW) is a solid-state welding process that produces coalescence of metals with heat and application of pressure sufficient to produce macroscopic deformation of workpieces." Vacuum or other shielding may be used to prevent severe oxidation contamination, which would interfere with obtaining metallic continuity. The two major embodiments of hot pressure welding are (1) pressure gas welding and (2) forge welding.

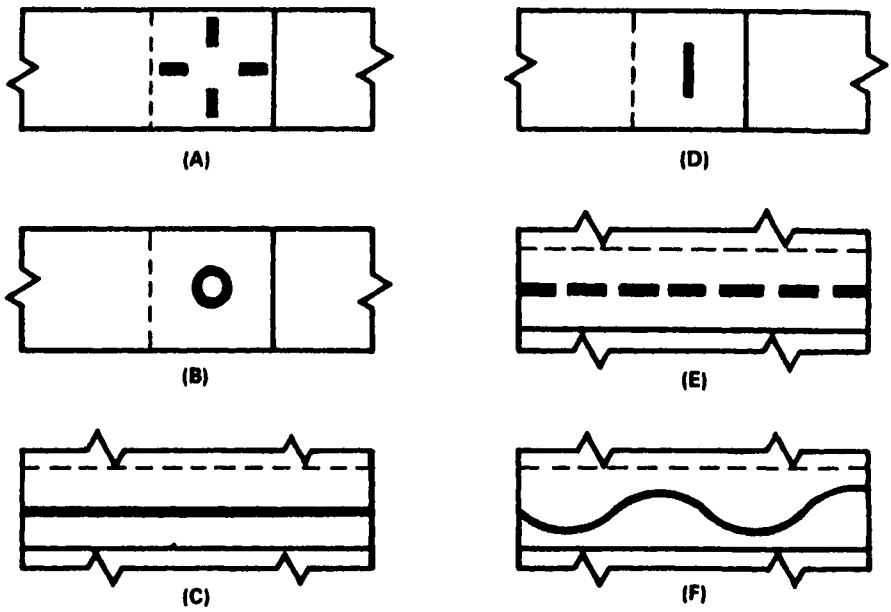


Figure 4.2 Schematic of typical lap joint weld indentor configurations used in cold welding. (From *Welding Handbook*, Vol. 2: *Welding Processes*, 8th ed., edited by R. L. O'Brien, published in 1991 by and used with permission of the American Welding Society, Miami, FL.)

4.2.2.1. Pressure Gas Welding. *Pressure gas welding* (*PGW*) employs oxy-fuel gas welding to heat faying surfaces at the same time pressure is applied to force the parts together to produce a solid-state weld. Two subforms are the (a) *closed joint* and (b) *open joint* methods. In the closed joint method, the faces of parts to be joined are tightly abutted, then heated under the simultaneous application of moderate pressure to cause a predetermined degree of upsetting and welding. In the open joint method, the faces of parts to be joined are heated while separated, and then are brought together under pressure to cause upsetting and welding. To achieve the level and consistency of heating needed at the joint, along with the pressure needed to force the parts together, the pressure gas welding process is always automated or, more properly, mechanized.

Typical joint designs for pressure gas welding are shown in Figure 4.3. Metals welded by this process include low- and high-carbon steels, low-alloy steels, stainless steels, and nickel–copper Monels. Upset pressures typically range from 3 to 10 ksi (20 to 70 MPa).

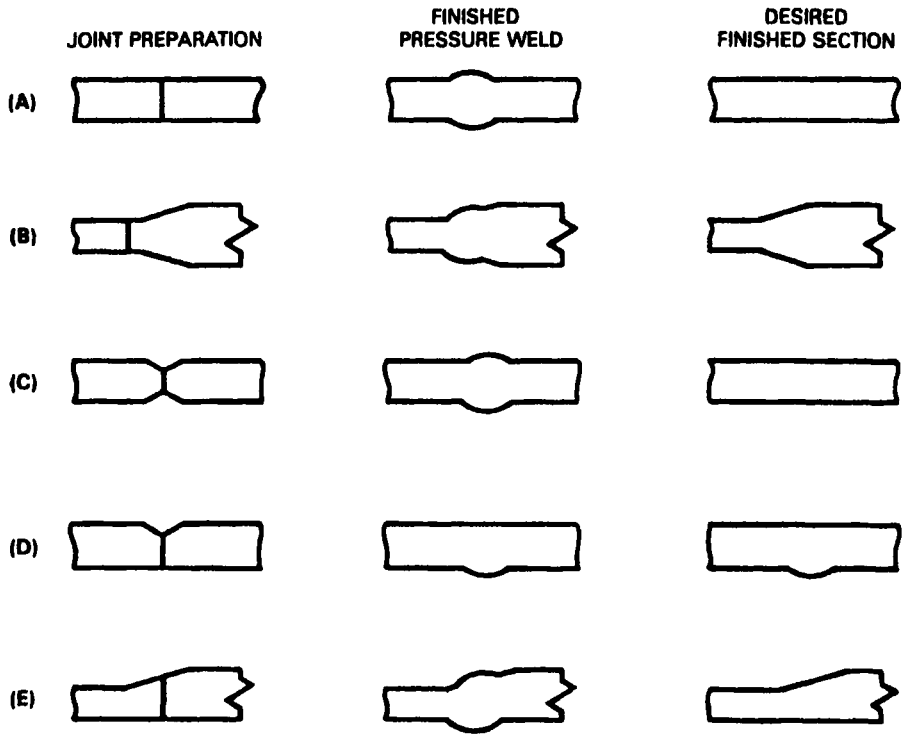


Figure 4.3 Schematic of typical joint designs for pressure gas welding. (From *Welding Handbook*, Vol. 2: *Welding Processes*, 8th ed., edited by R. L. O'Brien, published in 1991 by and used with permission of the American Welding Society, Miami, FL.)

4.2.2.2. Forge Welding. According to the AWS, "*Forge welding* (FOW) is a solid-state welding process that produces a weld by heating workpieces to welding [hot working] temperatures and applying blows sufficient to cause deformation at the faying surfaces." Without question, forge welding was the earliest form of welding, and is still used today by blacksmiths, among others. The well-known and highly regarded Damascus steel swords made by ancient Syrians are an excellent example of ancient forge welding, while hand-forged chains and wrought-iron products are good examples of modern forge welding by blacksmiths.

Parts to be forge welded can be heated in an actual forge or forging press, or in a furnace or by other means until malleable. These heated parts are removed from the heating source, placed in contact (usually by overlapping), and forced together by either repeated blows or by continuous pressure. The former process variant is called *hammer welding*; the latter is called *die welding*, because it usually takes place in a die to maintain the part/joint shape. Typical joint designs for manual and automated forge welding are shown schematically in Figure 4.4a and b, respectively.

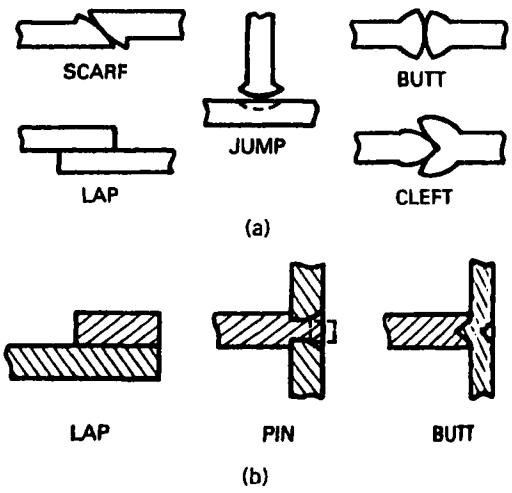


Figure 4.4 Schematic of typical joint designs for (a) manual and (b) automated forge welding. (From *Welding Handbook*, Vol. 2: *Welding Processes*, 8th ed., edited by R. L. O'Brien, published in 1991 by and used with permission of the American Welding Society, Miami, FL.)

Among metals that can be forge welded are low-carbon steels (which is by far the most commonly forge-welded metal), high-carbon steel, and aluminum alloys in extruded forms. (The latter is being looked at as one means of joining aluminum alloy extrusions to produce space frames for aluminum-intensive automobiles. Hydraulically or electrically-induced impulses and/or shockwaves are used to produce these welds.) To facilitate bonding during forge welding, fluxes are often used, the most common being borax and fine silica sand, singly or in combination.

4.2.3. Roll Welding

In *roll welding* (ROW), one workpiece, usually in plate or sheet form, is caused to form primary chemical bonds and welds with another by having large numbers of atoms brought into continuity by deforming the two pieces using pressure from squeezing rolls or rollers. While the process can be performed cold or hot, it is almost always performed hot to reduce the power required and to preclude work hardening by relying on dynamic recrystallization. In fact, it is recrystallization that causes nucleation of new grains at the original interface and growth across that interface to produce a high-quality weld (see Section 2.2).

A well-known example of roll welding is the production of clad metals such as those used in the manufacture of copper-bottomed steel or stainless steel pots and pans (e.g., Revereware). It turns out, there are a number of applications that require clad metals for obtaining required properties, one popular one being to clad pure copper onto structural steel to enable the fabrication of tanks used in electrochemical processing (e.g., plating or dissociation).

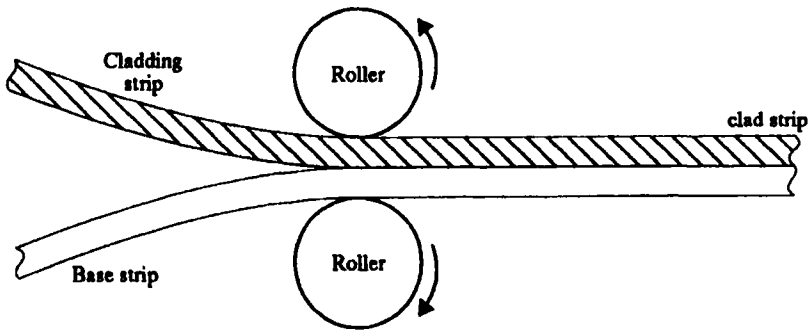


Figure 4.5 Schematic of a typical roll welding process producing clad metals.

Figure 4.5 schematically shows a typical roll welding process being used to produce clad metals.

4.2.4. Explosion Welding

Explosion welding (*EXW*) is a pressure-welding process that represents a special case. In explosion welding, the workpieces usually start out cold but heat significantly and extremely rapidly very locally at their faying surfaces during the production of the actual weld. As shown in Figure 4.6, the controlled detonation of a properly placed and shaped explosive charge causes the properly aligned workpieces (Figure 4.6a) to come together extremely rapidly at a low contact angle (Figure 4.6b). When this occurs, air between the workpieces is squeezed out at supersonic velocities. The resulting jet cleans the surfaces of oxides and causes very localized but rapid heating to high temperatures. Additional heating occurs as the result of high-strain-rate deformation in the immediate vicinity of the impacting pieces. The result of clean atoms coming together in large numbers is a metallurgical bond or weld. The weld bondline of explosion welds is typically very distorted locally, as shown in Figure 4.6b, reflecting severe but highly localized plastic deformation.

While not widely practiced because of the obvious requirement for intimate and highly specialized knowledge of explosives and their effects, explosion welding can provide some unique capabilities. Very heavy-section parts can be welded together, and over large surface areas, if required. Producing such welds would be virtually impossible by other means. Explosion welding is employed in the production of heavy-clad thick plates for use where heat, oxidation, corrosion, or wear resistance is needed, examples being AISI 304 clad to mild steel, and commercially pure (CP) titanium clad to mild steel. It is often performed under water to enhance the shock wave to move and deform material.

Explosion welding also has special value for producing transition joints for subsequent use in fusion welding two incompatible metals or alloys that cannot be directly welded. In such situations, explosion-welded combinations of two metals that are compatible with each substrate (i.e., one layer in the clad pair

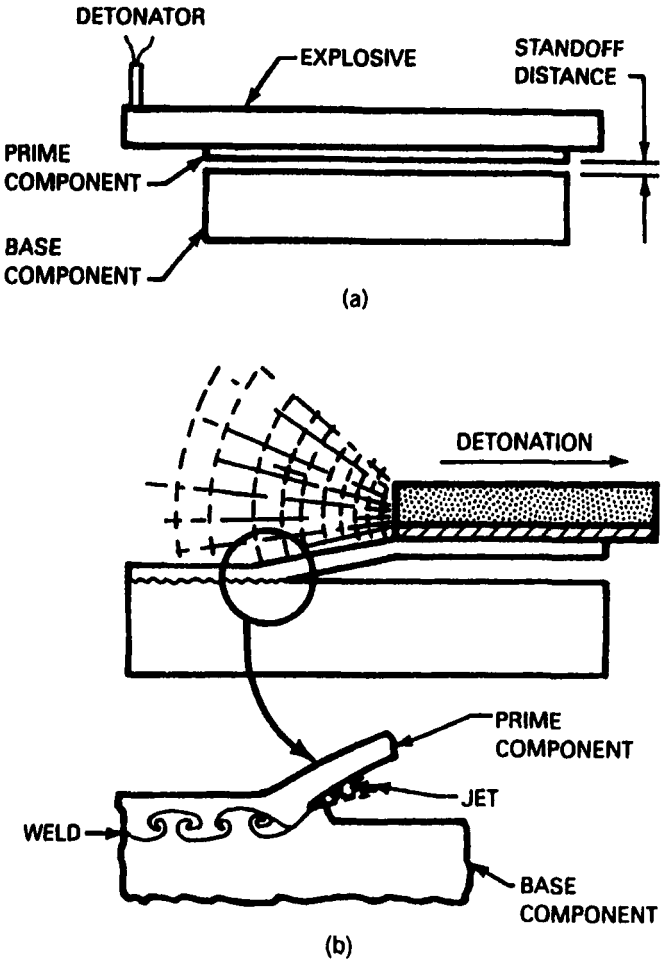


Figure 4.6 Schematic of explosion welding showing (a) typical component arrangement and (b) the action between components during welding. Note the turbulence that occurs at the interface to cause intermixing. (From *Welding Handbook*, Vol. 2: *Welding Processes*, 8th ed., edited by R. L. O'Brien, published in 1991 by and used with permission of the American Welding Society, Miami, FL.)

to one substrate, the other layer to the other substrate) make up the transition piece, and the transition piece is then welded by conventional means (usually using a fusion process) to each substrate. The transition piece acts as a bridging member. Examples are Cu-steel, Cu-stainless steel, Cu-Al, and Al-steel. The latter are occasionally used to allow automobile body parts made from aluminum alloy to be resistance spot welded to parts made from steel.

Figure 4.7 shows that a large number of commercially significant pure metals and alloys can be joined by explosion welding.

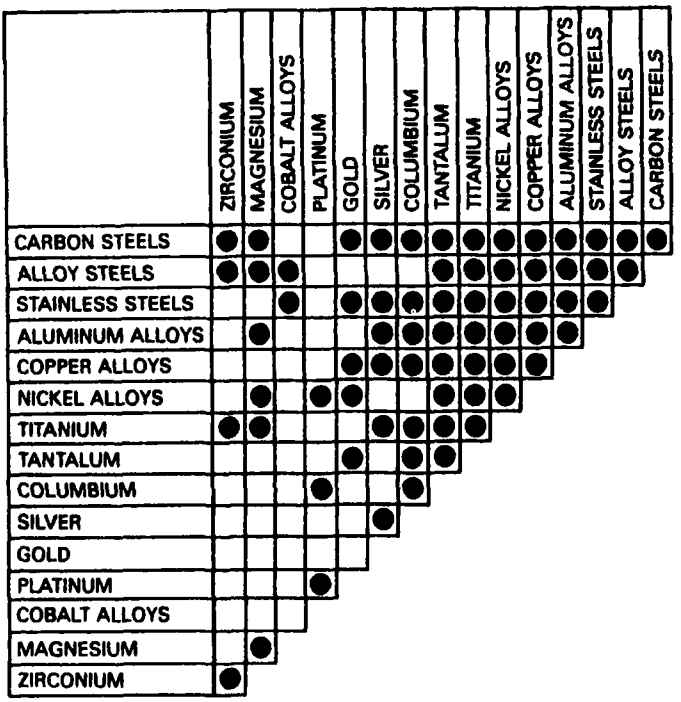


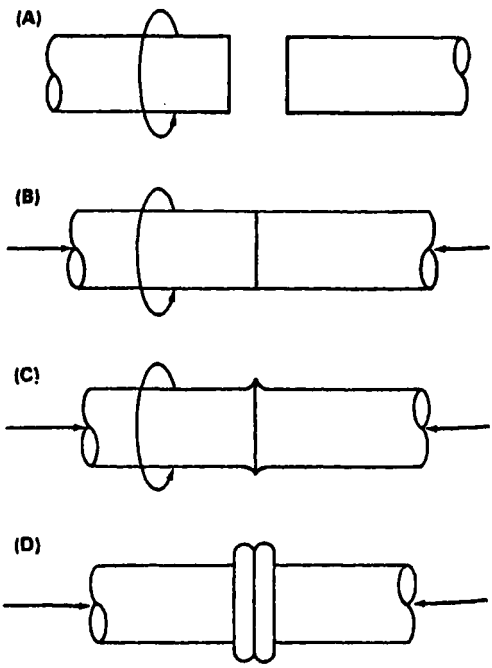
Figure 4.7 Commercially significant metals and alloys that can be joined by explosion welding. (From *Welding Handbook*, Vol. 2: *Welding Processes*, 8th ed., edited by R. L. O'Brien, published in 1991 by and used with permission of the American Welding Society, Miami, FL.)

4.3. FRICTION WELDING PROCESSES

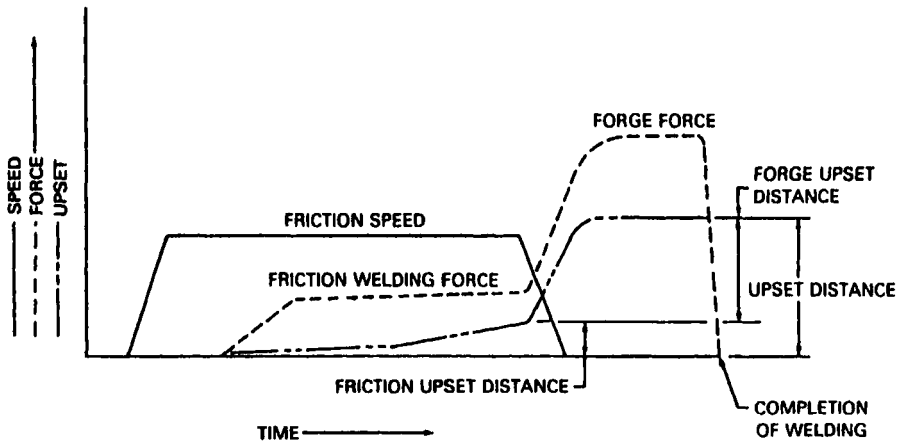
As a group, *friction welding* (*FRW*) *processes* employ machines that are designed to convert mechanical energy into heat at the joint to be welded using the relative movement between pieces. Coalescence of materials occurs under the compressive force of contact between workpieces moving relative to one another in rotation, or by angular or linear reciprocation.

Figure 4.8 schematically shows the basic steps involved in the friction welding process. The parts to be joined are moved relative to one another while under moderate pressure, frictional heating occurs and softens the material in the vicinity of the joint, and, then, an upsetting or forging pressure is applied to complete the weld. This final, forging step is what really establishes metallurgical continuity and bonding. The earlier steps cause heating and, simultaneously, scrub away any intervening oxide or tarnish.

There are three ways in which friction can be generated by the relative motion between workpieces, and these depend on the directions of that motion. The three motions are (1) rotation, (2) angular reciprocation, and (3) linear



(a)



(b)

Figure 4.8 Schematic of the basic steps (a) and direct drive parameter characteristics (b) involved in friction welding. (From *Welding Handbook*, Vol. 2: *Welding Processes*, 8th ed., edited by R. L. O'Brien, published in 1991 by and used with permission of the American Welding Society, Miami, FL.)

reciprocation. If the amplitude of relative motion is very small and the frequency very high, in the range of ultrasound (greater than around 30 kHz), the process is called *ultrasonic (friction) welding*. There is, in fact, a relatively new variant of friction welding in which the parts to be welded are held still and frictional heating is generated by a rapidly rotating tool placed between the pieces under pressure. This variation is called *(friction) stir welding*. Each of these variations is described very briefly.

4.3.1. Radial and Orbital Welding

When rotation is used to accomplish friction welding, the force applied to bring the parts into initial contact and then to forge them together can be either parallel to the axis of rotation (axial) or perpendicular to the axis of rotation (radial). When a radial force is to be used, either the parts can be rotated relative to one another in what is known as *orbital friction welding* or the parts can be held stationary while a concentric collar or sleeve is caused to rotate in what is known as *radial friction welding*. Figure 4.9 schematically shows radial versus orbital friction welding.

Regardless of the particular variation, whenever rotational motion is employed to produce friction to produce a weld, there are restrictions on the shape of parts that can be joined. Clearly, only parts with rotational symmetry can be welded using rotational motion.

4.3.2. Direct-Drive Versus Inertia-Drive (Friction) Welding

When an axial pressure/forging force is used with *rotational friction welding*, two predominant techniques are employed. In the first, more conventional technique, the moving part is held in a motor-driven collet and rotated at a constant speed against a fixed part while the axial force is applied to both parts. Rotation is continued until the entire joint is suitably heated, and, then, simultaneously, the rotation is stopped and an upsetting force is applied to produce a weld. Key process variables are rotational speed, axial force, welding time, and upset force or displacement. This variant is called *direct-drive welding*. In the second technique, called *inertia-drive* or simply *inertia welding*, energy is stored in a flywheel that has been accelerated to the required speed by a drive motor. The flywheel is connected to the motor through a clutch and to one of the workpieces by a collet. The weld is made by applying the axial force through the rotating part to a stationary part while the flywheel decelerates, transforming its kinetic energy into heat at the joint faying surfaces. When done properly, the weld is completed when the flywheel stops. Key process variables are the flywheel moment of inertia, the flywheel rotational speed, the axial force, and the upset force. The actual process for both techniques is usually automated. Sometimes rotational friction welding processes are called spin welding.

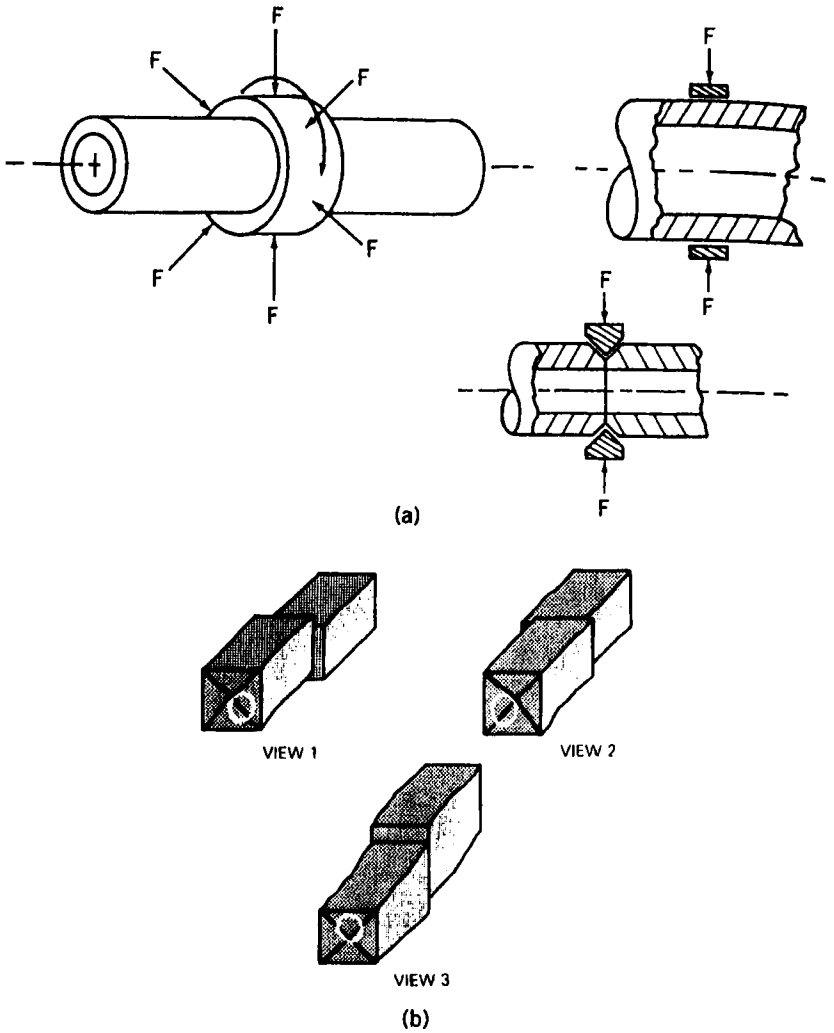


Figure 4.9 Schematic of (a) radial versus (b) orbital friction welding. (From *Welding Handbook*, Vol. 2: *Welding Processes*, 8th ed., edited by R. L. O'Brien, published in 1991 by and used with permission of the American Welding Society, Miami, FL.)

Typical arrangements of rotational friction welding, whether using direct or inertia drive, are shown schematically in Figure 4.10.

4.3.3. Angular and Linear Reciprocating (Friction) Welding

It is also possible to accomplish friction welding using reciprocating motion between workpieces in contact throughout the process. This reciprocating motion can be angular, in which case the process is called *angular* (*reciprocat-*

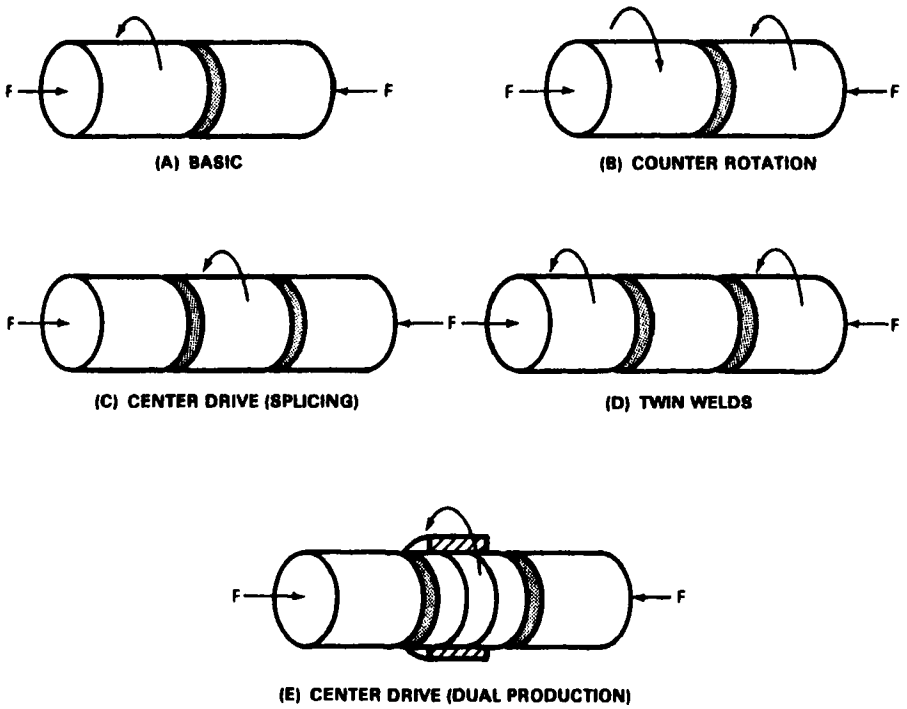


Figure 4.10 Schematic of typical arrangements of rotational friction welding. Note that the drive could be either direct or inertial for (A). (From *Welding Handbook*, Vol. 2: *Welding Processes*, 8th ed., edited by R. L. O'Brien, published in 1991 by and used with permission of the American Welding Society, Miami, FL.).

ing) *friction welding*, or linear, in which case the process is called *linear* (*reciprocating* or *vibration*) *friction welding*. Figure 4.11 schematically shows these two variations.

The fact that angular or linear reciprocating motion is being used to produce friction to produce a weld does not mean that there are not either restrictions on the shapes of parts that can be welded thereby, or that such welding will be trivial. The upset or forging force must be applied when reciprocation is halted and parts are properly aligned.

Figure 4.12 shows combinations of metallic materials that can be joined by friction welding. A variety of ceramic materials, as well as metal–ceramic combinations, can also be joined by this group of processes.

4.3.4. Ultrasonic (Friction) Welding

The source of motion in friction welding can be pure mechanical vibration or ultrasonically induced vibration. When ultrasonic vibration is employed, the

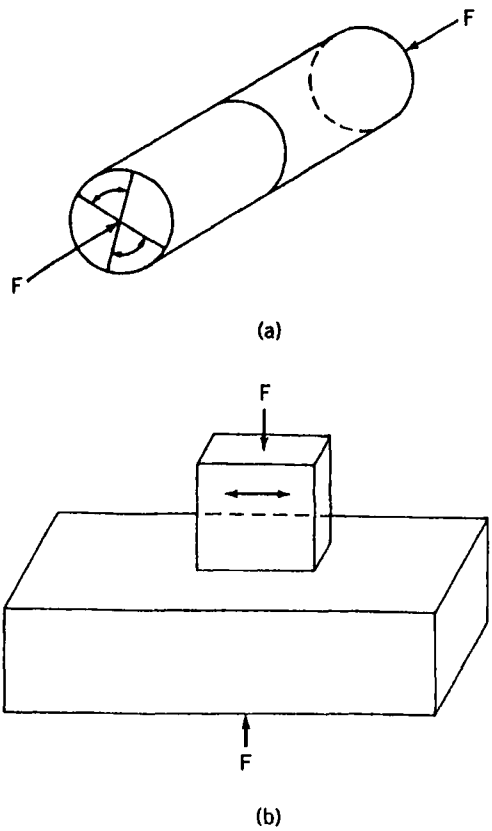


Figure 4.11 Schematic of (a) angular reciprocating friction welding and (b) linear reciprocating friction welding. (From *Welding Handbook*, Vol. 2: *Welding Processes*, 8th ed., edited by R. L. O'Brien, published in 1991 by and used with permission of the American Welding Society, Miami, FL.)

process is usually called *ultrasonic welding* (*USW*), and is often treated as an entirely different process, although it is not! The only real difference is the amplitude and frequency of motion compared to more conventional friction welding. For conventional friction welding, the amplitude of vibration is relatively large (fractions of to several millimeters) and the frequency is quite low (typically, 10^2–10^3 cycles per second). Ultrasonic vibration scrubs materials together, while under pressure, generates heat, and produces a weld usually without a distinct forging step. As can be seen in Figure 4.13, the ultrasonic energy is provided by a piezoelectric transducer.

There are, in fact, four variations of ultrasonic welding, according to the AWS, based on the type of weld produced: (1) spot, (2) ring, (3) line, and (4) seam. The names are fairly self-descriptive, and the different types are not

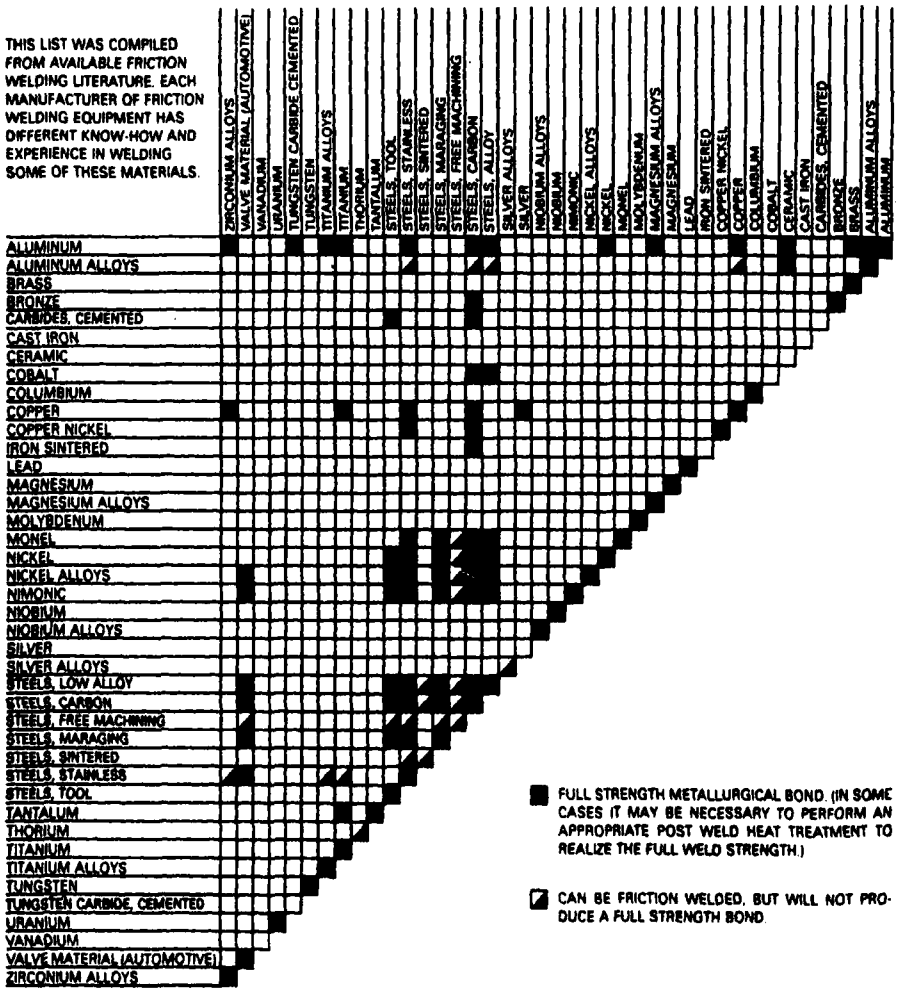


Figure 4.12 Material combinations that can be joined by friction welding. (From *Welding Handbook*, Vol. 2: *Welding Processes*, 8th ed., edited by R. L. O'Brien, published in 1991 by and used with permission of the American Welding Society, Miami, FL.)

detailed here. These process variations can be used to produce welds in a host of materials, including all thermoplastics and many metals (as shown in Figure 4.14).

Besides the above-mentioned variations, two special forms of ultrasonic welding are used explicitly for spot welding in microelectronic assembly: (1) *microminiature welding* and (2) *microminiature thermosonic welding*. In the former, the only difference compared to conventional ultrasonic welding is the scale of the welds. They are much smaller to allow welding of wires that range

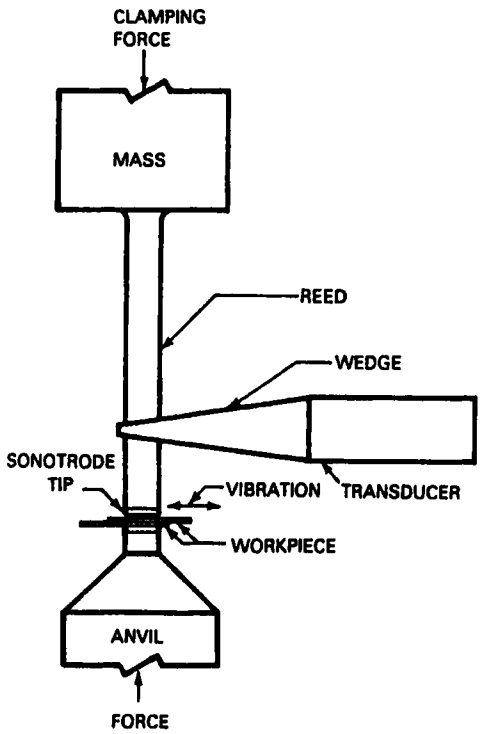


Figure 4.13 Schematic of a wedge–reed ultrasonic spot welding system. Note the piezoelectric transducer used to supply needed vibrational energy to cause frictional heating. (From *Welding Handbook*, Vol. 2: *Welding Processes*, 8th ed., edited by R. L. O'Brien, published in 1991 by and used with permission of the American Welding Society, Miami, FL.)

from 0.001 to 0.020 in. (25 to 500 μm). In the latter, the difference is that the microminiature ultrasonic welding is performed while the substrates are heated to temperatures between 215 and 400°F (100 and 200°C). The belief is that heating facilitates weld formation by both softening the substrates and helping remove any light oxide or tarnish layers that might be present after cleaning. Both of these process variations are often referred to as bonding rather than welding.

4.3.5. Friction Stir Welding

A relatively new variation of friction welding is *friction stir welding*. In this process, primarily developed at The Welding Institute (TWI) in England, a tool or tip is rapidly rotated while being squeezed between two abutting workpieces (as shown schematically in Figure 4.15). The combination of squeezing pressure and rapid rotation (i.e., relative motion between tool and work) leads

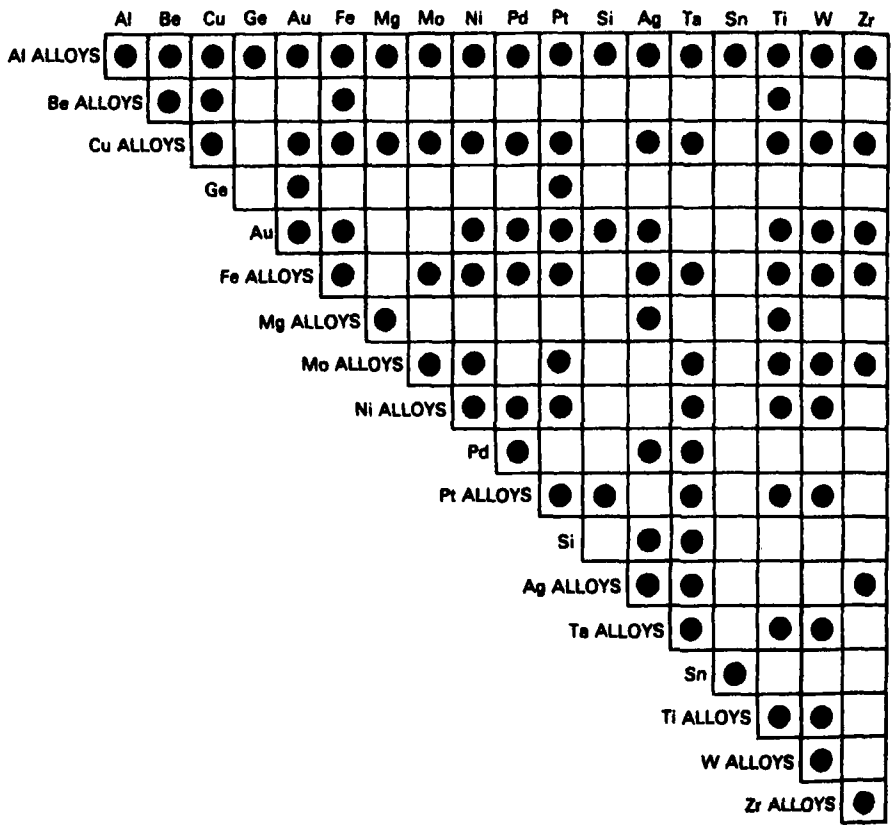


Figure 4.14 Metal combinations that can be ultrasonically welded. (From *Welding Handbook*, Vol. 2: *Welding Processes*, 8th ed., edited by R. L. O'Brien, published in 1991 by and used with permission of the American Welding Society, Miami, FL.)

to frictional heating and softening of the faying surfaces of the workpieces. Melting is a possibility, because the heating can become so intense. Whether melting occurs or the workpiece faying surfaces are just softened, material from each joint member is intermixed or stirred, hence the name. The result is a weld. A distinct advantage of the stir-welding process is that materials that might normally be incompatible if fused can be successfully intermixed and caused to weld.

To make the process work, the depth of tool plunge into the joint, rotational speed, rate of feed or translational motion, and squeezing pressure must all be carefully determined and controlled. As one might expect, there tends to be more heating and deformation or stirring on one side of the joint than on the other, due to the way in which the relative rotational and translational velocities add. Compensation can be made for this effect.

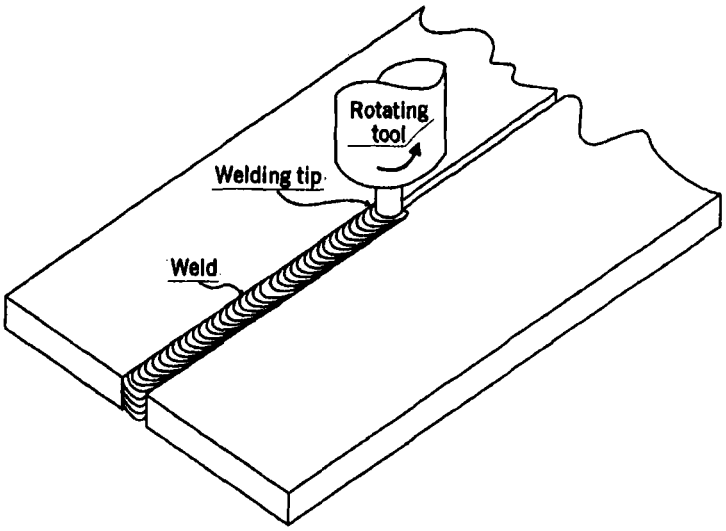


Figure 4.15 Schematic of friction stir welding.

4.3.6. Friction Surfacing

This variation on friction welding uses rotational motion of one part, but at the same time adds a relative motion in a direction perpendicular to the axis of rotation. This process is used to deposit material in a solid state to any of a variety of parts from flat plates to cylinders. The material being deposited comes from one of the parts involved in the process, usually the rotating one (as shown schematically in Figure 4.16) as a consumable, analogous to the way in which colored wax is deposited by a crayon. This material might be used to provide corrosion resistance or wear protection, so the process is really a surfacing process. The thickness that can be deposited is more limited than arc or beam fusion processes.

4.4. DIFFUSION JOINING PROCESSES

As mentioned at the beginning of this chapter and in Section 2.2, it is possible to obtain material continuity and produce a weld using only diffusion of atoms. When such diffusion takes place in the solid state, a weld is produced by what is called *diffusion welding*. When the diffusion process is enhanced or accelerated by the presence of a liquid, even if only in minute quantities for very short times (i.e., is transient), a joint is produced by what is properly called *diffusion brazing*. Both processes are popularly, but not properly, referred to as diffusion bonding.

Each process variation is described below, along with some special variations in which part forming and welding or bonding are accomplished simultaneously.

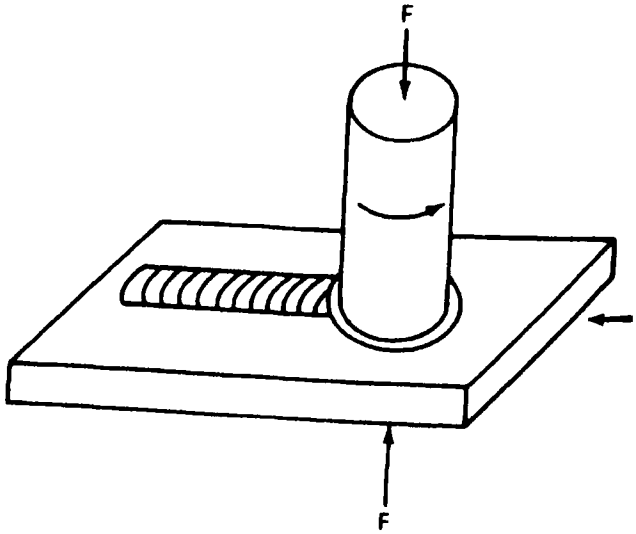


Figure 4.16 Schematic of friction surfacing. (From *Welding Handbook*, Vol. 2: *Welding Processes*, 8th ed., edited by R. L. O'Brien, published in 1991 by and used with permission of the American Welding Society, Miami, FL.)

4.4.1. Diffusion Welding

When properly defined, as by the AWS, "*Diffusion welding* (DFW) is a solid-state welding process that produces a weld by the application of pressure at elevated temperature with no macroscopic deformation or relative motion of the workpieces." A filler metal may or may not be inserted between the faying surfaces to facilitate weld formation by either helping to achieve more points or areas of intimate contact between substrates (through plastic accommodation), or speeding diffusion by providing a faster diffusing atomic species. The process is referred to by a number of other names, including diffusion bonding and solid-state bonding (which are both reasonable); pressure bonding, isostatic bonding, hot press bonding, and hot pressure welding (which are all reasonable, assuming that significant pressure is actually employed); and forge welding (which is usually not accurate, except for a particular variation of pressure welding in which diffusion plays an important role). In reality, diffusion is involved in every welding process, whether fusion or nonfusion, without or with pressure.

The diffusion welding process takes place in several steps as shown schematically in Figure 4.17 and as described in Chapter 2.

Diffusion welding offers some very special and often unique advantages: (1) metals as well as ceramics can be joined directly to form a completely solid-state weld, which has the potential (offered by no other process!) of producing a perfect weld—with a wrought structure, generally free of heat effect; (2) a

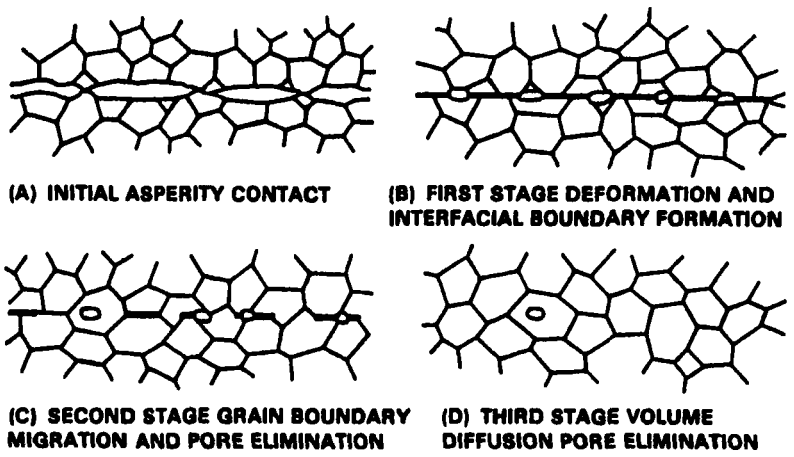


Figure 4.17 Schematic of the three-step mechanistic model of diffusion welding. (From *Welding Handbook*, Vol. 2: *Welding Processes*, 8th ed., edited by R. L. O'Brien, published in 1991 by and used with permission of the American Welding Society, Miami, FL.)

filler can be used to permit increased microdeformation to provide more contact for bond formation and/or promote more rapid diffusion by providing a faster diffusing species; (3) dissimilar materials either by class or type, including metal-to-ceramic joints, can be joined directly or with the aid of a compatible filler or intermediate; (4) large areas can be bonded or welded, provided uniform intimate contact can be obtained and sustained; and (5) there will be no heat-affected zone as such, since the entire assembly in which the diffusion weld is being made is virtually always heated to the same temperature. (This means that whatever heating to the diffusion welding or bonding temperature does to the microstructure of the joint elements or base materials, it does everywhere! This may not be as bad as a distinct heat-affected zone, because, at least, there is no metallurgical notch. This is true provided, of course, that the change in the microstructure caused by heating is acceptable.)

Among the key parameters of the process—temperature, time, and pressure—temperature is by far the most important, provided there is enough pressure to cause contact between joint elements! The reason temperature is so important is that diffusion occurs by an Arrhenius relationship, that is, exponentially with temperature:

$$D = D_0 e^{-Q/kT} \tag{4.1}$$

where D is the diffusion coefficient (of the diffusing species) at temperature T, D_0 is a constant of proportionality (dependent on the particular diffusing

species and host), Q (or frequently, Q_d) is the activation energy for diffusion to occur, k is Boltzmann's constant, and T is the temperature on an absolute scale (kelvin). In general, diffusion welding begins to take place at a reasonable rate when the temperature exceeds half the absolute melting point of the base or host material(s), and, as a rule-of-thumb, the rate of diffusion doubles every time the temperature is raised approximately 30°C or K (50°F).

Time is important because diffusion takes time to occur, since for atoms to jump from site to site takes time. Thus, the distance over which diffusion occurs depends on time:

$$x = C(Dt)^{1/2} \tag{4.2}$$

where x is the diffusion distance, D is the diffusion coefficient (as above), t is time, and C is a constant for the system.

Pressure is important from several standpoints, depending on which step of the process is considered. Initially, pressure is absolutely critical to establish point-to-point contact across which diffusion can occur; the higher the pressure, the more points and area of contact, so the more diffusion can occur for any particular temperature. Later in the process, pressure can help speed diffusion welding by being high enough to cause creep and/or sufficient plastic deformation that dynamic recrystallization occurs; the greater the deformation, the lower the recrystallization temperature. While certainly of secondary importance, pressure also enhances diffusion through a tension stress gradient concentration that expands the crystal lattice to make atom migration easier.

Besides these important process parameters, there are important metallurgical factors, including allotropic phase transformations (in some metals and alloys) that will speed diffusion both due to plastic accommodation at faying surfaces and faster diffusion as the transformation takes place; any microstructural condition that would tend to modify diffusion rates (e.g., occurrence of recrystallization); and ability to form dissimilar material joints (e.g., ceramic to metal), provided there is sufficient compatibility to allow mutual interdiffusion.

Heating during diffusion welding can be accomplished using a furnace, retort, autoclave, hot-platen press, or by resistance. Pressure can be applied by dead-weight loading, a press, differential gas pressure, or by differential thermal expansion of the parts or of tooling. Uniaxial methods of applying pressure limit welding to flat, parallel, planar surfaces, roughly perpendicular to the direction of load application. Isostatic pressurization, employing encapsulation or "canning," offers better pressure uniformity and is applicable to more complex geometry. (Remember that the principal purpose of applying pressure is to obtain contact at the interface to be joined. This contact initially occurs by plastic deformation of microscopic asperities, and later by creep.) Almost always, diffusion welding is made to take place in a protective, often inert, atmosphere. This is to prevent formation of interfering oxide or other tarnish layers after they have been removed prior to attempting to diffusion weld.

Components to be diffusion welded must be specially designed and carefully processed to produce successful joints consistently. The process is economical only when close dimensional tolerances, expensive materials, or special material properties are involved. Even then, not all metals can be easily diffusion welded or bonded. One excellent example, however, is titanium for aerospace applications. Titanium has the rather unusual characteristic of being able to dissolve its own oxide at a certain temperature (approximately 1000°C or 1800°F). Other metals and alloys that can be diffusion welded are nickel alloys, low-carbon steels, and aluminum alloys, although the persistent oxide associated with aluminum must be dealt with. Dissimilar metal combinations, as well as many combinations of ceramics of similar and dissimilar composition can be diffusion welded. Some ceramics can even be diffusion welded to some metals.

4.4.1.1. Conventional Diffusion Welding. What has just been described is what is referred to as *conventional diffusion welding.*

4.4.1.2. Deformation Diffusion Welding. There are variations of the diffusion welding process in which the degree of plastic deformation caused by the application of pressure is substantial. When this is the case, the process is often referred to as *deformation diffusion welding.* The impact of the severe plastic deformation is favorable in three ways: (1) Lots of contact is obtained from the outset of the process. (2) Severe plastic deformation is almost certain to break up oxide. This is especially important for materials that inherently form an aggressive and tenacious oxide, such as aluminum and its alloys do. (3) Lots of deformation means recrystallization at much lower temperatures. This will speed the effects of diffusion through new grain formation at and growth across the original interface.

4.4.1.3. Resistance Diffusion Welding. There is a variation of diffusion welding that is made to take place through the pressure and heating associated with the resistance spot welding (RSW) or resistance seam welding (RSEW) processes. It is called *resistance diffusion welding.* Other than the means by which heat and pressure are applied, there is no difference from conventional diffusion welding.

4.4.1.4. Continuous Seam Diffusion Welding. In *continuous seam diffusion welding* (CSDW), components are joined by yield-controlled diffusion welding. Parts are positioned so that their faying surfaces are properly abutted or overlapped, and then the assembly is passed through tooling consisting of four rollers. The rollers are usually made from molybdenum so that they can apply heat by resistance through the passage of current from the rollers through the parts and joints. The result is a continuous diffusion seam weld, an example of which appears in some built-up structural steel I-beams, where top and bottom members are CSD-welded to the web.

4.4.2. Diffusion Brazing

Diffusion brazing (DFB) is similar to conventional brazing, except that the filler metal and brazing temperature and time are selected so that the joint that results has physical and mechanical properties almost identical to the base metal. To do this, it is necessary to diffuse the braze metal almost completely into the base metal. The most important reason for doing this is to raise the remelt temperature of the joint once it is formed by brazing to well above the brazing temperature. A typical application is the diffusion brazing of nickel-base superalloy blades to an identical-composition disk.

In this process, liquid is formed at the joint interface through a eutectic reaction between the base metal or one of the base metal components and the filler or one of the filler components, as it must be for a process to be considered a brazing process. The liquid is normally quite transient, however, with solidification occasionally occurring isothermally.

4.4.3. Combined Forming and Diffusion Welding

It was found with commercially pure (CP) titanium and many titanium alloys (e.g., two-phase, alpha-beta, Ti-6Al-4V, Ti-6Al-2V-2Sn, and others) that diffusion welds could be made at the same time the material was hot formed. Undoubtedly, this discovery was made accidentally when two parts being formed were found to have welded together! Two process variations exist: (1) *creep isostatic pressing* (CRISP) and (2) *superplastic forming/diffusion welding* (SPF/DFW).

The reason these processes work is that, fortuitously, titanium and many of its alloys exhibit creep and superplasticity in the same temperature range in which they diffusion weld. (Recall that titanium also exhibits the rather unusual characteristic of being able to dissolve its own oxide before it melts, which means it self-cleans faying surfaces, even when tightly abutted.) Thus, while parts are being hot formed either by normal creep or superplastic behavior due to grain boundary sliding between alpha and beta phases, they also diffusion weld. After all, the temperature of both hot forming and diffusion welding is around 1700°F (925°C), which is over $0.50T_m$. Material flow by creep or superplasticity occurs at such low stresses that gas pressure (usually only hundreds of psi or a few MPa) can be used to cause forming, as well as to provide isostatic pressure to cause welding.

The forming and diffusion welding cycles can, in fact, be caused to occur in either order, depending on the particular design and process variation. That is, parts can be caused to diffusion weld and then formed, or formed and then diffusion welded. To prevent diffusion welding where it is not wanted, chemically inert and thermally stable oxides (e.g., yttria) are used as maskants.

Several materials besides titanium and some of its alloys can be made to simultaneously form and diffusion weld. Examples include some aluminum alloys (once specially processed to refine their grain structure considerably),

some nickel-base superalloys, pure copper and some copper alloys, and some ultra-fine-grained steels.

Figure 4.18 shows how SPF/DFW can be made to occur to produce complex shapes from titanium alloys for use in advanced aircraft, including both various possibilities for stabilizing skin structures (a) and replacing traditional design and fabrication techniques using either buildup (rivet-assembly) of details or machining (b).

4.5. SOLID-STATE DEPOSITION WELDING PROCESSES

While the underlying processes have been used for a long time, it has only recently been realized that *chemical deposition*, *electrochemical deposition* and *vapor deposition* can be used to weld materials together. These processes are or will be called *solid-state deposition welding processes.* For the most part, chemical bonds are formed as one material is deposited on another because the interface is atomically clean and contact is intimate which are the two requirements for producing a weld (see Chapter 2). Granjon (1991) spoke of this possibility when he wrote about the role of interfaces in causing welding (Section 2.4.4). While there are still only a few real applications, usually on very small scales where the boundary between a material and a structure becomes blurred, the future bodes well for these processes.

4.6. INSPECTION AND REPAIR OF NONFUSION WELDS

Nonfusion welding processes, as a group, pose a special challenge, despite their attractiveness to preserve microstructure and properties. The joints produced by all nonfusion welding processes tend to be thin compared to their fusion-welding counterparts and can involve much greater joint area. This makes nondestructive evaluation inherently difficult, whether by x-radiography, due to the thinness of planar defects relative to the thickness of the assembly, thereby exceeding resolution limits, or by ultrasound, due to the ease with which a significant proportion of sound can be transmitted by many very small connecting paths or ligaments. As if this isn't bad enough, once detected, it is often impossible to repair defects in nonfusion welds. This tends to be true because the joint often involves a large surface area, just because of the capability of such processes to produce such joints!

The designer and the process engineer must know what they are letting themselves in for in the way of inspection and repair when they choose nonfusion over fusion welding approaches. Nothing comes without a cost!

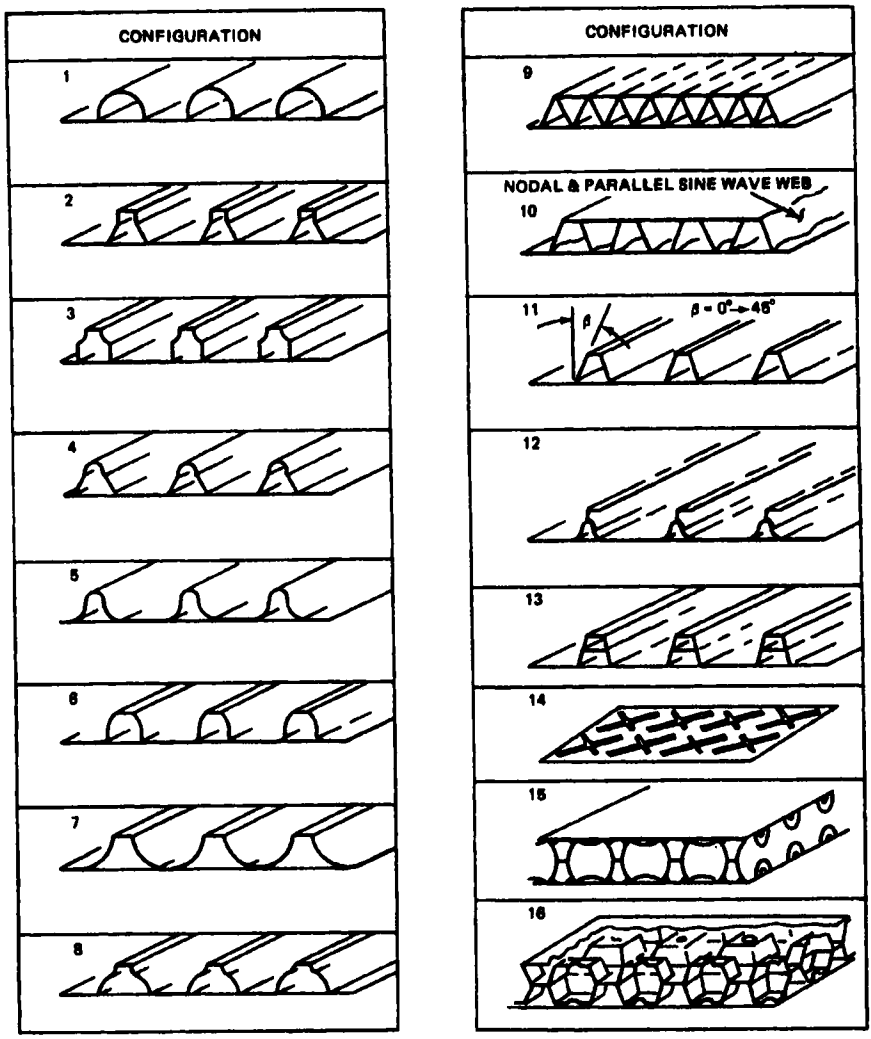
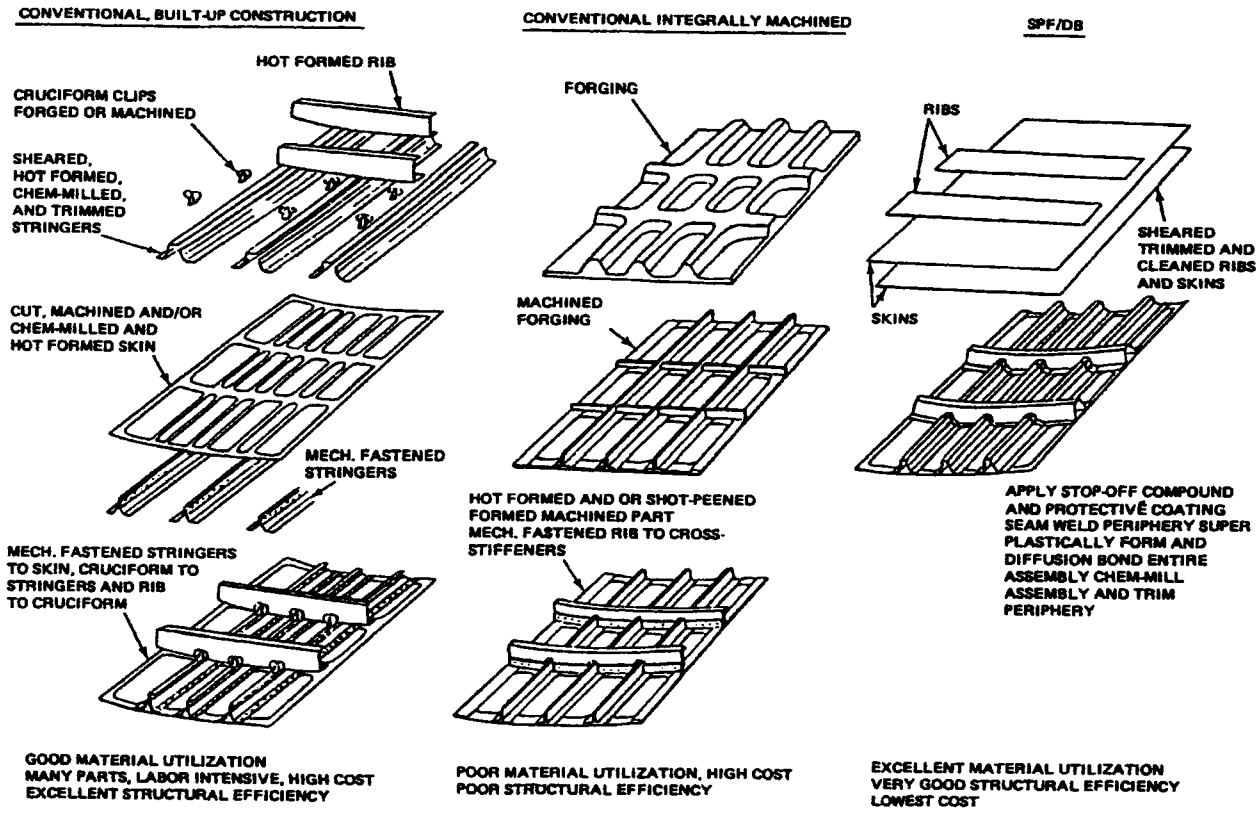


Figure 4.18a Schematic of superplastic forming/diffusion welding (SPF/DFW) of titanium alloy parts for an advanced aircraft: (a) various skin stabilization configurations made possible by SPF/DB and (b) comparison of conventional buildup or machining and SPF/DB design and fabrication techniques. (After original work by the author in the late 1970s).



(b)

Figure 4.18b Comparison of conventional buildup or machining and SPF/DFW or SPF/DB design and fabrication techniques. (After original work by the author in the late 1970s).

4.7. SUMMARY

Nonfusion welding processes offer a valuable alternative to fusion welding processes, enabling the joining of difficult, often dissimilar, materials to fairly precise tolerances, with little or no heat effect in the base material. Nonfusion welding processes rely on one of four factors to obtain material continuity and form welds: (1) pressure, (2) friction, (3) diffusion, or (4) solid-state deposition and chemical reactions. There are many variations on these basic approaches, yielding more and more specific processes every day. As materials continue to be more highly engineered in terms of chemical composition and microstructure, nonfusion welding processes will become more important and more prominent.

REFERENCES AND SUGGESTED READING

Suggested reading [by process]

Cary, H. B., 1998, *Modern Welding Technology*, 4th ed., Prentice Hall, Englewood, NJ. [Variety of processes]

Diffusion Bonding as a Production Process, 1979, Abington Publishing, Cambridge, UK. [DFW/DBW]

Exploiting Friction Welding Processes, 1979, Abington Publishing, Cambridge, UK. [FRW]. *Explosion Welding*, 1976, Abington, Cambridge, UK. [EXW]

O'Brien, R. L. (Editor), 1991, *Welding Handbook*, Vol. 2: *Welding Processes*, 8th ed., American Welding Society, Miami, FL. [Variety of processes]

This Page Intentionally Left Blank

PART II

THE PHYSICS OF WELDING

This Page Intentionally Left Blank

CHAPTER 5

ENERGY FOR WELDING

5.1. INTRODUCTION TO THE PHYSICS OF WELDING

By definition (see Section 1.1), welding requires the application of heat, pressure, or both to obtain sufficient continuity between the atoms (or ions or molecules) of one joint element or material and another to create chemical bonds in very large numbers. The result is a joint with strength that approaches the strength of the weaker base material or filler, if one is employed. Almost every imaginable exothermic source of heat energy has been used at one time or another to make welds; combustion and exothermic synthesis chemical reactions, electric arcs, electrical resistance, plasmas, electron beams, microwaves, light beams (lasers or focused IR or imaged arcs), mechanical friction, and mechanical plastic deformation by any of several means (see Section 2.2 and Chapters 3 and 4). Thus, it should not come as a surprise that the physics of welding deals with numerous and complex physical phenomena, including heat, electricity, magnetism, light, sound, and mechanical work.

Part two of this book deals with key aspects of this physics, beginning here with the energy for welding.

5.2. SOURCES OF ENERGY FOR WELDING

As described in Section 2.2, two forms of energy are necessary, in some combination from one extreme to the other, to produce a weld: (1) thermal energy or heat, and (2) mechanical energy in the form of pressure. These forms can be obtained from three fundamental sources (Section 2.4.3): thermal energy

from chemical, electrical, or mechanical sources, and, not surprisingly, mechanical energy from mechanical sources. Specific chemical sources are exothermic combustion of fuel gases by oxygen (oxyfuel gas welding), and exothermic solid-phase synthesis reactions (aluminothermic welding) (both described in Section 3.2) or combination reactions (reaction welding or brazing). Specific electrical sources are electric arcs (arc welding, described in Section 3.3), electrical resistance or Joule heating (resistance welding, described in Section 3.4), or high-intensity beam (high-energy beam welding) or radiant energy (radiant energy welding), (both described in Section 3.5). Specific mechanical sources for heat can be pressure, for some pressure welding (described in Section 4.2), or friction, for all friction welding (described in Section 4.3). Specific sources of pure mechanical energy (without heat) are cold pressure or explosions, for cold welding and explosion welding, respectively (described in Sections 4.2.1 and 4.2.4). Various potential fundamental and specific sources of energy for welding are listed in Table 5.1.

Diffusion welding, which depends entirely on interdiffusion between materials comprising mating joint elements to produce a weld, is a thermally driven process that can obtain the heat needed from a chemical (e.g., gas-fired furnace), electrical (radiant or convection electric furnace, electric resistance, etc.), or mechanical (friction or ultrasonic) energy source.

5.3. SOURCE ENERGY, TRANSFERRED POWER, ENERGY DENSITY, AND ENERGY DISTRIBUTION

5.3.1. Energy Available at a Source (Energy Level or Capacity)

The key feature of a source that enables welding to take place is that it provides energy, whether thermal (heat) or mechanical (pressure). In physics, energy is the capacity for doing work in a physical system in changing from one form to another. However, different sources, regardless of type, are capable of supplying both different amounts of energy and different intensity of energy. Let's look at the simpler case for a source of thermal energy, although a parallel case could be made for a source of mechanical energy.

A large oxyacetylene torch flame contains more thermal energy or heat and can supply more of that energy to a workpiece to heat it up to attempt to make a weld than a small oxyacetylene torch flame. Yet, both flames involve the same basic chemical reaction (see Eqs. 3.1–3.3) and have the same maximum temperature (see Table 3.1). In other words, one source contains a different amount of energy than the other, but is no more intense. The amount of energy available in a heat source is called its *energy level* or *energy capacity*. Depending on the nature of the energy source, energy level or capacity is measured in different units; e.g., calories (or Btus) for a flame, Watts for an arc, electrical resistance, or a beam — of either electrons or photons (in a laser).[1]

[1] In fact, 1 W = 0.2389 calories/second, and, what is being called energy is really power.

TABLE 5.1 List of the Various Fundamental and Specific Sources of Energy for Welding

Energy Source	Example Processes
Mechanical	
Friction	FRW, USW
Plastic deformation	
Cold work	CW, FOW, ROW
Warm or hot work	HPW, FOW, ROW, EXW[a]
Chemical	
Oxyfuel combustion	OFW, PGW,[b] AHW[c]
Aluminothermic reactions	TW, FOW[b]
Solid-state chemical reactions	Reactive brazing, chemical deposition/ reaction vapor deposition, electrochemical deposition[d]
Electrical	
Electric arc	AHW,[c] CAW, SMAW, FCAW, SW, GTAW, PAW, GMAW, SAW, EGW, MIAB[e]
Internal resistance (Joule heating)	RSW, RSEW, PW or RPW, PEW, UW,[e] FW,[e] IW, ESW[c]
Radiant energy	EBW, LBW, IR welding, imaging arc or arc image welding
Thermal (only)	
Diffusion welding or brazing	DFW,[g] DFB

[a] Workpieces are usually at room temperature, but work of pieces rapidly coming into contact raises the temperature at the faying surfaces due to localized deformation.
[b] Actually, heating from exothermic chemical reaction is followed by mechanical work of a pressing or forging process.
[c] Combustion actually occurs in the presence of an electric arc.
[d] Chemical reaction is enabled/aided by electrical energy.
[e] Initial heating of workpiece faying surfaces by an electric arc is followed by mechanical work and plastic deformation during an upset cycle.
[f] Initial heating of dry slag by an electric arc is followed by internal resistance heating of electrical-conductive molten slag.
[g] Thermally activated diffusion could be assisted by application of pressure, even to the point of causing microscopic or even macroscopic plastic deformation.

In an oxyacetylene flame, the available heat at the source is given by

$$Q\ (\text{W}) = 48\ \text{kJ/L acetylene} \times V_{\text{acetylene}} \times \text{h}/3600\ \text{s} \qquad (5.1)$$

where $V_{\text{acetylene}}$ is the volumetric flow rate of acetylene in liters (L) per hour (h), and the heat of combustion of acetylene (C_2H_2) is 48 kJ/L at a standard state of 25°C, 1 atm pressure. Similar equations apply to other oxyfuel gas combinations, simply substituting the heat of combustion for the particular fuel

gas, in kilojoules per liter, as given in Table 3.1. For an electric arc, the available heat at the source is given by:

$$Q\ (\text{W}) = EI \tag{5.2}$$

where E is the arc (or electron beam) voltage and I is the arc (or electron beam) current. There are similar relationships for electrical resistance sources, laser beams, and so on.

5.3.2. Transferred Power

For an oxyacetylene flame or any source of thermal energy (or mechanical energy, for that matter), the time you allow for energy to be deposited on or in the workpiece also has an effect.[2] The longer the energy is deposited on the workpiece, the greater the heating effect, at least to a limit at which losses from various causes prevent further heating. The energy delivered per unit of time from a heat source of a given energy level or capacity is known as the *transferred power*. The units of transferred power are calories per second for a flame or the sun, or watts per second for an arc or electrical resistance, but are usually reported as just calories or watts.

5.3.3. Source Intensity or Energy Density

When light from the sun strikes your hand, you feel some heat, regardless of the ambient temperature of the surroundings. If you place a magnifying glass lens between the sun and your hand, the same amount of light passes through the lens, dependent only on its size, regardless of how far the lens is from your hand. However, if you move the lens so that the point at which the light is focused to the smallest spot or area is on the surface of your hand, you will quickly discover the spot of light is much more intense—and so is the heat! The light energy is concentrated into a smaller area.

The transferred power per unit area of effective contact between a heat source and the workpiece (or your hand in the above analogy) is known as the *energy density*. The units of energy density are watts per square meter, square centimeter, square millimeter, or square inch. Energy density is the only true, completely unambiguous measure of "hotness," regardless of the energy source (e.g., flame, arc, plasma, or beam[3]), and it gives the best indication of the *source intensity*.

The significance of energy density as a property of an energy source cannot be overemphasized. The historical and technological evolution of welding processes has been the direct result of the ability to generate and apply energy sources with greater and greater energy density. As can be seen from revisiting the time line shown in Figure 1.1, progression from oxyacetylene to higher-

[2] The difference between depositing energy on (or onto) versus in (or into) a workpiece will become clear when the difference between the melt-in and keyhole modes are discussed in Section 5.8.

[3] The use of temperature as a measure of "hotness" has meaning for a flame or an arc, but has no meaning when one speaks about a beam of light (e.g., a laser) or electrons.

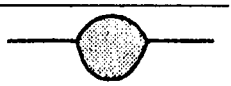
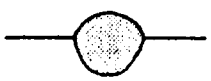
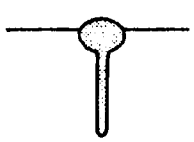
energy-density electric arcs almost completely displaced oxyacetylene. Likewise, for many applications where the melting point is high or thickness is great, very high-density plasmas or electron or laser beams supplant electric arcs as the welding source and process of choice; although certainly not displacing them altogether.

The density of the energy provided by heat sources varies over a wide range. Typical values of the energy density of various sources used for welding are shown in Table 5.2. The effects of energy density are described in Section 5.8.

5.3.4. Energy Distribution

The transfer of energy from a source to a workpiece is a complex process in which the true energy density of the welding heat source cannot be expressed as a precise number. The reason is that it is often difficult (more so for some

TABLE 5.2 Typical Values of Energy Density and the Type of Penetration for Various Sources Used in Welding

Process	Heat Source Intensity (Wm^{-2})	Condition	Fused Zone Profile
Flux-shielded arc welding	5×10^6 to 5×10^8		
Gas-shielded arc welding	5×10^6 to 5×10^8	Normal current	
		High current	
Plasma	5×10^6 to 5×10^{10}	Low current	
		High current	
Electron beam and laser	10^{10} to 10^{12}	Defocused beam	
		Focused beam	

Source: From *Welding of Metallurgy* by J. F. Lancaster, 4th ed., Table 2.2, page 12, Allen & Unwin, London, UK, 1987, with permission from Kluwer Academic Publishers, The Netherlands.

processes than for others) to identify and define the area of contact between the heat source and the workpiece. Think again of the focused spot of light from a magnifying glass. Where precisely is the edge or perimeter of the spot? The problem really is that the energy in the spot of light, as in any and every heat source, is nonuniformly distributed over the contact area. In fact, the energy is nonuniformly distributed within the source, whether that source is a flame, an electric arc, a plasma, or an electron or laser beam. For most sources, the energy density is highest near the center and drops off with distance from the center, usually (but not necessarily) with a Gaussian distribution.

The energy density distribution for an argon-shielded tungsten electric arc, an electron beam, and a laser beam is shown schematically in Figure 5.1. The distribution of energy in an oxyacetylene (or other oxyfuel gas) flame was alluded to in Section 3.2.1, where regions of primary and secondary combustion were described, and the different temperatures associated with each were given in Figure 3.1.

For some sources, the distribution of the energy density in or from the source is "engineered" to have a certain form. Such engineering or shaping of the energy density distribution can be accomplished for electric arcs and electron beams using electromagnetic coils, for plasma using constricting nozzles, and for lasers using optical lenses. The increased energy density associated with the plasma arc welding (PAW) process compared to the gas–tungsten arc welding (GTAW) process is largely the result of constricting the energy by the torch design (see Figure 3.8 and Table 5.2). Energy density shaping is most obvious for laser beams, used for welding, cutting, drilling, machining, surface heating, and so on. Examples of different energy density distributions possible in laser beams are shown schematically in Figure 5.1.

Like energy density, energy density distribution has an effect on the characteristics of the source and its effect on a material. These effects are discussed in Section 5.8.

5.4. ENERGY INPUT TO A WELD

Fundamental to the study of heat flow and how that heat flow affects the material being welded is the concept of *energy* or *heat input*. Here, an analogy is the well-known stunt of running our finger through a candle flame. If we move our finger quickly through the flame, there is little sensation of heat. If we move our finger more slowly, however, we may burn our finger! Clearly, the candle flame has a specific energy content or capacity and a particular temperature that is dependent on the combustion of paraffin wax. So, the difference is the amount of heat or energy input.

Inverting the candle is completely analogous to a welding source such as a flame. By moving the flame slowly across the workpiece, the net heat input per linear increment of movement is high compared to moving the flame across the

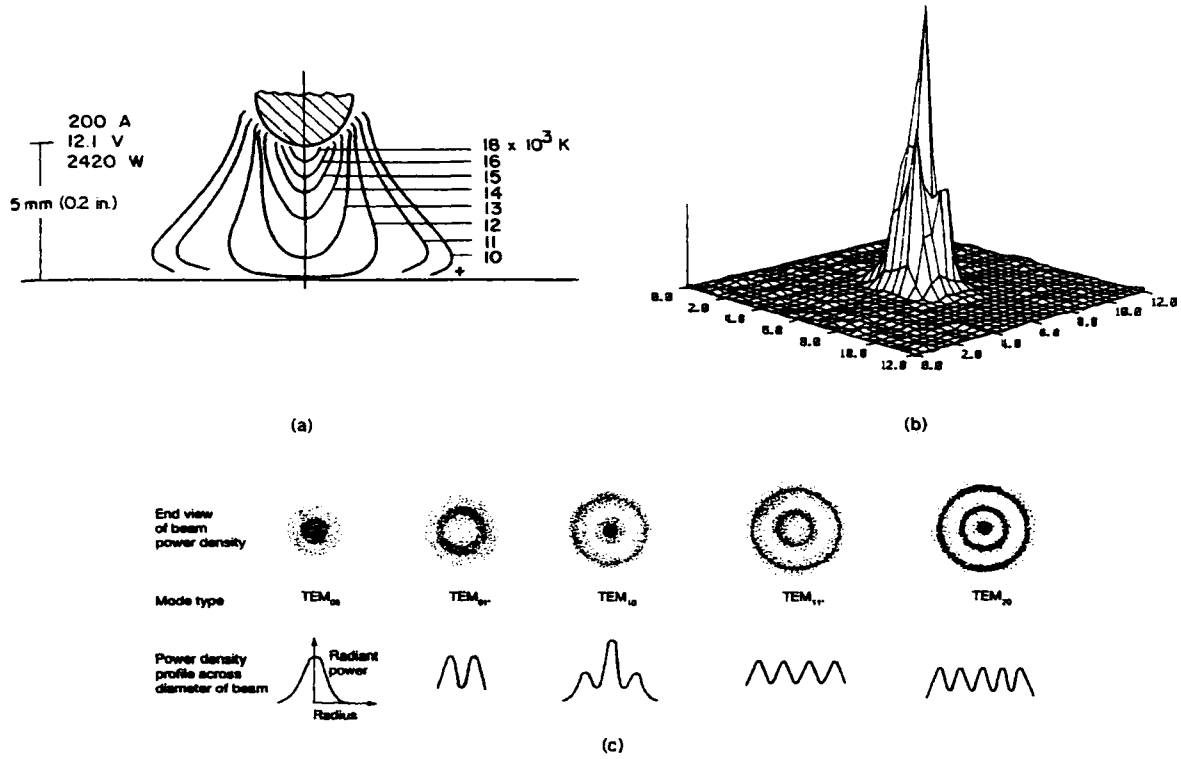


Figure 5.1 Typical energy density distribution for (a) an argon-shielded tungsten arc (From *Welding Handbook*, Vol. 1: *Welding Technology*, 8th ed., edited by L. P. Connor, published in 1987 by and used with permission of the American Welding Society, Miami, FL), (b) an electron beam (From *Electron Beam Welding* by H. Schultz, published in 1993 by and used with permission of Abington Publishing, Cambridge, UK), and (c) various different-purpose laser beams (From *Laser Welding* by C. Dawes, published in 1992 by and used with permission of McGraw-Hill/Abington Publishing, Cambridge, UK).

workpiece more rapidly. Thus, heat input or net heat input in welding is the quantity of energy introduced per unit length of weld from a traveling heat source, whether a flame, electric arc, plasma, or beam. The net energy input is computed as the ratio of the total input power of the heat source (in watts) to its travel speed:

$$H = \frac{P}{v} \tag{5.3}$$

where H = net energy input (in watt-seconds or joules per mm or inch), and P = total input power of the heat source (in watts), and travel or welding speed or velocity (in mm per second or inches per minute).

For an electric arc,

$$H = \frac{EI}{v} \tag{5.4}$$

where E = volts, I = amperes, to yield watts, and v = mm per second to yield watt-seconds (or joules) per mm (or, for v = inches per second, to yield watt-seconds or joules per inch, after conversion of minutes to seconds). A similar relationship applies to plasma arc and electron-beam welding.

The higher the net heat input to a workpiece, the greater the effect of the heat, both good and bad. Good and bad effects are discussed in Section 5.7.

5.5. CAUSES OF LOSSES DURING ENERGY TRANSFER FROM SOURCE TO WORK

When energy or heat is transferred from a source to the workpiece to produce a weld, the transfer is not perfect. There are many opportunities for energy to be lost between the welding source and the workpiece in fusion welding processes. There are also opportunities for loss within the workpiece. As can be seen from the schematic in Figure 5.2, there can be radiant losses in the form of infrared, visible, and/or ultraviolet light; convection losses to the air or shielding gases; and conduction losses to nonconsumable electrodes, filler wires, or the mass of the workpiece surrounding the region of energy deposition. There can also be losses of heat with loss of mass in the form of metal vapor or molten metal called spatter. Which of these possible causes actually lead to the loss of energy between the source and the workpiece, or within the workpiece, depends on the characteristics of the specific welding process and the workpiece, and the mode of energy deposition (i.e., melt-in conductor or keyhole).

5.6. TRANSFER EFFICIENCY OF PROCESSES

The sum of all losses (described in Section 5.5) determines the *energy* or *heat transfer efficiency* of the process. This transfer efficiency is expressed as a

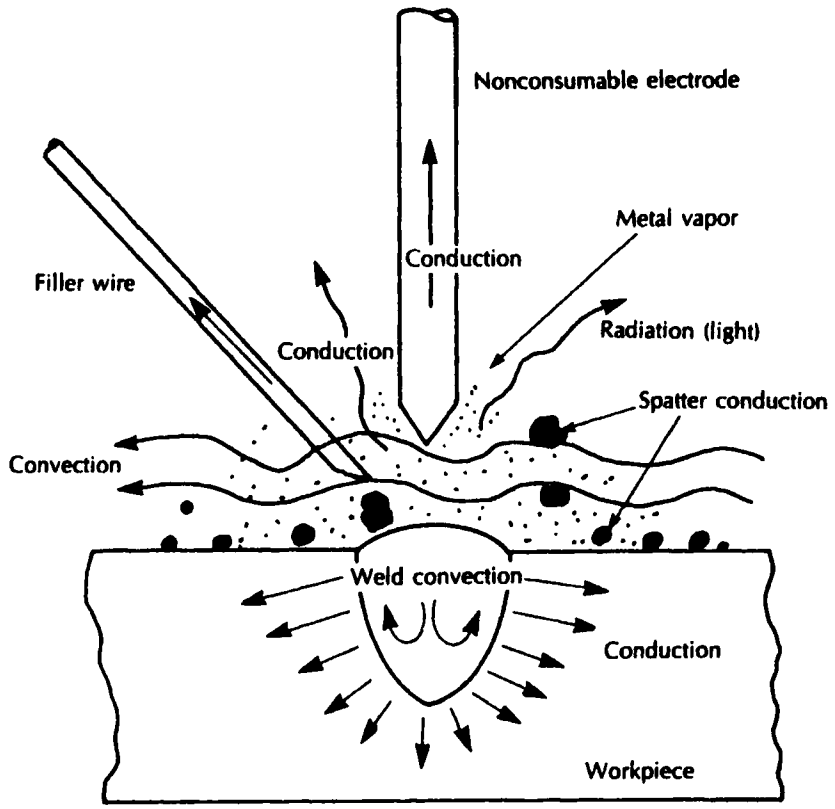


Figure 5.2 Causes of loss of energy during transfer from a welding source to the workpiece. (From *Joining of Advanced Materials* by R. W. Messler, Jr., published in 1993 by and used with permission of Butterworth-Heinemann, Woburn, MA.)

fraction ranging from 0.0 to 1.0, that lowers the *net energy* or *heat input* according to a modified form of Eq. 5.3 (or 5.4), to give

$$H_{net} = \eta \frac{P}{v} \tag{5.5}$$

or

$$H_{net} = \eta \frac{EI}{v} \tag{5.6}$$

Anything that prevents or reduces a loss, increases the energy transfer efficiency, η, to a maximum of 1.00 (or 100%). Some typical energy transfer efficiencies for various fusion welding processes are shown in Table 5.3.

As an example of how the characteristics of the process can affect the energy transfer efficiency, consider the submerged arc welding (SAW) process. Energy

TABLE 5.3 Typical Energy (or Heat) Transfer Efficiencies η for Various Fusion Welding Processes

Process	Transfer Efficiency
Oxyfuel gas	
Low combustion intensity fuel	0.25–0.50
High combustion intensity fuel	0.50–0.80
Gas–tungsten arc	
Low current DCSP mode	0.40–0.60
High current DCSP mode	0.60–0.80
DCRP mode	0.20–0.40
AC mode	0.20–0.50
Plasma arc	
Melt-in mode	0.70–0.85
Keyhole mode	0.85–0.95
Gas–metal arc	
Globular or short-arc transfer mode	0.60–0.75
Spray transfer mode	0.65–0.85
Shielded-metal or flux-cored arc	0.65–0.85
Submerged arc	0.85–0.99
Electroslag	0.55–0.85
Electron beam	
Melt-in mode	0.70–0.85
Keyhole mode	0.85–0.95+
Laser beam	
Reflective surfaces or vapors	0.005–0.50
Keyhole mode	0.50–0.75+

transfer efficiency is very high (0.85–0.99 from Table 5.3) because losses from radiation of light and heat, through convection of heat to the air and through metal vapor and spatter, are virtually eliminated. The material can play a role based on its thermal conductivity (which will contribute to heat loss by conduction from the point of energy deposition to the colder surrounding mass) or its tendency to reflect (as opposed to absorb) energy (as occurs with the laser process for some specular metals and certain laser wavelengths). The mode of energy deposition can also play a role, with better, more efficient transfer for the keyhole compared to the melt-in mode (see Section 5.8)

The transfer efficiency of a particular process is determined using calorimetric measurements. Various methods are employed, including wet and dry calorimetry. In wet calorimetry (Kou and Le, 1984), cooling water is used to remove the heat deposited into a special workpiece, usually in the form of a pipe. The transfer efficiency is determined from the temperature rise of the

water for a known flow rate:

$$WC(T_{out} - T_{in})dt = \eta EIt_{weld} \tag{5.7}$$

where W = mass flow rate of water (in g/s), C = specific heat of water (in $J/g°C^{-1}$), T_{out} = water temperature at the outlet of the calorimeter (°C), T_{in} = the temperature of the water at the inlet to the calorimeter (°C), t = time (in s), t_{weld} = welding time (in s), η = arc (or other source using a similar equation) transfer efficiency, E = welding voltage (in V), and I = welding current (in A). A schematic illustration of a wet calorimeter is shown in Figure 5.3.

In a dry calorimetric method (Malmuth et al., 1974), a specimen is subjected to a stationary (as opposed to moving) arc, and the transient thermal response of the specimen is recorded and compared to the theoretical response of the same specimen to deduce the amount of heat actually transferred from the arc

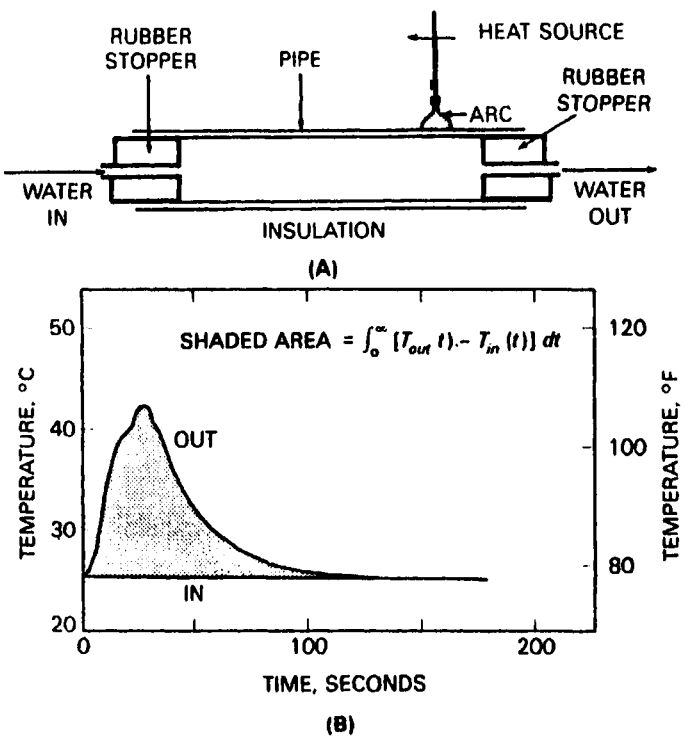


Figure 5.3 Schematic of a wet calorimeter being used to measure arc energy transfer efficiency for the GTA welding process: (a) calorimeter and (b) rise in cooling water temperature as a function of time (From *Welding Handbook*, Vol. 1: *Welding Technology*, 8th ed., edited by L. P. Connor, published in 1987 by and used with permission of the American Welding Society, Miami, FL.)

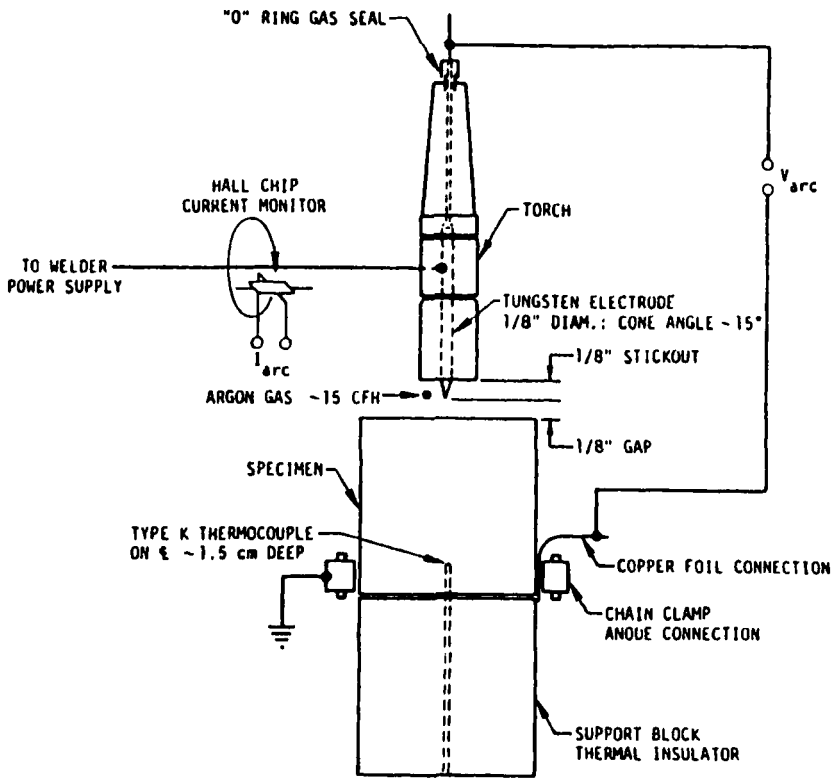


Figure 5.4 Schematic of a dry calorimetric apparatus for measuring arc energy transfer efficiency. (From "Transient thermal phenomena and weld geometry in GTAW" by N. D. Malmuth, W. F. Hall, B. I. Davis, and C. D. Rosen, *Welding Journal*, 53(9), 388s–410s, 1974, published by and used with permission of the American Welding Society, Miami, FL.)

to the specimen or workpiece. A schematic of a dry calorimetric apparatus for measuring arc energy transfer efficiency is shown in Figure 5.4.

Other similar devices and methods have been used to determine the efficiency of energy transfer for various welding processes under different conditions of their operation. Transfer efficiency is important because it strongly affects the input of heat to the workpiece and subsequent distribution of heat within the workpiece (described in Chapter 6).

5.7. EFFECTS OF DEPOSITED ENERGY: GOOD AND BAD

The primary function of a heat source for fusion welding is to melt material. For some nonfusion welding, where pressure is used but the required mechan-

ical power wants to be kept low and the rate of welding made faster, a heat source may be used or just the heat generated from mechanical work can be used to lower the flow strength in the vicinity of the weld interface to allow atoms to move by plastic deformation. Unfortunately, not all of the energy deposited from a heat source after considering transfer efficiency goes into causing this desired melting or plasticizing, that is, solid-phase softening by lowering of the yield strength, to occur. Some heat is lost to the surrounding mass of material through conduction, and the resulting heating can alter the microstructure in unfavorable ways. Let's look at these desirable and adverse effects in a little more detail.

5.7.1. Desirable Melting, Fluxing, or Softening

In fusion welding, melting is essential to the proper operation of the process and the proper formation of sound welds. The resulting liquid performs two functions: (1) It moves mass from the substrates and a filler, if one is used, to fill gaps in the joint, thereby establishing material continuity; and (2) it causes some cleaning of the faying surfaces of the joint through a fluxing action based on dissolution and, possibly, chemical reduction. Thus, causing melting is the primary function of the energy source.

Melting efficiency is the fraction of the net energy input (see Section 5.6, Eqs. 5.5 and 5.6), H_{net}, that is used for actually melting material. Figure 5.5 schematically illustrates the cross section of a typical bead-on-plate weld (i.e., a weld made in a plate without an actual joint being present). It shows three characteristic areas: (1) A_m = area of base material that was melted; (2) A_r = area of reinforcement, representing the volume of any filler material added in the molten condition; and (3) A_z = area of heat effect to the base material known as the heat-affected zone. The overall weld cross-sectional area, A_w, is:

$$A_w = A_m + A_r \tag{5.8}$$

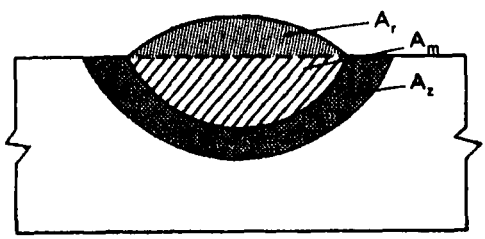


Figure 5.5 Schematic of the cross section of a bead-on-plate weld showing three key zones: (a) A_m = area of base material melted; (b) A_r = area of reinforcement, representing the volume of filler added in the molten condition; and (c) A_z = area of heat effect to the base material. (From *Welding Handbook*, Vol. 1: *Welding Technology*, 8th ed., edited by L. P. Connor, published in 1987 by and used with permission of the American Welding Society, Miami, FL.)

If no filler is added, that is, if the process is performed autogenously, then

$$A_w = A_m \tag{5.9}$$

A theoretical quantity of heat, Q, is needed to melt a given volume of metal, starting with the metal at ambient temperature. The amount is composed of (1) the heat needed to elevate the temperature of the solid metal to its melting point and (2) the extra, latent heat needed to convert the solid to liquid at the melting point, known as the heat of fusion. To a reasonable approximation, Q is given by

$$Q = \frac{(T_m + 273)^2}{300{,}000} \tag{5.10}$$

where T_m is the melting point or liquidus of the material (in °C). The melting efficiency, f, of a weld pass or energy deposition along a path in a given run can be determined by measuring the weld metal cross section and the net heat input. The melting efficiency, f, is the minimum amount of arc (or other source) heat needed for melting according to theory, divided by the net energy input:

$$f = \frac{QA_w}{H_{net}} = \frac{QA_w v}{\eta P} = \frac{QA_w v}{\eta EI} \tag{5.11}$$

Melting efficiency depends on both the welding process being employed and the material being welded, as well as other factors such as joint configuration and workpiece thickness (see Section 6.1). The higher the thermal conductivity of the base material being welded, the lower the melting efficiency. This is so because heat is lost to the surrounding mass rather than being used to cause melting. The effect is greater for low-energy-density sources than for high-energy-density sources. For example, in oxyacetylene welding, only about 2% of the heat delivered to the workpiece actually causes melting. The rest is lost by conduction to the surrounding workpiece mass. For this reason, it is difficult to weld aluminum and copper using oxyacetylene (or oxyfuel gas). For electron-beam welding, on the other hand, where energy density is very high (see Table 5.2), melting is virtually 100% efficient, which means that all of the energy delivered to the workpiece goes into melting and very little into the formation of a heat-affected zone.[4]

By rearranging Eq. 5.11 and substituting for H_{net} from Eq. 5.5 or 5.6, an important and simple relationship between weld area and net heat input results:

$$A_w = \frac{fH_{net}}{Q} = \frac{\eta fH}{Q} \tag{5.12}$$

[4] In fact, above an energy density of about 10^3 W/mm^2 or 10^9 W/m^2 (76.5 MW/in.^{2}), metals tend to boil, so vaporization rather than melting is favored. The result is that such sources (e.g., electron and laser beams) produce grooves or holes. In fact, electron beams and lasers are used for cutting, machining, and drilling.

Neither transfer efficiency (η) nor melting efficiency (f) changes very much with changes in welding parameters such as voltage or amperage or travel speed, only with process due to energy density of the source and operating mode (i.e., keyhole versus melt-in, as described in Section 5.8).

For some fusion welding processes (e.g., resistance flash welding), some nonfusion welding processes (e.g., explosion welding), and all brazing and, to a lesser degree, soldering processes, melting efficiency is poor, and only a small quantity of liquid is produced. This liquid, while not needed to provide mass, is used to clean the faying surfaces of any thin oxide or other tarnish layers that would otherwise interfere with obtaining needed metallurgical continuity. Thus, the liquid produced only serves as a fluxing agent (see Section 11.2.4). Molten base metal or filler, probably in the form of an intermediate layer, produced in the processes just mentioned fluxes faying surfaces by dissolving the oxide or tarnish compounds, possibly with some chemical reduction as well.

In nonfusion welding processes, not only is melting not required to obtain metallurgical continuity, it is often undesirable. In nonfusion welding, pressure is the key to obtaining metallurgical continuity. For many nonfusion welding processes, mechanical work from pressure or from friction generates heat (i.e., mechanical energy is converted to thermal energy). This heat, in turn, lowers the flow strength of the material and, thereby, facilitates movement of atoms to close gaps, obtain continuity, and produce a weld. For these processes, the desirable effect of heat, which, rather than being transferred to the workpieces from an energy source, is generated within the workpieces through the work done at their faying surfaces, is to plasticize material at the faying surfaces.

Thus, whether it is to cause melting or simply plasticize material at faying surfaces, thermal energy provided by energy sources is performing an important and desirable function.

5.7.2. Adverse Effects of Heat In and Around the Weld

Any heat that is lost to the surrounding mass of workpieces can and usually does result in adverse effects. The principal effects manifest themselves as a heat-affected zone. Heat-affected zones are discussed in detail in Chapter 16. Suffice it to say now that a heat-affected zone, or HAZ, is the region surrounding the actual weld (either the region of melting in a fusion weld or the region of bonding in a nonfusion weld) that has been subjected to and affected by heat lost to the surroundings by conduction. What specific effects take place depend on the fundamental response of the base material(s) to heat or temperature as a function of time. Rarely, however, are any changes that take place desirable. Almost without exception, material properties in an HAZ are degraded compared to the base material; if for no other reason than the designer almost certainly uses bases metal properties in sizing structure.

5.8. EFFECTS OF ENERGY DENSITY AND DISTRIBUTION

As described in Section 5.7.1, the density of energy deposited on workpieces is the prime determinant in the efficiency with which melting in fusion welding processes takes place. As the energy density increases, melting efficiency increases. Recall the example of electron-beam welding (EBW) versus oxyacetylene welding (OAW).

When energy is transferred to a workpiece from a flame or electric arc or beam, that energy strikes the surface and immediately causes heating by a combination of conduction of heat in the flame, arc, or, to a much lesser extent, beam, and conversion of kinetic energy. If the rate at which energy is being deposited exceeds the rate at which heat is being conducted away, the temperature will rise to eventually cause melting and produce a fusion weld. This mode of energy deposition and weld production is called the *melt-in mode* or the *conduction mode.* In the melt-in or conduction mode, the temperature is maximum at the point of deposition, on or near the surface. From that point outward into the mass of the workpiece, the temperature drops off. Depending on the total amount and rate of energy deposition, as well as the thermal conductivity and mass of the workpiece, heat energy is partitioned between melting to produce a fusion zone and just heating to produce a heat-affected zone.

If the density of the energy coming from a source is high enough, the rate at which it is deposited greatly exceeds the rate at which it is lost by being conducted into the workpiece(s). In this case, the material at the point of deposition rises in temperature not just to the melting point, but well above that. In fact, the temperature can rise to the boiling point, converting liquid to vapor, superheating the vapor. When this occurs, the energy source is said to be operating in the *keyhole mode.* This mode (as opposed to the melt-in mode) begins to occur at energy densities above around 10^9 W/m^2, 10^5 W/cm^2, or 10^3 W/mm^2.

Once vapor is formed by such high energy densities, it expands, is released upward away from the surface, and produces a reaction force that presses the melt downward and sideways. The result is a depression that permits additional photons (from a laser beam), electrons (from an electron beam), or electrons and ions (from a plasma arc) to impinge upon fresh material, which is then heated in the same way. The depression becomes larger and transforms to a keyhole, the entire central core of which consists of vapor surrounded on all sides by an envelope of liquid. For sufficient energy input, this keyhole will penetrate entirely through the thickness of the workpiece, even if this is several centimeters or inches. In this way, the faces of the two joint elements can be melted, the molten material flows back into the molten weld pool, metallurgical continuity is obtained, and solidification can occur to produce a weld. Figure 5.6 schematically shows the extremely rapid sequence of steps, while Figure 5.7 schematically shows the forces involved in the formation of the keyhole. Figure 5.8 presents an isometric illustration showing the movement of the keyhole to produce a weld.

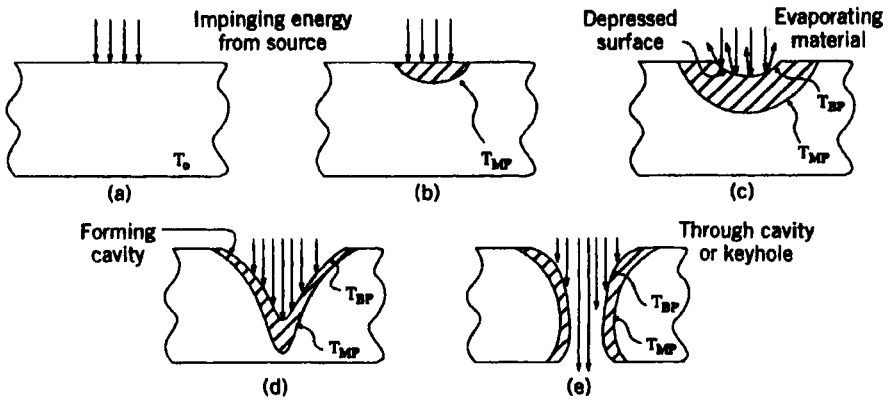


Figure 5.6 Schematic showing the extremely rapid sequence of steps leading to the formation of a keyhole when the density of energy being deposited is high enough: (a) initial deposition of impinging energy on the surface; (b) surface heating and inward propagating of heat to cause melting anywhere $T > T_{MP}$; (c) continued inward propagation of heat to raise a larger volume of material to above T_{MP}, and elevation of temperature near the surface to above T_{BP}, causing vaporization and a downward force on the liquid; (d) continued deposition of heat, increased vaporization and greater depression of liquid, and increased growth of melted volume; and (e) eventual penetration of vapor cavity through thickness to produce a keyhole of vapor surrounded by molten material.

While welding proceeds with a keyhole, hydrodynamic forces (particularly from gravity) intermittently cause the molten envelope surrounding the vapor cavity or keyhole to collapse. When this occurs, the stream of incoming energy is momentarily blocked, penetration is momentarily lost, and defects in the form of voids can be left entrapped. This possibility is shown schematically in Figure 5.9. This phenomenon occurs in electron-beam welding (although there are ways, using tandem beams, to ameliorate it) and plasma-arc welding. In laser-beam welding, this can also occur, as well as the intermittent blocking of the incoming beam by reflection from the metal vapor plume being emitted from the keyhole. This latter problem is one of coupling between the laser and the workpiece.

Figure 3.10 schematically compares the melt-in and keyhole modes of operation for plasma arc welding.

The distribution of energy density from a source has an effect on the way in which that energy interacts with the workpiece. This is best known for laser sources, where changing the energy density distribution of the laser beam using a combination of source design (in terms of laser spectral frequency distribution) and optical lenses is relatively simple. This was shown schematically in Figure 5.1. Different energy density distributions in laser beams are used to perform different functions, from surface heat treatment or other modification, welding, cutting, drilling, or machining. In a similar way, the energy density distribution of electron beams can differ, depending on the way in which the beam is generated and/or focused. However, while some distributions are more

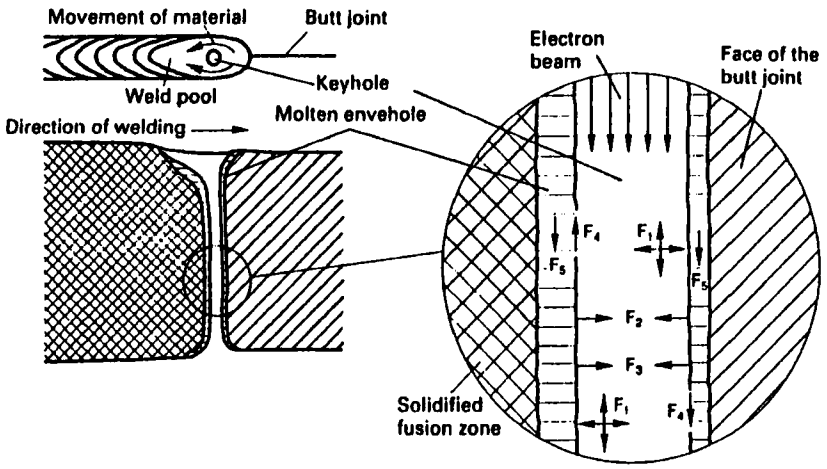


Figure 5.7 Schematic of the forces involved in the formation of a keyhole in electron-beam welding. (From *Electron Beam Welding* by H. Schultz, published in 1993 by and reprinted with permission of Abington Publishing, Woodhead Publishing, Cambridge, UK.)

undesirable that others, to the degree that corrections need to be made using focusing electromagnetic lenses, further investigation is needed to determine the relationship between the shape (i.e., energy density distribution) of the beam and the quality of the weld.

Figure 5.10 schematically shows the effect of energy (really power) density distribution on weld penetration and cross-sectional shape. In each case, the workpiece is 3.2-mm-thick aluminum alloy AA6061, while the welding heat input is a constant 880 W for a travel speed of 4.23 mm/s. Power density decreases from (a) to (d) in the figure.

More is said about the effects of the energy density distribution of a heat source impinging on a workpiece to produce a weld in Chapter 6.

5.9. SUMMARY

Only two fundamental forms of energy are used to make welds: heat (thermal) and pressure (mechanical). These forms can come from different sources, relying on chemical, electrical, or mechanical phenomena. To characterize the energy from a source, it is necessary to consider the total energy level or capacity of the source, as well as the rate of energy transfer or transferred power and energy density and density distribution. When the energy to produce a weld comes from a source external to the workpieces (as is the case for all fusion welding processes, except some aluminothermic welding), the

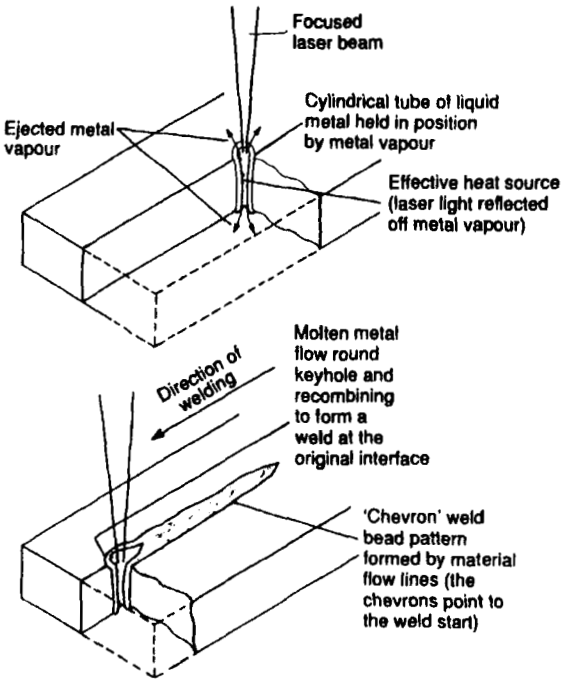


Figure 5.8 Isometric illustration of the movement of a keyhole in laser welding to produce a weld. (From *Laser Welding* by C. Dawes, published in 1992 by and used with permission of McGraw-Hill/Abington Publishing, Woodhead Publishing, Cambridge, UK.)

efficiency of energy transfer must also be considered by looking at all the possible causes of energy loss. This allows determination of the net heat input to the weld, which, in turn, helps determine the efficiency of melting. Energy density plays an important role because it determines the precise way in which energy enters the workpiece—by a melt-in or keyhole mode.

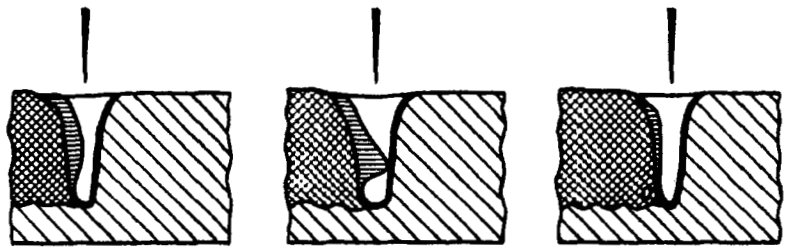


Figure 5.9 Possibility of interruption of beam penetration, with possible formation of voids, during keyhole welding with an electron beam. (From *Electron Beam Welding* by H. Schultz, published in 1993 by and used with permission of Abington Publishing, Woodhead Publishing, Cambridge, UK.)

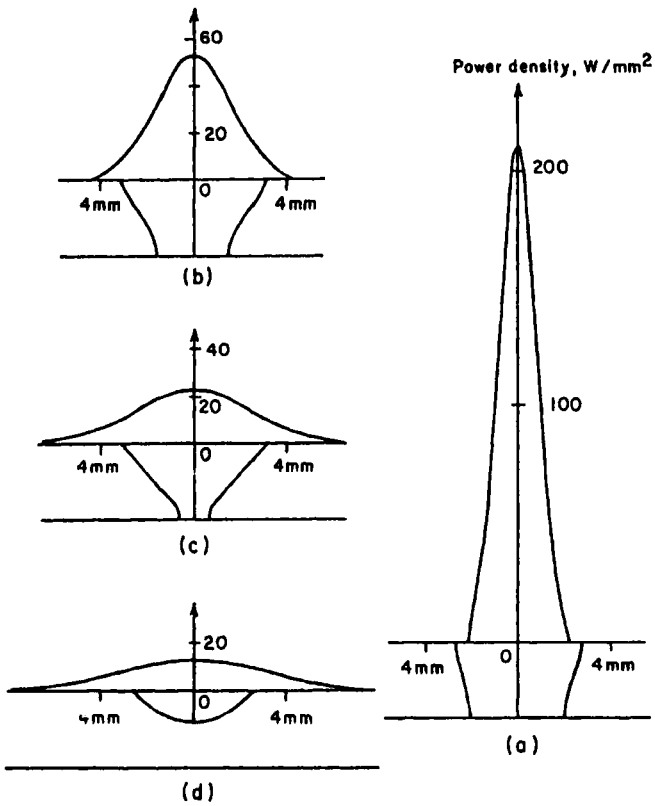


Figure 5.10 The effect of energy (really, power) density distribution of various heat sources on weld penetration and cross-sectional shape. The workpiece is a 3.2-mm-thick plate of aluminum alloy AA6061. Heat input is always 880 W, and travel speed is 4.23 mm/s. The energy (power) density decreases from (a), for EBW, to (b), for PAW, to (c) for GTAW operating with DCSP, to (d) for GTAW operating with DCRP. (From "Heat flow during the autogenous GTA welding of aluminum alloy pipes" by S. Kou and Y. Le, *Metallurgical Transactions A*, **15A**(6), 1165–1171, 1984, with permission of the ASM International, Materials Park, OH.)

REFERENCES AND SUGGESTED READING

Kou, S., and Le, Y., 1984, "Heat flow during the autogenous GTA welding of aluminum alloy pipes," *Metallurgical Transactions A*, **15A**(6), 1165–1171.

Malmuth, N. D., Hall, W. F., Davis, B. I., and Rosen, C. D., 1974, "Transient thermal phenomena and weld geometry in GTAW," *Welding Journal*, **53**(9), 388s–400s.

Suggested reading

AWS Handbook, Vol. 1: *Welding Technology*, 1987, 8th ed., edited by L. P. Connor, American Welding Society, Miami, FL.

Physics of the Welding Arc, 1966, Institute of Welding, London.

CHAPTER 6

THE FLOW OF HEAT IN WELDS

6.1. GENERAL DESCRIPTION OF THE FLOW OF HEAT IN WELDS

In fusion welding, a source of energy is necessary to cause the required melting of the materials to be joined. That source is usually chemical or electrical in nature, with losses occurring between the source and the workpiece (Section 5.5). Even after the net energy from the source is transferred to the workpiece as heat, not all of that heat contributes to cause melting to produce the weld. Some is conducted away from the point of deposition, raising the temperature of material surrounding the zone of fusion and causing unwanted metallurgical and geometric changes (Section 5.7.2). This surrounding region is called the heat-affected zone. The heat-affected zone is discussed in detail in Chapter 16.

In considering the effects of heat on melting and solidification in the fusion zone and in transformations and reactions in the surrounding heat-affected zone of a fusion weld, it is important to first consider how that heat is distributed once it reaches the workpiece, that is, how it flows. How that heat is distributed directly influences the rate and extent of melting, the rate of cooling and solidification in the fusion zone, and the rate and extent of peripheral heating and cooling in the heat-affected zone. The rate and extent of melting, in turn, directly affects the weld volume and shape, homogeneity through convection, the degree of shrinkage and attendant weldment distortion, and susceptibility to defects. The rate of solidification determines the solidification structure (including substructure) and, thus, properties. The rate and extent of peripheral heating affects the development of thermally induced stresses acting on the fusion zone (which contribute to fusion zone defect formation), the rate of cooling in the fusion zone (which controls solidification

mechanics and determines final fusion zone structure and properties), the rate and level of heating in the heat-affected zone (which can cause degradation of properties), the rate of cooling in the heat-affected zone (which determines the final structure and properties in this zone), and the degree and nature of distortion and/or residual stresses in the weldment.

The flow of heat (heat distribution) in fusion welds is addressed in the following subsections. What is described for fusion welding applies equally well to other joining processes employing heat, such as certain nonfusion welding processes and brazing or soldering.

6.2. WELD JOINT CONFIGURATIONS

One of the things that influences how the heat deposited (or generated) by an energy source flows and distributes in a weldment[1] is the size and shape of that weldment and, especially, weld joint. For this reason, weld joint configurations are briefly described here. The interested reader is referred to more specific references on this subject relating to weld joint design.

6.2.1. Types of Weld Joints

The loads in a welded structure are transferred from one member to another through welds placed in the joints. The type of joint, or the *joint geometry*, is predominantly determined by the geometric requirements or restrictions of the structure and the type of loading. Accessibility for welding, process selection, accessibility for inspection, and cost constraints, as well as the type of loading (e.g., uniaxial, biaxial, or triaxial; static or dynamic; tension, compression, shear, torsion or bending; single or combined) are other factors affecting the choice of joint type.

Weld joint configuration actually refers to more than just the joint geometry. Besides the shape or configuration of individual weld joints, it includes the location or placement of joints within the structure, that is, the structural arrangement. Together, joint configuration and the number and placement of weld joints determines ease of manufacture, cost, and structural integrity, including robustness against weld-induced distortion.

The fundamental types of welds are shown in Figure 6.1 and include groove welds, fillet welds, plug welds, and surfacing welds. Groove, fillet, and plug welds are used for joining structural elements. Surfacing welds are used for applying material to a workpiece by welding for the purpose of providing protection from wear or corrosion, or, perhaps, restoring dimensions lost

[1] A weldment is a structure containing welds or a structural assembly made by welding. It is important to know the difference between a weld and a weldment, although both the size, shape, number, placement, and sequence of producing welds and the size and shape of the weldment all influence heat flow and its effects.

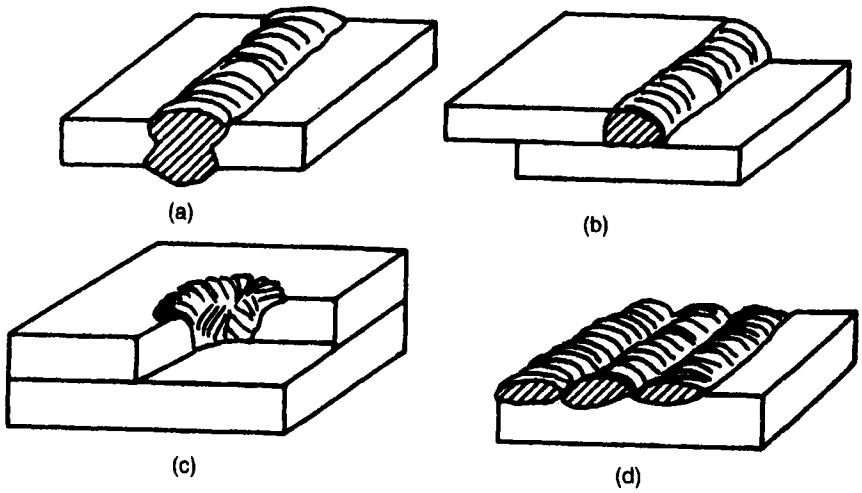


Figure 6.1 Fundamental types of welds, including (a) butt, (b) fillet, (c) plug, and (d) surfacing. (From *Joining of Advanced Materials* by R. W. Messler, Jr., published in 1993 by and used with permission of Butterworth-Heinemann, Woburn, MA.)

through wear or corrosion. The five basic joint designs for producing structures are (1) butt joints, (2) corner joints, (3) edge joints, (4) lap joints, and (5) tee (or T) joints, as shown in Figure 6.2. The plug weld is a special weld used to attach one workpiece to another locally through penetrations in the surface. While structural, plug welds generally do not provide the same degree of structural integrity as the other five weld joint types shown in Figure 6.2.

In practice, there are some variations of these five basic types that are worth mentioning. Butt welds or joints are also called square butts or straight butts when they are produced from joint elements prepared (before welding) with square or straight, 90° abutting edges. Such joints do not require filler metal, as they abut tightly, and are usually welded by an autogenous process such as GTAW, PAW, LBW, or EBW. For such welds, good fit-up, without gaps typically exceeding about $\frac{1}{16}$ in. or 1.5mm, is required, thereby placing additional constraints on preparation methods (usually machining versus sawing or thermal cutting). However, butt joints can have other preparations (by thermal or abrasive water-jet cutting, machining, or grinding) that can include single or double V's, single or double bevels, single or double J's, or single or double U's. These all require filler metal and so are performed by consumable electrode arc welding processes such as SMAW, FCAW, GMAW, or SAW. Likewise, corner joints can use no preparation, as in a single or double fillet, or have various preparations including a single V or a single V and a fillet. Edge welds can have no preparation, in which case they are called square edge welds, or a single V preparation. Lap or overlap joints can have single or double fillets, virtually always without any preparation. Finally, tee (T) joints

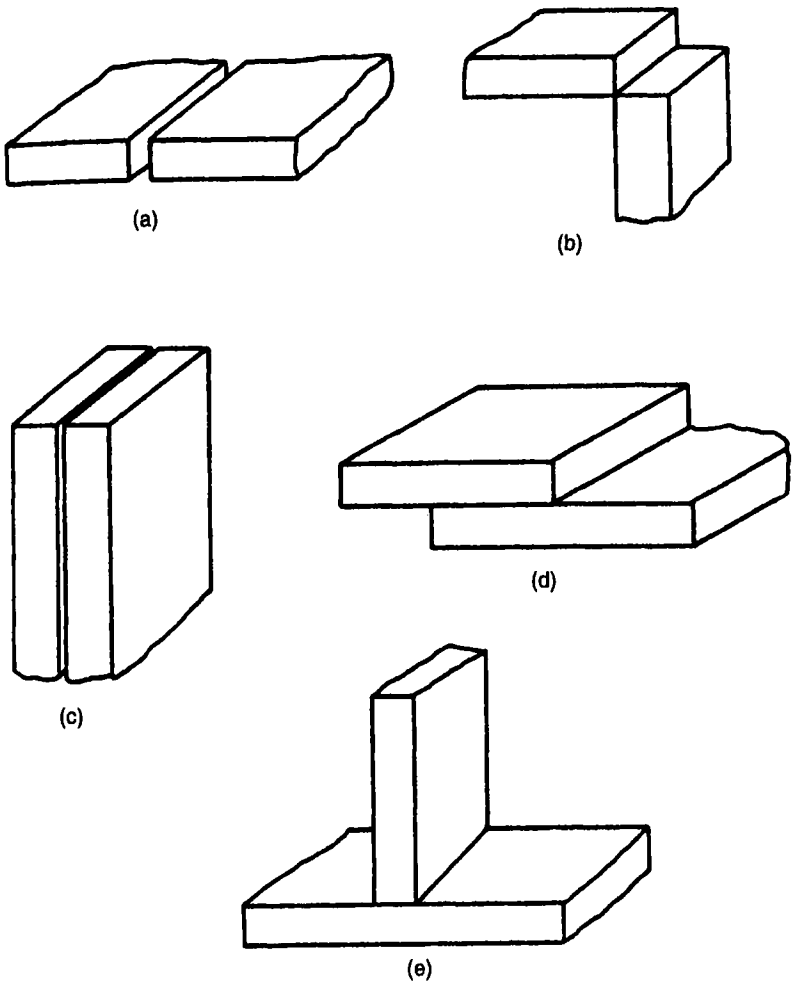


Figure 6.2 The five basic weld joint designs (other than plug welds) used in structural fabrication: (a) butt joint, (b) corner joint, (c) edge joint, (d) lap joint, and (e) tee joint. (From *Joining of Advanced Materials* by R. W. Messler, Jr., published in 1993 by and used with permission of Butterworth-Heinemann, Woburn, MA.)

can be made using double fillets, single or double bevels, or double J's. These variations of typical weld joints are shown in Figure 6.3.

Briefly, the square-groove is simple to prepare, economical to use, and provides satisfactory strength, but is limited by joint thickness. For thick joints, the edge of each member of the joint must be prepared to a particular geometry to provide accessibility for welding (torch tip and electrode or filler wire manipulation) and to ensure the desired weld soundness and strength. For economy, the opening or gap at the root of the joint and the included angle of

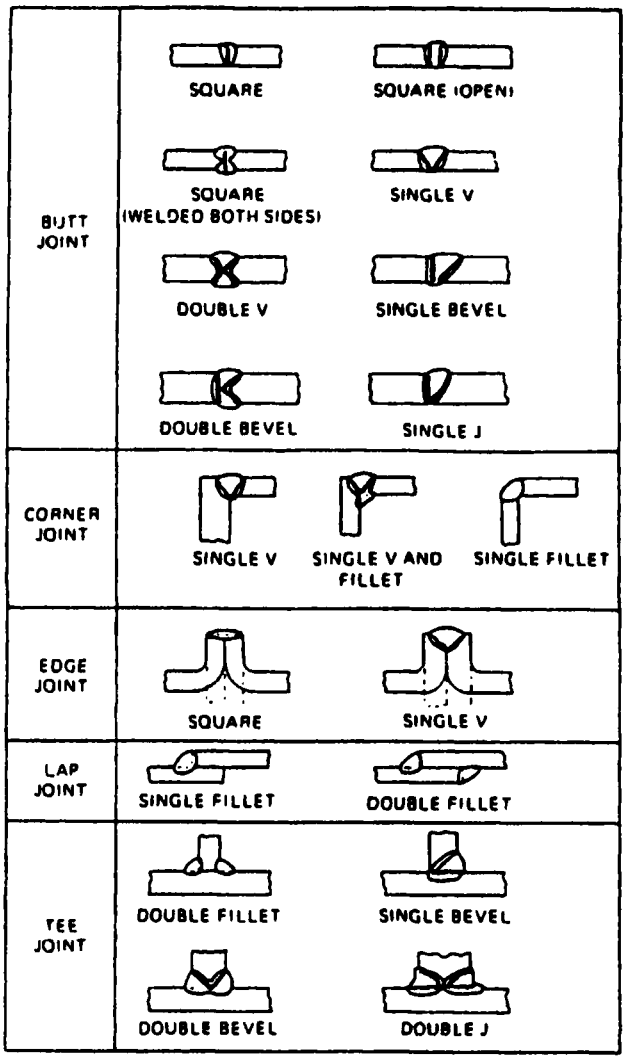


Figure 6.3 Some typical weld joint variations. (From *Joining of Advanced Materials* by R. W. Messler, Jr., published in 1993 by and used with permission of Butterworth-Heinemann, Woburn, MA.)

the groove should be selected to require the least weld metal necessary to give needed access and meet strength requirements. The J- and U-groove geometry minimizes weld metal requirements compared to V's, but adds to the preparation costs. Single-bevel- and J-groove welds are more difficult to weld than V- or U-groove welds because one edge of the groove is vertical. Figure 6.4 gives a schematic comparison of some of these shapes.

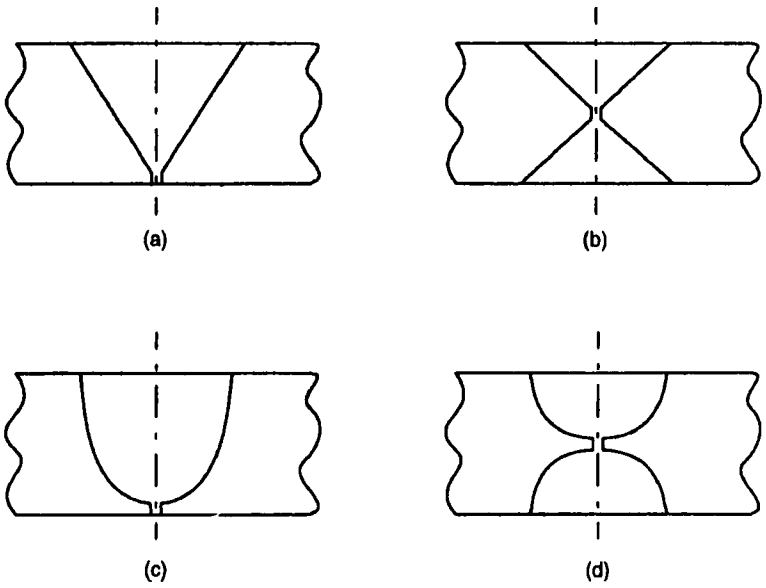


Figure 6.4 Schematic comparison of (a) single-V and (b) double-V joints and (c) single-U and (d) double-U joints.

Besides these basic weld joint shapes, welds (and the joints prepared to make those welds in or on) can be either *full penetration* or *partial penetration*, and *continuous* or *intermittent* (see Figure 6.5). Full penetration means melting all the way through the thickness of the joint, from entrance (or crown) to exit (or root), while partial penetration means less than through the thickness, or penetration without exit. Continuous means weld formation without any break, while intermittent means lengths of weld separated by lengths of joint that remain unwelded.

These basic joint types are used for all welding processes, with some types (e.g., straight butt) amenable to autogenous fusion processes (e.g., GTAW, PAW, EBW, or LBW) or some nonfusion processes (e.g., FRW, FOW), some (e.g., fillets and grooves) more amenable to arc fusion processes (e.g., SMAW, FCAW, GMAW, or SAW), and some (e.g., overlaps) to resistance (e.g., RSW) or certain nonfusion processes (e.g., EXW or USW).

The reason joint shape is so important to the flow of heat in a weldment is that the shape determines how much heat must be deposited to fill the joint, where that heat is deposited (at the surface or within the joint), and whether that heat flow will be one, two, or three dimensional (see Section 6.4).

6.2.2. General Weld Design Guidelines

The design of a joint for welding, as in other processes, should be selected primarily on the basis of load-carrying requirements. However, especially in

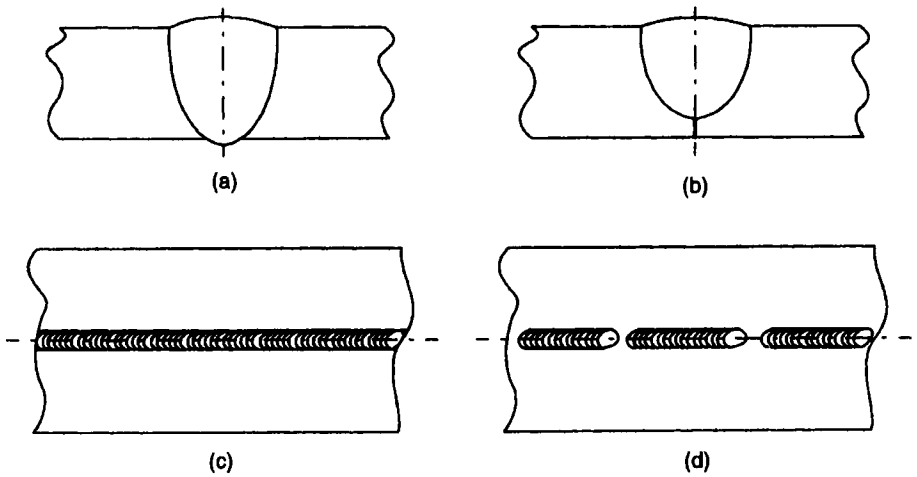


Figure 6.5 Schematic of (a) full- versus (b) partial-penetration and (c) continuous versus (d) intermittent welds.

welding, variables in the design and layout of joints can substantially affect the costs associated with welding, as well as the ability to carry loads safely, inherent susceptibility to the formation of certain defects, susceptibility to distortion, ability or facility to inspect quality, and other key properties (e.g., corrosion resistance, leak tightness, or hermeticity).

As a first guideline, always select the joint design that requires the least amount of weld metal. This will minimize distortion and residual stresses in the welded structure caused by weld metal shrinkage during solidification and due to thermal expansion and contraction under severe temperature gradients (as discussed in Chapter 7). Where possible, use square grooves (see Section 6.2.1) and welds that only partially penetrate the joint. Partial-penetration welds leave unmelted metal in contact throughout welding to help maintain dimensions (see Figure 6.5b). However, partial-penetration welds also leave behind a portion of unfused joint, which can act as a stress riser, much like an incipient crack, and cause problems, especially in fatigue. Use lap and fillet welds instead of groove welds when fatigue is not a design consideration. Use double-V or double-U instead of single-V or single-U groove welds on thick plates to reduce the volume of weld metal and control distortion (by balancing heat input on top and bottom surfaces). For corner joints in thick plates where fillet welds are not adequate, beveling of both members should be considered to reduce the tendency for lamellar tearing.[2] Finally, always design an assembly and its joints for good accessibility for any welding and inspection that will be required.

[2] Lamellar tearing is tearing in the plane of a plate caused by tensile stresses acting perpendicular to the plane of that plate and aggravated by the presence of processing-aligned nonmetallic inclusions in the plate (see Section 16.8.5).

6.2.3. Size of a Weld and Amount of Welding

Overdesign is a common error in welded structures, as is overwelding in production. Control of weld size and the amount of weld begins in design, but must be maintained during assembly and welding. Overdesign and overwelding both lead to excessive and unnecessary cost and weight. Adequate, but minimum size and length, welds should be specified for the forces to be transferred and stresses allowed. Oversize welds may cause excessive distortion and higher residual stresses, without improving suitability to service (see Chapter 7). The size of a fillet weld is especially important because the amount of weld required increases as the square of the weld fillet size increases.

For equivalent strength, a continuous fillet weld of a given size is usually less costly than a larger intermittent fillet or skip weld. Also, there are fewer weld terminations that are potential sites for flaws (e.g., "crater cracks"). An intermittent fillet weld can be used in place of a continuous fillet weld of minimum size when a static loading condition exists. An intermittent fillet weld should not be used under cyclic fatigue loading (to preclude defect formation and/or stress concentration at weld start and stop locations). For automatic welding, continuous welding is always preferred (to make both seam tracking and weld schedule planning simpler).

Welds should always be placed in the section of least thickness, and the weld size should be based on the load or other requirements of that section. (An exception is when the weld is placed in a section of slightly greater thickness i.e., a raised land), to lower the stress in the actual weld to satisfy demanding fracture toughness requirements.) The amount of welding should be kept to a minimum to limit distortion and internal stresses and, consequently, the need for postweld stress relieving and straightening. Welding of stiffeners or diaphragms should be limited to that required to carry the load.

There are many more important considerations in the design of welds, but those presented provide some appreciation of the problems. Again, the reader interested in weld design is referred to some specific references on the subject (see References and Suggested Reading).

6.3. THE WELDING THERMAL CYCLE

Most welding processes cause material in the workpiece to undergo a thermal excursion.[3] For fusion welding processes (on which we focus our attention in the remainder of this chapter, and most of the rest of this book), that excursion ranges from the ambient temperature of the work environment (e.g., shop, construction site, or shipyard), to above the liquidus temperature (possibly to the point of boiling and above for some very high-energy-density processes

[3] In fact, welding causes material in the workpiece to undergo combined excursions of temperature and pressure or force, the latter being much more important in nonfusion processes, and both being important in fusion processes.

operating in the keyhole mode). The severity of this excursion in terms of the temperatures reached and the times taken to reach them and remain at them completely determines the effects on structure (both microstructural for material changes and macrostructural for distortion). The *welding thermal cycle* must be known, because the thermal history influences the structure–property relationship.

If thermocouples are placed at various points along the path of a weld, presumed to have been started in the middle of a plate to avoid edge, effects, as shown in Figure 6.6a, then a series of thermal cycles are obtained, as shown in Figure 6.6b. Each individual thermocouple responds, in turn, to the approach of the heat source, with a rapid rise in temperature to a peak, a very short hold at that peak, and then a rapid drop in temperature once the source has passed by. Some short time after the heat from the source (say electric arc) begins being deposited, it can be seen that the peak temperature, as well as the rest of the thermal cycle, reaches a state of quasi-steady state. This quasi-steady state (or quasi-stationary condition) is the result of a balance having been achieved between the rate of energy input and the rate of energy loss or dissipation due to conduction into the cooler regions of the workpiece or loss to the environment. This also means that some short time after source (arc) initiation and heat deposition, and away from edges, the temperature isotherms surrounding a moving heat source remain steady and seem to move with the heat source. This is shown in Figure 6.7.

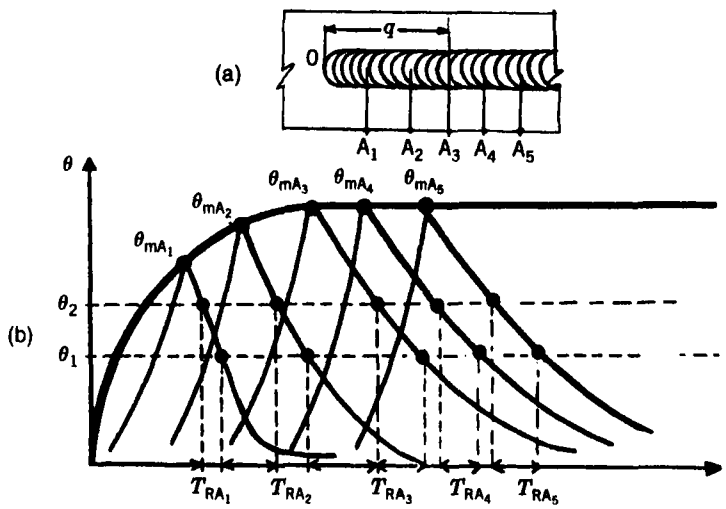


Figure 6.6 Schematic of (a) thermocouple placement along the path of a moving heat source and (b) the thermal cycle produced at each point to yield an overall response. (From *Fundamentals of Welding Metallurgy* by H. Granjon, published in 1991 by and used with permission of Abington Publishing, Woodhead Publishing, Cambridge, UK.)

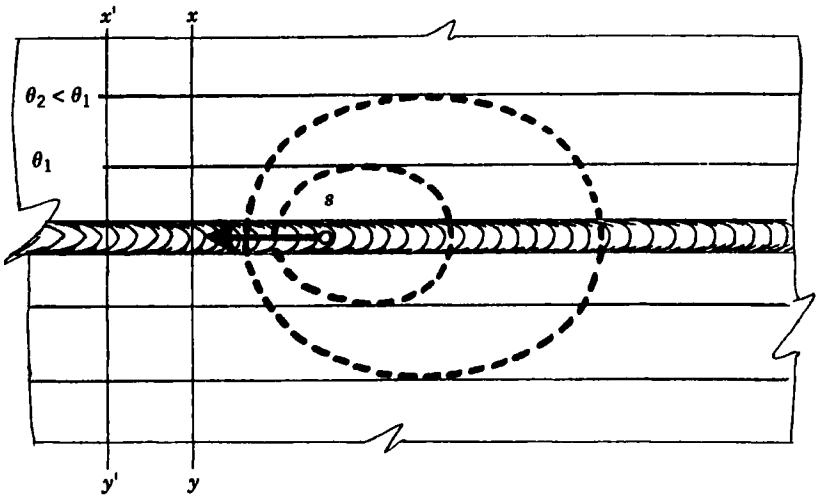


Figure 6.7 Schematic showing the establishment of quasi-steady-state (or quasi-stationary) condition in a weld made by moving a heat source after the passage of some time. (From *Fundamentals of Welding Metallurgy* by H. Granjon, published in 1991 by and used with permission of Abington Publishing, Woodhead Publishing, Cambridge, UK.)

Because of the establishment of quasi-steady state (even for a moving heat source), thermal cycles (temperature–time curves) can be determined for points distributed progressively further from the centerline of the path of the welding heat source along a line perpendicular or transverse[4] to the weld path. Temperature–time traces for three points, *A*, *B*, and *C*, are shown in Figure 6.8, with the following observations:

1. The temperature–time curves are situated one under the other, as the distance from the weld centerline increases. In particular, the maximum temperatures reaching above T_m decrease with increasing distance from the source, and more or less abruptly depending on the temperature gradient that characterizes the particular process (especially its energy density and distribution, and also its net heat input) and procedure (operating mode, manipulation, etc.). Every curve shows that temperature returns asymptotically to ambient.
2. The maximum temperatures reached (T_{mA}, T_{mB}, T_{mC}) decrease with distance from the weld line and occur at times (t_{mA}, t_{mB}, t_{mC}) that increase. This allows the peak temperature, T_p, to be plotted as a function of time. This peak temperature separates the heating portion of the welding thermal cycle from the cooling portion, and expresses the fact that points closest to a weld are already cooling, while points farther

[4] Longitudinal is in the direction of welding; transverse is perpendicular to that direction.

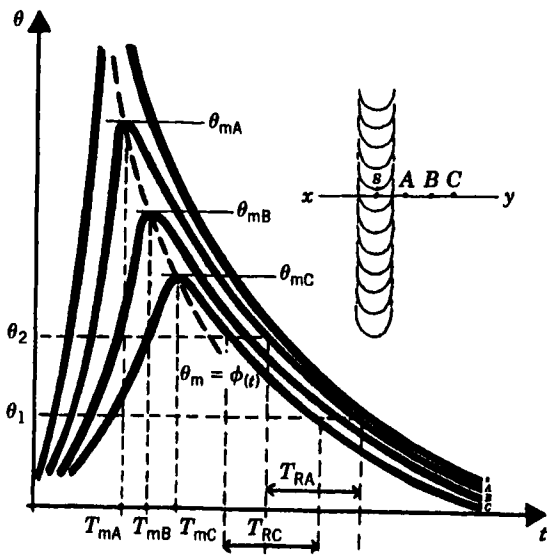


Figure 6.8 Schematic of temperature–time traces for three points located along a line perpendicular to a weld during passage of a moving welding heat source. Note the displacement in the times of occurrence of the maximum temperatures and the quasi-steady-state nature of cooling times in the lower portion of the curves. (From *Fundamentals of Welding Metallurgy* by H. Granjon, published in 1991 by and used with permission of Abington Publishing, Woodhead Publishing, Cambridge, UK.)

away are still undergoing heating. This phenomenon explains certain aspects of phase transformations that go on in the heat-affected zone, as well as differential rates and degrees of thermal expansion and contraction that lead to thermally induced stresses and, possibly, distortion.

3. Given the arrangement of the thermal history curves, the rate of cooling (measured from the maximum temperature) decreases with distance from the weld line. However, the cooling portion of curves rapidly produces tightly grouped rates as cooling progresses, so that by the time temperature drops to a certain point, the cooling rates are quite similar. This can be seen by comparing the times t_{RA} and t_{RC} for points A and C.

The overall spatial distribution of welding thermal cycles has been described by Portevin and Seferian (1935) as a "heat solid," as shown schematically in Figure 6.9. In this representation, S_x is the distance from the path of the welding heat source, known as the weld line, S_y is the distance along the weld line, and S_z is temperature. Because of quasi-steady state, the heat solid remains unchanged throughout the length of the weld line. If the heat solid is cut into planes parallel to xy through the origin at 0 (the xoy plane) and intersections are projected onto the xoy plane, contour lines of instantaneously equal

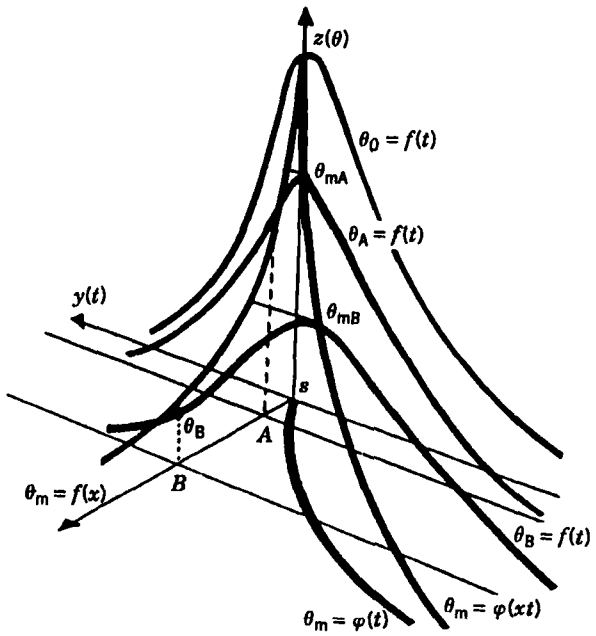


Figure 6.9 A schematic of the "heat solid" suggested by Portevin and Seferian. Distribution of the instantaneous temperatures around a heat source (moving under quasi-steady-state) at the moment it passes point S during movement along line S_y. Temperatures are plotted only along S_z for each distance x for the weld line. (From *Fundamentals of Welding Metallurgy* by H. Granjon, published in 1991 by and used with permission of Abington Publishing, Woodhead Publishing, Cambridge, UK.)

temperature are obtained. Movement of these curves produces isotherms parallel to the weld itself, as shown in Figure 6.10. The utility of the heat solid is that temperature, time, and distance can all be viewed to help understand what the material surrounding a weld goes through.

When a weld is made without moving the heat source, there is no quasi-steady state or quasi-stationary condition because the weld is produced by localized input of energy sufficiently intense not to be offset by conduction of heat away into the workpiece mass. Nevertheless, metallurgical phenomena can be interpreted by considering the temperature–time cycles (welding thermal cycles) as $T = f(t)$ and the distribution of final structure (and properties) by means of $T_m = f(x)$ or $T_m = f(r)$ in polar coordinates.

6.4. THE GENERALIZED EQUATION OF HEAT FLOW

The thermal conditions in and near the fusion zone of a fusion weld must be maintained within specific limits to control metallurgical structure, residual

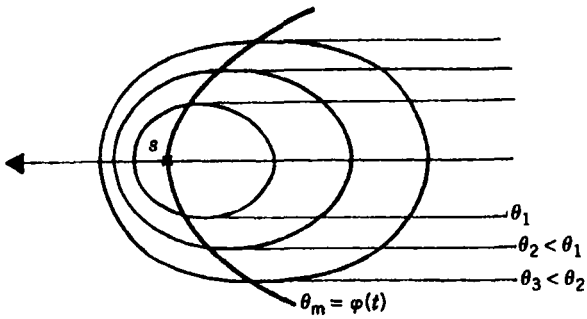


Figure 6.10 Formation of isotherms in the plane xsy by projection of curves of equal instantaneous temperature from a heat solid and the movement of that solid. (From *Fundamentals of Welding Metallurgy* by H. Granjon, published in 1991 by and used with permission of Abington Publishing, Woodhead Publishing, Cambridge, UK.)

stresses and distortions, and chemical reactions (e.g., oxidation) that result from a welding operation. Of specific interest are (1) the solidification rate of the weld metal, (2) the distribution of maximum or peak temperature in the weld heat-affected zone, (3) the cooling rates in the fusion and heat-affected zones, and (4) the distribution of heat between the fusion zone and the heat-affected zone.

The transfer of heat in a weldment is governed primarily by the time-dependent conduction of heat, which is expressed by the following general equation of heat flow:

$$\rho C(T)\frac{dT}{dt} = \frac{d}{dx}\left[k(T)\frac{dT}{dx}\right] + \frac{d}{dy}\left[k(T)\frac{dT}{dy}\right] + \frac{d}{dz}\left[k(T)\frac{dT}{dz}\right]$$

$$- \rho C(T)\left(V_x\frac{dT}{dx} + V_y\frac{dT}{dy} + V_z\frac{dT}{dz}\right) + Q \qquad (6.1)$$

where

x = coordinate in the direction of welding (mm)
y = coordinate transverse to the welding direction (mm)
z = coordinate normal to weldment surface (mm)
T = temperature of the weldment, (K)
$k(T)$ = thermal conductivity of the metal (or ceramic) (J/mm s^{-1} K^{-1}) as a function of temperature
$\rho(T)$ = density of the metal (or ceramic) (g/mm^3) as a function of temperature

$C(T)$ = specific heat of the metal (or ceramic) ($J/g^{-1}K^{-1}$), as a function of temperature

Vx, Vy, and Vz = components of velocity

Q = rate of any internal heat generation, (W/mm^3)

Despite its complexity, all the terms in this equation are straightforward, except Q, which deserves some explanation. For most processes, energy from the source is deposited on the surface of the workpiece, with heat then being conducted or generated and conducted inward, by a melt-in or conduction mode. For some processes, as the energy density of the source becomes higher, some, most, or all of the energy or heat, depending on how high the energy density is, is deposited below the surface. This is the case for processes operating in the keyhole mode (e.g., PAW, LBW, or EBW), as well as for some high-intensity arc processes like SAW.

Surface heating is usually characterized by a heat-flux distribution, $q(x, y)$ applied over a relatively small area of the workpiece surface (see Sections 5.3.3 and 5.8), rather than from internal generation (Q).[5] This distribution is given by:

$$k(T)\frac{dT}{dz} = q(x, y) \tag{6.2}$$

where $q(x, y)$ is given in W/mm^2 and is directed onto the surface at $z = 0$. Heat is then lost to the surroundings by a combination of radiation and convection and conduction (see Section 5.5)

Whether this general equation needs to be solved for one, two, or three dimensions depends on the weldment and weld geometry, including whether the weld penetrates fully or partially and is parallel sided or tapered, and the relative plate thickness (as shown in Figures 6.2, 6.3, and 6.5). A one-dimensional solution can be used for welding a thin plate or sheet with a stationary source or for welding under steady state (at constant speed and in uniform cross sections remote from edges) in very thin weldments. A two-dimensional solution is most useful in relatively thin weldments or in thicker weldments where the weld is full penetration and parallel-sided (as in EBW) to assess both longitudinal and transverse heat flow. A full, three-dimensional solution is required for a thick weldment in which the weld is partial penetration or non-parallel-sided (as is the case for most single or multipass[6] welds made with an arc source). Examples of situations requiring one-, two-, or three-dimensional solutions are given in Figure 6.11.

[5] Other distributions can be used to better reflect the energy density distribution of the source. For arc welding sources considered to have a normal (Gaussian) distribution, a commonly used distribution is $q(r) = \{3\eta EI/\pi r'^2\}\exp[-3(r/r')^2]$, where r' is a characteristic distance in radial coordinates that defines the region within which 95% of the heat flux is deposited.

[6] Multipass welds refer to welds that require more than one pass of the welding heat source to deposit sufficient filler to fill the joint.

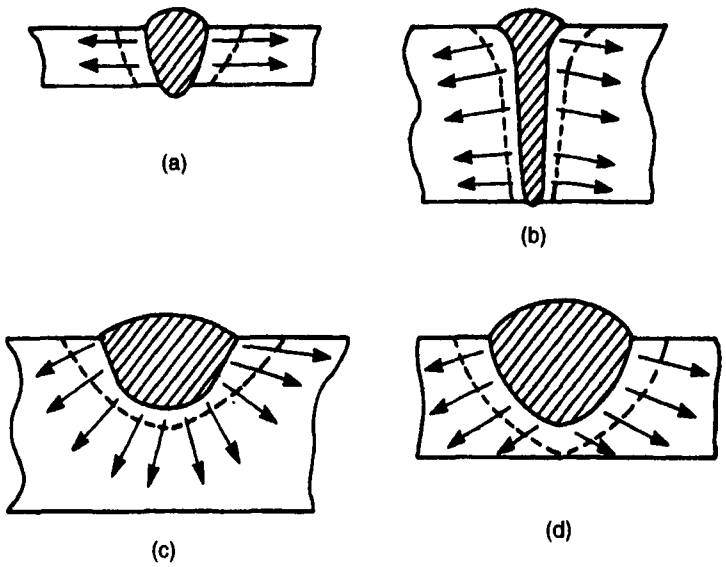


Figure 6.11 Schematic of the effect of weldment and weld geometry on the dimensionality of heat flow: (a) two-dimensional heat flow for full-penetration welds in thin plates or sheets; (b) two-dimensional heat flow for full-penetration welds with parallel sides (as in EBW and some LBW); (c) three-dimensional heat flow for partial-penetration welds in thick plate; and (d) an intermediate, 2.5-D, condition for near-full-penetration welds. (From *Joining of Advanced Materials* by R. W. Messler, Jr., published in 1993 by and used with permission of Butterworth-Heinemann, Woburn, MA.)

6.5. ANALYSIS OF HEAT FLOW DURING WELDING

Theoretical analyses of the weld thermal cycle, starting from the general heat flow equation (Eq. 6.1), have long been attempted. In the past, experimental results of weld heat transfer were fit to simplified equations suggested by heat transfer theory, and techniques were developed to calculate cooling rates, heat-affected-zone peak temperatures and dimensions, and solidification rates. These equations provided guidance for controlling the welding process and predicting specific properties that were desired. Once modern computers were developed, much of the need for fitting experimentally generated data to empirical curves was not necessary. Today, except for the most complicated situations (e.g., where heat flow in the weld is truly three dimensional and account must be taken of the strong temperature dependence of one or more thermophysical properties), the geometric weldment configuration can be modeled, and a solution to the generalized heat flow equation can be obtained numerically (e.g., using finite element and finite difference methods).

While computers can be used to solve the complex differential equations that model heat flow during welding, simplified equations supported by

engineering data still play a role in predicting fusion and heat-affected zone size and solidification and postsolidification (FZ or HAZ) cooling rates. After all, one can often get along quite well with a first-order approximation and general trends. Because of the complexity and highly specialized nature of the subject, details of computer-based modeling are left to the interested reader to seek out in appropriate welding literature. Given the mind-boggling rate at which progress in accuracy, sophistication, and speed of computation continues to be made, the best source of information is usually technical periodicals, such as the *Welding Journal*, *Journal of the Science and Technology of Welding and Joining*, and others devoted specifically to welding (as opposed to generalized computer-based modeling).

Ultimately, the value of reasonably accurate predictive models of heat transfer during welding is for enabling the intelligent automation of welding processes. Ideally, such models would operate, combined with sensors continuously monitoring the state of the weld and weldment, to control the process by making adjustments to key process parameters in real time in response to deviations from what is expected or wanted (Doumanidis and Hardt, 1990). However, it is worth remembering the anonymous adage: "It is not necessary or worthwhile to measure a manure pile with a micrometer." Crass as this may seem, there is a great lesson contained within: Only enough accuracy is needed in prediction to allow the process to operate properly and with consistency.

This being said, the subject of the analysis of heat flow during welding is approached from a more historical perspective here, with some useful rough-order-of-magnitude (ROM) predictive equations provided later. The goal is to provide an appreciation for what is involved, and an ability to obtain answers fast enough to allow a particular problem to be resolved without making huge investments in time or money for much more capable and accurate computer-based analysis. Obviously, if business warrants (either because of the number, volume, or value of different welded products), then computer-based modeling (and control) is the ultimate answer.

6.5.1. Rosenthal's Simplified Approach

It is worth looking briefly at one of the earliest, and still widely used simplified solutions of the generalized equation of heat flow, that of Rosenthal (1938, 1945, 1946). The key to Rosenthal's solution is the assumption of *quasi-* or *pseudo-steady state* (which was explained in Section 6.3).

Rosenthal's first critical assumption was that the energy input from the heat source used to make the weld was uniform and moved with a constant velocity v along the x-axis of a fixed rectangular coordinate system, as shown in Figure 6.12. This is not a bad assumption for many situations, provided heat flow is only considered some time after the welding source began depositing energy into the workpiece, and the workpiece is, from a heat flow standpoint, infinite (i.e., there are no edge effects). The net heat input to the weld under these

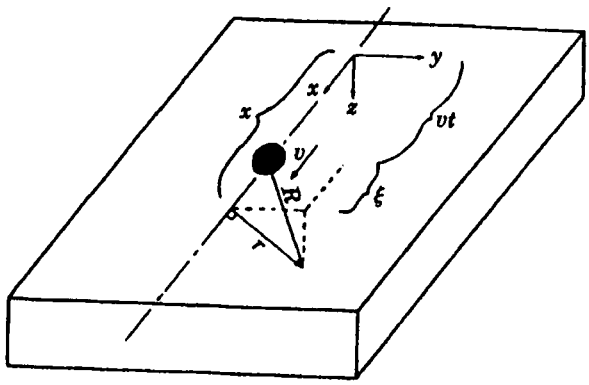


Figure 6.12 Coordinate system for Rosenthal's simplified, quasi-steady-state solution of the general heat flow equation. Welding is assumed to be done using a point source (q) moving at a constant velocity (v), so that, away from edges, steady-state isotherms that move with the source are formed. (From *Joining of Advanced Materials* by R. W. Messler, Jr., published in 1993 by and used with permission of Butterworth-Heinemann, Woburn, MA.)

conditions is given by

$$H_{net} = \frac{q}{v} \qquad \text{(in J/m)} \tag{6.3}$$

and the heat or energy q for an arc welding process is given by

$$q = \eta EI \tag{6.4}$$

where η is the the transfer efficiency of the process (see Section 5.6), E and I are the welding voltage (in V) and current (in A), respectively, and v is the velocity of welding or travel speed (in m/s). Rosenthal further assumed the heat source to be a point source, with all of the energy being deposited into the weld at a single point. This assumption avoided complexities with density distribution of the energy from different sources and restricted heat flow analysis to the heat-affected zone, beyond the fusion zone or weld pool boundary. (Given the importance of energy density distribution discussed in Sections 5.8 and 6.4, this is not a good assumption; rather it is one with possibly significant consequences, as suggested later.)

Rosenthal next simplified the general heat flow equation in two ways: (1) by assuming that the thermal properties (thermal conductivity, k, and product of the specific heat and density, $C\rho$) of the material being welded are constants; and, (2) by modifying the coordinate system from a fixed system to a moving system. The assumption that thermal properties are constants is seriously

flawed, as these properties typically change dramatically with temperature (often by as much as two to five times), especially considering the wide range of temperatures normally involved in fusion welding. (This shortcoming has only recently been dealt with using numerical solutions with computers.) The moving coordinate system was a perfectly reasonable simplification, replacing x with ξ, where ξ is the distance of the point heat source from some fixed position along the x axis, depending on the velocity of welding, v (where there is only a velocity component in the x direction) by

$$\xi = x - vt \tag{6.5}$$

where t is the time. This modified coordination system, using ξ instead of v, is also shown in Figure 6.11.

When the general heat flow equation (Eq. 6.1), with constant thermal properties, is differentiated with respect to ξ rather than x, the result is

$$\frac{d^2T}{d\xi^2} + \frac{d^2T}{dy^2} + \frac{d^2T}{dz^2} = -\frac{C\rho}{k} v \frac{dT}{d\xi} + \frac{C\rho}{k} \frac{dT}{dt} \tag{6.6}$$

where k is the thermal conductivity in $\mathrm{J/m\,s^{-1}\,K^{-1}}$, and v is the speed or velocity of welding in m/s. This equation can be further simplified, in accordance with Rosenthal, if a quasi-stationary temperature distribution exists. This means the temperature distribution around a point heat source moving at constant velocity will settle down to a steady form, such that $dT/dt = 0$, for q/v = a constant (see Section 6.4). The result is

$$\frac{d^2T}{d\xi^2} + \frac{d^2T}{dy^2} + \frac{d^2T}{dz^2} = -\frac{C\rho}{k} v \frac{dT}{d\xi} \tag{6.7}$$

This situation is, in fact, achieved in many welds (as explained above), so the simplified form given in Eq. 6.7 is reasonable except for the assumption of constant thermal properties, which can be dealt with in other ways (such as by using a weighted average of the property based on the welding thermal cycle, or solving the simplified heat flow equation several times using a value of the thermal property in a different temperature range each time and seeing the effect).

Rosenthal solved the simplified form of the heat flow equation above (Eq. 6.7) for both thin and thick plates in which the heat flow is basically two dimensional and three dimensional, respectively. The solutions are

$$T - T_0 = \frac{q}{2\pi k} e^{-v\xi/2\alpha} K_0 \frac{vR}{2\alpha} \tag{6.8}$$

for the thin plate, where

q = heat input from the welding source (in J/m)
k = thermal conductivity (in J/m s^{-1} K^{-1})
α = thermal diffusivity = $k/\rho C$, (in m^2/s)
K_0 = a Bessel function of the first kind, zero order[7]
$R = (\xi^2 + y^2 + z^2)^{1/2}$, the distance from the heat source to a particular fixed point (in m).

On the other hand, for the thick plate

$$T - T_0 = \frac{q}{2\pi kd} e^{-v\xi/2\alpha} \frac{e^{-vR/2\alpha}}{R} \tag{6.9}$$

where d = depth of the weld (which for symmetrical welds is half of the weld width, since $w = 2d$)

Equations 6.8 and 6.9 can each be written in a simpler form, giving the time–temperature distribution around a weld when the position from the weld centerline is defined by a radial distance, r, where $r^2 = z^2 + y^2$. For the thin plate, the time–temperature distribution is

$$T - T_0 = \frac{q/v}{d(4\pi k\rho Ct)^{1/2}} e^{-r^2/4\alpha t} \tag{6.10}$$

and for the thick plate is

$$T - T_0 = \left(\frac{q/v}{2\pi kt}\right) e^{-r^2/4\alpha t} \tag{6.11}$$

The form of the temperature distribution fields given by these equations is illustrated in Figure 6.13.

6.5.2. Modifications to Rosenthal's Solutions

Rosenthal's model is an infinite series solution to the heat dissipated by conduction in a semi-infinite workpiece with constant thermophysical properties. Since Rosenthal's outstanding early contribution in this area, there have been numerous refinements. Adams (1958) recognized the existence of the weld pool and other problems, and used the fusion line as the boundary condition to obtain expressions for the peak temperature at any distance (y) from this boundary. He did this for two- (i.e., thin plate) and three-dimensional (i.e., thick plate) heat flow conditions. One of Adams' solutions is given in Section 6.7 for peak temperatures.

[7] Bessel functions of zero order, as well as other orders, can be found in references on mathematical functions used in engineering, of which there are many.

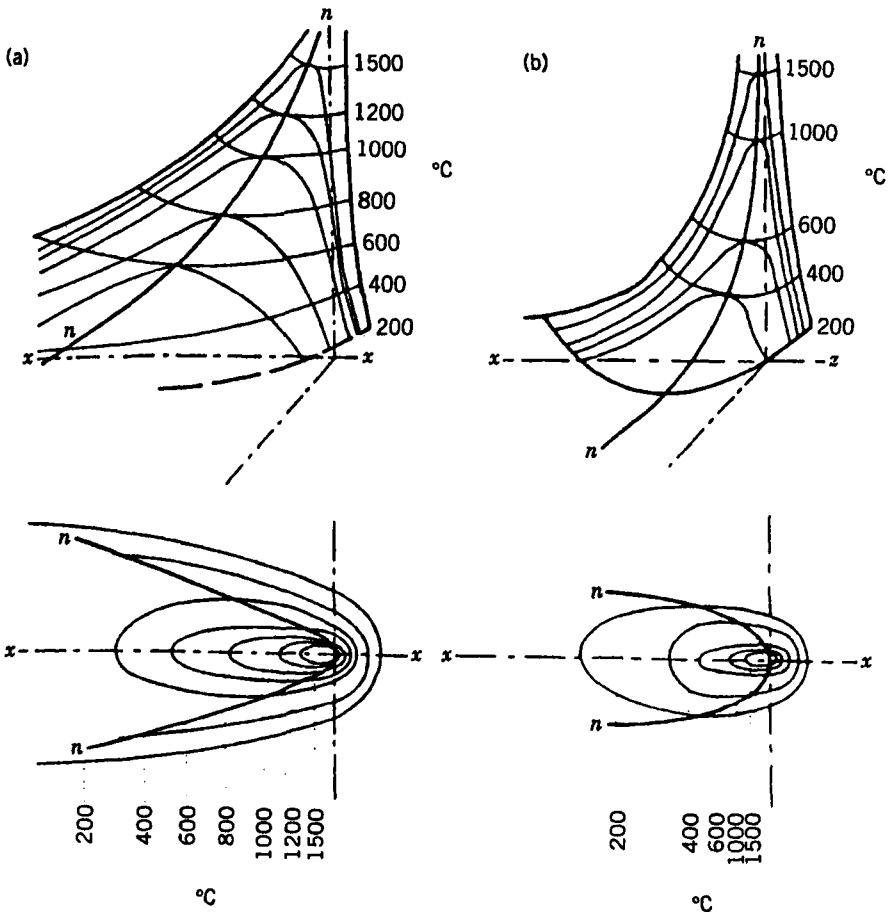


Figure 6.13 The temperature distribution fields obtained from solution of Rosenthal's simplified 2-D and 3-D equations for (a) thin and (b) thick plates, respectively. (From *Joining of Advanced Materials* by R. W. Messler, Jr., published in 1993 by and used with permission of Butterworth-Heinemann, Woburn, MA.)

Others, like Adams, tried to modify Rosenthal's solutions for two and three dimensions. Various early modifications of the two-dimensional solution were developed by Grosh et al. (1955), Grosh and Trabant (1956), Jhaveri et al. (1962), and Meyers et al. (1967). Later modifications were made by Swift-Hook and Gick (1973), Trevedi and Shrinivasan (1974), and Ghent et al. (1980). Various modifications of the three-dimensional solution were developed by Grosh and Trabant (1956), Jhaveri et al. (1962); and Malmuth et al. (1974). Even these early refined analytical models had several restrictive assumptions that are often hard to justify on the basis of the known physics of the process of welding.

For most of these, the complexity of the problem led to only limited success. Myers et al. (1967) reviewed many of the various analytical models and stated the simplifying assumptions that limit their use. In particular, heat flow and solidification rate in and immediately outside the weld pool (i.e., at the FZ/HAZ boundary) were still extremely difficult to handle, and predictions were inaccurate; often because good models of the heat source energy distribution were lacking. Neglecting convective heat transfer in the weld pool, considering conductive transfer only, caused the size of the weld pool to be underpredicted and the shape of the pool to be in error. (As seen in Chapter 10, fluid flow conditions in the weld pool, arising from contributions from electromagnetic and surface tension gradient forces, influence weld penetration, chemical homogeneity, porosity, and solidification structure.)

Again, much more realistic conditions of heat flow dimensionality (Goldak et al, 1986; Tekriwal and Mazumder, 1988; Kamala and Goldak, 1993), source energy density distribution (Goldak et al., 1984), weld pool convection (Zacharia et al., 1989, 1995), and temperature-dependent thermophysical properties can be dealt with today using modern computers and numerical solution approaches. The interested reader is referred to the abundant literature on this subject.

6.5.3. Dimensionless Weld Depth Versus Dimensionless Operating Parameter

Based on Rosenthal's solution of the simplified three-dimensional heat flow equation, Christiansen et al. (1965) derived theoretical relationships between a weld bead's cross-sectional geometry and the welding process operating conditions using dimensionless parameters. In Figure 6.14, the theoretical relationship between the dimensionless weld width, D, and dimensionless operating parameter, n, is shown, where

$$D = \frac{dU}{2\alpha_s} \tag{6.12}$$

and

$$n = \frac{QU}{4\pi\alpha_s^2 \rho C(T_m - T_0)} \tag{6.13}$$

In these equations, d is the depth of penetration of the weld, U is the welding speed, α_s is the thermal diffusivity ($k_s/\rho C_s$) of the base material (as a solid), Q is the heat input to the workpiece, T_m is the melting point of the base material (the workpiece), and T_0 is the temperature of the workpiece at the start of welding. For a symmetrical weld bead, the width of the weld bead is $w = 2d$, and the cross-sectional area of the weld bead can thus be determined. Equation

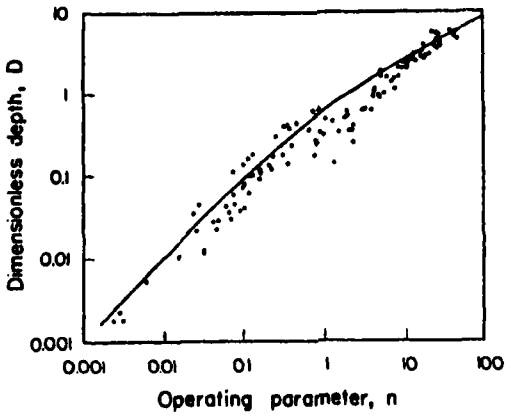


Figure 6.14 Dimensionless weld depth (D) as a function of dimensionless process operating parameter (n). The solid curve is the predicted relationship.. (From "Distribution of tempertures in arc welding" by N. Christiansen, V. de L. Davies, and K. Gjermundsen, 1965, *British Welding Journal*, 12, 54–75, used with permission of The Welding Institute, Cambridge, UK.)

6.13 can be applied to the heat-affected zone by simply substituting T_H for T_m, where T_H is the temperature of some relevant phase transformation that could take place.

The utility of the work of Christiansen et al. is that data obtained from different materials and processes can be interrelated through the dimensionless parameters for weld depth and weld operating parameter. This is shown well in Figure 6.15 after Shinoda and Doherty (1978).

6.6. EFFECT OF WELDING PARAMETERS ON HEAT DISTRIBUTION

The size and, especially, the shape of the melt region in a fusion weld affects the mechanics and kinetics of solidification and, therefore, the structure and properties of the resulting weld. The shape and, especially, the size of the weld pool, along with the size and shape of the surrounding heat-affected zone, also affects the thermally induced stresses that act on the weld, leading to the formation of defects or residual stresses or distortion. The size and, to a lesser degree, the shape of the heat-affected zone influences overall weld performance. Understanding the effect of the flow of heat and distribution of temperature (and associated thermally induced strains and stresses, as discussed in Chapter 7), on the size (or extent) and shape of this major zones comprising a weld is thus critically important to understanding, predicting, and, ultimately, controlling final weld and weldment properties and performance.

The shape of the melt, although not necessarily its physical size, is a function of material, welding speed, and welding power (voltage times current) and can

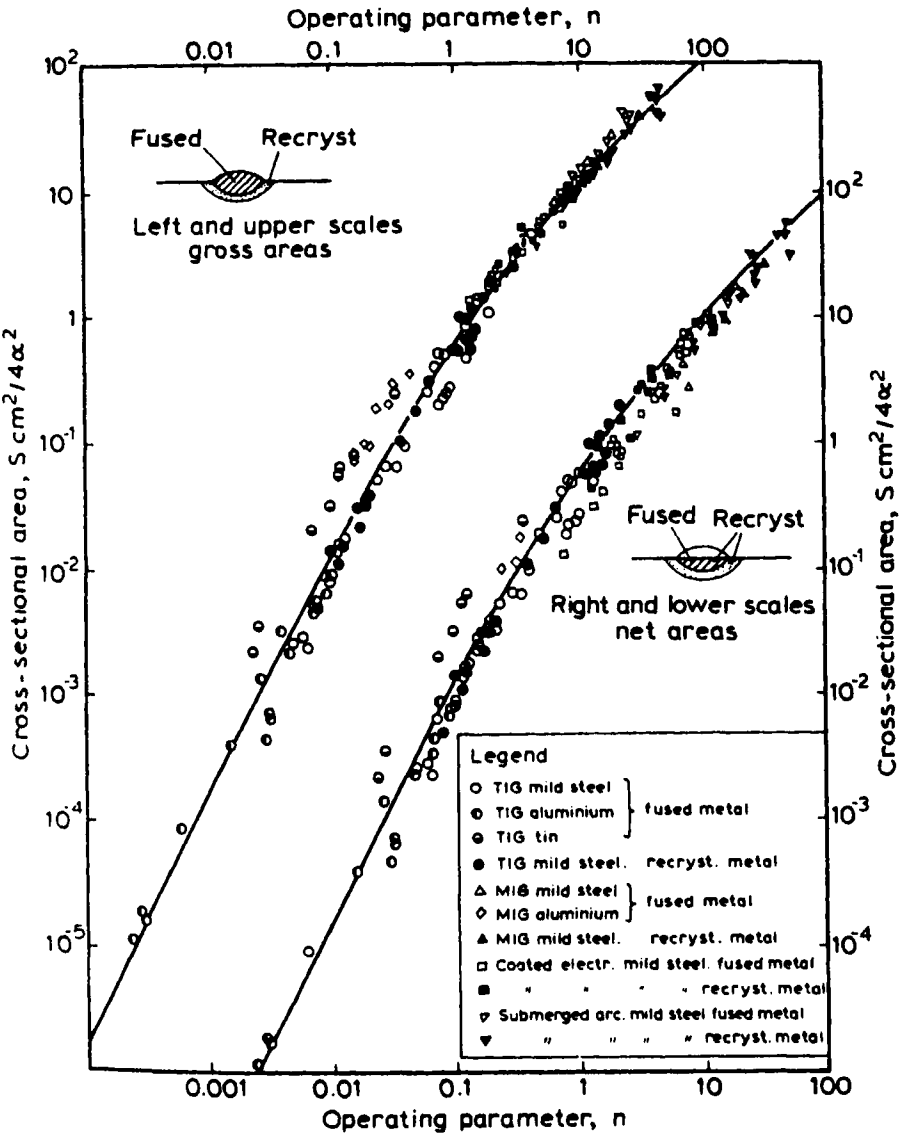


Figure 6.15 Comparison between predicted and measured weld cross-sections (given by S) for dimensionless operating parameter n, allowing various types of weld processes and materials to be compared on a single diagram. (After *The Relationship Between Arc Welding Processes and the Weld Bead Geometry* by T. Shinoda and J. Doherty, Report No. 74/1978/PE, published by The Welding Institute, London, UK, 1978, and used with permission of TWI, Cambridge, UK.)

be obtained from the isotherms predicted by the solutions to the heat flow equation. Figures 6.16, 6.17, and 6.18 show the effect on weld pool size and shape caused by changes in material (thermal properties), welding speed, and weldment plate thickness, respectively. Note that increasing thermal conductivity tends to cause deposited heat to spread, which can make welds smaller for a given heat input and melting temperature. The effect of melting temperature obviously cannot be ignored, however. For a given heat input, the lower the melting point, the larger the weld.

The effect of welding speed is to change both the weld pool and surrounding heat-affected zone shape. For a stationary (spot) weld, the shape in plan view, looking down on the workpiece from the source, is round, and approximately hemispherical in three dimensions (presuming a concentrated, heavy point energy source/deposit). Once the source is moved with constant velocity, the weld pool and surrounding HAZ become elongated to an elliptical plan form

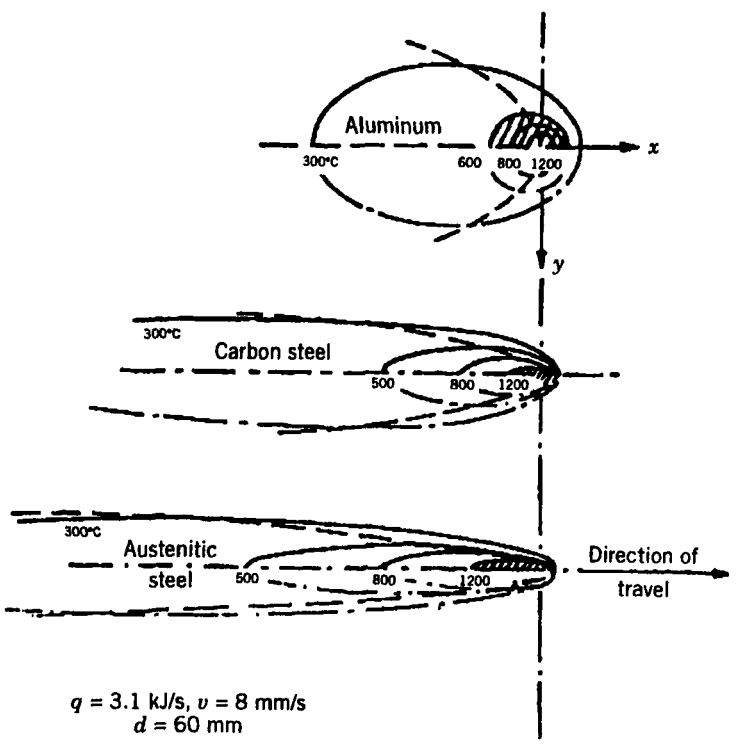


Figure 6.16 Effect of the thermal conductivity of a base material on weld pool (fusion zone) and surrounding heat-affected zone size and shape. (From *Joining of Advanced Materials* by R. W. Messler, Jr., published in 1993 by Butterworth-Heinemann, Woburn, MA, and after T. G. Gray et al., *Rational Welding Design*, originally published in 1975 by and used with permission of Butterworth-Heinemann, London.)

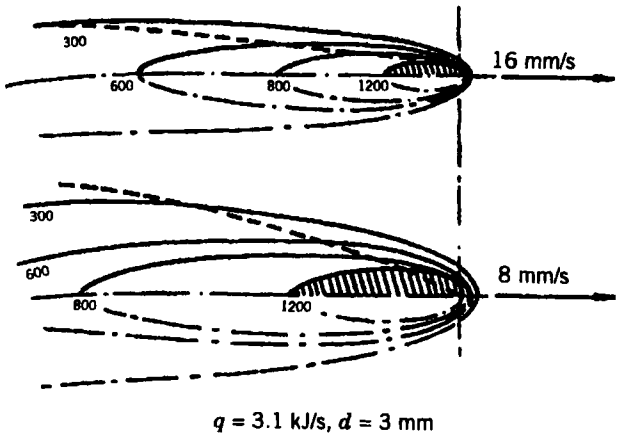


Figure 6.17 Effect of the speed of welding on the weld pool (fusion zone) and surrounding heat-affected zone size and shape. (From *Joining of Advanced Materials* by R. W. Messler, Jr., published in 1993 by Butterworth-Heinemann, Woburn, MA, and after T. G. Gray et al., *Rational Welding Design*, originally published in 1975 by and used with permission of Butterworth-Heinemann, London.)

and prolate spheroidal 3-D shape. With increased velocity, these zones become more and more elliptical and, finally, at some velocity (for each specific material), take on a tear drop shape, with a tail at the trailing end of the pool. The reason for this, which is explained in detail in Chapter 13, is the release of latent heat of solidification or freezing. Once a teardrop shape arises, the

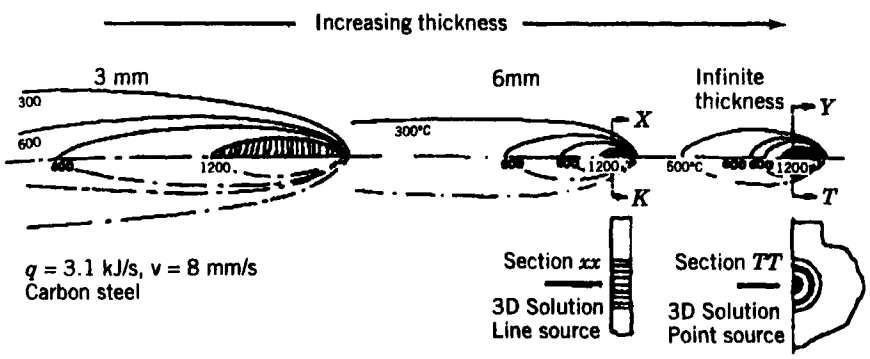


Figure 6.18 Effect of the thickness of a weldment on the weld pool (fusion zone) and surrounding heat-affected zone. (From *Joining of Advanced Materials* by R. W. Messler, Jr., published in 1993 by Butterworth-Heinemann, Woburn, MA, and after T. G. Gray et al., *Rational Welding Design*, originally published in 1975 by and used with permission of Butterworth-Heinemann, London.)

increasing velocity elongates the teardrop more and more, narrowing the fusion and heat-affected zone widths more and more (to keep overall melted volume constant). (At very high welding speeds, the tail of the teardrop weld pool can actually detach, isolate regions of molten metal, and lead to shrinkage-induced cracks along the centerline of the weld.) The effect of weldment thickness is to cause the weld pool and surrounding heat-affected zone to become smaller and smaller, without changing shape very much, as thickness increases toward infinity. This is due to the effect of thermal mass on heat distribution.

The final effect that needs to be mentioned is that of energy density for a given heat input, weldment material, and geometry. Increased energy density increases the efficiency of melting (see Section 5.7.1), thereby increasing the amount of melting (especially in the depth direction) and decreasing the extent of the surrounding heat-affected zone.

It should come as no surprise that the shape of the heat-affected zone is almost totally determined by the shape of the weld pool and that the shape of both can (and will be) distorted by any asymmetry around the joint. Such asymmetry might be the result of the relative thermal mass (e.g., thickness) of the joint elements as well as their relative thermal properties (including melting points, thermal conductivity, and heat capacities).

6.7. PREDICTION OF WELD ZONES AND WELD COOLING RATES

6.7.1. Zones in Fusion-Welded Materials

As shown in Section 2.4.1, Figure 2.4, and now in Figure 6.19, a fusion weld produces several distinct microstructural zones in a pure crystalline metal, ceramic, or crystalline alloy of one of these materials. These different zones correlate reasonably well with various transformations on appropriate phase diagrams except for where the resulting structure deviates from equilbrium significantly (e.g., martensite in steels). The *fusion zone* (or weld metal in a metal) is the portion of the weld that melted during welding, having been heated to above the temperature where melting just begins for the material being welded ($T_{melting}$ for the pure metal and $T_{solidus}$ for the alloy shown in Figure 6.19). The fusion zone is often designated as the FZ. In an alloy, there is a *partially melted zone* (*PMZ*) where the temperature rose to between the liquidus and the solidus temperature ($T_{solidus}$ and $T_{liquidus}$) for the alloy shown in Figure 6.19. Naturally, there is no PMZ in a pure material.

The *heat-affected zone* (*HAZ*) is the portion of the base material that was not melted but whose properties (and, usually, structure) were altered by the heat of welding through some phase transformation or reaction. The *unaffected base material* (*UBM*) is the portion of the base material wherein the welding heat did not exceed the minimum required to affect its structure or properties (below $T_{allotropic}$ for the pure metal and T_{solvus} for the alloy shown in Figure

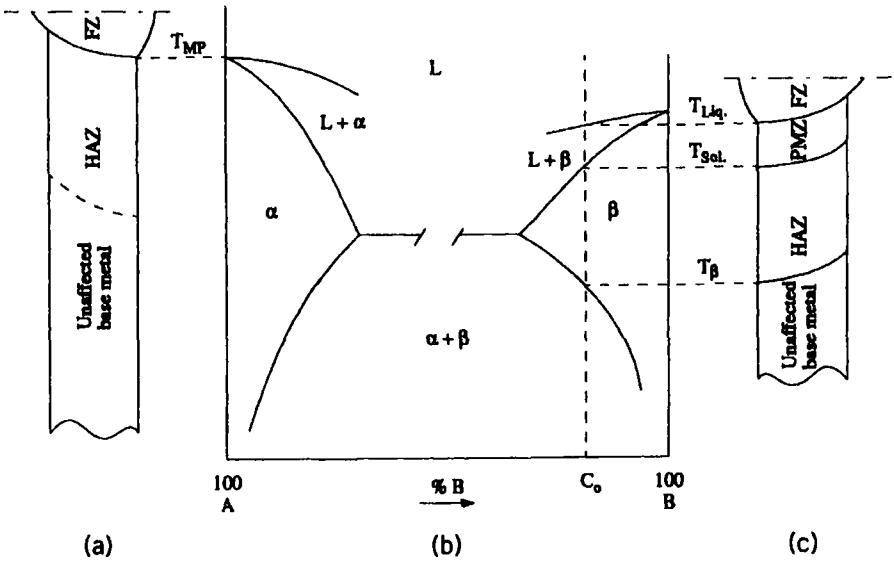


Figure 6.19 Schematic of the distinct zones in a fusion weld in a pure metal (a) and an alloy (c) as these correspond to phase regions in the hypothetical phase diagram shown (b).

6.19). The *weld zone* (WZ) encompasses the fusion, partially melted (if any), and heat-affected zones, since this is the region where base material properties are affected by welding.

6.7.2. Simplified Equations for Approximating Welding Conditions

In the past, as already stated, results of experiments were typically fit to simplified equations suggested by heat transfer theory, and techniques were developed to calculate important factors like peak temperatures to cause melting or produce heat affects, fusion and heat-affected zone widths, solidification rates, and cooling rates at various points from the weld fusion zone/heat-affected zone boundary. Later, simplifying assumptions, such as those of Rosenthal, allowed simplified analytical solutions. Computers can now be used to solve the complex differential equations that model heat flow in welding, and the general solution can be solved numerically, yielding remarkable correlation between predicted and measured fusion and heat-affected zone sizes and shapes, weld pool convection, and so on. However, simplified equations, supported by engineering data, still play an important role for approximating conditions especially in construction and fabrication of mundane welded structures. For this reason, several useful simplified equations are presented below.

6.7.2.1. Peak Temperatures. Predicting or interpreting metallurgical transformations (melting, austenitization, recrystallization of cold-worked material, etc.) at a point in the solid material near a weld requires some knowledge of the maximum or peak temperature reached at a specific location. For a single-pass, full-penetration butt weld in a sheet or a plate, the distribution of peak temperatures (T_p) in the base material adjacent to the weld is given by

$$\frac{1}{T_p - T_0} = \frac{(2\pi e)^{0.5}\rho C h y}{H_{net}} + \frac{1}{T_m - T_0} \tag{6.14}$$

where

T_0 = initial temperature of the weldment (K)
e = base of natural logarithms = 2.718
ρ = density of the base material (g/mm^3)
C = specific heat of the base material (J/g K^{-1})
h = thickness of the base material (mm)
y = 0 at the fusion zone boundary and where $T_p = T_m$
T_m = melting (or liquidus) temperature of the material being welded (K)

and H_{net} is obtained from Eq. 6.3 with 6.4.

6.7.2.2. Width of the Heat-Affected Zone. If one defines a peak temperature as the temperature at which the structure and properties of the base material are altered by some metallurgical transformation (creating a heat affect), then the peak temperature equation (Eq. 6.14) can be used to calculate the width of the heat-affected zone. The width of the heat-affected zone is determined by the value of y that yields a T_p equal to the pertinent transformation temperature (recrystallization temperature, austenitizing temperature, etc.). Equation 6.14 cannot be used to estimate the width of the fusion zone, since it becomes unsolvable when T_p equals T_m. This arises from the fact that Eq. 6.14 comes from Rosenthal's solution of the generalized equation of heat flow (Eq. 6.1), but where the assumption was made that heat was deposited at a point, and there was no melted region, just a heat-affected zone.

6.7.2.3. Solidification Rate. The rate at which weld metal (or ceramic) solidifies can have a profound effect on its microstructure, properties, and response to postweld heat treatment. The solidification time, S_t, in seconds, is given by

$$S_t = \frac{LH_{net}}{2\pi k\rho C(T_m - T_0)^2} \tag{6.15}$$

where L is the latent heat of fusion (J/mm^3), k is the thermal conductivity of the base material (J/m s^{-1} K^{-1}), and ρ, C, T_m, and T_0 are as before. S_t is the time (s) elapsed from the beginning to the end of solidification.

The solidification rate, which is derived from the solidification time, helps determine the nature of the growth mode (with temperature gradient) and the size of the grains (e.g., dendrite arm spacing) or the coarseness or fineness of the microstructure (see Chapter 13, Section 13.5.3.2).

6.7.2.4. Cooling Rates. The final metallurgical structure of a weld zone (FZ and HAZ) is primarily determined by the cooling rate from the peak temperature attained during the welding cycle (see Chapter 16). The rate of cooling influences the coarseness or fineness (scale) of the resulting solidification structure and the homogeneity, as well as the distribution and form of the phases and constituents in the microstructure, of both the fusion zone and the heat-affected zone for diffusion controlled transformations. When competing diffusionless or athermal transformations can occur (as in steels), cooling rate determines which transformation will occur and, thus, which phases or constituents will result. These, in turn, directly determine the properties of the resulting weld.

If cooling rates are too high in certain steels, hard, untempered martensite can result, embrittling the weld outright, and adding to the susceptibility to embrittlement by hydrogen. By calculating the cooling rate, it is possible to decide whether undesirable microstructures are likely to result. If so, preheat[8] can be employed to reduce the cooling rate. Cooling rate is primarily used to determine the need for preheat.

For a single weld pass used to make a butt joint between two plates of equal thickness, where the plates are relatively thick (requiring more than six passes[9]):

$$R = \frac{2\pi k(T_c - T_0)^2}{H_{net}} \tag{6.16}$$

where

R = cooling rate at the weld centerline (K/s)
k = thermal conductivity of the material (J/mm s^{-1} K^{-1})
T_0 = initial plate temperature (K)
T_c = temperature at which the cooling rate is calculated (K)

and where H_{net} is given by Eq 6.3, using Eq. 6.4.

[8] Preheat refers to the intentional elevation of the temperature of the base material of a weldment prior to welding to reduce the temperature gradient and the cooling rate in the fusion and heat-affected zones.

[9] It is often necessary to deposit weld metal in more than one step or "pass." When this is the case, welding is said to be multipass.

If the plates are relatively thin, requiring fewer than four passes, then

$$R = 2\pi k\rho C\left(\frac{h}{H_{net}}\right)^2 (T_c - T_0)^3 \tag{6.17}$$

where

h = thickness of the base material (mm)
ρ = density of the base material (g/mm^3)
C = specific heat of the base material (J/g K^{-1})
ρC = volumetric specific heat (J/mm^3 K^{-1})

Increasing the initial temperature, T_0, or applying preheat, decreases the cooling rate.

6.8. WELD SIMULATION AND SIMULATORS

The thermal cycles experienced in a workpiece during welding can be replicated in specimens more convenient for mechanical testing, using so-called weld simulators or, more generally, thermal simulators. These simulators, the most well known of which is the Gleeble (DSM, Inc., originally Duffers Scientific Instruments, Inc., Poestenkill, NY), evolved from an original device conceived and developed by Nippes and Savage (1949).

Figure 6.20 shows a schematic of a typical Gleeble apparatus. The specimen, usually a round tensile specimen (6.4 mm or $\frac{1}{4}$in. in diameter), is held in a pair of water-cooled copper grips, one of which is fixed and the other moveable. The specimen is heated by its own resistance to the passage of a preprogrammed cycle of current from a power transformer. The two copper grips serve as a means of introducing current to the specimen, apply a controlled, preprogrammed cycle of strain or stress, and ensure rapid heat extraction when the current is halted. By properly sequencing preprogrammed time cycles of temperature and displacement or force, the gauge region of the specimen develops the same microstructure as the weld (region) for which the thermal history is replicated, and is loaded to simulate shrinkage and contraction or apply tension (or compression) to test properties.

A thermocouple, previously percussion-welded to the middle of the specimen, allows electronic control of the current to cause a temperature–time response that closely simulates that of a real weld. If this thermal history can be spread over the entire gauge length of the specimen, a very narrow region of interest in a real weld can be replicated and tested in the Gleeble.

The Gleeble, and other thermal simulators, can be used for many purposes in welding, such as effect of strain on defect formation, formation of embrittled regions, and occurrence of constitutional liquation. They can also be used

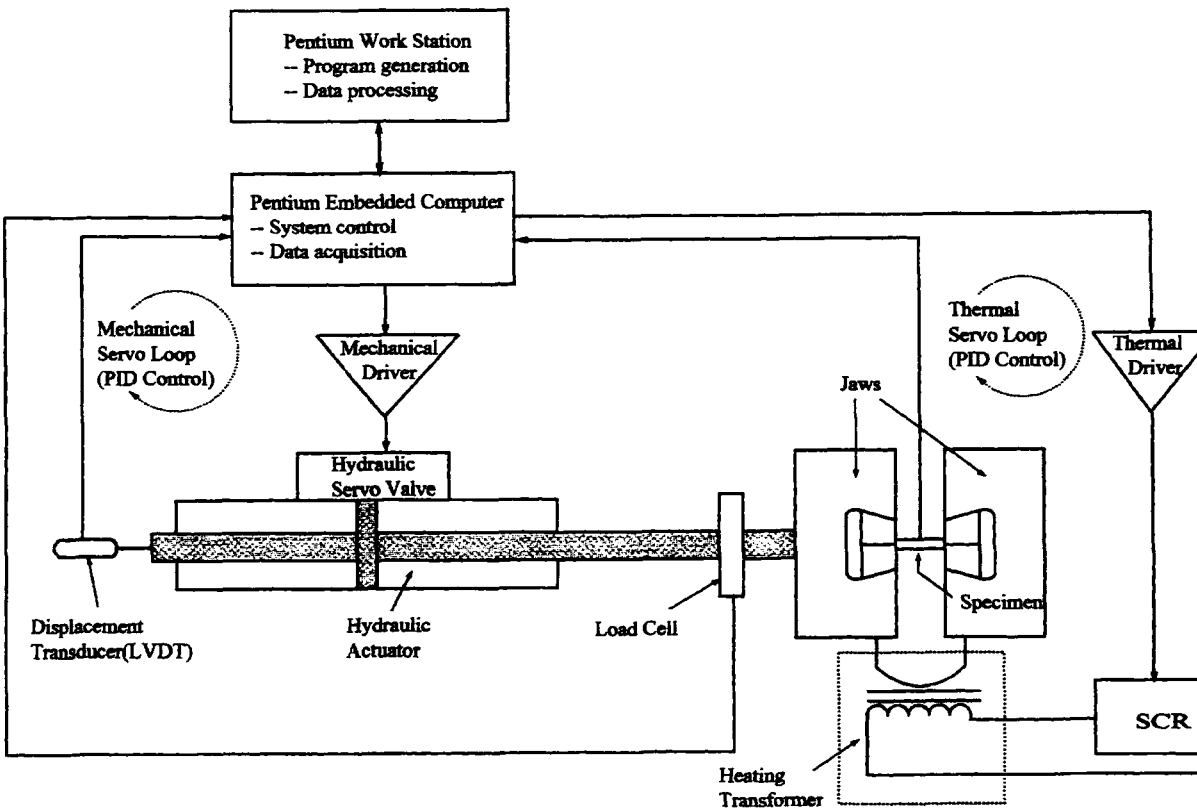


Figure 6.20 Schematic diagram of the digital control system for a modern (3000 Series) Gleeble weld thermal simulator. (Courtesy of and printed with the permission of DSI, Poestenkill, NY.)

beyond welding to simulate any thermomechanical process from continuous casting to continuous heat treatment to extrusion to generation of continuous cooling curves for conventional heat treatment.

Despite their obvious advantages of convenience, weld thermal simulators are not free of shortcomings. They are limited in their ability to cool specimens as fast as actual welds cool for high-energy-density processes (like EBW and LBW). There is also the difficult-to-avoid gradient in temperature (especially for very rapid heating and cooling) between the surface (where the monitoring/controlling thermocouple is located) and the interior of the specimen. The temperature gradient through the heat-affected zone in simulators is much less severe than in real welds, so the structure and properties in the simulated specimen differ from those in real welds due to differences in the degree of deviation from equilibrium. Finally, as pointed out by Dolby and Widgery (1972), the grain size in Gleeble specimens can be much larger than in real heat-affected zones, thus failing to completely simulate microstructure.

Once again, weld simulators are tools to be used to gain understanding, not to "measure manure piles with a micrometer."

6.9. SUMMARY

Once the thermal energy from a welding heat source reaches a weldment, it redistributes due to heat flow. Understanding how heat flows to establish a temperature distribution is critical to an understanding of melting, fusion zone size and shape, solidification rate (as it affects resulting structure and substructure), heat-affected zone size and shape, and cooling rates in the heat-affected zone (because these determine transformations and reactions that can occur). Modern computers enable quite realistic modeling for the purpose of prediction, understanding, and control. Modern weld thermal simulators enable convenient replication of thermal (and stress–strain) history to aid in understanding of postsolidification reactions and transformations on properties. But, both of these tools are only tools, they are not the real thing. Simulation is just that, and should not be used to "measure manure piles with micrometers."

REFERENCES AND SUGGESTED READING

Adams, C. M., Jr., 1958, "Cooling rates and peak temperatures in fusion welding," *Welding Journal*, **37**(5), 210s–215s.

Christiansen, N., Davies, V. de L., and Gjermundsen, K., 1965, "Distribution of temperatures in arc welding," *British Welding Journal*, **12**, 54–75.

Dolby, R. E., and Widgery, D. J., 1972, in *Weld Thermal Simulators for Research and Problem Solving*, edited by R. E. Dolby, Welding Institute, London, pp. M52–M70.

Doumanidis, C. C., and Hardt, D. E., 1990, "Simultaneous in-process control of heat-affected zone and cooling rate during arc welding," *Welding Journal*, **69**(5), 186s–194s.

Ghent, H. W., Roberts, D. W., Hermance, C. E., Kerr, H. W., and Strong, A. B., 1980, "Arc efficiencies in TIG welds," in *Arc Physics and Weld Pool Behaviour*, The Welding Institute, London, pp. 17–23.

Goldak, J. A., Chakravarti, A. P., and Bibby, M., 1984, "A new finite element model for welding heat sources," *Metallurgical Transactions*, **15B**, 299–315.

Goldak, J. A., Bibby, M., Moore, J. E., House, R., and Patel, B., 1986, "Computer modeling of heat flow in welds," *Metallurgical Transactions*, **17B**(9), 587–600.

Grosh, R. J., and Trabant, E. A., 1956, "Arc welding temperatures," *Welding Journal*, **35**(8), 396s–400s.

Grosh, R. J., Trabant, E. A., and Hawskins, G. A., 1955, "Temperature distribution in solids of variable thermal properties heated by moving sources," *Quarterly Journal of Applied Mathematics*, **13**, 161–167.

Jhaveri, P., Moffatt, W. G., and Adams, C. M., Jr., 1962, "The effect of plate thickness and radiation on heat flow in welding and cutting," *Welding Journal*, **41**(1), 12s–16s.

Kamala, V., and Goldak, J. A., 1993, "Error due to two-dimensional approximation in heat transfer analysis of welds," *Welding Journal*, **72**(9), 440s–446s.

Malmuth, N. D., Hall, W. F., Davis, B. I., and Rosen, C. D., 1974, "Transient thermal phenomena and weld geometry in GTAW," *Welding Journal*, **53**(9), 388s–400s.

Meyers, P. S., Uyehari, O. A., and Borman, G. L., 1967, "Fundamentals of heat flow in welding," *Welding Research Council Bulletin 123*, reprinted July 1976.

Nippes, E. F., and Savage, W. F., 1949, "Development of specimen simulating weld heat-affected zones," *Welding Journal*, **28**(11), 534s–546s.

Portevin, A. M., and Seferian, D., 1935, in *Symposium on the Welding of Iron and Steel*, 2–3 May 1935, London.

Rosenthal, D., 1945, "Mathematical theory of heat distribution during welding and cutting," *Welding Journal*, **20**(5), 220s–234s.

Rosenthal, D., 1946, "The theory of moving sources of heat and its application to metal treatments," *Transactions of the ASME*, **68**, 849–866.

Rosenthal, D., and Schmerber, R., 1938, "Thermal study of arc welding experimental verification of theoretical formulas," *Welding Journal*, **17**(4), 2s–8s.

Shinoda, T., and Doherty, J., 1978, *The Relationship between Arc Welding Processes and the Weld Bead Geometry*, Report No. 74/1978/PE, The Welding Institute, London, UK.

Swift-Hook, D. T., and Gick, A. E. F., 1973, "Penetration welding with lasers," *Welding Journal*, **52**(11), 492s–499s.

Tekriwal, P., and Mazumder, J., 1988, "Finite element analysis of three-dimensional heat transfer in GMA welding," *Welding Journal*, **67**(7), 150s–156s.

Trevedi, R., and Shrinivasan, S. R., 1974, "Temperature distribution around a moving cylindrical source," *Journal of Heat Transfer*, **96**, 427–428.

Zacharia, T., David, S. A., Vitek, J. M., and DebRoy, T., 1989, "Weld pool development during GTA and laser-beam welding of type 304 stainless steel, part 1: theoretical

analysis," *Welding Journal*, **68**(12), 499s–519s.

Zacharia, T., David, S. A., Vitek, J. M., and Kraus, H. G., 1995, "Surface temperature distribution of GTA weld pools on thin-plate 304 stainless steel," *Welding Journal*, **74**(11), 353s–362s.

Suggested readings [by topic]

Domey, J., Aidun, D. K., Ahmadi, G., Regal, L. L., and Wilcox, W. R., 1996, "Numerical simulation of the effects of gravity on weld pool shape," *Welding Journal*, **75**(8), 263s–269s. [Modeling weld pool shape].

Eager, T. W., and Tsai, N. S., 1983, "Temperature fields produced by traveling distributed heat sources," *Welding Journal*, **62**(12), 346s–355s. [Temperature fields].

Easterling, K., 1992, *Introduction to the Physical Metallurgy of Welding*, 2d ed., Butterworths, Oxford, UK, pp. 18–38. [General heat transfer].

Jones, D. K., Emery, A. F., and Marburger, S. J., 1993, "An analytical and experimental study of the effect of welding parameters on fusion welds," *Welding Journal*, **72**(2), 51s–59s. [Parameter effects].

Lundin, C. D., 1997, "Historical development of the high-speed time–temperature controller designed for welding research: the Gleeble™," from *Proceedings of the 7th International Symposium on Physical Simulation*, Tsukuba, Japan. [Gleeble history].

Paley, Z., and Hibbert, P. D., 1975, "Computation of temperatures in actual weld design," *Welding Journal*, **54**(11), 385s–392s. [Heat flow in weld design].

Prasad, N. S., and Narayanan, T. K. S., 1996, "Finite-element analysis of temperature distribution during arc welding using adaptive grid technique," *Welding Journal*, **75**(4), 123s–131s. [Modeling weld heat distribution].

Tsao, K. C., and Wu, C. S., 1988, "Fluid flow and heat transfer in GMA pools," *Welding Journal*, **67**(3), 70s–75s. [Heat transfer in weld pools].

Zacharia, T., David, S. A., Vitek, J. M., and DebRoy, T., 1989, "Weld pool development during GTA and laser-beam welding of type 304 stainless steel, part 1: theoretical analysis," *Welding Journal*, **68**(12), 499s–519s. [Modeling heat distribution and weld pool shape].

Zacharia, T., David, S. A., Vitek, J. M., and Kraus, H. G., 1995, "Surface temperature distribution of GTA weld pools on thin-plate 304 stainless steel," *Welding Journal*, **74**(11), 353s–362s. [Modeling surface temperature distribution in weld pools].

CHAPTER 7

THERMALLY INDUCED DISTORTION AND RESIDUAL STRESSES DURING WELDING

7.1. ORIGIN OF THERMAL STRESSES

Most stresses[1] that appear in a material or a structure arise from a mechanical source. These can include forces of external origin, such as wind acting on the walls of a building, the weight of snow on a roof, the weight of cars and trucks, trains, and/or people on bridges, and the shaking of buildings and bridges by an earthquake. Other examples of forces of external origin for machines or mechanisms are torque from a motor acting on a shaft or gear, forces from prime movers acting on linkages, and thrust from a jet engine acting on an aircraft fuselage through a mounting bulkhead, all to produce motion. Stresses from a mechanical source can also include forces of internal origin, such as the weight of the building or bridge itself. For example, the upper floors of the building produce forces, from weight, on the lower floors, and additional structure is needed beyond that to support the external loads to support the structure itself. These are known more generally as the inertia of parts of the structure itself, or inertial loads. Stresses can also arise from thermal sources and when they do, they are called thermal stresses.

Thermal stresses or *thermally induced stresses* arise from a material or mechanical structure being acted upon by a temperature gradient or a temperature change (and not simply temperature). There are three principal examples: (1) stresses induced by a volumetric change, either expansion or shrinkage, associated with some change of phase in the material of construction; (2) stresses induced by a difference in coefficient of thermal expansion (CTE) between two materials linked together, known as a CTE mismatch; and

[1] Recall that a stress is the result of a force acting on an area, so that stress = force/area.

(3) stresses induced by a temperature gradient resulting in differential rates of expansion (on heating) or contraction (on cooling) within the volume of the material or within the structure. For stresses to arise from a phase change, temperature must change to cause the phase change. For stresses to arise from a difference in coefficients of thermal expansion, the temperature may be changing or it may have stabilized. For stresses to arise from differential rates of expansion or contraction, the temperature must change and produce a gradient, which may or may not persist. Whether the temperature gradient persists or not, the thermally induced stresses from this source persist (ignoring relaxation processes that can occur in the material).

A well-known example of stresses induced by a phase change is the crushing of a wood- or fiberglass-hulled boat by ice formed in a lake, river, bay, or canal. Since the specific volume of water (its volume per unit mass) increases with a change from the liquid to the solid (ice) phase, the increased volume of the ice squeezes on the hull of the boat, which will likely give before the shoreline or bulkhead does. When a metal solidifies after having been made molten, unlike water, its specific volume decreases.[2] This volumetric shrinkage gives rise to thermally induced stresses in the surrounding metal, which must react somehow. If free to move, the surrounding metal will move to accommodate the shrinkage. If not free to move, the solidifying volume of metal will either yield or fracture by cracking in tension.

A well-known example of mismatched CTEs giving rise to a thermally induced stress is a bi-metal couple used in various temperature sensing/indicating devices (e.g., certain thermometers and thermostats). If strips of two metals with different coefficients of thermal expansion are joined along their length at some temperature, as the temperature changes from this point, the materials respond differently. On heating, one will expand faster than the other while the temperature is changing, and more than the other when the temperature change has ceased. On cooling, the reverse will occur: One will contract faster during cooling, and will have contracted more when cooling has ceased. The result will be a stress, with the higher CTE material causing bending of a straight two-layer strip toward the lower CTE material on heating. If the two-layer strip starts out straight while hot, the lower CTE material will cause bending of the couple toward itself on cooling. If motion or distortion cannot take place in response to the different CTEs, the stresses that would normally cause that motion or distortion will be trapped in the material as "locked-in" stresses. This source of thermally induced stress is commonplace, and, thus, must be carefully considered whenever two different materials are joined (which is probably far more often than one might think). If the joining process uses heat to be accomplished, as does fusion welding, brazing, and soldering, a thermally induced stress will arise during joining. If no heat is used in joining, as in mechanical fastening, thermally induced stresses will arise only if and when temperature is changed in service.

[2] There are exceptions, including but not being limited to Bi, Ga, Li, and Na, that expand upon solidifying.

A well-known example of thermally induced stresses arising as the result of a temperature gradient being present in a material or structure is when a very hot, dry glass cooking pot is suddenly placed into cold water. The outside of the walls and bottom of the glass pot cool faster than the insides as a result of thermal momentum exacerbated by glass' poor thermal conductivity, causing the outsides to contract faster and more than the insides. This places the outside layers of the pot's walls and bottom in tension, causing catastrophic fracture in such an inherently brittle material! A similar thing happens in any material or structure anytime there is a difference in temperature across any dimension, through the thickness or along a length or width, although sometimes the material (or part) yields (usually by bending or buckling) only if it has sufficient ductility. In fact, in all of these examples, and many situations in welding, thermally induced stresses are actually the result of thermally induced strains. The material undergoes some change in dimensions, locally, and a stress arises, more generally.

Illustrations of the examples cited above for the three sources of thermally induced stresses are shown schematically in Figure 7.1.

7.2. DISTORTION VERSUS RESIDUAL STRESSES

As mentioned above, if a thermally induced strain or stress is able to do so, it will cause a material or structure to respond by distorting. While the origin of thermally induced stresses often arises with relatively small dimensional changes, from some localized phenomena, the distortion that can result is often much more generalized, up to and including the entire structure. If thermally induced strains or stresses from one of the sources described in Section 7.1 are unable to cause a material or structure to respond by distorting macroscopically, it will either cause it to deform microscopically (e.g., yield or crack) or result in stresses that (as opposed to being applied) are "locked in." Locked-in stresses are called residual stresses.

An example of how distortion and residual stresses might arise from the same applied temperature change is shown schematically in Figure 7.2. *Note:* When stresses can cause macroscopic distortion, they will do so, and, in the process of causing this distortion, the thermally induced stresses are relieved; at least to below the yield stress, and, possibly, to lower levels due to creep. When stresses cannot cause macroscopic distortion, they either cause microscopic distortion or deformation (often in the form of cracking, but, possibly, in the form of localized yielding) to relieve themselves, or they are locked in to become residual stresses. In this last case, thermally induced stresses are *not* relieved, they are locked in! Not surprisingly, locked-in or residual stresses have consequences that are rarely good (described in Section 7.4), the exception being where compressive residual stresses can be induced to offset at least the initial levels of applied tensile stresses, as in prestressed cement or concrete, or thermally or chemically tempered glass.

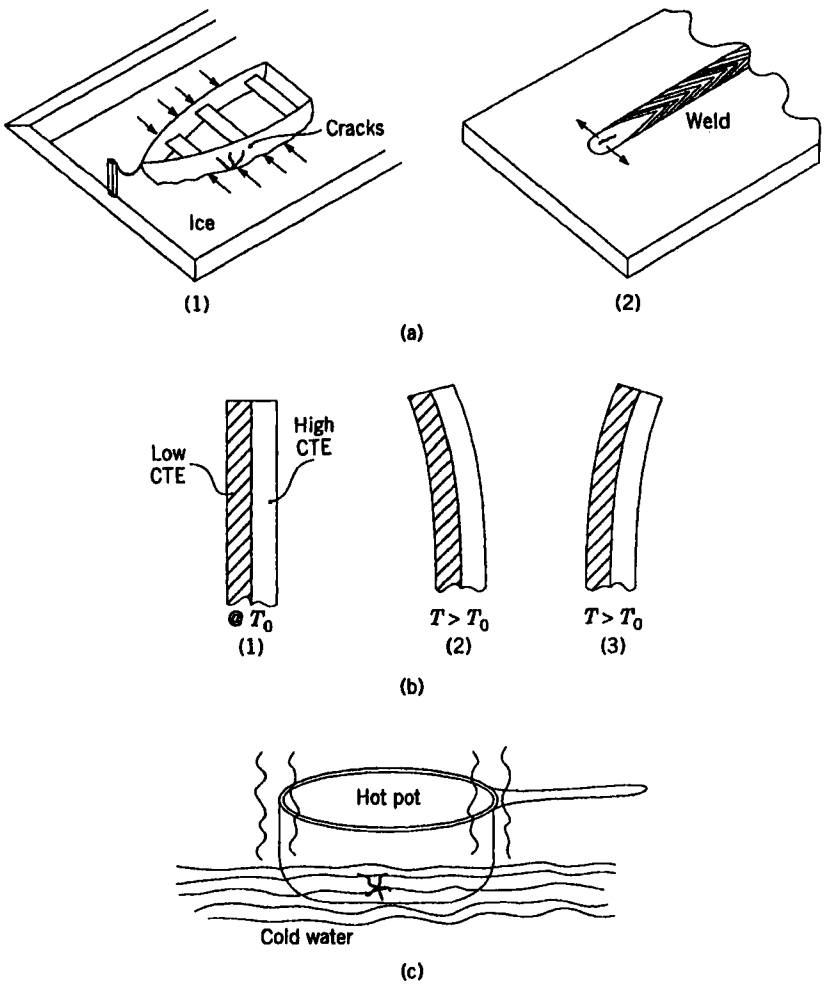


Figure 7.1 Schematic of thermally induced stresses from (a) volumetric change upon phase change (here, (1) liquid water expanding as it forms solid ice upon freezing, and (2) molten weld metal contracting as it solidifies to form a weld); (b) mismatched coefficients of thermal expansion (in a bimetal strip) (1) at room temperature, (2) on heating, and (3) on cooling; and (c) differential thermal expansion and contraction due to a temperature gradient.

Whether a particular material or structure is able to respond to thermally induced stresses by distorting macroscopically, or not, depends on its degree of constraint or restraint (discussed in Section 7.2.1). For convenience, the cause of residual stresses and distortion in weldments as a result of thermally induced stresses from welding are discussed in the opposite order in which these two fundamental responses to thermally induced stresses were introduced.

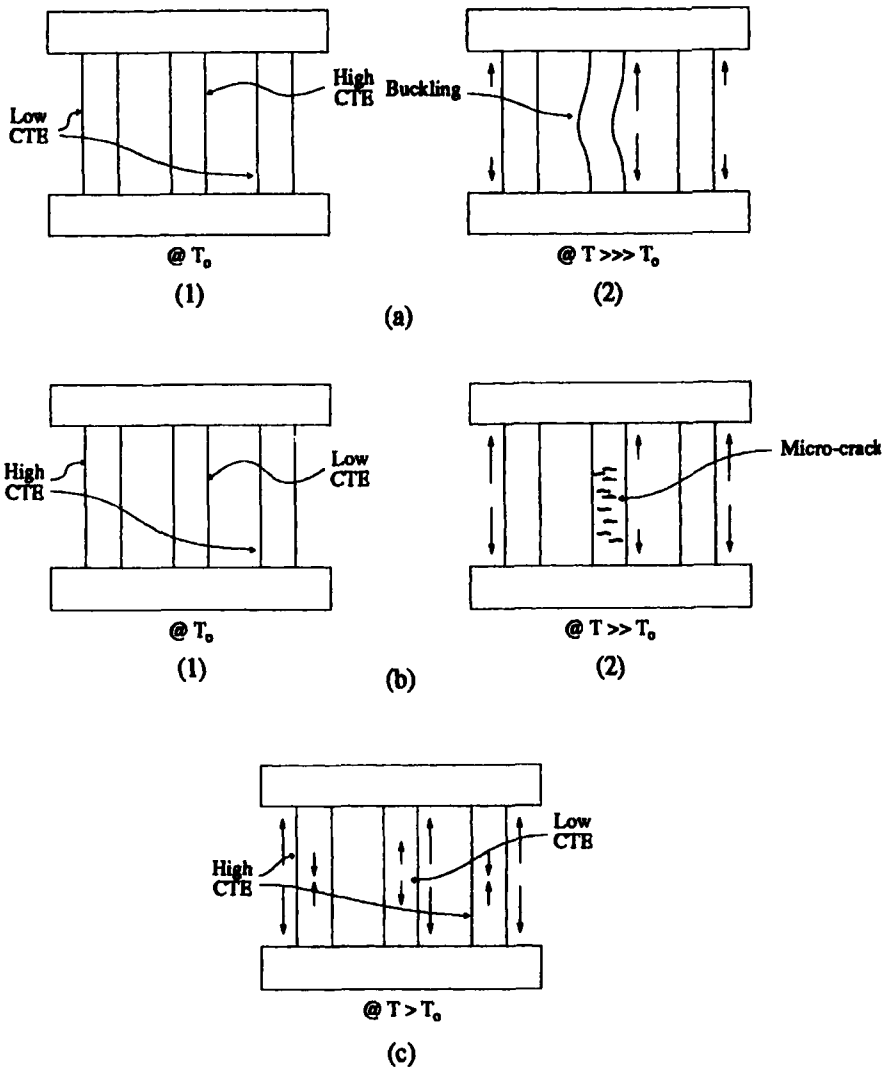


Figure 7.2 Illustration of thermally induced stresses leading to (a) macroscopic distortion, (b) microscopic distortion, or (c) residual stresses.

7.2.1. Causes of Residual Stresses in Weldments

Residual stresses are those stresses that would exist in a material or structure after all external loads are removed. Other names for residual stresses are *internal stresses* (not to be confused with stresses of internal origin to a structure, e.g., inertial loads), *initial stresses* or *inherent stresses* (since they are present in a material or structure before external loads are applied), *reaction stresses* (since they are the reaction to a localized or differential strain), and

locked-in stresses (which is probably the most descriptive name). Residual stresses can arise from any of several sources, but always as the result of an unbalanced situation of strain. Residual stresses can arise from nonuniform plastic deformation, especially when performed cold, during rolling or forging or forming, or from machining due to unbalanced local deformation caused by the material removal process; both of these are mechanical sources. They can also arise from thermal sources, as described in Section 7.1.

Thermally induced residual stresses can arise from any process that involves heat, whether that process is primarily a thermal process, such as heat treatment or welding, or not. In machining, for example, one source of residual stresses is localized heating from the friction of and work done by the cutting tool on the workpiece. When expansion and contraction associated with this heating and subsequent cooling is not free to take place because of constraint imposed by surrounding material that has not been heated, residual stresses develop. Proof that such stresses are induced is clear when a steel part is ground and cracks at its surface. But, just because cracks don't form, doesn't mean that no stresses were induced, only that they weren't high enough to cause cracking by exceeding the fracture strength of the material.

The most common sources of thermally induced residual stresses are thermal processes. Heat treatments at various stages in manufacturing can lead to residual stresses, as from quenching where the outside of the part cools (and thus contracts) faster than the inside, as is all too common with highly hardenable tool steels (e.g., "quench cracks"). Added to any unbalanced thermal contraction could be unbalanced stresses arising from localized phase transformations that result in a new phase with a different specific volume than the parent phase for materials that undergo such transformations.[3] Obviously, welding is an excellent source of residual stresses from both sources.

In structures that are welded (or brazed or soldered, for that matter), called weldments (or brazements or soldered assemblies), residual stresses arise from two situations and mechanisms: (1) structural mismatching and (2) uneven distribution of nonelastic strains whether from mechanical or thermal sources.

7.2.1.1. Residual Stresses From Mismatch. The simple example of residual stresses arising from structural mismatching is that of bars of different lengths being forcibly connected as shown in Figure 7.3. Tensile stress is produced in the shorter, middle bar, Q, as a result of joining by any method. At the same time, compressive stresses are produced in the longer, outboard

[3] Residual stresses that arise from phase transformations, or localized chemical reactions, often are referred to as microscopic residual stresses. Those that arise from other sources, mechanical or thermal, are often referred to as macroscopic residual stresses. Macroscopic residual stresses can arise from and exist on different scales, encompassing from all or most of the structure to only a region of the structure. An example of the former would be the distortion (and some locked-in stresses) of a large structure in earth orbit exposed to the heat (light) of the sun on one side (so that it thermally expands). An example of the latter would be localized distortion and locked-in stresses around a weld in a structure.

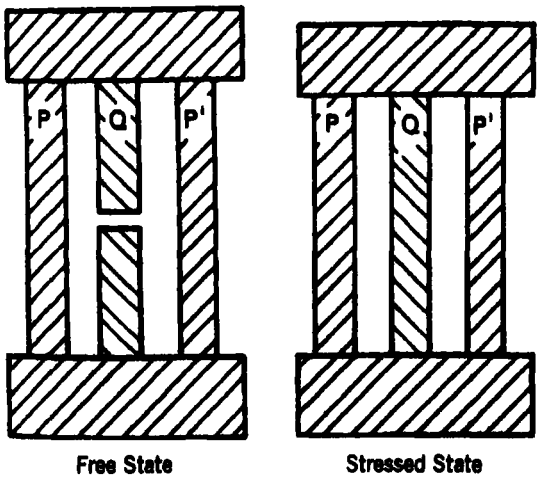


Figure 7.3 Residual stresses produced when bars of different lengths are forcibly joined into what is known as a "three-bar arrangement." (From *Welding Handbook*, Vol. 1: *Welding Technology*, 8th ed., edited by L. P. Connor, published in 1987 by and used with permission of the American Welding Society, Miami, FL.)

bars, P and P'. Compressive stresses arise to balance the tensile stress, so the overall system is in mechanical equilibrium. A similar situation arises when such a three-bar arrangement consists of a continuous middle bar of different composition and coefficient of thermal expansion than the two outboard bars. This is exactly the same as described for the case of the bimetal strip in Section 7.1.

A related situation, analogous to the situation that exists in a weldment, is that shown in Figure 7.4, taken from the *Welding Handbook*, 8th ed., Vol. 1. Here, three bars of the same carbon steel, having equal length and cross-sectional area, are connected at their ends by two rigid cap members (another 3-bar arrangement). The assembly produced is assumed to be free of any stresses following assembly. If the end members (or caps) and the middle bar are heated to 1100°F (595°C), in this example, and then cooled to room temperature while the two outside bars are kept at room temperature the whole time, the stress-versus-temperature response plotted in Figure 7.4 arises in the middle bar. These, as well as the stresses produced in the outside bars, are residual stresses. The two outside bars resist the deformation of the middle bar; first its expansion, then its contraction. The stress in each outside bar (where, for this example, the outside bars have equal cross-sectional areas) is half the value of the stress in the middle bar, but of opposite sign or type, that is, compression versus tension, or vice versa. When the middle bar is heated, compressive stresses arise in it because its expansion is restrained by the outside bars. As the temperature of the middle bar increases, the magnitude of the compressive stress that arises increases along line AB in Figure 7.4, until

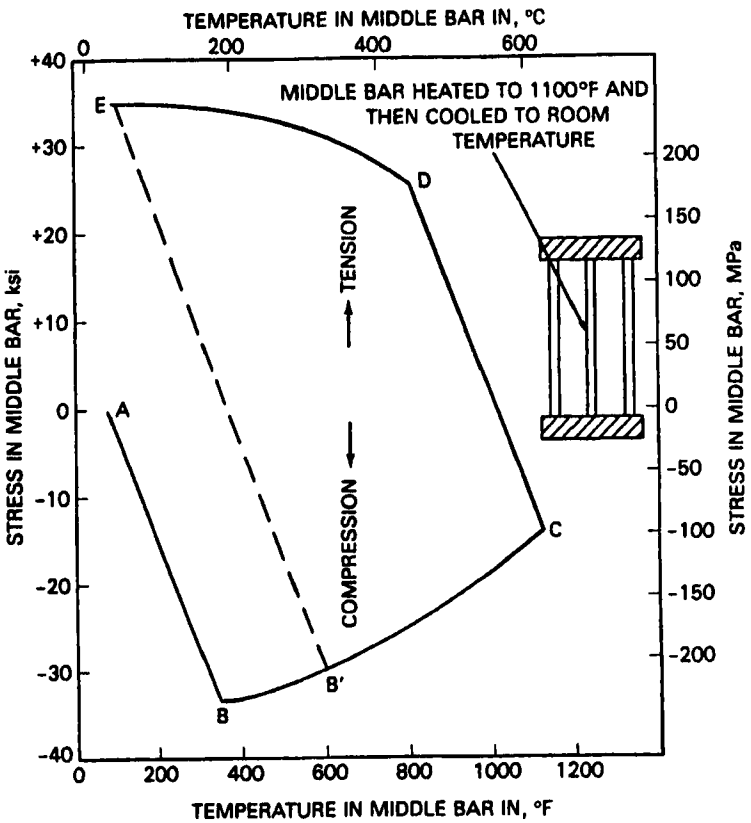


Figure 7.4 Effect on residual stresses of heating restrained bars (or volume elements in a weld). (From *Welding Handbook*, Vol. 1: *Welding Technology*, 8th ed., edited by L. P. Connor, published in 1987 by and used with permission of the American Welding Society, Miami, FL.)

at point *B* (approximately 340°F or 170°C) the yield strength in compression is reached. As the temperature increases beyond this level, the stress in the middle bar is limited to the yield strength, which decreases with increasing temperature as shown by curve *BC*. When the middle bar reaches 1100°F (595°C), heating is stopped (i.e., point *C* is reached).

As temperature decreases from point *C*, that is, as the middle bar cools and the response of the middle bar is elastic, the stress first drops rapidly, at some point changes to tension, and soon reaches the yield strength in tension (at point D). As temperature decreases further, stress in the middle bar is again limited by its yield strength (this time in tension), as shown by curve *DE*. Thus, a residual stress, equal to the yield strength in tension, is set up in the middle bar. Residual compressive stresses of half this value are set up in each outside bar to balance the system mechanically.

If heating of the middle bar had been stopped between points B and C, and the bar allowed to cool back to room temperature, tensile stresses would have developed elastically along a line parallel to $B'E$ until the yield strength was reached on curve DE. At room temperature, the final residual stress state would be the same, that is, residual tensile stress equal to the yield strength in the middle bar, and compressive stresses of half this value in the outside bars.

In welding, this three-bar arrangement can be envisioned as side-by-side-by-side volume elements of material running parallel to the weld line (with each base metal acting like the outside bars, and the weld acting like the middle bar), thereby showing how longitudinal residual stresses develop around welds.

7.2.1.2. Residual Stresses From Nonuniform, Nonelastic Strains. When a metal is heated uniformly, it expands uniformly, and no thermally induced stresses arise that can lead to either locked-in stresses or distortion. If, on the other hand, heating is done nonuniformly, thermal strains and stresses develop. These thermally induced stresses, which can become locked in as the result of the structure being restrained from distorting, obey the following relationships (for a plane-stress residual stress field where $\sigma_z = 0$).

1. Strains consist of elastic and plastic components given by:

$$\varepsilon_x = \varepsilon'_x + \varepsilon''_x \tag{7.1}$$

$$\varepsilon_y = \varepsilon'_y + \varepsilon''_y \tag{7.2}$$

$$\gamma_{xy} = \gamma'_{xy} + \gamma''_{xy} \tag{7.3}$$

   where ε_x, ε_y, and γ_{xy} are components of total strain; ε'_x, ε'_y, and γ'_{xy} are the elastic strain components; and ε''_x, ε''_y and γ''_{xy} are the plastic strain components.

2. Hooke's law applies to the stress and elastic strain, so that

$$\varepsilon'_x = \frac{1}{E(\sigma_x - \nu\sigma_y)} \tag{7.4}$$

$$\varepsilon'_y = \frac{1}{E(\sigma_y - \nu\sigma_x)} \tag{7.5}$$

$$\gamma_{xy} = \frac{1}{G\tau_{xy}} \tag{7.6}$$

   where ν is Poisson's ratio.

3. Stress must be in equilibrium, so that

$$\frac{d\sigma_x}{dx} + \frac{d\tau_{xy}}{dy} = 0 \tag{7.7}$$

$$\frac{d\tau_{xy}}{dx} + \frac{d\sigma_y}{dy} = 0 \tag{7.8}$$

4. The total strain must be compatible according to

$$\left(\frac{d^2\varepsilon_x'}{dy^2} + \frac{d^2\varepsilon_y'}{dx^2} - \frac{d^2\gamma_{xy}'}{dx\,dy}\right) + \left(\frac{d^2\varepsilon_x''}{dy^2} + \frac{d^2\varepsilon_y''}{dx^2} - \frac{d^2\gamma_{xy}''}{dx\,dy}\right) = 0 \tag{7.9}$$

Equations 7.7, 7.8, and 7.9 indicate that residual stresses exist when the value of R, called *incompatibility*, is not zero, where R is given by

$$R = -\frac{d^2\varepsilon_x''}{dy^2} + \frac{d^2\varepsilon_y''}{dx^2} - \frac{d\gamma_{xy}''}{dx\,dy} \tag{7.10}$$

In other words, incompatibility can be considered to be the cause of residual stresses.

Calculation of the stresses (σ_x, σ_y, and τ_{xy}) for given values of strain (ε_x'', ε_y'', and γ_{xy}'') requires that there be no applied stresses acting at the same time, and the history of residual stress formation must be known. With modern computer technology, solutions can be obtained from the temperature distribution as a function of time associated with a welding cycle (Chapter 6).

The preceding discussion was largely taken with permission from the *American Welding Society's Welding Handbook*, 8th ed., Vol. 1, Chapter 7, published in 1987, where residual stresses and distortion are treated in much more detail.

7.2.2. Causes of Distortion in Weldments

Distortion in a weldment can arise when thermally induced stresses (from situations described in Section 7.2.1) are unrestrained. Three fundamental dimensional changes taking place during welding can cause distortion in weld-fabricated structures or weldments: (1) transverse shrinkage that occurs perpendicular to the weld line, (2) longitudinal shrinkage that occurs parallel to the weld line,[4] and (3) any angular change that consists of rotation that occurs around the weld line.[5] These three-dimensional changes are shown in Figure 7.5.

The shrinkage and distortion that can occur during the fabrication of weldments is actually far more complex than illustrated in Figure 7.5. The amount and direction of shrinkage and distortion depends on mass distribution around the weld line (moment of inertia), the presence of other welds and their stress fields, and many other factors. The interested reader is referred to some specialized references given at the end of this chapter.

Transverse shrinkage in butt welds is uniform along the weld line, except as altered by through-the-thickness effects or variations and restraint from other

[4] Longitudinal stresses leading to longitudinal shrinkage distortion can be visualized from the three-bar analog.

[5] Rotation or angular distortion is the result of a nonuniformity of transverse shrinkage in the thickness direction.

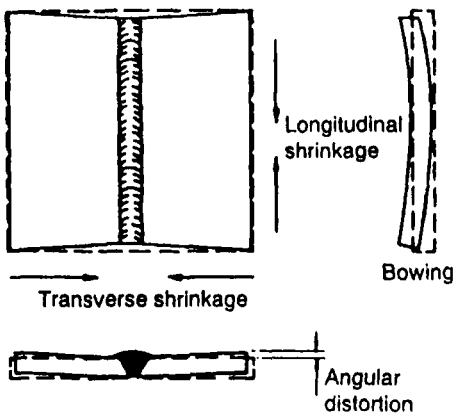


Figure 7.5 Fundamental dimensional changes that can take place in weldments: transverse shrinkage, longitudinal shrinkage, and angular distortion or bowing. (From *Introduction to the Physical Metallurgy of Welding*, 2d ed., by K. Easterling, published in 1992 by Butterworth-Heinemann, Oxford, UK and used with permission of the family.)

welds. The amount of transverse shrinkage that occurs is affected by the size (width and volume) of the weld and, so, the process, heat input, and joint configuration, the thermophysical properties of the base material(s), and the degree of restraint applied to the joint. External restraint can be considered to act like a system of transverse springs, the degree of restraint being expressed by the stiffness of the spring. The amount of shrinkage increases as the degree of restraint decreases. Since the amount of restraint almost always varies along the length of the weld, so, too, does the amount of transverse shrinkage. Normally, transverse shrinkage is greater in the center of a weld pass or run than near the ends. Longitudinal shrinkage in a butt joint is usually much less than transverse shrinkage, typically $\frac{1}{1000}$ of the weld length. Angular distortion is the result of nonuniformity of transverse shrinkage through the thickness. This is largely a function of the joint configuration and weld cross-sectional shape.

Distortion in fillet welds is similar to that in butt welds; namely, transverse and longitudinal shrinkage and angular distortion (across the weld) or bowing (along the weld) from unbalanced stresses in these welds (see Figure 7.5). Since fillet welds are most often used in combination with other welds in a weldment, specific resulting distortion can be very complex.

7.3. TYPICAL RESIDUAL STRESSES IN WELDMENTS

Typical changes in temperature and thermally induced stresses during welding are shown schematically in Figure 7.6, where a bead-on-plate weld is being

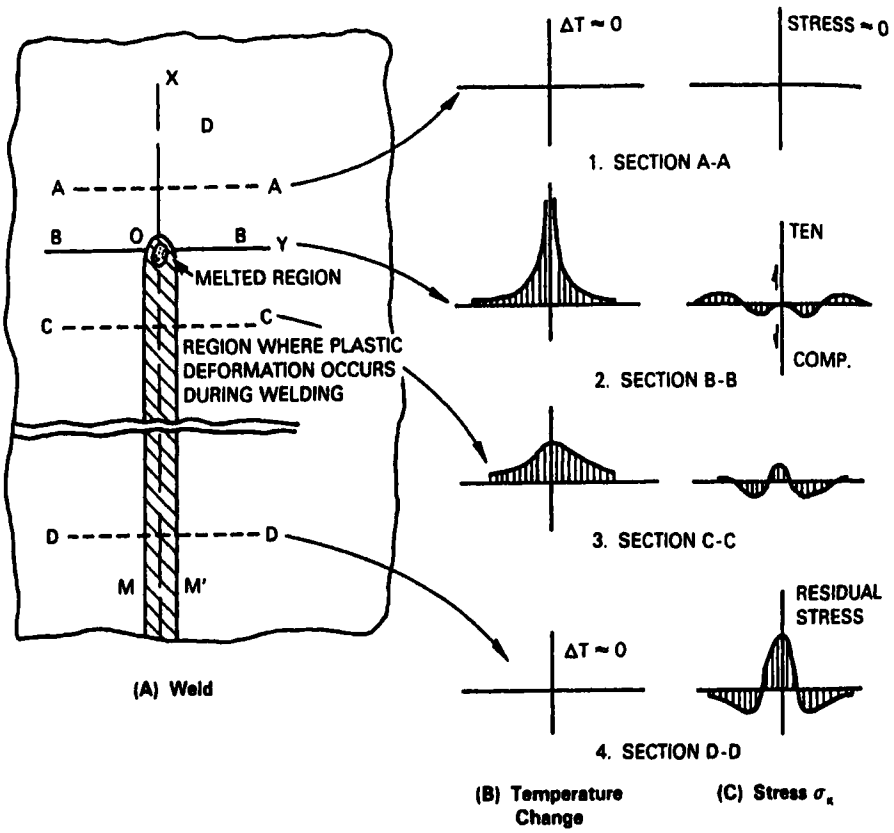


Figure 7.6 Typical distribution of temperature and stress at several locations in a bead-on-plate weld. (From *Welding Handbook*, Vol. 1: *Welding Technology*, 8th ed., edited by L. P. Connor, published in 1987 by and used with permission of the American Welding Society, Miami, FL.)

deposited along line x-x. The welding arc is moving at a constant speed, v, and, at the moment shown, is at the point O in Figure 7.6a. Let's take a look at the situation.

The distribution of temperature transverse to the weld line is shown in Figure 7.6b for four locations along the weld, A, B, C, and D. Along section A-A, which lies just ahead of the welding source, the temperature change due to the approaching arc is virtually zero. Along section B-B, on the other hand, the distribution of temperature is very steep, as this section passes through the arc. Some short distance behind the arc, the temperature distribution is less severe (since cooling has already begun), as shown for section C-C, and still further back, along section D-D, the temperature distribution along the line has dropped back to near that before welding was begun.

The distribution of stresses in the x direction, σ_x, at sections *A-A*, *B-B*, *C-C*, and *D-D*, is shown in Figure 7.6C. A stress in the y direction, σ_y, and a shearing stress, τ_{xy}, also exist, but these are not shown in Figure 7.6.

According to Chapter 7 in the *AWS Welding Handbook* (8th ed., Vol. 1), from which this discussion was taken nearly verbatim, with permission, the following occurs. At section *A-A*, thermally induced stresses due to welding are almost zero. Stresses in regions immediately below the arc and weld pool in section *B-B* are also almost zero because molten metal cannot support a load. Stresses in the heat-affected region on either side of the weld pool, however, do exist, and are compressive because thermal expansion in these very hot regions is restrained by surrounding metal at lower temperature, of higher strength, and without having experienced similar expansion. The limit of these compressive stresses is set by the yield strength of the metal in the heat-affected region. Where the temperature is the highest, which is nearest the fusion zone, the yield strength is lowest. The yield strength increases with increasing distance from the weld pool, so the compressive residual stress increases to its peak level. At some point away from the weld line, tensile stresses will arise to balance the compressive stresses induced by thermal expansion. This is essential for the system or weldment to be in mechanical equilibrium. The instantaneous stress distribution is shown in Figure 7.6c.2.

At section *C-C*, the weld and heat-affected zone have cooled considerably. As they did so, they tried to shrink, and tensile stresses developed in and near the fusion zone. These tensile stresses were again balanced by compressive stresses to maintain mechanical equilibrium. The stress distribution is shown in Figure 7.6c.3.

Very far behind the arc, the final, stable residual stress distribution for a bead-on-plate weld is shown in Figure 7.6c.4 for section *D-D*. High residual tensile stresses exist in the fusion and heat-affected zones, with compressive stresses in the unaffected base metal to balance the tensile stresses.

Once again, while difficult to do, the state of residual stress distribution can be calculated from the state of temperature distribution (discussed in Chapter 6). Numerical methods for estimating residual stresses are presented in section 7.8.

A typical distribution of both longitudinal and transverse residual stresses for a single-pass weld in a butt joint is shown in Figure 7.7. Typical residual stress patterns for some simple welded shapes are shown in Figure 7.8. According to Masubuchi and Martin (1961), the distribution of longitudinal residual stress (σ_x) can be approximated by

$$\sigma_x(y) = \sigma_m\left[1 - \left(\frac{y}{b}\right)^2\right]e^{-1/2(y/b)^2} \tag{7.11}$$

where σ_m is the maximum residual stress, which usually reaches no more than the yield strength of the base metal. The parameter b is the width of the tension zone of σ_x.

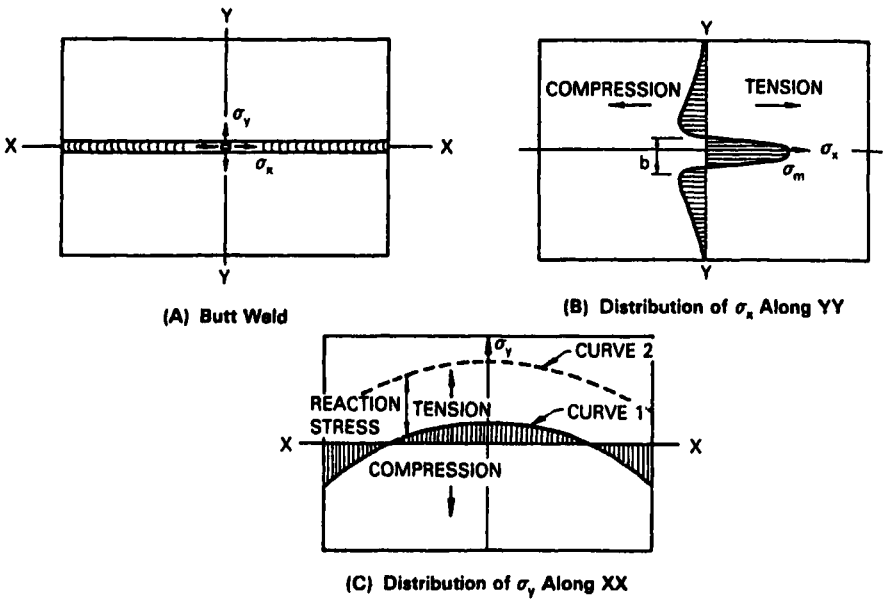


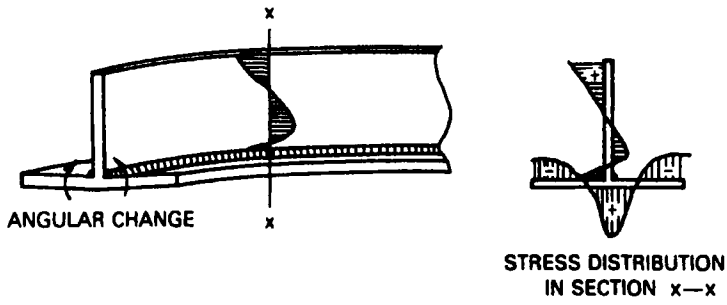
Figure 7.7 Typical distribution of residual stresses (b) longitudinal and (c) transverse to the butt weld line (a). (From *Welding Handbook*, Vol. 1: *Welding Technology*, 8th ed., edited by L. P. Connor, published in 1987 by and reprinted with permission of the American Welding Society, Miami, FL.)

7.4. EFFECTS OF DISTORTION

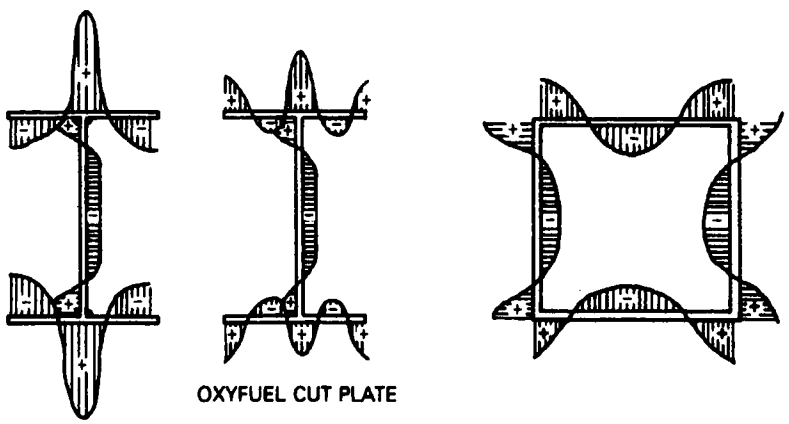
The effects of distortion as the result of welding are much more obvious than the effects of residual stresses (discussed in Section 7.5). Recall that distortion during or following welding is the result of unbalanced thermally induced stresses in unrestrained weldments. It arises from three fundamental dimensional changes that can occur during welding, singly or in combination: (1) transverse shrinkage that occurs perpendicular to the weld line, (2) longitudinal shrinkage that occurs parallel to the weld line, and (3) angular change that consists of rotation around the weld line. Examples of what can occur for butt and fillet welds are shown in Figure 7.5.

The degree or extent of distortion is affected by several factors, including (1) the geometry or configuration of the joint (butt, fillet, or T, etc.), as these each affects mass distribution; (2) the type of weld preparation (single- or double-V, J-, square-butt, etc.) (see Section 6.2); (3) the width or volume of the weld (related to the next factor); (4) the heat input from the process; (5) the arrangement of structural elements in the weldment (as these influence structural stiffness and restraint); and (6) the sequence in which welds are made (sequence can help balance or offset thermally induced stresses).

The obvious consequences or effects of distortion in weldments are (1) loss



Residual Stresses and Distortion of a Welded T-Shape



Residual Stresses in Welded H-Shapes

Residual Stresses in a Welded Box Shape

Figure 7.8 Typical residual stress patterns for some simple welded shapes. (From *Welding Handbook*, Vol. 1: *Welding Technology*, 8th ed., edited by L. P. Connor, published in 1987 by and used with permission of the American Welding Society, Miami, FL.)

of needed/required dimensions (especially those dimensions that determine shape); (2) misalignment of structural elements to allow proper support and transfer of applied loads; (3) inability to fit one welded subassembly onto, into, or with another (i.e., fit-up); (4) jamming or binding of a weldment in tooling used to hold structural elements in place during welding; and (5) loss of

aesthetics. Less obvious consequences during weld fabrication may include loss of structural integrity due to misalignment (related to factor (2); and loss of structural integrity of one or more structural elements due to localized buckling failure.

7.5. EFFECTS OF RESIDUAL STRESSES

The effects or consequences of residual stresses introduced into a structure by and during welding are often less obvious, but can be at least as detrimental as distortion. These effects often result from the way in which they alter applied stresses through interaction between the two. The major exception is effects on corrosion, which depend only on the residual stresses, unless they are altered by an applied stress in some way that either reduces or exacerbates the situation (to be described later).

Basically, applied stresses and residual stresses add vectorially, depending on both magnitude and relative direction. As a result, applied tensile stresses add to residual tensile stresses, but are reduced by residual compressive stresses. Applied compressive stresses are reduced by residual tensile stresses, but add to residual compressive stresses. The result may be that tensile fracture or compressive buckling (depending on which situation occurs) may take place at lower applied stresses than one might think, or have planned on and designed for. The effect of uniform external loads on the residual stress distribution of a welded butt joint is shown in Figure 7.9.

Based on analysis, the effects shown in Figure 7.9, may be summarized as follows:

1. The effect of weld-induced residual stresses on the performance of a welded structure is significant only for phenomena that occur at low applied stresses, such as brittle fracture, fatigue, and stress-corrosion cracking.
2. As the level of applied stress increases, the effect of residual stresses decreases. (This is because higher applied stresses overwhelm residual stresses by causing generally yielding.)
3. The effect of residual stress on the performance of welded structures under applied stresses greater than the yield strength is negligible.
4. The effect of residual stress tends to decrease after repeated loading.

Residual stresses affect the performance of weldments in several ways. They reduce the fracture strength of a weldment, often to very low levels, resulting in rapid, brittle fracture. The cause of brittle fracture is largely the complexity of the stress state (which is often triaxial), and residual tensile stresses cause more problem than residual compressive stresses. The situation is even worse as the rate of loading increases (approaching impact).

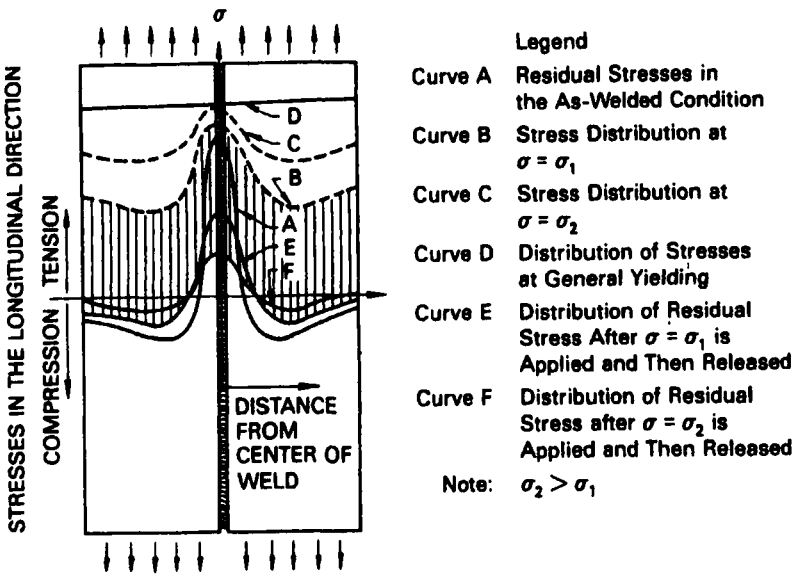


Figure 7.9 Effect of uniform external loads on the residual stress distribution of a welded butt joint. (From *Welding Handbook*, Vol. 1: *Welding Technology*, 8th ed., edited by L. P. Connor, published in 1987 by and used with permission of the American Welding Society, Miami, FL.)

Compressive residual stresses can cause buckling under compressive loading. This is a particular problem in thin columns or thin plates. In either case, localized buckling of a key structural member can lead to overall failure of the structure by shifting loads to other members, and exceeding their designed load limit.

Fatigue strength and life are affected in complex ways. They are increased in areas of compressive residual stresses, and decreased in areas of tensile residual stresses. Almost always, welding produces stress risers that aggravate fatigue, for example, undercut (near bead crowns or roots), ripples, pores, cracks, and metallurgical "notches" from sharp phase and property transitions.

Susceptibility to corrosion is increased by the presence of residual stresses almost without exception. This is particularly true for stress-corrosion cracking, which is exacerbated by the presence of residual tensile stresses.

7.6. MEASUREMENT OF RESIDUAL STRESSES IN WELDMENTS

Efforts to predict residual stresses arising from welding are pointless unless there is an effective way to measure such stresses; as neither analytical- nor numerical-based model simulations can be believed without experimental verification. Measuring residual stresses, including magnitude and sign (i.e.,

compression or tension), as a function of location, possibly in three directions, is far from trivial in reality, even if not in principle. In fact, there are many methods for measuring residual stresses in metals that are also generally applicable in weldments, and these can be divided into three classifications, as listed in Table 7.1: (1) stress–relaxation methods, (2) x-ray (and, more recently, neutron) diffraction methods, and (3) cracking methods. While no method is perfect, by any means, each has its merits, advocates, and appropriateness.

As a group, stress–relaxation methods determine residual stresses by measuring the magnitude sign and direction of strain released by cutting the sample containing these stresses and monitoring the strain released through some type of electrical or mechanical gauge. These methods provide reasonably accurate and reliable quantitative data, with some limitations imposed by sample geomerty (especially, 3-D complexity). Specific techniques exist for

TABLE 7.1 Classification Techniques for Measuring Residual Stresses

A1. Stress–relaxation using electric and mechanical strain gages	Techniques applicable primarily to plates	1. Sectioning technique using electric resistance strain gages
		2. Gunnert technique
		3. Mathar–Soete drilling technique
		4. Stablein successive milling technique
	Techniques applicable primarily to solid cylinders and tubes	5. Heyn–Bauer successive machining technique
		6. Mesnager–Sachs boring-out technique
	Techniques applicable primarily to three-dimensional solids	7. Gunnert drilling technique
		8. Rosenthal–Norton sectioning technique
A2. Stress–relaxation using apparatus other than electric and mechanical strain gages		9. Grid system-dividing technique
		10. Brittle coating-drilling technique
		11. Photoelastic coating-drilling technique
B. X-ray deffraction		12. X-ray film technique
		13. X-ray diffractometer technique
C. Cracking		14. Hydrogen-induced cracking technique
		15. Stress corrosion cracking technique

Source: From *Welding Handbook*, Vol. 1: *Welding Technology*, 8th ed., edited by L. P. Connor, published in 1987 by and used with permission of the American Welding Society, Miami, FL.

samples of different size and shape (essentially, thin, 2-D sheets or plates, or thick, 3-D solids), using different means and manner of cutting (e.g., drilling, boring, sectioning, and machine milling), and different means of monitoring strain release (e.g., physical distortion of overlying grids, mechanical measurement instruments or gauges, electrical-resistance strain gauges, photoeleastic or brittle coatings to provide visual indications of strain changes). Several different methods are described briefly, and one or two are described in more detail, in Section 7.6.1. For more information for stress–relaxation, as well as other specific methods, the interested reader is referred to specific references, some of which are listed at the end of this chapter.

As a group, x-ray diffraction (as well as more recently employed neutron diffraction) methods determine residual stresses by measuring their effect on the lattice parameter of the metal in which they are contained. Tensile residual stresses cause the lattice to expand, increasing the normal lattice parameter, while compressive residual stresses cause the lattice to contract, decreasing the normal lattice parameter, both in proportion to the magnitude of the stresses present. These methods generally suffer from being slow, requiring specialty equipment and skillful operators, and not being very accurate. A representative x-ray diffraction technique is described in Section 7.6.2.

A small group of techniques is available that monitor the effect of residual stresses on cracking induced by hydrogen (embrittlement) or stress corrosion. These methods, also given in Table 7.1, provide strictly qualitative data and are described in Chapter 17 as opposed to here.

7.6.1. Stress–Relaxation Techniques

As stated earlier, stress–relaxation methods for measuring residual stresses are all based on the fact that the straining that takes place during unloading (by removing or freeing material) is elastic, even when the material may have undergone plastic deformation. This being the case, it is possible to measure residual stresses even without knowing the history of the material.

A variety of specific techniques based on stress–relaxation are available, depending on sample size and shape, manner of cutting, and means of monitoring strain release. As summarized in Table 7.2, the first two techniques shown apply primarily to thin-plate samples; the next two techniques shown apply primarily to 3-D samples. The first two employ electrically resistive strain gauges, while the third employs a special mechanical gauge. The fourth also uses electric-resistance strain gauges. The fifth and last technique employs a photoelastic coating combined with a drilling procedure. Other methods use coatings that change color with different strains, or a brittle coating that exhibits strain release in the form (i.e., location, direction/pattern, and severity) of cracking in the coating.

7.6.1.1. A Sectioning Technique Using Electric-Resistance Strain Gauges. In this technique, gauges that measure strain (displacement) by the

TABLE 7.2 Specific Stress–Relaxation Techniques for Measuring Residual Stresses

Technique	Application	Advantages	Disadvantages
1. Sectioning technique using electric-resistance strain gages	Relative all-around use, with the measuring surface placed in any position	Reliable method, simple principle, high measuring accuracy	Destructive. Gives average stresses over the area of the material removed from the plate; not suitable for measuring locally concentrated stresses. Machining is sometimes expensive and time-consuming
2. Mathar–Soete drilling technique	Laboratory and field work use and on horizontal, vertical, and overhead surfaces	Simple principle, causes little damage to the test piece; convenient to use on welds and base metal	Drilling causes plastic strains at the periphery of the hole which may displace the measured results. The method must be used with great care
3. Gunnert drilling technique	Laboratory and field work use. The surface must be substantially horizontal	Robust and simple apparatus. Semidestructive. Damage to the object tested can be easily repaired	Relatively large margin of error for the stresses measured in a perpendicular direction. The underside of the weldment must be accessible for the attachment of a of a fixture. The method entails manual training
4. Rosenthal–Norton sectioning technique	Laboratory measurements	Fairly accurate data can be obtained when measurements are carried out carefully	Troublesome, time-consuming, and completely destructive method
5. Photoelastic coating-drilling technique	Primarily a laboratory method, but it can also be used for field measurements under certain circumstances	Permits the measurement of local stress peaks. Causes little damage to the material	Sensitive to plastic strains which sometimes occur at the edge of the drilled hole

Source: From *Welding Handbook*, Vol. 1: *Welding Technology*, 8th ed., edited by L. P. Connor, published in 1987 by and used with permission of the American Welding Society, Miami, FL.

change in electrical resistance in a coil of wire or foil are mounted on the surface of the test weldment. A very small piece of the material containing the strain gauges in or adjacent to the weld is then carefully removed by machining, so as not to introduce additional strains. By keeping the extracted piece small enough, no residual stresses can be sustained (or they are negligible in magnitude), so the strain measured by the gauges placed on the removed piece can be used to calculate the elastic strain resulting from the residual stresses distributed in the weldment. Gauges are generally mounted 120° apart to facilitate calulation using the following relations:

$$\begin{aligned} \bar{\varepsilon}_x &= -\varepsilon'_x \\ \bar{\varepsilon}_y &= -\varepsilon'_y \\ \bar{\gamma}_{xy} &= -\gamma'_{xy} \end{aligned} \tag{7.12}$$

where ε'_x, ε'_y, and γ'_{xy} are the elastic strain components of any residual stresses present and $\bar{\varepsilon}_x$, $\bar{\varepsilon}_y$, and $\bar{\gamma}_{xy}$ are the measured values of the strain components (the negative sign indicating that the stresses or strains involved are opposite one another, i.e., tensile residual stresses resulting in compressive elastic relaxation).

Residual stresses can be determined by substituting these strain values into the equations to satisfy mechanical equilibrium (Eqs. 7.7 and 7.8) and simultaneously solving these to get σ_x, σ_y, and τ_{xy} as

$$\begin{aligned} \sigma_x &= \frac{-E}{1-\nu^2}(\bar{\varepsilon}_x + \nu\bar{\varepsilon}_y) \\ \sigma_y &= \frac{-E}{1-\nu^2}(\bar{\varepsilon}_y + \nu\bar{\varepsilon}_x) \\ \tau_{xy} &= -G\bar{\tau}_{xy} \end{aligned} \tag{7.13}$$

To help negate any (bending) strains introduced by machine sectioning, it is advised that strain gauge measurements be made on both top and bottom surfaces. In this way, the mean measured value represents the normal stress component, while the difference in measured values represents any bending component.

7.6.1.2. The Rosenthal–Norton Section Technique. While out of order with the techniques listed in Table 7.2, the technique developed by Rosenthal and Norton (1945) is a close cousin of the sectioning technique. The difference is that the Rosenthal–Norton technique is intended for application to thick-section weldments. To work, two narrow blocks, the full thickness of the weldment, must be removed; one with its long dimension parallel to the weld direction (longitudinal) and the other with its long dimension transverse to the

weld direction. By measuring the strain release during block removal and the stresses remaining in the extracted blocks, developed formulas can be used to estimate the residual stresses in the interior of the weldment.

7.6.1.3. The Mathar–Soete Hole Drilling Technique. A hole drilling technique for measuring residual stresses first suggested by Mathar and refined and developed by Soete (1949) is shown schematically in Figure 7.10, with the modified residual stress pattern due to hole drilling shown in (b). When a hole is drilled in the midst of a rosette pattern of resistance strain gauges (a), the gauges register a change in strain. This is the result of localized removal of restraint by material removed from the hole, and concomitant localized distortion in response. The residual stress, σ_R, can be calculated if the distance between the hole and the gauge length is known, using the relationship between the measured strains in the 0, 45, and 90° directions, ε_1, ε_2, and ε_3. The maximum and minimum principal stresses are given by

$$\frac{\sigma_{max}}{\sigma_{min}} = -\frac{1}{K_1}\frac{E}{2}\left\{\left(\varepsilon_1 + \frac{\varepsilon_3}{1 - \nu K_2/K_1}\right)\right.$$
$$\left. \pm \frac{1}{1 + \nu K_2/K_1}[(\varepsilon_1 - \varepsilon_3^2 + 2\varepsilon_2 - (\varepsilon_1 + \varepsilon_3)^2]^{1/2}\right. \tag{7.14}$$

where K_1 and K_2 are calibration factors, which depend on the hole size and the distance between the strain gauges and the hole. These constants are given by

$$\frac{1}{K_1} - \frac{\varepsilon_A}{\varepsilon'_A} \sim 2.8 \qquad \text{for a 2-mm-diameter hole} \tag{7.15}$$

$$\frac{\nu K_2}{K_1} = -\frac{\varepsilon'_T}{\varepsilon'_A} \sim 0.3 \tag{7.16}$$

where ε_A is the applied strain in the axial direction, ε'_A is the relaxed strain in the axial direction (cause by drilling the hole), and ε'_T is the relaxed strain in the transverse direction.

The direction of the principal stresses Ψ is given by

$$\Psi = \tfrac{1}{2}\tan^{-1}\frac{\varepsilon_1 - 2\varepsilon_2 + \varepsilon_3}{\varepsilon_1 - \varepsilon_3} \tag{7.17}$$

Accuracy of the hole drilling technique using this approach is thought to be within 8–10% of the correct value (Parlane, 1977).

7.6.1.4. The Gunnert Drilling Technique. In this technique intended for thick-section weldments, four 3-mm (0.12-in.) through-thickness holes are

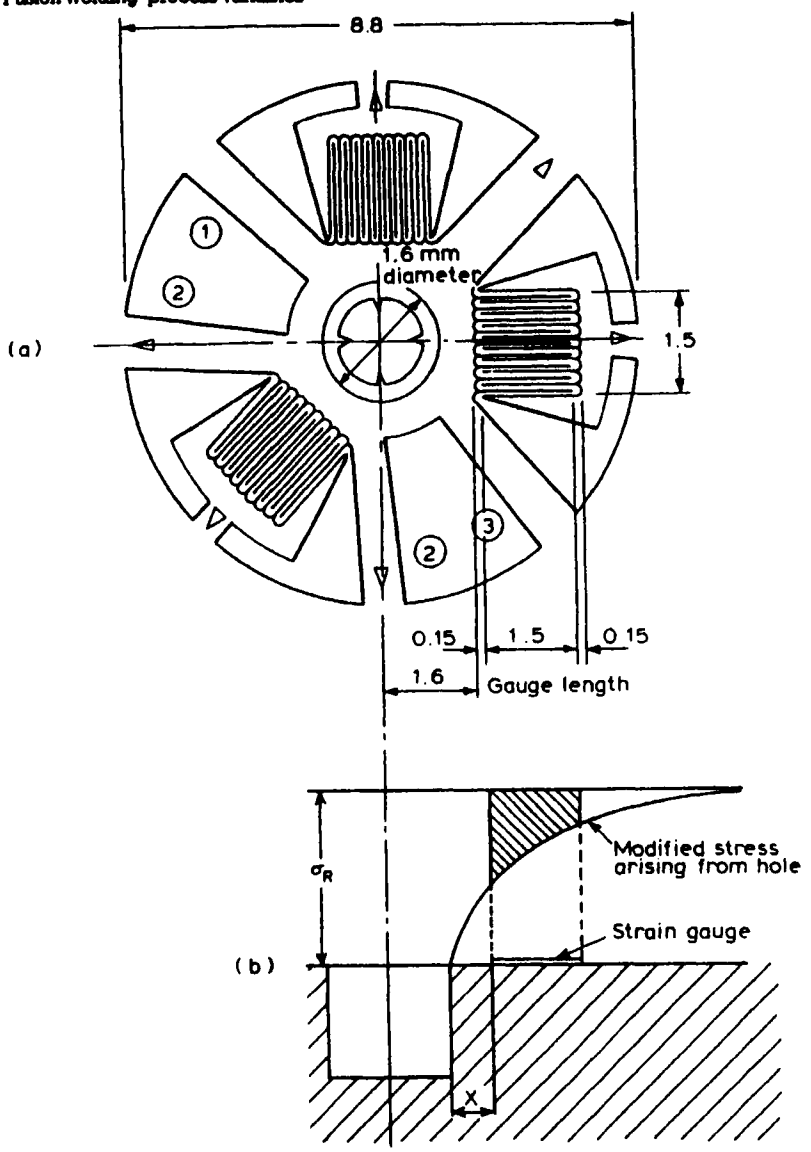


Figure 7.10 Schematic layout of the hole drilling technique for measuring residual stresses, in which the change in residual strain due to drilling is measured by the strain gauge rosette, as shown. (From *Introduction to the Physical Metallurgy of Welding*, 2d ed., by K. Easterling, published in 1992 by Butterworth-Heinemann, Oxford, UK, and used with permission of the Easterling family.)

drilled every 90° on a circle with a diameter of 9 mm (0.35 in.) perpendicular to the surface of the test weldment. The diametrical distance between holes at different depths below the surface is then measured by means of a specially designed mechanical gauge. The perpendicular distance between the plate surface and the gauge location at the different levels below the surface is also measured. A groove 16 mm (0.63 in.) from the measuring point is cut (or trepanned) around the holes in steps, and the same measurements described above are taken at each step. Residual stress is calculated at the interior of the weldment using developed formulas and measured data. This technique is shown schematically in Figure 7.11.

7.6.2. The X-ray Diffraction Technique

X-ray diffraction has been used to measure residual stresses for years. Obviously, the technique requires expertise, especially if high accuracy is required.

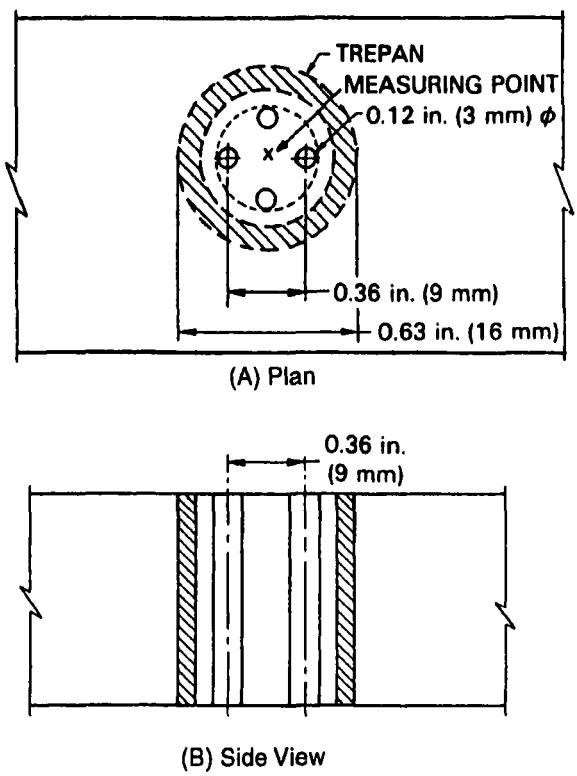


Figure 7.11 Schematic of the Gunnert drilling method for residual stress determination in thick-section weldments, plan (a) and side (b) views. (From *Welding Handbook*, Vol. 1: *Welding Technology*, 8th ed., edited by L. P. Connor, published in 1987 by and used with permission of the American Welding Society, Miami, FL.)

The technique relies on residual stresses (or any elastic stresses, for that matter) causing the normal lattice spacing of a crystal to change. Such a change can be measured using a back-reflection camera or suitable goniometer (of higher accuracy). The technique is shown schematically in Figure 7.12.

In one approach, stress-free and stressed states are compared, with the increase in stress from a reference or unstressed state given by

$$\sigma = K(2\Theta_0 - w\Theta_1) \tag{7.18}$$

where K is the bulk modulus $= E/(1 + \nu)$ (where ν is Poisson's ratio), Θ is defined in Figure 7.12, and Θ_0 and Θ_1 refer to the unstressed and stressed states, respectively. The technique is complicated in practice because it is difficult to measure the unstressed state, especially in welds. As a result, a double-exposure method is often used, comparing stress states before and after welding. In this case,

$$\sigma = K(2\Theta_{-} - \Theta_{\psi}) \tag{7.19}$$

where Θ_{-} is the angle of diffraction at zero angle of incidence to the principal strain direction, and Θ_{ψ} is the angle of incidence, usually 45°. Since K is a function of $\sin^2\Psi^{-1}$, this technique is often referred to as the $\sin^2\Psi$ method, the stress measured being proportional to the slope of the 2Θ versus $\sin^2\Psi$

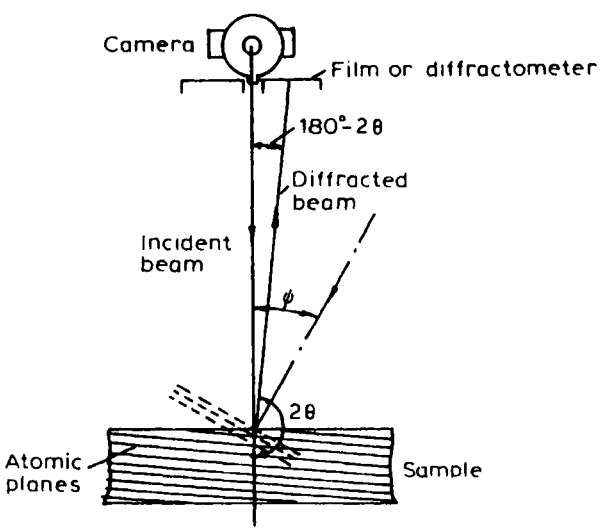


Figure 7.12 Schematic layout of the back-reflection x-ray technique used to measure residual elastic stresses in welds. (From *Introduction to the Physical Metallurgy of Welding*, 2d ed., by K. Easterling, published in 1992 by and used with permission of Butterworth-Heinemann, Oxford, UK, and used with permission of the Easterling family.)

curve. On this basis,

$$\sigma = K \frac{d(2\Theta)}{d(\sin^2 \Psi)} \tag{7.20}$$

The advantage of the x-ray diffraction method is that it is nondestructive compared to hole drilling or other trepanning methods, and the availability of portable commercial equipment enables field measurements to be made. Accuracy suffers, however, being only around 15–20%.

7.7. RESIDUAL STRESS REDUCTION AND DISTORTION CONTROL

That residual stresses and/or distortion occurs as a consequence of thermally induced stresses from all fusion and some nonfusion welding almost goes without saying. Thus, being able to deal with these residual stresses or this distortion is critical to producing quality weldments. To develop effective means for reducing residual stresses and distortion, it is essential to understand how they arise and how their formation is affected by design and welding procedures. Hopefully, the preceding sections provided this understanding. Now it is time to consider some practical approaches to the prevention or reduction of residual stresses and distortion.

7.7.1. The Interplay Between Residual Stresses and Distortion

From the discussion in Section 7.1, it should be clear that distortion and residual stresses both arise from thermally induced stresses, and, from Section 7.2, that the two are simply different manifestations of those thermally induced stresses. Distortion occurs as a result of unbalanced thermally induced stresses if the material or structure is free to respond to those unbalanced stresses, that is, if the material or structure is not restrained. Residual stresses occur as the result of unbalanced thermally induced stresses being prevented from causing distortion, and, thereby, being partially relieved, when the material or structure is restrained. Thus, it should come as no surprise that attempting to prevent or reduce distortion must be done in such a way that intolerable residual stresses do not result instead. Contrarily, attempting to relieve residual stresses once they have developed from welding must be done in such a way that unacceptable distortion does not result. In other words, design and process engineers must talk to one another to not end up "chasing their own tails."

7.7.2. Prevention Versus Remediation

Given the choice, it is always better to prevent a problem than to have to try to fix or remediate it. This is as true in welding as it is in medicine. Prevention, however, is not always practical, even if it is usually possible. Thus, good

engineering involves having knowledge and methods both to prevent and remediate the occurrence and adverse consequences of residual stresses and distortion.

7.7.3. Controlling or Removing Residual Stresses

Although the effects of residual stresses on the service performance of a welded structure vary significantly, depending on their severity and the impact of their occurrence, it is generally preferable to keep residual stresses to a minimum. Precautions to reduce residual stresses can take two forms: prevention or remediation. To prevent development of residual stresses it is crucial to reduce the effects of heat during welding. One way is to employ cold, nonfusion welding processes (see Section 4.2.1), but this is seldom a viable option. Another approach is to employ hot, nonfusion processes to eliminate shrinkage associated with solidification of any fusion zone. (There is still thermal contraction in any heat-affected zone that must be dealt with or tolerated, but the major source of residual stress, volumetric shrinkage upon solidification, is eliminated.) A third approach is to minimize the volume of molten weld metal so as to minimize shrinkage associated with solidification. This can be done by judicious choice of joint preparation. For example, a U-groove could be used in place of a V-groove, because U-grooves require less filler. It is also desirable to use the smallest groove size (regardless of geometry) and the smallest angle (for a V) and root opening that will still permit adequate accessibility for welding and production of a sound weld. Part of the effectiveness of a small root opening is to prevent or limit shrinkage across the joint (see Figure 6.4).

Attempting to keep the melting efficiency high to minimize the extent of a heat-affected zone by going to a high-energy-density welding process can, in fact, be counter-productive. The temperature gradient from the superheated center of the weld pool out into the unaffected base material is much steeper than that for a lower energy-density process, so a much more concentrated and severe residual stress pattern can result.

Remediation of residual stresses once they arise in a weldment is accomplished by postweld thermal treatment called thermal stress relief. Heating lowers the yield strength of the base material and allows localized relaxation of residual stresses, primarily by plastic deformation and secondarily by creep. The effects of time and temperature of stress relief are shown in Figure 7.13. To prevent the structure from distorting as a result of the residual stresses being redistributed, critical weldments should be stress relieved while still restrained in a fixture (sometimes, but not always, the same one in which they were welded).

It is also possible to relieve residual stresses by mechanical means,[6] or at

[6] The fundamental mechanism by which mechanical forces relieve residual stresses is the equivalence thermal and mechanical energy. Whether energy is added to a material from a thermal source or a mechanical source, dislocations can be caused to move, thereby causing residual stress to lower.

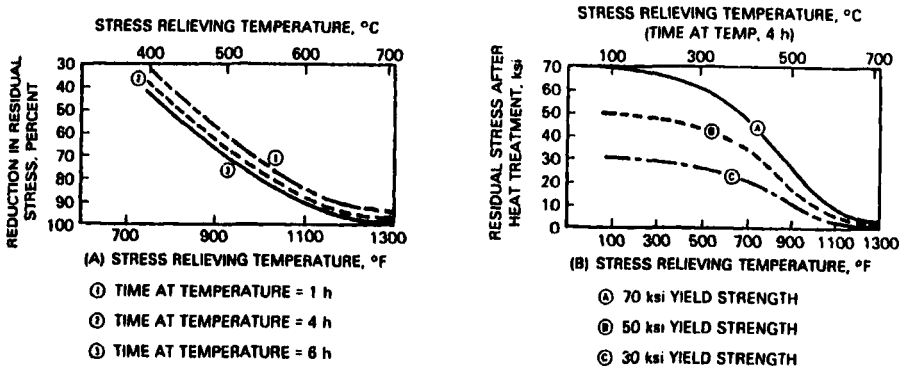


Figure 7.13 Effect of (a) time at temperature and (b) temperature of a thermal stress relieving treatment on residual stresses. (From *Welding Handbook*, Vol. 1: *Welding Technology*, 8th ed., edited by L. P. Connor, Figures 7.55A and 7.55B, page 263, published in 1987 by and used with permission of the American Welding Society, Miami, FL.)

least to redistribute these stresses to reduce peak levels. Proven methods includes, hammer peening, shot peening, and planishing. A method called vibratory stress relief uses the energy of elastic waves introduced by physically shaking a structure or impacting it with a transducer (e.g., ultrasonic) to cause stress reduction. However, the amplitude of vibration (often having to be at the frequency of natural resonance of the structure, or one of the harmonics of this frequency) can cause damage from fatigue. In many people's minds, the jury is still out on vibratory stress relief, but one should consider the results of Sonsino et al. (1996).

7.7.4. Controlling or Removing Distortion

To prevent distortion, there are several viable approaches. First, distortion can be minimized by proper design. This means, among other things (1) employing the minimum number of parts and, thus, a minimum amount of welding; (2) properly preparing the joint (especially for unrestrained butt joints) to minimize angular distortion (e.g., use double-V or double-U as opposed to single-V or single-U configurations to balance heat input and shrinkage); and (3) using minimum-sized fillet welds. Second, distortion can be minimized by proper assembly procedures, such as (1) presetting members to compensate for angular distortion from shrinkage; (2) assembling the weldment so that it is nominally correct before welding and then using some form of restraint to minimize distortion from welding; and (3) sequencing welding to balance heat input and create offsetting shrinkage/distortion. The advantage of presetting (shown in Figure 7.14a) is that there are few or no residual stresses once the part has been welded and seeks its own location. A consequence of rigid

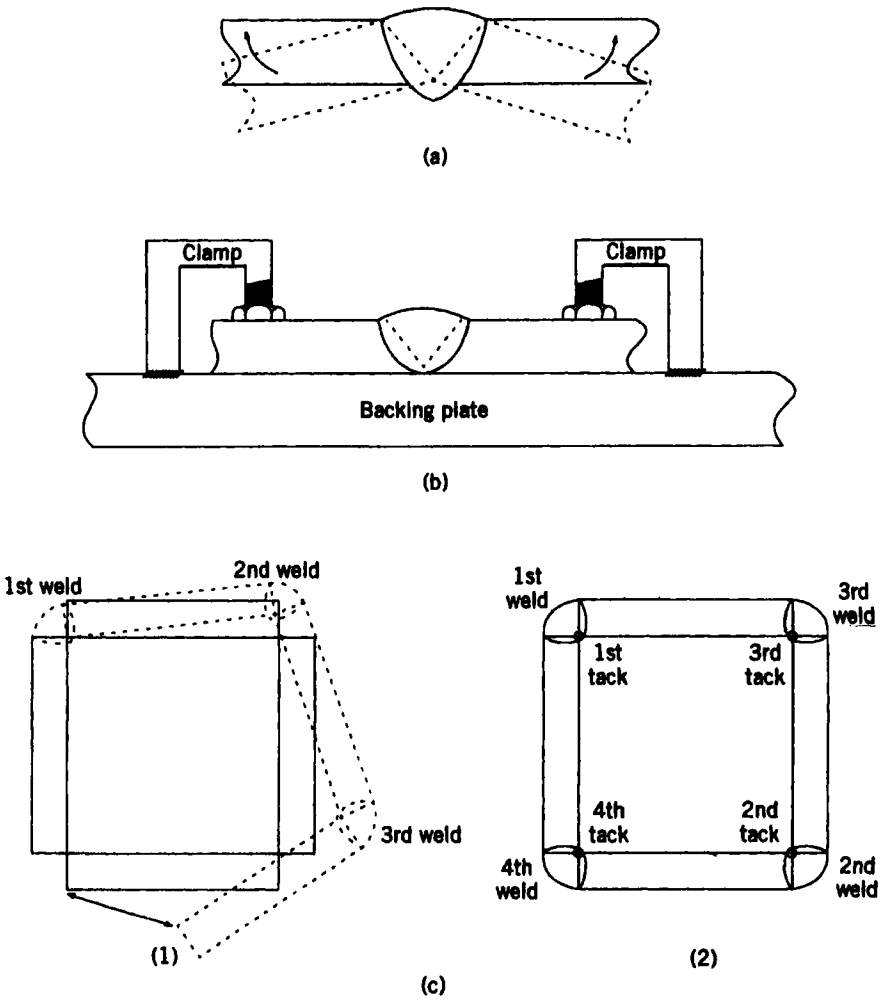


Figure 7.14 Techniques for preventing or minimizing distortion, including (a) presetting, (b) rigid fixturing, and (c) sequencing welds (or weld sequencing.)

fixturing is that it introduces residual stresses at the expense of freedom from distortion (Figure 7.14b). Proper sequencing certainly helps to minimize distortion, but also results in residual stresses, as the structure is eventually forced to fit together (Figure 7.14c). Preheating can be used to reduce distortion in a weldment by minimizing temperature gradients that lead to nonuniform elastic contraction (see Section 7.2.1.2).

Once distortion takes place and must be removed (remediated), there are two options: (1) thermal straightening using heat to cause compensating expansion and contraction (in what is called flame straightening) (see Section 2.5) or (2) mechanical straightening using presses or jacks. Mechanical

straightening is easier to understand, and is probably more common, unless structures get very large. Flame straightening is understandable in principle, much more "arty" in practice, but offers tremendous capability, even for very large, apparently immovable structures. (Here, in fact, is demonstration of just how powerful an effect thermally induced stresses can have on distortion. Historically, war-torn countries began the process of putting their industry, society, and economy back together by salvaging structural steel from bomb-ravaged buildings to rebuild those buildings, most notably power-generating and steel-making facilities, by cutting and flame straightening!)

Whatever is done, it is better to prevent problems than to have to fix them, and preventing one problem must be done so as not to introduce another problem.

7.8. NUMERICAL METHODS FOR ESTIMATING RESIDUAL STRESSES

Direct measurement techniques undoubtedly provide the most reliable estimates of residual stresses in welds and weldments, despite accuracy limitations mentioned in Section 7.6, but great benefit can be derived from predictions obtained from models. Such methods allow convenient assessment of the influences of process, process parameters, and procedures on the residual stress state that will develop. This knowledge, even though providing trends at best, can help in deciding on the need for and value of preheat or postheat on preventing or alleviating hydrogen cracking, for example.

Since residual stresses in welds involve both elastic and plastic deformation, any model must deal with this complex elastic–plastic treatment. Recent advances in computer technology and computing techniques based on finite-element methods have helped greatly, with agreement between predictions and measurements steadily improving. The computational procedure involves calculating the elastic–plastic strain increments of a network or mesh of volume elements surrounding and including the weld over a range of time intervals appropriate to the welding thermal cycle imposed. While accuracy increases with the use of smaller volume elements, this accuracy comes at the expense of capacity of the computer and time for computing.

The total strain increment over a temperature interval of interest is given by the matrix

$$\{d\varepsilon^{\mathrm{T}}\} = \{\alpha\}dT \tag{7.21}$$

where $d\varepsilon^{\mathrm{T}}$ refers to strain from thermal expansion. $d\varepsilon$ can be expressed in terms of elastic (ε^{e}), plastic (ε^{P}), and thermal (ε^{T}) strain contributions:

$$\{d\varepsilon\} = \{d\varepsilon^{\mathrm{e}}\} + \{d\varepsilon^{\mathrm{P}}\} + \{d\varepsilon^{\mathrm{T}}\} \tag{7.22}$$

The increment of stress is then obtained from the product of the matrix $[D]$

and the strain increment:

$$\{d\sigma\} = \{[D]d\varepsilon\} \tag{7.23}$$

after Ueda and Yamakawa (1971).

The stress change within a given volume element in the vicinity of a weld varies with temperature in accordance with the simplified equation:

$$\Delta\sigma = \alpha\Delta TE \tag{7.24}$$

where α is the coefficient of thermal expansion and E is the elastic modulus. The temperature change (ΔT) comes from the temperature distribution obtained from solution of the general equation of heat flow, simplified to the degree necessary and possible. This being the case, $\Delta\sigma$ depends on the thermal factors q and k (for all three orthogonal directions) and on the material properties of α, E and σ_y, all of which vary with temperature. If a phase transformation occurs during cooling, whether in the fusion zone or heat-affected zone, it contributes an additional factor, in terms of dilatation, given by

$$\varepsilon_d = \frac{5}{6}\left\{\left(\frac{\Delta V}{V}\right)\left(\frac{\sigma}{\sigma_y}\right)\right\} \tag{7.25}$$

where σ is the applied stress and σ_y the yield stress of the parent phase (e.g., austenite) before transformation. ΔV is the volume change associated with the phase change, while V is the volume of the parent phase. Typical results are shown in Figure 7.15.

While accuracy of results vary depending on the fineness of the mesh employed and on ability to incorporate properties as a function of temperature, they can be more than good enough to determine trends and aid in selection of process, parameters, and procedures. Figure 7.16 illustrates typical predicted versus measured results.

Some specific examples of finite element analysis to predict residual stresses and their effects can be found in the work of Majorana et al. (1988), Ueda and Yuan (1993), Roelens et al. (1994), and Nguyen and Wahab (1996), to name but a few.

7.9. SUMMARY

The severity of heating and cooling associated with the thermal cycles typical of fusion welding processes frequently result in high thermally induced strains and stresses. These can, in turn, lead to severe distortion if the material or structure is free to respond, or to severe residual stresses if the material or structure is restrained. For metals and alloys that undergo phase transformations in the fusion zone or heat-affected zone (or both), on cooling, the

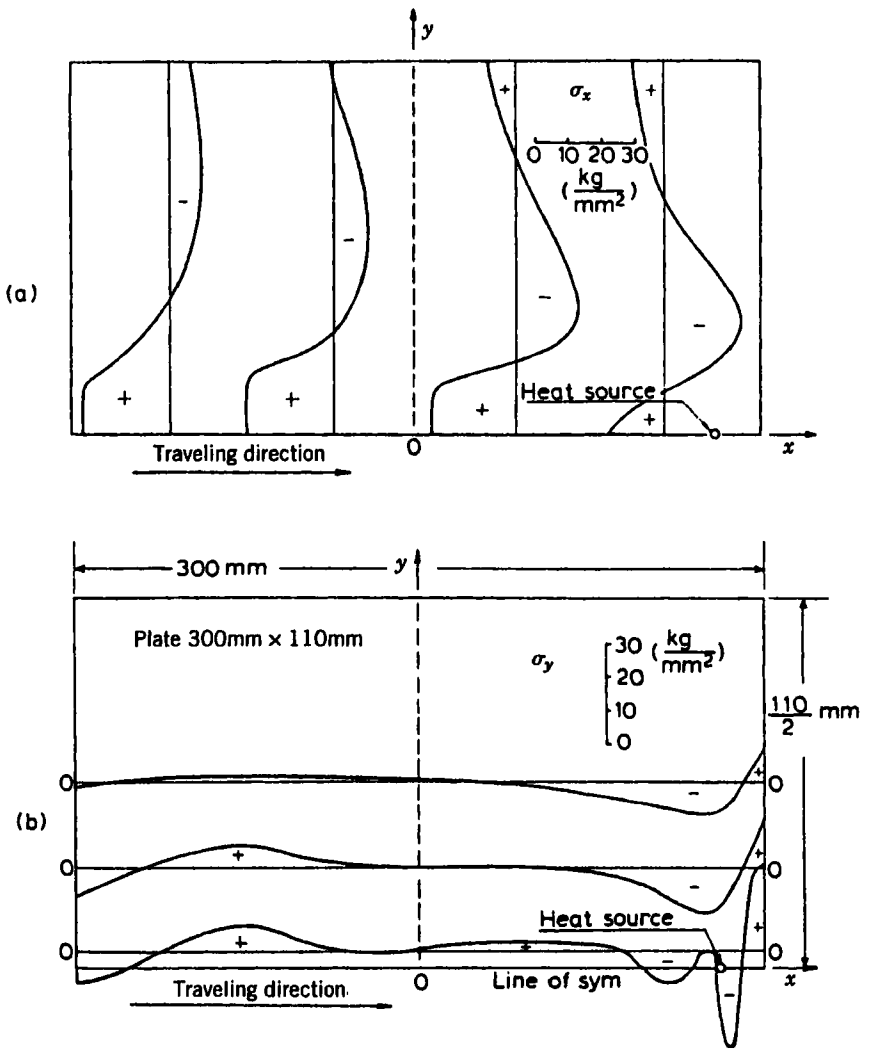


Figure 7.15 Residual stresses for a butt weld calculated using FEM techniques showing (a) changes in longitudinal stresses as a function of distance from the arc source and (b) changes in transverse stress at various distances from the weld centerline. (After "Mechanical characteristics of cracking of welded joints" by Y. Ueda and T. Yamakawa in *International Symposium on Cracking and Fracture in Welds*, 1971, Japanese Welding Society, Tokyo, Japan, p. IC5.1-13, used with permission of the Japanese Welding Society.)

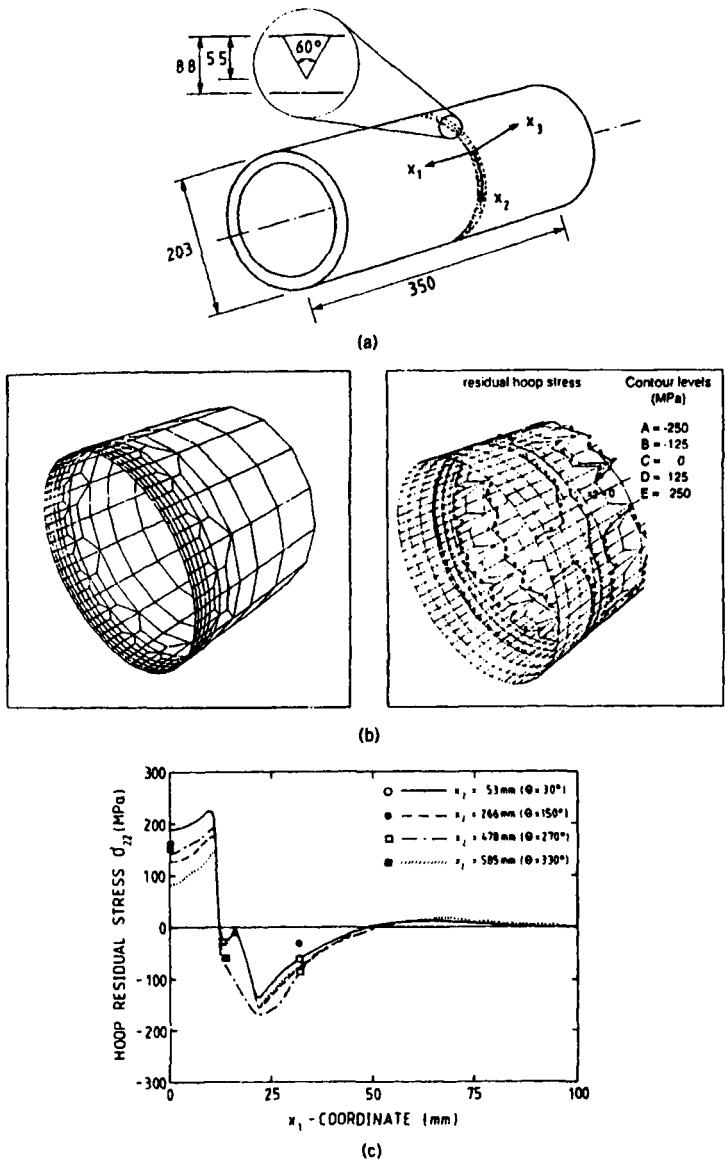


Figure 7.16 Comparison of calculated and measured hoop stresses at the outer surface, from the weld centerline, of a butt-welded pipe 203 mm in diameter by 350 mm long with a 5.5-mm-deep partial-penetration weld in a single-60°V groove in an 8.8-mm wall. (After "Residual stresses and deformations in a thin-walled pipe" by L. Karlsson, M. Jonsson, E. Lindgren, M. Nasstrom, and L. Troive in PVP, Vol. 173, *Weld Residual Stresses and Plastic Deformation*, edited by E. Rybicki, M. Shiratori, G. E. O. Widera, and J. Mihyashi, 1989, ASM, pp. 7–11, from *Introduction to the Physical Metallurgy of Welding*, 2d ed., by K. Easterling, published in 1992 by Butterworth-Heinemann, Oxford, UK, and used with permission of the Easterling family.)

residual stress pattern is further complicated by dilatational strains. Distortion poses obvious and usually immediate consequences relating to fit-up, shape integrity, proper performance (i.e., structural integrity), and aesthetics. Residual stresses pose more insidious problems with a tendency to reduce fracture strength and increase brittle behavior, alter and, usually, reduce fatigue life, and aggravate corrosion.

There are several ways of measuring and calculating residual stresses. Measurements can be made by relying on the relaxation of strain by hole drilling or trepanning (selective material removal), lattice distortion caused by stress and detected by x-ray diffraction, or cracking response in the presence of hydrogen or stress-induced corrosion. Calculations can be made by relying largely on numerical methods.

Attempts to prevent or remediate distortion must be done thoughtfully to avoid introducing unacceptable levels of residual stress. Both can be dealt with by proper joint design and setup, proper process selection and operation, proper sequencing of welding, and proper and expeditious use of postweld thermal or mechanical treatments.

REFERENCES AND SUGGESTED READING

Majorana, C. E., Navarro, G., and Schrefler, B. A., 1988, "Numerical and experimental analysis of the residual stresses in welding processes," *International Journal of Computer Applications Technology*, **1**(1–2), 96–104.

Nguyen, N. T., and Wahab, M. A., 1996, "The effect of undercut, misalignment, and residual stresses on the fatigue behaviour of butt welded joints," *Fatigue & Fracture of Engineering Materials & Structures*, **19**, 769–778.

Parlane, A. J. A., 1977, "The determination of residual stresses: a review of contemporary measurement techniques," *Conference on Residual Stresses in Welding Construction and Their Effects*, edited by R. W. Nichols, The Welding Institute, London, p. 63.

Roelens, J. B., Maltrud, F., and Lu, J., 1994, "Determination of residual stresses in submerged arc multi-pass welds by means of numerical simulation and comparison with experimental measurements," *Welding in the World* (*Le Soudage Dans Le Monde*), **33**(3), 152–159 (in English).

Rosenthal, D., and Norton, T, 1945, "A method for measuring residual stresses in the interior of a material," *Welding Journal*, **24**(5), 295s–305s.

Soete, W., 1949, "Measurement and relaxation of residual stresses," *Welding Journal*, **28**(8), 354s–364s.

Sonsino, C. M., Muller, F., Deback, J., and Gresnigt, A. M., 1996, "Influence of stress relieving by vibration on the fatigue behaviour of welded joints in comparison to post-weld heat treatment," *Fatigue & Fracture of Engineering Materials & Structures*, **19**, 703–708.

Ueda, Y., and Yamakawa, T., 1971, "Mechanical characteristics of cracking of welded joints," in *International Symposium on Cracking and Fracture in Welds*, Japanese Welding Society, Tokyo, Japan, p. IC5.1-13.

Ueda, Y., and Yuan, M. G., 1993, "Prediction of residual stresses in butt welded plates using inherent strains," *Journal of Engineering Materials and Technology, Transactions of the ASME*, **115**(4), 417–423.

Suggested readings on residual stresses and distortion, including relief and measurement techniques, in welding

Karlsson, L., Jonsson, M., Lindgren, E., Nasstrom, M., and Troive, L., 1989, "Residual stresses and deformations in a thin-walled pipe," in PVP, Vol. 173, *Weld Residual Stresses and Plastic Deformation*, edited by E. Rybicki, M. Shiratori, G. E. O. Widera and J. Mihyashi, ASM, Metals Park, OH, pp. 7–11.

Lu, J., Bouhelier, C., Lieurade, H. P., Baralle, D., Miege, B., and Flavenot, J. F., 1994, "Study of residual stress using the step–step hole drilling and x-ray diffraction method," *Welding in the World (Le Soudage Dans Le Monde)*, **33**(2), 118–128 (in English).

Masubuchi, K., 1970, "Control of distortion and shrinkage in welding," *Welding Research Council Bulletin 149*, Welding Research Council, New York.

Masubuchi, K., 1980, *Analysis of Welded Structures*, Pergamon Elmsford, NY.

Masubuchi, K., 1983, "Residual stresses and distortion," in *Metals Handbook, 9th ed.*, Vol. 6, American Society for Metals, Metals Park, OH, pp. 856–894.

Masubuchi, K., and Martin, D. C., 1961, "Investigation of residual stresses by use of hydrogen cracking," *Welding Journal*, **40**(12), 553s–563s.

Michaleris, P., and Sun, X., 1997, "Finite element analysis of thermal tensioning techniques mitigating weld buckling distortion," *Welding Journal*, **76**(11), 451s–457s.

O'Connor, L. P. (Editor), 1987, "Measurement of residual stresses in weldments," *Welding Handbook*, Vol. 1: *Welding Technology*, 8th ed., American Welding Society, Miami, FL, pp. 231–234.

Pavlovsky, V. I., and Masubuchi, K., 1994, "Research in the U.S.S.R. on residual stresses and distortion in welded structures," *Welding Research Council Bulletin 388*, Welding Research Council, New York, pp. 1–62.

Procter, E., 1981, "Measurement of residual stresses," *Residual Stresses*, The Welding Institute, London, p. 34.

Ruud, C. O., and Farmer, G. D., 1979, "Residual stress measurement by x-rays: efforts, limitations, and applications," *Nondestructive Evaluation of Materials*, edited by J. J. Burke and V. Weiss, Plenum, New York, pp. 101–116.

Scruby, C. B., Antonelli, G., Buttle, D. J., Dalzell, W., Gori, M., Gulliver, J. A., de Michelis, C., Ravenscroft, F. A., and Ruzzier, M., 1993, "Development of non-invasive methods for measurement of stress in welded steel structures," *PED Manufacturing Science and Engineering Proceedings of the 1993 ASME Winter Annual Meeting*, ASME Production Engineering Division, 28 November–3 December 1993, New Orleans, LA, pp. 855–859.

Smith, D. J., and Webster, G. A., 1997, "The measurement of prior plastic deformation in metallic alloys using the neutron diffraction technique," *Journal of Strain Analysis for Engineering Design*, **32**, pp. 37–46.

CHAPTER 8

THE PHYSICS OF WELDING ENERGY OR POWER SOURCES

The physics of welding deals with the complex physical phenomena associated with the process, including heat, electricity, magnetism, light, sound, and mechanical work. All welding processes require some form of energy to obtain continuity between the atoms, ions, or molecules of the materials being joined, that is, to form bonds and produce a weld. Alternative energy (or power) sources can include (1) electrical sources, in which the heat of an arc, a plasma, or internal resistance (or Joule heating) causes melting (at least for fusion welding) or softening or solid-phase diffusion (for nonfusion welding); (2) high-energy-density beams of electrons (for electron-beam welding) or light (for laser-beam welding); (3) chemical sources, in which heat of combustion or reaction causes melting (e.g., in oxyfuel and aluminothermic welding, respectively); or (4) mechanical sources, in which mechanical work is converted to heat to facilitate plastic deformation and interdiffusion (e.g., in pressure or friction welding). This chapter takes a look at some of the physics of these energy or power sources for accomplishing welding. Obviously, the treatment cannot be exhaustive; each source could be a book unto itself, and often is! But, enough will be said to aid understanding of future chapters, and to provide a ready reference for some quick answers.

8.1. ELECTRICITY FOR WELDING

Since electricity is essential to the operation of electric energy sources, and since so many and diverse welding processes rely on electric energy sources, it is only appropriate to briefly present some fundamentals on electricity for

welding. The electric circuit that allows an electric arc to form, or heat to be generated by resistance, is the same as any electric circuit, and, so, consists of three factors: (1) current, which is the flow of electricity; (2) voltage, which is the force or pressure that causes current to flow; and (3) resistance, which is a force that impedes the flow of current within a material, or, alternatively, allows the flow of current to be regulated. Let's look at each factor very briefly.

Current is actually the rate at which charge carriers (normally electrons, but possibly ions in plasmas or electrolytes, or holes, which are the absence of an electron, in semiconductor devices) flow in a circuit. Current is measured by the number of unit charges (in coulombs) that flow through a wire (or arc, plasma, or electrolytic solution) per second. One ampere (A) represents a flow of 1.6×10^{19} coulombs per second.[1] Current is designated by I and expressed in amperes.

Voltage is the force or pressure that causes charge carriers to move and a current to flow. The measure of this force or pressure is the volt. Voltage is actually the difference in the potential at two points to cause a current flow, so is often said to represent the potential difference. The force or potential is called the electromotive force or emf. One volt is the force that will cause one ampere of current to flow against a particular standard resisting force to the current flow present in all real materials.[2] Voltage or Emf is designated by E and expressed in volts.

Resistance is the obstacle or restriction presented to current flow in an electric circuit by the fact that the circuit consists of material elements or current paths, often, but not necessarily, wires. Every material offers resistance to current flow, with the degree or magnitude of resistance being a function of the material itself, the temperature of that material, and its physical size, including cross-sectional area and length. The inherent quality of a material to resist current flow is called resistivity, and arises from scattering of the electrons (or other charge carriers) by atoms (or ions or polar molecules) of the material. The effect of temperature is to increase resistivity in metals due to the increased incidence of scattering as atoms on the crystal lattice vibrate faster and at a greater amplitude. In other materials, like ceramics, glasses, and polymers, the origin of resistivity is more complicated, and, thus, so is the behavior as a function of temperature. Regardless of the type of material, if the resistivity of a material is low, it is said to be a conductor; if it is high, it is said to be a nonconductor or an insulator. (Incidentally, if it is somewhere between, it is a semi-conductor.) The effect of cross-sectional area and length are analogous to

[1] One ampere is actually the steady current that when flowing in straight parallel wires of infinite length and negligible cross section, separated by a distance of one meter in free space (i.e., a vacuum), produces a force between the two wires of 2×10^{-7} newtons per meter of length.

[2] In fact, real materials resist the flow of current except at extremely low temperatures, usually quite near absolute zero. This resisting force arises from the scattering of electrons by atoms and their electron clouds as they attempt to flow through a material, where atomic vibration ceases and scattering is minimized.

the area and length of a pipe to the flow of water; area constricts flow, length poses a frictional force to flow. Resistance is designated by R and is expressed in units called ohms. It is analogous to the viscosity of water.

In a simple electric circuit, shown in Figure 8.1, a voltage source is provided by a battery where the longer line represents the positive terminal or anode, and the shorter line the negative terminal or cathode. Outside the battery or voltage source (which could alternatively be a generator or transformer), which sets up an emf, a current flows. By convention (established by Benjamin Franklin), current is said to flow from positive to negative, although in reality, the electrons that constitute the current actually flow in the opposite direction, from the negative cathode to the positive anode. Current flow, I, can be measured using a low-resistance ammeter, and voltage, E, by a high-resistance voltmeter. Any resistance or resistor in the circuit is represented by the zigzag symbol, and the level of resistance could be measured by an ohmmeter (which is never used to make measurements when a current is flowing).

The relationship between current and voltage and resistance in this and any electric circuit is given by *Ohm's law*:

$$\text{current } (I) = \frac{\text{voltage } (E)}{\text{resistance } (R)} \tag{8.1}$$

or

$$\text{amperes} = \frac{\text{volts}}{\text{ohms}} \quad \text{or} \quad I = \frac{E}{R} \tag{8.2}$$

where I = current (flow) in amperes, E = voltage (pressure) in volts, and

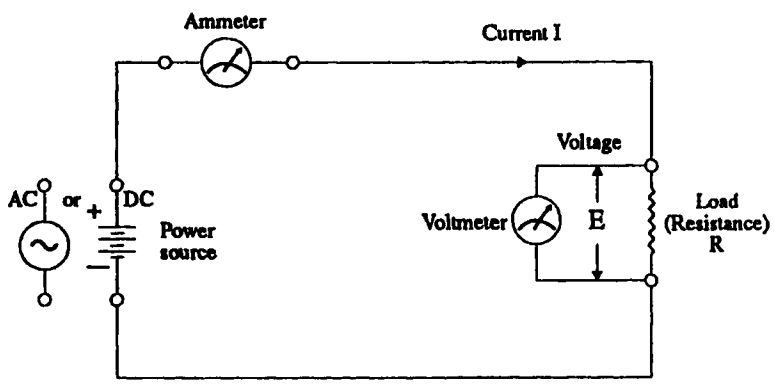


Figure 8.1 A typical, simple electric circuit showing a power source (here, a direct current battery, but, alternatively, an alternating current generator), current flow, current (I) and voltage (E) measurement using an ammeter and a voltmeter, respectively, and a resistance (or resistor).

R = resistance (restriction to current flow) in ohms. Ohm's law can be written in two other, rearranged forms:

$$E = IR \quad \text{or} \quad R = \frac{E}{I}$$

By simple mathematics, if any two values are known or measured, the third can be calculated.

For a typical, simple welding circuit (as shown in Figure 8.2), the battery (in Figure 8.1) is replaced by a welding power supply (e.g., a generator or transformer). The resistor (in Figure 8.1) is replaced by an electric welding arc. A welding arc poses a resistance to the flow of current due to collisions between electrons moving from the negative electrode or terminal to the positive electrode or terminal under an emf by air molecules in the arc gap.

As mentioned in Section 3.3.1.1, an electric welding arc can be operated in three ways: (1) with a direct current (DC) flow under the emf from a source with fixed polarity, with the welding electrode made to be negative (−) and the workpiece made to be positive (+); (2) with a direct current with the welding electrode made to be positive (+) and the workpiece made to be negative (−); or (3) with an alternating current (AC) flow under the emf from a source with periodically reversing or alternating polarity, where the welding electrode and workpiece each alternate between positive and negative. When a direct current (DC) power source is employed, welding is said to be operating in DC. When an alternating current (AC) power source is employed, welding is said to be operating in AC. For DC operation, when the welding electrode

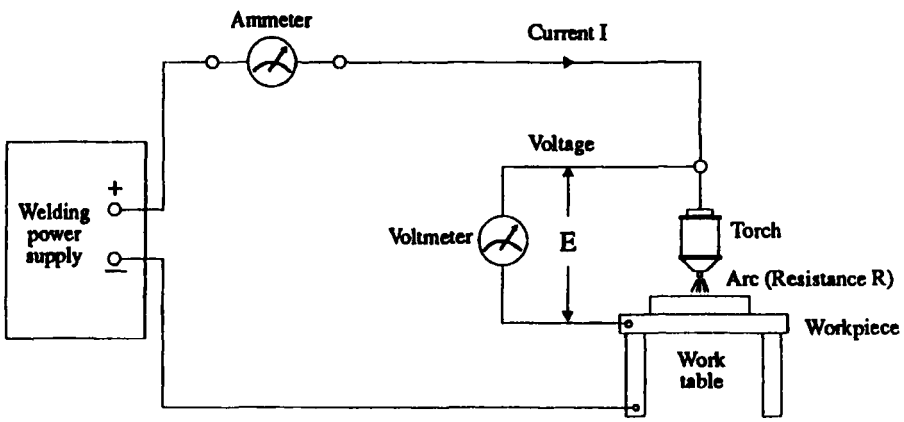


Figure 8.2 A typical, simple welding electrical circuit showing a welding machine as a power source and a welding arc as a resistance. This circuit is hooked up for DCSP or DCEN operation.

is negative, and electrons move to the positive workpiece, the DC operation is said to be occurring under straight polarity (or SP). This mode of operation is thus known as DCSP, DC (welding) electrode negative (or DCEN) or DC(−). For DC operation in which the welding electrode is made positive, electrons move from the negative workpiece to the welding electrode. This is referred to as DC reverse polarity, DCRP, or DC (welding) electrode positive (or DCEP) or DC(+). For AC operation there is, in fact, a net drift toward the positive anode (in the straight polarity direction) since electrons are more mobile than positive charge carriers.

These two DC operating modes result in very different distributions of heat, with the bulk (approximately two-thirds) of the heat being where the electrons give up their kinetic energy in collisions with atoms in the positive electrode. Details are given in Section 3.3.1.1, and the effects on weld appearance are given in Figure 3.5.

Referring back to Figure 8.2, the ammeter used to measure current in a welding circuit is in reality a millivolt-meter (calibrated in amperes) connected across a high current, very low resistance, calibrated shunt in the welding circuit. The voltmeter shown in Figure 8.2 will measure the voltage output of the welding machine and the arc, which are virtually the same, once the arc is struck and active. Before the arc is struck, or if the arc is broken, the voltmeter will read the voltage across the welding machine with no load applied, that is, with no current flowing in the circuit. This is known as the open-circuit voltage, and is higher than the arc voltage or the voltage across the welding machine when current is flowing.

An important unit to welding, and in electric circuits, is that of *power*. Power is the rate of producing or using energy, and is measured in watts. The power in an electric circuit or welding arc is the product of the current (in amperes) and the voltage (in volts):

$$\text{power} = \text{current} \times \text{voltage} \quad \text{or} \quad \text{watts} = \text{amperes} \times \text{volts}$$

or

$$P = IE \tag{8.3}$$

Power can be measured using a wattmeter, which is really a combination of an ammeter and a voltmeter.

Besides power, it is important to know the amount of work involved or being performed. Electrical *work* is the product of power and time, and is expressed in watt-seconds (or joules) or in kilowatt-hours.

As mentioned earlier in this section, electric current can also be operated in an alternating mode. Alternating current (AC) is electric current that flows back and forth in a circuit at regular intervals. During this alternation, current rises from zero to a peak value, returns to zero, reverses direction and rises to a peak in that new direction, and again returns to zero—comprising one full

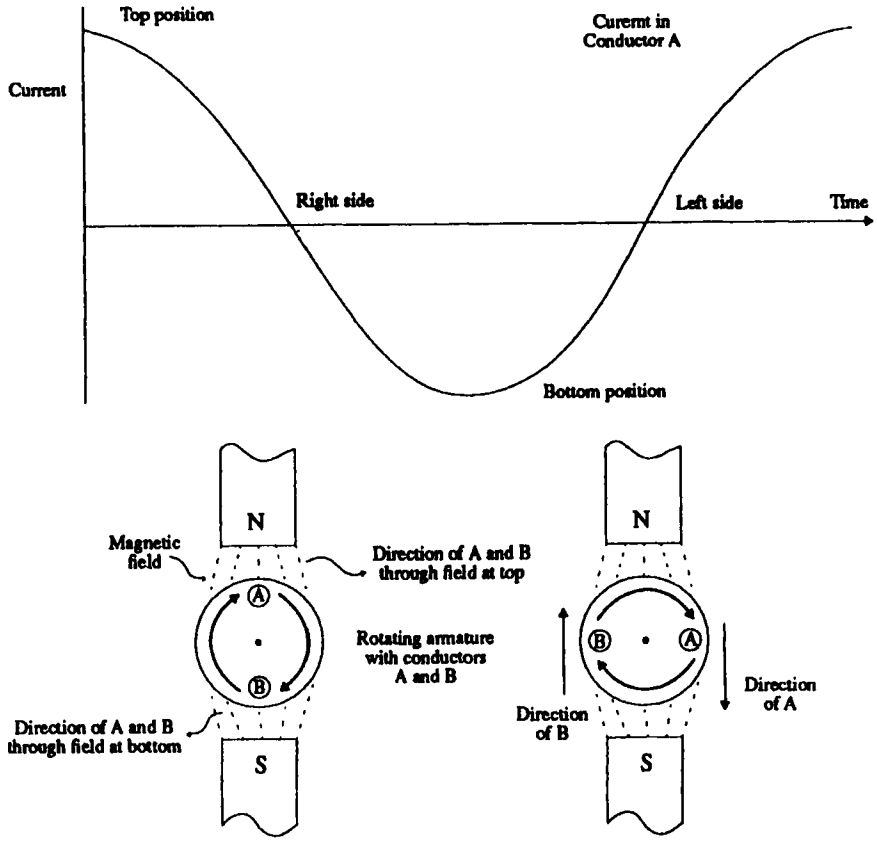


Figure 8.3 Sine-wave alternating current generation.

cycle. For convenience, a cycle is divided into 360 degrees of angle. Figure 8.3 shows such a cycle graphically. Note that the cycle takes a sine-wave form. This is usually the case because electricity is generated by one revolution of a single-loop coil armature in a two-pole alternating-current generator (shown along the bottom of Figure 8.3).[3] The maximum current value in one direction is reached at the 90° point, and in the other direction at the 270° point. The number of times such a cycle occurs per second is called the frequency of the alternating current. In the United States, this frequency is 60 cycles per second (cps), while in much of the rest of the world, it is 50 cps.

Alternating current for arc welding usually is of the same frequency as that provided by the power-generating utility over its transmission lines, that is, the line voltage or line current. While both the voltage and current in an AC welding arc follow the sine-wave form shown in Figure 8.3 and go through zero

[3] Recall that an emf is generated whenever an electrical conductor moves in a magnetic field so as to cut lines of force. This is the basis and explanation for alternating current generation. In welding generators, there are usually more than two poles and many hundreds of loops of wire in the coil.

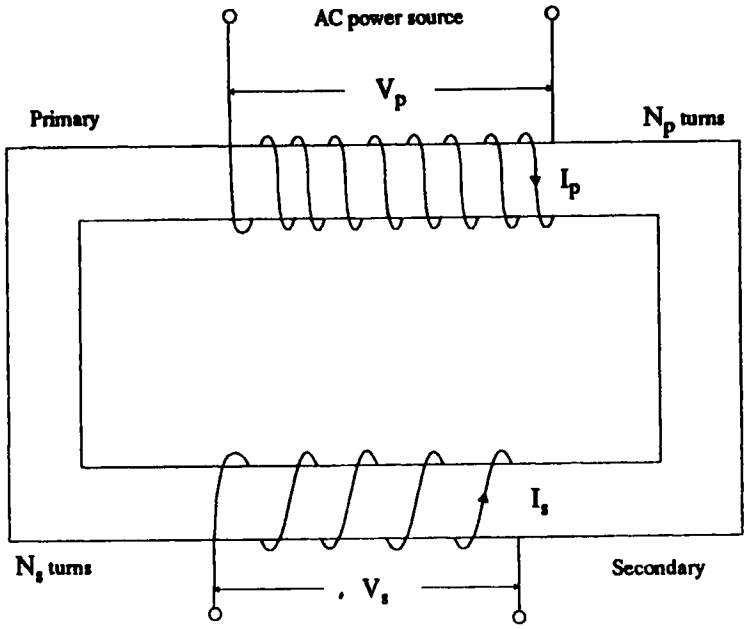
twice each cycle, the rate or frequency with which they do so is so fast that the arc appears continuous and steady to the unaided eye. Unless stated otherwise, the wave form of alternating current is taken to be a sine wave.[4]

When voltage or current need to be measured for AC, special meters are required to read both the positive and negative half-cycle peak values of the sine wave. Actually, an effective value or root-mean-square (rms) value is read, which is 0.707 times the maximum value. An alternating current has no unit of its own, but is defined in terms of the DC ampere. An alternating current, not being steady like a direct current, is said to be equivalent to a direct current when it produces the same heating effect under exactly similar conditions. This is done because the heating effect of a negative current is the same as that of a positive current. Ohm's law also applies to alternating current. However, for alternating current there is another important factor besides current, voltage, and resistance, namely inductance. Inductance arises from a magnetic circuit, analogous to an electric circuit.

Magnets have field lines of force running in arcs between the opposite (north and south) poles of the magnet. These can be seen by the alignment of a compass needle or fine iron fillings sprinkled on paper covering a magnet. Similar magnetic lines of force surround any conductor carrying an electric current. These lines of force are more intense for higher magnetic field strengths or currents, and are concentrated by ferromagnetic materials (such as iron) placed within a coil. *Inductance* expresses the results of a specific arrangement of electrical conductors, iron cores, and magnetic fields. It involves change, since it functions only when magnetic lines of force are cutting across electrical conductors. Thus, inductance is always important in alternating-current circuits; in direct-current circuits it is important only when they are first connected or disconnected, whereupon magnetic field lines expand or collapse across conductors and induce currents. For an alternating-current circuit, this "turning on" and "turning off" occurs four times with each cycle.

If a coil is connected to alternating current, the lines of force build to a maximum and then collapse, then build again in the opposite direction, and collapse again each cycle. If another coil is placed on the same iron core close to the first, the expanding and collapsing lines of force from the first cut across the conductors of the second and induce an alternating emf in it. The closer the coils, or the stronger the magnetic lines of force, the greater will be the induced emf. This is the principle of a transformer, shown schematically in Figure 8.4. By changing the magnetic coupling, the output of the second coil (called the secondary) and, thus, the output of the transformer can be controlled. This coupling can be increased by moving the coils closer together or by increasing the strength of the magnetic field between them. The strength of the magnetic field can, in turn, be increased by putting more iron into the area between the coils, or in some other ways not described here.

[4] The major exception in welding is the so-called square wave referred to in Section 3.3.1.1. The advantage of the square wave is explained there.



$$\frac{N_p}{N_s} : \frac{V_p}{V_s} : \frac{I_s}{I_p}$$

Figure 8.4 Principle of a transformer showing the relationship between the number of turns on the primary and secondary sides of the transformer and the primary and secondary voltage and current.

The output of a transformer-type welding machine is alternating current of the same frequency as the input power. Various techniques can be used to limit current flow to one direction, that is, convert it to direct current, by what is known as rectification. Once this was done by a rectifier consisting of a diode vacuum tube. Today, its done with solid-state diodes made from p-n junctions between doped semiconductors.

With this as background, we can proceed with a discussion of various electric power sources for welding.

8.2. THE PHYSICS OF AN ELECTRIC ARC AND ARC WELDING

8.2.1. The Physics of an Electric Arc

An electric arc is used as the heat source for more welding processes than any other energy source. This is because an arc produces a high intensity of heat

and is fairly easy to control. Because of its importance to welding, it is essential to understand the physics of an arc.

8.2.1.1. The Welding Arc. A *welding arc* is, in reality, a gaseous electrical conductor that changes electrical energy into heat. It involves electrical discharges formed and sustained by the development of conductive charge carriers in a gaseous medium. The current carriers in the gaseous medium are produced by thermionic emission; that is, by thermal activation and electric field extraction in which outer electrons from atoms in the gaseous medium and a permanent or consumable electrode or workpiece are stripped away to be free to contribute to current flow. Positive ions are formed in the gaseous medium as a consequence. Resulting arcs can be steady (from a direct current power supply), intermittent (due to occasional, irregular short circuiting), continuously unsteady (as the result of an alternating current power supply), or pulsing (as the result of a pulsing direct current power supply). It is this variety of possibilities that makes an electric arc such a useful heat source for welding and that results in so many processes and process variations.

8.2.1.2. The Arc Plasma. Current is carried in an arc by a plasma. A *plasma* is the ionized state of a gas, comprised of a balance of negative electrons and positive ions (both created by thermionic emission from an electrode and secondary collisions between these electrons and atoms in the gaseous medium being used, whether a self-generated or externally supplied inert shielding gas) to maintain charge neutrality. The electrons, which support most of the current conduction due to their smaller mass and greater mobility, flow from a negative (polarity) terminal called a cathode and move toward a positive (polarity) terminal called an anode. The establishment of a neutral plasma state by thermal means (i.e., collision processes) requires the attainment of equilibrium temperatures, the magnitude of which depend on the ionization potential (the ease or difficulty of forming positive ions by stripping away electrons) from which the plasma is produced (e.g., air, argon, helium).[5] The formation of plasma is governed by an extended concept of the ideal gas law and law of mass action, and is described in more detail in Section 8.3.

8.2.1.3. Arc Temperature. The temperature of welding arcs has been measured by spectral emission of excited and ionized atoms and normally is in the range of 5000 to 30,000 K, depending on the precise nature of the plasma and current conducted by it. Two important factors that affect the plasma temperature are what precisely constitutes the particular plasma, and its density. For shielded-metal and flux-cored arcs, a high concentration of easily ionized materials such as alkali metals, like sodium and potassium, from flux coatings or cores of the consumable electrodes used with these processes, result in a maximum temperature of about 6000 K. This temperature can be lowered even

[5] Recall that the higher work function or ionization potential of helium results from the tighter bonding of its outermost electrons compared to argon, for example, and, thus, in a hotter arc.

TABLE 8.1 Temperature of the Arc Column for Various Gases

Gas	Temperature (K) of Arc Column Close to Cathode
Alkali-metal vapor	4000
Alkaline-earth vapor	5000
Iron vapor	6000
Argon (200 A)	10,000–15,000

Source: From *Metallurgy of Welding*, 5th ed., by J. F. Lancaster, published in 1993 by Chapman & Hall, London and used with permission of Kluwer Academic Publishers, The Netherlands.

more by the presence of fine particles of molten flux (or slag) as well as molten metal and metal vapor, all of which absorb some heat. For pure inert gas-shielded arcs, such as those found in GTA welding, the central core temperature of the plasma can approach 30,000 K, except as lowered by metal vapor from the nonconsumable electrode and any molten metal particles from any filler used. Temperatures in the arc of the GMAW process would be lower due to the presence of large concentrations of metal ions and vapor and molten droplets. For a process where the plasma is pure and concentrated and there is no metal transfer, as in PAW, plasma core temperatures of 50,000 K could be attained. Table 8.1 gives the temperature of the arc column in various gases. An isothermal diagram of an argon-shielded gas-tungsten arc operating at 200 A is shown in Figure 8.5.

The actual temperature in an arc is limited by heat loss, rather than by any theoretical limit. These losses are discussed in Section 5.5, and include losses due to radiation, convection, conduction, and diffusion.

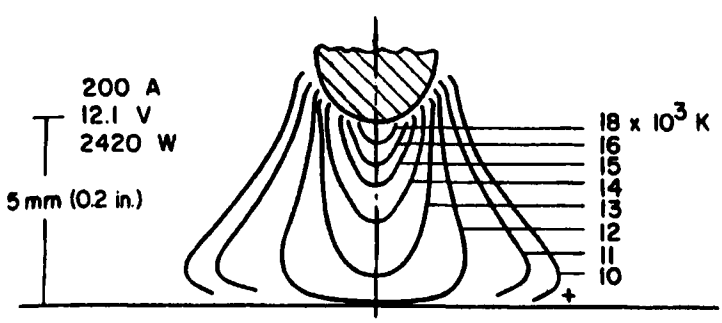


Figure 8.5 Isothermal diagram of an argon-shielded gas–tungsten arc operating at 200 A. (From *Welding Handbook*, Vol. 1: *Welding Technology*, 8th ed., edited by L. P. Connor, published in 1987 by and used with permission of the American Welding Society, Miami, FL.)

8.2.1.4. Arc Radiation. All electric arcs emit radiation, the amount and character of which depends on the atomic mass and chemical composition of the gaseous medium, the temperature, and the pressure. Spectral analysis shows bands due to vibrational and rotational states in molecules (for cellulosic-covered electrodes), as well as line and continuum emissions due to excited and ionized states of atoms and ions. As the energy input to an arc increases, higher states of ionization occur, and higher levels of radiation result.

Radiation from arcs is in the form of ultraviolet, visible, and infrared light. Loss from such radiation is normally about 10% of the total input to the arc, but can be as high as 20% for argon welding arcs. Since the intensity of radiation is high, arcs pose a hazard to operators and observers, even if exposure is only casual, such as reflection from light-colored walls. Ultraviolet radiation is particularly dangerous to the eyes but also can cause sunburn-like damage to exposed skin, while infrared radiation causes burning heat. Operators and observers must thus always employ proper eye and skin protection (see AWS Z49.1-94, *Safety in Welding, Cutting and Allied Processes*).

8.2.1.5. Arc Electrical Features. An electric welding arc is an impedance (related to the resistance of a circuit, but including contributions from capacitance and inductance as well) to the flow of electric current, just as all conductors of electricity are (see Section 8.1). The specific impedance at any point in an arc is inversely proportional to the density of the operative charge carriers and their inherent mobility. The total impedance depends on the radial and axial distribution of carrier density.

All electric arcs consist of three regions or spaces: (1) the cathode fall space (or drop zone); (2) the plasma column fall space (or drop zone); and (3) the anode fall space (or drop zone). These are shown schematically in Figure 8.6a as a plot of arc potential between the welding electrode and workpiece. There are also intermediate regions involved in expanding or contracting the cross section of the gaseous conductor to accommodate each of these main regions. As a consequence, welding arcs assume bell or cone shapes (as also shown in Figure 8.6a), and elliptical or some other noncylindrical contour. Factors that contribute to the particular shape of an arc are (1) shape of the arc terminals (i.e., pointed welding electrode producing a narrow arc focused at the electrode tip and flat workpiece electrode, which causes the arc to spread); (2) gravitational forces; (3) magnetic forces (from both internally generated and externally induced or applied sources); and (4) interactions between the plasma and ambient pressures. While the structure of the arc is always the same, the appearance differs slightly from one process to another, as shown in Figure 8.6b–d.

The area over which the current actually flows into the arc terminals is called *anode* and *cathode spots*. Although far less is understood about these regions than the plasma column, both have strong effects on the overall arc shape, as well as on the flow of heat into these terminals. The current density at the workpiece terminal is of particular importance to the size and shape (especially depth) of the fusion and heat-affected zones produced.

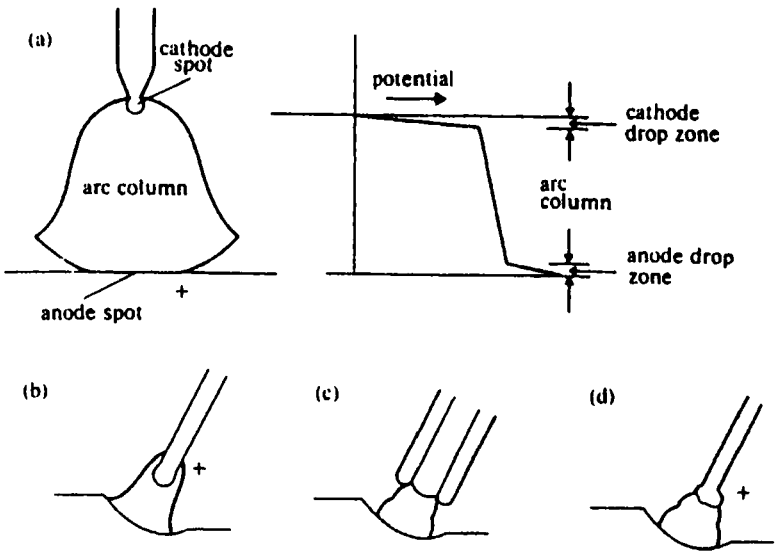


Figure 8.6 General arc appearance and structure, or potential (voltage) distribution between a welding electrode and workpiece (a), and arc appearance for (b) GTA, (c) SMA, and (d) CO_2-shielded GMA welding processes. (From *Metallurgy of Welding*, 5th ed., by J. F. Lancaster, published in 1993 by Chapman & Hall, London, and used with permission of Kluwer Academic Publishers, The Netherlands.).

The impedance of the plasma column is a function of temperature, but this is not so for the impedance in the regions near the arc terminals. The electrical power dissipated in each of the various regions or spaces of the arc is a product of the current flowing and the potential across the region given by

$$P = I(E_a + E_c + E_p) \tag{8.4}$$

where P is power (in watts); E_a is anode voltage, E_c is cathode voltage, and E_p is plasma column voltage (all in volts); and I is current (in amperes).

The total potential of an arc first falls with increasing current, and then rises with further increases in current, as shown in Figure 8.7. The initial increase is attributed to a growth of thermal ionization and thermally induced electron emission at the arc cathode. The total potential of arcs generally increases as the gap (*arc gap*) between the arc terminals (welding electrode and workpiece) increases. Since the arc column continually loses charge carriers to the cooler arc boundary by radial thermal migration, lengthening the arc exposes more of the arc column to cool boundary. This places a greater requirement on maintaining charge carriers, so applied voltage must be increased to offset losses.

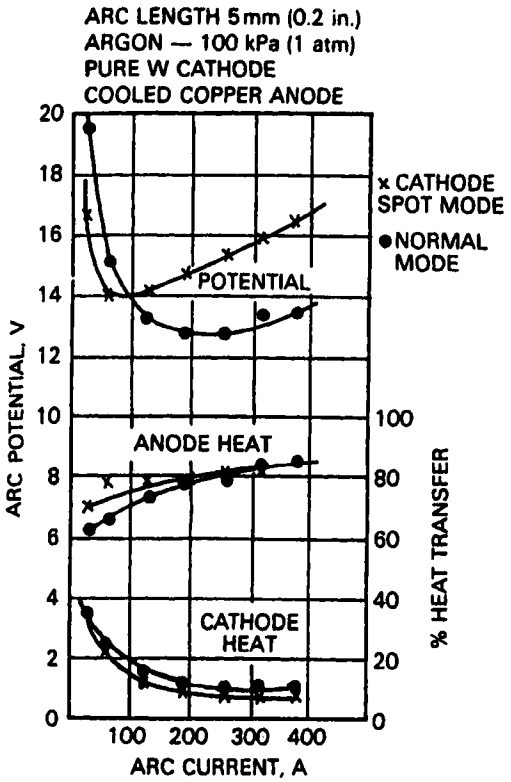


Figure 8.7 Typical volt–ampere and percent heat transfer characteristics of an argon-shielded tungsten arc. (From *Welding Handbook*, Vol. 1: *Welding Technology*, 8th ed., edited by L. P. Connor, published in 1987 by and used with permission of the American Welding Society, Miami, FL.)

8.2.1.6. Effect of Magnetic Fields on Arcs. As stated before, magnetic fields and electric currents in conductors interact (see Section 8.1), and some of this interaction as it pertains to welding arcs is detrimental and some is beneficial. Magnetic fields, regardless of their source (applied or induced), interact with arc current to produce a force that causes the arc to deflect. This phenomenon is known as arc blow when it becomes severe. Arc blow can be more than just annoying, when, under certain conditions, it has a tendency to force the arc away from the point of welding, making it difficult to impossible to make a satisfactory weld.

Arc blow arises from two basic conditions: (1) the change in direction of current flow as it leaves the arc and enters the workpiece to seek ground and (2) the asymmetrical arrangement of magnetic material around the arc. The former is shown schematically in Figure 8.8. The latter, shown schematically in Figure 8.9, arises because it is easier for magnetic flux to pass through certain

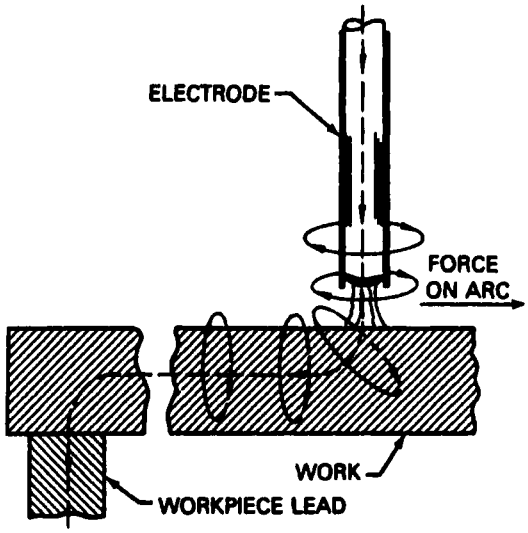
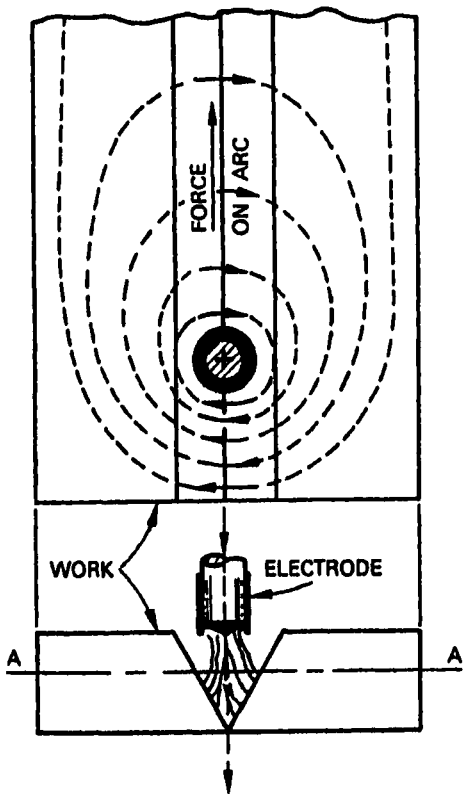


Figure 8.8 Force produced on an arc by the magnetic field induced as current flows to or from the ground location. (From *Welding Handbook*, Vol. 1: *Welding Technology*, 8th ed., edited by L. P. Connor, published in 1987 by and reprinted with permission of the American Welding Society, Miami, FL.)

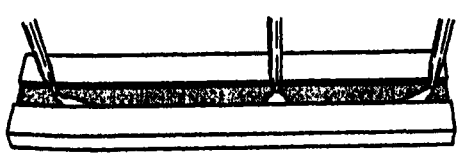
materials (especially ferromagnetic materials) than through air. Problems can be encountered in regions of section-thickness change, hold-down tooling, or the end of a weld as it exits a materials, where, in all cases, the distribution of mass is unbalanced. Arc blow is usually the combined result of both of these effects, so sources of each need to be considered to overcome problems. This means moving ground connections, attempting to balance ferromagnetic material mass distribution around the weld, or switching to AC operation where steady induced fields do not arise.

Other effects of permanent or induced magnetic field interactions with arc current are plasma streaming and some molten metal transfer (discussed in Chapter 9). Magnetic flux can be self-induced as a consequence of an arc current, or it can be produced by residual magnetism, in a workpiece being welded, or by an external source, such as permanent magnets or electromagnetic coils, both of which can be used to intentionally deflect or oscillate arcs or focus electron beams.

The effects of magnetic fields on welding arcs is determined by the Lorentz force, which is proportional to the vector cross-product of the magnetic field (**B**) and the current flow density (**J**), $\mathbf{B} \times \mathbf{J}$. The arc responds to this interaction by deflecting an amount that depends on the force produced and the arc's inherent stiffness. The direction of the Lorentz force (and arc deflection) is determined by *Fleming's left-hand rule*, illustrated in Figure 8.10. Arc deflection from the Lorentz force can promote molten metal transfer (as seen in



(a)



(b)

Figure 8.9 Distortion and imbalance of the induced magnetic field at the edge of a plate of ferromagnetic material (a) and the effect (in the form of "arc blow") on the welding arc (b). (From *Welding Handbook*, Vol. 1: *Welding Technology*, 8th ed., edited by L. P. Connor, published in 1987 by and used with permission of the American Welding Society, Miami, FL.)

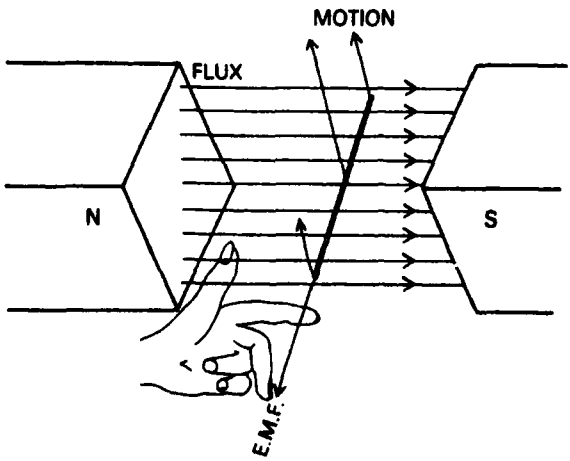


Figure 8.10 Fleming's left-hand rule for determining the Lorentz force and arc deflection. (From *Welding Handbook*, Vol. 1: *Welding Technology*, 8th ed., edited by L. P. Connor, published in 1987 by and used with permission of the American Welding Society, Miami, FL.)

Chapter 9), lead to favorable arc deflection in the direction of welding to improve crown bead appearance, or speed multiple-wire (multiple-arc) submerged arc welding. It can also lead to problems such as arc blow from sideways deflection or heavy undercutting and extensive crown bead reinforcement (mounding up) associated with backward deflection.

8.2.2. Volt–Ampere Characteristics for Welding

Arc welding involves low-voltage, high-current arcs between a permanent (nonconsumable) or consumable electrode and a workpiece. The means for reducing the voltage and simultaneously stepping up the current to conserve the power, EI, from a system (e.g., power-generating utility) may be a transformer, an electric generator, or an alternator driven by a gasoline or diesel engine or an electric motor. Details on such systems but can be found in the *AWS Welding Handbook*, along with information on modern, solid-state power supplies such as solid-state diodes, silicon-controlled rectifiers (SCRs), and thyristors, transistors, and solid-state inverters. What is described here are the volt–ampere characteristics for welding using these various power supplies.

The effectiveness of all arc welding power sources is determined by both static and dynamic characteristics. Static output characteristics are measured under conditions of steady state using conventional test procedures (see Section 8.1). A set of output-voltage versus output-current characteristic curves (*volt–ampere curves*) are used to describe static characteristics. Dynamic characteristics of an arc welding power source are determined by measuring

very short-duration (around 0.001 s) transient variations in output voltage and current that appear in the arc itself.

Transient effects in arc welding arise from several sources associated with the continually changing conditions: (1) during the striking of the arc; (2) during rapid changes in arc length (particularly with manual welding); (3) during the transfer of molten metal across the arc from a consumable electrode to the workpiece (discussed in detail in Chapter 9); and (4) in the case of AC welding, during arc extinction and reignition at each half-cycle. Power supplies must be capable of dealing with these transients and do so by (1) storing energy in parallel capacitors or by DC series inductors; (2) using feedback control in automatically regulating systems; or (3) modifying wave form or circuit operating frequencies.

As for static volt–ampere characteristics, two fundamentally different types of power source are employed, (1) constant-current and (2) constant-voltage, although a third combined-characteristic source is also possible.

8.2.2.1. Constant-Current Power Sources. The typical volt–ampere output curve for a *constant-current* (*CC*) power source is shown in Figure 8.11. Such sources are sometimes called "drooping sources" or "droopers" because of the substantial downward slope or droop of the V-A curves. The effect of the shape of V-A curves on power output is also shown in Figure 8.11, by comparing curve A (which is for an 80-V open-circuit voltage) and curve B (which is for a 50-V open-circuit voltage). In curve A, a steady increase in arc voltage from 20 to 25 V (25%) would result in a relatively small decrease in current from 123 to 115 A (about 6.5%). Thus, for a consumable electrode arc welding process, electrode melting or burn-off rate and metal deposition rate would remain fairly constant with slight changes in arc length. In curve B, a similar arc voltage or length change would produce a significantly greater (about 19%) change in current from 123 to 100 A. This would afford a skilled welder more control over current through arc length manipulation, but would pose more of a problem in current stability for a less-skilled welder.

Current control is used to provide lower output, resulting in V-A curves with greater slope, as illustrated by curves C and D in Figure 8.11. Such curves offer even better constant-current output, and greater tolerance to arc length variations. CC power sources are routinely used for manual SMAW and GTAW.

8.2.2.2. Constant-Voltage Power Sources. The typical V-A curve for a *constant-voltage* (*CV*) power source is shown in Figure 8.12. Like most CV sources, this does not have true constant voltage regardless of current, but exhibits some downward slope as current increases as a consequence of internal electrical impedance in the welding circuit. In fact, changing that impedance, as can be done in some power supplies by inserting a soft iron core farther into a coil (see Section 8.1), will alter the slope of the V-A curves.

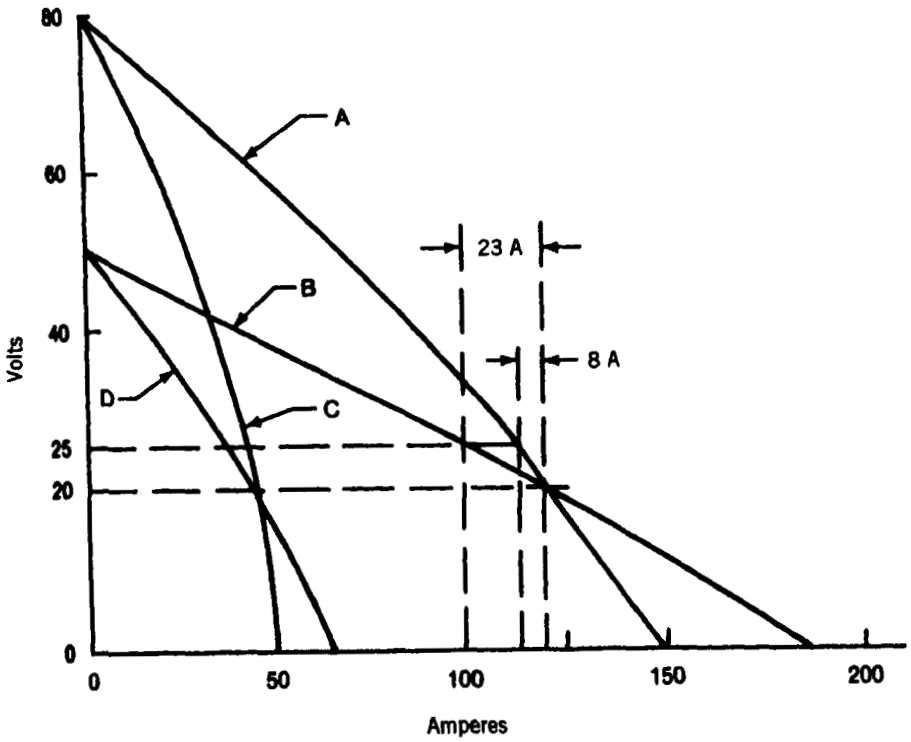


Figure 8.11 Typical volt–ampere characteristics of a "drooping" power source with adjustable open-circuit voltage used to provide near constant current during welding. (From *Welding Handbook*, Vol. 2: *Welding Processes*, 8th ed., edited by R. L. O'Brien, published in 1991 by and used with permission of the American Welding Society, Miami, FL.)

CV power supplies are attractive for constantly fed continuous electrode processes such as GMAW, FCAW, or SAW, to maintain near-constant arc length. A slight change in arc length causes a large change in current, so melting rate changes rapidly in response. This has the effect of self-regulation, increasing the melting rate as arc length is inadvertently shortened, and vice versa.

Short circuiting an electrode with such a power source would drop the arc length and the voltage to zero. This, in turn, would cause the current to rise to very high values very rapidly, with the result of causing the electrode to heat by Joule heating with great rapidity and explosive force, causing severe spatter and, possibly, lengths of unmelted wire stuck in the weld pool. To prevent this from occurring, impedance is built into such power supplies to limit the rate of current change, thereby reducing the likelihood of electrode overheating and explosion, and allowing short-circuiting transfer to take place (see Section 9.3).

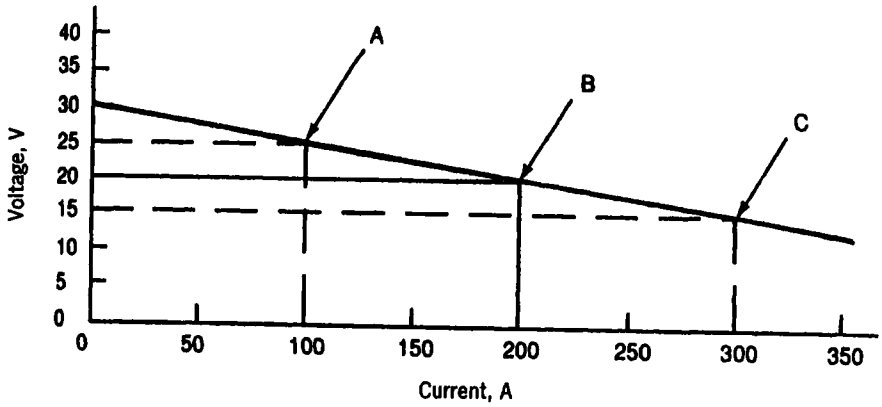


Figure 8.12 Typical volt–ampere output characteristic for a constant-voltage power source. (From *Welding Handbook*, Vol. 2: *Welding Processes*, 8th ed., edited by R. L. O'Brien, published in 1991 by and used with permission of the American Welding Society, Miami, FL.)

8.2.2.3. Combined Characteristic Sources. It is possible, through the use of electronic controls, to develop a single power supply that can provide either constant-voltage or constant-current as wanted. Such power supplies are advantageous in that they have utility for a variety of processes, and are actually a combination of the straight CV or CC types. As shown in Figure 8.13, the higher-voltage portion of the V-A curve is essentially constant current, while below a certain threshold voltage, the curve switches to a constant voltage type. Such a power supply is useful for SMA welding to assist in starting and avoid electrode sticking or stubbing in the weld pool should the welder use to short an arc length.

In other modern power supplies, their V-A characteristic can be manually switched from CV to CC, at will. Two different electronic control circuits are employed in such machines.

8.3. THE PHYSICS OF A PLASMA

As mentioned in Section 8.2.1.2, the formation of a plasma is governed by an extended concept of the ideal gas law and law of mass action. The operative equation is

$$\frac{n_e n_i}{n_0} = \frac{2Z_i(2\pi m_e kT)^{2/3}}{Z_0 h^3 e^{-V_i/kT}} \tag{8.5}$$

where n_e, n_i, and n_0 are the number of electrons, ions, and neutral atoms per

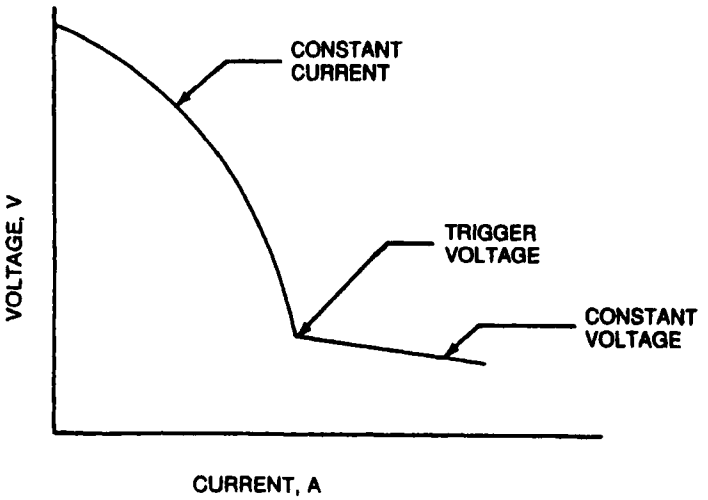


Figure 8.13 Combination V-A curve allowing CC operation at higher voltages and CV operation at lower voltages. (From *Welding Handbook*, Vol. 2: *Welding Processes*, 8th ed., edited by R. L. O'Brien, published in 1991 by and used with permission of the American Welding Society, Miami, FL.)

unit volume (i.e., the particle density), respectively, V_i is the ionization potential of the neutral atom, T is the absolute temperature (K), Z_i and Z_0 are partition functions for ions and neutral particles, h is Planck's constant (6.63×10^{-34} J/s), m_e is the mass of an electron (9.11×10^{-31} kg), and k is Boltzmann's constant (1.38×10^{-23}J/K). The density of the three kinds of particles can be determined from the welding current by assuming the plasma is electrically neutral and that the ions have a single positive charge, so $n_e = n_i$. The density and distribution of argon gas particles and electrons in an argon plasma between 0 and 30,000 K is shown in Figure 8.14.

Thermal equilibrium in an arc or plasma means that temperature is constant in the arc or plasma. This is not precisely true, although it is closely approached in real welding arcs. Effects of dominant energy transport by radiation, convection, conduction, or diffusion cause deviations from ideal, as do differences in degree of ionization from core to fringe or boundary of the arc or plasma.

A final comment about plasmas: The energy density in a plasma is so great (typically exceeding 10^9 W/m^2), and, thus, the temperature is so high (typically, 20,000 to 50,000 K), that not only does a solid material heat very quickly under impingement by a plasma, but it rapidly overheats to exceed the boiling point. This leads to the formation of vapor surrounded by a liquid layer. Pressure of escaping vapor pushes down on the liquid and forces even greater absorption of the energy of the impinging plasma. The end result is the formation of a vapor cavity that penetrates deeply into a material or entirely through a

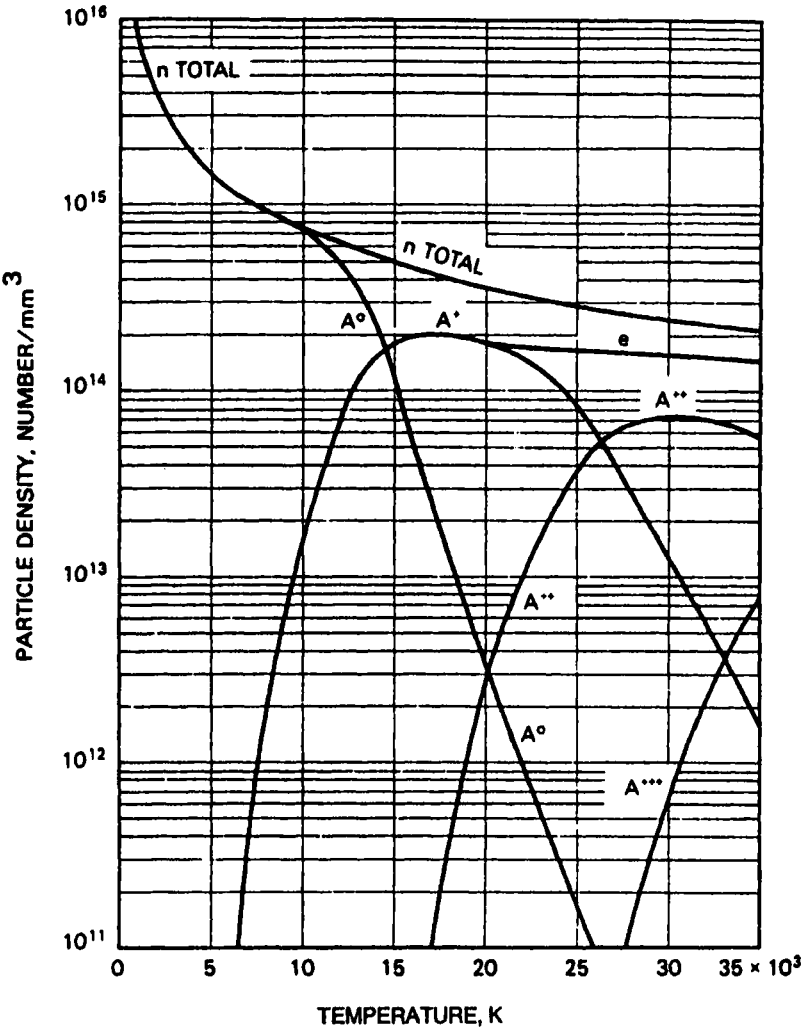


Figure 8.14 Density of various particles found in an argon plasma as a function of temperature for a pressure of 100 kPa (1 atmosphere). (From *Welding Handbook*, Vol. 1: *Welding Technology*, 8th ed., edited by L. P. Connor, published in 1987 by and used with permission of the American Welding Society, Miami, FL.)

material. When this occurs, the heating or energy deposition mode is said to be a *keyhole mode*. Once a vapor keyhole is formed, the superheated vapor cavity moves through the material (along with the energy source) causing further heating, melting, vaporization, and keyhole formation. Behind the vapor "keyhole," molten metal flows backward to close the gap, establish metallic continuity, and produce a weld once solidification takes place. Keyhole formation and movement is shown schematically in Figures 5.6–5.8. As

mentioned earlier, keyholing can occur for PAW and LBW, and almost always occurs for EBW.

8.4. THE PHYSICS OF RESISTANCE (OR JOULE) HEATING AND RESISTANCE WELDING

As described in Section 3.4, it is possible to weld a material by using its internal resistance to the passage of current to cause heating and melting.[6] To do this, the workpieces being joined are made part of the electric circuit, as shown in Figure 3.20. When this is done for a two-ply stack-up of workpieces, the circuit actually consists of a series of resistors representing (1) the upper (copper or copper-alloy) resistance welding electrode; (2) the upper electrode to upper workpiece interface; (3) the upper workpiece; (4) the upper to lower workpiece interface; (5) the lower workpiece; (6) the lower workpiece-to lower (copper or copper-alloy) resistance welding electrode; and (7) the lower electrode. Heating at each location occurs by what is known as Joule heating, and is shown schematically in Figure 8.15.

8.4.1. Joule Heating

The heat generated by passing an electric current through a conductor offering any resistance is referred to as Joule heating, and can be expressed as power (P) resulting from the product of the applied voltage (V) and passing

[6] Actually, internal resistance heating can also be used to cause brazing (in resistance brazing) or nonfusion welding by solid-state diffusion (in resistance diffusion welding).

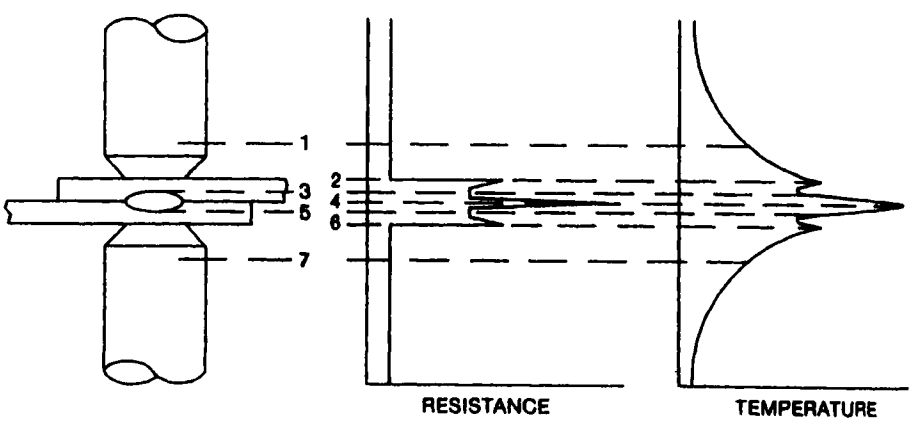


Figure 8.15 Graphs of resistance and temperature, as the result of Joule heating, as a function of location in a typical resistance welding arrangement. (From *Welding Handbook*, Vol. 2: *Welding Processes*, 8th ed., edited by R. L. O'Brien, published in 1991 by and used with permission of the American Welding Society, Miami, FL.)

current (I):

$$P = VI \tag{8.6}$$

By Ohm's law (Section 8.1), $V = IR$ (Eq. 8.1 or 8.2), where R is the resistance of the conducting path. The power dissipated is thus

$$P = I^2R \tag{8.7}$$

and is expressed in joules/second.

Assuming that a mass of material (m) has a current pass through it uniformly (which it rarely does because actual contact is not uniform over the area of contact, but, rather, is concentrated at points of contact between high points or asperities), the temperature rise can be estimated (assuming no losses) by the following steps: First, letting Q be the total heat energy supplied by applying power P (in joules/second) for time t (in seconds),

$$Q = Pt = I^2Rt \tag{8.8}$$

The temperature rise (ΔT) can then be calculated from the value of Q, the mass of the part m, and the heat capacity of the part material C_p:

$$\Delta T = \frac{Q}{mC_p} = \frac{I^2Rt}{mC_p} \tag{8.9}$$

In fact, since the resistance of a material increases with increasing temperature (due to increased scattering of conducting electrons by rapidly vibrating atoms), this computation underestimates the actual temperature rise. Then again, there are losses due to radiation, convection, conduction, and diffusion that offset this effect.

The heating process does not take place completely homogeneously within the interior volume of parts because the electrical path is not continuous. Rather, as just mentioned, real surfaces contain asperities that lead to only relatively few points of contact, across which heating would be very much more intense (see Section 1.4). The consequence of this is that interfacial regions will heat up faster and to generally higher temperatures than the bulk of parts. This is what leads to preferential heating, melting, and weld nugget formation at interfaces, exactly where it's wanted.

In practical resistance welding, heat is generated over a localized area approximated by the footprint of the electrode(s), and the path of current can be considered to be the geometric volume defined by the cross-sectional area of the electrode(s) and a straight path between the electrodes through the workpiece. The resistance in this volume is a function of the cross-sectional area (A) of the path, the length (L) of the path, and the inherent obstacle the

material presents to the current flow, known as resistivity, ρ:

$$R = \frac{\rho L}{A} \tag{8.10}$$

The rate of temperature rise in resistance heating is very rapid, being limited only by the power of the current source in relation to the size of the material volume to be heated, and the heat capacity (C_p) of the material. Rapid heating is advantageous not only because it makes the process more productive (i.e., allows welds to made more quickly), but also because it limits the time for which inherently heat-sensitive materials are exposed to elevated temperatures (see Chapter 16 on heat-affected zones), thus limiting kinetics for reactions or transformations.

8.4.2. The Resistance Welding Cycle

Resistance welding is a pressure fusion welding process, and the welding cycle for spot, seam, and projection resistance welding consists of four stages:

1. *Squeeze Time.* The time interval between timer initiation and the first application of current needed to assure that electrodes contact the work and establish full force.
2. *Weld Time.* The time for which welding current is applied (in single-impulse welding) to the work to make a weld.
3. *Hold Time.* The time during which force is maintained on the work after the last impulse of welding current ends to allow the weld nugget to solidify and develop strength.
4. *Off Time.* The time during which the electrodes are off the work and the work is moved to the next weld location for repetitive welding.

The full cycle or weld schedule is shown in Figure 8.16. This basic cycle can be enhanced to improve the physical and mechanical properties of a weld, as shown in Figure 8.16, where (1) precompression force is used to set electrodes and workpieces together; (2) preheat is applied to reduce thermal gradients at the start of weld time or to soften coatings such as zinc galvanize; (3) forging force is used to help consolidate the weld nugget; (4) quench and temper times are used to produce desired weld properties in hardenable steels; (5) postheat is used to refine weld nugget grain size and improve strength; and (6) current decay is used to retard cooling of aluminum alloys to help prevent cracking. Figure 8.17 also shows multiple-impulse welding, as opposed to single-impulse welding shown in Figure 8.16.

The strength of a weld nugget (shown schematically in Figure 8.18) made during resistance spot welding increases as current is applied for longer times, as the volume of melting and the size of the nugget formed increases

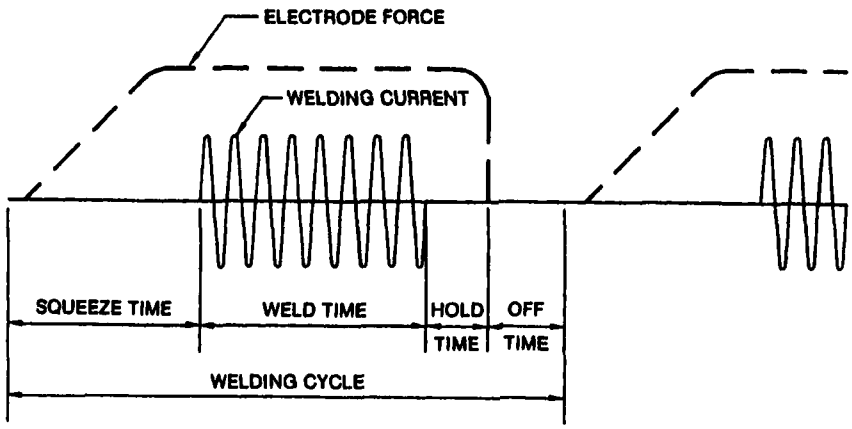


Figure 8.16 Basic single-impulse welding cycle for spot and projection welding. (From *Welding Handbook*, Vol. 2: *Welding Processes*, 8th ed., edited by R. L. O'Brien, published in 1991 by and reprinted with permission of the American Welding Society, Miami, FL.)

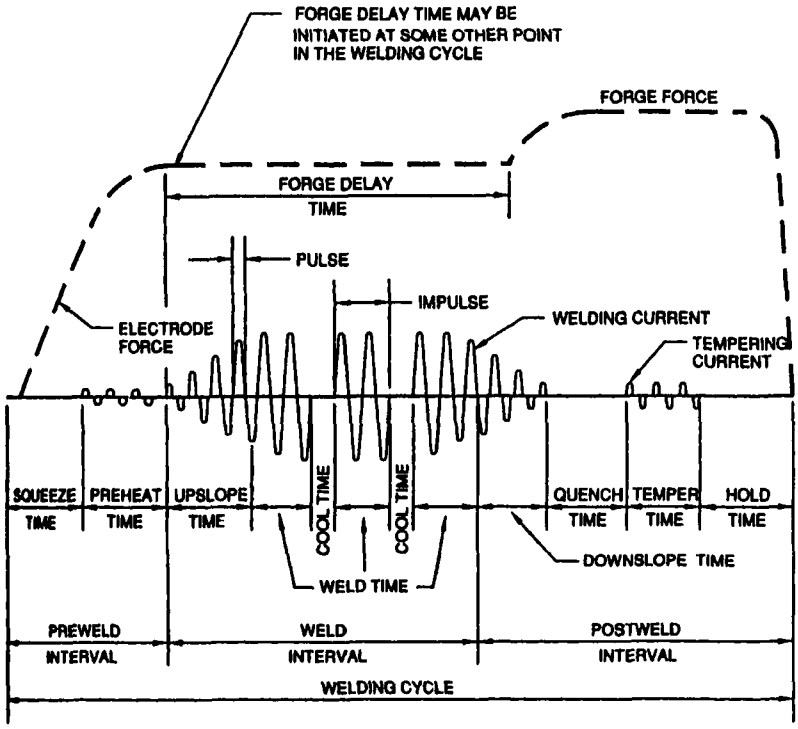


Figure 8.17 Enhanced welding cycle which includes preheat time, upslope time, downslope time, quench time, temper time, and forging time. (From *Welding Handbook*, Vol. 2: *Welding Processes*, 8th ed., edited by R. L. O'Brien, published in 1991 by and used with permission of the American Welding Society, Miami, FL.)

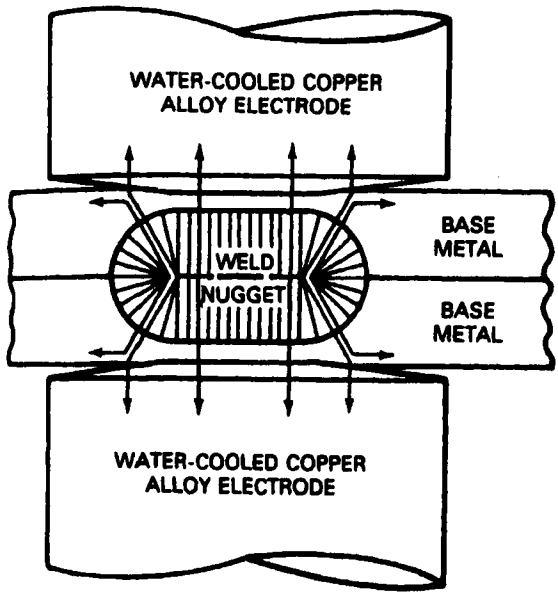


Figure 8.18 Nugget formation and heat dissipation into the surrounding base metal and electrodes during resistance spot welding. (From *Welding Handbook*, Vol. 2: *Welding Processes*, 8th ed., edited by R. L. O'Brien, published in 1991 by and used with permission of the American Welding Society, Miami, FL.)

accordingly. At some point, so much melting has occurred and the volumetric expansion of the molten metal compared to the solid metal from which it was produced becomes so great that the pressure applied by the electrodes cannot contain it. At this point expulsion or "spitting" occurs. When this occurs, molten metal is lost from within the nugget, and the final, solidified weld inevitably contains a void, thereby reducing the strength, perhaps dramatically. For this reason, welding time should be limited to prevent expulsion. This is shown in Figure 8.19.

8.4.3. Resistance Welding Power Supplies

Resistance welding (RW), regardless of the specific process, requires equipment to (1) provide the electric circuit, (2) control current and force, and (3) apply mechanical force. Because of the uniqueness of the process power requirements, it is important to look briefly at the power sources used.

Some resistance welding machines produce single-phase alternating current of the same frequency as the line power (e.g., 60 cps in the United States). These contain a single-phase transformer that provides very high current (1000–100,000 A) at low voltage (typically around 10 V). A typical single-phase AC spot welding circuit is shown in Figure 8.20.

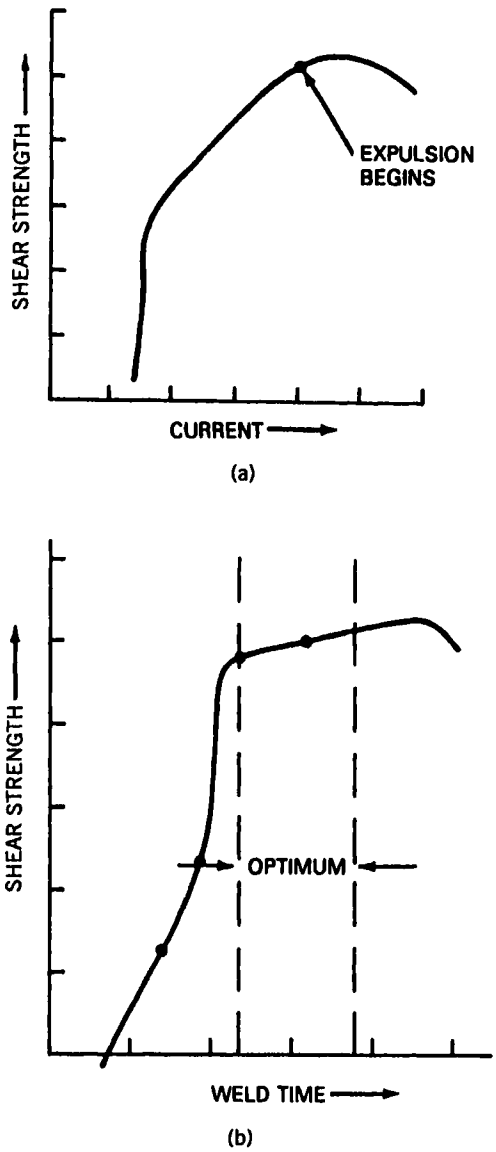


Figure 8.19 Development of weld strength as a function of current (a) and welding time (b). Note that molten metal expulsion from the nugget begins at a certain point, and welding current application should be ceased before this occurs. (From *Welding Handbook*, Vol. 2: *Welding Processes*, 8th ed., edited by R. L. O'Brien, published in 1991 by and us ed with permission of the American Welding Society, Miami, FL.)

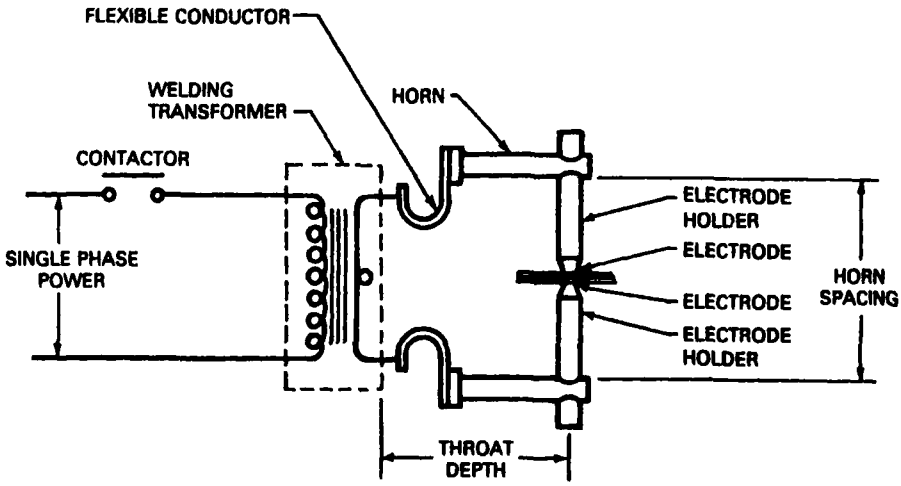


Figure 8.20 Typical single-phase AC spot welding circuit. (From *Welding Handbook*, Vol. 2: *Welding Processes*, 8th ed., edited by R. L. O'Brien, published in 1991 by and used with permission of the American Welding Society, Miami, FL.)

Welding machines can also produce direct current of continuous polarity, pulses of current of alternating polarity, or high-peaked pulses of current (the latter produced by energy stored in capacitor banks in a process called capacitor-discharge welding). Rectifier machines convert AC line power through a welding transformer and rectify that power to DC power. The system can be single-phase, or a three-phase transformer can be used. The latter makes it possible to use balanced three-phase line power. Related frequency converter-type machines use specially designed transformers with three windings, each of which is connected across one of the three phases of incoming power. There are half- and full-wave rectifier types. Examples of some of the electrical arrangements for such machines are shown in Figures 8.21 and 8.22.

8.5. THE PHYSICS OF ELECTRON BEAMS

As described in Section 3.5, there is a group of processes used for fusion welding (as well as cutting, drilling, machining, and surface texturing, heat treating, and alloying) that use the kinetic energy of particles in a high-intensity radiant beam to cause heating and, possibly, melting and vaporization as well. The two best-known examples of the *high-energy beam* (or *power-beam*) *welding processes* are electron-beam welding (EBW) and laser-beam welding (LBW). What may come as a surprise is that such high kinetic energy for conversion

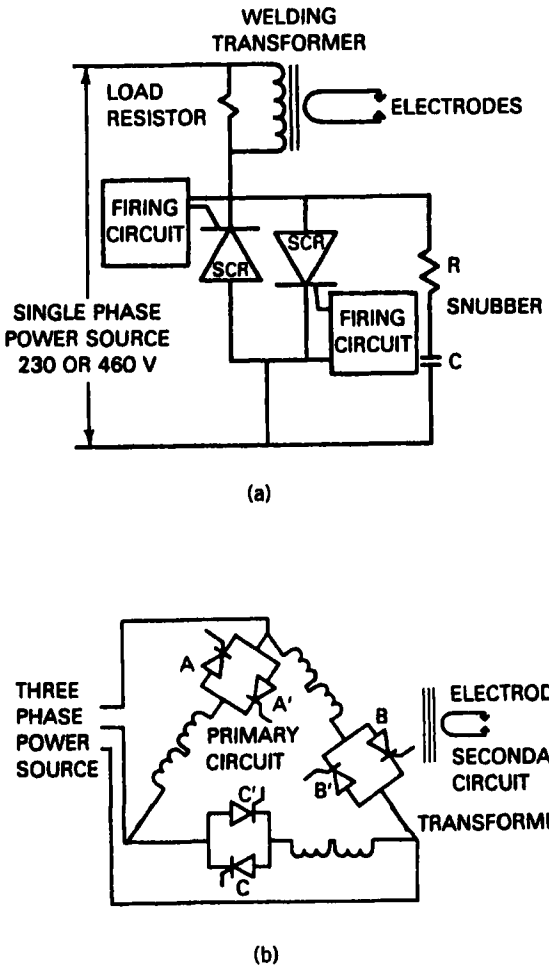
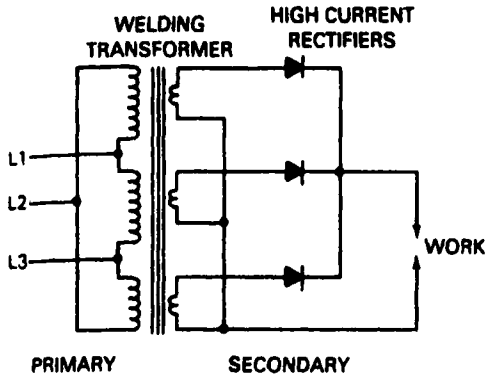
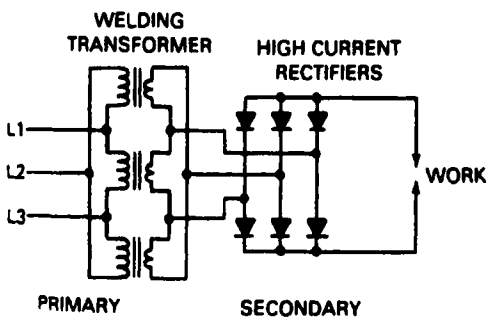


Figure 8.21 Schematic electrical arrangements of (a) single-phase and (b) three-phase frequency converter-type resistance welding machines with SCR contactors. (From *Welding Handbook*, Vol. 2: *Welding Processes*, 8th ed., edited by R. L. O'Brien, published in 1991 by and used with permission of the American Welding Society, Miami, FL.)

to such intense heating can be obtained from one of the lightest particles present in matter (an electron, with a mass of 9.1×10^{-31} kg) and a particle considered to be without mass (a photon). The answer lies in the speed to which an electron can be accelerated and at which a photon always travels (the speed of light). To understand how electrons and photons can produce welds, let's look at the physics of these two processes: electrons here, and photons in Section 8.6.



(A) HALF-WAVE RECTIFIER



(B) FULL-WAVE RECTIFIER

Figure 8.22 Schematic electrical arrangements for three-phase (a) half-wave and (b) full-wave DC rectifier-type resistance welding machines. (From *Welding Handbook*, Vol. 2: *Welding Processes*, 8th ed., edited by R. L. O'Brien, published in 1991 by and used with permission of the American Welding Society, Miami, FL.)

8.5.1. Electron-Beam Generation

The key to a beam of electrons being able to attain a kinetic energy high enough to cause melting and even vaporization in even the highest melting-point materials known (e.g., tungsten, 3390°C [6130°F], or carbon, 4730°C [8550°F], or several refractory carbides, nitrides, silicides, etc.), despite their small mass, lies in their electrical charge (-1.6×10^{-19} coulombs). This charge allows electrons to be accelerated by an electric field to phenomenally high velocities and, thus, kinetic energy levels. The relationship between the speed obtained and the accelerating voltage is shown in Figure 8.23. This speed, in fact, has two beneficial effects: the first directly on the kinetic energy, which is

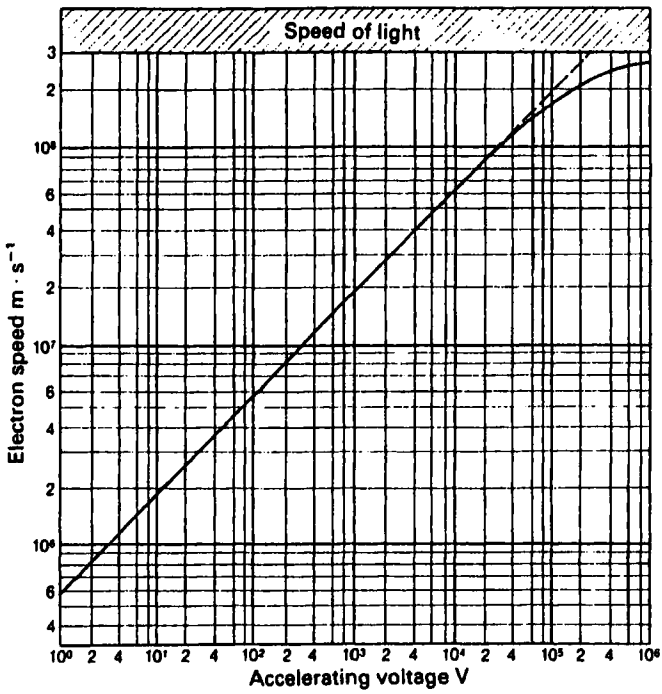


Figure 8.23 Relationship between the speed of an electron and the accelerating voltage. (From *Electron Beam Welding* by H. Schultz, published in English in 1993 by and used with permission of Abington Press, Woodhead Publishing, Cambridge, UK.)

given by $\frac{1}{2}m_e v^2$ (where m_e is the mass of an electron and v is its velocity); the second being the relative mass increase when their (or any object's) speed approaches the speed of light, c. For a fairly typical accelerating voltage of 150 kV in a reasonable vacuum (to preclude or minimize collisions with gas molecules that will cause loss of energy), electrons reach a speed of 2×10^8 m/s, two-thirds the speed of light (3×10^8 m/s). At this speed, the electrons have a relativistic mass increase of 35%.

To obtain electrons to accelerate and focus to produce a beam, they must be extracted by thermionic emission (so-called conduction electrons, being stripped from the loosely bound outer shells of atoms in a metal using thermal activation or heating). In practice, electrons are obtained by thermionic emission from cathodes, which, for electron-beam process sources, are normally either directly resistance- or Joule-heated thin metal strips (called strip cathodes), or indirectly heated by the impingement of electrons emitted from an auxiliary cathode (often called a bolt cathode for its shape). The objective in both cases is to obtain lots of electrons but without degrading the source too rapidly. (In fact, in an electron-beam gun, the only part to routinely wear out is the cathode, which is thus designed to be easily replaced.) Wear

degradation is minimized by proper material selection and shaping. According to Richardson's rule, thermionic emission of electrons rises exponentially to some limit (for the material) with increasing temperature. Thus, the material of choice for a cathode is inevitably a high-melting one, often with a relatively low ionization potential or work function either inherently or by alloying. Two prominent cathode materials are tantalum and tungsten alloyed with some rhenium.

Once electrons are obtained from a cathode by thermionic emission, the cathode develops a positive charge, so, unless something is done, the electrons collect near the cathode to form a cloud. To accelerate the electrons away from the cathode, a negative voltage is applied to the cathode and an annular anode at either earth potential (ground) or at some positive potential is mounted above or below the cloud (depending on one's perspective). This is shown schematically in Figure 8.24. The field between the cathode and the anode

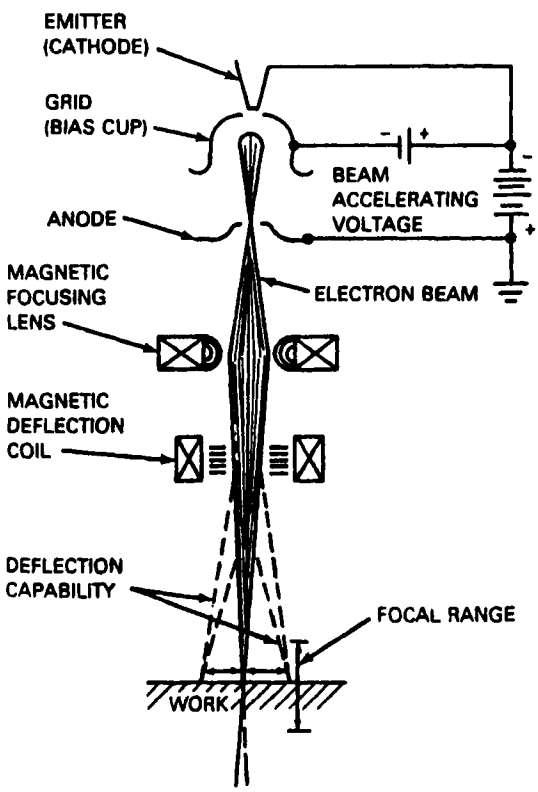


Figure 8.24 Schematic diagram of triode electron-beam generator system or gun. (From *Welding Handbook*, Vol. 2: *Welding Processes*, 8th ed., edited by R. L. O'Brien, published in 1991 by and used with permission of the American Welding Society, Miami, FL.)

accelerates electrons in the direction of the anode and by an amount that depends on the difference in potential. For very high accelerating voltages, a series of annular anodes is often used (i.e., cascading anodes) with acceleration boosts occurring between each subsequent pair. The accelerated electrons pass through the annular anode at constant velocity, with new electrons being supplied by the cathode. The result is a continuous beam of high-velocity, high-energy electrons. Once they strike the workpiece and give up their kinetic energy, electrons flow in a closed circuit from the workpiece, through the machine and earth connection, back to the high-voltage generator.

8.5.2. Electron Beam Control

While a cathode and an anode represent the simplest form of an electron-beam generator (known as a Pierce diode system), most systems employ an additional electrode for controlling beam current. Without such an electrode, beam current could be controlled only by changing either the accelerating voltage or the temperature of the cathode (i.e., the cathode or filament current). The typical control electrode, which creates a triode system, is commonly known as a Wehnelt cylinder. The actual annular control electrode is at the cathode's potential but can have a higher (more) negative voltage superimposed on it from a separate power supply. Once at higher negative potential, it repels electrons coming from the cathode back toward the cathode, in spite of the potential difference between the cathode and the anode(s). Varying this more negative potential in the control electrode causes the size of the emitting surface on the cathode to vary as shown in Figure 8.25. Adjustment of the beam current is thus possible by adjustment of the control electrode voltage.

There is a limit to how low the control voltage can be adjusted, because at some point the emitting surface expands to and around the edges of the face of the cathode (Figure 8.25d). This leads to severe beam divergence and distortion, which detract from beam effectiveness. The low-end limit on control voltage is the point at which a rotationally symmetrical electron beam is still just preserved.

The shape of the electron beam from a triode system is shown in Figure 8.26. Necking occurs just beneath the cathode's emitting face. The point of necking is called the point of real crossover. Once the beam of electrons passes through the anode(s) and into a region free of electrical fields, its shape remains constant until it is acted upon by a focusing lens. A point of intersection with the beam axis known as the point of virtual crossover is obtained by extending the tangents to the beam envelop backward beyond the cathode. This point has special significance in electron beam optics, as do imaginary focal points in regular optics. Figure 8.27 shows the situation schematically.

The electron field in the triode system shapes the beam to an initial focus, the crossover point, from which electrons then move through the anode(s) and diverge. This divergent beam does not have sufficient power density to produce welds. To do so, it must be refocused. This is accomplished using one or more

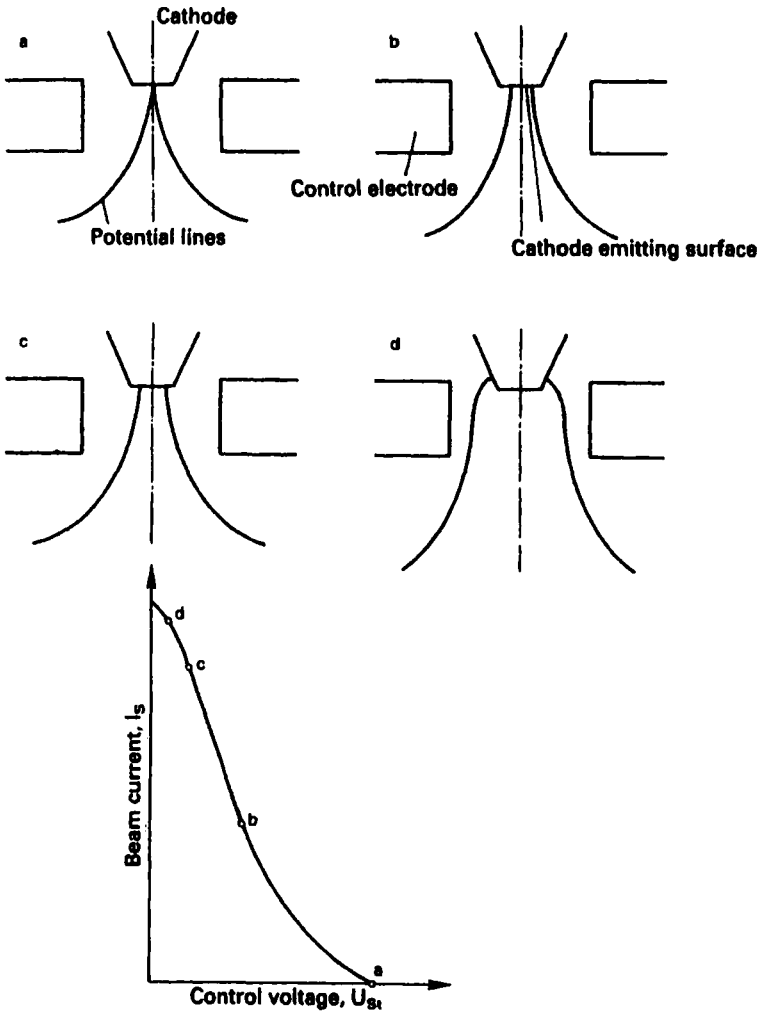


Figure 8.25 Schematic of the changes in the lines of potential as a result of an applied control (electrode) voltage to cause (a) blocking of beam current; (b) low beam current, I_s; (c) high beam current, I_s; and (d) (optical) distortion of the electron beam because of inadequate control voltage. (From *Electron Beam Welding* by H. Schultz, published in English in 1993 by and used with permission of Abington Press, Cambridge, UK.)

annular coils to influence the movement of the negatively charged electrons (current) by application of magnetic fields. A direct current in the windings of a magnetic coil (such as shown schematically in Figure 8.28) produces a magnetic field that acts inward from the coil focusing the beam of electrons.

Once electrons leave the magnetic lenses, without any change in velocity, they descend in a slightly curved, spiral path to meet at a focal point. The

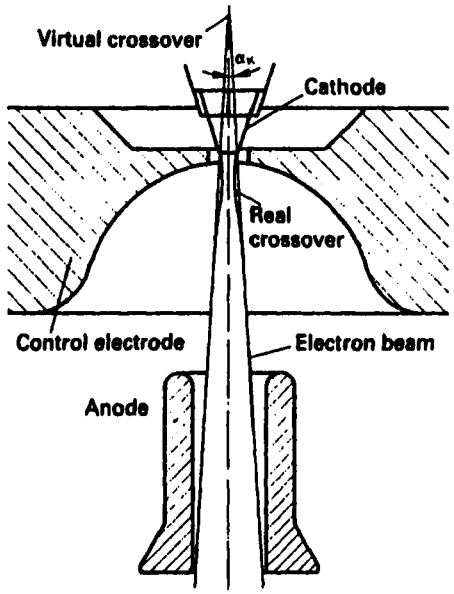


Figure 8.26 Schematic of the beam geometry in a triode system. (From *Electron Beam Welding* by H. Schultz, published in English in 1993 by and used with permission of Abington Press, Woodhead Publishing, Cambridge, UK.)

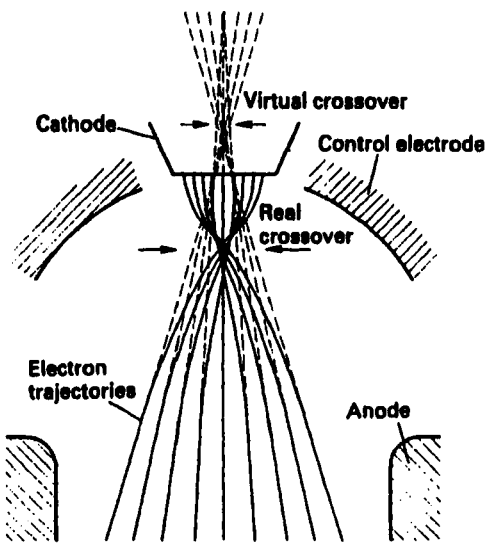


Figure 8.27 Schematic showing the trajectories of electrons that can lead to the occurrence of real and virtual crossovers. (From *Electron Beam Welding* by H. Schultz, published in English in 1993 by and used with permission of Abington Press, Woodhead Publishing, Cambridge, UK.)

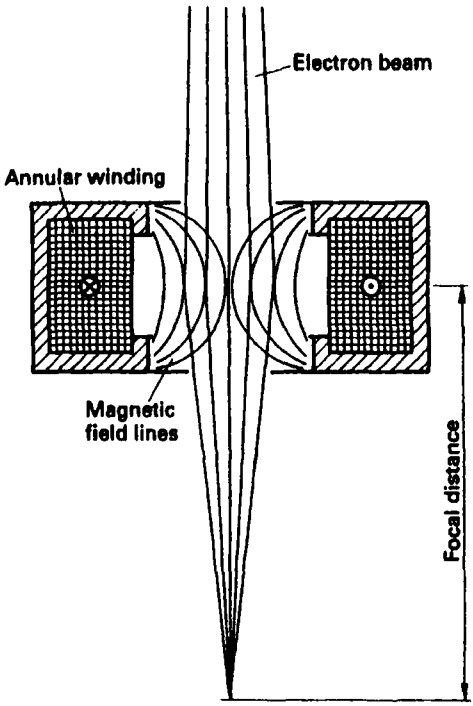


Figure 8.28 Schematic of an electromagnetic lens for focusing an electron beam. (From *Electron Beam Welding* by H. Schultz, published in English in 1993 by and used with permission of Abington Press, Woodhead Publishing, Cambridge, UK.)

diameter of this focal point is typically 0.1–1.0 mm, depending on the type of beam gun (larger-diameter, relatively high current, 100–1000 mA, lower voltage, 25–50 kV, range, typified by guns by Sciaky, or smaller-diameter, relatively low current less than 100–200 mA, higher voltage, 100–250 kV, range, typified by guns by Leybold-Heraeus), the beam power, and the focal distance. Under most circumstances, the focal point is placed at the surface of the workpiece, but can be adjusted slightly above or below the surface to achieve different effects on the weld profile and, especially, the weld bead contour. Additionally, magnetic lenses can be used to achieve additional corrections in the beam's optics, especially energy-density distribution for different purposes (e.g., surface heat treating versus welding versus drilling).

The final control of an electron beam is obtained from a deflection system. Again, an arrangement of electromagnetic coils is used (such as shown schematically in Figure 8.29). Deflection is used for several purposes, including (1) to correct unwanted beam deflection from induced magnetic fields and Lorentz forces from unbalanced ferromagnetic mass in workpieces or tooling,

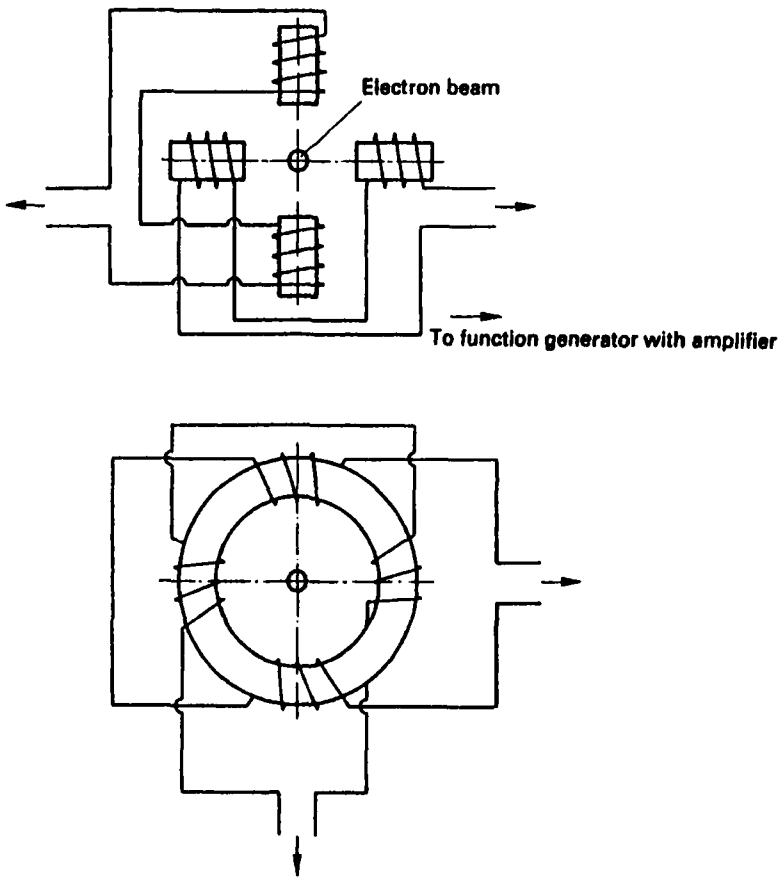


Figure 8.29 Typical beam deflection system consisting of main field coils (top) and subsidiary field coils (bottom). (From *Electron Beam Welding* by H. Schultz, published in English in 1993 by and used with permission of Abington Press, Cambridge, UK.)

and (2) to produce transverse, longitudinal, or rotational oscillation to affect weld substructure through convection and other effects.

An overall schematic of a typical electron-beam gun for welding was shown earlier in Figure 8.24.

8.5.3. Role of Vacuum in EB Welding

Since electrons interact with atoms, obtaining high-energy beams of electrons requires us to minimize such unwanted interactions by generating the beam and performing welding in a vacuum. The vacuum in the gun and welding chamber (shown schematically in Figure 8.30) plays three key roles: First, it excludes oxygen from contact with the cathode to prevent damage by oxida-

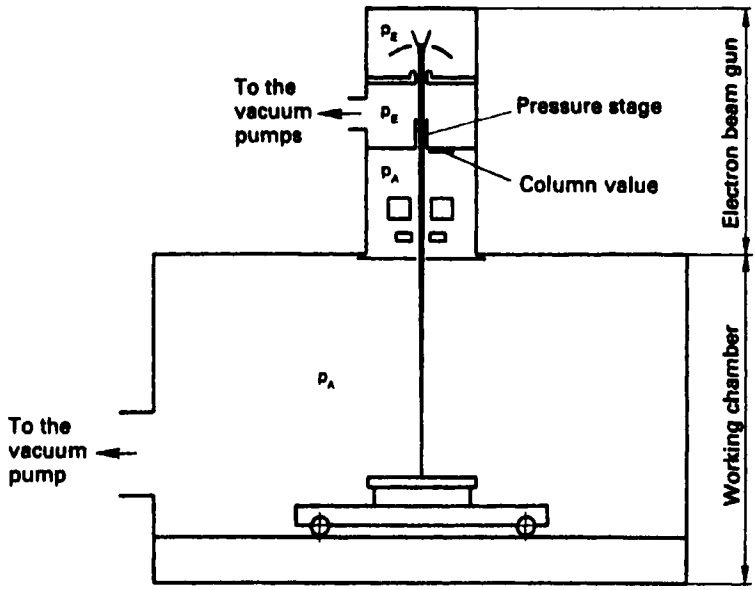


Figure 8.30 An electron-beam gun and working chamber incorporating pressure stages and column valve; with pressure p_E in the beam generator being two to three orders of magnitude lower than pressure p_A in the working chamber up to the pressure stage. (From *Electron Beam Welding* by H. Schultz, published in English in 1993 by and used with permission of Abington Press, Cambridge, UK.)

tion at high operating temperatures. Second, it minimizes collisions between electrons and heavy molecules in air to minimize scattering loss of energy. Third, it provides electrical insulation to high fields between cathode and anode and control electrode.

The highest acceptable pressure within the electron gun is 10^{-4} mbar (10^{-6} to 10^{-7} atm). Pressure in the working chamber can be one to three orders of magnitude greater, in which case the beam is directed through a pressure stage, as shown in Figure 8.30. The effect of operating pressure on material penetration by a beam of electrons (normalized for power) is shown in Figure 8.31.

8.5.4. Electron-Beam–Material Interactions

Understanding what happens when a beam of high-energy electrons strike and penetrate a metal is both one of the most important and one of the most difficult aspects of the physics of electron-beam welding. While the physical mechanisms are known in principle, the individual processes taking place are so complex they are not yet able to be quantitatively defined. One reason for this lack of precise understanding is the difficulty of observing the beam–material interaction process. Techniques like welding with contrasting ma-

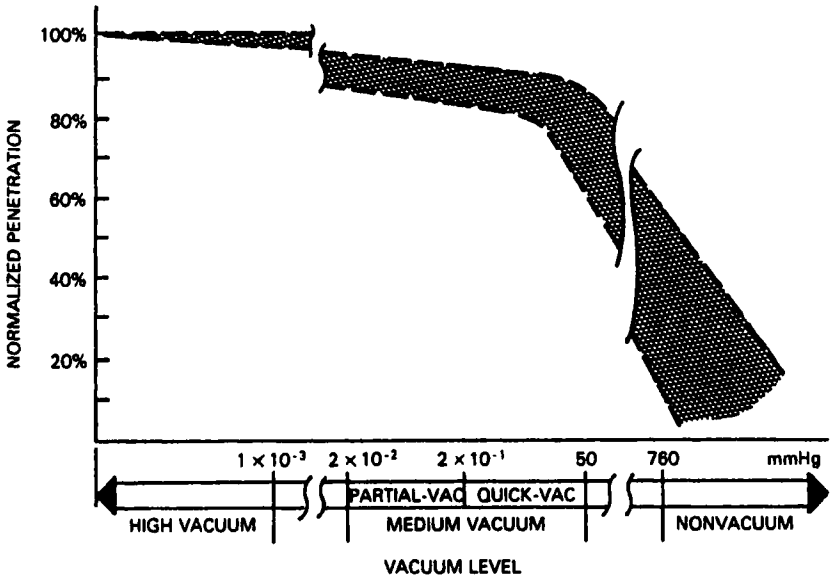


Figure 8.31 Electron-beam penetration as a function of operating pressure. (From *Welding Handbook*, Vol. 2: *Welding Processes*, 8th ed., edited by R. L. O'Brien, published in 1991 by and used with permission of the American Welding Society, Miami, FL.)

terials, real-time radiography, and measuring frequency of penetrating currents help, but are not completely adequate. This notwithstanding, let's look at the processes that occur.

When high-velocity electrons in a focused beam strike the surface of a workpiece, they transfer their kinetic energy to that workpiece in the form of heat. Progressive warming of a solid metal results in a progressive increase in the vibrational energy (frequency and amplitude) of atoms in the metal's crystal lattice. Because of their small mass, incoming electrons likely transfer their kinetic energy to electrons in the outermost shells and to free conduction electrons, rather than to much heavier nuclei. This step is followed by transfer of energy as excited conduction electrons pass energy to the lattice as lattice phonons. The observable result is that the temperature of the metal increases rapidly. When the rate of energy input greatly exceeds the rate of dissipation or loss by radiation, convection, or conduction to surroundings, given sufficiently high power density in the beam, temperature soon exceeds not only the point of melting, but also the point of boiling. In this resulting liquid and vapor, energy transfer continues even though there is no longer a lattice structure.

Not all electrons impinging on the workpiece transfer their kinetic energy to the lattice as heat. There are several other means by which energy is lost, including (1) elastic reflection of primary electrons, (2) ejection of secondary electrons; and other means shown in Figure 8.32.

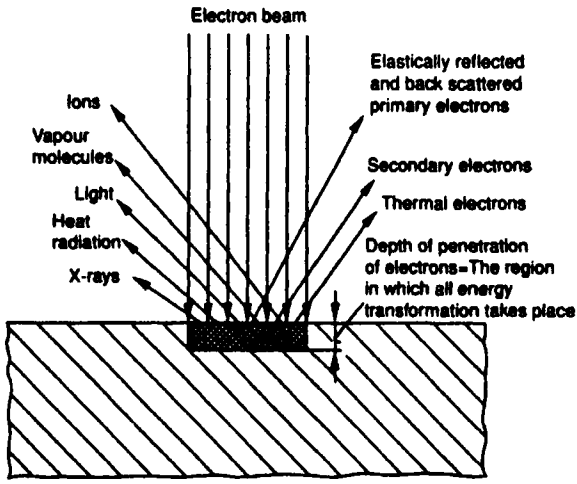


Figure 8.32 Processes occurring when a high-energy-density electron beam interacts with the surface of a metallic workpiece. (From *Electron Beam Welding* by H. Schultz, published in English in 1993 by and used with permission of Abington Press, Woodhead Publishing, Cambridge, UK.)

Once melting and vaporization begin, the process of keyholing (described in Section 5.8) occurs. In brief, pressure of vaporizing metal atoms forces liquid surrounding the vapor downward. Transfer of energy from incoming electrons tends to become more efficient as reflected primary electrons remain in the confines of the vapor cavity, as do secondary electrons from any of several sources. The result is rapid propagation of the vapor cavity into or through the workpiece to cause very deep penetration, especially relative to cavity or weld width or diameter. Figure 8.33 shows the rapid sequence of steps schematically.

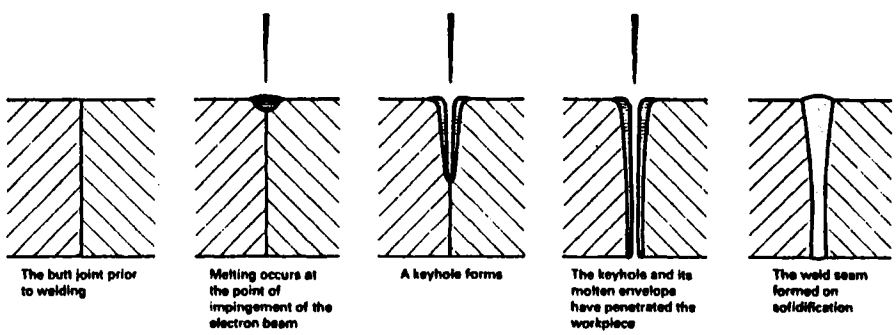


Figure 8.33 The rapid sequence of steps in the interaction between a beam of high-energy-density electrons and a material that leads to the formation of a keyhole. (From *Electron Beam Welding* by H. Schultz, published in English in 1993 by and used with permission of Abington Press, Woodhead Publishing, Cambridge, UK.)

How a vapor cavity surrounded by a concentric column of liquid metal moves through a material to produce a weld is very complex. Molten metal can occasionally drop back into the cavity to interfere with the incoming electrons, leading to intermittent loss of penetration. This phenomenon can be seen from the ragged, erratic penetration associated with some partial-penetration EB welds. If the keyholing process is stabilized, as it can be by suitable placement of the focal point relative to the surface, the depth of penetration remains quite constant and regular. More is said about keyhole formation and movement in the next section on laser beam interaction with materials.

8.6. THE PHYSICS OF LASER BEAMS

Light is a form of electromagnetic radiation or energy. It can be considered as either an energy wave or moving particles with quantized energy values. In fact, it is both at the same time as a consequence of wave–particle duality in physics. As waves, light exhibits different wavelengths, ranging from a minimum of about 5×10^{-9} to 4×10^{-7} m (0.005–0.4 μm) for light in the ultraviolet (UV) region of the spectrum, through 4×10^{-7} to 7×10^{-7} m (0.4–0.7 μm) for light in the visible region of the spectrum, to a maximum of 8×10^{-7} to 8×10^{-4} m (0.8 to 80 μm) for light in the infrared region of the spectrum. The shorter the wavelength (λ), the higher the frequency of the electromagnetic (light) wave (ν), as given by Planck's law that $\lambda = h\nu$, where h is Planck's constant ($= 6.63 \times 10^{-34}$ J/s). Regardless of its wavelength or frequency, or, for that matter, whether light is considered as a wave or particles, it moves at a constant velocity of 300,000 m/s, known as c. The speed of light, c, is, in fact, the upper limit at which anything can travel, according to Einstein's theory of relativity.

The ability of light of different wavelengths to give up energy in the form of heat when absorbed by different substances is the basis for using it to weld in so-called *high-intensity radiant-energy welding processes.* Of particular interest is the use of a special form of light called *laser light.*

8.6.1. Laser Light

Laser light is electromagnetic energy generally within the spectral frequency/wavelength range of normal light, but consists of almost parallel (collimated), single wavelength (monochromatic) light rays that are all in phase (coherent). This is shown in Figure 8.34, which compares normal light with laser light schematically.

8.6.2. Laser Generation

Laser light is produced from a special source known as a laser, which is an acronym standing for light (L) amplification (A) stimulated (S) by emission (E)

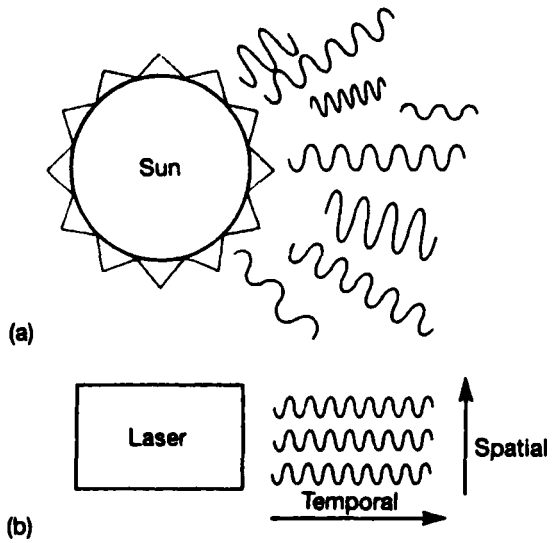


Figure 8.34 Coherent laser light (b) versus incoherent normal light (a). The random light waves from the sun, for example, are incoherent because they cannot achieve temporal and spatial symmetry. (From *Laser Welding* by C. Dawes, published in 1992 by and used with permission of McGraw Hill, Abington Publishing, Woodhead Publishing, Cambridge, UK.)

of radiation (R), referring to the way in which it is generated. Lasers are optical amplifiers that pump or excite an active medium between two mirrors, one of which is partially transparent to allow the laser light to exit the source, as shown in Figure 8.35. The active medium consists of specially selected atoms, molecules, or ions, which can be in the form of a gas, liquid, or solid. All have the common characteristic of emitting energy in the form of photons or light after being excited by a pumping source and then falling back to the normal, unexcited, ground state. Liquid and solid lasing sources are excited by normal

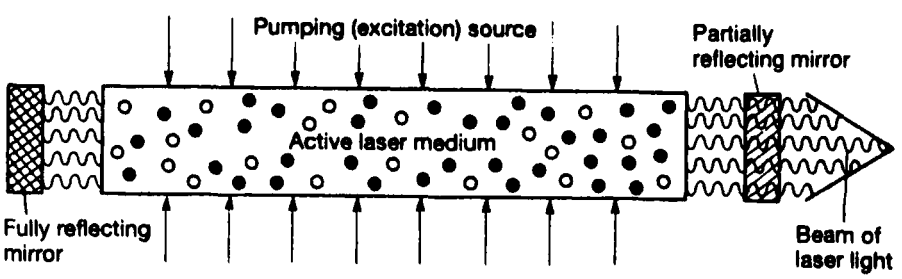


Figure 8.35 The basic elements of a laser. (From *Laser Welding* by C. Dawes, published in 1992 by and used with permission of McGraw Hill/Abington Publishing, Woodhead Publishing, Cambridge, UK.)

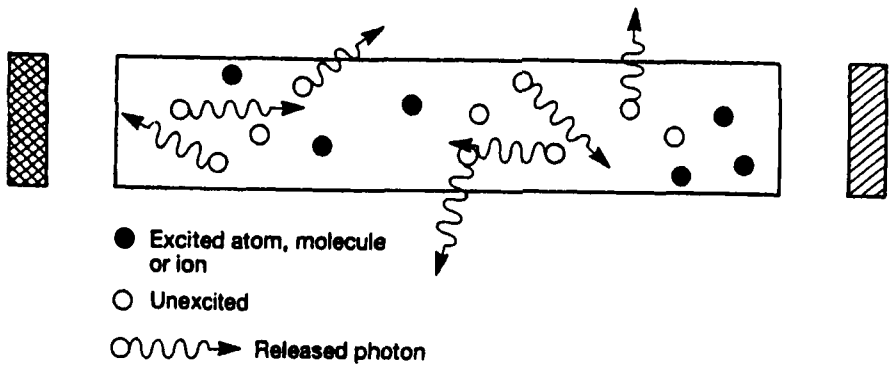


Figure 8.36 Spontaneous emission of photons from an excited active medium. Billions of excited atoms, molecules, or ions release their photons in all directions when they fall back to the ground states. (From *Laser Welding* by C. Dawes, published in 1992 by and used with permission of McGraw Hill/Abington Publishing, Woodhead Publishing, Cambridge, UK.)

light from an intense flash source, while gas lasing sources are excited by electrical discharges.

Atoms, molecules, or ions in the lasing medium absorb energy from the exciting source when pumped, and hold it for a very short and random time period. When they give up this excitation energy in the form of a photon, they return to their former normal, unexcited, ground state to be pumped (or excited) again. Such release is called *spontaneous emission*, with the released photons traveling in all directions relative to the optical axis of the laser (as shown in Figure 8.36). If, instead, photons collide with other excited atoms, molecules, or ions, they cause them to release their photon(s) prematurely. These photons then travel together in phase to cause further collisions, and the process continues. This action is called *stimulated emission*. Photons that do not travel parallel to the laser axis are generally lost from the system and process, while those that do travel parallel to the laser axis have their optical paths extended by repeated reflection (feedback) by the mirrors at each end of the laser source, before leaving through the partially transparent mirror. This action, shown schematically in Figure 8.37, amplifies photon generation by stimulated emission to achieve the required power level and collimate the resulting coherent laser light beam.

The two predominant types of lasers used for welding are (1) Nd:YAG solid-state lasers and (2) CO_2 gas lasers.

8.6.2.1. Nd:YAG Lasers. Nd:YAG (neodymium: yttrium–aluminum–garnet) solid-state lasers produce laser light with a wavelength of 1.06 μm, and are available with output powers ranging from approximately 100 W to over 3 kW. Although the average power of Nd:YAG solid-state lasers compared to CO_2 gas lasers is low, they can achieve very short-duration pulses with peaks of

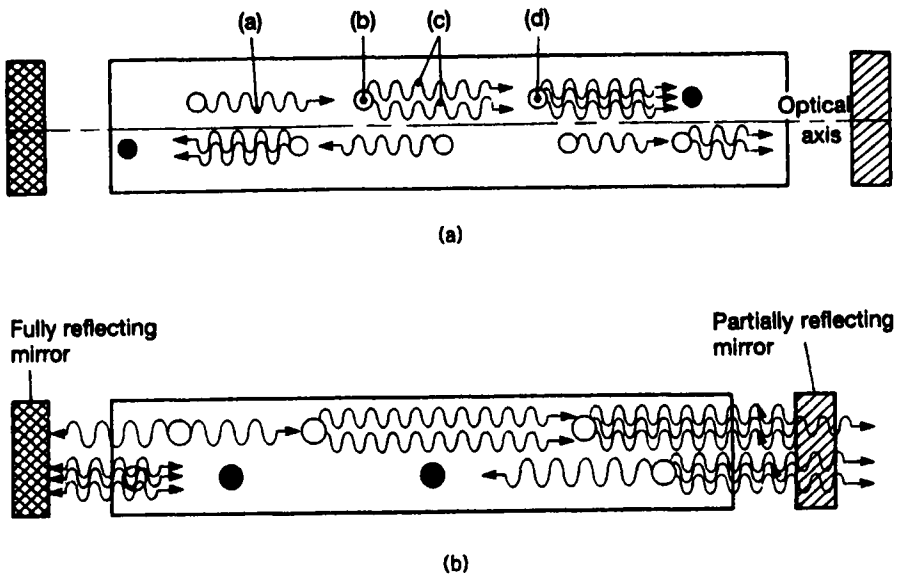


Figure 8.37 Stimulated emission of photons (a) and optical feedback of photons by mirrors to increase the path length for stimulated emission and thus amplify the laser power (b). (From *Laser Welding* by C. Dawes, published in 1992 by and used with permission of McGraw Hill/Abington Publishing, Woodhead Publishing, Cambridge, UK.)

10 kW. A 1-kW Nd:YAG laser machine (such as that shown schematically in Figure 8.38) could easily butt weld 4-mm-thick steel at 0.3 m/min. The greatest advantage of Nd:YAG lasers is that, because of the wavelength of laser light produced, energy can be transmitted through a fiber optic cable, thereby greatly simplifying control.

8.6.2.2. CO_2 Lasers. CO_2 gas lasers produce laser light with a wavelength of 10.6 μm, and are available with output powers of 0.5 to 25 kw. Examples of these machines are shown schematically in Figures 8.39 and 8.40. The higher energy range (say, 5–10 kW) of these lasers (compared to Nd:YAG lasers) allows continuous welding of steel 7–15 mm thick at speeds of 1 m/min, respectively.

The reader interested in knowing more about these and other lasers is referred to excellent sources by Koechner (1996) or Duley (1992).

8.6.3. Laser-Beam Control

Control in laser beams means two things: (1) Keeping the power density across the diameter of the laser output beam uniform, if that what is needed and wanted, or to have some special form for purposes like cutting or drilling, as opposed to welding; and (2) directing the laser light to the workpiece from the

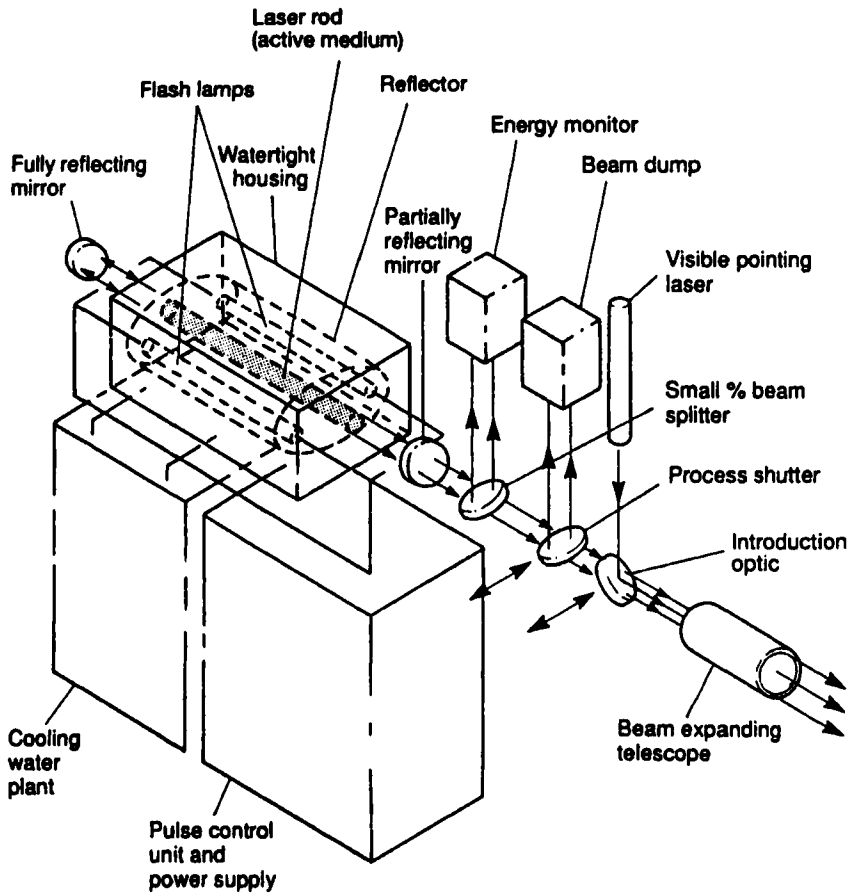


Figure 8.38 Schematic layout of an Nd:YAG solid-state laser. (From *Laser Welding* by C. Dawes, published in 1992 by and used with permission of McGraw Hill/Abington Publishing, Woodhead Publishing, Cambridge, UK.)

laser generator. The former is achieved by source design. The latter involves the use of special mirrors, mirror-guide tubes, and lenses (for CO_2), and fiber-optic cables and fiber-optic couplings (for Nd:YAG).

The reader interested in knowing more about the control of lasers is referred to the excellent works of Koechner (1996) or Duley (1992), as well as the reference by Schultz (1993).

8.6.4. Laser-Beam–Material Interactions

Like electron-beam welding, laser-beam welding is normally performed in a keyhole mode with very high-power density beams. To form a laser weld, the

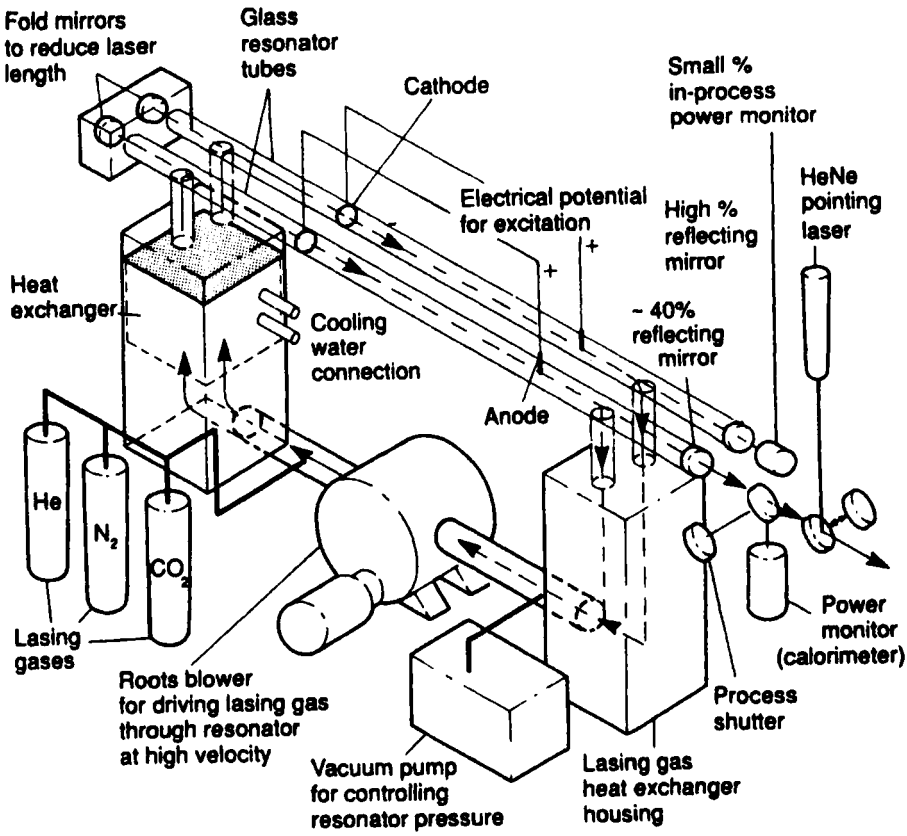


Figure 8.39 Schematic layout of an axial flow CO_2 gas laser. (From *Laser Welding* by C. Dawes, published in 1992 by and used with permission of McGraw Hill/Abington Publishing, Woodhead Publishing, Cambridge, UK.)

beam is focused on a spot on or near the surface of the workpiece. When focused on the surface, much of the incident energy is reflected, at least momentarily, because most metals are good reflectors of light. The small amount of laser-beam energy absorbed, however, quickly heats the metal surface. The mechanism for converting the kinetic energy of photons is largely the same as for electrons. Incoming photons excite the electrons in the outermost shells of surface atoms, including release and excitation of conduction electrons. These transfer their energy to the lattice as phonons or vibrational waves. Phonon excitation is revealed as rapid heating. Beyond this, however, surface heating and vapor formation rapidly accelerates the absorption process with photons. Figure 8.41 shows the depth of weld penetration as a function of laser-beam power density.

At focused power-density levels above 10^9–10^{10} W/m^2 (or about 10^4 W/mm^2), rapid vaporization leads to the formation of a small keyhole, which

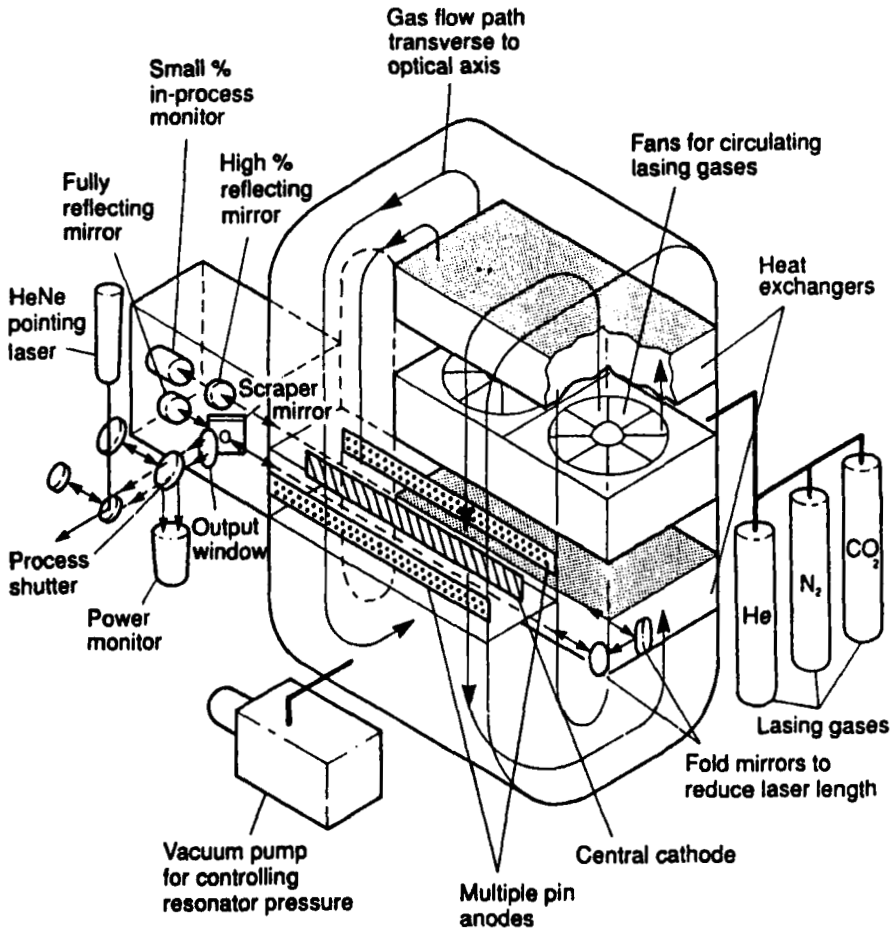


Figure 8.40 Schematic layout of a cross flow CO_2 gas laser. (From *Laser Welding* by C. Dawes, published in 1992 by and used with permission of McGraw Hill/Abington Publishing, Woodhead Publishing, Cambridge, UK.)

consists of a small-diameter cylindrical shaft, into the workpiece. As the keyhole penetrates deeper into the workpiece as a result of downward pressure of escaping vapor on the underlying liquid, photons of the laser light (as for electrons in EBW) are repeatedly reflected and scattered within the cavity. This increases the coupling of laser energy to the material. As long as energy is applied, the keyhole is held open by the pressure of escaping vapor, preventing the surrounding molten walls from collapsing. This is shown schematically in Figure 8.42.

When the laser is operated in a continuous-wave (as opposed to pulsed) mode and the beam is moved along a weld line, molten material at the leading edge of the keyhole produces a very small wave supported by surface tension.

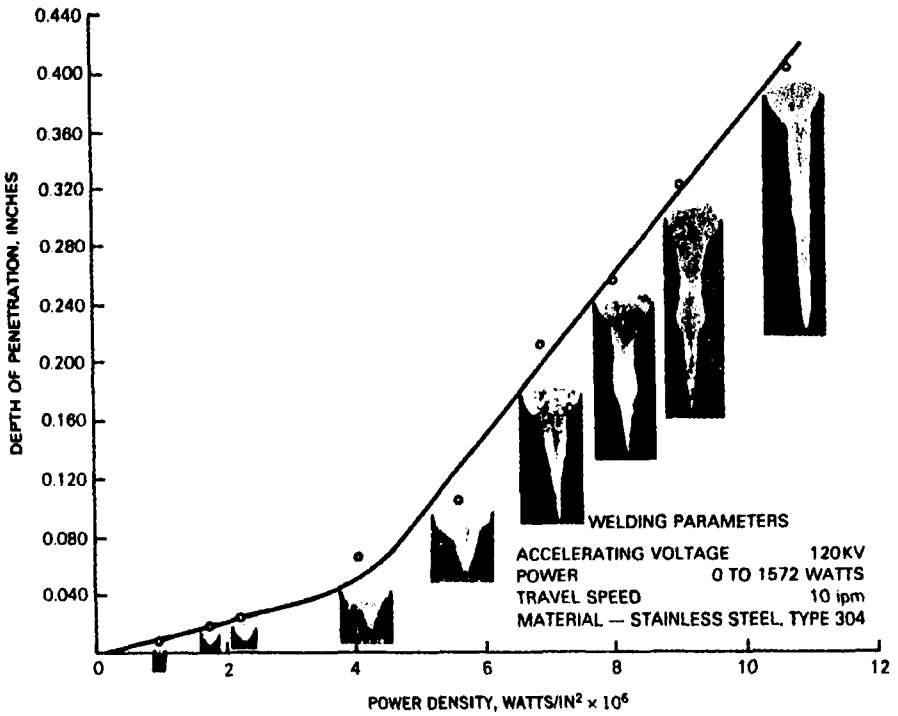


Figure 8.41 Depth of weld penetration as a function of laser-beam power density. (From *Welding Handbook*, Vol. 2: *Welding Processes*, 8th ed., edited by R. L. O'Brien, published in 1991 by and used with permission of the American Welding Society, Miami, FL.)

As the beam travels forward, this wave reorients around the edge of the keyhole and slumps to its trailing edge to come together (again by surface tension) to form a continuous liquid and solidify to form a continuous weld. Evidence that such a wave existed is found in the protruding top bead, which could also be the result of lateral shrinkage, however.

The laser-beam (like the electron-beam) keyhole welding technique transfers heat from the beam source into the material not just at the surface by conduction, but along a line extending into or through the material thickness. This gives rise to the internal heat generation term (q) in the generalized heat flow equation presented in Chapter 6.

8.6.5. Benefits of Laser-Beam and Electron-Beam Welding

Advantages shared by laser-beam and electron-beam welding are (1) deep-penetrating, narrow welds (i.e., high depth-to-width ratios); (2) high melting efficiency; (3) minimum heat effect to material surrounding the weld fusion

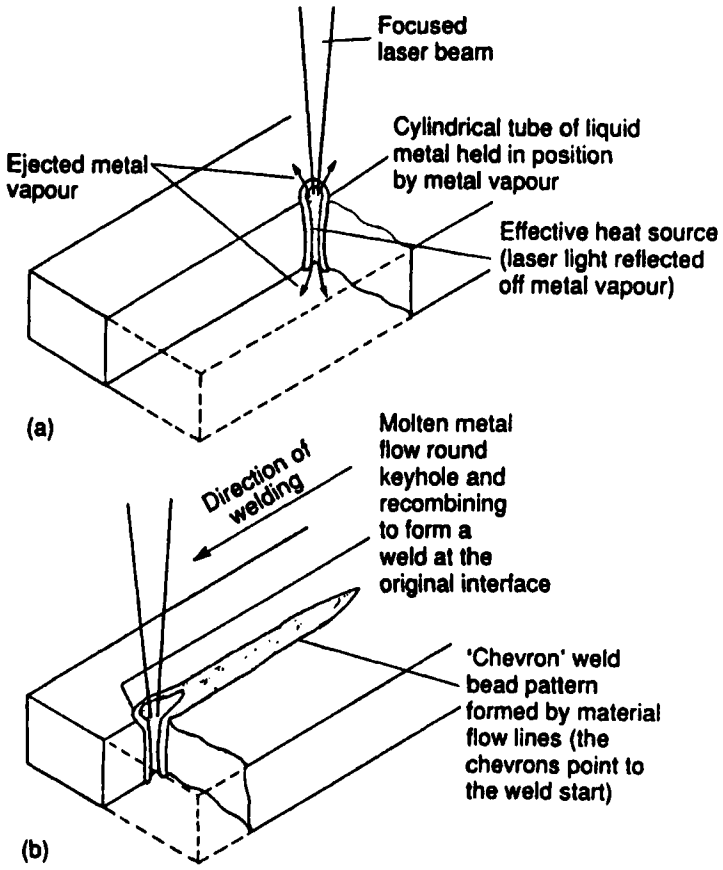


Figure 8.42 Schematic of (a) a laser weld keyhole and (b) its movement through a workpiece to recombine molten metal at its trailing edge to form a continuous weld. (From *Laser Welding* by C. Dawes, published in 1992 by and used with permission of McGraw Hill/Abington Publishing, Woodhead Publishing, Cambridge, UK.)

zone (i.e., the heat-affected zone); and minimal shrinkage- and thermal contraction-induced distortion. Disadvantages that they share are (1) the need for well-prepared, close-fitting square- or straight-butt joints due to the narrowness of the energy beams; and (2) the difficulty of introducing filler metal due to the high depth-to-width ratio of resulting welds. As a result, both tend to be used for specialized situations where one or more of the following are needed: (1) virtually unlimited melting capability (for refractory materials); (2) precise control of energy placement (for small or thin weld joints); (3) precise dimensional control (due to shrinkage or distortion); (4) high welding speed (made possible by the high-energy density); and (5) minimal heat effect (as a result of low net heat input).

8.7. THE PHYSICS OF A COMBUSTION FLAME

The combustion of a fuel gas in the presence of oxygen (normally, provided in pure form from a pressurized source) is the basis for oxyfuel welding and cutting. Commercial fuel gases have the common property of requiring oxygen to support combustion, but the suitability of one fuel gas over another depends on (1) providing a high flame temperature when burned with pure oxygen; (2) providing a high rate of flame propagation; (3) providing adequate heat content; and (4) causing minimal unwanted chemical reaction between the flame and base and filler metals. The first three of these involve physics as well as chemistry, while the fourth involves strictly chemistry. For this reason, the first three will be dealt with here. But, first, let's review the combustion process briefly (see Section 3.2.1).

8.7.1. Fuel Gas Combustion or Heat of Combustion

The combustion of hydrocarbon fuel gases (such as acetylene, but also methylacetylene–propadiene products, propylene, propane, natural gas [largely methane], and proprietary gases based on these) takes place in two stages described in more detail in Section 3.2.1. First, pure oxygen reacts with the hydrocarbon to cause it to dissociate into hydrogen and carbon, partially combusting the carbon to carbon monoxide and leaving the hydrogen uncombusted. This stage, called primary combustion, takes place in the core of the flame, known as the inner cone. Second, the carbon monoxide is oxidized to completion by oxygen from the air surrounding the flame, and the hydrogen is burned to form water vapor. This stage is called secondary combustion, and takes place in the outer portion of the flame, known as the outer flame. The total heat of combustion is divided between these two stages, depending on the particular chemistry of the fuel gas. Irrespective of the particular reactions, the heat of reaction is more concentrated in the inner cone, so the inner cone is at a higher temperature. By adjusting the molar ratio in the reaction (i.e., the combustion ratio), the flame can be rendered neutral (for a balanced molar ratio, based on the relevant chemical reactions), oxidizing (for an excess of oxygen), or reducing (for an excess of fuel gas). The relative benefits of each are described in Section 3.2.1.

8.7.2. Flame Temperature

The temperature of the flame of a combusted fuel gas varies according to both the fuel gas chemistry and the oxygen-to-fuel gas ratio. Typical flame temperatures are listed in Table 3.1. While the flame temperature gives an indication of the heating potential of the fuel gas, it is only one of many physical properties that is important. Flame temperatures are normally calculated, because measurement is difficult.

8.7.3. Flame Propagation Rate or Combustion Velocity

The velocity with which a flame front travels through adjacent unburned gas is known as the flame propagation rate or combustion velocity. The flame propagation rate influences the size and temperature of the primary flame and affects the maximum velocity at which gases can be made to flow from the torch tip without causing a flame standoff or backfire. Flame standoff is where combustion takes place some distance from the torch tip, rather than right at the tip. Backfire is the momentary recession of the flame into the torch tip, followed by either reappearance or complete extinction of the flame.

8.7.4. Combustion Intensity

Combustion intensity or specific flame output is a more meaningful way of assessing the effectiveness of a fuel gas for welding than flame temperature or heating values alone. Combustion intensity takes into account the burning velocity of the flame, the heating value of the fuel gas and oxygen mixture, and the area of the flame cone issuing from the torch tip (the effective contact area). Combustion intensity is expressed as

$$C_i = C_v C_h \tag{8.11}$$

where C_i is the combustion intensity (in $J/m^2 s^{-1}$ or $Btu/ft^2 s^{-1}$), C_v is the normal combustion velocity of the flame (in m/s or ft/s), and C_h is the heating value of the gas mixture under consideration (in J/m^3 or Btu/ft^3). Combustion intensity is maximum when the product of normal burning velocity and heating value of the mixture is maximum.

As for the heat of combustion, combustion intensity is really the sum of both primary and secondary combustion reactions, but, because of the concentration of energy at the cone, the primary reaction is more important. Figures 8.43, 8.44, and 8.45 show the rise and fall of primary, secondary, and total combustion intensity with oxygen-to-fuel gas ratio for various fuel gases, respectively.

8.8. THE PHYSICS OF CONVERTING MECHANICAL WORK TO HEAT

Pressure and friction nonfusion welding depend at least somewhat on heating to facilitate movement of material by plastic deformation at lower flow stresses to obtain the continuity required to produce a weld. Both achieve this heating by converting mechanical work to heat. All that needs to be said here about the physics of these processes is the following: First, mechanical energy and thermal energy (like all forms of energy) are equivalent. One form can be converted to another; in this case, mechanical energy (from macroscopic plastic

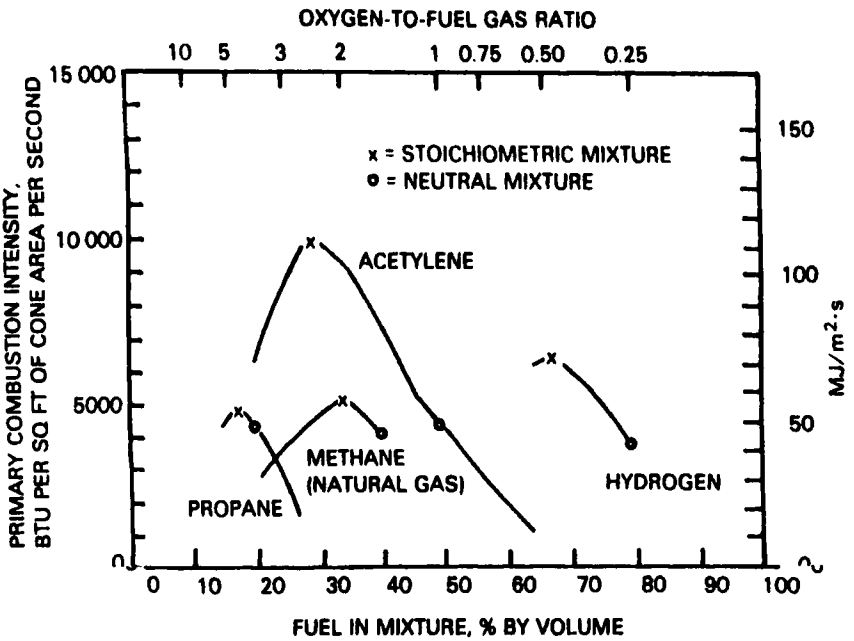


Figure 8.43 Primary combustion intensity of various fuel gas–oxygen mixtures. (From *Welding Handbook*, Vol. 2: *Welding Processes*, 8th ed., edited by R. L. O'Brien, published in 1991 by and used with permission of the American Welding Society, Miami, FL.)

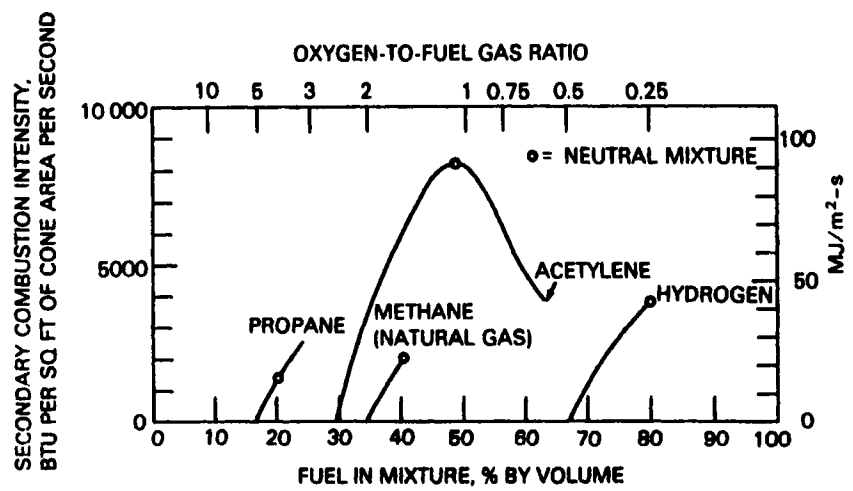


Figure 8.44 Secondary combustion intensity of various fuel gas–oxygen mixtures. (From *Welding Handbook*, Vol. 2: *Welding Processes*, 8th ed., edited by R. L. O'Brien, published in 1991 by and used with permission of the American Welding Society, Miami, FL.)

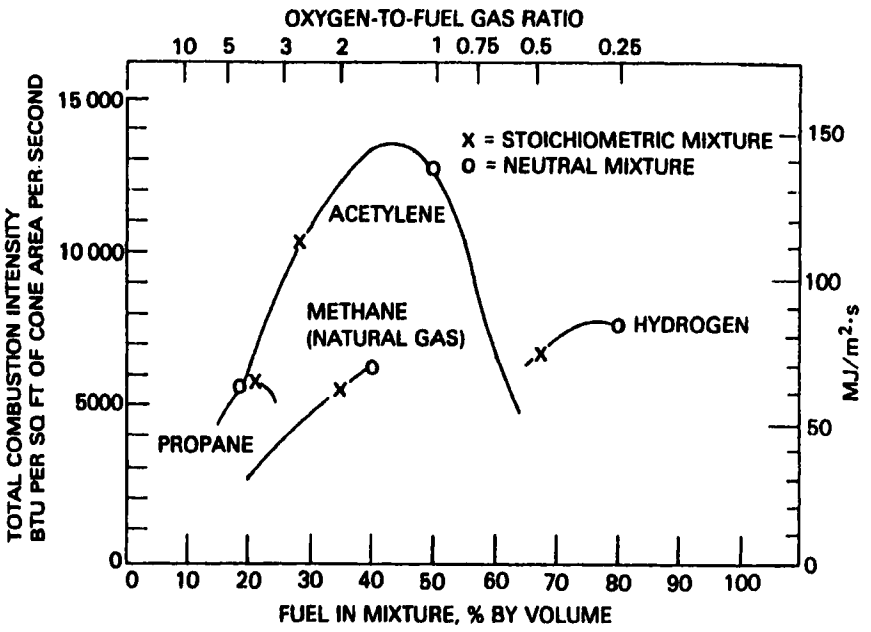


Figure 8.45 Total combustion intensity of various fuel gas–oxygen mixtures. (From *Welding Handbook*, Vol. 2: *Welding Processes*, 8th ed., edited by R. L. O'Brien, published in 1991 by and used with permission of the American Welding Society, Miami, FL.)

deformation from pressure or microscopic plastic deformation from friction) can be converted to heat. Second, the heat generated is not a property of the material or part from which it is obtained, nor is it contained in the material or part. Rather, heat is produced as a result of the conversion of mechanical work, and without limit. What that means is, keep adding work, and heat will continue to be generated.

8.9. SUMMARY

Welding requires the combined action of heat and pressure, from one extreme to the other. Thus, energy or power sources are required. These sources can be electric arcs, plasmas, high-energy-density beams of electrons or laser light, combustion flames, or mechanical work from pressure or friction. To understand welding requires understanding of the physics underlying the operation of these various sources. This involves understanding electricity, magnetism, light, optics, heat, and mechanical work. This chapter has provided an overview of the key concepts needed to proceed through the rest of this book.

REFERENCES AND SUGGESTED READING

Arata, Y., 1986, *Plasma Electron & Laser Beam Technology*, American Society for Metals, Metals Park, OH.

Dawes, C., 1992, *Laser Welding*, McGraw-Hill, New York (originally, Abington Press, Woodhead Publishing, Cambridge, UK).

Duley, W. W., 1992, *CO_2 Lasers: Effects and Applications*, Academic, London.

Johnson, K. I.(Editor) 1977, *Resistance Welding Control and Monitoring*, The Welding Institute, Cambridge, UK.

Koechner, W., 1996, *Solid State Laser Engineering*, 4th ed., Springer, Berlin.

Lewis, B., and Van Elbe, G., 1961, *Combustion Flames and Explosions of Gases*, Academic, New York.

Manz, A. F., 1973, *Welding Power Handbook*, Union Carbide Corporation, New York.

Schultz, H., 1993 (English), *Electron Beam Welding*, Abington Press, Woodhead Publishing, Cambridge, UK.

CHAPTER 9

MOLTEN METAL TRANSFER IN CONSUMABLE ELECTRODE ARC WELDING

9.1. FORCES CONTRIBUTING TO MOLTEN METAL TRANSFER IN WELDING

To occur at all, consumable electrode arc welding processes require that molten metal from the electrode be transferred to the workpiece, thereby providing filler besides simply heat to melt the substrate(s). To be most effective, this transfer should occur with minimal loss due to spatter, where *spatter* is molten metal from the consumable electrode that does not reach the weld pool, but goes elsewhere at random. At least part of the popularity of consumable electrode arc welding processes arises from the greater efficiency and higher rates at which filler metal is deposited compared to other welding processes.

One only need observe consumable electrode arc welding for a short time under different operating conditions of welding current and voltage to recognize that the precise manner in which molten metal transfers across an electric arc differs with these parameters, as well as for specific processes (e.g., flux-coated or flux-cored versus externally, inert gas-shielded welding), electrode compositions (e.g., steel versus aluminum), and, for gas-shielded processes, shielding gas composition (e.g., pure argon versus argon mixed with oxygen or carbon dioxide). The manner in which molten filler metal is transferred to the weld pool, in turn, can have profound effects on the performance and usefulness of a consumable electrode arc welding process. These effects include (1) the ease of (if not the ability for) welding in various positions (in a vertical plane or horizontally overhead as opposed to horizontally down-hand); (2) the extent of weld penetration; (3) the rate of filler

deposition and (4) heat input; (5) the stability of the weld pool; and (6) the amount of spatter loss.

To understand molten metal transfer in arc welding requires at least some understanding of the physics involved, even though the precise physics is not yet completely known. This should not come as a great surprise since arcs are small, arc temperatures are high, and the dynamics of molten metal transfer are high. Because of the difficulty in firmly establishing the precise mechanisms that lead to and influence the process, a great number of mechanisms have been suggested based on the following forces:

1. Pressure generated by the evolution of gas at the electrode tip (for flux-coated or flux-cored electrode processes).
2. Electrostatic attraction between the consumable electrode and the workpiece.
3. Gravity.
4. The "pinch effect" caused near the tip of the consumable electrode by electromagnetic field forces.
5. Explosive evaporation of a necked region formed between the molten drop and solid portions of the electrode due to very high conducting current density.
6. Electromagnetic action produced by a divergence of current in the arc plasma around a drop.
7. Friction effects of the plasma jet.
8. Surface tension effects once the molten drop (or electrode tip) contacts the molten weld pool.

The reality is, a combination of these forces (dependent on the process and operating conditions) act to detach a molten drop from the end of a consumable electrode and cause it to move toward, join with, and become part of a molten weld pool.

Before we examine the various ways in which molten metal transfer takes place, called transfer modes, let's look briefly at each of the forces just listed.

9.1.1. Gas Pressure Generated at Flux-Coated or Flux-Cored Electrode Tips

For those processes in which shielding gas is generated by thermal decomposition or dissociation of some of the ingredients in the coating (or covering) or core of the consumable electrode, that gas produces a pressure that helps both detach and propel a molten drop from the electrode's tip. Part of the force is simply that for every action, there is an equal and opposite reaction, which is Newton's second law. Another part is simply the effect of gas pressure on an unsupported volume of liquid that acts to form a neck to help detach the molten region from the solid region of the electrode.

9.1.2. Electrostatic Attraction

Oppositely charged entities attract one another electrostatically through Coulombic forces. With consumable electrodes, the molten drop is always attracted to the weld pool in the oppositely charged workpiece, regardless of operating mode (see Section 3.3.1.1). Since the drop is smaller (less massive) and better able to move (especially once it is detached from the electrode), it does move (usually, but not necessarily, to the workpiece).

9.1.3. Gravity

Gravity tends to detach a liquid drop from an electrode when that electrode points down to the source of the gravity, the earth, and is a retaining force when the electrode points upward. This is analogous to the effect on a water drop that forms at the end of a spigot or faucet when the valve or tap is barely opened. Gravity is taken for granted on earth, and must be dealt with, but its absence in the microgravity of space must also be considered when welding is to be performed there, as it almost surely will sooner or later.

9.1.4. Electromagnetic Pinch Effect

When an electric current flows through a conductor (such as a welding electrode), a magnetic field is set up around that conductor (see Section 8.1). An electromagnetic force is produced to act on a molten metal drop due to the interaction of such a welding current with its own magnetic field. When the cross-sectional area of a conductor varies, as it does at the molten tip of an arc welding consumable electrode, the direction of the electromagnetic force depends on the direction of the flow of the welding current. This force is known as the *Lorentz force.*

The Lorentz force acts in the direction of flow of current (positive to negative) when the cross-sectional area is increasing, and in the opposite direction to current flow when the cross-sectional area is decreasing. There are two ways in which the Lorentz force may act to detach a drop at the tip of a consumable electrode: First, when the drop is larger in diameter than the electrode and the electrode is positive (DCEP or DCRP), the magnetic force tends to detach the drop. Second, when there is a constriction or necking down, such as when the drop is about to detach, the magnetic force acts away from the point of the constriction in both directions. Thus, a drop that has started to detach will be given an acceleration, which increases the rate of separation. These two phenomena constitute the pinch effect and are shown schematically in Figure 9.1.

9.1.5. Explosive Evaporation

The force here is of the same type as that in Section 9.1.1, an action producing a reaction. Here, concentration of current (density) as necking takes place

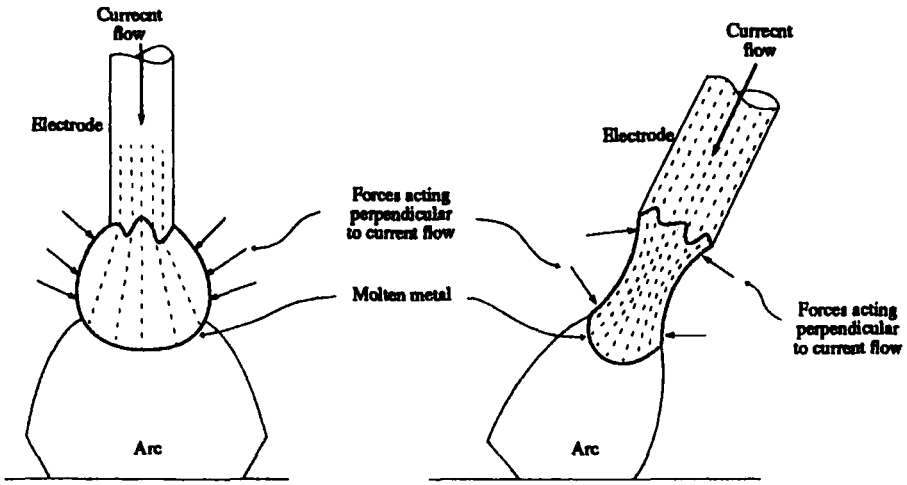


Figure 9.1 Electromagnetic (Lorentz) forces acting on the molten metal drop at the tip of a consumable welding electrode.

rapidly accelerates Joule (I^2R) heating to cause boiling evaporation at an explosive rate.

9.1.6. Electromagnetic Pressure

The magnetic force associated with current flow in the welding electrode also sets up a pressure within the molten metal drop. The maximum pressure is radial to the axis of the electrode and, at high currents, elongates the drop in the direction parallel to the electrode axis. This gives the drop what is referred to as stiffness and causes it to propel in line with the electrode, regardless of the direction the electrode is pointing, upward or downward.

9.1.7. Plasma Friction

Drops of molten metal, once detached from a consumable electrode, can be given an acceleration toward the plate electrode or workpiece by the plasma jet or plasma stream that exists within the core of an electric arc (see Section 8.2.1). This acceleration is the result of momentum transfer largely by friction between high-velocity particles in the plasma jet (ions and electrons) and the drop, so the force is often called the plasma friction force.

9.1.8. Surface Tension

Surface tension is a property of all liquids that arises from the fact that the surface of the liquid (actually, the interface between the liquid and the

surrounding phase, usually a gas in welding) has an energy. This energy is minimized by minimizing the surface area for any given volume. This, in turn, is accomplished by having the liquid take a spherical shape, since surface area-to-volume ratio is minimized for a sphere. Surface tension always tends to retain the molten metal drop that forms at the end of a consumable electrode in position, regardless of the welding position. Thus, surface tension naturally resists detachment. On the other hand, if the molten metal drop formed and being held at the tip of the electrode is caused to contact the molten metal in the weld pool, surface tension forces tend to pull the small drop into the large weld pool, just as it would a completely detached drop.

With this basic understanding of operative forces, let's look at the various molten metal transfer modes.

9.2. FREE-FLIGHT TRANSFER MODES

The different ways in which molten metal transfers from consumable electrodes during arc welding have been studied using high-speed cinematography and analysis of current and voltage traces versus time on an oscilloscope (or its printout, an oscillogram). Among many things observed, the most basic is that transfer can take place in either of two fundamental ways: (1) *free-flight transfer* or (2) *bridging transfer*. There is actually a third fundamental way of transferring molten metal that is not so easily observed, because it occurs only in processes employing molten slag as the transfer medium (e.g., submerged arc and electroslag welding, and to a lesser extent, shielded-metal and flux-cored arc welding). This third type is known as *slag-protected transfer*.

As the name implies, free-flight transfer involves complete detachment of the molten metal drop from the consumable electrode and, then, its flight to the workpiece and weld pool, without any direct physical contact. During this flight, the drops are free of both the consumable electrode and the workpiece, although certainly not forces emanating from each. In bridging transfer, molten metal drops are never completely free; rather they are always attached to the consumable electrode and the workpiece, momentarily bridging the two from a material standpoint—and electrically. Slag-protected transfer applies only to those consumable electrode welding processes that require the presence of a molten slag. The key point here is processes that require, rather than simply involve the presence of molten slag. In the former case, molten metal drops are literally transferred through the molten slag as opposed to with it. The best example is electroslag welding (ESW), in which an arc does not actually persist once the process is initiated (see Section 3.3.2.6), although another example is submerged arc welding (SAW).

It is useful, for simplicity, to start with molten metal transfer modes observed in argon-shielded gas–metal arc welding (GMAW) using a relatively small (1–1.3 mm) diameter steel solid wire operating in the down-hand or flat position and in the direct current electrode positive (DCEP) mode. Once an

understanding is obtained for this scenario, systems employing other shielding gas(es), other wires, other positions, or even other processes will be described.

9.2.1. Globular Transfer

At low welding currents (in the range of 50–170 A) in pure argon, molten metal from a small (1–1.3 mm) diameter solid steel wire electrode is transferred in the form of drops having a diameter larger than the wire. These large drops form at the electrode tip and detach, largely due to the force of gravity, like water dripping from a tap. Once detached, these large drops (also called globules) fall slowly (as determined by gravity) through the arc column and into the molten weld pool to be taken up by surface tension forces. The rate of drop or globule formation, detachment, and transfer is relatively slow, often ranging from less than one each second to a few (less than ten) per second. This mode of transfer is known as *globular* or *drop transfer*. It was once commonly referred to as gravitational transfer.

Not surprisingly, globular transfer occurs best in the down-hand position, where gravity acts to detach the drops. Contrarily, globular transfer is not very useful for out-of-position welding. For welding in a vertical plane, gravity acts to pull the drop from the electrode to cause it to fall to the ground. Depending on whether welding is being attempted horizontally, vertically up, or vertically down in a vertical plane, the effect of gravity can be more or less of a nuisance. For welding overhead, the problem is clearly the greatest, as gravity first tries to keep the molten drop from detaching from the consumable electrode (due to surface tension), then, after the drop has detached, causes it to fall to the ground or, worse yet, onto the welder's hand or down the welder's sleeve or shirt collar; an experience not soon forgotten.

As the welding current increases within the range of 50–170 A, the drops become progressively smaller, suggesting that electromagnetic forces are having an increasing effect on detachment. In fact, for DCEP, the drop size is roughly inversely proportional to the welding current. As welding current is increased, the rate of drop transfer also increases.

With a sufficiently long arc to minimize the likelihood of short circuits between the consumable electrode and the workpiece, globular or drop transfer is reasonably stable and fairly free of spatter loss. The arc has a rather nondistinctive sound: rather quiet with occasional crackling sounds. The arc appears somewhat soft but not wandering, and tends to exhibit some pulsation in size and brightness, becoming slightly smaller and less intense whenever a large globule has formed at the tip of the electrode and detaches to drop slowly through the arc column,[1] at which point the arc grows slightly in size and intensity.

[1] In fact, much can be learned from watching an electric arc, including size, relative softness (quiescence) or harshness (stiffness or drive), brightness (intensity), stability (steadiness, erratic pulsation, or wander), and occurrence of spatter in the form of free-rolling glowing-white balls or bursts of fine sparks. Listening to the arc tells us whether it is smooth and fairly silent or one of intense hissing or cracking and popping. These and other sensory clues are used by welders as feedback to judge how welding is occurring and for making needed adjustments.

9.2.2. Spray Transfer

When the welding current reaches a critical level,[2] individual drops no longer form, but, rather, the tip of the consumable electrode becomes pointed and a cylindrical stream of liquid metal flows toward the workpiece in line with the electrode. Near its tip (nearest the workpiece), this cylinder disperses into many very small drops or droplets. The rate at which droplets are transferred is hundreds per second. The current at which this transition occurs is called the *transition current*, and, often, as for steel, this transition is very sharp. This mode of transfer is called *streaming transfer* or, more recently and commonly, *axial spray transfer*.

The axial spray transfer mode is unique not only because of its excellent stability, but also because it is virtually free of spatter. This is because the droplets are actively propelled away from the consumable electrode and into the molten weld pool to be captured by surface tension force. Since the droplets are transferred in line with the electrode rather than across the shortest path between the electrode and the workpiece, filler metal can be directed exactly where it is needed. This is a great advantage when making vertical or overhead welds, where the propelling force offsets the disruptive effect of gravity.

The spray transfer mode also has associated with it a characteristic arc appearance and sound. The arc tends to seem firmer (or stiffer) and more steady, with little or no pulsation of any kind (assuming welding current is not intentionally being pulsed between two different levels). The arc also emits a steady hiss or "sshhhh!," which becomes more intense as the current is increased above the transition point.

The key to spray transfer is the pinch effect discussed in Section 9.1.4. This pinching Lorentz force, along with the explosive evaporation force, projects the droplets toward the workpiece, so this mode has also been called projected transfer. Often projected transfer refers to the mode that occurs just after transition from globular and before full streaming transfer.

Unfortunately or fortunately, depending on the situation, axial spray transfer also leads to a high net linear heat input to the workpiece. If high deposition rate and/or deep penetration is required, and the workpiece is massive enough to tolerate the heat by acting as a sink to dissipate it, this is an advantage of this mode. If heat is detrimental due to thinness of gauge or inherent metallurgical sensitivity, this can be a disadvantage.

At still higher currents above the transition current, other phenomena occur that give rise to some variations on the globular and axial spray transfer modes just described. These are described in Section 9.5.

Figure 9.2 schematically compares the sequence of drop formation and detachment for globular transfer (Figure 9.2a) and axial spray transfer (Figure 9.2b). Figure 9.3 shows various free-flight transfer modes schematically.

[2] The critical level depends on electrode and shielding gas composition, to mention the two major factors.

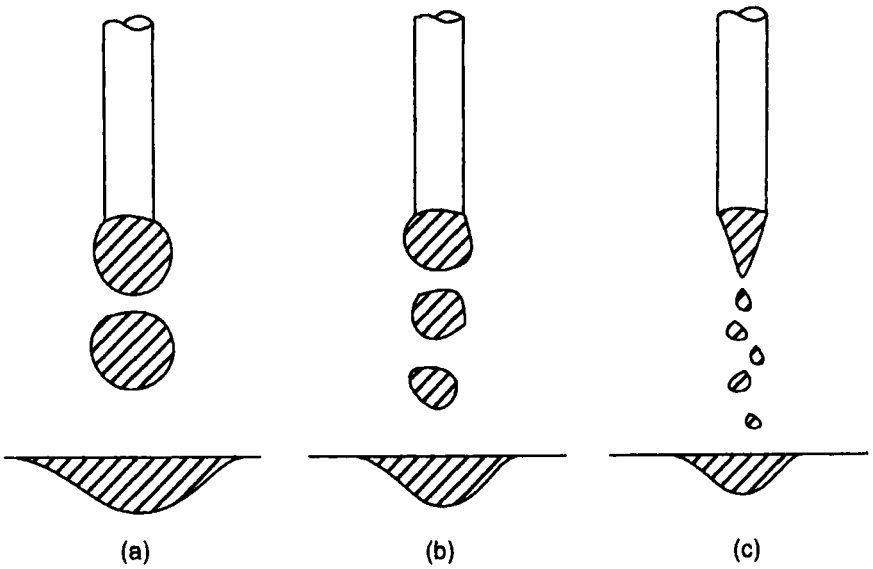


Figure 9.2 Individual drop formation and detachment sequence in (a) globular transfer and (b) projected and (c) streaming axial spray transfer.

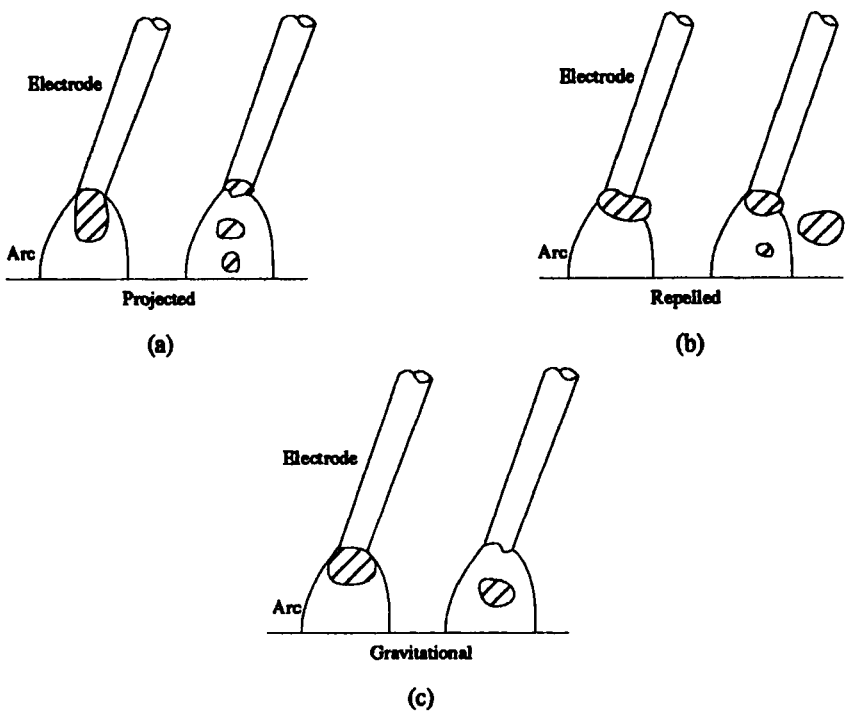


Figure 9.3 Three types of free-flight molten metal transfer in the welding arc from a consumable electrode: (a) projected, (b) repelled, and (c) gravitational.

9.3. BRIDGING OR SHORT-CIRCUITING TRANSFER MODES

Sometimes, for some consumable electrode materials such as steel, the transition current to achieve axial spray transfer is too high to be practical (e.g., 200–220 A for 1-mm-diameter steel wire) from the standpoint of heat input. Going to such high currents will overheat the workpiece, perhaps to the point that is glows intensely, and may cause severe distortion. Therefore, it has become necessary to modify the free-flight molten metal transfer mode in order to operate over a wider current range.

One means of doing this is by *short-circuiting transfer*. In this mode, the welding arc voltage is kept low (say 17–21 V versus 24–28 V for globular or spray free-flight transfer with steel wires) and the tip of the electrode periodically dipped into the molten weld pool. When this occurs, molten metal being formed at the electrode tip is transferred to the pool by a combination of surface tension and electromagnetic forces. The method works because a low voltage reduces the rate at which the electrode is melted (the burn-off rate) compared to the rate at which it is being fed from a wire feeder or wire pull-gun. Transfer is unfavorable if when the wire electrode dips into the weld pool it heats the wire back from the tip (by I^2R heating) to the point that it explodes due to rapidity of heating, possibly leaving a remnant of unmelted wire stuck in the weld, but always causing severe and violent spatter. Under proper operation, with a balance between wire feed rate and electrode burn-off rate, the wire dips into the weld pool to be continually melted and drawn in by surface tension. Because of the way in which this mode takes place, it is characterized by a fair amount of random, intermittent sparks from spatter, and a sound described as "frying bacon," consisting or irregular pops and crackles.

In the presence of carbon dioxide (CO_2) in shielding gas, the molten drop at the electrode tip is pushed upward, giving rise to what is known as *repelled transfer*. In this mode, short-circuiting captures the drop before it detaches in an unfavorable manner.

Short-circuiting transfer always involves bridging between the consumable electrode and the weld pool, so it is a bridging transfer mode. In fact, there are two subtle variations of short-circuiting transfer: one used with SMAW coated electrodes or GMAW wires known as short-arc, and the other known as bridging-without-interruption. The former simply employs a physically short arc and intermittent short circuiting. The latter involves continuous contact and is exemplified by some coated SMAW electrodes that can be operated in by dragging the electrode tip on the workpiece; this is called drag technique. The steps in short-circuiting molten metal transfer and arc operation are shown schematically in Figure 9.4.

Short-circuiting transfer offers several advantages over free-flight transfer modes, including (1) less fluid molten metal (due to less superheat) and (2) less penetration (due to lower welding voltage and lower net energy input). This allows the weld pool to be handled much more easily in all positions by welders, especially overhead, and for the joining of thin-gauge materials.

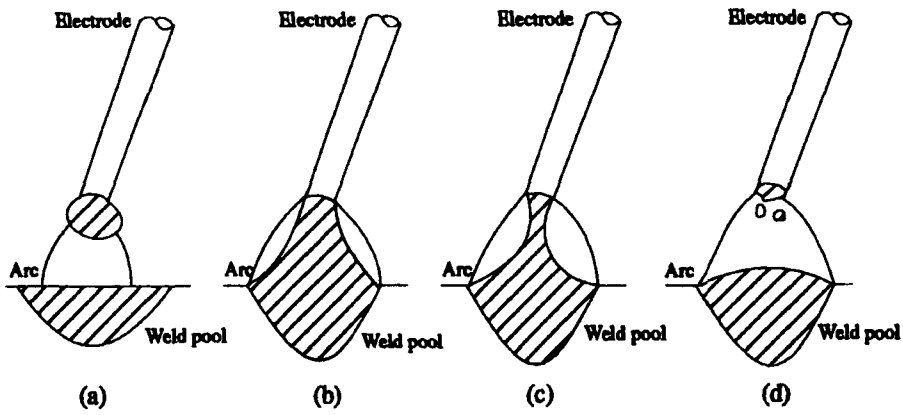


Figure 9.4 The sequence of events during short-circuiting transfer in a consumable electrode arc welding process: (a) globule of molten metal builds up on the end of the electrode; (b) globule contacts surface of weld pool; (c) molten column pinches off to detach globule; and (d) immediately after pinch-off, fine spatter may result.

Spatter normally associated with this mode can be kept to a minimum by using electrical inductance (see Section 8.1) to control the rate of current rise when the wire comes in contact with the weld pool. Because of the way in which molten metal transfer occurs in short-circuiting, this mode is also commonly referred to as the buried-arc technique.

Typical welding current and voltage traces during short-circuiting transfer are shown schematically in Figure 9.5.

9.4. PULSED-ARC OR PULSED-CURRENT TRANSFER

There is another technique for extending the operating range of molten metal transfer modes, particularly the axial spray transfer mode, namely *pulse arc transfer* or *pulsed current transfer*. Pulsed current transfer is achieved by employing a low, steady current to maintain the arc and a periodic current pulse to a higher level. When correctly timed, such a pulse detaches a drop and propels it into the weld pool, thereby giving the advantage of axial spray transfer at a lower average current, and, thus, lower net heat input. The time period of pulses must be short enough to suppress globular transfer, but long enough to ensure that transfer by the spray mode will occur. This pulsed mode differs from the normal spray mode in that (1) the molten metal transfer is interrupted between the current pulses and (2) the current to produce spray is below the normal transition current. Pulse shape (i.e., wave form, especially the rate of the rise and fall of current) and frequency can be varied over a wide range in modern, solid-state power sources. In fact, the rate of molten metal transfer can be adjusted to be one drop or a few drops per pulse.

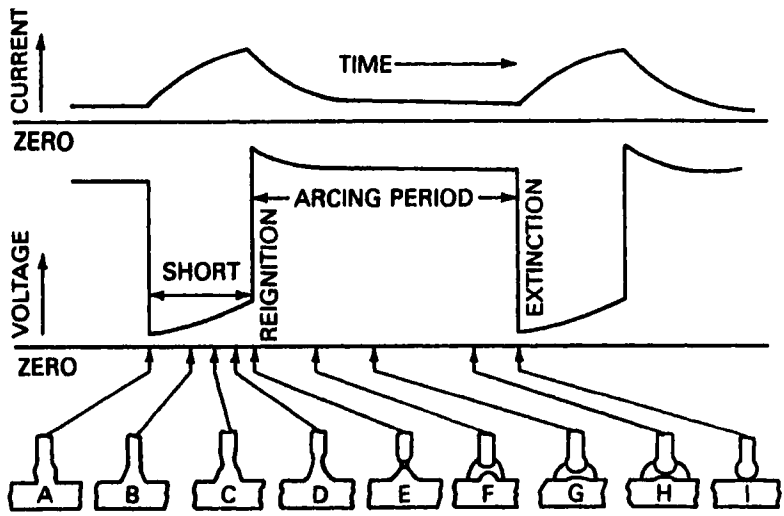


Figure 9.5 Schematic representation of short-circuiting molten metal transfer, and current and voltage trace, during consumable electrode arc welding. (From *Welding Handbook*, Vol. 1: *Welding Technology*, 8th ed., edited by L. P. Connor, published in 1987 by and used with permission of the American Welding Society, Miami, FL.)

A schematic showing what is taking place during pulsed current transfer is presented in Figure 9.6.

9.5. SLAG-PROTECTED TRANSFER

In some consumable electrode arc welding processes, the presence of a molten slag plays a major role in enabling molten metal transfer, not just in providing cleaning action, protection from oxidation, metallurgical refining, and containment of the weld pool until it solidifies—as if these weren't enough! This is particularly the case for what are properly called covered arc processes, which include electroslag welding (ESW) and submerged arc welding (SAW). In each of these, so much molten slag covers the weld pool that molten drops formed at the tip of the consumable electrode must transfer through this liquid to reach the pool. While the primary forces acting to cause drop detachment are the same as for many other consumable electrode arc welding processes (pinching force, electrostatic attraction, and gravity), transfer is never truly free-flight. Rather, the drops pass through the molten slag itself, thereby always being protected by it. While other consumable electrode arc welding processes employ slag, notably shielded-metal arc welding (SMAW) and flux-cored arc welding (FCAW), the sheer volume of slag coverage from these processes neither requires nor allows molten metal transfer to occur without at least some free flight. Figure 9.7 shows this mode of molten metal transfer schematically.

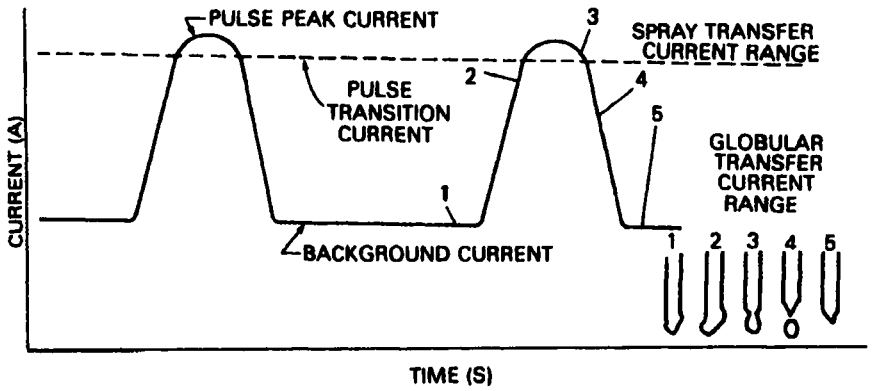


Figure 9.6 Output current wave form of a pulsed current power source and molten metal transfer sequence. (From *Welding Handbook*, Vol. 1: *Welding Technology*, 8th ed., edited by L. P. Connor, published in 1987 by and used with permission of the American Welding Society, Miami, FL.)

In fact, since the slag in submerged arc begins as a dry, granular flux, slag-protected transfer, this process is often referred to as flux-wall guided transfer.

9.6. VARIATIONS OF MAJOR TRANSFER MODES

As alluded to in Section 9.2.2, some variations of spray transfer occur at higher currents. As the welding current rises above the transition current, the liquid cylinder associated with axial spray transfer first collapses into a rotating spiral. This variation of streaming transfer is called *rotating transfer*. It has no particular benefit other than providing a high deposition rate, and no particular disadvantage either, except that it is the beginning of higher-order unstable modes identified based on formal mathematical analysis of liquid cylinders carrying an electric current. Rotating transfer is associated with what is referred to as a kink instability in such an analysis.

At very high welding currents, in the region of 400–500 A, or in the presence of a strong longitudinal magnetic field, streaming transfer is suppressed and a pair of mutually opposed, flattened drops appear at the tip of the consumable electrode. These detach and transfer at very high frequencies. This mode also tends to be quite unstable, and is referred to in formal analysis of liquid cylinders with flowing currents as the flute instability. This mode only offers very high deposition rates, provided the associated high heat input and difficult-to-control arc can be tolerated. These two modes are distinct from the earlier radial pinch modes discussed in Section 9.2.2. Figure 9.8 schematically illustrates these molten metal transfer modes.

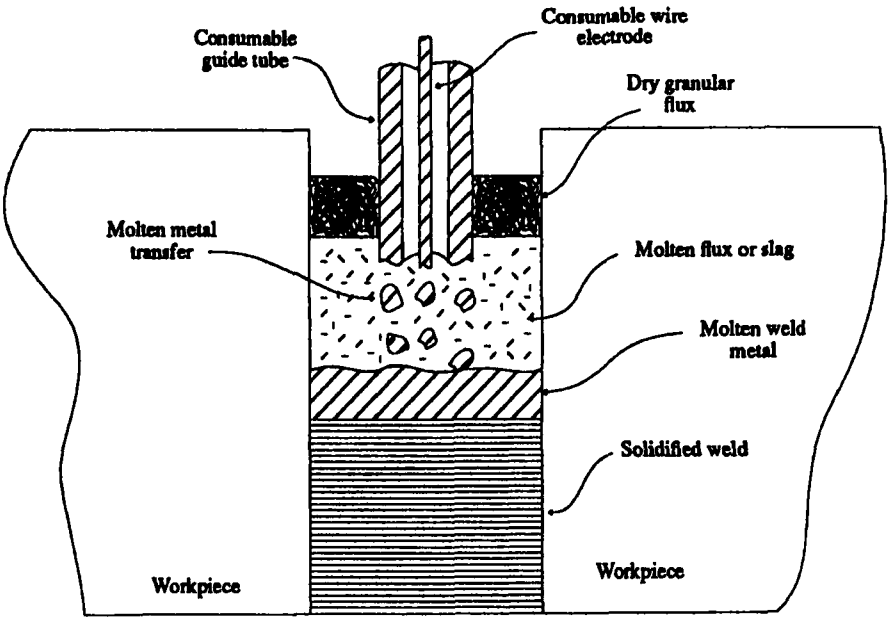


Figure 9.7 Slag-protected molten metal transfer during covered arc processes such as ESW.

Tables 9.1 and 9.2 present molten metal transfer modes in accordance with the IIW classification and in terms of the dominant forces involved, respectively.

9.7. EFFECT OF WELDING PROCESS PARAMETERS AND SHIELDING GAS ON TRANSFER MODE

9.7.1. Effects on Transition Current

The current at which transition from globular to spray transfer begins (the transition current) depends on a number of factors, including (1) the composition of the consumable electrode, (2) electrode diameter, (3) electrode extension, and (4) composition of shielding gas. A great difference in the transition current is found with different metal systems comprising the consumable electrode. Since they are the most widely used consumable electrode compositions, it is particularly interesting that there are great differences between steel and aluminum. Transition currents for various sizes of steel and aluminum electrodes are shown in Table 9.3. The transition current for a particular electrode material is approximately proportional to the diameter of the electrode, as shown in Figure 9.9. It turns out that the transition current is not dependent on current density, however, just current level. Values of transition current refer to the lower limit of useful current for spray transfer.

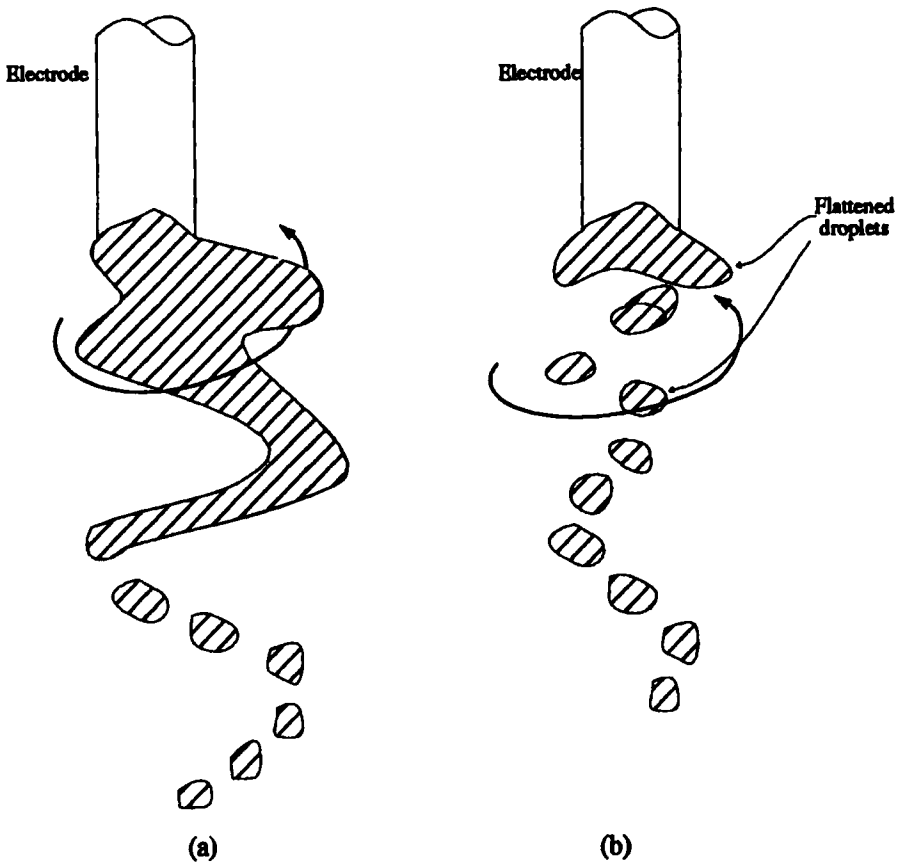


Figure 9.8 Rotating transfer associated with kink instability (a) and occurrence of flute instability (b) during molten metal transfer at very welding high currents.

The amount by which a consumable electrode extends past the contact tube in a gas–metal arc welding (GMAW) torch affects transition current, as shown in Figure 9.10. An increase in electrode extension or "stick-out" allows a slight decrease in the current at which spray transfer develops. In fact, while extensions to 2 in. (50 mm) are shown, a practical range is more like $\frac{1}{2}$–1 in. (12–25 mm).

In gas–metal arc welding (GMAW) of steels, spray transfer is usually done with argon-based shielding gas. However, small additions of oxygen (about 2 to 5%) lower the transition current, while additions of carbon dioxide (CO_2) raise it. The current at which axial spray disappears and rotational spray begins is also proportional to electrode diameter and varies inversely with electrode extension, as shown in Figure 9.10. At high welding current densities, where a rotating arc mode takes place, appropriate mixtures of shielding gases, proper wire feed rate control, and specially cooled welding torches or guns

TABLE 9.1 IIW Classification of Molten Transfer Modes

Designation of Transfer Type	Welding Processes (Examples)
1. Free-flight transfer	
1.1. Globular	
1.1.1. Drop	Low-current GMA
1.1.2. Repelled	CO_2 shielded GMA
1.2. Spray	
1.2.1. Projected	Intermediate-current GMA
1.2.2. Streaming	Medium-current GMA
1.2.3. Rotating	High-current GMA
1.3. Explosive	SMA (coated electrodes)
2. Bridging transfer	
2.1. Short-circuiting	Short-arc GMA, SMA
2.2. Bridging without interruption	Welding with filler wire addition
3. Slag-protected transfer	
3.1. Flux-wall guided	SAW
3.2. Other modes	SMA, cored wire, electroslag

Source: From *Metallurgy of Welding*, 4th ed., by J. F. Lancaster, published in 1987 by Allen & Unwin, London, and used with permission of Kluwer Academic Publishers, The Netherlands.

TABLE 9.2 Dominant Forces Associated With Molten Metal Transfer Modes

Transfer Type	Dominant Force or Mechanism
1. Free-flight transfer	
1.1. Globular	
1.1.1. Drop	Gravity and electromagnetic pinch
1.1.2. Repelled	Chemical reaction generating vapor
1.2. Spray	
1.2.1. Projected	Electromagnetic pinch instability
1.2.2. Streaming	Electromagnetic
1.2.3. Rotating	Electromagnetic kink instability
1.3. Explosive	Chemical reaction to form a gas bubble
2. Bridging transfer	
2.1. Short-circuiting	Surface tension plus electromagnetic forces
2.2. Bridging without interruption	Surface tension plus (hot wire) electromagnetic forces
3. Slag-protected transfer	
3.1. Flux-wall guided	Chemical and electromagnetic
3.2. Other modes	Chemical and electromagnetic

Source: From *Metallurgy of Welding*, 4th ed., by J. F. Lancaster, published in 1987 by Allen & Unwin, London, and used with permission of Kluwer Academic Publishers, The Netherlands.

TABLE 9.3 Approximate Arc Currents for Transition From Globular (or Drop) to Spray Transfer (i.e., Transition Currents)

Electrode Diameter		Transition Current,[a] A	
mm	in.	Steel Ar + 2%O_2	Aluminum Argon
0.75	0.030	155	90
0.90	0.035	170	95
1.15	0.045	220	120
1.6	0.062	275	170

[a]The transition current varies with electrode extension, alloy content, and shielding gas composition.

Source: From *Welding Handbook*, Vol. 1: *One, Welding Technology*, 8th ed., edited by L. P. Connor, published in 1987 by and used with permission of the American Welding Society, Miami, FL.

designed for high-speed operation allow deposition rates of 7 kg/h. (16 lb/h) and more for steel. The useful upper limit on welding current is where the rotational mode becomes unstable with loss of weld pool control and excessive spatter.

9.7.2. Shielding Gas Effects

Different gases can have quite different effects on the mode of molten metal transfer in consumable electrode welding compared to argon. Helium, for example, does not usually produce an axial spray, regardless of current level or polarity; transfer remains globular. Pure helium remains attractive, however, because helium-shielded arcs provide deeper penetration as a result of this gas' higher work function.[3] Spray transfer can be obtained by mixing relatively small quantities (starting at 20%, but usually 25%) of argon with the helium, without adversely affecting penetration. However, for thicker materials, less than 25% argon is preferred.

Spray transfer is also difficult to achieve with active gases such as nitrogen or carbon dioxide. Treatment of the wire electrode's surface with alkali metal compounds is necessary, but often not practical. Other problems arise with active gases, however, such as greater arc instabilities and chemical reactions between the gas and the superheated molten metal drops that cause considerable spatter. This difficulty can be overcome, at least to some degree, by employing the buried-arc, short-circuiting technique.

The harsh globular transfer and spatter associated with carbon dioxide as a

[3] Recall that work function refers to the energy (in electron volts) needed to remove electrons from an atom (usually from the outermost shell). For helium, both of its electrons are in the 1s shell; thus, binding energy is very high compared to argon, for example, where the outermost electrons are in a 3p shell.

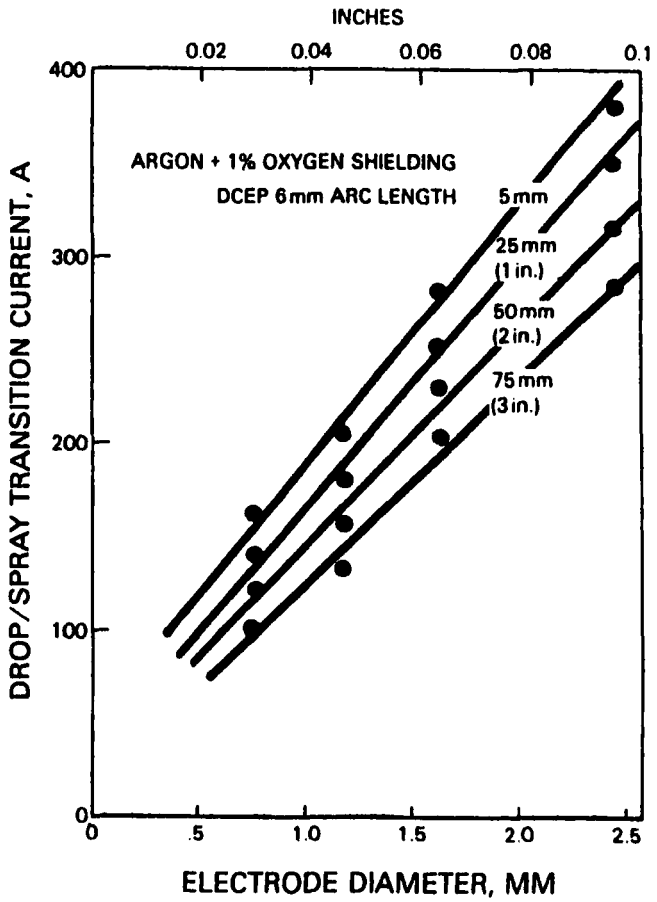


Figure 9.9 Influence of electrode diameter on globular-to-spray transition current for mild steel consumable electrodes for various electrode extensions. (From *Welding Handbook*, Vol. 1: *Welding Technology*, 8th ed., edited by L. P. Connor, published in 1987 by and used with permission of the American Welding Society, Miami, FL.)

shielding gas can be offset by adding argon to stabilize the arc and improve transfer. Short-circuiting transfer is optimized using mixtures of 20–25% carbon dioxide in argon, although higher percentages are typically used for welding thick steel plate.

Finally, small additions of oxygen (2–5%) or carbon dioxide (5–10%) are commonly added to argon to stabilize the arc, lower or raise the globular (or drop)-to-spray transition current, respectively, and improve wetting and bead shape, especially for welding steel.

Figure 9.11 schematically illustrates how different shielding gases lead to different types of molten metal transfer, weld bead contours, and weld penetration patterns.

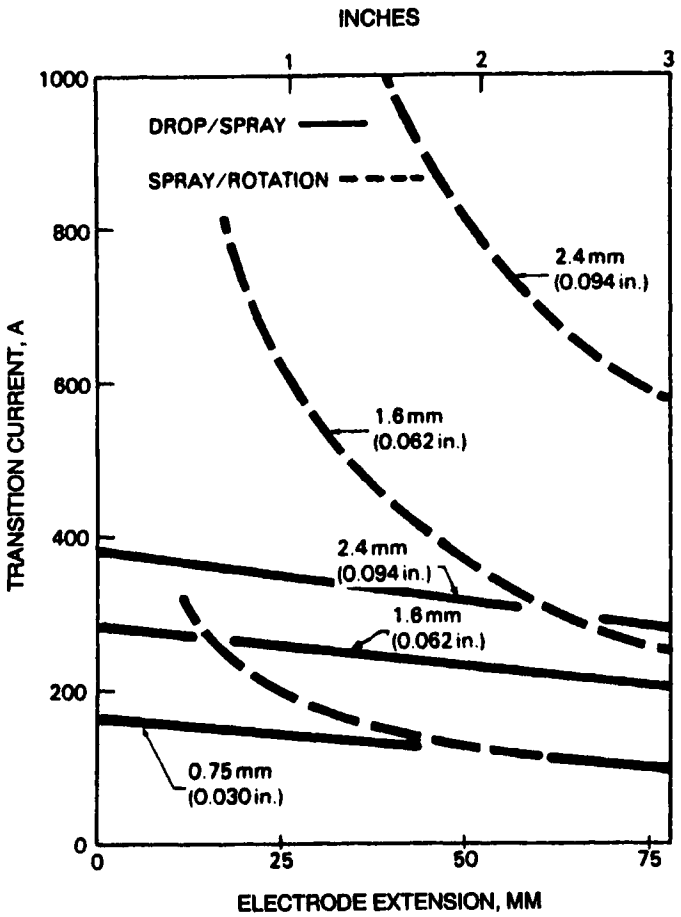


Figure 9.10 Effect of electrode extension on the transition current for mild steel consumable electrodes for various electrode diameters. (From *Welding Handbook*, Vol. 1: *Welding Technology*, 8th ed., edited by L. P. Connor, published in 1987 by and used with permission of the American Welding Society, Miami, FL.)

9.7.3. Process Effects

The mechanism of molten metal transfer with coated or covered electrodes in shielded-metal arc welding (SMAW), while difficult to observe because of fumes and particles of slag, is generally either globules that occasionally short-circuit the arc or a fine spray of both molten metal and molten slag; the latter is preferred, except that spatter can be problematic. The tendency for some covered electrodes (depending on specific coating formulation) to develop a cup at their tip is believed to help direct transfer through the effect of an extra push from gas pressure. Arc stability with SMAW is usually aided by the

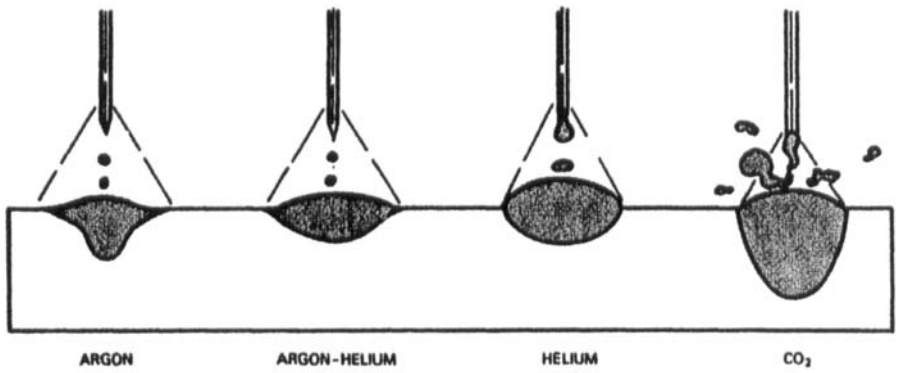


Figure 9.11 Effect of shielding gas composition on type of molten metal transfer, weld bead contour, and weld penetration. (From *Welding Handbook*, Vol. 2: *Processes*, 8th ed., edited by R. L. O'Brien, published in 1991 by and used with permission of the American Welding Society, Miami, FL.)

presence of easily ionized salts added as part of the formulation of the coating.

Not surprisingly, molten metal transfer with flux-cored arc welding (FCAW) is a combination of the basic transfer types and modes seen with GMAW and SMAW. Transfer can be globular, spray, short-circuiting, or pulsed-current; the preferred modes depending on the specific formulation of the flux core as well as on the arc voltage and current.

As mentioned earlier, direct observation of molten metal transfer in SAW is impossible because the arc is completely covered by a blanket of dry, granular flux. Since currents, and current densities, are high for this process, the arc plasma forms a vaporized core surrounded by a concentric zone of liquid flux or slag. Oscillographic studies indicate that molten metal is transferred simultaneously through both the ionized core and through the liquid slag; with the major portion likely occurring through the vapor because of fluid dynamics effects. Thus, both free-flight and slag-protected transfer are occurring in parallel. The form of the molten metal is globules or fine droplets, depending on the welding current.

9.7.4. Operating Mode or Polarity Effects

Since the GMAW process is almost always performed with direct current electrode positive (DCEP or DCRP) power, electrode negative operation is unlikely but possible. For DCEN (or DCSP), GMAW arcs tend to become unstable and spatter tends to be excessive. In this mode also, drop size is large and arc forces (due to the direction of current flow and interactions between current flow and magnetic fields surrounding the electrode) tend to propel drops away from the workpiece. In fact both effects are the result of low rates

of electron emission in the DCEN mode. Alkali metal compounds applied to the wire can help, but are generally of little practical consequence.

9.8. SUMMARY

For consumable electrode arc welding processes, it is necessary for molten metal from the electrode to transfer to the weld pool to provide filler and add heat to produce the weld. The manner in which molten metal transfers can vary, depending principally on operating current and secondarily on process, operating mode (steady direct current, EP or EN, or pulsed DC), and shielding gas composition. Three fundamental types of transfer exist: (1) free-flight, where drops pass through the arc gap between consumable electrode and workpiece; (2) bridging or short-circuiting, where drops are never free, but literally pass from the consumable electrode to the workpiece largely as the result of surface tension; and (3) slag-protected, where drops transfer directly through a molten slag in covered arc processes. Within these are major modes known as globular, (axial) spray, short-circuiting, slag-protected, and pulsed-current, with variations within some of these. All of these modes arise from eight different physical forces, usually acting in combination, but with one or two dominating: (1) evolved gas pressure, (2) electrostatic attraction, (3) gravity, (4) emf pinch effect (5) explosive evaporation, (6) electromagnetic pressure, (7) plasma friction, and (8) surface tension. As would be expected, each mode has its particular advantages and disadvantages, and together they provide increased flexibility to these processes.

REFERENCES AND SUGGESTED READING

The following are suggested for further reading on molten metal transfer modes:

Allemand, C. D., Schoeder, R., Pies, D. E., and Eager, T. W., 1985, "A method for filming metal transfer in welding arcs," *Welding Journal*, **64**(1), 45–47.

American Welding Society, *Welding Handbook*, Vol. 1: *Welding Technology*, 8th ed., American Welding Society, Miami, FL, 1987, pp. 50–57.

Brandi, S., Taniguchi, C., and Liu, S., 1991, "Analysis of metal transfer in shielded metal arc welding," *Welding Journal*, **70**(10), 261s–268s.

Essers, W. G., 1981, "Heat transfer and penetration mechanism with GMAW and plasma-GMAW," *Welding Journal*, **60**(2), 37s–42s.

Green, W. J., 1960, "An analysis of transfer in gas shielded welding arcs," *Transactions of AIEE*, Part 2, **7**, 194–203.

Heald, P. R., Madigan, R. B., Siewert, T. A., and Liu, S., 1994, "Mapping the droplet transfer modes for an ER-100S-1 GMAW electrode," *Welding Journal*, **73**(2), 38s–44s.

Jackson, C. E., 1960, "The science of arc welding," parts 1 and 2, *Welding Journal*, **39**(4 and 6), 129s–140s, 177s–190s.

Johnson, J. A., Carlson, N. M., and Smartt, H. B., 1990, "Detection of metal-transition mode in GMAW," in *Recent Trends in Welding Science & Technology*, ASM International, Materials Park, OH, pp. 377–381.

Johnson, J. A., Carlson, N. M., Smartt, H. B., and Clark, D. E., 1991, "Process control of GMAW: sensing of metal transfer mode," *Welding Journal*, **70**(4), 91s–99s.

Kim, Y.-S., and Eager, T. W., 1993, "Analysis of metal transfer in gas metal arc welding," *Welding Journal*, **72**(6), 269s–279s.

Kohn, G., and Siewert, T. A., 1987, "The effect of power supply response characteristics on droplet transfer in GMA welds," in *Advances in Welding Science & Technology, ASM International*, Materials Park, OH, pp. 299–302.

Lancaster, J. F., 1984, "Metal transfer and mass flow in the weld pool," in *The Physics of Welding*, edited by J. F. Lancaster, Pergamon, New York, pp. 204–267.

Lancaster, J. F., 1987, *Metallurgy of Welding*, 4th ed., Allen & Unwin, London, pp. 94–97.

Lesnewich, A., 1958, "Control of melting rate and metal transfer, part I: control of melting rate," *Welding Journal*, **37**(8), 343s–353s; and "Control of melting rate and metal transfer, part II: melting rate," *Welding Journal*, **37**(8), 418s–425s.

Liu, S., and Siewert, T. A., 1989, "Metal transfer in gas metal arc welding: droplet rate," *Welding Journal*, **68**(2), 51s–58s.

Liu, S., Siewert, T. A., and Lau, H.-G., 1990, "Metal transfer in gas metal arc welding," in *Recent Trends in Welding Science & Technology*, ASM International, Materials Park, OH, pp. 475–479.

Ma, J., and Apps, R. L., 1983, "Analyzing metal transfer during MIG welding," *Welding and Metal Fabrication*, **51**, 119–128.

Needham, J. C., and Carter, A. W., 1965, "Material transfer characteristics with pulsed current," *British Welding Journal*, **12**, 229–241.

Needham, J. C., Cooksey, C. J., and Milner, D. R., 1960, "Metal transfer in inert-gas shielded arc welding," *British Welding Journal*, **7**(2), 101–114.

Rhee, S., and Kannatey-Asibu, Jr., E., 1992, "Observation of metal transfer during gas metal arc welding," *Welding Journal*, **71**(10), 381s–386s.

Waszink, J. H., and Graat, L. H. J., 1983, "Experimental investigation of the forces acting on a drop of weld metal," *Welding Journal*, **62**(4), 109s–116s.

CHAPTER 10

WELD POOL CONVECTION, OSCILLATION, AND EVAPORATION

Fluids, whether in gaseous or liquid form, are subject to *convection*, where convection is defined as fluid motion caused by an external force.[1] It should come as no surprise, given the many forces present during welding, that there is considerable convection in a molten weld pool. Convection in the weld pool affects the pool's shape (as a result of fluid erosion aggravated by heat redistribution), mixing and, thus, homogeneity or heterogeneity (as a result of macrosegregation), and presence and distribution of porosity (as a result of gas dissolution, evolution, and entrapment). Convection also influences and aggravates preferential evaporation of certain alloying elements from the weld pool surface. Some of the forces that lead to convection in the weld pool also lead to weld pool oscillation, which also affects welding and welds. Understanding the origin of weld pool convection, oscillation and evaporation is essential to a full understanding of fusion welding processes and welding metallurgy.

10.1. ORIGIN OF CONVECTION

As defined by most popular dictionaries, convection is fluid motion caused by an external force (see Footnote 1). Convection is the result of forces all right, but these could just as well originate within the fluid as external to the fluid. In fact, in weld pools there are four different driving forces for convection; three of which have an external origin and one of which arises from within the weld pool. These four forces are (1) buoyancy or gravity force, (2) surface tension

[1] *The American Heritage Dictionary*, Second College Edition, Houghlin Mifflin Company, Boston, MA, 1982.

gradient force or Marangoni force, (3) electromagnetic or electromotive force (emf) or Lorentz force, and (4) impinging or friction force. All but the surface tension gradient force have an external origin. We will look at each in a moment, but first, let's look at some generalities of convection in weld pools.

10.1.1. Generalities on Convection in Weld Pools

The flow induced in the molten metal pool of a weld while it is being made is complex, as established by extensive observation and experiment. As shown schematically in Figure 10.1, immediately below an arc (as well as a beam and, to a much lesser extent, a gas flame) there is a depression, known as a *crater* or *pulsating arc cavity*, caused by the pressure of the impinging energy (in an arc or beam, ions, electrons, or photons with high kinetic energy and momentum). For arc welding processes, this depression can be quite deep; increasingly so for higher currents and current densities. This is because the momentum of the electrons and positive ions in the arc is fairly high. For electron-beam welding it is even deeper, given the even greater momentum due to much higher velocities of electrons, while for most laser beams and all gas flames, it tends to be less deep, as a result of much lower momentum due to much slower moving electrons and ions, or much less massive photons. Liquid metal flows rapidly around and under this depression or crater, then runs backward along the solid–liquid interface between the weld pool and unmelted base material, and, finally, reverses to produce a forward flow on the weld pool surface. This backward and forward flow is largely determined by the forward motion of the

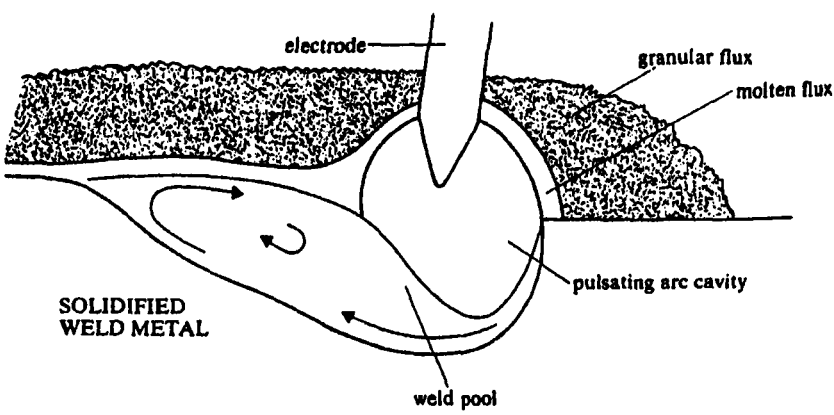


Figure 10.1 Schematic of the typical flow in a weld pool (shown here for submerged arc welding) from the forward (or leading) to trailing edge of the weld pool. There is also flow transverse to this direction due to one or more forces shown in Figures 10.2–10.5. (From *Metallurgy of Welding*, 5th ed., by J. F. Lancaster, published in 1993 by Chapman & Hall, London, and used with permission of Kluwer Academic Publishers, The Netherlands.)

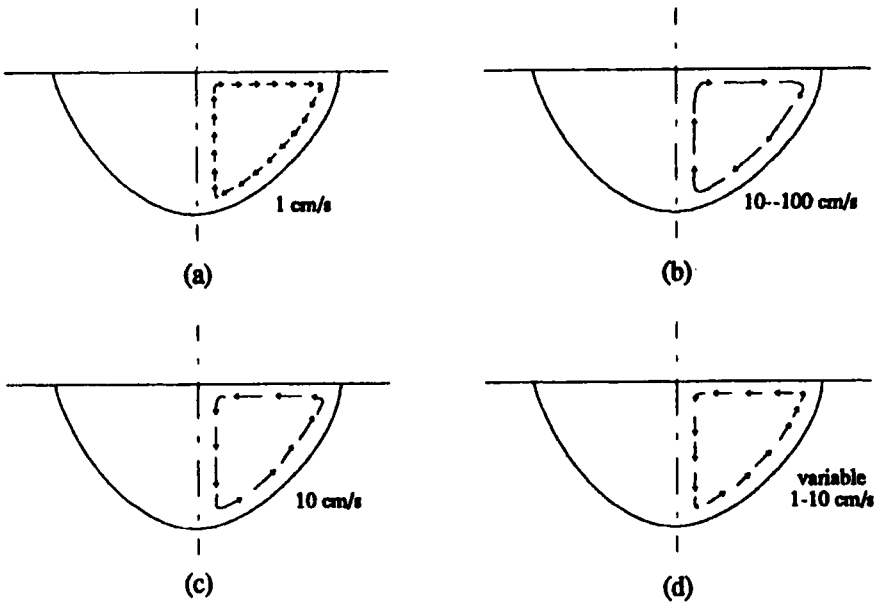


Figure 10.2 Schematic of the circulation or convection pattern induced by (a) only a buoyancy (or gravity) force; (b) only a surface tension gradient force or Marangoni force; (c) only an electromagnetic force (EMF) or Lorentz force; or (d) only an impinging force. The arrows shown direction, as well as relative velocity by their lengths.

arc (or other heat source) combined with the fact that there is a physical depression in the weld pool, both of which impose a rearward acceleration on the liquid metal.

Besides this fore-to-aft flow, flow can also be induced in a weld pool by the other forces mentioned earlier: buoyancy, electromagnetic, surface tension gradient, and/or friction. These forces produce flow in the cross section, as shown in Figure 10.2 for each individual force. This type of flow is generally referred to as *poloidal* or *meridional flow*. It can be generally inward across the weld pool surface, as shown in Figures 10.2c and d, in which case it is said to be *convergent*; or it can be outward, as shown in Figures 10.2a and b, in which case it is known as *divergent*. Convergent flows are inherently unstable and tend to break down into a spin. The reason for this is that as the flow reaches the central axis it becomes progressively more compressed, as well as being on a collision course with flow coming from the opposite direction. This causes the fluid to slip sideways to create a spin. Centrifugal forces associated with such spin set up pressure gradients that tend to oppose and slow down the convergent flow, but do not completely arrest it. The final result is *toroidal flow* (like flow around the surface of a donut into its center hole). This is the flow pattern normally seen when observing water flowing into a bucket from a hose

or in the atmosphere due to disturbances such as cyclones. Divergent flow does not suffer from such problems and is inherently stable.

10.1.2. Buoyancy or Gravity Force

The buoyancy force ($\mathbf{F}_b$) in weld pools, as elsewhere (e.g., atmospheric currents or weather, ocean currents, convection in castings), arises from gravity. It is defined as

$$\mathbf{F}_b = -\rho B g(T - T_0) \tag{10.1}$$

where ρ is the density of the liquid molten metal, B is the coefficient of thermal expansion of the liquid molten metal, g is the force of gravitational attraction, T is the temperature of interest, and T_0 is a reference temperature (normally, room temperature). It can be seen that this force has its origin in gravity as that force acts differently on regions of the weld pool fluid with different densities. Density differences in a molten weld pool can, in turn, have two origins: (1) the local temperature and (2) the local composition. While density differences due to differences in local composition can certainly play a role in leading to convection in a weld pool (due to chemical heterogeneity arising from macrosegregation, as discussed in Section 12.4), the density differences of greater general interest are more due to differences in local temperature.

Liquids are most dense just above the temperature at which they form, that is, the material's melting temperature. As temperature increases above the melting temperature, the density of a liquid decreases (because increased thermal motion acts to break down the attractive forces that tend to keep the atoms or molecules comprising the liquid together). Thus, hot, superheated regions of molten metal in a weld pool are of lower density than cooler regions. Cooler, more dense molten metal sinks under the force of gravity, causing hotter, less dense molten metal to be displaced and rise.

Like all forces, the force of buoyancy is a vector, meaning that it has both a magnitude and a direction (hence, the reason $\mathbf{F}_b$ and other forces leading to convection are shown in bold font). The magnitude is g and the direction is toward the center of the earth. The result of gravity or buoyancy in a weld pool is to cause circulation of the molten metal in the weld pool. Since molten metal in the pool is coolest and most dense nearest the fusion zone or pool boundary, molten metal near the edge of the pool sinks. This causes a circulation that causes hotter, less dense molten metal near the center of the weld pool to rise. Given the distribution of energy from most fusion welding sources, the center of a weld pool is almost always the hottest region (at least immediately upon the pool's formation). The resulting circulation or convection pattern is shown in Figure 10.2a.

As one can imagine, studying convection in hot, opaque, reactive molten weld metal is quite difficult; however, many studies have been attempted, with greater or lesser success. Research examining the mixing of dissimilar metal

droplets (Woods and Milner, 1971) or fine, inert, and refractory Al_2O_3 particles (Heiple and Roper, 1981, 1982) in weld pools has shown the relative velocity to be of the order of 1 cm/s.

As seen in Section 10.1.6, the major effort aimed at understanding in greater detail the dynamics of the heat and fluid flow in the weld pool so as to understand better the development of weld pool shapes and, eventually, predict weld geometries, relies on modeling.

10.1.3. Surface Gradient Force or Marangoni Convection

Every liquid has a surface tension, as discussed in Section 9.1.8. It turns out the surface tension of a liquid depends on the temperature of that liquid (for a uniform and constant composition) and increases with decreased temperature to become maximum just above the melting point. Thus, whenever a temperature gradient exists in a liquid, so too does a gradient in surface tension. This gradient exerts a force ($\mathbf{F}_\gamma$) given by

$$\mathbf{F}_\gamma = -\frac{d\gamma}{dT}\nabla T \tag{10.2}$$

where γ is the surface tension of the molten metal, T is the temperature, and ∇T is the temperature gradient at the weld pool surface.

Again, much work has concentrated on surface tension gradient effects and how they generate convective flows in the weld pool. The spatial variation of the surface tension (i.e, the gradient) present on the weld pool surface can cause the molten metal to be drawn along the surface from the region of low surface tension to the region of higher surface tension, with the variation really coming from two possible sources: temperature variation and composition variation. As temperature increases for a liquid of fixed composition, the surface tension decreases. Composition gradients act to complicate temperature effects, depending on how a change in the composition of any particular component affects the surface tension (these surface activating agents are discussed later).

Study of weld pool convection in GTA welding of stainless steel using fine particles of Al_2O_3 as markers (Heiple and Roper, 1981, 1982) revealed that surface tension gradients give rise to an extremely strong circulation at rates from 10 to 100 cm/s from the hotter, lower surface tension liquid at the center of the weld pool to the cooler, higher surface tension liquid at the pool edges. This circulation pattern, which is in the same direction as circulation for the buoyancy force, is shown schematically in Figure 10.2b.

Impurities in weld metal often alter the surface tension of the molten metal through their surface activity. Heiple and Roper (1981) and Heiple et al. (1983) showed that the surface tension gradient at the weld pool surface could be changed by the addition of surface-activating agents such as O, S, Se, and Te. The effect on molten stainless steel was to reverse the convection pattern, and, thus, weld pool shape, as shown in Figure 10.3.

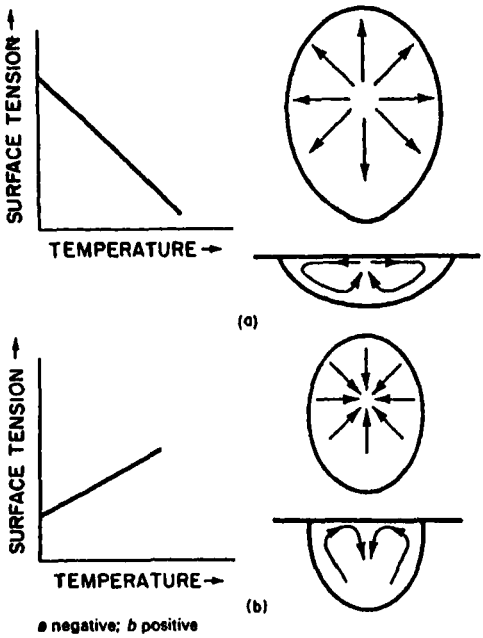


Figure 10.3 Different convective flow patterns produced by different temperature coefficients of surface tension. In (a), the pattern of convective flow without a surface-active agent; in (b) the effect of adding a surface-active agent. (From "Correlation between solidification parameters and weld microstructures" by S. A. David and J. M. Vitek, *International Materials Review*, 34(5), 213–245, 1989, with permission).

From these and other studies, the surface tension gradient force has been concluded to be the dominant force driving convection in weld pools. (This was made painfully obvious, and at great expense, in early studies of convection in the microgravity of earth orbit, where expected effects of greatly reduced buoyancy force were overwhelmed by surface tension gradient forces that caused circulation of the same general pattern.) The surface tension gradient force is also known as the Marangoni force, after its discoverer.

10.1.4. Electromotive Force or Lorentz Force

Electromagnetic theory predicts that electric and magnetic fields interact with one another to produce a force in an orthogonal direction when the electric force is crossed with the magnetic force using the right-hand rule.[2] This force

[2] In the right-hand rule, if the fingers of the open right hand are held in the direction of the electric field (current flow) and closed in the direction of the magnetic field, the extended thumb points in the direction of the resulting force. This process represents what is referred to in mathematics as the cross product of two vectors; one representing the electric field (current flow) and the other representing the magnetic field (flux lines).

is called the electromotive force or emf, and is also known as the Lorentz force (see Section 8.1). The emf is given by

$$\mathbf{F}_{em} = \mathbf{J} \times \mathbf{B} \tag{10.3}$$

where **J** is the vector of current density (with a direction the same as the current, positive to negative) and **B** is the vector of magnetic flux (with a direction the same as the flux lines). The effect is particularly pronounced due to the divergent current path in the weld pool and the magnetic field it generates.

Studies by Woods and Milner (1971) using dissimilar metal (indium) markers showed much more rapid circulation for gas–tungsten arc (GTA) welding in a (bismuth–tin eutectic) weld pool than for oxyacetylene (OA) welding and that the directions of circulation were opposite one another. The reason is that emf is induced in the weld pool by interaction between the magnetic field associated with current flow in the tungsten electrode and the induced electric current flow in the weld pool. The direction of the resulting circulation is from the edge to the center of the weld pool, as shown schematically in Figure 10.2c. The magnitude of this force leads to a circulation velocity of about 10 cm/s.

Obviously, electromagnetic or Lorentz forces are present only for processes using an electric energy source, namely arc, resistance, microwave, or electron-beam processes, and are totally absent for gas and laser-beam welding. The degree of stirring or circulation induced is proportional to the strength of the fields involved, so welding current (or voltage in EBW) plays a major role.

10.1.5. Impinging or Friction Force

Just as dropping pebbles into the center of a bucket filled with water will cause a circulating flow to develop from the edges to the center of the bucket (i.e., toroidal flow), so too will rapidly impinging particles from a welding source induce circulating flow in a weld pool. The impinging force is the result of momentum transfer through friction between impinging particles and metal atoms in the molten weld pool. Since most fusion welding processes use arcs, this force is often called the arc plasma force, but that term is too specific to be appropriate to all processes.

Whether the active particles are electrons or ions in arc, plasma, or electron-beam welding, or photons in laser-beam welding, they have kinetic energy (to be converted into heat upon collision with atoms in the workpiece) and they have momentum. Obviously, the momentum of rapidly moving electrons is greater than that of photons, even though photons move at the speed of light. The reason for this is that electrons (and ions) have much, much greater mass than photons. Thus, the magnitude of the impinging force depends on the process, but the flow pattern is always from edge-to-center of the weld pool, as shown in Figure 10.2d. This is because more energy is

deposited at the center of weld pools than near their edges as a result of the normal (Gaussian) distribution of energy in most sources (see Section 5.3.4).

10.1.6. Modeling Convection and Combined Force Effects

There have been many efforts to model weld pool convection because of its importance to weld pool and final weld profile or shape, homogeneity, and freedom from defects like porosity. These began with the work of Oreper et al. (1983) for two-dimensional convection for stationary arc (spot) weld pools. Work progressed with seminal studies by Heiple and Roper (1982) and Heiple et al. (1983–1985), and by many others, including Kou and Sun (1985), Oreper and Szekely (1984), and Chan et al. (1984). The first three-dimensional models were developed by Kou and Wang (1986), and much more elaborate and accurate models were developed by Zacharia et al. (1991) and others (e.g., Zhang et al., 1996; Lee and Na, 1997; Joshi et al., 1997; and Mundra et al., 1997).

The major observation of consequence is this: Weld pool convection is seldom the result of a single force (i.e., buoyancy, emf, surface tension gradient, or impinging friction), but is usually the result of combinations of forces that depend on (1) the individual process (e.g., gas, arc, or laser), (2) how that process is operated (e.g., polarity, current level, travel speed), and (3) material effects and interactions between the weld and its environment (including atmosphere and contaminants).

Velocity and temperature fields in a stationary GTA weld pool computed by Kou and Sun (1985) are shown for individual forces in Figure 10.4. Velocity and temperature fields in a stationary GTA weld pool also computed by Kou and Sun (1985) for combined forces are shown in Figure 10.5. Computed velocity and temperature fields for moving GTA weld pools are shown in Figures 10.6 and 10.7 (Kou and Wang, 1986). A simple schematic of the different flow patterns that can arise in gas–tungsten arc (GTA) welding, depending on the particular surface-tension gradient force is shown in Figure 10.8.

The key conclusion to be drawn from all models of combined forces is that circulation patterns can be complex. Note, for example, that the weld pool motion due to the combined effects of buoyancy, electromagnetic, and surface tension gradient forces (shown in Figure 10.8) consists of two flow loops in opposite directions: one near the weld pool surface dominated by the surface tension gradient, and one in the bulk of the pool dominated by emf versus buoyancy. As one can imagine, moving weld pools from moving heat sources exhibit even more complex and nonsymmetrical 3-D flow patterns.

10.2. EFFECTS OF CONVECTION

Convection in a weld pool, whether that weld pool is stationary or moving, has profound effects on the pool's shape (especially penetration), chemical homo-

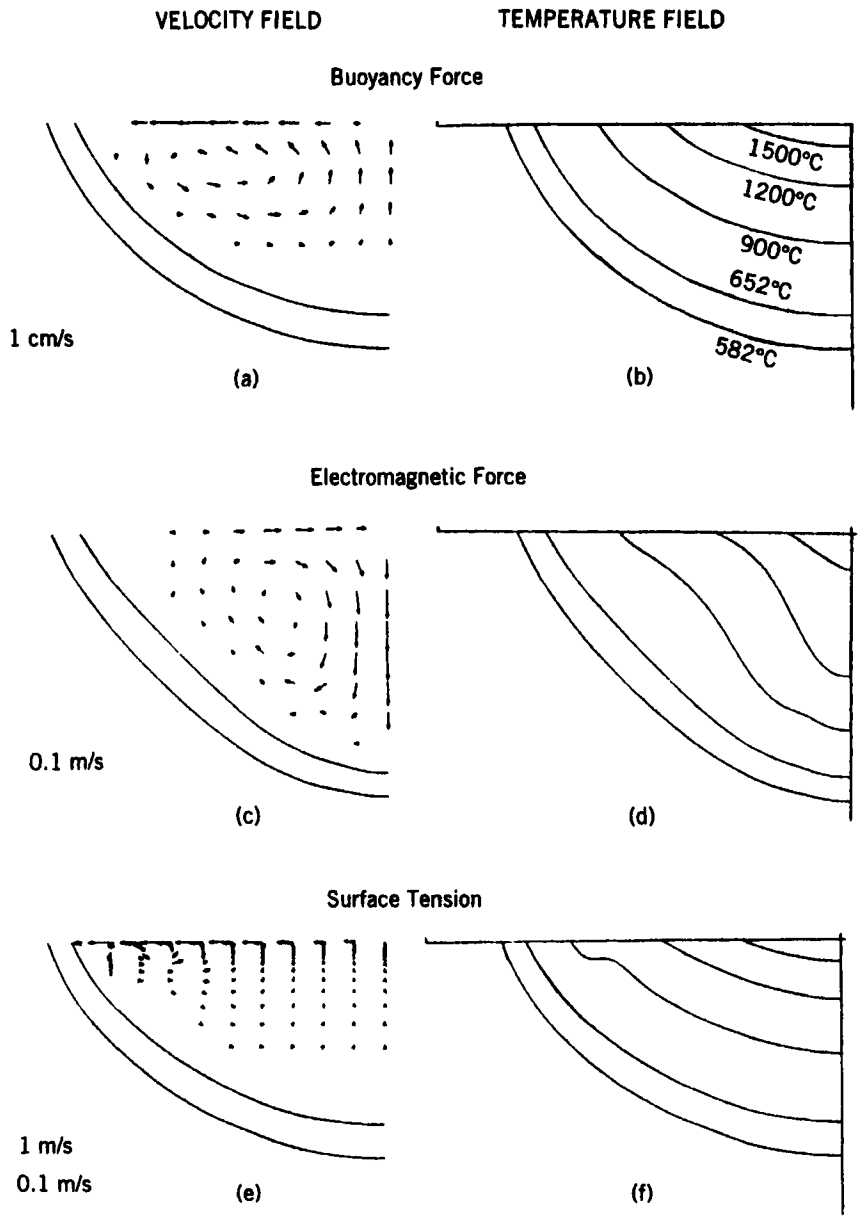


Figure 10.4 Computed velocity (on the left) and temperature (on the right) fields in a stationary GTA weld pool in AA6061 aluminum alloy due to individual driving forces of (a, b), buoyancy, (c, d) electromagnetic, and (e, f) surface tension gradient forces. The magnitudes of velocities are represented by the lengths of arrows. (From "Fluid flow and weld penetration in stationary arc welds" by S. Kou and D. K. Sun, *Metallurgical Transactions*, **16A**(Feb.), 203–213, 1985, published by and used with permission of the ASM International, Materials Park, OH.)

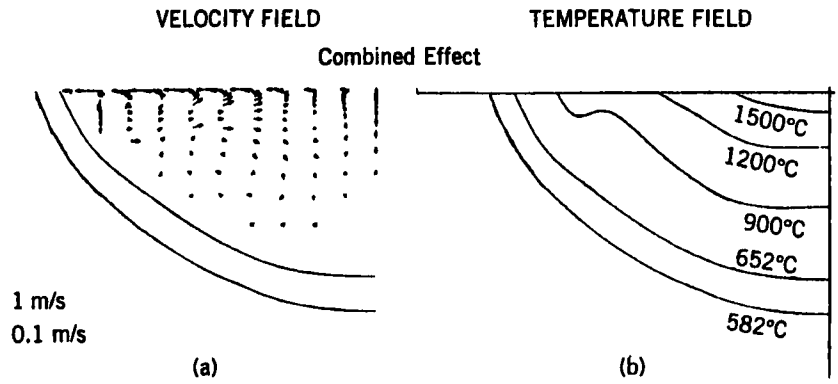


Figure 10.5 (a) Computed velocity and (b) temperature fields in a stationary GTA weld pool in AA6061 aluminum alloy due to the simultaneous action of buoyancy, electromagnetic, and surface tension gradient forces. The magnitudes of velocities are represented by the lengths of arrows. (From "Fluid flow and weld penetration in stationary arc welds" by S. Kou and D. K. Sun, *Metallurgical Transactions*, **16A**(Feb.), 203–213, 1985, published by and used with permission of the ASM International, Materials Park, OH.)

geneity, and porosity. Let's look at each effect, some of which can be favorable and some of which can be unfavorable.

10.2.1. Effect of Convection on Penetration

The pattern of fluid flow in a weld pool strongly affects the weld pool's shape, and especially its penetration. Moving fluid tends to erode surrounding unmelted base material, particularly since the moving molten weld metal redistributes superheat and can cause melting known as *recalescence*. Three effects are worth highlighting. First, when the electromagnetic force dominates (as it does for most arc welding processes), heat from the source is delivered to the top surface of the workpiece to produce a weld in the melt-in mode (see Section 3.3.1.2). The electromagnetic force causes downward circulation at the center of the weld pool, moving hot, superheated molten metal to the bottom of the pool at its center. This superheat causes additional melting here, leading to deeper than would be expected penetration without convection of this sort. The more pronounced (from increasing current level) and localized (from more concentrated current density) the emf effect, the more pronounced and localized the additional cratering. As a result, a deep spot can arise, as shown schematically in Figure 10.9a.

Second, buoyancy forces and, especially, surface tension gradient forces, which cause weld pool circulation in the same basic direction, resist the effect of any emf. The result is that, in the absence of an emf, or where emf is overwhelmed, the weld pool is caused to be wider and shallower than would

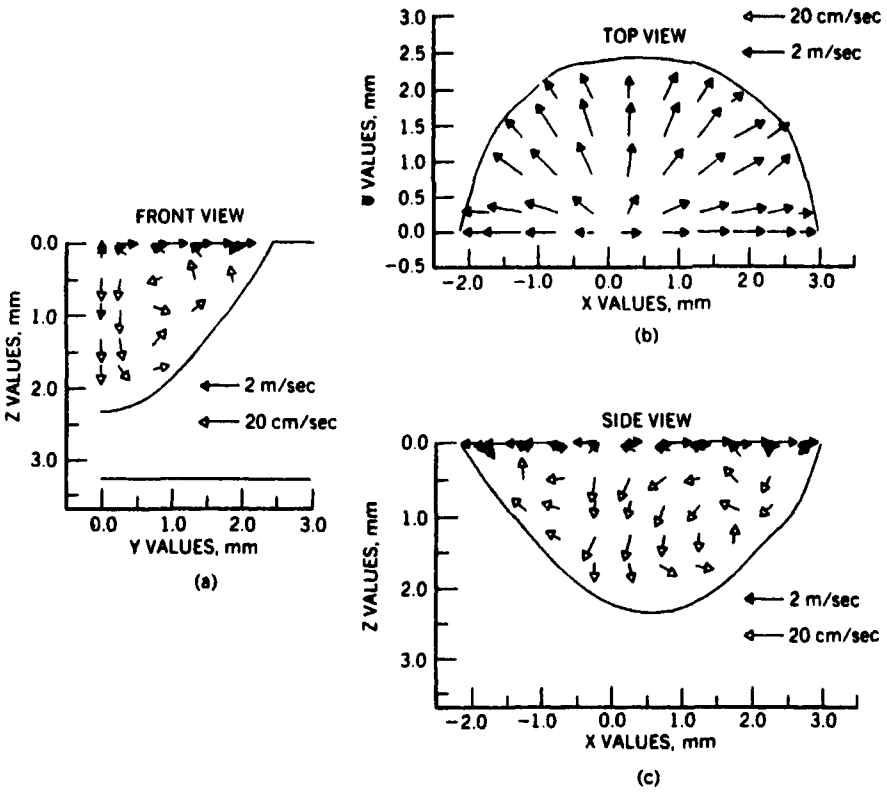


Figure 10.6 Computed velocity and temperature fields in a moving GTA weld pool of 3.2-mm-thick AA6061 aluminum alloy due to the simultaneous action of buoyancy, electromagnetic, and surface tension gradient forces. The coordinate system is such that the welding direction is perpendicular to the page in (a), and from right to left in (b) and (c), and the magnitudes of velocities are represented by the lengths of arrows. (From "Weld pool convection and its effects" by S. Kou and Y. H. Wang, *Welding Journal*, 65(2), 63s–70s, 1986, published by and used with permission of the American Welding Society, Miami, FL.)

be expected without convection. This effect is shown schematically in Figure 10.9b.

Finally, a dominant impinging force, such as is present in processes operating in the keyhole mode, results in exceptional penetration near the center of the weld pool at its bottom. This is shown schematically in Figure 10.9c.

10.2.2. Effect of Convection on Macrosegregation

If mixing in a weld pool due to convection is insufficient, macrosegregation can occur when either (1) heterogeneous filler is added (see Section 2.2.5) or (2)

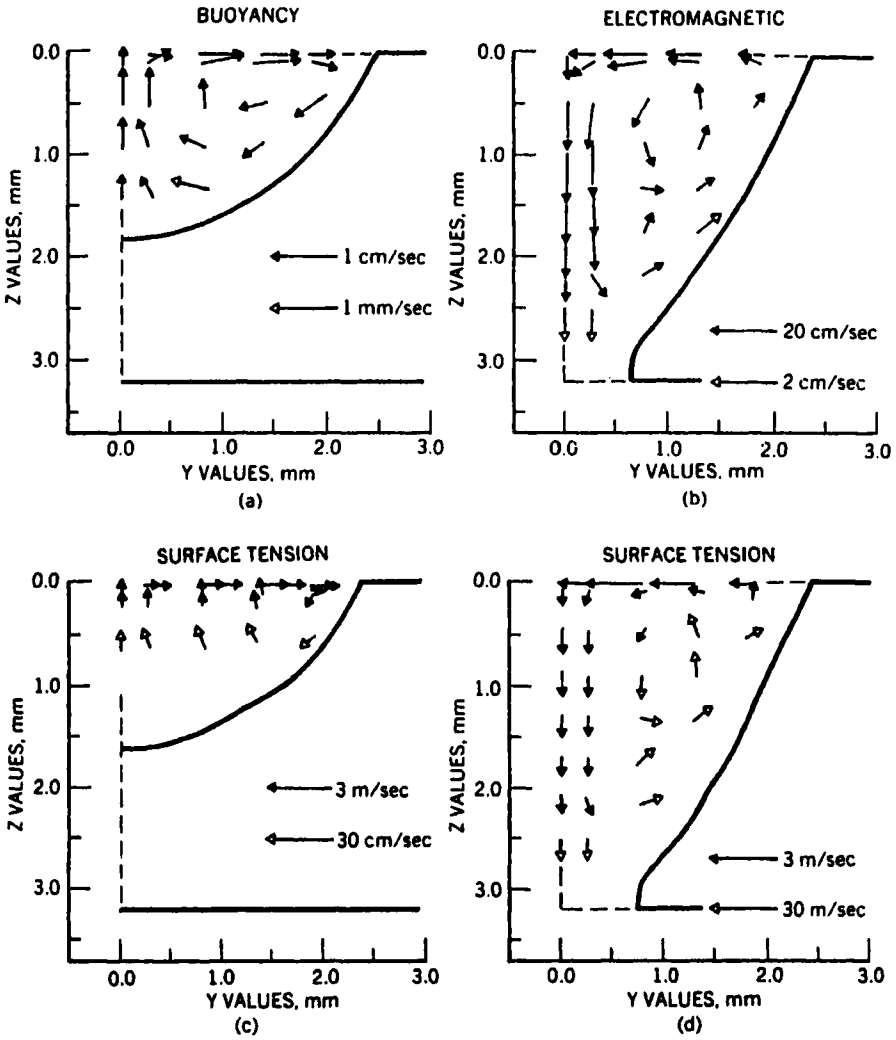


Figure 10.7 Front views of computed velocity fields in a moving weld pool of 3.2-mm-thick AA6061 aluminum alloy due to individual driving forces of (a) buoyancy, (b) electromagnetic, and (c) surface tension gradient forces with $d\gamma/dT = -0.35\,\text{kg/s}^2\,^\circ\text{C}^{-1}$, and (d) surface tension gradient with $d\gamma/dT = +0.35\,\text{kg/s}^2\,^\circ\text{C}$. The magnitudes of velocities are represented by the lengths of arrows. (From "Weld pool convection and its effects" by S. Kou and Y. H. Wang, *Welding Journal*, 65(2), 63s–70s, 1986, published by and used with permission of the American Welding Society, Miami, FL.)

dissimilar material substrates are welded together autogenously. This macrosegregation is especially pronounced in a plane transverse to the weld line, as shown schematically in Figure 10.10. Macrosegregation is distinctly different from microsegregation both in severity and origin. Microsegregation arises as the natural consequence of solute redistribution that takes place during the

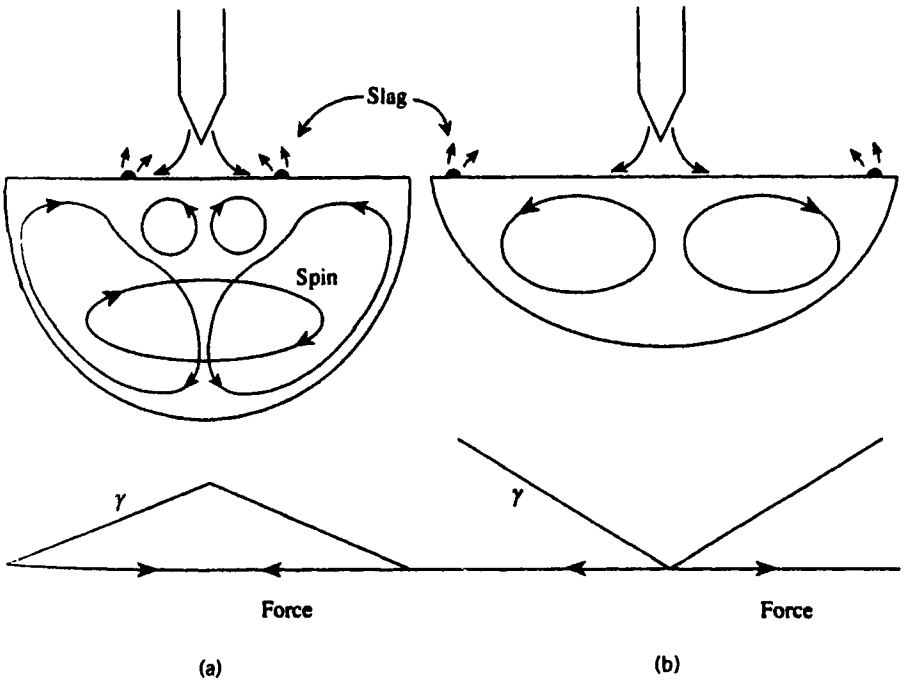


Figure 10.8 Simple schematic of the flow in a gas–tungsten arc weld pool under the combined effects of buoyancy and electromagnetic forces for a surface tension gradient force ($d\gamma/dT$) that is (a) positive and (b) negative. (From *Metallurgy of Welding*, 5th ed., by J. F. Lancaster, published in 1993 by Chapman & Hall, London, and used with permission of Kluwer Academic Publishers, The Netherlands.)

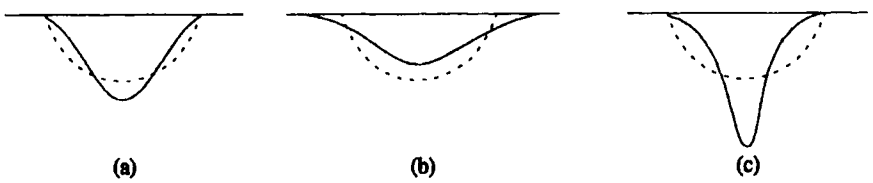


Figure 10.9 Schematic showing the effects of particular dominant driving forces for convection on weld pool shape, including (a) greater penetration at the bottom-center of a weld pool due to convection enhanced by a dominant electromagnetic (Lorentz) force, (b) shallower but wider penetration due to convection dominated by either a buoyancy or surface tension gradient force (or both together), and (c) pronounced deepening at the weld pool bottom due to convection enhanced by a dominant impinging force. A theoretical, semicircular cross section is shown by a dashed line for comparison.

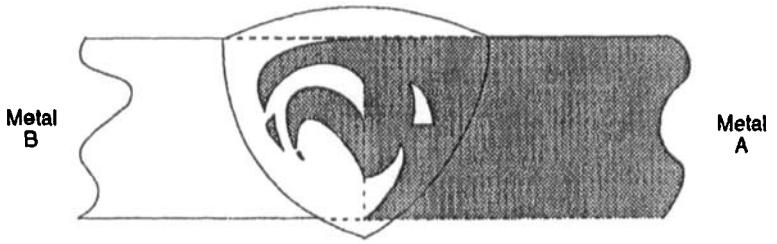


Figure 10.10 Schematic of macrosegregation in a weld pool, as affected by convection or its absence, when different base metals (A and B) are welded autogenously.

solidification of alloys under nonequilibrium conditions, as discussed in Chapter 13.)

The electromagnetic force in arc welding and the impinging force for EBW or PAW tend to promote mixing and reduce the tendency for macrosegregation. Macrosegregation can be quite severe, on the other hand, for laser-beam welding operating in the melt-in mode, because there is no electromagnetic force (due to the absence of an electric current flow) and little impinging force (due to the low momentum of photons). Surface tension gradient force tends to dominate. The effect is made worse by the typically high welding speeds possible with laser-beam welding due to its high energy density, and by the fact that laser welding is usually performed autogenously, so there is no opportunity for dilution of dissimilar base metals by added filler.

Regardless of the degree or intensity of convection present in a weld pool, there exists an unmixed zone, first reported by Lippold and Savage (1980). This thin layer of liquid metal near the weld pool boundary exists because of friction. The lack of mixing or stagnation causes this zone to differ significantly in composition from the bulk fusion zone, thereby frequently rendering it susceptible to preferential corrosive attack. More is said about this zone in Chapter 12.

10.2.3. Effect of Convection on Porosity

Convection in a weld pool is a two-edged sword. On the one hand, it promotes stirring and so tends to promote homogeneity. On the other hand, it exposes fresh, reactive molten metal to the surroundings at the weld pool surface, thus helping to promote any gas–metal reactions that might occur (see Section 11.1). Absorbed gases in molten weld metal can lead to porosity, among other things, upon solidification. Weld pool convection is generally viewed as helpful in reducing gas porosity in the final solidified weld because it is seen as sweeping it out of the circulating weld pool. But, this is not always true. It depends on the specific flow pattern of the convection.

The situation is shown schematically in Figure 10.11. Since most gases have lower solubility in cooler molten metals than in hotter ones, gas, in the form

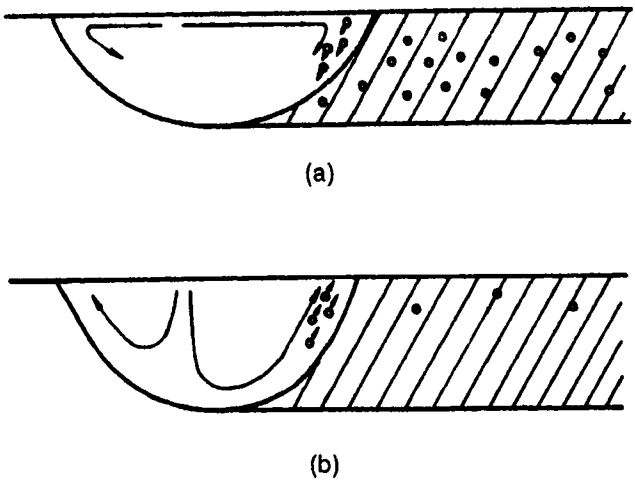


Figure 10.11 Schematic of the two possible effects of different convection pattern on gas porosity in a weld pool. (From *Welding Metallurgy* by S. Kou, published in 1987 by and used with permission of John Wiley & Sons, Inc., New York.)

of bubbles (to become pores in the final, solidified weld) are rejected at the solidification front, which is at the instantaneous edge of the weld pool. Depending on the convection pattern, these bubbles might be swept downward to become trapped by being frozen in throughout the weld, or they might be immediately swept toward the weld pool surface to escape to the surrounding atmosphere, never to become a trapped pore. When emf-induced flow occurs, there is an upward sweeping action acting on gas bubbles as they are formed at the weld pool edges (i.e., solidification front). Much of the gas escapes, resulting in much lower overall porosity.

10.3. ENHANCING CONVECTION

Convection can be enhanced by causing one of the driving forces to become larger and predominate. Every one of the four driving forces is fair game, in that any one can be preferentially increased, in theory, even if not, until recently (with space flight and microgravity), in practice.

The electromagnetic or electromotive force can be enhanced in three ways. First, switching from a nonelectric fusion welding process (e.g., oxyfuel gas welding) creates an emf where there was none. Second, raising the welding current increases **J** and **B** in Eq. 10.3. But doing this has consequences, not the least of which is greatly increased heat input. As discussed in Chapters 6 and 7 and later in Chapters 13, 15, and 16, increased heat input causes increased distortion and residual stresses and increased heat-induced, adverse changes in composition, microstructure, and metallurgical transformations. However, it is

possible to enhance the electromagnetic force without raising the welding current to unacceptable levels using a third approach. The principal method is to employ an external magnetic field around the weldment during welding to cause greater interaction between a larger **B** and **J** (see Eq. 10.3).

The impinging force can be enhanced by employing higher welding currents, for any arc welding process, by switching from a melt-in to a keyhole mode for processes where that is possible (e.g., PAW, EBW, and LBW), or by increasing the welding voltage, especially for EBW.

As mentioned earlier, the surface tension gradient force can be altered by adding surface-activating agents such as O, S, Se, or Te. The most preferred method is to add oxygen (in amounts of 2–5%) to argon in inert gas-shielded processes (especially GMAW). This, as well as addition of S, Se, or Te, is not without consequence, however, because oxygen can cause potent interstitial solid solution hardening, as well as possible phase stabilization in some alloy systems (namely, alpha-phase in Ti-based alloys), while S, Se, and Te all tend to promote low-melting constituents that can promote hot cracking during solidification (see Chapter 13).

Until the advent of space travel, control over the buoyancy force as a contributor to convection was virtually impossible. Today, however, welding (or other melt-processing) in the microgravity of earth orbit raises the possibility of removing this potentially problematic driver of convection. The best examples are the growth of fine crystals, and the growth of ultrapure materials.

Two other possibilities for inducing convection through the electromagnetic force need to be mentioned. First, arc oscillation, either transverse to the welding direction or in circulating patterns, tends to induce a circular flow in the weld pool that can be used to reduce macrosegregation, remove porosity, or alter solidification substructure by causing refinement due to dendrite fragmentation or grain detachment (see Chapter 13). Second, current pulsing can have a similar effect.

10.4. WELD POOL OSCILLATION

Besides the aforementioned forces that lead to convection, weld pools that are subject to a periodic force that acts normal to the surface may oscillate. In fact, a very large number of oscillation modes are possible, but the simplest are shown in Figure 10.12. Figure 10.12a, b illustrates axisymmetric modes for partial and full penetration, respectively, while Figure 10.12c illustrates an asymmetric mode for partial penetration that can arise in a moving weld pool.

Weld pool oscillation is particularly pronounced in the short-circuiting welding mode, where the small electrical explosion that occurs drives the center of the weld pool surface downward. On its return, the surface collides with the welding electrode and initiates another short-circuit. A portion of the spatter that is characteristic of this transfer mode comes from the weld pool in this

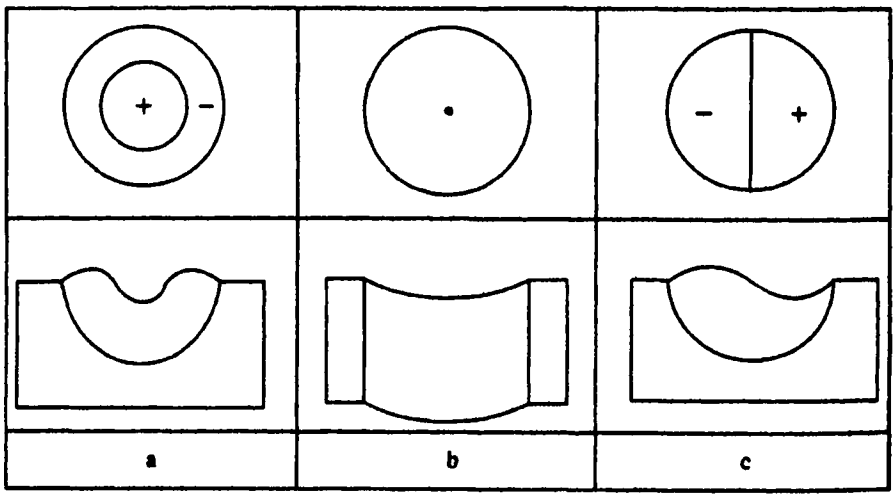


Figure 10.12 Schematic showing some possible oscillation modes for a weld pool: (a) axisymmetric, partial penetration; (b) axisymmetric, full penetration; and (c) asymmetric, partial penetration. (From *Metallurgy of Welding*, 5th ed., by J. F. Lancaster, published in 1993 by Chapman & Hall, London, and used with permission of Kluwer Academic Publishers, The Netherlands.)

way. The amount of spatter can thus be minimized if the frequency of electrical oscillation of the power source coincides with the natural oscillation frequency of the weld pool. Where this is not the case, the motion of the pool is erratic and some splashing of molten metal will occur. Alternatively, the electric circuit oscillation could be controlled to damp down weld pool oscillation. Weld pool oscillation occurring with SMAW and FCAW gives rise to the rippled appearance of the weld surface or crown bead, at least partially. Other sources of rippling and banding within the weld are discussed in Chapter 12.

The pools of gas–tungsten arc welds also oscillate when subjected to current fluctuations. The natural oscillation frequency of pools associated with partial penetration welds is much greater than that associated with full-penetration welds, as shown in Figure 10.13. Monitoring weld pool oscillation has therefore been studied as a means of feedback control of weld penetration (Xiao and den Ouden, 1993; Kovacevic et al., 1996; Anderson et al., 1997).

10.5. WELD POOL EVAPORATION AND ITS EFFECTS

Since the temperatures of heat sources used for welding are so high, significant metal vaporization can occur. Most of this evaporation, due either to exceeding the boiling point of the weld metal or causing the vapor pressure of a component of the weld metal to exceed its partial pressure in the surrounding atmosphere, takes place in molten metal drops or droplets during their transfer

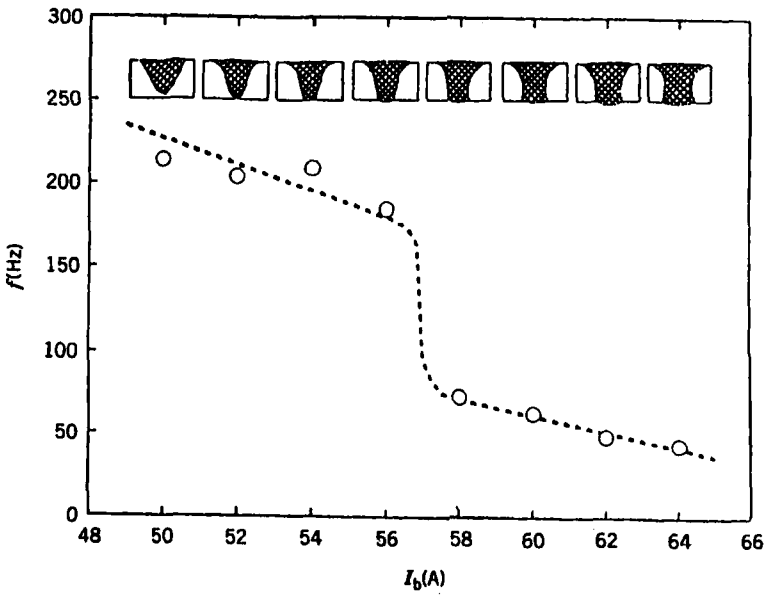


Figure 10.13 Oscillation frequency as a function of base current (I_b) for pulsed-current He-shielded GTAW (pulsed current 300 A, duration 2.4 ms). The drop in frequency occurs just above the current required for full penetration. (From *Metallurgy of Welding*, 5th ed., by J. F. Lancaster, published in 1993 by Chapman & Hall, London, and used with permission of Kluwer Academic Publishers, The Netherlands.)

through an arc to the weld pool. However, significant evaporation can also occur from the surface of weld pools, especially as exacerbated by convection.

Evaporation loss from weld pool surfaces occurs according to

$$r_A = 44.33\bar{P}_A\left(\frac{M_A}{T}\right)^{1/2} \quad (\text{g/s cm}^{-2}) \tag{10.4}$$

where r_A is the rate of evaporation of element A, M_A is the atomic weight of element A, T is the temperature (in K), and $\bar{P}_A$ is the partial pressure of element A in the gas phase above the weld at equilibrium. The partial pressure of element A in the gas phase is, in turn,

$$\log \bar{P}_A = \log P_A^0 + \log a_A \tag{10.5}$$

where P_A^0 is the standard pressure of element A in the atmosphere and a_A is the activity of element A in the weld pool. Preferential evaporation of some solute elements is quite high, including Mn (from steels and stainless steels), Mg (from aluminum alloys), and Zn (from brasses).

Figures 10.14a and b give vapor pressures for some key solute additions in aluminum alloys and steels, respectively. These were developed by Block-Bolten and Eager (1984) using existing activity data and simplifying assumptions in the applicable thermodynamics.

Evaporation of alloying elements is a potential problem not only because it changes the composition of a weld filler or weld pool, which could degrade properties (especially corrosion resistance), but also because evaporation removes heat, which can have adverse effects on solidification. The way to prevent evaporation is to employ a process in which molten metal transfer occurs by a slag-protected mode (e.g., SAW or ESW, and to lesser degrees,

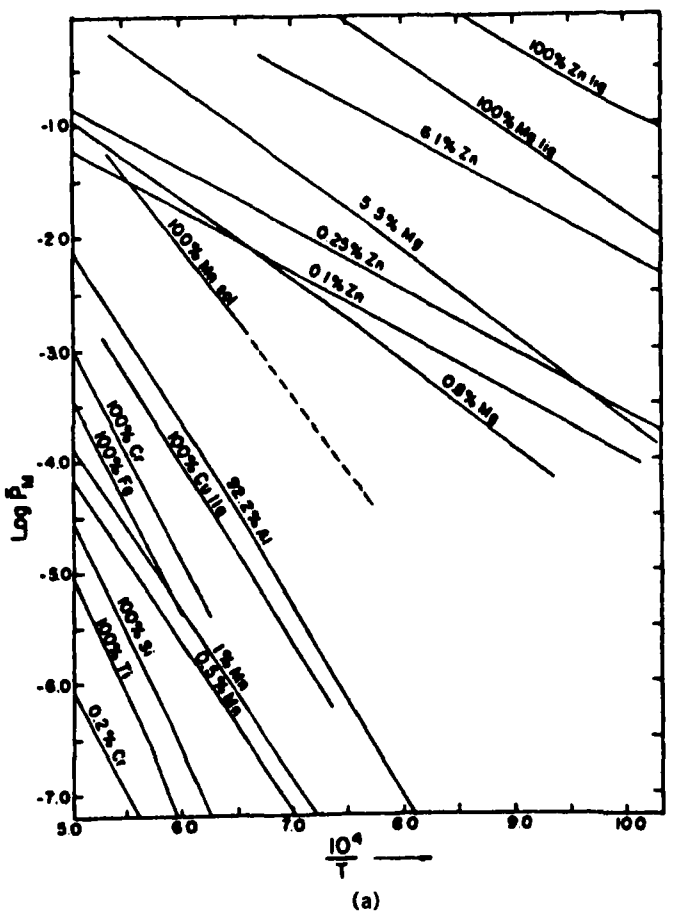


Figure 10.14 Vapor pressures for some constituent alloy additions in (a) aluminum alloys and (b) steels. (From "Metal vaporization from weld pools" by A. Block-Bolten and T. W. Eager, 1984, *Metallurgical Transactions*, **15B**(Sept.), 461–469, 1984, published by and with permission of the ASM International, Materials Park, OH.)

SMAW and FCAW). A way to offset the effects of evaporation is to use a filler that is richer in the volatile component than needed to match the base metal or meet service needs. In this way, any evaporative loss is made up for by having extra solute present in the first place.

10.6. SUMMARY

The weld pool in most fusion welding processes is subjected to several forces that lead to convection. The four possible driving forces are (1) buoyancy (due to gravity's effect on molten metal of different density because of its local temperature); (2) surface tension gradient (due to differences in surface tension of liquids because of differences in local temperature); (3) electromagnetic forces (due to the interaction between current flow and magnetic flux lines around conductors and the weld); and (4) impinging forces (due to friction between electrons, ions, or photons and atoms in the molten weld pool). Each force produces a particular flow pattern, in terms of direction and velocity. More often than not, multiple forces lead to complex flow patterns. Whatever the driving force, convection can have pronounced effects on weld pool shape (especially penetration), macrosegregation, and porosity presence and distribution. By understanding the driving forces and their effects on weld pools, it is possible to enhance one over another to achieve certain objectives. Some of the forces that lead to convection in the weld pool also cause the weld pool to oscillate. How that oscillation occurs is affected by penetration, and can be used as a means of penetration monitoring and control and can affect the way in which short-circuiting transfer occurs. An important consequence of convection is that it tends to promote evaporation from high vapor pressure solutes from weld metal, and this can also be problematic.

REFERENCES AND SUGGESTED READING

Anderson, K., Cook, G. E., Barnett, R. J., and Strauss, A. M., 1997, "Synchronous weld pool oscillation for monitoring and control," *IEEE Transactions on Industrial Applications*, **33**(Mar.–Apr.), 464–471.

Block-Bolten, A., and Eager, T. W., 1984, "Metal vaporization from weld pools," *Metallurgical Transactions*, **15B** (Sept.), 461–469.

Chan, C., Mazumder, J., and Chen, M. M., 1984, "A two-dimensional transient model for convection in a laser melted pool," *Metallurgical Transactions*, **15A** (Dec.), 2175–2184.

Choo, R. T. C., and Szekely, J., 1992, "Vaporization kinetics and surface temperature in a mutually coupled spot gas tungsten arc weld and weld pool," *Welding Journal*, **71**(3), 77s–93s.

Heiple, C. R., and Burgardt, P., 1985, "Effects of SO_2 shielding gas additions on gas tungsten arc weld shape," *Welding Journal*, **64**(6), 159s–162s.

Heiple, C. R., and Roper, J. R., 1981, "Effect of selenium on gas tungsten arc weld fusion zone geometry," *Welding Journal*, **60**(8), 143s–145s.

Heiple, C. R., and Roper, J. R., 1982, "Mechanism for minor element effects on gas tungsten arc fusion zone geometry," *Welding Journal*, **61**(4), 97s–102s.

Heiple, C. R., Roper, J. R., Stagner, R. T., and Aden, R. J., 1983, "Surface active element effects on the shape of GTA, laser, and electron beam welds," *Welding Journal*, **62**(3), 72s–77s.

Heiple, C. R., Burgardt, P., and Roper, J. R., 1984, in *Modeling of Casting and Welding Processes II*, edited by J. A. Dantzig and J. T. Berry, TMS, Warrendale, PA, 193–205.

Joshi, Y., Dutta, P., Schupp, P. E., and Espinosa, D., 1997, "Nonaxisymmetric convection in stationary gas tungsten arc weld pools," *Transactions of the ASME, Journal of Heat Transfer*, **119**(2), 164–172.

Kou, S., and Sun, D. K., 1985, "Fluid flow and weld penetration in stationary arc welds," *Metallurgical Transactions*, **16A**(Feb.), 203–213.

Kou, S., and Wang, Y. H., 1986, "Weld pool convection and its effects," *Welding Journal*, **65**(2), 63s–70s.

Kovacevic, R., Zhang, Y. M., and Li, L., 1996, "Monitoring of weld joint penetration based on weld pool geometrical appearance," *Welding Journal*, **75**(10), 317s–329s.

Kumar, S., and Bhaduri, S. C., 1994, "Three-dimensional finite element modeling of gas metal–arc welding," *Metallurgical Transactions*, **25B**(Jun.), 435–441.

Lee, S.-Y., and Na, S.-J., 1997, "A numerical analysis of molten pool convection considering geometric parameters of the cathode and anode," *Welding Journal*, **76**(11), 484s–491s.

Lippold, J. C., and Savage, W. F., 1980, "Solidification of austenitic stainless steel weldments, part 2: the effect of alloy composition on ferrite morphology," *Welding Journal*, **59**(2), 48s–58s.

Mundra, K, Debroy, T., Babu, S. S., and David, S. A., 1997, "Weld metal microstructure calculations from fundamentals of transport pheonomena in the arc welding of low-alloy steels," *Welding Journal*, **76**(4), 163s–171s.

Oreper, G. M., and Szekely, J., 1984, "Heat- and fluid-flow phenomena in weld pools" *Journal of Fluid Mechanics*, **147**, 53–79.

Oreper, G. M., Eager, T. W., and Szekely, J., 1983, "Convection in arc weld pools," *Welding Journal*, **62**(11), 307s–312s.

Pitscheneder, W., Debroy, T., Mundra, K., and Ebner, R., 1996, "Role of sulfur and processing variables on the temporal evolution of weld pool geometry during multikilowatt laser-beam welding of steels," *Welding Journal*, **75**(3), 71s–80s.

Tsao, K. C., and Wu, C. S., 1988, "Fluid flow and heat transfer in GMA weld pools," *Welding Journal*, **67**(3), 70s–75s.

Woods, R. A., and Milner, D. R., 1971, "Motion in the weld pool in arc welding," *Welding Journal*, **50**(4), 163s–173s.

Xiao, Y. H., den Ouden, G., 1993, "Weld pool oscillation during GTA welding of mild steel," *Welding Journal*, **72**(8), 428s–434s.

Zacharia, T., David, S. A., and Vitek, J. M., 1991, "Effect of evaporation and temperature-dependent material properties on weld pool development," *Metallurgical Transactions*, **22B**(Apr.), 233–241.

Zacharia, T., David, S. A., Vitek, J. M., and Kraus, H. G., 1991, "Computational modeling of stationary GTA weld pools and comparison to stainless steel 304 experimental results," *Metallurgical Transactions*, **22B**(Apr.), 243–253.

Zhang, Y. M., Cao, Z. N., and Kovacevic, R., 1996, "Numerical analysis of fully penetrated weld pools in gas tungsten arc welding," *Journal of Mechanical Engineering Science*, **210**, 187–195.

PART THREE

THE CHEMISTRY OF WELDING

This Page Intentionally Left Blank

CHAPTER 11

MOLTEN METAL AND WELD POOL REACTIONS

Most metals are inherently reactive, albeit some are far less or far more reactive than others. The so-called noble metals or precious metals, which include gold (Au), silver (Ag), platinum (Pt), and palladium (Pd), as well as some far less well-known types (e.g., rhenium (Re), iridium (Ir), and others), are quite inert. As a group, these exhibit superb resistance to oxidation[1] and corrosion, even when hot or molten. At the other extreme are reactive metals, which include beryllium (Be), niobium (Nb), titanium (Ti), and zirconium (Zr), as well as some of the refractory metals like molybdenum (Mo), hafnium (Hf), and tungsten (W), and light metals, which include lithium (Li), aluminum (Al), and magnesium (Mg). These metals react with many things, including gases, nonmetallic elements,[2] and even other metals.[3] Some do so at all temperatures, notably Ti and Zr, and all do so as they are heated and, especially, are made molten. All other metals, including copper (Cu), iron (Fe), nickel (Ni), and cobalt (Co), widely used as the base (or solvent) for engineering alloys, exhibit increasing reactivity with increasing temperature and, almost always, aggressive reactivity when molten. It should thus come as no surprise that the high

[1] Noble metals do, in fact, oxidize, but they do so very slowly and in a way that the oxide is not degrading, in that it is extremely tenacious and impermeable, thereby protecting from further, progressive oxidation.

[2] Nonmetallic elements, other than the gases, that react with metals include carbon (C), bromine (Br), iodine (I), sulfur (S), selenium (Se), and tellurium (Te), as well as semimetals or metalloids boron (B) and silicon (Si).

[3] Obviously, metallic sodium (Na), potassium (K), rubidium (Rb), cesium (Cs), and calcium (Ca) are also highly reactive, but are not used as solids, in either the pure state or as a base for alloying. Sodium, potassium, and cesium are used in liquid form as coolants in certain nuclear reactors and other heat devices, however, where their extreme reactivity and corrosiveness to other metals must be carefully considered and dealt with.

temperatures associated with fusion welding, in particular, cause chemical reactions to occur between molten weld metal and the surroundings, unless proper protection is provided. For some metals, protection must also be provided during heating to cause melting and during cooling immediately following solidification.

The need for protecting metals (especially when made molten) during welding became evident when the electric arc began to replace oxyfuel sources, such as oxyacetylene, for welding. These oxyfuel processes had been providing protection from air through their relatively nonreactive products of combustion, namely CO, CO_2, and H_2. When low-carbon steels were first arc-welded using bare wire electrodes and no shielding gas, the properties of the weld were notably inferior to either the base metal or the filler wire. As an example, in tests by Erokin (1964) to repeat early practice, the tensile strength of low-carbon steel only dropped from 390–400 N/mm^2 to 334–390 N/mm^2, but tensile ductility dropped from 25–30% to 5–10%, bend angle (as an indicator of ductility) from 180° to 20–40°, and impact toughness from greater than 147 J/cm^2 to 4.9–24.5 J./cm^2. Analysis showed severe pickup of oxygen (approaching 0.7 wt%) and nitrogen (approaching 0.2 wt%). Dissolved gas degraded ductility and toughness by the formation of brittle inclusions and caused fatigue (although not detailed by Erokin) by the formation of porosity. Clearly, providing protection to prevent reactions between the molten weld metal and the surroundings was essential.

Various techniques can be used to protect the molten weld pool during fusion welding, including inert gas, molten slag, gas and slag together, and vacuum. Each provides a different degree of protection and does so in different but related ways. Regardless of the particular technique selected, the key is always to prevent or minimize gas–metal reactions. Beyond this, some welding processes also rely on slag–metal reactions to provide either protection or an additional measure of metallurgical refinement or purification, or both. Each of these techniques is discussed in Section 11.2, but, first, let's look at gas–metal reactions.

11.1. GAS–METAL REACTIONS

Molten, and often just hot, metals react with almost any gas except the noble or inert gases, helium (He), neon (Ne), argon (Ar), krypton (Kr), xenon (Xe), and radon (Rn). This is the reason that Ar and He are used to provide shielding from the atmosphere for the so-called inert gas-shielded welding processes. To do so, however, requires that a gas be present. Thus, while reactions could take place with fluorine (F) gas, fluorine is rarely present in a welding environment, except as salts in electrode coatings, wire flux cores, or SAW fluxes. For this reason, gas–metal reactions normally arise for gases found in air, particularly nitrogen, N_2, which comprises 78% of air by weight, and oxygen, O_2, which

comprises about 21% of air by weight.[4] Gas–metal reactions also take place with hydrogen, H_2, which comes from the thermal or electrical dissociation of water from any of many sources, including humidity in the air.[5]

Gas–metal reactions can take one of two forms: (1) dissolution or (2) chemical. These two forms can lead to one or more of three effects: (1) Gas can dissolve to a solubility limit and remain dissolved; (2) gas can try to dissolve beyond a solubility limit and appear as porosity; and (3) gas can react chemically to form a brittle compound layer or inclusions. In fact, dissolved gas remaining in solution can have either (or both) of two effects: It can (1) cause solid solution hardening or (2) lead to preferential phase stabilization. Let's look at each effect for nitrogen, oxygen, and hydrogen.

11.1.1. Gas Dissolution and Solubility in Molten Metal

Gases, including nitrogen, oxygen, and hydrogen, dissolve in liquids, including molten metals. They do so by having gas molecules (or atoms or ions) occupy the many rather large spaces between atoms of the metal in liquid form. The amount of nitrogen, oxygen, or hydrogen that can dissolve in molten metal almost always increases with increasing temperature of the liquid,[6] and it does so as a function of the partial pressure of the gas species above the liquid. This is expressed by Sievert's law:

$$k = \frac{[\text{gas}]}{P^{1/2}\text{gas}_2} \tag{11.1}$$

where k is the equilibrium constant, [gas] is the concentration as weight percent (wt%) of a particular gas in the molten metal, and $P\text{gas}_2$ is the partial pressure of the particular gas in diatomic molecular form. This relationship, known as Sievert's law, applies to all diatomic gases,[7] including nitrogen (N_2), oxygen (O_2), and hydrogen (H_2). That it works is shown in Figure 11.1.

Plots showing the solubility of nitrogen and hydrogen in iron as a function of temperature are presented in Figures 11.2 and 11.3, respectively. Note that the equilibrium concentration of nitrogen in molten (liquid) iron at 1600°C is

[4] Argon makes up the majority of the remaining 1% of air, although there are also small to minute amounts of carbon dioxide, neon, krypton, xenon, and radon. Despite being the most abundant element in the universe, no free hydrogen is present in the air. Rather, it is always found combined with oxygen in the form of water vapor or humidity. He is found in deposits of natural gas, not in the air.

[5] More is said about possible sources of hydrogen in Section 11.1.5.

[6] This is not to be expected, however, as the amount of gas (such as carbon dioxide. but also oxygen and others) that can dissolve in liquid water decreases with increasing temperature. This is evidenced by the evolution of bubbles as cold carbonated soda water warms up.

[7] Certain gases take a diatomic form, forming a covalently-bonded molecule consisting of two atoms, to achieve a stable electron configuration in their outer shells by sharing electrons between the two atoms in covalent bonds.

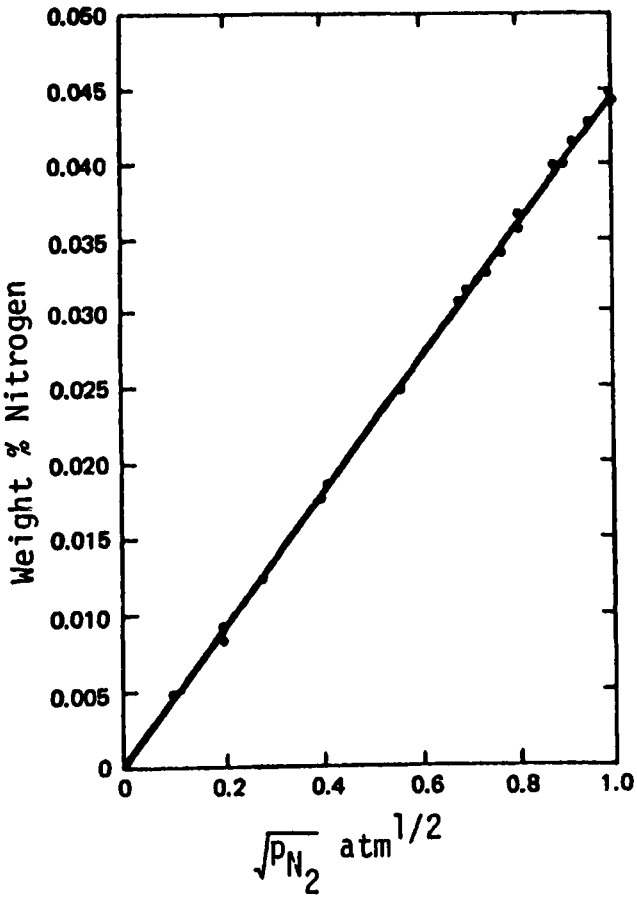


Figure 11.1 The solubility of nitrogen in molten iron as a function of the partial pressure of nitrogen at 1600°C. (Originally from "Solubility of nitrogen in liquid iron alloys, 1: thermodynamics" by R. Pehlke and J. F. Elliott, *Transactions of the Metallurgical Society AIME*, **218**, 1088–1101, 1960, with permission of the AIME, Warrensdale, PA.)

about 0.0445 wt% at one atmosphere of air pressure. These plots also show how solubility of nitrogen and hydrogen drop dramatically in the solid as soon as solidification takes place. This is because, in a solid, there is far less space between atoms in a crystal lattice for gas molecules (or atoms or ions) to occupy without leading to distortion of bonds and storing of and increase in energy in the system, which is thermodynamically unfavorable. Note also that solubility in the solid state of a metal depends on both the crystal structure (or allotropic form) and temperature. For iron, solubility of nitrogen is far higher in the face-centered cubic (fcc) γ-iron form than in the body-centered cubic (bcc) δ- or α-iron form. (At first this may seem counterintuitive, since the fcc structure is close-packed, while the bcc structure is not, but, in fact, the

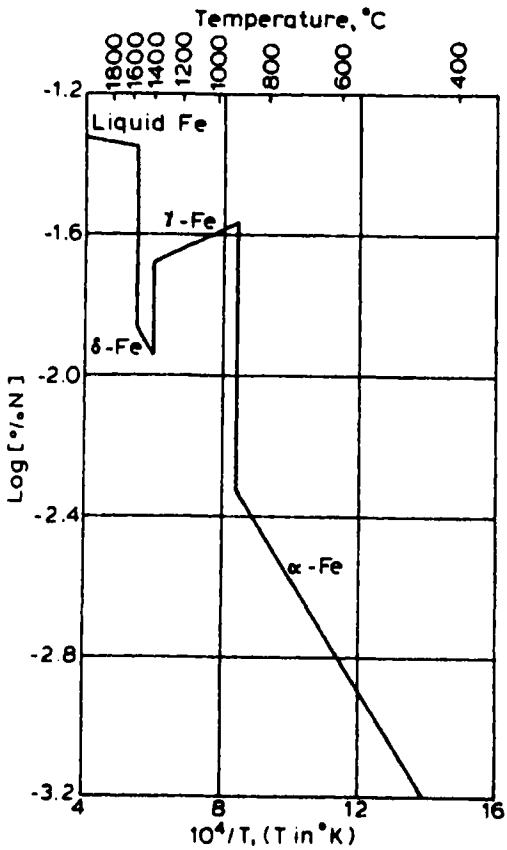


Figure 11.2 The solubility of nitrogen in iron as a function of temperature. (Originally from *The Making, Shaping and Treatment of Steel*, U.S. Steel Corporation, Pittsburgh, PA, 1971, with permission of the Association of Iron & Steel Engineers Foundation, Suite 2350, 3 Gate Way Center, Pittsburgh, PA 15222.)

octahedral, six-fold, interstitial sites in the fcc structure are larger than comparable octrahedral sites in the bcc structure; thereby, they can accommodate gas atoms with less strain energy.) A similar but less dramatic difference occurs for hydrogen.

The reason for different solubility in different crystalline (or allotropic) forms of a metal is due to differences in the number and size of interstitial sites. Figure 11.4 shows the solubility of hydrogen in aluminum. Normally, solubility within a particular allotropic form of a solid decreases with decreasing temperature, since the structure becomes tighter as a result of reduced lattice vibrations. This is not the case for nitrogen in γ-iron, as explained parenthetically above.

The presence of different alloying elements (known as solutes) in a molten metal can affect the solubility of a gas in that metal. This is shown in Figure

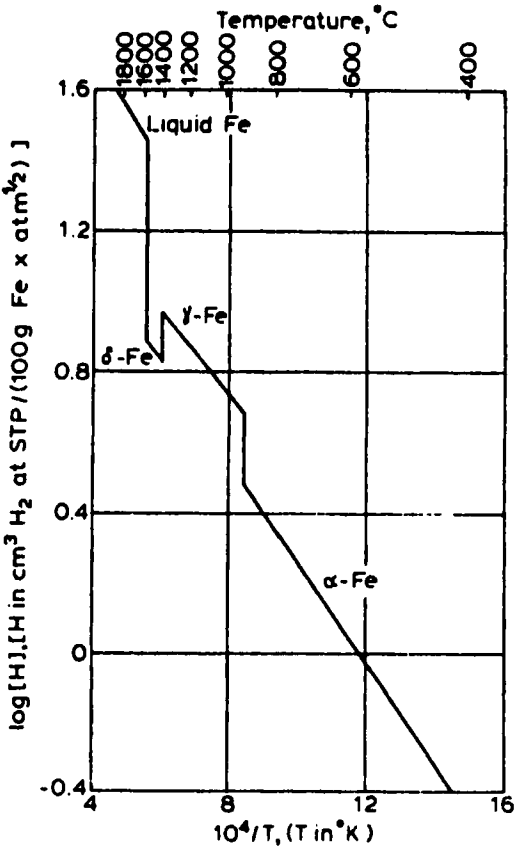


Figure 11.3 The solubility of hydrogen in iron as a function of temperature. (Originally from *The Making, Shaping and Treatment of Steel*, U.S Steel Corporation, Pittsburgh, PA, 1971, with permission of the Association of Iron & Steel Engineers Foundation, Suite 2350, 3 Gate Way Center, Pittsburgh, PA 15222.)

11.5 for nitrogen and Figure 11.6 for hydrogen. Some elements increase the solubility of a gas, while others decrease it; presumably as a result of misfitting strain effects in the liquid that are similar to (but less pronounced than) those found in the solid state.

As a result of the nonequilibrium conditions of fusion welding, the actual amount of a gas (such as nitrogen) found in both a molten metal (such as iron) and solidified welds is almost always different than that predicted by Sievert's law for equilibrium. In fact, it is almost always higher, which is strange because one of the key factors leading to nonequilibrium is the very short times at temperature. This can be seen by comparing the nitrogen content of various types of weld metal at ambient temperatures in Table 11.1 and the equilibrium value of 0.0455 wt% cited earlier. The reason for this discrepancy has been determined by Katz and King (1989) and Bandopadhyay et al. (1992) to be

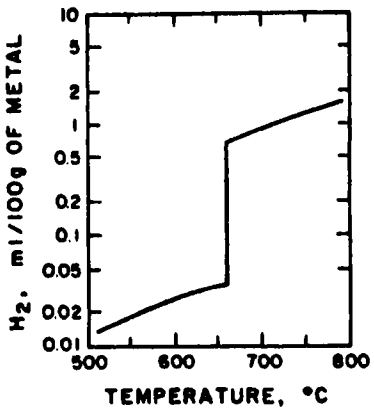


Figure 11.4 The solubility of hydrogen in aluminum as a function of temperature. (Originally from *Gases in Non-ferrous Metals and Alloys*, by L. W. Eastwood, 1953, American Society for Metals, Metals Park, OH, with permission of the ASM International, Materials Park, OH 44073.)

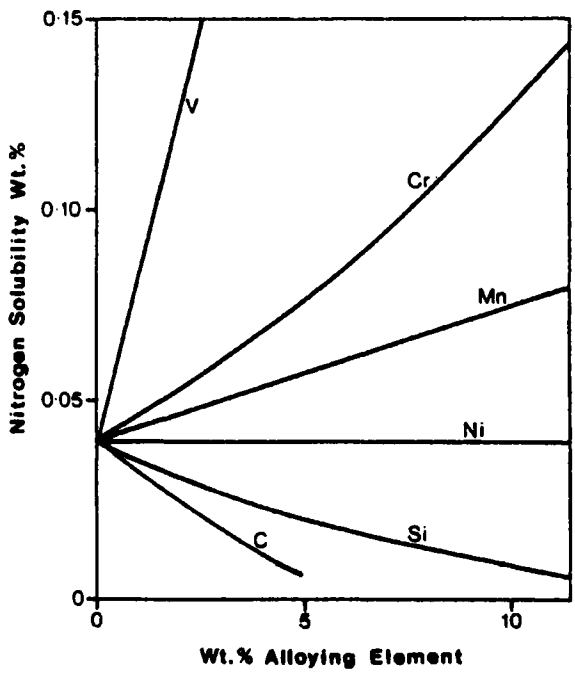


Figure 11.5 The effect of various alloying elements on the solubility of nitrogen in molten iron at 1600°C. (Originally from *Physical Metallurgy of Iron and Steel* by B. Kumar, 1968, Asia Publications, out of *Introduction to the Physical Metallurgy of Welding*, 2d ed., by K. Easterling, published in 1992 by Butterworth-Heinemann, Oxford, UK, and used with permission of the Easterling family.)

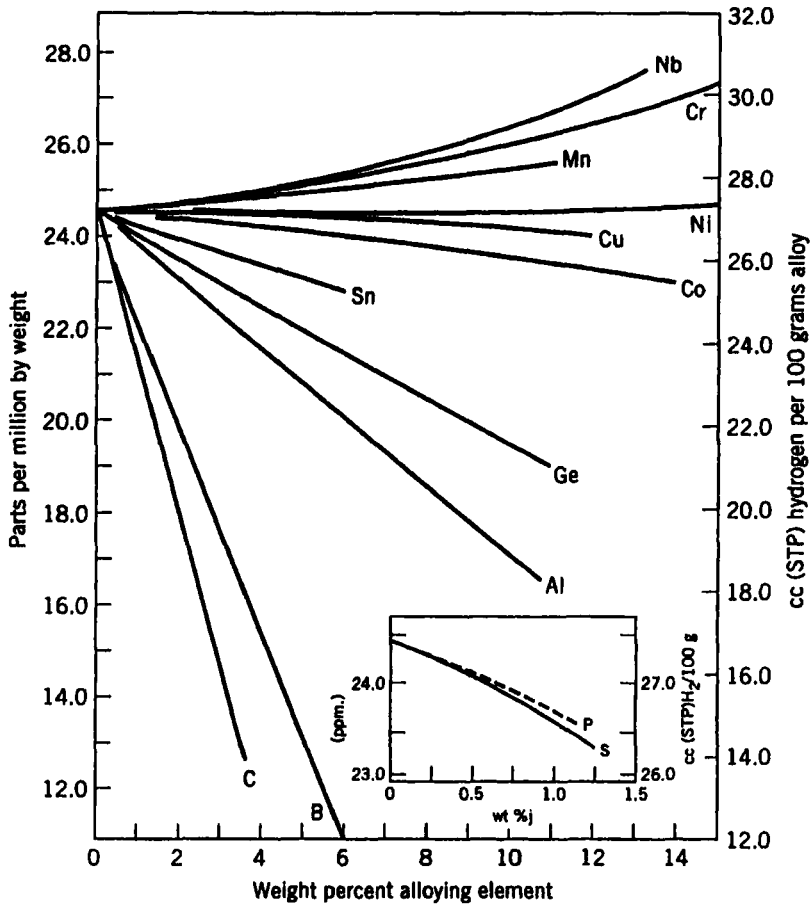


Figure 11.6 The solubility of hydrogen in various binary alloys of iron at 1592°C. (Originally from *The Making, Shaping and Treatment of Steel*, 1971, U.S. Steel Corporation, with permission of the Association of Iron & Steel Engineers Foundation, Suite 2350, 3 Gate Way Center, Pittsburgh, PA 15222.)

that in an electric arc, atomic or nascent and ionic as well as diatomic forms of a gas exist, and all dissolve in molten metal (even under nonequilibrium) to produce a concentration there and in final welds.

While data on oxygen solubility are extremely difficult to find, general behavior of oxygen closely parallels that of nitrogen and hydrogen. The effect of alloying additions to iron on the solubility of oxygen in molten iron, for example, is shown in Figure 11.7. Figure 11.8 shows the levels of dissolved oxygen and nitrogen in steel expected with several different arc welding processes, while Figure 11.9 shows the levels of hydrogen expected in steels as a function of process and process variables.

TABLE 11.1 Nitrogen Content in Various Types of Weld Metal at Ambient Temperature

Weld	Nitrogen Content (wt%)
Oxyacetylene welding, unalloyed steel	0.0016–0.002
Arc welding, unalloyed steel, using	
Basic electrode	0.001
Cellulose	0.0016–0.002
Rutile	0.002–0.0025
Acid	0.0027–0.003
Oxidizing	0.0035–0.004
Uncoated	0.01–0.022
Arc welding, 18-9 chrome–nickel steel, using	
Basic electrode	0.0055–0.0065
Rutile	0.006–0.0075
Submerged arc welding, melted powder (multirun)	0.0014

Source: Originally after *Welding Compendium* by N. Christensen, 1975, Norwegian Institute of Technology, Trondheim, Norway, reproduced from *Introduction to the Physical Metallurgy of Welding*, 2d ed., by K. Easterling, published in 1992 by Butterworth-Heinemann, London, and used with permission of the Easterling family.)

Once dissolved in molten metal, gases like nitrogen, oxygen, and hydrogen can lead to one or more of several things: (1a) they can remain in solution to cause hardening; (1b) they can remain in solution and stabilize a particular phase; (2) they can be rejected from the melt upon solidification (presuming solubility decreases, as it often does) to produce porosity; or (3) they can lead to formation of brittle compounds. Table 11.2 gives the solubility of hydrogen, nitrogen, and oxygen in various molten metals at their melting point. Let's look at each possibility.

11.1.2. Solid Solution Hardening and Phase Stabilization

Nitrogen and oxygen are potent solid solution strengtheners or hardeners to most metals, whether those metals are ferrous or nonferrous. These gases have this effect because they go into solution by occupying interstitial sites between atoms of the host or solvent. As small as the atoms of these gases are, they are still too large to fit into interstices without causing fairly substantial distortion of bonds and storing of energy. As a result, they increase strength by resisting the motion of dislocations by the repulsion between the strain field they produce and the strain field of dislocations trying to move in response to an applied stress.

The effectiveness of nitrogen as a strengthening addition is comparable to carbon in iron. This is evidenced by the replacement of carbon removed to

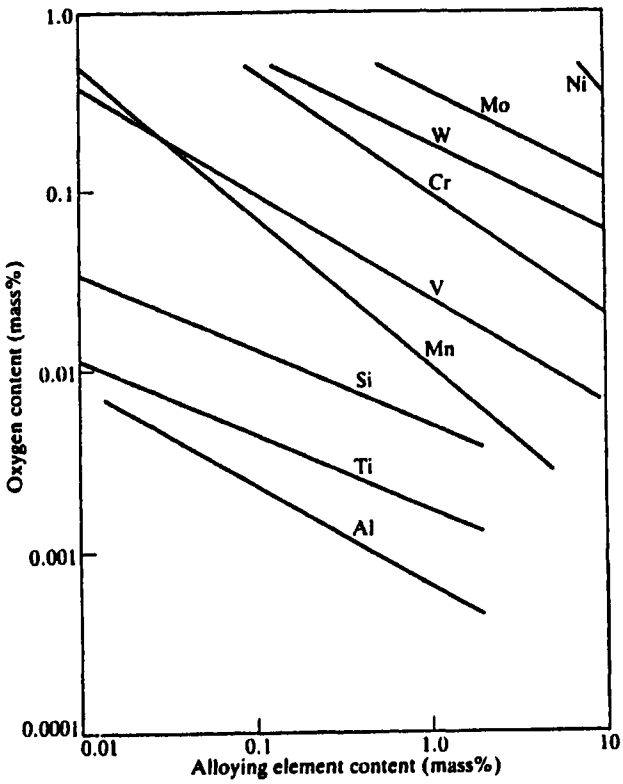


Figure 11.7 The effect of various alloying additions to iron on the solubility of oxygen. (Originally from *Y. Kasamatsu, Journal of the Japanese Welding Society*, **10**, 313–323, 1963, out of *Metallurgy of Welding*, 5th ed., by J. F. Lancaster, published in 1993 by Chapman & Hall, Oxford, UK, and used with permission of Kluwer Academic Publishers, The Netherlands.)

create low-carbon grades of austenitic stainless steel (e.g., 304L) to reduce susceptibility to sensitization (see Section 16.5) by adding nitrogen to restore lost strength in so-called 304LN grades. The effectiveness of oxygen as a strengthening addition is evidenced by its effect in copper (e.g., tough-pitch copper with 0.02–0.05 wt% of added oxygen).

Unfortunately, increased strength and hardness comes at the expense of ductility and toughness. This can be seen in Figure 11.10 for the effects of nitrogen on the room-temperature mechanical properties of mild steel. Strengthening by solid solution effects is limited for some gases since they react chemically to form brittle compounds that degrade not only ductility and toughness but also strength. This is discussed in Section 11.1.4.

Some gases dissolved in solid solution lead to stabilization of certain allotropic forms or phases of a metal or alloy. Dissolved nitrogen stabilizes

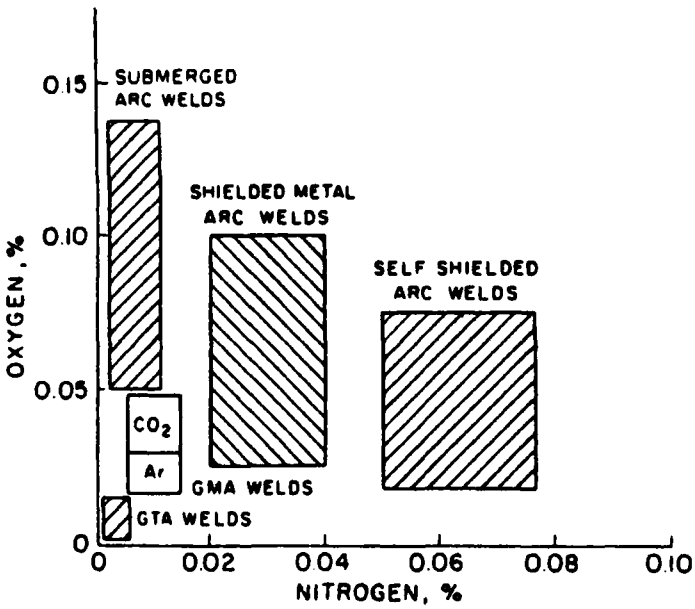


Figure 11.8 Oxygen and nitrogen levels expected in steel after welding using any of several different arc processes. (Originally from paper by R. H. Rein in *Proceedings of a Workshop on Welding Research Opportunities*, edited by B. A. McDonald, 1974, Office of Naval Research, AD-AO28395, Washington, DC, p. 92, reproduced from "Sources of weld metal oxygen contamination during submerged arc welding" by T. W. Eager, *Welding Journal*, 57(3), 76s–80s, 1978, published by and used with permission of the American Welding Society, Miami, FL.)

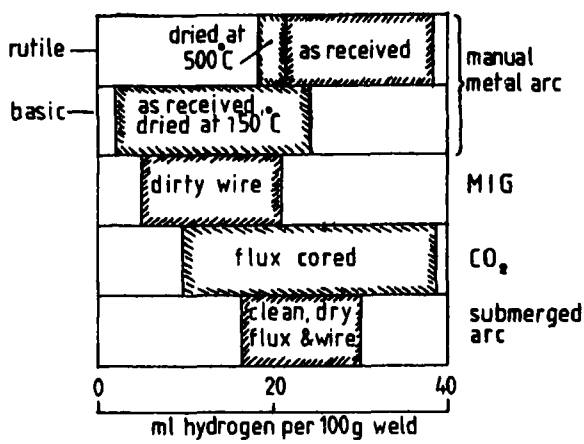


Figure 11.9 Amount of hydrogen found in welds in steel as a function of processes and process variables. (From *Introduction to the Physical Metallurgy of Welding*, 2d ed., by K. Easterling, published in 1992 by Butterworth-Heinemann, Oxford, UK, and used with permission of the Easterling family.)

TABLE 11.2 Solubilities of Hydrogen, Nitrogen, and Oxygen in Various Liquid Metals at Their Melting Point

		H	N	O
No compound formed (endothermic solution)	Gas soluble	Ag, Al, Be, Cd, Co, Cr, Cu, Fe, Mg, Mn, Mo, Ni, Pb, Pd, Pt, Rh, Ru, Sn, W, Zn	—	Ag
	Gas insoluble	Au, Hg	Rb, Cs, Cu, Ag, Au, Zn, Pb, platinum metals	Au, platinum metals
Compound formed (exothermic solution)	Compound very soluble	Sc, Y, rare earths, Ti, Zr, Hf, Th, V, Nb, Ta, U	Ti, Zr, Hf, Th, V, Nb, Ta, U	Ti, Zr, Hf, Th, V, Nb, Ta
	Compound moderately soluble	Alkali and alkaline-earth metals: Li, Na, K, Rb, Cs, Ca, Sr, Ba	Co, Cr, Fe, Mn, Mo, W	Alkali and alkaline-earth metals: Li, Na, K, Rb, Cs, Ca, Sr, Ba, Cu, Co, Cr, Fe, Mn, Mo, Ni, Pb, Sn, W
	Compound insoluble	—	Li, Na, K, Be, Mg, Ca, Zn, Al	Al, Mg, Be, Ca, Sr, Ba, Zn, Cd

Source: From *Metallurgy of Welding*, 4th ed., by J. F. Lancaster, published in 1987 by Allen & Unwin, London, and used with permission of Kluwer Academic Publishers, The Netherlands.

austenite in 18-8-type stainless steels.[8] Dissolved oxygen stabilizes the alpha phase in titanium alloys, producing what is known as alpha case, a very hard and brittle surface layer that makes machining difficult and promotes fatigue.

11.1.3. Porosity Formation

Beyond some limit (the solubility limit), every molten metal (just as every liquid) will be unable to dissolve any more of a particular gas. Furthermore, that solubility limit in the molten metal usually decreases with decreasing temperature, until at the melting point, upon solidification, the solubility drops precipitously. This is shown in Figures 11.2 and 11.3.

[8] 18-8 type refers to austenitic stainless steels containing 18 wt% Cr and 8 wt% Ni. This type is the basis for many derivatives.

As the solubility for a gas decreases in a liquid metal upon cooling, it comes out of solution in the form of bubbles. These bubbles form near the boundaries of the weld pool where the molten weld metal is almost always the coolest. Once formed in the liquid, these bubbles attempt to rise in the weld pool since they are buoyant. However, because of this buoyancy, they are also subject to convection, and, so, are swept through the liquid in a direction that depends on the direction of convective flow. This direction, in turn, depends on the particular force that dominates the convection — a buoyancy (or gravity) force, a surface tension gradient force, an electromagnetic force, or an impinging or plasma friction force (see Section 10.1). If, for example, the surface tension gradient force dominates, molten metal in the weld pool will move outward from the center and downward near pool edges, sweeping any gas bubbles back down into the depths of the pool. If, on the other hand, electromagnetic forces dominate, molten metal will move from the pool edges to the weld center, at which point, upon colliding with fluid flowing in the opposite direction from the other side of the weld pool, it will turn downward, strike the bottom of the pool, and turn outward and upward along the pool edges. This action will sweep any gas bubbles forming near the pool edges up to the pool surface to escape. These different actions are shown schematically in Figure 10.13.

Unfortunately, as often as not (perhaps more often than not), these gas bubbles never get to escape, regardless of the convection flow pattern. The reason is that solidification occurs first, trapping the bubbles to produce pores. Gas porosity, whether from nitrogen, oxygen, or hydrogen, is always problematic. First, it indicates that shielding was less than adequate, and that unwanted gas–metal reactions are occurring. Second, pores can easily act as stress risers, thereby promoting brittle (over ductile) fracture and aggravating susceptibility to cyclic loading (fatigue). The fact that a pore can act to arrest a propagating crack by blunting it, and, thereby, reducing the stress at its tip, is not justification for accepting porosity. Unless every pore is intentionally introduced and controlled in size and location (which is absurd!), the third and most significant reason porosity is always problematic is that its presence indicates that the process is not under proper control.

As an example of the effect of porosity on mechanical properties, Figure 11.11 shows the effect on tensile properties in aluminum welds.

11.1.4. Embrittlement Reactions

As if the possibility of porosity isn't bad enough, dissolved gases can chemically react with molten metal to form compounds that are almost always (1) undesirable (since they are nonmetallic) and (2) inherently brittle.[9] Nitrogen

[9] The reason compounds metals and gases are almost inherently brittle is that they are almost always ionically bonded. Ionic compounds, because they consist of alternating positive cations and negative anions in their crystal lattice, cannot deform by shear or slip between most planes of atoms. Instead of slipping, they cleave and fracture into pieces. Even if covalently bonded, slip is difficult and compounds are brittle.

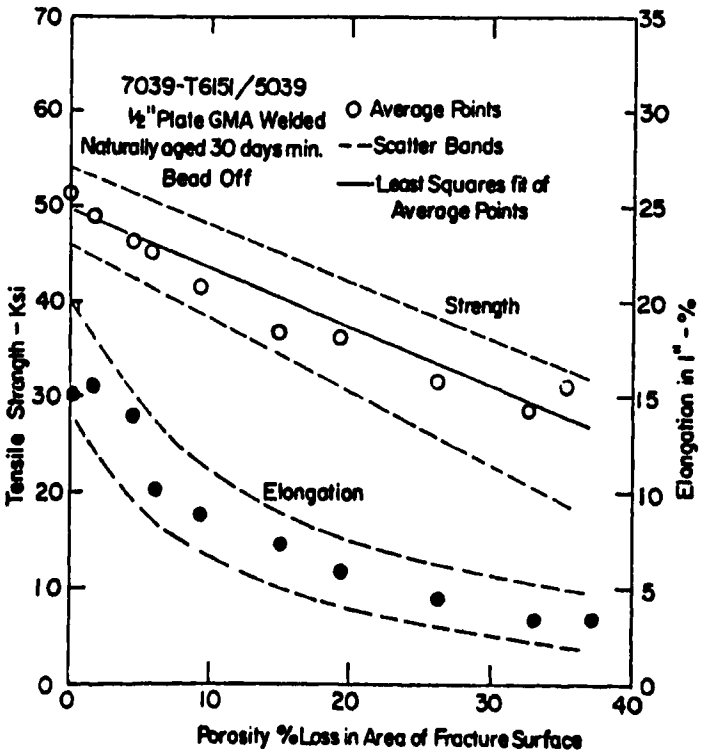


Figure 11.11 The effect of porosity on the tensile properties of aluminum welds. (Originally from a thesis by R. J. Shore, 1968, Ohio State University, Columbus, OH, used with permission of The Ohio State University.)

can form nitrides, and does in iron-based and iron-containing alloys to form acicular (needle-like) and crack-like Fe_4N, which acts to reduce ductility and impact toughness. Nitrides also form in aluminum-containing steels to form extremely hard, but less brittle, aluminum nitride, which is the basis for nitriding steels (with about 4 wt% of added Al) to improve their resistance to certain kinds of wear. Oxygen can form oxides, as it does in iron-based alloys, usually with silicon to form nonmetallic silicate inclusions, and in aluminum-based alloys to form aluminum oxide inclusions. Hydrogen can form hydrides, and does in titanium to cause severe embrittlement.

The adverse effect of oxide inclusion formation in mild steel welds is shown in Figure 11.10, while the adverse effect of nitride inclusions is shown in Figure 11.12.

11.1.5. Hydrogen Effects

Hydrogen is one of four or five elements (H, C, N, B, and, possibly, O) with a sufficiently small atomic diameter to dissolve interstitially in most metals. For

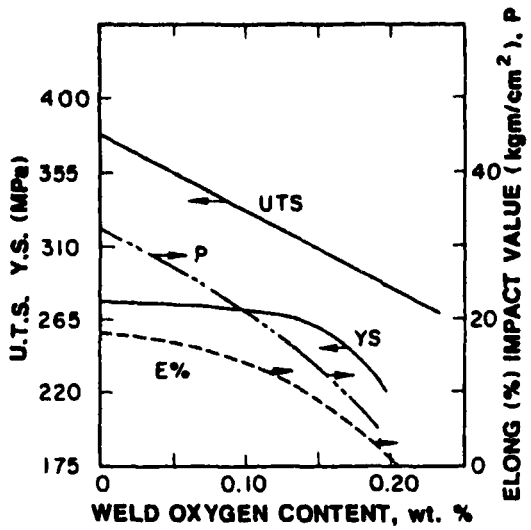


Figure 11.12 The effect of oxygen content on the mechanical properties of mild steel welds. (Originally from *The Metallurgy of Welding* by D. Seferian, 1962, Chapman & Hall, London, out of *Welding Metallurgy* by S. Kou, Figure 3.10, p. 70, published in 1987 by and used with permission of John Wiley & Sons, Inc., New York.)

reasons that will become clear later, this characteristic of hydrogen is of major importance in alloys based on the transition metals, that is, elements in groups IIIB through IIB in the periodic table, which have partially filled d electron states and, in some cases, one or two electrons in the next higher energy f shell. Of this group of alloys, the Fe-base construction steels are of greatest commercial importance, so the following discussion is based on the role of hydrogen in the welding of construction steels containing less than 5% total alloying addition.

The introduction of hydrogen into construction steels has three major deleterious effects: (1) hydrogen embrittlement, (2) hydrogen porosity, and (3) the formation of cold cracks and/or delayed cracks at ambient temperatures; each of which tends to impair the service behavior of weldments in construction steels. The following discussion summarizes the influence of hydrogen in each of the above phenomena.

11.1.5.1. Hydrogen Embrittlement. When dissolved in construction steels and, many other transition metal-based alloys, hydrogen tends to cause significant reduction in the ductility of these materials without causing noticeable effects on the elastic properties. The embrittlement due to the presence of hydrogen does not appear at all temperatures, however. In the vicinity of normal ambient or room temperature, say between about -100 and 60°C (-150 and 150°F), hydrogen in steels causes severe loss of ductility. Below this

range, the embrittling effect disappears. Similarly, when the temperature is raised much above room temperature, any embrittlement gradually disappears, primarily because the increase in temperature increases the diffusion rate of the hydrogen and promotes its escape to the surrounding atmosphere. The true fracture stress (i.e., load at fracture divided by the actual cross-sectional area at fracture) for a construction steel containing hydrogen can be reduced by 35–40% between −60 and +20°C (−75 and +75°F) and yet show little degradation at temperatures either far below or significantly above this range.

The rate of plastic deformation has been shown to have a marked influence on the extent of hydrogen embrittlement as well. Hydrogen embrittlement disappears at very rapid strain rates (above about $10^3 s^{-1}$) and becomes negligible at very slow strain rates (below $10^{-4} sec^{-1}$). Insidiously, the embrittlement due to dissolved hydrogen is most severe in the range of strain rates normally encountered in conventional tensile testing (i.e., 10^{-2} to $10^{-3} s^{-1}$) and service.

The degree to which hydrogen embrittles a steel has also been shown to be strongly dependent on the microstructure present. In general, microstructures produced by transformation of austenite at high temperatures or slower cooling are less severely embrittled than those that depart significantly from equilibrium, forming at temperatures well below the equilibrium eutectoid temperature or at high cooling rates. For example, untempered martensite loses almost all of its limited ductility in the presence of hydrogen, while lamellar pearlite loses about 40% of its ductility, and spheroidized pearlite loses less than 30% of its ductility. Bainite too can exhibit susceptibility to hydrogen embrittlement.

Hydrogen enters the Fe lattice in steels only in atomic form, and occupies interstitial sites. When in solution in Fe, there is strong evidence that hydrogen atoms give up their sole valence electron to become a hydrogen ion or proton, with a single positive charge and an extremely small diameter. Thus, hydrogen in solution in iron can diffuse very readily and rapidly by migrating in the lattice from interstice to interstice. In fact, the form that hydrogen ultimately takes when dissolved in a material depends on the size of the imperfection with which it associates. At vacancies and dislocation lines, the hydrogen probably exists in its ionized form as a proton. At dislocation pile-ups and small-angle grain boundaries, it probably exists as nascent or atomic hydrogen, while at voids, cracks, and in porosity, it probably exists as diatomic hydrogen (H_2) molecules or as gaseous hydrogen (Bastien, 1961).

Since hydrogen cannot enter the crystal (e.g., iron) lattice except in atomic or ionic form, reactions that provide a source of such nascent hydrogen or ions at the surface of a solid (or in liquid iron) can act as potent sources of hydrogen for embrittlement. Since the solubility of hydrogen varies with both the temperature and the state of aggregation (i.e., phase) of iron, as indicated in Figure 11.3, the majority of hydrogen involved in the degradation of properties of weldments is probably absorbed when the iron is in the molten state. The solubility of hydrogen in molten iron at 2795F (at 0.0024 wt%) is roughly 4 ×

that in δ-iron at 2795°C (at 0.00065 wt%). Furthermore, the solubility of hydrogen in austenite is greater than in ferrite.

Among the important sources of hydrogen in weldments are the following:

1. Nascent hydrogen produced by the dissociation of water (H_2O)⟨2H + O⟩ by the heat source in welding, with water arising from
   a. Condensate on the work
   b. Cooling water leaks in the welding torch
   c. Absorbed moisture in electrode coatings
   d. Water of hydration in fluxing compounds
   e. Absorbed moisture films on base metal or filler wire
   f. Moisture from the ambient atmosphere aspirated into the arc
   g. Combustion products of fuel gases in gas welding
   h. Decomposition and combustion of oil, grease, etc., on the work
   i. Decomposition and combustion of organic ingredients in coatings
2. Dissolved hydrogen present in the base metal and/or filler wire, as residue from the original production process.
3. Dissolved hydrogen picked up by the base metal and/or filler wire by electrochemical reactions accompanying prior chemical cleaning.
4. Contamination of inert shielding gases by improper storage and handling of compressed gas cylinders by supplier or user.
5. Use of polyethylene, rubber, or other polymeric hoses (which have not been properly cleaned and purged) after exposure to ambient atmosphere as carriers of shielding gases. (The inner surfaces of such hoses tend to adsorb moisture upon exposure to moist atmospheres and then liberate the moisture to the dry shielding gases.)

The mechanism responsible for hydrogen embrittlement, as well as the subsequent cracking that often follows, is discussed in Section 11.1.5.3.

11.1.5.2. Hydrogen Porosity. Another form of weld defect attributed to excessive hydrogen is porosity. Referring to Figure 11.3, note that the solubility of hydrogen in liquid metallic Fe-based alloys at the melting point is nearly four times that in solid δ-iron at the melting point (i.e., the equilibrium distribution coefficient, $k_0 = 0.00065\,\text{wt\%}/0.0024\,\text{wt\%} = 0.271$). Thus, during intervals of rapid growth at an advancing solid–liquid interface, the liquid at the interface can become supersaturated with and nucleate tiny bubbles of gaseous hydrogen. These bubbles often become entrapped in the spaces between dendrites, and grow as a result of rejection of additional hydrogen from the surroundings. Upon further cooling, more hydrogen is rejected by the solid as a result of the solubility of hydrogen decreasing with decreasing temperature, enters the tiny void, and builds up high hydrostatic pressures within the void. Even if the bubbles do not grow to visible size, the fracture

surface of a failed weld will often exhibit shiny circular patches, called fish-eyes. These are certain proof of excessive hydrogen pickup. If the amount of hydrogen dissolved in the liquid is sufficiently great, actual spherical voids, shiny on their interior surface, will be formed. This type of defect is called hydrogen porosity.

Porosity in welds, regardless of its source, tends to be formed in layers that delineate the instantaneous position of the trailing edge of the weld puddle at the time of their formation. Such observations suggest that the solidification process occurs by intermittent spurts rather than by the continuous, steady advance of the solid–liquid interface. Thus, the instantaneous velocity appears to vary from one instant to the next, although the average velocity of the interface is governed by the travel speed of the heat source during welding. It is likely that during the brief intervals of rapid growth, the liquid ahead of the advancing solid interface is enriched in hydrogen (and other solutes) far beyond what one would predict from the value of k_0 for hydrogen, thus causing hydrogen gas to be nucleated from solution.

11.1.5.3. Hydrogen Cracking. The fact that embrittlement associated with hydrogen dissolution disappears at high strain rates and low testing temperatures is indicative that such embrittlement, as well as any subsequent cracking, involves the transport of hydrogen to the neighborhood of an advancing crack. Thus, at fast strain rates and at low temperatures, the rate of diffusion of hydrogen through the crystalline lattice is too slow to cause embrittlement. Two types of transport have, in fact, been proposed: (1) interstitial diffusion of hydrogen ions (i.e., protons) and (2) group transport of hydrogen atoms or ions as an "atmosphere" associated with dislocations moving in the vicinity of a crack front. The fact that iron containing hydrogen exhibits a yield point at low temperatures is evidence of the tendency for it to form a Cottrell atmosphere by segregating into the expanded portions of the lattice directly below an edge dislocation, for example. At higher temperatures, where embrittlement is still observed, the yield point disappears, suggesting that the hydrogen is able to diffuse fast enough to keep up with the moving dislocations rather than pinning them to give rise to a yield-point phenomenon.

Over the years, several theories have been proposed for embrittlement and cracking by hydrogen, and, indeed, the mechanism of hydrogen-induced crack formation is still being investigated and debated. Several early hypotheses involving the buildup of hydrogen gas pressure in voids are now generally discredited. Preferred models involve the presence of preexisting defect sites in the material, including small cracks or discontinuities caused by minor phase particles or inclusions. In the presence of residual or applied stresses, such sites may develop highly localized regions of biaxial or triaxial stress concentration. Hydrogen diffuses preferentially to these sites because of the lattice expansion that exists. As the local hydrogen concentration increases, the cohesive energy and strength of the lattice decrease. When the cohesive strength falls below the local intensified stress level, spontaneous fracture occurs. Additional hydrogen

then evolves in the crack volume, and the process is repeated. A theory by Troiano (1960) suggests that certain sites act to concentrate stress to promote cracking, while a theory by Petch and Stables (1952) suggests that adsorption of hydrogen lowers surface energy to promote cracking. Both theories explain observed behavior quite well, and both make it clear that hydrogen must be avoided. Other theories have been proposed by Zapffe (1950), deKazinczy (1961), Vaughn and deMorton (1957), and Bastien (1961).

11.2. MOLTEN METAL SHIELDING

Given its extreme reactivity, it is essential to shield molten metal from gas–metal reactions during welding. In fact, while reactiveness is unquestionably greatest when a metal is molten, it is also high when the metal is solid but hot. Therefore, beyond providing shielding while a weld is molten, it is also important to provide a degree of shielding following welding as the weld cools, having just solidified.

Shielding in welding always involves removing potentially reactive gases from the vicinity of the weld. Provided the surfaces to be welded have been properly cleaned prior to actual welding, that may be all that is required. For some processes, however, cleaning and shielding must be or are accomplished simultaneously. Four fundamental approaches are used: (1) inert (or, at least, nonreactive) protective or shielding gases, (2) chemically reducing (cleansing) and protective molten slags, (3) protective vacuum, and (4) cleansing self-fluxing action. It is also possible to have a protective gas and a cleansing flux act together. Let's look at each fundamental approach very briefly.

11.2.1. Shielding Gases

Molten (or hot, solid) metal can be protected from adverse reactions with gases in the atmosphere (particularly oxygen and nitrogen) by excluding those gases. One of the most common and simplest methods is to displace atmospheric gases with inert gases, using what are called inert shielding gases and inert gas-shielded processes. The less rare of the truly inert (or noble) gases (found in group VIII of the periodic table) can be used, including pure argon (Ar), pure helium (He), and mixtures of the two (Ar + He). The advantages of using argon include higher density than air (so it excludes air very effectively, and tends to stay on the work), and relative abundance and, thus, low cost (being produced by fractional distillation of liquefied air). A clear disadvantage of using helium is its extremely low density compared to air, making it very difficult to keep it on the work. On the other hand, being a lighter, smaller atom, with only a full $1s^2$ shell of electrons, the ionization potential for helium is higher than for argon, so hotter arcs are produced, and the gas is fairly

abundant (being produced by liquefaction of helium found coexisting in natural gas deposits). Mixtures of argon and helium allow intermediate levels of arc heat or intensity, as well as other benefits such as lower net cost and better coverage than pure He.

Such inert gases are typically provided from either cylinders of high-pressure (compressed) gas or dewars of bulk, liquefied gases to shield nonconsumable or permanent electrodes (in GTAW and PAW) and torch components (e.g., contact tubes, nozzles), consumable electrodes, and torch components (in GMAW), and welds made by all three processes, by being fed to and through the welding torch itself (see Chapter 3 for details on each process). For more reactive metals, an extra degree of shielding is usually provided by purging a chamber of air and back-filling with inert gas(es), in what are called inert chambers, dry boxes, or glove boxes (given that rubber gloves sealed to the chamber allow access to equipment within the chamber). In lieu of such chambers, extended protection can be provided using special adapters on torches to provide leading and trailing shielding of welds during heating and cooling, prior to or following actual production of the molten weld pool.

Short of fully inert gases, a degree of shielding can also be provided by gases that are nonreactive with the base metal being welded. Examples are pure nitrogen (N_2) and pure carbon dioxide (CO_2). Obviously, key to the use of such less-expensive but less inert gases is that they not react adversely with the base metal (e.g., as carbon dioxide might react with steel to cause a degree of carburization, or as nitrogen might react to cause nitride formation in aluminum). Here too, either compressed gas or liquefied gas can be used as the supply.

It is not unusual for less inert or even reactive gases to be added to the noble gases (argon or helium, or mixtures of the two) to improve some characteristic of the arc or weld pool, or both, including heat intensity (from effects on ionization potential of the mixture); globular-to-spray transfer transition current (using carbon dioxide, for example); weld pool fluidity (as affected by surface-activating agents such as oxygen); or weld pool convection and weld shape (also using surface-activating agents such as oxygen). A comprehensive treatment of shielding gas mixtures can be found in several excellent sources, most notably the AWS's *Welding Handbook*, Vol. 2: *Welding Processes* and *ASM Handbook*, Vol. 6: *Welding, Brazing, and Soldering.*

In the extreme, relatively nonreactive gases such as carbon monoxide/carbon dioxide and hydrogen/water vapor, as well as some methane, produced by thermal decomposition of various flux coatings on electrodes in SMAW or ingredients contained in the core of tubular wires in FCAW, can be used. These gases are not as effective at preventing gas–metal reactions, since they are nowhere near as inert as the noble gases. However, they are certainly better than allowing the molten or hot weld to be exposed to air. In every case, however, from the most inert to the least inert shielding gases, the idea is to exclude atmospheric gases, especially oxygen.

11.2.2. Slags

In the primary production of metals from ore and the subsequent production of alloys from these metals, molten compounds of acidic, basic, or neutral oxides and halides (or oxide–halide mixtures) are used to remove unwanted nonmetallic impurities by oxidation–reduction, or redox, reactions. The starting ingredients are properly called a flux, while the flux once reacted is properly called a slag; however, the more general term slag is often used regardless of where it is in the process.

Not surprisingly, molten slags are also used in fusion welding to perform two major functions, as well as some secondary functions for some processes. First, dry flux ingredients in the coverings or coatings of consumable electrodes in SMAW, in the core of consumable tubular wire electrodes in FCAW, or covering the arc and weld in SAW melt in the heat of the arc to become extremely chemically reactive and protect or shield the molten weld pool from oxidizing gases in the surroundings. They do this by sacrificially reacting with or "gettering" these gases. At the same time, they perform a second function of removing nonmetallic impurities from the molten metal in the weld pool by scavenging or gettering these from within the molten weld pool, aided by convection. After potentially contaminating gases from the surroundings or nonmetallic impurities from within the weld pool have been scavenged, the resulting slag solidifies to form a friable, glass-like shell over the weld. This shell continues to exclude gases from the surroundings, preventing unwanted oxidation of the newly formed and still hot and reactive weld, and also provides a mold, which can help contain and shape the molten weld pool to form a solidified crown bead. For some processes, such as SAW and ESW, the slag also assists in heating to produce the weld by internal Joule (I^2R) heating, as well as to aid in transfer of molten metal from the consumable electrode to the weld pool.

The formulation and operation of slags to aid in metallurgical refinement is discussed in Section 11.3.

11.2.3. Vacuum

A sure-fire way of excluding gases from the atmosphere surrounding a weld is to eliminate the atmosphere altogether, by welding within a vacuum. The good news is that a vacuum precludes gas–metal reactions. The bad news is that a vacuum also precludes the possibility of producing an oxyfuel gas flame and an electric arc, the former because there is neither fuel gas nor oxygen in a vacuum, and the latter because there are no atoms in a vacuum from which to form ions to produce a plasma or arc. Consequently, the possibility of using a vacuum for shielding a weld is limited to processes other than oxyfuel or arc processes, and specifically to high-energy beam sources and almost exclusively electron-beam welding (EBW). The reason a vacuum is particularly needed

with EBW is that otherwise electrons emitted from a cathode and accelerated by annular anodes (see Sections 3.5.1 and 8.5) would collide with gas molecules in the air or any other gaseous atmosphere. In so doing, they would lose a portion of their kinetic energy, and, thereby, a portion of the heat they can ultimately produce from that kinetic energy by conversion in collisions with atoms comprising the workpiece. While a vacuum could also be used with laser-beam welding (LBW) or any focused light source, it is not used, because collisions of photons with molecules in the air have no adverse effect on photon beam energy delivered to the work. In such a case, a vacuum, as opposed to an inert atmosphere shield, would be too expensive and too confining, given the need for a vacuum chamber big enough to contain the work. Obviously, for welding in the vacuum of outer space, EBW and LBW will be two processes of choice.

The level of vacuum, that is, its perfection, has a definite effect on the degree of protection, with better protection provided by more perfect vacuums. For most materials that are to be EB welded, reducing pressure to 10^{-2} to 10^{-6} atm is fine, with only modest sacrifices in beam penetrating power in the higher pressure end of this range. However, when the more reactive metals or alloys (e.g., Ti-, Zr-, Nb-, or Be-based alloys) are to be welded using an electron beam, the lower the pressure (i.e., the higher the vacuum), the better the result. EB welding of titanium alloys at pressures of 10^{-5} to 10^{-4} atm still results in visible straw-gold or slightly purple heat tint, a sure sign of oxidation. When gas–metal reactions are not a primary concern, but EBW is still desired for high welding speeds or other benefits, softer vacuums (around 10^{-1} atm) can be used.

The obvious problem with providing vacuum is providing a chamber within which such a vacuum can be created. Inevitably, whatever size chamber you have, a need for a larger chamber will preclude being able to accept a potentially lucrative job. One answer is sliding-seal EBW as described in Section 5.1, in which the process is brought to the work, rather than the other way around.

11.2.4. Self-protection and Self-fluxing Action

There are some welding processes in which no inert or even nonreactive gas, no vacuum, and no molten slag are employed to protect the weld during and immediately after its formation. Yet somehow, some degree of cleaning to allow wetting between molten metal and substrate (to allow metallic continuity for bond formation to occur) and protection to prevent unacceptable levels of oxidation is still provided. Such processes are said to employ a self-fluxing action and are said to provide self-protection. Examples are resistance spot, seam, projection, flash, and upset welding, as well as MIAB welding.

Self-fluxing occurs when inherently reactive molten metal produced during the heating portion of the welding cycle serves to chemically reduce light layers of contamination at weld faying surfaces. Such self-fluxing occurs because

molten metal is itself reactive and will either dissolve or reduce thin layers of most oxides (the oxygen from such reduction being distributed through a greater volume of metal). Without question, this form of cleaning and subsequent protection is not as effective as some of the other means addressed above, but it is better than nothing; and for processes that rely on self-fluxing because of the way in which they are accomplished, there is really no other choice. Two other things that tend to allow self-fluxing to be good enough: (1) Much if not all of the molten metal that performs self-fluxing at the faying surfaces is subsequently expelled during a pressure upset cycle in many relevant processes; and (2) the heating cycle for some processes (e.g., RSW, RSEW, CDW) that rely on self-fluxing is very rapid, so time at temperature is very short, and time for reaction is extremely limited. For these latter processes, some help is also provided by at least a limitless supply of (albeit not all) air being excluded from the area of the weld by tightness of the joint.

11.3. SLAG–METAL REACTIONS

11.3.1. Deoxidizing/Denitriding (or Killing) Versus Protection

The handling of most molten metals in an air atmosphere requires protection from the detrimental effects of oxygen, nitrogen, and hydrogen (from water vapor or humidity), all of which can cause property degradation by adsorption or outright flaws like porosity or nonmetallic inclusions. The need for molten metal to be protected or shielded from such adverse interactions is as great for fusion welding as it is for bulk melt processing (e.g., steelmaking), only on a much smaller scale. Need for protection is most important during the transfer of molten metal from the tip of a consumable electrode or filler wire into the molten weld pool, because exposure occurs for a large surface area/volume ratio compared to the molten weld pool. Failure to provide suitable protection can result in unsound deposits due to the presence of porosity (primarily from nitrogen, but also from hydrogen from dissociated water), or less-than-optimal ductility and toughness due to gas–metal reactions that lead to embrittlement by dissociation (Section 11.1.2) or nonmetallic inclusion formation (Section 11.1.4).

As described in Section 11.2, there are, in principle, two extreme approaches to protection that can be taken: (1) virtual total exclusion of air from the environment of the weld by employing a vacuum, and (2) without any attempt at shielding, incorporation of a sufficient amount of elements whose affinity for oxygen and nitrogen (and, to a lesser extent, hydrogen[10]) is greater than the base metal. In practice, the total exclusion of air from the welding environment is usually not possible, except at that time in the future that welding is performed in the infinite vacuum of space.

[10] Hydrogen from water or a hydrocarbon must be dealt with differently than oxygen and nitrogen. is described in Section 11.1.5, all potential sources of hydrogen must simply be eliminated.

Despite the use of shielding gases, whether generated within the process from ingredients in consumable electrodes (e.g., in SMAW, FCAW, SAW, or ESW) or supplied from an external source (e.g., in GTAW, PAW, GMAW, and EGW), or vacuum (e.g., for EBW), some residual oxygen and nitrogen inevitably is present in base metal(s) and filler metal to be dissolved and diluted into the molten weld pool. For this reason, deoxidizing and denitriding elements (e.g., Mn, Si, Al, Ti, Zr, Ca, Mg and rare-earth metals, or REMs) are used in many processes, at least to some extent, depending on the process. For SMAW, FCAW, SAW, and ESW, use of deoxidizers/denitriders predominates over use of shielding gases, while for the inert gas-shielded processes, like GTAW, PAW, GMAW, and EGW, use of deoxidizers/denitriders is usually limited to small additions of Si, Mn, Al, or Ti, and so on. Such elements used in fillers, as well as in flux-bearing, slag-generating consumables (e.g., covered electrodes, flux-cored wires, granular SAW flux, or molten slag in ESW), are used to "kill" oxygen and nitrogen by tying it up as a benign compound floated away in the resulting slag.

In practice, a quantitative means for assessing the relative degree of protection versus killing in a particular process or welding consumable is the nitrogen scale. On this scale, residual nitrogen is used in this assessment. Reasons for the use of residual nitrogen in the weld metal as opposed to residual oxygen to assess shielding versus killing include the following: First, residual oxygen in the weld metal can come from too many internal sources (such as oxide inclusions in the filler or base metal, oxides in the flux, or oxidizing shielding gases like CO_2 as opposed to just air), which is not the case for nitrogen. Second, a substantial quantity of deoxidation products (oxides) always separate out of the weld metal before solidification, as opposed to nitrides, which tend to stay in the weld metal,[11] so residual oxygen gives no real indication of protection from air. Third, the more oxides that form, the more they tend to agglomerate and float out due to their lower density compared to the weld metal, thereby leaving residual oxygen low even when exposure to oxygen could have been high.

The relative positions of different arc welding processes and consumables on the nitrogen scale are shown in Figure 11.13. This figure summarizes nitrogen contents for numerous mild and C-Mn steel (ferritic) weld metals measured over a period of 20 years. At one extreme (on the left of the figure), are processes that rely on maximum protection with flux (e.g., SAW) or shielding gas (e.g., GTAW, GMAW, and SMAW with cellulose-coated E6010/11 electrodes), with residual nitrogen typically below 100 ppm. At the other extreme (on the right of the figure), are self-shielded solid wire processes that rely almost totally on killing, with residual nitrogen tending toward 1200 ppm. Between these two extremes are found the various flux-covered or flux-cored consumable electrode arc welding processes and consumables.

[11] The reason nitrides tend to remain in the weld metal while oxides tend to float out is that nitrides tend to form near, at, or below the solidification temperature, while oxides form well above it, thus becoming trapped.

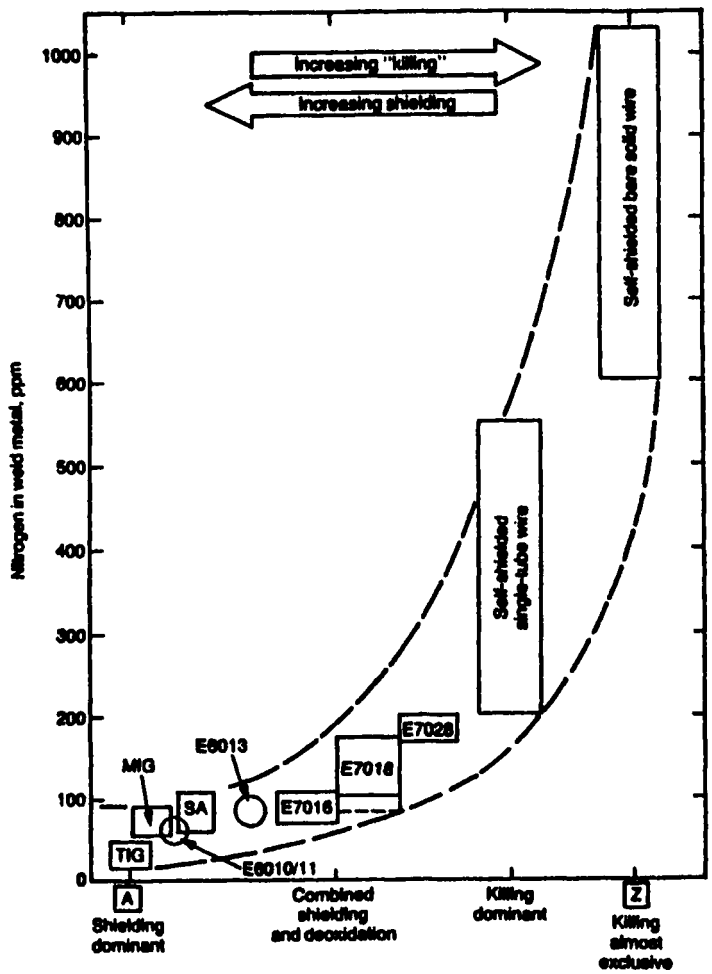


Figure 11.13 Residual nitrogen contents of ferritic steel weld metals deposited by different arc welding processes or consumables that rely on different degrees of either shielding protection or killing the molten weld pool contaminated by oxygen and nitrogen. (From *Self-Shielded Arc Welding* by T. Boniscewski, 1992, published by and used with permission of Abington Publishing Company, Woodhead Publishing, Cambridge, UK.)

11.3.2. Flux-Protected Welding Processes

As seen in Section 3.3.2, a number of arc welding processes employ a consumable electrode to produce a degree of gas and flux protection, as well as some flux killing refinement of the molten weld pool. In fact, there are three main types of such consumables and associated processes: (1) flux-coated or flux-covered stick electrodes (as used in shielded metal arc welding or SMAW);

(2) flux-cored continuous wire electrodes (as used in flux-cored arc welding or FCAW); and (3) fluxes (as used for submerged arc welding or SAW). Regardless of the specific type, these consumables should have the ability to

- Provide good arc initiation and stability (by controlling arc resistivity)
- Provide protection from oxidation/nitriding to molten metal droplets in transfer
- Maintain suitable melting temperature, viscosity, density, and surface tension
- Deoxidize/denitride molten weld metal
- Dissolve solute gases
- Protect the weld deposit by providing an impervious covering
- Assist in shaping the weld deposit (crown bead)
- Transfer alloying elements to the weld metal to offset evaporative losses
- Permit detachment (by being friable)
- Reduce spatter and fumes.

Given this long menu of desirable characteristics, it should come as no surprise that the formulation of fluxes and design of flux-containing consumables is very complex, riddled with mystique, shrouded in secrecy, and poorly understood in all but principle. Some discussion on flux formulation is presented in Section 11.3.7, but the interested reader is referred to specialized sources for more detailed information.

11.3.3. Shielding Capacities of Different Processes

The sheer mass of protective materials, including both fluxes and gases, applied to a weld by various welding processes and consumables gives the best correlation with the position of these processes or consumables on the nitrogen scale (Figure 11.13). Generally, the more, the better. Let's look at some specific processes and consumables within processes.

Submerged arc welding (SAW) tends to keep residual nitrogen very low, in the range of 60–110 ppm, as can be seen in Table 11.3. The reason is that the sheer volume or burden of flux that buries the arc and displaces air from around the arc and weld is very high. At average arc voltages, about 1 kg of flux is consumed per 1 kg of filler wire, and as the arc voltage increases (which tends to increase nitrogen pickup due to increased arc length) up to 2 kg of flux are consumed per 1 kg of wire. As long as the volume of flux is deep enough to completely bury the arc, the process has a self-regulating capability to consume more flux as arc length is increased.

In shielded metal arc welding (SMAW), the mass of flux from flux-covered electrodes that generates shielding gases and protective slag averages about 40% (ranging between 30 and 60%) of the total mass of the electrode. Thus,

TABLE 11.3 Comparison of Flux-Carrying Capacities, Consumption of Flux per Unit Mass of Metal, and Weld Metal Nitrogen Contents for Different Processes

Process	Flux-Carrying Capacity	Mass of Flux Consumed per 1 kg of Metal	Typical Nitrogen Contents in Weld Metal
Subarc	Unlimited	1–2 kg	60–110 ppm
Flux-covered electrode E7018	~40% of electrode	0.7 kg	80–150 ppm
Self-shielded tubular wire	~20% of electrode	0.25 kg	200–550 ppm

Source: From *Self-Shielded Arc Welding* by T. Boniscewski, 1992, published by and used with permission from Abington Publishing Company, Woodhead Publishing, Cambridge, UK.

on average, 0.7 kg of flux is generated per 1 kg of filler metal deposited for basic, low-hydrogen type E7018 electrodes. This lower flux/filler metal ratio compared to SAW results in less effective shielding, as can be seen in Table 11.3. Among electrode types, the cellulosic types produce much more voluminous gas shielding than the low hydrogen types; roughly 5.4 L/min versus 1.4 L/min). Thus, protection from nitrogen pickup is much better for the cellulosic types.

Flux-cored electrodes have an inherently more limited capacity for ingredients that can produce flux than covered electrodes, because these ingredients are contained within, as opposed to being applied to, the filler metal. The wall thickness of the tubular sheath holding the core ingredients must be sufficiently great to carry the stresses associated with drawing the wire to size. Usually, only about 30% maximum of the total electrode mass can be devoted to core ingredients in FCAW electrodes, compared to a maximum of 60% for SAW electrodes. Typical flux-cored wires produce 0.25 kg of flux per 1 kg of filler metal (as shown in Table 11.3), so shielding is much less effective than for SMAW and SAW. The specific form or geometry of the tubular flux-cored wire can vary, being single-walled or double-walled, and with several different folds. Thus, there is quite an effect of wire type on nitrogen content as well.

11.3.4. Slag Function

Fluxes are added to the welding environment, either as part of a consumable electrode (as in SMAW and FCAW) or as an essential complement to a consumable electrode (as in SAW), to provide a protective slag and refine or "kill" the weld pool.[12] Different ingredients in the flux system provide the

[12] In fact, as seen in Section 11.3.2, they perform several other functions as well.

process with different pyrometallurgical characteristics and, thus, different weld metal properties (Jackson, 1973). By covering molten or hot weld metal, the slag formed from flux protects the weld metal from the atmosphere and provides some metallurgical refinement in the molten weld pool. In brief, welding slag consists of the glass-forming components of a flux, as well as nonmetallic inclusions formed in the weld pool during deoxidation/denitriding, which coalesce and float to the weld pool surface due to their low density compared to molten metal (i.e., their buoyancy).

As hinted at earlier, the most important chemical agent in controlling weld or any melt-processed metal composition, microstructure, and properties is oxygen. It does so by reacting with alloying elements to alter their effective role, to reduce hardenability, produce inclusions, or promote porosity. Aside from oxygen that enters from the air surrounding a weld, oxygen is introduced to the weld pool at high temperatures through oxide fluxes that dissociate in the arc and by slag–metal reactions in the weld pool.

Slag–metal reactions have been estimated by pyrochemical analysis of slag and metal compositions to occur at temperatures around 1900°C (3450°F), near the hot arc root (see Section 8.2.1.1) at temperatures around 2200–2500°C (4000–5000°F) and above the melting point of the base metal (e.g., at temperatures around 1500°C or 2732°F for steels). During the short period of time (estimated at 3–8 s) that molten slag and molten metal are in contact, oxygen from arc "hot spot" reactions is distributed throughout droplets and reacts with metallic elements to form oxides. These oxides pass into the slag to allow slag–metal reactions to proceed toward equilibrium.

As already mentioned, slag is a mixture of glass and crystalline ceramic structures. Major slag formers are silicates, aluminates, and titanates. The high-valence cations (Si^{4+}, Al^{3+}, and Ti^{4+}) in these compounds produce a bonding network that promotes glass formation. Minerals used for slag formation are rutile (titanium dioxide), potassium titanate, ilmenite, alumina, fine silica (called "silica flour"), iron powder, fluorspar, feldspar, and manganese dioxide. Table 11.4 gives the elemental makeup of common minerals used in electrode coatings.

11.3.5. Slag–Metal Chemical Reactions

The thermochemistry and kinetics of slag–metal reactions is complicated and of a highly specialized nature. The field has its basis in pyrometallurgical processing, largely steelmaking. Details on slag–metal reactions are available in several excellent sources given at the end of this chapter. What follows is intended to provide some useful background and generalities.

11.3.6. Flux Types

Welding fluxes tend to be categorized into three groups according to the main constituents:

TABLE 11.4 Elemental Makeup of Common Minerals in Electrode Coatings

Chemical Name	Typical Chemical Composition
Ilmenite	$FeO\text{-}TiO_2$
Asbestos	$3MgO\text{-}4SiO_2\text{-}4H_2O$
Talc	$3MgO\text{-}4SiO_2\text{-}H_2O$
Bentonite	Complex Al, Mg, Ca, Fe Hydroxides
Silica, quartz	SiO_2
Cellulose	$(C_6H_{10}O_5)_x$
Alumina	Al^2O_3
Muscovite, mica	$K_2O.3Al_2O_3\text{-}6SiO_2\text{-}2H_2O$
Actinolite	$CaO.MgO\text{-}2FeO\text{-}4SiO_2$
Magnetite	Fe_3O_4
Hematite	Fe_2O_3
Rutile, titania	TiO_2
Dolomite	$MgO\text{-}CaO\text{-}(CO_2)_2$
Fluorspar, fluorite	CaF_2
Cryolite	Na_3AlF_4
Lime	CaO
Limestone, calcite, marble	$CaCO_3$
Zirconia	ZrO_2
Feldspar	$K_2O\text{-}Al_2O_3\text{-}6SiO_2$
Clay	$Al_2O_3\text{-}2SiO_2\text{-}2H_2O$
Sodium silicate	SiO_2/Na_2O ratio 3.22
Potassium silicate	SiO_2/K_2O ratio 2.11
Chrome oxide	Cr_2O_3

Source: From "Welding Flux: Nature and Behavior" by D. L. Olson, S. Liu, R. H. Frost, G. R. Edwards, and D. A. Fleming, Table VII, Report No. MT-CWR-093-001, Colorado School of Mines, Golden, CO, after G. E. Linnert, *Welding Metallurgy*, 1965, used with permission of D. L. Olson.

1. *Halide-type fluxes*, such as $CaF_2\text{-}NaF$, $CaF_2\text{-}BaCl_2\text{-}NaF$, $KCl\text{-}NaCl\text{-}Na_3AlF_6$, and $BaF_2\text{-}MgF_2\text{-}CaF_2\text{-}LiF$
2. *Halide/oxide-type fluxes*, such as $CaF_2\text{-}CaO\text{-}Al_2O_3$, $CaF_2\text{-}CaO\text{-}SiO_2$, $CaF_2\text{-}CaO\text{-}Al_2O_3\text{-}SiO_2$, and $CaF_2\text{-}CaO\text{-}MgO\text{-}Al_2O_3$
3. *Oxide-type fluxes*, such as $MnO\text{-}SiO_2$, $FeO\text{-}MnO\text{-}SiO_2$, and $CaO\text{-}TiO_2\text{-}SiO_2$

The halide types are free of oxygen, and so are preferred for welding reactive metals like titanium and aluminum. The halide/oxide types are slightly oxidizing, and so are used for welding high alloy steels. The oxide types can be quite oxidizing, and are generally used for welding low-carbon and low-alloy steels.

The oxides in a welding flux are categorized into acidic, basic, and amphoteric or neutral types, based on the nature of the anion complexes they

tend to form in the molten weld pool. Acidic-type oxides include, in order of decreasing acidity, SiO_2, TiO_2, P_2O_5, and V_2O_5. Basic-type oxides include, in order of decreasing basicity, K_2O, Na_2O, CaO, MgO, BaO, MnO, FeO, PbO, Cu_2O, and NiO. Neutral oxide types include Al_2O_3, Fe_2O_3, Cr_2O_3, V_2O_3, and ZrO.

11.3.7. Common Covered- and Cored-Electrode Flux Systems

As stated in Section 11.3.2, several different arc welding processes depend on welding fluxes, and each tends to require different formulations.

11.3.7.1. Shielded Metal Arc Welding Electrode Coatings. The shielded metal arc welding (SMAW) process employs fluxes as coverings on electrodes. Four fundamental coating formulations are employed as shown in Table 11.5: cellulosic, rutile, acid-core, and basic. Characteristics of each type are also given in this table as Comments.

Table 11.6 lists typical constituents in SMAW electrode coatings, along with the function of these constituents. Table 11.4, presented earlier, gives the elemental makeup of the common minerals used in electrode coatings. Table 11.7 gives typical chemical compositions for three different SMA welding electrodes: high cellulose, high titania, and low-hydrogen types.

11.3.7.2. Flux-Cored Arc Welding Fluxes. The flux-cored arc welding (FCAW) process uses a continuous, hollow wire electrode which is filled with fluxing as well as ferro-alloying additions. Tables 11.8 and 11.9 give typical composition for three types of carbon dioxide-shielded cored electrodes (used with gas-shielded FCAW), and for four types of self-shielded flux-cored electrodes, respectively.

11.3.7.3. Submerged Arc Welding Fluxes. Fluxes used for submerged arc welding (SAW) are made in three forms: bonded, agglomerated, and fused. Bonded types consist of nonmetallic ingredients and ferro-alloy additions mixed with a low-temperature binder to produce small particles. Agglomerated types are similar, except a high-temperature ceramic–glass binder is used. Fused fluxes are produced by pouring a homogeneous glass mixture into water to create a frit. Changing from bonded to agglomerated to fused fluxes improves control of weld metal composition, especially with respect to oxygen and hydrogen content.

The seven types of SAW fluxes are listed in Table 11.10, while typical compositions for several types are given in Table 11.11.

11.3.8. Basicity Index

The efficiency of the transfer of alloying elements from a consumable electrode through an arc to a weld pool depends strongly on the physical and chemical

TABLE 11.5 Coating Formulations of Shielded-Metal-Arc Electrodes

Specification	Electrode Designation	Electrode Coating Formulation	Comments
AWS 6010	Cellulosic	20–60% rutile, 10–50% cellulose, 15–30% quartz, 0–15% carbonates, 5–10% ferro-manganese	Cellulose promotes gas shielding in the arc region. Hydrogen increases heat at weld. Hydrogen content high (30–200 ppm). Deep penetration, fast-cooling weld.
AWS 6012	Rutile	40–60% rutile, 15–25% quartz, 0–15% carbonates, 10–12% ferromanganese, 2–6% organics	Slags mainly for slag shielding. Hydrogen content fairly high (15–30 ppm).
AWS 6013	Rutile	20–40% rutile, 15–25% quartz, 5–25% carbonates, 14–14% ferromanganese, 0–5% organics	High inclusion content in weld deposit
AWS 6020	Acid–ore	Iron ore–manganese ore, quartz complex silicates, carbonates, ferromanganese	Fairly high hydrogen content. High slag content in weld metal
AWS 7015	Basic	20–50% calcium carbonate, 20–40% fluorspar, 0–5% quartz, 0–10% rutile, 5–10% ferroalloys	Fairly low hydrogen levels ($\leqslant$10 ppm), hence commonly used in welding low-alloy construction steels. Electrodes should be kept dry. Low inclusion content in weld deposit

Source: Originally from "Welding Flux: Nature and Behavior" by D. L. Olson, S. Liu, R. H. Frost, G. R. Edwards and D. A. Fleming, Report No. MT-CWR-093-001, 1993, Colorado School of Mines, Golden, CO., after T. G. F. Gary, J. Spence, and T. H. North, *Rational Welding Design*, Butterworths, London, 1975, and later in *ASM Metals Handbook*, Vol. 6: *Welding, Brazing, and Soldering*, published in 1992 by the ASM International, with permission of both D. L. Olson and ASM International, Materials Park, OH.

TABLE 11.6 Typical Functions and Compositional Ranges of Constituents for Mild Steel Arc Welding Electrode Coatings

Constituent of Coating	Function of Constituent		Composition Range, for Coating on Electrode				
	Primary	Secondary	E6010, E6011	E6013	E7018	E7024	E7028
Cellulose	Shielding gas		25–40	2–12		1–5	
Calcium carbonate	Shielding gas	Fluxing agent		0–5	15–30	0–5	0–5
Fluorspar	Slag former	Fluxing agent			15–30		5–10
Dolomite	Shielding gas	Fluxing agent					5–10
Titanium dioxide (rutile)	Slag former	Arc stabilizer	10–20	30–55	0–5	20–35	10–20
Potassium titanate	Arc stabilizer	Slag former			0–5		0–5
Feldspar	Slag former	Stabilizer		0–20	0–5		0–5
Mica	Extrusion	Stabilizer		0–15		0–5	
Clay	Extrusion	Slag former		0–10			
Silica	Slag former						
Asbestos	Slag former	Extrusion	10–20				
Manganese oxide	Slag former	Alloying					
Iron oxide	Slag former						
Iron powder	Deposition rate	Contact welding			25–40	40–55	40–55
Ferrosilicon	Deoxidizer				5–10	0–5	2–6
Ferromanganese	Alloying	Deoxidizer	5–10	5–10	2–6	5–10	2–6
Sodium silicate	Binder	Fluxing agent	20–30	5–10	0–5	0–10	0–5
Potassium silicate	Arc stabilizer	Binder		5–15	5–10	0–10	0–5

Source: Originally from "Welding Flux: Nature and Behavior," by D. L. Olson, S. Liu, R. H. Frost, G. R. Edwards and D. A. Fleming, Report No. MT-CWR-093-001, 1993, Colorado School of Mines, Golden, CO., after T. G. F. Gary, J. Spence, and T. H. North, *Rational Welding Design*, Butterworths, London, 1975, and later in *ASM Metals Handbook*, Vol. 6: *Welding, Brazing, and Soldering*, published in 1992 by the ASM International, with permission of both D. L. Olson and ASM International, Materials Park, OH.

TABLE 11.7 Coverings for Mild Steel and Low-Alloy Steel Electrodes: Chemical Composition in Weight Percent

	High Cellulose, Gas Shielded (E6010)	High Titanium Gas–Slag Shield (E6012)	Low Hydrogen Iron Powder (E7018)
CaO			14.4
TiO_2	10.1	46.0	
CaF_2			11.0
SiO_2	47.0	23.6	20.5
Al_2O_3		5.0	2.0
MgO	3.2	2.0	1.0
Na_3AlF_3			5.0
Na_3O	5.1	2.4	1.2
FeO	1.3	7.0	
Si	1.5	1.5	2.5
Mn	2.8	2.5	1.8
Fe			28.5
CO and CO_2			12.0
Volatile matter	25.0	5.0	
Moisture	4.0	2.0	0.1

Source: Originally from "Welding Flux: Nature and Behavior," by D. L. Olson, S. Liu, R. H. Frost, G. R. Edwards and D. A. Fleming, Report No. MT-CWR-093-001, 1993, Colorado School of Mines, Golden, CO., after T. G. F. Gary, J. Spence, and T. H. North, *Rational Welding Design*, Butterworths, London, 1975, and later in *ASM Metals Handbook*, Vol. 6: *Welding, Brazing, and Soldering*, published in 1992 by the ASM International, with permission of both D. L. Olson and ASM International, Materials Park, OH.

properties of the molten flux present. It would be highly desirable to be able to correlate such transfer efficiency to the flux composition. Unfortunately, lack of complete understanding of the thermodynamic properties of slags makes such correlation imprecise. In lieu of a precise analytical approach, the concept of an empirical *basicity index, BI*, has been developed, proposed as follows:

$$\text{BI} = \text{CaO} + \text{CaF}_2 + \text{MgO} + \text{K}_2\text{O} + \text{Na}_2\text{O} + \text{LiO} + \frac{\frac{1}{2}(\text{MnO} + \text{FeO})}{\text{SiO}_2} + \frac{1}{2}(\text{Al}_2\text{O}_3 + \text{TiO}_2 + \text{ZrO}_2) \tag{11.2}$$

where all chemical compositions are given in weight percent.

When the basicity index, BI, is less than 1.0, the flux is considered acidic. An index between 1.0 and 1.2 is taken to mean the flux is neutral, while an index over 1.2 classifies the flux as basic. It has been found that the higher the basicity, the cleaner the resulting weld with respect to weld pool oxygen (as oxide inclusion) content. This correlation is shown in Figure 11.14. Given the

TABLE 11.8 Typical Flux Compositions of the Three Carbon Dioxide-Shielded Flux-Cored Electrode Types

	Composition (wt%)		
	Type 1	Type 2	Type 3
Compound or Element	Titania Type (nonbasic) Flux	Lime–Titania Type (basic or neutral) Flux	Lime Type (basic) Flux
SiO_2	21.0	17.8	7.5
Al_2O_2	2.1	4.3	0.5
TiO_2	40.5	9.8	
ZrO_2		6.2	
CaO	0.7	9.7	3.2
Na_2O	1.6	1.9	
K_2O	1.4	1.5	0.5
CO_2 (as carbonate)	0.5		2.5
C	0.6	0.3	1.1
Fe	20.1	24.7	55.0
Mn	15.8	13.0	7.2
CaF_2		18.0	20.5
AWS classification	E70T-1 or E70T-2	E70T-1	E70T or E70T-5

Source: Originally from "Welding Flux: Nature and Behavior," by D. L. Olson, S. Liu, R. H. Frost, G. R. Edwards and D. A. Fleming, Report No. MT-CWR-093-001, 1993, Colorado School of Mines, Golden, CO., after T. G. F. Gary, J. Spence, and T. H. North, *Rational Welding Design*, Butterworths, London, 1975, and later in *ASM Metals Handbook*, Vol. 6: *Welding, Brazing, and Soldering*, published in 1992 by the ASM International, with permission of both D. L. Olson and ASM International, Materials Park, OH.

correlation of high toughness with low oxygen content, the importance of basicity index is clear. What limits how high the basicity index of a flux can be made is poor slag behavior for high index values. The more acidic a flux (i.e., the lower the BI), the better the control of the weld pool and covering slag, the better the bead shape, the higher the deposition rate, and the better slag detachment.

The basicity index is unable to correlate weld strength and toughness when fluxes contain high concentrations of amphoteric oxides. Given the BI's origin in steelmaking, its true applicability to welding is still open to question.

11.3.9. Thermodynamic Model for Welding Slag–Metal Reactions

Fusion welding is a highly nonequilibrium process. Consequently, phase transformations and reactions also deviate from equilibrium, often consider-

TABLE 11.9 Typical Flux Compositions of the Four Types of Self-Shielded Flux-Cored Electrodes

	Composition (wt%)			
	Type 1	Type 2	Type 3	Type 4
Compound or Element	Fluorspar–Aluminum Flux	Fluorspar–Titania Flux	Fluorspar–Lime–Titania Flux	Fluorspar–Lime Flux
SiO_2	0.5	3.6	4.2	6.9
Al	15.4	1.9	1.4	
Al_2O_3				0.6
TiO_2		20.6	14.7	1.2
CaO			4.0	3.2
MgO	12.6	4.5	2.2	
K_2O	0.4	0.6		
Na_2O	0.2	0.1		0.6
C	1.2	0.6	0.6	0.3
CO_2 (as carbonate)	0.4	0.6	2.1	1.3
Fe	4.0	50.0	50.5	58.0
Mn	3.0	4.5	2.0	7.9
Ni			2.4	
CaF_2	63.5	22.0	15.3	22.0
AWS classification	E70T-4, E60T-7, E60T-8	E70T-3	E70T-6	E70T-5

Source: Originally from "Welding Flux: Nature and Behavior," by D. L. Olson, S. Liu, R. H. Frost, G. R. Edwards and D. A. Fleming, Report No. MT-CWR-093-001, 1993, Colorado School of Mines, Golden, CO., after T. G. F. Gary, J. Spence, and T. H. North, *Rational Welding Design*, Butterworths, London, 1975, and later in *ASM Metals Handbook*, Vol. 6: *Welding, Brazing, and Soldering*, published in 1992 by the ASM International, with permission of both D. L. Olson and ASM International, Materials Park, OH.

ably. Chemical reactions, such as the gas–metal reactions described in Section 11.1 and slag–metal reactions of interest here, do not achieve equilibrium during fusion welding. Available time for reaction is simply too short and temperature for reaction is nonuniform.

To attempt quantitative calculations relating to slag–metal reactions, investigators have devised the concept of effective equilibrium temperature. The effective equilibrium temperature is the temperature at which the equilibrium composition of the reacting system becomes identical to the actual weld composition after welding. Once obtained, this temperature can be used to calculate the weld metal composition using available thermodynamic information such as the activity coefficients of the components in the reaction system

TABLE 11.10 Fluxes for Submerged Arc Welding

Flux Type	Chemical Constituents	Advantages
Manganese silicate	$MnO + SiO_2 > 50\%$	Moderate strength, tolerant to rust, fast welding speeds, high heat input, good storage
Calcium–high silica	$CaO + MgO + SiO_2 > 60\%$	High welding current, tolerant to rust
Calcium silicate–neutral	$CaO + MgO + SiO_2 > 60\%$	Moderate strength and toughness, all current types, tolerant to rust, single or multiple-pass weld
Calcium silicate–low silica	$CaO + MgO + SiO_2 > 60\%$	Good toughness with medium strength; fast welding speeds, less change in composition and lower oxygen
Aluminate basic	$Al_2O_3 + CaO + MgO > 45\%$ $Al_2O_3 > 20\%$	Good strength and toughness in multipass welds. No change in carbon; loss of sulfur and silicon
Alumina	Bauxite base	Less change in weld composition and lower oxygen than for acid type, moderate to fast welding speeds
Basic fluoride	$CaO + MgO + MnO + CaF_2 > 50\%$ $SiO_2 < 22\%$, $CaF_2 < 15\%$	Very low oxygen, moderate to good low-temperature toughness

Source: Originally from "Welding Flux: Nature and Behavior," by D. L. Olson, S. Liu, R. H. Frost, G. R. Edwards and D. A. Fleming, Report No. MT-CWR-093-001, 1993, Colorado School of Mines, Golden, CO., after "The Physical and Chemical Behavior Associated with Slag Detachment during Welding," by D. L. Olson, G. R. Edwards, and S. K. Marya, *Ferrous Alloy Weldments*, Key Engineering Materials, Vol. 67–70, 1992, pp. 253–268, Trans. Tech. Publ. Zurich, Switzerland, and later in *ASM Metals Handbook*, Vol. 6: *Welding, Brazing, and Soldering*, with permission of both D. L. Olson and ASM International, Materials Park, OH.

and the equilibrium constant. Clearly, the effective equilibrium temperature is chosen for convenience of calculation and is not the temperature at which chemical reactions in the weld pool actually reach equilibrium, nor is it the average temperature of the weld pool during welding.

The concept of effective equilibrium temperature can be understood with the aid of Figure 11.15. If curves AB and $A'B'$ represent the composition–temperature relationship under actual and equilibrium conditions, respectively, and C_0 and C_d represent the initial and final concentrations of a particular component of interest in weld metal that solidifies at T_s, then composition C_d corresponds to temperature T_s and T_{eq} according to the actual and equilibrium conditions,

TABLE 11.10 (*Continued*)

Limitations	Basicity	Flux Form	Comments
Limited use for multipass welding, use where no toughness requirement, high weld-metal oxygen, increase in silicon on welding, low in carbon	Acid	Fused	Associated manganese gain; maximum current, 1100 A; higher welding speeds
Poor weld toughness, use where no toughness requirement, high weld metal oxygen	Acid	Agglomerated fused	Differ in silicon gain, some capable of 2500 A, wires with high manganese
	Neutral	Agglomerated fused	
Not tolerant to rust, not used for multiwire welding	Basic	Agglomerated fused	
Not tolerant to rust, limited to DCEP welding, poor slag detachability	Basic	Agglomerated	Usually manganese gain; maximum current ~1200 A; good mechanical properties
	Neutral	Agglomerated fused	
May present problems of slag detachability. May present problem of moisture pickup	Basic	Agglomerated fused	Can be used with all wires, preferably direct current welding, very good weld properties

respectively. The effective equilibrium temperature T_{eq} is not the real average temperature of the weld pool or the actual composition would be C' rather than C_d.

Eager (1978) and later Chai and Eager (1980, 1981) studied the thermodynamics of slag–metal reactions during welding. Using the definition of basicity index in Equation 11.2, but eliminating CaF_2 as a component of the flux, Eager and his coworker replotted data on weld oxygen content measured experimentally by Tuliani et al. (1969). The result of this replotting is shown in Figure 11.16. Based on the replotted data and on an effective equilibrium temperature of 2000°C (3600°F), Chai and Eager proposed a thermodynamic model for slag–metal reactions during submerged arc welding.

In this thermodynamic model, the activity of SiO_2 in the slag was calculated as a function of basicity index for SiO_2-CaO and SiO_2-CaO-FeO slags over Fe-Si welds made by SAW.[13] Results are shown in Figure 11.17. Using

[13] The work of Eager and Chai was all done using the following relationships: $k = A_{Si}a_{O_2}/a_{SiO_2}$ and $k = -28{,}360T^{-1} + 10.61$ for the reaction $SiO_{2(liq)} = [\%Si] + 2[\%O]$, and, also, for $Fe_{(liq)} + [\%O] = FeO_{(liq)}$, $k = a_{FeO}/a_{Fe}a_O$ and $k = 6372T^{-1} - 2.73$.

TABLE 11.11 Typical Submerged Arc Welding Fluxes

Flux	Composition (wt%)									Basicity Index (BI)
	Al_2O_3	SiO_2	TiO_2	MgO	CaF_2	CaO	MnO	Na_2O	K_2O	
A	49.9	13.7	10.1	2.9	5.7	—	15.1	1.6	0.2	0.4
B	24.9	18.4	0.2	28.9	24.2	—	1.8	2.1	0.07	1.8
C	19.3	16.3	0.8	27.2	23.6	9.8	0.08	0.9	1.1	2.4
D	18.1	13.2	0.5	28.2	31.8	4.5	0.1	0.9	0.9	3.0
E	17.0	12.2	0.7	36.8	29.2	0.7	8.9	1.6	0.1	3.5

Source: Originally from "Welding Flux: Nature and Behavior," by D. L. Olson, S. Liu, R. H. Frost, G. R. Edwards and D. A. Fleming, Report No. MT-CWR-093-001, 1993, Colorado School of Mines, Golden, CO., after "The Physical and Chemical Behavior Associated with Slag Detachment during Welding," by D. L. Olson, G. R. Edwards, and S. K. Marya, *Ferrous Alloy Weldments*, Key Engineering Materials, Vol. 67–70, 1992, pp. 253–268, Trans. Tech. Publ. Zurich, Switzerland, and later in *ASM Metals Handbook*, Vol. 6: *Welding, Brazing, and Soldering*, with permission of both D. L. Olson and ASM International, Materials Park, OH.

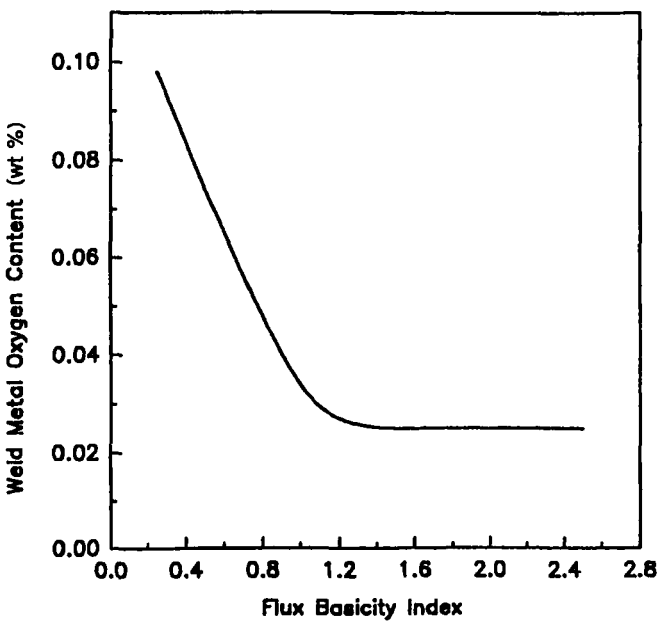


Figure 11.14 Correlation between the toughness of a weld metal and its residual oxygen content as influenced by basicity index of the welding flux employed. (From "Welding Flux: Nature and Behavior" by D. L. Olson, S. Liu, R. H. Frost, G. R. Edwards and D. A. Fleming, Figure 5, Report No. MT-CWR-093-001, 1993, Colorado School of Mines, Golden, CO, used with permission of D. L. Olson.)

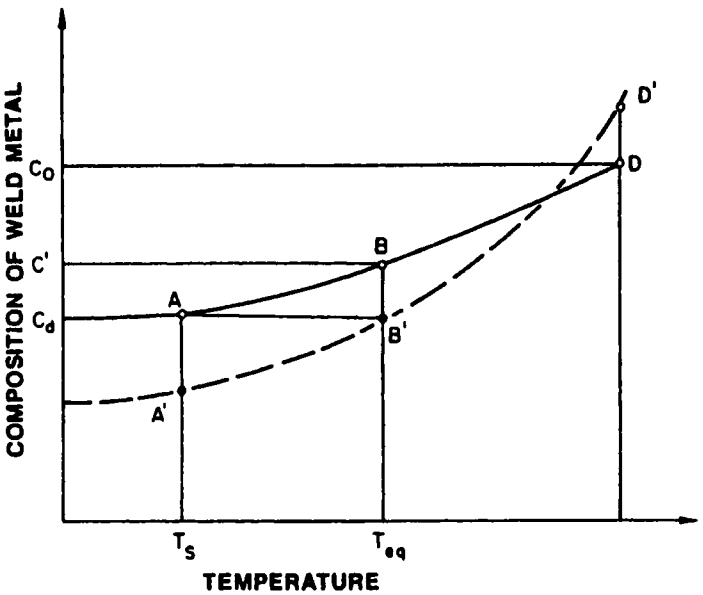


Figure 11.15 Schematic illustration of composition of weld metal versus temperature. (Originally from *Principles and Technology of the Fusion Welding of Metal*, Vol. 1, 1979, Mechanical Engineering Publishing Company, Peking, China, in Chinese, out of *Welding Metallurgy* by S. Kou, published in 1987 by and reprinted with permission of John Wiley & Sons, Inc., New York.)

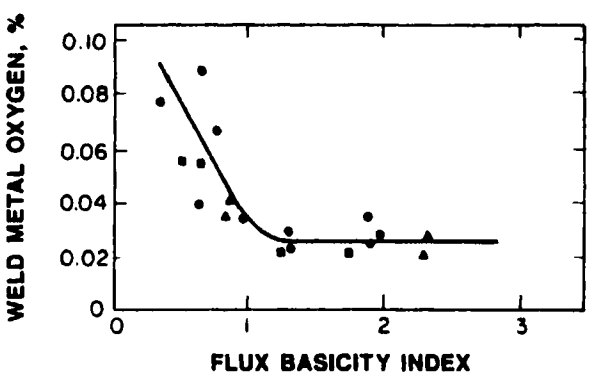


Figure 11.16 Weld metal oxygen content as a function of flux basicity (as defined by Eq. 11.2). (From "Slag–metal equilibrium during submerged arc welding" by C. S. Chai and T. W. Eager, *Metallurgical Transactions*, **12B**, 539–547, 1981, published by and used with permission of the ASM International, Materials Park, OH.)

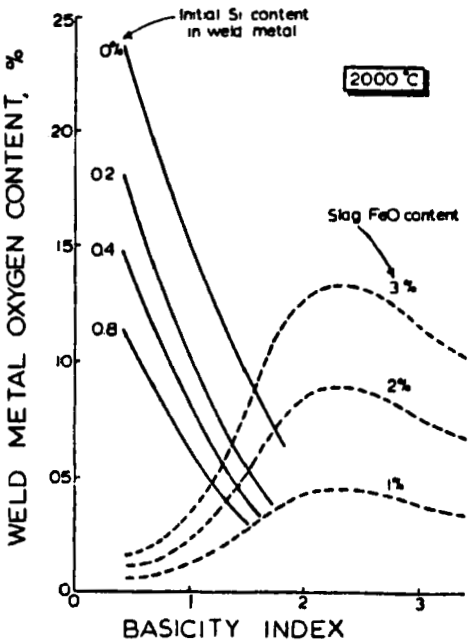


Figure 11.17 Dissolved oxygen equilibrium at 2000C as a function of basicity index in SiO_2–CaO and SiO_2–CaO–FeO slags over Fe–Si melts. (From "Sources of weld metal oxygen contamination during submerged arc welding" by T. W. Eager, *Welding Journal*, 57(3), 76s–80s, 1978, published by and used with permission of the American Welding Society, Miami, FL.)

available data for the activity coefficient of SiO_2 at 1600°C (2900°F), and assuming a regular solution model, the concentration of SiO_2 in the flux was calculated as a function of the flux BI for various levels of weld metal Si content. The results of the calculation are shown in Figure 11.18. Similar calculations were performed for MnO, as shown in Figure 11.19. According to Eager and Chai, these figures can be used to determine the Si and Mn content of welds under similar welding conditions.

Obviously, the thermodynamics of slag–metal reactions is complicated and, so, it is left to the interested reader to obtain details.

11.4. SUMMARY

Hot, no less molten, metals are extremely reactive, so it is no surprise that molten metal from fillers as well as base metals reacts with the environment surrounding the weld and weldment. For all fusion welding processes, reactions between molten metal as it is transferred from a consumable electrode, filler wire, or rod and molten metal in the weld pool produced by the heat source

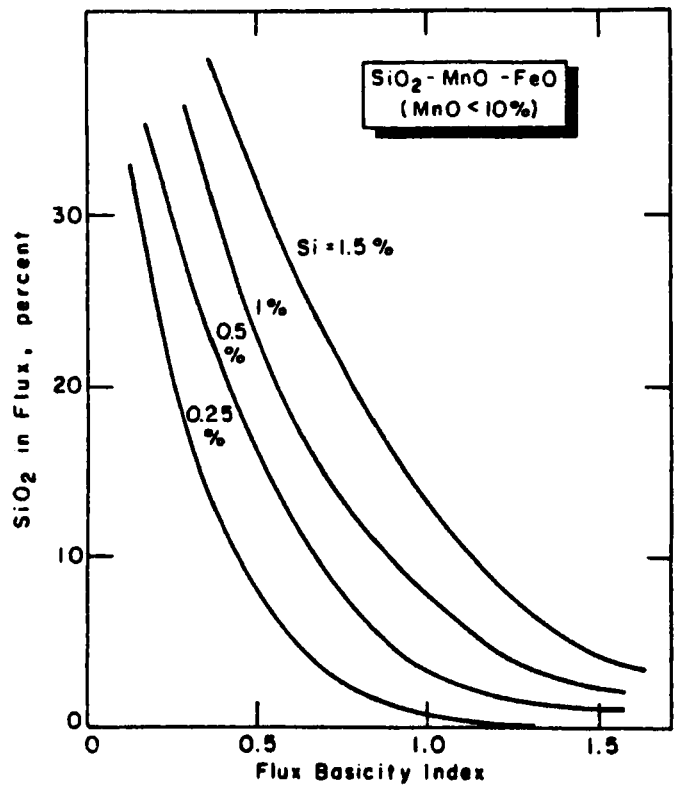


Figure 11.18 The relationship between the equilibrium SiO_2 content and the flux basicity index (BI) for a given weld metal Si content in the SAW flux system SiO_2–MnO–FeO at 2000°C. (From "The effect of SAW parameters on weld metal chemistry" by C. S. Chai and T. W. Eager, *Welding Journal*, **59**(3), 93s–98s, 1980, published by and used with permission of the American Welding Society, Miami, FL.)

occur with gases in the surroundings. In air, reactions between molten metals occur for oxygen, nitrogen, and hydrogen, the latter being generated from dissociation of water (or hydrocarbon-based oils, greases, etc.) by intense heat sources. Reactions can include dissolution of gas(es) into the molten weld pool that give rise to porosity as solubility for the gas decreases with decreasing temperature in the liquid; potent interstitial solid-solution strengthening; stabilization of certain solid phases; and formation of embrittling compounds in the form of nonmetallic inclusions.

To prevent such gas–metal reactions, either molten metal must be protected from air by excluding it, or potentially detrimental gases must be removed by element additions to fillers that have greater affinity for these gases than the base metal (in a process called killing). Given this general need, various means for protecting vs. killing were described, including the use of shielding gas(es),

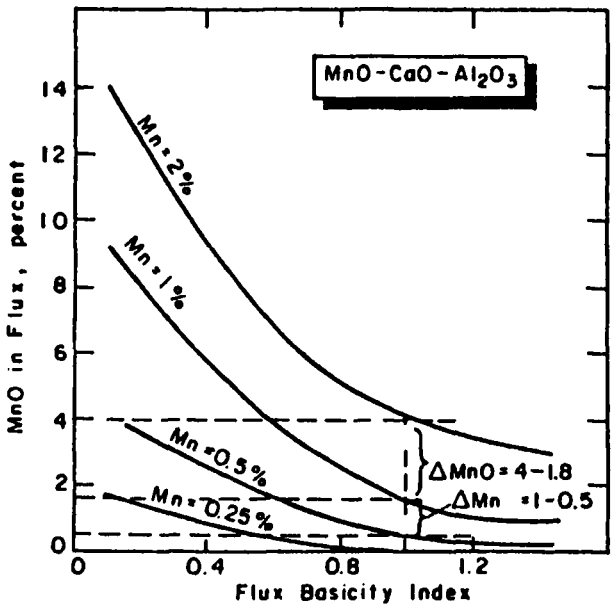


Figure 11.19 The relationship between equilibrium MnO content and the flux basicity index for a given weld metal Mn content in the $MnO-CaO-Al_2O_3$ system at 2000°C. (From "Slag–metal equilibrium during submerged arc welding" by C. S. Chai and T. W. Eager, *Metallurgical Transactions*, **12B**, 539–547, 1981, published by and used with permission of the American Welding Society, Miami, FL.)

vacuum, and flux and slag, and reliance on self-protection and self-fluxing. Particular attention was given to the use of fluxes and slag–metal reactions as a means of protecting and refining weld pools by killing.

A brief explanation of flux systems, assessment of their effectiveness using the concept of basicity index, and a thermodynamic model for slag–metal reactions occurring during welding were presented.

REFERENCES AND SUGGESTED READING

Bandopadhyay, A., Banerjee, A., and DebRoy, T., 1992, "Nitrogen activity determination in plasmas," *Metallurgical Transactions*, **23B**, 207–214.

Bastien, P. G., 1961, "Hydrogen in welding," *Welding Research Abroad*, February, 12–22.

Chai, C. S., and Eager, T. W., 1980, "The effect of SAW parameters on weld metal chemistry," *Welding Journal*, **59**(3), 93s–98s.

Chai, C. S., and Eager, T. W., 1981, "Slag–metal equilibrium during submerged rrc welding," *Metallurgical Transactions*, **12B**, 539–547.

Erokin, A. A., 1964, *Kinetics of Metallurgical Processes in Arc Welding*, Mashinostroenie (in Russian).

Eager, T. W., 1978, "Sources of weld metal oxygen contamination during submerged arc welding," *Welding Journal*, **57**(3), 76s–80s.

Easterling, K., 1992, *Introduction to the Physical Metallurgy of Welding*, 2d ed., Butterworth-Heinemann, London.

Eastwood, L. W., 1953, *Gases in Non-ferrous Metals and Alloys*, American Society for Metals, Miami, FL.

deKazinczy, F., 1961, "Crack formation in steel during electrolytic hydrogen absorption," *Teknisk-Vetenskaplig Forstening*, **32**(3), 159–162 (in Swedish).

Fumes and Gases in the Welding Environment, 1979, American Welding Society, Miami, FL.

Gary, T. G. F., Spence, J., and North, T. H., 1975, *Rational Welding Design*, Butterworths, London.

Jackson, C. T., 1973, "Fluxes and slags in welding," *Welding Research Bulletin No.* 190, Welding Research Council, New York.

Katz, J. D., and King, T. B., 1989, "The kinetics of nitrogen absorption and desorption from a plasma arc by molten iron," *Metallurgical Transactions*, **20B**, 175–185.

Kumar, B., 1968, *Physical Metallurgy of Iron and Steel*, Asia Publications.

Linnert, G. E., 1965, *Welding Metallurgy*, Vols. 1 and 2, 3d ed., American Welding Society, Miami, FL.

The Making, Shaping and Treatment of Steel, 1971, U.S. Steel Corporation, Pittsburgh, PA.

Pehlke, R., and Elliott, J. F., 1960, "Solubility of nitrogen in liquid iron alloys, 1: thermodynamics," *Transactions of the Metallurgical Society AIME*, **218**, 1088–1101.

Petch, N. J., and Stables, P., 1952, "Delayed fracture of metals under static load," *Nature*, **169**, 842–843.

Rein, R. H., 1974, in *Proceedings of a Workshop on Welding Research Opportunities*, edited by B. A. McDonald, Office of Naval Research, AD–AO28395, Washington, DC, p. 92.

Seferian, D., 1962, *The Metallurgy of Welding*, Chapman & Hall, London.

Troiano, A. R., 1960, "The role of hydrogen and other interstitials in the mechanical behavior of metals," *Transactions of the ASM*, **52**, 54–80.

Tuliani, S. S., Boniszewski, T., and Eaton, N. F., 1969, "Notch toughness of commercial submerged-arc weld metal," *Welding and Metal Fabrication*, **37**, 327–339.

Vaughn, H. G. and de Morton, M. E., 1957, "Hydrogen embrittlement of steel and its relation to weld cracking," *British Welding J.*, **4**(1), 40–61.

Zapffe, C. A., 1950, "How furnace moisture causes embrittlement," *Iron Age*, **166**(26), 60–65.

Suggested readings in shielding gases, fluxes and slag

ASM Handbook, Vol. 6: *Welding, Brazing, and Soldering*, 1993, American Society for Materials, Materials Park, OH. [Shielding gases]

AWS/ANSI Recommended Practices for Shielding Gases for Welding and Plasma Cutting, 1994, American Welding Society, Miami, FL. [Shielding Gases]

Boniscewski, T., 1992, *Self-Shielded Arc Welding*, Abington, Cambridge, UK. [Fluxes and slag].

O'Brien, R. L. (Editor), *Jefferson's New Welding Encyclopedia*, 1997, 18th ed., American Welding Society, Miami, FL. [Electrode formulation, fluxes, slag).

O'Connor, L. P. (Editor), 1992, *Welding Handbook*, Vol. 1: *Welding Technology*, American Welding Society, Miami, FL. [Shielding gases]

Olson, D. L., Liu, S., Frost, R. H., Edwards, G. R., and Fleming, D. A., 1993, "Welding Flux: Nature and Behavior," Report No. MT-CWR-093-001, Colorado School of Mines, Golden, CO. [Fluxes and slag]

CHAPTER 12

WELD CHEMICAL HETEROGENEITY

Conflicting phenomena occur during fusion welding that tend to cause the weld pool and final weld to become both more heterogeneous and more homogeneous at the same time. The result is that real welds are never completely homogeneous, and are often severely heterogeneous. The obvious desire, despite everything that tries to prevent it, is to obtain homogeneous welds. The goal is that welds end up homogeneous in chemical composition, homogeneous in (micro)structure, and, as a result of both of these, homogeneous in properties. Only then can a designer both get the most from the weld and be truly confident in his/her design.

The principal phenomenon that tends to cause heterogeneity is the rejection of solute from a molten alloy as it solidifies. This is a natural consequence of solute partitioning between the liquid and solid phase of an alloyed material expressed by the equilibrium distribution coefficient, k_0, where k_0 is the ratio of the composition of the solid and the liquid (i.e., $k_0 = C_S/C_L$) that would exist at equilibrium at any particular temperature during the process of solidification. Under true equilibrium, the weld pool throughout solidification, and the final weld after solidification, would be completely homogeneous.[1] It would have to be, since at equilibrium there can be no composition gradients. The reality of welding, however, is that solidification takes place under nonequilibrium conditions, often far removed from equilibrium. The result is incomplete solute redistribution both in the liquid weld pool and, at least partially as a consequence, in the final weld. This is all discussed in great detail in Chapter 13.

[1] As used here, homogeneous doesn't have to mean completely uniform and continuous, it just means generally homogeneous in overall composition and microstructure everywhere.

The principal phenomenon that tends to cause homogeneity in the weld pool is convection. Convection stirs the pool and, so, mixes the liquid in an attempt to remove any composition gradients. However, the process of convection never results in perfect mixing, as will be seen, and even if it did, there is still nonequilibrium solute redistribution and microsegregation to contend with. Convection was discussed in Chapter 10.

Let's look now at the various possible sources of chemical heterogeneity in a weld pool and final weld, leaving some details until Chapter 13.

12.1. WELD (POOL) DILUTION

In most instances, filler metal must be added to joints during fusion welding.[2] When it is, unless the filler is of exactly the same composition as the base metals, and the base metals are the same as one another, the weld deposit consists of a mixture of parent and filler metals. When filler has the same composition as the base metal(s), the process is known as homogeneous welding (see Section 2.4.5). When the filler is of a different composition than the base metals, and/or the base metals are not the same as one another, the process is known as heterogeneous welding

The reason for choosing a filler whose composition is the same as two identical base metals is to achieve what is called matching. Matching of filler and base metal compositions has several benefits, including (1) absolutely certain chemical, physical, and mechanical compatibility; (2) uniform chemical reactivity for equal corrosion resistance of base and weld metal[3]; (3) uniform mechanical properties in the weld and base metal, except for differences (especially in ductility and toughness and fatigue strength) affected by the cast structure as opposed to wrought structure of wrought base metal; and (4) no concerns pertaining to mixing.

Despite these advantages, heterogeneous filler is often required or preferred. When the base metals being joined are dissimilar, the filler obviously cannot be the same as both, but must be compatible with each. Dissimilar metal or alloy welding requires a heterogeneous filler. If the base metals are the same as one another, it may still be preferable to use a filler that is different (heterogeneous). A filler that is more heavily alloyed (or richer) than the base metal may be chosen to (a) compensate for any alloy loss by evaporation during molten metal transfer (see Section 10.5) or (b) offset any adverse effect of the cast structure of welds compared to the wrought structure of wrought base metals. This latter situation is called overmatching. The filler may be overmatched with regard to corrosion resistance or tensile strength or toughness or some other mechanical property; the reason being, in each case, to assure that the weld

[2] The exception, when no filler metal is added, is known as autogenous welding (see Section 2.4.5).
[3] In fact, minor losses of alloying elements in the filler largely by evaporation (see Section 10.5) can lead to mismatch, which can render the weld more susceptible to corrosion than the base metal.

does not fail before the base metal.[4] Contrarily, it could be preferable to undermatch a filler to force failure into the weld, thereby protecting the structural elements comprising the weldment either mechanically or from the standpoint of corrosion.

Since fusion welding requires or demands that a portion of each base metal or substrate involved in the joint melt along with the filler, heterogeneous fillers inevitably are diluted by the base metal(s). The degree of *dilution* depends on (1) the type of joint and joint edge preparation; (2) the welding process, process parameters (including operating current mode), and technique used; and (3) the mismatch between the filler and base metal(s). In general, dilution (D), expressed as a percentage, is defined as

$$D = \frac{100\% \times \text{weight of parent metals melted}}{\text{Total weight of fused metal}} \tag{12.1}$$

Weight in this relationship can be taken to be relative areas of a representative cross section of the weld, as shown in Figure 12.1.

Figure 12.2 schematically illustrates how the type of joint (fillet, groove, or overlap) and specific edge preparation (type of groove, e.g., U or V) make a difference in the degree of dilution. Figure 12.3 schematically illustrates how process, process operating mode, process operating parameters, and number of passes also make a difference in the degree of dilution. The key point is that dilution can be controlled! As a general rule, dilution is a maximum for single-pass welds made through sections with square- or straight-butt edge preparations in thin materials, and is minimum in fillet welds or in multipass welds with normal groove preparations.

Welding technique can also make a difference in degree of dilution. A series of overlapping, fine stringer beads (made with low heat input) result in less dilution than fewer heavy passes (made with high heat input) in multipass welds. A special technique used to minimize dilution is called buttering. In the

[4] A failure in the weld zone (consisting of the fusion and heat-affected zones) can make engineers reluctant to choose welding as the method for joining in future applications. Once burned, by any material or process, many designers will not take a second chance.

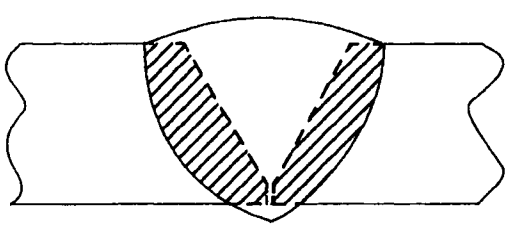


Figure 12.1 Schematic of a single-V groove showing the area of base metal melted versus the total area of the weld fusion zone; equivalent to weight percents of each.

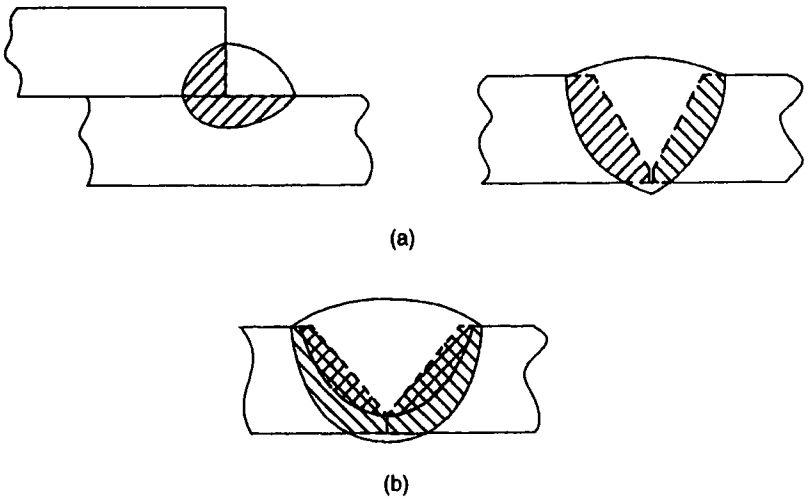


Figure 12.2 Schematic showing how (a) the type of joint (inside corner fillet versus single-V groove) and (b) edge preparation (single V-groove versus single U-groove) make a difference in the degree of dilution, *D*.

case where welding dissimilar base metals could result in metallurgical incompatibilities that could adversely affect weldability (e.g., produce hard spots, general embrittlement, or cracks), buttering is especially useful. The best example is probably welding a mild steel to a gray, malleable, or nodular cast iron containing 2–4 wt% C. If either a mild steel filler (that matches the mild steel base metal) or an austenitic stainless steel (which is simply compatible with the mild steel base metal) is used, carbon pickup from the cast iron by dilution could render the weld metal susceptible to transformation hardening to form brittle martensite, and would probably result in cracking in the weld. By buttering the cast iron joint faying surface with fine, side-by-side, overlapping stringer beads (made using very low arc energy and net heat input) of pure nickel (which will not be adversely affected by pickup of carbon), and then filling with either a mild steel or austenitic stainless steel, carbon pickup by the filler can be virtually eliminated. The buttering layer creates a cushion against intermixing between the cast iron and the filler.

Another place where dilution must be taken into account is in weld overlaying, also known as cladding, surfacing, or hardfacing, to provide protection against corrosion or wear. Too much dilution by the base metal can severely degrade the desired properties of the overlay. Multiple layers of overlay (to get past the dilution), or an intermediate, buttering or "cushion coat" (to block dilution) will help.[5]

[5] Cushion coats are also employed in hardfacing to provide some give or strain accommodation under hard, wear-resistant coatings that must also tolerate impact. A good example is the use of a softer, impact-resistant cushion coat under a wear-resistant coating on swing hammers used for crushing rock.

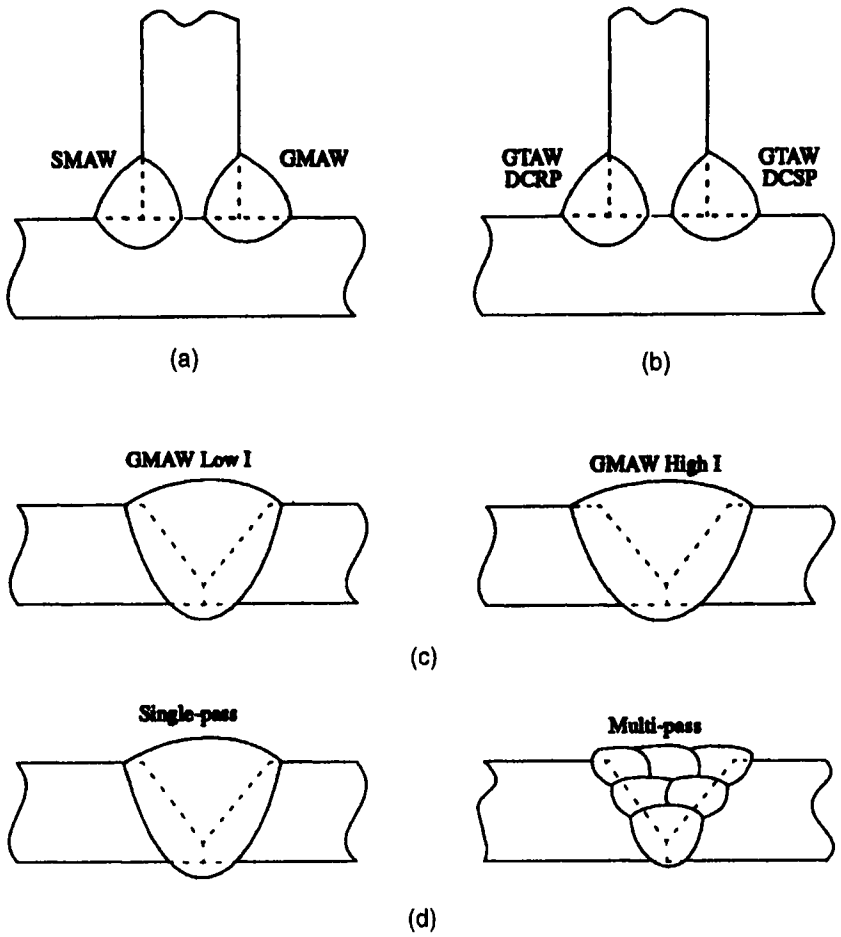
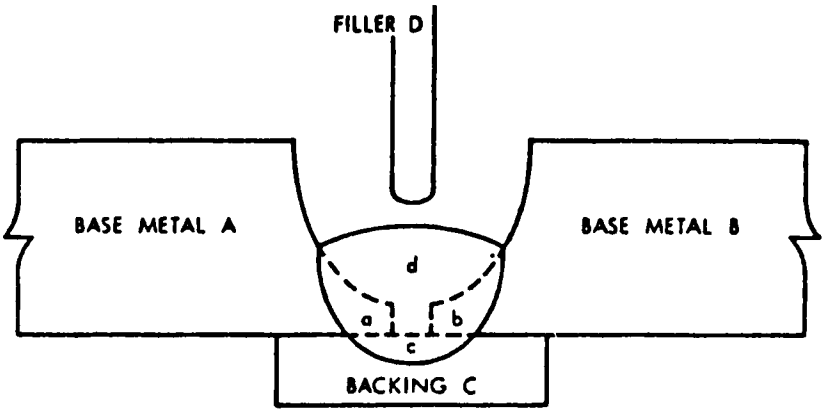


Figure 12.3 Schematic showing the effects of (a) process (e.g., SMAW versus GMAW), (b) operating mode (e.g., GTAW DCSP versus DCRP), (c) operating parameters (e.g., high versus low net heat input), and (d) single- versus multipass welds on dilution.

For multipass welds, Estes and Turner (1964) developed formulas for calculating filler metal dilution and, particularly, composition of the all-important root pass. These formulas are given in Figure 12.4, along with a schematic illustrating a typical joint to which the formulas apply.

12.2. MICROSEGREGATION AND BANDING IN THE WELD METAL

As stated at the start of this chapter and presented in detail in Chapter 13, microsegregation is the result of normal solute redistribution at the solid–liquid interface as an alloy solidifies. Under conditions other than equilibrium,



$$(1)\ \%\ \text{DILUTION} = \frac{a + b + c}{a + b + c + d} \times 100$$

$$(2)\ \%\ \text{ELEMENT E IN WELD BEAD} = \frac{1}{a + b + c + d}\left[a(\%\ \text{E in a}) + b(\%\ \text{E in b}) + c(\%\ \text{E in c}) + d(\%\ \text{E in d})\right]$$

Figure 12.4 Formulas for calculating dilution and percentage of each element in the root pass of a multipass weld developed by Estes and Turner (1964). (From "Dilution in multipass welding of AISI 4130 to type 304 stainless steel" by C. L. Estes and P. W. Turner, *Welding Journal*, 43(12), 541s–550s, 1964, published by and used with permission of the American Welding Society, Miami. FL.)

that is, nonequilibrium, this redistribution persists in the final weld, resulting in what is called dendritic coring or simply coring. Briefly, in dendritic coring, the first solid to form is leaner in solute than all subsequent solid that forms as cooling from the liquidus temperature (where solidification begins) to the solidus temperature (where solidification is completed) continues, with the last solid to form being the most rich in solute of all.

Besides the virtually unavoidable microsegregation and all of its consequences, given that welding is never performed under equilibrium conditions (or even close to them), solute segregation can also occur as the result of variations in growth rate of the solid as the solid–liquid interface advances. Suffice to say here that changing the rate of solidification changes the rate of solute rejection and subsequent redistribution. The result is called banding and shows up as phase-contrast in etched metallographic specimens and photomicrographs. The origin of banding is made clearer by referring to Figure 12.5, which shows a schematic trace of composition varying about the nominal alloy composition C_0 as a function of the movement of the solidification front for changing growth rates, R_1 and R_2. When the growth rate is suddenly increased from R_1 to R_2, an extra amount of solute is rejected into the liquid at the solid–liquid interface. The metal solidifying behind this interface right after this

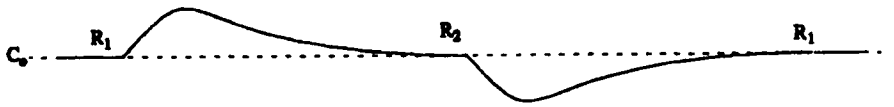


Figure 12.5 Schematic trace of local, average composition as a solid–liquid interface advances and changes in the rate of growth, R1 and R2, occur. (After figure in *Welding Metallurgy* by S. Kou, published in 1987 by and used with permission of John Wiley & Sons. Inc., New York.)

increase in growth rate thus has a higher concentration of solute than before the increase. For slower growth rates, $R_2 < R_1$, the opposite occurs. The solute concentration, in both cases, eventually resumes its steady-state value, as shown by the trace in Figure 12.5.

Growth rate changes leading to banding result from thermal fluctuations that arise during welding, which, in turn, can result from fluctuations in current, fluctuations in voltage, or erratic welding or travel speed. The consequence of banding need not be serious, although it could be, particularly because it could adversely affect corrosion resistance. The real problem, as for the occurrence of porosity, is evidence that the process is not under proper control.

12.3. UNMIXED AND PARTIALLY MIXED ZONES

Every fusion weld pool, regardless of how violent the convection, has a stagnate layer at its boundaries with the unmelted or partially melted surrounding region, as shown in Figure 12.6. The reason for this stagnate layer is

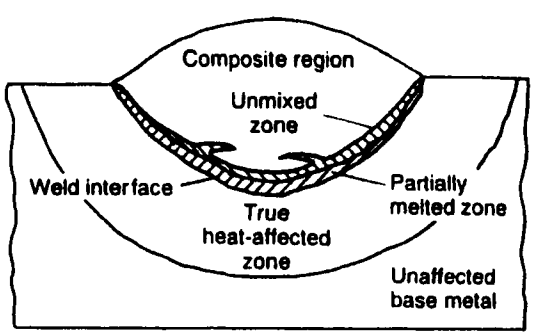


Figure 12.6 Schematic showing the different discrete regions present in a single-pass fusion weld, including the unmixed zone. (From ASM *Handbook*, Vol. 6: *Welding, Brazing, and Soldering*, published in 1993 by and used with permission of the ASM International, Materials Park, OH.)

friction. Molten metal, like any liquid, must have continuity with the solid (metal) with which it comes in contact. At the interface between the two, the velocity of the liquid must be the same as the velocity of the solid. If the solid isn't moving, the liquid can't be moving either.

In this stagnate layer, the melted base metal remains virtually unmixed with the molten filler metal. The region is known as the unmixed zone for this reason, and was discovered by Savage et al. (1976). Beyond the unmixed zone, as one approaches the main weld pool, there is a partially mixed zone, assuming that the bulk of the weld pool is rather completely mixed. This latter assumption is quite reasonable and valid for some processes, where the forces leading to convection, especially electromagnetic force and impinging force (see Chapter 10), are significant. Examples of such processes are most arc welding processes operating at higher currents, and EBW and LBW operating in the keyhole mode. For these processes, the unmixed and partially mixed zones would be narrow. For other processes, like oxyacetylene welding or laser-beam welding operating in the melt-in mode, the weld pool is fairly quiescent, so the unmixed and partially mixed zones can become large relative to the overall weld pool width. These zones can also be quite wide for fusion processes that produce very wide welds, such as SAW, EGW, and, especially, ESW.

The consequence of an unmixed zone (and, to a lesser extent, a partially mixed zone) is that it is unlike the bulk of the weld in composition and unlike the base metal in structure and, possibly, composition as a result of evaporative losses. Unmixed zones have been studied by many researchers and found to promote formation of undesirable phases such as martensite (when, for example, Cr-Ni-Mo steels are welded with 20 Cr–10 Ni austenitic stainless steel [Lippold and Savage, 1980]), hydrogen-induced cracking (Savage et al., 1976), or preferential corrosive attack (Lundin et al., 1997). Figure 12.7 shows an actual unmixed zone in a fusion weld.

Unfortunately, unmixed and partially mixed zones cannot be prevented or eliminated, although they can be kept to a minimum by maximizing convection.

12.4. IMPURITIES IN THE WELD METAL

Three general types of impurities that can be found in weld metal predominate: (1) gas porosity, (2) nonmetallic inclusions, and (3) foreign-metal inclusions. The origin of gas porosity was discussed at length in Section 11.1.3. Besides introducing stress risers, large gas pores can alter solidification substructure, since they are often surrounded by a finer planar or radially aligned cellular structure typical of a chill zone found in a casting than the coarser cellular–dendritic, columnar–dendritic, or equiaxed–dendritic structure comprising the bulk of welds. These substructures and their origin are discussed in Chapter 13.

Nonmetallic inclusions can easily arise during welding from slag entrapped within a weld. This is particularly a problem in multipass welds, where

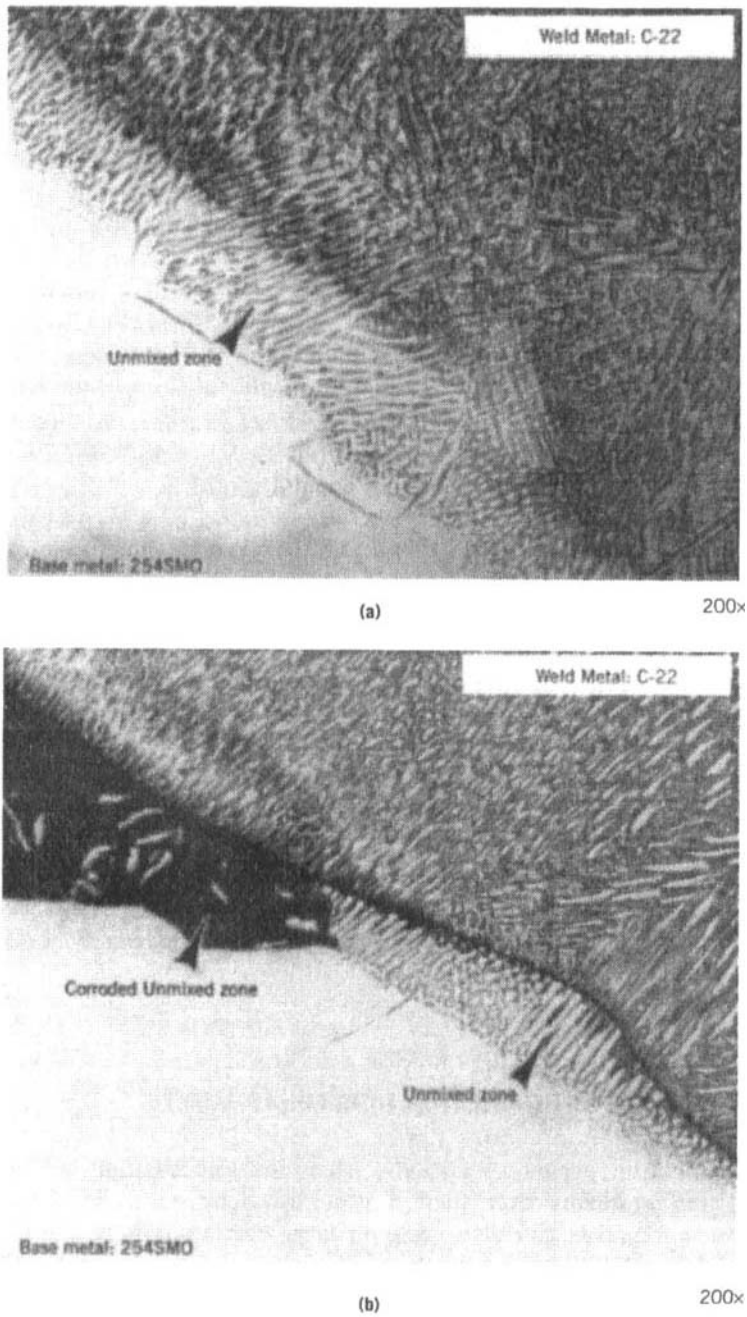


Figure 12.7 Photomicrograph of the unmixed zone at the extreme boundary of the weld fusion zone in Alloy 254SMO welded with Alloy C-22 filler (a) showing accelerated corrosion thereof (b). (Courtesy of C. D. Lundin, University of Tennessee at Knoxville, Knoxville, TN.)

remnants of slag from previous passes can become stuck in tight spaces between passes. It can also occur in single-pass welds as a result of slag being forced into the weld pool by either the torch and weld manipulation or convection and not given sufficient time to float to the surface before the weld solidifies. Nonmetallic inclusions can also come from (1) dirty base metal (preexisting nonmetallic stringers), (2) fragments of either flux or slag from covered electrodes or flux-cored wires, and (3) particles of dirt or other debris that fall into the weld during welding. The latter problem is not uncommon in field repair of rusty or mud-caked equipment.

Foreign-metal inclusions can occur as the result of either touching the tip of a tungsten nonconsumable electrode to the weld during GTA welding or as the result of a small particle of tungsten melting or being expelled and falling from the electrode into the weld. The former problem is one of the advantages of plasma arc over gas–tungsten arc welding, in that the likelihood of accidentally touching the tip of the electrode to the weld is precluded by it being recessed within the torch nozzle. The latter problem, which is more likely for DCRP than either DCSP or AC operation, can be minimized by proper tip preparation (e.g., "balling" of the tip for DCRP), torch cooling using water, and reduction of welding current.

Another source of foreign-metal inclusion can arise during consumable electrode arc welding in the short-circuiting transfer mode (see Section 9.3). If voltage and wire feed rate are not properly adjusted for GMAW, for example, the continuously fed wire electrode can stub into the weld and pieces can melt off and become stuck. These, as opposed to many of the other impurities, would almost certainly be detected by the operator, however, and so should normally not pose a problem in finished welds, provided they are removed or welded back over.

Whether inclusions are low-density nonmetallic compounds or high-density metals, they lead to stress concentration, especially under fatigue or impact loading. Figure 12.8 schematically illustrates the various types of weld heterogeneity, other than dilution.

12.5. MACROSEGREGATION IN DISSIMILAR WELDS

Microsegregation occurs in virtually all welds and castings and refers to composition gradients that span a grain or dendrite width. Much more extensive segregation can also occur in large castings, where a much larger volume of liquid existed and much longer times are involved in solidification. Such segregation is often referred to as macrosegregation as it spans many grains and often an entire ingot or weld width or length. Macrosegregation can also occur in fusion welds under certain circumstances.

One possible source of macrosegregation analogous to a source also found in cast ingots is convection of solute-rich liquid in the mushy

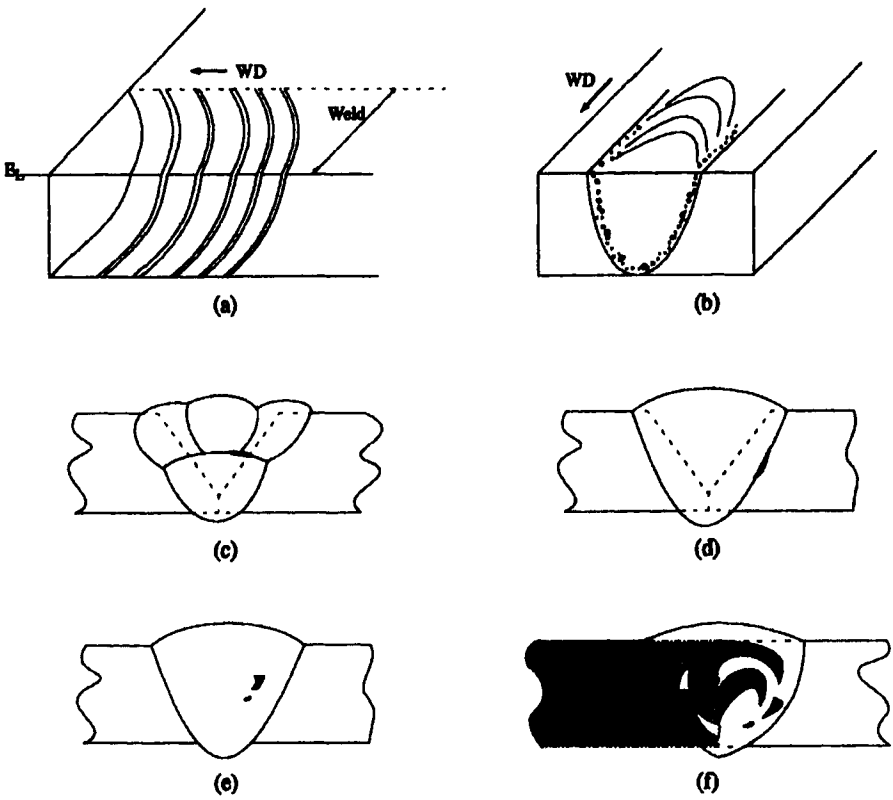


Figure 12.8 Schematic illustration of the various types of weld heterogeneity, other than dilution, including (a) banding, (b) gas porosity, (c) entrapped slag in multi-pass welds, (d) entrapped slag in a single-pass weld, (e) tungsten inclusion from the tip of the permanent electrode in GTAW, and (f) macrosegregation from welding dissimilar base metals.

zone,[6] interdendritically. Of course, since the mushy zone in welds is much smaller than it is for most ingots, the extent and severity of such segregation is less, but it does occur. Another source of macrosegregation occurs in some welds across their width as the centerline is approached. The origin of this centerline segregation is addressed in Chapter 13, but suffice to say here that it is largely the result of solute ahead of the solidification front advancing from each side of the weld being swept to the last liquid to remain at the centerline. In both welds and castings, this type of macrosegregation is further exacerbated by shrinkage of the liquid metal as it transforms to solid.

[6] The mushy zone is the region of a casting or weld pool formed when the temperature drops to between the liquids and solidus, at which time both newly formed solid dendrites and interdendritic liquid are present. Within the mushy zone, convection is severely restricted, but some mass transport, beyond that by diffusion, still occurs.

The most probable and pronounced source of macrosegregation encountered in welding occurs for fusion welds made between base metals of dissimilar composition. As molten metal obtained from each substrate tries to mix, with or without a filler, a marbling effect typically results. This type of weld macrosegregation can often be reduced by magnetically stirring the weld pool during welding using an externally applied magnetic field relying on Lorentz forces. Macrosegregation is more severe for very thick sections to be welded by multiple passes, being most severe in the root pass, and progressively less severe in subsequent passes. This was shown in Figure 12.4.

12.6. SUMMARY

There are conflicting phenomena at work during fusion welding that tend to cause weld pools and final welds to become more heterogeneous and more homogeneous at the same time. Heterogeneity tends to arise naturally on a microscopic scale due to solute rejection and redistribution in alloys solidifying under nonequilibrium conditions. Homogeneity tends to be promoted by convection in the weld pool arising from any of the four forces of buoyancy, surface tension gradient, electromagnetic force, and impingement or friction. Dilution of filler in weld pools by melted substrate(s), variations in composition due to variations in solidification rate (called banding), the presence and consequence of an unmixed and partially mixed zone in all welds, impurities in the form of gas porosity, nonmetallics, or foreign metals, as well as macrosegregation from several sources, but most especially welding of dissimilar base metals, were all described and discussed.

REFERENCES AND SUGGESTED READING

Estes, C. L., and Turner, P. W., 1964, "Dilution in multipass welding of AISI 4130 to type 304 stainless steel," *Welding Journal*, **43**(12), 541s–550s.

Flemings, M. C., and Nereo, G. E., 1967, "Macroesegregation, Part 1," *Transactions of the AIME*, **239**, 1449–1461.

Lippold, J. C., and Savage, W. F., 1980, "Solidification of austenitic stainless steel weldments; part 2: the effect of alloy composition on ferrite morphology," *Welding Journal*, **59**(2), 48s–58s.

Lundin, C. D., Liu, W., Zhou, G., and Qiao, C. Y. P., 1997, "Unmixed zone in arc welds: significance on corrosion resistance," Final Report, Welding Research Council High Alloys Committee/Stainless Steel & Corrosion Sub-Committee.

Savage, W. F., Nippes, E. F., and Szekeres, E. S., 1976, "Hydrogen induced cold cracking in a low alloy steel," *Welding Journal*, **55**(9), 276s–283s.

Suggested references on various topics

Davies, G. J., and Garland, J. G., 1975, "Solidification structures and properties of fusion welds," *International Metals Review*, No. 196, Vol. 20, ASM International, Materials Park, OH, p. 83.

Savage, W. F., 1980, "Solidification, segregation and weld imperfections," *Welding World*, **18**, 89.

This Page Intentionally Left Blank

PART FOUR

THE METALLURGY OF WELDING

This Page Intentionally Left Blank

CHAPTER 13

WELD FUSION ZONE SOLIDIFICATION

A fusion welding process produces several distinct zones in a pure crystalline material (e.g., metal or ceramic) or in a crystalline alloy of one of these materials. These different zones correlate with various transformations on appropriate equilibrium phase diagrams, adjusted for nonequilibrium heating and cooling effects on transformation temperatures and microconstituents. Figure 13.1 schematically illustrates these zones for a fusion weld made in (a) a metallic alloy and (b) a pure metal.

The *fusion zone* (or *weld metal*) in a pure metal or other crystalline material is the portion of the weld that completely melted during welding by having been heated by the welding thermal cycle to above the pure material's melting point. In an alloy, the fusion zone is the region heated above the liquidus temperature (T_{liquidus}). The fusion zone is often designated as the FZ or the weld metal (WM). It is important to the properties of the final weld because it has undergone melting and solidification, and so is quite different in structure and properties than the base material even if welding was autogenous. Base material structure is changed by the processes of melting and solidification, and composition can be changed by evaporation of certain components of an alloy. Obviously, if filler is employed in making the weld, the structure and composition, and thus the properties, of the fusion zone can be radically different than the base material, depending on how different the composition of the filler and base material(s) is and on how much dilution occurred (see Section 12.1).

At the outer extreme of the fusion zone is a narrow zone where convection forces in the weld pool could not overcome fluid friction forces, resulting in an *unmixed zone* (see Section 12.3). Composition in this unmixed zone can be quite different than in most of the fusion zone when the filler has a composition different than the base metal(s) (i.e., when welding was heterogeneous).

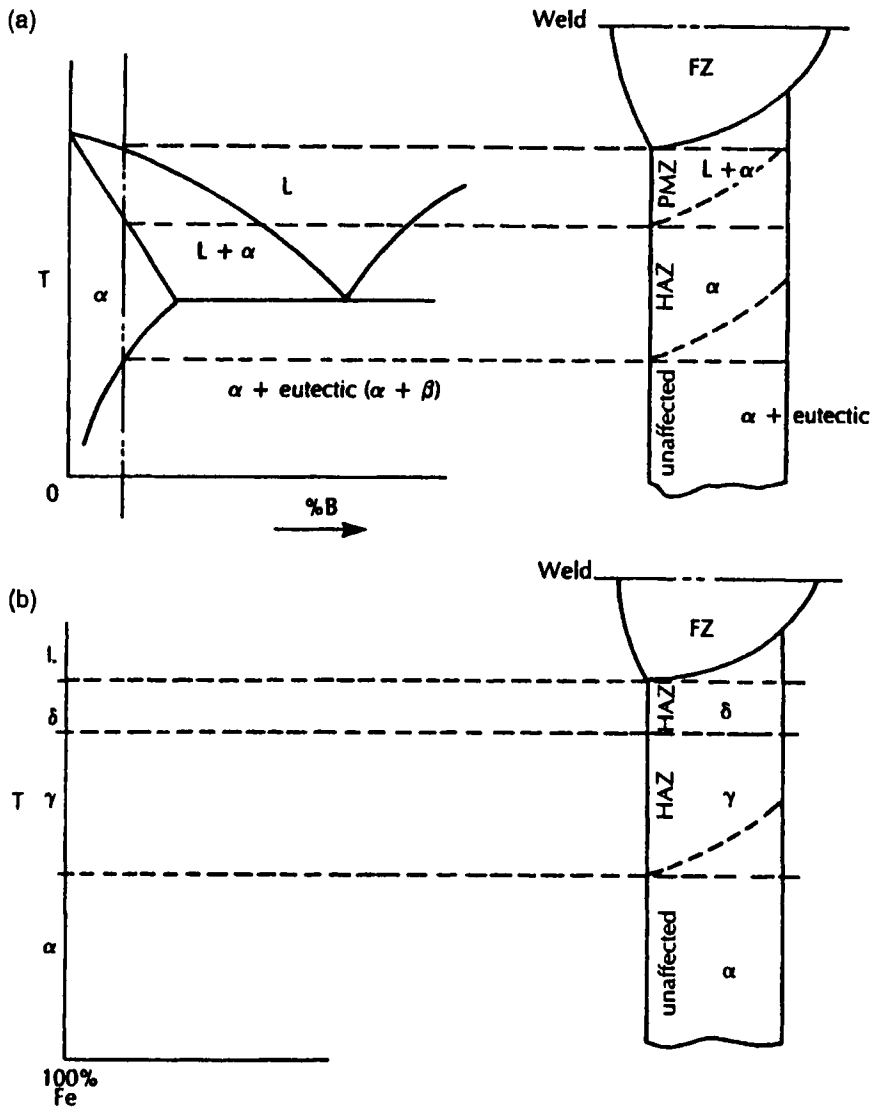


Figure 13.1 Schematic illustration showing the correlation between the various zones in a fusion weld in (a) an alloy and (b) a pure metal (or ceramic or polymer) and the corresponding equilibrium phase diagram. (From *Joining of Advanced Materials* by R. W. Messler, Jr., published in 1993 by and used with permission of Butterworth-Heinemann, Waltham, MA.)

For an alloy, there is a *partially melted zone* (or PMZ) where the welding thermal cycle caused the temperature of the base material to rise to between the liquidus (T_{liquidus}) and the solidus (T_{solidus}) for the alloy. In this zone, liquid and solid coexisted in proportions depending on what the peak temperature was between the solidus and liquidus. The higher the peak temperature, the greater the proportion of liquid. The PMZ is important to the properties of the weld because it too has undergone some degree of melting and solidification, thereby differing from the base material, but has been far less affected by dilution than the FZ. Naturally, no PMZ occurs in a pure material.

Somewhat farther away from the centerline of a fusion weld (where the maximum energy is normally deposited and the temperature is highest, as discussed in Section 5.3.4), there is a zone heated to near the solidus but never melted. This zone is known as the *heat-affected zone* (or HAZ). The heat-affected zone spans from the point where the peak temperature of a welding cycle reached the solidus down to a temperature high enough or long enough to alter the base material's structure through some solid-state transformation or reaction. As such, the heat-affected zone differs for each base material, depending on the mechanism by which the base material is strengthened and how it responds to elevated temperature.

Between the heat-affected zone and the fusion zone is the *fusion boundary* or *fusion line*. For a pure material, this line is well defined and easily recognized as being where melting from welding occurred. For an alloy, the fusion boundary or line is less well defined and distinct. It is usually taken to be where noticeable melting occurred and virtually all new structure has formed.

The *unaffected base material* (UBM) is that portion of the base material wherein the welding heat did not exceed the minimum required to affect its structure or properties. The structure, composition, and properties of this zone are unchanged by the production of a weld elsewhere. The so-called *weld zone* encompasses the fusion, partially melted (if any), and heat-affected zones, since this is the region where base material structure and properties have been altered by welding.

Since the processes of heating, melting, and solidification or solid-state phase transformations or reactions that take place during fusion welding are the keys to the structure and properties of the welds that result, Part IV of this book takes a look at each of the aforementioned zones. This chapter looks at the fusion zone, its formation and solidification. Chapter 14 looks at reactions that occur during the solidification of two-phase alloy systems, namely, peritectic and eutectic reactions, as well as postsolidification phase transformations that can occur in the fusion zone for some systems. Chapter 15 looks at the partially melted zone (PMZ), while Chapter 16 looks at the heat-affected zone (HAZ). Chapter 17 describes weldability and weld testing, just to compete the story.

13.1. EQUILIBRIUM VERSUS NONEQUILIBRIUM

It should be obvious by now, that fusion welding is a nonequilibrium process,[1] as are all real processes. During welding, heating not only deviates from equilibrium, but it often does so significantly. Cooling also deviates from equilibrium, usually significantly. For this reason, the processes of melting, weld pool mixing, solidification, postsolidification transformations, and heat-affected-zone solid-state transformations or reactions are all nonequilibrium events. What this means is that (1) equilibrium phase diagrams are often of limited utility in predicting what actually occurs in each of these processes or events, and (2) explanation and understanding of how structures change and properties develop is generally more complicated than for equilibrium.

The (micro)structure and properties of fusion welds depend significantly on the solidification behavior of the weld pool, and solidification behavior depends on cooling rate for real processes, as these deviate from equilibrium. Castings solidify under cooling rates ranging from 10^{-2} to 10^{2} deg K s^{-1}, with the rate within this range depending on the volume of molten metal, mold material (and, thus, thermal properties), metal being cast (and its thermophysical properties), and other conditions in the casting environment. As solidification processes go, cooling during casting is relatively slow, approaching equilibrium as a limit in very large castings. At the other extreme are rapid solidification processes, such as atomization to form powders, surface heat treatment and modification (e.g., using induction, or rastering laser or electron beams), and splat cooling techniques to produce amorphous metal alloys or metallic glasses. For such processes, cooling rate ranges from 10^{4} to 10^{7} deg K s^{-1}. Weld pool solidification lies between these two extremes.

Cooling rates in welds vary from 10 to 10^{3} deg K s^{-1} for conventional oxyfuel (at the lower end) and arc welding processes, including SMAW, FCAW, SAW, ESW, GTAW, and GMAW (at the higher end). Cooling rates of 10^{3} to 10^{6} deg K s^{-1}, depending on welding parameters, weldment geometry (mass and mass distribution), and material, occur for high-energy-density processes such as PAW (at the lower end) and LBW and EBW (at the higher end). Cooling rates can also vary significantly locally within a weld pool.

The features of real fusion welds that have to be taken into consideration because they can cause the fusion zone to deviate from equilibrium are (1) the weld pool can and usually does contain impurities or contaminants that may not show up on the phase diagram for the metal (or ceramic or polymer) or alloy; (2) dilution of filler (when used) by base material occurs; (3) there is usually considerable turbulence from convection and, therefore, reasonably

[1] Recall that equilibrium is the state a system achieves when it is in total balance, thermally, chemically and mechanically, so that no further changes occur. To achieve complete thermal and chemical equilibrium with a process requires very slow (really, infinitely slow) changes of temperature or composition, respectively. Nonequilibrium is when temperature is changed too rapidly to allow chemical composition to adjust. For processes such as welding, mechanical equilibrium is also a concern, but is usually secondary in relative importance.

good mechanical mixing in the molten region; (4) the volume of molten material is small compared to the volume of the overall base material, which acts as a mold within which solidification (analogous to casting) occurs; (5) the composition and structure of the molten region and mold are similar, even if not identical, and so they interact; (6) there are large temperature gradients across the melt, giving rise to nonequilibrium reactions and transformations; (7) since the heat source moves, weld solidification is a dynamic process, dependent on the welding speed; and (8) in welds made by high-energy processes or in multipass welds in which base material is preheated, temperature gradients, and, hence, solidification behavior are affected. Any one or all of these lead to nonequilibrium versus equilibrium behavior. In any case, current knowledge of weld pool solidification is really quite limited because of the harshness of the environment, with much of what is known coming from extrapolation of knowledge of solidification during casting (David and Vitek, 1989), or inference.

Before discussing solidification further, it is important to define three essential terms relating to material: phase, component, and constituent. A *phase* is a physically distinct, mechanically separable portion of a material, marked off in space by definable boundaries, within which the composition is either invariant or varies in a continuous fashion. A *component* is one of the pure species that comprises an alloy. It can be an element (as in metallic alloys) or a compound (as in intermetallics and ceramics and polymers). A *constituent* is any portion of an alloy, that, when viewed under a microscope, appears as a definite unit of the microstructure, examples being an eutectic or an eutectoid.[2] Constituents, however, contain more than one phase; they are not phases themselves.

Phase diagrams are plots or maps of the phase(s) that exist in equilibrium as a function of temperature, pressure, and composition; these three parameters or variables are called degrees of freedom. The number of degrees of freedom is the number of independent variables that must be specified to define the state of the system. The number of degrees of freedom (F) is a function of the number of components (C) and phases (P) in a system given by Gibbs' phase rule:

$$F = C - P + 2 \qquad \text{Gibbs' phase rule} \tag{13.1a}$$

The general relationship given in Gibbs' phase rule (Eq. 13.1a) assumes that both the temperature and pressure, as well as the composition, of a system are

[2] A eutectic is the product of a reaction in which a liquid (L) at one discrete temperature and a specific composition (C_{eutectic}) transforms to two different solids (S_1 and S_2) on cooling: $L \rightarrow S_1 + S_2$. These two solid phases are intimately mixed mechanically. A eutectoid is the product of a reaction in which one solid (S_1) at one discrete temperature and composition ($C_{\text{eutectoid}}$) transforms to two different solids (S_2 and S_3) on cooling: $S_1 \rightarrow S_2 + S_3$. Again, these two solid phases are intimately mixed mechanically. The solid phases, in either reaction, can be solid solutions or a compound (e.g., Fe_3C, iron–carbide cementite in the Fe-C system).

variable and affect the state of the system. For systems limited to incompressible phases, that is, liquids and solids, or so-called condensed systems, such as fusion-welded metals or ceramics or their alloys, pressure is not really a significant variable. This is revealed in the Clausius–Clapeyron equation:

$$\frac{\Delta T}{\Delta P} = \frac{T_E(V_2 - V_1)}{L} \tag{13.2}$$

where V_1 and V_2 are the specific volumes (or reciprocal densities) of the solid and liquid phases (in cm^3/g), respectively; T_E is the equilibrium melting temperature (in K); L is the latent heat of fusion (in dyne/cm); and ΔT is the resulting change in melting temperature for a pressure change of ΔP. As an example, consider the case for pure nickel (Ni) with the following properties: density of solid = 8.9 g/cm^3 at T_E; density of liquid = 8.4 g/cm^3 at T_E; latent heat of fusion = 74 cal/g; and the equilibrium melting temperature (T_E) = 1728 K, $\Delta T/\Delta P$) is 3.78×10^{-2} K/atm. Doubling the pressure on nickel at its melting point from 1 to 2 atm increases the melting point only about 0.0038 K![3] As a result of the Clausius–Clapeyron equation, pressure in Gibbs' phase rule can be ignored (except for extreme increases in pressure of thousands of atmospheres), so Gibbs' phase rule reduces to

$$F = C - P + 1 \tag{13.1b}$$

Applying Gibbs' phase rule modified for condensed systems (Eq. 13.1b) to a pure metal at the equilibrium melting point (T_E), solid and liquid can coexist in equilibrium, so $P = 2$, $C = 1$ (pure), and, if pressure is fixed or insignificant, $F = 1 - 2 + 1 = 0$. In other words, pure metals (or crystalline ceramics or crystalline polymers) must exhibit a discrete, single-valued melting temperature. We will come back to this when solidification of a pure material is discussed in Sections 13.2 and 13.3.

Nonequilibrium conditions of heating and cooling cause several important changes to equilibrium phase diagrams. First, the temperature at which a phase transformation takes place (e.g., melting begins at $T_{solidus}$, all solid disappears at $T_{liquidus}$, or a eutectoid reaction begins at $T_{eutectoid}$) progressively increases with increasing rates of heating. Second, the temperature at which a phase transformation takes place progressively decreases with increasing rates of cooling. Third, diffusion-controlled reactions or transformations can be sup-

[3] Whenever the liquid phase is less dense than the solid phase, as is the case for virtually all metals and alloys, except Bi, Ga, Li, Na, and a few other metals and their alloys, increasing the pressure raises the melting point. An important exception is water, where ice is less dense that water (i.e., it floats) and increased pressure lowers the melting point. This property is at least partially responsible for making ice skating possible, and survival of fish through the winter possible—since the ice doesn't collapse onto them.

pressed, sometimes completely. When this happens, diffusionless, athermal processes can sometimes occur and metastable phases can form. While none of this shows up on an equilibrium phase diagram, it must be recognized as occurring.

13.2. SOLIDIFICATION OF A PURE CRYSTALLINE MATERIAL

13.2.1. Criteria for Equilibrium at T_E and Constant Pressure

For the solid and liquid phases of a pure metal (or crystalline ceramic or polymer) to coexist in equilibrium at the discrete single-valued equilibrium melting temperature T_E, the Gibbs' free energy of these two phases must be equal

$$G_S = G_L \tag{13.3}$$

However, from thermodynamics,

$$G_S = H_S - T_E S_S \tag{13.4a}$$

and

$$G_L = H_L - T_E S_L \tag{13.4b}$$

where H_S and H_L are the enthalpies of the solid and liquid phases, respectively, and S_S and S_L are the entropies of the solid and liquid phases, respectively. Thus

$$H_S - T_E S_S = H_L - T_E S_L \tag{13.5a}$$

or, rearranging,

$$H_S - H_L = T_E(S_S - S_L)$$

or

$$\Delta H_F = T\Delta S_F) \tag{13.5b}$$

where subscript F refers to fusion, meaning at the melting point. But, $H_S - H_L$ is equal to the latent heat of solidification, L, which is the negative of the latent heat of fusion.[4] Thus,

$$(H_S - H_L) = \Delta H_F = -L \tag{13.6}$$

[4] Heat is liberated on freezing and absorbed during melting.

At the melting temperature, the average vibrational energy per atom is given by $3/2kT$, where k, Boltzmann's constant, is 1.38×10^{-16} erg/K. Furthermore, the entropy, which is a measure of disorder, increases upon melting. Thus, $S_S - S_L$ is always negative (i.e., $\Delta S < 0$). So,

$$\Delta S_F = S_S - S_L = \frac{-L}{T_E} \qquad \text{from } \Delta H_F = T\Delta S_F \tag{13.7}$$

and for any temperature T, for freezing to occur

$$\Delta G_F = G_S - G_L = (H_S - H_L) - T(S_S - S_L) = -L - T\left(\frac{-L}{T_E}\right) \tag{13.8}$$

or, rearranging,

$$\Delta G_F = -L(T_E - T)T_E = \frac{-L\Delta T}{T_E} \tag{13.9}$$

where ΔT is the supercooling below the equilibrium melting temperature.

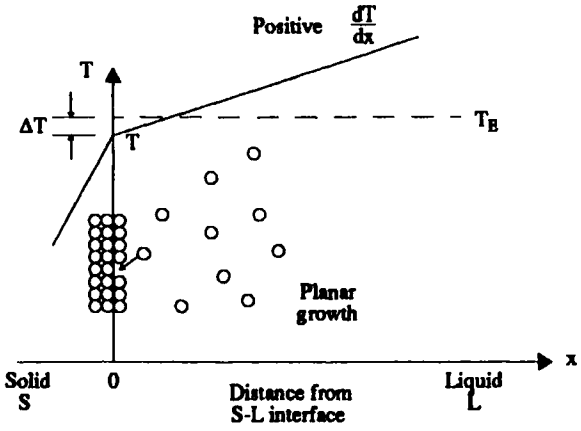
Equation 13.9 indicates that solidification can occur only if $T < T_E$, and that the latent heat of solidification must be dissipated. Restated, *the prerequisites for solidification of a pure metal (or ceramic) are as follows:*

1. The crystalline material must supercool to below T_E.
2. The latent heat of solidification must be dissipated by
   a. conduction through the solid to a heat sink (an unmelted region outside the weld pool in a weldment)
   b. conducted to the surrounding supercooled liquid until T rises to T_E, where T is the instantaneous temperature of the solid–liquid interface.

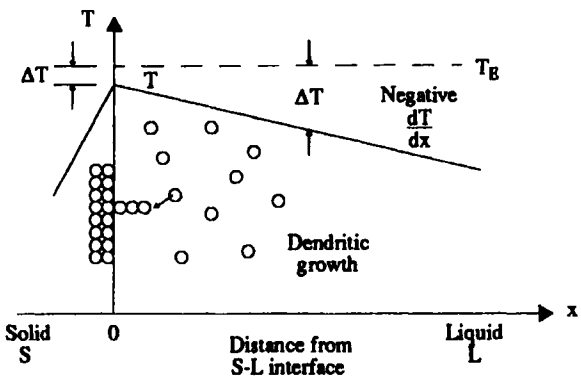
(A third, unusual possibility involves the Peltier effect, where, if an electric current can be made to flow across the solid–liquid interface in the proper direction, latent heat could be dissipated. This effect is not discussed further here.)

13.2.2. Pure Material Growth Modes

While welds are made far less frequently in pure metals than in alloys (see Section 16.2.2), it is worthwhile to consider the mechanics and kinetics of solidification and resulting growth modes or growth morphology in pure metals before discussing the more complicated case for alloys. Obviously, with no solute present, solute redistribution is not relevant. Only the prevailing thermal gradient affects solidification, with what happens depending on the effect of either a positive temperature gradient ahead of the advancing solid/liquid interface (where temperature increases with distance into the liquid) or a negative one. Later, it will be seen that it is the effect of such a gradient on the stability of the interface that matters.



(a)



(b)

Figure 13.2 Schematics of the possible temperature gradients that can occur in the liquid at a solid–liquid interface and the resulting solidification mode: (a) planar growth for a positive temperature gradient and (b) dendritic growth for a negative temperature gradient.

The two possibilites for growth of a pure crystalline solid are represented by Figure 13.2. In Figure 13.2a, heat flows down the gradient in the liquid, across the interface, into the solid. For the liquid,

$$\frac{\Delta T}{\Delta x} = \frac{Q}{K_L} \tag{13.10}$$

where Q is the heat flux and K_L is the thermal conductivity of the liquid. For the solid,

$$\frac{\Delta T}{\Delta x_S} = Q + \frac{L}{K_S} \tag{13.11}$$

where L is the latent heat of solidification, Q is the heat flux, and K_S is the thermal conductivity of the solid.

In Figure 13.2b, the liquid is supercooled throughout its volume, possibly by enhanced cooling from the surface, as one cools a cup of hot coffee by blowing on the surface because heat dissipation through the insulating walls of the cup is too slow. Therefore, any protuberance that forms (by chance) on the solid–liquid interface (as a result of atoms in the liquid attaching to the crystal lattice of the solid) can grow directionally or dendritically, in the direction of the maximum temperature gradient. While doing so, latent heat of solidification will be liberated to the supercooled liquid until the temperature of the solid–liquid interface reaches T_E. With the prevailing negative temperature gradient in the liquid, the amount of latent heat the liquid can accept before its temperature is raised to T_E and solidification must cease increases with increasing distance from the interface x.[5] Thus, dendritic growth prevails for pure materials with a negative temperature gradient into the liquid.

On the other hand, a chance protuberance formed on the solid–liquid interface in Figure 13.2a would find its tip in a liquid with a temperature T_E and would remelt. Thus, a positive temperature gradient into the liquid of a pure material causes a planar solid interface to be present during solidification. Growth of the pure solid (i.e., solidification) can progress only as fast a heat can be conducted away from the liquid through the newly formed solid.

In short, *only two modes of growth can occur for a pure crystalline material*[6]*: planar growth, in the presence of a positive temperature gradient into the liquid, and dendritic growth, in the presence of a negative temperature gradient into the liquid.*

13.2.3. Homogeneous Versus Heterogeneous Nucleation

13.2.3.1. Homogeneous Nucleation. For a crystalline solid to form from a liquid, randomly distributed atoms (or ions or molecules) in the liquid must take up the regular arrangement of the particular, stable crystalline structure

[5] This increase in the liquid temperature at the moving solid–liquid interface during dendritic solidification is called recalescence.

[6] While discussion in many texts is restricted to pure metals and ceramics, there are crystalline organic polymers that solidify exactly the same way. In fact, materials like succonitrile, camphene, and carbon tetrabromide are used to study solidification because (1) they are low melting (thereby making melting experiments easier) and (2) they are optically transparent (thereby facilitating observation). Examples of studies of solidification using organic analogs to metals are the classic works of Jackson and coworkers (1965, 1967), followed by Savage and Hrubec (1972) and the recent works of Glicksman and coworkers (1995, 1996).

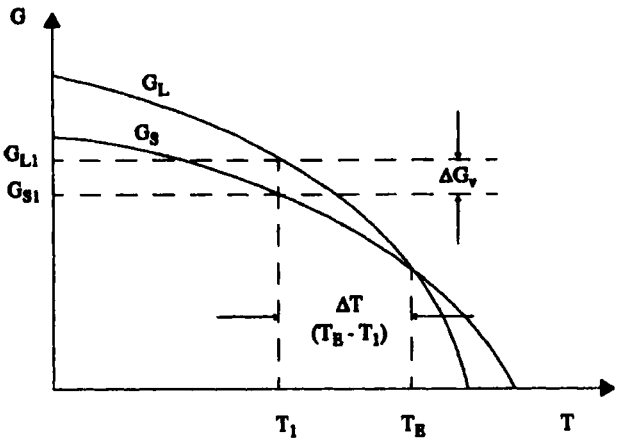


Figure 13.3 Schematic diagram of the effect of temperature on the Gibbs' free energy of the solid (G_S) and liquid (G_L) phases of a pure metal (or ceramic).

of the solid (face-centered cubic, body-centered cubic, or hexagonal close-packed in metals, for example). As cooling takes place and the temperature reaches and falls below the equilibrium melting temperature (T_E), such arrangements initially occur as small clusters by strictly probabilistic or chance events. If we assume the probability for the formation of a cluster or nucleus of a new phase is the same at all points in the parent phase,[7] and that these small-volume clusters or nuclei are of spherical shape[8] with radius r continuously forming by chance rearrangement of atoms of the parent phase to form the structure of the daughter phase, then we can determine whether such a nucleus is stable and will grow or is unstable and will disappear. Nucleation under such conditions is called *homogeneous nucleation*, because it occurs uniformly throughout a bulk parent phase.

Figure 13.3 is a schematic diagram of the effect of temperature on the Gibbs' free energy (G) of the solid and liquid phases of a hypothetical metal (or ceramic) that is pure. The volume free energy change for solidification if it were to occur at T_1 is given by

$$G_{S1} - G_{L1} = \Delta G_v^* \tag{13.12}$$

It is customary to define $T_E - T$ as ΔT, the *degree of supercooling*, where T_E is

[7] Here, we are talking about a solid as the new, daughter phase being formed from an original, liquid parent phase, but we could have been talking about a new solid (say β phase) being formed from a parent solid (say α phase) as in precipitation hardening.

[8] Assuming a spherical shape is not unreasonable because such a shape minimizes the surface area for any volume. Since the surface of the new phase (or interface between the new, daughter, and original, parent, phase) has an energy, minimizing surface (of interface) area minimizes surface (or interface) energy.

the equilibrium reaction temperature at which $G_L = G_S$ (the melting temperature) and T is the actual reaction temperature. Note that ΔT is positive when $T < T_E$, and increases with a decrease in the reaction temperature, while ΔG_v becomes more negative, the reaction thus becoming more favorable.

As soon as a new phase (here, a solid) forms within a parent phase (here, a liquid), there is an interface energy that did not previously exist (i.e., an interphase interface energy). The atoms adjacent to an interphase interface have a different number of near-neighbor bonds (here, fewer) than atoms in the bulk that are completely surrounded by other (like) atoms. This gives rise to an increase in their energy and requires expenditure of energy to create and maintain the interphase interface. For a liquid–solid interface, the surface energy ranges from about 24.4 ergs/cm^2 for mercury (Hg) to 255 ergs/cm^2 for nickel (Ni). On a per atom basis, the surface free energy is about one-half the latent heat of fusion per atom (for a liquid–solid interface at T_E) and does not change significantly over the range of temperature involved in the solidification of a pure metal (or ceramic).

Thus, the formation of a new phase tends to lower the volume free energy more and more as the new phase increases in volume, but simultaneously gives rise to a positive surface free energy that increases as the new phase grows and the surface or interphase area increases. These two energies compete. For a spherical nucleus, or embryo, of radius r, the change in volume free energy accompanying solidification is given by

$$\frac{4}{3}\pi r^3 \Delta G_v \rightarrow \frac{\Sigma \Delta G_v}{\text{embryo}} \tag{13.13}$$

For the same embryo size, the energy required to create the new solid–liquid (S–L) interface would be

$$4\pi r^2 \gamma \rightarrow \frac{\Sigma \gamma}{\text{embryo}} \tag{13.14}$$

The net change in the total free energy of the system associated with the formation of an embryo of radius r is, therefore, ΔG_T, where

$$\Delta G_T = \tfrac{4}{3}\pi r^3 \Delta G_v + 4\pi r^2 \gamma \tag{13.15}$$

Figure 13.4 shows, in schematic form, how each of these three quantities change with an increase in the radius of the embryo, that is, with growth. Note that ΔG_T has a maximum at r^*, defined as ΔG^*. The value of r^*, known as the *critical radius*, can be derived by differentiating ΔG_T with respect to r, yielding

$$\frac{d\Delta G_T}{dr} = 4\pi r^2 \Delta G_v + 8\pi r \gamma \tag{13.16}$$

and setting $d(\Delta G_T)/dr = 0$ and solving for r, so

$$4\pi r^2 \Delta G_v = -8\pi r \gamma \tag{13.17}$$

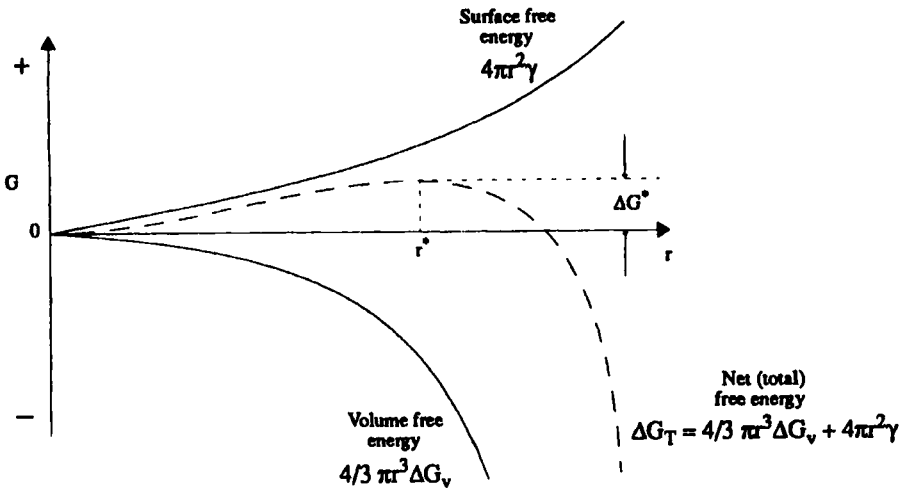


Figure 13.4 Schematic of the behavior of volume free energy (G_v), surface free energy (γ), and total free energy (G_T) with growth of an assumed spherical embryo of new phase of radius r.

and

$$r = r^* = -\frac{2\gamma}{\Delta G_v} \tag{3.18}$$

To obtain ΔG^*, substitute r^* into Eq. 13.15 for r, for ΔG_T, so

$$\Delta G_T = \Delta G^* = -\frac{32\pi\gamma^3}{3\Delta G_v^3}\Delta G_v + \frac{16\pi\gamma^2}{\Delta G_v}\gamma \tag{13.19}$$

or

$$\Delta G_T = \Delta G^* = \frac{16\pi\gamma^3}{3\Delta G_v} \tag{13.20}$$

The significance of all of this is that *there is a size for an assumed spherical nucleus or embryo of a new phase at which that phase becomes stable and grows as the result of volume free energy decreasing faster (proportional to r^3) than surface free energy increases (proportional to r^2), and that size is given by the critical radius r^*.*

The critical energy of formation of a stable nucleus, ΔG^*, represents the energy barrier to solidification. It is supplied by thermal fluctuations or other contributions to undercooling either at the solid/liquid interface or in the liquid (weld pool) not dependent on solute redistribution. To a first approximation, ΔG_v increases linearly with ΔT_{th}, the thermal component of supercooling or

undercooling below the equilibrium freezing temperature. Thus, from Eq. 13.20, it is seen that the thermodynamic barrier to nucleation decreases rapidly with increasing undercooling.

13.2.3.2. Super- or Undercooling. The term supercooling or undercooling really represents several different quantities. To avoid confusion, let's look at this term more closely.

The total supercooling of a liquid that leads to solidification consists of four quantities or components: (1) ΔT_{th}, representing pure thermal undercooling from random fluctuations in temperature at the interface as well as within the weld pool; (2) ΔT_c, representing constitutional supercooling arising from a change in the local composition of the liquid (by solute rejection from the newly formed solid) also present at the interface and within the weld pool; (3) ΔT_R, representing undercooling due to curvature of the solid–liquid interface (described in the next section); and (4) ΔT_k, representing kinetic undercooling arising from the rate at which atoms attach to the solid, and therefore present only at the interface. Thus, $\Delta T = \Delta T_{th} + \Delta T_c + \Delta T_R + \Delta T_k$.

Kinetic undercooling is quite small for weld pool solidification, and becomes significant only when the rate of growth is quite rapid (e.g., meters per second). Undercooling from curvature (also known as capillarity) is much more important in weld solidification as seen in the next section. Thermal undercooling, which represents the degree to which liquid is actually cooled below the equilibrium solidification temperature, is significant only when the barrier to nucleation is high. This is not the case in welds, as seen in Section 13.2.3.4, since nucleation is aided by the presence of a substrate on which new solid can grow. Constitutional supercooling is important in alloys, and is described in Sections 13.3 and 13.4.

Incidentally, measuring the degree of supercooling is a very difficult task, as can be imagined. This notwithstanding, there have been reasonable efforts by Kraus (1987) and Brooks et al. (1987).

13.2.3.3. Effect of Radius of Curvature on Supercooling. By definition, $G_S = G_L$ at T_E, and since $G = H - TS$, $H_S - T_E S_S = H_L - T_E S_L$. By rearranging, $H_S - H_L = T_E(S_S - S_L)$. But since $L = H_L - H_S$, $H_S - H_L = -L$, and, so, $S_S - S_L = \Delta S_F = -L/T_E$; both L and T_E being easily measured experimentally for a real system. For a temperature T,

$$\Delta G_F = G_S - G_L = (H_S - H_L) - T(S_S - S_L)$$

$$= -L - T\left(\frac{-L}{T_E}\right) \tag{13.8}$$

$$= -L\frac{T_E - T}{T_E} = -L\frac{\Delta T}{T_E} \tag{13.9}$$

where ΔT is supercooling and $\Delta T/T_E$ is fractional supercooling. Equation 13.9

indicates that (1) ΔT must be positive (i.e., $T < T_E$) for solidification to occur, and (2) the latent heat of solidification must be dissipated to the surroundings, as presented in Section 3.2.1 without proof.

From the earlier derivation of the critical radius r^* (Section 3.2.3.1), rearranging Equation 13.18 gives

$$\Delta G_v = -\frac{2\gamma}{r^*} \tag{13.21}$$

and, since $\Delta G_v = \Delta G_F$ for freezing or solidification, substituting gives

$$-L\frac{\Delta T}{T_E} = -\frac{2\gamma}{r^*} \tag{13.22}$$

This can, in turn, be rearranged to give

$$\Delta T = \frac{2\gamma T_E}{Lr^*} \tag{13.23}$$

and since $\Delta T = T_E - T$,

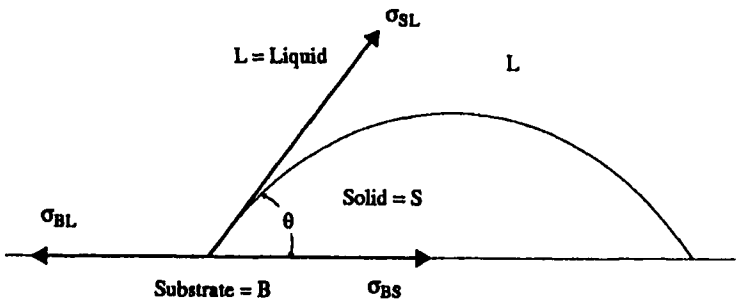
$$T = T_E - T_E\frac{2\gamma}{Lr} \tag{13.24}$$

or

$$T = T_E\left(1 - \frac{2\gamma}{Lr}\right) \qquad \text{Gibbs–Thompson equation} \tag{13.25}$$

Note that *the Gibbs–Thomson equation* (Eq. 13.25) indicates that the effective melting point T of a pure crystalline substance is decreased if the radius of curvature of the solid is decreased. Thus, in the presence of a positive temperature gradient, any protuberance would have its melting point decreased by an amount that is inversely proportional to its radius of curvature. In other words, *a positive temperature gradient in the liquid at a moving solid–liquid interface forces a planar solid interface* (i.e., $r = \infty$) *with no protuberances.* This supports the earlier conclusion that a planar growth mode would prevail for a positive temperature gradient in the liquid.

13.2.3.4. Heterogeneous Nucleation. While large degrees of supercooling have been obtained when solidification truly occurs as the result of homogeneous nucleation (Simpson, 1977), supercooling of more than a few degrees below the equilibrium freezing point is rare. The reason is that the presence of a substrate influences the nucleation of a new phase during solidification or any other transformation. Figure 13.5 shows in schematic form the influence of an



$$\sigma_{BL} = \sigma_{BS} + \sigma_{SL}\cos\theta$$

Figure 13.5 Schematic showing the balance of surface free energy vectors for a new solid (S) solidifying on a substrate (B) from a liquid (L) leading to heterogeneous nucleation.

interactive substrate. Note that a balance of surface free energy vectors exists when a solid (S) interacts with a substrate (B) within a liquid (L), such that

$$\gamma_{BL} = \gamma_{BS} + \gamma_{SL}\cos\theta \tag{13.26}$$

where γ_{BL}, γ_{BS} and γ_{SL} are values of the surface free energy for substrate–liquid, substrate–solid and solid–liquid, respectively, and θ is the *wetting angle* or *contact angle*. The contact or wetting angle differs for different energy balances, ranging from a maximum value of $\theta = 180°$ for a complete absence of interaction (or no wetting), where the solid beads up on the substrate, to a minimum value of $\theta = 0°$ for complete interaction (or complete wetting), where the solid spreads perfectly on the substrate. The lower the value of θ, the greater the interaction with the substrate, or what is called wetting.[9] Equation 13.26 is sometimes referred to as *Young's equation.*

The Gibbs–Thomson equation (Eq. 13.25) indicates that at a particular temperature T, the radius of an embryo of a new phase (here, a solid) can be considered to be the critical radius of curvature of the solid–liquid interface at equilibrium. Therefore, the volume of the critical nucleus or embryo will depend on the value of θ in Figure 13.5. At one extreme, $\theta = 180°$, and the substrate has no influence on nucleation. This is the case for *homogeneous nucleation.* However, consider the case where $\theta = 90°$. In this case, a hemisphere with radius r^* and volume V^* half that of a full sphere with the same radius (i.e., $\frac{2}{3}\pi r^{*3}$) would be stable. Obviously, a hemisphere of critical radius

[9] The term wetting comes from interactions between a liquid and a solid in the presence of a vapor or molten flux, as occurs with water beading or spreading on the hood of your car, adhesive bonding, or brazing and soldering.

r^* could be created with half as many atoms as would be needed to produce a full sphere with the same radius. Thus, in the presence of a suitable substrate, a spherical cap with radius r^* could represent the critical size nucleus, but with far fewer atoms required to produce it. This is illustrated in Figure 13.6.

If the ratio of the volumes of the spherical cap and a sphere of the same radius is defined as V_c/V_s, the following relationship can be derived:

$$\frac{V_c}{V_s} = 2\pi r^3(1 - \cos\theta) - \pi r^2 \sin^2\theta \cos\theta \tag{13.27}$$

For a unit radius, V_c/V_s for various values of θ (in degrees) is given in Table 13.1. This fraction can be viewed as the proportion of atoms that have to

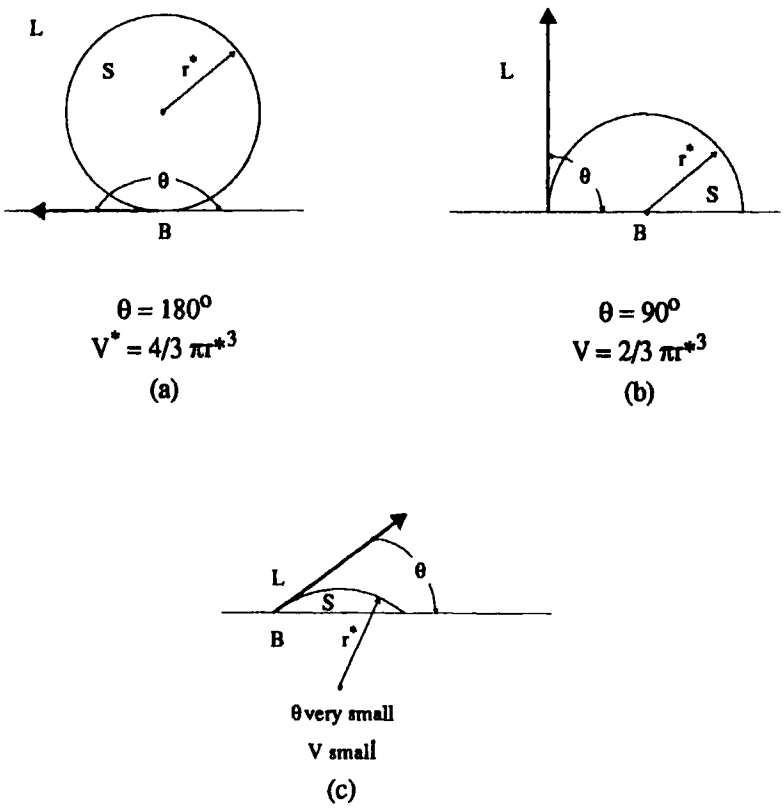


Figure 13.6 Schematic illustration of how interaction with a substrate (i.e., wetting) reduces the volume of the critical nucleus without changing the requirement that the radius be r^* for stable growth: (a) for $\theta = 180°$, (b) for $\theta = 90°$, and (c) for θ = a very low angle, say 10–15°.

TABLE 13.1 Ratio of the Volume of a Spherical Cap (V_c) to a Sphere (V_s) as Contact Angle (θ) Decreases

θ	V_c/V_s	θ	V_c/V_s
180°	1.0	40°	0.0349
90°	0.5	30°	0.0129
80°	0.371	20°	0.00267
70°	0.253	10°	0.000172
60°	0.156	5°	0.0000108
50°	0.0843	0°	0

cluster together for nucleation to take place heterogeneously. Note that there is an enormous decrease in the volume of the critical nucleus, or the number of atoms required, as θ approaches 0°; as wetting gets better.

Obviously, from a probabilistic point of view it is far easier to form a critical nucleus containing very few atoms in a small spherical cap than with very many atoms in a full sphere. For this reason, *in the presence of a suitable substrate, in which a new solid phase can interact with that substrate, heterogeneous nucleation will occur far more easily and long before homogeneous nucleation will*, i.e., the barrier to nucleation is significantly reduced.

A well-known example of just how potent a substrate can be for nucleating a new phase heterogeneously, where homogeneous nucleation has proved difficult to impossible, is seeding of clouds with silver iodide crystals to end a drought. Liquid water can nucleate on these crystals serving as substrates with far less supercooling below a given humidity level to cause saturation than without such substrates, that is, by normal homogeneous nucleation.

13.2.4. Epitaxial and Competitive Growth

When a liquid phase of a crystalline metal (or ceramic or polymer) and a substrate are at the same temperature and the liquid "wets" the substrate, the effective contact angle (θ) approaches 0°, and the critical nucleus size approaches atomic dimensions (see Eq. 13.27 or Table 13.1). Thus, solid growth into the liquid requires only that individual atoms in the liquid surrender their latent heat and join the existing crystal structure of the adjacent solid. This mechanism of growth is experienced in fusion welding (as well as brazing and soldering) processes (as well as other processes, such as crystal growth in the semiconductor industry) and is known as *epitaxial growth*. As a consequence of epitaxial growth, the grain boundaries in the solid that intersect the fusion boundary extend across that boundary as solidification proceeds and the crystalline lattices of the individual grains in the solid are extended into the previously molten volume. This is shown schematically in Figure 13.7.

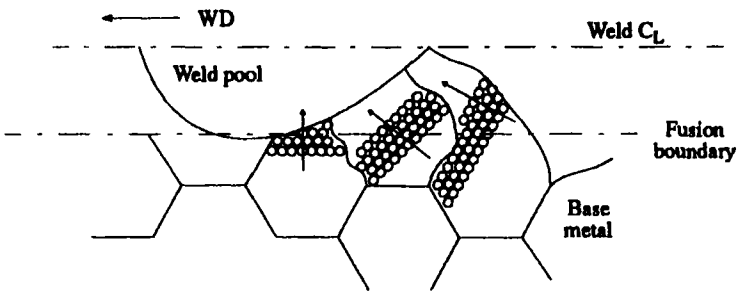


Figure 13.7 Schematic showing epitaxial growth in a weld (pool) from the base material (substrate).

Walton and Chalmers (1959) first demonstrated that when crystalline solids grow into a supercooled melt, growth occurs in characteristic crystallographic directions called *dendritic growth directions*, *preferred-growth directions*, or *easy-growth directions*. Figure 13.8 summarizes these directions for each of the three most common metallic crystal structures: body-centered cubic (bcc), ⟨100⟩; face-centered cubic (fcc), ⟨100⟩; and hexagonal close-packed (hcp), ⟨10$\underline{1}$0⟩.[10]

If one considers both positive and negative orientations of these three preferred growth directions, each of the three crystallographic forms (shown in Figure 13.8) has a total of six possible directions. At any instant, the operative growth direction will be that along which the steepest temperature gradient exists. This results from the necessity for dissipating latent heat of solidification that is liberated at the advancing solid–liquid interface. Therefore, within a given grain, the axes of the dendrite arms will correspond to the preferred growth direction most nearly parallel to the temperature gradient in the liquid at the solid–liquid interface. The result is *competitive growth*.

Savage and Aronson (1966) studied such competitive growth in a grain-oriented (cube-on-edge texture) silicon–iron sheet developed by careful thermomechanical processing. The structure is shown in Figure 13.9. There is a predominant ⟨100⟩ easy-growth direction in the plane of the sheet, and a ⟨110⟩ difficult-growth direction in the plane of the sheet at right angles to this ⟨100⟩. Autogenous, bead-on-plate welds were made parallel, perpendicular, and at 45° to the ⟨100⟩ easy-growth in-plane direction using the gas–tungsten arc process. Tracings for four such welds are shown in Figure 13.10. The welds in Figure 13.10a and b were made with a travel speed of 5 in./min using a current that produced a slightly elliptical weld pool. The light dashed lines in Figure 13.10a and b represent the ripple marks delineating successive locations of the trailing edge of the weld pool.

[10] Crystallographic directions, as well as planes, are designated using Miller indices. A description of Miller indices can be found in any basic textbook on material science and engineering (such as Callister or Shackleford) or textbook on crystallography (such as Cullity).

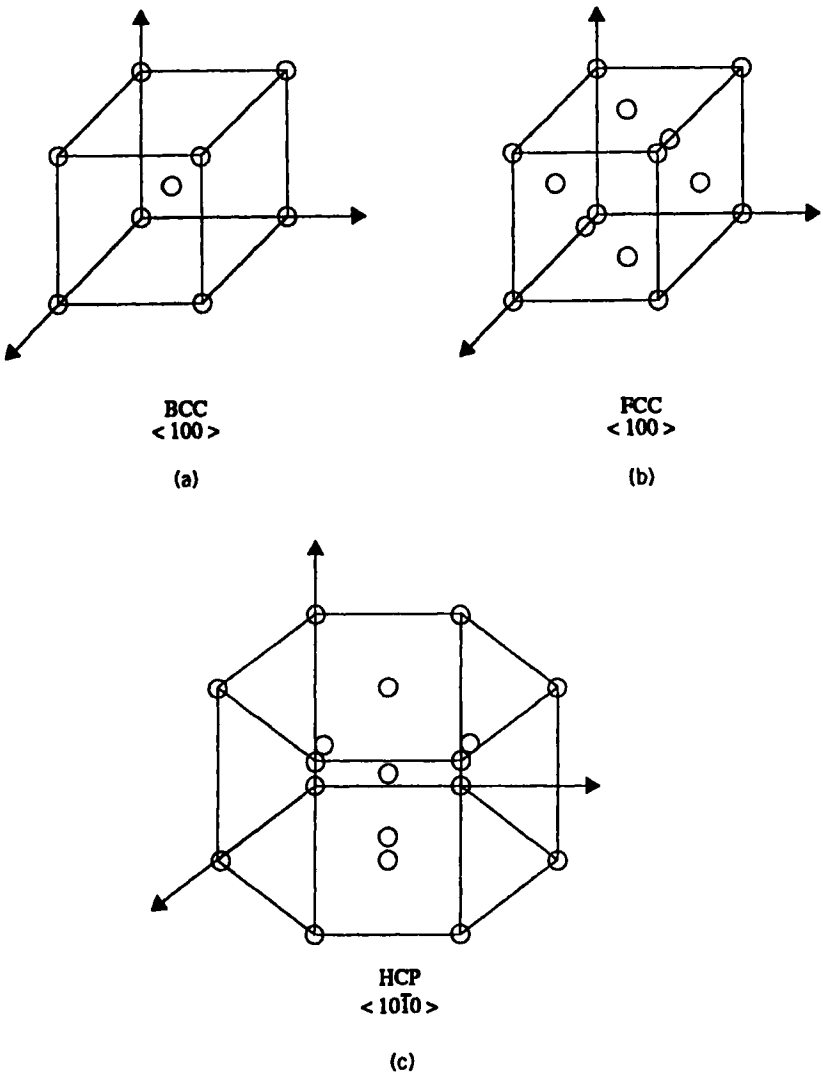


Figure 13.8 Schematic of the easy-growth directions for (a) body-centered cubic (bcc), (b) face-centered cubic (fcc), and (c) hexagonal close-packed (hcp); all being close-packed directions.

In Figure 13.10a, the easy-growth direction is parallel to the welding direction, so grains tended to align themselves as nearly as possible to the welding direction. On the other hand, in Figure 13.10b, the easy-growth direction is perpendicular to the welding direction, so grains tended to grow normal to the welding direction for a considerable fraction of the weld width. The sudden change in growth direction reflects a growth change to another

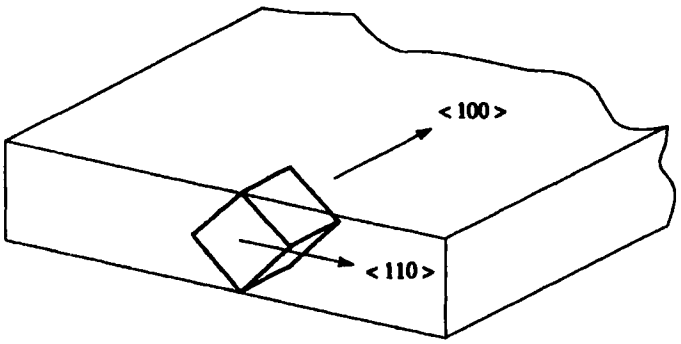


Figure 13.9 "Cube-on-edge" texture developed by careful thermomechanical processing of thin silicon–iron sheet for study of competitive growth.

⟨100⟩ direction at 45° to the texture, into or out of the plane of the sheet (see Figure 13.9). The grain marked A near the center of the weld happened to have a ⟨100⟩ parallel to the welding direction and was able to crowd out other grains since it had a steeper temperature gradient in the liquid on the opposite side of the solid–liquid interface.

Figures 13.10c and d are tracings of welds made at higher welding speeds of 22.5 in./min, as evidenced by more elliptical (tailed) weld pool ripple marks. Although growth is still epitaxial, the grain boundaries extend all the way to the centerline of the weld and are essentially perpendicular to the welding direction due to the direction of the temperature gradient for this tailed puddle.

Thus, once a grain begins to grow epitaxially from a substrate, it experiences different degrees of ease or difficulty of growth, depending on how its easy-growth direction just happened to be aligned relative to the prevailing maximum temperature gradient in the weld pool. Some grains are favorably oriented, compete well, and grow at the expense of grains that are less favorably oriented. This is shown schematically in Figure 13.11.

The competitive nature of growth has also been clearly demonstrated in more recent work by Rappaz et al. (1989) for autogeneous EB welds made in single crystals of low-residual Fe-15Cr-15Ni stainless steel.

13.2.5. Effect of Weld Pool Shape on Structure

Because growth following welding (or any process in which solidification takes place epitaxially) occurs competitively, the shape of the weld pool has a pronounced effect on the resulting solidification structure. In short, grains always attempt to grow such that an easy-growth crystallographic direction is aligned with the maximum temperature gradient and that gradient depends on the shape of the weld pool, which, in turn, depends predominantly on the welding velocity. Let's look at an example.

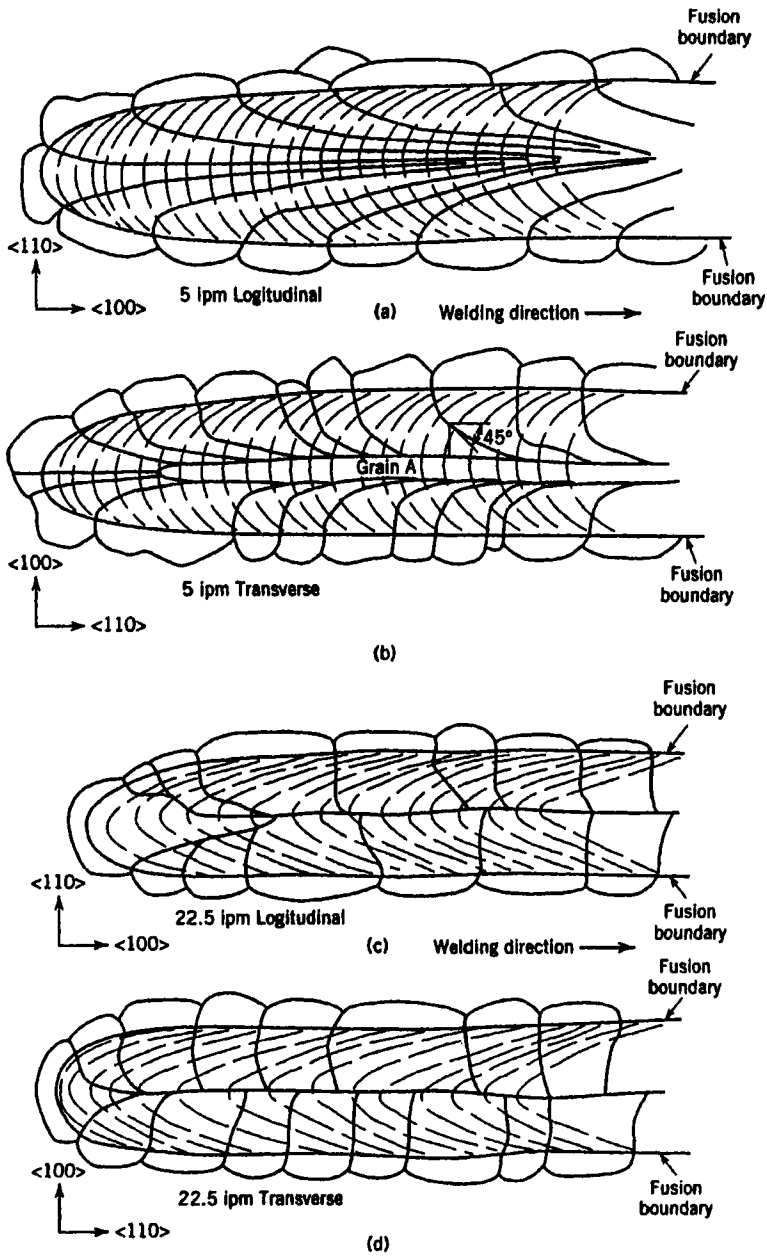


Figure 13.10 Tracings of autogenous, bead-on-plate GTA welds made at speeds of 5 ipm (a and b) and 22.5 ipm (c and d), both parallel or longitudinal (a and c) and perpendicular or transverse (b and d) to the ⟨100⟩ easy-growth directions in cube-on-edge texture silicon–iron sheet at two different welding speeds. (After original work by C. D. Lundin and W. F. Savage at Rensselaer Polytechnic Institute, Troy, NY, circa. 1963.)

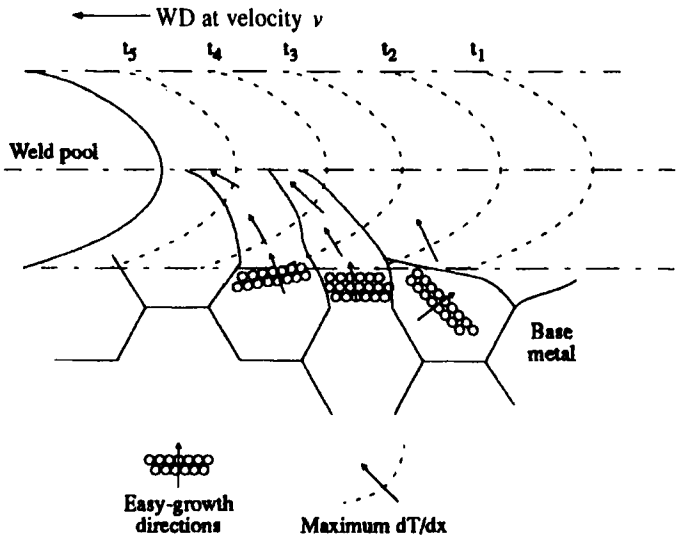


Figure 13.11 Schematic representation of favorably and unfavorably oriented grains growing epitaxially and competitively. Dotted lines show frailing edge of weld pool at progressive times t_1, t_2, and so on.

Unless a fusion weld is made with the heat source stationary, in which case the weld pool would be circular in plan view (and hemispherical in 3-D), during steady-state welding the resulting weld pool is always elliptical in plan view, at least until the welding velocity reaches some critical value, at which point the pool takes on a tear drop shape. For an elliptical weld pool, the rate of growth of the solid at the solid–liquid interface varies with location along the trailing edge of the pool. It should be obvious that solidification occurs only along the so-called trailing edge of the weld pool, which begins at a point approximately in line with the center of the heat source or energy deposition transverse to the direction of welding. At the forward edge of the weld pool, melting is occurring as the center of the source of heat is still approaching material ahead of the source. For constant welding velocity, v, if the welding voltage (E) and current (I) are held constant, the shape of the weld pool remains constant; i.e., energy input and energy losses come into balance to create a steady or quasi-steady state (see Section 6.3). The quasi-steady-state shape of the weld pool is most affected by the welding velocity, with voltage most influencing pool depth, and contributing to overall weld pool volume by multiplying with current. Since, on average, growth of the solid will occur parallel to the maximum temperature gradient (essentially normal to the moving solid–liquid interface at the trailing edge of the weld pool), the rate of growth R of the solid can be written:

$$R = v \cos \phi \tag{13.28}$$

where v is the welding velocity (in inches per minute or millimeters per second), and ϕ is the angle between the maximum temperature gradient in the liquid (i.e., the average growth direction) and the welding velocity. This is shown in Figure 13.12, where for an elliptical weld pool, ϕ varies from 90° at the sides of the pool to 0° at the weld centerline. Thus, the rate of growth of solid varies from 0 at the sides of the weld pool to a maximum of v (from $v \cos 0°$, where $\cos 0° = 1$) at the weld centerline.

Thus, in an elliptical weld pool, the maximum rate of growth, and, consequently, the maximum rate of evolution of latent heat, occurs at the centerline of the weld at the tail of the weld pool. Unfortunately, the temperature gradient in the solid at this point is parallel to the welding direction and is at a minimum. At the tail of the weld pool, material just behind the edge of the pool has just solidified, and so is at a temperature just below the melting point, while material just ahead of the trailing edge of the weld pool is still molten, but just above the melting point. Note that the maximum temperature gradient in the solid along the interface where solidification is occurring is found at the sides of the weld pool where growth falls to 0 (for $v \cos 90°$, where $\cos 90° = 0$).

Because the maximum rate of evolution of latent heat occurs where the temperature gradient in the solid is a minimum, the welding velocity cannot be increased beyond some critical value without rendering the weld pool unstable. At some critical velocity, the rate of evolution of latent heat at the centerline (or center point) of the trailing edge of the weld pool exceeds the ability of the system to dissipate it. When this happens, the rate of growth parallel to the welding direction decreases and the weld pool assumes a teardrop shape, as shown in Figure 13.13. Note in Figure 13.13 that the change in weld pool shape, from an ellipse to a teardrop increases the minimum value of ϕ from 0°

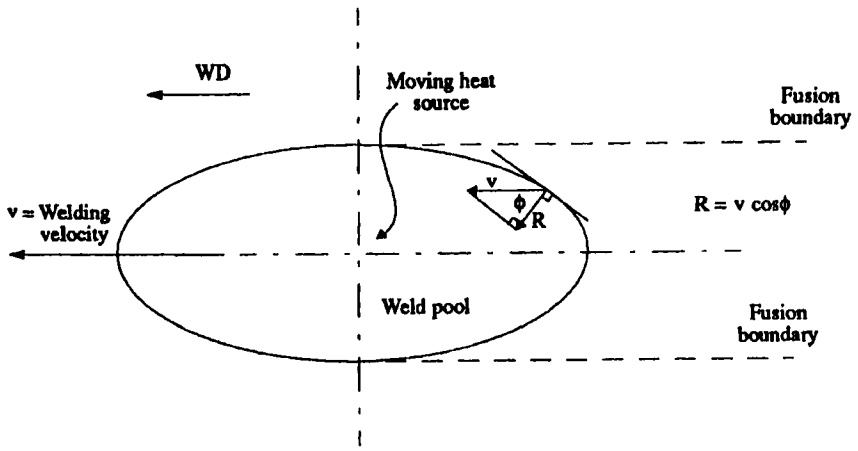


Figure 13.12 Schematic of an elliptical weld pool showing the relationship of rate of growth (R), welding velocity (v), and growth direction (ϕ).

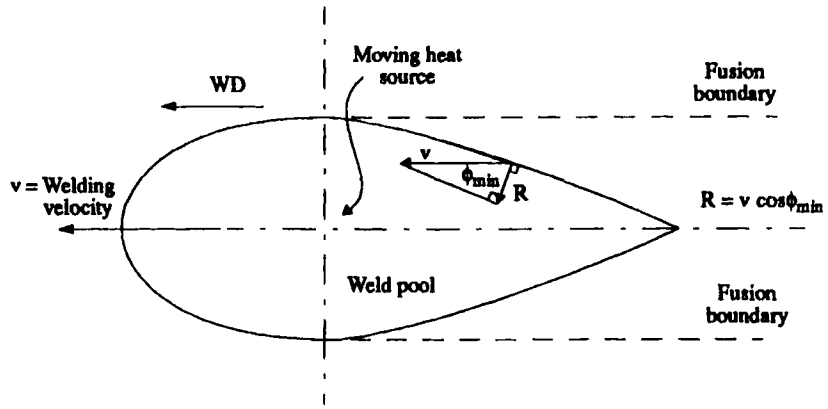


Figure 13.13 Schematic of weld pool becoming teardrop shaped as the welding velocity (v) reaches a critical limit where the rate of latent heat evolution tries to exceed the rate of growth (R) that can be attained at the trailing edge.

to some value that is directly proportional to the welding velocity. This, in turn, reduces the value of the maximum growth rate to $R = \cos \phi_{min}$.

As the welding velocity is increased, ϕ_{min} becomes larger and larger, the weld pool becomes longer and narrower, and grains continue to converge on one another along the centerline of the weld. At some critical velocity, which is inversely proportional to the thermal conductivity of the material being welded, a "neck" may appear at the weld centerline. This is shown schematically in Figure 13.14. Note in Figure 13.14 that along the length designated A-B, on both sides of the neck, $\phi = 90°$, and the transverse growth rate falls to 0. Unfortunately, this situation is also unstable, so the neck tends to freeze off, isolating molten regions that develop shrinkage cavities at their centers. Strings of intermittent cracks along the centerline of a fusion weld made at very high welding speeds (indicated by a very pronounced V-shape in ripple marks) are caused by this mechanism. High-rate production automated welding lines, such as used in tube-welding mills, often exhibit this problem, particularly when welding high-alloy materials which have inherently low thermal conductivity. In thin-walled tubes, these cracks can be through the wall, resulting in leaks, not to mention thin spots.

13.2.6. Competing Rates of Melting and Solidification

When a solid and a liquid are in contact at constant temperature, it is convenient to consider that any change in the amount of each phase present results from a difference in the rates of two competing processes: melting and solidification. For a solid to melt, an atom on the surface must fulfill the following criteria:

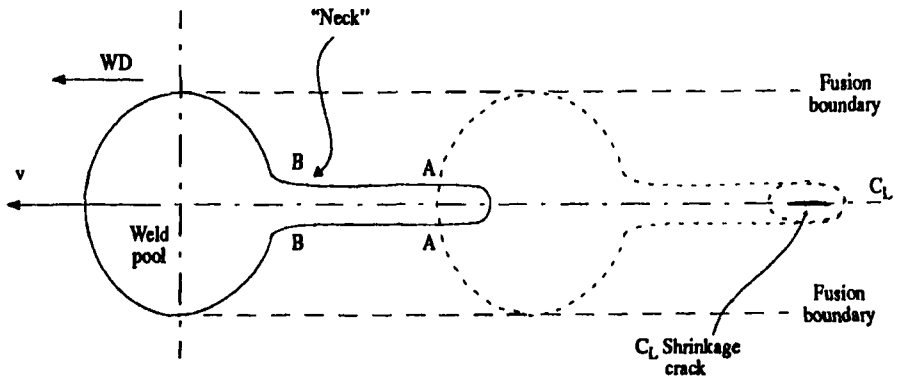


Figure 13.14 Schematic of a weld pool in which the welding velocity (v) has become so great that a pronounced tail forms, the pool becomes unstable, and portions of the tail neck down, pinch off, and become isolated from the main pool. When this occurs, cracks form at the center of these isolated areas as the result of there not being enough liquid to fill the volume once solid forms.

1. By chance, possess sufficient energy to break the bonds that bind it to neighboring atoms in the solid. The probability of this can be predicted from the Maxwell–Boltzmann distribution function:

$$p = \exp\left(\frac{-Q_m}{kT}\right) \tag{13.29}$$

   where k is Boltzmann's constant (1.38×10^{-16} ergs/K), Q_m is the energy required to break the bonds (often called the activation energy for melting), and T is absolute temperature.
2. By chance, be moving in the proper direction to escape at the instant it has the necessary energy to escape the solid. This can be expressed as a geometric probability, G_m, related to the crystal structure of the solid, since this determines the number of near neighbors or coordination.
3. By chance, find a suitable site in the liquid phase and give up some of its energy inelastically to its surroundings to be accommodated as part of the liquid. This can be expressed as the accommodation probability, A_m.

If the frequency of vibration of the atom in the solid is given by ν_s, then the number of "tries" the atoms has to escape the solid is equal to ν_s. If N_s equals the number of atoms per unit area of solid surface (in cm^2), then the number of tries/cm^2 of solid surface is equal to $N_s\nu_s$, and the rate of melting, R_m is given by

$$R_m = N_s v_s A_m G_m \exp\left(\frac{-Q_m}{kT}\right) \qquad \text{Rate of melting} \qquad (13.30)$$

For the rate of solidification, similar reasoning can be applied (for individual events occurring in the opposite direction), and R_s becomes

$$R_s = N_m v_m A_s G_s \exp\left(\frac{-Q_s}{kT}\right) \qquad \text{Rate of solidification} \qquad (13.31)$$

where N_m is the number of atoms/cm^2 on the molten interface, v_m is the number of vibrations per second for atoms in the melt, A_s is the accommodation probability for atoms that leave the liquid to join the solid, G_s is the geometric probability of an atom in the liquid to move toward the solid, and Q_s is the energy given up when bonds are formed as the atom joins the solid. The net rate of reaction at temperature T will be

$$R_{net} = N_s v_s A_m G_m \exp\left(\frac{-Q_m}{kT}\right) - N_m v_m A_s G_s \exp\left(\frac{-Q_s}{kT}\right) \qquad (13.32)$$

Plotting the rates of melting (Eq. 3.30) and solidification (Eq. 3.31) as a function of temperature gives Figure 13.15. The reaction, or process, which prevails on this plot is the one with the higher rate at any particular

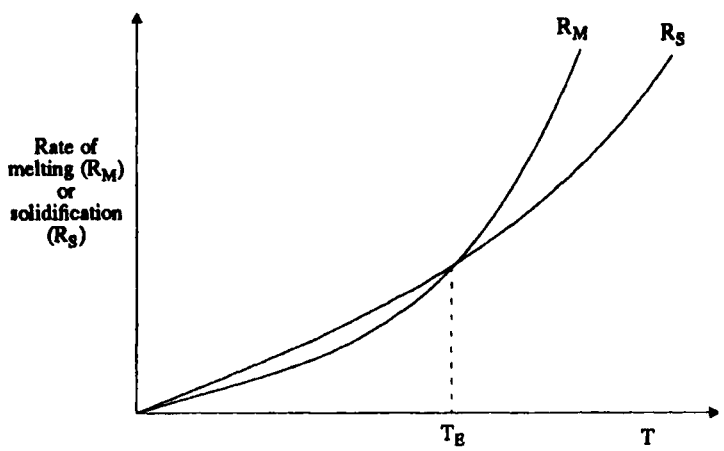


Figure 13.15 Plots of the rate of melting, R_m (from Eq. 3.30), and rate of solidification, R_s (from Eq. 3.31), as a function of temperature, with the equilibrium melting point shown by T_E. The net reaction, or process, is the one with the higher rate at any particular temperature, that is, melting above T_E and solidification below T_E. *Note:* While the rate of melting increases without limit as the degree of superheating increases, this is not so for the rate of solidification with supercooling.

temperature. Below T_E (the equilibrium melting temperature), $R_m < R_s$ and the net rate, R_n increases to a maximum and then decreases to zero. Therefore, solidification will occur, first with an increasing driving force as supercooling increases, but then with a decreasing driving force, reaching zero driving force at some point. Above T_E, $R_m > R_s$ and the net rate, R_n, increases in a continuous fashion with increase in temperature. For this reason, it is difficult to superheat a solid very much (plus an interphase interface exists from the outset).

On the other hand, Figure 13.15 predicts that if a liquid is supercooled sufficiently, the rate of solidification should go to zero, and it should be possible to retain the supercooled liquid as an amorphous phase. This is, in fact, accomplished when metallic glasses are produced by splat cooling or other means that cause the cooling rate to bring the liquid far below T_E very quickly. Typical cooling rates required to form amorphous metals are 10^6 K/s and higher. In welding, the only place this is even approached is when a thin surface layer of a thick solid substrate is rapidly heated by a laser beam, and the underlying cold metal causes a glazed layer to form. This process is called laser glazing, and is one of several ways in which high-energy-density beams are used to modify the surface of materials.

13.2.7. Effect of Nonequilibrium on Pure Material Solidification

About the only effect of nonequilibrium on the fusion welding of pure crystalline materials is the elevation and depression of melting point on heating and cooling, respectively. The reason no other effects tend to occur is that the rates at which atoms (or ions) in the melt can add to the crystal lattice of the solid epitaxially is quite high, and no redistribution of solute is necessary (as seen in Section 13.3) because there is no solute!

At very high cooling rates (around 10^6 deg/K s^{-1} and higher), as described in Section 3.2.6, it is possible that atoms in the melt do not have enough time to realign to take up a crystalline arrangement, but this never occurs in welding. This notwithstanding, cooling rate has significant effects on the mechanics and kinetics of solidification in alloys, where solute must be considered as well as heat.

13.3. EQUILIBRIUM SOLIDIFICATION OF AN ALLOY

Essentially all metals of commerce are actually alloys, in that they consist of two or more components. In the case of commercially pure metals (e.g., 1100 aluminum, oxygen-free/high-conductivity [OFHC] copper, Armco iron, and commercially pure [CP] titanium), the extra components are impurity elements that cannot be reduced below certain lower limits for economic reasons. Commercial alloys have, in addition to impurities or residuals, intentionally added components called solutes that improve certain properties such as

strength or corrosion resistance. From the standpoint of fusion welding, whether intentionally added or present as residuals, the presence of additional components invariably impairs weldability. But, because of the importance of alloying, it is essential to understand how alloys solidify, under equilibrium and nonequilibrium conditions. Let's look at equilibrium first.

13.3.1. Prerequisites for the Solidification of Alloys

Just as for the solidification of pure materials, there are prerequisites for the solidification of alloys. Besides requiring temperature to fall below an equilibrium melting temperature, which for alloys is the equilibrium liquidus temperature, and dissipating latent heat of fusion to the surroundings (either supercooled liquid or cooler solid), which are both heat transfer problems, there is an additional requirement: *The solute present in the alloy must be redistributed between the coexisting solid and liquid phases at the solid–liquid interface, which is a mass transfer problem.*

In most instances, the transport distance involved in the redistribution of solutes is many interatomic distances, rather than less than one atomic distance as is the case for the solidification of a pure metal, where atoms need move only from the liquid onto the crystal lattice of an embryo of solid. In the solid phase, adjustments in composition can occur only by diffusion, and the mean diffusion distance is proportional to $(Dt)^{1/2}$, where D is the diffusion coefficient of the diffusing species, and t is the diffusion time. The diffusion coefficient D is exponentially related to the absolute temperature, T, according to

$$D = D_0 \exp\left(\frac{-Q}{RT}\right) \tag{13.33}$$

where D_0 is the temperature-independent part of the expression indicative of the diffusing specie's inherent mobility in the host (and ranges from 0.02 to about 5.8), Q is the activation energy for diffusion (and ranges from about 10 to 68 kcal/mol), R is the universal gas constant (about 2 cal/g mol^{-1} K^{-1}), and T is absolute temperature (in K). Typical diffusion data are given in Table 13.2 for various diffusing solute species in iron near its melting point.

The key point is as follows: *For alloys to solidify, solute must be redistributed by diffusion, and that takes time, almost always more time than is available under nonequilibrium cooling!*

13.3.2. Equilibrium Solidification of a Hypothetical Binary Alloy (Case 1)

Consider a hypothetical binary alloy of solute element B in a solvent A, as shown in the hypothetical phase diagram in Figure 13.16. Note that an alloy of nominal composition C_0, would, upon cooling from the molten state under

TABLE 13.2 Typical Diffusion Data at the Melting Point of Pure Iron, 1774 K

	D_0	Q (kcal/mol)	D (cm^2/s)
Self-diffusion of γ-Fe	0.22	64.0	3.2×10^{-1}
Self-diffusion of α-Fe	2.0	57.5	1.8×10^{-7}
C in α-Fe	0.2	34.0	1.4×10^{-5}
C in γ-Fe	2.2	29.3	5.7×10^{-4}
Ni in γ-Fe	0.77	67.0	4.85×10^{-9}
Mn in γ-Fe	0.35	67.5	1.91×10^{-9}

equilibrium conditions, begin to form solid at temperature T_L, the intercept of the nominal composition with the liquidus.[11] At, or infinitesimally below, this temperature, the first nuclei of solid form, having a composition given by C_1, the intersection of a horizontal line (known as the tie-line) at this temperature between each single phase region (here, liquid L and solid solution S). The composition of this newly formed solid is lower in solute content than the homogeneous liquid from which it formed. The reason is the partitioning of solute between the liquid and the solid resulting from different solubility of solute in the two different phases. The more open structure of the liquid better accommodates foreign solute atoms than does the closer-packed structure of the crystalline solid. The relationship between the amount of solute contained in the solid and in the liquid from which it is formed is known as the equilibrium distribution coefficient, k_0, where

$$k_0 = \frac{C_S}{C_L} \qquad \text{at } T_i \tag{13.34}$$

Although in real systems, k_0 may vary with temperature because of curvature of the liquidus and solidus lines, for dilute solutions, k_0 can be assumed to be essentially constant. (As we will see, we are usually most interested in residual or trace elements, which are present in minor amounts, and, therefore, we can assume that k_0 is approximately constant for a given system.) Obviously, since mass (in the form of specific atomic species) must be preserved, any solute atoms that do not appear in the newly formed solid must be left behind to appear in the liquid, thereby raising the composition of the liquid along the liquidus line.

[11] The liquidus line on a phase diagram corresponds to the locus of points representing the liquidus temperature of various concentrations of solute B (at which point solid first begins to appear on cooling a liquid). The solidus line, similarly, corresponds to the locus of points representing the solidus temperature of various concentrations of solute B (at which point the last liquid disappears on cooling).

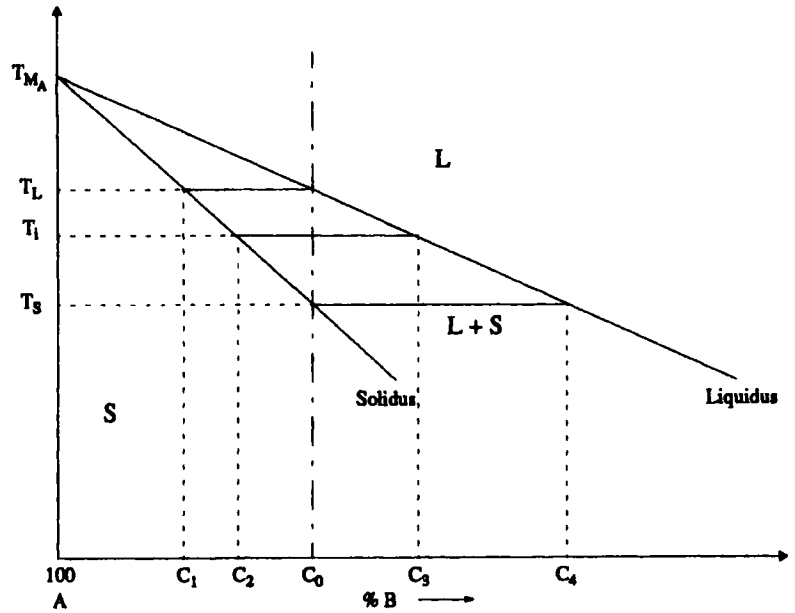


Figure 13.16 Hypothetical equilibrium phase diagram for a hypothetical binary alloy of solute B in solvent A. Solidification is considered for an alloy with a nominal composition of C_0.

As the temperature continues to fall at an infinitesimally slow rate to maintain equilibrium, the compositions of both the remaining liquid and the solid present adjust themselves by diffusion[12] in such a way that equilibrium prevails. According to equilibrium, at any intermediate temperature, T_i, the entire solid volume present would have a composition, C_2, as defined by the intercept of the T_i isotherm or tie-line with the solidus. The entire volume of liquid remaining would have a composition, C_3, as also defined by the T_i isotherm or tie-line with the liquidus. Furthermore, the amount of each phase can be calculated from the Lever rule[13] applied at T_i:

$$\%S = \frac{C_3 - C_0}{C_3 - C_2} \times 100 \tag{13.35}$$

[12] Recall that diffusion is the movement of atoms (at all temperatures above absolute zero) by random walk through a structure, whether the structure is that of a liquid or a solid. In a solid, for atoms to move, they must have a site to move to. This can be a vacancy on the crystal lattice or an interstice between atoms on the lattice. The former is called vacancy diffusion, and the latter interstitial diffusion. In the liquid, there are always spaces in the more open, near-random structure.

[13] An explanation and derivation of the Lever rule can be found in any basic textbook on material science. See Footnote 10 and the end of this chapter for examples.

and

$$\%L = \frac{C_0 - C_2}{C_3 - C_2} \times 100 \tag{13.36}$$

The reason the composition of solid progressively increases as solidification proceeds is that the liquid from which it forms continues to become progressively richer in solute rejected by solid formed earlier. The composition of the solid forming at any time or temperature is always determined by the equilibrium distribution coefficient k_0. The composition of all liquid present at any time is homogeneous as the result of equilibrium, which presumes that either mechanical mixing or diffusion or both together level the composition. The composition of all solid present at any time remains homogeneous as the result of equilibrium, which presumes enough time for diffusion to level the composition.

As the temperature falls further and further below the equilibrium liquidus toward the equilibrium solidus, the amount of solid increases, while the amount of liquid decreases. At just above T_s, the composition of the solid would be slightly to the left of C_0 (in Figure 13.16) and an infinitesimal volume of liquid with a composition slightly to the left of C_4 would be in equilibrium. If cooled to T_s at an infinitesimally slow rate, these two phases would interact and, by diffusion, convert the entire alloy to a composition of C_0; the starting composition. The resulting solid, regardless of its grain or sub-structure, thus exhibits no evidence of microsegregation.

Obviously, equilibrium of this sort never occurs in nature. However, equilibrium diagrams can be useful in predicting nonequilibrium behavior, as seen in the next section.

13.4. NONEQUILIBRIUM SOLIDIFICATION OF ALLOYS

In the real world, equilibrium solidification of alloys (or pure materials, for that matter) is never encountered. Solidification always occurs under conditions of nonequilibrium, with cooling rates ranging from a low of about 10^{-2} deg K s^{-1} (for large, voluminous castings) to a high of about 10^{7} deg K s^{-1} (for rapid-solidification processing). The questions are simply (1) How much does reality differ from equilibrium? and (2) Specifically, how does reality differ from equilibrium? We can begin to answer these questions by considering the boundary conditions under which solidification can take place.

13.4.1. Boundary Conditions for Solidification of Alloys

Four distinct boundary conditions have traditionally been differentiated to describe how the solidification of alloys can occur, not because these are

exactly the conditions under which real solidification of alloys occurs, but because they can be reasonably well modeled.

Case 1: Equilibrium Maintained at All Times
- a. $\Delta G = 0$.
- b. No composition gradient exists anywhere; $dc/dx = 0$ in both liquid and solid states.

Case 2: Complete Mixing in the Liquid
- a. Complete mechanical mixing takes place in the liquid, such that no composition gradient ever exists in the liquid, that is, $dc/dx = 0$ in the liquid.
- b. No diffusion occurs in the solid, so $dc/dt = 0$ in the solid.

Case 3: No Mixing in the Liquid
- a. No mechanical mixing takes place in the liquid.
- b. Changes in composition in the liquid occur by diffusion only.
- c. No diffusion occurs in the solid.

Case 4: Splat Cooling
- a. No mechanical mixing takes place in the liquid.
- b. No diffusion occurs in the liquid, so $dc/dt = 0$ in the liquid.
- c. Liquid is supercooled to a glassy (amorphous) state, rather than to a crystalline state.

We will look at cases 1, 2, and 3, leaving case 4 as an interesting, but far less relevant, situation.

13.4.2. Equilibrium Maintained Throughout the System at All Times: Microscopic Equilibrium (Case 1)

Case 1, where equilibrium is maintained throughout the system at all times, is described in Section 13.3.2. In the real world, case 1 is never encountered. However, for layers of solid and liquid only a few atoms thick on opposite sides of a moving solid–liquid interface, the free energy of the interface will be minimized if these vanishingly thin layers assume compositions that correspond to those predicted by the equilibrium phase diagrams. This condition, referred to as microscopic equilibrium, can be assumed to be present at all times during both case 2 and case 3 solidification. This does not imply that the compositions of the bulk solid and liquid will bear any relationship to the concentrations predicted by equilibrium, only that the first few atom layers adjacent to the solid–liquid interface will have compositions identical to those predicted by equilibrium concepts.

Case 1 is also interesting and important as it represents the ideal solidification process, and one of the major boundary conditions that can be described (or modeled) with precision.

13.4.3. Complete Liquid Mixing/No Diffusion in the Solid (Case 2)

The assumption of no or negligible diffusion in the solid with sufficient mechanical mixing in the liquid phase to render it completely homogeneous at all times, that is, the boundary conditions for case 2, has obvious relevance to fusion welding. Cooling of the weld pool following the rapid deposition of intense energy into a large thermal mass or heat sink can severely limit, even if not totally prevent, solid-state diffusion. Furthermore, convection in the weld pool can be severe enough to produce complete mechanical mixing and homogeneity of the liquid at all times, at least for some processes. For these reasons, case 2 represents an extremely important set of boundary conditions, both because it appears to have relevance and because, it turns out, it can be modeled without great difficulty.

Imagine the hypothetical binary phase diagram shown in Figure 3.17, in which the composition axis has been expanded for clarity. For an alloy with nominal composition C_0, the first solid forms at temperature T_L from homogeneous liquid of composition C_0 (the given composition for the alloy) on cooling from above the liquidus. The composition of this first solid to form is given by C_1 (from k_0C_0), obtained from the intersection of the horizontal isotherm or tie-line at T_L and the solidus curve. At any temperature, T_i, the composition of the solid interface in contact with the liquid is given by the intersection of the temperature isotherm at T_i with the solidus, C_3. However, since no diffusion is possible in the solid, a concentration gradient exists and

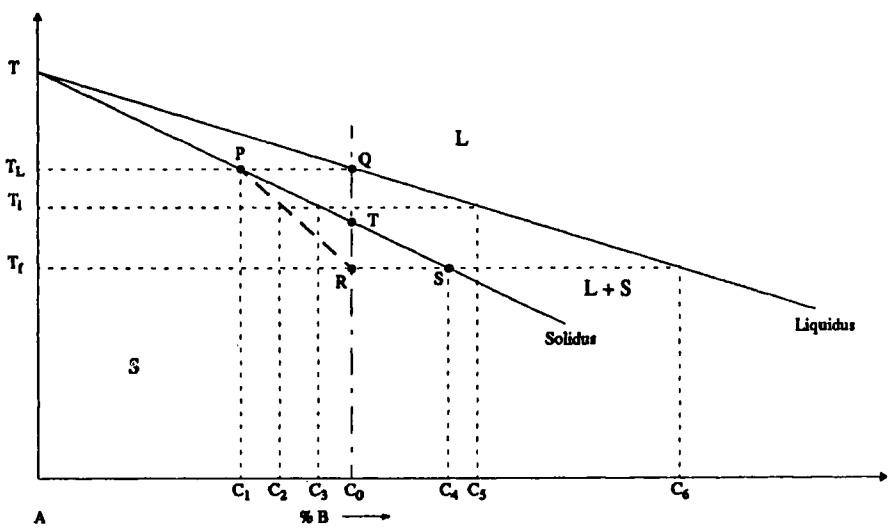


Figure 13.17 Hypothetical constitution diagram for a binary alloy of solute B in solvent A, with the composition axis expanded for clarity. Solidification under case 2 for an alloy of nominal composition C_0 is shown.

persists from C_1 at the point where the first solid formed to C_3 at the instantaneous location of the solid–liquid interface. The average composition of all of the solid formed until temperature T_i is reached somewhere (not necessarily halfway) between the first solid to form, C_1, and that present at the solid–liquid interface at T_i, C_3, shown here as C_2. Expressions for the composition of the solid at the advancing solid–liquid interface and for the average composition in the solid are given and derived later (subsections 13.4.3.1 and 13.4.3.2). The composition of the liquid at T_i is equal to C_5 and is obtained from the intersection between the isotherm at T_i and the liquidus. Recall, that complete mixing is assumed in the liquid, so the liquid phase is homogeneous at all times.

To determine how much solid has formed and how much liquid remains, the Lever rule must be applied between the average composition line (shown by *PR* in Figure 13.17) and the liquidus. Thus, for example, at T_i, the following calculations can be applied:

$$\%\text{solid at } T_i = \frac{C_5 - C_0}{C_5 - C_2} \times 100 \tag{13.37}$$

$$\%\text{liquid at } T_i = \frac{C_0 - C_2}{C_5 - C_2} \times 100 \tag{13.38}$$

where average composition is C_2 and homogeneous composition is C_5. This method of calculation is necessary to provide a material balance for the system.

At $T_f + \Delta T$, the following statements describe the situation: An infinitesimal quantity of liquid of composition $C_6 - \Delta C'$ throughout exists in contact with the solid phase. The balance of the system consists of a solid phase of composition varying from C_1 at its point of initial formation to $C_4 - \Delta C''$ at the instantaneous location of the solid–liquid interface. The average composition of the solid phase is $C_0 - \Delta C'''$. The previous compositions can be obtained from the intersection of an isotherm at $T_f + \Delta T$ with the liquidus, the solidus, and the locus of the average composition (line *PR*), respectively.

At T_f, the temperature defined by the intersection of the average composition line for the solid, *PR*, with the nominal composition of the alloy, C_0, the last remaining liquid disappears, the composition of the last solid to form is C_4, and the average composition of the entire solid mass reaches that of the given alloy, C_0. This latter point is necessary to satisfy the system's material balance.

Note that the solid mass constituting the weld metal or former fusion zone exhibits a concentration gradient ranging from C_1, at the point where the first solid formed, to C_4, at the point where the last solid formed. If the distances involved between points of minimum and maximum solute content are small (on the order of a grain diameter or dendrite arm width), such segregation is termed *microsegregation*. If, however, these distances are of the same order of size of the entire mass (i.e., weld width), the term *macrosegregation* applies (see Sections 12.2 and 12.5).

The above condition of solidification could, in theory at least, double the temperature range associated with the solidification process. That is to say, if the liquidus and solidus lines are straight or nearly so over the range of interest, triangles PQT and RST are congruent and QT is approximately equal to TR.

The specific consequences of solidification occurring under case 2, as well as more on the relevance of this case to actual fusion welding processes, are discussed in Section 13.5.

13.4.3.1. Expression for the Composition of Solid at the Advancing Solid–Liquid Interface. If one assumes that a rectangular volume of liquid of unit cross-sectional area is solidified unidirectionally by the passage of a planar solid–liquid interface that moves from left to right in Figure 3.18, then the following derivation leads to an expression for the composition of the solid at the advancing solid–liquid interface: If f_s is taken to be the fraction of the volume solidified, and the equilibrium distribution coefficient is k_0 for an alloy of nominal composition C_0, by conservation of matter, any solute not in the solid must be found in the remaining liquid. Thus, when an infinitesimal volume of solid, df_s, is formed from liquid by movement of the solid–liquid interface, the following can be written:

$$(C_L - C_S^*)df_s = (1 - f_s)dC_L \tag{13.39}$$

where C_L is the instantaneous composition of the liquid, f_s is the volume fraction solidified, and $C_S^* = k_0C_0$ at $f_s = 0$ and k_0C_L at all times later. Substituting gives

$$C_L - k_0C_L)df_s = (1 - f_s)dC_L \tag{13.40}$$

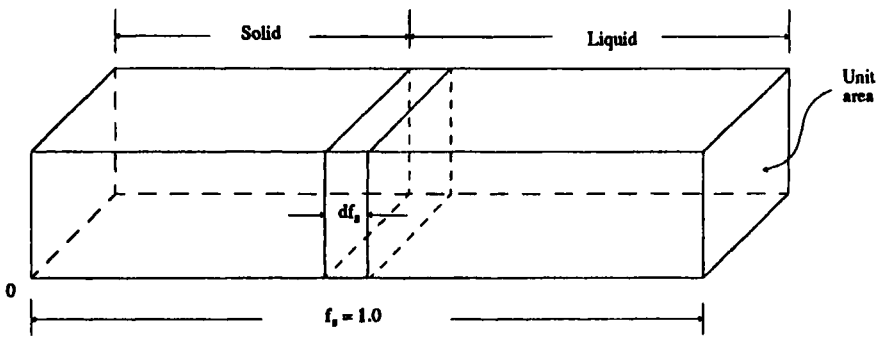


Figure 13.18 A rectangular volume of liquid with unit cross-sectional area within which a planar solid–liquid interface moves from left to right.

and rearranging gives

$$\frac{df_s}{1-f_s} = \frac{dC_L}{C_L(1-k_0)} \tag{13.41}$$

Integrating over the full range of fraction solidified gives

$$\int_0^{f_s} \frac{df_s}{1-f_s} = \int_{C_0}^{C_L} \frac{dC_L}{C_L(1-k_0)} \tag{13.42}$$

yielding

$$\ln(1-f_s) = \frac{1}{k_0-1} \ln \frac{C_L}{C_0} \tag{13.43}$$

so

$$(k_0-1)\ln(1-f_s) = \ln \frac{C_L}{C_0} \tag{13.44}$$

or

$$(1-f_s)^{k_0-1} = \frac{C_L}{C_0} \tag{13.45}$$

or

$$C_L = C_0(1-f_s)^{k_0-1} \tag{13.46}$$

But, since

$$C_S^* = k_0 C_L$$

$$C_S^* = k_0 C_0 (1-f_s)^{k_0-1} \tag{13.47}$$

This equation is known as the Scheil equation.

Assuming values of $k_0 = 0.2$ and $k_0 = 1.5$, values of C_S^*/C_0 versus f_s are given in Table 13.3.

13.4.3.2. Calculation of the Average Composition of the Solid for Case 2. Remember that under case 2 conditions, cooling rates are so rapid that there is virtually no time for changes in the composition of the solid formed to occur by diffusion. Thus, the average composition of the solid

TABLE 13.3 Calculated Values of C_s^*/C_0 Versus f_s for $k_0 = 0.2$ and 1.5 Using Eq. 13.47 Derived for the Composition of Solid at the Advancing Solid–Liquid Interface During Case 2 Solidification

	C_s^*/C_0	
Fraction Solidified f_s	For $k_0 = 0.2$	For $k_0 = 1.5$
0.0	0.2	1.5
0.1	0.2176	1.4230
0.2	0.2391	1.3416
0.3	0.2660	1.2550
0.4	0.3010	1.1619
0.5	0.3482	1.0607
0.6	0.4163	0.9487
0.7	0.5240	0.8216
0.8	0.7248	0.6708
0.9	1.2619	0.4743
0.99	7.9612	0.1500

Source: After Savage, circa 1966, unpublished notes.

present after a fraction f_s of the original liquid volume has solidified is given by

$$C_{Savg} = \frac{\int_0^{f_s} k_0 C_0 (1 - f_s)^{k_0 - 1} df_s}{\int_0^{f_s} df_s} \tag{13.48}$$

This gives

$$C_{Savg} = \frac{k_0 C_0 [1 - (1 - f_s)^{k_0}]}{f_s} \tag{13.49}$$

While not simple to solve without a computer, this equation can be (and was) solved by hand for various values of k_0 for values of f_s ranging from 0 to 0.999.

Note that the Lever rule applies if one writes

$$\% \text{ solid} = \frac{C_L - C_0}{C_L - C_{Savg}} \times 100 \tag{13.50}$$

$$\% \text{ liquid} = \frac{C_0 - C_{Savg}}{C_L - C_{Savg}} \times 100 \tag{13.51}$$

where C_L is the composition of the liquid at T_i (also equal to C_S^*/k_0), C_0 is the

nominal composition at T_i, and C_S is the solidus composition at T_i. Also, T_i can be written as

$$T_i = T_E + m_l \frac{C_S^*}{k_0} \tag{13.52}$$

where T_E is the melting point of the solvent element, m_l is the slope of the liquidus line, C_S^* is the composition of the solid at the solid–liquid interface at T_i, and k_0 is the equilibrium distribution coefficient. Thus, for any fraction solidified, it is possible to calculate C_S^*, $C_{S_{avg}}$, and the corresponding value of T_i.

13.4.4. No Liquid Mixing/No Diffusion in the Solid (Case 3)

The other set of boundary conditions that seemingly might apply to fusion welding are those assumed for case 3; namely, no diffusion in the solid and no mechanical mixing in the liquid, just diffusion in the liquid. Clearly, real fusion welds cool so quickly following welding, it is unlikely there is much diffusion occurring in the newly formed solid to alter its composition. There are also some fusion welding processes in which convection in the weld pool is minimal, such as oxyfuel gas welding. For these processes, any change that occurs in the composition of the weld pool must occur largely, even if not completely, by diffusion as opposed to mixing. Again, this case is interesting not only because it seems to represent some welding processes but because it, too, can be modeled with reasonable precision.

Imagine the hypothetical binary constitution diagram shown in Figure 3.19, and an alloy of nominal composition C_0 undergoing solidification under the above boundary conditions. The first solid to form will be of composition C_1 ($= k_0 C_0$) when the temperature of the melt falls to T_L, the liquidus temperature for composition C_0. Since this solid contains less solute than the nominal composition as a consequence of the equilibrium distribution coefficient k_0, the remaining liquid must be enriched in solute B. However, since there is no mechanical mixing in the liquid, this solute can only redistribute into the bulk of the liquid by diffusion. As a result, solute begins to build up right at the solid–liquid interface, creating a concentration gradient. As the interface advances, and more new solid forms, more solute is rejected into the liquid to accumulate near the interface, being redistributed into the liquid only as fast as diffusion allows. This takes time, and the concentration gradient continues to build up. This is shown schematically in Figure 13.20 for several sequential time steps. In the meantime, no changes occur to the composition of the solid formed as solidification continues, so, as in case 2, an average composition develops in the solid.

At some intermediate temperature, T_i, microscopic equilibrium (Section 13.4.2) dictates that the liquid and solid phase in contact at the solid–liquid interface be at C_{Li} and C_{Si}, respectively, such that $C_{Li} = C_{Si}/k_0$. The concen-

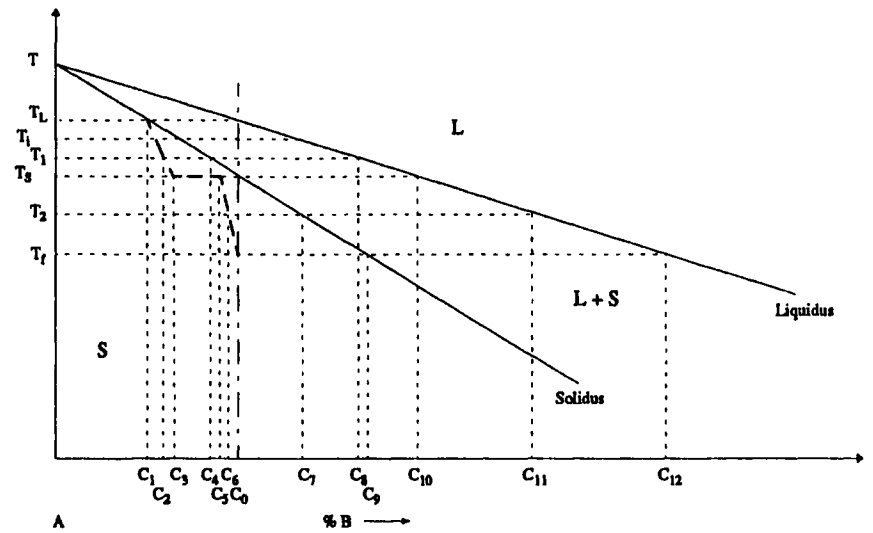


Figure 13.19 Hypothetical constitution diagram for a binary alloy of solute B in solvent A, with the composition axis expanded for clarity. Solidification for case 3 for an alloy of nominal composition C_0 is shown.

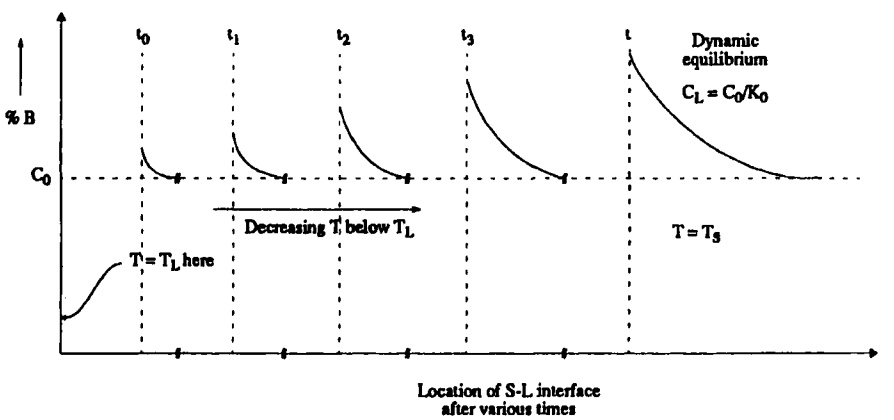


Figure 3.20 Schematic showing the buildup of a solute composition gradient or profile in the liquid ahead of an advancing solid–liquid interface under case 3, where there is no mixing in the liquid, only diffusion. Several sequential time steps are shown.

tration gradient in the liquid ahead of the moving solid–liquid interface therefore assumes the shape shown schematically in Figure 13.21. Note in this figure that liquid remote from the interface continues to exhibit a composition C_0, and that new solid is being formed from the solute-enriched liquid right at the interface.

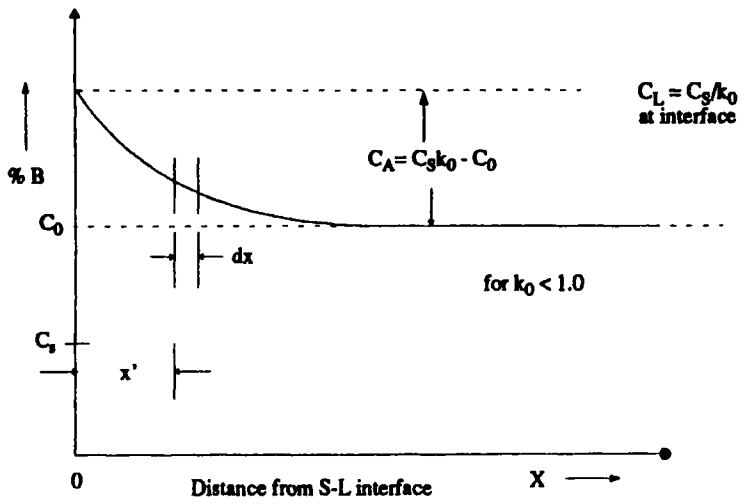


Figure 13.21 Schematic of the concentration gradient in the liquid ahead of a moving solid–liquid interface.

If a volume element dx is identified at some distance x'[14] from the moving solid–liquid interface along the concentration gradient (as it is in Figure 13.21), from Fick's second law of diffusion, then the net flux of solute atoms into or out of this volume element can be expressed as

$$J_D = D\frac{d^2c}{dx^2} \tag{13.53}$$

where J_D is the flux associated with diffusion only. However, the solid–liquid interface is moving from left to right (in Figure 13.21) at a rate R (cm/s). Therefore, the flux associated with the migration of the interface J_M can be expressed as

$$J_M = R\frac{dc}{dx} \tag{13.54}$$

When the composition of the liquid (C_L) at the moving interface reaches C_0/k_0, a condition of dynamic equilibrium is established, as shown in Figure 13.22 for $k_0 < 1.0$. At this point, the concentration gradient begins to move with but just ahead of the solid–liquid interface without change in shape so long as the conditions of solidification remain unchanged (see Section 12.5.1 on banding). For this to be the case, the rate of flow of solute atoms into the

[14] x' will be used to indicate the instantaneous distance from the moving interface, while x will indicate the distance from the beginning of solidification.

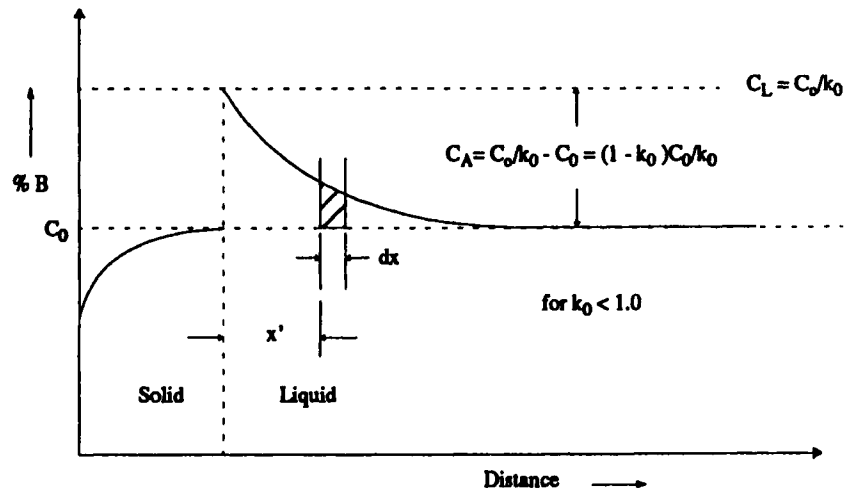


Figure 13.22 Schematic showing how a state of dynamic equilibrium is established when the composition of the liquid (C_L) at the moving interface becomes C_0/k_0.

volume element caused by interface migration, J_M (Eq. 13.54), must be equal to the rate of flow of solute atoms out of the volume element by diffusion, J_D (Eq. 13.53).[15] Thus, the following differential equation can be written:

$$R\frac{dc}{dx} + D\frac{d^2c}{dx^2} = 0 \tag{13.55}$$

The solution for this differential equation has the form

$$C_L = C_A \exp\left(-\frac{R}{D}x'\right) + C_0 \tag{13.56}$$

where C_A is shown in Figure 13.22 to be the amount by which solute at the peak of the concentration gradient builds above the background composition C_0. But since at dynamic equilibrium

$$C_A = \frac{C_0}{k_0} - C_0 = C_0\left(\frac{1 - k_0}{k_0}\right) \tag{13.57}$$

this reduces to

$$C_L = C_0\left[1 + \frac{1 - k_0}{k_0}\exp\left(-\frac{R}{D}x'\right)\right] \tag{13.58}$$

[15] For $k_0 > 1.0$, the signs of the flow would be reversed.

TABLE 13.4 Calculated Values of $\exp[(-R/D)x']$ as a Function of Multiples of the Characteristic Distance x'_c

x'	$\frac{R}{Dx'}$	$\exp\left(-\frac{R}{Dx'}\right)$
	0	1.0
x'_c	1	0.368
$2x'_c$	2	0.135
$3x'_c$	3	0.050
$4x'_c$	4	0.018
$5x'_c$	5	0.007
$6x'_c$	6	0.0025

Source: After Savage, circa 1966, unpublished notes.

where k_0 is the equilibrium distribution coefficient, R is the rate of growth or movement of the solid–liquid interface, D is the diffusion coefficient (approximately 5×10^{-5} cm^2/s), x' is the distance from the solid–liquid interface into the liquid, and C_0 is the nominal composition of the alloy and liquid.

For Eq. 13.58, it is convenient to define a characteristic distance, $x'_c = D/R$, to describe the shape of the concentration gradient in the liquid ahead of the moving solid–liquid interface. Table 13.4 summarizes the value of the exponential term, $\exp[(-R/D)x']$, in terms of integral multiples of the characteristic distance, $x'_c = D/R$. These data indicate that a change in $\exp[(-R/D)x']$ is virtually complete (i.e., within 1% of its final value of zero) when $x = 5x'_c$. Thus, the extent of the concentration gradient in the liquid that is associated with diffusion alone is approximately equal to $5x'_c$ or $5D/R$.

Table 13.5 summarizes the growth rates typical of three different fusion welding processes, with values of $5x'_c$ in both centimeters and inches. The values are based on the growth rate at the center of an elliptical weld pool where $v \cos\phi = R - v$, the welding velocity. Note that except for the electro-

TABLE 13.5 Growth Rates (R) and Stagnant Layer Widths (expressed as $5x'_c$ in centimeters or inches) for Three Different Welding Processes

Process	Typical Maximum Growth Rate R (cm/s)	Stagnate Layer Width $5x'_c$ (cm)	Stagnate Layer Width $5x'_c$ (in.)
ESW	2×10^{-3}	0.118	0.047
SMAW	2.5×10^{-1}	9.8×10^{-4}	3.86×10^{-4}
EBW	5	4.9×10^{-5}	1.93×10^{-5}

Source: After Savage, circa 1966, unpublished notes.

slag welding (ESW) process, the entire gradient is contained within a layer of liquid less than 0.001 in. or 0.025 mm thick ahead of the moving solid–liquid interface. Therefore, it is not difficult to imagine a stagnant layer of such small dimensions even if the weld pool experiences quite violent agitation. This means that Eq. 13.58 for the profile of C_L would be valid since the entire concentration gradient in the diffusion layer would be contained within the stagnate layer where no mechanical mixing would be possible.

As a generality, the steady-state concentration gradient established in the liquid ahead of the moving solid–liquid interface would be steeper for smaller values of D and faster growth rates R, since the characteristic distance $x' = D/R$.

What all of this means as far as how the concentration of the solid formed in the original fusion zone behaves is as follows and as shown in the steps in Figure 13.23, in which the abscissa in each illustration represents the width of the weld, with growth of the solid assumed to progress inward from both sides until impingement occurs at the centerline of the weld:

Step A. At $T_L - \Delta T$, the liquid is enriched slightly at the solid–liquid interface and the concentration of the solid and the liquid at the interface obey $C_S = k_0 C_0$.

Step B. The higher concentration of B in the solid at the solid–liquid interface at T_1 (corresponding to Figure 13.19) reaches C_4, and the liquid at the interface contains $C_8 = C_4/k_0 = C_4/0.5$ (for the situation shown in Figure 13.23).

Step C. The beginning of dynamic equilibrium occurs at $t = t_1$, $T = T_S$. C_L at the solid–liquid interface $= C_{10}$; $C_S = k_0 C_L = k_0 C_{10} = C_0$. Note the shape of the concentration spike in the liquid.

Step D. Note that at $t = t_2$, T still equals T_S and concentration spikes are just about to impinge on one another as they advance from opposite sides of the weld pool, although C_L still equals C_{10} and $C_S = k_0 C_L = C_0$.

Step E. Terminal transient enrichment of solid is well underway at T_2. Note that the liquid at the solid–liquid interface has composition C_{11} and adjoining solid $C_S = k_0 C_{11} = C_7$.

Step F. At $T_f - \Delta T$, solidification is complete. Note the terminal transient enrichment of solid at the centerline of the weld to C_9. Note also that the cross-hatched areas above and below C_0 are equal in all steps above, as required from a material balance in the system.

While what is shown in the various steps in Figure 13.23 are, in fact, highly idealized representations of the actual solute distribution during the solidification of a weld puddle by a case 3 process, they portray well the general phenomena.

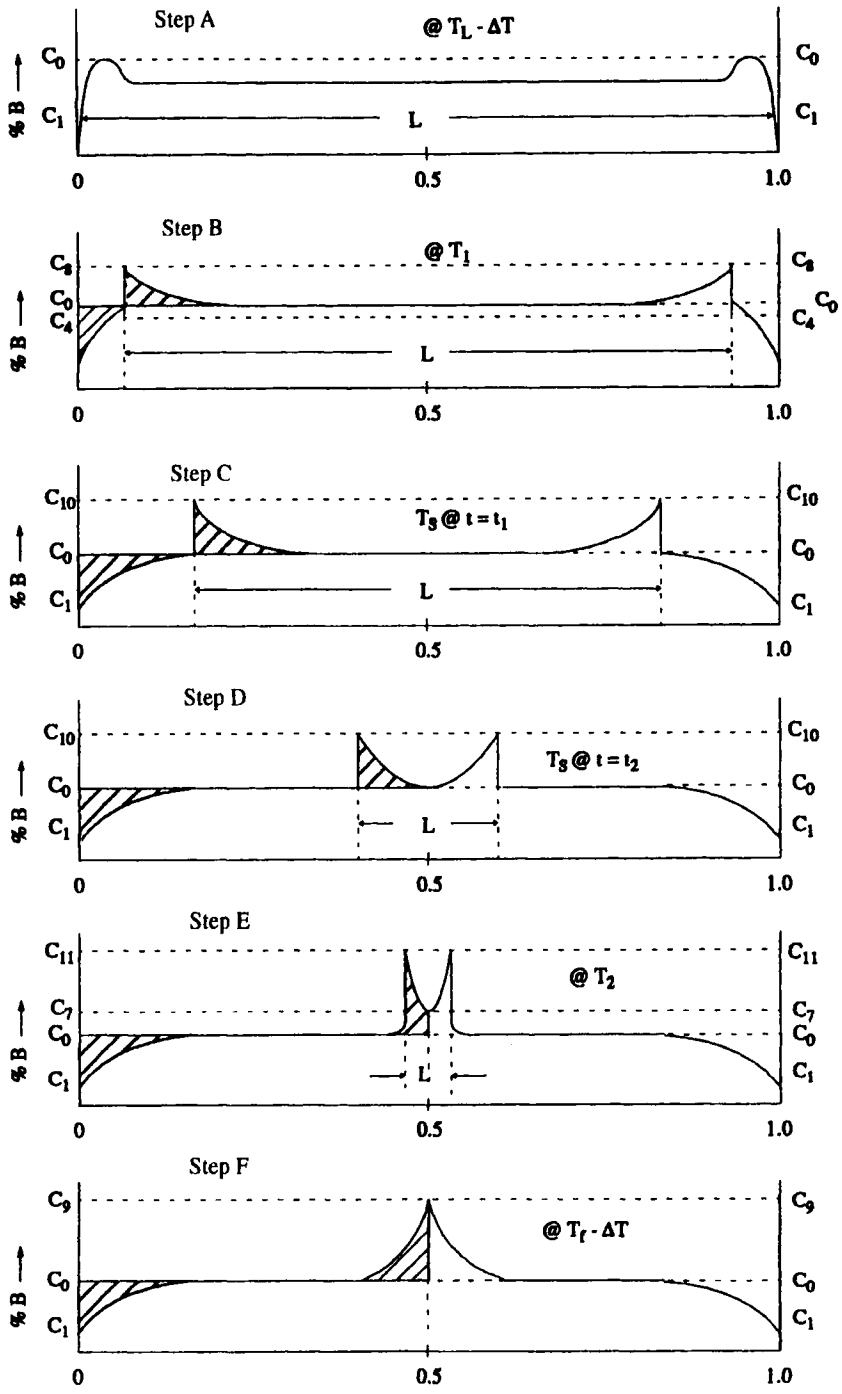


Figure 13.23 Schematic summary of case 3 solidification for $k_0 = C_S/C_L = 0.5$.

13.4.4.1. Trace of Average Composition in the Solid for Case 3. The overall trace of average composition in the solid formed as temperature drops is shown in Figure 13.19 by a heavy dashed line. The average composition of the solid falls precipitously in the range of temperature from T_L to T_S, while the initial transient of composition in the solid is decaying (see Section 13.4.4.2), that is, until the start of dynamic equilibrium. Upon completion of the decay of the initial transient, the temperature remains constant at T_S and the solid of composition C_0 forms from the liquid of composition C_{10} until some time t_2 (see step D in Figure 13.23) when the concentration spike in front of the solid–liquid interface growing from right to left meets the spike growing from left to right. During this interval from t_1 to t_2 (represented by steps C and D, respectively, in Figure 13.23), the rate of diffusion of solute away from the solid–liquid interface is exactly equal to the rate of growth of the solid phase, and, therefore, excess solute rejected by the liquid during the initial transient period is transported ahead of the growing interface. Thus, the area under the curve representing the concentration spike in the liquid must be equal to the area between the nominal composition level (C_0) and the initial transient. In other words, the latter area is a measure of the amount of solute displaced during the initial stages of solidification. Throughout this time interval, the average composition line progresses horizontally along the T_S isotherm (as shown in Figure 13.23).

When the two concentration spikes impinge upon one another, the solute content of the solid–liquid interface begins to rise (as shown in step E of Figure 13.23) and, therefore, the solid on the opposite side of the interface becomes enriched in solute until $C_S = k_0 C_L$. During this region of growth, the average composition line ceases to progress horizontally along the T_S isotherm and turns sharply downward, reflecting the increasing concentration of solute at the solid–liquid interface. As the two advancing solid interfaces meet at the center of the weld, the last liquid of composition C_{12} disappears by reacting with the solid interface to form the final bit of solid of composition C_9, and the average composition line crosses the nominal composition line C_0. Thus, the solidification is complete at T_f, and the resulting solid shows a distribution of solute as shown in step F of Figure 13.23.

13.4.4.2. Expression for the Initial Transient in the Composition of the Solid Formed. The first solid to form under case 3 conditions will have a composition $k_0 C_0$, according to the definition of k_0. Brody and Flemings (1966) and others proposed an approximate solution for the variation in the composition of the solid with distance from the initiation of solidification for unidirectional solidification with a planar solid–liquid interface given by

$$C_S = C_0\left\{(1 - k_0)\left[1 - \exp\left(-\frac{k_0 R}{D}\right)x\right] + k_0\right\} \tag{13.59}$$

where x is the distance from the initial solid–liquid interface in contrast to x', which referred to the distance from the moving solid–liquid interface.

According to this relationship, the concentration of the solid changes from k_0C_0 in the first solid to C_0 over a distance of about five characteristic distances, where the characteristic distance $x_c = D/k_0R$. The length of this initial transient variation in the composition of the solid depends on both k_0 and R, whereas the solute gradient in the liquid was independent of k_0 and dependent only on R.

Smith, Tiller, and Rutter (1948, 1953, 1956) later developed an exact solution to the initial transient variation in the composition of the solid:

$$C_S = 2C_0 \left\{ 1 + \operatorname{erf} \sqrt{\frac{R}{2D}}\, x + (2k_0 - 1) \exp\left[-k_0(1 - k_0) \frac{R}{D} x \right] \times \operatorname{cerf}\left[\frac{(2k_0 - 1)\sqrt{\dfrac{R}{D}}}{2} x \right] \right\} \tag{13.60}$$

Both Brody and Flemings' far simpler and Smith, Tiller, and Rutter's exact solutions predict virtually the same length of the initial transient, which is what is of greatest concern, and both assume the same initial and final concentrations.

13.4.4.3. Some Limitations of the Classic Models. A problem with the Scheil equation (Eq. 13.47) is that, unless a limit is placed on the solid solubility of the solidifying alloy, and the remaining materials solidify at a fixed temperature, such as occurs for an eutectic composition, the final composition approaches infinity. Another shortcoming is failure to account for the diffusion that actually takes place in the solid state during solidification. Brody and Flemings (1966) took this into account and modified Schiel's equation for the case where solid-state diffusion does occur, yielding

$$C_s^* = k_0 C_0 \left(1 - \frac{f_s}{1 + \alpha k_0} \right)^{(k_0 - 1)} \tag{13.61}$$

where $\alpha = 4D_s t_F/d^2$, and d is a volume element length, D_s is the solid-state diffusion coefficient, t_F is the local solidification time, and all other terms are as defined previously.

For the simpler Schiel equation and the more elaborate Brody and Flemings' equation, microsegregation is predicted across dendrites only, and no allowance is made for constitutional supercooling at dendrite tips. It is assumed that initial solidification takes place at the liquidus temperature corresponding to the overall composition of the liquid (i.e., alloy). While this latter failing causes neither model to be very accurate at describing the dendrite

core composition if appreciable supercooling takes place at the dendrite's tip, they remain useful for predicting concentration across dendrites in any case. Interested readers are referred to experimental studies of Lippold and Savage (1980) and Brooks and Baske (1987).

13.4.5. Other Effects of Rapid Solidification

Solidification under fast cooling rates, typical of most welding, but especially welding using high-energy-density sources, leads to two important nonequilibrium effects not yet discussed. The first is the effect on the distribution or solute partition coefficient. The second is on the phases produced, with nonequilibrium phases not found on equilibrium phase diagrams being most important.

13.4.5.1. Nonequilibrium Solute Partitioning. Under normal solidification conditions, it is not unreasonable to assume that microequilibrium is maintained at the solid–liquid interface (as was the case until now). In such a case, the equilibrium distribution or partition coefficient, k_0, can be obtained by taking the ratio of the solid to liquid compositions given by the appropriate tie-line on the phase diagram. Such is clearly not the case as cooling rate increases significantly (such as prevails for EBW and LBW). At such high rates, diffusion is limited, and the solid and liquid compositions near the interface tend to converge. Several models have been developed that allow for a nonequilibrium partition coefficient, k', and its variation with solidification (growth) velocity (Boettinger and Coriell, 1984). Basically, the nonequilibrium partition coefficient is allowed to vary between the equilibrium value applicable at low growth velocities and a value of 1 at extremely high growth velocities. When $k' = 1$, the solid forming at any instant of time has the same composition as the liquid from which it just formed, and, so, solidification is said to be "partitionless." Figure 13.24 gives the nonequilibrium partition coefficient as a function of growth rate for several models. These values of k' have been verified by experiment.

As the result of less solute redistribution at high solidification rates, the newly formed solid is more uniform in composition. As a consequence, the normally occurring second phase may not appear and, therefore, the solubility limit is in effect extended. One favorable effect can be a reduced tendency for hot cracking arising from microsegregation of low-melting constituent, which has been observed by the author during EB welding of advanced titanium alloys (Messler, 1981).

13.4.5.2. Nonequilibrium Phases. A variety of nonequilibrium phases may be produced as a result of rapid solidification, ranging from extended ranges of stability and/or altered limits on solubility, to massive (shear) transformations, to even amorphous phases. These are broadly documented in the literature (Jones, 1973), and there is a fine review of the correlation between solidification parameters and weld microstructure by David and Vitek (1989).

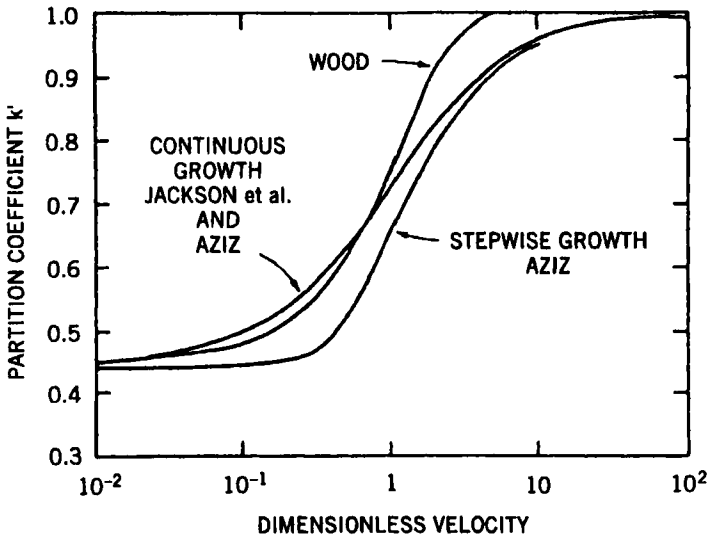


Figure 13.24 Calculated variation of partition coefficient, k', with velocity using various models. (From "Mechanisms of microsegregation-free solidification" by W. J. Boettinger and S. R. Coriell, *Materials Science & Engineering*, **65**, 27–35, 1984, used with permission.)

13.5. CONSEQUENCES OF NONEQUILIBRIUM SOLIDIFICATION

If alloys solidified under equilibrium conditions, there would be no particular problem. The final structure would be of uniform microstructure, consisting of phases and constituents in accordance with phase diagrams, and, within phases, composition and properties would be uniform. Unfortunately, as we have seen, in the real world, solidification of alloys takes place under nonequilibrium conditions, with the degree of deviation varying from process to process, and from practice to practice within a process. Deviation from equilibrium leads to several consequences that are now discussed.

13.5.1. Interdendritic Microsegregation

Solidification of an alloy under nonequilibrium conditions always gives rise to microsegregation within the dendritic structure formed, whether nonequilibrium conditions are best approximated by case 2 or case 3. Recall that in case 2, the liquid in the weld pool from which solid forms is assumed to be completely mixed mechanically. In case 3, there is no mixing in the liquid; only diffusion in the liquid allows solute to be redistributed. In both cases, it is assumed that there is no diffusion in the solid once it has formed. This latter assumption is borne out by observation: There is always a degree of microsegregation within the dendritic structure formed in welds.

Microsegregation is the direct consequence of the unavoidable redistribution or partitioning of solute between the liquid and the solid arising from the equilibrium distribution coefficient k_0. Unlike for equilibrium, however, where this redistribution is of no consequence because composition of both the liquid and the solid are each always homogeneous, under nonequilibrium this microsegregation persists, appearing as what is known as dendritic coring or simply coring. Coring is shown schematically in Figure 13.25 for two substructure modes found in alloys described in Section 13.5.3: cellular (or cellular dendritic) and dendritic (or equiaxed dendritic).

Incidentally, solute is rejected from any solid into the surrounding liquid, not just at the solid–liquid interface representing the primary weld solidification front. The identical process occurs as new solid is formed as spikes or dendrites, with the dendrite becoming the solid in the solid–liquid interface, and the liquid surrounding it becoming the liquid in this new interface. Thus,

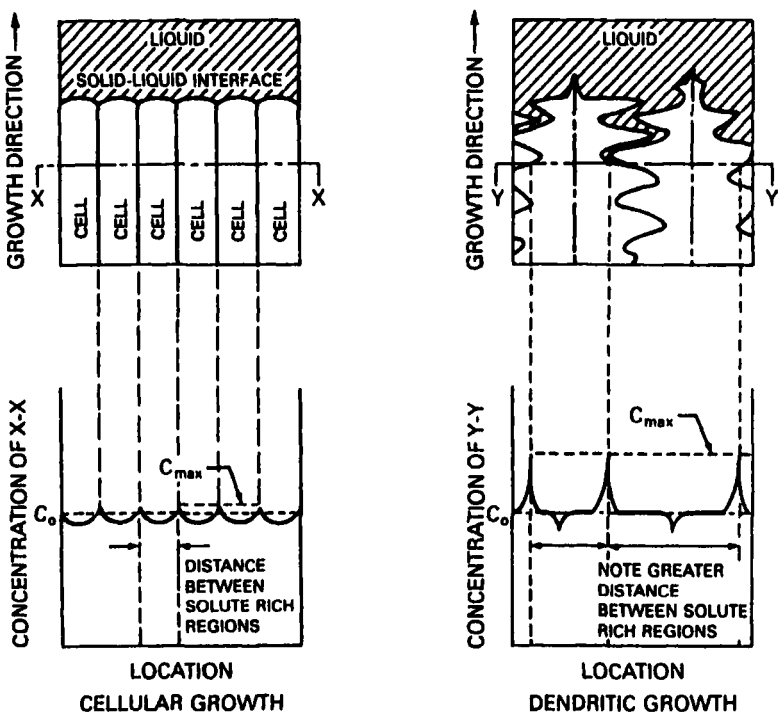


Figure 13.25 Schematic of solute redistribution or coring for cellular and dendritic growth resulting from nonequilibrium solidification under either case 2 or case 3 boundary conditions. (From *Welding Handbook*, Vol. 1, *Welding Technology*, 8th Ed., edited by L. P. Connor, published in 1987 by and used with permission of the American Welding Society, Miami, FL.)

microsegregation occurs everywhere—ahead of the advancing primary solid–liquid interface and between all dendrites, regardless of their particular modality (discussed in Section 13.5.3). Interdendritic microsegregation, in fact, is what leads to interdendritic cracking during solidification (see Section 13.6).

There are several consequences of coring, one being the nonuniformity and unpredictability of precise properties, including varying resistance to corrosion, and another being cracking during solidification. Cracking during solidification is discussed separately in Section 13.6.

Some degree of microsegregation is unavoidable in fusion welding. The only way to reduce the severity of microsegregation is to perform postweld heat treatment involving prolonged exposure to elevated temperatures to attempt to homogenize the structure, but this is usually impractical.

13.5.2. Solidus Suppression

As can be seen from Figure 13.17 for case 2 and Figure 13.19 for case 3, rather than being complete at the equilibrium solidus temperature, T_S, solidification continues to well below the equilibrium solidus under nonequilibrium conditions. The point was made in Section 3.4.3 for case 2, that the range over which solidification takes place under nonequilibrium conditions can easily be double the range for equilibrium solidification. The reason (in both cases) is that solidification isn't complete until all the solute present in the original liquid of the weld pool (i.e., in the alloy) is accounted for in the newly formed solid. Given the occurrence of coring and associated average composition in the solid that follows the heavy dashed lines in Figures 13.17 and 13.19, solidification continues below T_S to the point where the average composition line intersects the nominal composition C_0.

The consequence of an extended range of solidification is serious. First, because the longer it takes for solidification to be completed, the greater the thermally induced stresses that develop from thermal contraction in the presence of a temperature gradient. Tensile components of these stresses act to tear open the still molten interdendritic network, causing cracks (see Section 13.6). Second, the lower the temperature at which final solidification takes place, the lower the temperature at which this same solid can remelt in service. This is particularly disturbing if the welded assembly is to be exposed to severely elevated temperatures in service. For example, if nickel-base superalloy gas turbine blades were welded to compatible nickel-base superalloy disks under highly nonequilibrium conditions, severe microsegregation or coring could be expected. Assuming nothing is done to alleviate this situation (say by postweld normalization or homogenization heat treatment), operating the welded blade-disk assembly to what might be presumed by the designer to be a safe temperature, say 100°C below the equilibrium solidus, could lead to unexpected and intolerable melting at lower temperatures. The results could be catastrophic.

13.5.3. Substructure Formation

The mark of a good theory is that it accurately predicts or explains reality. For theories of weld solidification, both case 2 and case 3 accurately predict (1) the existence of dendritic coring as a consequence of nonequilibrium solute redistribution and (2) suppression of the final solidification temperature to well below the equilibrium solidus. Two other situations appear in real fusion welds, however: (3) substructures (from growth modes) other than planar and dendritic predicted for pure metals, and (4) pronounced segregation along the centerline of the weld. Neither of these is predicted by case 2, but both are predicted by case 3.

During the solidification of a pure crystalline material, the solid–liquid interface is usually planar, as there is almost always a positive temperature gradient in the liquid ahead of that interface (see Section 13.2.2). Unless severe undercooling of the liquid is imposed, the dendritic or, more properly, the "equiaxed dendritic" mode is not observed. During the solidification of an alloy, however, the solid–liquid interface, and hence the mode of solidification, can vary considerably, with several additional modalities depending on the solidification conditions and material system involved. Two major theories have been proposed to quantitatively describe the breakdown of a planar solid–liquid interface during solidification: (1) constitutional supercooling (by Tiller et al., 1953), which considers only thermodynamics, and (2) interface stability (by Mullins and Sekerka, 1964), which also considers kinetics and heat transfer. Let's look at each theory.

13.5.3.1. Constitutional Supercooling. Recall, under case 3, that the liquid in the weld pool is assumed not to mix, but, rather, only to undergo composition changes as the result of diffusion. As a result, a concentration gradient of solute builds up in the liquid ahead of the moving solid–liquid interface. The situation is made clear in Figure 13.26. As shown in Figure 13.26b, solidification takes place from left to right at a rate R. Because of the lower solubility of the solid phase (S), solute atoms are rejected into the liquid phase (L) during solidification, and a solute-enriched composition gradient or boundary layer is formed in front of the advancing solid–liquid interface. The composition profile in the liquid is $C_L(x)$ and the compositions of the liquid and solid at the interface are C_L^* and C_S^*, respectively. With the help of the equilibrium liquidus line (defined as $T_L = f(C_L)$ of the phase diagram in (a), the equilibrium liquidus temperature (or effective liquidus) profile in the liquid, $T_L(x)$, can be obtained as shown in (c) of the figure.

Assuming that local microscopic equilibrium exists at the solid–liquid interface, and that there is no diffusion occurring in the solid phase, this gradient of the equilibrium liquidus temperature profile at the interface follows the relationship

$$\frac{dT_L(x)}{dx} \qquad @\, x = 0 = -\frac{Rm_L}{D_L(C_L^* - C_S^*)} \tag{13.62}$$

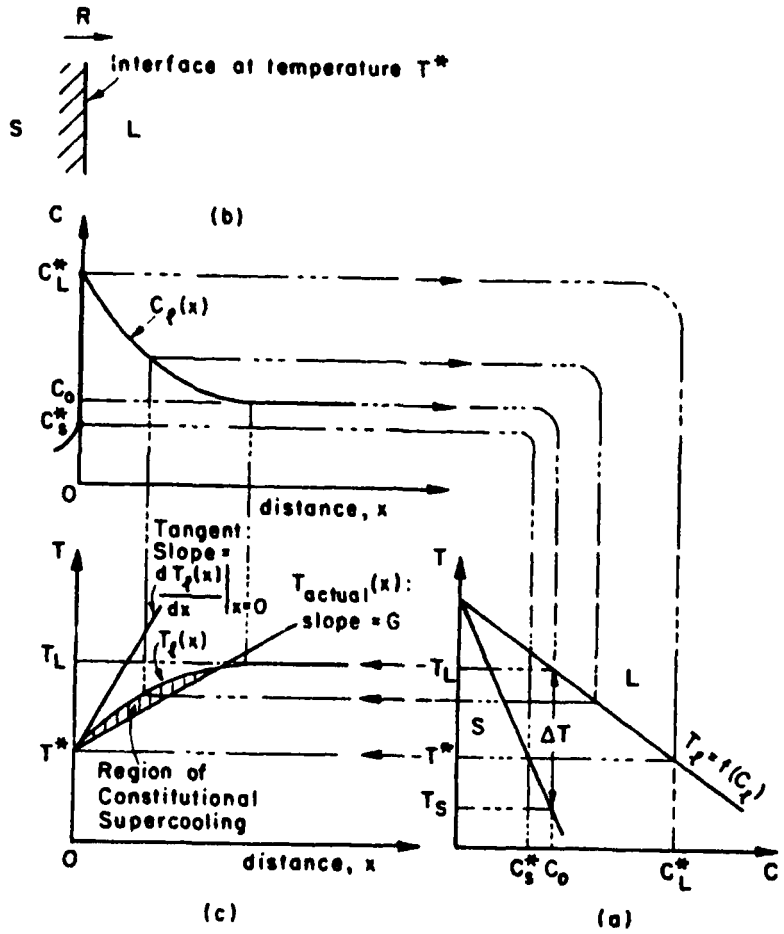


Figure 13.26 Origin of constitutional supercooling during alloy solidification, as explained by (a) the phase diagram for a hypothetical binary alloy system (lower right), (b) the creation of a solute concentration gradient in the liquid ahead of the advancing solid–liquid interface (upper left), and (c) constitutional supercooling relative to the corresponding effective liquidus profile associated with this solute gradient (lower left). (From *Welding Metallurgy* by S. Kou, published in 1987 by and used with permission of John Wiley & Sons, Inc., New York.)

where m_L is the slope of the liquidus line dT_L/dC_L, R is the rate of growth, D_L is the diffusion coefficient of solute in the liquid, and C_L^* and C_S^* are defined as before.

If the actual temperature of the liquid near the solid–liquid interface, $T_{actual}(x)$, is such that its gradient, G, is less than $dT_L(x)/dx$ @ $x = 0$, there exists in the front of the solid–liquid interface a region in which $T_{actual}(x)$ is lower than the equilibrium liquidus temperature, $T_L(x)$. This is shown by the shaded area in Figure 13.26c. This region is said to be *constitutionally supercooled* (i.e.,

supercooled relative to the effective liquidus temperature due to the liquid's "constitution" or composition). Such *constitutional supercooling* leads to different solidification growth modes, other than planar. This is because any protuberance that forms by chance on the solid–liquid interface will find itself in liquid below the effective liquidus, at least for some distance, and will tend to grow.

Figure 13.27 shows the various growth modes that can occur for differing degrees of constitutional supercooling. When the actual temperature gradient in the liquid is so steep it does not fall below the effective liquidus profile anywhere (i.e., it is tangent to the effective liquidus profile), the *planar mode* familiar from pure metals prevails. The planar growth mode is fully epitaxial and completely replicates (in crystal structure and orientation) the substrate grain from which it emanates. Only grain boundaries present in the substrate appear in the planar growth structure. As the actual temperature gradient becomes less steep (i.e., less positive), a small region of constitutional supercooling leads to a new, *cellular growth mode.* Cellular growth is characterized by a number of narrow, parallel, pencil-like subgrains. A single cluster of cells

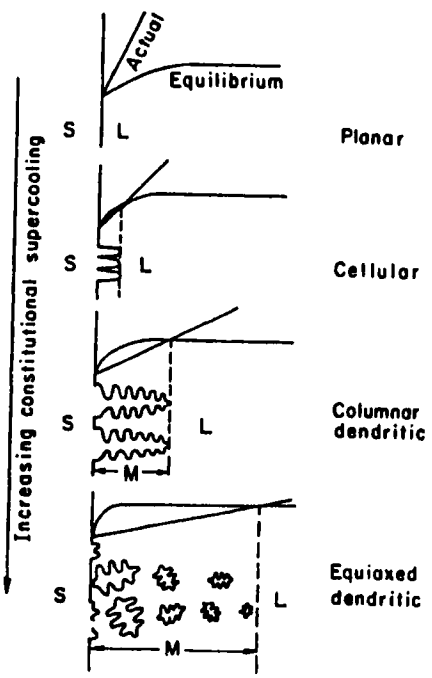


Figure 13.27 Various solidification growth modes as a function of the relative degree of constitutional supercooling, showing interface morphology during solidification of an alloy. L, S, and M denote solid, liquid, and mushy (mixed) zones. (From *Welding Metallurgy* by S. Kou, published in 1987 by and used with permission of John Wiley & Sons, Inc., New York.)

emanates from a grain in the substrate by epitaxial growth, each individual cell deviating very slightly in crystallographic orientation from adjacent cells. From one cluster of cells to another, emanating from another substrate grain, crystallographic orientation can vary significantly. Grain boundaries in the substrate propagate into the weld as a result of epitaxial growth, with some alteration as the result of competitive growth.

As the actual temperature gradient in the liquid becomes still less steep (less positive), cells in the cellular mode first become thicker or wider, then begin to develop secondary branches or arms. At some point, the structure appears columnar, and the mode of growth is referred to as *columnar dendritic*. Once this mode is fully developed, individual columnar dendrites emanate from each substrate grain by epitaxial growth.

Finally, for some very shallow, positive, actual temperature gradients, constitutional supercooling exists for a considerable distance ahead of the advancing solid–liquid interface, and new grains nucleate homogeneously. The resulting growth mode is called *equiaxed dendritic*, and is fully analogous to the same mode observed in pure metals.

Some researchers refer to a fifth mode between the cellular and columnar dendritic mode, in which the cells have just begun to develop secondary branches or dendrite arms. They refer to this mode as *cellular dendritic*. Whether this is a distinct mode or not is moot. Transition from cellular growth to columnar dendritic growth is likely a continuous process, and so distinguishing one mode from another becomes largely a relative matter.

The term *substructure* is often used in reference to the solidification structure of fusion welds. The reason becomes clear after seeing what kinds of growth modes can develop as a result of constitutional supercooling. Clearly, cellular growth involves substructure, with a cluster of like-oriented parallel cells emanating from a single substrate grain or heterogeneous nucleation site. The same can be said about cellular dendritic growth, and, possibly, columnar dendritic growth, at least until the columnar dendrites grow so thick that there is only one for each substrate grain from which they grew epitaxially.

To avoid constitutional supercooling, and, therefore, maintain a planar solid–liquid interface, the following constitutional supercooling criterion must be met:

$$\frac{G}{R} \geqslant \frac{-m_L(C_L^* - C_S^*)}{D_L} \tag{13.63}$$

where C_L^* and C_S^* are related by the equilibrium distribution coefficient or partitioning ratio, $k_0 = C_S^*/C_L^*$. Under a steady-state solidification condition, the composition of the solid at the solid–liquid interface becomes the composition of the bulk liquid: $C_S^* = C_0$, so $C_L^* = C_0/k_0$. Thus,

$$\frac{G}{R} \geqslant \frac{-m_L C_0(1 - k_0)}{k_0 D_L} \tag{13.64}$$

Note that $[m_L C_0(1 - k_0)]/k_0$ is the equilibrium freezing range, that is, the

difference between T_L and T_S or ΔT, so

$$\frac{G}{R} \geqslant \frac{\Delta T}{D_L} \tag{13.65}$$

In general, the theory of constitutional supercooling predicts fairly closely the conditions required to initiate the breakdown of a planar interface in alloys with isotropic surface energy. No present theory can quantitatively predict the transition from the cellular to columnar dendritic or from columnar dendritic to equiaxed dendritic modes of solidification. However, the greater the degree of constitutional supercooling (i.e., the smaller the ratio of G/R), the greater the tendency for a given material to switch from the cellular to the dendritic mode of solidification. When G/R is very low, the region of constitutional supercooling is so wide that some solid nuclei form well in front of the advancing solid–liquid interface and grow into equiaxed dendrites as solidification proceeds.

Incidentally, the region in which dendrites, whether columnar or equiaxed, coexist with the liquid phase is called the mushy zone, denoted by M in Figure 13.27. Also, as was noted for microsegregation earlier, the creation of a solute gradient in the liquid and associated constitutional supercooling occurs at every solid–liquid interface, not just at the primary solidification front. It is this that gives rise to secondary, and even ternary, branch or arm formation on dendrites.

13.5.3.2. Effect of Cooling Rate on Substructure. The ratio of the temperature gradient, G, to the growth rate, R, in G/R, governs the mode of solidification. The product of these terms, GR (sometimes RG), governs the scale of the solidification structure or, even more correctly, substructure. The greater the product GR, the finer the cellular, cellular dendritic (if you like), columnar dendritic, and equiaxed dendritic structure. This is so because the product GR is equivalent to cooling rate, both having units of °C/s. (from °C/mm for G, and mm/s for R). The effect of cooling rate on dendrite arm spacing, a favorite measure of the scale of dendritic structure, is shown in Figure 13.28. During the growth of dendrites, large dendrite arms grow at the expense of smaller ones as solidification proceeds, since smaller arms have more surface area, and thus energy, per unit of volume. The slower the cooling rate during solidification, the longer the time available for this mechanism to operate, resulting in larger arm spacing. This is called the coarsening effect.

The effect of temperature gradient G and solidification rate R can be summarized in the schematic in Figure 13.29.

Work by Hunt (1979) and Flemings (1974) has shown that the functional dependence of the spacing of primary dendrite arms, d_1, and of secondary dendrite arms, d_2, on G and R are likely different, and given by

$$d_1 = a_1(G^2R)^{-1/4} \tag{13.66}$$

$$d_2 = a_2(GR)^{-n} \tag{13.67}$$

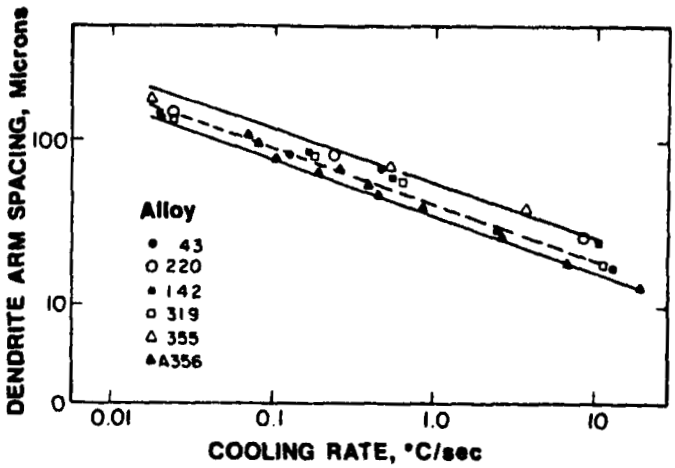


Figure 13.28 Effect of cooling rate on dendrite arm spacing in commercial aluminum alloys. (After R. E. Spear and G. R. Gardner, *Transactions of the American Foundryman Society*, **71**, 209, 1963, with permission of the American Foundryman Society, Inc., Des Plaines, IL.)

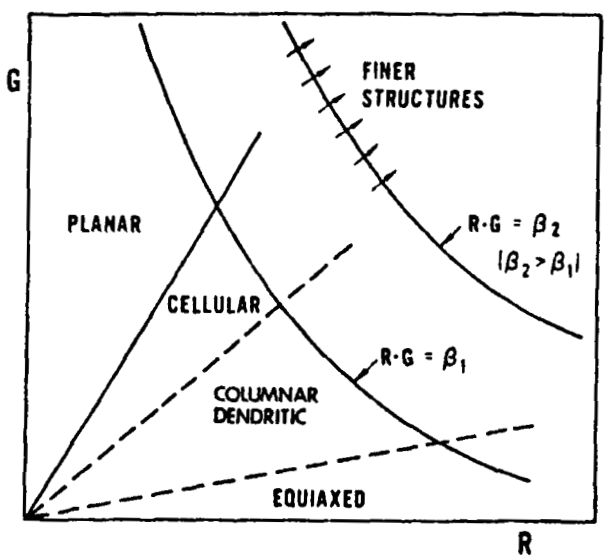


Figure 13.29 Schematic growth rate (R) vs. temperature gradient (G) map showing transitions in solidification growth mode as well as the refining effect of high cooling rates. (From *New Trends in Materials Processing* by A. F. Giamei, E. H. Kraft, and F. D. Lemkey, published by and used with permission of the ASM International, Materials Park, OH.)

where a_1 and a_2 are coefficients where values depend on the alloy system, and $n = \frac{1}{3}$ to $\frac{1}{2}$. Other work on dendrite arm spacing is nicely reviewed by David and Vitek (1989), along with much more relating to the effect of solidification parameters on weld microstructure.

13.5.3.3. Interface Stability. In their original experimental study of the breakdown of a planar solid–liquid interface into cellular undulations during the unidirectional solidification of a dilute binary alloy, Rutter and Chalmers (1953) proposed a criterion that predicted instability of the planar interface whenever growth conditions produced an adjacent layer of constitutionally supercooled liquid. The conditions under which constitutional supercooling occurs were subsequently made quantitative by Tiller et al. (1953). This quantitative criterion successfully predicted the dependence of breakdown in several experiments based on growth rate and the temperature gradient in the liquid. However, the theoretical status of this criterion remains uncertain, since it was premised on equilibrium arguments. Mullins and Sekerka (1964) tackled this shortcoming by developing a rigorous theory of the stability of a planar interface by calculating the time dependence of the amplitude of a sinusoidal perturbation[16] of infinitesimal initial amplitude into the plane. The interface is deemed unstable if any sinusoidal perturbation grows and stable if none grow.

As before for case 2 and case 3, and constitutional supercooling arising as part of case 3, analysis assumed isotropy of bulk and surface properties and local microscopic equilibrium at the interface, which is reasonable. The critical mathematical simplification is the use of steady-state values for the thermal and diffusion fields, which is valid provided the interface moves at constant velocity or, in other words, welding is done at a truly constant velocity.

Interface stability theory differs in two main respects from the theory of constitutional supercooling. First, stability theory yields an interface stability criterion based on the dynamics (e.g., heat flow in the solid, latent heat of fusion associated with solidification) of the entire system (liquid and solid), not just on the thermodynamics of the liquid. The theory of constitutional supercooling deals with which state, solid or liquid, is thermodynamically favorable in the region of the liquid ahead of the moving solid–liquid interface, while the real question is what state is dynamically achievable. Second, stability theory provides a description of the time evolution of a perturbed interface and the accompanying temperature and concentration fields, which is valid as long as the perturbation and its effects remain sufficiently small to be described by a linear theory.

By assuming the solidification of a dilute binary alloy at constant velocity or growth rate R with a macroscopically planar front separating solid and liquid, as shown in Figure 13.30, and taking a coordinate system that moves

[16] A sinusoidal perturbation was assumed because it simplifies the mathematics by permitting the decomposition of any perturbation into a collection of juxtaposing sinusoidal waves using Fourier analysis, and since all relevant equations turn out to be linear.

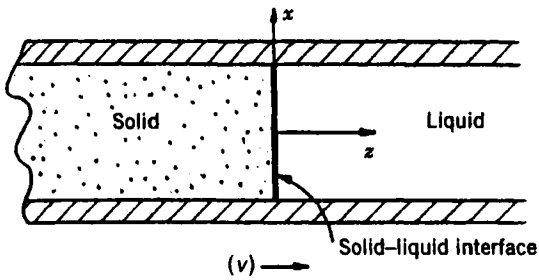


Figure 13.30 Schematic representing unidirectional solidification at constant velocity (v) or growth rate (R) for a planar solid–liquid interface. The xz coordinate system moves at constant velocity v or R so that the plane $z = 0$ is always at the unperturbed interface. (From "Morphological stability" by R. F. Sekerka, 1968, *Journal of Crystal Growth*, 3(4), 71–81, 1968, with kind permission of Elsevier Science-NL, Sara Burgerhartstraat 25, 1055 KV Amsterdam, The Netherlands.)

with the interface such that the z axis is along the direction of growth and the plane at $z = 0$ is the unperturbed interface, the concentration and temperature fields are given by

$$C^0(z) = \frac{G_c D}{R}\left[1 - \exp\left(-\frac{R_z}{D}\right)\right] + C_0 \qquad \text{in the liquid} \qquad (13.68a)$$

$$T^0(z) = \frac{GD_{th}}{R}\left[1 - \exp\left(-\frac{R_z}{D_{th}}\right)\right] + T_0 \qquad \text{in the liquid} \qquad (13.68b)$$

$$T'^0(z) = \frac{G_S D'_{th}}{R}\left[1 - \exp\left(-\frac{R_z}{D'_{th}}\right)\right] + T_0 \qquad \text{in the solid} \qquad (13.68c)$$

with

$$T_0 = T_M - m_L C_0 \qquad (13.69a)$$

$$C_\infty = k_0 C_0 = \frac{G_C D}{R} + C_0 \qquad (13.69b)$$

and

$$R = \frac{1}{L}(K_S G_S - K_L G_L) = \frac{K}{L}(\mathscr{G}' - \mathscr{G})$$

$$= \frac{D}{C_0(k_0 - 1)} G_L = \frac{Dk_0}{C_\infty(k_0 - 1)} G_C \qquad (13.69c)$$

where R is the growth velocity; G_L and G_S are the average temperature gradients in the liquid and solid at the interface; G_C is the average composition gradient in the liquid at the interface; k_0 is the equilibrium distribution

coefficient; K_L and K_S are the thermal conductivity of the liquid and solid; K is the average thermal conductivity given by $K = \frac{1}{2}(K_L + K_S)$; T_M is the absolute melting point of the pure solvent; L is the latent heat of fusion per unit volume of solid; C_0 is the nominal alloy composition; C_∞ is the concentration of solute in the liquid far from the interface; m_L is the slope of the liquidus line on the appropriate phase diagram; D_{th} and D'_{th} are the thermal diffusivity of the liquid and solid; D is the solute diffusivity in the liquid; and $\mathcal{G}$ is the weighted gradient in the liquid at the interface ($= G_L[K_L/\bar{K}]$), while $\mathcal{G}'$ is the weighted gradient in the solid at the interface ($= G_S[K_S/\bar{K}]$).

Plots of Eqs. 13.68a–c are shown in Figure 13.31 for the case where $k_0 < 1$. Since D_{th}/D is typically 10^4 for real systems, the temperature plot shows only very little curvature. Equations 13.69a–c arise from satisfying the interface boundary conditions.

The theory proceeds by assuming that Eqs. 13.68 and 13.69 describe the system, and then calculates the response of the system to small perturbations, either of the shape, as was done by Mullins and Sekerka (1964), the concentration field, as was done by Delves (1966), or, in fact, not admitting to any specific perturbation, just dealing with the homogeneous problem, as was done by Voronkov (1965). The result is essentially the same. It does not matter what triggers instability; a particular perturbation is only an artifact used to get the calculation started in the analysis.

The task from here is to solve the perturbed problem and determine if the perturbation decays or is enhanced in time. The detailed mathematics are involved, although not overwhelming in complexity, but are, in any case, beyond the scope of this book. Thus, these details are left to the interested

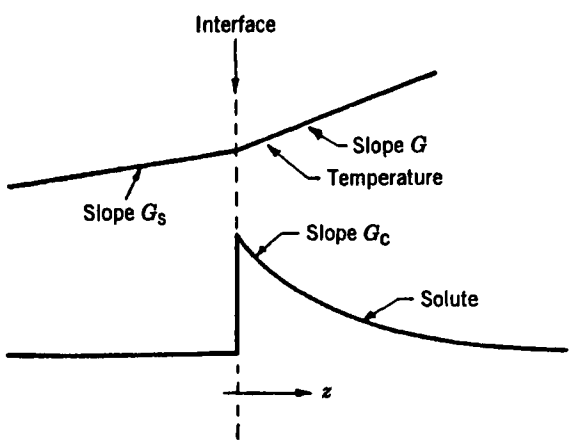


Figure 13.31 Temperature and solute profiles as a function of distance z from the solid–liquid interface. (From "Morphological stability" by R. F. Sekerka, *Journal of Crystal Growth*, 3(4), 71–81, 1968, with kind permission of Elsevier Science-NL, Sara Burgerhartstraat 25, 1055 KV Amsterdam, The Netherlands.)

reader to pursue in the original references given at the end of the chapter, most notably that by Sekerka in the *Journal of the Physical Chemistry of Solids* (1967). Suffice to say here, the interface stability theory predicts that the original planar interface shape, when perturbed by an infinitesimal sinusoidal wave, evolves in time as:

$$\Phi(x, t) = \frac{1}{2}\pi \int_{-\infty}^{+\infty} e^{i\omega x}\Phi_0\omega e^{tf\omega}d\omega \tag{13.70}$$

where $\omega = 2\pi/\lambda$, the spatial frequency of the sinusoidal perturbation, with λ the wavelength of the sinusoidal perturbation. Analysis of $f(\omega)$ gives a stability criterion and the detailed time evolution of the interface shape.

Sketches of $f(\omega)$ versus ω are shown in Figure 13.32. *For stability, $f(\omega)$ must never be positive for any value of ω. The condition for this to occur leads to the following criterion for instability:*

$$\frac{1}{2}\frac{\mathscr{G}' - \mathscr{G}}{m_L G_C} < \mathscr{S} \tag{13.71}$$

the so-called stability function shown in Figure 13.33, and having values between 0 and 1. $\mathscr{S}$ is itself a function of the equilibrium distribution coefficient k_0 and the parameter A, given by

$$A = \frac{k_0^2}{1 - k_0}\frac{\Gamma R}{D}\frac{T_M}{-m_L C_\infty} \tag{13.72}$$

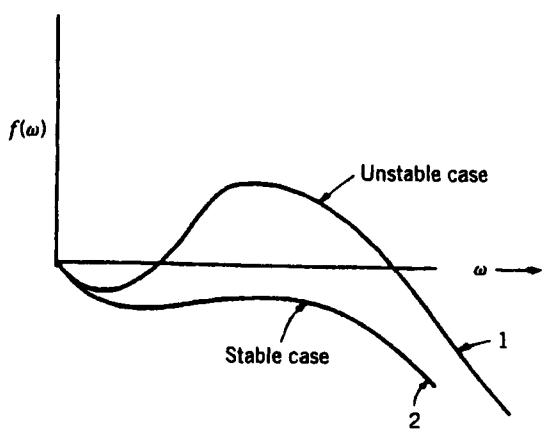


Figure 13.32 Sketches of $f(\omega)$ versus ω for an unstable case (curve 1) and a stable case (curve 2). (From "Morphological stability" by R. F. Sekerka, *Journal of Crystal Growth*, 3(4), 71–81, 1968, with kind permission of Elsevier Science-NL, Sara Burgerhartstraat 25, 1055 KV Amsterdam, The Netherlands.)

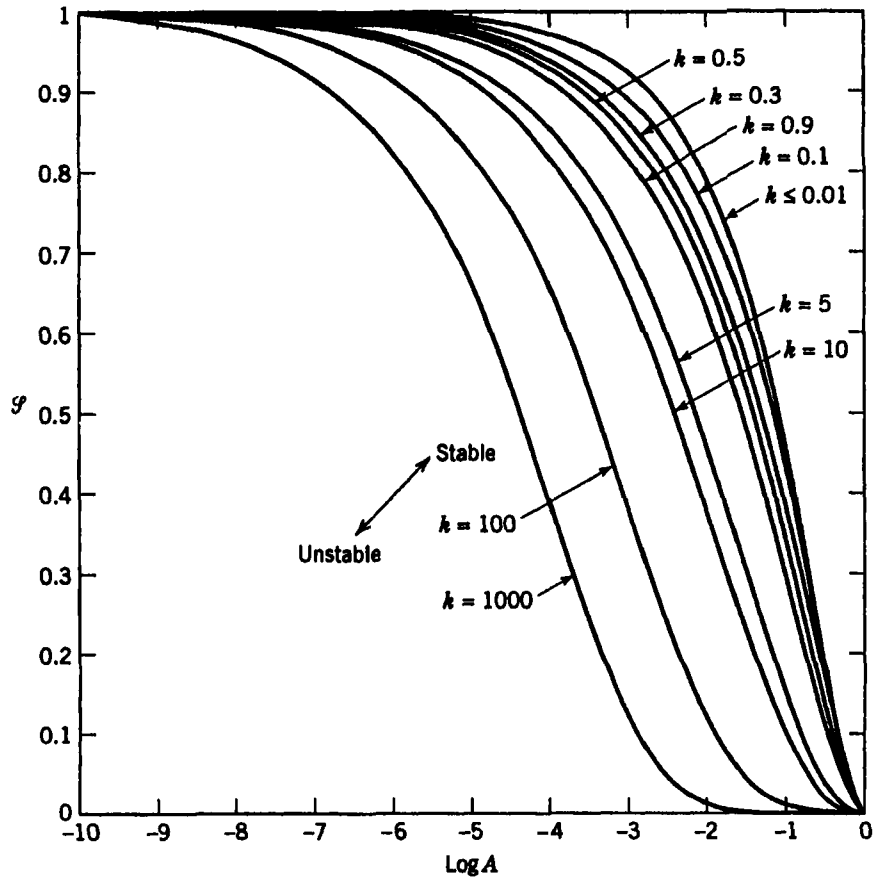


Figure 13.33 Plot of the stability function $\mathscr{S}$ versus log A for several values of k_0. The difference between $\mathscr{S}$ and i represents the tendency of solid–liquid surface tension to stabilize the interface shape. (From "Morphological stability" by R. F. Sekerka, *Journal of Crystal Growth*, 3(4), 71–81, 1968, with kind permission of Elsevier Science-NL, Sara Burgerhartstraat 25, 1055 KV Amsterdam, The Netherlands.)

where $\Gamma = \gamma/L$, the length associated with capillarity, where γ is the solid–liquid surface free energy, and all other terms are as before. Parameter A varies linearly with the solid–liquid surface free energy (or surface tension) through Γ and is typically 10^{-3} or less. Hence, $\mathscr{S}$ is typically 0.8 to 0.9, whereas for negligibly small solid–liquid surface free energy, $\mathscr{S} = 1$. The difference of $\mathscr{S}$ from unity therefore represents the expected tendency of the surface free energy to stabilize the interface. Imagine tension forces pulling in opposite directions within the plane of the interface, which would tend to keep it planar.

Besides the effect of surface tension above, the instability criterion from Eq. 13.72 differs from the theory of constitutional supercooling in other areas as well. First, G in the theory of constitutional supercooling is effectively replaced

by

$$\frac{1}{2}(\mathscr{G}' + \mathscr{G}) = \frac{K_S G_S + K_L G_L}{K_S + K_L} \tag{13.73}$$

which is a weighted average of thermal conductivity that can have values quite different than G. Depending on the material system, the gradient in the solid can dominate stability considerations. No effect from the solid was considered in the theory of constitutional supercooling. Finally, there is a contribution from surface diffusion, or really interface diffusion, in stability theory not considered in constitutional supercooling theory.

Further studies have attempted to extend the work of Mullins and Sekerka (1964) from a planar interface to an interface with other shapes, including spheres, cylinders, and paraboloids of revolution that closely approximate real needle crystals.

The predictions of stability theory have been borne out by experiment, albeit not many. Some examples include those of Seidensticker and Hamilton (1963), Williamson and Chalmers (1967), and Townsend and Kirkaldy (1968). The best confirmation has been from elegant experiments by Hardy and Coriell (1968).

At high solidification rates, rigorous analyses have shown that an absolute stability limit (i.e., maximum rate) exists beyond which a planar front is again stable, which is unexplainable by the theory of constitutional supercooling. At high growth rate R, the characteristic diffusion length is short (as there is not much time available). Thus, for any perturbation to be stable, its size would have to be smaller than the diffusion length so that variation in composition, and corresponding variation in liquidus temperature, can be used to promote any constitutional supercooling at the solidification front. But for perturbations with small wavelengths, the influence of surface effects would dominate and such small perturbations would require too much surface energy. Thus, a planar front would be stable once again.

For most purposes, the conceptually far simpler theory of constitutional supercooling suffices. It predicts planar breakdown for most cases with sufficient accuracy. However, there are those cases that this simpler theory does not explain. This point was made clear to the author when unexpected changes in the mode of solidification were observed in type 347, Nb-stabilized austenitic stainless steel. While studying the effects of Nb, C, and N, as well as residual S and P on solidification and liquation cracking in the heat-affected zone, a change in growth mode was observed for a change in S from around 0.030 to below 0.010 wt %. Since weldment geometry, process operating parameters, and heat chemistries were virtually identical otherwise, this change in growth mode can only be explained based on the effect of S on surface tension, which is well known in austenitic stainless steels in other work on convection (for example, Messler and Li, 1998, to be published).

13.5.3.4. Nucleation of New Grains Within the Fusion Zone. Knowing that equiaxed dendrites are the result of homogeneous as opposed to heterogeneous nucleation makes it hard to believe they can ever occur in welds, no less appear with any frequency. Yet, the growth of columnar dendrites is fairly frequently interrupted by the formation of new, equiaxed grains. In fact, much of the time, what appears to be equiaxed dendritic growth in a weld is likely the result of some other mechanism. Several possible mechanisms for the formation of new, equiaxed grains in the fusion zone of welds have been suggested.

Dendrite fragmentation presumes that the fine, fragile tips of cellular or columnar dendrites are broken off by convective flow in the weld pool, and these serve as heterogeneous nuclei for growth of equiaxed dendrites. Three possible ways in which convection could break off fragile tips are (1) remelting (or recalescence) as hot liquid, above the liquidus temperature for the dendrites, sweeps by; (2) friction forces from fluid flow; and (3) impact by particles of solid contaminant entrained in the convective flow.

Grain detachment presumes that convective flow causes partially melted grains in the substrate to melt out as superheated liquid sweeps by. These detached grains then act as sites for heterogeneous nucleation of equiaxed dendrites.

Outright *heterogeneous nucleation* can lead to growth of new, equiaxed grains from foreign solid particles in the weld pool. Such particles could be detached pieces of tungsten from a GTAW torch, small particles of unmelted flux from an SMAW or FCAW electrode or in SAW, or particles of dust or debris found at many welding sites.

Finally, preferential cooling at the surface of a weld pool, by convection currents of air or impinging shielding gas, could lead to *surface nucleation* of new grains homogeneously.

These various mechanisms for formation of new, equiaxed grains are shown schematically in Figure 13.34.

13.5.3.5. Controlling Substructure. Formation of fine structure or substructure in the fusion zone of a weld offers two major advantages: (1) reduced susceptibility to solidification cracking (as will become clear in the next section) and (2) improved mechanical properties (especially ductility and toughness) based on the Hall–Petch relationship that strength increases inversely proportional to the square root of the average grain diameter. Techniques for refining the structure or substructure of welds include the following, largely based on what was just described in the previous subsection.

Weld pool stirring, using arc oscillation (David and Liu, 1982; Scarborough and Burgan, 1984), arc current pulsation (Slavin, 1974) or applied magnetic fields (Jayarajan and Jackson, 1972), or weld vibration, using mechanical shaking or ultrasonic excitation (Brown et al., 1962), results in what is known as dynamic grain refining. The way stirring helps is to either fragment dendrites or detach grains (see Section 13.5.3.4). Related to this is the controlled

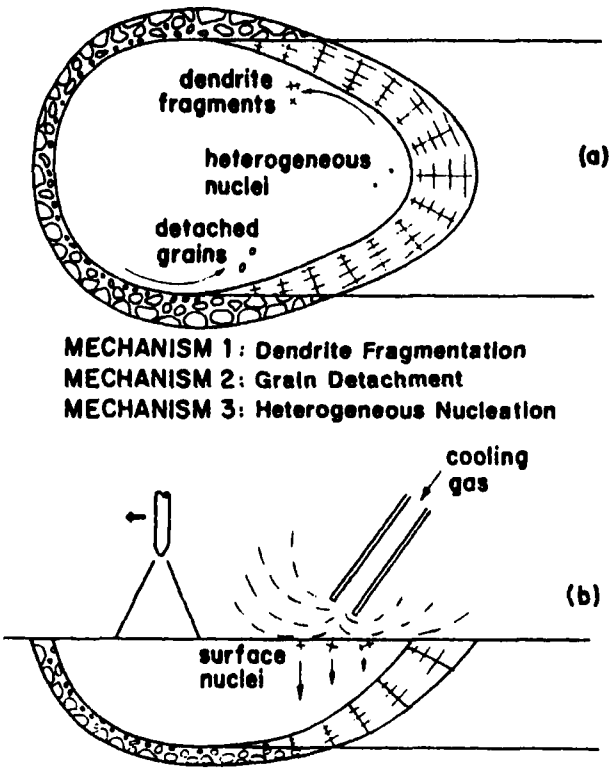


Figure 13.34 Schematic illustrating the various mechanisms that could lead to the formation of new, equiaxed grains in a weld fusion zone: (a) top and (b) side views. (From "Improving weld quality by low frequency arc oscillation" by S. Kou and Y. Le, *Welding Journal*, **64**(3), 51–55, 1985, published by and used with permission of the American Welding Society, Miami, FL.)

alteration of grain growth direction by altering weld pool shape through arc oscillation. Surface nucleation can be promoted by employing forced undercooling of the surface liquid using a jet of cooling gas (preferably inert), thereby refining substructure. Finally, while seemingly a bit far-fetched, nucleation agents can be added to the weld pool by what is known as 'inoculation' (Davies and Garland, 1975; Pearce and Kerr, 1981; Heintz and McPherson, 1986). When this is done, the inoculates are in particulate (or powdered) form.

The relationship between the solidification or growth rate R and the welding speed v gives another clue on how to refine weld structure or substructure. This relationship is

$$R = \frac{v \cos\phi}{\cos(\phi - \psi)} \tag{13.74}$$

where ϕ is the angle between the welding direction and the normal to the weld pool boundary (taken to be the direction of the maximum temperature gradient), and ψ is the angle between the welding direction and the actual solidification growth direction, as shown in Figure 13.35. Since $\phi = 0$ and 90° at the weld centerline and the fusion line, respectively, the solidification rate R is greatest at the weld centerline and lowest at the fusion line. Because of the elongated shape of moving weld pools, the distance between the heat source and the pool boundary is greater at the centerline than at the fusion line. Therefore, the temperature gradient G is smallest at the weld centerline and greatest at the fusion line.

From the preceding, G/R is greatest at the fusion line and decreases toward the weld centerline. Weld subgrain structure (another common term for substructure) changes from planar to cellular and then to columnar dendritic as the degree of constitutional supercooling in the weld increases, and can vary significantly from the fusion zone boundary to the centerline of the weld. Thus, growth mode changes from planar to cellular, and even columnar dendritic. In fact, rarely is planar growth observed in real welds made in alloys, except for the highest energy-density processes, EBW and LBW. Figure 13.36 schematically illustrates the effect of the degree of constitutional supercooling on weld subgrain structure.

Just as the solidification mode can vary across a weld, so too can cell spacing vary. Where the cooling rate through the solidification range is higher, the fineness of the substructure is greater. Figure 13.37 shows where cooling rate is higher for typical weld thermal cycles.

As shown in Table 13.6, at a particular, constant welding speed (say, 2 inches/min or 1 mm/s), the weld subgrain structure changes from cellular to

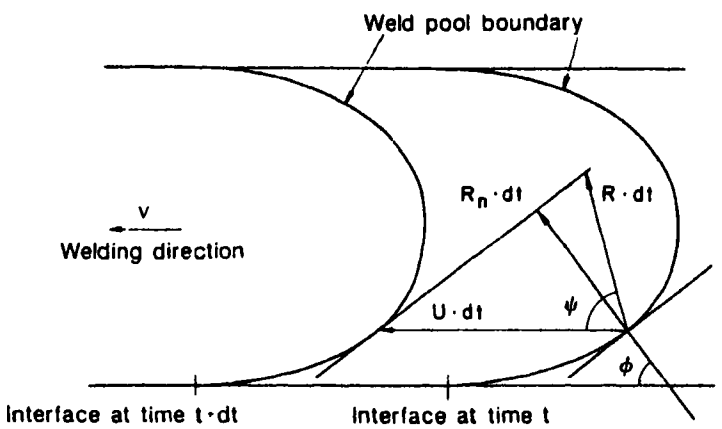


Figure 13.35 Relationship between welding velocity (v) and actual solidification growth rate. (After Nakagawa et al., 1970, from *Welding Metallurgy* by S. Kou, published in 1987 by and used with permission of John Wiley & Sons, Inc., New York.)

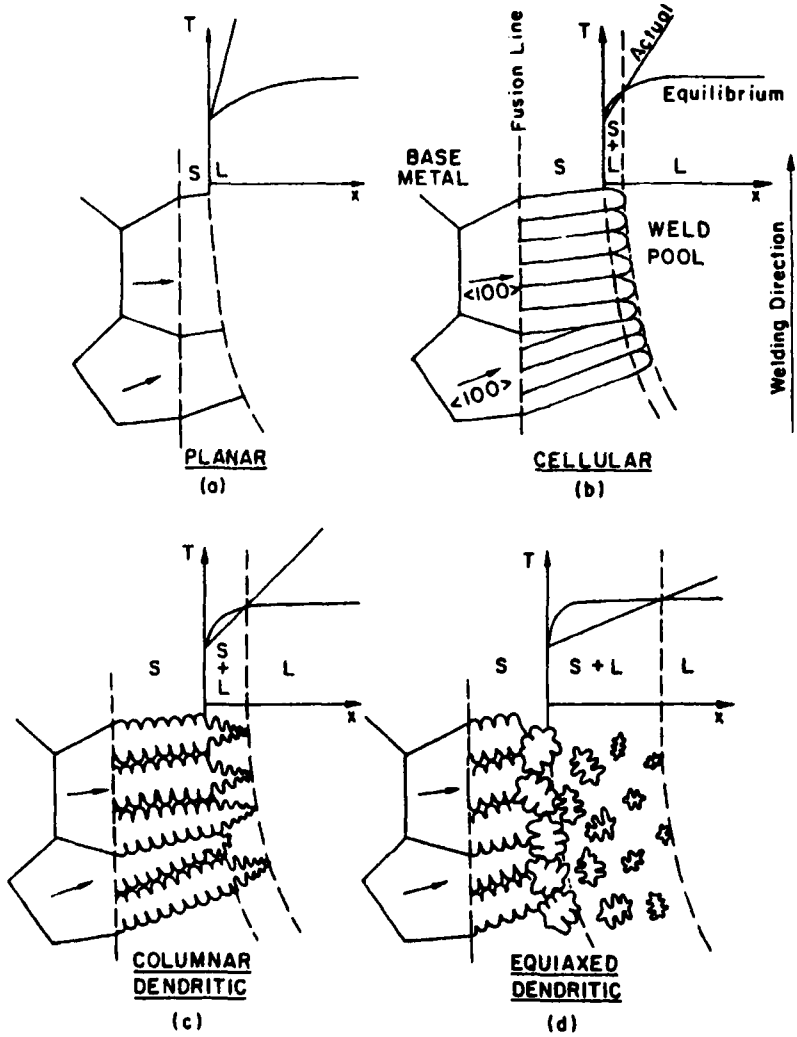


Figure 13.36 Schematic illustrating the effect of constitutional supercooling on weld subgrain structure, the degree of supercooling increasing from (a) to (d). Arrows in grains in the base material indicate the easy-growth direction, say ⟨100⟩ in fcc or bcc metals or alloys. (From *Welding Metallurgy* by S. Kou, published in 1987 by and used with permission of John Wiley & Sons, Inc., New York.)

dendritic when the welding current is increased (from 150 to 450 A). For constant weld velocity (v), the higher the heat input (Q), the lower the temperature gradient G, and, hence, the lower the G/R ratio. Therefore, at high welding heat inputs, the G/R ratio is low and dendritic growth prevails. At low heat inputs, the G/R ratio is high and cellular growth prevails. The effect of

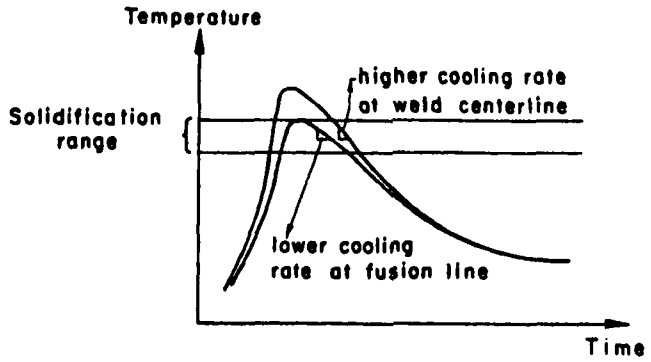


Figure 13.37 Schematic showing typical thermal cycles at the weld centerline and at the weld fusion line. (From *Welding Metallurgy* by S. Kou, published in 1987 by and used with permission of John Wiley & Sons, Inc., New York.)

heat input may, at first, seem counterintuitive, but a little thought helps. Long, slow delivery of energy (i.e., high heat input) heats material surrounding the weld more, so that the temperature gradient between the weld and the surrounding base metal is actually low.

At a constant welding current (say 150 A), the substructure becomes finer as the welding speed increases. Under the same heat input (Q), the cooling rate and growth rate R increases with increasing welding velocity (v). With higher heat inputs per unit length of weld, the subgrain structure becomes more coarse.

Once again, finer subgrain structure is normally advantageous because it results in (1) higher yield strength (from the Hall–Petch relationship), (2)

TABLE 13.6 Effect of Current and Travel Speed on the Growth Mode of HY-80 Steel Welds

	Current		
Travel Speed	150 A	300 A	450 A
2 ipm	Cellular	Cellular dendritic	Coarse cellular dendritic
4 ipm	Cellular	Fine cellular dendritic	Coarse cellular dendritic
8 ipm	Fine cellular	Cellular slight undercutting	Severe undercutting
16 ipm	Very fine cellular	Cellular undercutting	Severe undercutting

Source: After Savage et al., 1968, from *Welding Metallurgy* by S. Kou, published in 1987 by and reprinted with permission of John Wiley & Sons, Inc., New York.

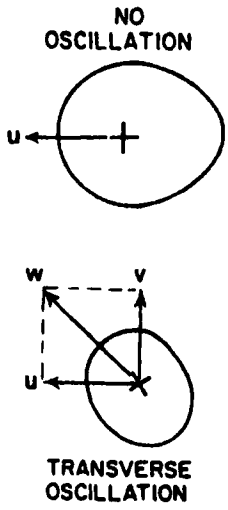


Figure 13.38 Schematic showing how transverse arc oscillation results in a higher resolved welding speed and, thus, finer subgrain structure. (From "Improving weld quality by low frequency arc oscillation" by S. Kou and Y. Le, *Welding Journal*, **64**(3), 51–55, 1985, published by and with permission of the American Welding Society, Miami, FL.)

higher ductility, and (3) reduced tendency to solidification cracking (owing to greater dilution of crack-causing residual elements in greater grain or subgrain boundary area, as seen in Section 13.6). The predominant technique for refining subgrain structure is by increasing the welding speed or velocity. Transverse arc oscillation also helps, because it results in a higher resolved speed, as shown in Figure 13.38.

13.5.4. Centerline Segregation

The final observation made of real welds is that they frequently suffer from micro- (albeit fairly pronounced) segregation along their centerlines. Such segregation is, in fact, also predicted or explained by nonequilibrium solidification under the conditions of case 3, that is, no mixing in the liquid in the weld pool. The explanation for centerline segregation is given in Section 13.5.4 and shown in Figure 13.23, step F.

13.6. FUSION ZONE HOT CRACKING

Solidification cracking, which is observed frequently in castings and ingots, can also occur in fusion welds. Such cracking can be characterized as follows: (1) It is intergranular, that is, occurs along grain and subgrain boundaries; (2) it

occurs at the terminal stages of solidification when the shrinkage-induced stresses from both weld metal solidification and nonuniform thermal contraction become the highest; and (3) severity increases with both the degree of constraint on the weld and thickness of the weldment.

13.6.1. Mechanism of Hot Cracking

The accepted theory of solidification cracking in welds as well as castings is that a coherent, interlocking solid network separated by essentially continuous thin liquid films is ruptured by tensile stresses arising from thermal contraction. If sufficient liquid metal is present near the cracks when they form, they can backfill or heal. If not, the cracks appear as open tears. For this reason, solidification cracks are also called hot tears, or, most commonly, hot cracks.

The terminal stage of solidification refers to the point at which the fraction of solid is close to 1.0, rather than the point at which the temperature nears the lower limit of the freezing range for an alloy. In some alloys, depending on the nature of their fraction solid–temperature relationship, the fraction of solid can be close to 1.0 and an essentially complete solid network can form, just below the liquidus temperature (e.g., some carbon steels and some stainless steels).

Several factors favor solidification cracking, some of which are metallurgical in origin and some of which are mechanical in origin. Metallurgical factors that aggravate solidification cracking susceptibility include: (1) freezing temperature range, (2) presence of low-melting eutectics, (3) grain or subgrain structure in the fusion zone, and (4) surface tension of the grain boundary liquid. Mechanical factors that aggravate solidification cracking are (1) contraction stresses and (2) degree of restraint. Let's look at each of these factors.

In general, the wider the freezing range for an alloy, the larger or wider the mushy zone and the larger the area that is weak and susceptible to weld solidification cracking. The freezing range of an alloy can be increased either by intentional additions (e.g., Cu, Mg, or Zn in Al) or by the presence of undesirable impurities (e.g., S and P in steels or Ni-based alloys). In fact, different amounts of an intentional or unintentional solute can have different effects. For example, in aluminum alloys, sensitivity to solidification cracking is greatest at intermediate levels of common solutes (as shown in Figure 13.39). This is because, at very low levels, there is very little effect on the freezing range and little or no tendency to form cracks, since pure aluminum is resistant to cracking. At much higher levels, there is such a large effect and so much liquid is present that any cracks that form are backfilled. In between is the worst case: enough eutectic liquid to form a continuous film at grain boundaries and render the alloy crack susceptible, but not enough to backfill incipient cracks.

The effect of impurities, such as S or P in steels, is to widen the freezing range considerably, but without producing large volumes of liquid to permit backfilling. Such residuals tend to segregate to grain boundaries, where diffusion rates are almost always higher due to the more open nature of lattice

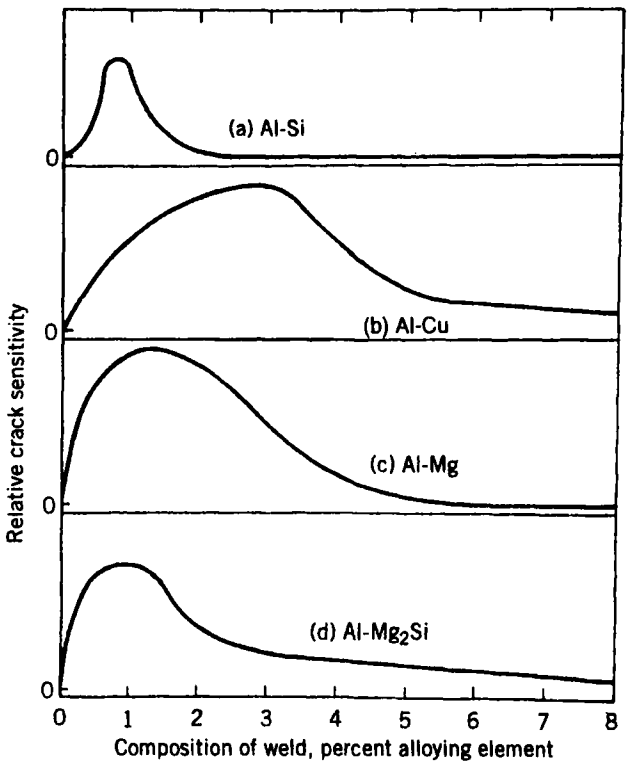


Figure 13.39 Susceptibility of some aluminum alloys to solidification cracking as a function of major solute content. (From "Preventing weld cracks in high-strength aluminum alloys" by J. H. Dudas and F. R. Collins, *Welding Journal*, **45**(6), 241s–249s, 1966, published by and with permission from the American Welding Society, Miami, FL.)

structure in these areas, and form low-melting compounds that lead to cracking. In plain carbon steels, for example, FeS films would form and lead to severe cracking if not for intentional additions of Mn leading to preferential formation of harmless globules of MnS. For this reason, Mn/S ratio is carefully controlled in steels.

Coarse columnar grains are more susceptible to solidification cracking than fine equiaxed grains for several reasons. First, fine, equiaxed grains can better deform to accommodate contraction stresses, relieving stress across interdendritic boundaries. Second, liquid can be more effectively fed to incipient cracks to promote healing in fine-grained materials, where grain boundaries run in all directions. And, third, when the grain boundary area is greater, the concentration of potentially harmful low-melting-point segregates is reduced, hopefully to below the threshold that causes cracking. Besides these effects, head-on impingement of columnar dendrites growing from opposite sides of a weld can

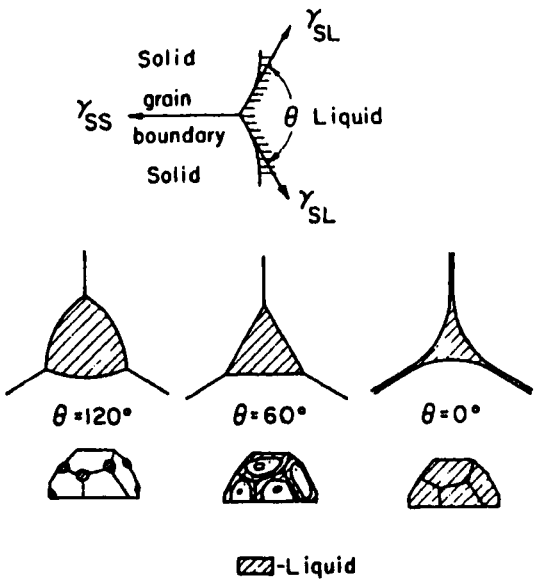


Figure 13.40 Relationship between the surface tension of a liquid, the dihedral angle, and the distribution of the liquid in grain boundaries. (From "Grains, phases, and interfaces: an interpretation of microstructure" by C. S. Smith, *Transactions of the AIME*, **175**, 15–51, 1948, published by and with permission from the AIME, Warrensdale, PA.)

lead to sever centerline segregation through a plowing effect. This is a particular problem in austenitic stainless steels.

It is not just the presence and amount of a low-melting-point phase or segregate that leads to solidification hot cracking, it is also the surface tension of this liquid. If the surface tension between the solid grain and the grain boundary liquid is very low, a thin liquid film forms by wetting the grain boundaries. For this situation, susceptibility to cracking is very great. If, on the other hand, the surface tension of the liquid is high, it will tend to ball up to form globules and will not coat the grain boundaries with a continuous film. This greatly reduces the susceptibility to cracking. The effects of different surface tensions on liquid wetting and distribution is shown in Figure 13.40.

From a mechanical standpoint, stress, particularly tensile stress, is all important. Without a tensile stress acting, no cracking would occur. There are two internal sources of tensile stresses in fusion welding: (1) shrinkage as liquid transforms to solid, and (2) contraction due to the thermal coefficient of expansion. Both sources were described in detail in Section 7.1. As a result of both of these, aluminum alloys exhibit more incidents of solidification cracking than mild steels.

The other major mechanical factor contributing to solidification cracking is the degree of restraint of the weld while it is solidifying. Suffice to say, for the same joint design and material, the greater the degree of restraint of the workpiece by fixturing or other structure in the weld assembly, or the weld from material thickness or mass, the more likely that solidification cracking will occur.

13.6.2. Remediation of Hot Cracking

Solidification cracking can be minimized by knowing where it comes from and by doing whatever can be done to remediate these sources. There are three basic approaches: (1) control the composition of the weld metal, (2) control the solidification structure, and (3) weld under favorable conditions. Let's look at each approach.

13.6.2.1. Control of Weld Metal Composition. In autogenous welding, where no filler is used, weld metal composition is determined by the composition of the base metal, and to a much lesser extent, the composition of the shielding atmosphere (which would affect the extent of oxidation, and thus loss, of certain alloying elements). To effectively avoid or reduce solidification cracking in autogenous welds, avoid base metal compositions that are prone to cracking.

When filler metals are used, the weld composition is essentially controlled by the composition of the base metal, the composition of the filler metal, and the dilution ratio, and can be affected to a lesser extent by the composition of shielding flux or gas. The dilution ratio is the amount of base metal melted and dissolved to the total amount of metal in the fusion zone (see Section 12.1). Dilution ratio can vary significantly from one type of joint to another, so joint design, as well as welding process and procedure, must be carefully selected. If dilution by base metal will almost certainly lead to cracking, the use of "buttering" layers is recommended (see Section 12.1). For example, layers of nickel or austenitic stainless steel are often used in high (>1.0%) C steels or cast irons to prevent pick up of unacceptable levels of C in the weld metal.

Filler metal composition, flux or shielding gas, process, operating parameters, and welding procedures, including prevention of dilution, must all be carefully considered and selected to control weld metal composition to minimize solidification cracking. Some examples of what to watch for include

- Cu in Al alloys to control freezing range and amount of eutectic liquid
- Residual element contents, such as S and P in steels or Ni-based alloys
- Mn content in steels to control the distribution of low-melting segregates such as FeS
- Alloy content to control fusion zone structure, such as keeping 5–10% δ-ferrite in austenitic stainless steels (see Chapter 14)
- Controlling C level in steels, keeping it low to avoid martensite formation.

13.6.2.2. Control of Solidification Structure. Another way to reduce the incidence of solidification cracking is to control the solidification structure, in terms of both mode or morphology through G/R ratio and scale or coarseness through GR product. Almost without exception, control of structure means attempting to minimize grain size. By reducing grain size, any potentially detrimental microsegregation and/or low-melting phase or constituent is spread across more grain boundary area. This might reduce the level of segregate to below the threshold that will cause a continuous liquid film to form, thereby preventing cracking. Some specific techniques that might be considered are

- Selecting the appropriate process, favoring those providing low linear heat input, for example, high-energy-density processes like PAW, LBW, or EBW
- Adding grain refining agents, such as, Ti or Zr, to Al-alloys (Davies and Garland, 1975; Pearce and Kerr, 1981; Heintz and McPherson, 1986)
- Vibrating or stirring the weld pool during solidification, causing dendrite fragmentation (Brown et al., 1962; Jayarajan and Jackson, 1972; Slavin, 1974)
- Employing transverse arc oscillation to increase the resolved welding velocity and, thus, growth rate (David and Liu, 1982; Scarborough and Burgan, 1984).

13.6.2.3. Use of Favorable Welding Conditions. Last, but by no means least, solidification cracking can be avoided by using favorable welding conditions. These include the following:

- Employing high-intensity, high-energy density, low heat input processes (such as PAW, LBW, or EBW)
- Minimizing restraint
- Preheating to reduce stress and cooling rates for materials that form inherently brittle phases or constituents athermally
- Controlling weld profile and bead shape

This last point, controlling weld profile and bead shape, deserves some further discussion.

Concave, single-pass fillet welds solidify to produce surface under tension, so cracks tend to form, whereas fillets with convex contours tend to be more resistant to cracking. In multipass welding, keep passes narrow and convex. This is shown in Figure 13.40. Finally, watch weld width-to-depth ratios, keeping welds shallow and wide. This is also shown in Figure 13.41.

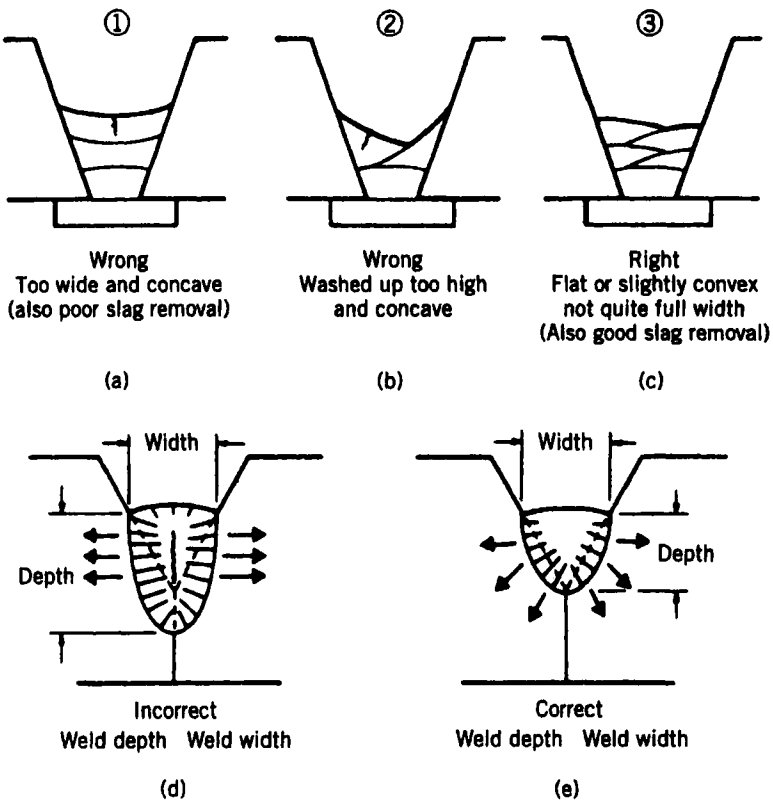


Figure 13.41 The effect of weld bead shape on solidification cracking in multipass welds, in (a), (b), and (c), and weld width-to-depth ratio in (d) and (e). (From *Welding Innovations Quarterly*, 2(3), 1985, O. Blodgett, courtesy of the James F. Lincoln Arc Welding Foundation, Cleveland, OH.)

13.7. SUMMARY

Melting and solidification are critical to the formation of fusion welds. Understanding how melting and solidification occur in real welds, where the rates of heating and cooling mean that these processes take place under conditions that deviate from equilibrium, is key to understanding and controlling real processes and real welds. After differentiating between equilibrium and nonequilibrium, the processes of melting and solidification were described for pure crystalline materials, using pure metals as the example. The complication of adding a solute to produce an alloy was then described, first under the ideal conditions of equilibrium, and then under two different conditions of nonequilibrium. The origin and consequences of microsegregation in the resulting weld structure, the extension of the range over which solidification

occurs, the origin of growth modes different than observed in pure materials, and the origin and consequences of centerline segregation were all described. The two major theories of alloy solidification, the simpler theory of constitutional supercooling and the more complicated but precise theory of interface stability were explained in detail. Finally, reasons and means for controlling weld solidification structure and substructure, in terms of both mode and scale, were described.

REFERENCES AND SUGGESTED READING

Blodgett, O. W., 1985, *Welding Innovations Quarterly*, **2**(3), 4.

Boettinger, W. J., and Coriell, S. R., 1984, "Mechanism of microsegregation-free solidification," *Materials Science & Engineering*, **65**, 27–35.

Bower, T. F., Brody, H. D., and Flemings, M. C., 1966, "Measurements of solute redistribution in dendritic solidification," *Transactions of the AIME*, **236**, 625–634.

Brody, H. D., and Flemings, M. C., 1966, "Solute redistribution in dendritic solidification," *Transactions of the AIME*, **236**, 615–624.

Brooks, J. A., Baskes, M., and Greulich, F., 1991, "Solidification modeling and solid-state transformations in high-energy-density stainless steel welds," *Met-Trans.*, **22A**(4), 915–926.

Brown, D. C., Crossley, F. A., Rudy, J. F., and Schwartzbart, H., 1962, "The effect of electromagnetic stirring and mechanical vibration on arc welds," *Welding Journal*, **41**(6), 241s–250s.

David, S. A., and Liu, C. T., 1982, "High-power laser and arc welding of thorium-doped iridium alloys," *Welding Journal*, **61**(5), 157s–163s.

David, S. A., and Vitek, J. M., 1989, "Correlation between solidification parameters and weld microstructures," *International Materials Reviews*, **34**(5), 213–245.

Davies, G. J., and Garland, J. G., 1975, "Solidification structures and properties of fusion welds," *International Metallurgical Review*, No. 196, **20**, 83–93.

Delves, R. T., 1966, *Physical Status of Solidification*, **16**, 621.

Dudas, J. H., and Collins F. R., 1966, "Preventing weld cracks in high-strength aluminum alloys," *Welding Journal*, **45**(6), 241s–249s.

Flemings, M. C., 1974, *Solidification Processing*, McGraw-Hill, New York.

Garland, J. G., 1974, "Weld pool solidification control," *Metals Construction*, **6**, 121–127.

Giamei, A. F., Kraft, E. H., and Lemkey, F. D., 1976, in *New Trends in Materials Processing*, American Society for Metals, Metals Park, OH, p. 48.

Glicksman, M. E., Singh, N. B., Mani, S. S., Adam, J. D., Coriell, S. R., Duval, W. M. B., Santoro, G. J., and DeWitt, R., 1996, "Direct observations of interface instabilities," *J. of Crystal Growth*, **166**, 364–369.

Glicksman, M. E., Koss, M. B., Bushnell, L. T., LaCombe, J. C., and Winsa, E. A., 1995, *ISIJ International*, **35**(6), 604–610.

Hardy, S. C., and Coriell, S. R., 1968, "Morphological stability and ice-water interface free energy," *Journal of Crystal Growth* **3**(4), 569–573.

Heintz, G. N., and McPherson, R., 1986, "Solidification control of submerged arc weld in steels by inoculation of Ti," *Welding Journal*, **65**(3), 71s–82s.

Huang, S.-C., and Glicksman, M. E., 1981, "Fundamentals of dendritic solidification, I: steady-state tip growth" and "II: development of sidebranch structure," *Acta Metallurgica*, **29**, 710–715, 717–734.

Hunt, J. D., 1979, *Solidification and Casting of Metals*, The Metals Society, London.

Jackson, K. A., and Hunt, J. D., 1965, "Transparent compounds that freeze like metals," *Acta Metallurgica*, **13**, 1212–1215.

Jackson, K. A., Uhlmann, D. R., and Hunt, J. D., 1967, "On the nature of crystal growth from the melt," *Journal of Crystal Growth*, **1**, 1–36.

Jayarajan, T. N., and Jackson, C. E., 1972, "Magnetic control of gas tungsten-arc welding process," *Welding Journal*, **51**(8), 377s–385s.

Jones, H., 1973, *Rep. Prog. Phys.*, **36**, 1425.

Kou, S., and Le, Y., 1983, "Three-dimensional heat flow and solidification during autogenous GTA welding of Al plates," *Metallurgical Transactions A*, **14A**, 2245–2253.

Kou, S., and Le, Y., 1985, "Improving weld quality by low frequency arc oscillation," *Welding Journal*, **64**(3), 51–55.

Kraus, H. G., 1987, "Experimental measurement of thin plate 304 stainless steel GTA weld pool surface temperature," *Welding Journal*, **66**(12), 353s–359s.

Lippold, J. C. and Savage, W. F., 1980, "Solidification of austenitic stainless steel weldments: Part 2—The effect of alloy compulitron on ferrite morphology," *Welding Journal*, **59**(2), 485–585.

Messler, R. W., Jr., 1981, "Electron-beam weldability of advanced titanium alloys," *Welding Journal*, **60**(5), 79s–84s.

Messler, R. W., Jr., and Li, L., 1998, "Comparison of fusion zone solidification and heat-affected zone liquation cracking in type 347 stainless steel," 79th Welding Convention and Exposition, Detroit, MI, 20–24 April 1998; to be published in the *Welding Journal*.

Mullins, W. W., and Sekerka, R. F., 1964, "Stability of a planar interface during solidification of a dilute binary alloy," *Journal of Applied Physics*, **35**(2), 444–452.

Nakagawa, H., et al., 1970, *Journal of the Japanese Welding Society*, **39**, 94.

Pearce, B. P., and Kerr, H. W., 1981, "Grain refinement in magnetically stirred GTA welds of luminum alloys," *Metallurgical Transactions*, **12B**, 479–486.

Rappaz, M., David, S. A., Vitek, J. M., and Boatner, L. A., 1989, "Development of microstructures in Fe-15Ni-15Cr single-crystal electron beam welds," *Metallurgical Transactions*, **20A**, 1125–1138.

Rutter, J. W., and Chalmers, B., 1953, "A prismatic substructure formed during solidification of metals," *Canadian Journal of Physiology*, **31**, 15–25.

Savage, W. F., and Aronson, A. H., 1966, "Preferred orientation in the weld fusion zone," *Welding Journal*, **45**(2), 85s–89s.

Savage, W. F., and Hrubec, R. J., 1972, "Synthesis of weld solidification using crystalline organic materials," *Welding Journal*, **51**(5), 260s–271s.

Savage, W. F., Lundin, C. D., and Aronson, A. H., 1965, "Weld metal solidification mechanics," *Welding Journal*, **44**(4), 175s–181s.

Scaborough, J. D., and Burgan, C. E., 1984, "Reducing hot-short cracking in iridium GTA welds using four-pole oscillation," *Welding Journal*, **63**(6), 54–56.

Seidensticker, R. G., and Hamilton, D. R., 1963, "Growth mechanisms in germanium dendrites: three twin dendrites; experiments on and models for the entire interface," *Journal of Applied Physics*, **34**, 3113–3120.

Sekerka, R. F., 1965, "A stability function for explicit evaluation of the Mullins-Sekerka interface stability criterion," *Journal of Applied Physics*, **36**(1), 264–268.

Sekerka, R. F., 1967, "Application of the time-dependent theory of interface stability to an isothermal phase transformation," *Journal of the Physical Chemistry of Solids*, **28**, 983–994.

Sekerka, R. F., 1968, "Morphological stability," *Journal of Crystal Growth* **3**(4), 71–81.

Simpson, R. P., 1977, "Controlled weld-pool solidification structure and resultant properties with yttrium inoculation of Ti-6Al-6V-2Sn welds," *Welding Journal*, **56**(3), 67s–77s.

Slavin, G. A., 1974, "Control of the solidification process by means of a dynamic action of the arc," *Welding Production*, **21**(8), 3–4.

Smith, C. S., 1948, "Grains, phases, and interfaces: an interpretation of microstructure," *Transactions of the AIME*, **175**, 15–51.

Smith, V. G., Tiller, W. A., and Rutter, J. W., 1955, "A mathematical analysis of solute redistribution during solidification," *Canadian Journal of Physics*, **33**, 723–745.

Tiller, W. A., and Rutter, J. W., 1956, "The effect of growth conditions upon the solidification of a binary alloy," *Canadian Journal of Physiology*, **34**, 96–104.

Tiller, W. A., Jackson, K. A., Rutter, J. W., and Chalmers, B., 1953, "The redistribution of solute atoms during the solidification of metals," *Acta Metallurgica*, **1**, 428–437.

Townsend, R. D., and Kirkaldy, J. S., 1968, "Widmanstaetten ferrite formation in Fe-C alloys," *ASM Transactions*, **61**(3), 605–619.

Turnbull, D., and Cech, R. E., 1950, "Microscopic observations of the solidification of small metal droplets," *Journal of Applied Physics*, **21**, 804–810.

Vitek, J. M., and David, S. A., 1988, "The effect of cooling rate on ferrite in type 308 stainless steel weld metal," *Welding Journal*, **67**(5), 95s–102s.

Voronkov, V. V., 1965, *Soviet Physics—Solid State*, **6**, 2378.

Walton, D., and Chalmers, B., 1959, "Origin of preferred orientation in the columnar zone of ingots," *Transactions of the Metallurgical Society of AIME*, **215**(3), 447–457.

Williamson, R. B., and Chalmers, B., 1967, in *Crystal Growth*, edited by H. S. Peiser, Pergamon, Oxford, UK, p. 739.

Suggested readings on basic material science, including crystal structure, Miller indices, phase diagrams and Lever rule

Callister, W. D., Jr.. 1997, *Materials Science and Engineering: An Introduction*, 4th ed., Wiley, New York.

Cullity, B. D., 1978, *Elements of X-ray Diffraction*, 2d ed., Addison-Wesley, Reading, MA.

Shackleford. J. F., 1996, *Introduction to Materials Science for Engineers*, 4th ed., MacMillan, New York.

Smith, W. F., 1996, *Principles of Materials Science and Engineering*, 3d ed., McGraw-Hill, New York.

Suggested readings on the general area of solidification and solidification cracking

Chalmers, B., 1964, *Principles of Solidification*, Wiley, New York.

Davies, G. J., and Garland, J. G., 1975, "Solidification structures and properties of fusion welds," *International Metallurgical Review*, No. 196, **20**, 83–93.

Flemings, M. C., 1974, *Solidification Processing*, McGraw-Hill, New York.

Goodwin, G. M., 1988, "The effects of heat input and weld process on hot cracking in stainless steel," *Welding Journal*, **67**(4), 88s–94s.

Liu, W., Tian, X., and Zhang, X., 1996, "Preventing weld hot cracking by synchronous rolling during welding," *Welding Journal*, **75**(9), 297s–304s.

Ogborn, S. J., Olson, D. L., and Cieslak, M. J., 1995, "Influence of solidification on the microstructural evolution of nickel base weld metal," *Materials Science and Engineering A: Structural Materials Properties, Microstructure and Processing*, **203**(Nov.), 134–139.

Rajasekhar, K., Harendranath, C. S., Raman, R., and Kulkarni, S. D., 1997, "Microstructural evolution during solidification of austenitic stainless steel weld metals: a color metallographic and electron microprobe analysis study," *Materials Characterization*, **38**(Feb.), 53–65.

Savage, W. F., 1968, in *Weld Imperfections*, edited by A. R. Pflunger and R. E. Lewis, Addison-Wesley, Reading, MA, 13.

Savage, W. F., 1980, "Solidification, segregation and weld imperfections," *Welding in the World*, **18**, 89.

Zacharia, T., 1994, "Dynamic stresses in weld metal hot cracking," *Welding Journal*, **73**(7), 164s–172s.

CHAPTER 14

EUTECTIC, PERITECTIC, AND POSTSOLIDIFICATION FUSION ZONE TRANSFORMATIONS

For many important alloy systems, the transformation that takes place during solidification is more complex than simply a liquid phase changing to a single solid-phase alloy. The first of these important transformations (or reactions, really) is the *eutectic reaction* in which a single liquid phase transforms at a specific temperature and composition to an intimate mixture of two solid phases. Because such reactions in two-phase alloys are so commonplace in systems of engineering importance, including all brazes and solders, they are described first. Another important reaction associated with solidification is also one of the least well understood by most materials or welding specialists, namely, the *peritectic reaction*, in which a liquid and a solid phase that has formed from that liquid react at a particular temperature and composition to produce a new solid phase. While this reaction occurs in many alloy systems of importance in engineering, most notably the iron–iron carbide system, which includes all steels, rarely is it discussed in the treatment of welding metallurgy. That will not be the case here: The peritectic reaction is described in the second section of this chapter.

Even after a liquid has completely transformed to solid, as a single phase or a mixture of phases, producing a solidification structure or substructure, further transformations can occur in the solid state. These so-called *postsolidification phase transformations* can significantly alter the structure and substructure of the fusion zone of a weld, and, thus, the properties of the final weld. For this reason, it is just as important to know that such postsolidification transformations occur and understand how they occur and how they change

structure and properties as it is to understand the solidification process itself. In this chapter, several important postsolidification phase transformations occurring in the iron–iron carbide system are discussed, including δ-ferrite versus austenite primary solidification in stainless steels, and austenite decomposition to ferrite and pearlite, bainite, or martensite in carbon or low-alloy steels. Finally, a couple of other important postsolidification phenomena are briefly described.

14.1. EUTECTIC REACTIONS OR SOLIDIFICATION OF TWO-PHASE ALLOYS

Many binary alloy systems of importance in engineering consist of two phases in equilibrium at room temperature, in which each phase exhibits partial solid solubility for the relevant solute, that is, B in solid solution of A (usually known as the α phase, and A in solid solution in B (usually known as the β phase). These phases often form together upon solidification of the liquid in what is known as an eutectic reaction or transformation, where $L \rightarrow S_1 + S_2$ on cooling, and $S_1 + S_2 \rightarrow L$ on heating. The reaction or transformation takes place at a specific temperature (known as the eutectic temperature, $T_{eutectic}$, or here, simply, T_E) and composition (known as the eutectic composition or $C_{eutectic}$), together known as the eutectic point. As such, the reaction is said to be invariant; i.e., the temperature and composition are fixed, and the transformation or reaction occurs at a discrete temperature, not over a temperature range.

An important characteristic of eutectic transformations in binary systems (as well as more complex systems, such as ternaries consisting of three components) is that the eutectic is the lowest melting constituent in the system, lower melting than either (or, for more complex systems, any) component. As such, alloys of eutectic composition (or near-eutectic composition, where there is a narrow freezing range) are often used as braze or solder fillers (often selected for their low melting range), but are also used when castability is important. Important examples of the former are the Al-Si braze fillers and Sn-Pb solders, and of the latter is cast iron. The reasons are fairly obvious: (1) possibility of melting without melting substrates being brazed or soldered, and (2) no or little mushy zone to impede mold filling or lead to segregation during casting.

A typical binary eutectic is shown in Figure 14.1 for a hypothetical alloy system. Let's look at how solidification takes place in such a two-phase alloy system, first under conditions of equilibrium, then under nonequilibrium when cooling is rapid.

14.1.1. Solidification at the Eutectic Composition

Under conditions of equilibrium, solid solution phases S_1 and S_2 would form from liquid of composition C_0 simultaneously at temperature T_E. The compo-

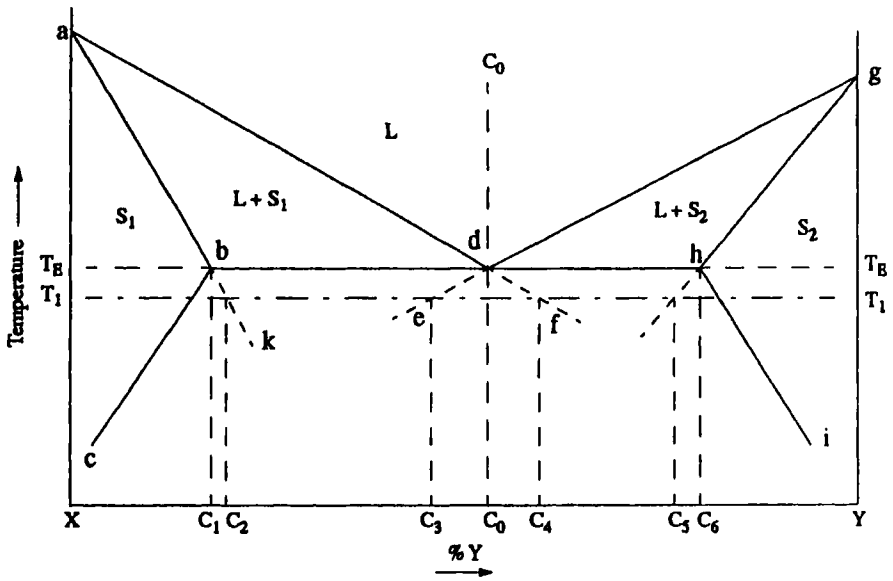


Figure 14.1 Hypothetical binary phase diagram for a two-phase alloy containing a eutectic reaction at the eutectic composition, Co. (From unpublished notes of W. F. Savage, 1965–67, Rensselaer Polytechnic Institute, Troy, NY, with permission of Mrs. H. L. Savage.)

sitions of the solid solution phases would be C_1 and C_6, respectively. However, in the usual case, some supercooling would be necessary to produce nuclei of solid from the melt, and the degree of supercooling would depend largely upon the rate of cooling (with more supercooling being needed for faster cooling rates) and the condition of the melt (e.g., homogeneity, presence of impurities to act as sites for heterogeneous nucleation, etc.) Assuming that the solid phases experience no diffusion and that changes in composition in the liquid (melt) are achieved solely by diffusion (i.e., there is no mixing), the sequence of events would be as follows.

At a temperature T_1, slightly below T_E, sufficient supercooling would occur to create a nucleus of greater than the critical nucleus size of either S_1 or S_2, depending strictly on chance variations of the localized concentration of the liquid. Assume for the point of discussion that a nucleus of S_1 of composition slightly less rich in Y than C_1 forms (as defined by the intersection of the particular temperature isotherm, here T_1, with the solvus line *bc*). This nucleus of solid S_1 would proceed to grow, rejecting excess Y (due to the system's distribution coefficient, $k_o = C_{solid}/C_{liquid}$) to the surrounding liquid, until sufficient Y was present in the liquid to nucleate solid S_2 on either side of the original nucleus of S_1 (as shown in Figure 14.2). Once nuclei of S_2 were formed, they, in turn, would grow into the surrounding liquid rejecting excess X to the adjacent liquid until the concentration of X in the surrounding liquid became

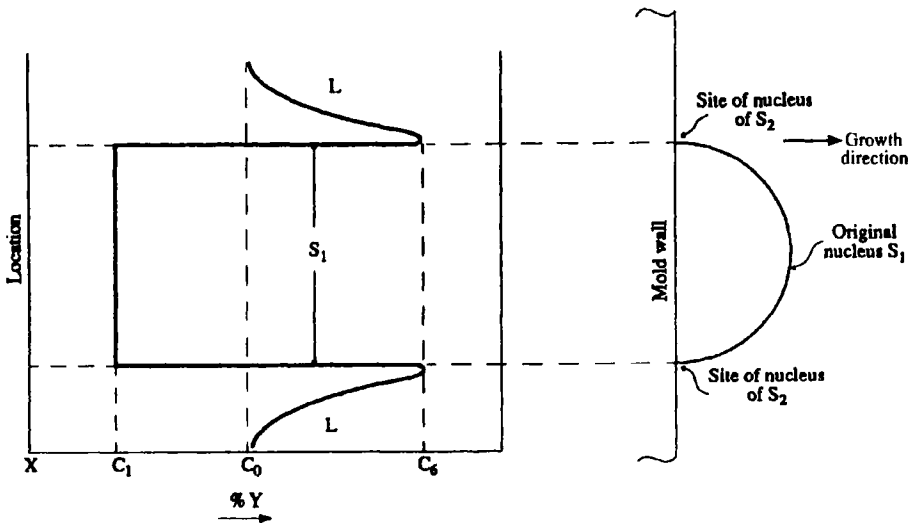


Figure 14.2 Schematic showing the buildup of solute concentration profiles in the liquid surrounding an advancing lamella of solid S_1. (From unpublished notes of W. F. Savage, 1965–67, Rensselaer Polytechnic Institute, Troy, NY, with permission of Mrs. H. L. Savage.)

sufficiently high to nucleate additional particles of S_1. This process would continue creating nuclei alternately of S_1 and S_2 at the original mold wall or weld solidification front. The existing nuclei would, meanwhile, grow in a direction approximately normal to the mold wall or advancing weld solidification front, rejecting solute to the adjacent liquid (Y from solid S_1; X from solid S_2), and causing constitutional supercooling of the liquid in contact with each solid.

Near the center of the laminations of S_1 that formed, the liquid phase ahead of the growing lamination would tend to assume a composition C_4 determined by the intersection of the temperature isotherm, T_1, with the extended liquidus *adf* (assuming that the temperature of the molten liquid has decreased to T_1). The solid phase that would be formed from this liquid would be of composition C_2, determined by the intersection of the actual temperature isotherm T_1 with the projected solidus *abk*. By the same token, the liquid in contact with the centers of the S_2 laminations would assume a composition C_3, while the solid would form with composition C_5. The liquid some distance from the advancing solid interfaces would remain essentially of composition C_0, and concentration gradients similar to those shown in Figure 14.3 would exist along the dashed lines. Note that liquid in front of S_2 has less Y than the nominal composition C_0, while that in front of S_1 has more Y than the nominal composition C_0, the compositions being C_3 and C_4, respectively.

At the same time as all of the above is going on, the extra X rejected in front

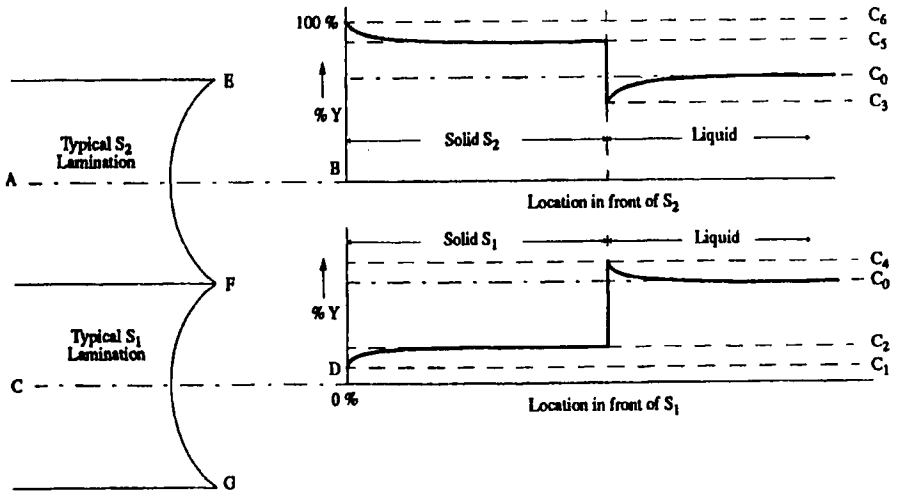


Figure 14.3 Schematic showing concentration gradients in the liquid ahead of advancing adjacent lamella of S_1 and S_2. (From unpublished notes of W. F. Savage, 1965–67, Rensselaer Polytechnic Institute, Troy, NY, with permission of Mrs. H. L. Savage.)

of advancing S_2 diffuses through the liquid toward points *E* and *F* in Figure 14.3, while the extra Y rejected in front of advancing S_1 also diffuses toward points *G* and *F*. This tends to produce a lateral or transverse concentration gradient in front of the growing solid interfaces similar to that shown by the dashed line in Figure 14.4. Note that the liquid composition at the interface between the two solid phases (i.e., at *F*, *G*, *E*) is approximately equal to C_0, the nominal composition of the alloy. Since the composition of the liquid phase next to points *E*, *F*, and *G* is equal to C_0, the liquid at these points (also at temperature T_1) is supercooled more than the liquid at locations near the center of each advancing solid phase. Therefore, the rate of growth of the lamellae is slightly faster and the solid interface develops a series of cusps at the solid phase junctions *E*, *F*, and *G*.

One additional consequence of the concentration gradients in front of the advancing solid interface is the tendency for the solute enriched liquid to nucleate the opposing solid phase, as shown in Figure 14.5. Note that the liquid in front of S_1 of composition C_4 (refer to previous figures) is markedly supercooled with respect to S_2. That is, liquid of composition C_4 has an equilibrium liquidus of T_2 (as shown by point *m*), and would be in equilibrium with solid S_2 at composition C_7 (see Figure 14.5). This corresponds to a supercooling of $T_2 - T_1 = \Delta T$, and the chances are good for nucleation of S_2 at this point.

As a consequence of this last point, the growth of the individual laminations of a eutectic constituent does not normally proceed uninterrupted very far before the supercooling described leads to nucleation of the opposing phase.

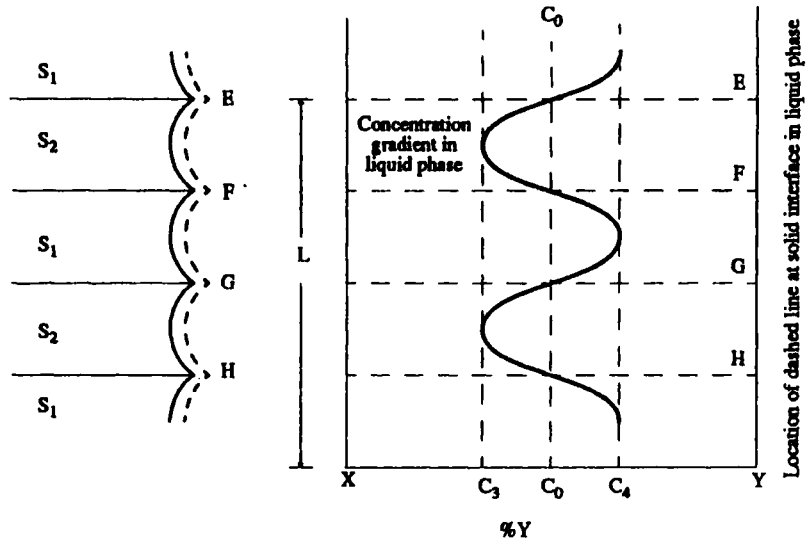


Figure 14.4 Schematic showing the tendency for cusp formation between adjacent lamella of S_1 and S_2 in a growing eutectic. (From unpublished notes of W. F. Savage, 1965–67, Rensselaer Polytechnic Institute, Troy, NY, with permission of Mrs. H. L. Savage.)

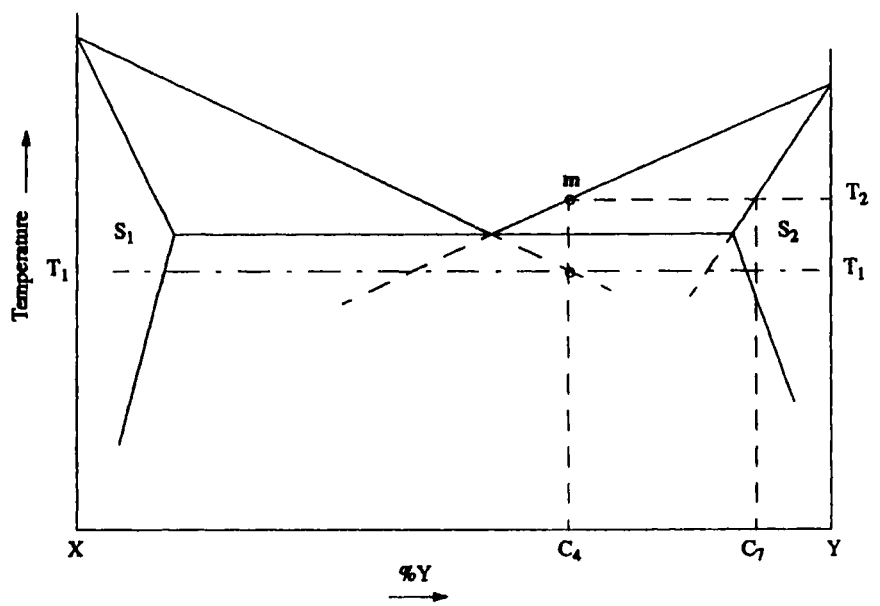


Figure 14.5 Schematic showing the supercooling ahead of advancing lamella in a growing eutectic leading to nucleation of the opposing phase. (From unpublished notes of W. F. Savage, 1965–67, Rensselaer Polytechnic Institute, Troy, NY, with permission of Mrs. H. L. Savage.)

14.1.2. Solidification of Two-Phase Alloys at Noneutectic Compositions

As often as not, two-phase alloys exhibiting an eutectic are caused to solidify at a composition off the eutectic composition, that is, at a noneutectic composition. Therefore, it is important to consider the solidification process for such compositions. Referring to the hypothetical binary phase diagram in Figure 14.6, an alloy of composition C_2 caused to solidify under conditions of equilibrium would form the first solid S_1 of composition C_0 at temperature T_1 from liquid of composition C_2. The remaining liquid would change composition along the liquidus line to point *d* at the eutectic temperature as solidification proceeded. Meanwhile at any temperature, the solid and liquid in equilibrium would be defined at any temperature by the intersection of the particular temperature isotherm with the solidus and liquidus lines (*ab* and *ad*, respectively). When the composition of the liquid phase reached C_4, the eutectic composition at the eutectic temperature, under equilibrium conditions, the remaining liquid would transform isothermally to a mixture of S_1 and S_2 as discussed for equilibrium solidification of the eutectic alloy (Section 14.1.1). Thus, the resulting solid would consist of solid of composition C_1 (produced between T_1 and the eutectic temperature) imbedded in or surrounded by the eutectic constituent.

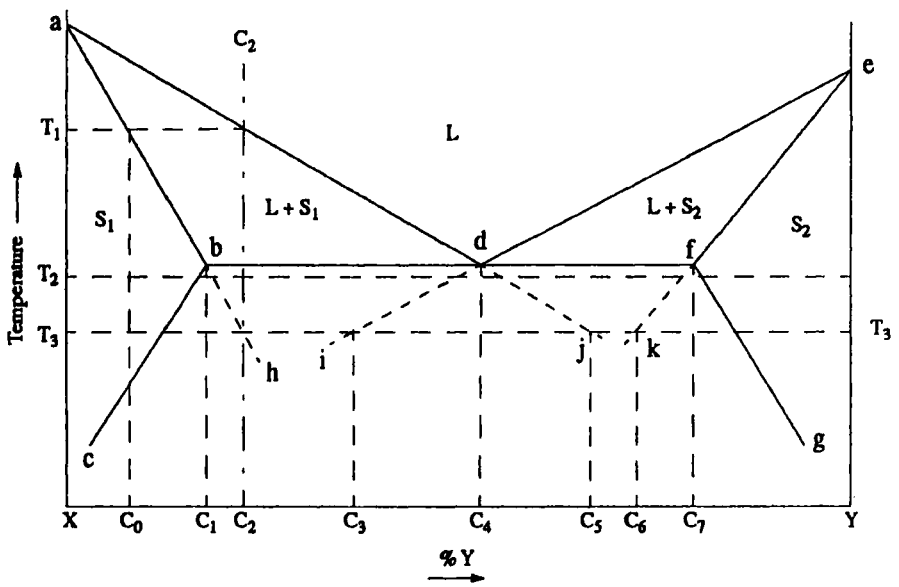


Figure 14.6 Hypothetical binary phase diagram for a system containing a eutectic showing situation for solidification of an alloy C_2 of noneutectic composition. (From *unpublished* notes of W. F. Savage, 1965–67, Rensselaer Polytechnic Institute, Troy, NY, with permission of Mrs. H. L. Savage.)

Under nonequilibrium conditions of rapid cooling, the sequence of events with alloy C_2 would be modified. (Note that the maximum possible degree of constitutional supercooling is always defined by the intersection of the nominal composition line with the solidus temperature or projection of the solidus temperature in cases such as this.)

Again, assuming no diffusion in the solid phases, and assuming that adjustment of the liquid composition can occur only by diffusion (not by mixing), an alloy C_2 would tend to form the first solid S_1 at a temperature slightly below T_1 and of composition slightly richer in Y than C_0. The rejection of solute Y from the solid nucleus would rapidly enrich the liquid in contact with the solid S_1 along the liquidus line *adj* to a composition of Y slightly greater than the eutectic composition C_4. If the temperature of the solid metal interface was continuously lowered by conduction of heat to the mold wall (or surrounding base metal for a weld), the temperature of the liquid at the interface might be reduced to, say, T_2. At this temperature, the liquid and solid in contact at the interface would be of compositions given by the intersection of the T_2 isotherm with the projection of the liquidus line *adj* and the solidus line *abh*, respectively. Note, however, that the liquid phase of the above composition would be supercooled with respect to S_2 (as argued earlier in Section 14.1.1), and would thus tend to nucleate solid S_2 of composition slightly less rich in Y than C_7. Once a nucleus of S_2 had formed, it would, in turn, reject X to the surrounding liquid, and the solid and liquid at the interface of S_2 would change composition along the projection of the solidus *efk* and the projection of the liquidus *edi*, respectively. This event would cause the liquid in contact with solid S_2 to again become supercooled with respect to solid S_1, and another nucleus of S_1 would tend to form.

Since the above process would be occurring at many separate growth interfaces, the net result would be the simultaneous formation of both S_1 and S_2 as a mechanical mixture in proportions differing slightly from the eutectic composition from a liquid whose nominal composition is still C_2. Thus, an eutectic-like constituent can be formed in a rapidly cooled alloy of other than eutectic composition long before the composition of the liquid phase is adjusted by formation of primary (or proeutectic) solid. As a limiting case, it could be imagined that the composition of the liquid in contact with solid S_1 could achieve composition C_5 and form a nonequilibrium solid S_1 of composition C_2 at the interface at a temperature T_3. This would correspond to the maximum possible constitutional supercooling. If now a nucleus of solid S_2 were to grow parallel to the lamella of S_1 formed as described above, diffusion of solute Y from the S_1-to-liquid interface into the liquid in front of the growing S_2 could maintain the composition of the latter liquid at C_3 and sustain the growth of the S_2 lamella. Thus, a balance could be struck whereby the X rejected at the interface of S_2 diffused away only to be replaced by the Y rejected from the neighboring lamella of S_1. It would be expected that the volume of S_2 formed under such circumstances could be less than that formed by equilibrium decomposition of liquid of eutectic composition. Nonetheless,

the structure would appear eutectic-like, and the proportion of the constituent formed in this way would far exceed that expected under equilibrium conditions.

14.1.3. Morphology of Eutectic Phases

While one tends to think of eutectics as lamellar structures, the shape or morphology of the phases comprising an eutectic constituent can differ depending on the relative proportions and growth rates of each. Without going into great detail, here are some guidelines. The interested reader can find more details on the morphology of eutectic phases in any good physical metallurgy textbook.

When one phase is present in minor proportions due to the composition of the eutectic, the minor phase tends to form as discrete particles, as spheres, rods, or plates, in a matrix of the phase present in the larger volume proportion. When both phases are produced in approximately equal proportions and grow at approximately the same rate, a lamellar structure results.

When, on the other hand, both phases are present in about the same volume proportions, but one grows faster than the other, the faster growing phase tends to grow around the slower growing phase to produce a spiral eutectic.

Finally, when the nominal composition is only slightly greater than the maximum solubility of one solid phase comprising a portion of the eutectic, solidification may produce a "divorced eutectic." Here, the second phase normally comprising the eutectic may form near the end of the solidification process as discrete particles instead of as a mechanical mixture with the first.

14.2. PERITECTIC REACTIONS

When a liquid phase and a solid phase react at a particular temperature and composition to produce a new, single solid phase, a *peritectic reaction* has occurred. Generically, the peritectic reaction can be written: $L + S_1 \rightleftharpoons S_2$. As can be seen, the reaction is reversible, depending on whether the system is being cooled or heated. In fusion welding, the cooling reaction is of particular interest. The temperature at which the reaction occurs is called the peritectic temperature, while the composition at which the reaction occurs is called the peritectic composition.

Undoubtedly, the best known and probably most important peritectic reaction is the one that occurs in the iron–carbon, Fe-C (or, more practically, iron–iron carbide, Fe-Fe_3C) system. In this system, the following reaction occurs:

$$L + \delta\text{-ferrite (or } \delta) \rightleftharpoons \text{austenite (or } \gamma) \tag{14.1}$$

The peritectic temperature is 1492°C (2818°F), while the peritectic composition

is 0.18 wt% *C*. The Fe-Fe_3C system is important because it is the system within which low-, medium-, and high-carbon plain and low-alloy steels are found, as well as being the basis for high-alloy, tool, and stainless steels, and even cast irons. The peritectic reaction is important in the fusion welding of all of these except the cast irons, which have high enough carbon that they involve only an eutectic reaction at 1147°C (2097°F) and 4.3 wt% *C* (where the eutectic is known as ledeburite). This can all be seen in Figure 14.7, the Fe-Fe_3C phase diagram. Peritectic reactions occur in other alloy systems important to engineering, most notably the Cu-Sn and Cu-Zn systems of bronzes and brasses.

Despite being important and prevalent in engineering alloys, the peritectic reaction is rarely discussed in treatises on welding metallurgy, at least not explicitly, understandably, and comprehensively; an exception is provided in the classic reference by Fhines (1956). Without doubt, the finest treatment of the peritectic reaction was and is that of Warren F. "Doc" Savage, long-time gifted teacher and researcher at Rensselaer Polytechnic Institute (RPI). Doc Savage described the peritectic reaction under equilibrium for all generic compositions below, at, and above the peritectic composition. He also described the reaction under nonequilibrium conditions of no diffusion in the solid and complete mixing in the liquid, as in case 2 in Section 13.4.1. Having been fortunate enough to have been taught peritectic reactions by Doc, the author will share that understanding in the following subsections, taken almost verbatim from Doc's famous and priceless (but unpublished) purple-on-white mimeo notes. The nonequilibrium condition where there is assumed to be no diffusion in the solid and no mixing, only diffusion, in the liquid, as in case 3 in Section 13.4.2, is not be described for reasons given at the end of this section. Permission to use this material from Doc's charming and gracious widow, Helen L. Savage, is gratefully acknowledged.

14.2.1. Equilibrium Conditions (Case 1)

Although equilibrium conditions never exist in the real world of welding, as we have seen from discussions of solidification in Sections 13.1 and 13.3, equilibrium is an essential and excellent starting point. For the purpose of the following subsections, variations of the hypothetical phase diagram for a peritectic in a binary alloy system as shown in Figure 14.8 will be used. The behavior of alloys in various key composition ranges relevant to the generic peritectic reaction is described.

14.2.1.1. Alloys Below the Solubility Limit of the Solid Phase in the Peritectic. Consider an alloy C_0 in Figure 14.8. On cooling, at T_1, the first solid α that forms from liquid of composition C_0 has composition C_S. As cooling continues from T_1 to T_2, the proportion solidified increases and the instantaneous equilibrium concentrations of the solid and the liquid present are always given by the compositions at the intersection of the temperature isotherm or tie-line with the solidus and liquidus lines, respectively (i.e.,

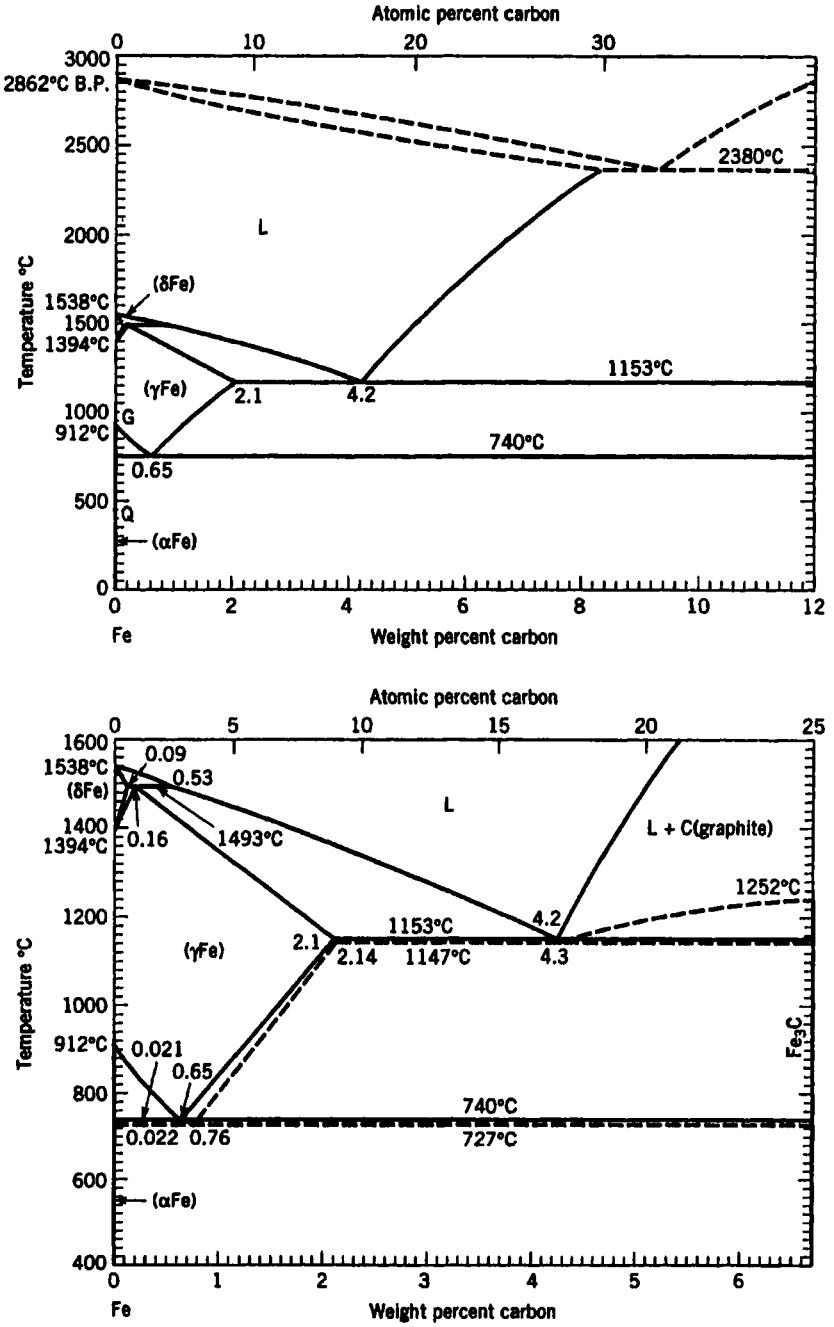


Figure 14.7 Equilibrium phase diagram for the Fe–Fe_3C system showing the peritectic reaction near the upper-left-hand corner of the diagram, where liquid + δ-ferrite δ reacts to form austenite γ on cooling. (From *ASM Handbook*, Vol. 3: *Alloy Phase Diagrams*, published in 1993 by and used with permission of the ASM International, Materials Park, OH.)

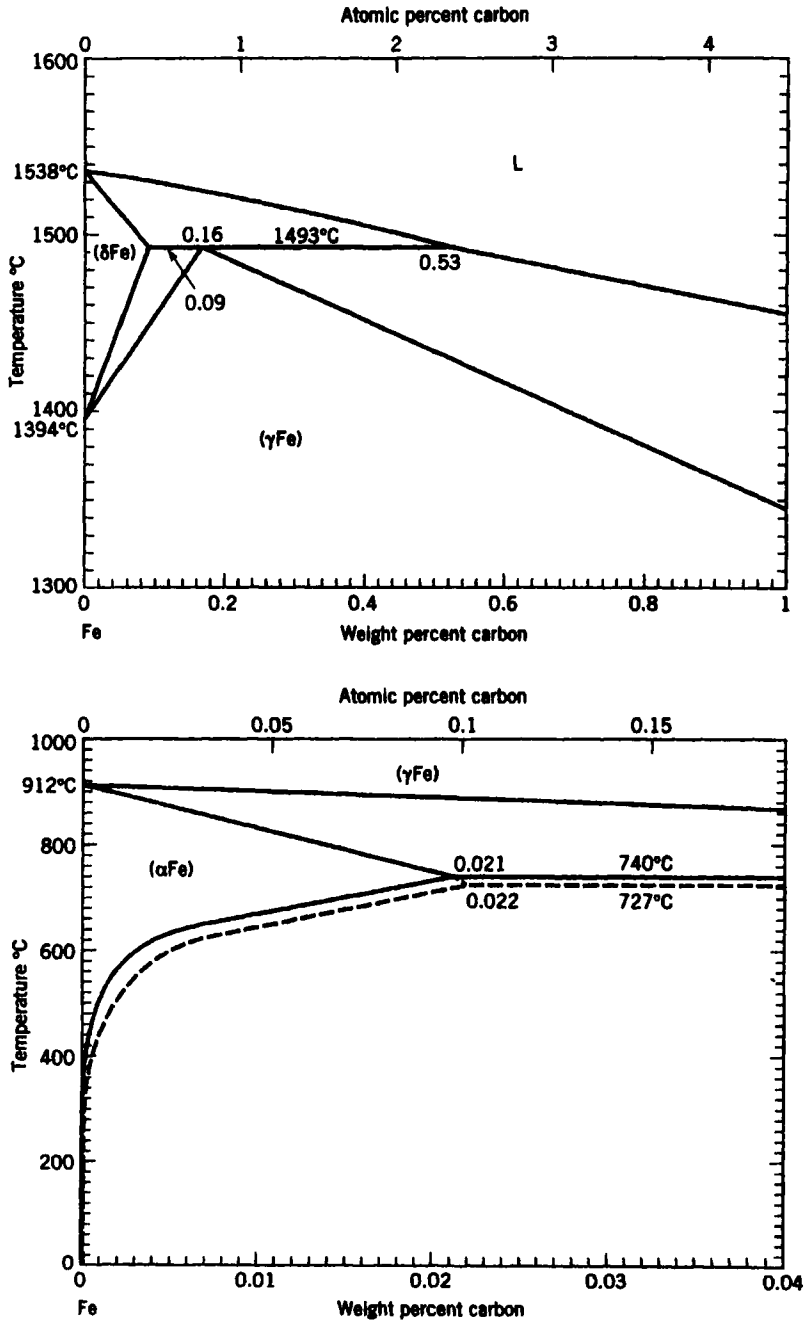


Figure 14.7 (*Continued*)

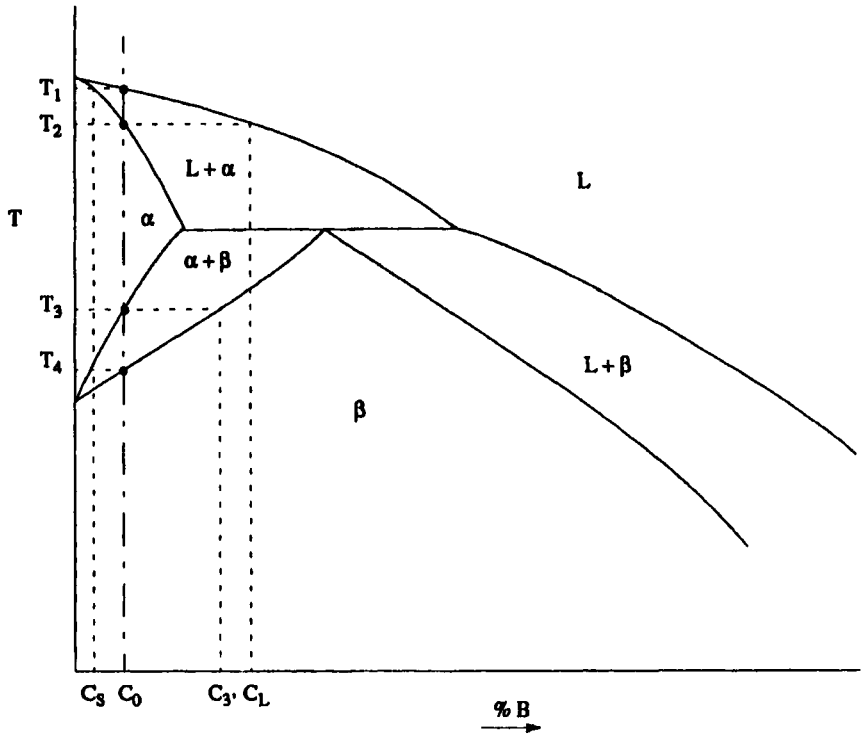


Figure 14.8 Hypothetical phase diagram showing just the region of a peritectic reaction, where liquid + $\alpha > \beta$ on cooling. Here, an alloy with nominal composition C_0 below the solubility limit of the α solid phase is treated.

microscopic equilibrium prevails). At T_2, the last liquid, of composition C_L, disappears and the nominal composition of the solid reaches C_0. Note that at all times, the composition of the *entire* solid present is equal to the equilibrium value predicted by the diagram, a condition possible only if diffusion is allowed to remove all concentration gradients in the solid phase. By the same token, the composition at all points in the liquid is that predicted by equilibrium, a condition possible only if complete mixing or diffusion is achieved in the liquid phase.

At T_3, β of composition C_S, begins to form from the α of composition C_0, and the amount of β formed increases in accordance with the Lever rule as cooling continues below T_3 until all β of composition C_0 exists at and below T_4. Between T_3 and T_4, the composition of the α and β present are given by the intersections of the horizontal tie-line (or temperature isotherm) and the boundaries of the single-phase, α and β, regions.

14.2.1.2. Alloys Between the Solubility Limit and the Peritectic Composition. Consider an alloy C_0 in Figure 14.9. On cooling, at T_1, the first solid

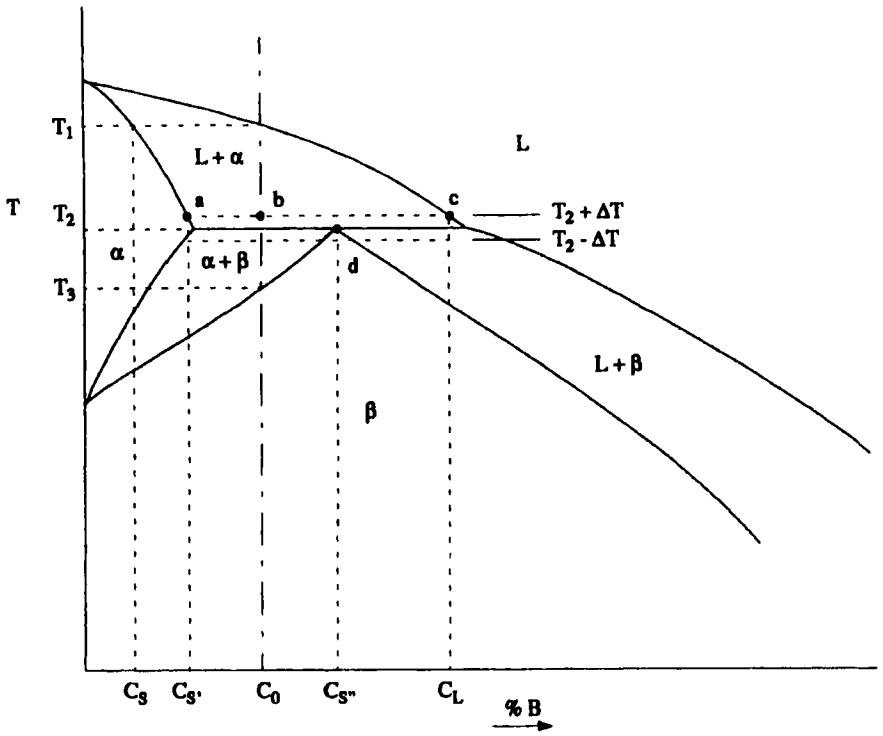


Figure 14.9 Hypothetical phase diagram showing just the region of a peritectic reaction, where liquid + $\alpha > \beta$ on cooling. Here, an alloy with nominal composition C_0 between the solubility limit of the α solid phase and the peritectic composition is treated.

α that forms from liquid of composition C_0 has composition C_S. As cooling continues from T_1 to T_2 (the peritectic temperature), the proportion of solid increases in accordance with predictions of the Lever rule, until at $T_2 + \Delta T$, the alloy consists of $100 \times bc/ac\%$ of solid α of composition $C_{S'}$ and $100 \times ab/ac\%$ of liquid of composition C_L. At $T_2 - \Delta T$, the remaining liquid reacts with solid α and, if sufficient time for diffusion is allowed, the alloy consists of $100 \times bd/ad\%$ solid α of composition $C_{S'}$ and $100 \times ab/bd\%$ solid β of composition $C_{S''}$. On cooling from T_2 to T_3, the amount of α decreases in accordance with the Lever rule until at T_3, the alloy consists of 100% β of composition C_0.

14.2.1.3. Alloys With the Peritectic Composition. Consider the alloy C_0 in Figure 14.10. On cooling, at T_1, the first solid α that forms from liquid of composition C_0 has composition C_S. Again, the proportion of solid and liquid, and the composition of each, can be predicted by the Lever rule as above (in Section 14.2.1.2). However, at T_2 (the peritectic temperature), the last remaining liquid of composition C_L reacts with solid α of composition $C_{S'}$ to form

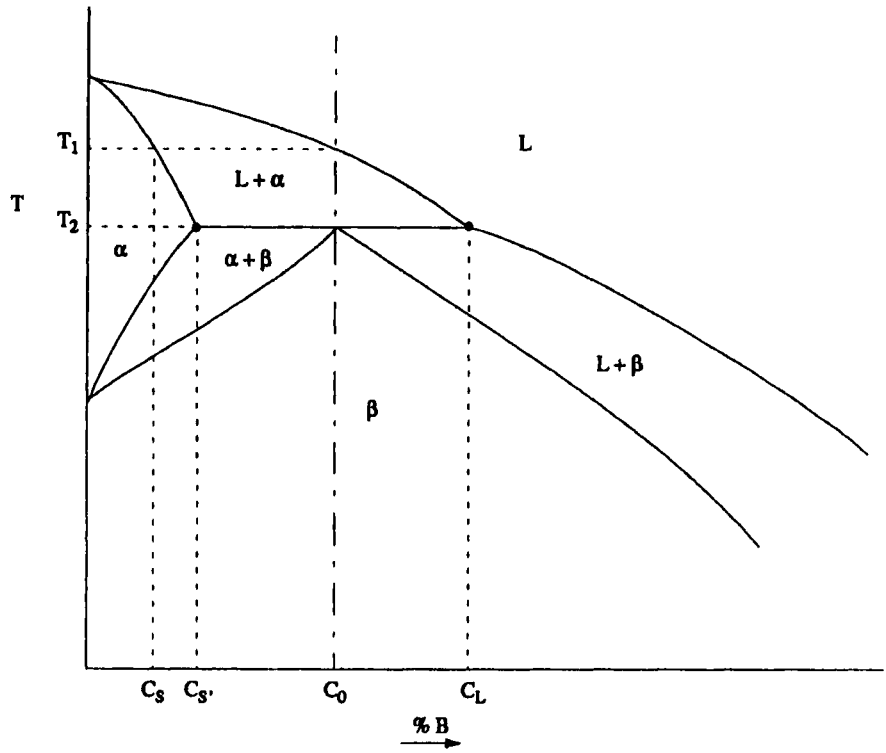


Figure 14.10 Hypothetical phase diagram showing just the region of a peritectic reaction, where liquid + $\alpha > \beta$ on cooling. Here, an alloy with nominal composition C_0 at the peritectic composition is treated.

100% β of composition C_0, providing that sufficient diffusion time is allowed to remove all concentration gradients. Below T_2, the system is 100% β, so no changes occur.

14.2.1.4. Alloys Beyond the Peritectic Composition, but Within the L + S Range. Consider an alloy C_0 in Figure 14.11. On cooling, at T_1, the first solid α that forms from liquid of composition C_0 has composition C_S. On cooling from T_1 to T_2, more solid α forms until at $T_2 + \Delta T$, there is 100 × *cd/ad*% solid α of composition $C_{S'}$ in equilibrium with 100 × *ac/ad*% liquid of composition C_L. At $T_2 - \Delta T$, all the solid α present reacts with all the liquid present to form 100 × *cd/bd*% β of composition $C_{S''}$ and 100 × *bc/bd*% liquid of composition C_L. On cooling from T_2 to T_3, the amount of β increases in accordance with the Lever rule prediction and the concentration of B in β increases along the line *be* until, at T_3, the entire alloy is solid β and has composition C_0. The last remaining liquid at $T_3 + \Delta T$ would be of composition $C_{L'}$. Below T_3, the system is 100% β, so no changes occur.

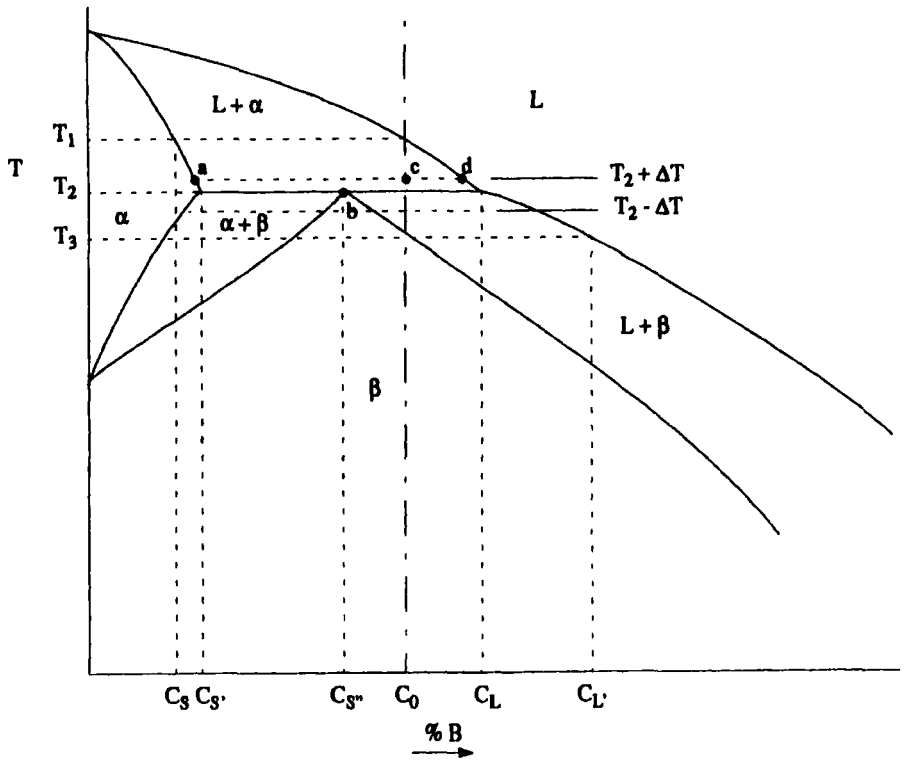


Figure 14.11 Hypothetical phase diagram showing just the region of a peritectic reaction, where liquid + $\alpha > \beta$ on cooling. Here, an alloy with nominal composition C_0 beyond the peritectic composition but within the L + α range is treated.

14.2.1.5. Alloys Past the L + S Range of a Peritectic in the Liquid Field. Consider alloy C_0 in Figure 14.12. In this case, at T_1, the liquid would transform directly to β of composition C_{B1} on cooling, just as would any normal solid-solution-type alloy. With further cooling from T_1 to T_2, the proportion of β would increase relative to the amount of remaining liquid, and the composition of the β phase would become progressively richer in solute along the line *ab* until it reached the composition C_0 at T_2. Below T_2, there would be no further changes in the β until some other reaction occurred. In the Fe-Fe_3C system, this is the occurrence of the eutectic reaction at 1153°C and 4.2 wt% *C*.

14.2.2. Nonequilibrium Conditions

As discussed in Section 13.1, solidification never occurs under equilibrium conditions in the real world. Rather, solidification is always a nonequilibrium

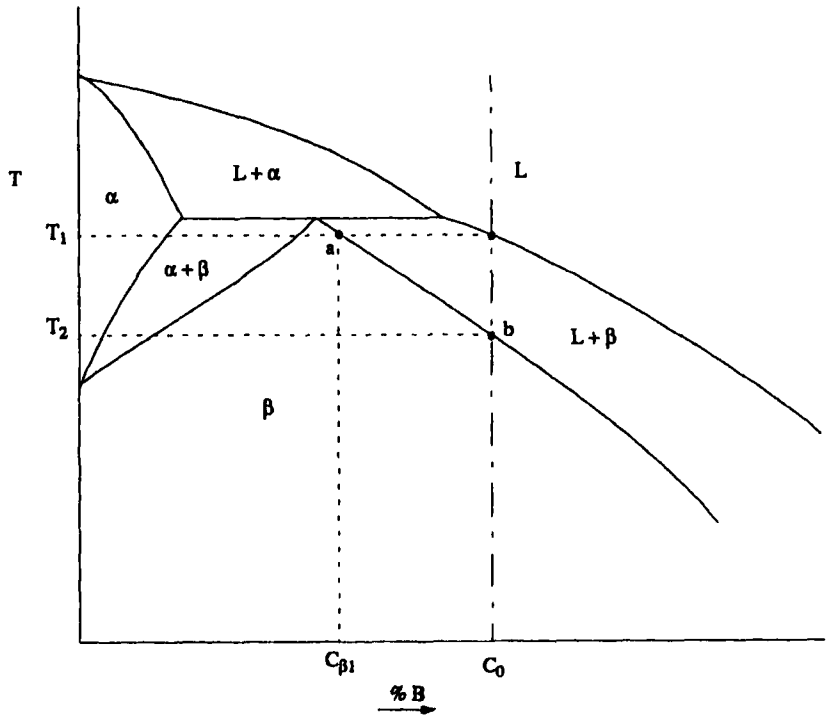


Figure 14.12 Hypothetical phase diagram showing just the region of a peritectic reaction, where liquid + $\alpha > \beta$ on cooling. Here, an alloy with nominal composition C_0 to the right of the L + α range, in the all liquid range, is treated.

process, especially in welds. For this reason, as in Section 13.4, the peritectic reaction must also be considered under nonequilibrium conditions. Once again, as in Section 13.4, two different sets of boundary conditions can be considered to represent the situation in nonequilibrium solidification, case 2 and case 3, as defined in Section 13.4.1. Let's follow the same path here for the peritectic reaction.

14.2.2.1. No Diffusion in the Solid/Complete Mixing in the Liquid (Case 2). Consider alloy C_0 in Figure 14.13. The first solid forms at T_1 of composition C_S from liquid of composition C_0. Since no diffusion of B is allowed in the solid, line *ac* represents the locus of average composition of solid (as was previously described for a solid solution in Section 13.4.1). Thus, when temperature T_2 is reached, the average composition of the solid is less rich in B than C_0 (shown by point *e*), and, so, some liquid of composition C_L still remains. Note that the composition of the solid in contact with the liquid is at all times given by line *ad*, and the composition of the remaining liquid is at all times given by the line *af*.

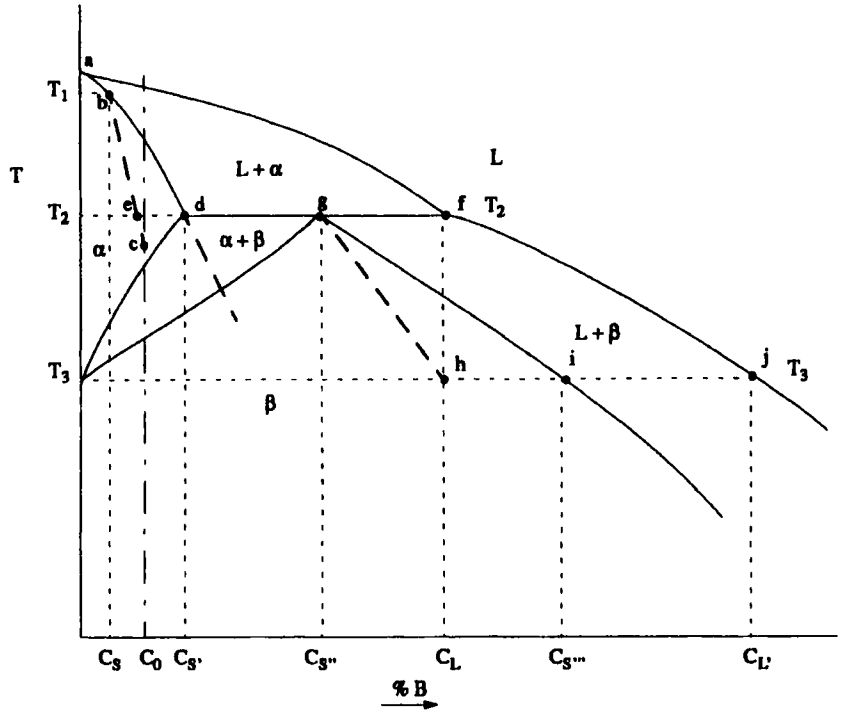


Figure 14.13 Hypothetical phase diagram showing just the region of a peritectic reaction, where liquid + $\alpha > \beta$ on cooling. Here, an alloy with nominal composition C_0 is considered to be solidifying under nonequilibrium conditions where there is assumed to be no diffusion in the solid and complete mixing in the liquid (i.e., case 2).

At temperature T_2, an infinitesimally thin layer of β of composition $C_{S''}$ forms on the surface of the existing α. This walls off the solid α from the liquid, however, and, so, prevents further peritectic reaction from occurring by $L + \alpha > \beta$. The remaining liquid then transforms directly to β as would any solid solution alloy. The instantaneous composition of the solid β and liquid in contact with it below T_2 are given by *gi* and *fj*, respectively. The average composition of the solid β is given by line *gh* (constructed such that $gf = hi$), and the last solid forms with composition $C_{S'''}$ from liquid of composition $C_{L'}$ at temperature T_3. Thus, the alloy is not completely solid until temperature T_3, which is considerably below the peritectic temperature. Note also that if no diffusion is allowed, the α formed on cooling from T_1 to T_2 is retained as a supersaturated solid solution, and the alloy at T_3 would consist of (1) particles of α ranging from C_S at their center to $C_{S'}$ at their surface, and each particle would be surrounded by a thin film of β of composition $C_{S''}$; and (2) the space between the α particles would consist of β ranging in composition from $C_{S''}$ to $C_{S'''}$ which formed from the last remaining liquid.

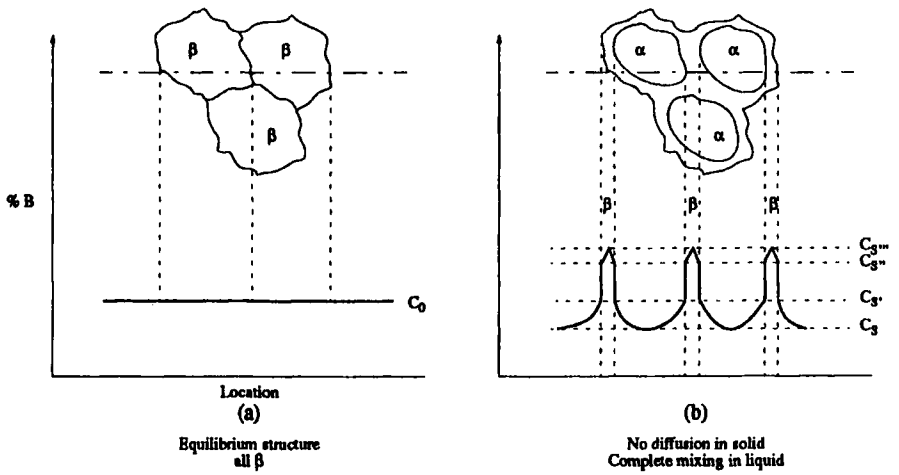


Figure 14.14 Schematic comparison of the structures formed under conditions of (a) equilibrium versus (b) nonequilibrium as defined by case 2.

Compare this nonequilibrium situation with the equilibrium situation described in the previous subsection, using Figure 14.14. Note that the alloys described in Sections 14.2.1.1–14.2.1.4 would all consist of α and β when solidified under conditions permitting complete mixing in the liquid and no diffusion in the solid. However, the amount of α produced decreases as the amount of β increases in the original alloy. Thus, the richer the alloy is in solute, the sooner the composition of the liquid reaches the point where β can form directly from the liquid. For this situation, the concentration gradients for alloys such as described in Section 14.2.1.4 might look like the structure shown schematically in Figure 14.15.

14.2.2.2. No Diffusion in the Solid/No Mixing, Only Diffusion in the Liquid (Case 3). Doc Savage said in his lectures and stated in his infamous mimeo-notes: "In the interest of our collective sanity, I shall not attempt to consider the peritectic for case 3, where there is no diffusion in the solid and no mixing in the liquid. In fact, no one really knows what happens in this case." It is no exaggeration to say that if Doc didn't know, no one knew! In reality, real peritectic reactions take place somewhere between the boundary conditions of case 2 and case 3, which explains some of the problems encountered in welding, no less understanding, peritectic alloys in commercial practice.

14.3. TRANSFORMATIONS IN FERRITE + AUSTENITE OR DUPLEX STAINLESS STEELS

Fully austenitic stainless steels based on 18 wt% Cr and 10 wt% Ni (or 18–10 types) are particularly prone to solidification hot cracking during fusion

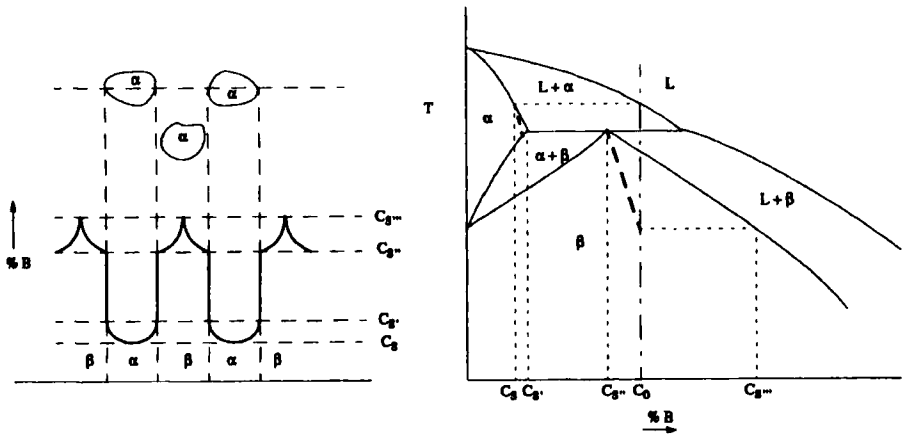


Figure 14.15 Schematic representation of the structure of an alloy rich in solute, as described in Section 14.1.1.4, but for nonequilibrium under case 2.

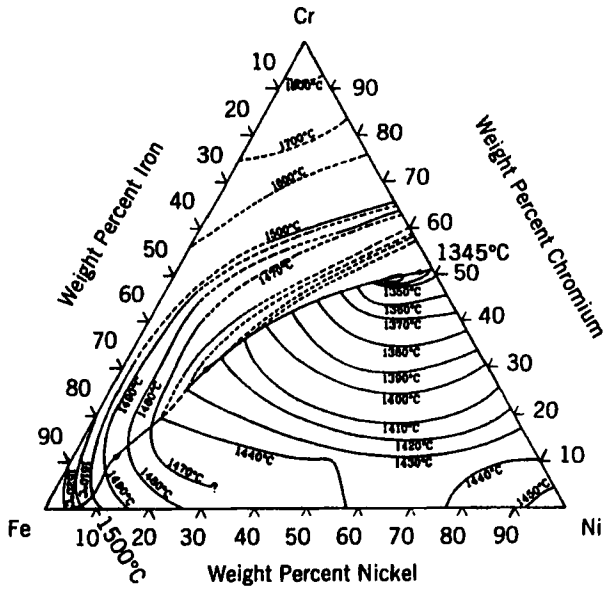
welding. This is largely the result of segregation of residual elements or impurities such as P and S to form low-melting constituents at grain boundaries in the austenite. A common, successful remedy is to employ a filler that contains 5–10 vol% δ-ferrite as the result of added ferrite stabilizers[1] (principally Cr, but also Mo). The fine dispersion of δ-ferrite as a second phase within the austenite produces a *duplex, ferrite + austenite structure.* This increases interphase boundary area, thereby lowering the concentration of these segregates to below the threshold that causes a continuous film of liquid to form and render the structure crack sensitive.[2] The duplex, ferrite + austenite, structure in stainless steels derives from the solidification characteristics of Fe-Cr-Ni alloys.[3] However, solidification of such duplex alloys is somewhat complex, and so deserves some discussion.

By referring to what is known as a pseudobinary phase diagram for Fe-Cr-Ni alloys, the source of the complex nature of solidification of duplex stainless steels can be seen. The pseudobinary diagram is a vertical slice or section of the full ternary phase diagram for the Fe-Cr-Ni system at some composition of interest. The full Fe-Cr-Ni (really, Cr-Fe-Ni, which is identical) ternary is shown in Figure 14.16, with the liquidus and solidus surfaces shown

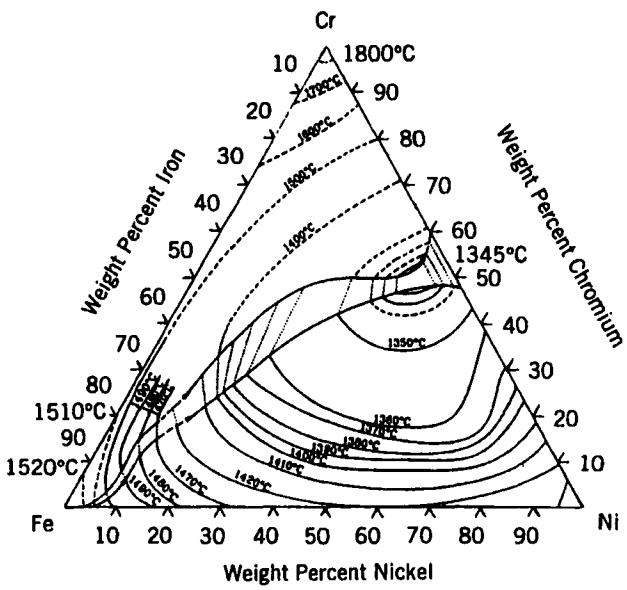
[1] Solute additions that stabilize the body-centered cubic δ-ferrite phase in steels themselves have body-centered cubic crystal structures and include Cr, Mo, Nb, W, and V. Solute additions that stabilize the face-centered cubic austenite phase in steels themselves have face-centered cubic crystal structures and include Ni and Mn. Diamond-cubic Si also stabilizes δ-ferrite, while carbon (C) and nitrogen (N) are potent austenite stabilizers. Development of ferritic versus austenitic stainless steels relies on preferential stabilization of δ-ferrite or austenite, respectively.

[2] δ-ferrite (as well as α-ferrite, the virtually identical and far more common, room-temperature form of iron and steel) also scavenges P and S, taking them into solution, where they are harmless.

[3] In fact, duplex, ferrite + austenite stainless steels are now produced as base metals, and enjoy great success in certain applications.



(a)



(b)

Figure 14.16 Ternary phase diagram for the Cr-Fe-Ni system, showing (a) the liquidus and (b) solidus surfaces. (From *ASM Handbook*, Vol. 3: *Alloy Phase Diagrams*, published in 1993 by and used with permission of the ASM International, Materials Park, OH.)

in (a) and (b), respectively. For 18–10-type alloys, a vertical section at 70 wt% Fe (or close to that) is commonly used, as shown in Figure 14.17. Opposing ranges of Cr and Ni content are shown at the bottom, along the horizontal axis of the pseudobinary, where the sum of Cr + Ni is 30 wt% at any point (70 wt% Fe plus 30 wt% Cr + Ni = 100 wt%). Ternary compositions richer in Cr, a ferrite stabilizer, tend toward the δ-ferrite (δ) or α-ferrite (α) or, simply, ferrite structure. Compositions richer in Ni, an austenite stabilizer, tend toward the austenite or γ structure.

For ternary alloys with compositions that fall between the end points of the bottom (horizontal) side of the triangular region of L + γ + δ in Figure 14.17, typified by the ferrite-containing fillers referred to earlier, solidification leads to δ-ferrite + austenite, but with either δ-ferrite or austenite solidifying first, depending on the precise (Cr + Ni) composition. That is, sometimes δ-ferrite forms first and then transforms to austenite on cooling, while other times austenite forms immediately upon solidification. If solidification initiates as

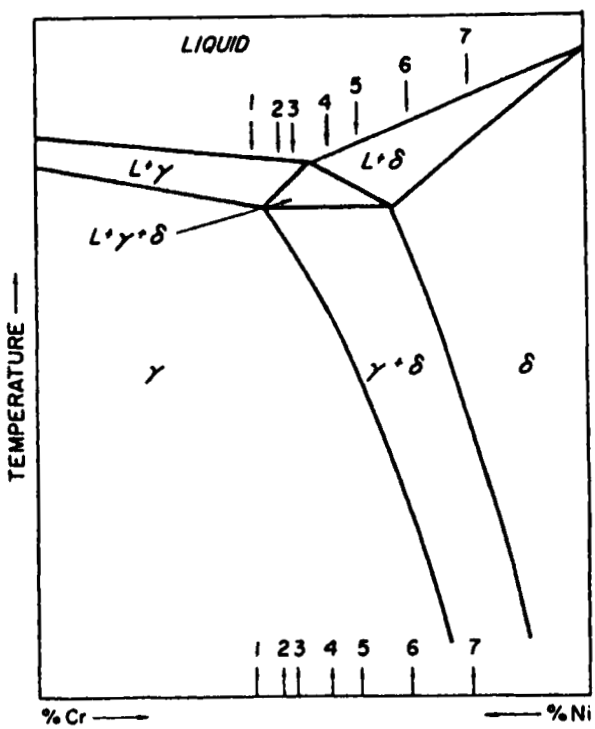


Figure 14.17 Pseudobinary phase diagram obtained from a vertical slice or section through the Cr-Fe-Ni ternary diagram in 14.16 at a (Cr + Ni) content of 30 wt%. (From "Weldability and solidification phenomena of cast stainless steel" by M. J. Cieslak and W. F. Savage, *Welding Journal*, **59**(5), 136s–146s, 1980, published by and used with permission of the American Welding Society, Miami, FL.)

δ-ferrite, it is said to be primary delta solidification; if it initiates as austenite, it is said to be primary austenite solidification. Strictly speaking, the first phase formed is, in fact, determined by the structure of the base metal at its melting point, not by the filler metal or diluted weld metal composition, the reason being that weld solidification is initially epitaxial. Thus, if the base metal is austenite, the initial growth structure is also austenite. The duplex structure is expected to develop during the planar-to-cellular growth breakdown stage.

The three-phase eutectic triangle containing $L + \gamma + \delta$ is obtained by connecting the three intersections between the vertical section (at 70 wt% Fe) and the heavy curved lines on the liquidus and solidus surfaces of the ternary diagram (Figure 14.16). For alloys that lie to the Ni-rich (left) side of the apex of the three-phase eutectic triangle, γ-austenite is the primary solidification phase. For such alloys, grains or dendrites of austenite form, with δ-ferrite (δ) developing along grain or dendrite boundaries during the final stage of solidification.

For alloys that lie to the Cr-rich (right) side of the apex of the three-phase eutectic triangle, on the other hand, δ-ferrite is the primary solidification phase. For such alloys, δ-ferrite is at the core of dendrites, which form at the start of solidification, and the core is very rich in Cr. As solidification proceeds, the outer portions of these dendrites have lower Cr contents. When the temperature drops to the point that the three-phase eutectic region is entered, austenite begins to form at boundaries among the δ-ferrite dendrites. Upon cooling to below the solidification range into the $\delta+\gamma$ and then γ regions, the outer portions of the dendrites transform to austenite as a result of their lower Cr content, leaving behind "skeletons" of δ-ferrite at the dendrite cores. This same gradient in Cr content that renders the interdendritic boundaries Cr-lean can lead to preferential corrosive intergranular (really, interdendritic) attack in the weld.

Very detailed discussions of the morphology of δ-ferrite in austenitic stainless steels appear in several excellent papers by Cieslak and Savage (1980), David (1981), Okagawa et al. (1983), and Brooks and Thompson (1991). Figure 14.18 shows typical microstructures for various compositions and solidification modes from Cieslak and Savage (1980), while Figure 14.19 schematically illustrates solidification and transformation behavior resulting in a range of ferrite morphologies in austenitic stainless steel welds from Brooks and Thompson (1991).

The resulting structure of duplex stainless steel fillers or base metals was made less complicated and quantitative, first by Schaeffler (1949) and then by Delong (1974), and, most recently, by the WRC (1992). Figures 14.20a and b and 14.21 are constitution diagrams by Schaeffler, DeLong, and the WRC, respectively. These each show the relationship between the δ-ferrite content and the weld metal composition for stainless steels, expressed as nickel-equivalent (for austenite stabilizers) on the vertical axis against chromium-equivalent (for ferrite stabilizers) on the horizontal axis. Austenite formers with

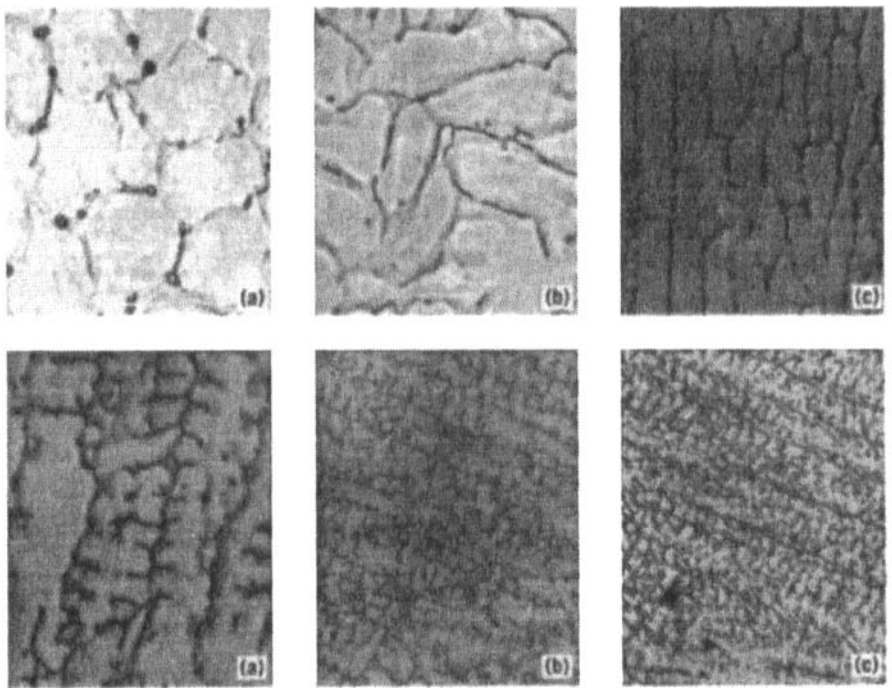


Figure 14.18 Photomicrographs of stainless steels with different compositions showing the different solidification structures that can result. Top row: (A) alloy 1, (B) alloy 2, (C) alloy 3; bottom row: (A) alloy 4, (B) alloy 5, and (C) alloy 6. (From "Weldability and solidification phenomena of cast stainless steel" by M. J. Cieslak and W. F. Savage, *Welding Journal*, **59**(5), 136s–146s, 1980, published by and used with permission of the American Welding Society, Miami, FL.)

various equivalencies to Ni (at 100%) include C and Mn. Ferrite formers with various equivalencies to Cr (at 100%) include Mo, Si, and Nb.[4] The DeLong diagram differs from the Schaeffler diagram in that nitrogen (N), a strong austenite stabilizer often added to offset strength losses associated with reduced C content to avoid sensitization (see Section 16.5), is included in the former. Nitrogen pickup, either from the air during inadequate shielding or from its addition to shielding gas, can significantly reduce the ferrite content of weld metal, as reported by Lundin et al. (1980), Cieslak et al. (1982), and Okagawa et al. (1983). The DeLong diagram also switched to the use of the WRC ferrite number (FN), which has proven to be far more reproducible than the ferrite content as a percentage, and is now acclaimed as the most accurate ferrite

[4] Niobium, Nb, is the modern, internationally accepted name for what was formerly called Columbium, Cb. Cb is sometimes still used instead of Nb, because it is on the original, Schaeffler and the DeLong diagrams.

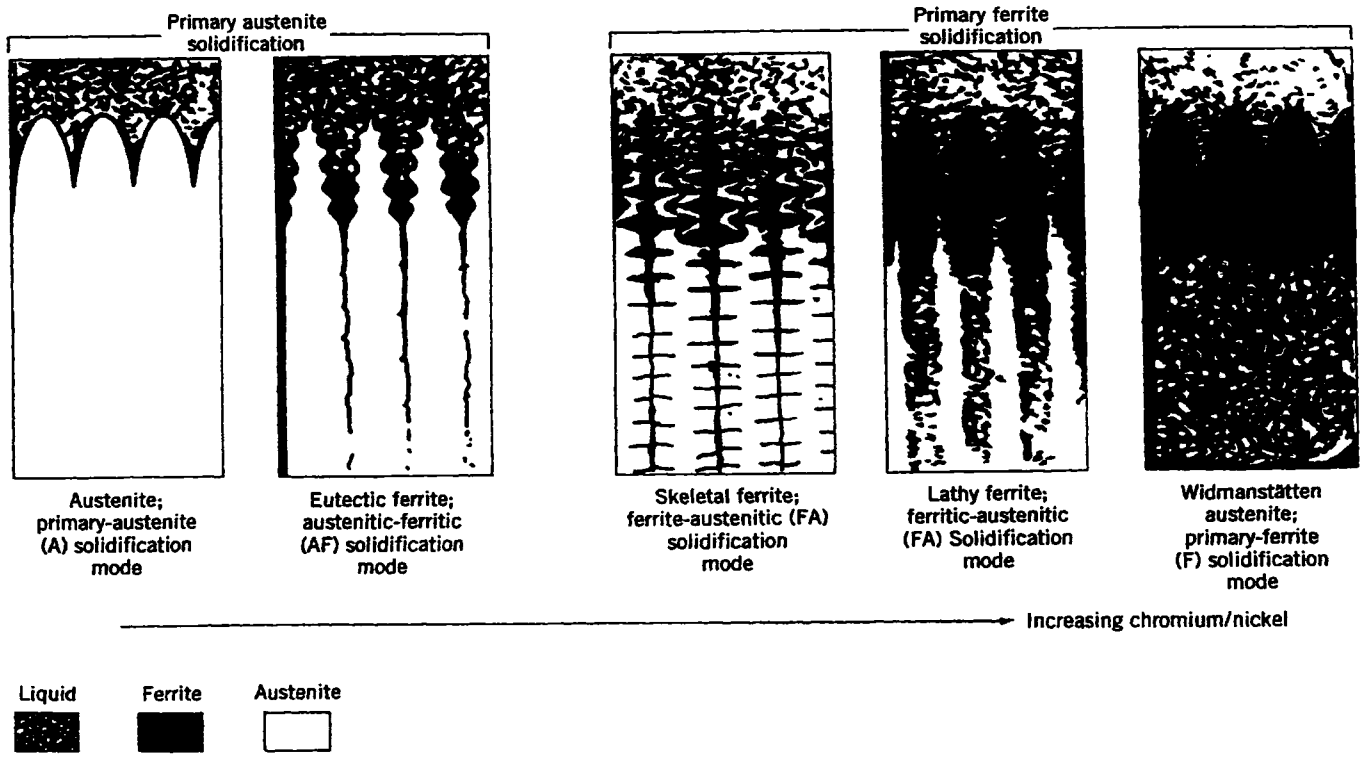
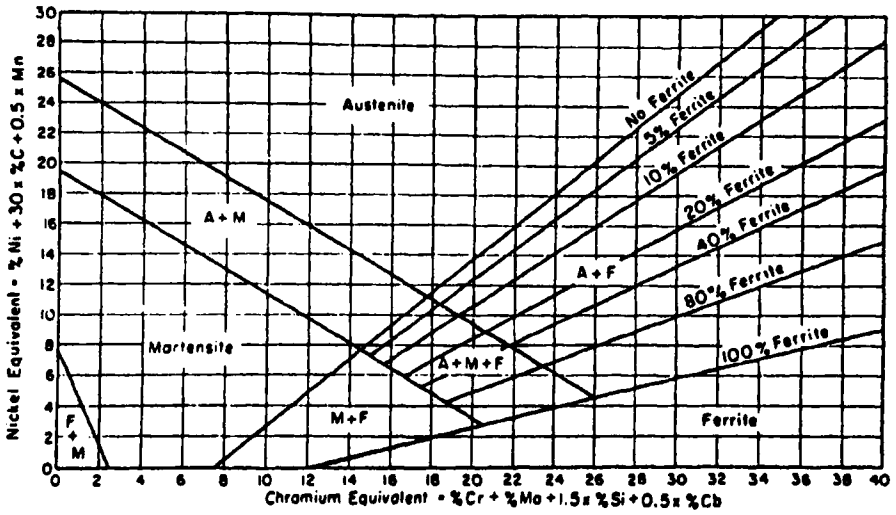
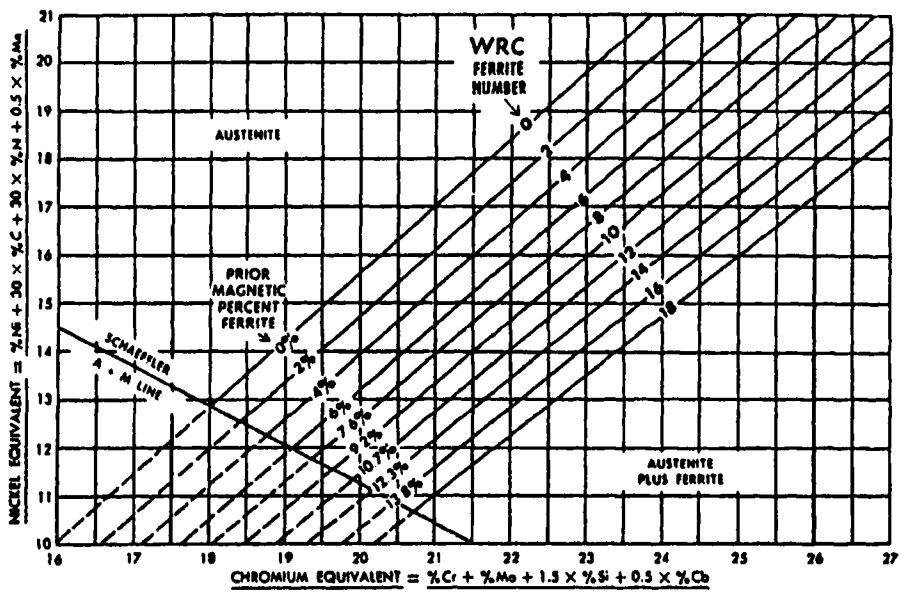


Figure 14.19 Schematic showing solidification and transformation behavior resulting in a range of ferrite morphologies in austenitic stainless steel welds. (Originally from "Microstructural development and solidification cracking susceptibility in austenitic stainless steel welds" by J. A. Brooks and A. W. Thompson, *International Materials Review*, **36**(1), 16–44, 1991, out of *ASM Handbook*, Vol. 6: *Welding, Brazing, and Soldering*, published in 1993 by and used with permission of ASM International, Materials Park, OH.)



(a)



(b)

Figure 14.20 Ferrite constitution diagrams developed by (a) Schaeffler (1949) and (b) Delong (1976) showing ferrite content (as percent) and ferrite number (FN), respectively, as a function of Cr- vs. Ni-equivalents. (After (a) A. L. Schaeffler, *Metals Progress*, **56**, 49, 1949, published by and used with permission of the ASM International, Materials Park, OH; and (b) W. T. DeLong, *Welding Journal*, **53**(7), 273s–286s, 1974, published by and used with permission of the American Welding Society, Miami, FL.)

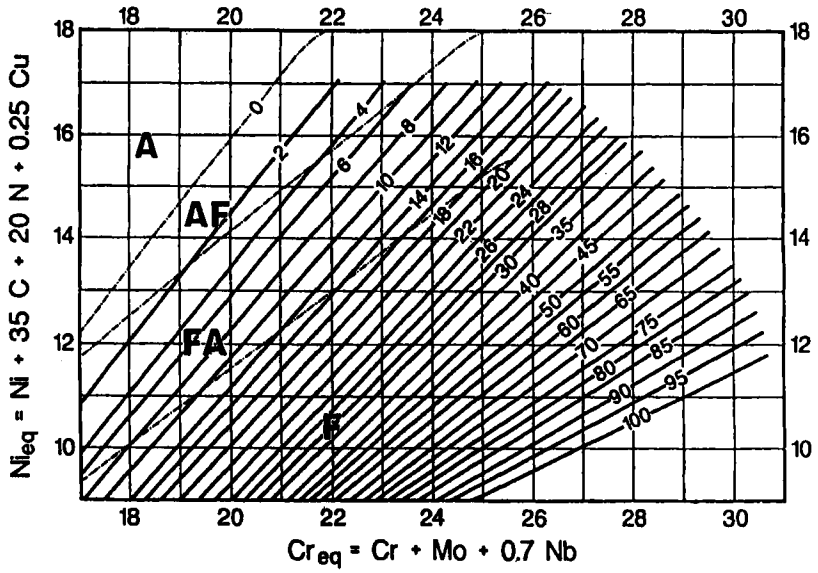


Figure 14.21 Ferrite constitution diagram developed by the WRC in 1992 showing ferrite number in weld metal during cooling and at ambient temperature. (From "WRC-1992 constitution diagram for stainless steel weld metals: a modification of the WRC-1988 diagram" by D. J. Kotecki and T. A. Siewert, *Welding Journal*, **71**(5), 171s–178s, 1992, published by and used with permission of the American Welding Society, Miami, FL.)

predictive constitution diagram.[5] The WRC 1992 diagram also incorporates the Ni-equivalent for Cu, an important minor alloying addition to many stainless steels to improve corrosion resistance to certain media (Thomas and Messler, 1997). Unlike the Schaeffler and DeLong diagrams, it shows the structures existing during solidification, as well as the ferrite, measured in FN, at ambient temperatures.

Use of the Schaeffler, DeLong, or WRC diagrams for predicting δ-ferrite content in the weld metal from weld metal composition is, unfortunately, not

[5]The problem with ferrite percentage is that different methods of measurement yield different results. While in much of the literature prior to 1970, the amount of ferrite is designated as a percentage, it has been aptly said: "No two people on the face of the planet can agree on a percent ferrite value for a weld. When ferrite is stated as a percent, that value must be interpreted based on how it was 'determined'. On the other hand, Ferrite Number (FN) can be determined with known precision" (Kotecki, 1996). The concept of ferrite number grew out of dissatisfaction with ferrite percent and the results of extensive round-robin measurements on numerous specimens, with results determined on constitution diagrams and by several different instruments. Most recently, correlations of FN have been able to be made to special international standards (Messler and Thomas, 1997).

completely reliable. Both solidification mode and the rate of postsolidification cooling to room temperature can affect the ferrite content in the weld (Lippold and Savage, 1979). These are, in turn, both sensitive to both the welding process and welding parameters. David et al. (1987) showed that high cooling rates (as encountered in laser welding) significantly alter the weld solidification structure, shifting the solidification mode from primary ferrite to primary austenite as cooling rate in increased.

In multipass welding, the heat of a subsequent pass can drastically alter the properties of weld metal deposited in an earlier pass (Lundin and Chou, 1985). Ferrite number and ductility are both lowered, increasing susceptibility to cracking under stress. The embrittled region is called the hazard HAZ. The explanation for the hazard HAZ in austenitic stainless steel welded with multiple passes, or where welds are repaired, is as follows: The heat of a subsequent weld pass dissolves δ-ferrite in the region of 1200°C. The higher the reheating temperature, the greater the dissolution of δ-ferrite. As the reheating temperature increases above the γ-solvus, δ-ferrite starts to reform. The higher the reheating temperature above the γ-solvus, the greater the reformation of δ-ferrite. The result is a region of low δ-ferrite a short distance away from the fusion zone of the later pass. It is believed elements such as S, P, and Si, known to promote hot cracking and normally having higher solubility in δ-ferrite than austenite, are released during the dissolution of δ-ferrite. Once released, these solutes are free to migrate to austenite/austenite grain boundaries, form low-melting or simply brittle constituents, and degrade ductility and promote fissuring.

14.4. KINETICS OF SOLID-STATE PHASE TRANSFORMATIONS: NONEQUILIBRIUM VERSUS EQUILIBRIUM

Rapid cooling rates following fusion welding mean that postsolidification transformations involving solid phases, not just solidification, can occur under nonequilibrium conditions to a greater or lesser extent, depending on process, operating parameters, and procedures. As a result, equilibrium phases or constituents are altered, either in morphology and distribution or form, which includes metastable types.

Just as for the formation of new solid phase from a liquid phase, a new daughter solid phase must nucleate from an original parent solid phase. This nucleation, as for the solid from liquid (Section 13.2.1), requires a certain minimum energy as a driving force to accommodate or offset the surface energy of the new phase boundary. For solid-state transformations, it is also necessary to accommodate strain energy caused by the daughter phase within the parent phase, when the specific (or per unit mass) volumes as well as the crystal structures and lattice parameters of the two phases are different, whether

smaller or larger.[6] This is expressed in the relationship

$$\Delta G \geqslant -\Delta G_v + \Delta G_s + \Delta G_E - \Delta G_D \tag{14.2}$$

where ΔG is the molar free energy for the transformation, ΔG_v is the chemical volume free energy of the nucleus of the new phase and is negative because it assists the transformation, ΔG_s is the increase in surface free energy between daughter and parent phase, and ΔG_E is the increase in strain energy due to the lattice dilatation (expansion or contraction) involved. For two solid phases, the relationship between the two molar free energies is shown in Figure 14.22. T_0 in Figure 14.22 refers to the temperature at which the free energy of the two phases is equal. ΔG_D in Eq. 14.2 implies that the transformation is heterogeneous and refers to the energy donated to nucleation by an existing heterogeneity in the high temperature (parent) phase (e.g., a grain boundary). ΔT in Figure 14.22 refers to the undercooling below T_0 needed for ΔG to become sufficiently large for the new phase to nucleate.

Since some rearrangement of solute atoms, often by diffusion, is needed before the nucleus has the structure and composition and stable size (critical radius) appropriate to the new phase, and because this rearrangement requires some time, it is clear that ΔT depends on the cooling rate of the alloy, needing to be greater for faster cooling rates.

To see how ΔT is related to the nucleus size and to ΔG, consider a new phase β nucleating on the grain boundary of α, as shown in Figure 14.23. The nucleus of β tries to adjust its shape to minimize surface energy (ΔG_s), provided the strain energy term (ΔG_E) is negligible, as it tends to be for diffusion-controlled processes. The optimum shape if the α/β interphase boundary is incoherent[7] is described by

$$\cos \Psi = \frac{\gamma_{\alpha/\alpha}}{2\gamma_{\beta/\alpha}} \tag{14.3}$$

[6] If interatomic bonds are viewed as springs connecting the two adjacent atoms, a strain is introduced and (strain) energy is stored whether those springs (bonds) are forced to compress to accommodate a larger near neighbor or stretch to accommodate a smaller near neighbor.

[7] An incoherent interface is one where the crystal structures and/or lattice parameters of solid parent and daughter phases are so different that for one to distort to attempt to match the other is impossible. Consequently, there is virtually no lattice matching across an incoherent interface. With no attempt of one to match the other, there is no accommodation and no strain energy associated with this interface. In a coherent interface, the crystal structures and/or lattice parameters of the solid parent and daughter phases are so closely matched that planes of one are easily able to adjust and distort to match the other. Consequently, there is complete lattice matching across a coherent interface, but at the cost of strain energy stored in the distorted region. A semicoherent interface is somewhere between these two extremes; that is, there is partial lattice matching across the interface and some stored energy.

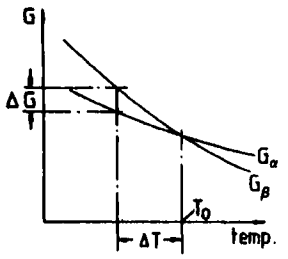


Figure 14.22 Relationship between the molar free energies of two solid phases: the higher temperature parent phase (α), and the lower temperature daughter phase (β). (From *Introduction to the Physical Metallurgy of Welding*, 2d ed., by K. Easterling, published in 1992 by Butterworth-Heinemann, Oxford, UK, and used with permission of the Easterling family.)

where $\gamma_{\alpha/\alpha}$ and $\gamma_{\beta/\alpha}$ are the various surface energies between α and α and α and β. In fact, this equation can be derived from Young's equation (Eq. 13.26). As was shown in Eq. 13.18, the critical radius, r^*, of the embryo (or nucleus) for a new phase to become stable is

$$r^* = \frac{2\gamma_{\beta/\alpha}}{\Delta G_v} \tag{14.4}$$

If the interface between β and α is oriented so that it is coherent or semicoherent (as shown in Figure 14.23), and a low-energy orientation relationship exists between the two phases, then $\gamma_{\beta/\alpha}$ (coherent) $<$ $\gamma_{\beta/\alpha}$ (incoherent), and r^* can be correspondingly smaller.

Thus, the ability of any imperfection in a crystalline material to reduce ΔG

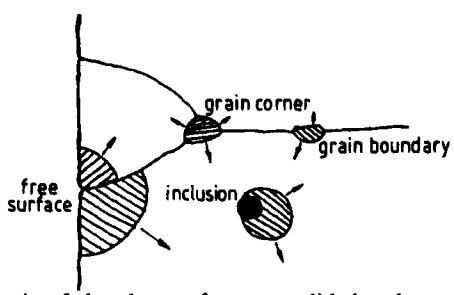


Figure 14.23 Schematic of the shape of a new solid daughter phase growing heterogeneously on a grain boundary of a solid parent phase shows that shape depends on the relative surface free energies. The situation is shown for (a) an incoherent particle of daughter phase and (b) a semicoherent particle of daughter phase. (From *Introduction to the Physical Metallurgy of Welding*, 2d ed., by K. Easterling, published in 1992 by Butterworth-Heinemann, Oxford, UK, and used with permission of the Easterling family.)

depends on its potency as a nucleation site, measured by the ratio of $\gamma_{\alpha/\alpha}/\gamma_{\beta/\alpha}$. The relative potency of various crystalline imperfections as nucleation sites is, in descending order,

1. free surface
2. grain corners (e.g., triple-points)
3. grain boundaries
4. inclusions
5. dislocations, including stacking faults (which are special dislocation pairs)
6. vacancy clusters

The overall proportion of a parent phase to transform to a daughter phase is not just a function of the potency of the nucleation site, however, but also depends on the number of sites available. If the concentration of nucleation sites available per unit volume of parent phase is C_1, then the nucleation rate N is given by

$$N = \nu C_1 \exp\frac{\Delta G_M}{kT} \exp\frac{\Delta G^*}{kT} \tag{14.5}$$

where N is in nuclei/m^3 s^{-1}, ν is the frequency of vibration of atoms, $\exp(\Delta G_M/kt)$ relates to the activation energy for atomic migration to occur (for rearrangement) to form a nucleus, k is Boltzmann's constant, and $\exp(\Delta G^*/kT)$ relates to the probability of creating a nucleus of critical size (r^*) during heterogeneous nucleation. The rate of nucleation thus follows a C-shaped curve. The rate is low just below the equilibrium transformation temperature because the driving force for formation of a lower energy phase is small. Rate increases with further cooling due to the increased driving force provided by greater undercooling. Finally, the rate decreases again since needed rearrangement becomes increasingly more difficult as the rate of diffusion drops exponentially, despite a tremendous driving force for the transformation.

When the rate of nucleation (N) and the rate of growth (G) of a phase are considered, the overall transformation rate also follows a C-curve. This is because the overall rate is the product of the rates of nucleation and growth, the former having a C-shape and the latter decreasing exponentially with temperature just as the diffusion rate does. The relationship between the driving force to cause transformation or phase instability, the rate of diffusion, and the nucleation rate is shown in Figure 14.24. The relationship between overall transformation rate and the rates of nucleation (N) and growth (G) is shown in Figure 14.25. The net rates for a transformation to be 1 and 99% complete, as well as the fraction transformed at two temperatures, T_1 and T_2, are shown in Figure 14.26. The latter behavior is said to follow an Avrami

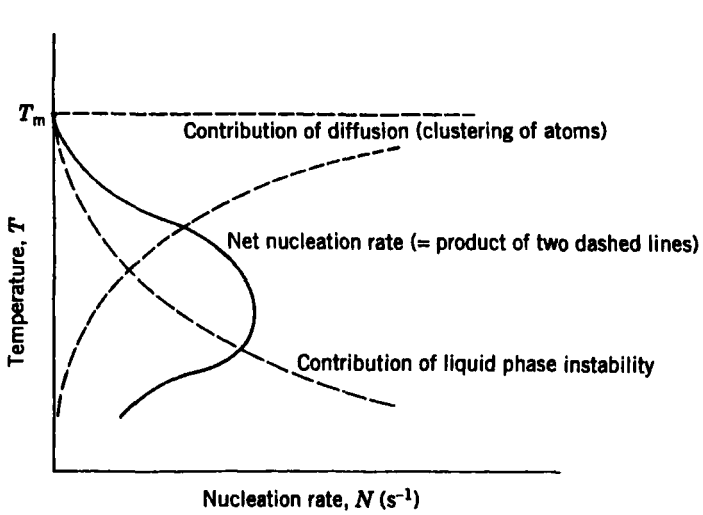


Figure 14.24 The dependence of the rate of nucleation (N) on the driving force for a new phase to form (i.e., phase instability) (I) and the rate of diffusion (D) for atomic rearrangement is shown. A C-shape curve results. (From *Materials Science & Engineering*, 4th ed., by W. D. Callister, published in 1997 by and used with permission of John Wiley & Sons, Inc., New York.)

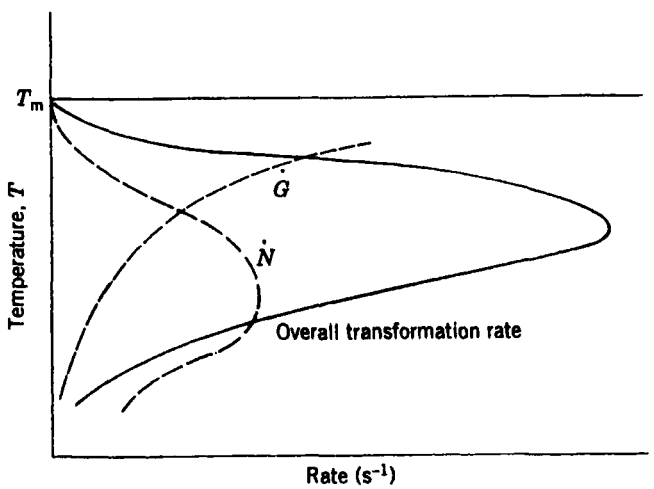


Figure 14.25 The overall transformation rate is the product of the nucleation rate (N) and the growth rate (G), which depends on the rate of diffusion, and also follows a "C-curve." (From *Materials Science & Engineering*, 4th ed., by W. D. Callister, published in 1997 by and used with permission of John Wiley & Sons, Inc., New York.)

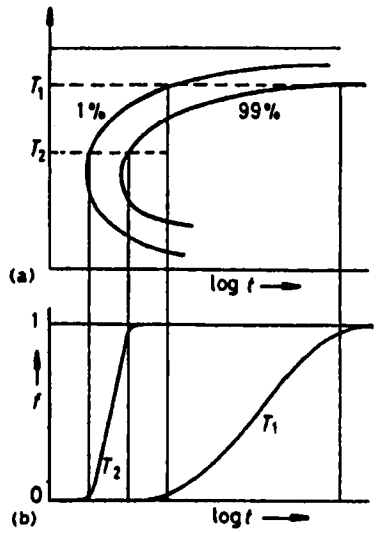


Figure 14.26 The net rate for a transformation to be 1 and 99% complete (a) and the fraction transformed (b). (From *Introduction to the Physical Metallurgy of Welding*, 2d ed., by K. Easterling, published in 1992 by Butterworth-Heinemann, Oxford, UK, and used with permission of the Easterling family.)

relationship, where

$$\text{fraction transformed } y = 1 - \exp(-kt^n) \tag{14.6}$$

where k and n are time-independent constants for the particular reaction, with n varying between 1 and 4, depending on the type of nucleation involved. By convention, the rate of transformation is taken as the reciprocal of the time required for the transformation to proceed halfway to completion.

Many solid-state transformations that depend on nucleation and growth follow an Avrami relationship, including recrystallization, precipitation, and decomposition of austenite to various products. (In fact, human population also follows an Avrami relationship: When there are very few people, no amount of procreation has much of an effect on the population, and at some point the population begins to saturate as resources needed to sustain that population are not available.)

If the rate of cooling is increased, other types of transformation product can develop, based on different morphologies, different modes of growth, different compositions, or different lattice structures. Each product has its own characteristic C-curve. A classic example is shown in Figure 14.27 for the continuous

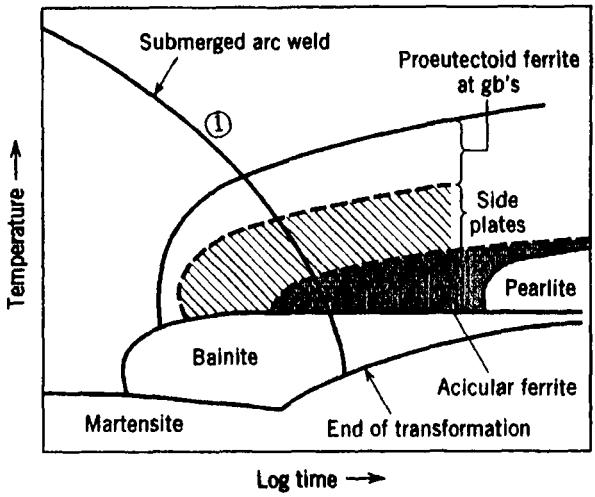


Figure 14.27 Schematic continuous cooling transformation (CCT) diagram for a typical steel weld showing the variety of different transformation products that can result, depending on cooling rate. (From *Introduction to the Physical Metallurgy of Welding*, 2d ed., by K. Easterling, published in 1992 by Butterworth-Heinemann, Oxford, UK, and used with permission of the Easterling family.)

cooling transformation (CCT) curves for a steel weld metal, in which austenite can decompose or transform to any of several different products.[8] It can be seen that the peak rate or minimum time for transformation for each product's transformation is simply displaced to lower temperatures.

The final volume fraction of various possible transformation products is determined by the rate of nucleation, the rate of growth, the density and distribution of nucleation sites, the overlap of diffusion fields from adjacent products, and the physical impingement of adjacent volumes of product. Another important factor in weld metals, however, is the initial columnar grain size from which transformation products must form. The problem is defining a grain size from a columnar dendrite, given that grains are normally equiaxed and columnar dendrites are long and relatively thin (i.e., they have very

[8] Continuous cooling transformation (CCT) diagrams denote transformations that occur in samples that are cooled to progressively lower temperatures without interruption by continuous extraction of heat into a quenching medium. Continuous cooling by quenching is far more common than isothermal transformation, in which a sample is quenched into a medium at a particular (normally elevated) temperature, forced to cool quickly to that temperature, and then held at that temperature to allow transformation(s) to take place strictly as a function of time. Such transformation is called time–temperature transformation and generates TTT curves. The use of CCT diagrams is clearly more appropriate to the development of solidification structure in and immediately surrounding welds.

high length-to-width aspect ratios). What is usually done is to use an equivalent or effective grain size obtained from regression equations that include composition and heat input terms. One example presented in Easterling (1992) is

$$\bar{d}\text{columnar (in mm)} = 64.5 - 445.8(\text{wt\% C}) + 139(\text{wt\% Si}) - 7.6(\text{wt\% Mn}) + 16(\text{heat input, kJ/mm}) \tag{14.7}$$

The effect of initial (columnar) grain size is to displace the cooling rate curves in CCT diagrams to the right or left a large grain size increasing hardenability and shifting the curve to the left to shorter transformation times.

Under some processing conditions, the rate of cooling is so rapid that there is not enough time for the long-range rearrangement of solute atoms by either vacancy or interstitial diffusion to allow a new phase to nucleate and grow. Nevertheless, the new phase is energetically favored (i.e., its molar chemical free energy is lower than that of the parent), progressively so for greater and greater supercooling. Thus, there is still a strong driving force for transformation. When this is the case, there is sometimes still a possibility for transformation to an intermittent, metastable phase, provided this intermittent phase can be obtained by a diffusionless transformation relying on shear to rearrange atoms. For such transformations, no single atom moves more than one lattice spacing. The daughter phase thus has the same composition as the parent phase, but a different crystal structure. The best-known example of a diffusionless shear transformation is the martensite transformation that occurs in the Fe-C system, as well as in some other alloy systems.

In martensite formation, the parent austenite phase shears, in one or two directions, to form a new lattice that is coherent with the parent lattice. For ferrous martensite, the face-centered cubic (fcc) austenite lattice tries to shear to the body-centered cubic (bcc) α-ferrite lattice, but becomes stuck at an intermittent point. Carbon in solution in the austenite and occupying six-fold octahedral interstitial sites at the midpoint of cube edges in the fcc lattice not only is unable to precipitate out (due to lower solubility) and form Fe_3C cementite particles, but is unable to move to favored six-fold octahedral interstitial sites at the center of faces of the bcc lattice of ferrite. Instead, it becomes stuck along the cube edges in the new bcc lattice obtained by shear. In these sites, the carbon causes considerable distortion of the cube in one direction, resulting in a body-centered tetragonal (bct) lattice. This severe lattice strain results in significant strengthening due to the effect on the strain field of dislocations attempting to cause slip-based plastic deformation, but also pronounced brittleness. The resulting martensite is supersaturated with carbon and severely distorted.

In time, the carbon atoms stuck in solution in unfavorable sites will rearrange to preferred, equilibrium six-fold sites and allow the distorted lattice

to relax and the martensite to become softer and less brittle. This process is called tempering and can be accelerated by raising the temperature of the martensite during a *tempering heat treatment* process. Such tempering greatly reduces the likelihood of cracking and dramatically reduces susceptibility to hydrogen cracking that plagues untempered martensite. The resulting product is called tempered martensite. In equilibrium, of course, tempering goes too far, and all strength is lost as a mixture of normal α-ferrite and Fe_3C cementite results. The objective in tempering is to reduce brittleness only as much as necessary to maintain as high a strength or hardness as possible.

There are several variations of the martensite morphology, including plate, lath, and needle types. Each has a slightly different common or "habit" plane with the parent austenite and each arises from slightly different conditions of nucleation and growth, but all have fairly similar macroscopic properties.

14.5. AUSTENITE DECOMPOSITION TRANSFORMATIONS

Under equilibrium conditions, austenite will revert or decompose to α-ferrite and Fe_3C cementite or, simply, iron carbide, when it is cooled. Under nonequilibrium conditions, the mode of distribution of the hard carbide constituent in the inherently soft α-ferrite changes, until for very high cooling rates formation of the carbide as a precipitate is suppressed. As each particular distribution results in a different structure, so too does each result in different mechanical properties of strength, hardness, ductility, and toughness. During heat treatment, cooling conditions are controlled to control the final products of austenite decomposition, and, thus, the final properties. For other processes, such as hot rolling, forging, or welding, the cooling conditions are either not controlled or not controlled as well. For these processes, the final structure (and, thus, properties) are the result of a more or less automatically determined rate of cooling dictated by the mass of the material being cooled and the environment in which it is being cooled. While technically this is not heat treatment, metallurgically it is, because in practice it is reproducible.

When carbon steels are cooled at exceeding slow rates (a few degrees per hour), the transformation of austenite will occur nearly in accord with the equilibrium diagram (within 5–10°), an applicable portion of which is shown in Figure 14.28. With increased rates of heating or cooling, a lag in the transformations occurs, as shown in Figure 14.29. Faster and faster heating and cooling rates cause greater and greater lags. The structure is equally influenced by the rate of cooling, and, after all, it is the structure in which we are interested.

The decomposition of the solid-solution austenite does not begin instantly when its temperature is lowered. Instead, there is a definite lag until nuclei of the new phase have a chance to form. The degree of undercooling required to cause the transformation to occur depends on the rate of cooling, needing to

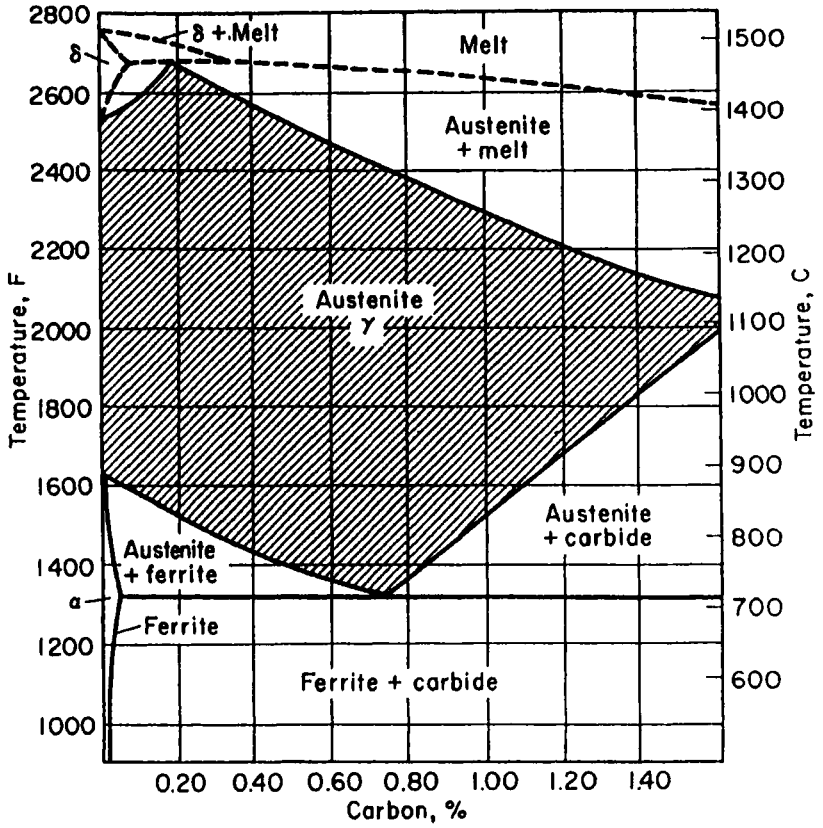


Figure 14.28 The austenite region in carbon steels, alone with regions of ferrite and other phases. (From *Alloying Elements in Steel*, by E. C. Bain and H. W. Paxton, published in 1966 by American Society for Metals, Metals Park, OH, and used with permission of the ASM International, Materials Park, OH.)

be greater for faster cooling. When a new austenite decomposes on cooling, the decomposition phases are always (or, in the case of martensite, are always trying to be) α-ferrite and carbide. The form and distribution of the carbide differs, however, as does the morphology of the ferrite. The result of these different structural arrangements of otherwise identical phases is different properties. In general, the carbide can appear as films, filaments, or particles, each having a very different effect on properties, just as different arrangements (e.g., small balls, fine wires, large-diameter reinforcing bars) of steel in cement lead to different properties in reinforced concrete.

Let's look at the various possible products of decomposition of austenite, first under conditions of equilibrium and then under conditions that deviate more and more from equilibrium.

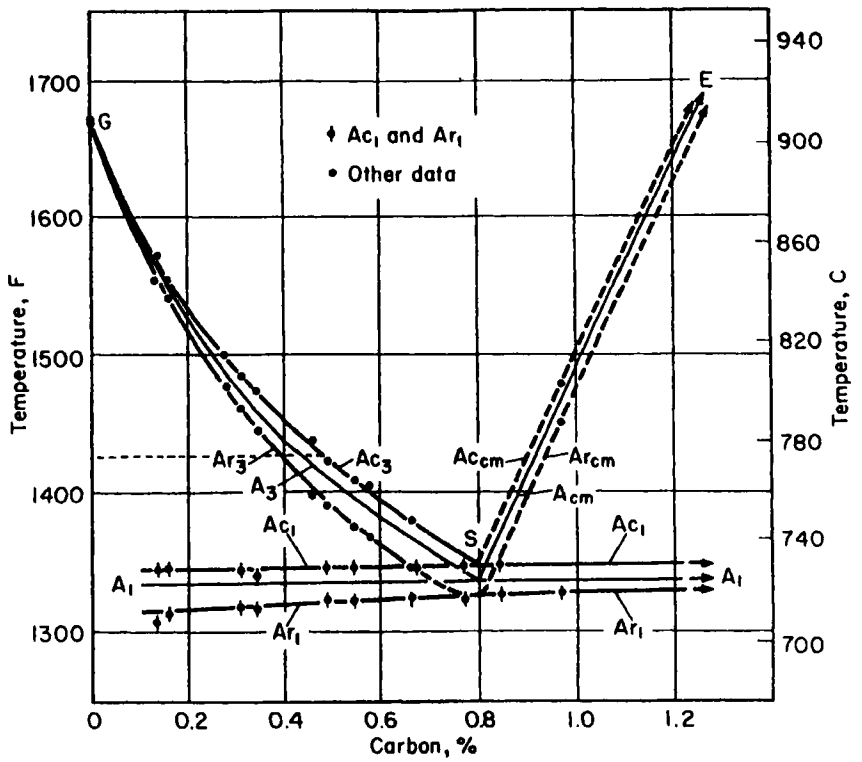


Figure 14.29 The effect of 0.125°C per minute heating (subscript c) and cooling (subscript r) rate on the transformation temperatures of pure Fe-C alloys (after Mehl and Wells, 1937). Faster rates would have greater effects, but in the same general directions. (From *Alloying Elements in Steel*, by E. C. Bain and H. W. Paxton, published in 1966 by American Society for Metals, Metals Park, OH, and used with permission of the ASM International, Materials Park, OH.)

14.5.1. Equilibrium Decomposition to Ferrite + Pearlite (The Eutectoid Reaction)

Under infinitesimally slow rates of cooling, regardless of the nominal composition of the starting alloy and austenite, once a temperature of 727°C is reached, all of the remaining austenite transforms by a solid-state reaction called an eutectoid reaction. Generically, an *eutectoid reaction* involves a solid phase transforming to two new solid phases upon cooling: $S_1 \rightarrow S_2 + S_3$. The reaction is reversible on heating, and takes place at an *eutectoid temperature* and *eutectoid composition*. In the Fe-C system, the eutectoid transformation that occurs on cooling to below 727°C is called the *pearlite transformation*, with the reaction that occurs being γ-austenite $\rightarrow$ α-ferrite + Fe_3C cementite as an intimate mixture of the two phases forming a constituent called *pearlite*. Prior

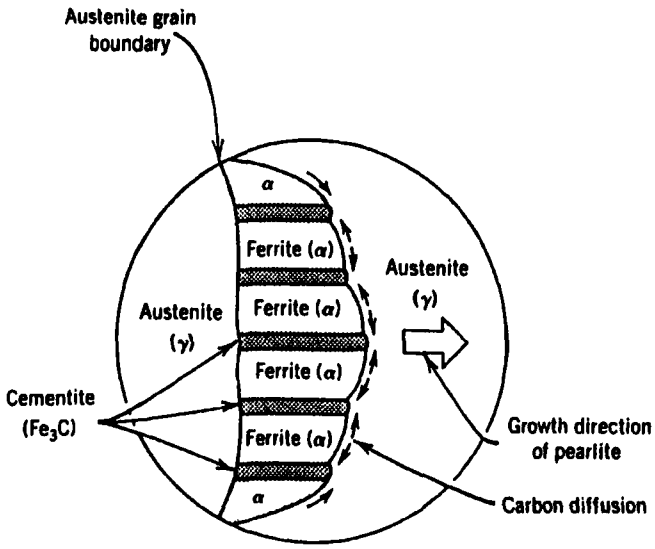


Figure 14.30 Schematic of the growth of the eutectoid in the Fe-C system, showing both forward and sideways growth of lamellae, starting with the nucleation of ferrite heterogeneously at high-energy sites. (From *Materials Science & Engineering*, by W. D. Callister, published in 1985 by and used with permission of John Wiley & Sons, Inc., New York.)

to the eutectoid reaction or transformation, either α-ferrite or Fe_3C cementite will form from the austenite by diffusion, depending on whether the nominal alloy composition has a C-content below or above the eutectoid composition, that is, whether it is hypoeutectoid or hypereutectoid, respectively. This α-ferrite or Fe_3C cementite is called *proeutectoid ferrite* or *proeutectoid cementite*, respectively.

The way the eutectoid transformation occurs is essentially as follows: Upon cooling to A_1 or slightly below, nuclei of cementite form heterogeneously at austenite grain corners or boundaries. Transformation of γ- to α-iron takes place rapidly compared to the time required for diffusion of carbon to allow formation of cementite. Thus, edgewise growth of alternate plates of ferrite and cementite takes place into the austenite grains as time goes by, until, finally, the entire austenite grain is transformed. Ferrite plates nucleate as carbon is depleted out beside the growing cementite. Carbon rejection from this ferrite also occurring beside the ferrite, nucleates new, secondary cementite; and the process repeats. The end result is a lamellar arrangement of ferrite and cementite. A schematic of the process is shown in Figure 14.30. In reality, since nucleation and growth never occur under equilibrium, there are some details missing from the preceding explanation, but it will do.

14.5.2. Nonequilibrium Decomposition to Other Ferrite Morphologies (Very Slow to Moderately Slow Cooling Rates)

During very slow, but nonequilibrium, cooling of a low-carbon (hypoeutectoid) steel, ferrite nucleates heterogeneously at high-angle grain corners and boundaries in the austenite. This requires only very slight undercooling below the A_3. Once formed, the ferrite grows into the austenite as a planar front, with carbon being rejected into the immediately surrounding austenite due to its lower solubility limit in ferrite than austenite. The redistribution of carbon is quite efficient. At such high temperatures (just below the A_3), the diffusion rate of C in austenite is about 10^{-11} m^2s^{-1}, so buildup to a characteristic distance x[bar] of about 2 μm occurs in less than 0.1 s. This is a short time, even by weld cooling rate standards.

A typical profile of the carbon in the austenite during very slow cooling is shown in Figure 14.31. For the situation just described, the carbon content of the austenite at the growing interface is within area *I* of Figure 14.31a.

As temperature decreases below A_3, carbon continues to diffuse into austenite with the growth of so-called "blocky" ferrite. This continues to occur until the temperature falls below the A_1 eutectoid temperature. Here, austenite regions enriched in carbon to an amount that lies within the eutectoid triangle *xyz* in Figure 14.31a are transformed to pearlite by the eutectoid reaction described above. Not surprisingly, the enrichment of the austenite at the advancing transformation front leads to cementite nucleation as the means of triggering the eutectoid transformation.

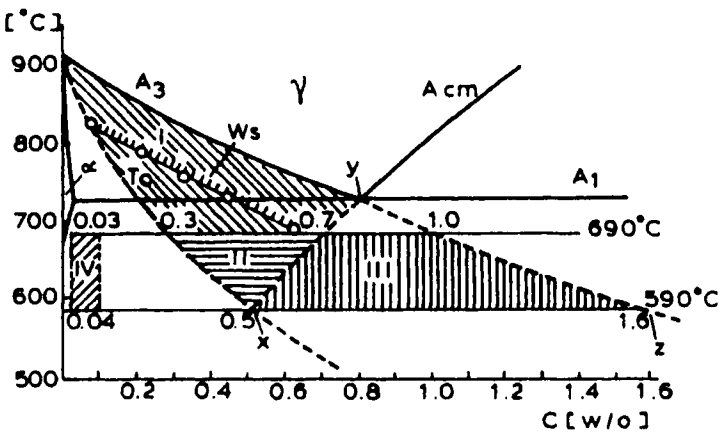


Figure 14.31 (a) Quasi-equilibrium diagram for the Fe-Fe_3C system showing the various transformation regions that can occur during nonequilibrium cooling of austenite, and (b) the carbon profiles at the [gamma]/α interface for various cooling rates. (Originally after Räsänen and Tenkula, 1972, out of *Introduction to the Physical Metallurgy of Welding*, 2d ed., by K. Easterling, published in 1992 by Butterworth-Heinemann, Oxford, UK, and used with permission of the Easterling family.)

As the rate of cooling of austenite increases slightly, but remains moderately slow, more undercooling (below A_3) is needed to initiate nucleation of ferrite, but such nucleation does occur. Again, nucleation begins at high-angle grain corners or boundaries in the austenite, and growth occurs along a front that moves into the austenite. However, at these slightly higher cooling rates, carbon redistribution is not as efficient, so the carbon solute gradient into the austenite at the growth front is steeper (as shown in Figure 14.31b). The morphology of the resulting ferrite is, at some rate, no longer blocky. In fact, it is referred to as proeutectoid ferrite (which is a little confusing), and quickly decorates grain boundaries in the austenite.

Once the austenite undercools to below the line W_s in Figure 14.31a, only individual needles of ferrite are able to break through the carbon–solute barrier. These needles are known as *Widmanstätten side plates*. Growth of these side plates is very rapid since solute is efficiently redistributed to the sides of the growing tips, avoiding solute pile-up problems. On further cooling below A_1, cementite begins to nucleate alongside these ferrite plates, as described in Section 14.5.1.

Still another morphology of ferrite is possible for still more rapid cooling in the vicinity of the A_1 temperature, namely, *acicular ferrite*. This form of ferrite is more equiaxed and its formation is favored by a high density of intragranular as well as intergranular (i.e., grain boundary) nucleation sites. Examples of such sites are inclusions.

14.5.3. Nonequilibrium Transformation to Bainite (Faster Cooling Rates)

At medium-high cooling rates, undercooling to below the A_1 becomes necessary before any decomposition product of austenite can nucleate. In this regime, the initial growth rate of ferrite is so rapid that the carbon concentration gradient at the interface enters the region of the *xyz* triangle in Figure 14.31a and assumes a profile like that shown in Figure 14.31b, bottom left. The austenite becomes unstable relative to ferrite and cementite, so when a small amount of carbide precipitates, the ferrite grows, establishes another carbon profile, and the process repeats in what is known as a periodic pearlite reaction.

For still faster cooling rates, the amount of undercooling needed to begin decomposition falls to around 690°C. At this temperature, carbon does not have a sufficiently high diffusion rate and there is insufficient time for it to diffuse into the austenite as grain-boundary ferrite nucleates. Thus, the carbon builds up at the phase boundary (as shown in Figure 14.31b, bottom right) and the austenite transforms to ferrite by a *massive transformation* mechanism. Massive transformation occurs by movement of a high-angle phase boundary, moving atoms from the parent phase to the product lattice by short-range diffusion across the boundary. For this to happen, the carbon distribution in parent and daughter phases must be the same.

As the cooling rate increases further, and supercooling to the range between about 550°C and 200–300°C is necessary to cause nucleation for decomposition of the austenite, a structure is produced in which ferrite and cementite are arranged not in lamellar form, but, rather, in either a feathery or acicular (needle-like) pattern where both phases are barely resolvable by optical light microscopy. This structure, generically known as *bainite*, has the feathery appearance when the transformation occurs in the upper region of the temperature range between 550 and 200–300°C, blending into a more acicular appearance when the transformation occurs in the lower portion of this range. The *feathery bainite* is also called *upper bainite*, while the *acicular bainite* is also called *lower bainite*, corresponding to the range in which each is formed.

The mechanism by which bainite forms is different from that involved in the transformation of austenite to pearlite by the eutectoid reaction. Pearlite is nucleated by cementite, and the formation of this cementite is accompanied by the formation of ferrite. Bainite, on the other hand, is nucleated by ferrite, which leads to precipitation of cementite. In fact, as the transformation of austenite is forced to lower and lower temperatures by faster and faster cooling rates, the rate of diffusion of carbon becomes so slow that only edgewise growth is possible and some massive shear transformation also occurs. This change in mechanism of transformation of austenite accounts for the difference in appearance as well as properties.

Figure 14.32 schematically shows the differences in the transformation mechanism for upper and lower bainite, as well as the effect of these different mechanisms on the final morphology.

14.5.4. Nonequilibrium Transformation to Martensite (Very Fast Cooling Rates)

At very fast cooling rates, undercooling must reach near 500°C before decomposition can commence. This is near the martensite start temperature or M_s. In this temperature regime, the diffusion rate of carbon is very slow, so any transformation of austenite to a lower energy phase must occur without diffusion, that is, be diffusionless. One possibility is to form lath martensite by shear that follows the Kurdjumov–Sachs orientation relationship of shared or habit planes: $(111)_\gamma // (011)_{\alpha'}$ and $[10\bar{1}]_\gamma // [\bar{1}1\bar{1}]_{\alpha'}$. Alternatively, if there is sufficient diffusion (i.e., if the temperature is high enough, above M_s), an interface-controlled transformation to *lower bainite* is possible. Here, carbon diffusion is so slow that very short-range diffusion takes place to form carbides with an orientation relationship to the ferrite. Ferrite plates thicken more easily by repeated precipitation of carbide.

Alloy content, beyond just carbon, as well as the presence of inclusions can influence the aforementioned transformations. While these will not be dealt with here in much detail, there are a few points that need to be mentioned. First, almost all alloying additions in steels (a notable exception being C_0), increase the hardenability; that is, the transformation C-curves shift to the left.

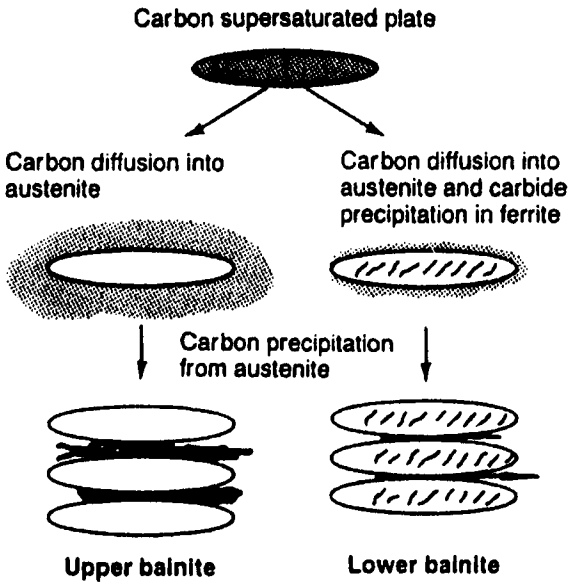


Figure 14.32 Schematic showing the differences in the transformation mechanism for upper and lower bainite, as well as the effect these different mechanisms have on the final morphology. (Originally from Bhadashira and Svensson, 1993, out of *ASM Handbook*, Vol. 6: *Welding, Brazing, and Soldering*, published in 1993 by and used with permission of the ASM International, Materials Park, OH.)

The consequence of this is that every welding process acts as if it is causing a faster cooling rate in terms of the structures produced. Second, the nose (or peak rates) of the bainite C-curve can be shifted relative to that of the pearlite C-curve, usually moving it to the left more than the pearlite curve moves. The consequence of this is that the bainite curve is now not masked by the pearlite curve, so that it becomes more likely that bainite will form on continuous cooling. This is not the case for low-C steels. Third, the temperatures for martensite start (M_s) and martensite finish (M_f) are generally increased by the addition of alloying additions (with C_0 again being a notable exception). The consequence of this is greater susceptibility to quench cracking, arising from a difference in the cooling rates between the surface and the interior, and less likelihood of retained austenite. Retained austenite can transform later on in processing or service, often by the application of mechanical energy in the form of plastic deformation (e.g., from machining). The result is dimensional instability, since martensite has a larger specific volume than austenite, and possible cracking.

Figure 14.33 gives schematics that show the Dubé classification of ferrite morphologies produced by various cooling conditions. Figure 14.34 shows that

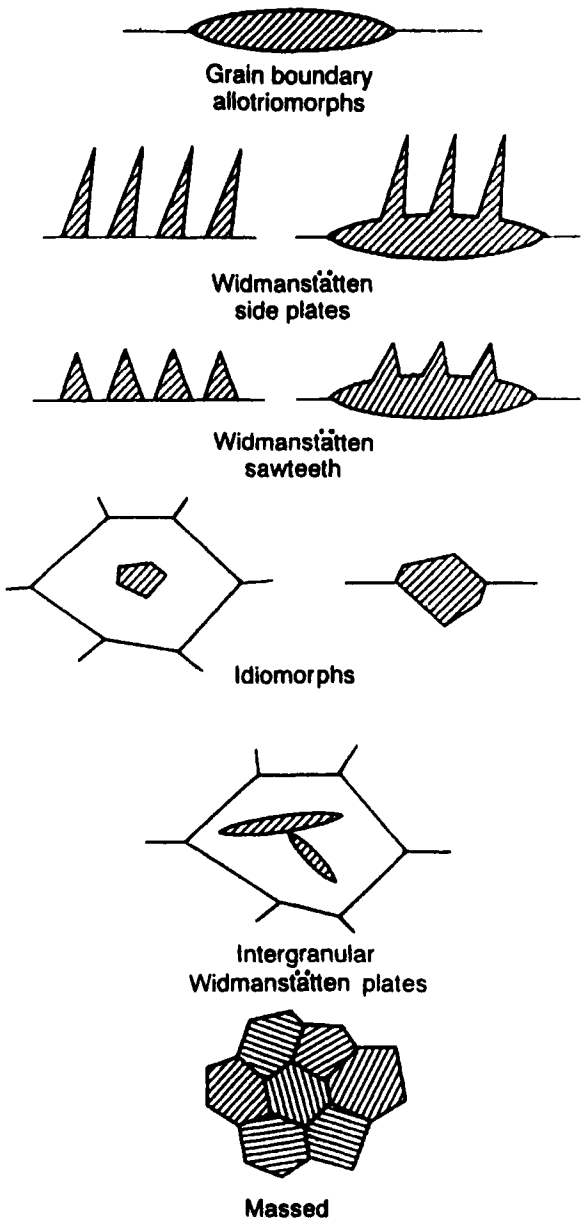


Figure 14.33 Schematic illustrations of the various possible morphologies for ferrite as classified by Dubé. (Originally from *Optical Microscopy of Carbon Steels*, by L. E. Samuels, 1980, American Society for Metals, Metals, Park, OH, out of *ASM Handbook*, Vol. 6: *Welding, Brazing, and Soldering*, published in 1993 by and used with permission of the ASM International, Materials Park, OH.)

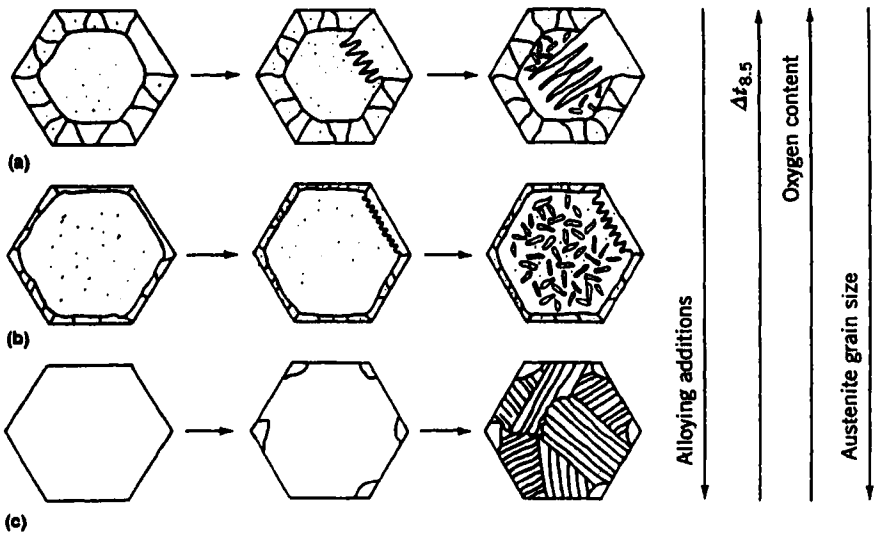


Figure 14.34 Schematic showing the effect of alloy composition, $\Delta t_{8.5}$ (cooling rate), oxygen content, and prior austenite grain size on the development of microstructure in ferritic steel weld metals. (Originally from "Modeling the evolution of microstructure in steel weld metal" by H. K. D. H. Bhadeshia and L. E. Svensson, in *Mathematical Modeling of Weld Phenomena*, edited by H. Cerjak and K. Easterling, 1993, The Institute of Metals, London, out of *ASM Handbook*, Vol. 6: *Welding, Brazing, and Soldering*, published in 1993 by and used with permission of the ASM International, Materials Park, OH.)

other factors, besides cooling rate, affect ferrite morphology, including alloying additions, oxygen content, and prior austenite grain size.

14.6. SIGMA AND CHI PHASE FORMATION

During certain postweld heat treatments of duplex austenitic stainless steels or weld metal, say for stress relief of heavy sections, or during elevated-temperature service, certain embrittling phases can form. In the range of 600–900°C, transformation of ferrite to σ and χ phases can occur, along with precipitation of complex, $M_{23}C_6$ carbides.

Formation of both σ and χ phases is promoted by high Cr and Mo, such as found in type 316 (nominal composition 17.0Cr-12.0Ni-2.5Mo), as well as in type 309 (23Cr-13Ni) and 310 (25Cr-20Ni) fillers. Sensitivity to σ and χ phases can be seen in Figure 14.17. When susceptible compositions are being welded or used as fillers, care must be exercised during both postweld heat treatment and service.

14.7. GRAIN BOUNDARY MIGRATION

In some alloys, the migration of grain boundaries in postsolidified structure can be significant. As a result, the structure of the fusion zone can change significantly. The driving force is reduction of surface energy associated with grain boundaries, and the mechanism for migration is solid-state diffusion. No particular problem arises from grain boundary migration, other than the possibility of what appears to be anomalous cracking, when in fact, what is occurring is cracking due to interdendritic microsegregation, but after boundaries have moved. A phenomenon known as ghost boundaries associated with so-called hot ductility dips in some austenitic stainless steels, is one manifestation of grain boundary migration. The ghost boundaries are sites where segregate was left behind after the boundary moved from its original location.

14.8. SUMMARY

Solidification of a liquid phase into a solid phase is certainly not all that is involved in establishing fusion zone structure. First, in many alloy systems (e.g., virtually all braze fillers and solders, as well as cast iron and other important engineering alloys), the solid that forms upon solidification is not a single phase, but, rather, consists of two phases in an intimate mixture formed by what is known as an eutectic reaction. Second, for some alloy systems, most notably the Fe-C system, solidification is made even more complicated by the occurrence of a peritectic reaction, in which a liquid phase and solid phase react to form a new solid phase on cooling. Both reactions complicate solidification even under conditions of equilibrium, but especially complicate solidification under conditions of nonequilibrium. There is also the possibility that solid-state transformations or reactions will take place in the previously solidified fusion zone. One prime example involves the δ-ferrite/austenite transformation modes that can arise in stainless steels with a duplex ferrite + austenite structure. Another is the critically important decomposition of austenite upon cooling, which depends on cooling rate. Of other significance are formation of brittle phases or structure that change as the result of grain boundary migration in the solid state.

REFERENCES AND SUGGESTED READING

Bhadeshira, H. K. D. H., and Svensson, L. E., 1993, "Modeling the evolution of microstructure in steel weld metal," in *Mathematical Modeling of Weld Phenomena*, edited by H. Cerjak and K. Easterling, The Institute of Welding, London.

Brooks, J. A., and Thompson, A. W., 1991, "Microstructural development and solidification cracking susceptibility of austenitic stainless steel welds," *International Materials Review*, **36**(1), 16–44.

Cieslak, M. J., and Savage, W. F., 1980, "Weldability and solidification phenomena of cast stainless steels," *Welding Journal*, **59**(5), 136s–146s.

Cieslak, M. J., Ritter, A. M., and Savage, W. F., 1982, "Solidification cracking and analytical electron microscopy of austenitic stainless steel weld metals," *Welding Journal*, **62**(1), 1s–8s.

David, S. A., 1981, "Ferrite morphology and variations in ferrite content in austenitic stainless steel welds," *Welding Journal*, **60**(4), 63s–71s.

David, S. A., Vitek, J. M., and Hebble, T. L., 1987, "Effect of rapid solidification on stainless steel weld metal microstructure and its implication on the Schaeffler diagram," *Welding Journal*, **66**(10), 289s–300s.

DeLong, W. T., 1974, "Ferrite in austenitic stainless steel weld metal," *Welding Journal*, **52**(7), 273s–286s.

Easterling, K., 1972, *Introduction to the Physical Metallurgy of Welding*, 2nd ed., Butterworth-Heinemann, London.

Fhines, F. N., 1956, *Phase Diagrams in Physical Metallurgy*, McGraw-Hill, New York, pp. 83–91. [Peritectic solidification/reactions.]

Kotecki, D., 1996, private communication.

Lippold, J. C., and Savage, W. F., 1979, "Solidification of austenitic stainless steel weldments, part 1: a proposed mechanism," *Welding Journal*, **58**(12), 362s–374s.

Lundin, C. D., and Chou, C. P. D., 1985, "Fissuring in the "hazard HAZ" region of austenitic stainless steel welds," *Welding Journal*, **64**(4), 113s–118s.

Lundin, C. D., Chou, C. P. D., and Sullivan, C. J., 1980, "Hot cracking resistance of austenitic weld metals," *Welding Journal*, **59**(8), 226s–232s.

Mehl, R. F., and Wells, C., 1937, "Constitution of high purity iron-carbon alloys," *Metals Technology* (June).

Okagawa, R. K., Dixon, R. D., and Olson, D. L., 1983, "The influence of nitrogen from welding on stainless steel weld metal microstructure," *Welding Journal*, **62**(8), 204s–209s.

Samuels, L. E., 1986, *Optical Microscopy of Carbon Steels*, American Society for Metals, Metals Park, OH.

Schaeffler, A. L., 1949, "Constitution diagram for stainless steel weld metal," *Metals Progress*, **56**(5), 680, 680B.

Suggested readings on postsolidification phase transformations.

Davies, G. J., and Garland, J. G., 1975, "Solidification structures and properties of fusion welds," *International Metals Review*, **20**, 83.

Linnert, G., 1965 and 1967, *Welding Metallurgy*, Vols. 1 and 2, 3d ed., American Welding Society, Miami, FL.

Porter, D. A., and Easterling, K. E., 1992, *Phase Transformations in Metals and Alloys*, 2d ed., Chapman & Hall, London.

Savage, W. F., 1980, "Solidification, segregation and weld imperfections," *Welding in the World*, **18**(5/6), 89–113.

Thomas, R. D., Jr., and Messler, R. W., Jr., 1997, *Welding of 347 Stainless Steels*, Interpretive Report 421, Welding Research Council, New York.

CHAPTER 15

THE PARTIALLY MELTED ZONE

Probably the least understood region of a fusion weld is the partially melted zone, or PMZ, that exists in alloys. As the region between the unmelted but heat-affected zone and the fully melted fusion zone, it is here that solidification usually begins. Yet, its presence complicates the solidification process in ways still not fully understood. As such, the PMZ remains the most needed and fertile area for research in welding, although it poses many daunting analytical and experimental challenges. Let's look at the PMZ and see why.

15.1. ORIGIN AND LOCATION OF THE PARTIALLY MELTED ZONE

The *partially melted zone* or *PMZ* is the area of a fusion weld in an *alloy* subjected to localized melting along grain boundaries and, to a lesser extent, in grain interiors (usually at interphase boundaries). The PMZ forms from thermal cycles associated with welding that heat an alloy to temperatures between the liquidus and solidus, or to above its effective solidus if prior nonequilibrium solidification resulted in pronounced interdendritic microsegregation of solute. Pure metals do not exhibit partially melted zones since melting occurs at a single, discrete temperature (the melting point) and, thus, along a line (the fusion line) not over a region.

The thermal cycles that cause partial melting have peak temperatures lower than those that cause complete melting in the fusion zone, but above those that do not cause melting but affect the microstructure of the solid surrounding the

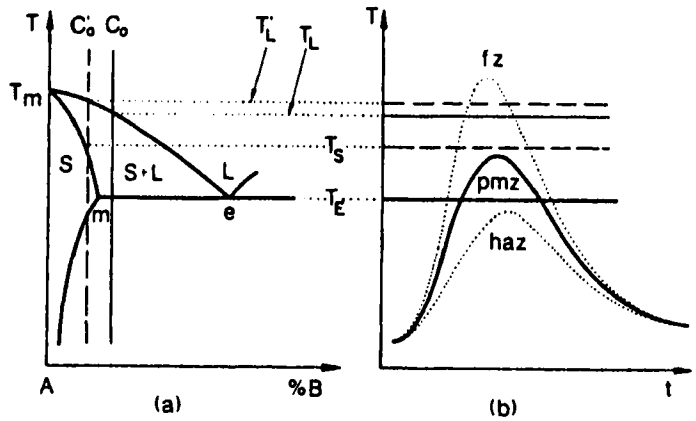


Figure 15.1 Relationship between (a) a portion of an eutectic phase diagram and (b) welding thermal cycles in the fusion zone (curve fz), partially melted zone (curve pmz), and heat-affected zone (curve haz). (From *Welding Metallurgy* by S. Kou, published in 1987 by and used with permission of John Wiley & Sons, Inc., New York.)

fusion zone, that is, the heat-affected zone or HAZ (discussed in Chapter 16). This can be seen in Figure 15.1 by comparing curves fz, pmz, and haz in (b). These thermal cycles in (b) are related to a portion of an eutectic phase diagram in (a).

The partially melted zone is located in the region surrounding the weld pool where the temperature rose to between the nonequilibrium solidus ($T_{S_{eff}}$) or eutectic temperature ($E_{E_{eff}}$) and the nonequilibrium liquidus ($T_{L_{eff}}$), where the subscript "eff" refers to the effective temperature of any particular transformation as altered by nonequilibrium. Since the liquidus temperature is not suppressed by microsegregation from earlier casting or welding, it is usually quite close to the equilibrium liquidus, except for some depression due to nonequilibrium cooling-induced transformation lag.[1]

Thus, under nonequilibrium conditions, the values of T_S or T_E (or $T_{eutectic}$) and T_L are very slightly higher during heating at the leading portion of a weld pool, and lower (possibly considerably lower) during cooling at the trailing portion of the weld pool. However, for a moving heat source and weld pool, the instantaneous region of partial melting ahead of the source and pool is destroyed and completely melted as the pool advances. The location of the instantaneous partially melted zone around a moving weld pool is shown in Figure 15.2. Remember, real welds are three dimensional, not two dimensional,

[1] Recall that phase transformation and reaction temperatures are altered by nonequilibrium heating and/or cooling in a direction that causes the transformation or reaction to lag the equilibrium case. This reflects the need under nonequilibrium for some additional driving force to cause the transformation or reaction, more so on cooling than on heating (see Section 13.2.6). Thus, transformation or reaction temperatures are higher for nonequilibrium heating and lower for nonequilibrium cooling, more so for faster rates.

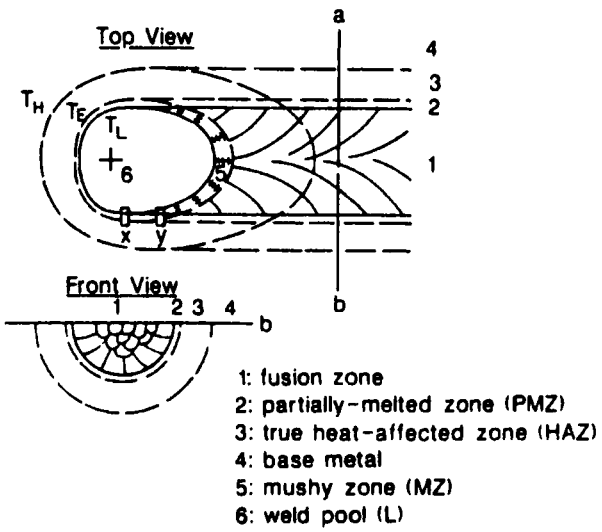


Figure 15.2 Schematic showing the location of the partially melted zone around a weld pool (a) in plan view both instantaneously ahead of the pool (where the PMZ is destroyed as the pool advances) and permanently after solidification along both sides of the weld pool path, as well as in (b) cross section. (From *Welding Metallurgy* by S. Kou, published in 1987 by and used with permission of John Wiley & Sons, Inc., New York.)

so there is a partially melted zone all around the surface perimeter or boundary of a weld pool, beneath as well as alongside.

Once a moving heat source and weld pool have advanced, solidification occurs along the trailing edge. Thus, in the volume path swept by the fusion zone, there is no remnant of partial melting, only solidification of completely melted material. There is, however, a mushy zone at the trailing edge of the weld pool during the time period that the temperature drops below the liquidus but is still above the solidus, as affected by nonequilibrium cooling.[2]

Along both sides as well as all around the underside of the pool of a fusion weld, remnants of the partially melted zone persist after solidification. Thus, any phase transformation or reaction that occurs in the partially melted zone that alters the melted structure or affects the solidification process or structure persists all around the boundary of the weld fusion zone.

The width or extent of the PMZ depends on the heat flow around the weld (see Chapter 6). Major factors affecting the width of the PMZ are (1) the liquidus and solidus temperature (melting range) of the alloy being welded; (2) the thermal conductivity of the material being welded; (3) the welding process being employed (especially heat capacity and intensity or energy density); (4)

[2] The effect of mixed liquid and solid in the mushy zone on convection, solute redistribution, solidification mechanics, and defect formation is complex, as alluded to in Chapter 13.

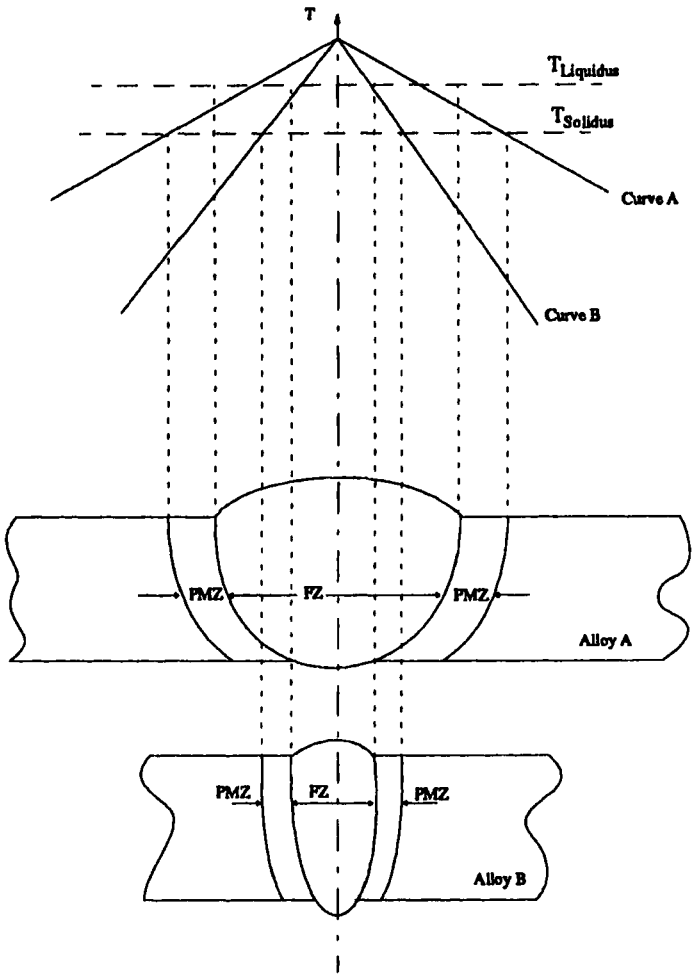


Figure 15.3 Schematic showing the effect of base alloy thermal conductivity on the temperature gradient into the base material for a high thermal conductivity (curve A) and low thermal conductivity (curve B).

the operating parameters for the process (as these affect net linear heat input); and (5) the operating conditions (i.e., preheat, source manipulation as by weave or oscillation). The wider the melting range, the wider the PMZ, for all other factors the same. The higher the thermal conductivity, the wider the PMZ, as shown in Figure 15.3 for the shallow gradient (curve A) produced in a material with high thermal conductivity versus the steep gradient (curve B) produced in a material with a low thermal conductivity. The higher the energy density of the heating source, the narrower the PMZ, since melting occurs more efficiently and results in a steeper gradient for such sources. Operating parameters that increase the net linear heat input increase the width of the PMZ for reasons

related to the preceding. Likewise, any operating condition that alters the temperature gradient surrounding the weld pool will also affect the PMZ width. Examples are (1) a wider PMZ when preheating is employed (as the temperature gradient is made shallower to lower the cooling rate), and (2) a narrower PMZ when arc oscillation is employed (as the resolved welding speed is higher, so the net linear heat input is lower).

15.2. CONSTITUTIONAL LIQUATION

Certainly one of the reasons for the existence of partially melted regions around fusion zones is that alloys melt and solidify over a range of temperatures rather than at a single temperature. But there is another reason. Occasionally, partially melted grain boundary films are observed significantly below the bulk equilibrium solidus of an alloy. Pepe and Savage (1967, 1970) attributed this phenomenon to *constitutional liquation.* Here's where the phenomenon has its origin.

The constitutional diagram in Figure 15.4 represents a hypothetical alloy system exhibiting the behavior necessary for constitutional liquation to occur. In this diagram, A_xB_y is a second-phase precipitate, such as an complex

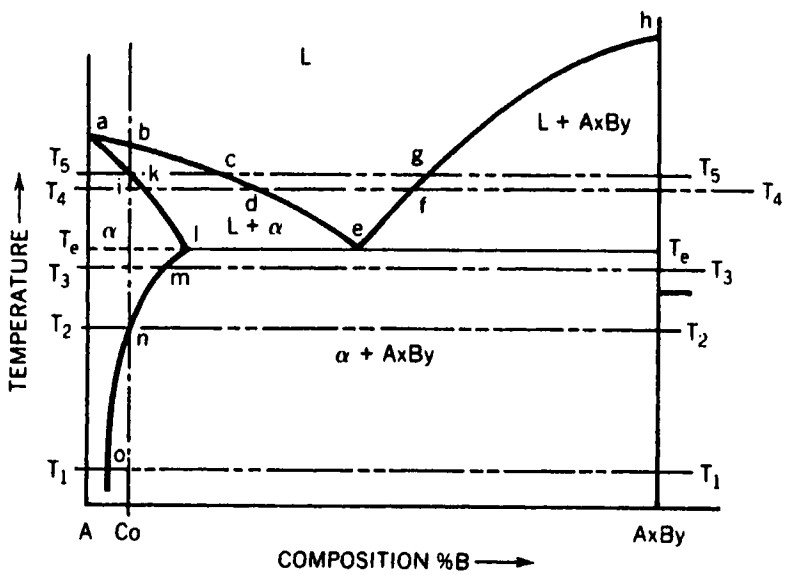


Figure 15.4 Portion of a constitutional diagram for a hypothetical alloy system exhibiting the necessary characteristics for constitutional liquation. (Originally from "Effects of constitutional liquation in 18Ni maraging steels" by J. J. Pepe and W. F. Savage, *Welding Journal*, **46**(9), 411s–422s, 1967, published by and used with permission of the American Welding Society, Miami, FL.)

carbide, nitride, carbo-nitride, phosphide, sulfide, or silicide inclusion, distributed in the α solid solution, which serves as a matrix phase. When an alloy of nominal composition C_0 is heated very slowly (so that equilibrium is maintained approximately), the solubility of solute B in the α matrix increases until the solvus temperature T_2 is reached. The particles of A_xB_y shrink as B atoms leave this B-rich phase to become part of the solid solution matrix. At T_2, the last remaining A_xB_y disappears, converting the alloy to a homogeneous, single-phase solid solution consisting entirely of α of composition C_0.

If heating is rapid, however, as occurs in fusion welding, A_xB_y particles do not have enough time to dissolve by having B atoms enter solid solution in the α phase, and nonequilibrium prevails. Thus, some portion of larger particles remain in the α matrix even when the temperature rises above the equilibrium solvus temperature T_2, say to T_3. Upon further heating to the eutectic temperature, T_{eutectic} or, simply, T_e, liquid phase of the eutectic composition begins to form at the interface between dissolving A_xB_y particles and the α matrix. The reason is that somewhere in the region of this interface, the solute concentration of the α matrix exceeds the eutectic composition in the solute profile that develops. Further heating to T_4 would allow additional time for further dissolution of A_xB_y and the formation of more liquid phase around particles. In fact, at this temperature, every particle of A_xB_y remaining undissolved should be completely surrounded by a liquid film of varying composition from f at the A_xB_y particle boundary to d at the interface of the α matrix. This is shown in Figure 15.5b, and a simplified hypothetical phase diagram like that in Figure 15.4 is shown in Figure 15.5a.

In short, localized melting is possible at temperatures significantly below the equilibrium solidus temperature T_5. This localized melting is called constitutional liquation,[3] and can have profound adverse effects on weldabililty because it promotes cracking.

Constitutional liquation is observed in many important engineering alloys during nonequilibrium heating, such as during fusion (and some nonfusion) welding and some hot processing (e.g., rolling, forging, extrusion, or drawing). Examples include the following: heat-treatable, age-hardenable Al alloys in the Al-Cu or Al-Cu-Mg systems (2000-series alloys), Al-Mg-Si system (6000 series), and Al-Zn-Mg system (7000 series), with the second-phase culprit being Al_2Cu or Al_2CuMg, Mg_2Si, or Zn_2Mg, respectively; some heat-treatable, age-hardenable Ni-based superalloys such as Udimet 700 (0.15maxC, 3.7–4.7Al, 3.0–4.0Ti, 4.5–5.7Mo, 13–17Cr, 17–20Co, trace B, bal. Ni), Waspalloy (20Cr, 13Co, 4Mo, 3Ti, 1Al, bal. Ni), Hastelloy X (21Cr, 1Co, 18Fe, 1W, 9Mo, bal. Ni), and Inconel 718 ((52.5Ni, 0.04C, 0.18Mn, 18.5Fe, 0.008S, 0.18Si, 0.15Cu, 19.0Cr, 0.50Al, 0.90Ti, 3.05Mo, and 5.13Nb+Ta), where the operative A_xB_y second phases are complex MC and M_6C carbides; and 18Ni-maraging steel (0.02C, 0.4–0.7Mn, 0.020S max, 0.010P max, 0.10–0.20Si, 17.5–18.5Ni, 7.5–8.5Co,

[3]The term constitutional liquation actually derives from liquation or melting arising from the constitution or composition profile.

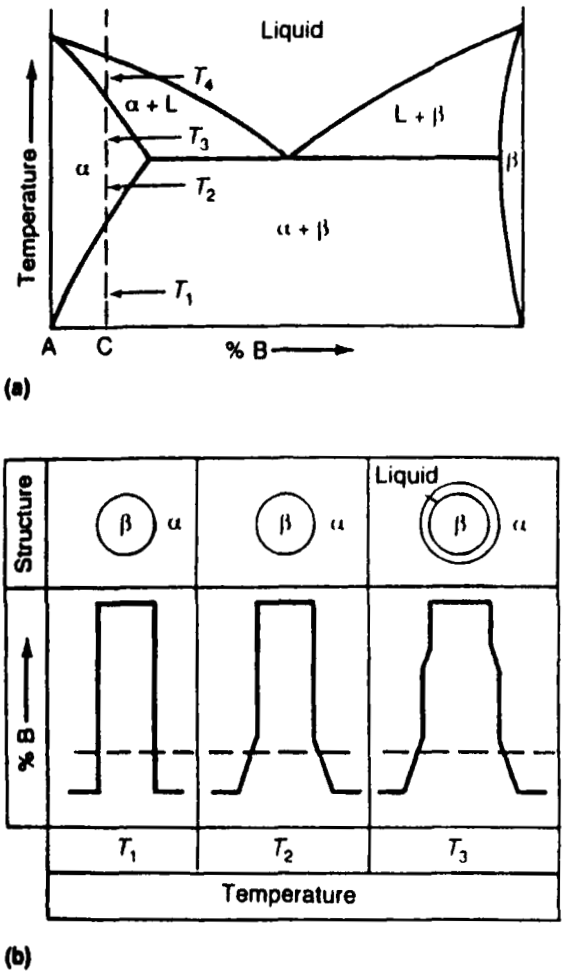


Figure 15.5 Extension of the partially melted zone by constitutional liquation of particles of beta phase (b) as these progressively dissolve at three temperatures shown in the simplified phase diagram from a hypothetical binary alloy (a). (From "Joining" by W. Yeniscavitch in *Superalloys II*, edited by C. T. Sims, N. S. Stoloff, and W. C. Hagel, 1987, John Wiley & Sons, Inc., New York, with permission.)

4.5–5.0Mo, 0.010–0.015Al, and 0.30–0.45Ti), where the operative second-phase is Ti-sulfide inclusions. Another important example is certain austenitic stainless steels such as AISI 347, where stabilizing Nb forms various compounds with carbon, nitrogen, carbon and nitrogen, sulfur, phosphorus, and silicon, all of which can liquate as described earlier. A suggested sequence for the occurrence of hot cracking in the PMZ arising from low-melting compounds of Nb is shown schematically in Figure 15.6.

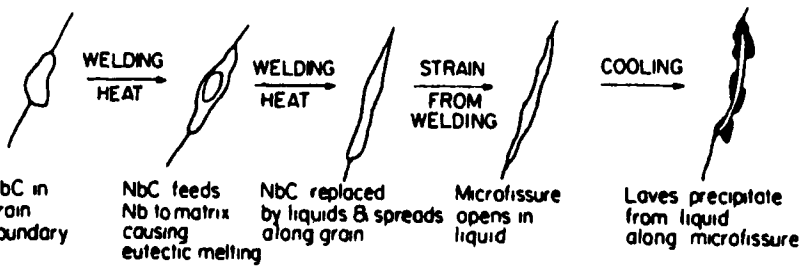


Figure 15.6 Schematic of the suggested sequence for development of microfissuring in Nb-containing Inconel 718 and other austenitic alloys. (From "The relationship between grain size and microfissuring in alloy 718" by R. G. Thompson, J. R. Dobbs, D. E. Mayo, and J. J. Cassimus, *Welding Journal*, 64(4), 91s–96s, 1985, published by and used with permission of the American Welding Society, Miami, FL.)

In some alloys, the occurrence of constitutional liquation is indicated by the appearance of solute-rich ghost grain boundaries or grain boundary networks. These are caused by the pinning of migrating grain boundaries during non-equilibrium heating. A schematic representation of how ghost boundaries arise from constitutional liquation is shown in Figure 15.7. Ghost boundaries have been found to be associated with cracking in some alloy systems, one example being austenitic stainless steels (such as type 347) at intermediate temperatures, leading to what is known as a [hot] ductility dip.

15.3. DEFECTS ARISING IN THE PMZ

Partially melted zones in welds in alloys can suffer from several problems, including (1) conventional hot cracking, (2) liquation cracking, (3) loss of ductility (or grain boundary embrittlement), and (4) hydrogen cracking. Let's look at each of these briefly.

15.3.1. Conventional Hot Cracking and Liquation Cracking in the PMZ

Conventional hot cracking is usually the most prevalent problem associated with the partially melted zone. As for solidification hot cracking in the fusion zone (Section 13.6.1), hot cracking in the PMZ is intergranular. Also as for fusion zone hot cracking, the cause of hot cracking in the PMZ is the combination of grain boundary liquation (as opposed to residual liquid before solidification is completed), especially as aggravated by microsegregation from prior processing or lack of processing, such as, welding or casting, and lack of mechanical working, and the stresses induced by both volumetric liquid-to-solid shrinkage during solidification and thermal contraction during cooling

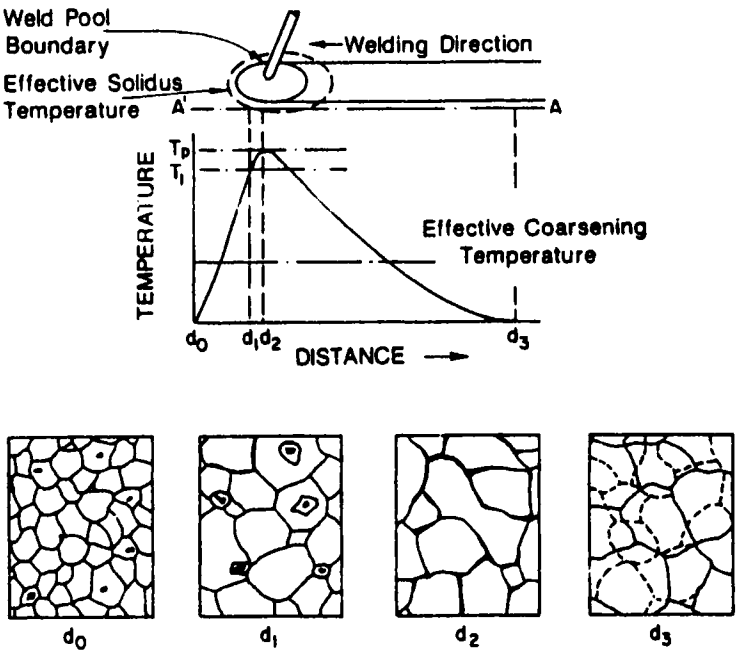


Figure 15.7 Schematic representation of the formation of a ghost boundary network formed by constitutional liquation and solute segregate left behind following grain boundary migration. (From "The heat-affected zone of the 18Ni maraging steels" by J. J. Pepe and W. F. Savage, *Welding Journal*, **49**(12), 545s–553s, 1970, published by and used with permission of the American Welding Society, Miami, FL.)

following welding. With the grain boundary liquated, the partially melted zone, like the partially solidified fusion zone, has little strength or ductility to resist tensile stresses. The effect of thermally induced stresses is, not surprisingly, critical (Section 13.6.1).

Related to conventional hot cracking in the fusion zone and PMZ is liquation cracking. In fact, the term liquation cracking is often used to refer to normal hot cracking in the PMZ, but should really be reserved for use for cracking arising from constitutional liquation (as described in Section 15.2). As for conventional hot cracking, cracking arising from constitutional liquation occurs when tensile stresses act on liquated films (Lu et al., 1996).

15.3.2. Loss of Ductility in the PMZ

Many eutectics are inherently hard and brittle, and, thus, lower the ductility of a material. The reason for this is twofold: First, in binary systems, eutectics always consist of an intimate mechanical mixture of two phases, one of which is often much stronger, harder, and more brittle than the other. The result, of

course, is that the weaker, softer, but tougher phase is strengthened and hardened. However, the resulting two-phase mixture or constituent is also made less tough and less ductile. Second, the interface between the two phases is extensive, often in the form of alternating layers in what are called lamellar eutectics. The large shared interface between an inherently tough phase and an inherently brittle phase inevitably limits the toughness of the combination. The reason is that for loading along or parallel to the lamellae, the maximum strain that can be tolerated is limited by the less ductile phase (for a condition of isostrain). It should come as no surprise, then, that once extensive segregation of a eutectic constituent to grain boundaries occurs, as is the case in the PMZ of many alloys, the ductility of the PMZ following solidification is lowered considerably.

The above problem is made worse by the fact that to reduce the embrittling effect means removing or drastically altering the structure of the eutectic. The only way to do this is by heat treatment. Unfortunately, redissolving an eutectic requires temperatures that are well beyond what is normally considered reasonable for postweld heat treatment, that is, into the solutionizing range where a single-phase solid solution is formed above the solvus temperature. Another option, of course, is to attempt to modify the structure of a lamellar eutectic. This can be done by long-time soaks at elevated temperatures, causing the second phase to form spherical particles within the matrix of the first phase. The driving force for this is the reduction of interphase energy, and the process is called spheroidization. Again, while theoretically possible, the temperatures required are usually unacceptable for weldments, because loss of dimensions due to warpage or unwanted alteration of other structure elsewhere in the weld will adversely affect overall properties.

15.3.3. Hydrogen-Induced Cracking in the PMZ

In some steels, such as high-yield, 80-ksi yield strength, HY-80 steel (0.18C, 0.1–0.4Mn, 2.0–3.25Ni, 1.0–1.8Cr, 0.2–0.6Mo, 0.002Ti, 0.02V, 0.25Cu, bal. Fe) and other high-yield steels of this type,[4] hydrogen-induced cracking is observed in both the partially melted zone and the adjacent fusion zone, where, in both regions, mixing between the molten filler and melted base metal is incomplete. . Savage et al. (1976) attributed this behavior to the following mechanism: Liquated films form in the grain boundaries of the PMZ and provide easy paths for hydrogen diffusion from the weld metal to pump across the fusion boundary. Since these boundaries contain molten iron that can dissolve 3–4 times as much nascent hydrogen as the surrounding solid, these areas become supersaturated with hydrogen upon resolidification. Since these liquated grain boundaries are also solute enriched as a result of solute rejection, they are more hardenable and more prone to formation of martensite than either the fusion

[4] HY-100 (100-ksi yield strength) with 0.2C, 0.1–0.4Mn, 2.25–3.5Ni, 1.0–1.8Cr, 0.2–0.6Mo, 0.02Ti, 0.02V, 0.25Cu, bal. Fe, and HY-130 (130-ksi yield strength) with 0.12C, 0.6–0.9Mn, 4.75–5.25Ni, 0.4–0.7Cr, 0.3–0.65Mo, 0.02Ti, 0.05–0.10V, 0.15Cu, bal. Fe.

zone or the heat-affected base metal. The result is that untempered martensite forms right where the hydrogen content is the highest and in the presence of some of the highest residual tensile stresses found anywhere around the weld. The three essential criteria for hydrogen embrittlement couldn't be better met if one tried!

15.4. REMEDIATION OF DEFECTS IN THE PMZ

Knowing the sources of several defects prevalent in the partially melted zone helps only a little in their remediation. Remedies for problems associated with the PMZ can be grouped into four general categories: (1) the heat source, (2) restraint, (3) the base metal, and (4) the filler metal.

As stated earlier, the size of the PMZ and the extent of grain boundary liquation increase with increasing net linear heat input. Thus, to minimize difficulties associated with the PMZ, minimize the size of the PMZ by (1) selecting processes offering inherently low net linear heat input as a consequence of the high energy density of their source (e.g., LBW, EBW, PAW, or even GTAW); (2) use multipass welding techniques to minimize the heat input for each pass; and (3) employ transverse arc oscillation to increase the resolved welding speed and, thereby, decrease the net linear heat input.

Since both hot cracking and hydrogen-induced cracking in the PMZ are caused by the combination of a susceptible microstructure and the presence of tensile stresses, the sensitivity of the PMZ to both types of cracking can be reduced by decreasing the level of restraint. Methods for doing this are described in Section 7.7.3.

The composition, grain structure, and preexisting solute segregation of the base metal can significantly affect the susceptibility of the PMZ to cracking. Of course, selection of the base metal is commonly done by the designer and usually cannot be changed, or even fully known in many cases (such as in the repair of old equipment for which records no longer exist) by the welding engineer and welder. However, to the degree that it is possible, select base metals with the lowest levels of residual elements possible. This includes, especially, keeping the levels of S and P low in steels and nickel-based alloys, where both elements, singly or in combination, promote the formation of low-melting eutectics and widen the freezing range significantly.

Susceptibility to hot cracking in the PMZ (as well as the FZ) is obviously greater when, due to prior processing (e.g., casting or welding), a condition of segregation already exists. Such segregation already renders such base metals prone to formation of low-melting eutectics in grain boundaries.

To minimize possible effects of low-melting eutectics regardless of their source, keep grain boundary area as large as possible by refining the base metal microstructure as much as possible. In steels, this can be accomplished by the process of normalization, in which the steel is heated to just above the A_1 or $A_{1,3}$ temperature, depending on whether it is hypo- or hypereutectoid. The favorable effect of grain size reduction is shown in Figure 15.8.

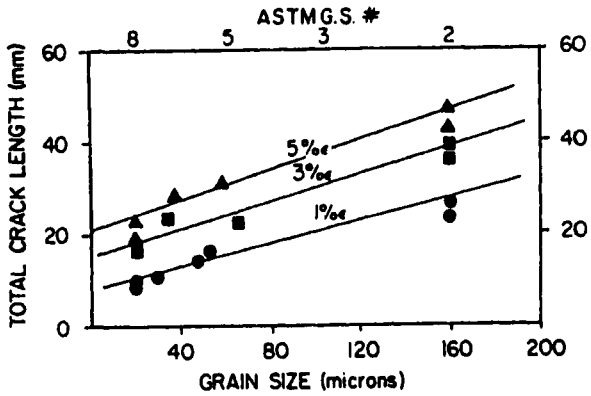


Figure 15.8 The favorable effect of reducing grain size on the tendency to hot cracking in the partially melted zone. (From "The relationship between grain size and microfissuring in alloy 718" by R. G. Thompson, J. R. Dobbs, D. E. Mayo, and J. J. Cassimus, *Welding Journal*, 64(4), 91s–96s, 1985, published by and used with permission of the American Welding Society, Miami, FL.).

Finally, one can attempt to minimize cracking in the PMZ by choosing a proper filler metal. However, since there is little or no mixing in the PMZ because the high fraction of solid present severely retards convection, attempting to adjust the composition of the weld metal to prevent cracking is not a viable approach. Instead, cracking can be reduced by selecting a filler whose melting range assures that solidification throughout the PMZ will be completed before weld metal in the fusion zone solidifies. In employing this tactic, care must still be taken to be sure that the filler does not render the weld metal more susceptible to solidification cracking. The difference between success and chasing one's tail is often small.

15.5. SUMMARY

Just outside the fusion zone of alloys there is a region in which the welding cycle caused temperatures to reach a peak above the solidus, but below the liquidus. In this region melting was never complete, and a partially melted (as opposed to partially solidified, mushy) zone or PMZ results. The partially melted zone is critical to the solidification of a weld since it is here that epitaxial growth of new structure into the fusion zone begins. Unfortunately, less is known about the PMZ than either the fusion or heat-affected zones because of both analytical and experimental difficulties associated with its study. Nevertheless, it is known that besides melting along grain boundaries to produce a situation in which hot cracking can occur on cooling, there is also localized melting around certain second-phase particles due to constitutional

liquation arising from nonequilibrium heating. Embrittlement and cracking can also arise in the PMZ from the presence of solidified eutectic films or enhanced hardenability and hydrogen cracking in steels. Remediation of problems in the PMZ is possible by minimizing its size through proper selection of process and operating parameters, and by minimizing restraint. Avoidance of base metals prone to the formation of low-melting eutectics is another possibility, as is selecting a filler metal that allows the PMZ to solidify completely before the fusion zone does.

REFERENCES AND SUGGESTED READING

Lu, Z. J., Evans, W. J., Parker, J. D., and Birley, S. S., 1996, "Simulation of microstructure and liquation cracking in 7017 aluminum alloy," *Materials Science and Engineering A: Structural Materials Properties, Microstructure, and Processing*, **220**(Dec.), 1–7.

Pepe, J. J., and Savage, W. F., 1967, "Effects of constitutional liquation in 18Ni maraging steels," *Welding Journal*, **46**(9), 411s–422s.

Pepe, J. J., and Savage, W. F., 1970, "The heat-affected zone of the 18Ni maraging steels," *Welding Journal*, **49**(12), 545s–553s.

Savage, W. F., Nippes, E. F., and Szekeres, E. S., 1976, "Hydrogen induced cold cracking in a low alloy steel," *Welding Journal*, **55**(9), 276s–283s.

Thompson, R. G., Dobbs, J. R., Mayo, D. E., and Cassimus, J. J., 1985, "The relationship between grain size and microfissuring in alloy 718," *Welding Journal*, **56**(4), 91s–96s.

Yeniscavitch, W., 1987, "Joining," in *Superalloys II*, edited by C. T. Sims, N. S. Stoloff, and W. C. Hagel, Wiley, New York, 495–516.

Suggested readings on constitutional liquation

Hermann, R., Birley, S. S., and Holdway, P., 1996, "Liquation cracking in aluminum alloy welds," *Materials Science and Engineering A: Structural Materials Properties, Microstructure, and Processing*, **212**(July), 247–255.

Lin, W., Lippold, J. C., and Baeslack III, W. A., 1993, "Heat-affected zone liquation cracking susceptibility, part I: development of a method for quantification," *Welding Journal*, **72**(4), 135s–143s.

Lippold, J. C. Baeslack, W. A. III, and Varol, I., 1992, "Heat-affected zone liquation cracking in austenitic and duplex stainless steels," *Welding Journal*, **71**(1), 1s–14s.

Robinson, J. L., and Scott, M. H., 1980, "Liquation cracking during the welding of austenitic stainless steels and nickel alloys," *Philosophy Transactions of the Royal Society of London*, **A295**, 105.

Tamura, H., and Watanabe, T., 1973, "Mechanism of liquation cracking in the heat-affected zone of austenitic stainless steels," *Transactions of the Japan Welding Research Institute*, **4**(1), 30.

CHAPTER 16

THE WELD HEAT-AFFECTED ZONE

16.1. HEAT-AFFECTED ZONES IN WELDS

For any welding process that employs heat to obtain continuity between the atoms, ions, or molecules of abutting workpieces, there can be an effect on the microstructure and properties, even if there is no melting of the base materials.[1] The region affected by the heat of welding is called the *heat-affected zone*, commonly abbreviated *HAZ*. The heat-affected zone lies outside the fusion zone (FZ) in pure metals and outside the partially melted zone (PMZ) in alloys. As distance from the centerline of the weld increases, the heat-affected zone begins where the peak temperature of the welding cycle is just below the solidus temperature (as altered by nonequilibrium as described in Section 13.1) and extends to a point where the peak temperature is high enough long enough (under conditions of nonequilibrium) to cause some change in the microstructure of the base material(s) that alters one or more properties. A temperature that is high enough long enough, is terribly important, because high temperature in and of itself is not a problem, so long as the structure and, thus, the properties are not altered. Since virtually all phase transformations and reactions take time for nucleation to occur, and for the transformation or reaction to progress, time at temperature is important. Herein is where deviation from the ideal conditions of equilibrium alters structure and properties in real materials processed in the real world.

The exact effect of exposure to elevated temperature on the microstructure and properties of a base material depends on what that base material is and

[1] What is being said about welding processes also applies to brazing and soldering processes to the extent that these processes heat the base material.

how it obtains its properties, that is, the operative strengthening mechanism(s). Metals and alloys of engineering interest, to which we will restrict our attention in this treatment, are generally strengthened by one or more of the following basic mechanisms: (1) grain refinement, (2) work or strain hardening or cold working, (3) solid solution strengthening or alloying, (4) second-phase strengthening by precipitation hardening or aging, (5) transformation hardening (sometimes called quench hardening, since for most systems such transformations are brought about by quenching an elevated-temperature phase to room temperature or below to produce a nonequilibrium phase), and (6) second-phase strengthening by a dispersoid or dispersion strengthening. Especially affected by heat are work-hardened, precipitation-hardened, and transformation-hardened materials. Relatively unaffected are solution-hardened and dispersion-strengthened materials, except for some grain growth effects in the former, and to a lesser extent in the latter. To the degree that crystalline ceramics are strengthened by the same mechanisms or processes, they will respond to heat in a similar way. Crystalline polymers, which tend to obtain their strength from different mechanisms, respond differently.

A complete understanding of welding demands an understanding of the effects of heat on the structure and properties of materials in the weld heat-affected zone. Let's begin by looking at the heat-affected zone for generic metallic materials strengthened by each of the various possible mechanisms.

16.2. THE HAZ IN WORK-HARDENED OR COLD-WORKED METALS AND ALLOYS

16.2.1. The Physical Metallurgy of Cold Work/Recovery/Recrystallization/Grain Growth

When a metal or metallic alloy is plastically strained (i.e., stressed beyond its elastic limit or yield strength) at temperatures less than approximately 0.35–0.5 of its absolute melting point, new imperfections are generated in its crystalline lattice and existing imperfections interact to alter properties. Point or zero-dimensional imperfections in the form of vacancies and crowd ions are generated, which, while they have little effect on mechanical properties, lower electrical conductivity by causing scattering of electrons participating in conduction (conduction electrons). Existing one-dimensional or line imperfections (known as dislocations) in the crystal structure are set in motion to enable plastic deformation by slip. As these available dislocations become unable to accommodate all of the strain required by the imposed stresses, new dislocations are generated from various sources, including free surfaces, grain boundaries, Frank–Reed sources, and others. Preexisting dislocations and new dislocations eventually interact when they encounter obstacles such as grain boundaries or second-phase particles (or their boundaries) and pile up, or when they simply cross one another's paths on intersecting active slip planes

to form immobile tangles or jogs. Once they are pinned by obstacles, tangles, or jogs, further dislocation motion is hindered, and the resistance of the metal or alloy to further plastic strain is increased; that is, the material is strengthened. Pure metals or metallic alloys strengthened by such cold work are said to have experienced *work hardening* or *strain hardening*.

The phenomenon of work hardening or strain hardening is shown in Figure 16.1a and b for a typical ferrous and nonferrous material, while Figure 16.1c shows an "ideal" metal or alloy in which there is no work hardening. Note in Figure 16.1a and b how the stress needed to cause further strain in an engineering stress–engineering strain diagram increases to the point of fracture. Releasing the load at any point allows recovery of the elastic portion of strain, but not the plastic portion, and upon reloading, the stress to cause yielding by further dislocation motion is increased. The reason for this increase is that all dislocations able to move at lower stresses have moved (since temperature is

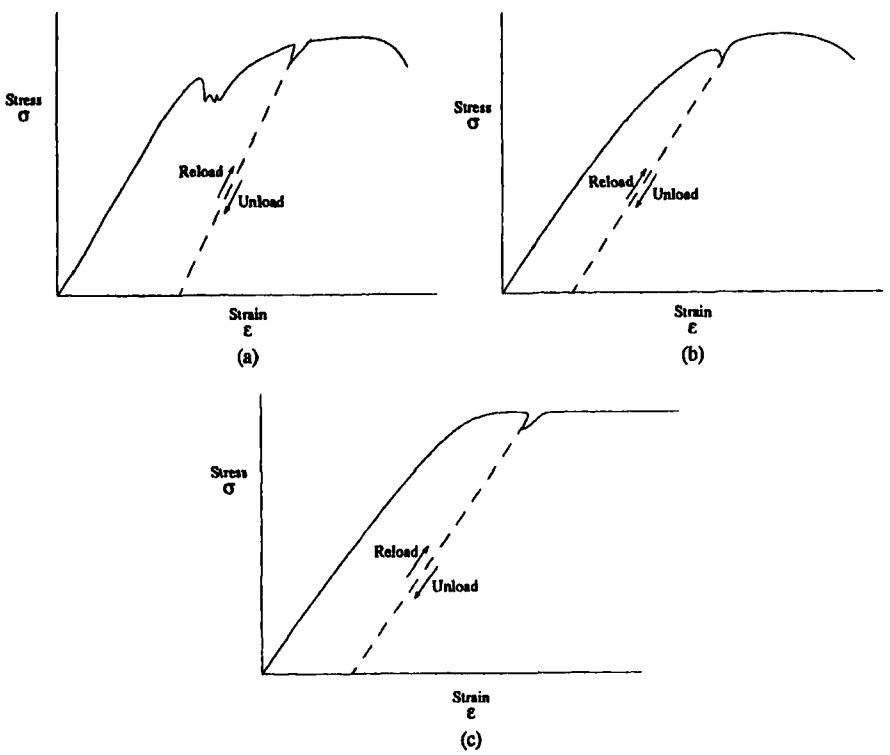


Figure 16.1 Strain hardening or work hardening can be seen in the engineering stress–engineering strain diagram for a typical (a) ferrous and (b) nonferrous metal or alloy. Note how the stress to cause continued strain increases, and how releasing the load at any point causes the stress to cause further yielding upon reloading to be increased. The behavior of a hypothetical material that does not exhibit work hardening is shown in (c).

too low to allow any recovery process relying on diffusion to occur). To move these now piled-up or tangled dislocations farther, or to move other dislocations, requires a higher stress or driving force.

In certain forming operations, strain hardening is a hindrance, since it makes continued plastic deformation of the material more difficult and may require unacceptably high forces to secure the desired deformation. On the other hand, strain hardening may be advantageous because it increases the elastic limit of the material. Two examples where such behavior is desirable are, (1) in the manufacture of springs, where direct proportionality between applied stress and resulting strain makes division of the stress scale simple, and (2) to eliminate the presence of an upper and lower yield point in ferrous materials (as can be seen to occur in Figure 16.1a).

With an upper and lower yield point present, such as occurs in plain carbon and low-alloy steels, localized deformation follows attainment of the upper yield point, in which dislocations pinned by atmospheres of interstitial carbon suddenly break away and cause nonuniform, localized deformation. Such deformation, known as Lüder's bands, appears as stretch marks, and produces an "orange peel" surface texture. Such behavior is unacceptable where the surface finish of a cold-worked part is important (e.g., automobile exterior body panels). Upper and lower yield points are eliminated by stretching a sheet to a strain level above the lower yield point strain level, then either unloading and forming the part in a reasonably short time period, or immediately as an integral step of the same operation (stretch forming). This process is known as stretch leveling. Waiting too long following stretch leveling, allows carbon (Cottrell) atmospheres to reform, with reappearance of upper and lower yield points. This phenomenon is known as strain aging.

Most of the energy expended in plastically deforming a material appears as heat, through the conversion of work to heat (see Section 8.8). A small fraction, typically around 3–8%, of the work done is stored as strain energy in the crystal lattice, that is, as distortion in bond lengths, imagined to be springs stretched or compressed from their relaxed position at the equilibrium spacing of the atoms comprising the lattice (see Sction 1.3). This stored energy creates an energetically unfavorable condition that is metastable at best. This behavior is shown in Figure 16.2.

When a work-hardened metal (or alloy) is exposed to temperatures greater than approximately $0.4T_{\text{MPabsolute}}$ (or $0.4T_{\text{solidus}}$ in absolute degrees), the deformed grains tend to nucleate[2] new strain-free grains in a process generally called annealing and specifically known as recrystallization annealing or simply

[2]This process of nucleation is essentially identical to the process of nucleation that takes place during solidification. A new phase tries to form since it has a lower volume free energy, resulting in a negative volume free energy change. The creation of a new phase results in the creation of an interface between the new daughter phase and the original parent phase, and gives rise to a positive surface free energy. In fact, additional positive energy is required to cause the parent phase to strain to accommodate the daughter phase, whether the daughter phase's specific volume is smaller or larger than the parent's. At some critical size for the new nuclei, the total of these opposing energies reaches a maximum, and further growth results in a stable structure.

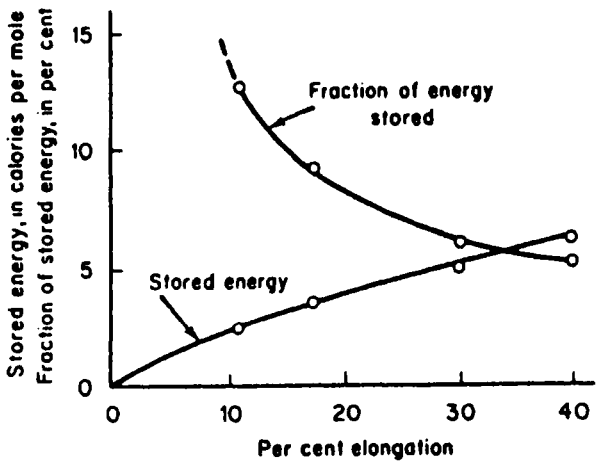


Figure 16.2 Conversion of mechanical work to stored energy in the form of lattice strain. (From "Microcalorimetric investigation of recrystallization of copper" by P. Gordon, *Transactions of the AIME*, **203**, 1955, 1043–1052, with permission of the AIME, Warrensdale, PA.)

recrystallization. The driving force for recrystallization is the reduction of stored strain energy, which is reduced as the new, strain-free grains are formed. With the onset of recrystallization, mechanical properties change drastically. Strength decreases, hardness decreases, and ductility and toughness increases. This is shown in Figure 16.3.

Even before recrystallization begins, certain less obvious changes occur. Specifically, zero-dimensional, point imperfections (e.g., crowd ions and vacancies) are reduced in number, or are "annealed out," and certain properties change. Most notably, electrical resistivity decreases as scattering sites to charge carriers are reduced, hence, electrical conductivity increases (or, really, is restored to its original level before cold work), as shown in Figure 16.3. This process, known as *recovery*, is usually of little concern in welding, but is important generally as a predecessor of recrystallization.

The extent of recrystallization increases with increasing annealing temperature and/or time according to an Avrami relationship (see Figure 14.20), and the rate at which recrystallization occurs is greater (or the temperature could be lower) for more severely cold-worked materials or for purer materials (which have lower yield strengths than alloys). During welding, this means that the extent of recrystallization increases as the peak temperature increases as the distance from the fusion zone boundary is reduced.

Once recrystallization is complete, the newly formed, strain-free grains grow in order to reduce the surface energy associated with grain boundaries (which are two-dimensional, planar imperfections). Grain growth also increases with increased temperature and time at temperature, and so is greatest very close to

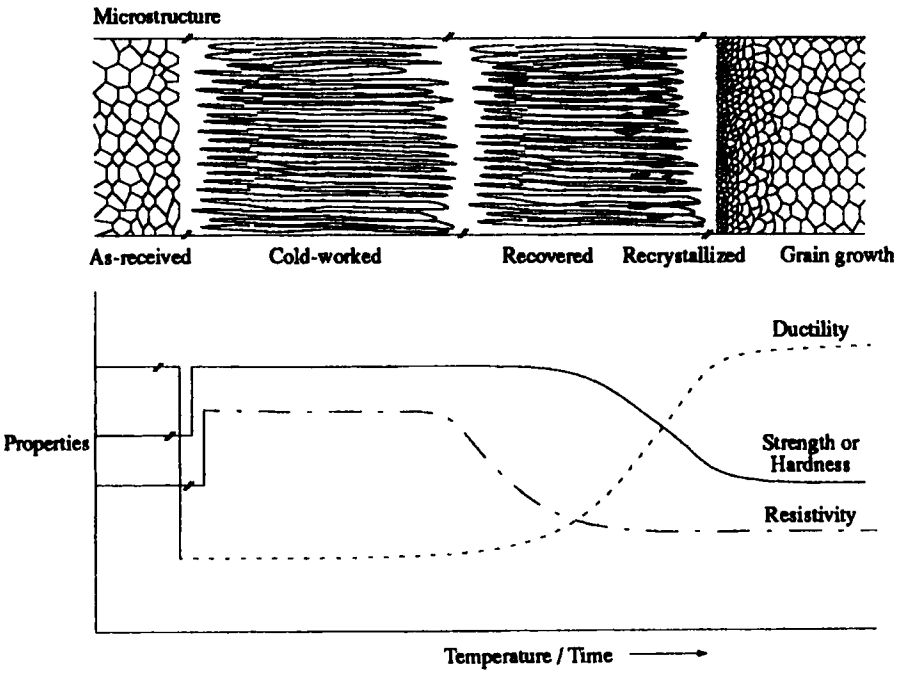


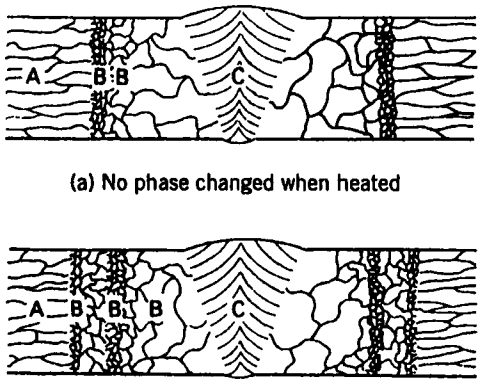
Figure 16.3 Schematic illustration of the change in microstructure and change in properties as the sequential processes of recovery, recrystallization and grain growth occur following cold working.

the fusion zone boundary and as the net linear heat input is increased. All materials exhibit grain growth on heating, regardless of whether they have been cold worked.[3] Grain growth reduces yield strength (more than tensile strength), ductility, and toughness, but the effect is usually not noticeable unless the width of the region of grain growth becomes great or the size to which grains grow becomes excessive (thereby reducing available slip systems and altering the critical resolved shear stress needed to cause slip).

If cold-worked materials undergo an allotropic transformation or solid-state phase change when heated, the effects of welding are more complex, as shown in Figure 16.4. Steel, titanium, and certain other alloys that exhibit allotropic transformations may have two recrystallized zones, as shown in Figure 16.4b. The first fine-grained zone results from recrystallization of the cold-worked, lower-temperature alpha phase. The second fine-grained zone results from the allotropic transformation to the high-temperature phase, not from recrystallization, as is often stated.

The effect of work hardening is completely lost in the fusion zone and

[3]The only time grain growth does not occur is when the grain boundaries are pinned by thermodynamically stable particles, such as carbides or nitrides, or, better yet, dispersed oxides or other phases. This phenomenon is discussed in Section 16.7.



(a) No phase changed when heated

(b) Allotropic transformation when heated

Figure 16.4 Schematic of recrystallization of cold-worked grains in the heat-affected zone of (a) a single-phase material in which no solid-state phase change occurs on heating and (b) of a material that undergoes an allotropic transformation on heating. (From *Welding Handbook*, Vol. 1: *Welding Technology*, 8th ed., edited by L. P. Connor, published in 1987 by and used with permission of the American Welding Society, Miami, FL.)

partially melted zone owing to melting and solidification, and is partially lost in the heat-affected zone due to recrystallization and grain growth. Table 16.1 gives the recrystallization temperatures for several important metals as a guide for assessing the heat effect to be expected following welding. Figure 16.5 schematically illustrates how the width of a heat-affected zone, such as occurs in a cold-worked metal, is affected by the net linear heat input during welding.

16.2.2. Cold-Worked Metals and Alloys in Engineering

Examples of metals and alloys commonly used in a cold-worked condition are listed in Table 16.2 along with some of their properties. While cold working is used with various aluminum alloys (giving rise to the -H temper designations), Cu-Zn brasses, plain low- and high-carbon steels, and austenitic stainless steels, it is also particularly useful for strengthening certain pure metals where alloying would unacceptably degrade other important properties (e.g., electric conductivity).[4] Examples are copper, aluminum, titanium, nickel, and some refractory metals such as W or Mo. Metals and alloys in a cold-worked condition are often designated by terms such as "$\frac{1}{4}$-hard," "$\frac{1}{2}$-hard," "$\frac{3}{4}$-hard," "full-hard," "spring-hard," or "spring-temper," which refer to progressively greater degrees of cold working.

[4]Cold working, in and of itself, degrades electrical conductivity by impeding the flow of charge carriers by increasing scattering. However, the degradation of electrical conductivity is often less than would be caused by alloying to achieve the same increase in yield strength.

TABLE 16.1 Recrystallization Temperatures for Some Important Metals

Metal	Approximate Minimum Recrystallization Temperature
Lead (Pb)	Below room temperature, 20°C (68°F)
Tin (Sn)	Below room temperature, 20°C (68°F)
Cadmium (Cd)	Room temperature, 20°C (68°F)
Zinc (Zn)	Room temperature, 20°C (68°F)
Magnesium (Mg)	150°C (300°F)
Aluminum (Al)	150°C (300°F)
Copper (Cu)	200°C (390°F)
Gold (Au)	200°C (390°F)
Silver (Ag)	200°C (390°F)
Iron (Fe)	450°C (840°F)
Platinum (Pt)	450°C (840°F)
Nickel (Ni)	600°C (1100°F)
Titanium (Ti)	650°C (1200°F)
Beryllium (Be)	700°C (1290°F)
Molybedenum (Mo)	900°C (1650°F)
Tantalum (Ta)	1000°C (1830°F)
Tungsten (W)	1200°C (2200°F)

Source. Originally, Jeffries and Archer, *The Science of Metals*, McGraw-Hill Book Company, 1924, p. 86.

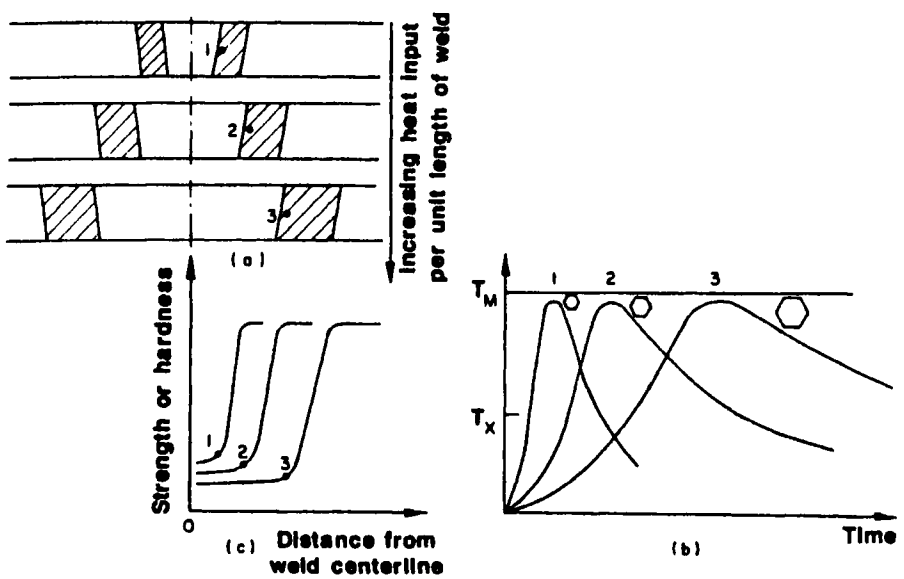


Figure 16.5 Schematic illustration of the effect of net linear heat input to a weld on (a) the size of the HAZ, along with (b) the welding thermal cycles near the fusion zone boundary for various net linear heat inputs, and (c) strength or hardness profiles across the HAZ. (From *Welding Metallurgy* by S. Kou, published in 1987 by and used with permission of John Wiley & Sons, Inc., New York.)

TABLE 16.2 Examples of Pure Metals and Alloys Commonly Used in the Cold-Worked Condition (Along with Yield and Ultimate Tensile Strength in ksi)

	Cold-worked		Annealed	
	YS	UTS	YS	UTS
Aluminum and aluminum alloys				
EC-H19	24	27	4	12
1xxx-H12, H14, H16, or H18	18–22	19–24	4–5	10–13
3xxx-H18	27–36	29–41	6–10	16–26
5xxx-H18, H38, or H113	33–37	42–46	13–21	28–40
Copper and copper alloys				
Pure Cu				
$\frac{1}{2}$-hard	37–46			30–38
Hard	43–52			
Spring hard	50–58			
Extra spring-hard	52+			
Mn-bronze	45–60	75–80	30	65
70Cu-30Zn (cartridge brass)				
Hard	63	76	17	49
Spring hard	65	90		
85Cu-15Zn (red brass)				
Hard	57	70	14	41
Spring hard	63	84		
Cupronickel (70Cu-30Ni)	70	75	25	60
Be-Cu (approx. 2% Be)[a]	70	107	25	72
Iron and iron alloys				
Low-C steels				
$\frac{1}{4}$-hard/hard		55/80		45
Austenitic stainless (60% work)		190		100
Magnesium and magnesium alloys				
AZ31B (and others)	24–32	38–42	24	38
Nickel and nickel alloys				
Pure Ni (cold drawn)	50–130	100–150	30–60	90–120
Monel (67Ni-30Cu)	55–120	85–125	25–40	70–85
Precious metals and alloys				
Gold/Au alloys	nil	19	30	32
Platinum/Pt alloys	nil	17–26	N/A	38–52

[a]Be-Cu alloys can also be artificially aged to even higher strenghs (see Table 16.3).

A proper combination of cold work and precipitation hardening (discussed in Section 16.4) can result in strength and hardness unattainable by either process alone. This is shown for beryllium–copper sheet in Table 16.3. As seen in Section 16.4, cold work increases the uniformity of precipitation by increasing the number of nucleation sites along dislocations and at dislocation tangles.

TABLE 16.3 Effect of Combined Cold Work and Precipitation Hardening on the Strength and Hardness of Beryllium–Copper Sheet

Condition	Tensile Strength (psi)	Elongation in 2 inches (%)	Brinell Hardness (3000 kg)
As annealed	70,000	45	110
Annealed and cold worked	120,000	4	220
Annealed and aged only	170,000	6	340
Annealed, cold worked, and aged	200,000	2	365

Source. Originally from Clark and Varney, *Physical Metallurgy for Engineers*, D. Van Nostrand Company, Princeton, NJ, 1962, p. 480.

16.2.3. Avoiding or Recovering Property Losses in Work-Hardened Metals or Alloys

The effect of weld heat on the heat-affected zone of a work-hardened material can be seen in Figure 16.6, where the thermal cycle at each of three points, as well as a hardness traverse showing the location of these three points, are shown. Note that the closer to the fusion boundary, where the peak temperature of the thermal cycle is higher, and the longer the retention time above the effective recrystallization temperature, T_x, the greater the reduction of hardness. Hardness and strength continues to decrease as the fusion boundary is approached, since the hardness and strength of a work-hardened material decreases with increasing annealing temperature and time. Incidentally, grain growth and its effects are greatest nearest the fusion boundary where peak temperatures were highest and where time at temperatures above T_x was longest.

Both the width of the heat-affected zone within which peak temperatures of the welding cycle are high enough to cause recovery, recrystallization, and grain growth in cold-worked metals and alloys, and the retention time above the effective recrystallization temperature (T_x) increase with increasing heat input per unit length of weld. As a result, the loss of strength in the HAZ becomes more extensive and more severe as the net linear heat input to the weld is increased. Again, the effect of heat input on size of the HAZ is shown in Figure 16.5, while the effect on the hardness in the HAZ of a work-hardened aluminum alloy AA5356 (essentially, Al-5Mg) is shown in Figure 16.7.

There are always two fundamental approaches to minimizing the adverse effects of the heat of welding on the base material microstructure surrounding a weld (the HAZ): (1) is prevention or avoidance of the problem, and (2) remediation of the problem by attempting to recovery properties. (We've discussed this before!) Prevention in engineering, as in medicine and law, is fundamentally better than remediation, and perhaps nowhere is this more true

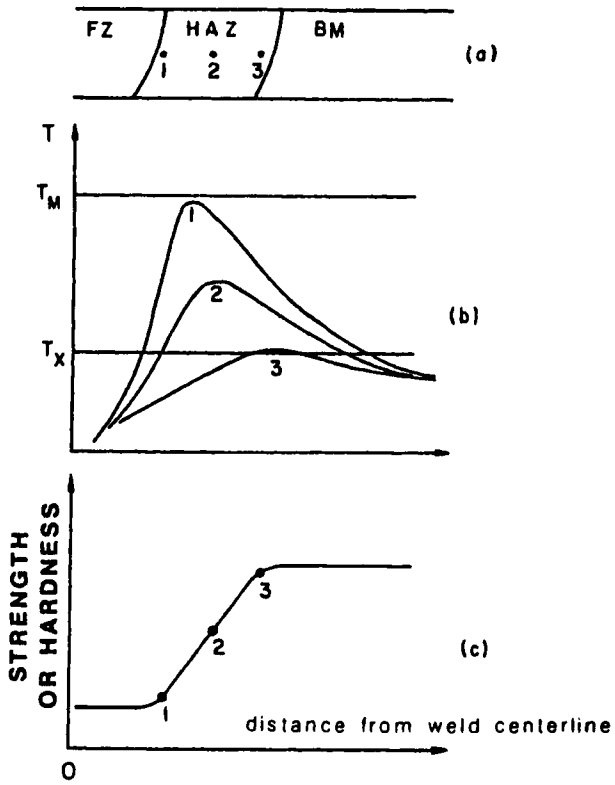


Figure 16.6 Plot showing the softening of a work-hardened material due to welding (c) at three locations in the heat-affected zone (a) for three corresponding weld thermal cycles (b). (From *Welding Metallurgy* by S. Kou, published in 1987 by and used with permission of John Wiley & Sons, Inc., New York.)

than for work-hardened metals and alloys. The reason is that once a cold-worked structure has experienced recrystallization and lost strength and hardness, the only way to restore those properties is to rework the affected area mechanically. This is often, although not always, impossible, and is always difficult and less effective than the original working.

Options for restoring cold work include (1) rolling or roll-planishing the raised weld crown and root beads, as well as the surrounding heat-affected zone (i.e., reducing the thickness by cold processing); and (2) locally cold working the weld region (i.e., fusion and heat-affected zones) by hammer peening (perhaps with a pneumatic riveting gun) or shot peening. The reason this is difficult, and perhaps impossible, is that such reworking will change the shape and dimensions of the assembly, even if there is sufficient access to allow the needed working.

The better, more practical approach is to prevent or minimize loss of properties by minimizing the degree of recrystallization. This can be accom-

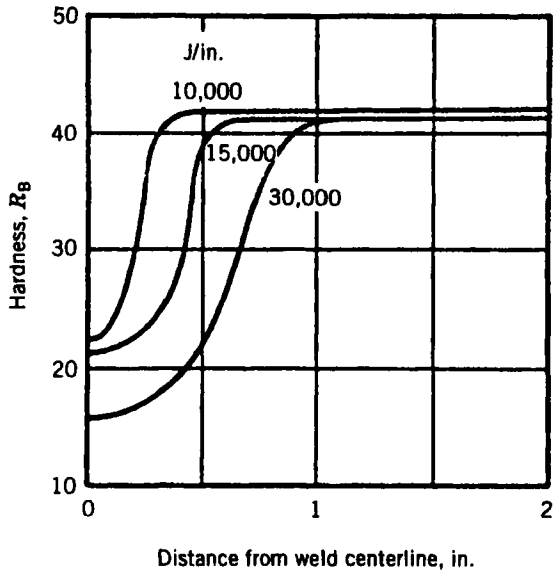


Figure 16.7 Plots showing the effect of net linear heat input on the hardness in the HAZ in cold-worked AA5356 (essentially, Al-5Mg) aluminum alloy. (From "Plastic properties of aluminum-magnesium weldments" by S. S. White, R. E. Manchester, W. G. Moffatt, and C. M. Adams, *Welding Journal*, 39(1), 10s–19s, 1960, published by and used with permission of the American Welding Society, Miami, FL.)

plished by (1) keeping net linear heat input as low as possible, (2) selecting a source with the highest energy density possible, and (3) minimizing the time at temperature. Minimizing net linear heat input usually means welding as fast as possible. Selecting a high-energy-density source usually means employing LBW, EBW, PAW, or, possibly, GTAW. Minimizing time at temperature usually means employing a high-energy-density source, but could be achieved by employing resistance welding techniques, especially using stored energy sources (e.g., capacitor-discharge welding). Of course, it's also possible to prevent recrystallization of work-hardened metals or alloys by not allowing the temperature to rise above approximately 0.4 of the absolute melting point (or solidus temperature). This might mean relying on cold nonfusion processes, but could also mean resorting to brazing (or, less likely, soldering) to accomplish joining.

16.2.4. Development of a Worked Zone in Pressure-Welded Materials

When pressure is used to bring the atoms of metals and alloys together by plastic deformation to produce welds without fusion, there is a localized effect on the microstructure. Such processes are called nonfusion, pressure-welding processes. The effect on the microstructure depends on the temperature at

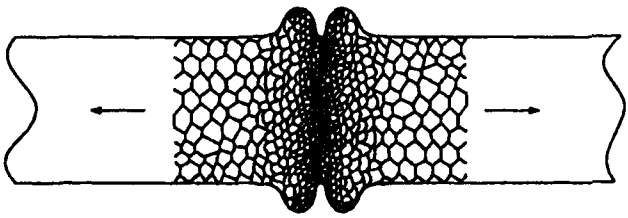


Figure 16.8 Schematic showing the effect of dynamic recrystallization in the vicinity of the original interface between two materials being welded using pressure at temperatures above approximately $0.4T_{\text{MPabsolute}}$. Note the region of grain refinement.

which the pressure is applied and under which plastic deformation is caused to take place. If the temperature is below approximately $0.4T_{\text{MPabsolute}}$, material in the vicinity of the interface will be cold worked, exhibiting the characteristic deformed grain pattern and work hardening of such a structure. This would be the case for so-called cold welding processes. On the other hand, if the temperature at which pressure is applied, or to which the material rises as a result of the work converted to heat, exceeds $0.4T_{\text{MPabsolute}}$ for sufficient time, material in the vicinity of the interface will undergo plastic deformation and immediate recovery and/or recrystallization, depending on how high the temperature is. This process is called dynamic recrystallization, and is exactly the same as normal recrystallization, except that it occurs at the same time that work is introduced. In other words, as soon as dislocations are caused to move, pile up, or entangle, and multiply by generation, the strain energy of the crystal lattice is increased, the driving force for recrystallization is present, and the process of recrystallization occurs almost all at once, but, really, in rapid sequence.

The consequence of dynamic recrystallization accompanying hot pressure, nonfusion welding processes is usually evidenced by fine-grained structure right near the original interface between the materials being joined. This is shown schematically in Figure 16.8.

16.3. THE HAZ OF A SOLID-SOLUTION-STRENGTHENED METAL OR OF AN ALLOY

16.3.1. The Physical Metallurgy of Solid-Solution Strengthening or Alloying

If grain refinement (relying on the Hall-Petch relationship) or work hardening do not provide enough strength to a metal, there are other alternatives, most of which rely on addition of foreign atoms to produce alloys. The addition of foreign atoms to a pure metal produces solid solutions in which the foreign atoms occupy either sites on the lattice of the host metal or solvent normally

occupied by atoms of the host, or interstitial sites or spaces among these atoms. In both cases, the strength and hardness of the host or solvent is increased by the presence of the foreign or solute atoms. The reason is that the solute atoms are rarely the same size as the solvent atoms, so when they substitute for solvent atoms they create strain in the host lattice by disrupting normal, equilibrium bond lengths (again, picture bonds as springs that expand or contract to attach to a substitutional solute atom). For solute atoms that are larger than the solvent atoms, compression of the bonds gives rise to a compressive strain field. For solute atoms smaller than the solvent atoms, extension of the bonds (to maintain bonding) gives rise to a tensile strain field. Either strain field around solute atoms interacts with either the tensile or compressive portion of the strain field always associated with a dislocation, thereby impeding the dislocation's motion by repulsion and causing the modified host material to be stronger and harder.

For solute atoms that occupy interstitial sites, because they are small enough to do so without leading to too much strain, significant strain (which is always compressive) is also produced. Thus, for these solutes too, dislocation motion is impeded and the host material is strengthened. The mechanism of strengthening described here and shown schematically in Figure 16.9 is known as *solid solution strengthening* or *alloying*.

For metals alloyed to form single-phase solid solutions, the heat of welding causes no change other than grain growth, provided the alloy is not also work-hardened. In a work-hardened, single-phase, solid-solution-strengthened alloy, the heat of welding will lead to recovery, recrystallization, and grain growth, as shown in Figure 16.4a. The result of grain growth in the high-

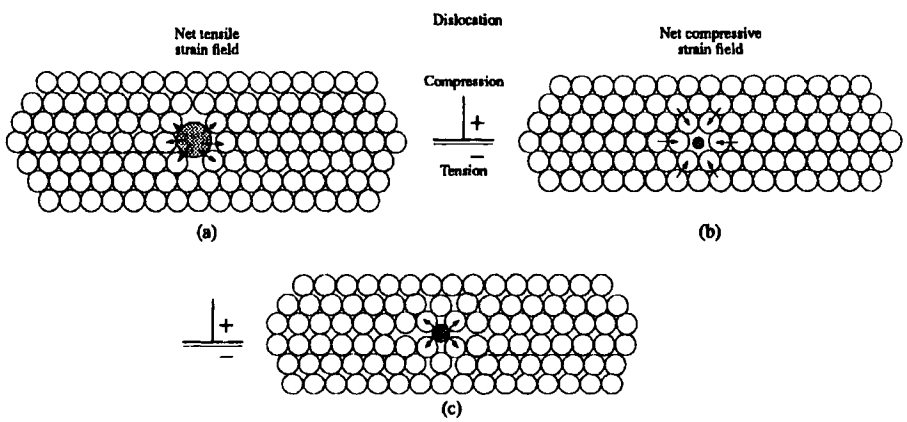


Figure 16.9 Schematic illustration of dislocation motion being hindered by interaction between the strain field of (a) a larger or (b) a smaller substitutional solute atom, or (c) an interstitial solute addition to a host crystal lattice leading to solid solution strengthening.

temperature region of a heat-affected zone is once again reduced yield strength and reduced ductility and toughness, as seen in Section 16.2.1. With melting and oxidation especially when the weld pool is super-heated and stirred by convection, composition could change as high vapor pressure of oxidation-prone solute(s) are lost. An example are Zn-bearing brasses.

As progressively greater concentrations of solute are added to a host metal, the amount of strain created in the host lattice progressively increases, whether that solute goes into solution substitutionally or interstitially. For all interstitial solutes and for those substitutional solutes whose atoms are more than 8% different in size (even if inherent crystal structures of the host solvent and added solute are the same) than the solvent atoms, a limit is reached where no more lattice strain can be accommodated. At this point, the solution is said to be saturated with solute, and the solubility limit (for that solute in the host) has been reached. Increasing the solute content beyond this solubility limit results in formation of a second phase, almost always having a different crystal structure. The situations for (a) unlimited or complete solid solubility and (b) limited solid solubility are shown in Figure 16.10, where the situation for no

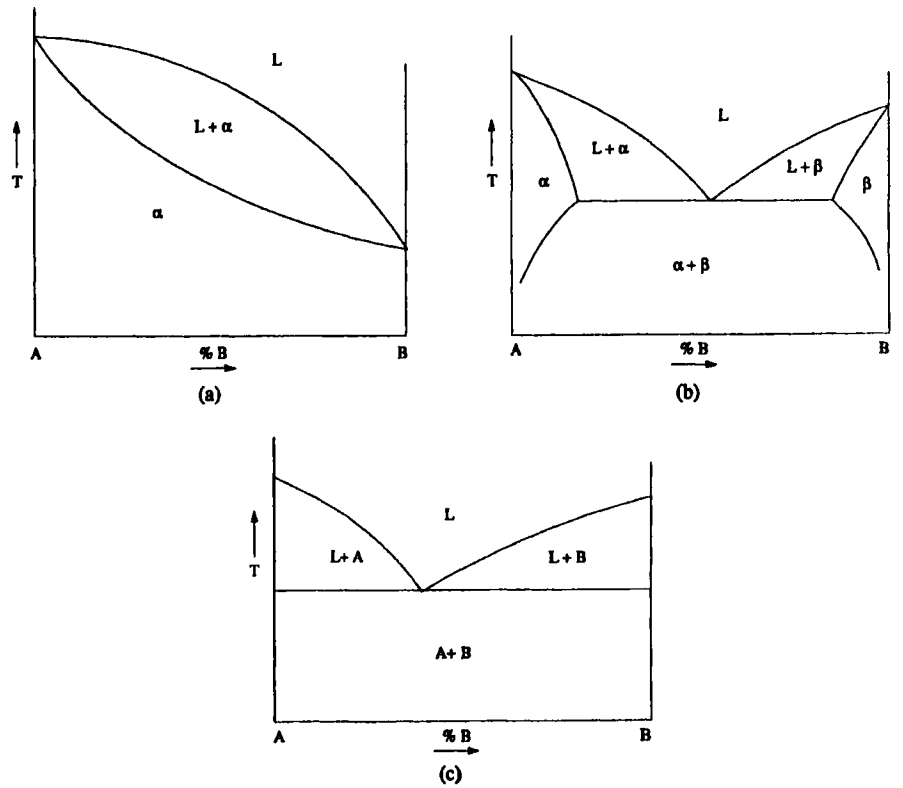


Figure 16.10 Hypothetical phase diagrams for binary alloy systems in which a solute has (a) unlimited or complete solubility, (b) limited solubility, and (c) no solubility in the host.

solubility is also shown (c). The last case is, obviously, not very interesting, since there would be no benefit from solid solution strengthening, but there would be from second-phase strengthening (as occurs in some solder systems).

16.3.2. Major Engineering Alloys Consisting of Single-Phase Solid Solutions

There are a number of alloys of engineering importance that consist of single-phase solid solutions. A few exist in binary systems in which the solute has unlimited solid solubility in the solvent (e.g., Cu-Ni), since the inherent crystal structures of Cu and Ni are the same (i.e., fcc) and less than 8% different in size. Many others simply have solute concentrations that place the alloy in a single-phase terminal solid-solution region near the solvent. Still others are intermediate solid solutions at higher concentrations of solute than for terminal solid solutions, at intermediate locations in the phase diagram's composition axis. Several examples of such alloys, of all three types, are listed in Table 16.4. Single-phase alloys that derive their strength (or other properties) from such simple solid-solution strengthening are called non-heat-treatable alloys, since they cannot be further strengthened either by developing a second phase precipitate or a metastable transformation phase.

16.3.3. Maintaining Properties in Single-Phase Solid-Solution-Strengthened Alloys

Other than being careful to prevent contamination or solute loss by improper shielding and/or cause excessive grain growth by excessive heat input, no special precautions are needed to weld single-phase, non-heat treatable, solid-solution-strengthened alloys. In fact, such alloys are considered highly weldable. The only exception to this is the occurrence of hot cracking associated with low-melting-point eutectics or compounds that segregate to grain boundaries in alloys that, while binary or ternary by design or appearance, contain small amounts of other elements that were either added or present as impurity (e.g., as in fully austenitic, as opposed to duplex, stainless steels).

16.4. THE HAZ IN PRECIPITATION-HARDENED OR AGE-HARDENABLE ALLOYS

16.4.1. The Physical Metallurgy of Precipitation- or Age-Hardenable Alloys

In some alloys, addition of solute beyond a certain limit (the solubility limit) leads to the formation of a second phase with much higher solute content. When that second phase forms from a parent phase as the result of precipitation, the

TABLE 16.4 Examples of Non-Heat-Treatable, Single-Phase Solid-Solution Strengthened Alloys of Engineering Importance

Aluminum alloys	
1xxx (commercial purity, >99% Al)	
3xxx Al-Mn (with added strength from fine, Mn, $FeAl_6$ dispersoids)	
4xxx Al-Si (predominantly used as filler metals, not in wrought form)	
5xxx Al-Mg must avoid formation of continuous β-Mg_3Al_2 in grain boundaries	
Copper alloys	
Phosphorus-deoxidized coppers	(99.9Cu, 0.008 to 0.02P)
Copper-Cd	(high-strength, high-conductivity alloy)
Low-zinc brasses	
Gilding	(95Cu, 5Zn)
Commercial bronze	(90Cu, 10Zn)
Red brass	(85Cu, 15Zn)
Low brass	(80Cu, 20Zn)
High-zinc brasses	
Cartridge brass	(70Cu, 30Zn)
Yellow brass	(65Cu, 35Zn)
Tin brasses	
Admiralty brass	(71Cu, 28Zn, 1Sn)
Special brasses	
Aluminum brass, arsenical	(77.5Cu, 20.5Zn, 2Al, 0.06As)
Phosphor bronzes	(90–98.7Cu, 10–1.3Sn, 0.2P)
Silicon bronzes	(97–98.5Cu, 1.5–3Si)
Copper–nickel (Cupronickels)	(70–88Cu, 9–30Ni)
Magnesium alloys	
Many Al-Zn (AZ) grades[a]	
Th-Zr (HK) grades	
Nickel alloys	
Low-alloy nickels	(99 + %Ni, plus Co, Fe, Cr, Mo, W, V, Ti, or Al)
Nickel–copper alloys (Monels)[a]	(30–67Ni, 37–68Cu, 1–2Fe or Mn or both)
Some Ni-Cr, annealed	
Some Ni-Cr-Fe, annealed	
Some Ni-Cr-Mo, annealed	
Titanium alloys	
Commercially pure (CP) Ti	(98.5–99.5Ti)
Alpha alloys	
Ti-5Al-2.5Sn	
Ti-6Al-2Sn-4Zr-2Mo	
Ti-5Al-5Sn-2Zr-2Mo	
Ti-6Al-2Nb-1Ta-1Mo	
Ti-8Al-Mo-1V	
Some beta alloys[a] (in the annealed condition)	
Refractory alloys of W, Mo, Ta, Hf	
Zirconium alloys	
Some Zr alloys	(95.5–99.2Zr + Hf, 4.5Hf)

[a]Some of these alloys can be precipitation-hardened.

alloy is said to be *precipitation-hardened* or *age-hardened.* Second phases always increase the strength of an otherwise single-phase alloy by hindering dislocation motion because of the interfacial strain energy they introduce.

Three conditions must exist for an alloy to be precipitation- or age-hardenable: (1) The solute must exhibit limited solubility in the solvent, (2) this solubility must decrease with decreasing temperature, and (3) the alloy of interest must have a nominal solute concentration (i.e., a composition) below the maximum limit of solubility. These three conditions are shown in Figure 16.11.

To develop the second-phase precipitate, the following steps must be followed in order:

Step 1: The alloy of nominal composition $C_0 < C_{max}$ must be heated into the single-phase α region, that is, above the solvus temperature, and held there to equilibrate. This step is called the solution heat treatment, solution anneal, or solutionizing step.

Step 2: The alloy must be cooled rapidly enough to allow insufficient time for the second-phase β to form (or, at least, grow very much) as the temperature falls below the solvus temperature, thereby retaining more solute in solution than permitted under equilibrium. The resulting condition is said to be supersaturated with respect to solute B in solvent A, and this step is called the quench treatment or quenching step.

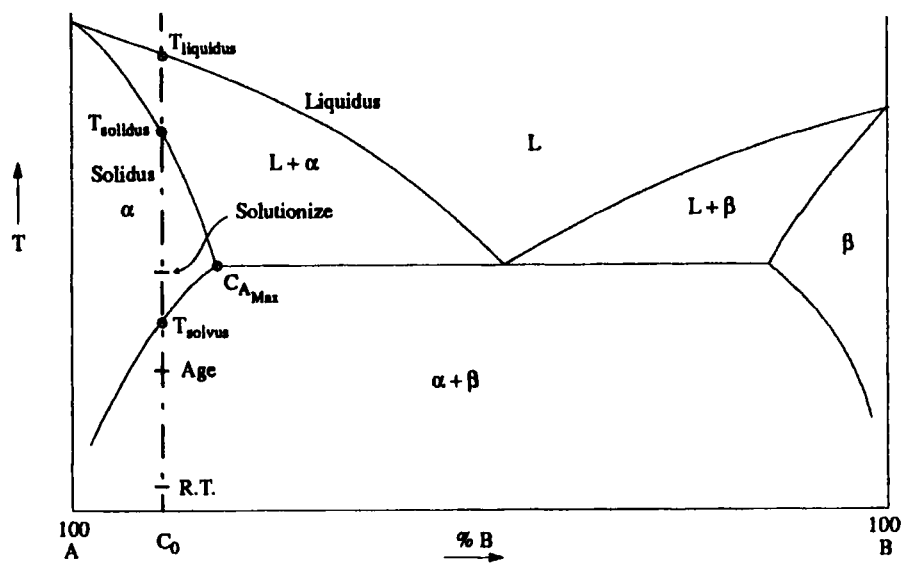


Figure 16.11 Hypothetical binary phase diagram for an alloy (nominal composition, $C_0 < C_{max}$) that can be precipitation or age hardened.

Step 3: The supersaturated alloy must be given sufficient time to allow second-phase β to nucleate and grow (or simply grow more from incipient nuclei) as a precipitate. This process, called the aging heat treatment or aging step, can be accelerated by heating the supersaturated solution to nearer but below the solvus temperature, thereby speeding diffusion of B in A.

The process of precipitation of a second phase involves the steps of nucleation and growth, and depends on diffusion of solute to obtain the composition necessary to produce the second phase. Thus, not surprisingly, the process of developing a new second phase takes time and, in fact, occurs in several progressive steps. These steps are shown below for a simple Al-4 wt% Cu alloy:

$$\text{Supersaturated SS} \rightarrow \text{GP1} \rightarrow \text{GP2}\ (\theta'') \rightarrow \theta \rightarrow \theta(Al_2Cu) \qquad (16.1)$$

In the first step, solute atoms begin to migrate to form a small cluster with solvent atoms which begins to approach the composition, and, perhaps, crystal structure of the new, stable precipitate phase, which is body-centered tetragonal Al_2Cu θ for this alloy system. These minute clusters, called Guinier–Preston zones (or GP zones in general and GP1 here), extend only up to about a 100 or so atom diameters in size and maintain coherency or lattice matching with the parent, supersaturated α phase. In doing so, they almost always cause some lattice distortion, producing some strain energy, that interferes with dislocation motion to cause some degree of strengthening. Nucleation, even at this early stage, while probabilistic, tends to occur heterogeneously on high-energy sites, such as grain corners, grain boundaries, and dislocations.

With increased time or temperature, these clusters grow in size as the result of further solute diffusion. As they grow, their composition continues to approach that required for the new precipitate phase (here, 33 at% Cu in Al_2Cu) and their crystal structure continues to approach that of the new phase (here, body-centered tetragonal). Coherency is still maintained, although the degree of lattice distortion and level of strain energy increases to cause even more strengthening effect by impeding dislocation motion even more effectively. These larger clusters, although not always differentiated in precipitation transformations, are called GP2 zones. The newly forming precipitate at this stage is often designated as a distinct, albeit metastable, phase, here θ''.

After still more time or still higher temperature and more diffusion of solute atoms to the GP zones, the newly forming phase becomes so large it begins to lose coherency, being unable to maintain lattice matching. In its semicoherent form, the new phase continues to grow in both size and number, with new nuclei forming heterogeneously on less potent, secondary sites. As growth continues, coherency continues to be lost, and the precipitates become less effective at impeding dislocation motion, that is, at strengthening the matrix

phase. At this stage, the alloy is said to be beginning to overage. For the Al-4 wt% Cu example, the phase at this stage is called θ'.

In the final stages of aging, the stable precipitate phase (here, θ) can form either from a metastable precursor (here, θ') or directly. In either case, lattice matching is totally lost, and the stable phase is incoherent with the solid solution matrix phase. The effectiveness of this incoherent precipitate is poor compared to the coherent phase.

The sequence of the formation and growth of a new, precipitate phase is shown schematically in Figure 16.12. Note the attempt to maintain coherency

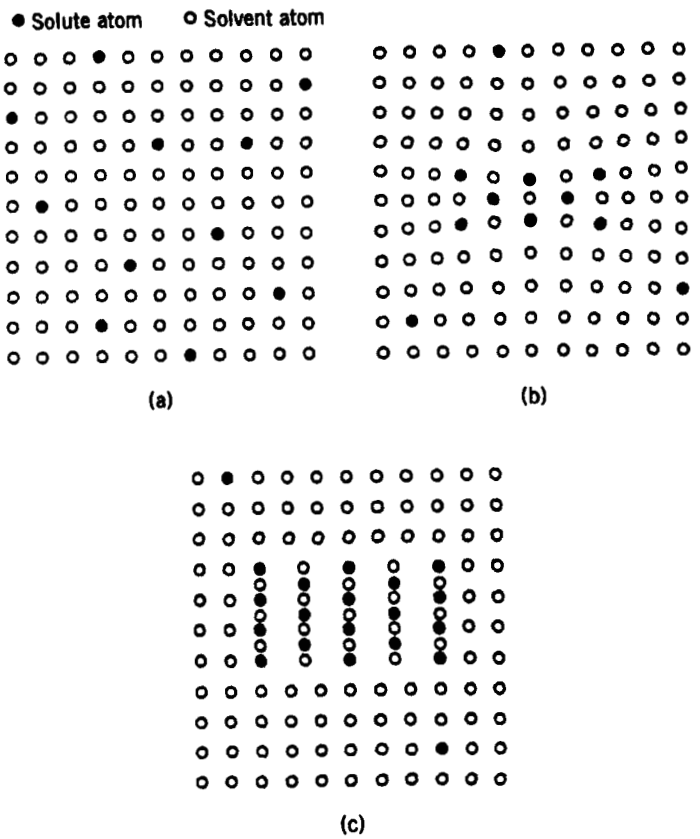


Figure 16.12 Schematic illustration of the sequence of steps in forming a precipitate, including (a) formation of a cluster (known as a Guinier–Preston or GP zone) that approaches the equilibrium composition and crystal structure of the new precipitate phase from the supersaturated solid solution; (b) growth of this cluster in size as equilibrium composition and structure is attained, maintaning coherency, and optimally strengthening the matrix (in what is usually known as a GP2 stage); and (c) attainment of the final phase, but with total loss of coherency with the onset and progress of overaging. (From *Elements of Physical Metallurgy* by A. G. Guy, 1959, Addison-Wesley, Reading, MA, used with permission of Addison-Wesley Publishing Company.)

as long as possible as the full, equilibrium composition and structure of the new phase is reached, producing optimum strengthening or optimum aging, then the loss of coherency during overaging.

The correlation of hardness or strength with the development with time of a precipitate during aging at various temperatures is shown schematically in Figure 16.13 for a generic alloy, and in Figure 16.14 for the Al-4 wt% Cu alloy used as an example. Note the following points:

1. Increasing the time at any temperature causes the general process to progress, first increasing the hardness and strength, then reaching at peak, and then decreasing with overaging.

2. The hardening or strengthening effect is greatest for any temperature of aging (or *aging temperature*) when the metastable, coherent phase (here, GP2 or θ'') is formed to its maximum concentration.

3. Increasing the temperature of aging causes the process to accelerate exponentially (because diffusion-controlled processes obey an Arrhenius relationship), bringing on peak or optimum aging, and subsequent overaging, sooner, and, often, not allowing the peak hardness or strength to reach as high a value (because of reduced numbers of particles as a consequence of fewer nucleation events).

It can now be understood how cold working before aging enhances the effect of precipitates. Cold work produces a greater number of and more potent nucleation sites by generating more dislocations and dislocation tangles.

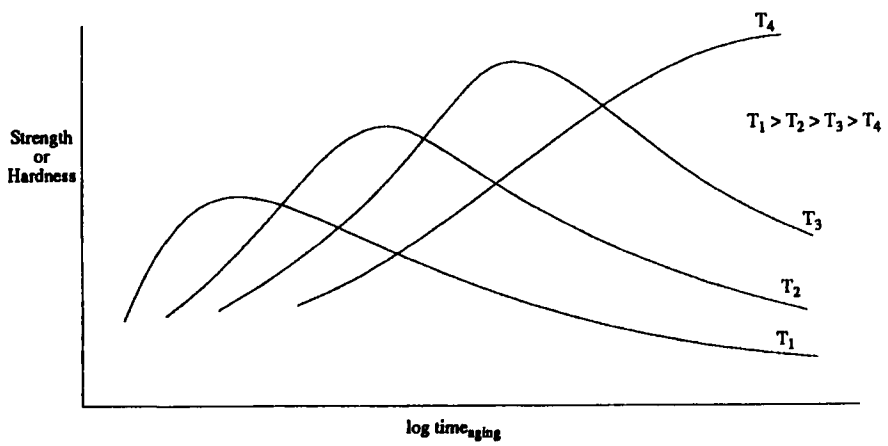


Figure 16.13 Generic correlation of the hardness (or strength) of an alloy with time for various aging temperatures.

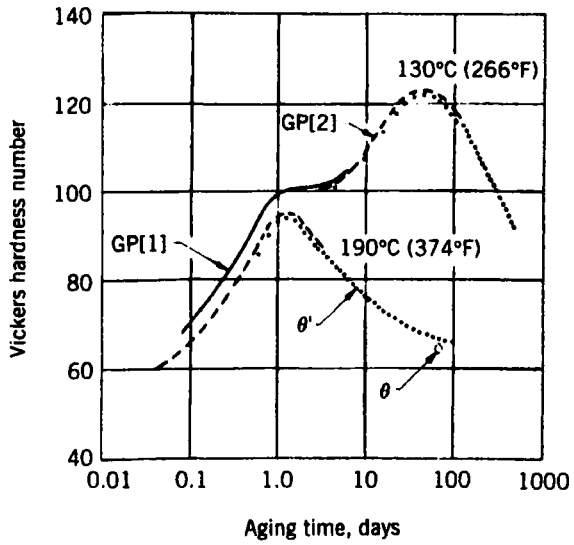


Figure 16.14 Correlation of structures and hardness of Al–4 wt% Cu alloy aged at two temperatures. (From "Structural ageing characteristics of binary aluminum–copper" by J. M. Silcock, J. J. Heal, and H. K. Hardy, *Journal of the Institute of Metals*, **82**, 239–248, 1953, published by and used with permission of the American Welding Society, Miami, FL.)

Other alloys exhibit a very similar sequence of structure and property development to that described for Al-4 wt% Cu, although the composition and structure of the final, stable precipitate obviously differs, and there may be some minor differences in the intermediate steps or stages. Further examples are given below for three popular, heat-treatable aluminum alloys and one heat-treatable nickel-based alloy:[5]

$$\text{Al-Cu-Mg (2024):} \quad \text{SS} \rightarrow \text{GP} \rightarrow \sigma'(\text{Al}_2\text{CuMg} \rightarrow \sigma\text{Al}_2\text{CuMg}) \tag{16.2}$$

$$\text{Al-Mg-Si (6061):} \quad \text{SS} \rightarrow \text{GP} \rightarrow \beta'(\text{Mg}_2\text{Si}) \rightarrow \beta(\text{Mg}_2\text{Si}) \tag{16.3}$$

$$\text{Al-Zn-Mg (7075):} \quad \text{SS} \rightarrow \text{GP} \rightarrow \eta'(\text{Zn}_2\text{Mg}) \rightarrow \eta(\text{Zn}_2\text{Mg}) \tag{16.4}$$

[5]For aluminum- and nickel-based (as well as some other) alloys, the term heat-treatable refers to the fact that these alloys can have their hardness and strength (or perhaps other properties, such as corrosion resistance) developed by thermal processing to cause precipitation or aging. Other times, the term heat-treatable may refer to the ability to develop properties by the development of various different arrangements of second phases (e.g., isothermal continuous cooling transformation of austenite to ferrite and pearlite or ferrite and bainite) or formation of a metastable phase by a diffusionless transformation (e.g., martensite in steels). The latter cases are described in Section 14.4.

Ni-Cr-Co-Mo (Udimet 700):

$$(Ni,Cr,Co,Mo,Al,Ti)\gamma \rightarrow Ni_3(Al,Ti)\gamma' + (Cr,Co,Mo) \text{ matrix} \qquad (16.5)$$

The key to selecting an appropriate combination of temperature and time to age a precipitation-hardenable alloy involves several considerations. First and foremost, the aging temperature during heat treatment must be higher than the maximum expected service temperature to preclude excessive overaging in service. This is usually not particularly difficult, since the rate of any diffusion-controlled transformation (such as precipitation), which follows an Arrhenius relationship with temperature, approximately doubles for every 30°C (50°F) increase in temperature. Therefore, to prevent excessive overaging in service, choose an aging temperature that is sufficiently high that service temperatures will result in diffusion rates several orders of magnitude slower (depending on expected exposure time and needed life). Second, choose a temperature high enough to allow attainment of optimum or peak strength or hardness in a reasonable heat treatment period. In industry, this usually means a period of time as short as possible, and within an 8-h or 16-h work shift for practicality. Third, avoid too high an aging temperature so that the time to attain peak strength is not too short. This could pose problems with obtaining reproducible results from run to run due to minor differences in heat treatment furnace temperature, exposure time, part size, precise alloy composition, and so on. Finally, the heat treatment time and especially temperature can influence the composition, morphology, and distribution of the precipitate.

16.4.2. Important Precipitation-Hardenable Alloys in Engineering

Many alloys of engineering interest develop their properties by precipitation or age hardening. By far the most important are (1) various heat-treatable Al-based alloys with Cu, Cu + Mg, Mg + Si, Zn + Mg, Si, and Li; (2) various heat-treatable Ni-based alloys with Cr, Cr + Nb, Cr + Mo, Cr + Co + Mo, Cr + Co + W, all relying on formation of nickel–aluminide/nickel–titanium intermetallic precipitates; (3) heat-treatable Mg-based alloys with aluminum; (4) precipitation-hardenable or PH austenitic, semiaustenitic or ferritic stainless steels, relying on various complex carbides as well as other (usually Cu-based) intermetallic precipitates; and (5) Ni-maraging steels, relying on various complex carbides and Cu-containing intermetallics. Important examples of these as well as a few other alloys are listed in Table 16.5.

16.4.3. Avoiding or Recovering Property Losses in Age-Hardenable Alloys

Alloys that derive their hardness and strength from the formation of a precipitate upon aging respond to the heat of welding by annealing, where

annealing is a general term in material science meaning to soften.[6] The response of the heat-affected zone of an age-hardened alloy during welding tends to be complex because the different thermal cycles imposed on different regions of the heat-affected zone have different effects, depending on peak temperature and dwell time above certain critical temperatures. Basically, however, what happens to the structure of an optimally age-hardened alloy happens in the microcosm of the heat-affected zone. This is shown schematically in Figure 16.14.

The heat-treating sequence for precipitation hardening a susceptible alloy is solution treat, quench, and age. In the heat-affected zone shown schematically in Figure 16.15, optimum, coherent precipitates in the base material are caused to dissolve, that is, go into solution, anywhere the peak temperature exceeds the solvus temperature (T_{solvus}) for sufficient time (i.e., retention time). The result of such re-solution, dissolution, or so-called reversion is pronounced softening due to the loss of all second phase as a hindrance to dislocation motion. Those regions of the heat-affected zone below the solvus temperature can cause overaging to occur, provided the temperature is high enough, long enough. In these regions, lying outside the region of reversion, the structure is also softened, due to loss of coherency of the precipitate phase. While the degree of softening is not as pronounced, it can be significant, especially closer to the reverted region. If the heat of welding does not raise the temperature in the heat-affected zone above the original aging temperature, or does so for only a very short time, the mechanical properties are not significantly affected.

The effect of welding heat on an optimally aged base metal thus causes the strength or hardness to vary from the centerline of the weld, through the fusion and partially melted zone, where all effect of aging is lost due to melting, through heat-affected zone regions of reversion, then severe overaging, then modest overaging, to unaffected base material. This is shown schematically in Figure 16.16.

With this understanding of what can happen in the HAZ of an optimally aged, age-hardenable alloy, there are several approaches to attempting to prevent loss of properties, as well as several approaches for attempting to recover properties. Let's begin with the always preferred prevention methods.

Since both re-solution (or reversion) and overaging of optimally aged precipitates takes both time and temperature, the two fundamental ways to

[6]In fact, there are many different kinds of annealing heat treatments, all of which result in softening. This requires the user to be more specific to make it clear how softening is being made to occur, whether on purpose (as in heat treatment) or accidentally (as in welding). Major specific annealing processes are recrystallization annealing, in which recrystallization of a cold-worked structure results in softening; stress-relief annealing, in which relaxation of residual stresses results in some softening, but more in improvement in fatigue and corrosion resistance; homogenization, in which composition is made uniform by allowing diffusion to reduce gradients from segregation; normalization, in which grain size is refined; and solution annealing, in which a soft, single-phase solid solution is formed, usually prior to subsequent aging or other transformation, as in decomposition of austenite in steels.

TABLE 16.5 Typical Quenched and Tempered Steels

ASTM Specification or Common Designation	Grade Type, or Class	Composition (%)										Min Strength (ksi)	
		C	Mn	P	S	Si	Cr	Ni	Mo	Cu	Others	Tensile	Yield
A514/A517	A	0.15–0.21	0.80–1.10	0.035	0.04	0.40–0.80	0.50–0.80		0.18–0.28		Zr,0.05–0.15; B, 0.0025		
	B	0.12–0.21	0.70–1.00	0.035	0.04	0.20–0.35	0.40–0.65		0.15–0.25		V, 0.03–0.08 Ti, 0.01–0.03; B, 0.0005–0.005		
	C	0.10–0.20	1.10–1.50	0.035	0.04	0.15–0.30			0.20–0.30		B, 0.001–0.005		
	D	0.13–0.20	0.40–0.70	0.035	0.04	0.20–0.35	0.85–1.20		0.15–0.25	0.20–0.40	Ti, 0.004–0.10[b]; B, 0.0015–0.005		
	E	0.12–0.20	0.40–0.70	0.035	0.04	0.20–0.35	1.40–2.00		0.40–0.60	0.20–0.40	Ti, 0.04–0.10[b]; B, 0.0015–0.005		
	F	0.10–0.20	0.60–1.00	0.035	0.04	0.15–0.35	0.40–0.65	0.70–1.00	0.40–0.60	0.15–0.50	V, 0.03–0.08; B, 0.0005–0.006	100–130/ 105–135	90/100
	G	0.15–0.21	0.80–1.10	0.035	0.04	0.50–0.90	0.50–0.90		0.40–0.60		Zr, 0.05–0.15; B, 0.0025		
	H	0.12–0.21	0.95–1.30	0.035	0.04	0.20–0.35	0.40–0.65	0.30–0.70	0.20–0.30		V, 0.03–0.08; B, 0.0005–0.005		
	J	0.12–0.21	0.45–0.70	0.035	0.04	0.20–0.35			0.50–0.65		B, 0.001–0.005		
	K	0.10–0.20	1.10–1.50	0.035	0.04	0.15–0.30			0.45–0.55		B, 0.001–0.005		
	L	0.13–0.20	0.40–0.70	0.035	0.04	0.20–0.35	1.15–1.65		0.25–0.40	0.20–0.40	Ti, 0.04–0.10[b]; B, 0.0015–0.005		
	M	0.12–0.21	0.45–0.70	0.035	0.04	0.20–0.35		1.20–1.50	0.45–0.60		B, 0.001–0.005		
	N	0.15–0.21	0.80–1.10	0.035	0.04	0.40–0.90	0.50–0.80		0.25		Zr, 0.05–0.15; B, 0.0005–0.0025		
	P	0.12–0.21	0.45–0.70	0.035	0.04	0.20–0.35	0.85–1.20	1.20–1.50	0.45–0.60		B, 0.001–0.005		
	Q	0.14–0.21	0.95–1.30	0.035	0.04	0.15–0.35	1.00–1.50	1.20–1.50	0.40–0.60		V, 0.03–0.08		

A533	A	0.25	1.15–1.50	0.035	0.040	0.15–0.30			0.45–0.60			80–125	50–82.5
	B	0.25	1.15–1.50	0.035	0.040	0.15–0.30		0.40–0.70	0.45–0.60				
	C	0.25	1.15–1.50	0.035	0.040	0.15–0.30		0.70–1.00	0.45–0.60				
	D	0.25	1.15–1.50	0.035	0.040	0.15–0.30		0.20–0.40	0.45–0.60				
A537	2	0.24	0.70–1.60	0.035	0.040	0.15–0.30	0.25	0.25	0.08	0.35		70–100	46–60
A543	B	0.23	0.40	0.020	0.020	0.20–0.40	1.50–2.00	2.60–4.00	0.45–0.60		V, 0.03	90–135	70–100
	C	0.23	0.40	0.020	0.020	0.20–0.40	1.20–1.50	2.25–3.50	0.45–0.60		V, 0.03		
A678	A	0.16	0.90–1.50	0.04	0.05	0.15–0.50	0.25	0.25	0.08	0.20[d]		70–90	50
	B	0.20	0.70–1.60	0.04	0.05	0.15–0.50	0.25	0.25	0.08	0.20[d]		80–100	60
	C	0.22	1.00–1.60	0.04	0.05	0.20–0.50	0.25	0.25	0.08	0.20[d]		85–115	65–75
HY-80		0.12–0.18	0.10–0.40	0.025	0.025	0.15–0.35	1.00–1.80	2.00–3.25	0.20–0.60	0.25	V, 0.03; Ti, 0.02	—	80
HY-100		0.12–0.20	0.10–0.40	0.025	0.025	0.15–0.35	1.00–1.80	2.25–3.50	0.20–0.60	0.25	V, 0.03; Ti, 0.02	—	100
HY-130		012	0.60–0.90	0.010	0.015	0.15–0.35	0.40–0.70	4.75–5.25	0.30–0.65		V, 0.05–0.10	—	130

[a]When a single value is shown, it is a maximum limit.
[b]Vanadium may be substituted for part or all of titanium content on a one for one basis.
[c]Limiting values vary with the plate thickness.
[d]When specified.

Source. From *AWS Welding Handbook*, 7th ed., Vol. 4: *Metals and Their Weldability*, edited by W. H. Kearns, published in 1982 by and used with permission of the American Welding Society, Miami, FL.

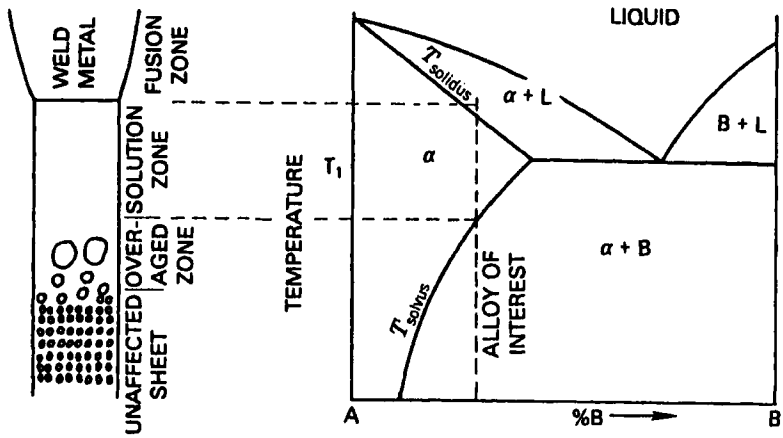


Figure 16.15 Effect of the heat of welding on the structure in the heat-affected zone of an optimally aged precipitation-hardenable alloy. HAZ structure is shown as it correlates to various temperatures on the equilibrium phase diagram. Remember, however, heating and cooling during welding deviate from equilibrium, so such a diagram must be used with caution. (From *Welding Handbook*, Vol. 1, *Welding Technology*, 8th ed., edited by L. P. Connor, published in 1987 by and used with permission of the American Welding Society, Miami, FL.)

prevent loss of properties are (1) keep the temperature below levels that will cause either reversion (the solvus temperature) or overaging; or (2) keep the time at elevated temperatures short. The first approach could be completely accomplished only by employing a nonfusion process, and one that doesn't cause much heating at that. While it is certainly worthwhile to minimize the extent of the heat-affected zone by keeping net linear heat input low for a fusion process, any softening that results from reversion or overaging is detrimental, as there is now a weak link where there was none before. In fact, one could make a fairly convincing argument that a narrow band of severe softening might be worse than a wide one, in that the narrow band acts more like a stress- (actually, strain-) concentrating notch. The second, far more practical approach is to employ a fusion process that causes very rapid heating and allows very rapid cooling, the idea being to keep the time at temperature so short that there is no time for the kinetics of degrading, diffusion-controlled processes to take place. This can be achieved using fast processes like capacitor discharge or even conventional spot, resistance welding, and, possibly high-energy-density EBW or LBW.

There is really a third approach to preventing loss of aged properties during welding, and that is to not age the weldment until after welding. In other words, whether the original material or parts comprising the weldment have been aged or not, following welding, solutionize the entire weldment, quench it, and optimally age it. This technique is expensive and risky to say the least,

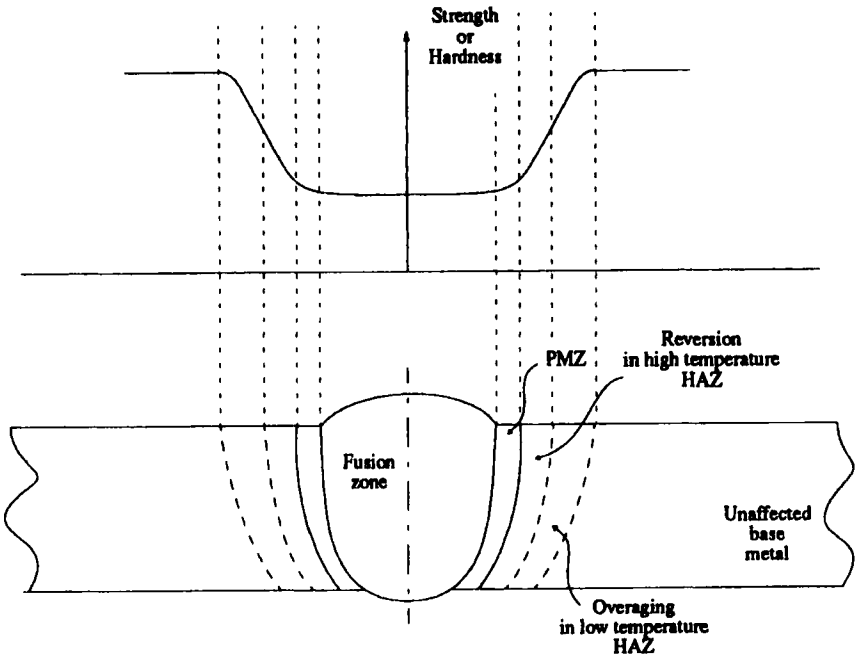


Figure 16.16 Schematic of the strength (or hardness) from the centerline of a fusion weld through the partially melted zone and high-to-low temperature heat-affected zone to the unaffected base metal of an optimally aged alloy.

as the high value-added weldment could be ruined by irreparable distortion or cracking, and is often impractical since solutionizing temperatures are so high they soften the structure to the point that shape and dimensions can be lost. Nevertheless, it may be a possibility.

If the material comprising parts to be welded has already been aged before welding, it will be necessary to try to recover properties lost due to reversion and/or overaging in the heat-affected zone. For such recovery, there are two approaches. First, following welding, re-age the weldment, either in its entirety, or locally, whichever is tolerable. Re-aging in a postweld heat treatment process will cause aging to take place in the fusion zone, where there was never any aging, presuming the filler is itself age-hardenable. It will also cause aging to take place in the partially melted zone and reverted region of the heat-affected zone. Anywhere aging takes place, there will be some recovery of strength and hardness, albeit perhaps not optimal. In the overaged regions of the HAZ, postweld aging will cause some additional overaging, which will probably further lower strength and hardness, and will definitely not improve the situation. The effect of such an aged + weld + postweld age (A + W + PWA) approach is shown in Figure 16.17, comparing aged before welding (curve A), previously aged/as-welded (curve B), and previously aged/

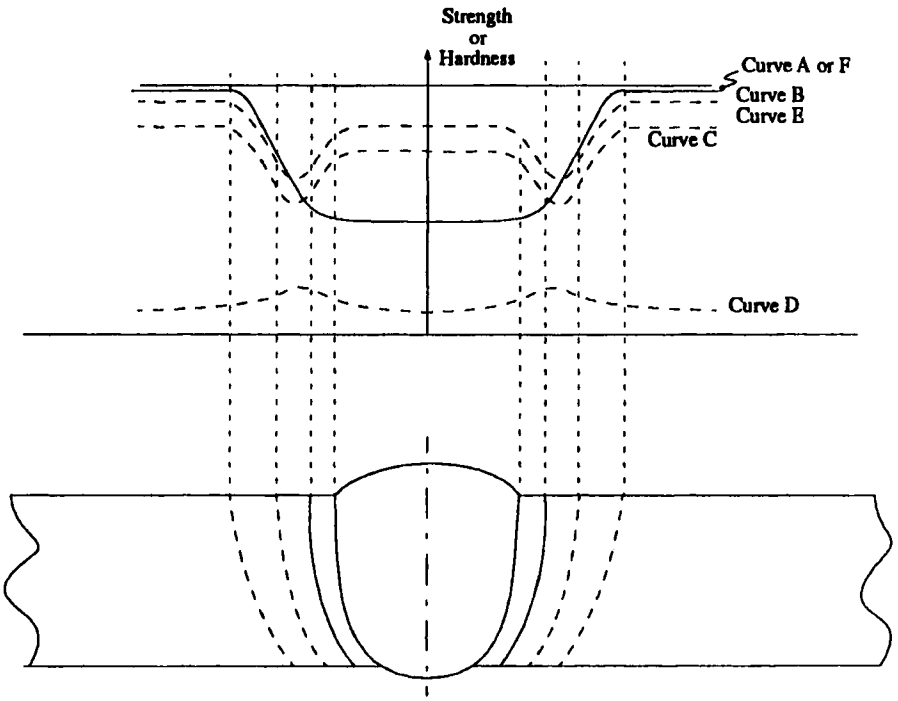


Figure 16.17 Schematic showing the effect of two approaches to attempt to recover strength and hardness in a fusion-welded, optimally aged alloy, that is, weld + postweld age and solution-treat + weld + postweld age: curve A, aged before welding; curve B, previously aged, as-welded; curve C, previously aged after welding plus postweld aging; curve D, solution treated before welding; curve E, previously solutionized, as-welded; and curve F, solutionized after welding plus postweld aging.

welded/postweld aged. The end result may be better, or may not, depending on the precise material, welding conditions, aging response, and design/service requirements.

The second approach for recovering properties is to weld the alloy in the solution-treated (ST) condition and then age following welding. The result of such an approach is that the fusion zone (assuming the filler is age-hardenable, or welding was autogenous), partially melted zone, and entire heat-affected zone will all age together. The only minor deviation from this is that the heat of welding could have caused some aging to take place somewhere in the heat-affected zone, as the temperature was high, but the time short. The results of such a solution treat + weld + postweld age (ST + W + PWA) are shown in Figure 16.17 in curves D, E, and F, representing the as-solutionized, solutionized as-welded, and solutionized + welded + postweld aged conditions. This approach is more practical than postweld solution treatment and aging since the temperature for aging is far lower and potentially less damaging to the weldment's shape and dimensions.

Another approach used to avoid problems, which might be suitable for some design and service situations, is to weld parts made from overaged material. The result after welding and postweld aging will be a weldment, including all welds, that is overaged, and less than optimum but of fairly uniform strength, hardness, and ductility. This was the practice with alpha-beta Ti-6Al-4V EB welded to produce wing carry-through structures (or wing boxes) on the Navy's F-14 fighter built in the 1970s and 1980s.

Throughout the preceding discussion it went without saying that the weld metal (i.e., fusion zone) was unaged after welding. Several ways were given for attempting to restore properties to the HAZ that would also help the fusion (and partially melted) zone in autogenous welding. For welding using filler, remember there is always the possibility of obtaining needed strength in the weld metal by choosing a filler alloy that is nearly as strong or stronger than the base metal without aging, or that can be aged. Admittedly, however, this is not easy for some alloys, such as the heat-treatable aluminum alloys.

16.5. THE HAZ IN TRANSFORMATION-HARDENABLE ALLOYS

16.5.1. The Physical Metallurgy of Transformation-Hardenable Alloys

Alloys are said to be transformation-hardenable when they form a particularly hard, high-strength, nonequilibrium phase on cooling. Almost inevitably, such phases are produced by diffusionless, athermal,[7] martensitic transformations occurring by massive shear (see Section 14.2.4). Materials that develop their strength from such transformations under controlled conditions during heat treatment are prone to similar, but uncontrolled transformation during cooling following welding. Uncontrolled transformations are rarely good, and often cause problems. Thus, transformation-hardenable alloys are prone to some particular problems in their heat-affected zones.

Carbon and low-alloy steels epitomize alloys that develop their maximum strength and hardness through transformation hardening, when both types form martensite upon cooling at rates exceeding the critical cooling rate for the particular alloy. Alloys with higher carbon and/or alloy content are more difficult to weld because they are prone to uncontrolled transformation to brittle martensite, with attendant quench cracking from thermal shock and stresses induced by pronounced temperature gradients or hydrogen cracking from both inherent sensitivity to hydrogen and high locked-in or residual tensile stresses. For steels that have been transformation-hardened and tempered to produce tempered martensite by controlled heat treatment prior to

[7]A transformation is athermal when the degree or extent to which it occurs (or goes to completion) depends only on the temperature and not the time. Ferrous martensite is the prime example, with transformation beginning at the M_s and being completed at the M_f, independent of time at any temperature between these two.

welding, it is possible that this structure and its properties will be severely altered by the uncontrolled heating and cooling associated with welding. Let's look at the underlying physical metallurgy of steels to understand the potential problems and cures.

Welding exposes steels to much more severe conditions in the heat-affected zone than normal heat treatment in two ways. First, peak temperatures encountered during welding (e.g., >1400°C in the HAZ near the fusion zone) are much higher than those encountered during heat treatment (typically, less than 950–1000°C maximum). Such high peak temperatures can result in (1) partial melting from segregation or constitutional liquation (see Section 15.2), (2) severe grain coarsening, especially near the fusion zone, and (3) reaustenitization or solutionizing, with attendant, subsequent phase transformations. The combination of reaustenitization and grain coarsening poses a particular problem, because transformation to brittle, untempered martensite occurs more easily (i.e., at lower critical cooling rates) in coarse-grained as opposed to fine-grained austenite. Obviously, the kinetics of reactions and transformations at very high temperatures are very fast.

The second way in which welding produces conditions more severe than heat treatment is that heating rates are much faster and retention times at peak temperatures are much more brief, accentuating nonequilibrium effects. High heating rates make diffusional transformations, such as ferrite + pearlite → austenite, more difficult, increasing effective transformation temperatures (such as the lower critical temperature, A_{C1}, and the upper critical temperature, A_{C3}, on the Fe-Fe_3C diagram, see Figure 14.1). The effect of heating rate is more pronounced in steels with greater amounts of carbide-forming elements (such Cr, Mo, V, and W) because these elements have low diffusion rates themselves and hinder diffusion of carbon, thereby retarding diffusional transformations.

High heating rates with short high-temperature retention times can also result in the formation of nonhomogeneous austenite. This occurs as the result of rapid dissolution of carbides, including Fe_3C cementite from pearlite or elsewhere, and localized carbon enrichment with no time for diffusion leveling or homogenization. Upon subsequent rapid cooling, as is typical following welding, such inhomogeneity can result in the formation of localized high-carbon martensite areas and widely scattered hardness in the HAZ.

Continuous cooling transformations in steels can be very different during welding than during normal heat treatment, as was explained in Section 14.4. Austenite can decompose to ferrite with different morphologies than are usually observed (e.g., Widmanstätten and acicular forms), as well as upper and lower forms of bainite. Near the M_s (martensite start) temperature, the transformation curves for diffusional transformation decomposition products are shifted to lower temperatures and longer times, so that, for the same cooling rate, the ability to form martensite (i.e., the hardenability of the steel) is greater. This is probably because welding coarsens grain structure and reduces the number of favorable, potent nucleation sites for pearlite.

16.5.2. Some Important Engineering Alloys Exhibiting Transformation Hardening

While transformation of the beta phase of titanium alloys on cooling resembles the decomposition of austenite, including the formation of a martensitic phase by a diffusionless, massive shear transformation, by far the most important engineering alloys in which transformation hardening occurs are steels. Important steels prone to transformation hardening include (1) carbon steels, including mild and higher-carbon steels; (2) low-alloy steels, including so-called high-strength low-alloy, HSLA steels; (3) high-alloy steels, including heat-resisting grades and tool steels; and (4) martensitic stainless steels. The next section addresses carbon and alloy steels.

16.5.3. Welding Behavior of Carbon and Alloys Steels

16.5.3.1. Behavior of Carbon Steels. Carbon steels are those steels that achieve their properties principally from carbon as an alloying addition. They may contain up to 1.65 wt% Mn (to tie up residual sulfur in benign globular inclusions, as opposed to a low-melting iron–sulfide grain-boundary film), 0.60 wt% Si (for improved fluidity and working and as a residual of steel-making), and 0.60 wt% Cu, in addition to very small amounts of some other elements. Mild steels are carbon steels with less than 0.30 wt% C, while higher-carbon steels are those with over 0.30 wt%.

Typical regions in the microstructure of a mild steel (say AISI 1018, containing 0.18 wt% C) are shown schematically in Figure 16.18, with each region correlated to the hypoeutectoid portion Fe-Fe_3C phase diagram. The heat-affected zone consists of partially grain-refined (point 3), grain-refined (point 2), and grain-coarsened (point 1) regions corresponding to just above the A_{C1}, just above the A_{C3}, and well above the A_{C3}, respectively. In the partially grain-refined region (corresponding to point or region 3), prior pearlite colonies transform to austenite and expand slightly into prior ferrite grains upon heating above A_{C1}. Upon cooling, this region decomposes into very fine colonies and grains of pearlite and ferrite. The prior untransformed ferrite remains essentially unchanged upon postweld cooling.

In the grain-refined region (corresponding to point or region 2), transformation of pearlite and ferrite to new grains of austenite is complete. Upon cooling, these austenite grains decompose into small pearlite colonies and ferrite grains, as described in Section 14.4.2. The distribution of the resulting pearlite and ferrite is nonuniform because heating during welding was rapid, preventing complete diffusion and leveling of carbon. In the grain-coarsened region (corresponding to point or region 1), the austenite grains formed from prior pearlite colonies and ferrite grains are large because the temperature was well above the A_{C3}. Because of the high cooling rates in this highest-temperature HAZ region, and because of the large grain size, acicular ferrite, rather

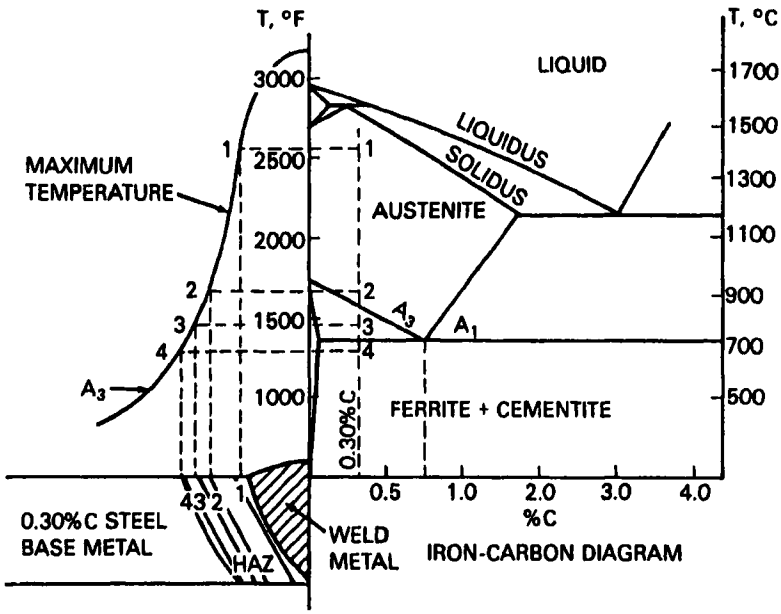


Figure 16.18 Schematic of the various microstructural regions of a typical mild steel (say AISI 1018), showing correlation to the hypoeutectoid portion of the Fe-Fe_3C phase diagram. (From *Welding Handbook*, Vol. 1, *Welding Technology*, 8th ed., edited by L. P. Connor, published in 1987 by and used with permission of the American Welding Society, Miami, FL.)

than blocky ferrite, forms at grain boundaries, in what is often called a Widmanstätten structure. Although the HAZ of this mild steel consists of both fine and coarse grains, its average grain size is smaller than the coarse columnar grains of the fusion zone. For this reason, fusion zone structure is refined by exposure to the HAZ of subsequent passes.

If postweld cooling rates are very high, as they can be for high-energy-density processes like EBW or LBW, martensite can form in the HAZ in regions where former pearlite colonies existed and C diffusion was incomplete. The greatest likelihood for martensite formation is in the coarse-grained region, where both cooling rate (as a result of the high peak temperature of the prevailing weld thermal cycle) and the inherent higher hardenability of coarse (versus fine) grains will favor martensite formation.

In higher-carbon steels, welding is plagued by many more problems than in mild steels, most particularly formation of hard, brittle untempered martensite in the HAZ, raising the possibility of what is referred to as underbead cracking. As in mild steels, the HAZ of higher-carbon steels consists of partial grain-refined, grain-refined, and grain-coarsened regions (as shown in Figure 16.18 by points or regions 3, 2, and 1, respectively). In the grain-coarsened region (region 1), both the higher cooling rate associated with the thermal cycle in this

location and the larger grain size of the austenite promote the formation of martensite. In the grain-refined region (region 2), both the lower cooling rate and smaller grain size discourage the formation of martensite and encourage the formation of pearlite and ferrite.

Potential problems from martensite formation can be prevented by preheating the weldment, at least in the vicinity of the weld. Preheating increases the size of the HAZ, but decreases the cooling rate, hopefully to below the critical cooling rate at which martensite is formed. The favorable effect of preheat on HAZ as-welded hardness is shown in Figure 16.19.

16.5.3.2. Behavior of Alloy Steels. The higher content of alloying additions besides carbon in these steels dramatically alters the CCT curves (such as shown in Figure 14.20) and results in very different microstructures in the HAZ compared to carbon steels. So-called quenched and tempered (Q&T) alloy steels usually have low (0.10–0.25 wt%) C contents, so are relatively easy to weld, requiring low or no preheating, and, usually, no postweld heat treating. Q&T steels are furnished in the heat-treated condition with yield strengths ranging from 50 to 150 ksi (345 to 1035 MPa), depending on chemical composition, thickness, and heat treatment, which always involves austenitizing, quenching, and tempering. Some Q&T steels are precipitation hardened after they are quenched and tempered and welded. Table 16.5 gives the composition and strength of several important Q&T steels.

The low carbon content of these steels minimizes the hardness and brittleness of any martensite that forms, since the hardness of untempered martensite is a function of carbon content up to a content of about 0.55 wt%, at which point the hardness reaches about Rockwell C65. It also causes the M_s to be high, allowing any martensite that forms to "autotemper" during cooling between the M_s and M_f temperatures.[8] Hardenability, in the meantime, which is the ease with which martensite will form as the result of both a higher M_s and M_f temperature and slower critical cooling rate (from as rightward shift of the CCT curve), is provided by additions of Mn, Cr, Ni, and Mo.

In some quenched and tempered steels, such as T-1, if cooling rates are too low, ferrite forms, rejecting carbon into the surrounding austenite and leading to martensite with high carbon. The result can be a brittle HAZ at surprisingly low cooling rates. For this reason, both heat input and preheat should be limited with Q&T steels. This behavior can be seen by referring to Figure 16.20, between curve p and the cross-hatched area. If, on the other hand, the cooling rate is too fast, that is, left of curve z in Figure 16.20, insufficient time is available for autotempering, so susceptibility to hydrogen cracking is high. To

[8]The M_s temperature can be determined from composition using any of a number of different empirical relationships. Some of these relationships are $M_s(°F) = 1000–650C–70Mn–35Ni–70Cr–50Mo$ (with all compositions in wt%), by Grange and Stewart (*Trans. AIME*, **167**, 467, 1946); and $M_s(°C) = 561–474C–33Mn–17Ni–17Cr–21Mo$ (with all compositions in wt%) by Steven and Haynes (*Journal of the Iron and Steel Institute*, **183**, 349, 1956; with M_f being 325–475°F (175–265°C) below the M_s.

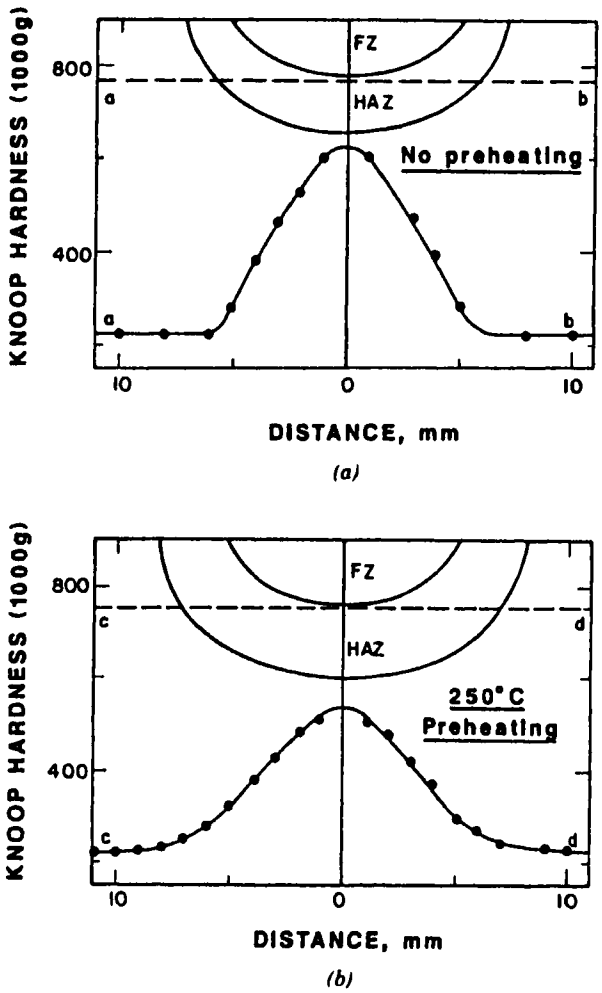


Figure 16.19 Hardness profile across the HAZ of an AISI 1040 steel (a) without preheating and (b) with 250°C preheating. (From *Welding Metallurgy* by S. Kou, published in 1987 by and used with permission of John Wiley & Sons, Inc., New York.)

avoid problems in this regard, low-hydrogen SMAW electrodes, processes, or procedures should be employed, along with some preheating.

To meet the requirements of both limited heat input and proper preheating, thick sections of Q&T steels should be welded using multiple passes. Preheat is then maintained as interpass temperature, and subsequent passes temper prior passes. This latter technique is known as the temper bead technique.

So-called heat-treatable alloy steels usually contain 0.30–0.50 wt% carbon and have higher strength and lower toughness than Q&T alloy steels. They are usually welded in the annealed (really, homogenized) and normalized condition

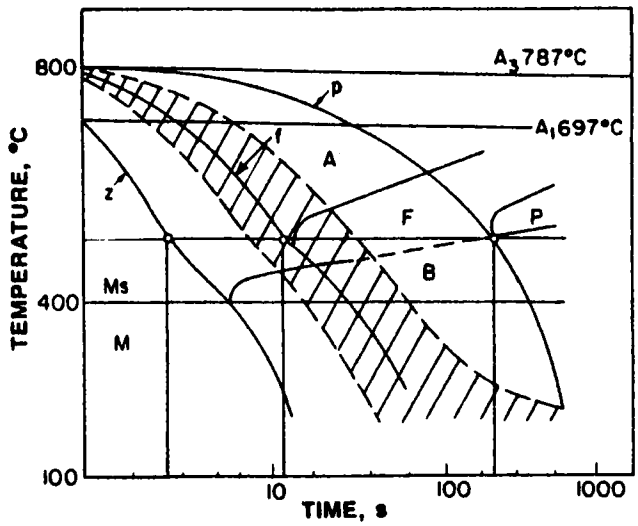


Figure 16.20 CCT curves for T-1 steel. Curves p, f, and z represent the critical cooling rate for the formation of pearlite (P), ferrite (F), and bainite (B), respectively. The cross-hatched area represents the region of optimum cooling rates. (From *Welding Metallurgy* by S. Kou, published in 1987 by and used with permission of John Wiley & Sons, Inc., New York, after *Fusion Welding Processing* by M. Inagaki et al., 1971 [in Japanese].)

(see Footnote 6) and are then heat-treated after welding to attain their final high strength and required toughness. For this reason, any filler metal must be carefully matched to the base metal so that the fusion zone (FZ) also responds to heat treatment.

Proper preheating and low-hydrogen electrodes or processes and procedures should be used to avoid hydrogen-induced underbead cracking. Preheating requirements can be determined from what are called carbon equivalents. Carbon equivalents give a measure of the hardenability and, thus, hydrogen cracking susceptibility. Various empirical equations exist for determining carbon equivalent, such as

$$\text{Equivalent C content} = \text{wt\% C} + \text{wt\% Mn}/4 + \text{wt\% Si}/4 \qquad (16.6)$$

Typical preheat temperatures versus equivalent C contents are:

Equivalent C Content	Suggested Preheat
Up to 0.45 wt%	Optional
0.45–0.60 wt%	200–400°F (94–205°C)
Above 0.60 wt%	400–700°FF (205–382°C)

Heat-treatable alloy steels should usually be stress relieved immediately following welding, preferably prior to cooling to room temperature in order to temper the martensite formed simultaneous with relief of weld-induced stresses. After this, the alloy weldment can be postweld heat-treated to develop strength and toughness by austenitizing, suitably quenching, and tempering.

Prior to stress relieving, as just advised, the weld heat-affected zone should be cooled to below the M_f temperature to prevent untransformed austenite from decomposing to pearlite and ferrite. The reason is twofold: First, tempered martensite is the desired final structure, and, second, pearlite and ferrite mixed with martensite severely degrades toughness against impact loads.

If, for any reason, stress relief cannot be accomplished immediately upon cooling following welding, the weldment should be heated to 750°F (400°C) for about 1 h to transform any untransformed austenite to bainite versus martensite. If weldments of these alloys cannot be postweld heat-treated, and they must be welded in the heat-treated condition, softening and hydrogen cracking can both be serious problems. Such problems can be minimized by (1) lowering the heat input per unit length of weld as much as possible, and (2) keeping preheat, interpass, and stress relief temperatures at least 90°F (50°C) below the tempering temperature of the base metal.

16.6. THE HAZ IN CORROSION-RESISTANT STAINLESS STEELS

16.6.1. The Physical Metallurgy of Stainless Steels

Stainless steels are a class of iron-based alloys with high corrosion and oxidation resistance achieved through extensive solid-solution alloying, typically with 12–27 wt% Cr, 1–2 wt% Mn, often 6–22 wt% Ni, and sometimes a few weight percent of Mo. The Cr is principally responsible for corrosion and oxidation resistance, provided by its leading to the formation of a thin, tenacious, and impermeable surface oxide, but also serves to strengthen by a solid-solution mechanism, and, to a lesser degree, by formation of carbide precipitates under certain conditions. Cr, having a bcc crystal structure, also acts to stabilize the bcc ferrite α and δ phases of iron. Mo, also a bcc metal, stabilizes ferrite relative to austenite, increases strength by both its solid-solution effect and formation of carbides under certain conditions, and improves resistance to corrosion in some environments. Mn and Ni, both fcc metals, stabilize the austenite phase and act as solid-solution strengtheners. Ni also imparts some corrosion resistance. A small amount of carbon, in the range of 0.03–0.25 wt%, is also present, either deliberately added as a potent solid-solution strengthener, or, before steelmaking practice reached the level it has today, as an unavoidable impurity.

Stainless steels are conveniently classified into four major categories based on their primary structure: (1) ferritic, (2) martensitic, (3) austenitic, and (4) duplex, ferrite + austenite. *Ferritic stainless steels* are characterized by a

body-centered cubic (bcc) solid solution of ferrite produced by the stabilization of the α and δ phases of iron by addition of bcc Cr to form a closed γ loop as shown in Figure 16.21. The ferritic stainless steels must have sufficient Cr (greater than 12 wt%) to remain outside the γ-loop, but not so much (less than 27 wt%) that brittle σ-phase is formed (see Section 14.5). Ferritic grades are attractive because they are fairly inexpensive (compared to more highly alloyed austenitic and duplex grades) and exhibit greater resistance to stress corrosion cracking than the austenitic types.

Martensitic stainless steels are characterized by a body-centered tetragonal structure of martensite formed in Fe-Cr alloys containing less than 12 wt% Cr. For such Cr contents, alloys fall within the γ loop, and so form δ-iron upon solidification, γ on initial cooling, and then martensite on further rapid cooling. Martensitic stainless steels are employed because of their combination of high strength, hardness, and good corrosion resistance, making them ideal for corrosion-resistant knives, surgical instruments, shears, chopping or shredding blades, and so on. Hardness increases rapidly with increased carbon content.

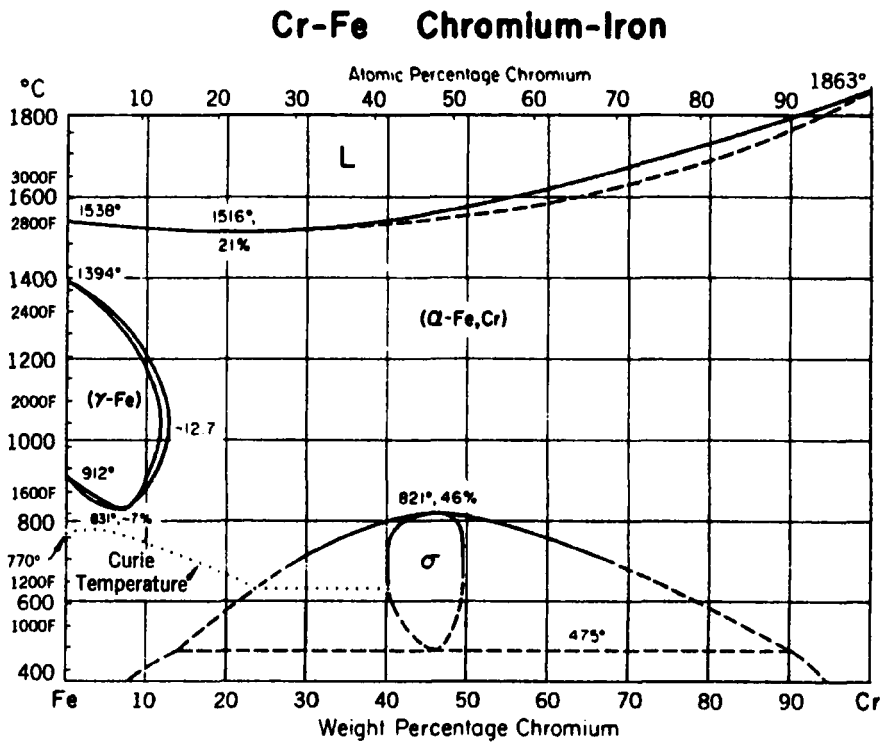


Figure 16.21 Cr-Fe phase diagram showing closure of the γ loop resulting from the stabilization of the α and δ phases of iron by the addition of bcc Cr. (From *Metals Handbook*, Vol. 8, 8th ed., published by the American Society for Metals in 1973, and used with permission of the ASM International, Materials Park, OH.)

Austenitic stainless steels are characterized by a face-centered cubic solid-solution austenite. The austenite (or γ) phase is rendered stable by balancing the composition to have more than 15 wt% bcc Cr, needed to impart corrosion resistance through the formation of a tenacious Cr-oxide layer, with 6–22 wt% fcc Ni to stabilize the austenite phase. As can be seen in the constitution diagrams for binary Fe-C, binary Fe-Cr, and pseudobinary 70 vol% Fe/30 vol% (Ni + Cr) in Figure 16.22, martensite does not form because the austenite is stable well below room temperature, that is, the M_s temperature is below (often, well below) room temperature. Austenitic stainless steels are attractive for their corrosion resistance, nonmagnetic character, and exceptional cryogenic properties, the latter arising from the fcc structure of the alloy.

Duplex stainless steels are characterized by a structure consisting of a mixture of ferrite and austenite. This duplex structure is obtained through the addition of more Ni (beyond about 22 wt%), as seen in the pseudobinary in Figure 16.22c. These alloys offer improved hot working and welding and excellent corrosion resistance in a number of environments.

Precipitation hardening or *PH stainless steels* are Fe-Cr-Ni alloys with corrosion resistance that is superior to hardenable 400 series stainless steels

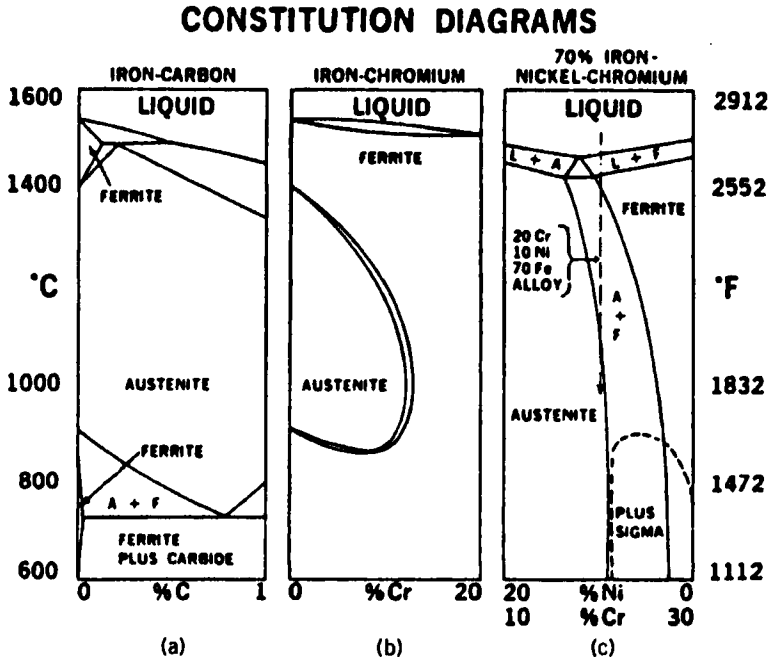


Figure 16.22 Constitution diagrams for (a) the Fe-C binary, (b) the Fe-Cr binary, and (c) the pseudo-binary for 70 vol% Fe/30 vol% Cr + Ni. (From "Ferrite in austenitic stainless steel weld metal" by W. T. Delong, *Welding Journal*, 53(7), 273s–286s, 1974, published by and used with permission of the American Welding Society, Miami, FL.)

and yield strengths of around 600 to nearly 1800 MPa (85–260 ksi). These high levels of strength are obtained by precipitation hardening a martensitic, austenitic, or semiaustenitic (i.e., with subzero M_s temperature so they can consist of mixtures of tough, ductile austenite and hard martensite) matrix with second-phase particles composed of one or more of Cu, Al, Ti, Nb, or Mo.

16.6.2. Major Stainless Steels Used in Engineering

Table 16.6 lists major stainless steels used in engineering by class, such as, ferritic, martensitic, austenitic, and duplex (ferrite + austenite), as well as precipitation hardening (PH) types.

16.6.3. Sensitization of Austenitic Stainless Steels by Welding

Austenitic stainless steels containing more than about 0.1 wt% C are often susceptible to intergranular corrosion in the HAZ of any welds. The phenomenon is known as *sensitization*, for the way the alloy is rendered sensitive to corrosive attack, or *weld decay*, for the way the sensitized region in the HAZ is eaten away by corrosion.

Sensitization is caused by the precipitation of $M_{23}C_6$ Cr,Fe-carbides preferentially along grain boundaries,[9] thereby depleting or "denuding" the Cr in solution surrounding these carbides and in grain boundaries to below the level required to provide corrosion resistance (about 14 wt%). This is shown schematically in Figure 16.23. The Cr-depleted region along the grain boundaries becomes anodic compared to the bulk of the grains, which leads to greater susceptibility to corrosive attack. The rate of carbide formation is most rapid in the range of temperature between 600 and 850°C (about 1100 and 1550°F), known as the sensitization range. Sensitization is more severe when (1) the austenitic stainless contains higher amounts of carbon, (2) weld heat input is high, (3) the alloy is deformed (cold-worked) prior to welding, and (4) there are no alloying additions with greater affinity for C than Cr.

Sensitization occurs only in a narrow band or temperature range because at cooling rates above a certain level (curve *a* in Figure 16.24), precipitation cannot occur because the time available for diffusion in the sensitization range is too short. Also, if the peak temperature of a weld thermal cycle is too low (curve *c* in Figure 16.24), precipitation cannot occur because nucleation does not occur.

When the mechanism responsible for sensitization and weld decay is known, there are three ways of avoiding the problem. First, a small amount of an

[9]Precipitation is favored along grain boundaries for two reasons: (1) because the combined energy increase of grain boundary, planar imperfections, and coherent precipitate interfaces is lower than if these same precipitates formed away from grain boundaries (i.e., the grain boundaries provide a suitable site for heterogeneous nucleation); and (2) the rate of diffusion in grain boundaries is higher than in bulk structure because the atomic structure is more open in boundaries. This higher rate of diffusion particularly favors growth, but also helps with nucleation.

TABLE 16.6 Major Stainless Steels Used in Engineering Applications

Martensitic types (wrought and cast)	
Ferritic types (wrought and cast)	
Austenitic types (wrought and cast)	
Duplex types	
Fe-23Cr-4Ni-0.1N	(2304)
Fe-22Cr-5.5Ni-3Mo-0.15N	(2205)
Fe-25Cr-5Ni-2.5Mo-0.17N-Cu	(Ferralium 255 or Zeron 25)
Fe-25Cr-7Ni-3.5Mo-0.25N-Cu-W	(2507 or Zeron 100)
Precipitation-hardening types	

Source. From *AWS Welding Handbook*, 7th ed, Vol 4: *Metals and Their Weldability*, edited by W. H. Kearns, published in 1982 by and used with permission of the American Welding Society, Miami, FL.

Chemical Composition of Typical Martensitic Stainless Steels

Type	UNS Number	Composition[a] (%)							
		C	Mn	Si	Cr	Ni	P	S	Other
Wrought alloys									
403	S40300	0.15	1.00	0.50	11.5–13.0		0.04	0.03	
410	S41000	0.15	1.00	1.00	11.5–13.0		0.04	0.03	
414	S41400	0.15	1.00	1.00	11.5–13.5	1.25–2.50	0.04	0.03	
416	S41600	0.15	1.25	1.00	12.0–14.0		0.04	0.03	
420	S42000	0.15 min	1.00	1.00	12.0–14.0		0.04	0.03	
422	S42200	0.20–0.25	1.00	0.75	11.0–13.0	0.5–1.0	0.025	0.025	0.75–1.25Mo; 0.75–1.25W; 0.15–0.3V
431	S43100	0.20	1.00	1.00	15.0–17.0	1.25–2.50	0.04	0.03	
440A	S44002	0.60–0.75	1.00	1.00	16.0–18.0		0.04	0.03	0.75Mo
440B	S44003	0.75–0.95	1.00	1.00	16.0–18.0		0.04	0.03	0.75Mo
440C	S44004	0.95–1.20	1.00	1.00	16.0–18.0		0.04	0.03	0.75Mo
Casting alloys									
CA-6NM	J91540	0.06	1.00	1.00	11.5–14.0	3.5–4.5	0.04	0.04	0.40–1.0Mo
CA-15	J91150	0.15	1.00	1.50	11.5–14.0	1.0	0.04	0.04	0.5Mo
CA-40	J91153	0.20–0.40	1.00	1.50	11.5–14.0	1.0	0.04	0.04	0.5Mo

[a]Single values are maximum.

Chemical Compositions of Typical Ferritic Stainless Steels

Type	UNS Number	Composition[a] (%) C	Mn	Si	Cr	Ni	P	S	Other
Wrought alloys									
405	S40500	0.08	1.00	1.00	11.5–14.5		0.04	0.03	0.10–0.30Al
409	S40900	0.08	1.00	1.00	10.5–11.75		0.045	0.045	Ti min — 6 × %C
429	S42900	0.12	1.00	1.00	14.0–16.0		0.04	0.03	
430	S43000	0.12	1.00	1.00	16.0–18.0		0.04	0.03	
434	S43400	0.12	1.00	1.00	16.0–18.0		0.04	0.03	0.75–1.25Mo
436	S43600	0.12	1.00	1.00	16.0–18.0		0.04	0.03	0.75–1.25Mo; (Ch + Ta)min — 5 × %C
442	S44200	0.20	1.00	1.00	18.0–23.0		0.04	0.03	
444	S44400	0.025	1.00	1.00	17.5–19.5	1.00	0.04	0.03	1.75–2.5Mo; 0.035M max; (Cb+Ta)min — 0.2+4(%C+%N)
446	S44600	0.20	1.50	1.00	23.0–27.0		0.04	0.03	0.25N
26-1	S44626	0.06	0.75	0.75	25.0–27.0	0.50	0.04	0.020	0.75–1.50Mo; 0.2–1.0Ti; 0.04N; 0.2Cu
29-4	S44700	0.010	0.30	0.20	28.0–30.0	0.15	0.025	0.020	3.5–4.2Mo, 0.020Ni, 0.15Cu
29-4-2	S44800	0.010	0.30	0.20	28.0–30.0	2.0–2.5	0.025	0.020	3.5–4.2Mo; 0.020Ni, 0.15Cu
Casting alloys									
CB-30	J91803	0.30	1.00	1.50	18.0–21.0	2.0	0.04	0.04	
CC-50	J92616	0.50	1.00	1.50	26.0–30.0	4.0	0.04	0.04	

[a]Single values are maximum.

Compositions of Typical Wrought Austenitic Stainless Steels

Type	UNS Number	Composition[a] (%)							
		C	Mn	Si	Cr	Ni[b]	P	S	Other
201	S20100	0.15	5.5–7.5	1.00	16.0–18.0	3.5–5.5	0.06	0.03	0.25N
202	S20200	0.15	7.5–10.0	1.00	17.0–19.0	4.0–6.0	0.06	0.03	0.25N
301	S30100	0.15	2.00	1.00	16.0–18.0	6.0–8.0	0.045	0.03	
302	S30200	0.15	2.00	1.00	17.0–19.0	8.0–10.0	0.045	0.03	
302B	S30215	0.15	2.00	2.0–3.0	17.0–19.0	8.0–10.0	0.045	0.03	
303	S30300	0.15	2.00	1.00	17.0–19.0	8.0–10.0	0.20	0.15 min	0–0.6Mo
303Se	S30323	0.15	2.00	1.00	17.0–19.0	8.0–10.0	0.20	0.06	0.15Se min
304	S30400	0.08	2.00	1.00	18.0–20.0	8.0–10.5	0.045	0.03	
304L	S30403	0.03	2.00	1.00	18.0–20.0	8.0–12.0	0.045	0.03	
305	S30500	0.12	2.00	1.00	17.0–19.0	10.5–13.0	0.045	0.03	
308	S30800	0.08	2.00	1.00	19.0–21.0	10.0–12.0	0.045	0.03	
309	S30900	0.20	2.00	1.00	22.0–24.0	12.0–15.0	0.045	0.03	
309S	S30908	0.08	2.00	1.00	22.0–24.0	12.0–15.0	0.045	0.03	
310	S31000	0.25	2.00	1.50	24.09–26.0	19.0–22.0	0.045	0.03	
310S	S31008	0.08	2.00	1.50	24.0–26.0	19.0–22.0	0.045	0.03	
314	S31400	0.25	2.00	1.5–3.0	23.0–26.0	19.0–22.0	0.045	0.03	
316	S31600	0.08	2.00	1.00	16.0–18.0	10.0–14.0	0.045	0.03	2.0–3.0Mo
316L	S31603	0.03	2.00	1.00	16.0–18.0	10.0–14.0	0.045	0.03	2.0–3.0Mo
317	S31700	0.08	2.00	1.00	18.0–20.0	11.0–15.0	0.045	0.03	3.0–4.0Mo
317L	S31703	0.03	2.00	1.00	18.0–20.0	11.0–15.0	0.045	0.03	3.0–4.0Mo
321	S32100	0.08	2.00	1.00	17.0–19.0	9.0–12.0	0.045	0.03	5 × %C Ti min
329	S32900	0.10	2.00	1.00	25.0–30.0	3.0–6.0	0.045	0.03	1.0–2.0Mo
330	N08330	0.08	2.00	0.75–1.5	17.0–20.0	34.0–37.0	0.04	0.03	
347	S34700	0.08	2.00	1.00	17.0–19.0	9.0–13.0	0.045	0.03	C
348	S34800	0.08	2.00	1.00	17.0–19.0	9.0–13.0	0.045	0.03	0.2Cu[c,d]
384	S38400	0.08	2.00	1.00	15.0–17.0	17.0–19.0	0.045	0.03	

[a]Single values are maximum unless indicated otherwise.
[b]Higher percentages are required for certain tube manufacturing processes.
[c](Cb + Ta)min — 10 × %C.
[d]Ta — 0.10% max.

Composition of Typical Cast Austenitic Stainless Steels

Alloy Designation	UNS Number	Similar Wrought Type[b]	Composition[a] (%)					
			C	Si	Cr	Ni	Mo[c]	Others
CE-30	J93423	312	0.30	2.00	26–30	8–11	—	—
CF-3	J92700	304L	0.03	2.00	17–21	8–12	—	—
CF-3M	J92800	316L	0.03	1.50	17–21	9–13	2.0–3.0	—
CF-8	J92600	304	0.08	2.00	18–21	8–11	—	—
CF-8C	J92710	347	0.08	2.00	18–21	9–12	—	d
CF-8M	J92900	316	0.08	1.50	18–21	9–12	2.0–3.0	—
CF12M	—	316	0.12	1.50	18–21	9–12	2.0–3.0	—
CF-16F	J92701	303	0.16	2.00	18–21	9–12	1.5	0.20–0.35Se
CF-20	J92602	302	0.20	2.00	18–21	8–11	—	—
CG-8M	—	317	0.08	1.50	18–21	9–13	3.0–4.0	—
CH-20	J93402	309	0.20	2.00	22–26	12–15	—	—
CK-20	J94202	310	0.20	2.00	23–27	19–22	—	—
CN-7M	J95150	—	0.07	1.50	18–22	27.5–30.5	2.0–3.0	3–4Cu
HE	J93403	—	0.2–0.5	2.0	26–30	8–11	—	—
HF	J92603	304	0.2–0.4	2.0	19–23	9–12	—	—
HH	J93503	309	0.2–0.5	2.0	24–28	11–14	—	0.2N
HI	J94003	—	0.2–0.5	2.0	26–30	14–18	—	—
HK	J94224	310	0.2–0.6	2.0	24–28	18–22	—	—
HL	J94604	—	0.2–0.6	2.0	28–32	18–22	—	—
HN	J94213	—	0.2–0.5	2.0	19–23	23–27	—	—
HP	—	—	0.35–0.75	2.0	24–28	33–37	—	—
HT	J94605	330	0.35–0.75	2.5	15–19	33–37	—	—
HU	—	—	0.35–0.75	2.5	17–21	37–41	—	—

[a]Single values are maximum.
Manganese — 1.50% max in CX-XX types; 2.0% max in HX types.
Phosporus — 0.04% max except for Cf-16F — 0.17% max.
Sulfur — 0.04% max.

[b]Compositions are not exactly the same.
[c]Molybdenum in HX types is 0.5% max.
[d]Cb — 8 × %C (1.0% max), or Cb + Ta — 9 × %C (1.1% max).

Nominal Compositions of Typical Precipitation-Hardening Stainless Steels

Type	Designation[a]	UNS Number	Nominal Composition (wt%)							
			C	Mn	Si	Cr	Ni	Mo	Al	Others
Martensitic (moderate strength)	17-4PH	S17400	0.04	0.30	0.60	16.0	4.2	—	—	3.4Cu, 0.25Cb
	15-5PH	S15500	0.04	0.30	0.40	15.0	4.5	—	—	3.4Cu, 0.25Cb
	Custom 450	S45000	0.03	0.25	0.25	15.0	6.0	0.8	—	1.5Cu, 0.3Cb
	Stainless W	S17600	0.06	0.50	0.50	16.75	6.25	—	0.2	0.8Ti
Martensitic (high strength)	PH 13-8Mo	S13800	0.04	0.03	0.03	12.7	8.2	2.2	1.1	—
	Custom 455	S45500	0.03	0.25	0.25	11.75	8.5	—	—	2.5Cu, 1.2Ti, 0.3Cb
Semi-austenitic	17-7PH	S17700	0.07	0.50	0.30	17.0	7.1	—	1.2	—
	Ph 15-7Mo	S15700	0.07	0.50	0.30	15.2	7.1	2.2	1.2	—
	PH 14-8Mo	S14800	0.04	0.02	0.02	15.1	8.2	2.2	1.2	—
	AM-350	S35000	0.10	0.75	0.35	16.5	4.25	2.75	—	—
	AM-355	S35500	0.13	0.85	0.35	15.5	4.25	2.75	—	—
Austenitic	A-286	K66286	0.05	1.45	0.50	14.75	25.25	1.30	0.15	0.30V, 2.15Ti, 0.005B
	17-10P	—	0.10	0.60	0.50	17.0	11.0	—	—	0.30P
	HNM	—	0.30	3.50	0.50	18.50	9.50	—	—	0.25P

[a]Some of these designations are registered trademarks.

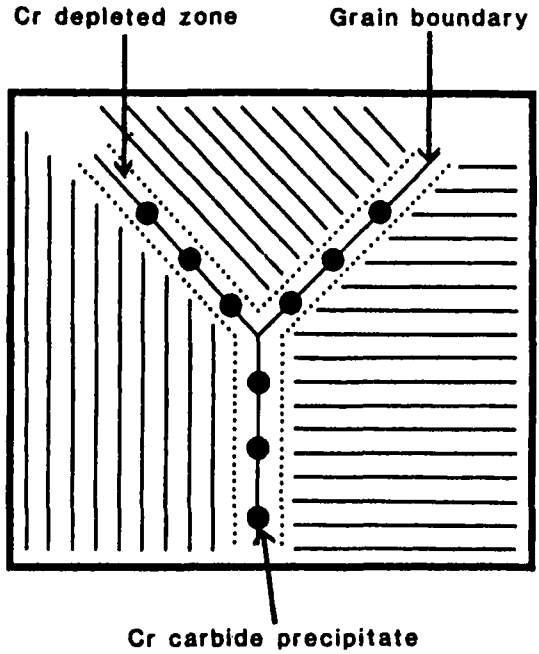


Figure 16.23 Schematic of the depletion of Cr in the region of grain boundaries in austenitic stainless steel caused by the preferential precipitation of $M_{23}C_6$-type Cr,Fe-carbides in these regions. This depletion renders the grain boundary regions anodic and sensitizes the area to corrosive attack in a phenomenon known as "sensitization". (From *Welding Metallurgy* by S. Kou, published in 1987 by and used with permission of John Wiley & Sons, Inc., New York.)

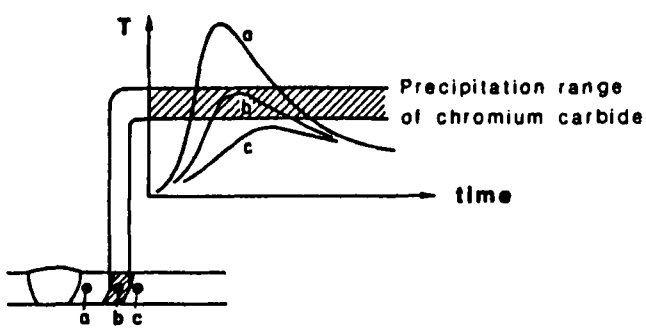


Figure 16.24 Schematic showing plots of various weld thermal cycles and the sensitization range of an austenitic stainless steel. (From *Welding Metallurgy* by S. Kou, published in 1987 by and used with permission of John Wiley & Sons, Inc., New York.)

element having greater affinity for C than Cr can be added, examples being Ti to type 304 to produce type 321, and Nb to type 304 to produce type 347. By forming Ti-carbides or Nb-carbides preferentially to Cr, Fe-carbides, Cr depletion is prevented and the alloy is said to be stabilized. Second, the carbon content can be reduced to decrease the amount of Cr, Fe-carbide that can form, and thereby the amount of Cr that can be removed from the matrix. This approach is used in so-called low-carbon or L grades, such as type 304L and type 316L, both having C below 0.035 wt%. To offset the loss of strength caused by reducing the C content, small amounts (0.01 to 0.03 wt%) of nitrogen (N) can be added, N being a potent, interstitial solid-solution strengthener, as well as austenite stabilizer, like C. Grades with intentionally added N are designated, by an N postscript, such as type 304LN. Third and last, once sensitization has occurred following welding, the weldment can be postweld heat-treated to redissolve the Cr, Fe-carbides in a solutionizing process. This requires heating to 1000–1100°C (1800–2000°F) for 1 h per inch of thickness, followed by rapid quenching to retain the Cr in solution. This last approach obviously has limited practicality due to problems from distortion of large and/or complex weldments exposed to such high temperatures and such rapid quenches.

16.6.4. Welding the Ferritic and Martensitic Stainless Steels

Ferritic stainless steels are generally less weldable than austenitic stainless steels, but are attractive for their lower cost and greater resistance to stress corrosion cracking (see Section 16.8.4). Some grades of ferritic stainless steel (such as 430 and 446) exhibit sensitization. The sensitization temperature range is much higher than for the unstabilized austenitic grades, however, typically above 925°C (1750°F), so weld decay, when it occurs, occurs very near the fusion zone boundary. Immunity to preferential intergranular corrosive attack is restored by solution annealing at 650–815°C (1200–1500°F) for 15 to 60 min, both sensitization and recovery ranges being generally opposite those for austenitic grades. Also unlike for the austenitic grades, lowering the carbon content even to just below 0.010 wt% fails to prevent sensitization, although the addition of Ti or Nb is helpful for stabilizing Cr in solution.

The reason for the apparent strange behavior of the ferritic versus austenitic grades is the inherently higher diffusion rate of C in the more open lattice of bcc ferrite than in fcc austenite. As a result, even rapid cooling in the vicinity of 925°C (1750°F) fails to suppress grain boundary precipitation of Cr, Fe-carbides. Similarly, lowering the C content fails to effectively prevent Cr, Fe-carbide precipitation, unless the level is dropped to extremely low concentrations around 0.002 wt%. Postweld solution annealing has been found to restore corrosion resistance, allegedly by allowing Cr remaining in the matrix in the bulk of grains to diffuse to depleted regions in grain boundaries.

The typical weld HAZ of a ferritic stainless steel comprises two distinct regions; both of which can contain embrittling martensite, and one of which

can exhibit severe grain coarsening. The origin of these regions can be seen from Figure 16.25. Farther from the fusion zone, where the peak temperature of the weld thermal cycle entered the ($\delta + \gamma +$ carbide) and ($\gamma + \delta$) regions, some fine-grained austenite forms along ferrite grain boundaries. Upon rapid cooling following welding, this austenite transforms to martensite. Nearer the fusion zone, where the peak temperature of the weld thermal cycle entered the δ region, much more grain growth occurred, more austenite forms along δ-ferrite grain boundaries upon cooling following welding. This austenite tends

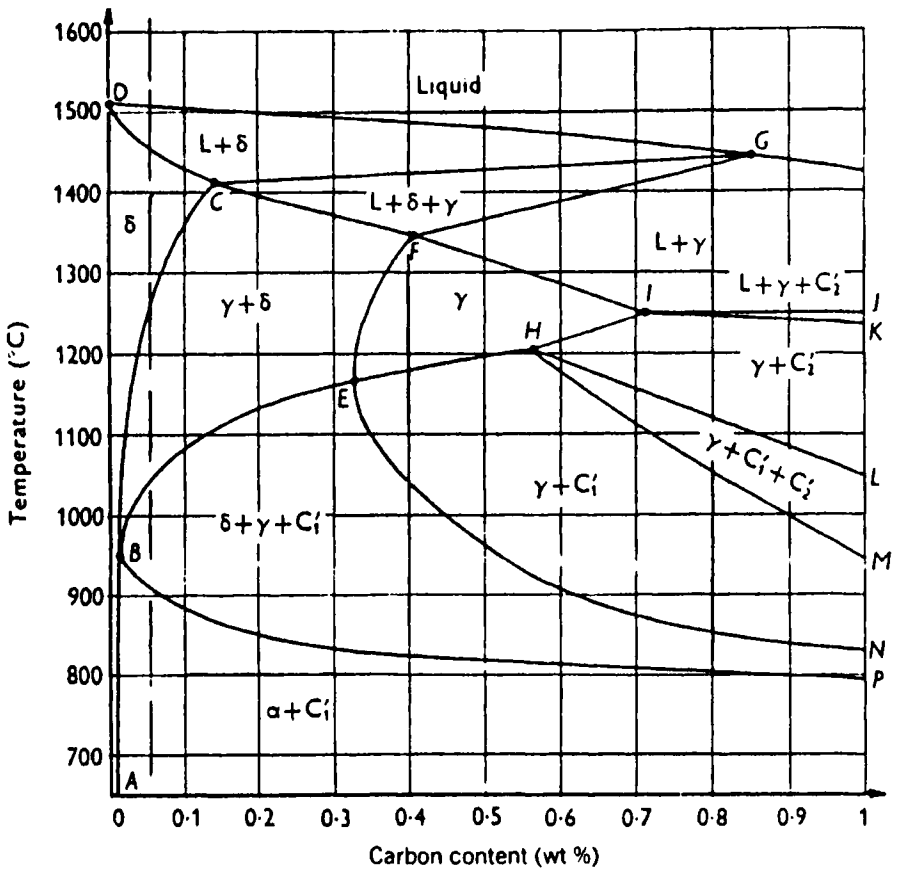


Figure 16.25 A vertical section (or pseudobinary) at 17 wt% Cr for the Fe-Cr-C ternary phase diagram showing the origin of two distinct regions in the HAZ of ferritic stainless steels: (a) a region containing some martensite along grain boundaries where the weld thermal cycle entered the ($\delta + \gamma +$ carbide) and ($\gamma + \delta$) regions and (b) a region containing considerable amounts of coarse-grained martensite along grain boundaries where the weld thermal cycle entered the δ region. (From *Welding Metallurgy of Stainless and Heat-Resisting Steels* by R. Castro and J. J. DeCadenet, 1974, Cambridge University Press, London, used with permission of the Cambridge University Press.)

to have an acicular morphology due to the coarse grain structure from which and the rapid rate at which it is formed. Upon further cooling, this inherently more hardenable, coarse-grained, acicular austenite transforms to brittle acicular martensite. As a result, the notch toughness of as-welded ferritic stainless steels can be quite low. Postweld tempering at around 800°C (1500°F) tends to improve toughness significantly.

Undesirable martensite formation can be suppressed by adding 0.5 wt% Ti or 1.0 wt% Nb, either of which tends to stabilize the δ-ferrite, thereby suppressing austenite formation and, consequently, subsequent transformation to martensite. Both elements also tend to form carbides stable at high temperatures, so also tend to lower the C content in the matrix, thereby lowering hardenability. Problems from excessive grain growth can be minimized by employing low heat inputs, as well as by using alloys with small additions of grain-growth inhibitors such as B, Al, V, or Zr.

Martensitic stainless steels, typically containing 13 wt% Cr and more than 0.08 wt% C, exhibit a much more extensive austenite region than their 17 wt% Cr, lower C ferritic cousins, as can be seen by comparing Figure 16.26 to Figure 16.25. Consequently, these stainless grades exhibit a much greater tendency to form martensite upon rapid cooling. Since the hardness of martensitic stainless steels increases rapidly with increased C content (as is typical for all ferrous martensite), grades with higher C contents are especially susceptible to underbead cracking. The term underbead cracking derives from the fact that cracks appear in the HAZ surrounding a weld, under the weld bead. Cracking results from the generation of high internal stresses associated with the approximate 10% volume increase as austenite transforms to martensite. These stresses can be so severe that cracking can occur even without excessive restraint or further embrittlement by hydrogen, although both clearly would make matters worse. For this reason, martensitic stainless steels containing more than 0.25–0.30 wt% C are generally considered unweldable.

Underbead cracking problems can be minimized using a combination of preheating and postweld tempering between 600 and 850°C or 1100 and 1550°F, as well as by employing an austenitic filler. The latter allows some accommodation of stresses (really, strains) associated with the austenite-to-martensite transformation since the austenite is softer and more ductile than the base metal, and acts as a sponge to any hydrogen that might be present, benignly taking it into solution. As in the case of alloy steels (discussed in Section 16.5.3.2), martensitic stainless steels are usually not permitted to cool directly to room temperature upon the completion of welding to prevent underbead cracking.

The welding of the PH grades of stainless steels is involved, because there are martensitic, austenitic, and semiaustenitic types, so the interested reader is directed to references such as the *ASM Handbook*, Vol. 6, *Welding, Brazing, and Soldering*, published in 1993 by the ASM International, Materials Park, OH, pp. 482–494.

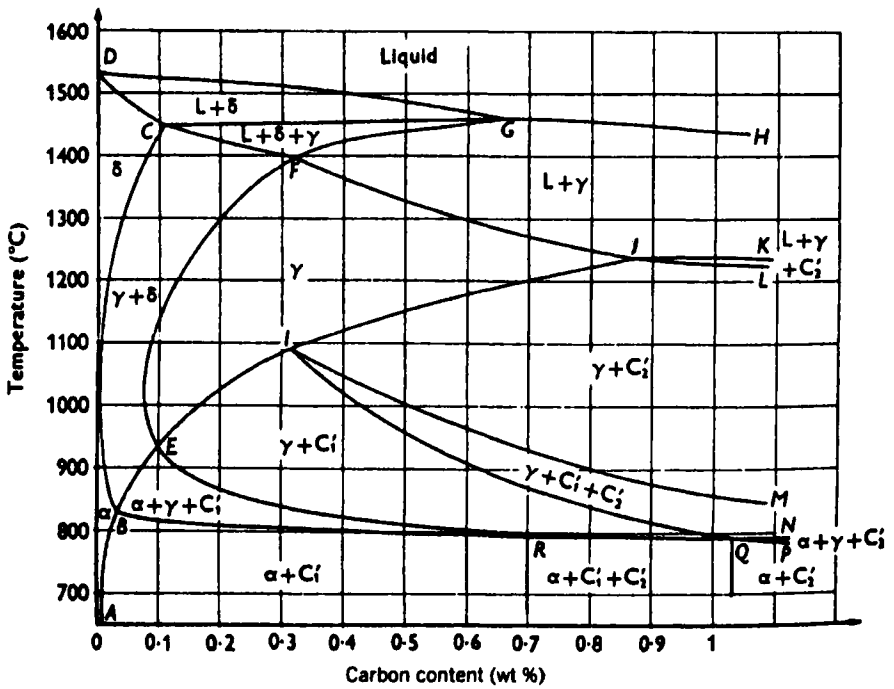


Figure 16.26 A vertical section (or pseudobinary) at 13 wt% Cr for the Fe-Cr-C ternary phase diagram showing the existence of a much more extensive austenite region in typical martensitic compared to 17 wt% Cr ferritic stainless steels. (From *Welding Metallurgy of Stainless and Heat-Resisting Steels* by R. Castro and J. J. DeCadenet, 1974, Cambridge University Press, London, used with permission of the Cambridge University Press.)

16.7. THE HAZ IN DISPERSION-STRENGTHENED OR REINFORCED ALLOYS

There are alloys as well as essentially pure metals that derive their strength from the effect of a dispersed, stable second phase on dislocation motion, as well as metals and alloys strengthened by incorporation of reinforcing particles, fibers, or filaments; the latter are called metal–matrix composites or MMCs. Among the former are oxide-dispersion-strengthened (ODS) metals and alloys and mechanically alloyed (MA) materials containing thermally stable oxides, carbides, nitrides, or complex intermetallic compounds. In ODS alloys, the oxide may be developed by internally oxidizing a reactive solute addition (such as yttrium, Y, or thorium, Th), while in MA alloys, oxides or other phases are mechanically mixed and consolidated into the matrix alloy by powder processing techniques. The advantages of both types of materials is retention of strength and/or modulus) to elevated temperatures. This is achieved by the effect of the stable dispersoid or reinforcement, which had to be added just

TABLE 16.7. Some Important Dispersion-Strengthened/Mechanically Alloyed, and Reinforced Metals and Alloys

Oxide Dispersion Strengthed (ODS)/Mechanically Alloyed (MA) Metals and Alloys	
Oxide- and carbide-dispersion strengthened/MA aluminum alloys	
7090 and 7091	(6.5–8.0Zn, 2.5Mg, 1.0–1.5Cu, 0.4–1.5Co)
CW67 and 7064	(as above, plus Zr)
Al-9052 and 905XL	(4Mg, 0.4–0.5O, 1.1C: latter with 1.3Li)
X8009 (or FVS alloys)	(Al-Fe-V-Si)
X8019	(Al-Fe-Ce)
Al-Ti alloys	
Al-Cr alloys	
Oxide-dispersion strengthened copper	
ODS Cu	
ODS/MA iron alloys	
MA956	(Fe-20Cr, plus 1 vol% Th_2O_3)
ODS/MA nickel and nickel alloys	
MA754, 758, 760, 6000	(Ni-20Cr, plus 1 vol% Th_2O_3)
Metal–Matrix Composites (MMCs)	
Al–matrix composites:	
B/6061 Al	(48 vol% B)
SCS-2/6061 Al	(47 vol% SiC)
P100Gr/6061 Al	(43.5 vol% Gr)
FP/Al-2Li	(55 vol% α-Al_2O_3, sapphire)
SiC/Al-4Cu-1.5Mg	
Cu–matrix composites:	
P120Gr/Cu	(60 vol% Gr)
Mg–matrix composites:	
Mg-Gr	
Mg-Al_2O_3	
Mg-SiC	
Mg-B_4C	
Ti–matrix composites:	
SiC/Ti	
Intermetallic compound–matrix composites:	
SiC, Al_2O_3, TiC, TiB_2, or refractory metal fibers in NiAl	

because to be thermally stable it probably could not be developed by conventional precipitation. Table 16.7 lists some important metals and alloys in this category.

As a result of the way in which these metals or alloys obtain their properties, the heat of fusion welding often has little or no effect. For most oxide-dispersion-strengthened alloys and many MA alloys the dispersed, strengthening phase is so thermally stable it is unaffected by heat in the HAZ. In fact, in some materials (such as Al_2O_3-reinforced Al-alloys), the oxide is so thermally

stable it can even survive melting in the PMZ and FZ. In other MA alloys, thermal stability might not be this great, so some degradation (either by dissolution, decomposition, or interaction with the matrix) can occur in the high-temperature HAZ. This is the case, for example, in some of the so-called high-temperature aluminum or HTA alloys. Often, the only effect observed in the HAZ is grain growth, and even this can be minimal as a result of the pinning of grain boundaries by particles of the stable phase. In a new class of microalloyed, oxide-dispersion-strengthened steels, for example, there is no recognizable grain growth in even the high-temperature portion of the HAZ nearest the fusion boundary. The presence of fine oxide dispersoids, however, causes the morphology of the ferrite to tend toward acicular.

In the case of metal–matrix composites, the situation can be much more complex, depending on the type and form of the reinforcement and the nature of the matrix. For some systems, where the reinforcement is very stable and the matrix is fairly nonreactive, there can be little or no adverse effects of heat. For other less stable reinforcements, or more reactive matrices, there can be degrading interfacial interactions. This subject is beyond the scope of this book; the reader should seek out needed information on specific systems as they evolve.

16.8. HAZ DEFECTS AND THEIR REMEDIATION

Like the fusion zone (FZ) and partially melted zone (PMZ), the heat-affected zone (HAZ) is not free of problems from defect formation during welding. Table 16.8 provides a general list of the types of defects that can be encountered, as well as a list of major materials in which each is apt to appear.

16.8.1. Liquation Cracking

The width of the partially melted zone can be extended into what is arguably the heat-affected zone by the phenomenon of constitutional liquation. By this phenomenon, melting can occur even where the peak temperature of the local weld thermal cycle is less than the equilibrium solidus, hence supporting the argument that the phenomenon occurs in the HAZ. As explained in Section 15.2, constitutional liquation occurs during nonequilibrium heating (as always found with fusion welding), with the development of a solute gradient around second-phase particles into the matrix phase leading to melting at the eutectic temperature, even though the nominal alloy composition lies in a single-phase terminal solid–solution region. Tensile stress induced by volumetric shrinkage as liquid transforms to solid in the fusion zone, along with nonuniform thermal contraction in the heat-affected zone act on constitutionally liquated films surrounding second-phase particles and in grain boundaries to produce hot cracks called liquation cracks.

Liquation cracking has been seen to occur in the high-temperature region of weld heat-affected zones in maraging steels, austenitic stainless steels, and

TABLE 16.8 Major Types of Defects Found in Weld HAZs, Along With Materials in Which Each Is Apt to Appear

Defect	Alloy
Hydrogen (cold or delayed) cracking	Medium- and high-C steels
	Low-alloy steels
	High-alloy steels
	Tool steels
	Martensitic stainless steels
	Some transition metal alloys (Ti, W, Mo, V)
Strain-age or reheat cracking	Age-hardenable Al alloys 2xxx, 6xxx, 7xxx
	Age-hardenable Ni alloys
	Maraging steels
	PH-stainless steels
Lamellar cracking	Low-grade mild steels
	Corrosion- and heat-resisting steels
Weld decay	Unstabilized austenitic stainless steels
Knife-line attack	Stabilized austenitic stainless steels
Low HAZ toughness (due to grain growth)	Carbon and low-alloy steels
	Ferritic stainless steels
	Refractory metals and alloys

heat-treatable (i.e., age-hardenable) aluminum- and nickel-based alloys. The occurrence of liquation cracking can be particularly dramatic in the weld HAZs of cast irons. Formation of the Fe-C eutectic ledeburite (at 4.3 wt% C) leads to liquation cracking if heat input or preheat or both are too high, such conditions being employed to prevent formation of brittle martensite. To overcome liquation cracking in such cast irons, a technique called quench welding is used in which several small stringer beads are made intermittently without preheat so as to maintain the interpass temperature below 80°C (175°F).

Liquation cracking tends to exhibit an intergranular mode, since it is along grain boundaries that many second-phase particles precipitate preferentially and constitutionally liquate, and the liquid formed spreads to produce a continuous or discontinuous grain boundary film. Intragranular cracking can also be found, however, as the result of cracking around particles or inclusions around which liquation occurs.

16.8.2. Reheat or Strain-Age Cracking

Cracking is sometimes found to occur during the postweld heat treatment of certain age-hardenable alloys, most notably nickel-based superalloys. The

purpose of such postweld heat treatment is twofold: (1) to relieve weld-induced residual stresses and (2) to develop maximum strength by aging. To age the weldment, however, it must first be solutionized, then quenched, and then aged. During solutionizing, residual stresses in the weldment are relieved. However, it is quite possible for some aging to occur in regions of the heat-affected zone that were solutionized by the heat of welding, since aging occurs at lower temperatures than stress relief. When this is the case, cracking can occur as the alloy in this region age hardens, becomes stronger but less ductile, and is acted upon by stress to cause cracking. The phenomenon is called strain-age cracking or simply reheat cracking. The mechanism is shown schematically in Figure 16.27. Reheat cracks usually, but not always, initiate in the HAZ and propagate intergranularly into the regions unaffected by welding heat.

Susceptibility to strain-age cracking in Ni-based alloys has been found to increase with increased Al and Ti content, the active solutes for developing the γ' strengthening precipitate. This susceptibility as a function of (Al + Ti) content is shown schematically in Figure 16.28.

In fact, several mechanisms have been proposed for the low ductility in the HAZ leading to strain-age or reheat cracking, including (1) embrittlement of the grain boundaries due to either liquation or solid-state reactions during welding (Hughes and Berry, 1967); (2) embrittlement of grain boundaries by oxygen during heat treatment (Thompson et al., 1968); and (3) a change in deformation mode from transgranular slip to grain boundary sliding (Owczarski et al., 1966). The sources of high strain in the HAZ are the obvious thermal expansion and contraction associated with welding, as well as contraction associated with the precipitation process in Ni-based alloys itself (Schwenk and Trabold, 1963).

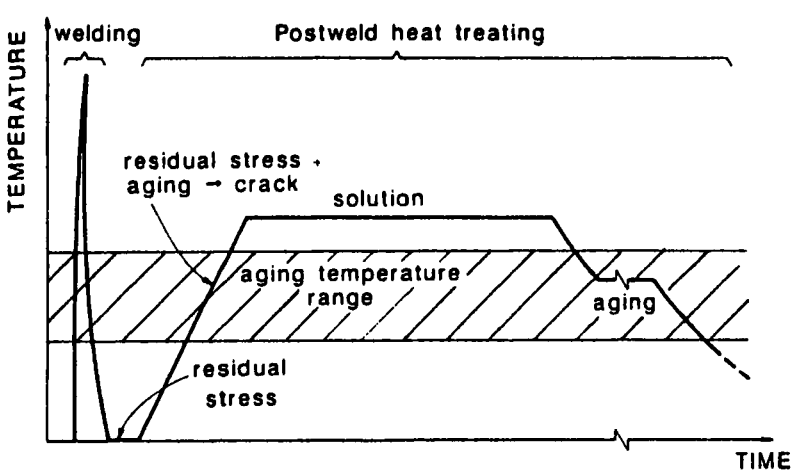


Figure 16.27 Schematic illustration of postweld heat-treatment reheat or strain-age cracking in heat-treatable Ni-based alloys. (From *Welding Metallurgy* by S. Kou, published in 1987 by and used with permission of John Wiley & Sons, Inc., New York.)

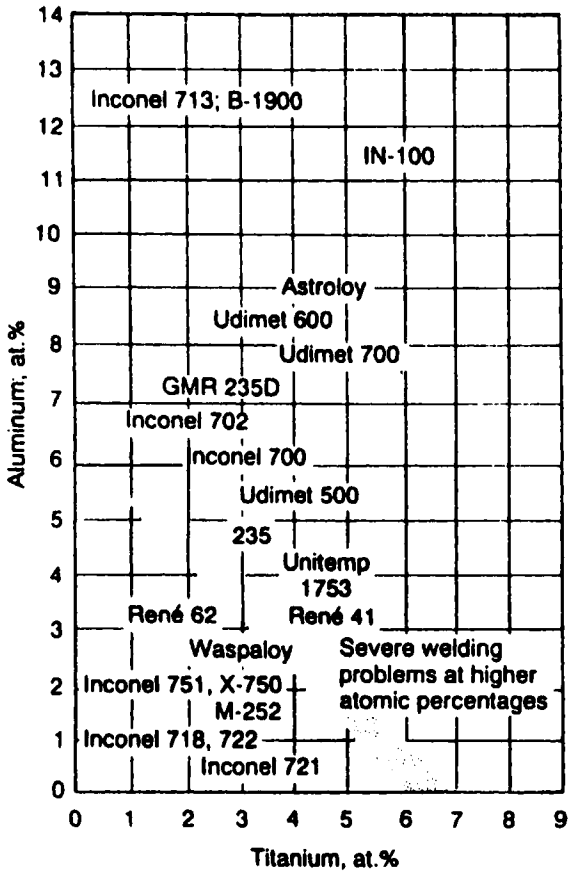


Figure 16.28 Plot of Al versus Ti content indicating susceptibility to strain-age cracking when (Al + Ti) exceeds about 6% in Ni-based alloys. (From *ASM Handbook*, Vol. 6: *Welding, Brazing, and Soldering*, published in 1993 by and used with permission of the ASM International, Materials Park, OH.)

Extensive study by Franklin and Savage (1974) concluded that the weld HAZ of heat-treatable Ni-based alloys responds to postweld heat treatment quite differently than the base metal. While the base metal tends to stress relax during postweld heat treatment without being interrupted by precipitation reactions if it is overaged rather than solution-annealed prior to welding, stress relaxation in the weld HAZ is always interrupted by precipitation reactions regardless of the preweld heat treat condition.

Postweld heat treatment (reheat) cracking can be avoided in Ni-based alloys by any of several methods, including (1) proper base alloy selection to keep (Al + Ti) content below 6%; (2) preweld overaging via multistep overaging processes or by slow cooling from the solutionizing temperature; (3) use of specific solutionizing and aging treatment cycles for particular alloys; (4) using

vacuum or inert gas atmosphere during heat treatment to prevent oxygen embrittlement along grain boundaries; and (5) use of low-restraint joint designs.

16.8.3. Quench Cracking and Hydrogen Cold Cracking

The formation of untempered martensite in weld heat-affected zones occurs for several important classes of steels, including higher-carbon steels, quenched and tempered (Q&T) alloy steels, heat-treatable alloy steels and ferritic and martensitic stainless steels, as well as cast irons. Any time untempered martensite is formed during welding, there is a good chance cracking will result, either upon rapid cooling immediately following welding or some time after cooling to room temperature. The former cracking is called quench cracking, and arises from high, and often nonuniform, tensile stresses that develop in association with the volume expansion as austenite transforms to martensite, as was described for higher C martensitic stainless steels in this chapter. The latter cracking arises from the formation of this susceptible microstructure and the simultaneous presence of residual or applied tensile stresses and hydrogen, and is called hydrogen cold cracking. The critical difference is that the latter requires the presence of hydrogen to cause embrittlement and cracking of the martensite in the presence of tensile stresses, while the former does not, just high tensile stresses.

Prevention of quench cracking involves prevention of the formation of brittle, untempered martensite and high tensile residual stresses at the same time. This means preventing the formation of martensite, generally by preheating to slow cooling rates to less than the critical cooling rate, or preventing the buildup of high tensile stresses by reducing temperature gradients using a hold above the M_s, and making every effort to minimize restraint.

The mechanisms for hydrogen cracking in the heat-affected zone or elsewhere in a weld were presented in Sections 11.5 and 15.3.3, but it is worthwhile to repeat the three prerequisites for such cracking: (1) presence of martensite (or other susceptible microstructure in other alloy systems), (2) presence of tensile stresses, and (3) presence of hydrogen. It is also worthwhile to repeat some sources of hydrogen in welding and various ways of preventing the problem.

Hydrogen can be present in the heat-affected zone of a weld either because it was present in the base metal in the first place, independent of and prior to welding, or because it found its way into the heat-affected zone through the fusion zone from either the welding process (including the welding environment) or the weld deposit (filler). Hydrogen can be dissolved in the base metal either during primary metal production (e.g., principally from acid pickling to remove mill scale) or during subsequent, secondary processing of parts or structural elements (e.g., also from acid cleaning following heat treatment or prior to welding, from chemical milling, or from electroplating). To preclude problems from hydrogen it must be removed prior to welding by a process of baking at slightly elevated temperatures, typically between 125 and 375°C (250

and 700°F), preferably under a vacuum (i.e., vacuum degassing) to take advantage of Sievert's law (see Section 11.1.1).

Hydrogen can be introduced into the fusion zone or weld metal from the process (as hydrogen itself or water vapor in shielding gas or from water absorbed in fluxes), from filler wire (either as hydrogen dissolved in the filler wire or from decomposition of hydrocarbon contaminants, such as rust-protective oils), from the weldment (by dissociation of any form of water on workpiece surfaces or hydrated surface oxides or by dissociation of hydrocarbon oils, paints, marking materials), or from the environment (humidity, rain, or snow). If hydrogen is introduced into the weld during welding, it often migrates or "pumps" to lower temperature regions, but need not, such as when an austenitic filler is used to keep hydrogen benignly in solution. Regardless of where it is introduced, hydrogen has the insidious behavior of migrating up a tensile stress gradient to the region of highest stress. The reason is that the crystal structure is more open in such regions, and thus more accommodating to interstitially dissolved gases.

While effort should always be made to minimize potential sources of hydrogen, the problem of hydrogen cracking can be avoided by preventing martensite formation by preheating (to slow cooling rates to below the critical cooling rate) or immediately tempering any martensite that forms. It is also possible to minimize the introduction of residual stresses by minimizing restraint or immediately stress relieving the weldment.

Throughout this book, hydrogen-induced cracking has been alternatively referred to as hydrogen cracking (after its major driver), hydrogen embrittlement (after its inherent nature), cold cracking (after the fact that it occurs only after the temperature has dropped enough for martensite to form), delayed cracking (after the fact that considerable time might be required for crack initiation), as well as underbead cracking (after its typical location). The purpose of this was not to confuse the reader, but to increase awareness.

Two last points regarding hydrogen cracking: (1) It can be devastating and (2) it is avoidable.

16.8.4. Weld Decay, Knife-Line Attack, and Stress Corrosion Cracking

The occurrence of weld decay in the heat-affected zone of austenitic or ferritic stainless steels is the result of prior sensitization during welding. No more will be said about weld decay, except that some care must be exercised in attempting to prevent it. The reason is that, depending on the approach used, it is possible to fix one problem and create another. Knife-line attack, like weld decay, is the result of carbide precipitation along grain boundaries, depletion of Cr content to below the level needed for providing corrosive attack (about 14%), and exposure to a corrosive environment. Knife-line attack is so-named because it occurs in a very narrow band or knife-line in an area immediately adjacent to the weld fusion zone, and it occurs in stabilized grades of austenitic stainless steel!

The mechanism responsible for knife-line attack is shown schematically in Figure 16.29. The area corresponding to thermal cycle *a* is very close to the fusion boundary, and is subjected to both a very high peak temperature and very rapid cooling during welding. Being above the solvus temperature for Ti- or Nb-carbide, these carbides are dissolved. Because of rapid cooling through its precipitation range, new Ti- or Nb-carbide does not reprecipitate during cooling, thus leaving abundant carbon in solution. Upon reheating into the lower-temperature Cr, Fe-carbide formation range during stress relief treatment or in service, Ti- or Nb-carbide does not form because the temperature is not high enough. However, Cr, Fe-carbide does form at grain boundaries, rendering them susceptible to corrosion. At lower peak temperatures, such as for thermal cycle *b* in Figure 16.29, the Ti- or Nb-carbides do not dissolve. Knife-line attack can also occur as the result of multipass welding when one pass dissolves Ti- or Nb-carbides and another causes subsequent Cr, Fe-carbide precipitation. Thus, care must be taken in deciding on weld sequence in areas of weldments where exposure to a corrosive environment is expected. Likelihood of knife-line attack can be reduced by (1) additions of rare-earth elements (La and Ce) to stabilized austenitic grades, because accelerated precipitation of carbides of these elements leaves less carbon in solution to form unwanted Cr-carbides; (2) using low C grades; and (3) postweld solutionizing and quenching, when practical.

Susceptibility to both weld decay and knife-line attack can be evaluated by

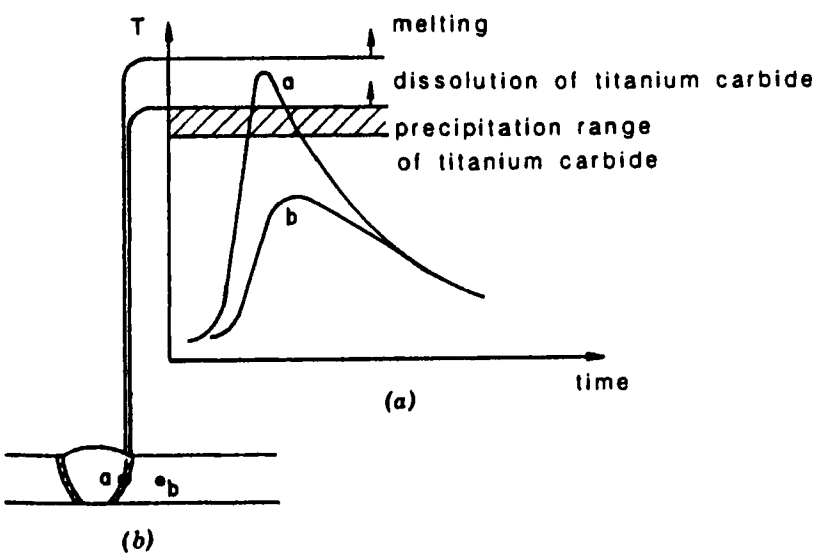


Figure 16.29 Schematic showing (a) the thermal cycles responsible for the formation of (b) knife-line attack in a region where carbides with the stabilizing solute addition are dissolved during welding. (From *Welding Metallurgy* by S. Kou, published in 1987 by and used with permission of John Wiley & Sons, Inc., New York.)

exposing sensitized materials to corrosive agents using either the Huey test (with boiling 65% nitric acid) or the Strauss test (using aqueous copper sulfate solution). Attack can be detected by metallographic analysis or by dropping the exposed piece and listening for a metallic ring. If there is none, the sample has been severely attacked.

As a consequence of their inherently low thermal conductivity and high coefficient of thermal expansion compared to mild steels, austenitic stainless steels are prone to the development of severe residual stresses during welding. In the presence of such severe residual stresses, branched, transgranular cracking often occurs in chloride-containing media, especially in the HAZ. Such cracking is known as stress-corrosion cracking, and can be prevented by suitable postweld stress relief.

16.8.5. Lamellar Tearing

Metals and alloys, most notably wrought iron and mild and low-alloy steels with nonmetallic inclusion contents, can exhibit lamellar tearing. *Lamellar tearing* in welded structure is the result of a combination of high localized stresses due to weld contraction and low ductility of the base metal in its through-thickness direction parallel to the rolling direction due to the presence of elongated stringers of nonmetallic inclusions. Tearing is triggered by decohesion of these inclusions, which are usually silicates or sulfides. The problem is particularly severe just outside the fusion and partially melted zones. The situation leading to lamellar tearing is shown schematically in Figure 16.30a.

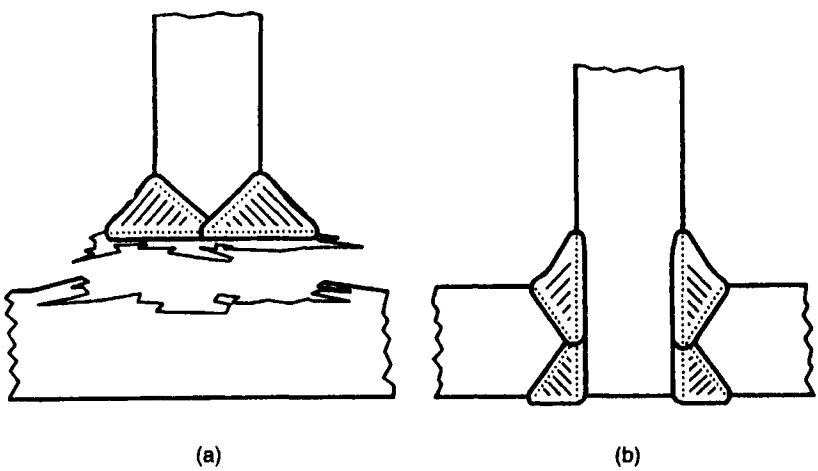


Figure 16.30 Schematic illustration of (a) lamellar tearing across nonmetallic inclusions due to weld-induced stresses in a T-joint and (b) orientation of the weld joint to minimize such opening stresses. (From *Welding Metallurgy* by S. Kou, published in 1987 by and used with permission of John Wiley & Sons, Inc., New York.)

Two practical ways of avoiding lamellar tearing, given the general impracticality of changing to a less "dirty" base metal, are (1) employing joint designs that cause contraction stresses to act along rather than across the rolling direction of susceptible materials (see Figure 16.30b), and (2) grinding or machining away the volume of the workpiece where tearing is anticipated and "buttering" the cutaway portion with a softer, better strain-accommodating weld metal.

Tests for susceptibility to lamellar tearing include the Lehigh cantilever lamellar tearing test, Cranefield lamellar tearing test, and tensile lamellar tearing test. More about these and other tests of weldability are presented in Chapter 17.

16.9. SUMMARY

Outside the region of melting (or partial melting) and solidification caused by fusion welding, the microstructure of base materials is altered when heat causes the temperature to rise sufficiently to cause solid-phase transformations or reactions. This region is called the heat-affected zone or HAZ. Since changes in the structure in this zone result in changes in properties, the effect of heat on structure must be understood. What changes take place depends on how the base metal attains strength and other properties, that is, on the mechanisms of strengthening that are operative. The expected effects of heat on pure metals or alloys that obtain strength from a fine-grain structure, from cold work through work or strain hardening, or from dispersion of a stable second phase were described. The heat effects on metals obtaining strength throuh solid solution strengthening or alloy, and alloys that obtain additional strength beyond solid solution strengthening by precipitation, age hardening, transformation hardening were also discussed. The possibility, types, causes, and means of preventing defects in the heat-affected zone were explored.

REFERENCES AND SUGGESTED READING

Castro, R., and DeCadenet, J. J., 1974, *Welding Metallurgy of Stainless and Heat-Resisting Steels*, Cambridge University Press, London.

Delong, W. T., 1974, "Ferrite in austenitic stainless steel weld metal," *Welding Journal*, **53**(7), 273s–286s.

Franklin, J. G., and Savage, W. F., 1974, "Stress relaxation and strain-age cracking in René 41 weldments," *Welding Journal*, **53**(9), 380s–387s.

Gordon, P., 1955, "Microcalorimetric investigation of recrystallization of copper," *Transactions of the AIME*, **203**, 1043–1052.

Hughes, W. P., and Berry, T. F., 1967, "A study of the strain-age cracking characteristic of René 41, phase I," *Welding Journal*, **46**(8), 361s–370s.

Owczarski, W. A., DuVall, D. S., and Sullivan, C. P., 1966, "A model for heat-affected zone cracking in nickel base superalloys," *Welding Journal*, **45**(4), 145s–155s.

Schwenk, W., and Trabold, A. F., 1963, "Weldability of René 41," *Welding Journal*, **42**(10), 460s–465s.

Silcock, J. M., Heal, J. J., and Hardy, H. K., 1953, "Structural ageing characteristics of binary aluminum-copper," *Journal of the Institute of Metals*, **82**, 239–248.

Thompson, E. G., Nunez, S., and Prager, M., 1968, "Practical solutions to strain-age cracking of René 41," *Welding Journal*, **47**(7), 299s–313s.

Suggested readings on grain refinement, cold work and work hardening, recovery/recrystallization/grain growth, solid solution strengthening, precipitation or age hardening, transformation hardening, and dispersion strengthening

ASM Handbook, Vol. 6: *Welding, Brazing and Soldering*, 1993, American Society for Metals, Materials, Park, OH. [Also defects]

Callister, W. D., Jr., 1997, *Materials Science and Engineering: An Introduction*, 4th ed., Wiley, New York.

Reed-Hill, R. E., 1973, *Physical Metallurgy Principles*, Van Nostrand, New York. [More advanced]

Shackelford, J. F., 1996, *Introduction to Materials Science for Engineers*, 4th ed., MacMillan, New York.

Smith, W. F., 1996, *Principles of Materials Science and Engineering*, 3d ed., McGraw-Hill, New York.

White, S. S., Manchester, R. E., Moffatt, W. G., and Adams, C. M., 1960, "Plastic properties of aluminum–magnesium weldments," *Welding Journal*, **39**(1), 10s–19s.

Suggested readings on the physical metallurgy and welding metallurgy of aluminum and aluminum-based alloys, nickel and nickel-based alloys (or superalloys), steels, and stainless steels

Hatch, J. E. (Editor), 1990, *Aluminum: Properties and Physical Metallurgy*, American Society for Metals (ASM International), Materials Park, OH. [Aluminum and aluminum alloys]

Leslie, W. C., 1981, *The Physical Metallurgy of Steels*, McGraw-Hill, New York. [Steels]

Linnert, G. E., 1965 and 1967, *Welding Metallurgy*, Vols. 1 and 2, 3d ed., American Welding Society, Miami, FL. [Steels]

Linnert, G. E., 1976, *Source Book on Stainless Steels*, American Society for Metals, Metals Park, OH. [Stainless steels].

Mondolfo, L. F., 1976, *Aluminum Alloys: Structure and Properties*, Butterworths, London. [Aluminum and aluminum alloys]

Oldland, P. T., Ramsay, C. W., Matlock, D. K., and Olson, D. L., 1989, "Significant features of high-strength steel weld metal microstructures," *Welding Journal*, **68**(4), 158s–168s. [High-strength steels]

Peckner, D., and Bernstein, I. M., 1977, *Handbook of Stainless Steels*, McGraw-Hill, New York. [Stainless steels]

The Superalloys, edited by C. T. Sims and W. C. Hagel, Wiley, New York. [Nickel-based alloys]

Suggested reading on in-process control of heat-affected zone microstructure

Doumonidis, C. C., and Hardt, D. E., 1990, "Simultaneous in-process control of heat-affected zone and cooling rate during arc welding," *Welding Journal*, **69**(5), 186s–193s.

Suggested readings on general weldability of metals and alloys by type

ASM Handbook, 1993, Vol. 6: *Welding, Brazing, and Soldering*, ASM International, Materials Park, OH.

Welding Handbook, 1997, Vol. 3, 9th ed., American Welding Society, Miami, FL.

CHAPTER 17

WELDABILITY AND WELD TESTING

At first glance, all that seems to be involved in producing a welded structure is to weld together structural elements. But, there is more; much more! There are the obvious steps of (1) defining the problem to be resolved by welding; (2) designing the various structural elements, weld joints, and joint edge preparations to join these elements by welding into assemblies and subassemblies into an assembly; (3) selecting the proper (and, hopefully, best) process, which really needs to be done as part of the design process; (4) selecting or developing (by weld procedure qualification or WPQ) the proper welding or operating parameters (current mode, current, voltage, and travel speed for arc welding, for example), conditions (cleanliness, protection from the environment, etc.), and procedures (e.g., fixturing, positioning, heat source manipulation); (5) performing the actual welding following proper joint preparation, assembly, and welder certification; (6) postweld heat treating (and/or machining or finishing) the welds and weldment; and (7) inspecting the welds and various weldment dimensions to see that they meet requirements (e.g., specifications).

However, before all this can begin, there are two other key items that will not only assure that what you want, you'll get, but will make the entire process easier and more successful: (1) assessing, by testing, the weldability of the materials and configuration involved; and (2) testing representative welds and weld joints to assure properties are acceptable. This chapter looks at weldability and weld testing to help understand why and how each is performed.

17.1. WELDABILITY TESTING

According to the definition developed by the American Welding Society, "Weldability is the capacity of a material to be welded under the imposed fabrication conditions into a specific suitably designed structure and to perform satisfactorily in the intended service." By this definition, some base metals or alloys may exhibit good weldability under some conditions, but poor weldability under other conditions. A good example is heat-treatable, quenched and tempered (Q&T) steels, such as ASTM A514 construction steel. In the heat-treated condition, where a yield strength of 689 MPa (100 ksi) has been developed by appropriate quenching and tempering, this alloy exhibits good weldability provided the base metal is sufficiently preheated (to prevent cooling at rates high enough to produce untempered martensite), that low-hydrogen welding procedures are employed, and that allowable heat input limits are not exceeded. Fail at any of these, and the weldability is considered to be poor.

While weldability depends on the process, operating parameters (especially, net linear heat input), procedures, degree of restraint, and environment (especially presence of hydrogen from any form of water or hydrocarbon), the most important factor is base metal chemical composition. Composition can determine inherent weldability, with some alloys being inherently weldable, others being inherently difficult to weld, and still others being essentially unweldable. For those materials that are inherently difficult to weld, special attention and care must be given to the conditions under which welds are to be made, most particularly the degree of restraint, but also the net heat input. For those few materials (or assemblies) that are unweldable, an alternative method of joining must be sought.

To assess the weldability of a base material, or filler for that matter, it is essential to employ a technique that replicates the conditions that will be present during weld fabrication as closely as possible. This means replicating (1) joint configuration (fillet or groove, groove type, etc.), (2) degree of inherent restraint as imposed by base metal thickness or general mass, and (3) degree of imposed restraint from fixturing or other structure in the welded assembly.

Weldability tests can be classified into two broad categories: (1) direct tests and (2) indirect tests. *Direct weldability tests* make use of an actual sample of the weld metal or entire weld zone made in the intended service material, replicating process, process operating parameters, and operating conditions, as well as base material conditions (e.g., cast versus wrought, machined versus forged, state of heat treatment), geometry and dimensions, and restraint as closely as possible. For this reason, direct weldability tests are also referred to as actual welding tests. *Indirect weldability tests*, on the other hand, utilize basic metallurgical principles to examine welding parameters on a sample, and then infer the effects of those welding variables on the actual final product. They usually do so by simulating the weld thermal cycle so as to create a simulated weld zone, at least in terms of microstructure. For this reason, indirect weldability tests are also referred to as simulated tests.

Direct weldability tests are of greater practical importance to the process engineer and designer because they are designed to closely approximate actual production welds and welding conditions. While more removed from actual fabrication conditions, indirect weldability tests nevertheless provide valuable metallurgical information that might be impractical or impossible to obtain through direct methods. Results from indirect tests should always be considered by a welding or materials engineer.

Weldability testing offers a rational and, in reality,[1] economical way to investigate the effects of the process, physics, chemistry, and metallurgy of welding on the quality, properties, and performance of actual weldments. To be effective, however, a weldability test should provide (1) information that has direct relevance to a production weld, (2) sensitivity to the effects of welding variables, (3) a high degree of reproducibility, and (4) simplicity of operation.

17.2. DIRECT WELDABILITY OR ACTUAL WELDING TESTS

A wide variety of tests have been devised to directly investigate or assess the weldability of base metals and alloys—arguably, as will be seen, too many! (Sometimes, a test for every possible situation can be as disconcerting as no test at all!) Usually, these tests are used to assess the weldability of particular alloys, grades, or individual heats of base materials. When this is the case, specimen geometry, dimensions, and welding conditions (process, parameters, procedure, etc.) are held constant to make the base material the only variable. Alternatively, these tests may be used to establish compatible combinations of base material, filler, and welding conditions (including process, parameters, and procedure) that will produce acceptable results in the test and, hopefully, in practice.

Another way of thinking about direct weldability or actual welding tests is (1) those used to assess weldability during fabrication and (2) those used to assess properties of the weldment. We look at the former here, and the latter in the section on weld testing.

Fabrication weldability tests are designed to assess the susceptibility of the welded joint to cracking, and usually are grouped according to the type of cracking they produce. For this reason, fabrication weldability tests are also called crack-susceptibility tests. Hence, crack-susceptibility tests can be categorized by the zone in which they assess cracking; such as *fusion zone, partially melted zone, and heat-affected zone crack-susceptibility tests.* Or, better still, they can be categorized by whether the cracks form above the solidus temperature, that is, supersolidus cracking, and involve melting, or whether the cracks form below the solidus, that is, subsolidus cracking, and occur without melting being

[1] At first glance, performing weldability tests might seem to add to the cost of producing a product, and it does. But with information from a properly selected and conducted weldability test, this cost will be recovered many times over in terms of production cost, including yield, throughput, customer satisfaction, and liability. And, this is true for high-value one-of-a-kind products, like pressure vessels or bridges, as well as for high-volume products, like automobile bodies.

involved. The former are often called hot-cracking tests, and the latter are often called cold-cracking tests, not to be confused with just hydrogen-induced cold cracking, but also including reheat or strain age cracking and lamellar tearing.

Here, fusion and partially melted zone hot-cracking tests are discussed together, then heat-affected zone general cold cracking tests are described.

17.2.1. Fusion and Partially Melted Zone Hot-Cracking Tests

Tests designed to assess susceptibility to cracking that occurs during solidification in the fusion zone or partially melted zone are called hot-cracking or supersolidus crack-susceptibility tests. There are many, widely different tests, some of which are strictly qualitative to allow comparison of one base material to another, and some of which are semiquantitative-to-quantitative to allow assessment based on some measurable characteristic such as prevailing strain. Within both hot-cracking and cold-cracking test classifications, there are self-restraint and externally-loaded types, with the latter yielding more quantitative results. Futhermore, some tests are suitable for assessing either or both hot and cold cracking. Those suitable to both types of cracking are identified.

Popular tests include the following, with reference to the figure number where a schematic can be found:

- Finger (crack-susceptibility) test (Figure 17.1)
- Houldcroft (crack-susceptibility) test (Figure 17.2)
- Battelle (crack-susceptibility) test (Figure 17.3)
- Lehigh restraint (crack) test (Figure 17.4)
- Varestraint (crack-susceptibility) test (Figure 17.5)
- Murex hot-cracking test (Figure 17.6)
- Root-pass crack test (Figure 17.7)
- Keyhole-slotted-plate restraint test (Figure 17.8)
- Navy circular-fillet-weldability (NCFW) test (Figure 17.9)
- Circular-groove cracking test (Figure 17.10)
- Segmented-groove (or modified circular restraint) cracking test (Figure 17.11)
- Circular-patch (crack-susceptibility) test (Figure 17.12)
- Restrained-patch (crack-susceptibility) test for sheet metal (Figure 17.13)
- Sigmajig test (Figure 17.14)

The basic intent and value of each of these tests is given in very brief statements below, while Table 17.1 lists these tests, as well as heat-affected zone tests for cold-cracking mechanisms, along with (1) general purpose, (2) material normally evaluated, (3) important variables, and (4) data obtained. References specific to each test are given at the end of the chapter.

TABLE 17.1 Major Weld Cracking-Susceptibility (Weldability) Tests

Test	Applicable Material	Applicable Process	Purpose
Finger (hot-cracking)	High-alloy steels; superalloys	Metal arc GMAW	Effect transv. cracks (FZ)
Houldcroft (hot-cracking)	Al and steels	GTAW	Effect range of restraint (FZ)
Battelle (hot-cracking)	Plain-C, low-alloy, HS and UHS steels	GMAW	Semi-quant. restraint (FZ)
Lehigh restraint (hot-cracking)	Steels	Metal arc	Quant. effect restraint (FZ)
Varestraint (hot-cracking)	Low- and high-alloy steels	GTAW (BOP)	Quant. effect strain (FZ/HAZ)
Murex hot-cracking	Steels	Metal arc	Evaluate filler metals
Root pass	Steel fillers	GMAW	Evaluate root-pass cracking
Submerged-arc welding	Steels	SAW	Hot-cracking in SAW
Keyhole slotted-plate	Steels	Metal arc	Semi-quant. FZ and HAZ
Naval circular-fillet-weldability (NCFW)	Low alloy, HS steels	GMAW	Effect of self-restraint
Controlled thermal severity (CTS)	Steels	Metal arc	Effect of HAZ cooling rate
Circular groove/ segmented groove	Steels	Metal arc	FZ/HAZ hot & cold cracking
Restraint patch	Age-hardenable alloys High-temp. sheet alloys	GTAW	Strain-age cracking
U.S. Navy circular patch	Steels	Metal arc	Hot & cold cracking
Cruciform	Armor steels	Metal arc	Restraint; hydrogen cracking
BWRA	Cr-Ni austenitic steels	Metal arc	HAZ cracking
Wedge	Med-C/low-alloy steels	Metal arc	Effect of cooling rate
Implant	Hardenable steels	Metal arc GTAW	HAZ hydrogen cracking, stress relief cracking
G-BOP	Hardenable steels	Metal arc GTAW	HAZ hydrogen cracking
Tekken	Hardenable steels	Metal arc GTAW	HAZ hydrogen cracking
Spiral notch	All	Metal arc GTAW	Pinpoint brittle zone; strain-age cracking
Vinkier	Age-hardenable alloys	Metal arc GTAW	Strain-age cracking
Compact tension	Age-hardenable alloys	Metal arc GTAW	Strain-age cracking
Cranfield	Low-grade steels	Metal arc	Lamellar tearing
Lehigh cantilever	Low-grade steels	Metal arc	Lamellar testing
Tensile lamellar	Low-grade steels	Metal arc	Lamellar tearing

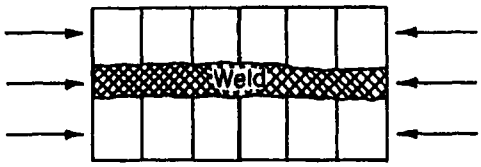


Figure 17.1 Schematic of the finger-test crack-susceptibility test. (From "Weldment Evaluation Methods," by J. J. Vagi, R. P. Meister, and M. D. Randall, *DMIC Report 244*, August 1968, courtesy of Advanced Materials and Processes Technology Information Analysis Center (AMPTIAC), 201 Mill Street, Rome, NY.)

17.2.1.1. Finger Test. These tests (shown in Figure 17.1) involve depositing a weld bead across tightly compressed bars, simulating transverse base metal cracks by the gaps between the bars. Different degrees of severity of weld-induced strain can be developed by varying the width of the fingers (more strain for more narrow fingers). Performance is based on the percentage of the bead width that contains cracks.

17.2.1.2. Houldcroft and Battelle Hot-Crack Susceptibility Tests. These tests (shown in Figures 17.2 and 17.3) each provide a wide range of restraint in a single test specimen, the Houldcroft being developed to evaluate cracking tendency of sheet materials to GTAW with or without filler, and the Battelle being developed to evaluate the cracking tendency of fillers deposited under conditions of high restraint. The tests are made by depositing a weld bead along the length of the specimen, complete penetration being required in the Houldcroft Test, and partial-penetration for the Battelle test. Performance is

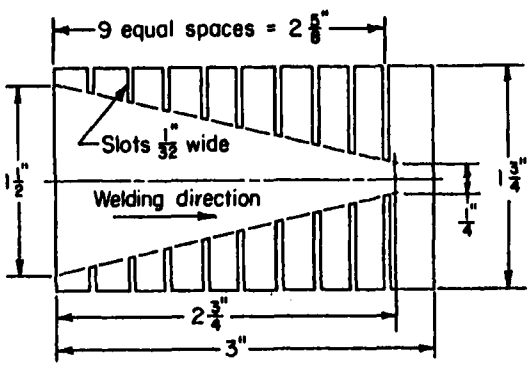


Figure 17.2 Schematic of the Houldcroft (crack-susceptibility) test. (From "Weldment Evaluation Methods," by J. J. Vagi, R. P. Meister, and M. D. Randall, *DMIC Report 244*, August 1968, courtesy of Advanced Materials and Processes Technology Information Analysis Center (AMPTIAC), 201 Mill Street, Rome, NY.)

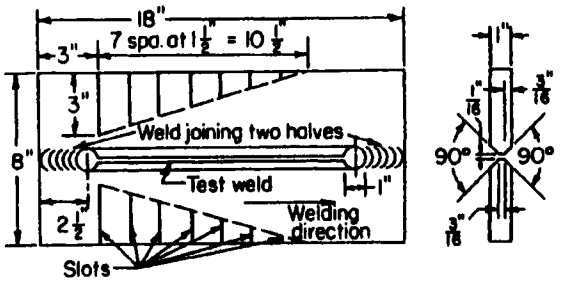
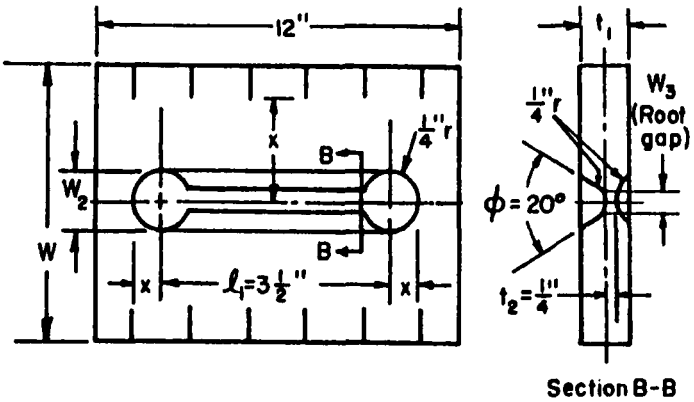


Figure 17.3 Schematic of the Battelle (crack-susceptibility) test. (From "Weldment Evaluation Methods," by J. J. Vagi, R. P. Meister, and M. D. Randall, *DMIC Report 244*, August 1968, courtesy of Advanced Materials and Processes Technology Information Analysis Center (AMPTIAC), 201 Mill Street, Rome, NY.)

based on crack length in the Houldcroft specimen and on the point of crack initiation in the Battelle specimen.

17.2.1.3 Lehigh Restraint Test. The test (shown in Figure 17.4) provides a quantitative measure of the degree of restraint necessary to produce weld-metal fusion zone hot cracking as well as cold cracking in either the fusion or heat-affected zone. The degree of restraint is varied by changing the length of slots extending inward from the edges of the test plate toward the weld groove (with longer slots imposing greater restraint); each level of restraint requires a separate test plate. Cracking is detected by examining the cross section of welds. Performance is based on the minimum distance between the ends of opposing slots that just results in cracking.

17.2.1.4. Variable-Restraint (or Varestraint) Test. The test (shown in Figure 17.5) is conducted by depositing a weld on a cantilevered specimen, beginning at the free end (left in the figure), and continuing until the arc reaches a point near the point of tangency between the cantilevered specimen and an underlying radius block (point *A* in the figure). The cantilevered section is then bent (using a pneumatically actuated ram) to conform to various curved dies or radius blocks, and the welding arc continues to point *C* in the figure, at which point it is extinguished. After cooling, the as-welded face surface of the specimen is examined at 60× magnification, and the length of each crack recorded. Performance is based on one or more of the following: (1) the minimum augmented strain (calculated from the specimen thickness and the form-block radius) to just cause cracking (the cracking threshold); (2) the maximum crack length (MCL), indicative of susceptibility to fusion zone hot-cracking; and (3) the total crack length (TCL), obtained by adding the lengths of all cracks observed in both the fusion and heat-affected zones, indicative of both fusion zone hot-cracking and HAZ liquation cracking. There is a variant of this test called the spot varestraint test, also known as the



Dimensions, inches									
ℓ_1	L	W	X	W_2	W_3	t_1	t_2	ϕ[a]	R
3-1/2	12	8	Var.	1/2	1/16	<1	1/4	20°	1/4
5-1/2	12	8	Var.	1/2	1/16	>1	1/4	20°	1/4

Dimension X usually varied in 1/2-inch increments. Temperature of base plate at time of depositing test weld varied depending on condition studied, i.e., preheat, ambient temperature, etc. Small specimen illustrated.

Figure 17.4 Schematic of the Lehigh restraint-cracking test. (From "Weldment Evaluation Methods," by J. J. Vagi, R. P. Meister, and M. D. Randall, *DMIC Report 244*, August 1968, courtesy of Advanced Materials and Processes Technology Information Analysis Center (AMPTIAC), 201 Mill Street, Rome, NY.)

TIG-A-MA-JIG, used to assess hot cracking susceptibility in stationary GTAW spot welds. In this variation, the test specimen is loaded as a 3-point beam, with the central point at which the spot weld is made being bent over a known radius block to fix the augmented strain level.

17.2.1.5. Murex Hot-Cracking Test. The test (shown in Figure 17.6) is used for obtaining comparative information on similar (or different) welding fillers. The test is performed by depositing a fillet weld in a V-groove formed between two 0.5-in.-thick plates. Five seconds after welding has started, one of the plates is rotated about the point of the vee by a predetermined amount, usually 30°. The speed of rotation is adjusted to control straining of the weld metal. Performance is measured based on lengths of cracks appearing as a result of straining.

17.2.1.6. Root-Pass Crack Test. This test (shown in Figure 17.7) was specifically designed to evaluate susceptibility to cracking in the root pass of multipass SMA welding of thick sections. A similar, related test, called the

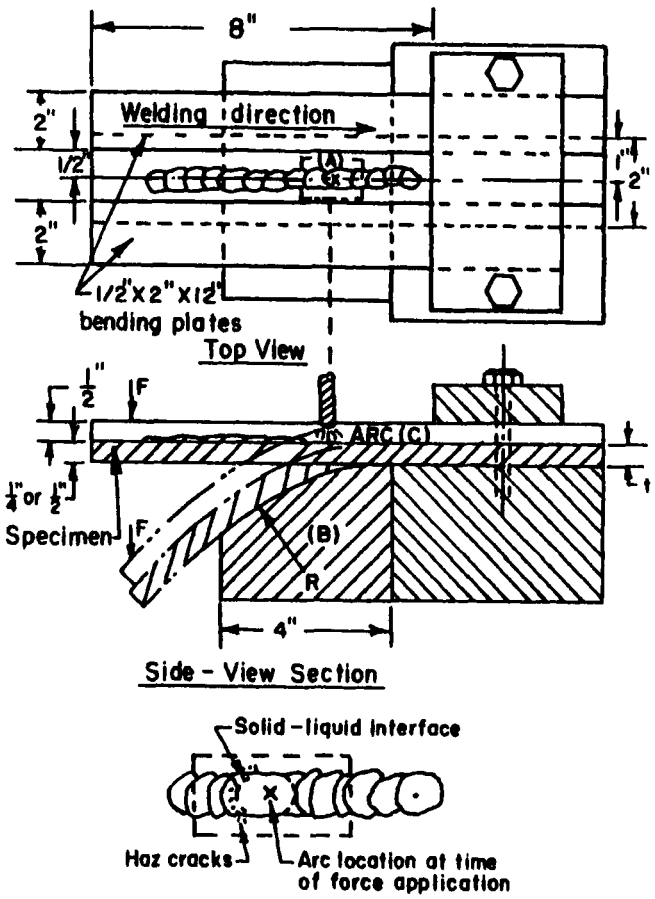


Figure 17.5 Schematic of the Varestraint (crack-susceptibility) test. (From "Weldment Evaluation Methods," by J. J. Vagi, R. P. Meister, and M. D. Randall, *DMIC Report 244*, August 1968, courtesy of Advanced Materials and Processes Technology Information Analysis Center (AMPTIAC), 201 Mill Street, Rome, NY.)

submerged-arc-weld crack test, was developed for evaluating the same thing for root passes made by SAW. After deposition of the first pass of weld metal, slag removal, and cooling to 100°F (39°C), the specimen is examined visually, by dye penetrant, or by x-radiography. Performance is based on the extent of weld-metal cracking.

17.2.1.7. Keyhole-Slotted-Plate Test. The test (shown in Figure 17.8) is used to evaluate susceptibility to a mixture of weld metal and base metal to hot and cold cracking under restrained conditions. The presence of a notch at the bottom of a weld groove is representative of a root pass in a restrained weld. Self-restraint from the specimen is varied by varying key dimensions of

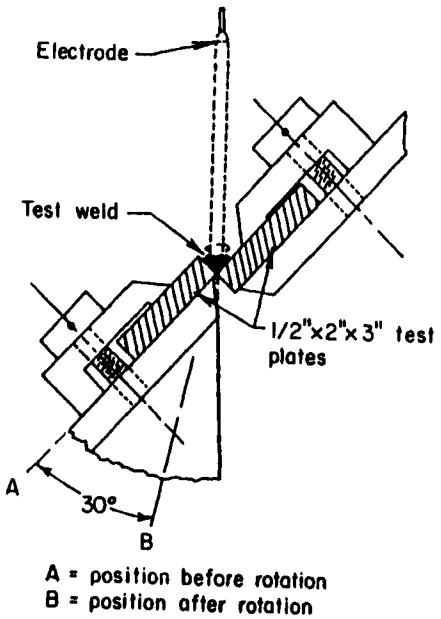
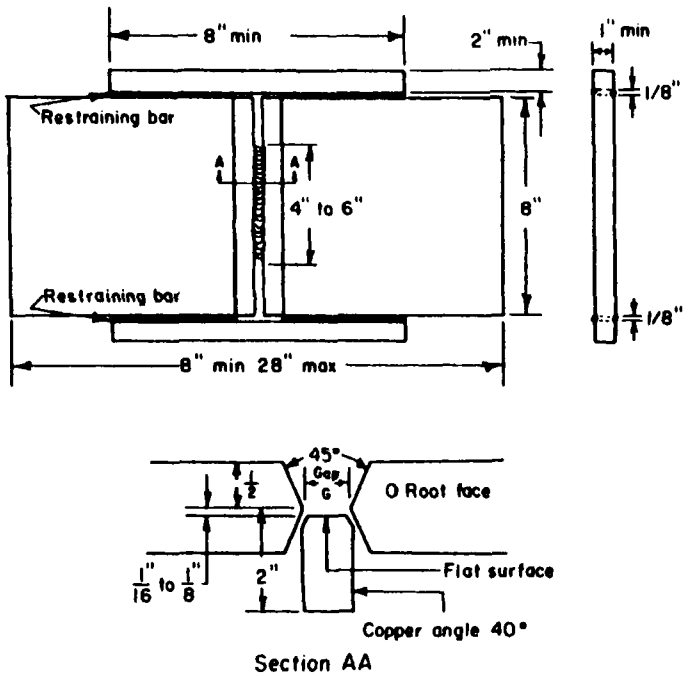


Figure 17.6 Schematic of the Murex hot-crack test. (From "Weldment Evaluation Methods," by J. J. Vagi, R. P. Meister, and M. D. Randall, *DMIC Report 244*, August 1968, courtesy of Advanced Materials and Processes Technology Information Analysis Center (AMPTIAC), 201 Mill Street, Rome, NY.)

the plate as shown in the figure. The test is performed by depositing weld metal to within $\frac{1}{4}$ in. (6 mm) of the hole at the end of the slot, and examining for cracking. Inspection for cracks is repeated at several intervals after welding has ceased, to determine whether cold cracking is occurring. Performance is based on the length of cracks, time of cracking, and location of cracks.

17.2.1.8. Navy Circular-Fillet-Weldability (NCFW) Test. This test (shown in Figure 17.9) also employs a specimen developing self-restraint, and is used to evaluate hot-cracking susceptibility in both the fusion and heat-affected zones. Here, stress increases with the number of weld layers deposited. The layer at which cracking first occurs, along with the type, quantity and size of cracks are all considered in evaluation of results. Performance is based on comparison of results obtained from other material combinations tested.

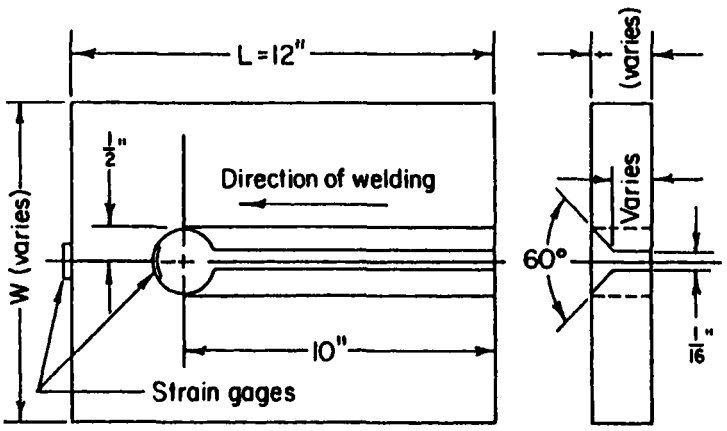
17.1.1.9. Circular-Groove Cracking and Segmented-Groove Tests. The circular-groove test (shown in Figure 17.10) is a simple "go/no-go" test designed to evaluate weld-metal and heat-affected zone cracking in various base metal/filler metal combinations. Weld metal is deposited into a circular groove machined into a square plate and the extent of cracking is expressed as a percentage of total weld length. The test can be made semiquantitative by



Electrode Diameter, in.	Root Gap (G), in.	Root-Bead Thickness, in.
5/32	3/16	0.160 - 0.200
3/16	1/4	0.185 - 0.240
1/4	5/16	0.250 - 0.330
5/16	3/8	0.280 - 0.360

Figure 17.7 Schematic of the root-pass crack-susceptibility test. (From "Weldment Evaluation Methods," by J. J. Vagi, R. P. Meister, and M. D. Randall, *DMIC Report 244*, August 1968, courtesy of Advanced Materials and Processes Technology Information Analysis Center (AMPTIAC), 201 Mill Street, Rome, NY.)

varying the diameter of the machined groove or by varying the plate dimensions. The segmented-groove test (shown in Figure 17.11) is a modification of the circular groove test designed to simulate the notch extension cracking encountered in welding various components in gas turbines. The specimen consists of four segments, usually with abutting faces machine finished. The segments are first tacked together, and then the test weld is deposited in a single pass. The extent of cracking is determined by breaking apart the segments and noting oxide areas as indicative of preexisting cracks.



Restraint varied by varying L, W, and t; normally L held constant; example - for t = 1/2 inch, W varied from 6 to 10 inches.

Figure 17.8 Schematic of the keyhole-slotted-plate restraint-test. (From "Weldment Evaluation Methods," by J. J. Vagi, R. P. Meister and M. D. Randall, *DMIC Report 244*, August 1968, courtesy of Advanced Materials and Processes Technology Information Analysis Center (AMPTIAC), 201 Mill Street, Rome, NY.)

17.1.1.10. Circular-Patch Test. The test (shown in Figure 17.12) was designed to investigate weld-metal cracking, but is also used to evaluate both hot and cold cracking in the HAZ. The specimen consists of welding a circular disk back into a square plate from which it was cut. It is another "go-no go" test, in which performance is assessed by how small a disk can be welded without cracking. Closely akin to this test is the U.S. Navy circular patch test, the major difference being the precise sequencing of welding for the latter test.

17.1.1.11. Restrained-Patch Test. This test (shown in Figure 17.13) uses a full-penetration, circular bead-weld deposit to assess cracking susceptibility in sheet materials. It is essentially identical in principle to the circular-patch test.

17.1.1.12. Sigmajig Test. This test for hot-cracking susceptibility in sheet-gauge materials, developed at the Oak Ridge National Laboratory, applies a transverse normal stress (known as sigma stress or simply σ, hence the name), to a 50 × 50-mm (2 × 2-in.) specimen as shown in Figure 17.14. Several specimens are welded autogenously, one after the other, along their longitudinal centerline using GTAW. Applied stress is increased between tests until centerline cracking occurs. The threshold stress needed to produce 100% cracking is used as the measure of cracking susceptibility.

While these and many other tests are used to evaluate susceptibility to hot

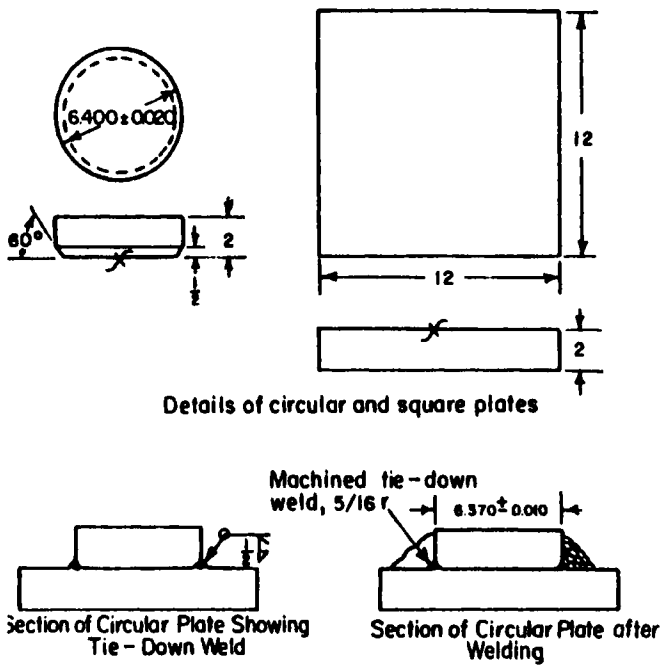


Figure 17.9 Schematic of the Navy circular-fillet-weldability (NCFW) test. (From "Weldment Evaluation Methods," by J. J. Vagi, R. P. Meister, and M. D. Randall, *DMIC Report 244*, August 1968, courtesy of Advanced Materials and Processes Technology Information Analysis Center (AMPTIAC), 201 Mill Street, Rome, NY.)

cracking in the fusion zone or partially melted zone of fusion welds, the most popular by far are the Houldcroft and Battelle tests, the Lehigh restraint test, and the varestraint test.

17.2.2. Heat-Affected Zone General Cold-Cracking Weldability Tests

Cracking that occurs in the heat-affected zone is always classified as *subsolidus cracking*, because it is the equilibrium solidus temperature that delineates the high-temperature extreme of this zone. Furthermore, most such cracking is also generically classified as cold cracking, in that it occurs after solidification is complete and the material has cooled toward room temperature. The only exception is liquation cracking that involves tearing along liquated boundaries formed below the equilibrium solidus as a consequence of nonequilibrium heating (see Section 15.2). Like other cracking involving liquid films, liquation cracking is really hot cracking, and, as such, can be evaluated using the hot-cracking weldability tests just described.

Subsolidus, solid-state cracking in the heat-affected zone can be of three general types: (1) hydrogen-induced cold or delayed cracking, (2) postweld heat

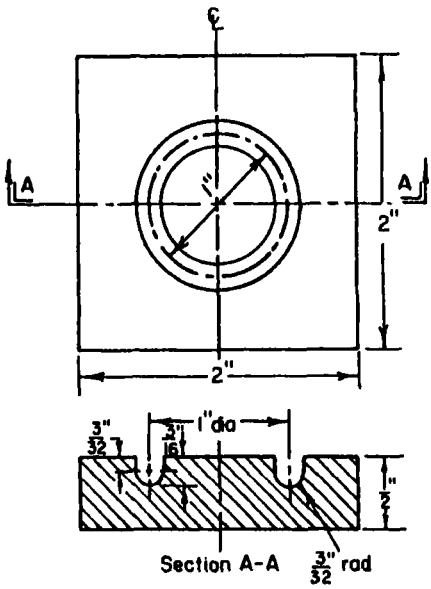
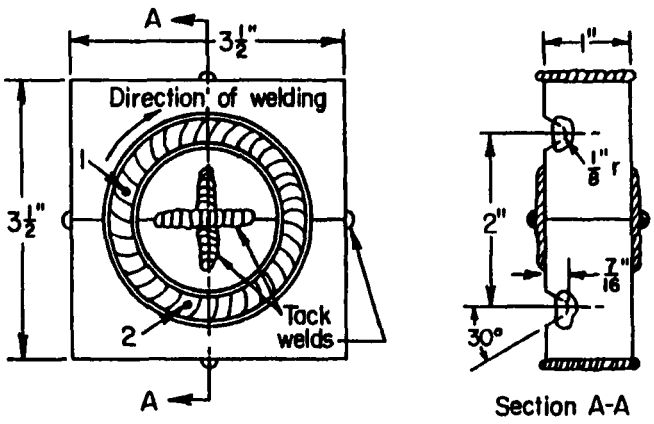
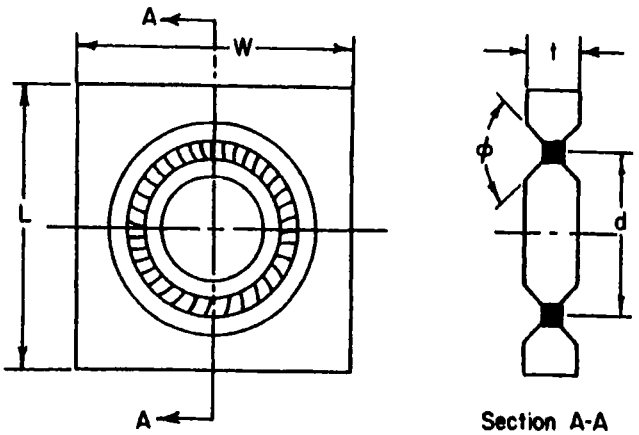


Figure 17.10 Schematic of the circular-groove cracking test. (From "Weldment Evaluation Methods," by J. J. Vagi, R. P. Meister, and M. D. Randall, *DMIC Report 244*, August 1968, courtesy of Advanced Materials and Processes Technology Information Analysis Center (AMPTIAC), 201 Mill Street, Rome, NY.)



Dimensions varied; tests made at room temperature in air.

Figure 17.11 Schematic of the segmented-groove cracking test (modified circular restraint test). (From "Weldment Evaluation Methods," by J. J. Vagi, R. P. Meister, and M. D. Randall, *DMIC Report 244*, August 1968, courtesy of Advanced Materials and Processes Technology Information Analysis Center (AMPTIAC), 201 Mill Street, Rome, NY.)



Dimensions, inches				
L	W	ϕ	d	t
12 5	12 5	90° 0°	Var. 2	Var. 0.076

Dimensions varied greatly but dimensions shown are recommended for plates (1/4 inch and thicker) and sheets; the variable dimensions are discussed in Remarks below. Tested in air at room or preheat temperature.

Figure 17.12 Schematic of the circular-patch (crack susceptibility) test. (From "Weldment Evaluation Methods," by J. J. Vagi, R. P. Meister, and M. D. Randall, *DMIC Report 244*, August 1968, courtesy of Advanced Materials and Processes Technology Information Analysis Center (AMPTIAC), 201 Mill Street, Rome, NY.)

treatment or reheat or strain-age cracking, or (3) lamellar tearing. (Other causes of postweld cracking, such as stress corrosion, are not considered weld cracking, although they may be the result of changes in the material brought about by welding.) Hydrogen-induced cracking tends to occur in transformation-hardenable alloys,[2] most notably steels, as the result of martensite formation on rapid cooling and embrittlement by hydrogen present in the weld. Reheat or strain-age cracking occurs in age-hardenable alloys during their postweld heat treatment to simultaneously relieve stress and cause aging, where the two processes compete. Lamellar tearing occurs in alloys (such as certain steels) when weld-induced stresses act to open nonmetallic inclusions drawn out into stringers by thermomechanical processing such as rolling.

Let's look at testing techniques to evaluate susceptibility to each.

[2]Hydrogen-induced cracking is not restricted to alloy microstructures formed by transformation hardening, but is certainly most prevalent in such structures.

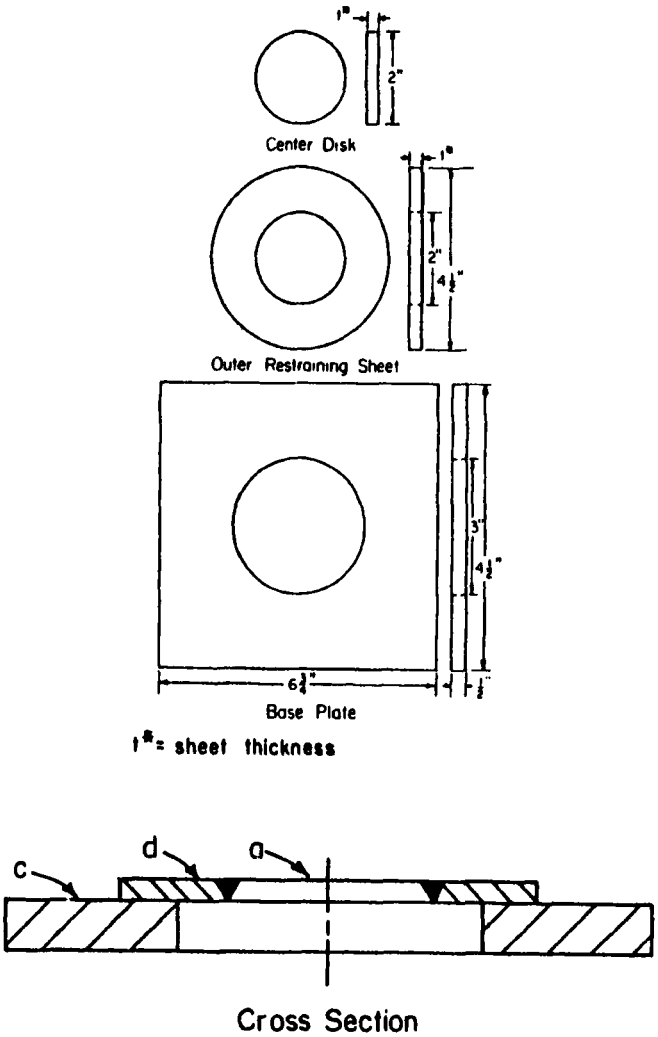


Figure 17.13 Schematic of the restraint-patch (crack-susceptibility) test. (From "Weldment Evaluation Methods," by J. J. Vagi, R. P. Meister, and M. D. Randall, *DMIC Report 244*, August 1968, courtesy of Advanced Materials and Processes Technology Information Analysis Center (AMPTIAC), 201 Mill Street, Rome, NY.)

17.2.3. Hydrogen-Cracking Testing

To repeat the key points about hydrogen cracking, it occurs when four factors are present simultaneously (1) hydrogen in the weld zone (including the fusion, partially melted, and heat-affected zones); (2) high tensile stresses (whether residual or applied); (3) susceptible microstructure (such as ferrous martensite); and (4) relatively low temperature (typically between 200 and $-100°C$ [400

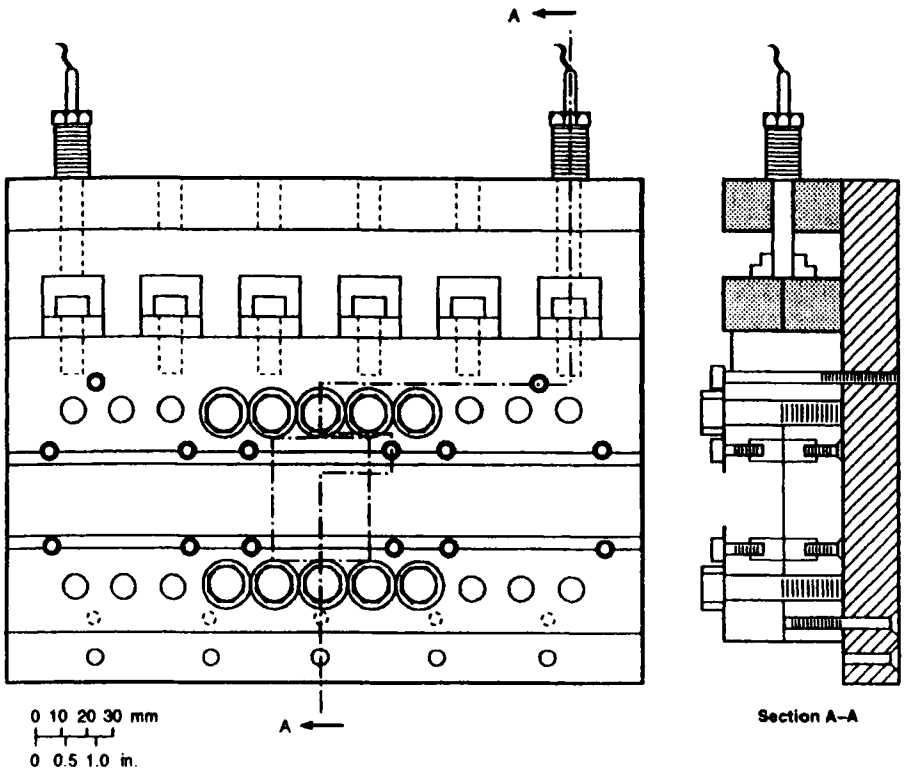


Figure 17.14 Schematic of the Sigmajig test specimen and loading fixture. (From *ASM Handbook*, Vol. 6: *Welding, Brazing, and Soldering*, published in 1993 by and with permission of ASM International, Materials Park, OH.)

and $-150°F$]). The cause and effect of each of these factors has been described before (Section 11.1.5). Hydrogen cracking is alternatively known as cold cracking, because of the necessity for the weld to have cooled to below the range where martensite begins to form, the M_s temperature; delayed cracking, because of the incubation time needed for nucleation in some cases; hydrogen embrittlement, because of the inherent highly brittle nature and transgranular mode of fracture; underbead cracking, because of its common occurrence in the heat-affected zone surrounding, and under a weld bead, where the cooling rate was the fastest and the hardenability the greatest; and toe cracking or root cracking, because of increased likelihood in regions of stress concentration, such as is found in these locations. Figure 17.15 shows underbead-, toe-, and root-cracking locations schematically.

As stated in Section 11.1.5, the exact mechanism for hydrogen cracking is not resolved, but there are several theories, each of which has some merit. The two predominant theories are (1) that hydrogen promotes crack growth by reducing the cohesive strength in the crystal lattice (after Troiano, 1960); and

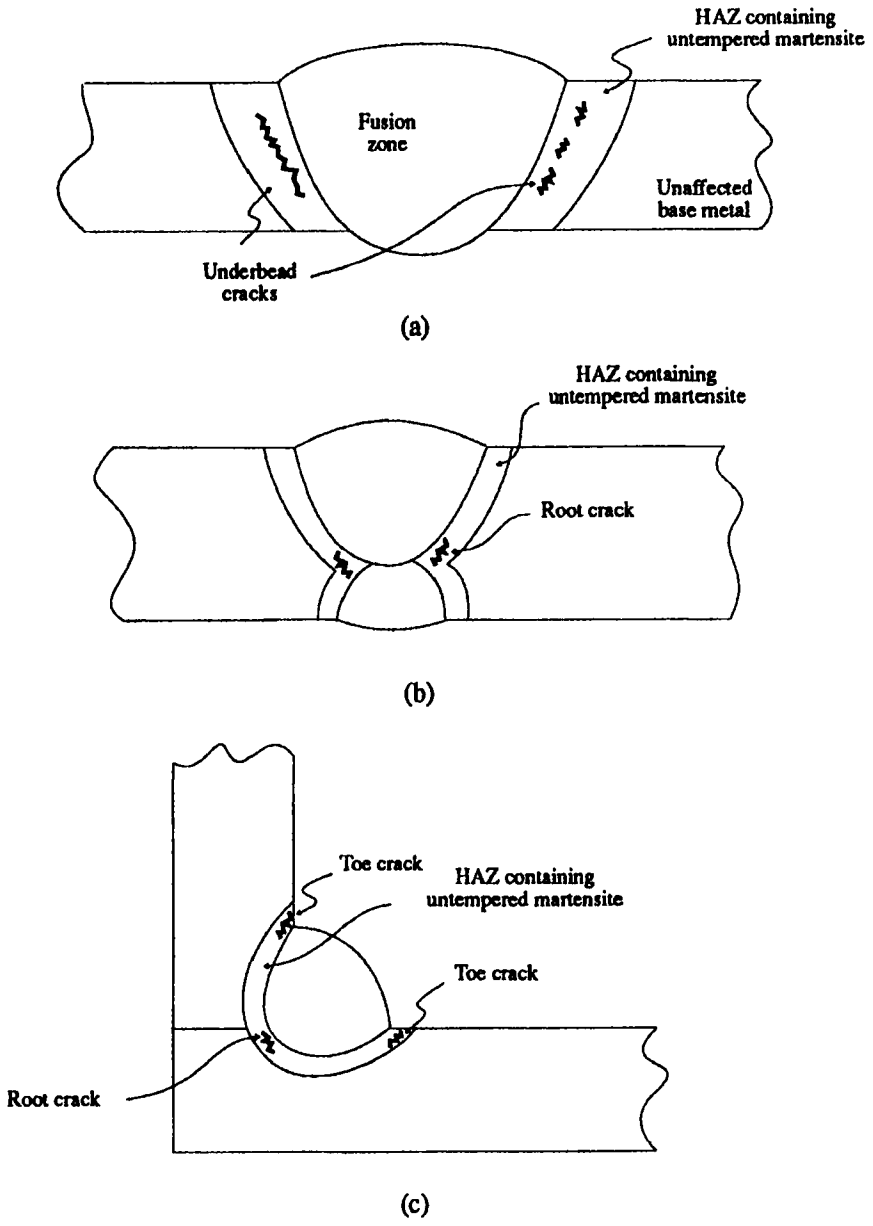


Figure 17.15 Schematic showing the location of hydrogen-induced cracking leading to the alternative names of (a) underbead cracking" (b) toe cracking, and (c) root cracking.

(2) that hydrogen promotes crack growth by lowering the surface free energy of the crack (after Petch, 1952). The interested reader is referred to specific references given at the end of this chapter.

There are several methods for testing susceptibility to hydrogen cracking, especially in steels, including the following:

- Implant test (Figure 17.16)
- Lehigh restraint test (Figure 17.4)
- RPI augmented strain cracking test (Figure 17.17)
- Controlled-thermal-severity test (Figure 17.18)
- Lehigh slot weldability test (Figure 17.19)
- Wedge test (Figure 17.20)
- Tekken test (Figure 17.21)
- G-BOP test (Figure 17.22)

Several other tests that have dual-applicability to both hot- and cold-cracking evaluation were described earlier (e.g., keyhole-slotted-plate test, Navy circular-fillet-weldability test, circular-groove test, segmented-groove test, circular-patch test, and restrained-patch test). Each of the methods not described are briefly described now.

17.2.3.1. Implant Test. In this test (shown in Figure 17.16), a cylindrical specimen is notched around its circumference near one end and inserted into a close-fitting machined hole in a plate made from similar material. A weld is deposited over this inserted specimen, located so its top becomes part of the fusion zone and a notch lies in the heat-affected zone. Immediately following welding, but before the weld is cold, a load is applied to the free end of the specimen. Time to cracking is determined for a range of applied stresses to assess hydrogen-cracking susceptibility.

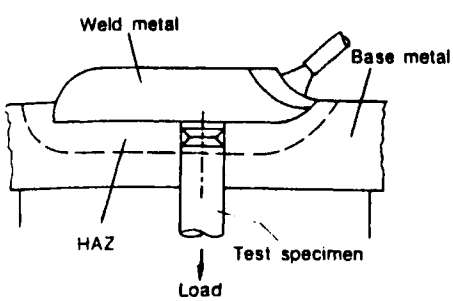


Figure 17.16 Schematic of the implant test, showing proper positioning of the implant relative to the weld deposit. (From *Welding Metallurgy* by S. Kou, published in 1987 by and used with permission of John Wiley & Sons, Inc., New York.)

17.2.3.2. RPI Augmented Strain Cracking Test. This test was designed to produce a known reproducible strain in the outer fibers of a transverse section of a weld (as shown in Figure 17.17). Welded specimens are forced to conform to the surface of a radius die block by tightening the bolt. Bending must be completed before a specimen stored in liquid nitrogen (−196°C or −320°F) immediately after welding has had time to warm to the range where hydrogen-assisted cracking occurs (−100–200°C or −150–400°F). The critical diffusible hydrogen content required to induce cracking in a particular microstructure with a given magnitude of augmented strain is used as the index of susceptibility of a steel to hydrogen cracking.

17.2.3.3. Controlled-Thermal-Severity (CTS) Test. This test (shown in Figure 17.18) is used to evaluate the effect of heat-affected zone cooling rate, and not restraint, on cold cracking. The test is based on the assumption that such cracking is based on the cooling rate at about 300°C (572°F) in the HAZ.

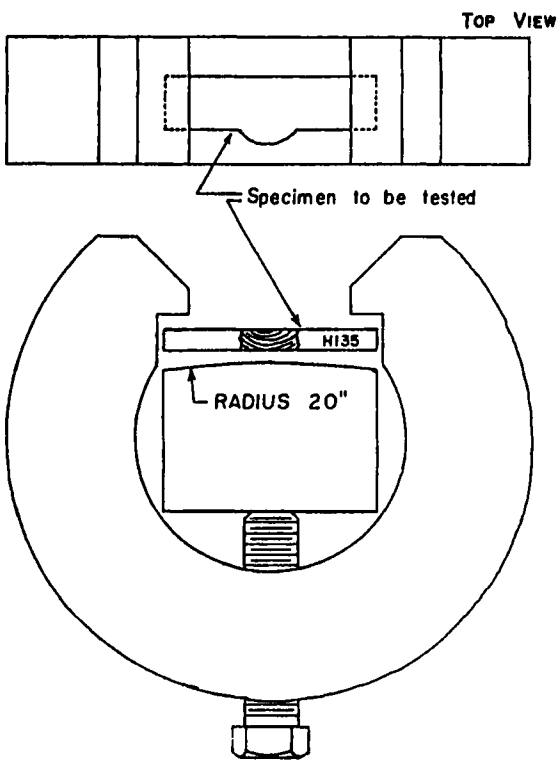
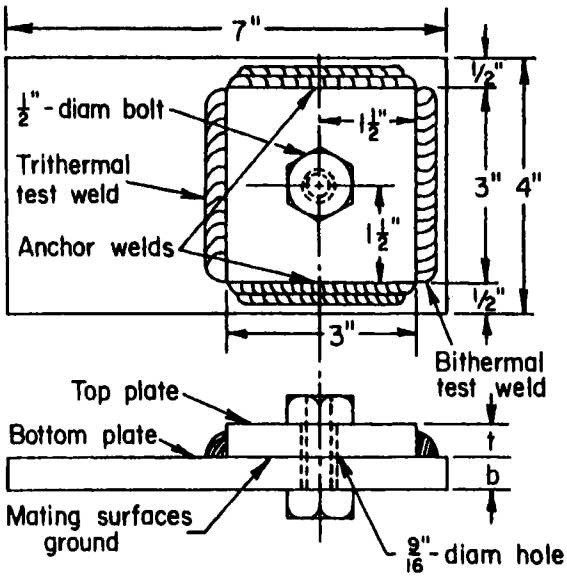


Figure 17.17 Schematic of the RPI augmented strain cracking test. (From "Hydrogen-assisted cracking in HY-130 weldments" by W. F. Savage, E. F. Nippes, and E. I. Husa, *Welding Journal*, **61**(8), 233s–242s, 1982, published by and used with permission of the American Welding Society, Miami, FL.)



Dimensions t and b varied to change thermal severity; the thermal severity number is obtained from the following formula:

TSN = 4(t+b) for bithermal welds

TSN = 4(t+2b) for trithermal welds.

After specimen assembled and anchor welds deposited, assembly allowed to cool to room temperature for depositing bithermal test weld; similarly, specimen cooled to room temperature before trithermal weld deposited; severity of cracking determined by measurements of crack length on metallographic sections.

Figure 17.18 Schematic of the controlled-thermal-severity (CTS) test. (From "Weldment Evaluation Methods," by J. J. Vagi, R. P. Meister, and M. D. Randall, *DMIC Report 244*, August 1968, courtesy of Advanced Materials and Processes Technology Information Analysis Center (AMPTIAC), 201 Mill Street, Rome, NY.)

The specimen consists of two plates ground and tightly bolted together to provide intimate thermal contact. The plates are held rigidly in place by anchor welds along opposite edges. So-called bithermal fillet welds are deposited along one remaining unwelded edge after the assembly has cooled following anchor welding. The assembly is again allowed to cool, and then a trithermal fillet weld is deposited. The bithermal and trithermal test welds are welds in which heat can flow away into the assembly. Thermal-severity numbers are calculated on the basis of the cross-sectional areas of the plates through which heat flows away. Performance is based on crack lengths observed in transverse weld cross sections as a function of thermal-severity number.

17.2.3.4. Lehigh Slot Weldability Test. In this test (shown in Figure 17.19), designed specifically to field-test welds in steel pipelines, a weld bead is deposited over a saw-cut slot in a piece of plate extracted from the pipeline steel. The weld bead must extend 25 mm beyond the end of the slot. Quantitative measurement of the extent of cracking is obtained by heat-tinting crack surfaces with a 500°C/24-h heat treatment and breaking the weld open.

17.2.3.5. Wedge Test. This test (shown in Figure 17.20), like the CTS test, evaluates hydrogen-cracking susceptibility as a function of cooling rate, but this time a simple wedge-shaped specimen is used. Following deposition of a weld from the thin to the thick end of the wedge, the weld is sectioned longitudinally along its centerline to reveal the HAZ. Cracks are then measured and equated to cooling rates based on thickness.

17.2.3.6. Tekken Test. This test for HAZ cold cracking susceptibility, developed in Japan, expands upon (or modifies) the Lehigh restraint test (Section 17.2.1.3) by using specimens of several different dimensions and joint designs. Specifically, a Y-shaped joint provides more self-restraint than either single- or double-U designs (Figure 17.21). Preheat and welding parameters are varied to alter the stress state and assess cracking severity.

17.2.3.7. Gapped-Bead-on-Plate or G-BOP Test. The cold-cracking susceptibility of weld metal as a function of chemical composition, preheat, cooling rate, and measured hydrogen level can be studied using the gapped-bead-on-plate or G-BOP test. Two blocks with a machined recesses are

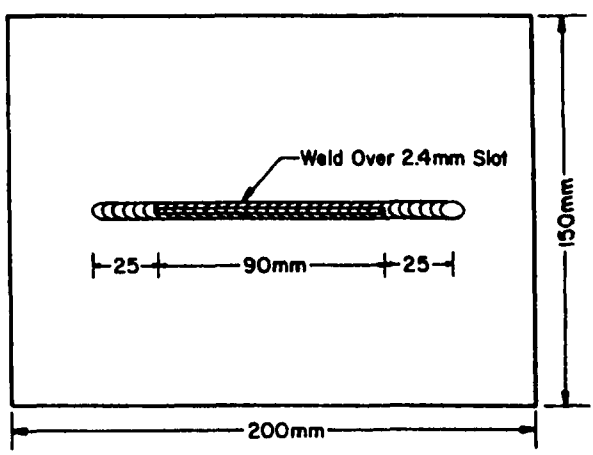


Figure 17.19 Schematic of the Lehigh slot weldability test. (From "A field weldability test for pipeline steels" by R. D. Stout, R. Vasudevan, and A. W. Pense, *Welding Journal*, 55(4), 89s–94s, 1976, published by and used with permission of the American Welding Society, Miami, FL.)

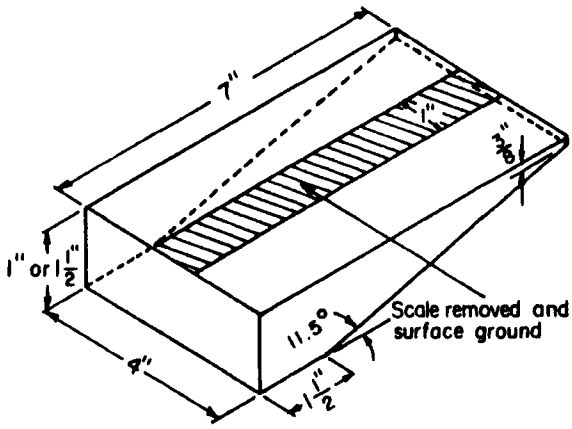


Figure 17.20 Schematic of the wedge test. (From "Weldment Evaluation Methods," by J. J. Vagi, R. P. Meister, and M. D. Randall, *DMIC Report 244*, August 1968, courtesy of Advanced Materials and Processes Technology Information Analysis Center (AMPTIAC), 201 Mill Street, Rome, NY.)

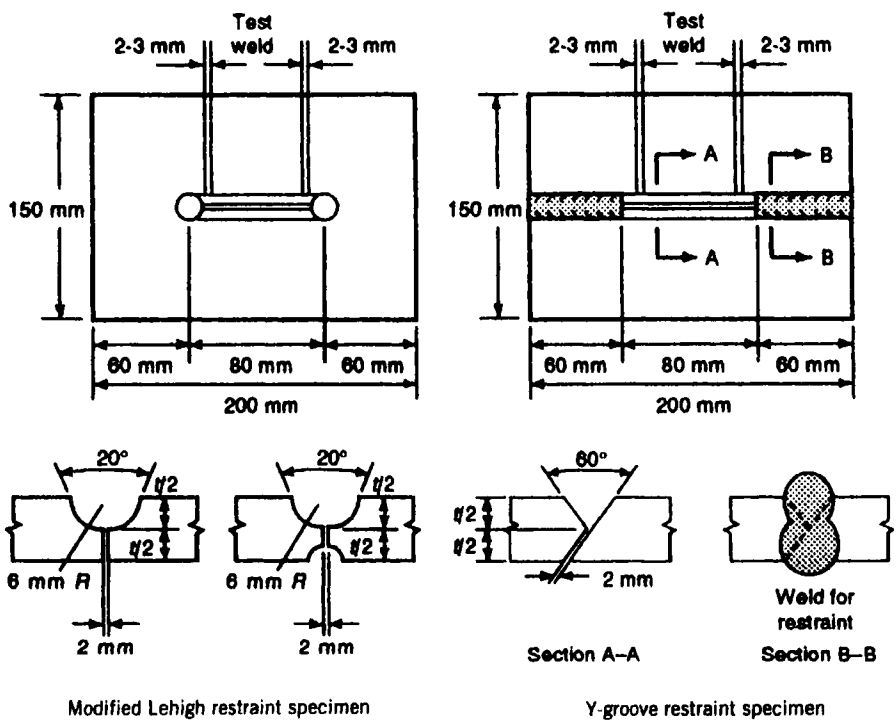


Figure 17.21 Schematic showing sample specifications for the Tekken test. (From *ASM Handbook*, Vol. 6: *Welding, Brazing, and Soldering*, 1993, published in 1993 by and used with permission from ASM International, Materials Park, OH.)

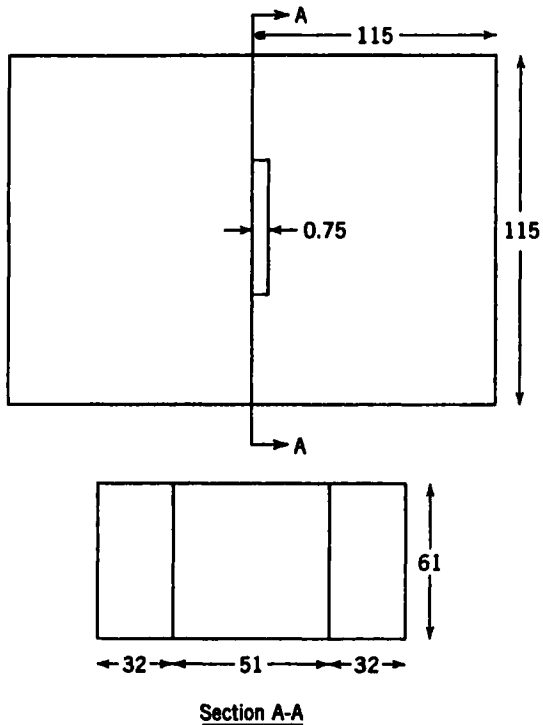


Figure 17.22 Schematic of the G-BOP test. (From "Evaluation of weld metal cold cracking using the G-BOP test" by A. P. Chakravarti and S. R. Bala, *Welding Journal*, 68(1), 1s–8s, 1989, published by and used with permission of the American Welding Society, Miami, FL.)

welded across while clamped together (Figure 17.22). The welded blocks are left in the clamping fixture for 24 h, then are removed from the clamps and left another 24 h to see if cold cracks develop. Following this controlled delay, the blocks in the vicinity of the gap are gas-torch heated to a dull-red heat level. After cooling to room temperature, the weld bead is snapped open to reveal any cold cracking by heat tinting of their free surfaces from torch heating. Results are analyzed statistically to determine welding parameters suitable for minimizing (or, ideally, avoiding) cold cracking.

Historically, most tests for cracking susceptibility utilize the restraint (or stress that develops as the result of restraint) within the weld specimen to cause weld-metal or base-metal cracking. Since no external loading occurs, such tests are called self-restraint tests. Examples from the group just discussed include (but are not limited to) Lehigh restraint test, keyhole restraint test, Houldcroft crack susceptibility test, keyhole slotted-plate restraint test, Tekken test, circular-patch and Navy circular-patch test, and controlled-thermal-severity (CTS) test. The other important group of tests that have tended to emerge more recently are externally loaded tests. By applying a known external stress,

a more quantitative measurement of stress and cracking susceptibility can be obtained. Examples from tests described include implant test, varestraint and spot varestraint test, and sigmajig test.

17.2.4. Reheat or Strain-Age Cracking Tests

Reheat cracking, which is also known as strain-age cracking, postweld heat treatment (PWHT) cracking, or stress rupture cracking, occurs in several nonferrous, age-hardenable alloys (e.g., heat treatable Al- and Ni-based alloys), as well as along prior austenite grain boundaries in the grain-coarsened region of the HAZ of some stainless steels (such as type 347) and alloy steels (such as $1\frac{1}{4}$Cr-$\frac{1}{2}$Mo). It can occur either during postweld heat treatment or in service at elevated temperatures. In steels, in particular, it is virtually always associated with discontinuities in the weld such as lack of fusion and entrapped slag, where such discontinuities act as severe stress raisers or notches (Lundin et al., 1996).

There are many tests for evaluating susceptibility to reheat cracking, but most suffer from one or more of the following problems: (1) poor reproducibility, (2) poor correlation with field experience, (3) difficulty in quantifying susceptibility, (4) key factors in the field are missing in the tests, (5) only an extremely narrow region of the HAZ becomes the focus, with no accounting for effects from the weld metal, other regions of the HAZ, or base metal), and (6) expensive instrumentation and elaborate testing facilities (Lundin et al., 1996). This notwithstanding, two traditional methods and one new method are described: the compact tension test, Vinckier test, and spiral notch test. The interested reader is referred to the relevant literature for more detail.

17.2.4.1. Compact Tension test. One way of evaluating susceptibility to reheat cracking is to measure the extent of crack growth into a compact tension specimen, relying on fracture mechanics (Gooch and King, 1980). In this approach (shown schematically in Figure 17.23), crack extension is monitored in the compact tension specimen using the DC potential drop technique. There is a related method that uses Charpy impact energy in a V-notch specimen for evaluating reheat cracking susceptibility (Batte and Murphy, 1979). Both tests suffer from difficulty in placing the notch in the precise region where embrittlement by strain aging is the greatest.

17.2.4.2. Vinckier Test. This test (shown in Figure 17.24) consists of a specimen made by welding two pieces of 50-mm-thick plates together. The ends of the test specimen are then welded to a stainless steel block. Upon PWHT or reheating, the test specimen is subjected to tensile loading induced by the higher coefficient of thermal expansion of the stainless steel block compared to the steel test pieces. Overall strain can be calculated from the relation

$$\varepsilon_1 = \frac{\sigma_1}{E_1} = \frac{(\alpha_2 - \alpha_1)T}{E_1 A_1 / E_2 A_2 + 1} \tag{17.1}$$

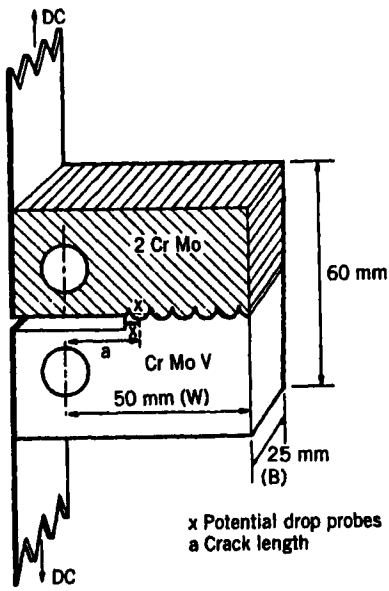


Figure 17.23 Schematic of the compact tension test for evaluating susceptibility to reheat cracking by monitoring crack growth rate. (From "Creep crack growth in controlled nicrostructure Cr-Mo-V heat-affected zones" by T. J. Gooch and B. L. King, *Welding Journal*, **59**(1), 10s–18s, 1980, published by and used with permission of the American Welding Society, Miami, FL.)

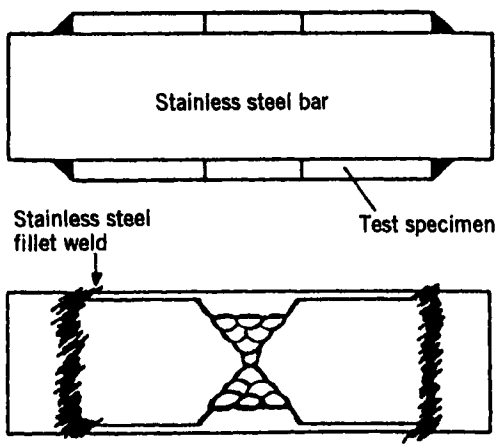


Figure 17.24 Schematic of the Vinckier test for evaluating susceptibility to reheat cracking using differential thermal expansion for applying strain. (From "Assessment of resistance of low-alloy steels to reheat cracking using the Vinckier test" by A. G. Glover, W. K. C. Jones, and A. T. Price, *Metals Technology*, **4**, 326–332, 1977, published by and used with permission of the AIME, Warrendale, PA.)

where subscript 1 refers to the test material and subscript 2 to the stainless steel support plate, with α being the coefficient of thermal expansion, E the modulus of elasticity, and A the cross-sectional area.

17.2.4.3. Spiral Notch Test. The spiral notch test was developed to overcome the numerous deficiencies of available tests for reheat cracking susceptibility (Lundin et al., 1996). By use of a machined notch that spirals around a test specimen (as shown in Figure 17.25), traversing the entire heat-affected zone of a weld (whether produced by simulation or actual welding), this test can simultaneously evaluate susceptibility to reheat cracking in all regions of the HAZ. The notch is considered of paramount importance to the mechanism of reheat cracking, at least in steels.

Notched specimens with a simulated coarse-grained HAZ region near their gage center are tested in the as-simulated or as-welded and postweld heat-treated condition. Loading is done in a standard creep rupture frame at a given stress with the specimen heated under control to 1150°F (625°C) in 1 h and held at this temperature until rupture occurs. Rupture time and total specimen extension are recorded and the fracture surface is examined to determine fracture mode. The specimen is usually reassembled and sectioned longitudinally to determine the precise location of the fracture within the HAZ. Selection of applied stress is based on the material being tested and the fact that residual stress in a weldment approximates the yield strength at the PWHT temperature.

17.2.5. Lamellar Tearing Tests

Recall that the cause of lamellar tearing in the HAZ of susceptible materials (e.g., steels) is the combination of high localized stresses due to weld contraction and low ductility of the base metal in its through-the-thickness direction due to the presence of elongated stringers of inherently weak and brittle nonmetallic inclusions oriented parallel to the rolling direction (Section 16.8.5). Therefore, tests for lamellar tearing susceptibility must develop such stresses in susceptible material. Three popular tests are the

- Lehigh cantilever lamellar tearing test
- Cranefield lamellar tearing test
- Tensile lamellar tearing test

The first and last are briefly described below.

17.2.5.1. Lehigh Cantilever Lamellar Tearing Test. This test (shown in Figure 17.26) employs a multipass weld made in a V-groove between the test material and a beveled, 50-mm (2-in.)-thick beam set at right angles to it. Upon loading, the newly formed weld pulls on the test plate, tending to open any incipient cracks from embrittling nonmetallic inclusions.

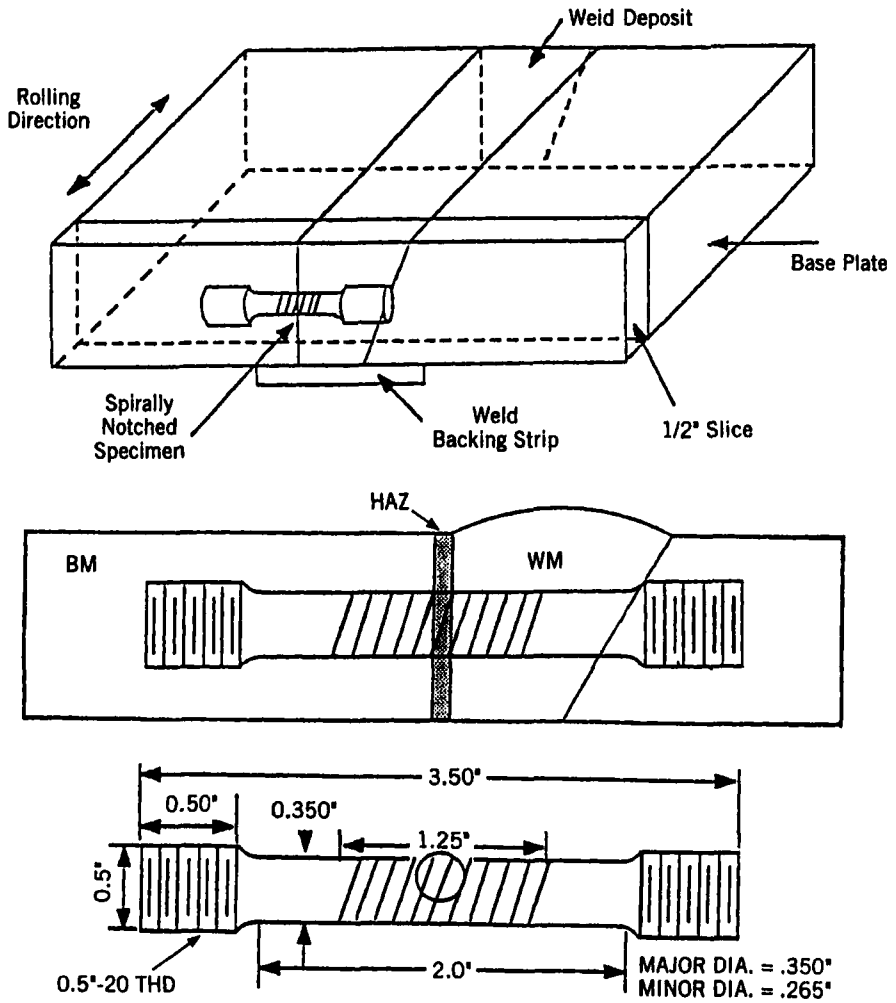


Figure 17.25 Schematic of the specimen and location from which it is extracted from a weldment for conducting the spiral notch test for reheat cracking susceptibility, especially in steels. (From "Overview of Results From PVRC Programs on Half-bead/Temper-bead/Controlled Deposition Techniques for Improvement of Fabrication and Service Performance of Cr-Mo Steels" by C. D. Lundin, *WRC Bulletin 412*, published in 1996 by and used with permission of the Welding Research Council, New York, NY.)

17.2.5.2. Tensile Lamellar Tearing Test. This test (shown in Figure 17.27) uses a weld made in test plates to allow machining of a standard tensile specimen containing that weld oriented transverse at the center of its gage length. When this specimen is pulled in tension, susceptibility to lamellar tearing can be assessed by the degree of degradation of normal tensile strength. For this test to work, the weld filler must have a higher strength than the test

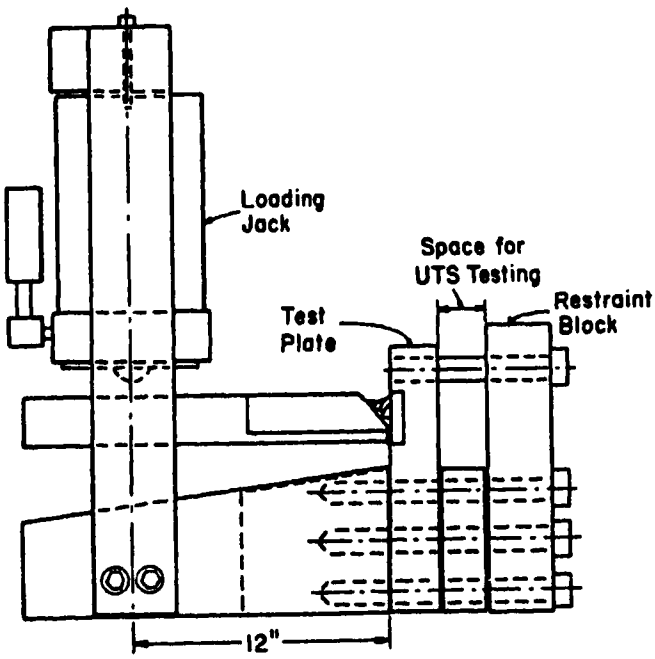


Figure 17.26 Schematic of the Lehigh cantilever lamellar tearing test. (From "An evaluation of factors significant to lamellar tearing" by E. J. Kaufman, A. W. Pense, and R. D. Stout, *Welding Journal*, **60**(3), 43s–49s, 1981, published by and used with permission of the American Welding Society, Miami, FL.)

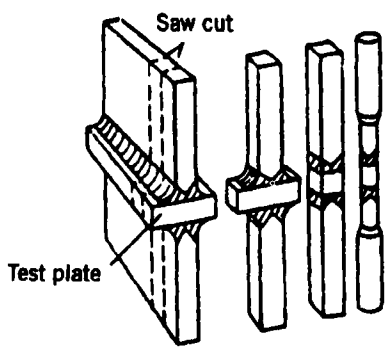


Figure 17.27 Schematic of the tensile lamellar tearing test. (Originally from paper by G. Wold and T. Kristoffersen in *Sverseteknikk*, **27**, 33, 1972 out of *Welding Metallurgy* by S. Kou, published in 1987 by and used with permission of John Wiley & Sons, Inc., New York.)

plate (so it doesn't fail first), and the weld should be free of slag inclusions or lack of fusion defects. Also, for reliable results, the tensile specimen should not be made too small.

17.3. INDIRECT WELDABILITY TESTS OR TESTS OF SIMULATED WELDS

The idea behind simulated tests is to replicate the heat effect from welding on a base material to create a region of material extensive enough to test mechanically by conventional means (methods, specimens, or both). There are two fundamental ways to do this. In the first method, a base material sample or specimen is heated and cooled according to a predetermined temperature–time profile that replicates the weld thermal cycle. The underlying premise is that two identical starting materials subjected to the same temperature–time histories will end up with the same microstructure and properties. The difficulty in attempting to replicate the temperature–time history of a weld zone is the speed at which heating and cooling occur and the extremely short time at peak temperature, all leading to highly nonequilibrium behavior. Conventional heat-treating facilities (e.g., ovens and furnaces) are unable to achieve these rates. However, special apparatus are available, known as thermal simulators. Most use internal resistance heating to simulate the weld cycle.

In the second method, a specimen is not only heated and cooled to simulate the welding cycle, but is also simultaneously loaded in tension to reproduce the strain conditions accompanying welding. The best-known example of an apparatus to accomplish this is the Gleeble. General operation of the Gleeble was described in Section 6.8. More detailed information is available in several references at the end of this chapter.

While simulated tests provide very useful data regarding mechanical properties in various areas of the HAZ, during as well as after the welding cycle (e.g., on-heating versus on-cooling hot ductility, and stress relaxation), they cannot account for residual and reaction stresses, contamination, and other conditions that can be imposed on real actual welds in practical production environments and situations.

17.4. WELD POOL SHAPE TESTS

It is often desirable to assess the three-dimensional shape and size of a weld pool to determine the role of process and material factors or variables. Metallographic techniques have been shown to be not only inefficient but inaccurate and/or incomplete as well (Walsh et al., 1986). Early work to decant the weld pool using gravity or gunshot blasts lack speed or cause contamination (with pool-altering, surface-activating sulfur, for example), so have been largely abandoned. A favored approach uses a high-pressure impulse jet of inert argon gas. The technique, known as impulse decanting, empties the pool of molten metal, leaving the instantaneous shape as a cavity

that is usually replicated with a silicone rubber casting. The resulting replica or cast allows study of weld pool length, width, depth, volume, shape, and surface area.

17.5. WELD TESTING

Without question, the most important criterion of all for judging the performance of a weldment is whether it performs the functions required for its intended service. The real final test is that of performing in service (the service performance test). However, the need for weldment evaluation exists long before the final structure is complete and actual service begins. Waiting until the weldment is finished is far too late, because too much value has been added to find a mistake has been made, whether that mistake is in design or manufacture. Clearly, some type of test during fabrication that will provide information on how the product will perform in service must be used prior to fabrication to provide indications of the efficiency of design, welding procedures, expected mechanical properties, and behavior during service.

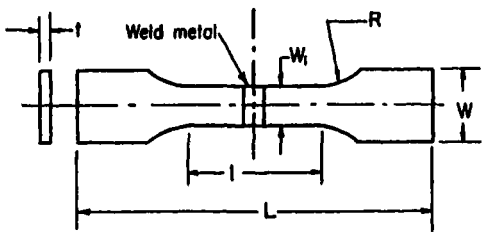
Weldment evaluation is quite complex. A great variety of testing methods and specimens exist for evaluating the performance of welds and welded joints[3]. There are tests of tensile and compressive and shear strength, bend ductility, impact toughness, fracture toughness, fatigue resistance, creep resistance, and corrosion resistance. For each of these tests, however, only a limited number of specimens are considered to be standards, because fabricated structures and service environments are difficult to reproduce in detail under controlled laboratory or shop conditions. Attempts are often made, therefore, to develop special test specimens designed to be as representative of the actual structure as possible.

It has been stated that the faithful execution of a testing procedure should provide a rational basis for the establishment of materials, procedures, and techniques, and, hopefully, a reasonable evaluation of expected service performance (Randall et al., 1961). A number of factors are important, not only in the evaluation of the testing procedure, but also in reporting on the information obtained: (1) the purpose of the test, (2) intended service conditions, (3) allowable (values of) properties, (4) specimen design, (5) specimen preparation method and finishing, (6) source of the specimen (part and location), (7) ambient conditions (atmosphere, temperature, humidity, pressure, geographic location, etc.), (8) rates of loading (test machine cross-head speed), (9) test materials, (10) material condition (state of heat treatment, etc.), (11) testing equipment, (12) methods for making measurements and/or observations, (13) scales involved, (14) failure characteristics (e.g., type, location, size, geometry, etc.), (15) interpretation of results and basis for these interpretations, and (16) conclusions. When the above details are omitted from reports on test data, the data lose usefulness.

[3]As used here, "welds" refers to the fusion, partially melted, and heat-affected regions of a material subjected to welding. "Welded joint" refers to the portion of a structure containing a weld, but also containing unaffected base material.

17.5.1. Transverse and Longitudinal-Weld Tensile Tests

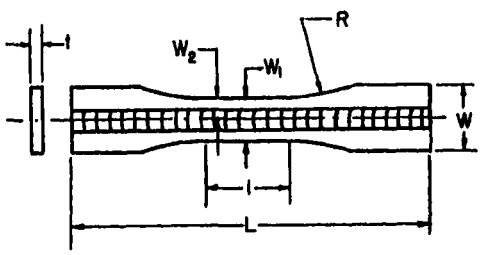
Uniaxial tension tests are used more for evaluating weldments than any other type of tensile test. There are two fundamentally different types: (1) transverse-weld tests and (2) longitudinal-weld tests. As can be seen in Figure 17.28a and b, these differ in the location of the weld relative to the specimen's loading axis. *Transverse-weld* specimens (which can be flat for welded sheet metal, or round



Dimensions, inches				
W	W_1	l	L	R
3/4	0.500 ± 0.010	2-1/4 min	8 min	1/2 min
2	1-1/2 ± 0.01	9 min	16[a]	1-3

Dimensions shown are ASTM standard for unwelded base plate; smaller specimen used for t from 0.005 to 5/8 inch; larger specimens used for t of 3/16 inch and over; used for all temperatures and all atmospheres; tested with and without weld reinforcement, preferably without.

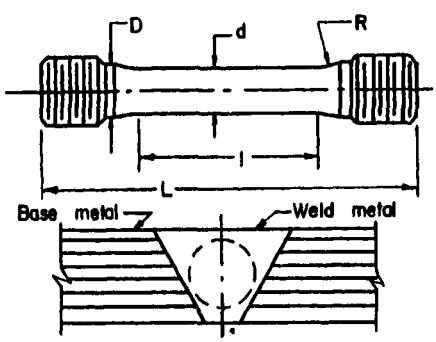
(a)



Dimensions, inches						
W	W_1	W_2	l	L	t	R
3/4	1/2	1/4	2-1/4	8	t	1
1-1/2	1	1/2	4	12	t	2

Smaller dimensions used for t up to 1/4 inch; larger dimensions used for t greater than 1/4 inch; usually tested in air at 70 F but limited use at elevated temperatures; usually tested without weld reinforcement.

(b)



Dimensions, inches				
d	D	l	L	R
0.505	3/4	2-1/4	5-1/2	3/8
0.357	1/2	1-3/4	3-1/2	3/8
0.252	3/8	1-1/4	3	1/4
0.160	5/16	3/4	2	1/4
0.113	1/4	5/8	1-5/8	1/4

Dimensions shown are MIL-STD-418; usually tested at room temperature in air.

Figure 17.28 Schematic illustrations of (a) transverse-weld, (b) longitudinal-weld, and (c) all-weld-metal tensile specimens. (From "Weldment Evaluation Methods," by J. J. Vagi, R. P. Meister, and M. D. Randall, *DMIC Report 244*, August 1968, courtesy of Advanced Materials and Processes Technology Information Analysis Center (AMPTIAC), 201 Mill Street, Rome, NY.)

for welded plate, thick-section castings or forgings, etc.) provide an excellent measure of joint efficiency (i.e., strength of the welded joint to the strength of the welded base material), but do not provide a measure of weld ductility. This is because ductile regions of the weld zone, being oriented transverse to the direction of loading, can accommodate strain preferentially to less ductile (or even brittle) regions. This is particularly true if the weld-metal strength exceeds that of the base metal. For such situations, the majority of plastic strain will occur in the unwelded region of the gage length, with resultant necking and failure outside the weld area, with base-plate failure providing no basis for evaluating weld strength or ductility. For a weak weld metal, almost all strain concentrates in the weld, thereby reducing the elongation measured for the composite gage length.

The *longitudinal-weld* test forces all zones of the joint to strain simultaneously and equally. Thus, weld metal, regardless of its strength, elongates with the base metal until failure occurs at the limiting strain. Poor weld-metal ductility forces fracture at strength levels considerably below the unwelded base metal, while highly ductile weld metals are able to sustain loads to strength levels comparable to the base metal.

Because of these differences, full evaluation of the strength and ductility of a weldment requires that both types of specimens be tested.

17.5.2. All-Weld-Metal Tensile Tests

A tensile specimen extracted from the weld fusion zone so that it contains only weld metal is called an *all-weld-metal* specimen; an example is shown in Figure 17.28c. Such a specimen permits accurate evaluation of weld-metal strength and ductility, and so is ideal for comparing different fillers. Contamination by base metal through dilution must be carefully avoided to obtain representative results. Contamination can be avoided by building up multiple layers of weld metal on a base plate to reduce dilution to near zero; usually three to five layers are sufficient. Both flat and round bars are used, depending on the form of the base material.

17.5.3. Bend Ductility Tests

Bend tests or *bend-ductility tests* are widely used to evaluate welds, largely because of their simplicity yet reliability. Bend ductility is usually expressed in terms of the angle of bend just prior to failure in the form of tearing or complete fracture, although it is far more meaningful to express ductility in terms of the measured or calculated elongation. For tests employing a flat specimen of thickness t, elongation in the outer fibers for a bend radius of R is given by

$$e = \frac{t}{2R + t} \tag{17.2}$$

Bend ductility tests are performed on specimens with welds oriented transverse and longitudinal to the long axis of the specimen, and can be bent with either the face or the root of the weld located at the outer fiber of the bend. These are called transverse, longitudinal face, or root bends, respectively. The same considerations apply to bend tests that apply to tensile tests regarding weld orientation effects on measured ductility. The reason for bending with either the face or root at the outer fibers of the bend is to accentuate the strain at one or the other of these areas to force open any defect. Bending can be forced to conform to a standard radius block or form, or be allowed to bend to whatever radius they choose in what are called guided-bend and free-bend tests. Special side-bend tests are used to expose defects near the midthickness of a weld that might not contribute to failure in face- or root-bend tests. Side-bend tests are particularly widely used in evaluating multipass welds.

Examples of transverse- and longitudinal-weld face- or root-bend, and transverse-weld side-bend guided-bend tests are shown in Figure 17.29a, b, and c, respectively. A longitudinal-weld face- or root-bend free-bend test is shown in Figure 17.30.

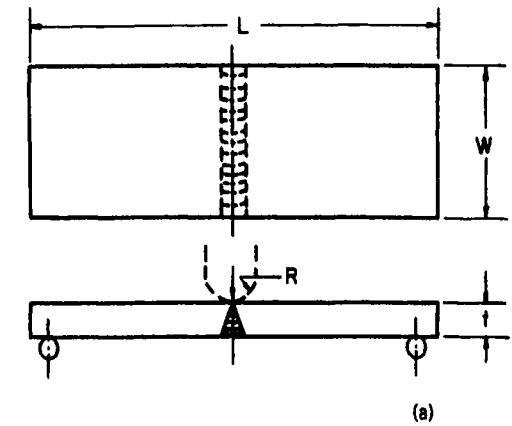
17.5.4. Impact Tests

Impact tests are used to measure the toughness of a material, which is a function of both its strength and ductility as obtained from the area under a true-stress/true-strain curve, toughness being the ability to absorb energy without failure. The simplest and best-known test is the Charpy impact test, which can employ a V-notched or keyhole-notched specimen cut from thick-section plate, casting, or forging (as shown in Figure 17.31). There is also a specimen configuration of testing sheet materials. Many tests were conceived to determine the ability of weld-fabricated structures to absorb loading under severe conditions of strain rate, through a combination of elastic strain, plastic strain, and inertia of the parts. For this reason, there are many specialized tests, such as (1) drop-weight test (Figure 17.32); (2) U.S. Navy explosion-bulge impact test (Figure 17.33), specifically designed to test resistance of depth charges; and (3) U.S. Army Ordnance ballistic-impact test (Figure 17.34), specifically designed to test resistance to impact from projectiles.

Of particular importance for all impact tests is the effect of test temperature on the toughness. This is especially important for metals and alloys that exhibit ductile-to-brittle transitions as temperature decreases, the notable examples being body-centered cubic materials.

17.5.5. Other Mechanical Tests

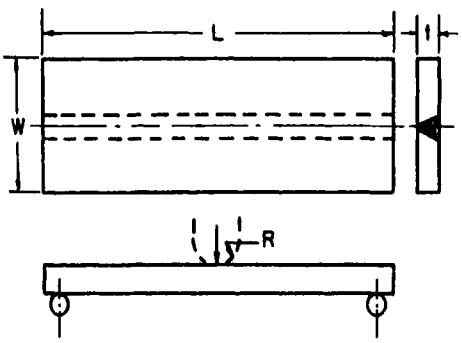
There are several other mechanical properties of welds and weldments that can be important to a particular design. Examples include shear strength, fracture toughness, fatigue strength and life, and stress-rupture and creep. The strength



(a)

Dimensions, Inches			
L	W	t	R
10	1-1/2	3/8	3/4
4	1-1/2	<1/4	Var.

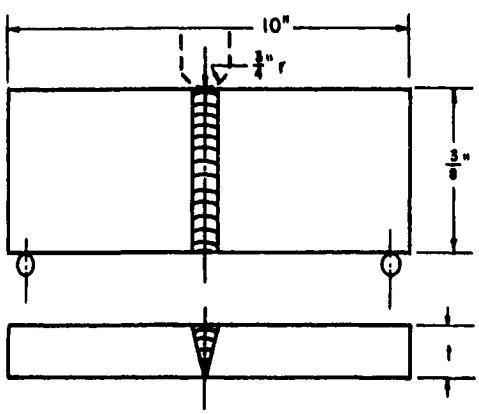
Dimensions varied greatly. First set of dimensions shown are AWS standard. Second set of dimensions used for sheet with series of varying radii dies. Usually tested at room temperature in air with welds ground flush.



(b)

Dimensions, Inches			
L	W	t	R
10	1-1/2	3/8	3/4
4	1-1/2	<1/4	Var.

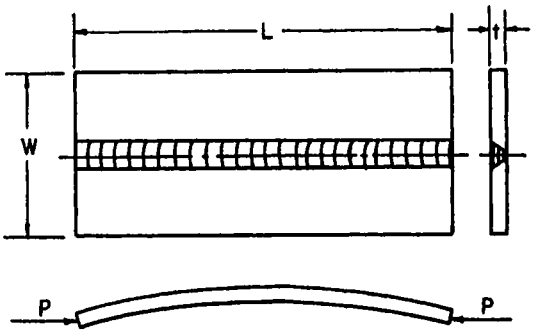
Dimensions varied greatly, first dimensions shown are AWS standard. Second dimensions used for sheet with series of varying radii dies (see below); usually tested at room temperature in air with welds ground flush.



(c)

For plates 3/4 to 1-1/2-inch thick, specimen t equals actual plate t (less any surface grinding); for plates over 1-1/2 inch thick, cut specimen into about equal strips 3/4 to 1-1/2 inch wide and test each strip; test not applicable to plates less than 3/4 inch thick. Usually tested at room temperature in air. Root and face of weld should be machined to prevent premature edge failure.

Figure 17.29 Schematic illustrations of (a) transverse-weld and (b) longitudinal-weld face- or root-bend tests, and (c) transverse-weld side-bend test. (From "Weldment Evaluation Methods," by J. J. Vagi, R. P. Meister, and M. D. Randall, *DMIC Report 244*, August 1968, courtesy of Advanced Materials and Processes Technology Information Analysis Center (AMPTIAC), 201 Mill Street, Rome, NY.)



Dimensions, inches		
L	W	t
6	3/8	1/4
8	9/16	3/8
9	3/4	1/2
10	15/16	5/8
11	1-1/8	3/4
12	1-1/2	1
13-1/2	1-7/8	1-1/4
15	2-1/4	1-1/2
18	3	2
21	3-3/4	2-1/2

Dimensions shown are MIL-STD-418 for transverse-weld specimen. Usually tested in air at room temperature.

FINAL BEND FOR FREE-BEND SPECIMENS

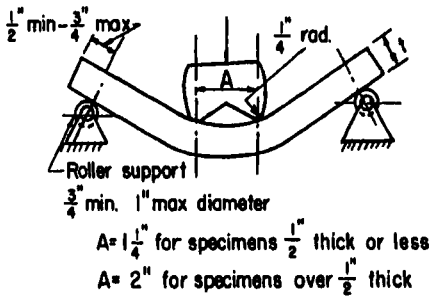


Figure 17.30 Schematic of a longitudinal-weld face- or root-bend free-bend test. (From "Weldment Evaluation Methods," by J. J. Vagi, R. P. Meister, and M. D. Randall, *DMIC Report 244*, August 1968, courtesy of Advanced Materials and Processes Technology Information Analysis Center (AMPTIAC), 201 Mill Street, Rome, NY.).

of a weld joint in shear is important for some designs, and, when it is, joint strength should be tested in shear. A number of specimens and tests have been designed for this purpose, with particular applicability for certain welded steel structures. The problem in conducting shear tests is keeping the shear as near to pure as possible, which means avoiding bending caused by eccentric loads.

Testing a material for its fracture toughness is of ever-increasing importance, with the maturation of fracture mechanics analysis in design. The underlying philosophy of fracture mechanics is as follows: All materials contain flaws, or should be assumed to, so a structure should be able to contain a flaw smaller than some readily detectable size (using nondestructive evaluation techniques) without catastrophic propagation up to some design stress intensity. Testing welds for their fracture toughness is complicated by the variety of structures and properties present across the weld zone (i.e., the fusion, partially melted, and various heat-affected regions). The three biggest problems are (1) placing

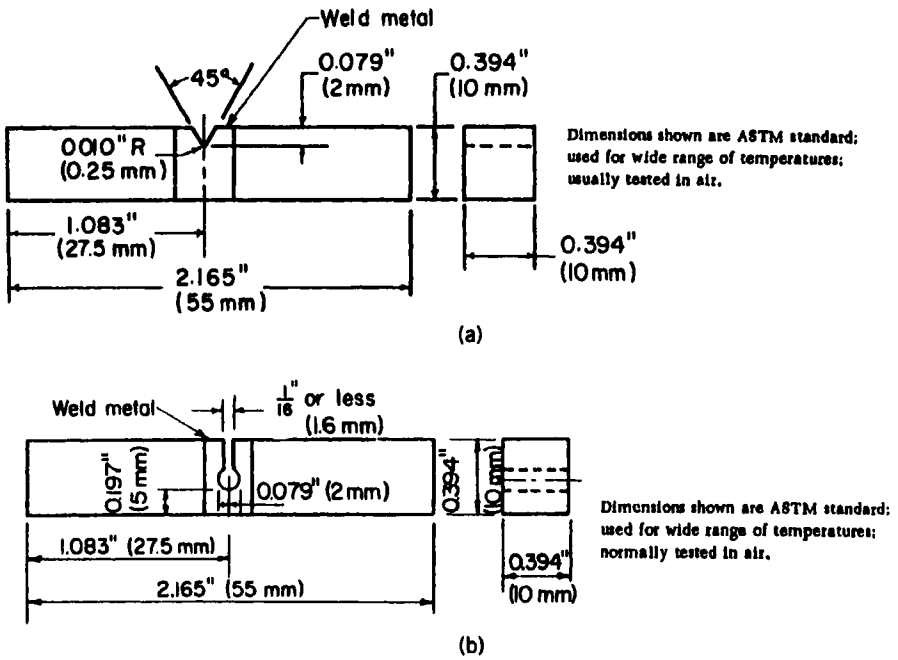
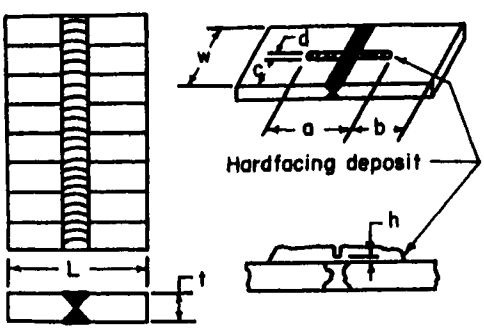


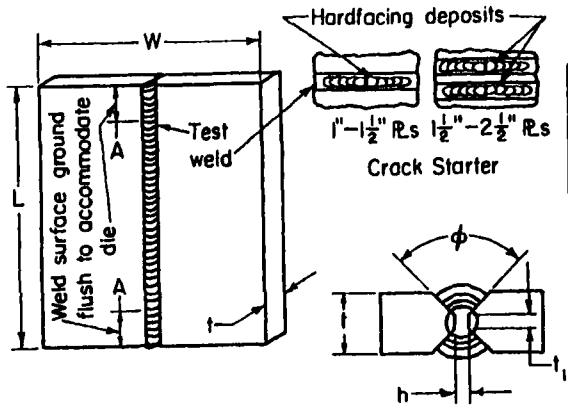
Figure 17.31 Schematic illustrations of the Charpy impact test using specimens with (a) V-notch and (b) keyhole-notch. (From "Weldment Evaluation Methods," by J. J. Vagi, R. P. Meister, and M. D. Randall, *DMIC Report 244*, August 1968, courtesy of Advanced Materials and Processes Technology Information Analysis Center (AMPTIAC), 201 Mill Street, Rome, NY.)



Dimensions, inches							
L	W	t	a	b	c	d	h
14	3-1/2	1/2 to 1-1/4	2-1/2	5-3/4	1-1/2	1/2	1/16
5	2	1/2	2	1-1/2	3/4	1/2	1/16

NRL reference standard specimen is 14 by 3-1/2 by 1 inch with a 12-inch span and a 0.3-inch anvil stop. Smaller specimens used for materials thinner than 3/4 inch but at least 1/2 inch. Testing done over wide range of temperature in air.

Figure 17.32 Schematic of the drop-weight impact test. (From "Weldment Evaluation Methods," by J. J. Vagi, R. P. Meister, and M. D. Randall, *DMIC Report 244*, August 1968, courtesy of Advanced Materials and Processes Technology Information Analysis Center (AMPTIAC), 201 Mill Street, Rome, NY.)



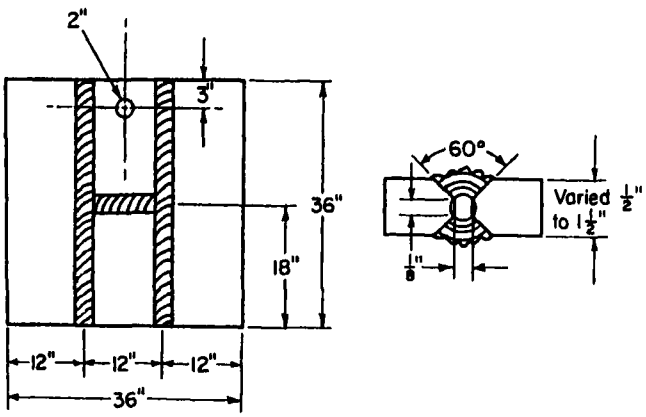
Dimensions, inches						
L	W	t	t1	h	φ	A
20	20	1 to 1-1/2	1/16	3/32	60°	5
30	30	1-1/2 to 2-1/2	1/16	3/32	60°	7

Dimensions shown are NRL standard; the over-all dimensions generally are adhered to; weld-joint dimensions varied; tested over wide range of temperature.

Figure 17.33 Navy explosion-bulge test. (From "Weldment Evaluation Methods," by J. J. Vagi, R. P. Meister, and M. D. Randall, *DMIC Report 244*, August 1968, courtesy of Advanced Materials and Processes Technology Information Analysis Center (AMPTIAC), 201 Mill Street, Rome, NY.)

the initial specimen notch at the point where the fracture toughness will be the lowest, (2) forcing the crack to follow an acceptable path to give meaningful results (as severe deviation in path from straight is unacceptable), and (3) finding a sample big enough to give meaningful results (i.e., exhibit plane strain behavior).

Determining the stress to which a weldment can be loaded without exhibiting failure under a given number of repeated load cycles, predicting the



Generally tested at 70 F in air. Some testing over a range of temperature for developmental purposes.

Figure 17.34 Army Ordnance ballistic-impact test. (From "Weldment Evaluation Methods," by J. J. Vagi, R. P. Meister, and M. D. Randall, *DMIC Report 244*, August 1968, courtesy of Advanced Materials and Processes Technology Information Analysis Center (AMPTIAC), 201 Mill Street, Rome, NY.)

number of load cycles a welded structure can endure (i.e., its life), and determining the effect of any defects is of obvious interest in many welded designs. Test specimens do not differ much from those used to assess tensile strength. The greatest problem is to obtain a reasonable idea of the adverse effect of any welding defects without making the test results look any better or worse than the likely real-world situation.

For those applications where welded structures are to be used at elevated temperatures, stress-rupture and creep behavior can be critically important. When this is the case, fairly standard stress-rupture and creep specimens are used with fairly standard tests. The problem, once again, is trying to assess these properties in a microstructure that is representative of what is found in real welds.

The complexity of all of these special situations should drive the interested reader to specialized sources. Table 17.2 lists the major mechanical tests employed for evaluating welds and weldments.

17.5.6. Corrosion Tests

Corrosion is the chemical attack of a material (or structure made therefrom) by the environment. Eight unique forms of corrosion are usually said to exist, although several are interrelated (Fontana, 1986): (1) uniform or general corrosion or attack, (2) galvanic or two-metal corrosion, (3) crevice corrosion, (4) pitting corrosion, (5) intergranular corrosion, (6) selective leaching or parting, (7) erosion corrosion, and (8) stress corrosion. All of these can occur in weldments, but general corrosion, crevice corrosion, pitting corrosion, intergranular corrosion, and stress corrosion are the most common, and are described briefly here.

17.5.6.1. General Corrosion and Its Testing. As implied by the name, *general corrosion* or *uniform attack* is normally characterized by chemical or electrochemical reaction that proceeds fairly uniformly over the entire exposed surface or a large area of that surface. As a result of such corrosion the metal becomes thinner and eventually fails by having insufficient cross-sectional area to carry loads or by allowing fluid to leak through corroded-through holes. Tests of general corrosion involve controlled exposure to corrosive media expected to be present in the service environment, and measuring the rate of metal loss per unit of time (often expressed as mils [of thickness] per year or mpy). During such tests, solution composition (i.e., active corrosives and contaminants), concentration, temperature, solution agitation and aeration, as well as test piece surface preparation are a few important parameters to be controlled.

General corrosion is of more interest to the base metal than it is to the weld zone, and, so, is normally tested for the base metal. What is important for welds is how any disruption of the microstructure and/or surface condition (e.g., heat tint oxidation) affects the general corrosion rate in the vicinity of the weld. The

TABLE 17.2 Major Mechanical Tests Used to Evaluate Welds

Tension tests
Transverse-weld tension
Longitudinal-weld tension
All-weld-metal tension
Spot-weld cross tension
Brazed joint tension
Nick-break (for soundness)
Shear tests
Fillet-weld shear
Spot-weld shear
Brazed joint shear
Bend tests
Longitudinal-weld guided-bend
Transverse-weld guided-bend
Free-bend
Fillet-weld tee-bend
Notched-bend
Progressive-bend
Fatigue tests (rotating beam and axial)
Transverse-weld fatigue
Longitudinal-weld fatigue
Fillet-weld fatigue
Spot-weld fatigue
Brazed joint fatigue
Notched toughness
Charpy vee-notch impact
Charpy vee-notch impact (sheet material)
NRL drop-weight
Drop-weight tear
Explosion-bulge
Army Ordnance ballistic-impact (H-Plate)
Drop-weight bulge
Fracture toughness
Double-edge-notch tension
Central-through-notch tension
Precracked bend
Compact K_{Ic}-type fracture toughness
Surface-notch tension
Single-edge-notch tension
Stress rupture and creep
Transverse- and longitudinal-weld stress-rupture and creep

rate of general corrosion can also be accelerated by stress, and so can be higher in the vicinity of welds than elsewhere.

17.5.6.2. Crevice Corrosion and Its Testing. Intensive localized corrosion often occurs within protected areas on metal surfaces exposed to corrosives. Such areas can include holes, lap joints, corners, surface deposits, and crevices under bolt heads, nuts, washers, and weld crown and root bead reinforcements. The phenomenon is called *crevice corrosion*, and, in brief, the mechanism for the accelerated attack often seen is a change in the oxidation–reduction potentials and reactions as oxygen is depleted from such protected areas where the corrosive changes due to its stagnation.

Many methods exist for testing for crevice corrosion behavior, all of which share the common characteristic of creating an artificial crevice with a gasket of some type. Examples include the use of clamped gaskets, grooved Delrin washers, contouring silicone-rubber cylinders, and other schemes. Susceptibility is evaluated by comparing the degree and nature of attack in the crevice to the general attack elsewhere.

17.5.6.3. Pitting Corrosion and Its Testing. *Pitting* is a form of extremely localized attack that results in holes in the surface of the metal. These holes can be small or large, but are usually small, having a depth comparable to their diameter. Pits can be clustered and so dense as to cause the surface to appear rough, or can be isolated. Pitting corrosion is considered particularly problematic because it can quickly result in perforation of a structure's wall, with little loss of weight (or thickness) to the general structure. The mechanism for the formation of pits is autocatalytic; that is, the conditions for the anodic reaction for corrosion to occur is self-stimulating, in that high concentrations of positive charge in the pit attack corrosive anions (such as chloride ions).

Testing for susceptibility to pitting is made difficult by the highly probabilistic nature of its occurrence, highly localized character, and long incubation times. Testing must, therefore, involve large samples and very long test times. Test solutions depend on expected service environment. Once again, if welds are being evaluated, the surface of the weld should be left in the same condition as it will be in during service—heat-tint removed or left on, weld crown machined or not, and so on.

17.5.6.4. Intergranular Corrosion and Its Testing. Preferential attack of grain boundary regions by corrosives leads to *intergranular corrosion* or *attack.* Mechanisms for rendering grain boundary regions susceptible to such attack were described in Section 16.6.3 under sensitization and as in Section 16.8.4 under "weld decay" and "knife-line attack."

In fact, any test could be considered a test for susceptibility to intergranular attack because the test specimen should be examined for localized pitting or intergranular attack as well as for generalized attack. However, three tests are used to specifically evaluate for sensitization: (1) the Huey test (ASTM A-262)

TABLE 17.3 Standard ASTM Tests Used to Evaluate Resistance of Welds to Various Forms of Corrosion

Standard	Method	Solution	Applicability of Test	Results	Criteria
ASTM A 262	A 262 A	10% oxalic acid	Wrought or cast stainlessl steels	Screening test	Etch structures
	A 262 B	Ferric sulfate–sulfuric acid	Wrought or cast stainless steels	Intergranular attack	Weight loss
	A 262 C	Nitric acid	Wrought or cast, e.g., 304, 304L, and CF-8, CF-3	Intergranular attack	Weight loss
	A 262 D	Nitric hydrofluoric acid	Wrought or cast, weld metal, e.g., 316, 317	Intergranular attack	Weight loss Corrosion rate ratio
	A 262 E	Copper–copper sulfate–16% sulfuric acid	Wrought stainless steels, e.g., 201, 316, 321, 347; weld metal	Intergranular attack	Fissures or cracks in bend test
	A 262 F	Copper–copper sulfate–50% sulfuric acid	Mo-bearing cast, weld and heat treated austenitic stainless steels CF-8M, CF-3M	Screening test intergranular attack	Weight loss

ASTM G 28	G 28 A	Boiling ferric sulfate–50% sulfuric acid	Wrought Ni, Cr alloys, not applicable to castings	Intergranular attack	Weight loss Metallographic examination
	G 28 B	23% H_2SO_4 + 1.2% HCl + 1% $FeCl_3$ + 1% $CuCl_2$	Wrought N10276 (alloy C-276), not applicable to castings	Intergranular attack	Weight loss Metallographic examination
ASTM G 48	G 48 A	6% $FeCl_3$ (Na_2 EDTA stabilized)	Wrought or cast stainless steels, Ni, Cr-bearing alloys	Pitting	Visual exam. CPT
	G 48 B	6% $FeCl_3$ (Na_2 EDTA stabilized)	Wrought or cast stainless steels, Ni, Cr-bearing alloys	Pitting and crevice	Visual exam. Weight loss CPT, CCCT
ASTM G 61		3.56% NaCl	Fe, Ni, or Co-based alloys	Localized corrosion	Polarization curves, E_c
ASTM G 78		Seawater	Fe or Ni-based stainless steels	Crevice corrosion	Visual exam. Weight loss

Source. From "Fabrication and Corrosion Behavior of High Alloy Cast Materials: A State-of-the-Art Review" by C. D. Lundin, L. Li, G. L. Lu, and W. Liu, Table 4, pp. 39–40, University of Tennessee–Knoxville for Steel Founders' Society of America, November 1995.

TABLE 17.4 Other than ASTM Tests Used to Evaluate Resistance of Welds to Various Forms of Corrosion

Standard	Solution	Applicability of Test	Results	Criteria
Du Pont	10% HCl	Cast high alloys: CW12M, CW7M, CW2M	Intergranular attack	Etch structures Weight loss
	20% HCl	Cast high alloys: N-12M-1, N-12M-2	Intergranular attack	Etch structures Weight loss
INCO Alloy	Saturated SO_2 + 26% NaCl	Ni-Cr-Mo corrosion-resistant alloys: 622, 686, C-22, C-276, and weld filler metals	Pitting test	Visual exam. CPT
	11.9% H_2SO_4 + 1.3% HCl + 1% $FeCl_3$ + 1% $CuCl_2$	Ni-Cr-Mo corrosion-resistant alloys: 622, 686, C-22, C-276, and weld filler metals	Pitting test	Visual exam. CPT
	10% H_2SO_4 + 2% HCl	Ni-Cr-Mo corrosion-resistant alloys: 622, 686, C-22, C-276, and weld filler metals	General corrosion	Corrosion rate
Allegheny and Trent Tube	"Yellow death" solution: 4% NaCl + 1% $Fe_2(SO_4)_3$ +0.01 M HCl	AL-6XN and other wrought or cast austenitic stainless steels	Pitting test	CPT
	10% ferric chloride	AL-6XN and other wrought or cast austenitic stainless steels	Pitting and crevice test	CPT; CCCT
Haynes	60 vol% H_2SO_4 + 20 vol% HCl + 15 vol% HNO_3 + 1 vol% HF + 1% $FeCl_3$	Cast or wrought nickel alloys: C-22, C-4C, C-276	General corrosion	Corrosion rate

Source. From "Fabrication and Corrosion Behavior of High Alloy Cast Materials: A State-of-the-Art Review" by C. D. Lundin, L. Li, G. L. Lu, and W. Liu, Table 5, p. 41, University of Tennessee–Knoxville for Steel Founders' Society of America, November 1995.

for stainless steels, employing exposure to boiling 65% nitric acid for five 48-h periods and evaluating mils loss per year after each exposure; (2) the Streicher test (ASTM A-262-55T) for screening susceptible stainless steels (to subsequently be tested using the Huey test), employing an electrochemical etch in 10% oxalic acid for 1.5 min under an applied current density of 1 A/cm^2, and examining at 250–500× magnification to detect grain boundary trenching; and (3) the Warren test for type 316L stainless steel (due to its unfair disadvantage in the Huey test due to the presence of sigma phase), employing 10% nitric acid/3% hydrochloric acid mixture at 70–80°C for two 2-h or $5\frac{1}{2}$-h periods of exposure. There are also variants of the Huey test using other solutions (e.g., the Strauss test using aqueous copper sulfate) and the Streicher test.

17.5.6.5. Stress Corrosion and Its Testing. When localized, as opposed to general, corrosive attack and intergranular cracking occurs in the presence of residual or applied tensile stresses, the phenomenon is called *stress-corrosion cracking*. Since stress almost always accelerates corrosion, the important point that distinguishes stress-corrosion cracking is severe localized attack with little or no generalized attack. While the precise mechanism is still subject to debate, a preferred model involves the formation of pits (as in pitting corrosion) and the progressive rupture of the passivating film near the stressed tip of an initially incipient and then growing crack.

Susceptibility to stress corrosion is usually evaluated by immersing a specimen into a suitable (based on expected service) corrosive medium under sustained stress. U-bend, hairpin and horseshoe type specimens are typically used, in what are classified as constant load, constant strain, and constant strain-rate tests.

Tables 17.3 and 17.4 list various tests for evaluating the susceptibility of welds to various forms of corrosion. Table 17.3 lists tests standardized by ASTM, and Table 17.4 lists tests other than ASTM-standardized tests. Potential problems from corrosion can be so severe, and the mechanisms so complex, that the interested reader is strongly encouraged to seek out specialize references, such as those at the end of this chapter.

17.6. SUMMARY

It is neither prudent nor sufficient to simply weld a material or a structure. Before beginning to weld an actual structure, it is important to know whether the material to be welded will be easy or difficult to weld, by its inherent nature, under the kinds of mechanical restraint that will be encountered during welding, and in the environment within which welding must take place. Such knowledge is gained from weldability tests. These allow assessment of the possible problems in the fusion zone or partially melted zone from so-called hot-cracking mechanisms or in the heat-affected zone from so-called cold

mechanisms, including hydrogen cold cracking, postweld heat treatment reheat or strain-age cracking, or lamellar tearing.

It is also essential after a material or structure has been welded to know its properties, and it is helpful to have such knowledge even before weld fabrication begins. For this reason weld testing is critical. Welds should be tested for those properties that are either essential or important for satisfactory performance of the finished product, including both mechanical properties and corrosion behavior. Mechanical properties that can be tested include tensile strength and ductility, bend ductility, resistance to impact, shear strength, fracture toughness, fatigue strength and life, and stress-rupture and creep response. Corrosion behavior of interest includes general corrosion, crevice corrosion, pitting, intergranular corrosion due to sensitization from welding, and stress corrosion due to the stresses induced by welding.

REFERENCES AND SUGGESTED READING

Batte, A. D., and Murphy, M. C., 1979, "Reheat cracking in 2.25Cr-1Mo weld metal: influence of residual elements and microstructure," *Metals Technology*, **6**, 62–68.

Fontana, M. G., 1986, *Corrosion Engineering*, 3d ed., McGraw-Hill, New York.

Glover, A. G., Jones, W. K. C., and Price, A. T., 1977, "Assessment of resistance of low-alloy steels to reheat cracking using the Vinckier test," *Metals Technology*, **4**, 326–332.

Gooch, T. J., and King, B. L., 1980, "Creep crack growth in controlled microstructure Cr-Mo-V heat-affected zones," *Welding Journal*, **59**(1), 10s–18s.

Lundin, C. D., Liu, P. Qiao, C. Y. P., Zhou, G., Khan, K. K., and Prager, M., 1996, "An experimental study of causes and repair of cracking in 1-1/4Cr–1/2Mo steel equipment," *Welding Research Council (WRC) Bulletin 411*, Welding Research Council, New York.

O'Connor, L. P. (Editor), 1987, *Welding Handbook*, Vol. 1: *Welding Technology*, 8th ed., American Welding Society, Miami, FL.

Petch, H. J., 1952, "Delayed fracture of metals under static load," *Nature*, **169**, 842–843.

Randall, M. D., Monroe, R. E., and Rieppel, P. J., 1961, *Methods of Evaluating Welded Joints*, Defense Materials Information Center, Report No. 165, Battelle Memorial Institute, Columbus, OH.

Savage, W. F., Nippes, E. F., and Husa, E. I., 1982, "Hydrogen-assisted cracking in HY-130 weldments," *Welding Journal*, **61**(8), 233s–242s. [RPI Augmented Strain Cracking Test]

Stout, R. D., Vasudevan, R., and Pense, A. W., 1976, "A field weldability test for pipeline steels," *Welding Journal*, **55**(4), 89s–94s. [Lehigh Slot Weldability Test]

Troiano, A. R., 1960, "The role of hydrogen and other interstitials in the mechanical behavior of metals," *Transactions of the ASM*, **52**, 54–80.

Vagi, J. J., Meister, R. P., and Randall, M. D., August 1968, *Weldment Evaluation Methods*, DMIC Report 244, Advanced Materials and Processes Information Analysis Center (AMPTIAC), 201 Mill Street, Rome, NY.

Suggested readings on various weldability tests

Abplett, W. R., and Pellini, W. S., 1954, "Factors which influence hot cracking," *Welding Journal*, **33**(2), 83s–90s. [Finger test].

Ballass, J. T., Freedman, B. J., and Goodman, S., 1967, "Submerged arc welding of Army armor," *Welding Journal*, **46**(3), 105s–113s. [Root-pass crack test]

Borland, J. C., 1960, "Cracking test for assessing weldability," *British Welding Journal*, **7**(10), 623–628. [Houldcroft Test]

Chakravarti, A. P., and Bala, S. R., 1989, "Evaluation of weld metal cold cracking using the G-BOP test," *Welding Journal*, **68**(1), 1s–8s. [G-BOP test]

Cottrell, C. L. M., 1953, "Controlled thermal severity cracking test simulating practical weld joints," *Welding Journal*, **32**(6), 257s–272s. [Controlled-thermal-severity (CTS) test]

Gittos, N. F., and Scott, M. H., 1981, "Heat-affected zone cracking of Al-Mg-Si alloys," *Welding Journal*, **60**(6), 95s–103s. [Circular-patch test]

Goodwin, G. M., 1987, "Development of a new hot-cracking test: the sigmajig," *Welding Journal*, **66**(2), 33s–38s. [Sigmajig test]

Hackett, J. E., and Seaborn, L. O., 1952, "Evaluation of the circular-patch weld test," *Welding Journal*, **31**(8), 387s–392s. [Circular-patch test]

Henry, A., and Clausson, G. E., 1949, *Welding Metallurgy*, 2d ed., revised by G. E. Linnert, American Welding Society, Miami, FL. [Circular-groove test]

Hoerl, A., and Moore, T. J., 1957, "The welding of type 347 steel," *Welding Journal*, **36**(10), 442s–448s. [Segmented-groove test).

Houldcroft, P. T., 1955, "A simple cracking test for use with argon arc welding," *British Welding Journal*, **2**(10), 471–475. [Houldcroft test].

Jones, P. W., 1957, "The Murex hot cracking test," *British Welding Journal*, **36**(4), 189–197. [Murex Hot Cracking Test]

Kaufman, E. J., Pense, A. W., and Stout, R. D., 1981, "An evaluation of factors significant to lamellar tearing," *Welding Journal*, **60**(3), 43s–49s. [Lehigh cantilever lamellar tearing test]

Liptax, J. A., and Baysinger, F. R., 1968, "Welding dissimilar aluminum alloys," *Welding Journal*, **47**(4), 173s–180s. [Houldcroft test]

Lundin, C. D., Lingenfelter, G. E., Lessmann, G. G., and Matthews, S. J., 1982, "The varestraint test," *WRC Bulletin No. 280*, Welding Research Council, New York. [Varestraint test]

Mishler, H. W., Monroe, R. E., and Rieppel, P. J., 1959, "Determination of the Causes of Weld-Metal Cracking in High-Strength Steels and the Development of Heat-Treatable Low-Alloy Steel Filler Wires for Use With the Inert Gas-Shielded Arc-Welding Process," Battelle Memorial Institute, WADC Technical Report 59-531 (AF Contact No. 33(615)-5878) [Battelle test]

Savage, W. F., and Lundin, C. D., 1965, "The varestraint test," *Welding Journal*, **44**(10), 433s–442s. [Varestraint test]

Stern, I. L., and Quattrone, R., 1967, "A multiple test approach to the prediction of weldment cracking," *Welding Journal*, **46**(5), 203s–216s. [Navy Circular-fillet-weldability (NCFW) test]

Stout, R. D., and Doty, W. D., 1953, *Weldability of Steel*, Welding Research Council, New York. [Lehigh restraint cracking test]

Walsh, D. W., Campbell, R. D., and Savage, W. F., 1986, unpublished research, Rensselaer Polytechnic Institute, Troy, NY. [Impulse decanting]

Watkinson, F., 1961, "Welding medium carbon steels," *British Welding Journal*, **8**(3), 93–103. [Wedge test]

Weiss, S., Hughes, W. P., and Macke, H. J., 1962, "Welding evaluation of high-temperature sheet materials by restrained patch testing," *Welding Journal*, **41**(1), 17s–22s. [Restrained-patch test]

White, S. S., Moffat, W. G., and Adams, C. M., Jr., 1958, "Dynamic measurement of stress associated with weld cracking," *Welding Journal*, **37**(4), 185s–192s. [Keyhole-slotted-plate restraint test]

Suggested readings on weld simulation

Nippes, E. F., and Savage, W. F., 1949, "Development of specimen simulating weld heat-affected zones," *Welding Journal*, **28**(11), 534s–546s.

Weld Thermal Simulators for Research and Problem Solving, 1972, edited by R. E. Dolby, The Welding Institute, Cambridge, U.K.

CLOSING THOUGHTS

Welding is a critically important process in modern construction and manufacturing from both a technological and an economic standpoint. It has been estimated that more than half the gross national product of all the industrialized countries in the world comes either directly or indirectly from welding. The process may be used to join materials into parts and parts into structures or assemblies and it may be used to build the machines that make those materials and parts.

A little reflection on our world makes it clear just how essential welding is. Huge welded offshore drilling platforms tap new reserves of oil and natural gas in the wilds of the Arctic, the fury of the North Sea, and the warm waters of the Gulf of Mexico. Welded steel pipelines transport natural gas and oil from the Bering Sea across Alaska and Canada to the Pacific Northwest of the United States, across the barren steppes of Siberia to Western Russia and across the Ural Mountains to Western Europe, and across the great deserts of the Mideast to ports on the Red Sea and Mediterranean Sea. Giant 100,000-ton supertankers with welded hulls and superstructures ply the oceans, moving oil around the world. Welded reaction vessels, cracking and distillation towers, and storage tanks enable conversion of crude oil and natural gas into critical fuels, lubricants, solvents, plastics, and other products that have become essential to the world. Welding is used to construct our buildings of manufacture, trade, commerce, service, and residence, and large electric generators, high-voltage transmission towers, and microelectronic devices that provide

energy to our homes and businesses and information to our minds. Welding is involved in the manufacture of our cars, buses, trucks, RVs, trains, ships, and airliners. We use welding to construct bridges that span gorges, rivers, and ravines, and to manufacture giant rocket boosters, space stations, and reentry vehicles that allow us to bridge the distances to our past and our future. The list goes on and on, and the import and impact of welding is obvious.

If we have progressed to the degree that we have by using welding with far less-than-optimum understanding, just think of how fast and to what level we could progress with full understanding. Hopefully, this book has brought you a little closer.

APPENDICES

This Page Intentionally Left Blank

APPENDIX A

TABLE A1 Designation of Welding and Allied Processes by Letter

Welding and Allied Processes	Letter Designation	Welding and Allied Processes	Letter Designation
Adhesive bonding	ABD	dip brazing	DB
Arc welding	AW	flow brazing	FLB
atomic hydrogen welding	AHW	furnace brazing	FB
bare metal arc welding	BMAW	induction brazing	IB
carbon arc welding	CAW	infrared brazing	IRB
gas	CAW-G	resistance brazing	RB
shielded	CAW-S	torch brazing	TB
twin	CAW-T	Other welding processes	
electrogas welding	EGW	electron beam welding	EBW
flux cored arc welding	FCAW	high vacuum	EBW-HV
gas metal arc welding	GMAW	medium vacuum	EBW-MV
pulsed arc	GMAW-P	nonvacuum	EBW-NV
short circuiting arc	GMAW-S	electroslag welding	ESW
gas tungsten arc welding	GTAW	flow welding	FLOW
pulsed arc	GTAW-P	induction welding	IW
plasma arc welding	PAW	laser beam welding	LBW
shielded metal arc welding	SMAW	percussion welding	PEW
stud arc welding	SW	thermit welding	TW
submerged arc welding	SAW	Oxyfuel gas welding	OFW
series	SAW-S	air acetylene welding	AAW
Brazing	B	oxyacetylene welding	OAW
arc brazing	AB	oxyhydrogen welding	OHW
block brazing	BB	pressure gas welding	PGW
carbon arc brazing	CAB	Resistance welding	RW
diffusion brazing	DFB	flash welding	FW

TABLE A1 (*Continued*)

Welding and Allied Processes	Letter Designation	Welding and Allied Processes	Letter Designation
projection welding	PW	arc cutting	AC
resistance seam welding	RSEW	air carbon arc cutting	AAC
high frequency	RSEW-HF	carbon arc cutting	CAC
induction	RSEW-I	gas metal arc cutting	GMAC
resistance spot welding	RSW	gas tungsten arc cutting	GTAC
upset welding	UW	metal arc cutting	MAC
high frequency	UW-HF	plasma arc cutting	PAC
induction	UW-I	shielded metal arc cutting	SMAC
Soldering	S	electron beam cutting	EBC
dip soldering	DS	laser beam cutting	LBC
furnace soldering	FS	air	LBC-A
induction soldering	IS	evaporative	LBC-EV
infrared soldering	IRS	inert gas	LBC-IG
iron soldering	INS	oxygen	LBC-O
resistance soldering	RS	oxygen cutting	OC
torch soldering	TS	chemical flux cutting	FOC
wave soldering	WS	metal powder cutting	POC
Solid-state welding	SSW	oxyfuel gas cutting	OFC
coextrusion welding	CEW	oxyacetylene cutting	OFC-A
cold welding	CW	oxyhydrogen cutting	OFC-H
diffusion welding	DFW	oxynatural gas cutting	OFC-N
explosion welding	EW	oxypropane cutting	OFC-P
forge welding	FW	oxygen arc cutting	AOC
friction welding	FRW	oxygen lance cutting	LOC
hot pressure welding	HPW	Thermal spraying	THSP
roll welding	RW	arc spraying	ASP
ultrasonic welding	USW	flame spraying	FLSP
Thermal cutting	TC	plasma spraying	PSP

Source. From *Welding Handbook*, Vol. 1, 8th ed., 1990, with permission of the American Welding Society, Miami, FL.

TABLE A2 Alphabetical Cross Reference to Table A1

Letter Designation	Welding and Allied Processes	Letter Designation	Welding and Allied Processes
AAC	air carbon arc cutting	CAB	carbon arc brazing
AAW	air acetylene welding	CAC	carbon arc cutting
ABD	adhesive bonding	CAW	carbon arc welding
AB	arc brazing	CAW-G	gas carbon arc welding
AC	arc cutting	CAW-S	shielded carbon arc welding
AHW	atomic hydrogen welding	CAW-T	twin carbon arc welding
AOC	oxygen arc cutting	CEW	coextrusion welding
ASP	arc spraying	CW	cold welding
AW	arc welding	DB	dip brazing
B	brazing	DFB	diffusion brazing
BB	block brazing	DFW	diffusion welding
BMAW	bare metal arc welding	DS	dip soldering

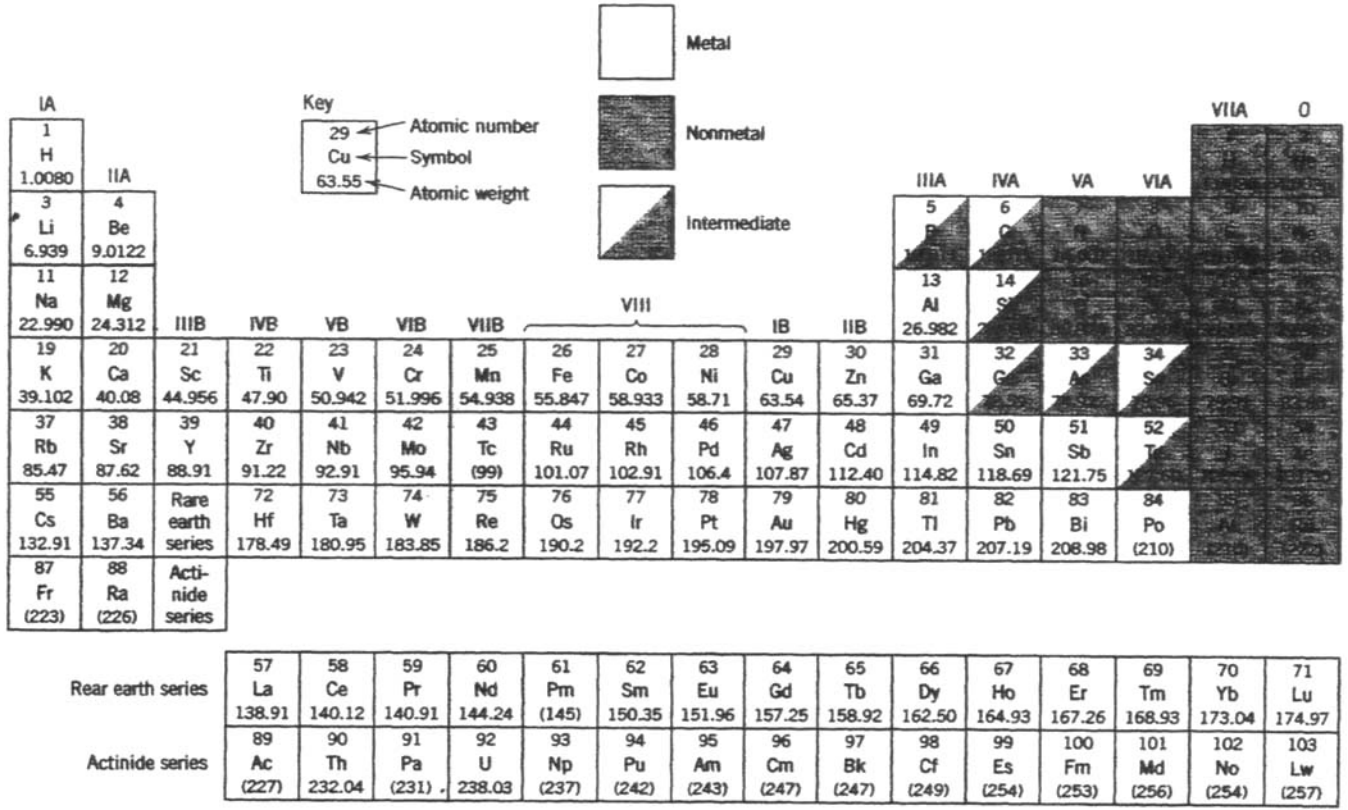
TABLE A2 *(Continued)*

Letter Designation	Welding and Allied Processes	Letter Designation	Welding and Allied Processes
EBC	electron beam cutting	LOC	oxygen lance cutting
EBW	electron beam welding	MAC	metal arc cutting
EBW-HV	electron beam welding-high vacuum	OAW	oxyacetylene welding
		OC	oxygen cutting
EBW-MV	electron beam welding-medium vacuum	OFC	oxyfuel gas cutting
		OFC-A	oxyacetylene cutting
EBW-NV	electron beam welding-nonvacuum	OFC-H	oxyhydrogen cutting
		OFC-N	oxynatural gas cutting
EGW	electrogas welding	OFC-P	oxypropane cutting
ESW	electroslag weldingB	OFW	oxyfuel gas welding
EXW	explosion welding	OHW	oxyhydrogen welding
FB	furnace brazing	PAC	plasma arc cutting
FCAW	flux cored arc welding	PAW	plasma arc welding
FLB	flow brazing	PEW	percussion welding
FLOW	flow welding	PGW	pressure gas welding
FLSP	flame spraying	POC	metal powder cutting
FOC	chemical flux cutting	PSP	plasma spraying
FOW	forge welding	PW	projection welding
FRW	friction welding	RB	resistance brazing
FS	furnace soldering	RSEW	resistance seam welding
FW	flash welding	RSEW-HF	resistance seam welding-high frequency
GMAC	gas metal arc cutting		
GMAW	gas metal arc welding	RSEW-I	resistance seam welding-induction
GMAW-P	gas metal arc welding–pulsed arc	RSW	resistance spot welding
		ROW	roll welding
GMAW-S	gas metal arc welding–short circuiting arc	RW	resistance welding
		S	soldering
GTAC	gas tungsten arc cutting	SAW	submerged arc welding
GTAW	gas tungsten arc welding	SAW-S	series submerged arc welding
GTAW-P	gas tungsten arc welding-pulsed arc	SMAC	shielded metal arc cutting
HPW	hot pressure welding	SMAW	shielded metal arc welding
IB	induction brazing	SSW	solid-state welding
INS	iron soldering	SW	stud arc welding
IRB	infrared brazing	TB	torch brazing
IRS	infrared soldering	TC	thermal cutting
IS	induction soldering	THSP	thermal spraying
IW	induction welding	TS	torch soldering
LBC	laser beam cutting	TW	thermit welding
LBC-A	laser beam cutting-air	USW	ultrasonic welding
LBC-EV	laser beam cutting-evaporative	UW	upset welding
		UW-HF	upset welding-high frequency
LBC-IG	laser beam cutting-inert gas		
LBC-O	laser beam cutting-oxygen	UW-I	upset welding-induction
LBW	laser beam welding	WS	wave soldering

Source. From *Welding Handbook*, Vol. 1, 8th ed., 1990, with permission of the American Welding Society, Miami, FL.

APPENDIX B

Periodic Table of the Elements With Metallic, Nonmetallic, and Intermediate Types Designated



Source. From *Materials Science and Engineering* by William D. Callister, 2d ed., 1985 with permission of John Wiley & Sons, Inc., New York.

APPENDIX C

Some Physical and Chemical Properties of Selected Elements

Element	Symbol	Atomic No.	Atomic Wt. (amu)	Radius (nm) Atom	Radius (nm) Ion	Density Solid @ 20°C (g/cm^3)	Crystal Structure (20°C)	Allotropic Transformations	Melting Point (°C)	L-S Vol. Change (%)	CTE @ 20°C ($10^{-6}\,°C^{-1}$)
Aluminum	Al	13	26.98	0.143	0.057(3+)	2.7	fcc	none	660.452	−6.5	23.6
Antimony	Sb	51	121.75	0.138	0.090(3+)	6.69	rhombo.	none	630.755	N/A	8–11
Arsenic	As	33	74.92	0.125	0.069(3+)	5.78	rhombo.	NA	603	N/A	5–6
Barium	Ba	56	137.33	0.217	0.143(2+)	3.59	bcc	N/A	729	N/A	18
Beryllium	Be	4	9.012	0.113	0.034(2+)	1.85	(hcp) α	β bcc @ 1270°C	1289	N/A	11.6
Bismuth	Bi	83	208.98	0.120	0.120(3+)	9.80	rhombo.	none	271.4	+(N/A)	13.2
Boron	B	5	10.81	0.097	0.023(3+)	2.34	rhombo.	none	2030	N/A	1.1
Cadmium	Cd	48	112.40	0.148	0.065(2+)	8.65	hcp	N/A	321	−4.74	31.3
Calcium	Ca	20	40.08	0.197	0.106(2+)	1.55	fcc α	β bcc @ 467°C	846	N/A	22.3
Carbon (graphite)	C	6	12.011	0.071	<0.02(4+)	2.25	hex.	none	3550	N/A	~0
Cesium	Cs	55	132.905	0.190	0.165(1+)	1.87	bcc	none	28.7	N/A	N/A
Chromium	Cr	24	52.00	0.128	0.064(3+)	7.19	bcc	fcc @ 1840°C	1875	N/A	6.2
Cobalt	Co	27	58.93	0.125	0.072(2+)	8.85	hcp α	β fcc @ 417°C	1498	N/A	13.8
Copper	Cu	29	63.54	0.128	0.096(1+)	8.96	fcc	none	1083	−4.92	16.5
Gallium	Ga	31	69.72	0.135	0.062(3+)	5.91	ortho.	none	29.8	+3.2	11.5
Germanium	Ge	32	72.59	0.139	0.044(4+)	5.32	dc	none	937	N/A	2.3
Gold	Au	79	196.97	0.144	0.137(1+)	19.3	fcc	none	1063	N/A	14.2
Hydrogen	H	1	1.00797	0.046	0.154(1−)	—	(hex.)	none	−259	N/A	—
Indium	In	49	114.82	0.162	0.092(3+)	7.31	fc tetrag.	none	157	−2.5	24.8
Iridium	Ir	77	192.2	0.135	0.066(4+)	22.4	fcc	none	2454	N/A	6.8
Iron	Fe	26	55.85	0.124	0.077(2+)	7.87	bcc α	γ fcc @ 912°C δ bcc @ 1394°C	1536	−3.4	11.8
Lead	Pb	82	207.19	0.175	0.132(2+)	11.34	fcc	none	327	N/A	29.3
Lithium	Li	3	6.939	0.152	0.068(1+)	0.53	hcp α	β bcc @ 193°C	180	+1.5	56.0
Magnesium	Mg	12	24.31	0.160	0.078(2+)	1.74	hcp	none	650	−4.2	25.2

Some Physical and Chemical Properties of Selected Elements (*Continued*)

Element	Symbol	Atomic No.	Atomic Wt. (amu)	Radius (nm) Atom	Radius (nm) Ion	Density Solid @ 20°C (g/cm^3)	Crystal Structure (20°C)	Allotropic Transformations	Melting Point (°C)	L-S Vol. Change (%)	CTE @ 20°C (10^{-6} °C^{-1})
Manganese	Mn	25	54.94	0.112	0.067(2+)	7.43	cubic α γ @ 1087°C δ @ 1138°C	β @ 707°C	1245	−1.7	21.3
Mercury	Hg	80	200.59	0.155	0.112(2+)	14.19	rhombo.	none	−38.4	N/A	—
Molybdenum	Mo	42	95.94	0.136	0.068(4+)	10.2	bcc	none	2610	N/A	0.4
Nickel	Ni	28	58.71	0.125	0.069(2+)	8.9	fcc	none	1453	N/A	13.3
Niobium	Nb	41	92.91	0.143	0.069(5+)	8.6	bcc	none	2415	N/A	7.3
Nitrogen	N	7	14.007	0.071	0.01/.02(5+)	1.03	hex.	N/A	−240	N/A	—
Osmium	Os	76	190.2	0.135	0.067(4+)	22.57	hcp	none	2700	N/A	3.2
Oxygen	O	8	15.9994	0.060	0.132(2−)	1.43	cubic	N/A	−218	N/A	—
Palladium	Pd	46	106.4	0.137	0.050(2+)	12.0	fcc	none	1552	N/A	11.8
Phosphorus	P	15	30.974	0.110	0.035(5+)	1.83	ortho.	N/A	44.2	N/A	—
Platinum	Pt	78	195.09	0.139	0.080(2+)	21.4	fcc	none	1769	N/A	9.1
Potassium	K	19	39.102	0.238	0.133(1+)	0.86	bcc	none	63.9	−2.41	N/A
Rhenium	Re	75	186.2	0.138	0.072(4+)	21.0	hcp	none	3180	N/A	6.6

Rhodium											
	Rh	45	102.905	0.134	0.068(3+)	12.4	fcc	none	1966	N/A	8.3
Ruthenium	Ru	44	101.1	0.125	0.065(4+)	12.2	hcp	none	2500	N/A	5.05
Scandium	Sc	21	44.96	0.160	0.083(2+)	2.99	fcc	none	1539	N/A	N/A
Selenium	Se	34	78.96	0.140	0.191(2−)	4.79	hex. α	β monocl. @ 209°C	217	N/A	49
Silicon	Si	14	28.09	0.117	0.039(4+)	2.34	dc	none	1410	N/A	2.6
Silver	Ag	47	107.670	0.144	0.113(1+)	10.5	fcc	none	961	−5.0	19.0
Sodium	Na	11	22.990	0.192	0.098(1+)	0.97	bcc β	α hcp @ −237°C	97.8	+1.8	68.93
Strontium	Sr	38	87.62	0.215	0.127(2+)	2.60	fcc α	β bcc @ 557°C	76.8	N/A	N/A
Sulfur	S	16	32.064	0.104	0.174(2−)	2.07	ortho.	none	119	N/A	—
Tantalum	Ta	73	180.95	0.143	0.068(5+)	16.6	bcc	none	2996	N/A	6.5
Tin	Sn	50	118.69	0.158	0.074(4+)	7.30	tetrag. α	β bcc @ 13.2°C	232	−3.2	20–23
Titanium	Ti	22	47.90	0.147	0.064(4+)	4.51	hcp α	β bcc @ 882.5°C	1668	N/A	8.41
Tungsten	W	74	183.85	0.141	0.068(4+)	19.3	bcc	none	3410	N/A	1.1
Uranium	U	92	238.03	0.138	0.105(4+)	19.0	ortho. α γ bcc @ 1042°C	β tetrag. @ 934°C	1132	N/A	25.3
Vanadium	V	23	50.94	0.136	0.065(3+)	6.1	bcc	none	1900	N/A	8.3
Zinc	Zn	30	65.37	0.137	0.083(2+)	7.13	hcp	none	419.5	−7.28	15.0
Zirconium	Zr	40	91.22	0.160	0.087(4+)	6.49	hcp α	β bcc @ 862°C	1852	N/A	5.81

This Page Intentionally Left Blank

INDEX

Acetylene feather, *see* Oxyfuel gas welding
Acicular bainite, *see* Bainite formation
Acicular ferrite, *see* Ferrite morphologies
Adaptive metallurgy, 6
Adhesive (or adhesive bonding), 4
Adjustment of oxyacetylene flames, *see* Oxyfuel gas welding
Adsorbed (layers of) gases (on surfaces), 21, 22
Age-hardened alloys, 529–536
  aging sequence, 534–536
  aging (temperature-time) cycles, 534–535
  aging or aging (heat) treatment, 532
  Al alloys, 534–536
  Arrhenius relationship, 536
  avoiding property losses (in the HAZ), 536–541
  coherent precipitates, 532, 533
  dissolution (in the HAZ), 537
  Gunnier–Preston (GP) zones, 532
  heat-treatable alloys, 535
  incoherent precipitates, 533
  loss of coherency, 532–533
  mechanism of hardening or strengthening, 532–536
  Ni-alloys, 537
  nucleation and growth, 532–533
  optimum aging, 534
  overaging, 532–535
  precipitation hardening heat treatment steps, 531–532
  prerequisites for, 531
  quenching or quenching treatment, 531
  re-aging (to recover lost properties), 541
  recovering property losses (in the HAZ), 536, 541–543
  reversion (in the HAZ), 537
  semicoherent precipitates, 532, 533
  solution heat treatment (or solutionizing treatment) or solution anneal, 531
  supersaturated state (or supersaturated solid solution), 531
  temperature (of aging) effect, 534, 536
  time (of aging) effect, 534, 536
Allied processes (to welding), 31, 35–37
  heat (or thermal or flame) straightening or shaping, 36
  surface heat treatment (or modification), 36
  thermal cutting, 36
  thermal spraying, 36
Alloying, *see* Solid solution strengthening
Alloy solidification, *see* Solidification
Alloy steels, 543, 547–550
All-weld-metal tensile tests, *see* Weld testing
Alternating current (AC) arc welding, 52
Aluminothermic (or Thermit) welding, 32, 46–48
  combustion synthesis, 48
  exothermic brazing, 48
  exothermic welding, 48
  process arrangement, 48
  reactions (for Fe and for Cu), 47

Aluminothermic (*Continued*)
self-propagating high-temperature synthesis (SHS), 48
temperatures achieved, 47–48
Aluminum alloys, 534–536. *See also* Age-hardened alloys
Amount of welding, 154
Analysis of heat flow (during welding), 161–168
Annealing treatments
homogenizing anneal (or homogenizing heat treatment), 537
normalizing anneal (or normalizing heat treatment), 537
recrystallization annealing, 537
solution annealing (or solutionizing heat treatment), 537
stress-relief annealing, 537, 550
Angular (reciprocating) friction welding, 108–109, 110
Anode fall space or drop zone, 226–227
Anode spot, 226–227
Arc blow, 68, 228–229, 231
Arc (thermal) cutting, *see* Shielded-metal arc welding; Gas-tungsten arc welding
Arc, electric (for welding), *see* Electric arc
Arc gap, 227
Arc image welding, *see* Imaged arc welding
Arc (metal arc) spraying, *see* Thermal spraying
Arc oscillation, 438
Arc plasma, 224
Arc plasma force, *see* Metal transfer modes; Weld pool convection
Arc pulsation (or arc current pulsation), 438
Arc radiation, 226–227
Arc stud welding, *see* Stud arc welding
Arc temperature, 224–225
Arc terminals, 226–227
Arc welding, 31, 35
Arc welding processes, *see* Electric arc welding processes
Arrhenius relationship, 536
Asperities (on real surfaces), 11, 12, 25
Atomic hydrogen welding, 50
Austenite decomposition (or reversion), 488–498
bainite formation, 494–496. *See also* Bainite formation
equilibrium decomposition (eutectoid transformation), 491–492
eutectoid composition, 491
eutectoid reaction, 491–492
eutectoid temperature, 492
ferrite morphologies, 493–494
habit plane, 489
martensite formation, 488–489, 495
metastable phase formation, 488
nonequilibrium decomposition/transformation, 493–496
pearlite formation, 491–492
proeutectoid cementite, 492
proeutectoid ferrite, 492
retained austenite, 496
tempered martensite, 489
tempering (or temper heat treatment), 489
untempered martensite, 489
Austenite stabilizers, 473, 550
Austenitic stainless steels, *see* Corrosion-resistant stainless steels; Stainless steels
Autogenous welding, 30, 32
Automated welding, 14
Autotempering, 547
Avrami relationship, 484, 486
AWS classification of welding and allied processes, 37–38
Axial spray transfer, *see* Metal transfer modes

Backfilled cracks, 444–446, 511
Bainite formation, 494–496
acicular (lower) bainite, 495, 496
feathery (upper) bainite, 495, 496
Baking (to remove hydrogen), 570
Ballistic-impact test (U.S. Army Ordnance), *see* Weld testing
Banding, 307, 364–365, 369
Basicity index (BI), *see* Slag-metal reactions
Battelle test, *see* Hot cracking tests
Beam welding processes, 80–87. *See also* High-density beam welding processes
electron-beam welding (EBW), 77, 80, 82. *See also* Electron-beam welding
focused IR welding, 80
imaged arc (or arc image) welding, 80
laser-beam welding (LBW), 77, 80, 82. *See also* Laser-beam welding
microwave welding, 80
Bend ductility (or bend) tests, *see* Weld testing
Bevel joints, *see* Joint configurations
Binding energy (in atomic bonds), 11
Bithermal and trithermal test welds, 597
Bonding, *see* Chemical bond formation
Bonding force, 11
Bond formation, *see* Chemical bond formation
Brazing (or brazing processes), 20, 30
Braze welding, 20, 30, 31
Bridging transfer modes, *see* Metal transfer modes
Bridging-without-interruption, *see* Metal transfer modes

Buoyancy (or gravity) force (in convection), *see* Weld pool convection
"Buttering" (or "buttering layers"), *see* Dilution
Butt joint or welds, *see* Joint configurations

Calorimetry, dry and wet (to measure energy transfer efficiency), 136–138
Capacitor-discharge welding, *see* Percussion welding
Capillarity (in solidification), 388
Carbon arc welding (CAW), 50
Carbon equivalence, 549
Carbon steels, 543, 545–547
Case 1 solidification of alloy under equilibrium, *see* Solidification
Case 2 nonequilibrium solidification of alloy, complete mixing in liquid, *see* Solidification
Case 3 nonequilibrium solidification of alloy, no mixing in liquid, *see* Solidification
Casting processes, *see* Foundry processes
Cast irons, 567
Cathode fall space or drop zone, 226, 227
Cathode spot, 226, 227
Cellular or cellular dendritic growth, *see* Solidification
Centerline segregation in welds, 422, 443. *See also* Solidification
Charpy impact test, *see* Weld testing
Chemical bond formation, 4, 9
  covalent bonds, 4
  dipole bonds (induced or permanent), 4, 9, 10
  extended covalent bonds, *see* metallic bonds
  hydrogen bonds, 4
  ionic bonds, 4
  ionic-covalent bonds, *see* mixed bonds
  metallic bonds, 4, 10
  mixed bonds, 4
  primary bonds, 4
  secondary bonds, 4
  van der Waals bonds, 4
Chemical fusion welding processes, 41–48
  aluminothermic (thermit welding), 46–48
  oxyfuel gas and oxyacetylene welding, cutting, gouging, or piercing, 41–46. *See also* Oxyfuel gas welding
Chemical heterogeneity (in welds), 359–370
  banding, 364–365, 369
  "buttering", 362
  centerline segregation (in welds), 369
  "cushion coats" or "cushion layers", 362
  dilution (in welds), 360–363. *See also* Dilution
  dissimilar metal welding, 360
  entrapped slag, 366, 368
  feed-wire stubbing, 369
  foreign-metal inclusions, 366, 368
  heterogeneous welding, 360
  homogeneous welding, 360
  impurities (in weld metal), 366, 368
  macrosegregation (in dissimilar welds), 368–370
  matching of filler to base metal, 360
  microsegregation, 363–364, 368
  nonmetallic inclusions, 366, 368
  overmatching (filler), 360–361
  porosity, 366, 368, 369
  tungsten (electrode) inclusions, 369
  undermatching (filler), 361
  unmixed zone, 365–367
Chemical sources for welding, *see* Energy sources for welding
χ phase formation, 498
Circular-groove cracking test, *see* Hot cracking tests
Circular-patch test, *see* Hot cracking tests
Classification schemes for welding, 17, 23, 27, 37–38
Classifying welding, *see* Classification schemes for welding
Clausius–Clapeyron equation, 380
Cleanliness (in welding), 12–13, 22
Closed-joint method of pressure gas welding, 100
CO_2 (gas) laser, 85, 88
Coherent interfaces, 482
Cold cracking, *see* Hydrogen
Cold cracking tests, 589–605
  controlled-thermal-severity (CTS) test, 595–597
  G-BOP (gapped bead-on-plate) test, 595, 598–600
  hydrogen cracking susceptibility (testing for), 592–600
  implant test, 595
  Lehigh restraint test, 595
  Lehigh slot weldability test, 595, 598
  RPI augmented strain cracking test, 595, 596
  Tekken test, 595, 598, 599
  wedge test, 595, 598, 599
Cold (pressure) welding processes, 20, 26, 97, 98, 100
  indentor configurations for, 100
  joint configurations for, 97, 98
Cold-worked metals and alloys, 20, 515–526
  aging after cold work (combined effect), 522–523, 534

Cold-worked metals and alloys (*Continued*)
allotropic transformations (effects of), 519, 520
avoiding property losses due to welding, 523–525
cold work, 20, 515–518
engineering metals and alloys that are cold worked, 520–522
grain growth (stage), 518–520
lower yield point, 516, 517
Lüders bands, 517
nucleation and growth, 517
peening, 524
planishing (or roll-planishing), 524
recovering properties after welding, 524–525
recovery (stage), 518
recrystallization (stage), 517–520
shot peening, 524
stored energy (of cold work), 517, 518
strain aging, 517
strain hardening, *see* work hardening
stretch leveling, 517
upper yield point, 516, 517
worked zone in pressure welded materials, 525–526
work hardening, 515–517
Columnar dendritic growth, *see* Solidification
Combined characteristic (CC/CV) power supplies, 54, 234, 235
Combined forming and diffusion welding, 119
Combustion flame, physics of, 265–266
Combustion (or oxygas) spraying, *see* Thermal spraying
Combustion synthesis, *see* Aluminothermic welding
Compact tension test, *see* Reheat tests
Competitive growth, 21, 29
Computer modeling of welding, 161–162, 167, 173, 210–213, 298
Conduction mode, *see* Melt-in mode
Constant current (CC) power supplies, 54, 232, 233
Constant voltage (CV) power supplies, 54, 232–234
Constitutional liquation, *see* Partially-melted zone
Constitutional supercooling (theory of), 426–430
Constricted arc (in plasma arc welding), 55
Consumable electrode arc welding (processes), 35, 60–71. *See individual processes*
electrogas welding (EGW), 60, 69–70
electroslag welding (ESW), 60, 70–71
flux-cored arc welding (FCAW), 60, 66–67
gas-metal arc welding (GMAW), 60–64
shielded-metal arc welding (SMAW), 60, 64–66
submerged arc welding (SAW), 60, 68–69
Contaminating (or contaminant) layers, 12, 21, 22
Continuity, metal or material, 3, 4, 18, 20, 21, 27
Continuous cooling transformation (CCT) curves and diagrams, 487
Continuous consumable electrode arc welding (processes), 35
Continuous seam diffusion welding (CSDW), 118
Continuous welds or welding, 14, 152–153
Continuous wire welding, *see* Continuous consumable electrode arc welding
Contour of welds, 63
Controlled-thermal-severity (CTS) test, *see* Cold cracking tests
Convection, *see* Weld pool convection
Conventional diffusion welding, 118
Convergent flow, *see* Weld pool convection
Conversion of mechanical work to heat, 266–267
Cooling rate (around welds), 175–176
Corner joint or welds, *see* Joint configurations
Corrosion-resistant stainless steels, 550–564
austenite stabilizers, 550
austenitic stainless steels, 550, 552, 554, 557, 558
denuded zone, 553, 560
depleted zone, *see* denuded zone
duplex stainless steels, 550, 552, 554
ferrite stabilizers, 550
ferritic stainless steels, 550–551, 554, 556, 561–563
gamma loop, 551
intergranular corrosive attack, 561
low-carbon (L) grades, 561
martensite formation, 563
martensitic stainless steels, 550, 551, 554, 555, 563–564
nitrogen-strengthened (N) grades, 561
precipitation-hardening (PH) stainless steels, 544, 552–553, 559
pseudo-binary phase diagrams, 552, 562, 563
semiaustenitic stainless steels, 553
sensitization (or weld decay), 553, 560–561
solutionizing, 561
stabilization, 561
stabilizing elements, 561
stress-corrosion cracking, 561
thermal (welding) cycles, 560
weld decay, *see* sensitization

Corrosion tests, 615–621
crevice corrosion, 617
forms of corrosion, 615
generalized corrosion, 615
Huey test, 617, 621
intergranular corrosion, 617
pitting corrosion, 617
Streicher test, 621
stress corrosion, 621
Warren test, 621
Covered arc processes, 280
Cranefield lamellar tearing test, *see* Lamellar tearing tests
Crater (or pulsing arc crater), *see* Weld pool convection
Creep isostatic pressing (CRISP), 119
Crevice corrosion, 617
Critical cooling rate (for martensite formation), 547
Current (or operating) modes for electric arc welding, 52–53
"Cushion coats" or "cushion layers", *see* Dilution)
Cutting, thermal, *see* Allied processes

DC electrode negative (also DCSP), *see* Direct current straight polarity
DC electrode positive (also DCRP), *see* Direct current reverse polarity
DC reverse polarity, *see* Direct current reverse polarity
DC straight polarity, *see* Direct current straight polarity
Decanting (of weld pools), 606
Defects in welds and welding
cold cracking, *see* hydrogen cracking
delayed cracking, *see* hydrogen cracking
embrittled region, 562–563
grain coarsening (severe), 562
hydrogen (cold or delayed) cracking, 510–511, 567, 570–571, 593
intergranular corrosive attack, 561
knife-line attack, 567, 571–573
lamellar tearing or cracking, 567, 573–574
liquation cracking, 509, 566
loss of ductility (in PMZ), 509
low (HAZ) toughness, *see* grain growth
oxygen embrittlement of grain boundaries, 573
quench cracking, 570
reheat (or strain-age) cracking, 567, 568–570, 600
root cracking, 593, 594
solidification (hot) cracking, 508–509
strain-age, *see* reheat cracking
stress-corrosion cracking, 561, 573
stress-rupture cracking, 600
toe cracking, 593, 594
underbead cracking, 546, 549, 563, 591
weld decay (in stainless steels), 553, 560–561, 567, 571
Deformation diffusion welding, 118
Delayed cracking, *see* Hydrogen
DeLong diagram, 479
Δ ferrite, 473. *See also* Primary ferrite vs. primary austenite solidification
Dendrite fragmentation, 438
Dendritic growth (mode), *see* Solidification
Denuded (or depleted) zones (in the HAZ), 553, 560
Deoxidizing/denitriding (or killing), 337–339
Design guidelines for welds, 152
Detonation spraying, *see* Thermal spraying
Die (forge) welding, 101
Diffusion (to obtain continuity in welding), 20, 22, 25, 28
Diffusional transformations, 544
Diffusion bonding, *see* Diffusion welding
Diffusion brazing (DFB), 32, 114, 119
Diffusionless transformations, 545
Diffusion joining processes, *see* Diffusion brazing; Diffusion welding
Diffusion welding (DFW), 32, 114, 115
Diffusion welding (processes), 20, 32
combined forming and diffusion welding, 119
continuous seam diffusion welding, 118
conventional diffusion welding, 118
creep isostatic pressing (CRISP), 119
deformation diffusion welding, 118
process equipment, 117
process parameter effects, 116
resistance diffusion welding, 118
steps in the process, 115, 116
superplastic forming/diffusion bonding (SPF/DB), 119, 121, 122
Dilution (in fusion welds), 360–363, 447
"buttering" or "buttering layers" to reduce, 362, 447, 574
"cushion coats" or "cushion layers" to reduce, 362
effect of joint geometry or preparation, 361
effect of welding technique, 361–362, 363
formulas to calculate, 363, 364
Direct current reverse polarity (DCRP) arc welding, 52
Direct current straight polarity (DCSP) arc welding, 52
Direct-drive friction welding, 107

Direct weldability test, *see* Weldability tests
Discontinuous consumable electrode arc welding (processes), 35
Dispersion-strengthened metals and alloys, 564–566
  high-temperature Al (HTA) alloys, 566
  mechanically-alloyed metals and alloys, 564–566
  metal-matrix composites (MMCs), 564–566
  oxide-dispersion strengthened (OSD) metals and alloys, 564–566
  reinforced metals and alloys, 564–566
Dissimilar metal welding, *see* Chemical heterogeneity
Dissolution (in the HAZ), *see* Age-hardened alloys
Distortion, thermal (due to welding), 183–190, 194–196
Distribution coefficient, equilibrium, 404. *See also* Solidification
Divorced eutectic, 462
Drag technique, *see* Metal transfer modes
Drooping power supply or drooper, *see* Constant-current power supply
Drop-globular transfer, 64. *See also* Metal transfer modes
Droplet transfer (during welding), *see* Metal transfer modes
Drop-weight impact test, *see* Weld testing
Dry boxes, *see* Shielding
Duplex stainless steels, *see* Corrosion-resistant stainless steels; Stainless steels
Dynamic equilibrium (during alloy solidification), *see* Solidification
Dynamic recrystallization (in welding), 20, 102, 117, 526

Edge joints or welds, *see* Joint configurations
Efficiency of joints, *see* Joint efficiency
Efficiency of melting (during fusion welding), 139–140
Electric arc (for welding), 26, 224
Electric arc welding processes, 49–71. *See individual processes*
  consumable electrode arc welding processes, 60–71. *See individual processes*
  nonconsumable electrode arc welding processes, 50–59. *See individual processes*
Electrical sources for welding, *see* Energy sources for welding
Electricity (for welding), 216–223
  capacitance, 226
  current, 217
  impedance, 226
  inductance, 222
  Ohm's law, 218–219
  power, 220
  resistance, 217
  root-mean-square (rms) current or voltage (in AC), 222
  voltage, 217
  welding circuit, 219
Electrode negative (also DCSP), *see* Direct current straight polarity
Electrode positive (also DCRP), *see* Direct current reverse polarity
Electrogas welding (EGW), 69–70
Electromagnetic force or emf, *see* Lorentz force
Electron-beam (thermal) cutting, *see* Allied processes
Electron-beam interactions (with materials), 253–256
Electron-beam welding (EBW), 31, 80–89, 243–256
  accelerating voltage, 246
  anodes for, 247–248
  beam control, 248–252
  beam deflection systems, 251–252
  beam generation, 81
  cathodes for, 246
  comparison to laser-beam welding (LBW), 85, 89
  cross-over (of beam), 248, 250
  efficiency of, 81
  electron speed vs. accelerating voltage, 246
  energy density range for, 80
  filament (or cathode) current, 248
  focal point (of beam), 251
  focusing (lens), 251
  gun or generator (EB gun), 246–248
  hard-vacuum arrangement, 83
  heating mechanism, 80
  keyholing, 255–256
  nonvacuum arrangement, 84
  penetration vs. operating pressure, 254, 255
  physics of electron beams and EB welding, 243–256
  shielding in, 80
  sliding-seal electron-beam (SSEB) welding, 84–85
  thermionic emission, 247
  vacuum (role of), 252–256
  vacuum modes, 85–86
  weld characteristics, 80
  working chamber, 253
Electroslag welding (ESW), 70–71
Elements, properties of, 635–637
Energy, 128

Energy capacity (of a welding source), 128–130
Energy density (for welding), 80, 130–131, 142–144
Energy density distribution (within a source), 131–133, 142–144, 146
Energy input, *see* Heat input
Energy level (or capacity), 128–130
Energy sources for welding, 26, 29, 127–130
  chemical sources, 26
  electrical sources, 26,
  mechanical sources, 26, 128. *See also* Mechanical energy sources
  source intensity, *see* Energy density
  thermal energy sources, 127–128. *See also* Thermal energy sources
Energy transfer at the interface (of various welding processes), 31–33
  chemical reaction (transfer), 32
  diffusion (transfer), 32
  electric arc transfer, 31
  gas transfer, 31
  passage of a current, 32
  radiation transfer, 31
  transfer by mechanical effect, 31
Energy transfer efficiency (during welding), 134–138
  measurement of, 136–138
Energy transfer losses (during welding), 134, 135
Epitaxial growth (during welding) or epitaxy, 21, 29
Equiaxed dendritic growth (mode), *see* Solidification
Equilibrium vs. nonequilibrium, 378–381
Equilibrium interatomic distance or spacing, *see* Interatomic distance or spacing
Evaporation, *see* Weld pool evaporation
Evolution of welding, *see* Historical evolution of welding
Eutectic reactions or transformations, 379, 454–462
  cusp formation at growth front (tendency for), 458–459
  divorced eutectic, 462
  equilibrium solidification, 460
  eutectic composition, 455
  eutectic temperature, 455
  morphology of eutectic phases, 462
  noneutectic or off-eutectic compositions (solidification at), 460–462
  nonequilibrium solidification, 461–462
  solidification sequence, 455–459
Eutectoid reaction, 379, 491–492
  proeutectoid cementite, 492
  proeutectoid ferrite, 492
Explosion-bulge impact test (U.S. Navy), *see* Weld testing
Explosion welding (EXW), 32, 103–104
  applicability to various metals and alloys, 105
  process arrangement, 104
  process operation/mechanism, 103
Expulsion or "spitting" (in resistance spot welding), 73, 241, 242
Exothermic brazing, *see* Aluminothermic welding
Exothermic (chemical) reactions (for welding), 26
Exothermic welding, *see* Aluminothermic welding
Extinguishing oxyfuel gas torches, *see* Oxyfuel gas welding

Fe-Fe_3C peritectic, 464, 465
Feathery bainite, *see* Bainite formation
Ferrite morphologies, 478, 493–494
Ferrite number (FN), 477, 480
Ferrite stabilizers, 473, 550
Ferritic stainless steels, *see* Corrosion-resistant stainless steels; Stainless steels
Filler, categories of, 30
  heterogeneous (or unmatched) filler, 30, 360
  homogeneous (or matched) filler, 30, 360
  matched (or homogeneous) filler, 30, 360
  overmatched (heterogenous) filler, 30, 360
  unmatched (or heterogeneous) filler, 30
  undermatched (heterogeneous) filler, 30, 360
Filler material (or filler metal, or filler), 5, 13
Fillet welds and welding, *see* Joint configurations
Fit-up (of a joint), 149
Finger test, *see* Hot cracking tests
Flame (thermal) cutting, *see* Allied processes
Flame shaping (or straightening), *see* Allied processes
Flame straightening (or shaping), *see* Allied processes
Flame temperatures (in oxyfuel gas torches), *see* Oxyfuel gas welding
Flash welding (FW), 32, 75, 77, 78
Fleming's left-hand rule, 229, 231
Flow of heat (during welding), *see* Heat flow
Flute instability (in molten metal transfer), 281, 283
Flux-assisted gas-tungsten arc welding (GTAW), 55

Flux-cored arc (or open arc) welding (FCAW), 66–67
advantages over SMAW, 66, 67
gas-shielded mode, 67
operation of, 67
self-shielded mode, 66
Fluxing (in fusion welding), 23
Flux protected (welding) processes, 339
FN (ferrite number), 477, 480
Focused infrared (IR) welding (or solar welding), 31, 86, 87
through-transmission IR welding, 87
Forge welding (FOW), 99, 101–102
die welding, 101
hammer welding, 101
joint designs for, 102
Foundry (or founding) processes, 6
Fracture toughness testing, 612, 614–615
Free-bend test, *see* Weld testing
Free-flight transfer modes, *see* Metal transfer modes
Friction (as a source of heat for welding), 26
Friction (or impinging) force, *see* Weld pool convection
Friction stir welding, 112–114
Friction surfacing, 114
Friction welding (FRW) processes, 105–114
angular (reciprocating) friction welding, 108–110
applicable metals and alloys, 111
basic steps in, 105–106
direct-drive friction welding, 107
friction stir welding, 112–114
friction surfacing, 114
inertia-drive or (inertia) friction welding, 107
linear (reciprocating) friction (or vibration) welding, 109, 110
microminiature thermosonic welding, 111–112
microminiature welding, 111–112
orbital (friction) welding, 107
process variations, 105–106
radial and orbital (friction) welding, 107
reciprocating friction welding, 108–112
rotational friction welding, 107–108
thermosonic welding, 111–112
typical direct-drive characteristics, 106
ultrasonic (friction) welding, 109–113
vibration welding, 109–112
Full-penetration welds or welding, 152–153
Fusing (of glass), 5
Fusion, 13, 23
Fusion bonding (of glass), 5
Fusion boundary or fusion line, *see* Microstructural zones
Fusion welding processes, 23, 29, 30, 32, 40–41. *See specific types*
aluminothermic (exothermic) or thermit welding processes, 41
beam welding processes, *see* high-intensity radiant energy processes
chemical fusion welding processes, 40, 41–48
consumable electrode arc welding processes, 41, 60–71
electric arc welding processes, 41, 50–71
exothermic welding processes, *see* aluminothermic welding processes
gas (or oxyfuel gas) welding processes, 40, 41–46
high-intensity radiant energy (or beam) processes, 41, 77–92
nonconsumable electrode arc welding processes, 41, 50–59
resistance welding processes, 41, 71–77
thermit welding, *see* aluminothermic welding processes
Fusion zone (FZ), 23, 24, 147, 172, 173, 375. *See also* Chapter 13

G/R effects during solidification, *see* Solidification
$G \times R$ effects during solidification, *see* Solidification
Gamma loop (in Fe-Cr/Ni pseudo-binary phase diagrams), 551
Gap, weld (or opening), 150–151
Gas cutting, *see* Oxyfuel gas welding
Gas lasers, 85, 88
Gas-metal arc welding (GMAW), 61–64
advantages of, 61–62
globular transfer mode, 62
molten metal transfer modes in, 62–64
operating (current) mode, 61
pull-type (or pull-gun) wire feeders, 61
pulsed-arc or pulsed-current mode, 62
push-type wire feeders, 61
role of shielding gas, 61
short-circuiting mode, 62
spatter of molten filler, 62, 63
spray transfer mode, 62
types of power supply, 61
Gas-metal reactions, *see* Molten metal reactions
Gas-tungsten arc welding (GTAW), 50–55
AC operation, 52
current (or operating) modes, 52–53

DCRP (or DCEP or DC+) operation, 52
DCSP (or DCEN or DC−) operation, 52
flux-assisted (or fluxed) GTAW, 55
"hot wire" GTAW, 55
inert shielding gases for, 54–55
operating modes, 52–53. *See also* current modes
square-wave AC, 53
tungsten electrodes for, 54
wave balancing in AC, 53
weld and welding characteristics for various operating modes, 52–53
G-BOP (gapped bead-on-plate) test, *see* Cold cracking tests
General corrosion, 617
Generalized equation of heat flow, *see* Heat flow
Ghost boundaries, 499, 508, 509
Gibbs' phase rule, 379–380
Gibbs-Thompson equation, 389
Gleeble thermal simulator, *see* Thermal simulators
Globular mode, *see* Metal transfer modes
Glove boxes, *see* Shielding
GP zones, *see* Age-hardened alloys
Grain boundary migration, 499
Grain-coarsened region, *see* Heat-affected zone
Grain-coarsening (loss of toughness from), *see* Defects
Grain detachment, 438
Grain growth, 518–520, 567
Grain-refined region, *see* Heat-affected zone
Gravitational transfer mode, *see* Metal transfer modes
Gravity (or buoyancy) force, *see* Weld pool convection
Growth modes (during solidification), *see* Solidification
Guided-bend tests, *see* Weld testing
Gunnert technique, *see* Residual stresses, measurement
Gunnier–Preston (GP) zones, *see* Age-hardened alloys

Hall–Petch relationship, 438, 526
Hammer (forge) welding, 101
Hardenability (of steels), 547, 549
Hardenable alloys, *see* Transformation-hardened alloys
Hardening by cold work or strain, *see* Work hardening
Hazard HAZ, 481
Heat (to aid welding) or heating, 13, 22
Heat-affected zone (HAZ), 24, 141, 147–148, 170, 173, 377, 514–576
age-hardenable alloys, *see* Age-hardened alloys
avoiding property losses due to welding, 523–525, 536–541, 561
cold-cracking, *see* Defects
cold-worked metals or alloys, 515–526. *See also* Work-hardened metals and alloys
defects, *see* Defects. *See also specific types*
delayed cracking, *see* Defects
denuded (or depleted) zones (in stainless steels), 553, 560
dispersion-strengthened metals and alloys, *see* Dispersion-strengthened metals and alloys
grain-coarsened region (loss of toughness in), 545. *See also* Defects
grain refined metals or alloys, 515, 526
grain-refined region, 545
hardenability (of steels), 547, 549
high-temperature heat-affected zone, 24
hydrogen cracking, *see* Defects
intergranular corrosive attack, *see* Defects
knife-line attack, *see* Defects
lamellar tearing or cracking, *see* Defects
liquation cracking, *see* Defects
location of, 514
loss of ductility, *see* Defects
low-temperature heat-affected zone, 24
low toughness, *see* Defects
martensite formation, 563
metal-matrix composites, 565–566
oxygen embrittlement, *see* Defects
partially-refined region, 545
precipitation-hardenable alloys, *see* Age-hardened alloys
preheating effect, *see* Preheat or preheating
recovering properties in, 524, 525, 536, 541–543, 561
reheat cracking, *see* Defects
retention time effects, 514, 523
sensitization, *see* Corrosion-resistant stainless steels
size and shape, 168, 170, 174
solidification cracking, *see* Defects; Hot cracking
solid solution strengthened (or alloyed) metals, 526–529
steels, *see* Transformation-hardened alloys
strain-age cracking, *see* Defects
stress-corrosion cracking, *see* Defects
tempering, 563
transformation-hardenable alloys, *see* Transformation-hardened alloys
weld decay, *see* Defects

Heat distribution (around a weld), 147
Heat flow (during welding), 147–148, 154–172
  analysis of, 161–168
  Christiansen's analysis, 167–168
  computerized modeling of, 161–162, 167, 173
  cooling rates (following welding), 159, 175
  1-dimensional heat flow, 160–161
  2-dimensional heat flow, 160–161
  3-dimensional heat flow, 160–161
  dimensionless weld depth vs. dimensionless operating parameters, 167–168
  effect of base metal thermal conditions, 170–172
  effect of welding parameters, 168–172
  effect of weldment thickness, 170–172
  generalized equation of heat flow, 158–160
  HAZ shape, 168, 170
  HAZ size, 168, 170
  "heat solid" (visualization of temperature distribution), 157–158
  intelligent automation of welding, 162
  internal heat generation (role of), 160
  isotherms (in and around welds), 159, 166
  modifications to Rosenthal's solutions, 165–167
  multipass welds or welding, 160, 175
  peak (or maximum) temperature (during welding), 156–157, 159, 174
  quasi-steady-state condition, 156, 158, 162–165
  Rosenthal's solutions (of generalized heat flow equation), 162–165
  steady-state condition, *see* quasi-steady-state condition
  weld (pool) shape, 168, 170
  weld (pool) size, 168–170
Heat forming, *see* Allied processes, heat shaping
Heat input (or net heat input), 132, 133
Heat of combustion (in a flame), 265
Heat shaping or straightening, *see* Allied processes
"Heat solid" (visualization of temperature distribution), 157–158
Heat straightening or shaping, *see* Allied processes
Heat transfer efficiency, *see* Transfer efficiency
Heat-treatable alloys, *see* Age-hardened alloys; Transformation-hardened alloys
Heli-arc welding, *see* Gas-tungsten arc welding
Heterogeneity, *see* Chemical heterogeneity
Heterogeneous (or unmatched) filler, see Filler
Heterogeneous nucleation, 389–392
Heterogeneous welds or welding, 4, 32, 34, 360
High-carbon steels, 546–547
High-density beam welding processes, 80–87. *See also* Beam welding processes
High-energy beam (as a source for welding), 26
High-frequency dielectric (or microwave) welding, 88, 91–92
High-frequency resistance seam welding (RSEW-HF), *see* Resistance seam welding
High-intensity radiant energy welding processes, 77–92
  arc image welding, 80, 86, 87
  electron-beam welding (EBW), 77, 80, 82–89
  focused IR welding, 80, 86
  imaged arc (or arc image) welding, 80, 86, 87
  laser-beam welding (LBW), 77, 80, 82
  microwave welding, 80, 88, 91–92
  solar welding, 80, 86
High-strength low-alloy (HSLA) steels, *see* Transformation-hardened alloys
High-temperature Al alloys (HTAs), 566
Historical evolution of welding, 6–8
History of welding, 6–8
Homogeneous (or matched) filler, *see* Filler
Homogeneous nucleation, 384–389
Homogeneous welds or welding, 4, 32, 34, 360
Hot cracking (or solidification cracking), 443–444, 508–509
  contraction stress effect, 444–447
  factors involved in, 444–447
  freezing range effect, 444–445
  liquation cracking, 509
  low-melting constituents (effect of), 444–447
  mechanism of, 444
  remediation of, 447–449
  restraint effect, 444–447
  surface tension (of liquid) effect, 444–447
  structure or substructure effect, 444–447
Hot cracking (weldability) tests, 580–589
  Battelle test, 580, 581, 582–583
  circular-groove cracking test, 580, 581, 586–587, 590
  circular-patch test, 580, 581, 588, 591
  finger test, 580, 581, 582
  Houldcroft test, 580–583
  keyhole-slotted-plate restraint test, 580, 581, 585–586, 588
  Lehigh restraint test, 580, 581, 583, 584
  modified circular restraint cracking test, *see* segmented-groove cracking test
  Murex hot-cracking test, 580, 581, 584, 586
  Navy circular-fillet-weldability (NCFW) test, 580, 581, 586, 589
  restrained-patch test, 580, 581, 588, 592

root-pass test, 580, 581, 584–585, 587
segmented-groove cracking test, 580, 581, 586–587, 590
sigmajig test, 580, 581, 588–589, 593
spot varestraint (or TIG-A-MA-JIG) test, 583–584
submerged arc weld cracking test, 585
TIG-A-MA-JIG test, *see* spot varestraint test
U.S. Navy circular patch test, *see* circular patch test
variable restraint (or varestraint) test, 580, 581, 583–585
Hot deformation welding processes, 20
Hot press bonding, *see* Diffusion welding
Hot pressure welding, 97, 100–101
closed-joint method of pressure gas welding, 100
joint designs for, 101
open-joint method of pressure gas welding, 100
pressure gas welding (PGW), 99, 100
Hot wire gas-tungsten arc welding (GTAW), 55
Houldcroft test, *see* Hot cracking tests
Huey test, 573, 617, 621
Hydrogen (in welds), 328–333
baking (to remove), 570
cold cracking, *see* hydrogen cracking
delayed cracking, *see* hydrogen cracking
"fish-eyes", 332
hydrogen cracking, 332–333, 510–511, 567, 570–571, 593
hydrogen embrittlement, 329–331
hydrogen porosity, 331–332
sources of, 331
theories of hydrogen-induced embrittlement/cracking, 332–333
vacuum degassing (to remove), 571
Hypereutectoid steels, 545, 546
Hypoeutectoid steels, 545, 546

Ideal weld, 7, 10, 12
Imaged arc (or arc image) welding, 31, 86, 87
Impact tests, *see* Weld testing
Impediment(s) (to making ideal welds), 10
Impinging (or friction) force, *see* Weld pool convection
Implant test, *see* Cold cracking tests
Impulse decanting, 606
Incoherent interfaces, 482
Incompatibility (during welding), 190
Indirect weldability tests, *see* Weldability tests
Induction (as a source of heat for welding), 26
Induction seam welding (RSEW-I), *see* Resistance seam welding
Inert gas chambers, *see* Shielding
Inertia-drive (friction) welding, 107
Inertia (friction) welding, 107
Inner cone (in an oxyfuel gas flame), *see* Oxyfuel gas welding
Inoculation of welds, 439
In-position welding, 63
Intelligent automation of welding, 162
Interatomic distance or spacing (at equilibrium), 10
Interface relationships (and classification) for welding, 27–30, 33
liquid/solid, 29–30, 33
solid/solid, 29–30, 33
solid/vapor, 30, 33
Interface stability theory, 432–438
Intergranular corrosion, 617, 621
Intermediate material (or intermediary), 5
Intermittent (or skip) welds or welding, 152–153
Internal stresses, *see* Residual stresses
Interpass temperature, 548
Ionization potential (or work function), 224, 285
Isostatic bonding, *see* Diffusion welding

J-groove welds, *see* Joint configurations
Joint configurations (or geometry or preparations), 148–152
bevels (single- and double-), 152
butt (or straight butt or square butt) joints, 149–151
continuous welds, 152–153
corner joints, 149–150
edge joints, 149–150
fillets (single- and double-), 152
fillet welds, 148
full-penetration (welds), 152–153
groove welds, 148
intermittent (or skip) welds, 152–153
J-grooves (single- and double-), 152
lap (or overlap) joints, 149–150, 152
partial-penetration (welds), 152–153
plug welds, 148–149
skip welds, 152–153
square butt joints, 149–150
square edge, 152
straight butt joints, 149–150
surfacing welds, 148–149
tee (or T) joints or welds, 149–150, 152
U-grooves (single- and double-), 152
V-grooves (single- and double-), 152
Joint efficiency, 11, 14
Joint fit-up, 149
Joint geometry, *see* Joint configurations

Joint preparations, *see* Joint configurations
Joule heating, 71, 237–239

Keyhole mode, 56, 58, 142–145, 235–237, 255, 256, 261–264
  EB welding (keyholing mode), 255, 256
  forces involved in formation, 143–144
  interruption of, 143, 145
  LB welding (keyholing mode), 261–264
  movement of, 145
  steps in the formation of, 143–144
Keyhole-slotted-plate restraint test, *see* Hot cracking tests
Killing (for deoxidizing/denitriding using slag systems or fluxes), 337–339
Kinetics of solid-state phase transformations, 481–489
Kink instability (in molten metal transfer), 281, 283
Knife-line attack, 567, 571–573
Kurdjamov-Sachs orientation, 495

Lamellar tearing or cracking, 153, 567, 573–574
Lamellar tearing tests, 603–606
  Cranefield lamellar tearing test, 604, 605
  Lehigh cantilever lamellar tearing test, 603, 605
  tensile lamellar tearing test, 604, 605
Lap (or overlap) joints or welds, *see* Joint configurations
Laser, *see* Laser beam welding
Laser beam interactions (with materials), 260–263
Laser-beam welding, 31, 80, 82–89, 256–264
  axial flow lasers, 261
  beam control, 260
  CO_2 (gas) laser, 85, 88, 259, 261
  comparison to electron-beam welding (EBW), 85, 89
  continuous laser, *see* CO_2 laser
  cross-flow (or transverse flow) lasers, 262
  efficiency of, 81
  energy density range for, 80
  excimer laser, 85
  excitation (or pumping) source (for lasing), 257
  fast-axial flow (gas laser), 85, 88
  gas lasers, 85, 88, 259, 261
  heating mechanism, 80
  keyholing during LBW, 261–264
  laser beam generation, 85, 256–259
  lasing (or laser light), 256, 257
  lasing media, 258
  Nd:YAG laser, 80, 258–259, 260
  physics of laser beams, 256–264
  pulsed lasers, *see* Nd:YAG laser
  shielding for, 80
  slow-axial flow (gas laser), 85, 88
  solid-state (Nd:YAG) laser, 85, 87, 258–260
  spontaneous emission, 258
  stimulated emission, 258
  transverse flow (gas laser), 85, 88, 262
  weld characteristics, 80
Laser (thermal) cutting, *see* Allied processes
Leading (torch) shields, *see* Shielding
Lehigh cantilever lamellar tearing test, *see* Lamellar tearing tests
Lehigh restraint test, *see* Cold cracking tests; Hot cracking tests
Lehigh slot weldability test, *see* Cold cracking tests
Lever rule or lever law, 404, 405
Lighting (and extinguishing) oxyfuel gas torches, *see* Oxyfuel gas welding
Linear (reciprocating) friction welding, 109, 110
Liquation cracking, 509, 566
Liquid/solid interfaces (for welding), *see* Interface relationships
Liquid-to-solid volume change (for elements), 635–637
Liquidus temperature or line, 404, 405. *See also* Solidification
Locked-in stresses, *see* Residual stresses
Longitudinal-weld face- or root-bend test, *see* Weld testing
Longitudinal-weld tensile test, *see* Weld testing
Lorentz (or electromotive or electromagnetic) force, 229. *See also* Weld pool convection
Low-carbon (L) grades of stainless steels, 561
Lower bainite, *see* Bainite formation
Lower yield point, 516, 517
Low (HAZ) toughness, *see* Defects
Lüder's bands, 517

Macrosegregation (in dissimilar welds), *see* Chemical heterogeneity
Magnetically-impelled arc butt (MIAB) welding, 31, 50, 57–59
Magnetic fields (effects on welding arcs), 228, 229, 231
Magnetic stirring, 438
Manual welding, 14
Marangoni (or surface tension gradient) force, *see* Weld pool convection
Martensite formation, 494–496, 543–544, 547. *See also* Austenite decomposition

Martensitic stainless steels, *see* Corrosion-resistant stainless steels; Stainless steels
Mash welding, *see* Resistance seam welding
Massive shear transformations, 543–544
Mass transport, 21
Matched filler, *see* Filler
Mather–Soerte technique, *see* Residual stresses, measurement
Maximum crack length (MCL), 583
Mechanical energy sources for welding, 128. *See also* Energy sources for welding
Mechanically-alloys (MA) metals, 564–566
Mechanical relief of residual stresses, 207–208
Mechanical vibration (effects on solidification), 438–439
Mechanical work (conversion to heat), *see* Conversion of mechanical work to heat
Melt-in (or conduction) mode, 56, 58, 142
Melting (to form a weld), 12, 22
Melting efficiency (during welding), 139–140
Melting vs. solidification, rates of, 399–402
Meridional (or poloidal) flow, *see* Weld pool convection
Metal arc spraying (or metallizing), *see* Thermal spraying
Metal inert gas (MIG) welding, *see* Gas-metal arc welding
Metallizing, *see* Thermal spraying
Metal-matrix composites (MMCs), 565–566
Metal (molten) transfer modes, 62–64, 270–289
  axial spray (or streaming) transfer mode, 276, 277
  bridging transfer modes, 274, 278–279, 280
  bridging-without-interruption, *see* bridging transfer modes
  buried-arc transfer technique, *see* bridging transfer modes
  covered arc processes, 280
  drag technique, 278
  drop formation and detachment sequence, 276–277
  drop transfer mode, *see* globular transfer mode
  effect of operating mode or polarity, 288
  effect of process, 287–288
  effect of shielding gas, 285–286, 288
  effect of welding parameters, 282–283, 285–287
  electromagnetic pinch (or Lorentz) force, 272, 273
  electromagnetic pressure force, 273
  electrostatic attraction force, 272
  explosive evaporation force, 272
  flute instability, 281, 283
  flux-walled guided transfer, 281
  forces contributing to, 270–274, 284
  free-flight transfer modes, 274–277
  generated gas pressure force, 271
  globular (or drop) transfer mode, 275, 277
  GMAW modes, 62–64
  gravitational transfer mode, *see* globular transfer mode
  gravity force, 272
  kink instability, 281, 283
  pinching force, *see* electromagnetic pinch force
  plasma friction force, 273
  repelled transfer mode, 277, 278
  rotating transfer, 281, 283
  short-arc technique or transfer mode, *see* bridging transfer modes
  short-circuiting (or short-circuit) transfer mode, *see* bridging transfer modes
  slag-protected transfer mode, 274, 280–282
  spatter (or spatter loss) with, 270, 275, 276, 279, 287, 288, 306–307
  spray transfer mode, *see* axial spray transfer mode
  steps in short-circuiting transfer, 279
  streaming transfer mode, *see* axial spray transfer mode
  surface tension force, 273–274
  transition current (for globular to spray mode), 276–277, 279, 282–283, 285–287
  variations in major transfer modes, 281, 283
M_f temperature, 547
Microminiature (ultrasonic) welding, 111–112
Microminiature thermosonic (ultrasonic) welding, 111–112
Microsegregation, 363–364, 368, 423–425
Microscopic equilibrium, 407
Microstructural zones (in and around welds), 375–376. *See also individual zones*
  fusion boundary or fusion line, 377
  fusion zone (FZ), 375
  heat-affected zone (HAZ), 377
  partially-melted zone (PMZ), 377
  unaffected base metal (UBM), 377
  unmixed zone (UMZ), 375
  weld metal (WM), *see* fusion zone
  weld zone (WZ), 377
Microwave (high-frequency dielectric) welding, 88, 91–92
Mild steels, *see* Carbon steels
Modified circular restraint cracking test, *see* Hot cracking tests
Molten metal reactions, 315–356
  basicity index, *see* Slag-metal reactions

Molten metal reactions (*Continued*)
deoxidizing/denitriding (or killing), 337–339
dry (or glove) boxes, 334
embrittlement reactions, 327–329
"fish-eyes", 332
flux-protected (welding) processes, 339
flux types, *see* Slag-metal reactions
gas dissolution and solubility (in molten metals), 317–323, 326
gas-metal reactions, 316–336
glove boxes, *see* dry boxes
hydrogen cracking, 332–333
hydrogen effects, 328–333
hydrogen embrittlement, 329–331
hydrogen porosity, 331–332
inert gas chambers (or dry boxes), 334
leading gas shields, 334
molten metal shielding, 333–337
nitrogen scale, 338–339
phase stabilization (by gas dissolution), 324, 325
porosity formation and effects, 326–328
self-fluxing (action), 336–337
self-protection, 333–334
shielding gases, 333–334
shielding molten metal, *see* molten metal shielding
Sievert's law, 317
slag-metal reactions, 337–356
slags for molten metal shielding, 335
solid solution hardening (by gas dissolution), 323–324
solubility of gases in molten metals, *see* gas dissolution and solubility
sources of hydrogen in welding, 331
sweeping out of gas bubbles (by convection), 327
theories of hydrogen-induced cracking, 332–333
trailing gas shields, 334
vacuum as a shield, 335–336
vacuum level (or perfection), 336
M_s temperature, 547
Multipass welds and welding, 160, 175
Murex hot-cracking test, *see* Hot cracking tests
Mushy zone, 369, 503

Navy circular-fillet-weldability (NCFW) test, *see* Hot cracking tests
Nd:YAG (solid-state) laser, 85, 87
Net energy input, *see* Heat input
Net heat input, *see* Heat input
Neutral flame (with oxyfuel gas), *see* Oxyfuel gas welding
Ni-based alloys, 537, 567–570. *See also* Age-hardened alloys
Nitrogen scale (in slag-metal reactions), 338–339
Nitrogen-strengthened (N) grades of stainless steels, 561
Nonconsumable (or permanent) electrode arc welding (processes), 35, 49–59, *see individual processes*
Nonequilibrium vs. equilibrium, 378–381
Nonfusion welding processes, 23, 30, 32, 94–122. *See also specific types*
advantages over fusion welding, 95, 97
cold (pressure) welding, 95, 97. *See also* Cold welding
deposition welding, 95, 120
diffusion brazing, 95, 114–120
diffusion joining processes, 95, 114–120
diffusion welding processes, 94, 114–120. *See also* Diffusion welding processes
disadvantages of, 97
explosion welding, 95, 103–104
friction welding processes, 94, 105–114. *See also* Friction welding processes
hot pressure welding, 95, 97–103. *See also* Hot pressure welding
inspection of, 120
mechanism of bond formation, 94
pressure welding processes, 94, 97–104
repair (of defects in), 120
roll (pressure) welding, 95, 102–103
solid-state deposition welding processes, 94, 120
Nonpressure welding, 25, 26
Nontransferred arc plasma mode, 55, 58
Nucleation and growth, 517, 532–533
Nucleation of new (equiaxed) grains in welds, 438
Nucleation sites (potency of), 484

Ohm's law, 218–219
Open arc welding, *see* Flux-cored arc welding
Open-joint method of pressure gas welding, 100
Oscillation, *see* Arc oscillation; Weld pool oscillation
Outer flame (in an oxyfuel gas flame), *see* Oxyfuel gas welding
Out-of-position welding, 63, 275
Overdesign of a weld, 154
Overwelding, 154
Overmatched filler, *see* Filler
Oxide (contaminant) layers, 12, 20, 22
Oxide-dispersion strengthened (OSD) metals

and alloys, 564–566
Oxidizing flame (with oxyfuel gas), *see* Oxyfuel gas welding
Oxyacetylene torch, *see* Oxyfuel gas welding
Oxyacetylene welding, *see* Oxyfuel gas welding
Oxyfuel gas cutting, *see* Oxyfuel gas welding
Oxyfuel gas torch, *see* Oxyfuel gas welding
Oxyfuel gas welding 41–46, 265–268
  acetylene feather (in oxyacetylene flame), 44
  adjusting a flame, 44–45
  backfire, 266
  combustion intensity, 266–268
  combustion velocity, 266
  flame propagation rate (or combustion velocity), 266
  flame stand-off, 266
  flame temperatures (of oxyfuel gas processes), 41, 44–45, 265–266
  inner cone (of an oxyfuel gas flame), 42, 265
  lighting and extinguishing a torch flame, 44–45
  neutral flame, 43–44
  outer flame (of an oxyfuel gas flame), 42, 265
  oxidizing flame, 43–44
  oxyacetylene torch, 45–46
  oxyacetylene welding, 41–46
  primary combustion (at inner cone), 41–42, 43, 265
  reducing flame, 43–44
  secondary combustion (in outer falme), 42, 43, 265
  specific flame output, *see* combustion intensity
  torch for welding and cutting, 45–46
Oxygen embrittlement (of grain boundaries in HAZs), 568

Partially-melted zone (PMZ), 23, 24, 172, 173, 377, 501–513
  alloy systems prone to constitutional liquation, 506
  constitutional liquation, 505–508
  defects in, 508–512
  eutectic temperature, 506
  extent of, 503–505
  ghost boundaries, 508, 509
  location of, 501–503
  origin of, 501–503
  remediation of PMZ defects, 511
  solvus temperature, 506
  spheroidization, 510
  thermal cycle leading to, 601
Partially-refined region, 545
Partial-penetration welds or welding, 152–153
Partitioning of solute (during alloy solidification), *see* Solidification
Peak temperature (during welding), 174. *See also* Heat flow
Pearlite transformation/formation, 491–492
Peening, 208, 524. *See also* Shot peening
Percussion welding (PEW) or capacitor-discharge welding, 77, 79
Perfect weld, *see* Ideal weld
Periodic table of elements, 633
Peritectic reactions or transformations, 454, 462–472
  equilibrium conditions (Case 1), 463–469
  Fe-Fe_3C peritectic, 464, 465
  important peritectic alloy systems, 463
  nonequilibrium peritectic solidification (Cases 2 and 3), 470–472
  peritectic composition, 462
  peritectic temperature, 462
  solidification at various compositions at the peritectic temperature, 463–470
  "walling off" during the peritectic transformation, 471
Pierce diode system, *see* Electron-beam welding, gun or generator
Pitting corrosion, 617
Planar growth (mode), *see* Solidification
Planishing (or roll-planishing), 208, 524
Plasma (for welding), 26
Plasma arc welding (PAW), 50, 55–57
  advantages over gas-tungsten arc welding (GTAW), 55–57
  comparison to gas-tungsten arc welding (GTAW), 57
  conduction (or melt-in) mode of operation, 56, 58
  constricted arc, 55
  keyhole mode of operation, 56, 58
  melt-in (conduction) mode of operation, 56, 58
  nontransferred arc (plasma) mode, 55, 58
  operating modes of, 56
  plasma cutting, 55
  plasma spraying, 55
  shielding gases for, 55
  torch for, 56
  transferred arc (plasma) mode, 55, 58
Plasma column fall space or drop zone, 226, 227
Plasma physics, 234–236
Plasma spraying, *see* Thermal spraying
Plasma (thermal) cutting, *see* Allied processes
Plastic deformation (to aid welding), 13, 18, 22, 23, 25, 28

Poloidal (or meridional) flow, *see* Weld pool convection
Porosity, 326–327, 328
  formation and effects, 326–327, 328
  sweeping out of weld pools, *see* Weld pool convection
Post-solidification transformations (in the fusion zone), 454–499
  austenite decomposition, 489–498. *See also* Austentite decomposition
  χ phase formation, 498
  ghost boundaries, 499
  grain boundary migration, 499
  growth rate, 484, 485
  kinetics of, 481
  nucleation rate, 484, 485
  nucleation sites (potency of), 484
  percentage of transformation, 484–486
  primary ferrite vs. primary austenite solidification, 472–473, 475–488. *See also* Primary ferrite vs. primary austentite solidification
  sigma phase formation, 498
  transformation rate and proportion, 484–486
Post-weld heat treatment (PWHT)
  baking, *see* Baking
  recrystrallization (anneal), *see* Recrystallization
  solutionizing, *see* Age-hardened alloys; Corrosion-resistant stainless steels
  stress-relief, *see* Stress relief
  tempering, *see* Transformation-hardened alloys
Precipitation-hardened alloys, *see* Age-hardened alloys
Precipitation-hardening (PH) stainless steels, *see* Corrosion-resistant stainless steels; Stainless steels
Preheat (or preheating), 175, 210, 547–549, 563, 570, 571
Pressure (to obtain continuity in welding), 13, 22, 25
Pressure bonding processes, 25. *See also* Diffusion brazing; Diffusion welding
Pressure gas welding (PGW), 99–101
  closed-joint method, 100
  joint designs for, 101
  open-joint method, 100
Pressure welding processes, 25–27, 97–104
  cold (pressure) welding, 97. *See also* Cold pressure welding
  die welding, 101
  dynamic recrystallization during, 102
  explosion welding, 103–104
  forge welding, 99, 101–102
  hammer welding, 101
  hot pressure welding, 97. *See also* Hot pressure welding
  pressure gas welding, 99–101
  roll welding, 102–103
Primary combustion, *see* Oxyfuel gas welding
Primary δ-ferrite vs. primary austenite solidification (in stainless steels), 472–478
  austenite stabilizers (in stainless steels), 474
  Avrami relationship, 484, 485
  DeLong diagram, 479
  δ-ferrite, 473
  ferrite morphologies, 478
  ferrite number (FN), 477, 480
  ferrite percentage (vs. FN), 480
  ferrite stabilizers (in stainless steels), 473
  hazard HAZ, 481
  morphology of δ-ferrite in austenitic stainless steels, 476–478
  primary austenite solidification, 476
  primary δ-ferrite solidification, 476
  pseudobinary phase diagrams, 475
  Schaeffler diagram, 479
  WRC-1992 diagram, 480
Projected spray transfer, 64. *See also* Metal transfer modes
Projection welding (PW), 71, 73–74, 76
Pseudobinary (Fe-Cr/Ni) phase diagrams, 552, 562, 563
Pulsed-arc or Pulsed-current welding, *see* Metal transfer modes
Pure metal (or material) solidification, *see* Solidification, pure crystalline materials

Quench cracks or cracking, 186, 570
Quenched and tempered (Q&T) steels, *see* Transformation-hardened alloys
Quenching treatments, 531
Quench welding, 567

Radial (friction) welding, 107
Radiation (as a source of heat for welding), 26
Radiation, arc, *see* Arc radiation
Rapprochement, 18
Rare-earth stabilization (against knife-line attack), 572. *See also* Knife-line attack
Rate of growth, *see* Primary ferrite vs. primary austenite solidification
Rate of nucleation, *see* Primary ferrite vs. primary austenite solidification
Rate of (overall) phase transformation, *see* Primary ferrite vs. primary austenite solidification

Reaction bonding, 32
Recalescence, 384
Reciprocating (friction) welding, 108–110
Recovery (during recrystallization), 24, 25, 518
Recrystallization, 20, 517–520
Recrystallization, dynamic, *see* Dynamic recrystallization
Redistribution of solute (during alloy solidification), *see* Solidification
Reducing flame (with oxyfuel gas), *see* Oxyfuel gas welding
Reheat (or strain-age) cracking, *see* Defects
Reheat (or strain-age) cracking tests, 600–604
  compact tension test, 601–602
  spiral notch test, 603–604
  Vinckier test, 601–602
Reinforced metals and alloys, *see* Dispersion-strengthened metals and alloys; Metal-matrix composites
Repelled-globular transfer, 64. *See also* Molten metal transfer
Residual stresses (from welding), 183–213
  definition of, 183–184
  effect of, 196–197
  measurement of, 197–206
  microscopic vs. macroscopic, 186
  modeling, 210–211, 212, 213
  numerical methods for estimating, 210–211
  prevention of, 206–208
  reduction of, 206–208
  three-bar analog for, 186–189
  typical distributions in weldments, 191–195, 197
  various sources of, 186–190
Resistance diffusion welding, 118
Resistance heating, 26. *See also* Joule heating
Resistance seam welding (RSEW), 71, 73
  mash welding, 73
Resistance spot welding (RSW), 71–74
  expulsion (or spitting), 73
  resistive elements in welding circuit, 72
  role of pressure (or forging cycle), 73
  series-welding technique, 72, 74
  shunting, 73
  spitting (or expulsion), 73
  weld nugget formation, 73
Resistance welding cycle, 239–241
  downslope, 239, 240
  expulsion (or spitting), 241, 242
  forging force, 239, 240
  hold time, 239
  off time, 239
  postheat period, 239, 240
  precompression force, 239, 240
  preheat period, 239, 240
  quench and temper periods, 239, 240
  squeeze time, 239
  upslope, 239, 240
  weld time, 239
Resistance welding physics, 237–239
Resistance welding power supplies, 241–245
Resistance welding (RW) processes, 71–77
  capacitor-discharge welding (or percussion welding), 77, 79
  current path (or circuit elements), 73
  flash welding (FW), 71, 74–75
  high-frequency resistance seam welding (RSEW-HF), 71
  high-frequency upset welding (UW-HF), 71, 75
  induction (resistance) seam welding (RSEW-I), 71
  induction upset welding (UW-I), 71
  Joule heating, 71
  percussion welding (PEW), 71, 75
  process variables, 71
  projection welding (PW), 71, 73–74, 76
  resistance seam welding (RSEW), 71, 73
  resistance spot welding (RSW), 71
  upset welding (UW), 71, 75
Restrained-patch test, *see* Hot cracking tests
Retained austenite, 496
Reversion, *see* Age-hardened alloys
Richardson's rule (of thermionic emission), 247
Right-hand rule (for Lorentz force direction), 296
Ripples or rippling (of weld beads and welds), 307
Roll (pressure) welding (ROW), 102, 103
Root cracking, *see* Defects
Root-pass test, *see* Hot cracking tests
Rosenthal–Norton technique for measuring residual stresses, *see* Residual stresses, measurement
Rosenthal's solution of generalized heat flow equation, 162–167
Rotational (friction) welding, 107–108
Rotating arc welding, *see* Magnetically-impelled arc butt welding
Rotating spray transfer, 64. *See also* Metal transfer modes
RPI augmented strain test, *see* Cold cracking tests

Schaeffler diagram, 479
Scheil equation, 411
Secondary flame, *see* Oxyfuel gas welding

Segmented-groove cracking test, *see* Hot cracking tests
Self-fluxing (action) in welding, *see* Shielding
Self-protection, *see* Shielding
Self-propagating high-temperature synthesis (SHS), *see* Aluminothermic welding
Semiaustenitic stainless steels, *see* Corrosion-resistant stainless steels; Stainless steels
Semiautomated welding, 14
Semicoherent interfaces, 482
Sensitization or weld decay (in stainless steels), 553, 560–561
Shape welding, 36
Shielded-metal arc (or stick) welding (SMAW), 64–66
  advantages of, 66
  coating (or covering) function, 65–66
  core wire function, 65
  electrode design, 65
  operating (current) mode, 66
  shortcomings of, 66
Shielding (in welding), 13, 333–337
  dry boxes, 334
  glove boxes, 334
  inert gas chambers, 334
  leading gas shields (on torches), 334
  self-fluxing (action), 334
  self-protection, 336–337
  shielding gases, 333–334
  trailing gas shields (on torches), 334
  vacuum shielding, 335–336
Short-arc technique, *see* Metal transfer modes
Short-circuiting transfer mode, *see* Metal transfer modes
Shot peening, 524
Sievert's law, 317
Sigmajig test, *see* Hot cracking tests
σ phase formation, 498
Simulated weld tests, *see* Weldability tests
Simulation of welds and welding, *see* Thermal simulators
Size of a weld, *see* Weld size
Skip welds or welding, 152–153
Slag-metal reactions, 337–356
  acidic fluxes, 347
  basic fluxes, 347
  basicity index (BI), 344–348, 352–356
  deoxidizing/denitriding (or killing), 337–339
  fluxes for FCAW, 344, 348, 349
  fluxes for SAW, 344, 350–352
  fluxes for SMAW, 344–347
  flux shielding capacities, 340–341
  halide-oxide-type fluxes, 342–344
  halide-type fluxes, 342–344
  killing, 337–339
  neutral fluxes, 347
  oxide-type fluxes, 342–344
  role of flux ingredients and fluxes, 340
  slag formers, 342, 343
  slag function, 341–342
  thermodynamic model for, 348–354
Slag-protected transfer, *see* Metal transfer modes
Solar (or focused IR) welding, 31, 86
Solidification (of weld fusion zones), 375–450
  alloy solidification, 402–443
  applied magnetic field effect, 438
  arc current pulsation effect, 438
  arc oscillation effect, 438
  average composition line in alloys under nonequilibrium, 408–410, 422
  boundary conditions for, 406–407
  capillarity (effect on solidification), 389
  Case 1—solidification of alloy underequilibrium, 403–406
  Case 2—nonequilibrium solidification of alloys, complete mixing in liquid, 408–413
  Case 3—nonequilibrium solidification of alloys, no mixing in liquid, 413–422
  cellular or cellular dendritic (growth) mode, 420–430
  centerline segregation (origin of), 422, 443
  Clausius–Clapeyron equation, 380
  columnar dendritic (growth) mode, 428–430
  composition at solid-liquid interface of alloys, 410–411
  constitutional supercooling (theory of), 426–430
  controlling substructure, 438–443
  coring or dendritic coring, 423–425
  criteria for equilibrium, 381–382
  critical nucleus size (or critical radius), 386
  dendrite fragmentation, 438
  dendritic (or equiaxed dendritic) growth (mode), 383–384, 428–430
  diffusion (role of), 405
  distribution coefficient, equilibrium, 404
  dynamic equilibrium (during), 415–418, 422
  equilibrium vs. nonequilibrium, 378–381
  eutectic or eutectic reaction, 379. *See also* Eutectic reaction
  eutectoid or eutectoid reaction, 379. *See also* Eutectoid reaction
  forced (surface) cooling effect, 439
  G/R effects, 430, 431

$G \times R$ effects, 430, 432
Gibbs' phase' rule, 379–380
Gibbs-Thompson equation, 389
grain detachment, 438
growth modes, 382–384, 428–430
growth rate vs. temperature gradient relationships, 430–432
heterogeneous nucleation, 389–392, 438
homogeneous nucleation, 384–389
hot cracking, 443–449. *See also* Hot cracking
impurities, 438
initial transient in composition of alloy solid, 422–423
inoculant effects, 439
interdendritic microsegregation, 423–425
interface stability theory, 432–438
lever rule or lever law, 404, 405
limitations of various models of alloy solidification, 421–422
liquidus temperature or line, 404, 405
melting vs. solidification, rates of, 399–402
microequilibrium, 407
nonequilibrium vs. equilibrium, 378–381
nonequilibrium effects on, 378–379, 402, 423–443
nonequilibrium phases or constituents, 422
nonequilibrium solidification of alloys, 406–422
nucleating agent effects, 439
nucleation of new (equiaxed) grains within welds, 438
partitioning of solute, 404
planar growth (mode), 383–384, 428–430
prerequisites for, 382, 403
pure crystalline materials, 381–384
organic analogs to, 384
rapid solidification (effects of), 422–423
recalescence, 384
redistribution of solute in an alloy, 404
refinement (of structure) techniques, 438–439
Scheil equation, 411
solidus suppression, 425
solidus temperature or line, 404, 405
solute redistribution (during alloy solidification), 403–406
stirring effects, 438
substructure formation, 426–443
supercooling, 385–388
surface nucleation, 438
tie line (or horizontal tie line), 404
vibration effects, 438–439
welding speed (or resolved speed) effects, 439–440
Solidification cracking, *see* Hot cracking
Solidification of two-phase alloys, *see* Eutectic reactions or transformations
Solidification rate (in fusion welds), 174–175. *See also* Heat flow
Solid-phase weld or welding, 24, 29, 32
Solid/solid interfaces (for welding), *see* Interface relationships
Solid solution strengthening (or alloying), 526–529
  effect of welding on, 527–528
  nonheat treatable alloys, 530
Solid-state deposition welding processes, 120
  chemical deposition, 120
  chemical vapor deposition, 120
  electrochemical deposition, 120
  physical vapor deposition, 120
  vapor deposition, 120
Solid-state (Nd:YAG) lasers, 85, 87
Solid-state weld or welding, *see* Solid-phase weld or welding
Solidus temperature or line, 404, 405. *See also* Solidification
Solid/vapor interfaces (for welding), *see* Interface relationships
Solubility of gases (in welds), 317–323, 326
Solution anneal or solution heat treatment or solutionizing, *see* Age-hardened alloys
Solvus temperature or line, 506, *see* Age-hardened alloys
Source intensity, *see* Energy density
Sources (of energy) for welding, *see* Energy sources
  arc, *see* Electric arc
  friction, *see* Friction
  high-energy beam, *see* High-energy beam
  plasma, *see* Plasma
  radiation, *see* Radiation
  resistance, *see* Resistance
Spatter (of molten metal during consumable electrode arc welding), 62, 63, 270, 275, 276, 279, 287, 288, 306–307
Spiral notch test, *see* Reheat cracking tests
Spitting, weld, *see* Resistance spot welding
Spot varestraint (or TIG-A-MA-JIG) test, *see* Hot cracking tests
Spray forming, *see* Thermal spraying
Spray (axial spray) transfer mode, *see* Metal transfer modes
Square butt joint or weld, *see* Joint configurations
Square-wave AC, 53
Stabilization (of stainless steels), 561

Stabilizing elements (in stainless steels), 561, 572
Stagnant layer, 417–418
Stainless steels, 550–553. *See also* Corrosion-resistance stainless steels
  austenitic stainless steels, 550, 552, 554, 557, 558
  duplex stainless steels, 550, 552, 554
  ferritic stainless steels, 550–551, 554, 556, 561–563
  gamma loop, 551
  martensitic stainless steels, 550, 551, 554, 555, 563–564
  precipitation-hardenable (PH) stainless steels, 544, 552–553, 559
  pseudo-binary phase diagrams, 552, 562, 563
  semiaustenitic stainless steels, 553
  sensitization (or weld decay), 553, 560–561
Steels, *see specific types*, e.g., Carbon steels
Stick welding, *see* Shielded-metal arc welding
Straight butt joint or weld, *see* Joint configurations
Strain age (or reheat) cracking, *see* Defects
Strain aging, 517
Strain hardening, *see* Work hardening
Strauss test, 573
Streaming transfer, 64. *See also* Metal transfer modes
Streicher test, 621
Stress-corrosion, 621
Stress-corrosion cracking, *see* Defects
Stress relaxation, 569
Stress relief, *see* Residual stresses, relief
Stretch leveling, *see* Cold worked metals and alloys
Stringer bead technique, 567
Structural integrity (of welds and welded structures), 14
Stud arc (or arc stud) welding, 50
Submerged arc weld cracking test, *see* Hot cracking tests
Submerged arc welding (SAW), 68–69
  flux compensation (of filler metal losses), 69
  operation of, 68
  superior efficiency of, 68
Superplastic forming/diffusion bonding (SPF/DB), 119, 121, 122
Surface contamination, *see* Contaminating layers
Surface heat treatment (or modification), *see* Allied processes
  electron-beam surface modification, 36
  flame hardening, 36
  induction hardening, 36
  laser-beam surface modification, 36
Surface tension gradient force, *see* Weld pool convection

Tarnish layers, *see* Oxide layers
Taxonomy (of welding processes), 17, 28
Tekken test, *see* Cold cracking tests
Temper bead technique, 548
Tempering, *see* Transformation-hardened alloys
Tensile lamellar tearing test, *see* Lamellar tearing tests
Thermal bonding (of polymers), 5
Thermal (flame, plasma, laser, or electron-beam) cutting, *see* Allied processes
Thermal cycle (for a weld), *see* Welding thermal cycle
Thermal distortion, *see* Distortion, thermal
Thermal energy sources (for welding), 127–128
Thermal history (of a weld), *see* Welding thermal cycle
Thermally-induced stresses, 181–184
  origins of, 181
  various sources, 181–184
Thermal shaping or straightening, *see* Allied processes
Thermal simulators and thermal simulation (of welding), 176–178
Thermal spraying, *see* Allied processes
  arc (or metal arc) spraying, 36
  combustion (oxygas) spraying, 36
  detonation spraying, 36
  metal arc (or arc) spraying or metallizing, 36
  metallizing, *see* metal arc spraying
  oxygas or combustion spraying, 36
  plasma spraying, 36
  spray forming, 36
Thermal straightening or shaping, *see* Allied processes
Thermionic emission, 224, 246
Thermit (or thermite) welding, *see* Aluminothermic welding
Thermosonic welding, *see* Microminiature thermosonic welding
Through-transmission IR (focused IR) welding, 87
Tie line (or horizontal tie line), 404
TIG-A-MA-JIG (or spot varestraint) test, *see* Hot cracking tests
Toe cracking, *see* Defects
Torches (for oxyfuel gas welding), *see* Oxyfuel gas welding
Toroidal flow, *see* Weld pool convection
Total crack length (TCL), 583

Trailing (torch) shields, *see* Shielding
Transfer efficiency (or energy transfer efficiency), 134–136
Transfer losses during welding, 134, 135
Transferred arc plasma mode, 55, 58
Transferred power (from a welding source), 130
Transformation-hardened alloys, 543–550
  alloy steels, 543, 547–550
  autotempering, 547
  carbon equivalence, 549
  carbon steels, 543, 545–547
  coarsened region (in the HAZ), 545
  critical cooling rate (for steels), 547
  diffusional transformations, 544
  diffusionless transformations, 545
  grain-refined region (in the HAZ), 545
  hardenability (of steels), 547, 549
  high-carbon steels, 546–547
  high-strength, low-alloy (HSLA) steels, *see* alloy steels
  hypereutectoid steels, 545, 546
  hypoeutectoid steels, 545, 546
  interpass temperature, 548
  martensite transformation, 543–544
  massive shear transformation, 543–544
  mild steels, *see* carbon steels
  M_f temperature, 547
  M_s temperature, 547
  partially-refined region (in the HAZ), 545
  preheating, 547–549
  quenched and tempered (Q&T) steels, 538–539, 547, 550
  steels, *see specific types*
  temper bead technique, 548
  transformation-hardenable alloys, 545
  underbead cracking, 546, 549
  Widmanstatten structure, 546
Transformers (for welding), 222–223
Transient liquid (bonding), 30, 32
Transition current (for globular to spray), *see* Metal transfer modes
Transverse-weld face- or root-bend test, *see* Weld testing
Transverse-weld side-bend test, *see* Weld testing
Transverse-weld tensile test, *see* Weld testing
Tungsten (permanent or nonconsumable) electrodes (for GTAW), 54
Tungsten inert gas (TIG) welding, *see* Gas-tungsten arc welding

U-grooves, *see* Joint configurations
Ultrasonic welding (USW), 109–113
Unaffected base metal or material (UBM), 24, 25, 172, 173, 377
Underbead cracking, *see* Defects
Undermatched filler, *see* Filler
Uniform corrosion, 615, 617
Unmixed zone, 365–367
Upper bainite, *see* Bainite formation
Upper yield point, 516, 517
Upset welding (UW), 78, 79, 375
U.S. Navy circular patch test, *see* Hot cracking tests

Vacuum (in welding), *see* Shielding, also see Electron-beam welding
Vacuum degassing (to remove hydrogen), 571
Variable restraint (or Varestraint) test, *see* Hot cracking tests
V-grooves, *see* Joint configurations
Vibratory stress relief, 208
Vibration (friction) welding, 109–112
Vinckier test, *see* Reheat cracking tests
Volt-ampere (V-A) characteristics (for welding power supplies), 231–235
  combined charcteristics, 234, 235
  constant-current (CC), 232, 233
  constant-voltage (CV), 232–234
  drooper or drooping source, 232, 233
  transient effects, 232
Volume change, liquid to solid (for various elements), 635–637

Warren test, 621
Wave balancing in AC, 53
Wedge test, *see* Cold cracking tests
Wehnet cylinder, *see* Electron-beam welding, beam control
Weldability, 578
Weldability testing and tests, 577–606. *See also* Cold cracking tests; Hot cracking tests
  actual welding tests, *see* Direct weldability tests
  cold cracking tests, 580, 589–605. *See also* Cold cracking tests
  crack-susceptibility tests, 579
  direct weldability (or actual welding) tests, 578–606
  externally-loaded crack-susceptibility tests, 599
  fabrication weldability tests, 579. *See also* direct weldability tests
  fusion zone (FZ) cracking tests, 580, *see* Hot cracking tests
  hot cracking tests, 580–589. *See also* Hot cracking tests

Weldability testing and tests (*Continued*)
indirect weldability (or simulated) tests, 578, 606
lamellar tearing or cracking tests, 580, 604–605. *See also* Lamellar tearing tests
maximum crack length (MCL), 583
partially-melted zone (PMZ) cracking tests, 580
reheat (or strain-age) cracking tests, 580, 600–604. *See also* Reheat cracking tests
self-restraint crack-susceptibility tests, 599
simulated (welding) tests, *see* indirect weldability tests
solidification cracking tests, *see* Hot cracking tests
strain-age cracking tests, *see* reheat cracking tests
sub-solidus crack-susceptibility tests, *see* Cold cracking tests
super-solidus crack-susceptibility tests, *see* Hot cracking tests
total crack length (TCL), 583
Weld contour, 63
Weld decay, *see* Sensitization
Weld deposit (amount), *see* Amount of welding
Weld design guidelines, 152
Weld fit-up, 149
Weld gap, *see* Weld opening
Welding, advantages and disadvantages, 14–15
Welding, autogenous, *see* Autogenous welding
Welding cold, *see* Cold welding processes
Welding, definition of, 3
Welding, fusion, *see* Fusion welding processes, or *specific types*
Welding, nonfusion, *see* Nonfusion welding processes, or *specific types*
Welding processes, *see specific types*, e.g., Gas-tungsten arc welding
aluminothermic welding, *see* Aluminothermic welding
angular (reciprocating) friction welding, *see* Friction welding processes
arc image welding, *see* Imaged arc welding
arc welding, *see* Arc welding
atomic hydrogen welding, *see* Atomic hydrogen welding
capacitor-discharge welding, *see* Percussion welding
carbon arc welding, *see* Carbon arc welding
cold welding, *see* Cold welding
combined forming and diffusion welding (or bonding), *see* Diffusion welding
consumable electrode welding, *see* Consumable electrode arc welding
continuous electrode (or wire) welding, *see* Continuous electrode welding
continuous seam diffusion welding, *see* Diffusion welding
conventional diffusion welding, *see* Diffusion welding
deformation diffusion welding, *see* Diffusion welding
deposition welding, *see* Solid-state deposition welding
diffusion brazing, *see* Diffusion brazing
diffusion welding, *see* Diffusion welding
direct-drive (friction) welding, *see* Friction welding processes
discontinuous electrode welding, *see* Discontinuous electrode arc welding
electrogas welding, *see* Electrogas welding
electron-beam welding, *see* Electron beam welding
electroslag welding, *see* Electroslag welding
exothermic brazing, *see* Aluminothermic welding
exothermic welding, *see* Aluminothermic welding
explosion welding, *see* Explosion welding
flash welding, *see* Flash welding
flux-cored arc welding, *see* Flux-cored arc welding
focused infrared (IR) welding, *see* Focused infrared welding
forge welding, *see* Forge welding
friction stir welding, *see* Friction welding processes
friction surfacing, *see* Friction welding processes
friction welding, *see* Friction welding processes
gas-metal arc welding, *see* Gas-metal arc welding
gas-tungsten arc welding, *see* Gas-tungsten arc welding
heli-arc welding, *see* Gas-tungsten arc welding
high-frequency seam welding, *see* Resistance seam welding
hot pressure welding, *see* Hot pressure welding
imaged (or imaging) arc welding, *see* Imaged arc welding
induction seam welding, *see* Resistance seam welding
inertia (or ineria-drive) welding, *see* Friction

welding processes
infrared welding, *see* Focused infrared welding
laser-beam welding, *see* Laser beam welding
linear (reciprocating) friction welding, *see* Friction welding processes
magnetically-impelled arc butt welding, *see* Magnetically-impelled arc butt welding
metal inert gas (MIG) welding, *see* Gas-metal arc welding
microwave welding, *see* Microwave welding
nonconsumable electrode arc welding, *see* Nonconsumable electrode arc welding
open-arc welding, *see* Flux-cored arc welding
orbital (friction) welding, *see* Friction welding processes
percussion welding, *see* Percussion welding
permanent electrode welding, *see* Consumable electrode arc welding
plasma arc welding, *see* Plasma arc welding
pressure gas welding, *see* Pressure gas welding
projection welding, *see* Projection welding
radial (friction) welding, *see* Friction welding processes
reaction bonding, *see* Reaction bonding
resistance diffusion welding, *see* Diffusion welding
resistance seam welding, *see* Resistance seam welding
resistance spot welding, *see* Resistance spot welding
resistance welding, *see* Resistance welding
roll welding, *see* Roll welding
sliding-seal EB welding, *see* Beam welding
solar welding, *see* Solar welding
solid-state deposition welding, *see* Solid-state deposition welding
stud arc welding (or arc stud welding), *see* Stud arc welding
submerged arc welding, *see* Submerged arc welding
thermit (or thermite) welding, *see* Aluminothermic welding
tungsten inert gas (TIG) welding, *see* Gas-tungsten arc welding
ultrasonic welding, *see* Friction welding processes
upset welding, *see* Upset welding
vibration (or vibratory) welding, *see* Friction welding processes
Welding thermal cycle, 154–158, 176, 501, 521, 560, 572
Weld joint configurations, *see* Joint configurations
Weldment, 148
Weld nugget, 239, 241, 242
Weld opening, 150–151
Weld pool convection, 291–298
arc plasma force, *see* impinging force
buoyancy (or gravity) force, 294–295
combined force effects, 298
convergent flow, 293
crater (or pulsating arc crater), 292
divergent flow, 293
effects of convection, 298–305
electromagnetic (or Lorentz) force, 296–297
enhancing convection (in weld pools), 305–306
forces causing convection, *see* origin of convection
friction force, *see* impinging force
gravity force, *see* buoyancy force
impinging (or friction) force, 297–298
Marangoni force, *see* surface tension gradient force
meridional flow, *see* poloidal flow
modeling convection, 298
patterns of flow, 293, 296, 299–303
poloidal (or meridional) flow, 293
origin of convection (in the weld pool), 291
surface activating agents (in weld pools), 295, 296, 306
surface tension gradient (or Marangoni) force, 295–296
toroidal flow, 293
Weld pool dilution, *see* Dilution
Weld pool evaporation, 307–310
consequences of, 309
evaporative losses from weld pool, 308–309
prevention of, 309–310
vapor pressures of solutes (in Al and steels), 309–310
Weld pool oscillation, 306–308
asymmetric partial-penetration, 307
axisymmetric full-penetration, 307
axisymmetric partial-penetration, 307
frequency of (vs. mode), 308
use in penetration control, 307
Weld pool shape tests, 606
Weld pool, size and shape, 168, 170
Weld pool reactions, *see* Molten metal reactions
Weld preparations, *see* Joint configurations
Weld simulators and simulation, *see* Thermal simulators

Weld size, 154
Weld solidification, *see* Solidification
Weld testing, 577, 607–621
  all-weld-metal tensile tests, 608–609
  ballistic-impact test (U.S. Army Ordnance), 610, 614
  bend ductility (or bend) tests, 609–610
  Charpy impact test, 610, 613
  corrosion tests, *see* Corrosion tests
  drop-weight impact test, 610, 613
  explosion-bulge test (U.S. Navy), 610, 614
  fracture toughness testing, 612, 614–615
  free-bend tests, 610, 612
  guided-bend tests, 610
  impact tests, 610, 613, 614
  longitudinal-weld face- or root-bead tests, 610–612
  longitudinal-weld tensile tests, 608–609
  transverse-weld face- or root-bead tests, 610–611
  transverse-weld side-bend tests, 610–611
  transverse-weld tensile tests, 608–609
Weld zone (WZ), 173, 377
Wire feeders, 61
  pull-type, 61
  push-type, 61
Work function, *see* Ionization potential
Work-hardened metals and alloys, *see* Cold-worked metals and alloys
Work (or strain) hardening, 18, 515–517
WRC-1992 diagram, 480
Wrought iron, 573

Zones (in and around welds), *see* Microstructural zones